Earth Mechanics

Fugro - Earth Mechanics
A JOINT VENTURE

GROUND MOTION REPORT

SAN FRANCISCO-OAKLAND BAY BRIDGE EAST SPAN SEISMIC SAFETY PROJECT

Prepared for

CALIFORNIA DEPARTMENT OF TRANSPORTATION

March 2001

Earth Mechanics

Fugro - Earth Mechanics
A JOINT VENTURE

February 28, 2001
EMI Project No. 97-146

California Department of Transportation
Engineering Service Center
Office of Structural Foundations
5900 Folsom Boulevard
Sacramento, California 95819-0128

Attention: Mr. Mark Willian
Contract Manager

Subject: **Ground Motion Report**
SFOBB East Span Seismic Safety Project
Contract 59A0053, Task Order 4

Dear Mr. Willian:

Transmitted is our report on ground motion studies for the new East-Span San Francisco-Oakland Bay Bridge (SFOBB) Seismic Safety Project. The report is applicable for the entire bridge structure ranging from the Yerba Buena Island (YBI) structure through Oakland Mole approach.

On behalf of the project team, we appreciate the opportunity to provide geotechnical services on the subject project. If you have any questions or comments regarding this report, please contact our offices.

Sincerely,
EARTH MECHANICS, INC.
(on behalf of Fugro-Earth Mechanics, a Joint Venture)

Earth Mechanics

Fugro - Earth Mechanics
A JOINT VENTURE

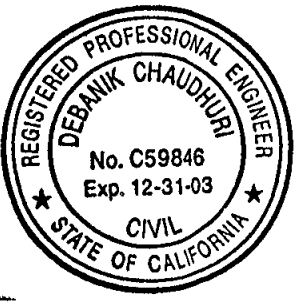

Debanik Chaudhuri, CE 59846
Project Engineer, Earth Mechanics

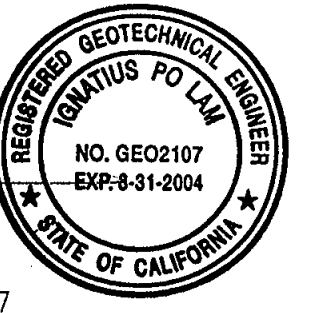

Ignatius Po Lam, GE 2107
Principal, Earth Mechanics

Hubert Law, CE 55784
Senior Engineer, Earth Mechanics

DC:HL:ipl:ss

Attachment

Copies Submitted:
Mr. Mark Willian, Caltrans (1 bound, 1 unbound reproducible)
Mr. Reid Buell, Caltrans (4)
Dr. Brian Maroney, Caltrans (1)
Mr. Ade Akinsanya, Caltrans (1)
Mr. Rafael Manzanarez, TY Lin (1)
Mr. Al Ely, Moffatt & Nichol (1)
Mr. Tim Dunne, Fugro (2)

GROUND MOTION REPORT
SAN FRANCISCO OAKLAND BAY BRIDGE
EAST SPAN SEISMIC SAFETY PROJECT

Task Order No. 4
State Contract No. 59A0053

Prepared for:

CALIFORNIA DEPARTMENT OF TRANSPORTATION

Submitted by:

FUGRO-EARTH MECHANICS
A JOINT VENTURE

February 28, 2001

EXECUTIVE SUMMARY

The development of seismic design criteria for the proposed San Francisco–Oakland Bay Bridge (SFOBB) East Span Replacement Project has involved a team of geologists, seismologists, geotechnical and structural engineers. This has made it possible to incorporate leading-edge developments in the understanding of earthquake ground motion while at the same time maintaining the balance and sense of perspective required in a robust and cost-effective engineering design process.

SEISMIC DESIGN CRITERIA TEAM

Caltrans has established a Seismic Safety Peer Review Panel (SSPRP) which meets regularly with the structural design team to review the design. The SSPRP includes Dr. I.M. Idriss, Dr. Freider Seible, Mr. Gerry Fox, Professor Ben C. Gerwick and Mr. Joe Nicoletti who serves as Chairman. An Ad Hoc Committee on Ground Motions has also been appointed by the SSPRP Chairman to establish the overall ground motion design criteria. The Ad Hoc Committee on Ground Motions includes Professor Bruce Bolt, Chairman, Professor Joseph Penzien, Dr. Roger Borcherdt and Dr. Norm Abrahamson.

Dr. Norm Abrahamson also serves as the lead seismologist for the geotechnical team and was responsible for the probabilistic seismic hazard (PSHA) and rock motion generation effort. Other key personnel contributing to the seismic hazard and ground motion efforts included Dr. Brian Maroney, Dr. Abbas Abghari and Dr. Mahmoud Khojasteh from Caltrans and Dr. Robert Pyke, Dr. Hubert Law and Mr. Po Lam of Earth Mechanics, Inc. Other subcontractors who contributed to the project included Dr. Walt Silva, Dr. Paul Sommerville and Professor John Anderson who all conducted fault-rupturing simulations to improve our understanding of fault-rupture directivity effects.

BRIDGE DESCRIPTION

The proposed East Span San Francisco-Oakland Bay Bridge (SFOBB) is located along the N6 alignment between the Yerba Buena Island (YBI) and Oakland. The structure is approximately 4.0 km long from the YBI Tunnel to the toll plaza in Oakland Mole. The entire bridge project can be divided into following four segments;

YBI Structure: A transition structure from the tunnel portal to the self-anchored suspension bridge

Main Bridge: A self-anchored cable suspension bridge extending offshore from Yerba Buena Island

Skyway Structure: A multiple-frame structure linking the cable suspension bridge to Oakland Mole

Oakland Mole Structure: An approach structure connecting Skyway Structure to the toll plaza at Oakland Mole.

SEISMIC SOURCES

The dominant earthquake sources for the SFOBB East Span Replacement Project are the Hayward fault at 9 kilometers east of the Oakland Toll Plaza and the San Andreas faults at 18 kilometers west of Yerba Buena Island.

SEISMIC HAZARD DESIGN CRITERIA

The Ad Hoc Committee on Ground Motions recommended that a probabilistic approach be adopted to define the ground motion design criteria for the East Span SFOBB project. The committee recommended a 1,500-year mean return period for the Safety Evaluation Earthquake (SEE), corresponding to a 10-percent probability of exceedance over the 150-year expected life span of the East Span structures.

Based on the deaggregated hazard, the seismic hazard at the bridge is dominated by a magnitude 7.8 event at 18 to 21 km distance on the San Andreas fault and a magnitude 7.0 event at 9 to 12 km distance on the Hayward fault. The deaggregated hazard also showed that at the 1,500-year return period, the controlling earthquakes would be associated with forward rupturing events. Therefore, the time histories should represent large magnitude earthquakes at short distances with forward fault rupturing.

The Ad Hoc Committee also recommended that the structures be checked using six sets of multiple-support ground motions with the rock motions spectrum-compatible to the 1,500-year return period spectra: three sets for San Andreas earthquake scenarios and three sets for Hayward earthquake scenarios. The committee also expressed a strong preference that the time histories be based on actual recordings rather than on synthetic motions.

DESIGN GROUND MOTIONS

Experience from recent toll bridge seismic retrofit projects suggests that motions containing a large velocity pulse or fling from forward rupturing earthquakes can be particularly damaging to bridge structures. Therefore, a major effort has been made to research the near-fault rupture directivity effects. These effects are considered in the design ground motions.

Six sets of spectrum-compatible rock motions (three each for the San Andreas and the Hayward event) were adopted for design analysis. Start-up motions for five sets were actual records chosen based on the appropriate seismological features and the remaining was an artificial record. Due to the lack of existing records for a magnitude 8 event, two sets of start-up motions for the San Andreas event were developed by splicing two actual records and the third was from the artificial record. All three start-up motions for the Hayward event are actual

records. The six sets of time histories were selected to introduce a variety of ground motions characteristics but in particular they show significant differences in the rupture directivity pulses.

Multiple-support time histories for the six sets of motions were generated at each of the bridge piers based on latest techniques. The following considerations have been included in the development of the multiple-support rock motions:

Wave-passage effects to account for travelling waves.

Compatibility with a coherency function to account for scattering and complex wave propagation phenomena as observed in closely spaced linear array data.

Attenuation of shaking amplitude with distance from the earthquake source.

Cross-correlation issues between the two orthogonal horizontal components.

Spectrum-compatibility not only at the two orthogonal horizontal reference directions but also over 360-degree rotations.

DESIGN SCENARIO

The self-anchor suspension bridge is designed by time history analyses. The Skyway structure is initially designed by ARS criteria and is later verified by multiple-support time history analyses. The YBI and Oakland Mole structures are designed by ARS criteria.

The ARS design criteria for the Skyway structure were developed by means of grouping of soil conditions along the alignment as the structure is situated in an area with thick soil sediments with variable properties. Then site response and kinematic soil-structure interaction analyses were performed to derive robust ARS curves. A similar approach was taken to develop the ARS curves for the Oakland Mole structure. However, the supports for the YBI structure are founded in rock or near bedrock, the reference rock spectra are adopted for design.

SITE RESPONSE AND SOIL-STRUCTURE INTERACTION ANALYSES

The multiple-support rock motions were used in free-field site response analyses to develop input motions for soil-structure interaction analyses and for input to the global bridge response model. The site response analyses were conducted with one-dimensional equivalent liner program SHAKE. Also, nonlinear site response analyses were conducted using TESS to appreciate effects of permanent ground displacement.

The geologic conditions at the location of the self-anchored suspension bridge (immediately offshore Yerba Buena Island) are rather complex. It is known that ground motions are sometimes amplified in such geologic conditions (commonly referred to as basin edges) due to trapping and focusing of seismic energy within the dipping near-surface sediments, resulting in amplified motions at long period and extended durations of shaking. To investigate potential

basin edge effects, two-dimensional site response analyses were conducted using QUAD4M. The results from the two-dimensional site response analyses form the basis for time history analyses of the self-anchored suspension bridge.

The vertical component spectrum-compatible rock outcrop motions were used directly for input to structural response analysis. Wave passage effect is incorporated by shifting the vertical input motion in time along the embedded pile length in accordance with an apparent wave speed close to the measured compressional wave velocity. The above adopted vertical motion approach is considered conservative because no credit is taken for the reduction in shaking amplitude with depth and the adopted wave speed is high in comparison to what is observed from downhole strong-motion data.

The soil-structure interaction analyses were performed to compute effective shaking levels at the foundation level. The approach is based on the kinematic analysis where pile foundations are supported on multiple soil layers (soil springs) that are excited by depth-varying free-field motions. The kinematic interaction analysis provides a rational means to develop appropriate seismic excitation that retains the characteristics of the depth varying motions. Mathematical derivation to compute the kinemtaic forcing function (also kinematic motion) as a result of soil-structure interaction due to depth-varying input ground motions is presented.

SEISMIC COEFFICIENT FOR GROUND STABILITY

Significant level of effort has also been placed on evaluation of liquefaction and lateral ground spread at the Oakland Mole. The same sets of ground motions developed for structural design have also been used for assessing edge-stability of the existing and proposed fills that comprise the Eastern approaches to the structures. Two-dimensional site response analyses were used to compute the average history of driving accelerations on a specified slip surface. These time histories were then used to evaluate of permanent slope displacements using the Newmark method.

TABLE OF CONTENTS

SECTION **PAGE**

EXECUTIVE SUMMARY ES-1
Seismic Design Criteria Team ES-1
Bridge Description ES-1
Seismic Sources ES-2
Seismic Hazard Design Criteria ES-2
Design Ground Motions ES-2
Design Scenario ES-3
Site Response and Soil-Structure Interaction Analyses ES-3
Seismic Coefficient for Ground Stability ES-4
1.0 INTRODUCTION 1-1
1.1 Project Limit 1-1
1.2 Background on Ground Motion 1-1
1.3 Acknowledgment 1-2
1.4 Organization of the Report 1-4
2.0 PROBABILISTIC SEISMIC HAZARD 2-1
2.1 Design Philosophy 2-1
2.2 Seismic Sources 2-1
2.2.1 Fault Sources 2-1
2.2.2 Magnitude Density Distribution 2-3
2.2.3 Rupture Dimension Relations 2-4
2.2.4 Time Dependent Earthquake Recurrence 2-4
2.3 Recurrence Relationships 2-4
2.4 Attenuation Relations 2-4
2.5 Rupture Directivity Effects 2-5
2.6 PSHA for Safety Earthquake Event 2-6
2.7 Functional Earthquake and Temporary Structures Design Criteria 2-8
2.8 Summary of SEE and FEE Spectra 2-9
3.0 REFERENCE ROCK MOTIONS 3-1
3.1 Selection of Initial Rock Motions for Subsequent Matching 3-1
3.2 Spectrum Compatible Reference Rock Motions 3-1
3.3 Cross-Correlation and Shaking Intensity Under Rotation 3-3
4.0 INCOHERENT MULTIPLE-SUPPORT ROCK MOTION TIME HISTORY 4-1
4.1 Wave Passage Effect 4-1

4.2 Spatial Coherency Effect 4-2
4.3 Attenuation 4-2
4.4 Generation of Multiple Support Ground Motions 4-3
5.0 FREE-FIELD SITE RESPONSE ANALYSES 5-1
5.1 General 5-1
5.2 Subsurface condition 5-2
5.2.1 Yerba Buena Island 5-2
5.2.2 Offshore Marine Area 5-2
5.2.3 Oakland Mole Area 5-3
5.3 Shear Wave Velocity 5-4
5.4 Modulus Reduction and Damping Curves 5-4
5.5 Site Response Analysis 5-5
5.5.1 YBI Structure 5-5
5.5.2 Suspension Bridge 5-5
5.5.3 Skyway Structure 5-6
5.5.3.1 Site Response Analyses for ARS Design Criteria 5-6
5.5.3.2 Pier Specific Site Response Analyses 5-7
5.5.4 Oakland Mole 5-8
6.0 KINEMATIC SOIL-PILE INTERACTION 6-1
6.1 Concept for Substructuring 6-1
6.2 Theoretical Background 6-1
6.3 Development of Kinematic Motion and Condensed Stiffness Matrix 6-3
6.4 Treatment of Mass and Damping 6-5
7.0 DEVELOPMENT OF ARS DESIGN CRITERIA 7-1
7.1 YBI Structure 7-1
7.2 Suspension Bridge 7-1
7.3 Skyway Structure 7-1
7.3.1 Sensitivity Studies 7-1
7.3.2 Other Considerations 7-2
7.4 Oakland Mole Structure 7-3
7.5 Vertical ARS Spectra 7-3
8.0 MULTIPLE SUPPORT KINEMATIC MOTION 8-1
8.1 Analytical Procedure 8-1
8.2 Soil Springs and Pile Properties 8-1
8.3 Treatment of Vertical Motion 8-2
8.4 Implementation 8-2
8.5 Results of kinematic motions 8-3
9.0 SUMMARY AND CONCLUSIONS 9-1
10.0 REFERENCES 10-1

APPENDICES

Appendix A Probabilistic Seismic Hazard Assessment, Mathematical Details
Appendix B Attenuation Relations
Appendix C Non-stationary Spectral Matching Program, RSPMATCH
Appendix D Spectral Matching Example
Appendix E Characteristics of Initial Startup Motions and SEE Reference Motions
Appendix F Empirical Plane-wave Coherency Models for Horizontal and Vertical Components
Appendix G Guidelines for Generation of Response-Spectrum Compatible Rock Motion Time Histories for Application to Caltrans Toll Bridge Seismic Retrofit Projects

LIST OF TABLES

2-1	Seismic Sources Based on Deterministic Model	2-2
2-2	Sources and Source Parameters Used in Hazard Analysis	2-3
2-3	Rock Outcrop SEE Design Spectra at 5 Percent Damping	2-7
2-4	Percentage Contribution to Seismic Hazard	2-8
2-5a	Deaggregation of Hazard by Source	2-10
2-5b	Deaggregation of Hazard by Distance	2-11
2-6	Earthquake Scenario for SEE Design	2-11
3-1	Candidate Time Histories for Initial Rock Motions	3-1
3-2	Peak Ground Motion Values for Six Sets of Reference Rock Motions	3-2
4-1	Parameters for Multiple Support Ground Motion	4-4
7-1	Parameters Used for Sensitivity Study	7-1
7-2	ARS Curves for Skyway Structure for Vertical Piles at 5 % Damping	7-4
7-3	ARS Curves for Skyway Structure for Battered Piles at 5% Damping	7-6
7-4	Scaling Factors for Different Levels of Damping for Skyway ARS Curves	7-8
8-1	Sectional Properties of Piles	8-2

PLATES

1-1 Project Location Map
2-1 Fault Map Around the Project Site
2-2 Comparison of Probabilistic Hazard Solutions from Prior (Retrofit) and Present Studies
2-3 East and West Side PSHA : Fault Normal Spectra for SEE
2-4 Three Components of Target Rock Spectra for SEE
2-5 Comparison Between 1,500-Yr PSHA and MCE Spectra
2-6a Deaggregated Hazard According to Source at 0.5 Sec Period : FP
2-6b Deaggregated Hazard According to Source at 1.0 Sec Period : FP
2-6c Deaggregated Hazard According to Source at 2.0 Sec Period : FP
2-6d Deaggregated Hazard According to Source at 3.0 Sec Period : FP
2-6e Deaggregated Hazard According to Source at 5.0 Sec Period : FP

2-7a Deaggregated Hazard According to Source at 0.5 Sec Period : FN
2-7b Deaggregated Hazard According to Source at 1.0 Sec Period : FN
2-7c Deaggregated Hazard According to Source at 2.0 Sec Period : FN
2-7d Deaggregated Hazard According to Source at 3.0 Sec Period : FN
2-7e Deaggregated Hazard According to Source at 5.0 Sec Period : FN
2-8a Deaggregated Hazard According to Distance at 0.5 Sec Period : FP
2-8b Deaggregated Hazard According to Distance at 1.0 Sec Period : FP
2-8c Deaggregated Hazard According to Distance at 2.0 Sec Period : FP
2-8d Deaggregated Hazard According to Distance at 3.0 Sec Period : FP
2-8e Deaggregated Hazard According to Distance at 5.0 Sec Period : FP
2-9a Deaggregated Hazard According to Distance at 0.5 Sec Period : FN
2-9b Deaggregated Hazard According to Distance at 1.0 Sec Period : FN
2-9c Deaggregated Hazard According to Distance at 2.0 Sec Period : FN
2-9d Deaggregated Hazard According to Distance at 3.0 Sec Period : FN
2-9e Deaggregated Hazard According to Distance at 5.0 Sec Period : FN
2-10 Comparison Between 92-Year PSHA and Deterministic FEE Spectra
2-11 Target Rock Outcrop Spectra for SEE
3-1 Startup Time Histories for Spectral Matching : FN Component
3-2 Reference Rock Outcrop Motion, Set1, FN Component, San Andreas Event
3-3 Reference Rock Outcrop Motion, Set1, FP Component, San Andreas Event
3-4 Reference Rock Outcrop Motion, Set1, Vertical Component, San Andreas Event
3-5 Reference Rock Outcrop Motion, Set2, FN Component, San Andreas Event, Synthetic
3-6 Reference Rock Outcrop Motion, Set2, FP Component, San Andreas Event, Synthetic
3-7 Reference Rock Outcrop Motion, Set2, Vert. Component, San Andreas Event, Synthetic
3-8 Reference Rock Outcrop Motion, Set3, FN Component, San Andreas Event, Composite Landers
3-9 Reference Rock Outcrop Motion, Set3, FP Component, San Andreas Event, Composite Landers
3-10 Reference Rock Outcrop Motion, Set3, Vert. Component, San Andreas Event, Composite Landers
3-11 Reference Rock Outcrop Motion, Set4, FN Component, Hayward Event, West Pico Canyon
3-12 Reference Rock Outcrop Motion, Set4, FP Component, Hayward Event, West Pico Canyon
3-13 Reference Rock Outcrop Motion, Set4, Vert. Component, Hayward Event, West Pico Canyon
3-14 Reference Rock Outcrop Motion, Set5, FN Component, Hayward Event, LPGC Record
3-15 Reference Rock Outcrop Motion, Set5, FP Component, Hayward Event, LPGC Record
3-16 Reference Rock Outcrop Motion, Set5, Vert. Component, Hayward Event, LPGC Record
3-17 Reference Rock Outcrop Motion, Set6, FN Component, Hayward Event, Saratoga Record
3-18 Reference Rock Outcrop Motion, Set6, FP Component, Hayward Event, Saratoga Record
3-19 Reference Rock Outcrop Motion, Set6, Vert Component, Hayward Event, Saratoga Record
3-20 Cross-correlation of Horizontal Components of Motion, Set1, San Andreas Event

3-21 Cross-correlation of Horizontal Components of Motion, Set2, San Andreas Event
3-22 Cross-correlation of Horizontal Components of Motion, Set3, San Andreas Event
3-23 Cross-correlation of Horizontal Components of Motion, Set4, Hayward Event
3-24 Cross-correlation of Horizontal Components of Motion, Set5, Hayward Event
3-25 Cross-correlation of Horizontal Components of Motion, Set6, Hayward Event
4-1a Coherency Functions for Horizontal Component Motion
4-1b Coherency Functions for Vertical Component Motion
5-1 Cross-section Location Map, YBI
5-2a Cross-section AA'
5-2b Cross- Section BB'
5-3 Cross-section Location Map, Skyway
5-4 Cross-section Location Map, Skyway
5-5 Subsurface Cross-section A_1-A'_1
5-6 Subsurface Cross-section A_2-A'_2
5-7 Subsurface Cross-section A_3-A'_3
5-8 Subsurface Cross-section A_4-A'_4
5-9 Subsurface Cross-section A_5-A'_5
5-10 Cross-section Location Map, Oakland Mole
5-11a Subsurface Cross-section A-A'
5-11b Subsurface Cross-section B-B'
5-12 Shear Wave Velocity Profile Pier E02
5-13 Shear Wave Velocity Profile Pier E03
5-14 Shear Wave Velocity Profile Pier E04
5-15 Shear Wave Velocity Profile Pier E05
5-16 Shear Wave Velocity Profile Pier E06
5-17 Shear Wave Velocity Profile Pier E07
5-18 Shear Wave Velocity Profile Pier E08
5-19 Shear Wave Velocity Profile Pier E09
5-20 Shear Wave Velocity Profile Pier E10
5-21 Shear Wave Velocity Profile Pier E11
5-22 Shear Wave Velocity Profile Pier E12
5-23 Shear Wave Velocity Profile Pier E13
5-24 Shear Wave Velocity Profile Pier E14
5-25 Shear Wave Velocity Profile Pier E15
5-26 Shear Wave Velocity Profile Pier E16
5-27 Modulus Reduction vs. Shear Strain for Young Bay Mud
5-28 Modulus Reduction vs. Shear Strain for Old Bay Mud
5-29 Damping Ratio vs. Shear Strain for Young Bay Mud
5-30 Damping Ratio vs. Shear Strain for Old Bay Mud
5-31 2-D Finite Element Mesh for QUAD4M Analysis at Main Span Location
5-32 Selected Results from QUAD4M Analyses
5-33 Representative Soil Profile Location Map
5-34 Representative Soil Profiles
5-35 Pile Group Configuration Pier E03

5-36 Pile Group Configuration Pier E04
5-37 Pile Group Configuration Pier E05
5-38 Pile Group Configuration Pier E06
5-39 Pile Group Configuration Pier E07
5-40 Pile Group Configuration Pier E08
5-41 Pile Group Configuration Pier E09
5-42 Pile Group Configuration Pier E10
5-43 Pile Group Configuration Pier E11
5-44 Pile Group Configuration Pier E12
5-45 Pile Group Configuration Pier E13
5-46 Pile Group Configuration Pier E14
5-47 Pile Group Configuration Pier E15
5-48 Pile Group Configuration Pier E16
6-1 Schematic of Single and Multiple Degrees of Freedom Systems
6-2 Kinematic Motion and Condensed Matrices
7-1 ARS Design Curves for Skyway Structures, FN
7-2 ARS Design Curves for Skyway Structures, FP
7-3 ARS Spectra for Oakland Mole, FN
7-4 ARS Spectra for Oakland Mole, FP
8-1 Schematic of Pile Group Configuration for Kinematic Soil-Structure Interaction Analysis
8-2 Plate Showing Linearization Procedure
8-3 Pile Layout of Piers E02 through E14
8-4 Pile Layout for Piers E15 and E16
8-5 Abstract of Computer Program, KIPS
8-6 Kinematic and Depth-varying Free Field Motions at Pier E02, Set 1, FN
8-7 Kinematic and Depth-varying Free Field Motions at Pier E02, Set 1, FP
8-8 Kinematic and Depth-varying Free Field Motions at Pier E02, Set 2, FN
8-9 Kinematic and Depth-varying Free Field Motions at Pier E02, Set 2, FP
8-10 Kinematic and Depth-varying Free Field Motions at Pier E02, Set 3, FN
8-11 Kinematic and Depth-varying Free Field Motions at Pier E02, Set 3, FP
8-12 Kinematic and Depth-varying Free Field Motions at Pier E02, Set 4, FN
8-13 Kinematic and Depth-varying Free Field Motions at Pier E02, Set 4, FP
8-14 Kinematic and Depth-varying Free Field Motions at Pier E02, Set 5, FN
8-15 Kinematic and Depth-varying Free Field Motions at Pier E02, Set 5, FP
8-16 Kinematic and Depth-varying Free Field Motions at Pier E02, Set 6, FN
8-17 Kinematic and Depth-varying Free Field Motions at Pier E02, Set 6, FP
8-18 Kinematic and Depth-varying Free Field Motions at Pier E03, Set 1, FN
8-19 Kinematic and Depth-varying Free Field Motions at Pier E03, Set 1, FP
8-20 Kinematic and Depth-varying Free Field Motions at Pier E03, Set 2, FN
8-21 Kinematic and Depth-varying Free Field Motions at Pier E03, Set 2, FP
8-22 Kinematic and Depth-varying Free Field Motions at Pier E03, Set 3, FN
8-23 Kinematic and Depth-varying Free Field Motions at Pier E03, Set 3, FP
8-24 Kinematic and Depth-varying Free Field Motions at Pier E03, Set 4, FN
8-25 Kinematic and Depth-varying Free Field Motions at Pier E03, Set 4, FP

8-26 Kinematic and Depth-varying Free Field Motions at Pier E03, Set 5, FN
8-27 Kinematic and Depth-varying Free Field Motions at Pier E03, Set 5, FP
8-28 Kinematic and Depth-varying Free Field Motions at Pier E03, Set 6, FN
8-29 Kinematic and Depth-varying Free Field Motions at Pier E03, Set 6, FP
8-30 Kinematic and Depth-varying Free Field Motions at Pier E04, Set 1, FN
8-31 Kinematic and Depth-varying Free Field Motions at Pier E04, Set 1, FP
8-32 Kinematic and Depth-varying Free Field Motions at Pier E04, Set 2, FN
8-33 Kinematic and Depth-varying Free Field Motions at Pier E04, Set 2, FP
8-34 Kinematic and Depth-varying Free Field Motions at Pier E04, Set 3, FN
8-35 Kinematic and Depth-varying Free Field Motions at Pier E04, Set 3, FP
8-36 Kinematic and Depth-varying Free Field Motions at Pier E04, Set 4, FN
8-37 Kinematic and Depth-varying Free Field Motions at Pier E04, Set 4, FP
8-38 Kinematic and Depth-varying Free Field Motions at Pier E04, Set 5, FN
8-39 Kinematic and Depth-varying Free Field Motions at Pier E04, Set 5, FP
8-40 Kinematic and Depth-varying Free Field Motions at Pier E04, Set 6, FN
8-41 Kinematic and Depth-varying Free Field Motions at Pier E04, Set 6, FP
8-42 Kinematic and Depth-varying Free Field Motions at Pier E05, Set 1, FN
8-43 Kinematic and Depth-varying Free Field Motions at Pier E05, Set 1, FP
8-44 Kinematic and Depth-varying Free Field Motions at Pier E05, Set 2, FN
8-45 Kinematic and Depth-varying Free Field Motions at Pier E05, Set 2, FP
8-46 Kinematic and Depth-varying Free Field Motions at Pier E05, Set 3, FN
8-47 Kinematic and Depth-varying Free Field Motions at Pier E05, Set 3, FP
8-48 Kinematic and Depth-varying Free Field Motions at Pier E05, Set 4, FN
8-49 Kinematic and Depth-varying Free Field Motions at Pier E05, Set 4, FP
8-50 Kinematic and Depth-varying Free Field Motions at Pier E05, Set 5, FN
8-51 Kinematic and Depth-varying Free Field Motions at Pier E05, Set 5, FP
8-52 Kinematic and Depth-varying Free Field Motions at Pier E05, Set 6, FN
8-53 Kinematic and Depth-varying Free Field Motions at Pier E05, Set 6, FP
8-54 Kinematic and Depth-varying Free Field Motions at Pier E06, Set 1, FN
8-55 Kinematic and Depth-varying Free Field Motions at Pier E06, Set 1, FP
8-56 Kinematic and Depth-varying Free Field Motions at Pier E06, Set 2, FN
8-57 Kinematic and Depth-varying Free Field Motions at Pier E06, Set 2, FP
8-58 Kinematic and Depth-varying Free Field Motions at Pier E06, Set 3, FN
8-59 Kinematic and Depth-varying Free Field Motions at Pier E06, Set 3, FP
8-60 Kinematic and Depth-varying Free Field Motions at Pier E06, Set 4, FN
8-61 Kinematic and Depth-varying Free Field Motions at Pier E06, Set 4, FP
8-62 Kinematic and Depth-varying Free Field Motions at Pier E06, Set 5, FN
8-63 Kinematic and Depth-varying Free Field Motions at Pier E06, Set 5, FP
8-64 Kinematic and Depth-varying Free Field Motions at Pier E06, Set 6, FN
8-65 Kinematic and Depth-varying Free Field Motions at Pier E06, Set 6, FP
8-66 Kinematic and Depth-varying Free Field Motions at Pier E07, Set 1, FN
8-67 Kinematic and Depth-varying Free Field Motions at Pier E07, Set 1, FP
8-68 Kinematic and Depth-varying Free Field Motions at Pier E07, Set 2, FN
8-69 Kinematic and Depth-varying Free Field Motions at Pier E07, Set 2, FP

8-70 Kinematic and Depth-varying Free Field Motions at Pier E07, Set 3, FN
8-71 Kinematic and Depth-varying Free Field Motions at Pier E07, Set 3, FP
8-72 Kinematic and Depth-varying Free Field Motions at Pier E07, Set 4, FN
8-73 Kinematic and Depth-varying Free Field Motions at Pier E07, Set 4, FP
8-74 Kinematic and Depth-varying Free Field Motions at Pier E07, Set 5, FN
8-75 Kinematic and Depth-varying Free Field Motions at Pier E07, Set 5, FP
8-76 Kinematic and Depth-varying Free Field Motions at Pier E07, Set 6, FN
8-77 Kinematic and Depth-varying Free Field Motions at Pier E07, Set 6, FP
8-78 Kinematic and Depth-varying Free Field Motions at Pier E08, Set 1, FN
8-79 Kinematic and Depth-varying Free Field Motions at Pier E08, Set 1, FP
8-80 Kinematic and Depth-varying Free Field Motions at Pier E08, Set 2, FN
8-81 Kinematic and Depth-varying Free Field Motions at Pier E08, Set 2, FP
8-82 Kinematic and Depth-varying Free Field Motions at Pier E08, Set 3, FN
8-83 Kinematic and Depth-varying Free Field Motions at Pier E08, Set 3, FP
8-84 Kinematic and Depth-varying Free Field Motions at Pier E08, Set 4, FN
8-85 Kinematic and Depth-varying Free Field Motions at Pier E08, Set 4, FP
8-86 Kinematic and Depth-varying Free Field Motions at Pier E08, Set 5, FN
8-87 Kinematic and Depth-varying Free Field Motions at Pier E08, Set 5, FP
8-88 Kinematic and Depth-varying Free Field Motions at Pier E08, Set 6, FN
8-89 Kinematic and Depth-varying Free Field Motions at Pier E08, Set 6, FP
8-90 Kinematic and Depth-varying Free Field Motions at Pier E09, Set 1, FN
8-91 Kinematic and Depth-varying Free Field Motions at Pier E09, Set 1, FP
8-92 Kinematic and Depth-varying Free Field Motions at Pier E09, Set 2, FN
8-93 Kinematic and Depth-varying Free Field Motions at Pier E09, Set 2, FP
8-94 Kinematic and Depth-varying Free Field Motions at Pier E09, Set 3, FN
8-95 Kinematic and Depth-varying Free Field Motions at Pier E09, Set 3, FP
8-96 Kinematic and Depth-varying Free Field Motions at Pier E09, Set 4, FN
8-97 Kinematic and Depth-varying Free Field Motions at Pier E09, Set 4, FP
8-98 Kinematic and Depth-varying Free Field Motions at Pier E09, Set 5, FN
8-99 Kinematic and Depth-varying Free Field Motions at Pier E09, Set 5, FP
8-100 Kinematic and Depth-varying Free Field Motions at Pier E09, Set 6, FN
8-101 Kinematic and Depth-varying Free Field Motions at Pier E09, Set 6, FP
8-102 Kinematic and Depth-varying Free Field Motions at Pier E10, Set 1, FN
8-103 Kinematic and Depth-varying Free Field Motions at Pier E10, Set 1, FP
8-104 Kinematic and Depth-varying Free Field Motions at Pier E10, Set 2, FN
8-105 Kinematic and Depth-varying Free Field Motions at Pier E10, Set 2, FP
8-106 Kinematic and Depth-varying Free Field Motions at Pier E10, Set 3, FN
8-107 Kinematic and Depth-varying Free Field Motions at Pier E10, Set 3, FP
8-108 Kinematic and Depth-varying Free Field Motions at Pier E10, Set 4, FN
8-109 Kinematic and Depth-varying Free Field Motions at Pier E10, Set 4, FP
8-110 Kinematic and Depth-varying Free Field Motions at Pier E10, Set 5, FN
8-111 Kinematic and Depth-varying Free Field Motions at Pier E10, Set 5, FP
8-112 Kinematic and Depth-varying Free Field Motions at Pier E10, Set 6, FN
8-113 Kinematic and Depth-varying Free Field Motions at Pier E10, Set 6, FP

8-114 Kinematic and Depth-varying Free Field Motions at Pier E11, Set 1, FN
8-115 Kinematic and Depth-varying Free Field Motions at Pier E11, Set 1, FP
8-116 Kinematic and Depth-varying Free Field Motions at Pier E11, Set 2, FN
8-117 Kinematic and Depth-varying Free Field Motions at Pier E11, Set 2, FP
8-118 Kinematic and Depth-varying Free Field Motions at Pier E11, Set 3, FN
8-119 Kinematic and Depth-varying Free Field Motions at Pier E11, Set 3, FP
8-120 Kinematic and Depth-varying Free Field Motions at Pier E11, Set 4, FN
8-121 Kinematic and Depth-varying Free Field Motions at Pier E11, Set 4, FP
8-122 Kinematic and Depth-varying Free Field Motions at Pier E11, Set 5, FN
8-123 Kinematic and Depth-varying Free Field Motions at Pier E11, Set 5, FP
8-124 Kinematic and Depth-varying Free Field Motions at Pier E11, Set 6, FN
8-125 Kinematic and Depth-varying Free Field Motions at Pier E11, Set 6, FP
8-126 Kinematic and Depth-varying Free Field Motions at Pier E12, Set 1, FN
8-127 Kinematic and Depth-varying Free Field Motions at Pier E12, Set 1, FP
8-128 Kinematic and Depth-varying Free Field Motions at Pier E12, Set 2, FN
8-129 Kinematic and Depth-varying Free Field Motions at Pier E12, Set 2, FP
8-130 Kinematic and Depth-varying Free Field Motions at Pier E12, Set 3, FN
8-131 Kinematic and Depth-varying Free Field Motions at Pier E12, Set 3, FP
8-132 Kinematic and Depth-varying Free Field Motions at Pier E12, Set 4, FN
8-133 Kinematic and Depth-varying Free Field Motions at Pier E12, Set 4, FP
8-134 Kinematic and Depth-varying Free Field Motions at Pier E12, Set 5, FN
8-135 Kinematic and Depth-varying Free Field Motions at Pier E12, Set 5, FP
8-136 Kinematic and Depth-varying Free Field Motions at Pier E12, Set 6, FN
8-137 Kinematic and Depth-varying Free Field Motions at Pier E12, Set 6, FP
8-138 Kinematic and Depth-varying Free Field Motions at Pier E13, Set 1, FN
8-139 Kinematic and Depth-varying Free Field Motions at Pier E13, Set 1, FP
8-140 Kinematic and Depth-varying Free Field Motions at Pier E13, Set 2, FN
8-141 Kinematic and Depth-varying Free Field Motions at Pier E13, Set 2, FP
8-142 Kinematic and Depth-varying Free Field Motions at Pier E13, Set 3, FN
8-143 Kinematic and Depth-varying Free Field Motions at Pier E13, Set 3, FP
8-144 Kinematic and Depth-varying Free Field Motions at Pier E13, Set 4, FN
8-145 Kinematic and Depth-varying Free Field Motions at Pier E13, Set 4, FP
8-146 Kinematic and Depth-varying Free Field Motions at Pier E13, Set 5, FN
8-147 Kinematic and Depth-varying Free Field Motions at Pier E13, Set 5, FP
8-148 Kinematic and Depth-varying Free Field Motions at Pier E13, Set 6, FN
8-149 Kinematic and Depth-varying Free Field Motions at Pier E13, Set 6, FP
8-150 Kinematic and Depth-varying Free Field Motions at Pier E14, Set 1, FN
8-151 Kinematic and Depth-varying Free Field Motions at Pier E14, Set 1, FP
8-152 Kinematic and Depth-varying Free Field Motions at Pier E14, Set 2, FN
8-153 Kinematic and Depth-varying Free Field Motions at Pier E14, Set 2, FP
8-154 Kinematic and Depth-varying Free Field Motions at Pier E14, Set 3, FN
8-155 Kinematic and Depth-varying Free Field Motions at Pier E14, Set 3, FP
8-156 Kinematic and Depth-varying Free Field Motions at Pier E14, Set 4, FN
8-157 Kinematic and Depth-varying Free Field Motions at Pier E14, Set 4, FP

8-158 Kinematic and Depth-varying Free Field Motions at Pier E14, Set 5, FN
8-159 Kinematic and Depth-varying Free Field Motions at Pier E14, Set 5, FP
8-160 Kinematic and Depth-varying Free Field Motions at Pier E14, Set 6, FN
8-161 Kinematic and Depth-varying Free Field Motions at Pier E14, Set 6, FP
8-162 Kinematic and Depth-varying Free Field Motions at Pier E15, Set 1, FN
8-163 Kinematic and Depth-varying Free Field Motions at Pier E15, Set 1, FP
8-164 Kinematic and Depth-varying Free Field Motions at Pier E15, Set 2, FN
8-165 Kinematic and Depth-varying Free Field Motions at Pier E15, Set 2, FP
8-166 Kinematic and Depth-varying Free Field Motions at Pier E15, Set 3, FN
8-167 Kinematic and Depth-varying Free Field Motions at Pier E15, Set 3, FP
8-168 Kinematic and Depth-varying Free Field Motions at Pier E15, Set 4, FN
8-169 Kinematic and Depth-varying Free Field Motions at Pier E15, Set 4, FP
8-170 Kinematic and Depth-varying Free Field Motions at Pier E15, Set 5, FN
8-171 Kinematic and Depth-varying Free Field Motions at Pier E15, Set 5, FP
8-172 Kinematic and Depth-varying Free Field Motions at Pier E15, Set 6, FN
8-173 Kinematic and Depth-varying Free Field Motions at Pier E15, Set 6, FP
8-174 Kinematic and Depth-varying Free Field Motions at Pier E16, Set 1, FN
8-175 Kinematic and Depth-varying Free Field Motions at Pier E16, Set 1, FP
8-176 Kinematic and Depth-varying Free Field Motions at Pier E16, Set 2, FN
8-177 Kinematic and Depth-varying Free Field Motions at Pier E16, Set 2, FP
8-178 Kinematic and Depth-varying Free Field Motions at Pier E16, Set 3, FN
8-179 Kinematic and Depth-varying Free Field Motions at Pier E16, Set 3, FP
8-180 Kinematic and Depth-varying Free Field Motions at Pier E16, Set 4, FN
8-181 Kinematic and Depth-varying Free Field Motions at Pier E16, Set 4, FP
8-182 Kinematic and Depth-varying Free Field Motions at Pier E16, Set 5, FN
8-183 Kinematic and Depth-varying Free Field Motions at Pier E16, Set 5, FP
8-184 Kinematic and Depth-varying Free Field Motions at Pier E16, Set 6, FN
8-185 Kinematic and Depth-varying Free Field Motions at Pier E16, Set 6, FP

SECTION 1.0
INTRODUCTION

1.0 INTRODUCTION

1.1 PROJECT LIMIT

The proposed N6 alignment for the new East Span San Francisco-Oakland Bay Bridge (SFOBB) is approximately 4.0 km long from the Yerba Buena Island Tunnel to the toll plaza on the Oakland Mole. The entire bridge project can be divided into following four segments;

YBI Structure: A transition structure from the tunnel portal to the self-anchored suspension bridge

Main Bridge: A self-anchored cable suspension bridge extending offshore from Yerba Buena Island

Skyway Structure: A multiple-frame structure linking the cable suspension bridge to Oakland Mole

Oakland Mole Structure: An approach structure connecting Skyway Structure to the toll plaza at Oakland Mole.

Plates 1-1, 5-3 and 5-4 show the alignment of the bridge and division of the segments. The YBI structure is supported on spread footings where rock outcrop exists and on piles where thick soil sediment overlies the rock. The self-anchored suspension structure (also known as the Main Bridge) is 565 meters long extending offshore from the tip of the Yerba Buena Island. This signature structure is asymmetric with a longer East Span and the shorter West Span, and is supported on three piers; denoted as West Pier (W2), Main Pier (E1), and East Pier (E2). The proposed Skyway Structure is approximately 2.4 km long, consisting of two parallel structures to carry the eastbound and westbound traffic independently. Both eastbound and westbound structures are supported on 14 piers (piers E3 through E16). All the piers for the Main Bridge and Skyway Structure are supported on piles. The piles at Pier W2 and Pier E1 are constructed in rock while those at Pier E2 and the entire Skyway piers are founded in soil sediments. The Oakland Mole portion consists of bridge structures supported on piles and embankment fill approaches.

1.2 BACKGROUND ON GROUND MOTION

The 30 percent type-selection design phase of work for the SFOBB East Span Replacement Project was conducted based on a set of ground motions and ARS design criteria developed for the seismic retrofit of the existing Bay Bridge structure by the Office of Structural Foundation (OSF) of Caltrans.

To incorporate new geologic and geotechnical data obtained from the Fugro-EMI geologic investigation contract and recent recommendations from the Ground Motion Ad Hoc

Committee of the Seismic Safety Advisory Board, new ground motions and ARS criteria have been developed for the final design of the SFOBB replacement structure. Development of the new ground motion criteria is described in this report. The new ARS design criteria guided much of the initial Skyway design and to some extend the East Pier design. The initial design of the Skyway based on the ARS procedure would eventually be proven against six sets of multiple-support input motions. Generation of multiple-support input motions is also an element in the ground motion studies.

The task of developing ground motions for the SFOBB replacement project was divided into two phases to meet the schedule and contractual constraints:

Phase I: An interim phase to furnish the ARS criteria to allow initial design and sizing of structural components by response spectrum approach.

Phase II: A second phase to furnish multiple-support input motion for dynamic response analyses, for final checking of the designed structure.

With the above mentioned objectives, the following individual tasks were performed in the course of the ground motion studies:

- Probabilistic seismic hazard analysis to define resultant target rock motion design spectra.
- Generation of spectrum-compatible reference rock motions from actual earthquake records as seed motions.
- Generation of coherency function compatible rock motions for the Main Bridge and Skyway Structure.
- Studies on site response analyses to understand wave propagation phenomena and to compute depth-varying free-field motions.
- Development of ARS design criteria using several representative soil profiles to establish effective shaking intensity at the foundation level which formed a basis for response spectrum analyses.
- Development of multiple support free-field and kinematic motion arising from soil-pile interaction to be used in time-history analyses.

1.3 ACKNOWLEDGMENT

It is truly a team effort to address the highly complex seismic loading criteria for the SFOBB replacement structure, involving:

- Caltrans Personnel -

Dr. Brian Maroney, Caltrans's SFOBB Project Manager, Dr. Abbas Abghari and Dr. Mahmoud Kojasteh, Mr. Reid Buell and Mr. Ronnie Gu of the Office of Structure Foundations

who served as reviewer and provided background information and many suggestions in the course of performance of this project.

- Ad Hoc Committee for SFOBB Ground Motion -

An Ad Hoc Committee appointed by Joe Nicoletti, Seismic Safety Peer Review Panel Chairman, established the basic ground motion criteria guidelines. The committee comprises: Professor Bruce Bolt, Chairman, Professor Joseph Penzien, Chairman of Seismic Safety Advisory Board, Dr. Roger Borcherdt of USGS and Dr. Norm Abrahamson.

- Seismic Safety Peer Review Panel -

Caltrans also established the Seismic Safety Peer Review Panel to provide review and guidance to the overall project. Dr. Idriss of the Peer Review Panel worked closely with the Bay Bridge seismological and geotechnical team in numerous informal meetings and provided many valuable suggestions on various technical issues.

- TY Lin-Moffatt&Nichol JV Team -

Mr. Gerry Houlahan assisted coordination efforts with the structural engineers while Dr. Tim Ingham provided valuable feedbacks from the structural analyses over the course of the development of ARS design criteria.

- Fugro-EMI JV Team -

The following members served as subcontractor to the Fugro-EMI JV geologic investigation team and performed various subtasks for the project:

Po Lam, Hubert Law and Bob Pyke of Fugro-EMI were responsible for the overall coordination, and performed site response and soil-structure interaction analyses and organized the overall ground motion subtask in the project. Debanik Chaudhuri conducted computations on multiple support kinematic motions.

Tom McNeilan of Fugro-EMI led the geologic and geotechnical characterization task.

Dr. Norm Abrahamson, serving as a subcontractor to the Fugro-EMI JV Team was the lead seismologist for the project. He also served on the Ground Motion Ad Hoc Committee and also was responsible for the probabilistic seismic hazard (PSHA) and rock motion generation effort. Dr. Abrahamson also co-authured this report.

Dr. Walt Silva of Pacific Engineering assisted in the project on various facets, including conducting fault-rupturing simulations to increase our understanding of the fault-rupture directivity effects. He conducted some wave propagation analyses to appreciate the SV-wave propagation phenomena and furnished miscellaneous strong motion data (e.g. various downhole and outcrop strong motion records) and also assisted in addressing various elements of ground motion attenuation relations.

Other subcontractors who contributed in the project included Dr. Paul Sommerville of Woodward Clyde Consultants and Professor John Anderson of University of Nevada at Reno.

Both group conducted fault-rupturing simulations to improve our understanding on the fault-rupture directivity effects.

1.4 ORGANIZATION OF THE REPORT

In addition to this introduction section, this report has been organized into the following sections:

Section 2	Probabilistic seismic hazard study to develop target rock motion response spectra.
Section 3	Documentation of reference rock motions that are spectrum-compatible to the target spectra developed in Section 2.
Section 4	Descriptions of multiple-support rock motions for the main span bridge and skyway structure.
Section 5	Free-field site response analyses conducted for development of ARS criteria and multiple-support motions. It also contains two-dimensional site response studies for East Pier (E2).
Section 6	Discussion of kinematic soil-pile interaction analyses and mathematical derivation of kinematic motion from depth varying free-field ground motions.
Section 7	Development of ARS criteria to account for variations of soil profiles, uncertainties of soil properties, and needs to envelop the six sets of design motions.
Section 8	Multiple-support input motions for time-history analysis of the global bridge model.
Section 9	Summary and conclusion
Appendix A	Probabilistic Seismic Hazard Assessment, Mathematical Details
Appendix B	Attenuation Relations
Appendix C	Non-Stationary Spectral Matching Program RSPMATCH
Appendix D	Spectral Matching Example
Appendix E	Characteristics of Initial Startup Motions
Appendix F	Empirical Plane-Wave Coherency Models for Horizontal and Vertical Components
Appendix G	Guidelines for Generation of Response-Spectrum-Compatible Rock Motion Time Histories for Application to Caltrans Toll Bridge Seismic Retrofit Projects

Earth Mechanics FUGRO

649000

648500

648000

647000

TREASURE ISLAND

YERBA BUENA ISLAND

OAKLAND MOLE

E22

E18

E10

E5

E3

E2

1836000

1836500

1837000

1837500

1838000

N

W

E

S

SCALE: 1:10000

0 200 m 400 m

LEGEND

- 1998 Phase 2 Borings
- 1998 Phase 1 Borings
- Pre-1998 Borings
- Caltrans Survey Corridor
- Approximate Limits of 3-D Survey Coverage
- San Francisco-Oakland Bay Bridge
- N6 Alignment

PROJECT LOCATION MAP
SFOBB East Span Seismic Safety Project

PLATE 1-1

SECTION 2.0
PROBABILISTIC SEISMIC HAZARD

2.0 PROBABILISTIC SEISMIC HAZARD

2.1 DESIGN PHILOSOPHY

A Ground Motion Ad Hoc Committee provided overall guidance on appropriate ground motion criteria for the East Bay Bridge project. This Committee met periodically with Caltrans' representatives to review interim results and to provide recommendations to the project team. A major focus of the discussions was the relative merits of the probabilistic and deterministic approaches to computing ground motions. The Ad Hoc Committee recommended adopting the probabilistic ground motion approach for the Bay Bridge Safety Evaluation Earthquake (SEE).

The probabilistic seismic hazard analytical technique follows a standard approach first developed by Cornell (1968). This approach has been further expanded to fully treat both, the randomness (aleatory variability) and the scientific uncertainty (epistemic uncertainty) of ground motion prediction. The mathematical formulation for the hazard analysis used in this study is described in Appendix A.

The analysis requires characterizing seismogenic sources (faults) in terms of their geometry (strike, dip, length, down-dip width), maximum magnitude, slip rate, and recurrence. The development of these parameters is discussed fully in Appendix A. The assumptions made in the East Bay Bridge analysis are summarized below.

2.2 SEISMIC SOURCES

Plate 2-1 presents a map of major active faults in the Bay Area extracted from the latest fault map developed by Caltrans (Mualchin, 1996). Both Quaternary (last rupture up to 2 to 3 million years) and Holocene active faults (last rupture within the last 11,000 years) have been plotted. The majority of the faults shown on the map are Holocene faults. Table 2-1 summarizes the closest distance that several of these faults approach the East Bay Bridge.

2.2.1 Fault Sources

The source model adopted for the probabilistic seismic hazard analysis (PSHA) was synthesized from models developed by Geomatrix Consultants for assessment of the West Bay Bridge ground motions and by the California Division of Mines and Geology (CDMG). Many of the model details incorporated in the Geomatrix and CDMG models are not included in our model described herein. (A typical simplification is our assumption of a single downdip seismogenic width for each modeled fault, as opposed to Geomatrix's assumption of a range of widths with assigned weights.) These simplifications do not result in significantly different ground motions for the same hazard levels. At a period of 3 seconds (of importance in the Bay Bridge analysis), the hazard results described below lie within about 5 percent of the CDMG model results (Peterson et al., 1996), when the effects of directivity are ignored. Plate 2-2 presents a comparison for the 5-percent damped spectral acceleration at 3 second (based on the

standard horizontal component attenuation relation without directivity effects) at Yerba Buena Island between the 1992 Geomatrix study and the current study. It can be observed that the two solutions are quite comparable indicating that very similar assumption in the seismic sources (i.e. the major faults and their recurrence rates) between the Geomatrix and this current study. However, directivity effects, incorporated in the attenuation model for the present study based on recent advancements in this subject, is the cause of most of the difference in the shaking level for design. The 1,500-year fault normal and fault parallel spectral accelerations for the Safety Earthquake Event (SEE) at 3-second period ultimately developed for this current project have been shown on Plate 2-2 as solid circles. From the Plate, it can be observed that as a result of latest advancement in treatment for directivity effects, the design shaking level is increased by about 30 percent as compared to prior study conducted for seismic retrofit.

Table 2-1. Seismic Sources Based on Deterministic Model

Fault	Maximum Credible Magnitude, M_w	Closest Distance to Site
San Andreas (Northern Segment)	8	18 Km to Yearba Buena Island
Hayward	7.5	9 Km to Toll Plaza
San Gregorio	7.0	21 kM to Yerba Buena Island
Rogers Creek - Healdsburg	7.0	37 Km to Toll Plaza
Calaveras	7.5	30 Km to Toll Plaza
Greenville	7.25	36 Km to Toll Plaza
Green Valley	6.75	37 Km to Toll Plaza

NOTE :
Above maximum credible magnitude is based on Mualchin (1996). This table is presented for reference only. The probabilistic seismic hazard analysis for the bay bridge was conducted utilizing a range of potential maximum magnitude in conjunction with the geologic slip rates as shown in Table 2-2.

For the East Bay Bridge, the dominant sources are commonly known to be the Hayward and San Andreas faults due to their high activity rates and relatively close distances to the Bridge. Several additional faults are also included in the hazard analysis although they do not contribute significantly to the hazard. All fault sources considered in this hazard analysis are shown in Plate 2-1 and the source parameters are summarized in Table 2-2. A logic tree approach was adopted to incorporate an assumed distribution of values for fault slip rate, width, and maximum magnitude. The various parameter values and their weights are included in Table 2-2.

Areal sources are also commonly included into seismic hazard assessments to account for seismicity not associated with identified faults. However their addition in the assessment has a negligible effect on the total hazard compared to the faults listed in Table 2-2 and consequently they are not incorporated in the source model. The minimum magnitude used in the hazard

calculation is 5.0. Smaller magnitude events do not contribute significantly to ground motions of engineering interest.

Table 2-2. Sources and Source Parameters Used in Hazard Analysis

Fault	Slip Rate (mm/yr)	Fault Width (Km)	Maximum Magnitude
Calaveras (Northern Segment)	2.0 (0.25) 6.0 (0.5) 8.0 (0.25)	12.0 (1.0)	6.9 (1.0)
Calaveras (Southern Segment)	13.0 (0.25) 15.0 (0.5) 17.0 (0.25)	12.0 (1.0)	7.0 (1.0)
Green Valley-Cedar Roughs	1.5 (0.2) 4.0 (0.6) 5.0 (0.2)	12.0 (1.0)	6.85 (1.0)
Hayward	7.0 (0.25) 9.0 (0.5) 11.0 (0.25)	12.0 (0.5) 15.0 (0.5)	7.05 (0.5) 7.35 (0.5)
Marsh Creek- Greenville-Arroyo Complex	0.50 (0.25) 2.0 (0.5) 3.0 (0.25)	12.0 (1.0)	6.9 (1.0)
Rodgers Creek	6.0 (0.25) 8.0 (0.5) 11.0 (0.25)	12.0 (1.0)	7.25 (1.0)
San Andreas	19.0 (0.2) 24.0 (0.6) 29.0 (0.2)	15.0 (1.0)	7.8 (0.8) 8.0 (0.2)
San Gregorio	1.0 (0.25) 2.0 (0.25) 3.0 (0.25)	15.0 (1.0)	7.25 (1.0)

Notes:
1. Ranges of values assumed for each parameter are shown with weights in parenthesis.
2. All faults are vertical strike-slip with Richter b-value = 0.90.
3. Rupture Area Relation: $\log_{10}(A) = -3.49 + 0.91\,M$ $\sigma(\log_{10}A) = 0.24$
   Rupture Width Relation: $\log_{10}(W) = -1.01 + 0.32\,M$ $\sigma(\log_{10}W) = 0.15$
4. Characteristic recurrence model weighted 0.9; exponential recurrence model weighted 0.1.
5. For characteristic recurrence, $\Delta M_1 = 1.0$, and $\Delta M_2 = 0.5$ (Appendix A).

2.2.2 Magnitude Density Distribution

Two magnitude density functions are possible: the characteristic model and the truncated exponential model (see Appendix A). For Bay Area faults, the characteristic model is weighted 0.9 and the truncated exponential model is weighted 0.1. This weighting reflects the observation that use of an exponential model for faults for which the activity rate is computed from slip-rate leads to a large over-prediction of the historical recurrence of moderate magnitude events.

2.2.3 Rupture Dimension Relations

The rupture dimension is modeled using the relations for fault area and fault width developed by Wells and Coppersmith (1994) for all source types. These relations are provided in Table 2-2. Rupture length is computed from the area divided by the width.

2.2.4 Time Dependent Earthquake Recurrence

In this study, earthquake recurrence is modeled as a Poisson process. Time dependent recurrence models have been considered by the U. S. Geological Survey Working Group on California Earthquake Probabilities (WGCEP, 1990) in the San Francisco Bay Area. For cases in which the exposure time and the recurrence intervals are similar (such as the case here with a 150 year exposure time), there is not a large difference between the computed hazard from time dependent and Poisson models. For short exposure times, such as for the temporary structures, there can be a large difference between the computed hazard from time dependent and Poisson models.

2.3 RECURRENCE RELATIONSHIPS

Fault area and fault slip rate (Table 2-2) are the primary parameters defining earthquake recurrence in our model. For all faults in the PSHA, we assumed a preferred slip rate and upper and lower limits to the slip rate. In general, single values of fault width and maximum magnitude were assumed. The characteristic recurrence model of Youngs and Coppersmith (1985) allows a convenient conversion of these parameters to earthquake recurrence intervals.

Using the source model described above, the recurrence intervals for the characteristic earthquakes on the San Andreas (M=7.8) and Hayward (M=7.0) faults are about 250 years and 300 years, respectively.

2.4 ATTENUATION RELATIONS

For design of long-period structures such as the new Bay Bridge, characterization of long-period motion is essential. Extra effort has been made to incorporate the latest state-of-the-art development of rock motion attenuation relations incorporating strong motion records and lessons from recent earthquakes including the 1989 Loma Prieta earthquake, 1992 Landers earthquake, 1994 Northridge earthquake and 1996 Kobe earthquake.

The rock motion attenuation relationships adopted for the PSHA include: 1) the Abrahamson and Silva (1997) model, 2) the Geomatrix (1995) model (sponsored by Caltrans), and 3) the Idriss (1991) model (equal weight among the three models). These models combine empirical data from rock sites and shallow soil sites (less than 20 m of soil over rock) into a single rock category because there are not enough data to develop separate models for either category. These relations are fully described in Appendix B. For each relation, the log-normal distribution was truncated in the analysis at three standard deviations.

The Idriss model does not include attenuation relations for vertical motions. To obtain vertical motions, a ratio of vertical-to-average horizontal motion was computed using the empirical models of Geomatrix and Abrahamson and Silva. These V/H ratios were computed for the events dominating the hazard at the Toll Plaza and YBI sites. These ratios were then scaled by the geometric mean of the fault normal and fault parallel components (Ave H) to define the vertical target spectrum.

2.5 RUPTURE DIRECTIVITY EFFECTS

The three horizontal motion attenuation relations were adjusted to account for near-fault directivity effects using a modified form of the Somerville et al. (1997) fault-rupture directivity model (described in Appendix B). Somerville et al. (1997) developed an empirically-based model, quantifying the effects of rupture directivity on horizontal response spectra, that can be used to scale the average horizontal component computed from attenuation relations. The Somerville et al. (1997) model comprises of two period-dependent scaling factors that may be applied to any ground motion attenuation relationship. One of the factors accounts for the increase in shaking intensity in the average horizontal component of motion due to near-fault rupture directivity effects. The second factor reflects the directional nature of the shaking intensity using two ratios: fault normal (FN) and fault parallel (FP) versus the average (FA) component ratios. The fault normal component is taken as the major principal axis resulting in an FN/FA ratio larger than 1 and the fault parallel component is taken as the minor principal axis with an FP/FA ratio smaller than 1. The two scaling factors depend on whether fault rupture is in the forward or backward direction, and also the length of fault rupturing toward the site.

Prior to 1991, no adjustments to ground motions were made to Caltrans bridges to account for rupture directivity. Beginning in 1991, ground motion evaluations for Caltrans bridges considered only the increase in the fault normal ground motion. For most toll bridges evaluated in 1991-1995, the fault parallel component was not reduced since this was a new issue for ground motion prediction and there was not sufficient confidence in the directivity-predicting relations to reduce the ground motion. However, the most recent ground motions for the West Bay Bridge (Nov. 1997) included a decrease in the fault parallel ground motion as well as an increase in the fault normal ground motion as confidence in the methods has grown.

In past Caltrans toll bridge retrofit projects, PSHA were conducted using attenuation relationships without directivity effects. The resultant horizontal target spectrum was scaled to the FN/FA and FP/FA ratios deterministically (assuming that the design event be a forward rupture event). In this contract for the new Bay Bridge, the PSHA incorporated directivity effects within the probabilistic analyses taking into account that both forward and backward directivity rupturing scenarios are possible (Appendix A). Also, the directivity model we used was first modified to reflect results of a review study conducted for this project (Appendix B).

2.6 PSHA FOR SAFETY EARTHQUAKE EVENT

The Ad Hoc Committee evaluated the appropriate return period (hazard) level for design analyses at the SEE. The SEE is intended to reflect a performance level at which significant structural damage may occur, but not structural collapse. Four return periods were considered: 500, 1000, 1500, and 2000 years which correspond roughly to a 10 percent probability of exceedance over 50-, 100-, 150-, and 200-year expected life spans of the East Bay Bridge structures. The Committee recommended the SEE correspond to a 1500-year return period event.

The 1500-year ground motion spectra (fault normal component) at Yerba Buena Island (western limit) and the Toll Plaza (eastern limit) are presented in Plate 2-3. Differences in long period (T>0.5 sec) probabilistic ground motions at the western-most and the eastern-most limits of the bridge alignment are small and may be neglected. The Toll Plaza motions were higher than the YBI motions at short periods, but these short-period motions are not important for the response of the bridge, particularly for the self-anchored suspension bridge and the skyway which are long-period structures. In addition, the site response differences between the soils at the two ends compensate for the difference (with more attenuation of the high frequency content at the Toll Plaza site). The target spectrum at YBI has been selected for reference because it is more appropriate for the self-anchored suspension bridge and skyway which are more inherent for design. The SEE motions for all three components (fault normal, fault parallel, and vertical) at YBI are shown in Plate 2-4. The spectral ordinates are listed in Table 2-3.

For comparison purposes, Plate 2-5 shows the SEE spectrum (fault normal component) and deterministic spectra for the San Andreas and the Hayward faults based on the Maximum Credible Earthquake (MCE) used in the previous Bay Bridge Retrofit studies (Geomatix, 1992). The MCE spectra are 84th percentile spectra including forward directivity effects.

The overall strike angle for both the San Andreas and the Hayward faults is about N35°W. Therefore, the fault normal and fault parallel directions are N55°E and N35°W, respectively. The longitudinal axis of the main span signature structure is oriented very close to the fault normal direction and the bridge alignment varies by about 15° from an average alignment along its length. Thus the longitudinal and the transverse bridge directions may be loosely regarded as the fault normal and fault parallel directions, respectively.

The 1500-year hazard results were deaggregated and show that the hazard is dominated by the San Andreas and Hayward faults (Table 2-4). Deaggregation according to source is shown in Plates 2-6a through 2-6e (fault parallel component) and Plates 2-7a through 2-7e (fault normal). Deaggregation according to distance is shown in Plates 2-8a through 2-8e (fault parallel) and Plates 2-9a through 2-9e (fault normal). Suites of Plates, a through e, correspond to spectral periods at 0.5, 1, 3, 4 and 5 second. The primary contributions to hazard arise from faulting at 5 to 15 Km distance and magnitude 7 and from 15 to 30 km distance and magnitude 7.75 - faulting on the Hayward and San Andreas faults. These faults are closest to the bridge, are

capable of larger magnitude earthquakes than other more distant regional faults, and are considered more active than other regional faults.

Table 2-3 Rock Outcrop SEE Design Spectra at 5 Percent Damping at YBI

PERIOD	Spectral Acceleration (g)			Relative Displacement (in)		
(SEC)	1500-Yr FN	1500-Yr FP	FV Target	1500-Yr FN	1500-Yr FP	FV Target
0.010	0.627	0.627	0.646	0.001	0.001	0.001
0.020	0.627	0.627	0.646	0.002	0.002	0.003
0.030	0.627	0.627	0.646	0.006	0.006	0.006
0.050	0.820	0.820	1.038	0.020	0.020	0.025
0.075	1.036	1.036	1.255	0.057	0.057	0.069
0.100	1.236	1.236	1.304	0.121	0.121	0.128
0.120	1.360	1.360	1.290	0.192	0.192	0.182
0.150	1.546	1.546	1.262	0.340	0.340	0.278
0.170	1.591	1.591	1.198	0.450	0.450	0.339
0.200	1.658	1.658	1.123	0.649	0.649	0.440
0.240	1.654	1.654	1.034	0.933	0.933	0.583
0.250	1.653	1.653	1.017	1.011	1.011	0.622
0.300	1.626	1.626	0.935	1.432	1.432	0.824
0.400	1.480	1.480	0.799	2.318	2.318	1.251
0.500	1.277	1.277	0.675	3.125	3.125	1.651
0.750	1.008	0.978	0.550	5.550	5.385	3.030
1.000	0.794	0.755	0.441	7.772	7.390	4.320
1.500	0.576	0.508	0.312	12.685	11.188	6.867
2.000	0.444	0.373	0.235	17.383	14.604	9.216
3.000	0.270	0.220	0.156	23.785	19.380	13.725
4.000	0.186	0.148	0.106	29.129	23.178	16.663
5.000	0.140	0.108	0.079	34.258	26.428	19.258
6.000	0.105	0.080	0.059	36.999	28.189	20.931
7.000	0.081	0.063	0.047	38.805	30.063	22.318
7.500	0.072	0.055	0.043	39.405	30.046	23.399
8.000	0.065	0.048	0.037	40.680	30.252	23.429
9.000	0.053	0.039	0.030	42.187	31.087	23.626
10.000	0.045	0.032	0.024	44.046	31.322	23.687

Table 2-4. Percentage Contribution to Seismic Hazard

Period (sec)	Northern San Andreas	Hayward	Other Faults
Fault Normal			
0.5	38	62	Small
1.0	52	48	Small
2.0	61	39	Small
3.0	65	35	Small
5.0	70	30	Small
Fault Parallel			
0.5	38	62	Small
1.0	54	46	Small
2.0	70	30	Small
3.0	76	24	Small
5.0	83	17	Small

The mode of the magnitude (accounting for all magnitudes and their corresponding weights) - distance and magnitude - source distributions is represented by the peaks in Plates 2-6 through 2-9. The mean values for these distributions were computed from the deaggregated results. Tables 2-5a and 2-5b list both mean and mode values of magnitude according to given source and distance, respectively, for different spectral periods.

Using the deaggregation results, two scenario earthquakes for SEE design were chosen that correspond to faulting on the San Andreas and the Hayward faults (Table 2-6). The scenario events are based on the mode of the distributions in Plates 2-6 through 2-9. These scenarios are the basis for developing spectrum-compatible time histories (Section 3).

2.7 FUNCTIONAL EARTHQUAKE AND TEMPORARY STRUCTURES DESIGN CRITERIA

The appropriate ground motion criteria for design at a functional earthquake performance level (minimal damage; Functional Earthquake Event, FEE) were discussed between Caltrans and the Peer Review Panel. Due to the long design life of 150 years and the high activity rate for the San Andreas and the Hayward faults, Caltrans selected a 92-year return period earthquake for the functional event corresponding to a 50 percent probability of experiencing up to 2 earthquakes within the 150-year design life. Plate 2-10 presents the 92-year return period equal hazard spectrum for the fault normal component rock motion. The spectrum is similar to median ground motions from a magnitude 6.5 earthquake on the Hayward fault at 10 Km from the

Oakland Toll Plaza. Therefore the FEE was defined as a magnitude 6.5 event on the Hayward fault.

For simplicity, the above magnitude 6.5 event on the Hayward fault also serves as the appropriate ground motion design criterion for the planned temporary structures at the Yerba Buena Island for a Safety Earthquake Event (SEE) performance goal (i.e. significant damage). Peer Review recommended that, for temporary structures, the ground motion criterion can be set at a probabilistic earthquake of 10 percent exceedance for a time exposure about 5 to 10 times the expected duration of operation of these temporary structures; this is consistent with the 92-year return period. The above criterion for the FEE and for temporary structures should be adopted rather than other presumptive criteria (i.e. a 0.25g minimum threshold seismic coefficient level). The Bay Bridge structures are unusual structures - its fundamental period is much longer than most common bridge structures - and therefore the presumptive force coefficient level for design is inappropriate.

2.8 SUMMARY OF SEE AND FEE SPECTRA

Plate 2-11 presents the resultant design spectra, including the 1,500-year SEE spectra and the FEE spectra (Magnitude 6.5 at 10 Km) fault normal spectrum, which roughly corresponds to a 92-year return period.

Table 2-5a Deaggregation of Hazard by Source

Source	Period (Sec)	Mean Magnitude	Mode Magnitude
Fault Normal			
Northern San Andreas	0.5	7.69	7.75
	1.0	7.68	7.75
	2.0	7.72	7.75
	3.0	7.75	7.75
	5.0	7.74	7.75
Hayward	0.5	6.97	6.95
	1.0	7.02	7.05
	2.0	7.11	7.25
	3.0	7.16	7.25
	5.0	7.16	7.25
Fault Parallel			
Northern San Andreas	0.5	7.69	7.75
	1.0	7.68	7.75
	2.0	7.70	7.75
	3.0	7.67	7.75
	5.0	7.67	7.75
Hayward	0.5	6.97	6.96
	1.0	7.01	7.05
	2.0	7.10	7.25
	3.0	7.09	7.25
	5.0	7.11	7.25

Table 2-5b Deaggregation of Hazard by Distance

Distance	Period (Sec)	Mean Magnitude	Mode Magnitude
Fault Normal			
5-15 Km	0.5	6.97	7.25
	1.0	7.02	7.25
	2.0	6.99	7.25
	3.0	7.16	7.25
	5.0	7.17	7.25
15-30 Km	0.5	7.68	7.75
	1.0	7.67	7.75
	2.0	7.58	7.75
	3.0	7.73	7.75
	5.0	7.72	7.75
Fault Parallel			
5-15 Km	0.5	6.97	7.25
	1.0	7.01	7.25
	2.0	7.10	7.25
	3.0	7.09	7.25
	5.0	7.11	7.25
15-30 Km	0.5	7.68	7.75
	1.0	7.67	7.75
	2.0	7.70	7.75
	3.0	7.68	7.75
	5.0	7.67	7.75

Table 2-6 Earthquake Scenario for SEE Design

Earthquake Scenario	Magnitude	Closest Distance to Fault
San Andreas	7.75	18 Km to YBI
Hayward	6.95	9 Km to Oakland Toll Plaza

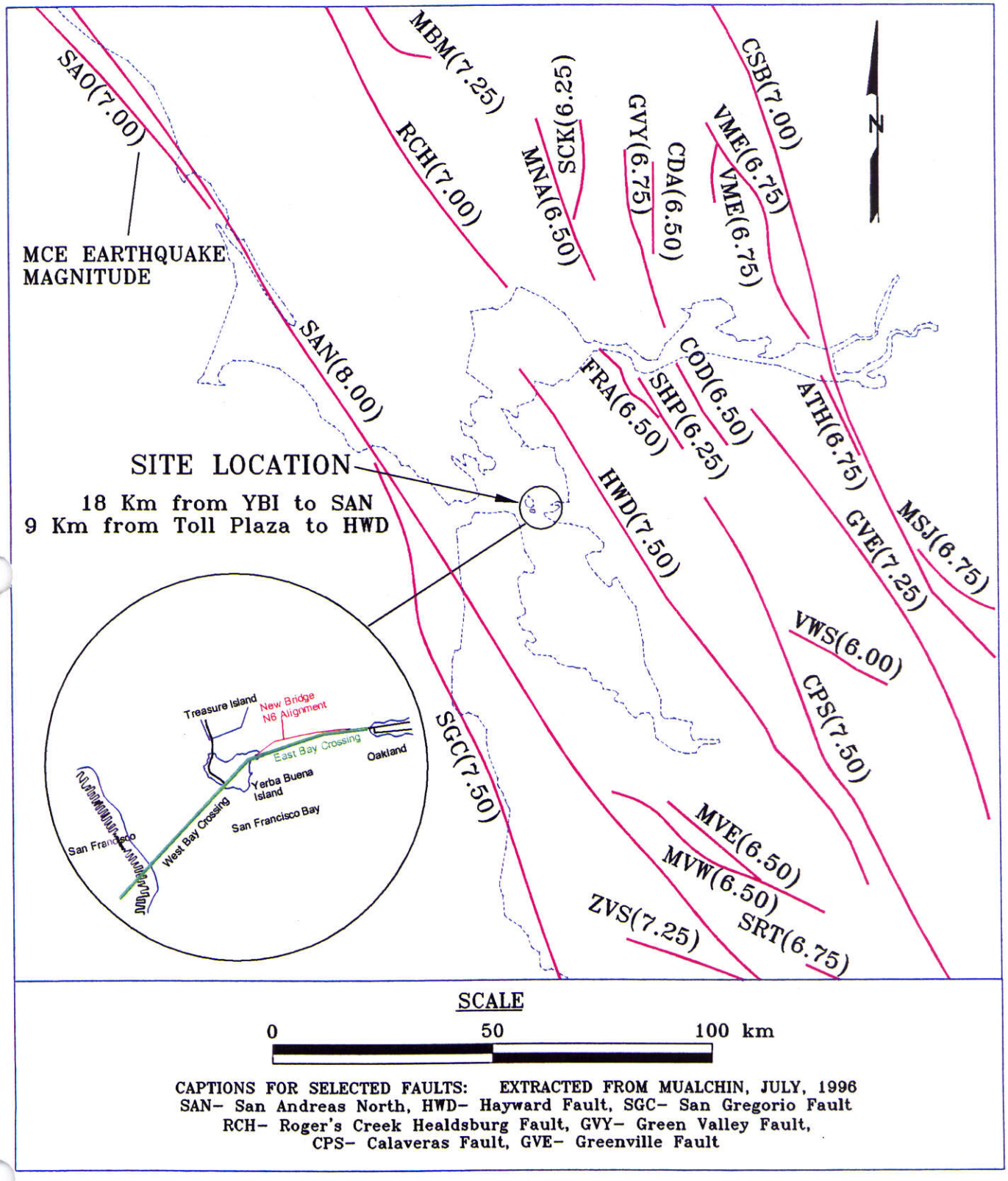

CAPTIONS FOR SELECTED FAULTS: EXTRACTED FROM MUALCHIN, JULY, 1996
SAN– San Andreas North, HWD– Hayward Fault, SGC– San Gregorio Fault
RCH– Roger's Creek Healdsburg Fault, GVY– Green Valley Fault,
CPS– Calaveras Fault, GVE– Greenville Fault

FAULT MAP AROUND PROJECT SITE
SFOBB East Span Seismic Safety Project

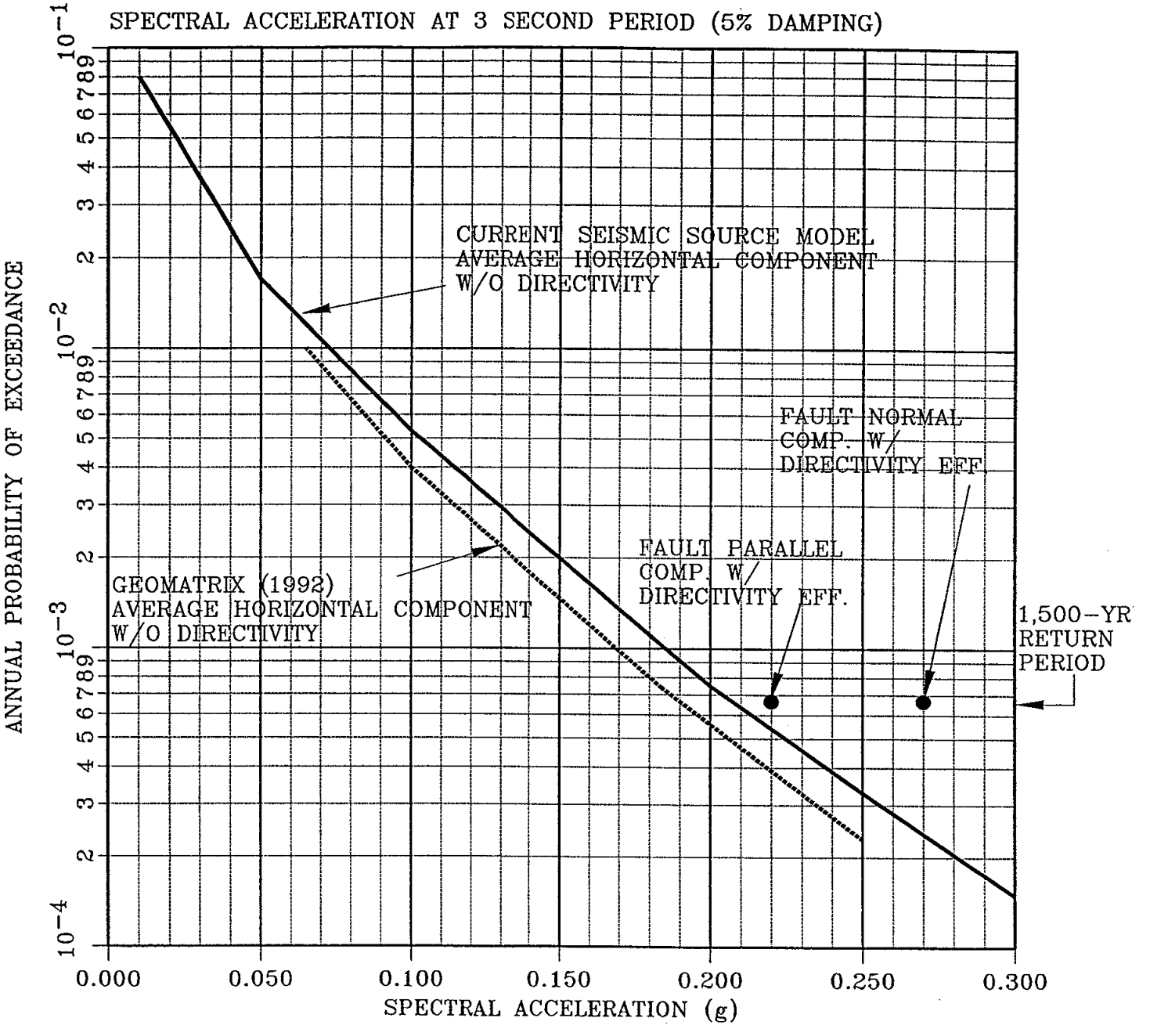

COMPARISON OF PROBABILISTIC HAZARD SOLUTIONS FROM PRIOR (RETROFIT) AND PRESENT STUDIES

SFOBB East Span Seismic Safety Project

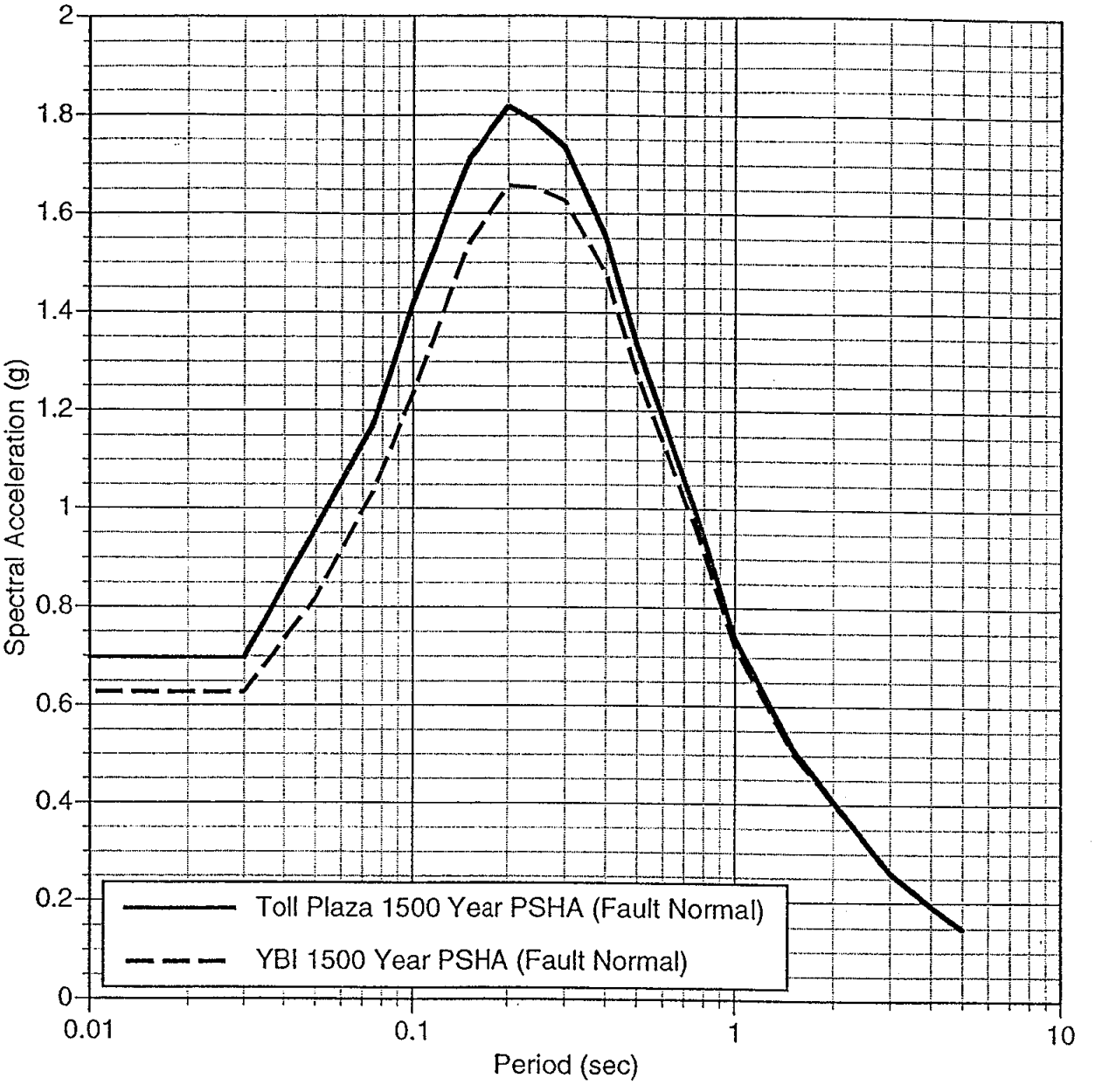

EAST AND WEST SIDE PSHA: FAULT NUMBER SPECTRA FOR SAFETY EVALUATION EARTHQUAKE (SEE)
SFOBB East Span Seismic Safety Project

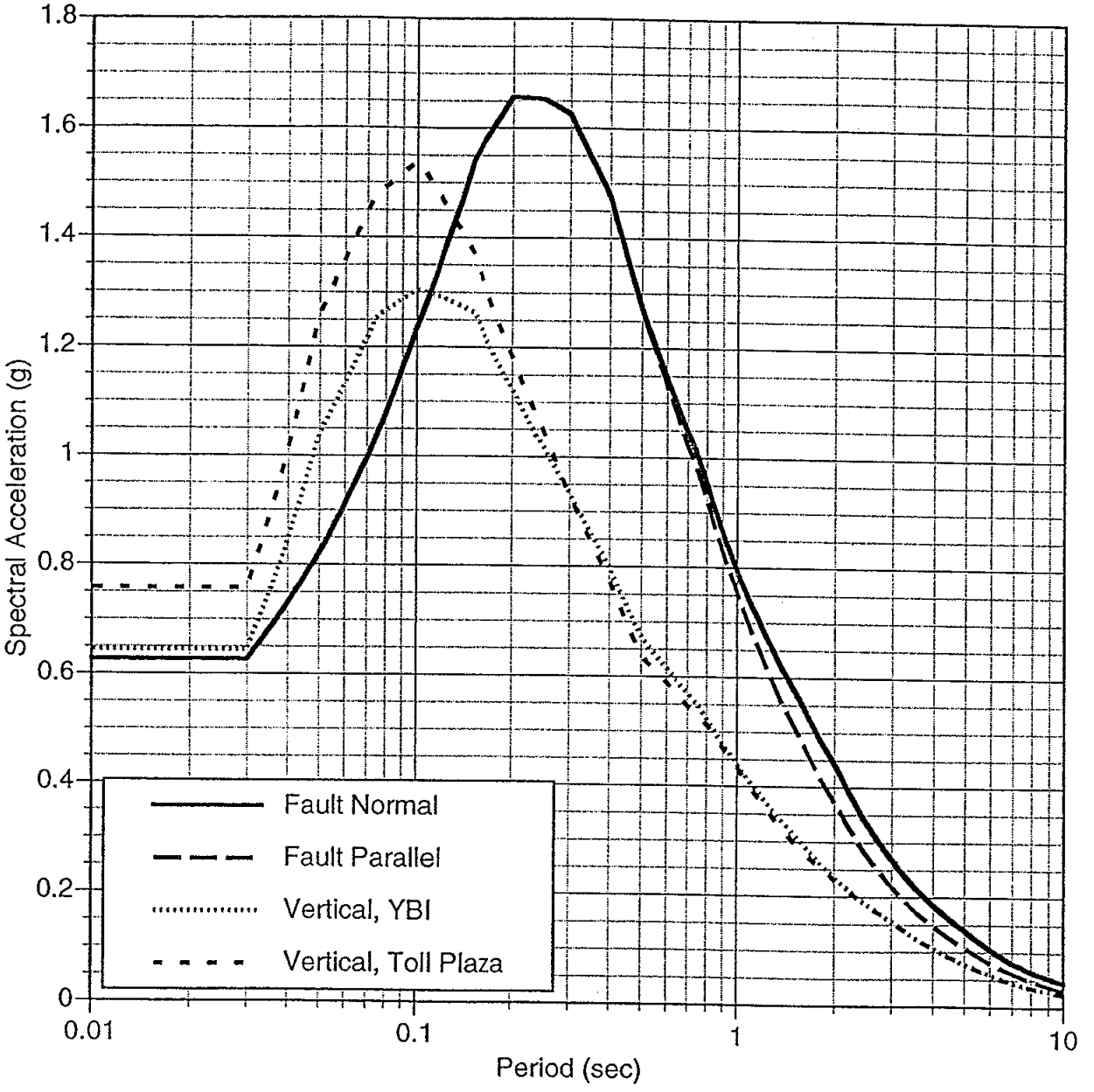

THREE COMPONENTS OF TARGET ROCK SPECTRA FOR SAFETY EVALUATION EARTHQUAKE (SEE)
SFOBB East Span Seismic Safety Project

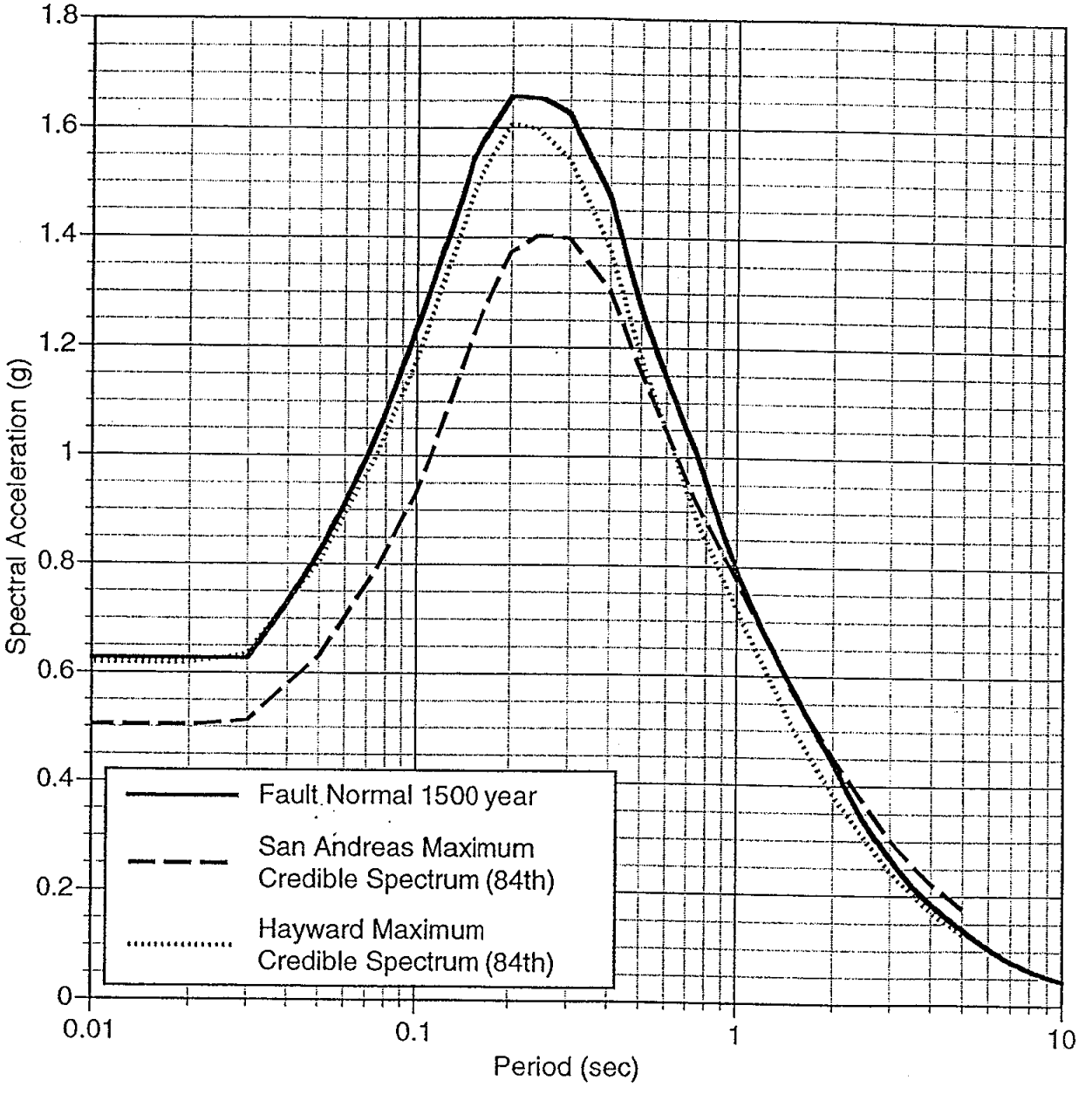

COMPARISON BETWEEN 1,500-YR PSHA AND MCE SPECTRA
SFOBB East Span Seismic Safety Project

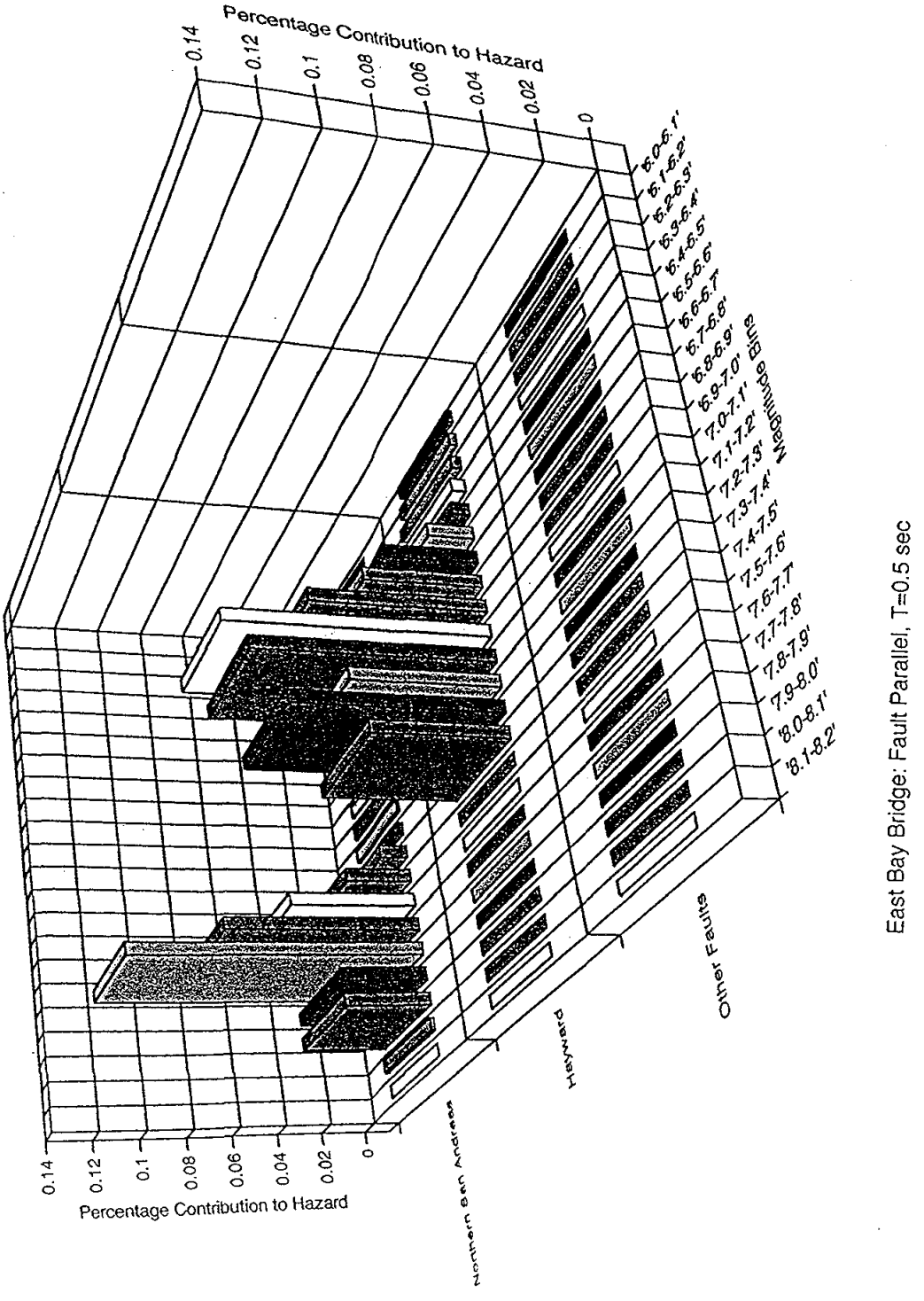

DEAGGREGATED HAZARD ACCORDING TO SOURCE AT 0.5 SEC PERIOD: FAULT PARALLEL

SFOBB East Span Seismic Safety Project

Earth Mechanics

FUGRO

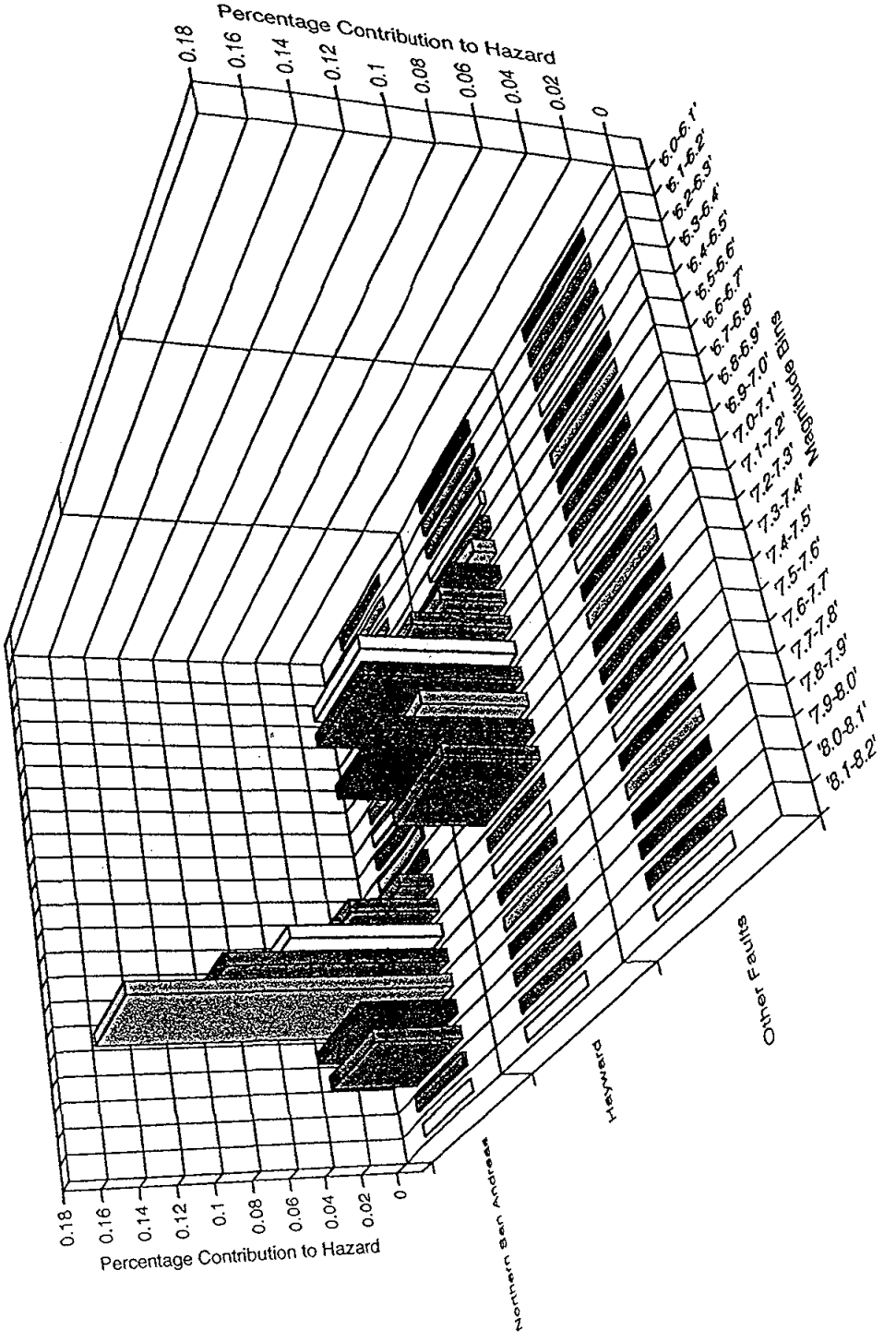

DEAGGREGATED HAZARD ACCORDING TO SOURCE AT 1.0 SEC PERIOD: FAULT PARALLEL

SFOBB East Span Seismic Safety Project

Earth Mechanics FUGRO

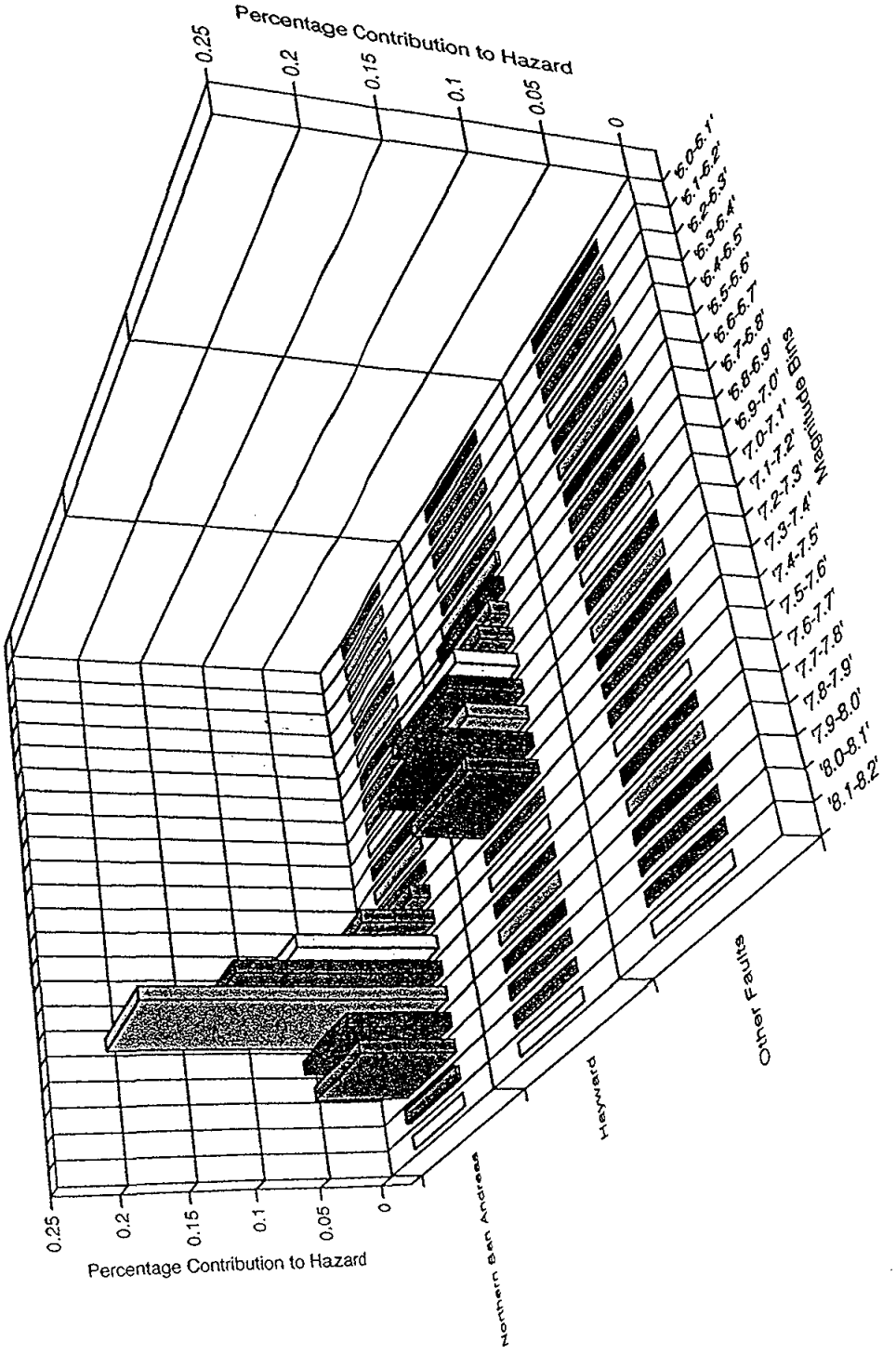

East Bay Bridge: Fault Parallel, T=2.0 sec

DEAGGREGATED HAZARD ACCORDING TO SOURCE AT 2.0 SEC PERIOD: FAULT PARALLEL

SFOBB East Span Seismic Safety Project

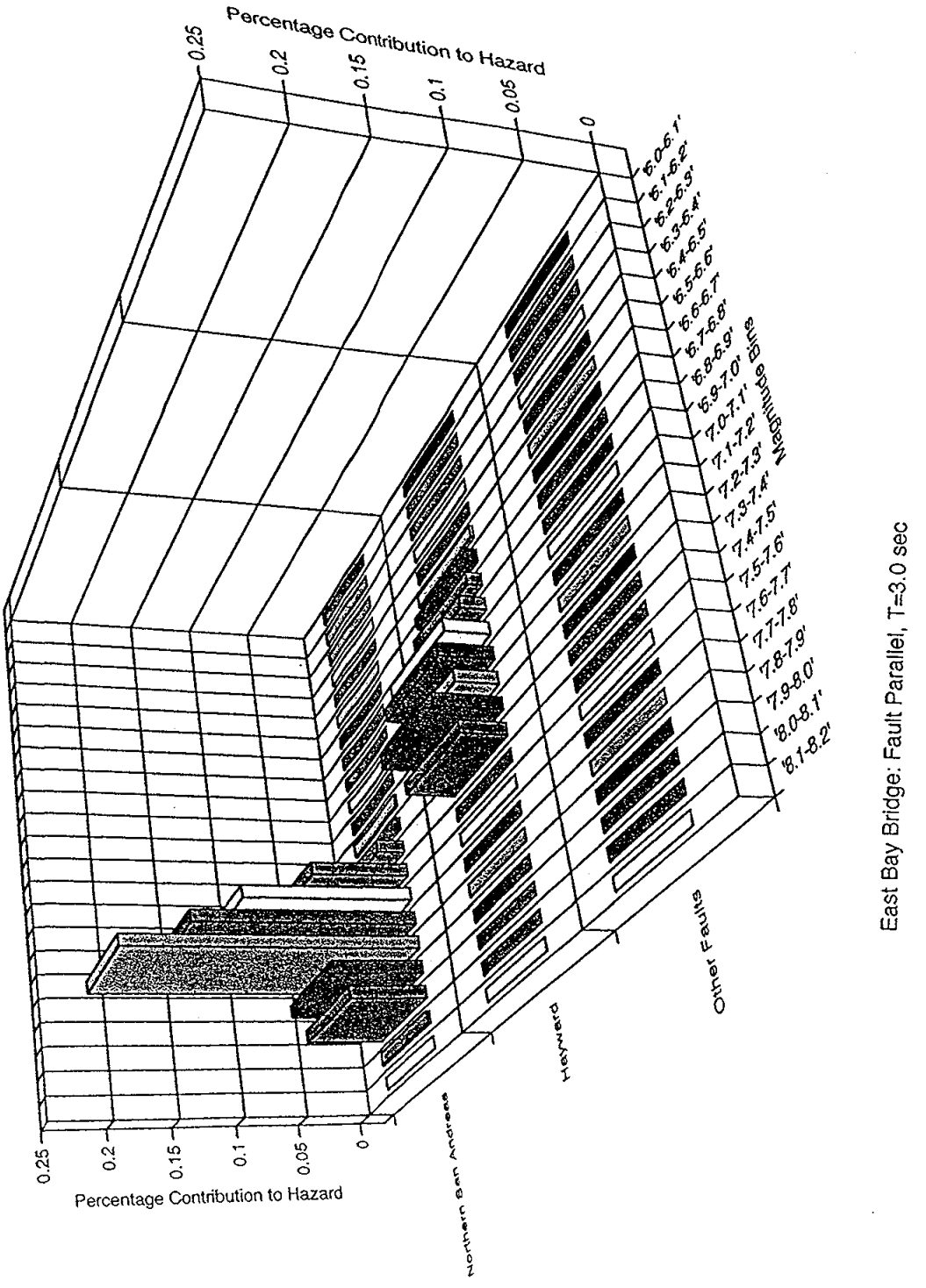

DEAGGREGATED HAZARD ACCORDING TO SOURCE AT 3.0 SEC PERIOD: FAULT PARALLEL

SFOBB East Span Seismic Safety Project

Earth Mechanics

FUGRO

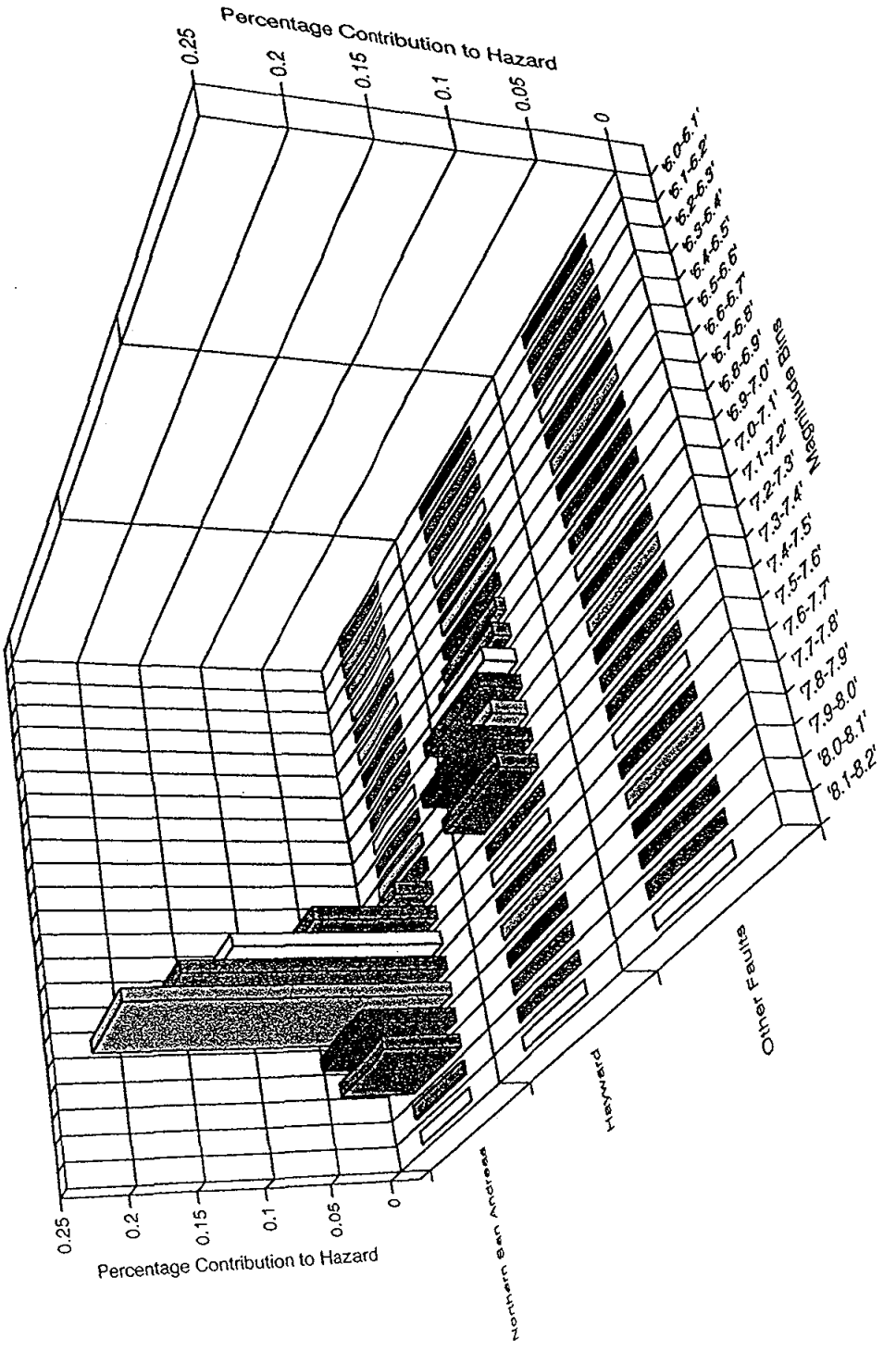

East Bay Bridge: Fault Parallel, T=5.0 sec

DEAGGREGATED HAZARD ACCORDING TO SOURCE AT 5.0 SEC PERIOD: FAULT PARALLEL

SFOBB East Span Seismic Safety Project

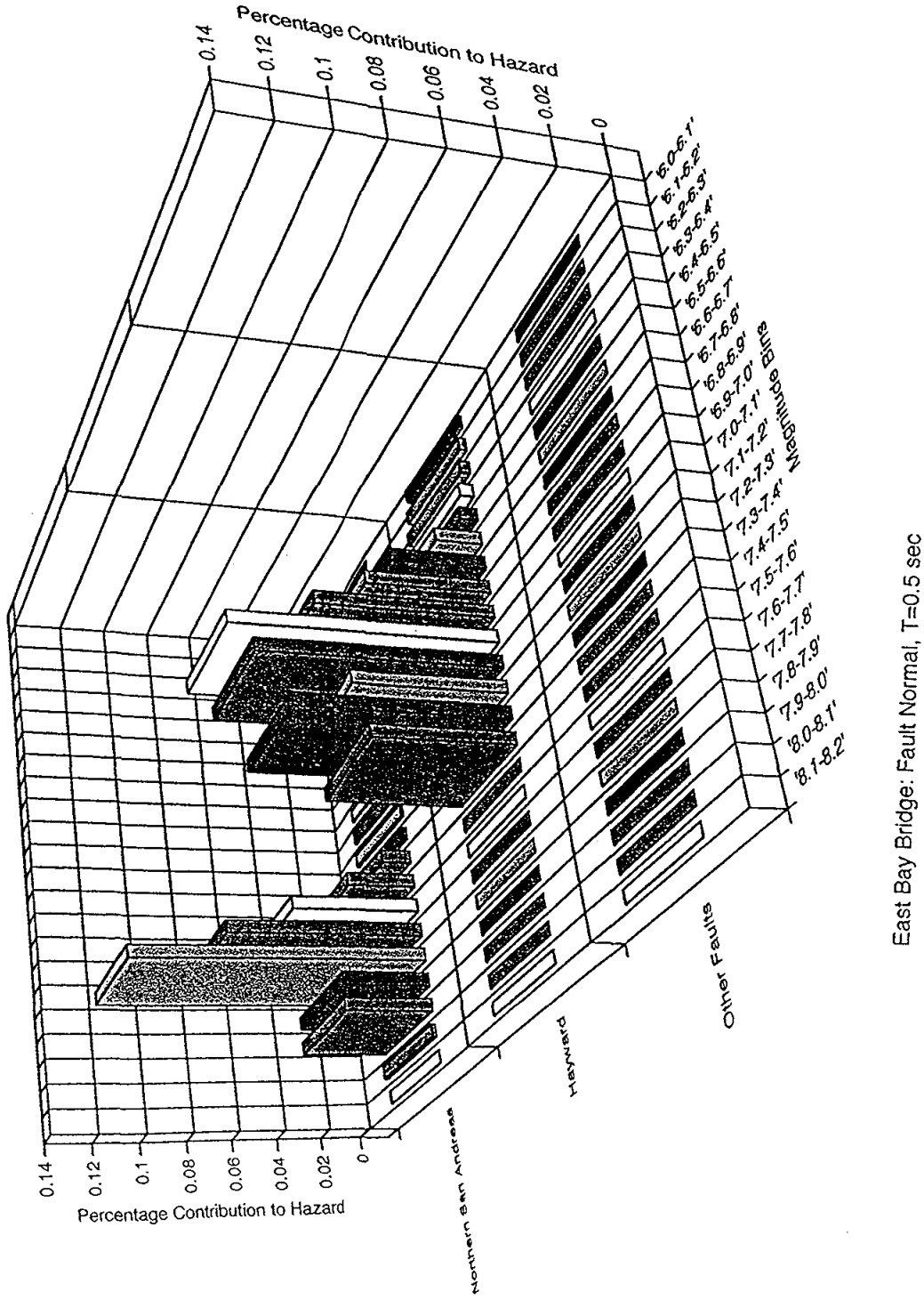

DEAGGREGATED HAZARD ACCORDING TO SOURCE AT 0.5 SEC PERIOD: FAULT NORMAL

SFOBB East Span Seismic Safety Project

Earth Mechanics FUGRO

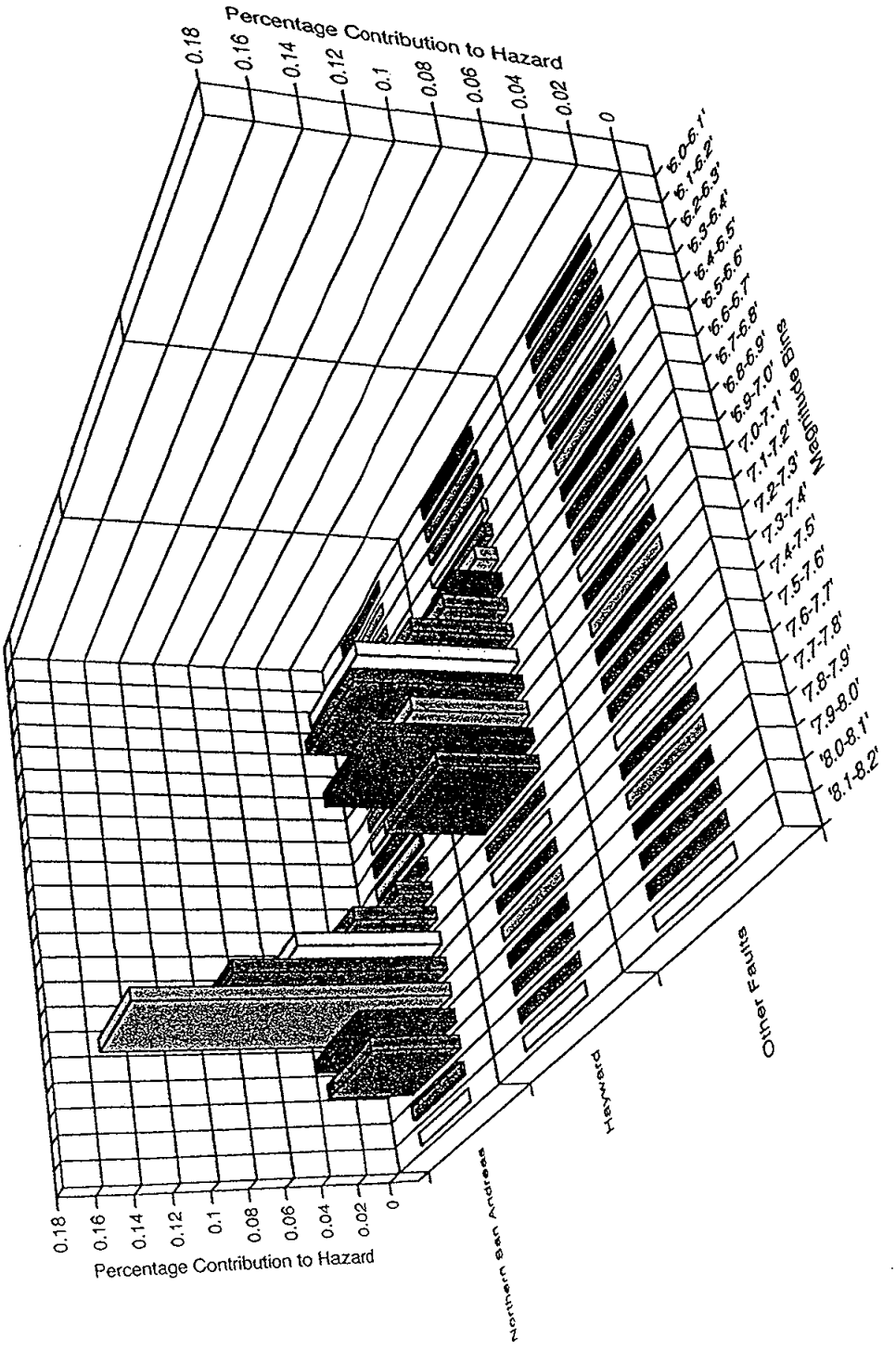

DEAGGREGATED HAZARD ACCORDING TO SOURCE AT 1.0 SEC PERIOD: FAULT NORMAL

SFOBB East Span Seismic Safety Project

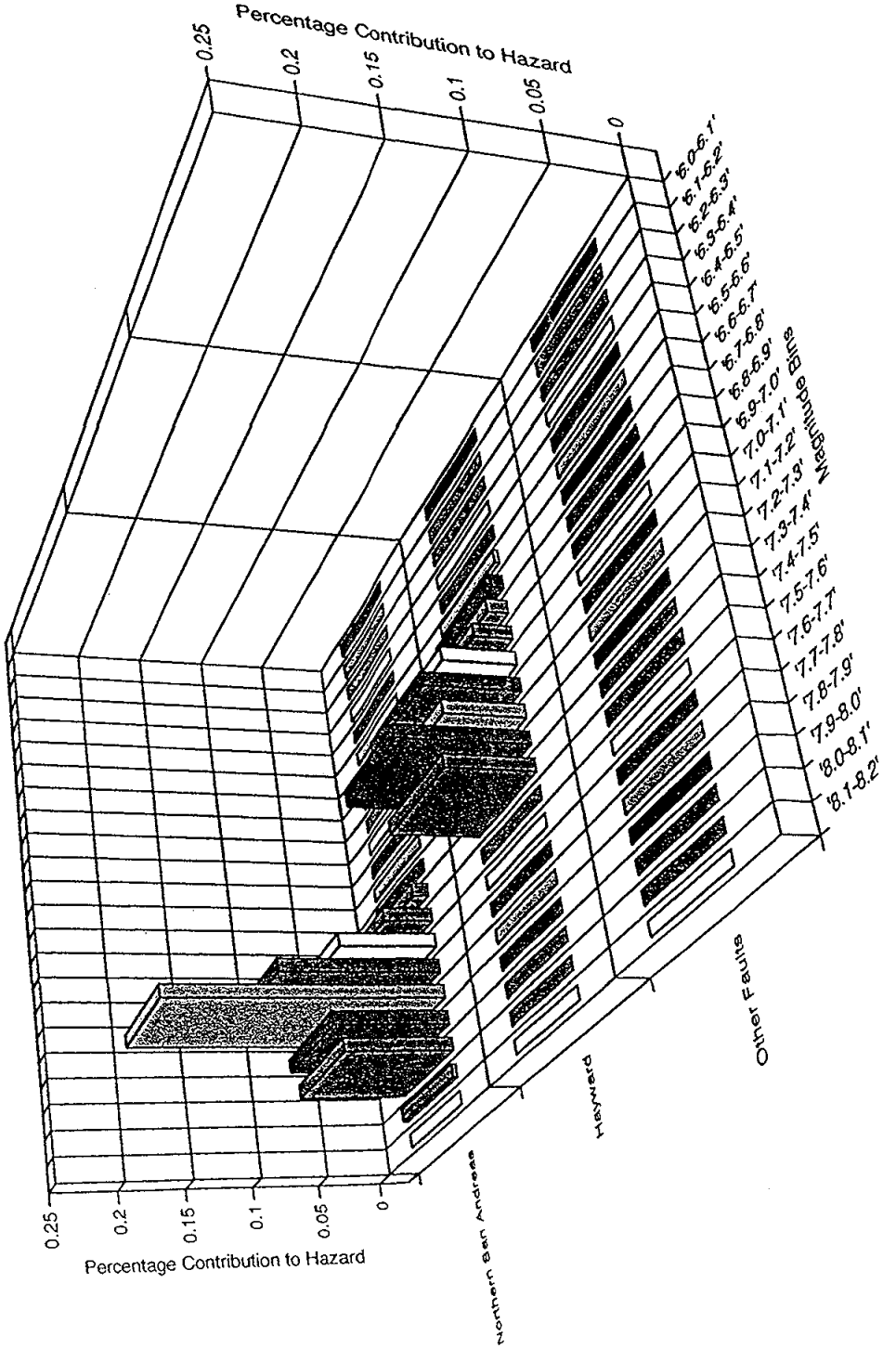

DEAGGREGATED HAZARD ACCORDING TO SOURCE AT 2.0 SEC PERIOD: FAULT NORMAL

SFOBB East Span Seismic Safety Project

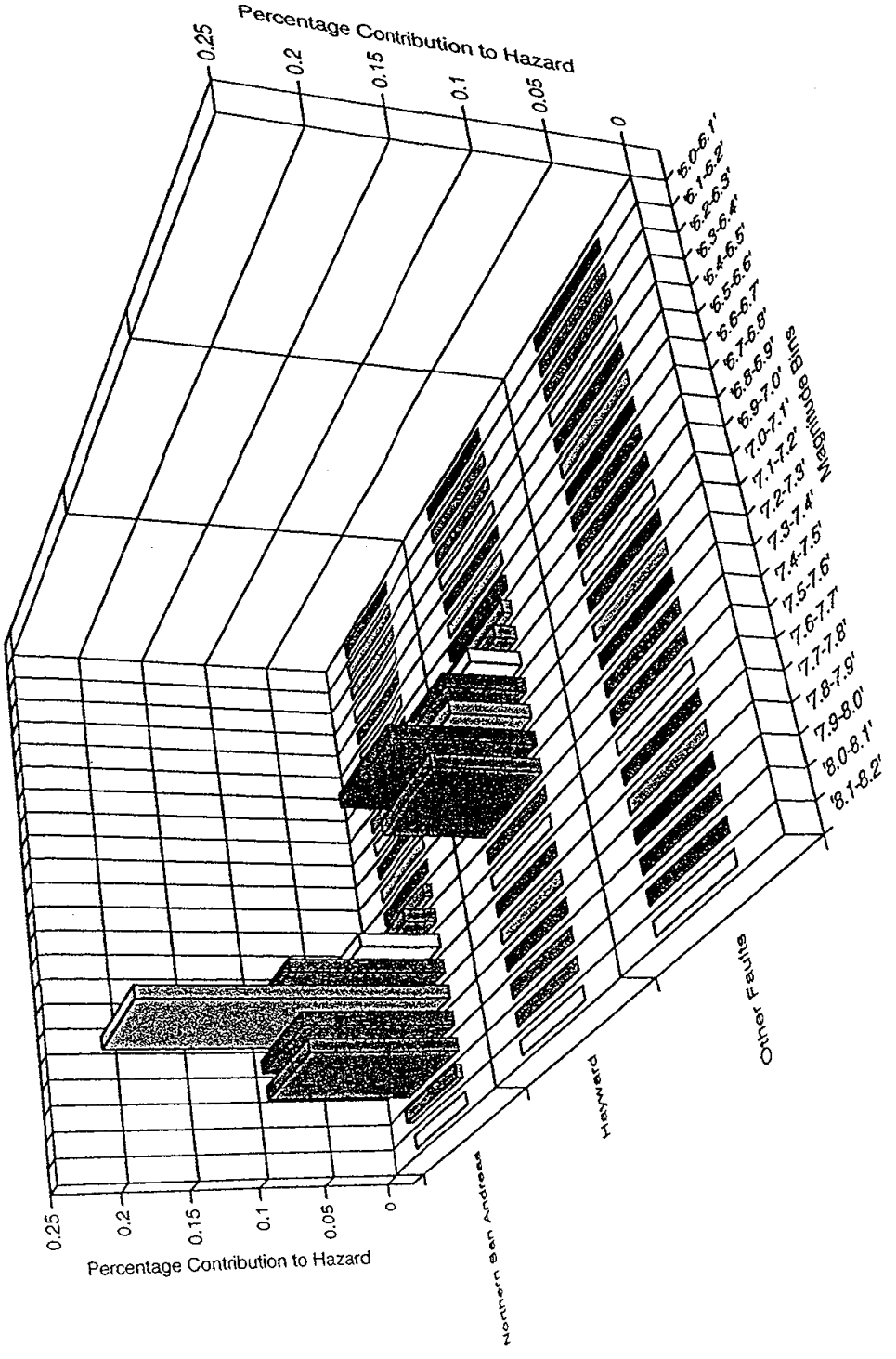

East Bay Bridge: Fault Normal, T=3.0 sec

DEAGGREGATED HAZARD ACCORDING TO SOURCE AT 3.0 SEC PERIOD: FAULT NORMAL

SFOBB East Span Seismic Safety Project

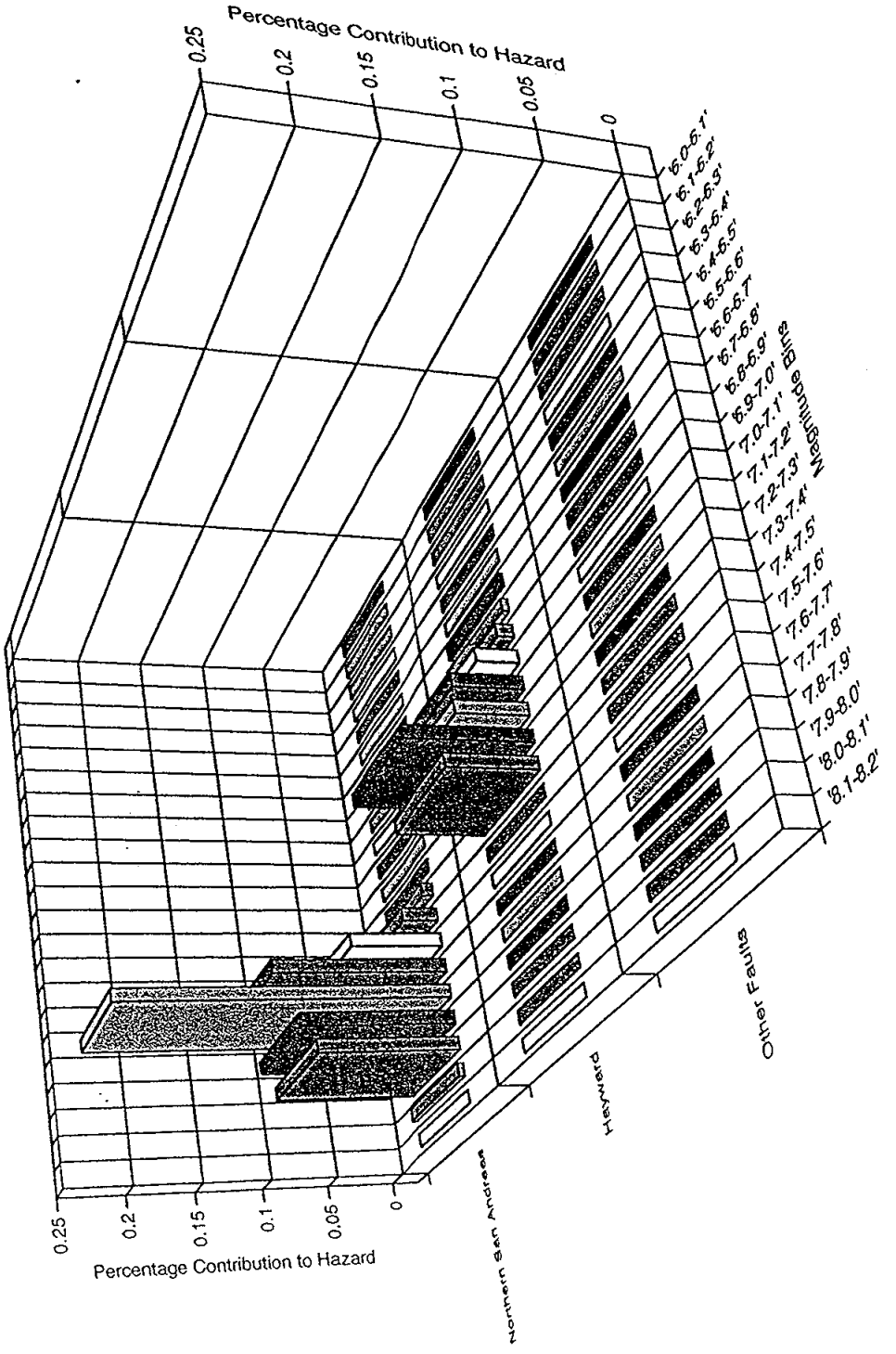

DEAGGREGATED HAZARD ACCORDING TO SOURCE AT 5.0 SEC PERIOD: FAULT NORMAL

SFOBB East Span Seismic Safety Project

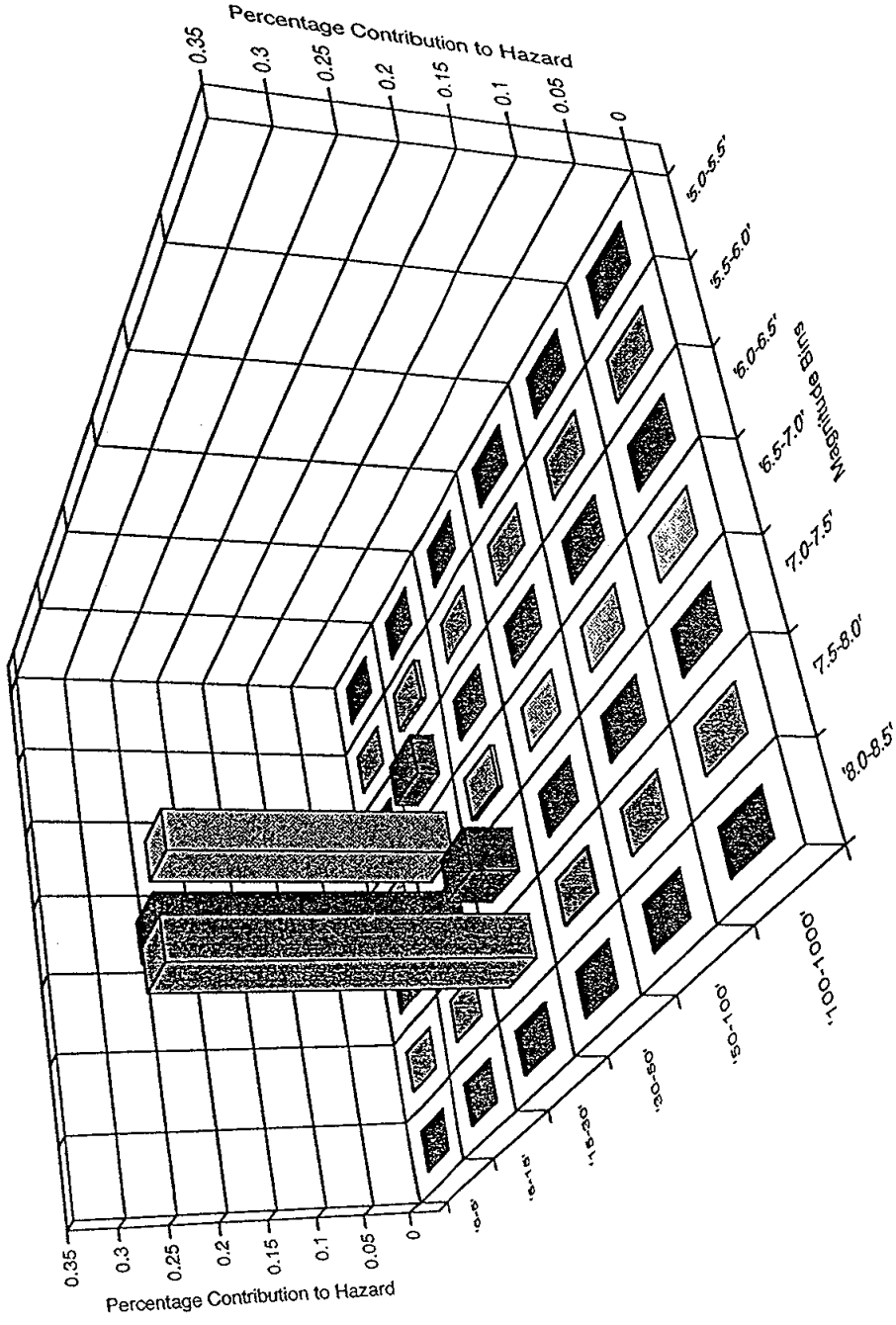

DEAGGREGATED HAZARD ACCORDING TO DISTANCE AT 0.5 SEC PERIOD: FAULT PARALLEL

SFOBB East Span Seismic Safety Project

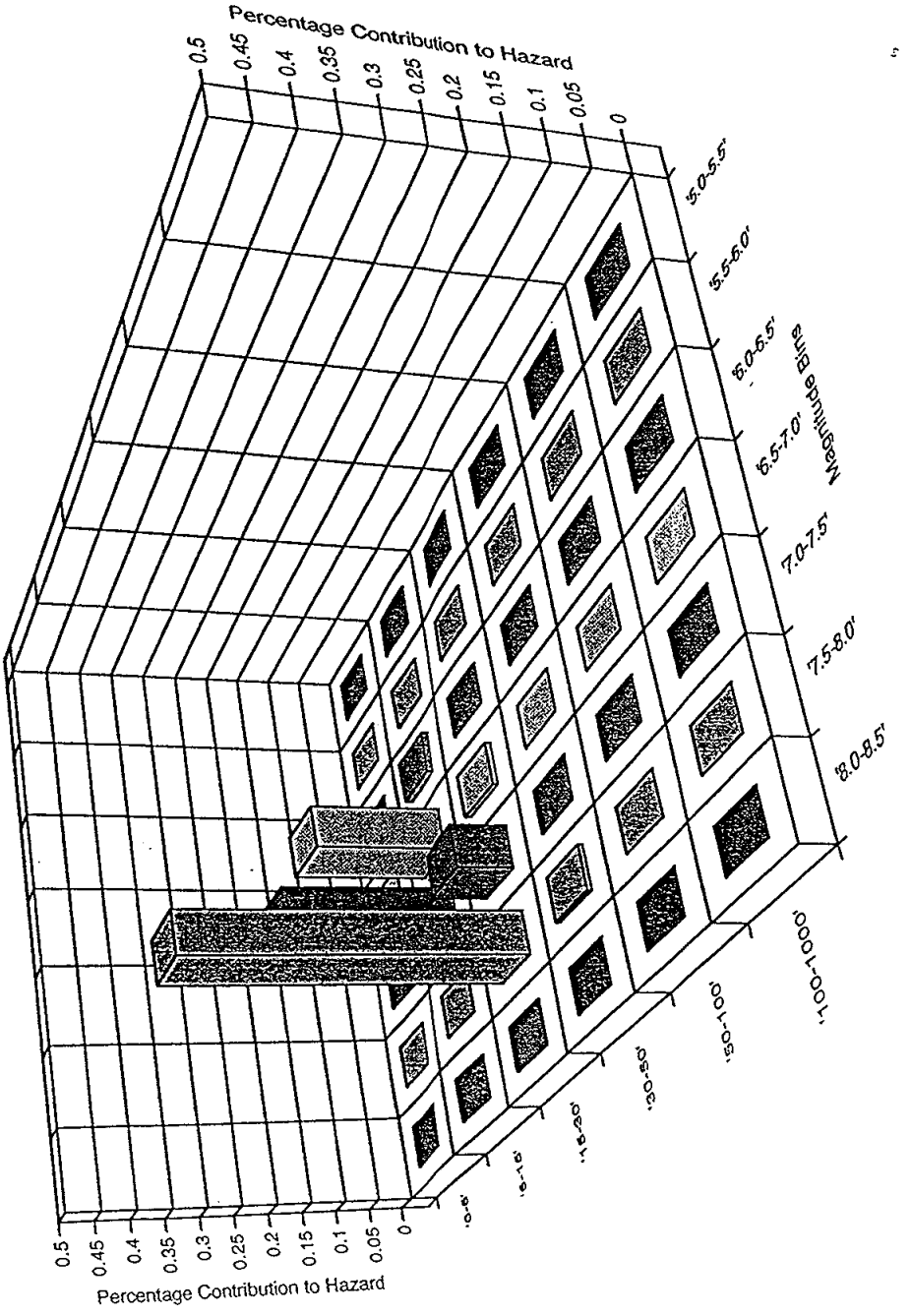

DEAGGREGATED HAZARD ACCORDING TO DISTANCE AT 1.0 SEC PERIOD: FAULT PARALLEL

SFOBB East Span Seismic Safety Project

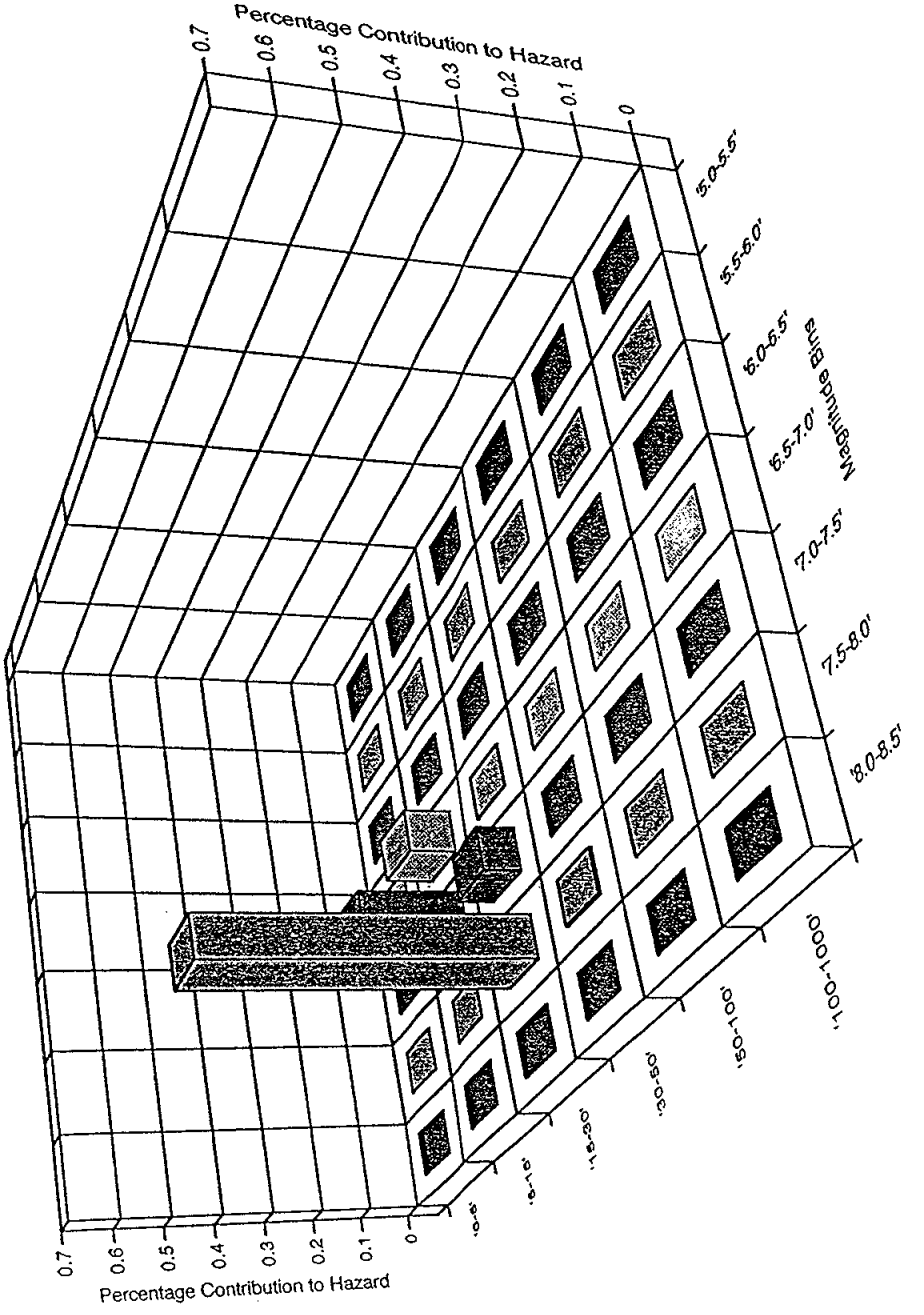

DEAGGREGATED HAZARD ACCORDING TO DISTANCE AT 2.0 SEC PERIOD: FAULT PARALLEL

SFOBB East Span Seismic Safety Project

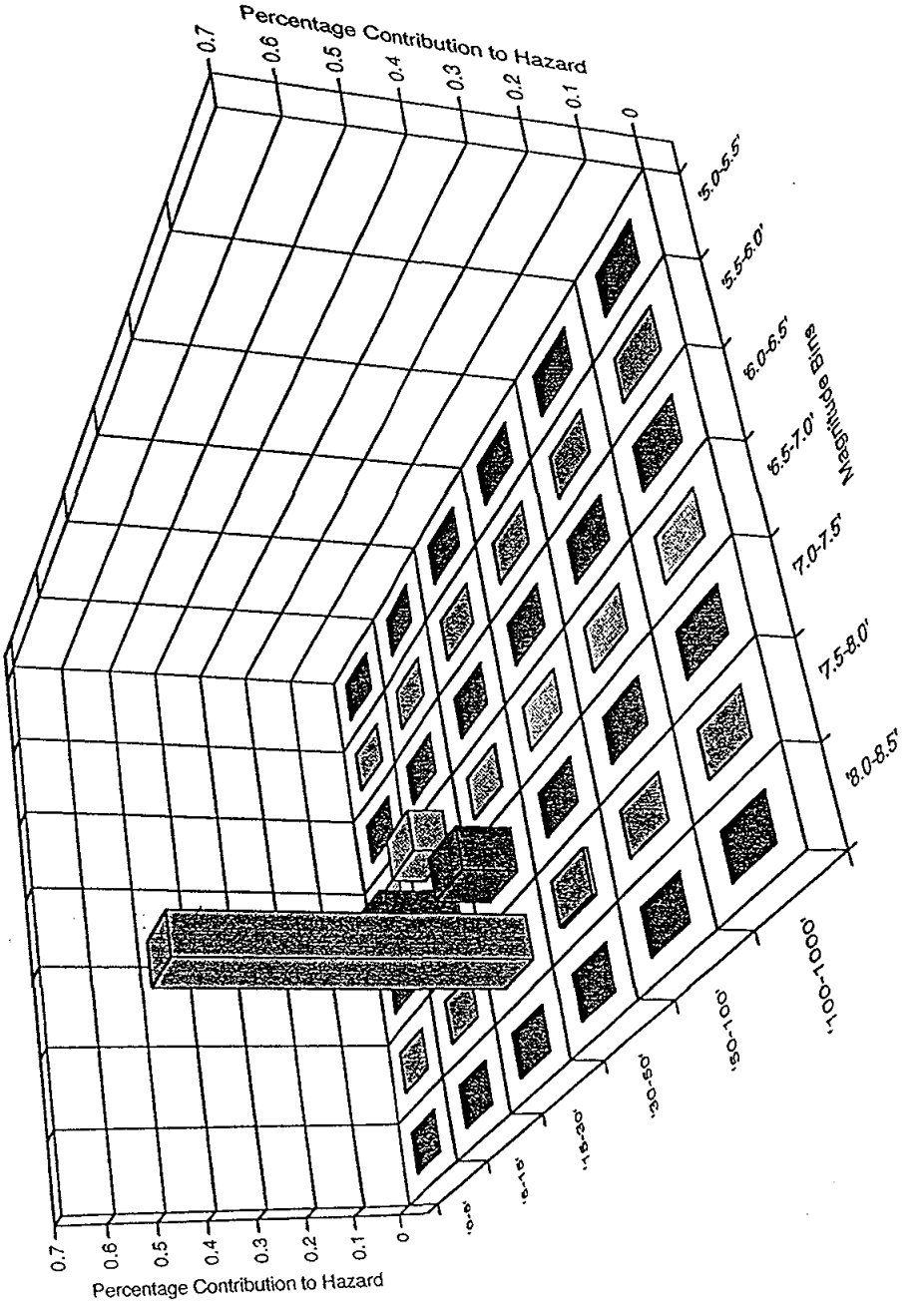

DEAGGREGATED HAZARD ACCORDING TO DISTANCE AT 3.0 SEC PERIOD: FAULT PARALLEL

SFOBB East Span Seismic Safety Project

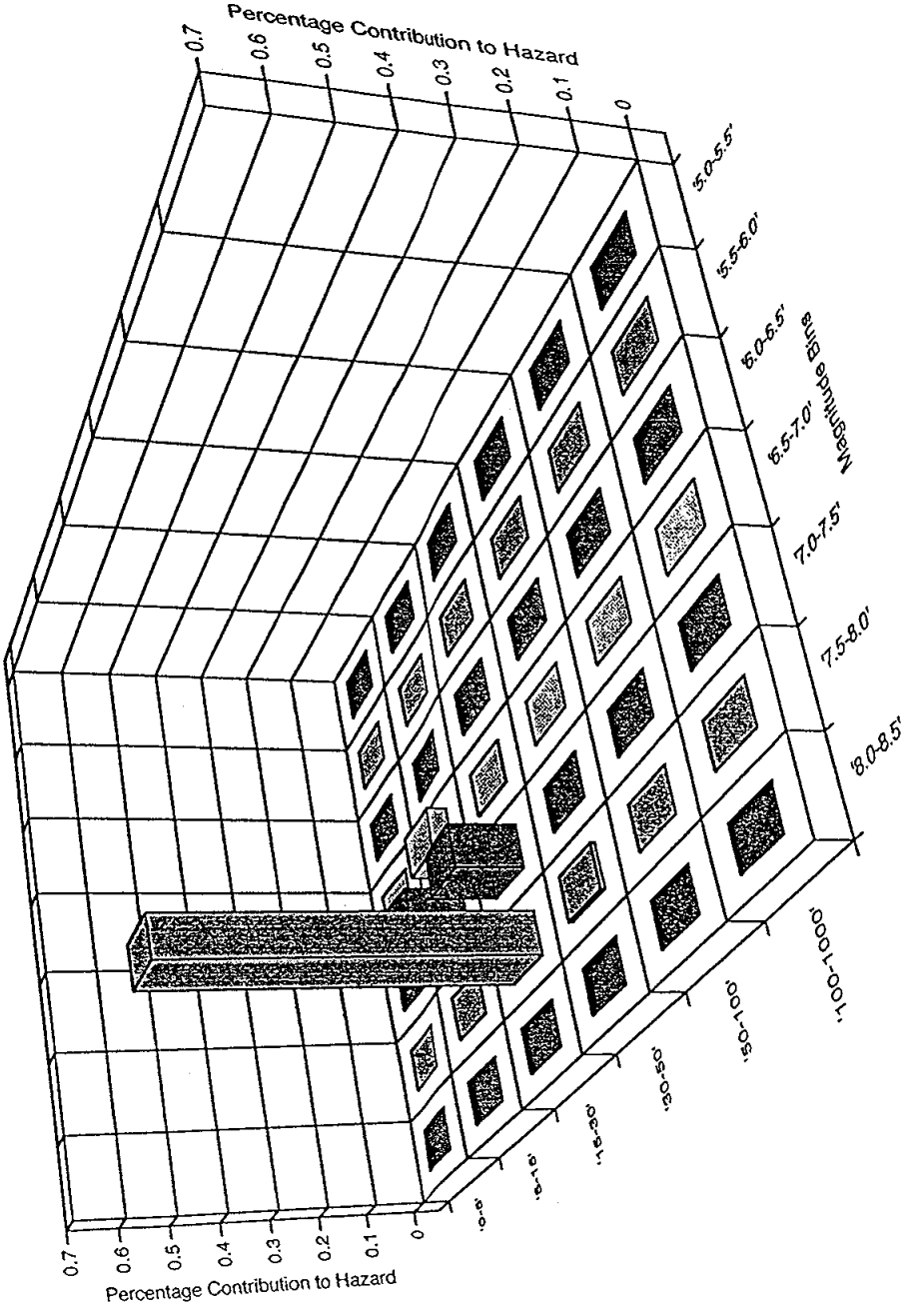

DEAGGREGATED HAZARD ACCORDING TO DISTANCE AT 5.0 SEC PERIOD: FAULT PARALLEL

SFOBB East Span Seismic Safety Project

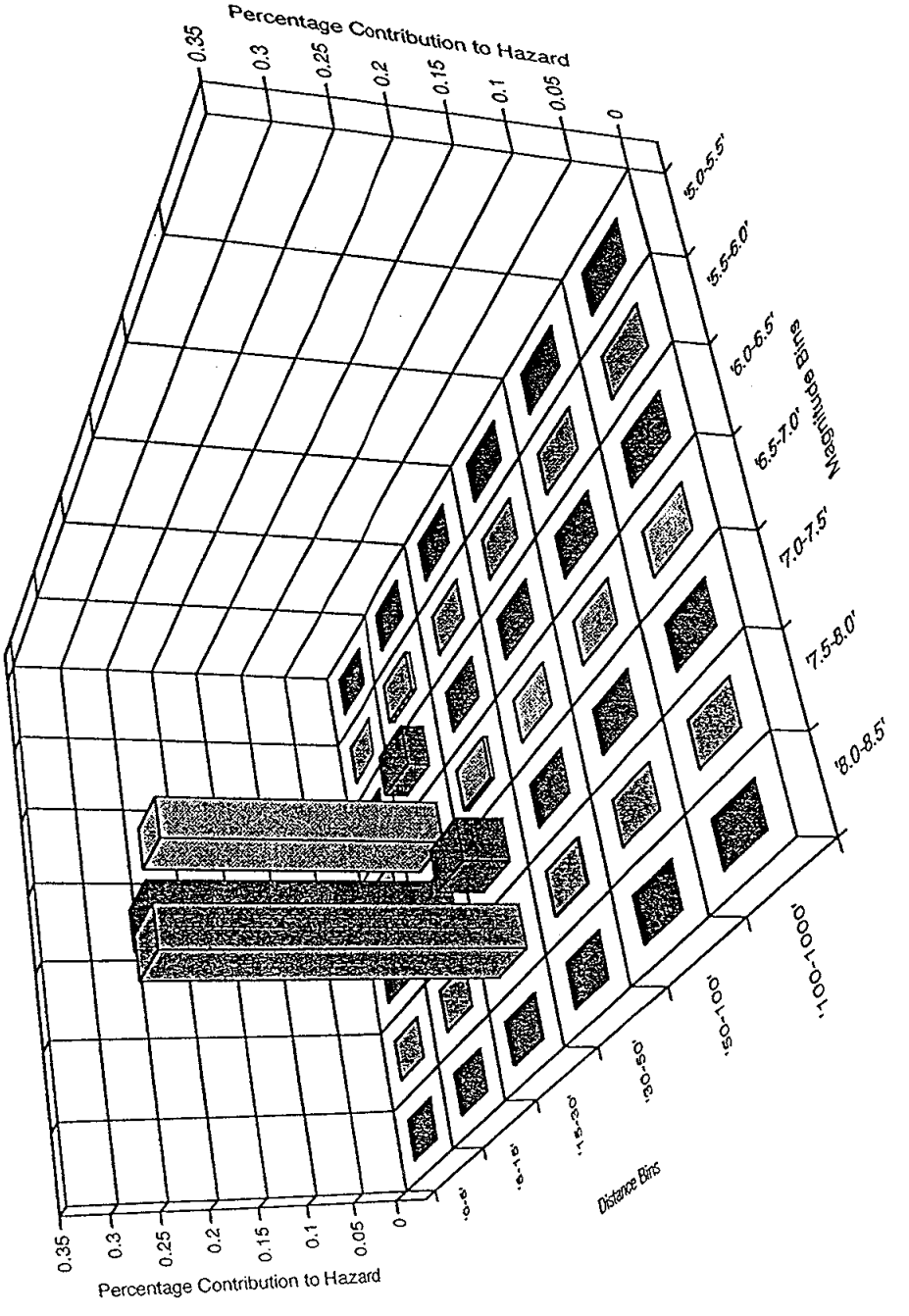

DEAGGREGATED HAZARD ACCORDING TO DISTANCE AT 0.5 SEC PERIOD: FAULT NORMAL

SFOBB East Span Seismic Safety Project

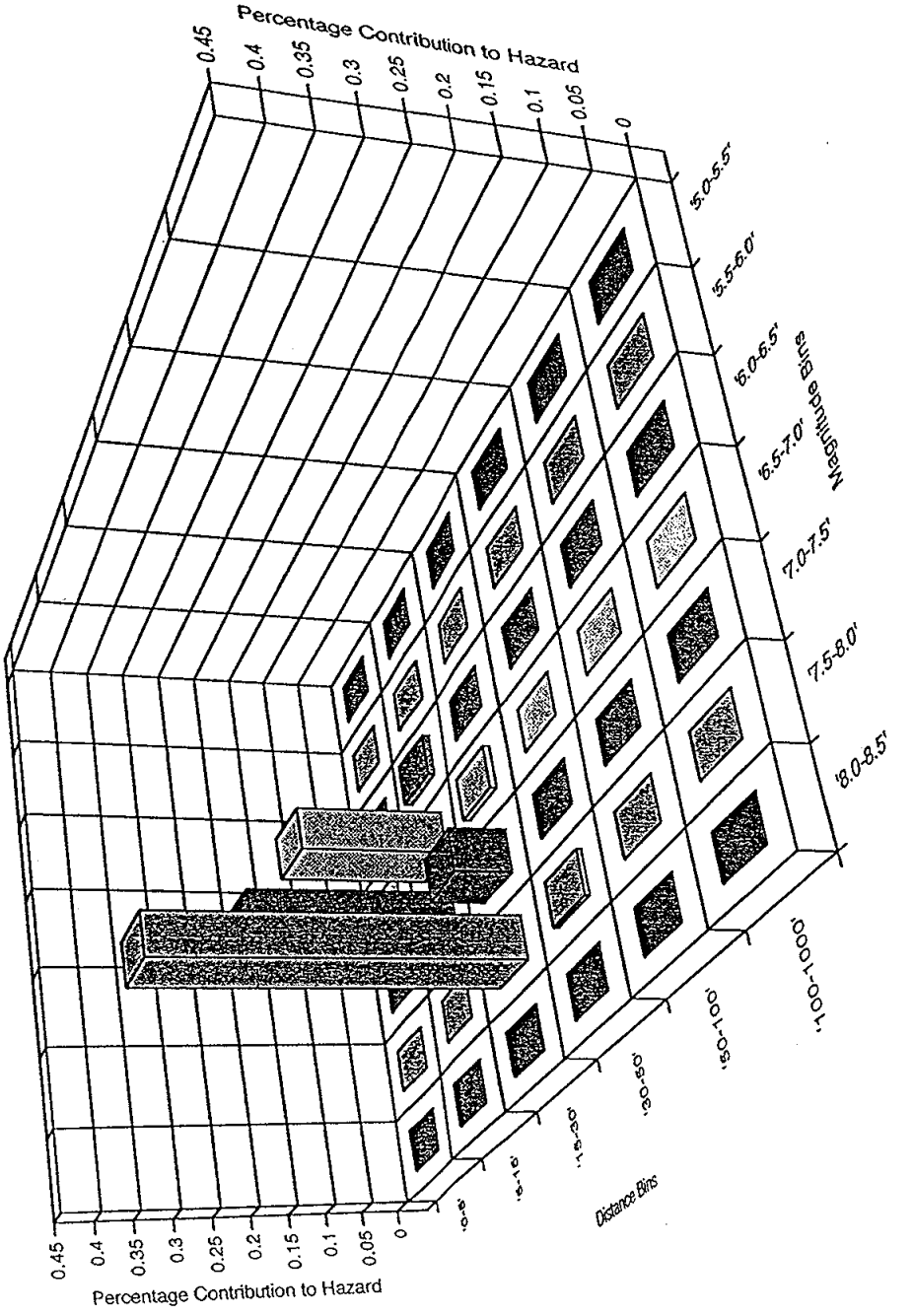

DEAGGREGATED HAZARD ACCORDING TO DISTANCE AT 1.0 SEC PERIOD: FAULT NORMAL

SFOBB East Span Seismic Safety Project

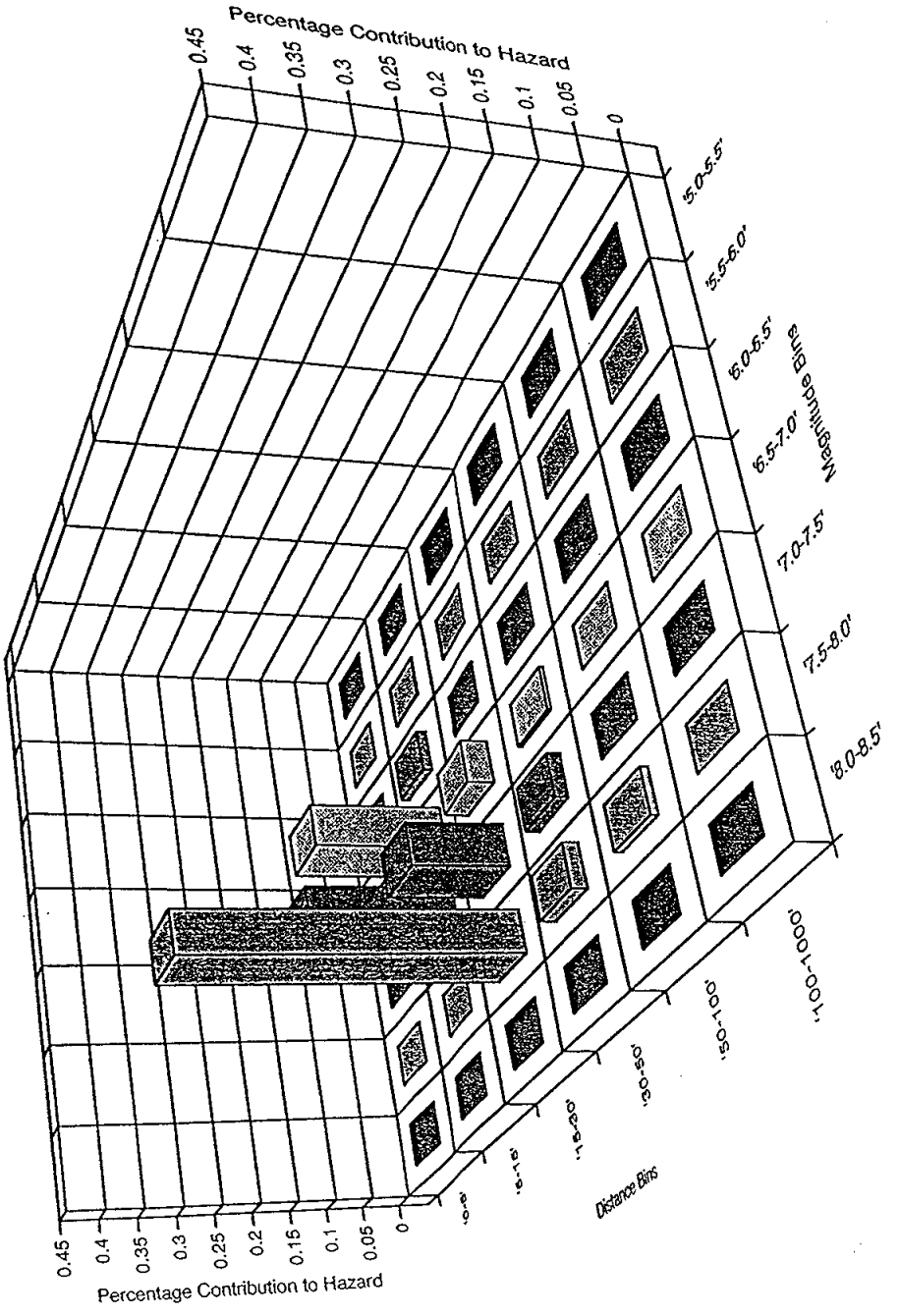

East Bay Bridge: Fault Normal, T=2.0 sec

G:\Data2\HO17\8\East_Baybridge_3\98\Hazard\Haz2dm_10\98\tiol_In_fltdeag.gg

DEAGGREGATED HAZARD ACCORDING TO DISTANCE AT 2.0 SEC PERIOD: FAULT NORMAL

SFOBB East Span Seismic Safety Project

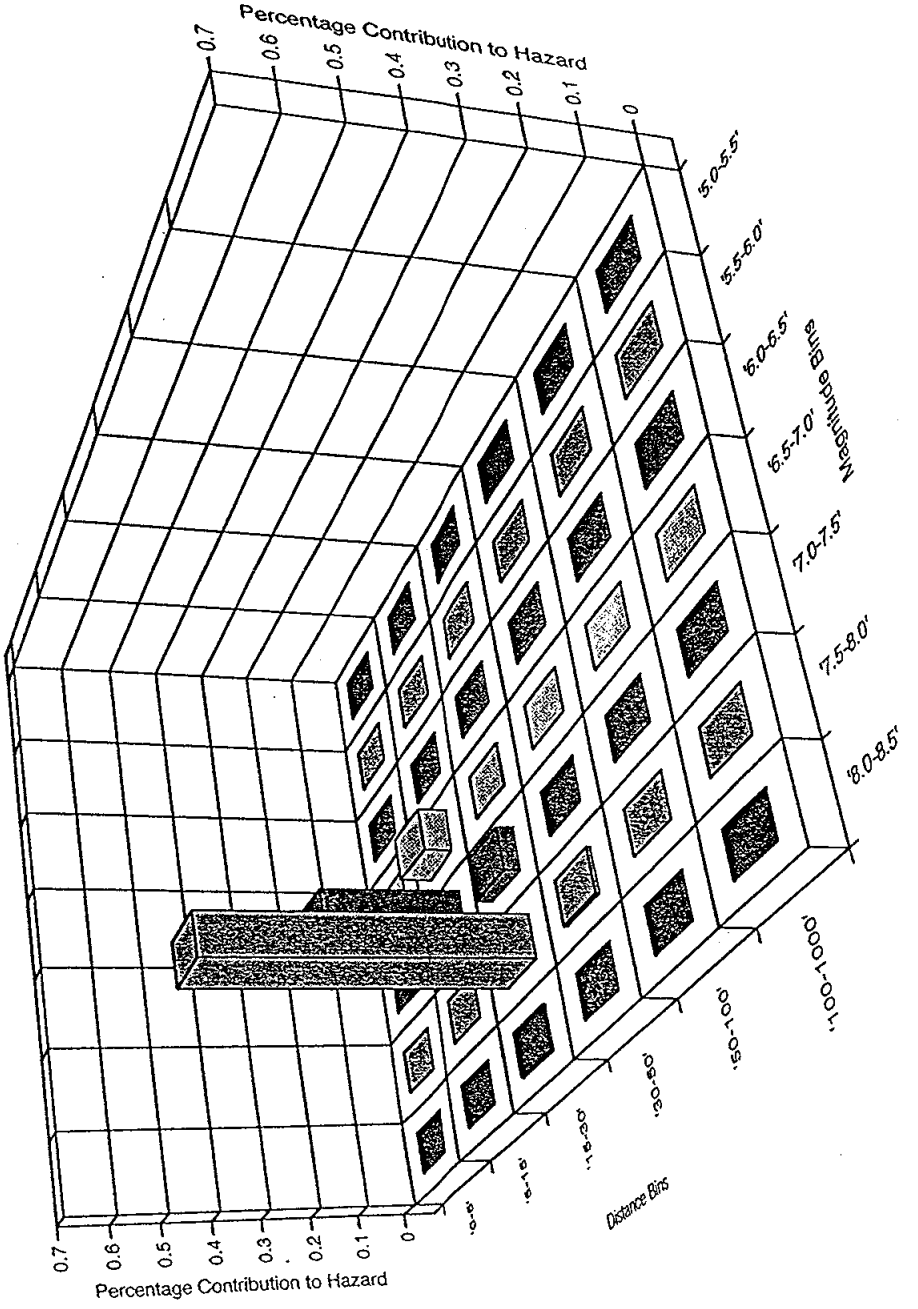

DEAGGREGATED HAZARD ACCORDING TO DISTANCE AT 3.0 SEC PERIOD: FAULT NORMAL

SFOBB East Span Seismic Safety Project

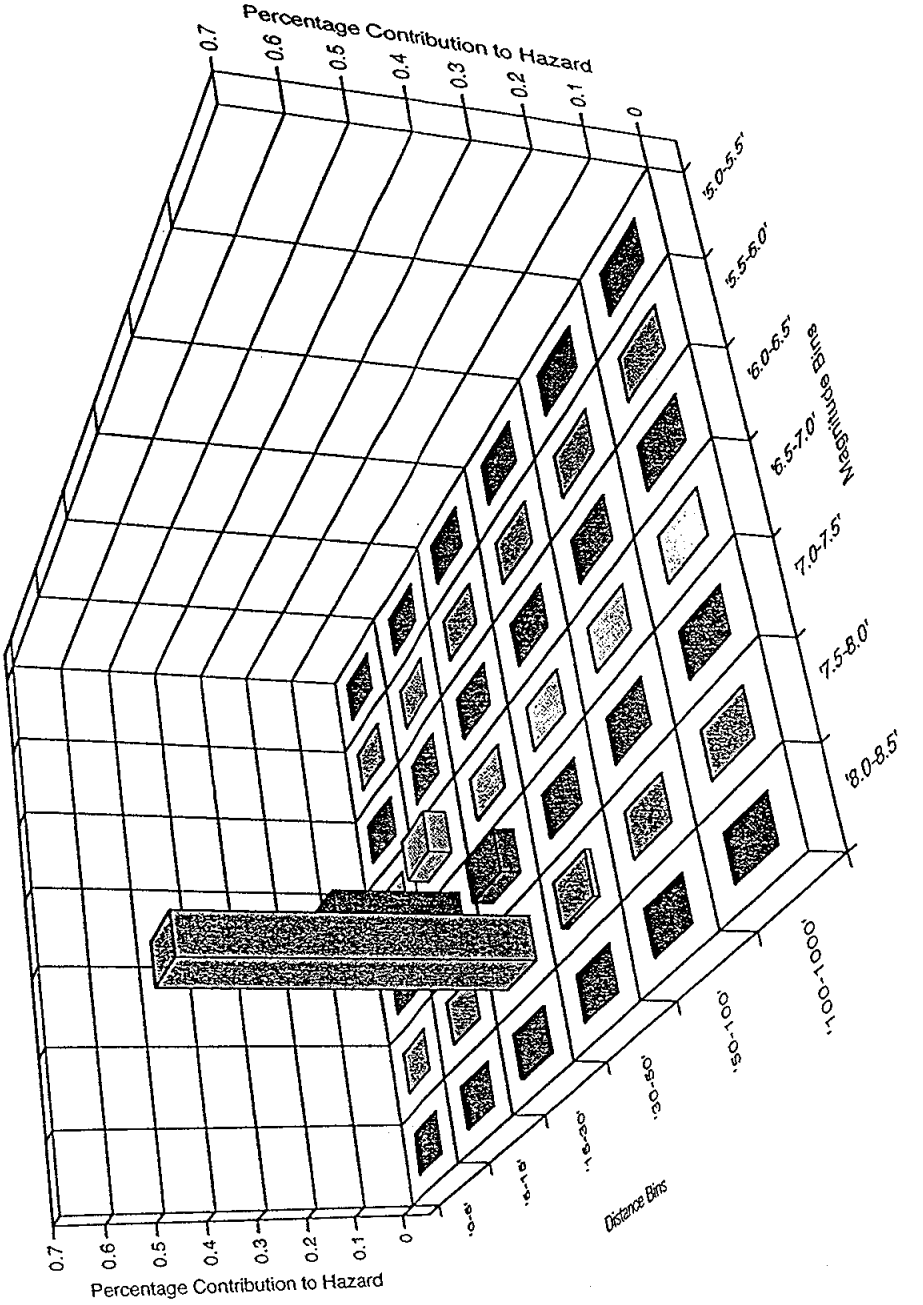

DEAGGREGATED HAZARD ACCORDING TO DISTANCE AT 5.0 SEC PERIOD: FAULT NORMAL

SFOBB East Span Seismic Safety Project

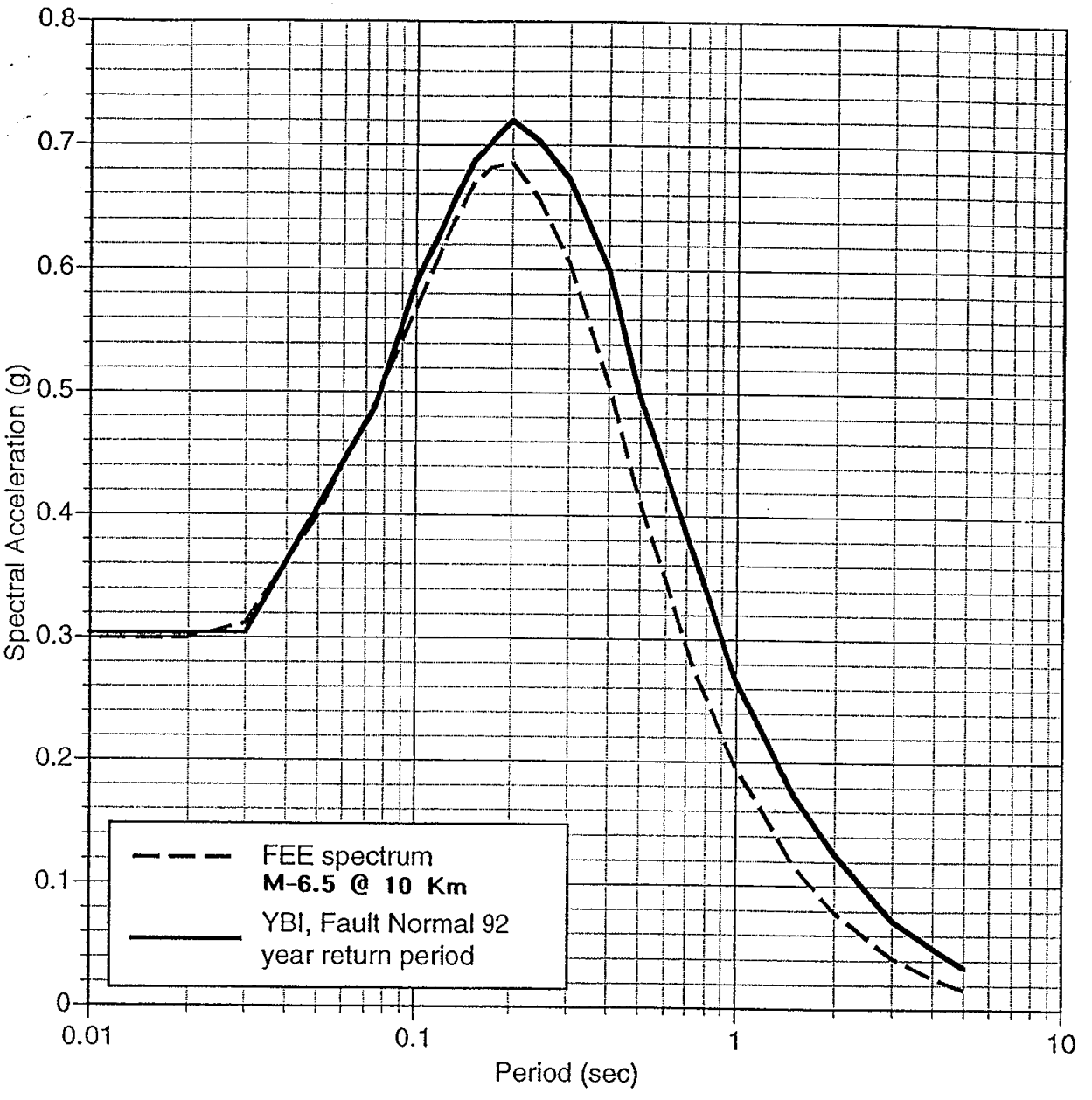

COMPARISON BETWEEN 92-YEAR PSHA AND DETERMINISTIC FEE SPECTRUM
SFOBB East Span Seismic Safety Project

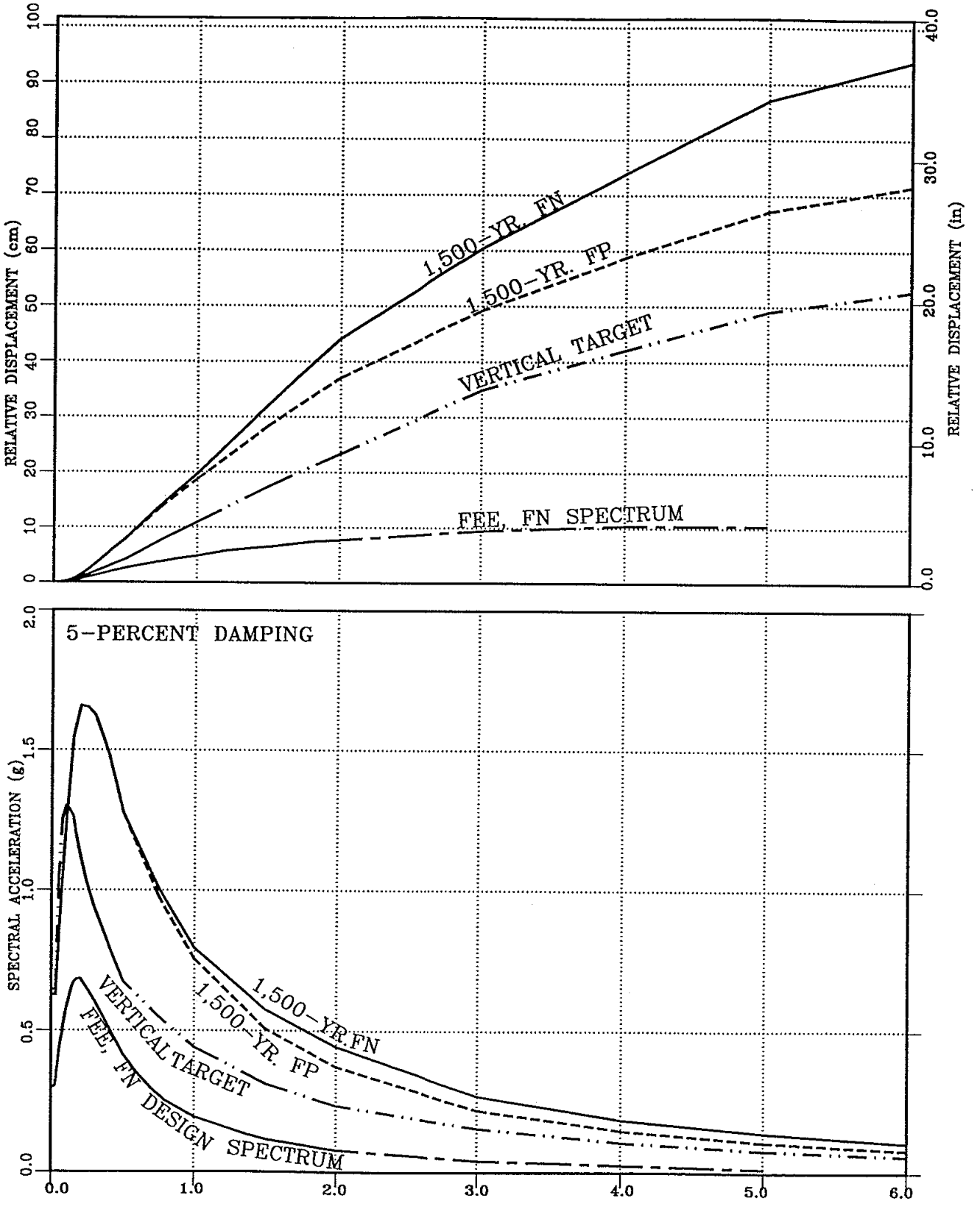

TARGET ROCK OUTCROP SPECTRA FOR SEE

SFOBB East Span Seismic Safety Project

PLATE 2-11

SECTION 3.0
REFERENCE ROCK MOTIONS

3.0 REFERENCE ROCK MOTIONS

The Ground Motion Ad Hoc Committee evaluated several key issues related to development of reference rock time histories for use in design. These key issues included:

- Number of time histories to be used for design analyses,
- Selection of records for use as initial motions for spectra matching,
- Appropriate approach to develop spectrum-compatible reference rock motions.

The Ad Hoc Committee recommended that the structural design be checked against 6 sets of multiple-support ground motions: three sets for San Andreas scenarios and three sets for Hayward Scenario. The Ad Hoc Committee also recommended that the reference rock motions be spectrum compatible. There was also a strong preference that the initial time histories be based on empirical recordings rather than synthetic recording when appropriate empirical time histories are available. The implementation of these recommendations is described below.

3.1 SELECTION OF INITIAL ROCK MOTIONS FOR SUBSEQUENT MATCHING

Based on the deaggregated hazard, the seismic hazard at the bridge is dominated by a magnitude 7.8 event at 18-21 km distance on the San Andreas fault and a magnitude 7.0 event at 9-12 km distance on the Hayward fault. Therefore, the initial time histories should be for large magnitude earthquakes at short distances.

The available empirical ground motions for events with magnitude greater than 6.5 and recorded at distances of less than 30 km are listed in Table 3-1. Both rock and soil site time histories are considered (for a wider selection) because the spectral matching will correct for frequency content differences between soil and rock.

First, the horizontal components of the startup motions are rotated to their principal major and minor directions to minimize the cross-correlation between the two orthogonal components. After rotating the motions to their principal directions, the major principal direction motion (generally the direction of maximum spectral response for long period motions) is used for the fault normal component and the minor direction motion is used for the fault parallel component. Each record was then classified based on the characteristics of the fault normal displacement time history. They were subdivided into three sets: one-sided pulses, two-sided pulses, and multiple cycle pulses.

Near-fault time histories with forward directivity (e.g. rupture heading toward the site) have a characteristic of large velocity and displacement pulses. Near-fault recordings exhibiting forward directivity effects were selected because the deaggregation of the long period hazard showed that at a 1500 year return period, the long period hazard is dominated by forward rupture.

Table 3-1 Candidate Time Histories for Initial Rock Motions

Name	Date	STATION ID	Station	FN Comp	FP Comp	M	Distance (km)	Soil/Rock
One-Sided								
Imperial Valley	5/19/40	ELC	El Centro Array #9	255	345	7.0	8.3	Soil
Nahanni	12/23/85	S1	Site 1	310	040	6.8	6.0	Rock
Loma Prieta	10/18/89	COR	Corralitos	055	145	6.9	5.1	Rock
		GOF	Gilroy - Historic Bldg.	260	170	6.9	12.7	Soil
		G03	Gilroy Array #3	105	015	6.9	14.4	Soil
Cape Mendocino	4/25/92	CPM	Cape Mendocino	005	095	7.1	8.5	Rock
Landers	6/28/92	LUC	Lucerne	275	360	7.3	1.1	Rock
Northridge	1/17/94	ARL	Arleta, Nordhoff Fire Stn.	055	145	6.7	9.2	Soil
		LOS	Canyon Country, W. Lost	075	345	6.7	13.0	Soil
		WPI	W. Pico Canyon Rd.	051	321	6.7	7.1	Soil
		SCE	Sylmar, Converter Stn. (East)	092	182	6.7	6.2	Soil
		SCS	Sylmar, Converter Stn.	333	063	6.7	6.1	Soil
Two-Sided								
Tabas	9/16/78	TAB	Tabas	Long + 45	Trans + 45	7.4	3.0	Rock
Loma Prieta	10/18/89	GIL	Gilroy - Gavilan College	097	007	6.9	11.6	Rock
		G01	Gilroy Array #1	045	135	6.9	11.2	Rock
		STG	Saratoga - Aloha Ave	070	160	6.9	13.0	Soil
Erzinkan	3/13/92	ERZ	Erzinkan	NS + 45	EW + 45	6.7	2.0	Soil
Cape Mendocino	4/25/92	PET	Petrolia	100	010	7.1	9.5	Soil
Northridge	1/17/94	JEN	Jensen Filter Plant	012	102	6.7	6.2	Soil
		NWH	Newhall, Fire Station	160	070- FP	6.7	7.1	Soil
		PUL	Pacoima Dam, Upper Left	199	109	6.7	8.0	Rock

TABLE 3-1 Contd.

Multi-Pulse								
Gazli	5/17/76	GAZ	Gazli	035	125	6.8	3.0	Rock
Superstition Hills	11/24/86	ICC	El Centro, Imperial County	045	135	6.7	13.9	Soil
		WAM	Westmoreland Fire Station	150	240	6.7	13.3	Soil
Loma Prieta	10/18/89	BRAN	U. C. Santa Cruz Station	175	085	6.9	10.3	Rock
		CAP	Capitola	160	070	6.9	14.5	Soil
		G02	Gilroy Array #2	055	145	6.9	12.7	Soil
		LGPC	Los Gatos, Presentation	010	100	6.9	6.1	Rock
Landers	6/28/92	JOS	Joshua Tree	095	005	7.3	11.6	Soil
Northridge	1/17/94	BLF	Montebello, Bluff Rd.	301	211	6.7	12.3	Soil
		CLD	North Hollywood, Cold Water	285	195	6.7	14.6	Soil
		PAC	Pacoima Dam, Downstream	215	305	6.7	8.0	Rock
		KAG	Pacoima Dam, Kagel Canyon	090	360	6.7	8.2	Rock
		RRS	Rinaldi Receiving Station	048	298	6.7	7.1	Soil
		SPV	Sepulveda VA	020	290	6.7	8.9	Soil
		KAT	Simi Valley, Katherine Rd.	025	115	6.7	14.6	Soil
		ROS	Sun Valley, Roscoe Blvd.	135	045	6.7	12.3	Soil
		SYL	Sylmar, Olive View Med.	145	055	6.7	6.4	Soil
Kobe	1/16/95	KJM	KJMA	140	050	6.9	0.6	Rock
		KBU	Kobe University	165	075	6.9	0.2	Rock
		AMA	Amagasaki	120	030	6.9	10.2	Soil

For the Hayward scenarios, there are empirical time histories that can be directly used as initial time histories. The following three empirical recordings were selected: the West Pico Canyon records from the 1994 Northridge earthquake, the LGPC records from the 1989 Loma Prieta earthquake, and the Saratoga records from the 1989 Loma Prieta Earthquake. The fault normal displacement time histories for these three initial time histories are shown in Plate 3-1.

For the San Andreas scenarios, there are no empirical time histories that are directly applicable to the magnitude and distance range. To develop initial time histories for these scenarios, two approaches were used: splicing together empirical time histories and numerical simulations. Given the strong preference for empirical data, two of the sets were developed based on splicing together empirical time histories and one set was developed using numerical simulations. Care was taken in splicing the records to avoid introducing discontinuities in the acceleration, velocity, or displacement time histories.

The first set was based on the 1940 Imperial Valley earthquake recorded at El Centro. When rotated to the principal axes, the fault normal displacement has two one-sided pulses separated by 20 seconds. To increase the duration to be appropriate for a magnitude 7.8 earthquake, the recording from the 1979 Imperial Valley earthquake recorded at EC #6 was added to the end. The other empirical set (set 3) was based on the 1992 Landers earthquake recorded at Lucerne. This time history has a single one-sided displacement pulse on the principal axis component. The Lucerne recording has a large high frequency site resonance at about 12 Hz that was filtered out of the record. To increase the duration, the recordings from the Joshua Tree site were appended to the filtered Lucerne recordings.

The numerical simulation (set 2) was adopted from the retrofit study of the East Bay Bridge. This simulation, developed by Woodward-Clyde was for a magnitude 8.0 earthquake on the San Andreas fault at a distance of 18 km. Several alternative simulations were generated. A simulation for the case of forward rupture directivity was selected (Simulation #4). This three component time history was used without modification as the initial recording for the spectral matching.

The fault normal components of these three San Andreas scenario initial displacement time histories are also shown in Plate 3-1. Comparing the six sets, there are significant differences in the character of the directivity pulses.

3.2 SPECTRUM COMPATIBLE REFERENCE ROCK MOTIONS

The time histories were modified to match the target spectrum using the time domain spectral matching procedure described in Appendix C. This procedure is used to preserve the gross non-stationary characteristics of the acceleration, velocity and displacement time histories. The spectral matching is performed independently for each component. The spectral matching is a multi-step process. As an example, Appendix D gives a step-by-step description of the spectral matching process used for one component of one set.

Table 3-2 Peak Ground Motion Values for Six Sets of Reference Rock Motions

Motion	PGA (g)	PGV (cm/sec)	PGD (cm)
Set 1 : San Andreas, Composite El Centro and Imperial Valley			
Fault Normal	0.62	88	84
Fault Parallel	0.58	73	24
Vertical	0.60	36	28
Set 2 : San Andreas, Synthetic Record			
Fault Normal	0.78	109	96
Fault Parallel	0.52	75	34
Vertical	0.58	45	25
Set 3 : San Andreas, Composite Landers			
Fault Normal	0.62	86	45
Fault Parallel	0.60	70	26
Vertical	0.64	50	30
Set 4 : Hayward, West Pico Canyon			
Fault Normal	0.67	98	58
Fault Parallel	0.66	86	35
Vertical	0.71	57	27
Set 5 : Hayward, LGPC			
Fault Normal	0.62	76	40
Fault Parallel	0.63	61	33
Vertical	0.75	42	27
Set 6 : Hayward, Saratoga			
Fault Normal	0.60	100	47
Fault Parallel	0.62	83	37
Vertical	0.72	53	23

Although each of the six sets is spectrum compatible, there is a range of peak velocities and peak displacements for the six sets. These are listed in Table 3-2. The largest peak displacements are associated with the time histories with one-sided directivity pulses. The characteristics of initial start-up motion are presented in Appendix E.

Plates 3-2 to 3-19 present the resulting 6 sets of SEE motions in terms of their displacement, velocity and acceleration time histories and their acceleration and displacement

response spectra. The corresponding rock target spectra have also been included in the Plates for comparison. Plates 3-20 to 3-25 present characteristics of the shaking intensity pattern under rotation. The upper 6 shaking intensity patterns were obtained by rotating the fault normal and fault parallel motion by 10-degree rotations (merely applying directional cosines). Response spectra are then computed for the rotated motion. The resulting spectral amplitude is plotted against the corresponding orientation in a polar coordinate plot. The angle in the polar plot denotes the angle of rotation and the radial distance (distance from the origin) denotes the spectral amplitude after they are normalized by the response in the fault normal direction for the given structural period. Tabulation of the spectral displacement used for normalization has been tabulated along with the target fault normal and fault parallel spectral displacement (from the PSHA rock target spectra). The polar coordinate shaking intensity plots are presented for 6 periods at 1, 1.5, 2, 3, 4 and 5 second of structural response.

3.3 CROSS-CORRELATION AND SHAKING INTENSITY UNDER ROTATION

Other than matching of response spectrum for each of the ground motion components developed for structural designs, checking of cross-correlation of the two horizontal orthogonal directions is also important for ensuring no deficiency in shaking level at any rotated axis. Cross correlation is a comparison of two signals as a function of a time shift between them. It is defined in signal processing as:

$$c_{xy}(\tau) = \lim_{T\to\infty} \frac{1}{T} \int_T x(t)y(t+\tau)dt \qquad (3.1)$$

where x(t) and y(t) are two signals, and τ is a time shift. For comparison of earthquake records, a zero time shift ($\tau = 0$) is used. It is computed as multiplying two earthquake records together at each instant in time and adding up all the products. If the two records are dissimilar, then some of the products would be positive and some would be negative. There would be a tendency for the products to cancel, so the final sum would be small. If the two signals are identical, every product is positive and the resulting sum is large. In other words, if two earthquake records are unrelated, the cross correlation value is small while if they are related, the cross correlation value is large. It is also possible to normalize the cross correlation so that the absolute value of the coefficient would range from 0 to 1. In this case, the cross correlation coefficient of 0 means totally unrelated; that of 1 means the two records are totally related. A discrete form of cross correlation, after normalization with auto correlation, can be expressed as

$$c_{xy}(0) = \frac{\frac{1}{N}\sum_{n=1}^{N} x(n\Delta t)y(n\Delta t)}{\sqrt{\frac{1}{N}\sum_{n=1}^{N} x^2(n\Delta t)}\sqrt{\frac{1}{N}\sum_{n=1}^{N} y^2(n\Delta t)}} \qquad (3.2)$$

where $c_{xy}(0)$ is the cross correlation coefficient without time shift, Δt is time step of digital data and $(N\Delta t)$ is record length.

The cross-correlation computation of the two orthogonal horizontal reference rock motions is shown in the lower part of the Plate in Plates 3-20 to 3-25. Computations have been presented for all the acceleration, velocity and displacement time histories. In addition to solutions at the fault normal/fault parallel axes, computations have been conducted for motions rotated in 360-degree angles at every 10-degree increment. Again, the computed cross-correlation coefficient values were plotted against their corresponding angular rotation in polar coordinate plots.

From the presented data, it can be observed that the resultant 6 sets of reference rock motion have relatively low cross-correlation coefficients within limits specified in the guidelines set by the Ad Hoc Committee. The Committee recommended cross coefficients to be limited to 0.1, 0.2 and 0.3 for acceleration, velocity and displacement records, respectively. A copy of the Ad Hoc Committee guidelines is included in Appendix G.

However, it appeared that a low cross-correlation coefficient is merely an indicator that the two orthogonal motions are not closely related. They might not be sufficient as the indicator to ensure adequate shaking level at any rotated axis needed for design applications. It seems appropriate to check the feature of the motion by the shaking intensity pattern at the upper portion of the presented Plates to ensure that the resultant motion is sufficiently close to the intended target not only in the coordinate axis used for matching target spectrum, but also in other rotated directions. Such checks are needed to give some degree of control so that the resultant motion when used in response spectrum approach (involving some superposition principals such as the square roots of sum of squares, SRSS) can be compared with time history solutions in a three-dimensional response analysis.

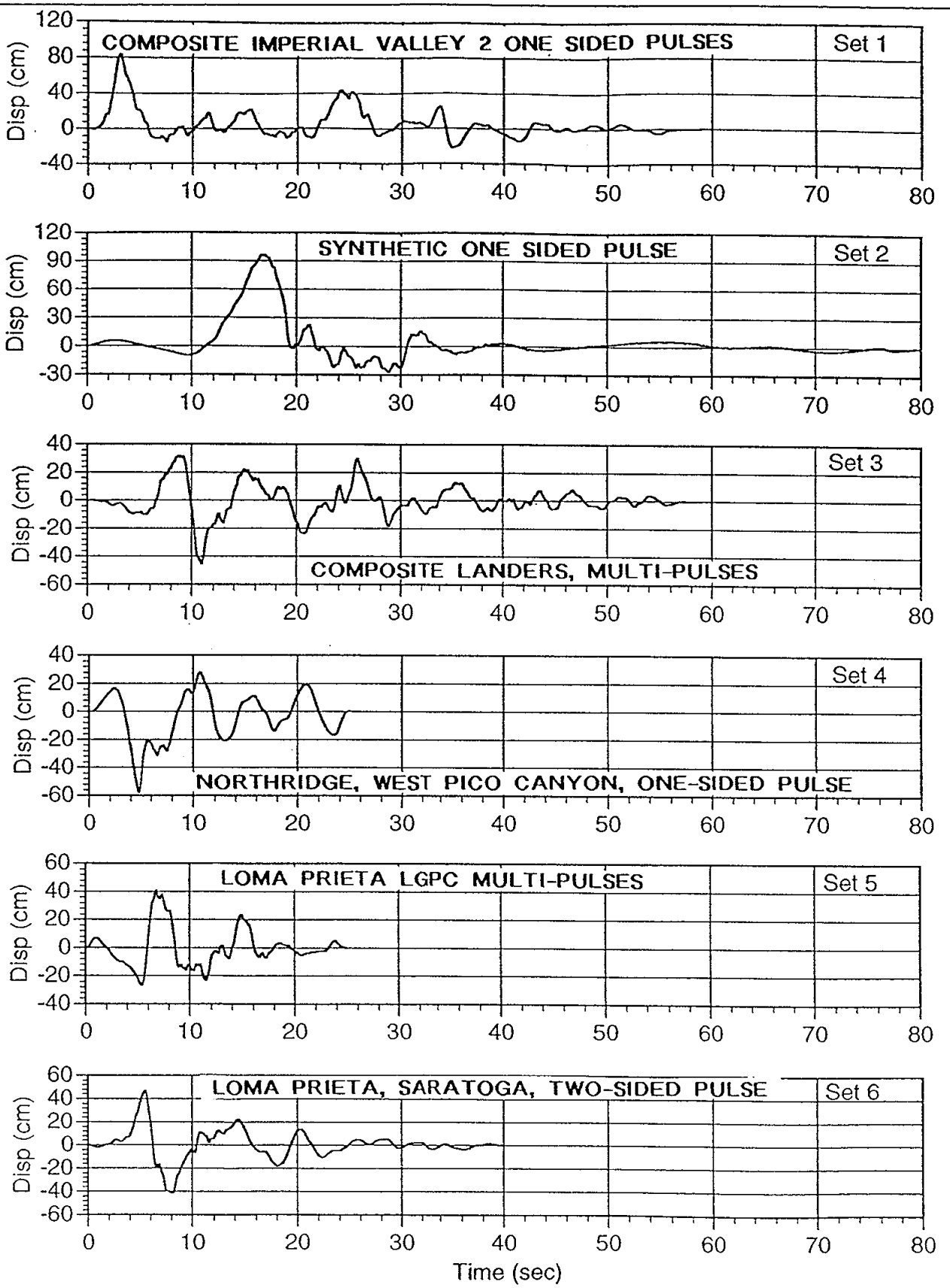

STARTUP TIME HISTORIES FOR SPECTRAL MATCHING : FN COMPONENT

SFOBB East Span Seismic Safety Project

PLATE 3-1

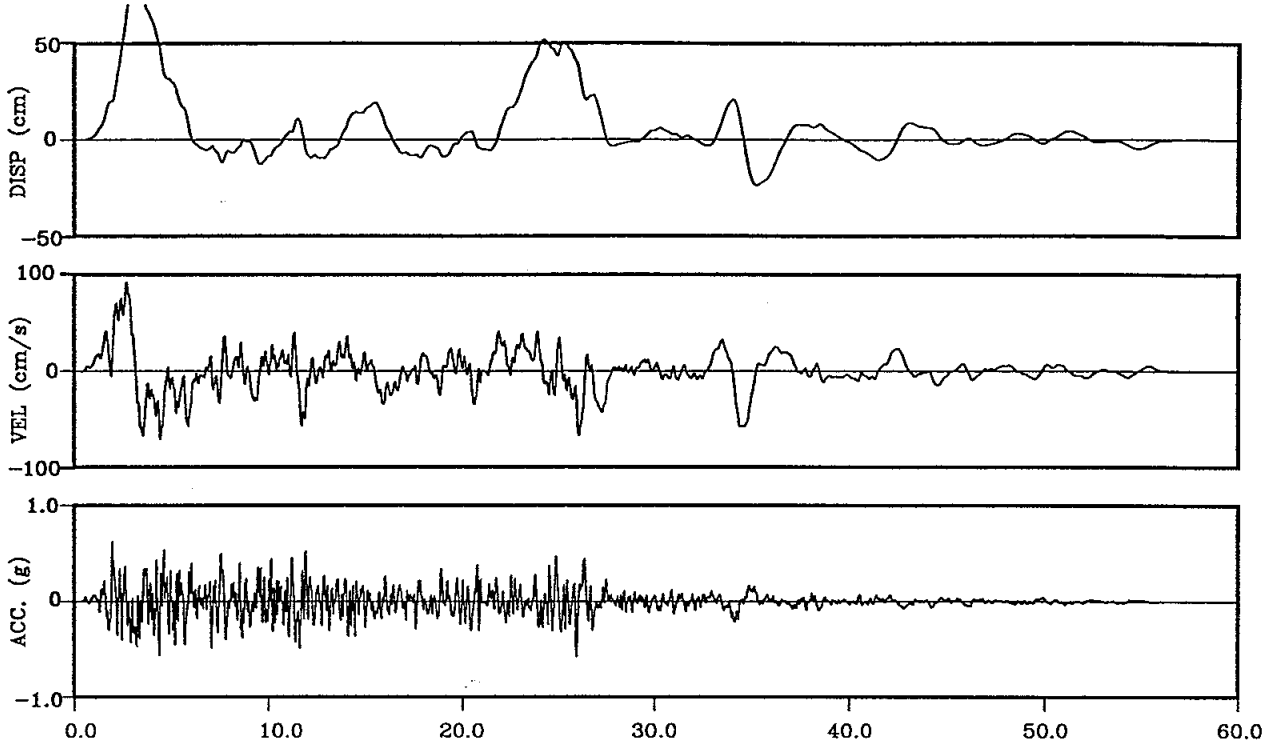

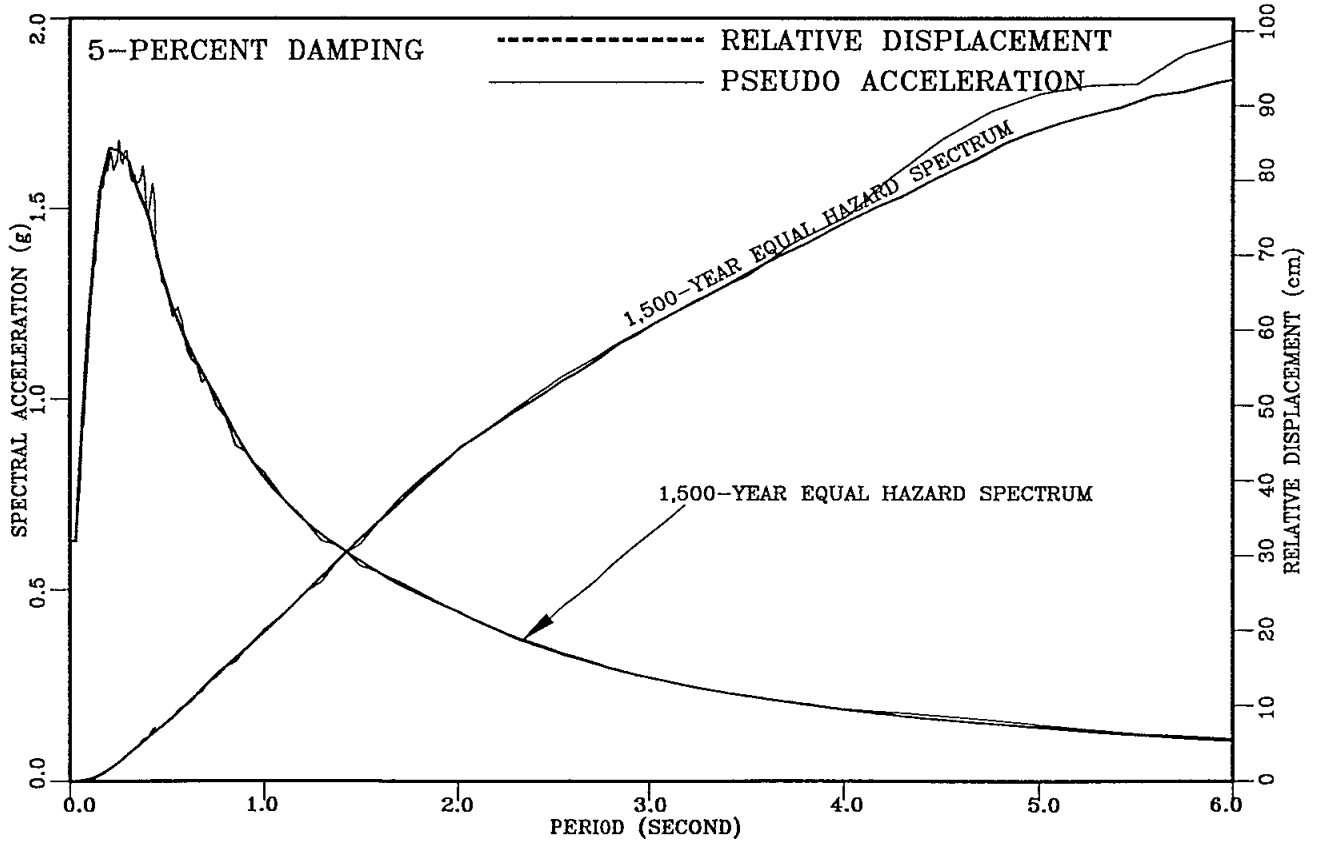

REFERENCE ROCK OUTCROP MOTION, SET1, FN COMPONENT, SAN ANDREAS EVENT

SFOBB East Span Seismic Safety Project

PLATE 3-2

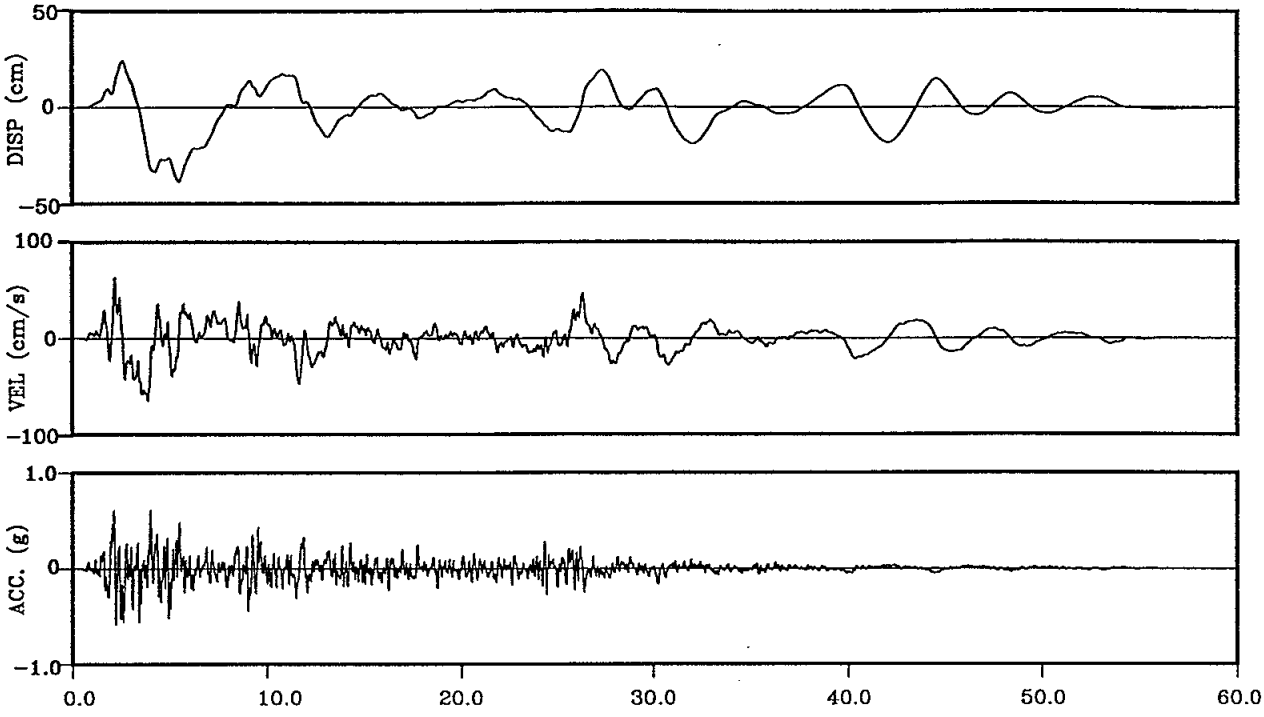

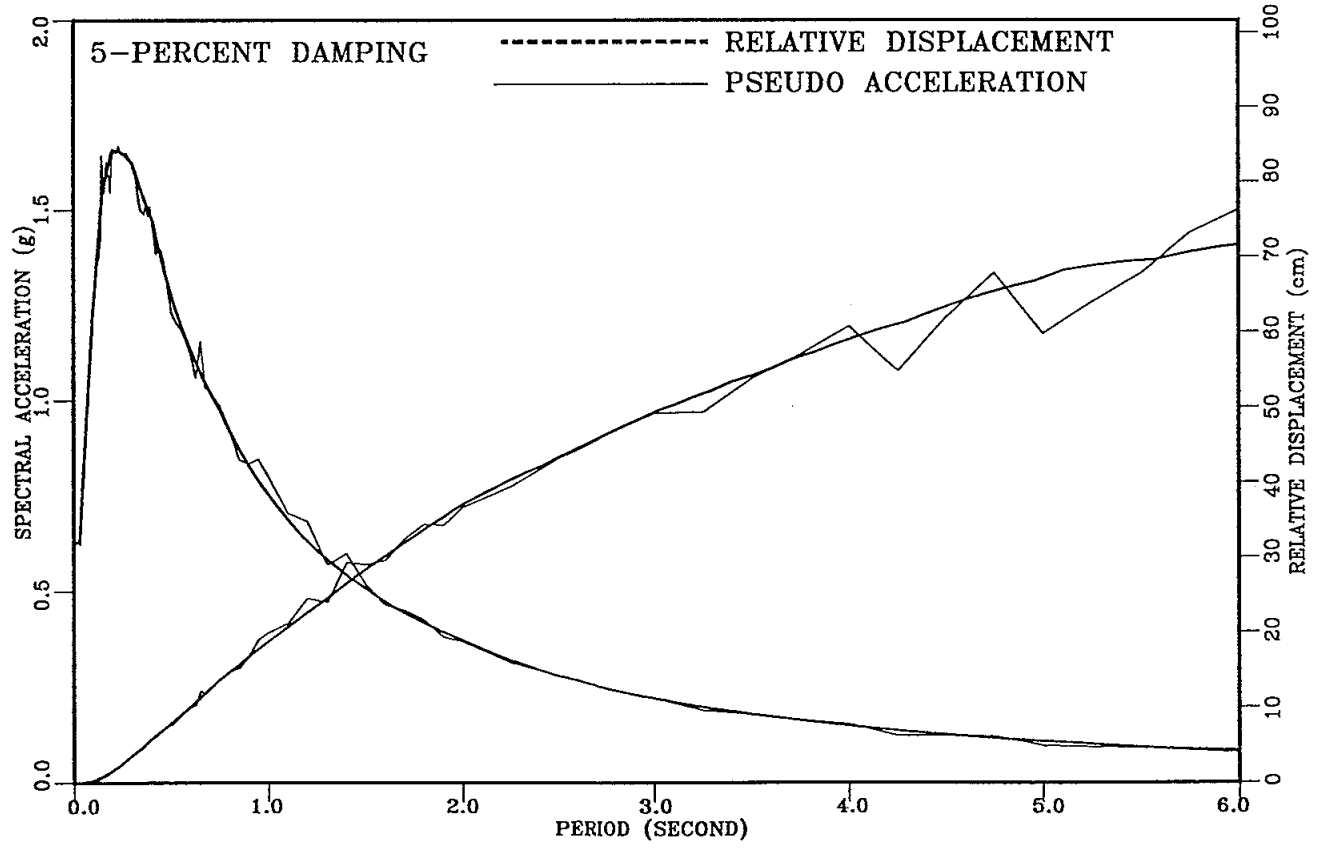

REFERENCE ROCK OUTCROP MOTION, SET1, FP COMPONENT, SAN ANDREAS EVENT

SFOBB East Span Seismic Safety Project

PLATE 3-3

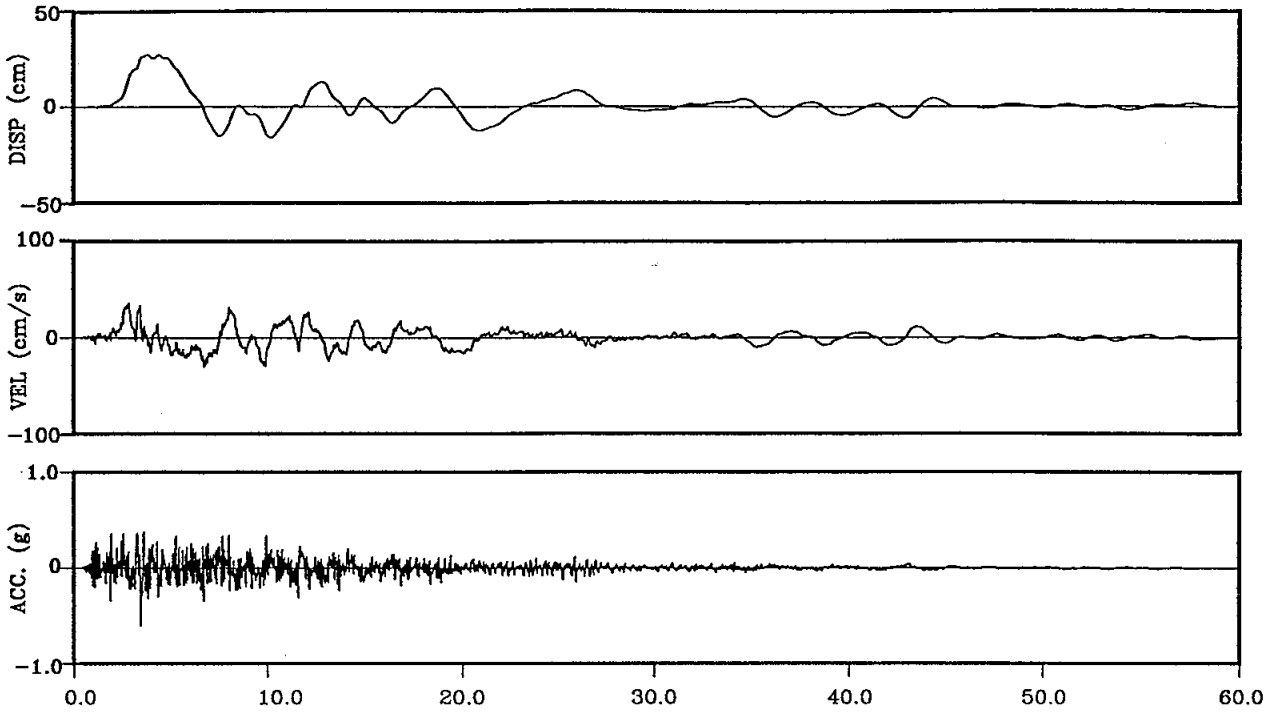

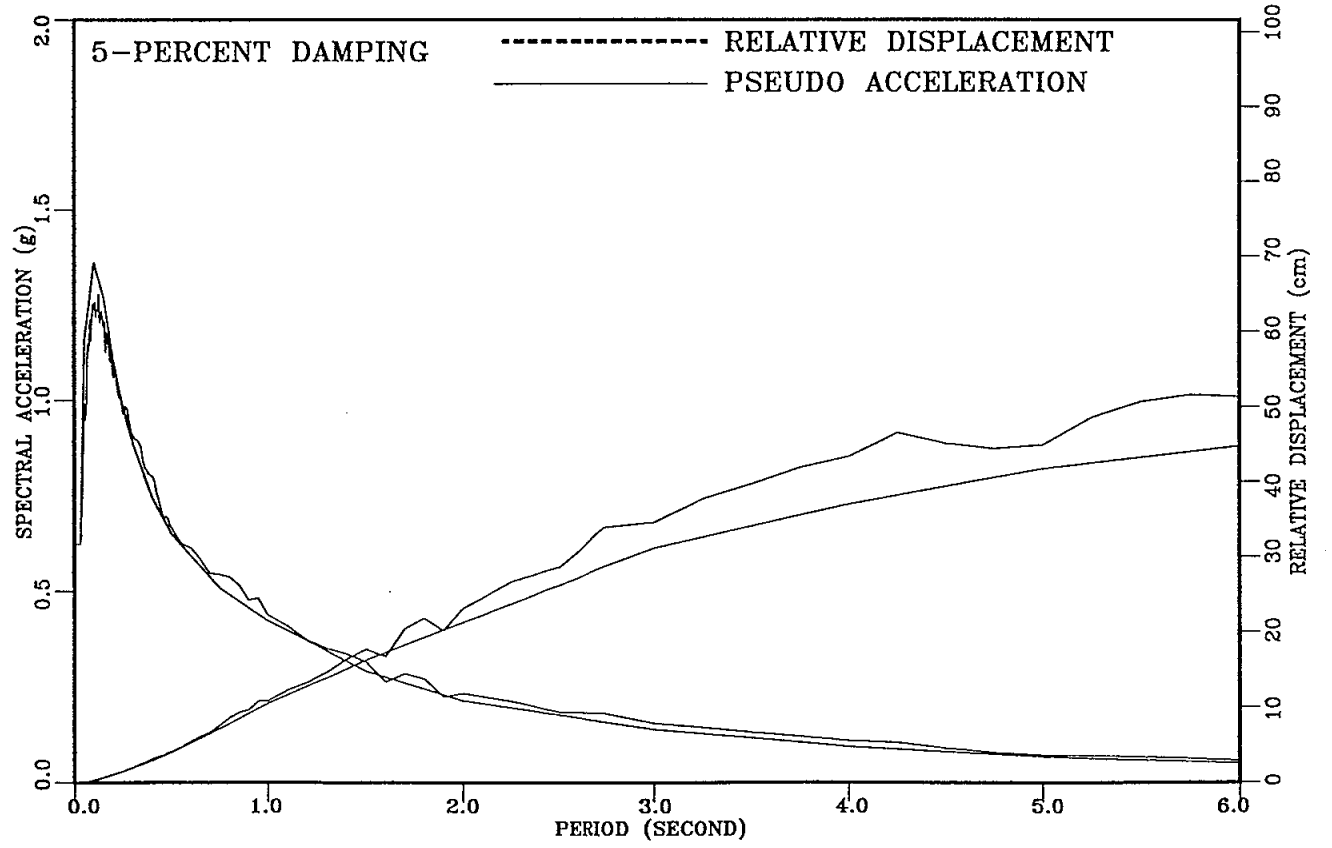

REFERENCE ROCK OUTCROP MOTION, SET1, VERTICAL COMPONENT, SAN ANDREAS EVENT

SFOBB East Span Seismic Safety Project

PLATE 3-4

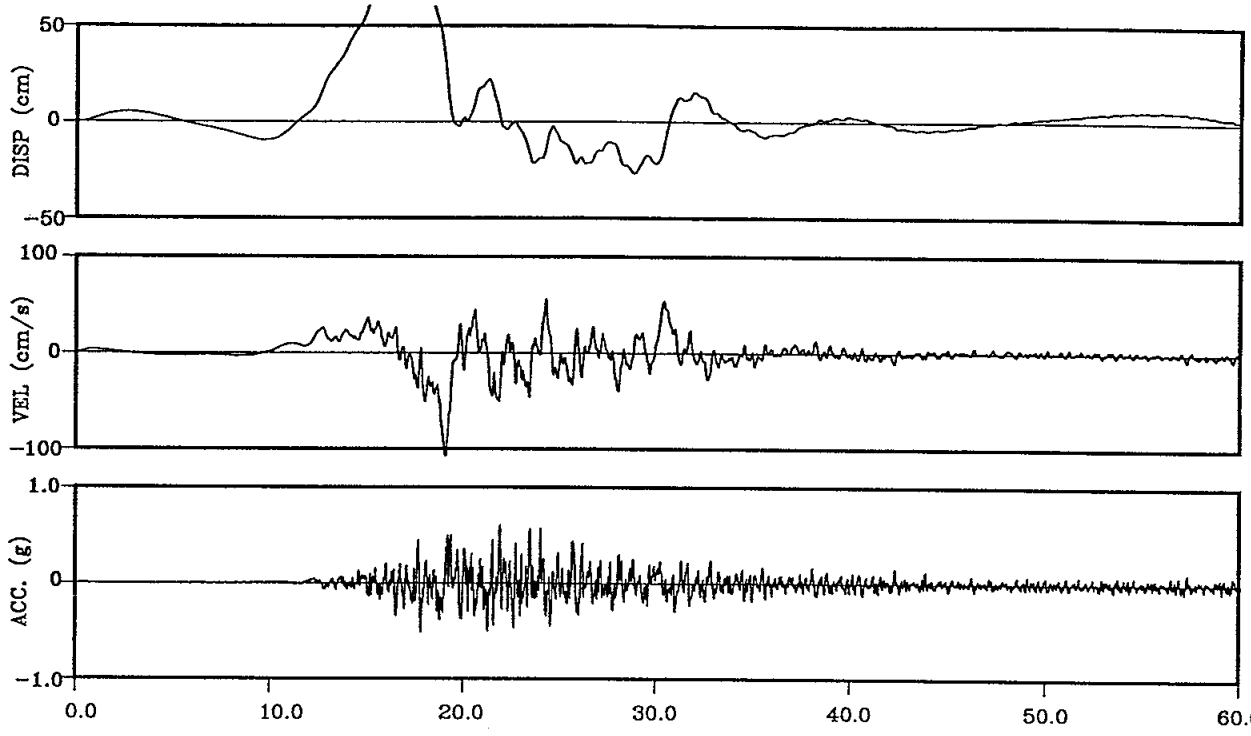

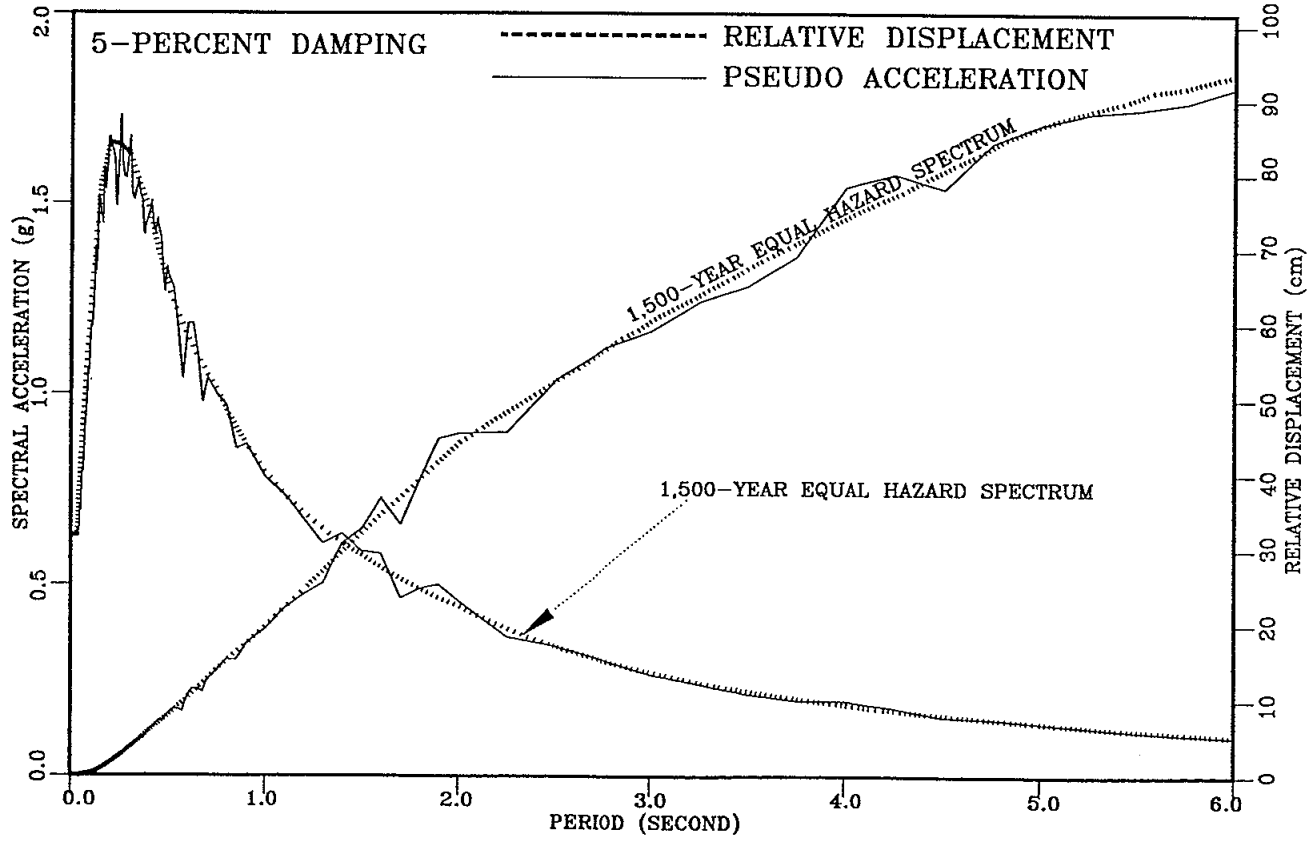

REFERENCE ROCK OUTCROP MOTION, SET2, FN COMPONENT, SAN ANDREAS EVENT, SYNTHETIC

SFOBB East Span Seismic Safety Project

PLATE 3-5

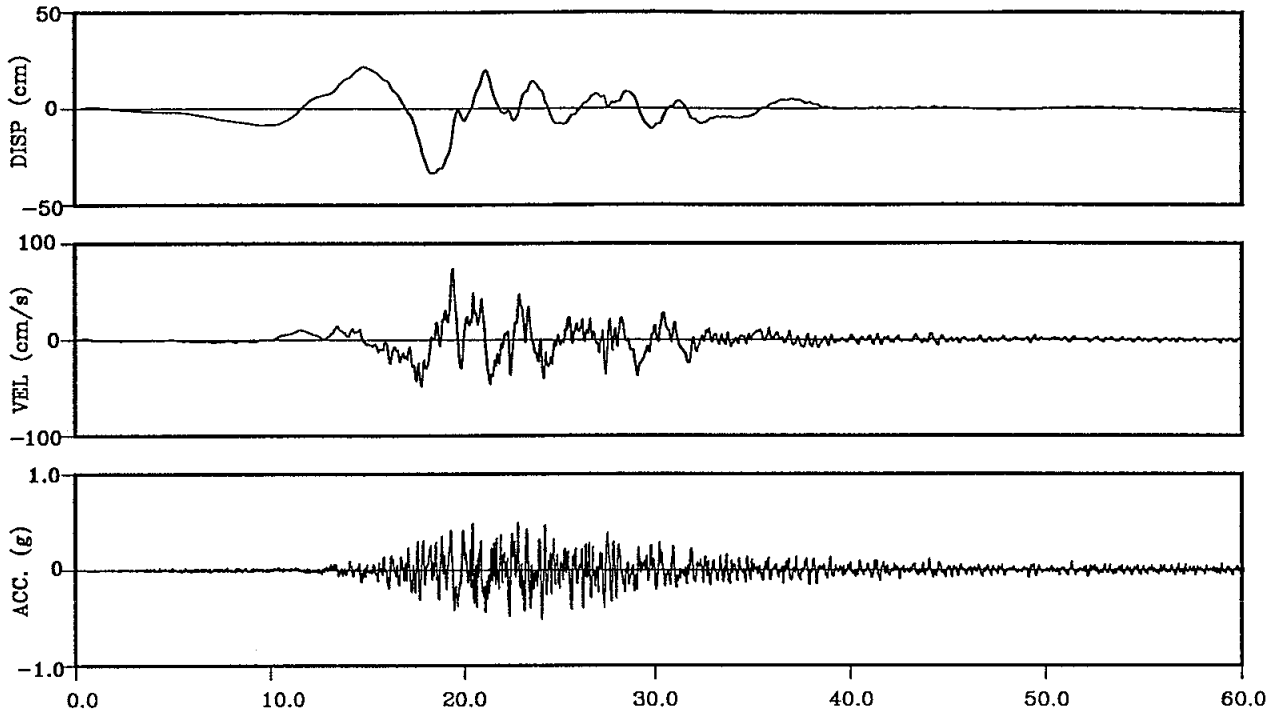

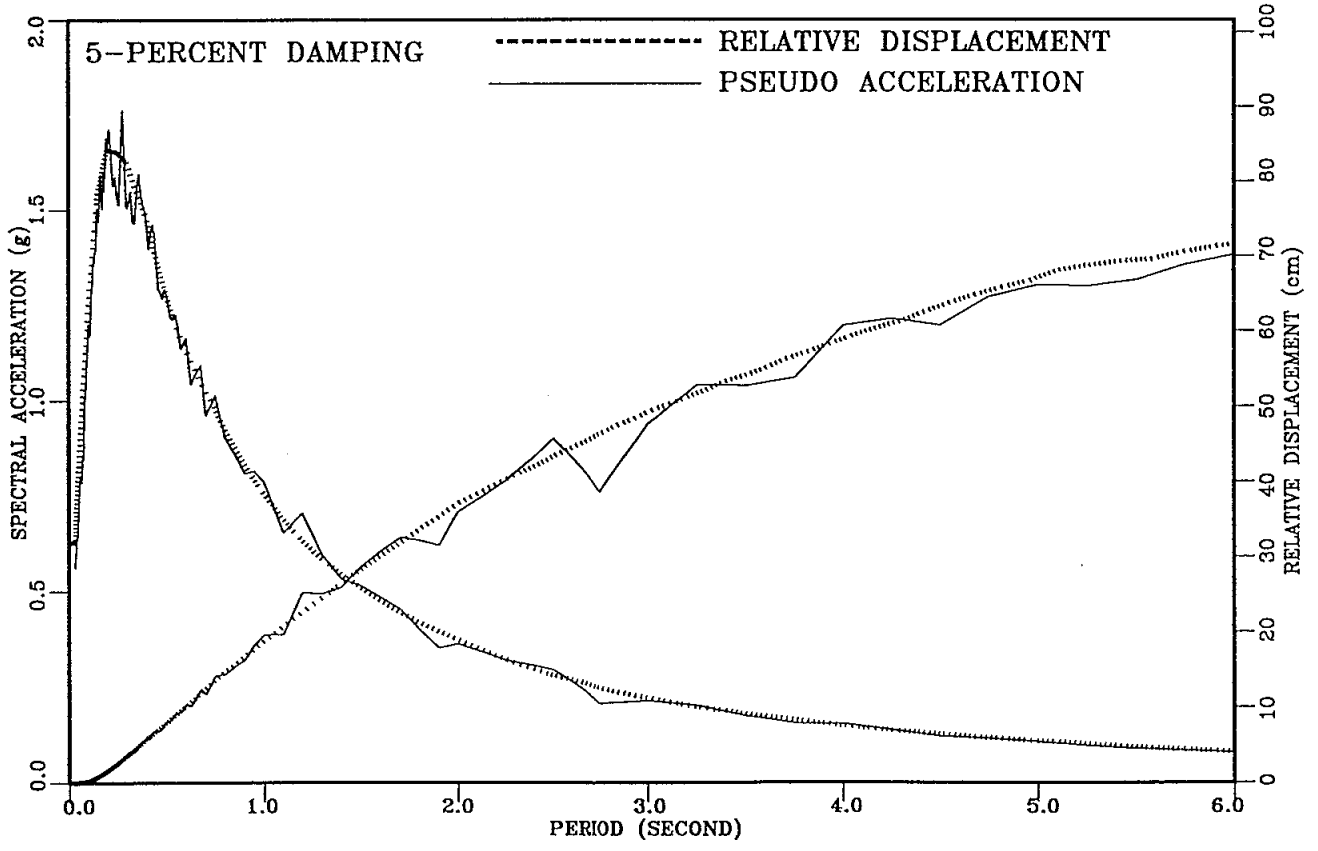

REFERENCE ROCK OUTCROP MOTION, SET2, FP COMPONENT, SAN ANDREAS EVENT, SYNTHETIC

SFOBB East Span Seismic Safety Project

PLATE 3-6

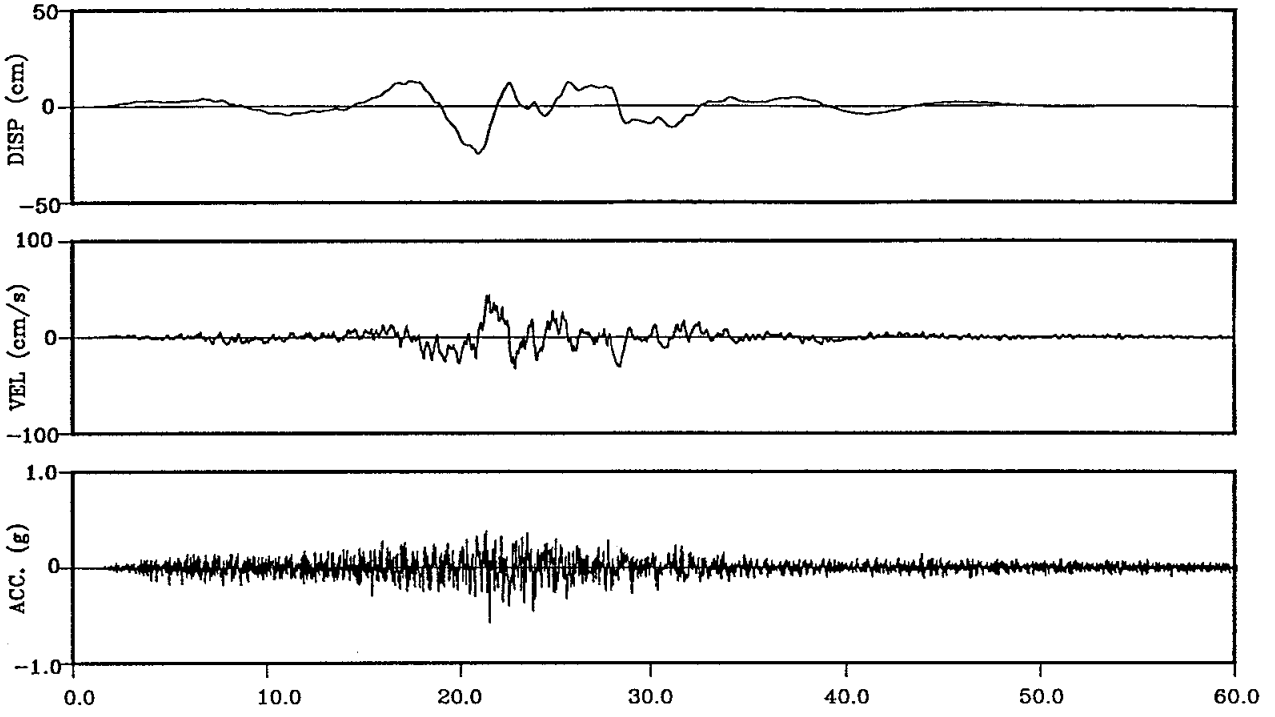

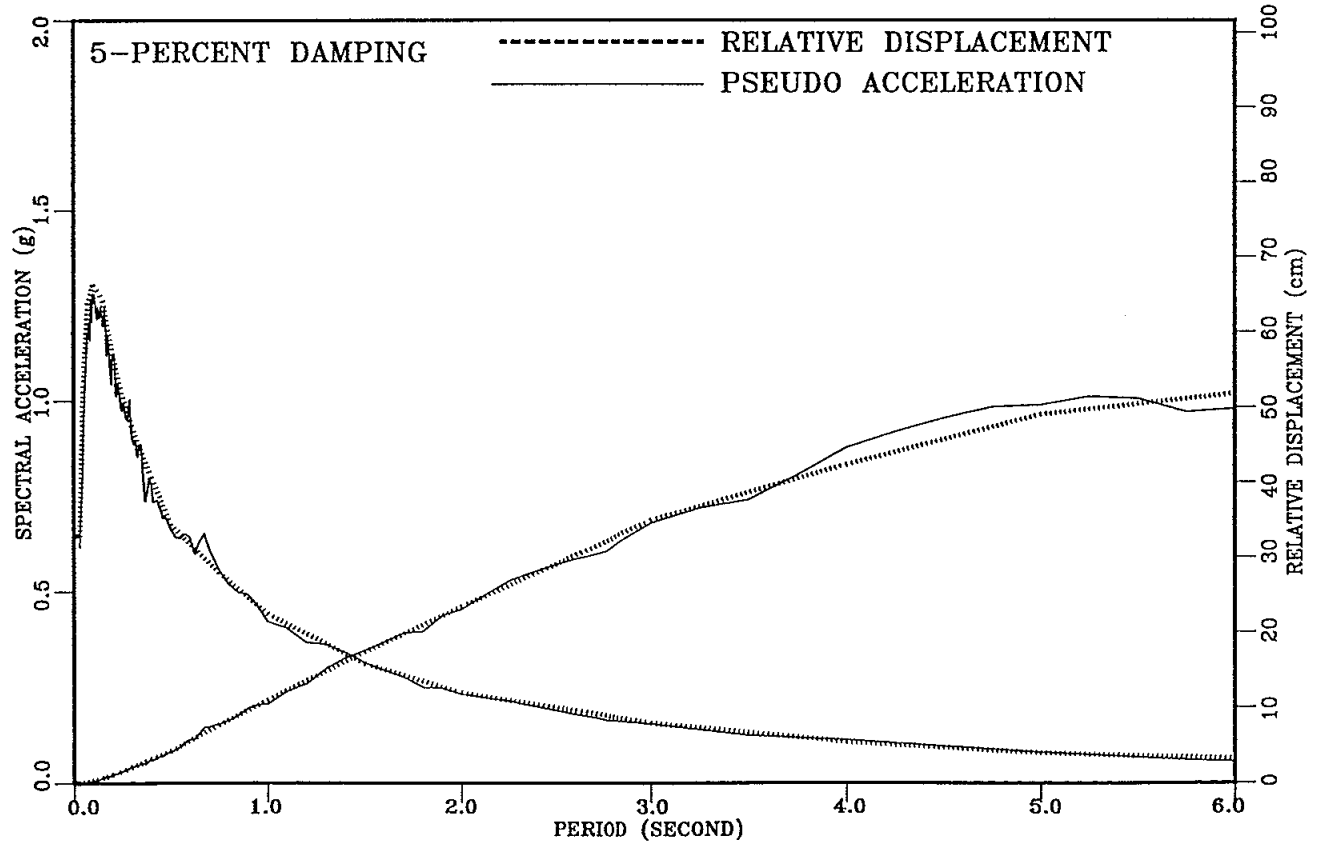

Reference Rock Outcrop Motion, Set2, Vert. Component, San Andreas Event, Synthetic
SFOBB East Span Seismic Safety Project

PLATE 3-7

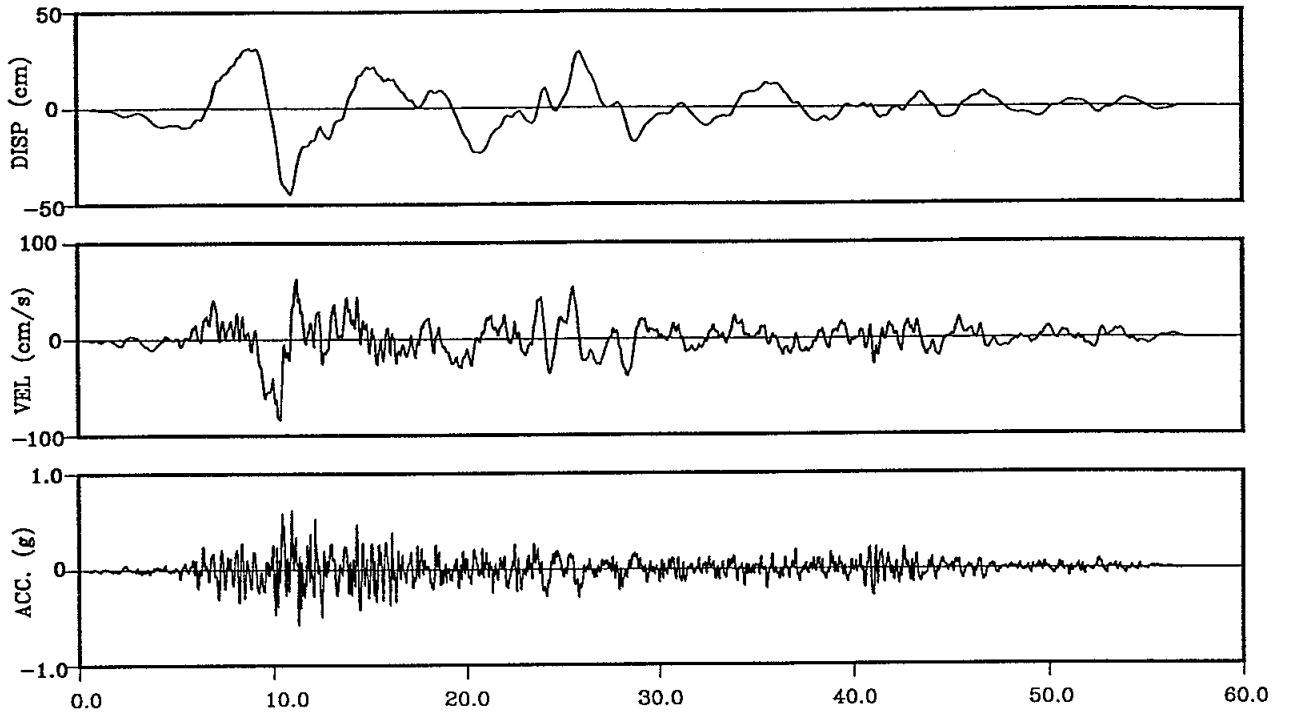

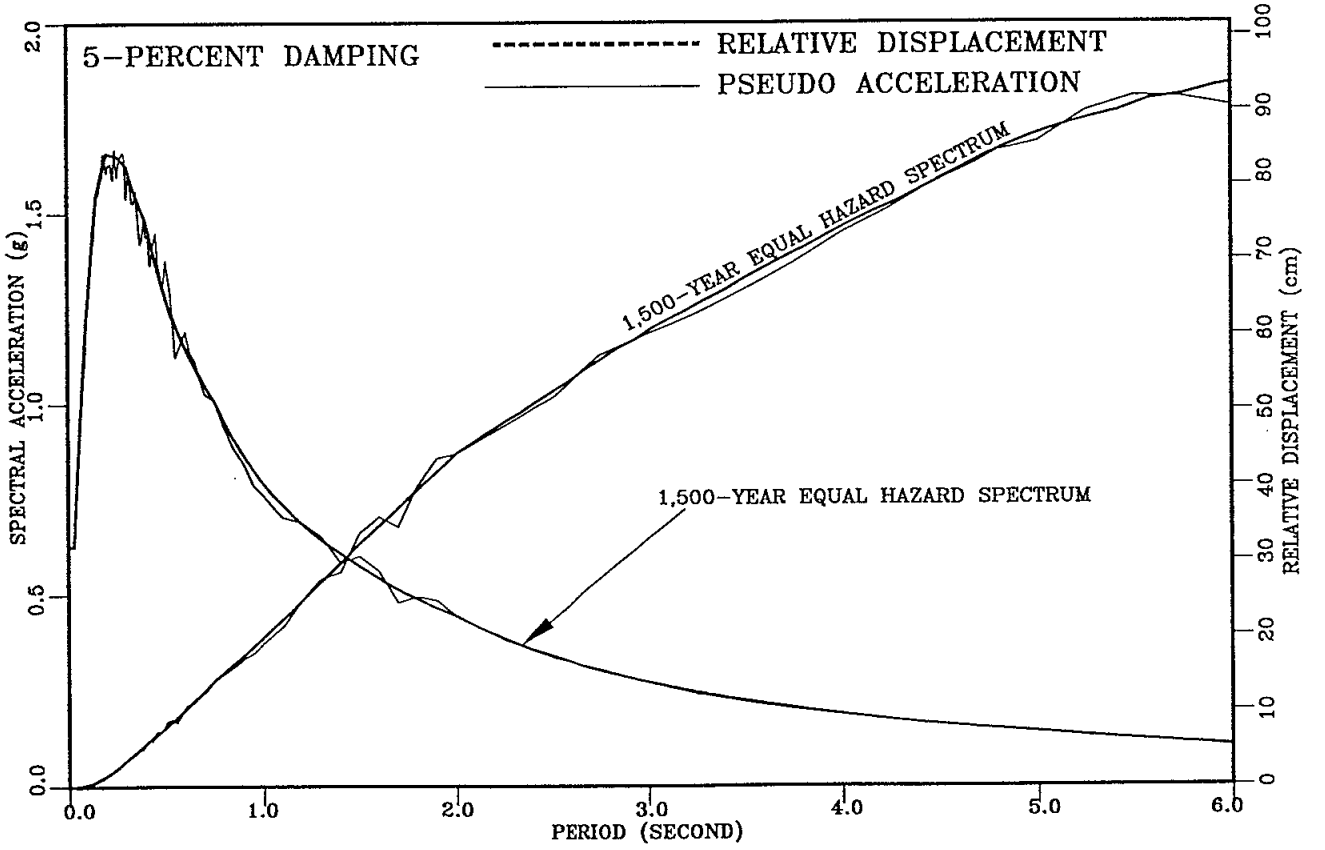

REFERENCE ROCK OUTCROP MOTION, SET3, FN COMPONENT, SAN ANDREAS EVENT, COMPOSITE LANDERS

SFOBB East Span Seismic Safety Project

PLATE 3-8

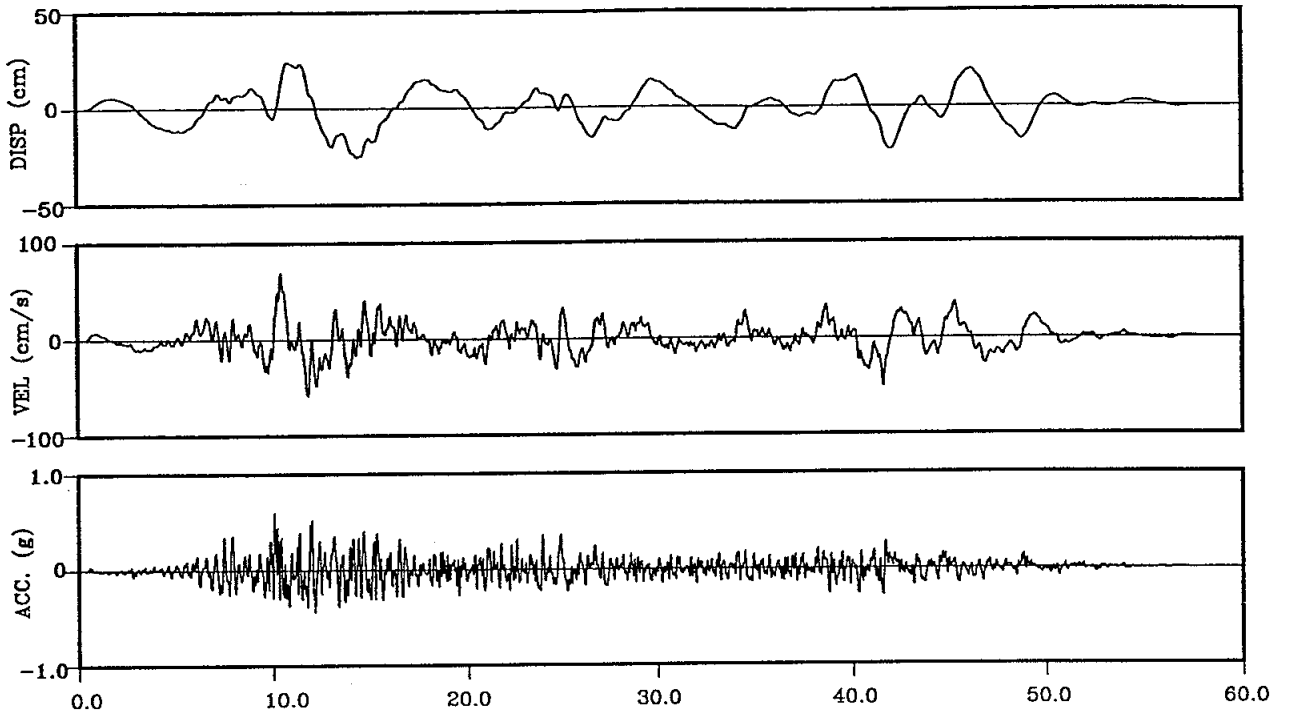

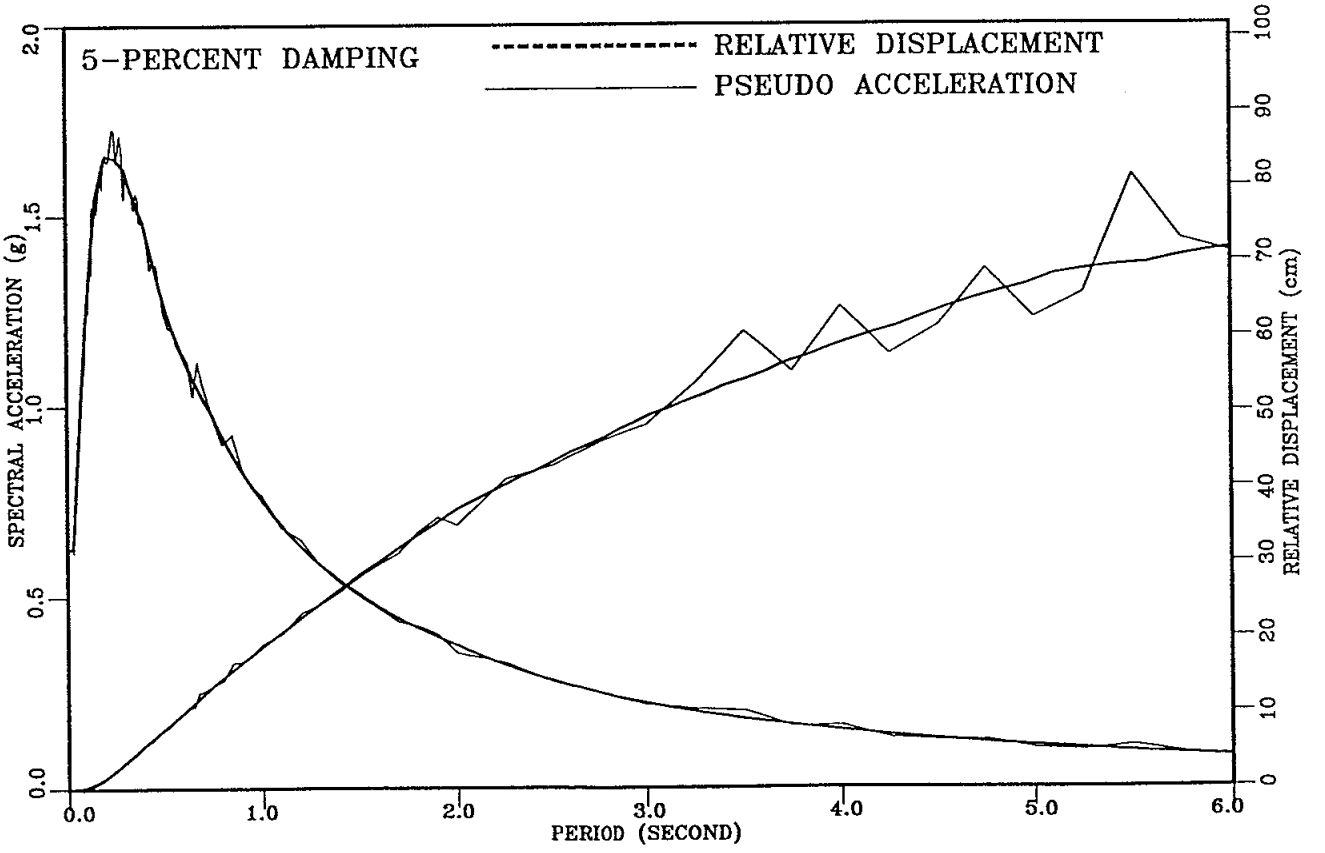

REFERENCE ROCK OUTCROP MOTION, SET3, FP COMPONENT, SAN ANDREAS EVENT, COMPOSITE LANDERS

SFOBB East Span Seismic Safety Project

PLATE 3-9

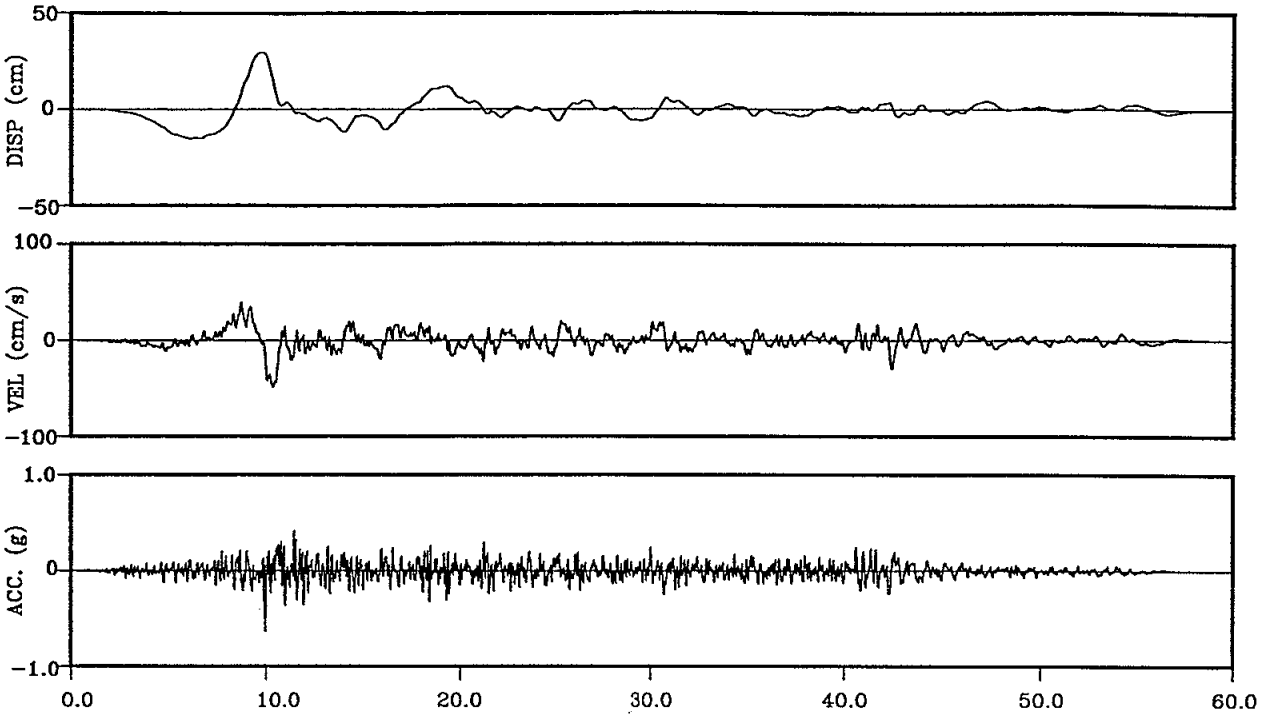

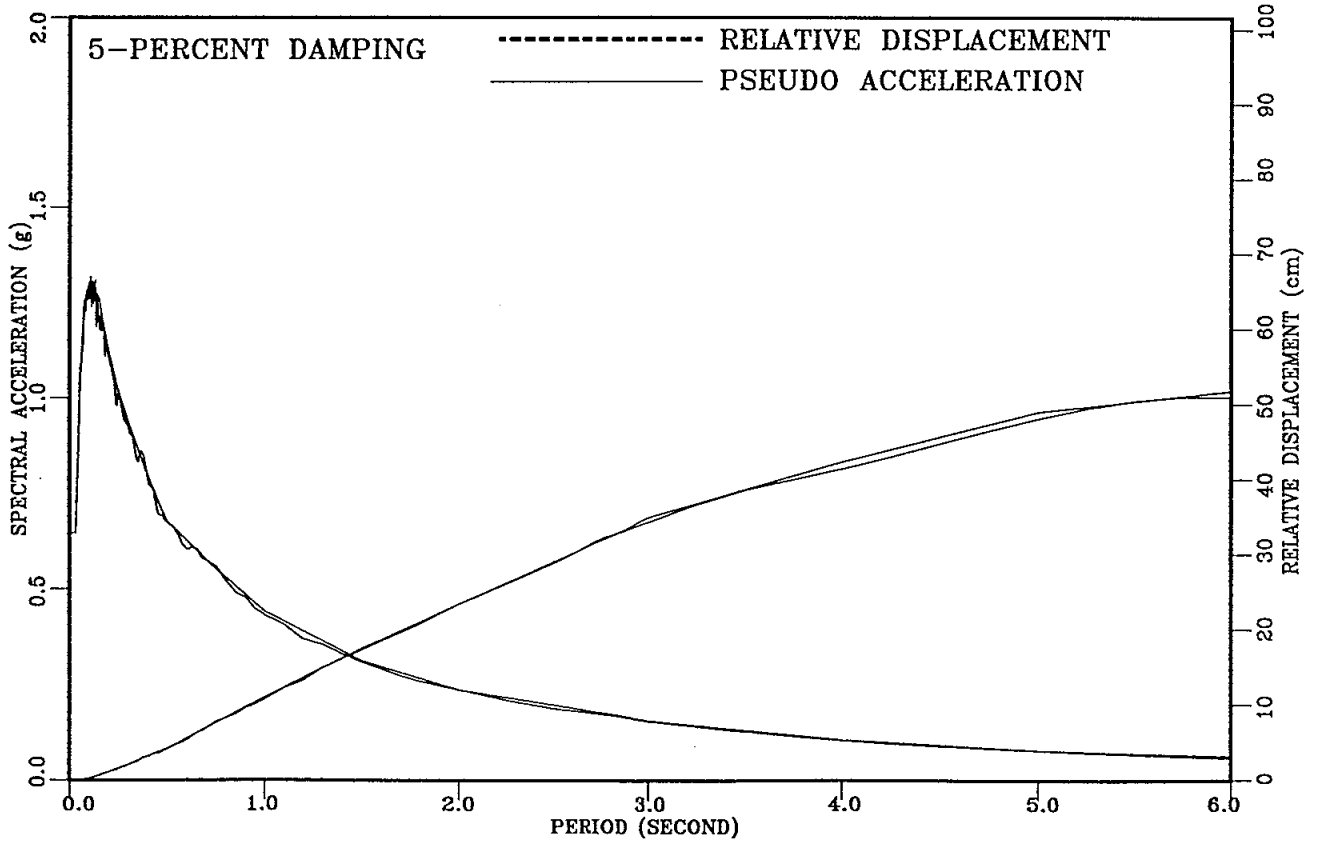

REFERENCE ROCK OUTCROP MOTION, SET 3, VERT. COMPONENT, SAN ANDREAS EVENT, COMPOSITE LANDERS

SFOBB East Span Seismic Safety Project

PLATE 3-10

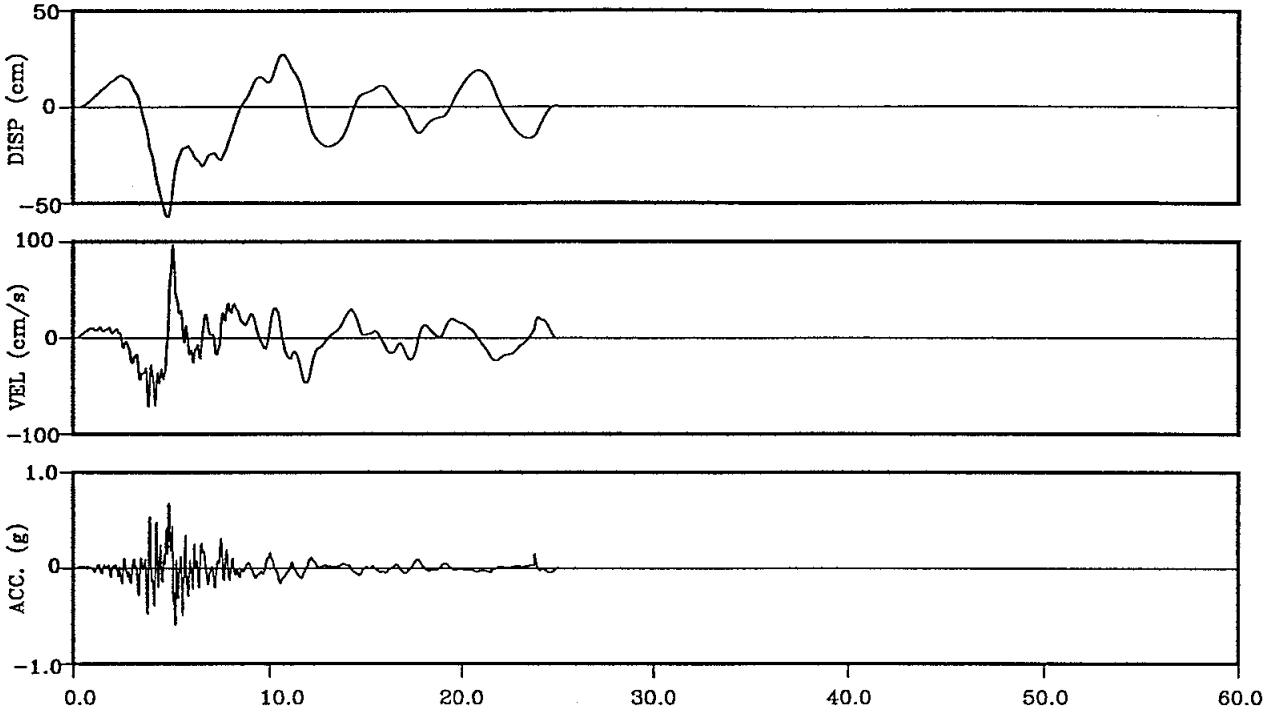

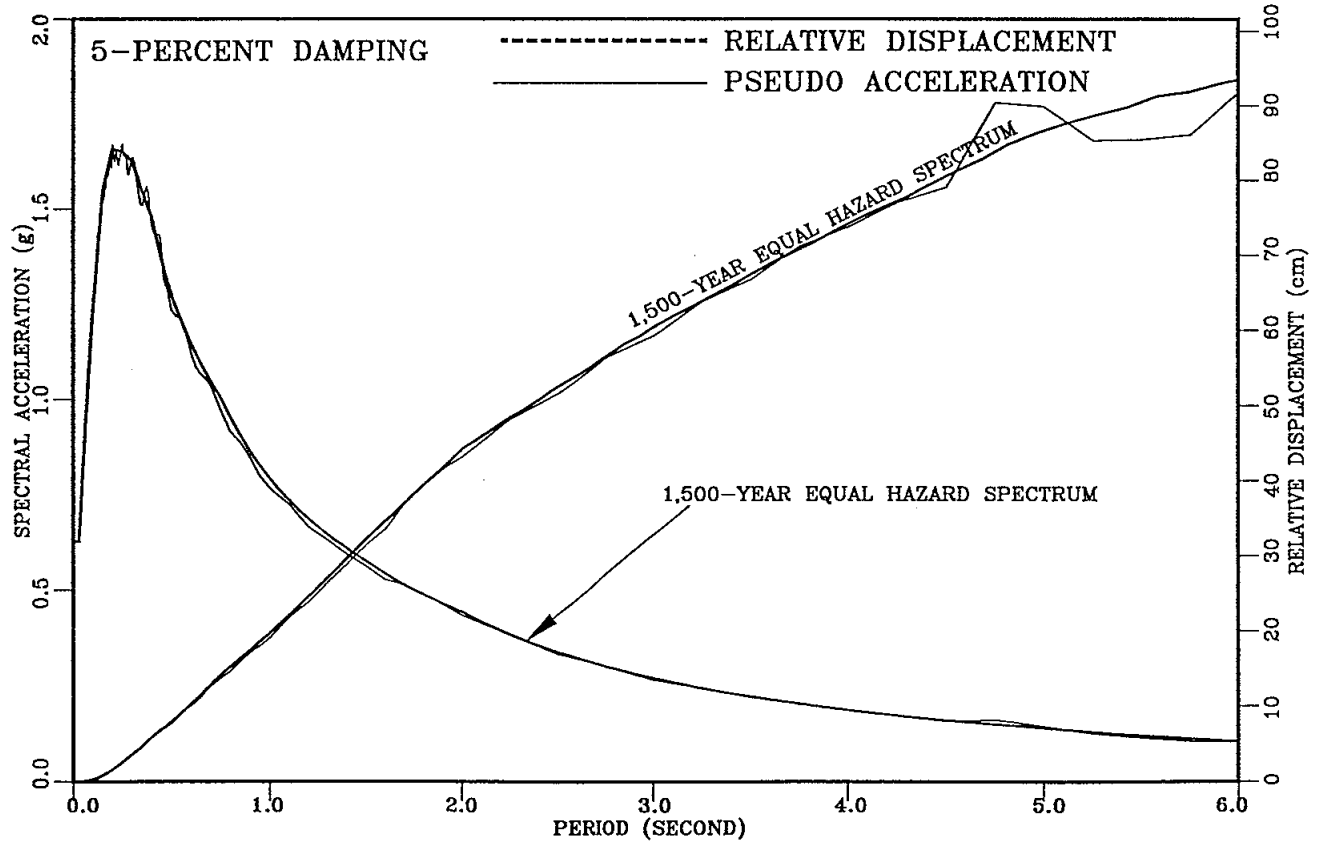

REFERENCE ROCK OUTCROP MOTION, SET4, FN COMPONENT, HAYWARD EVENT, WEST PICO CANYON

SFOBB East Span Seismic Safety Project

PLATE 3-11

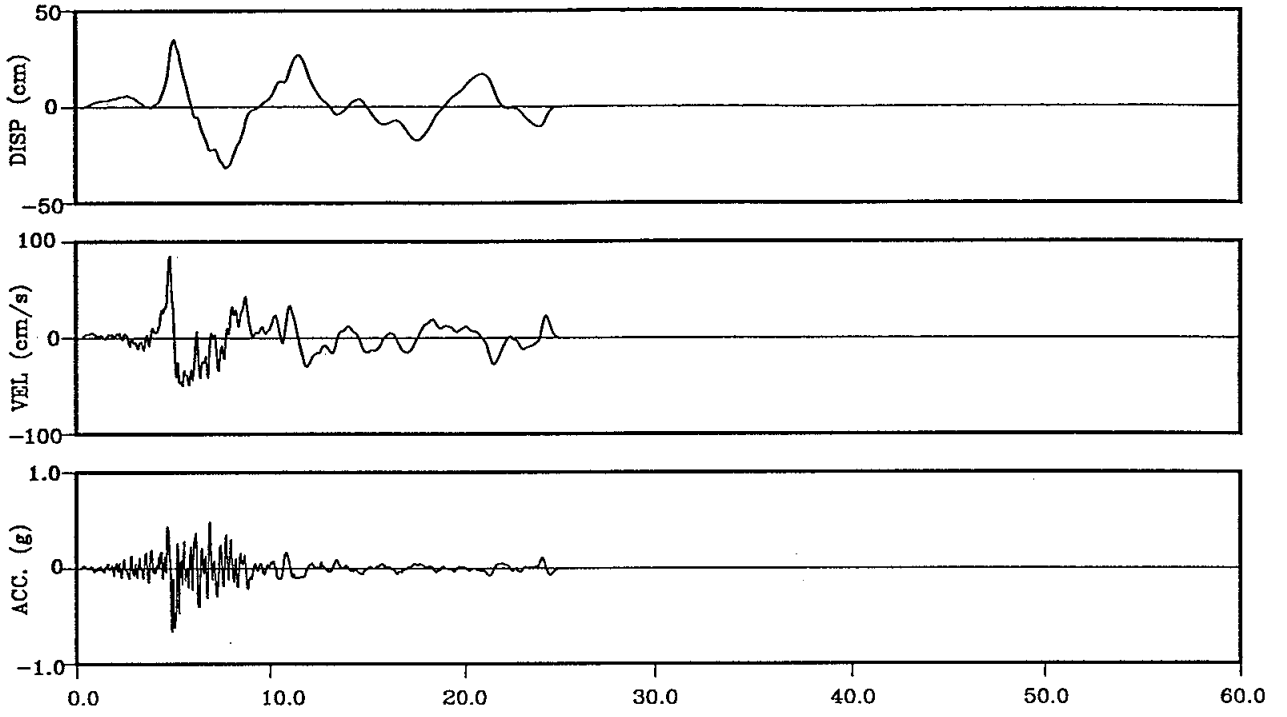

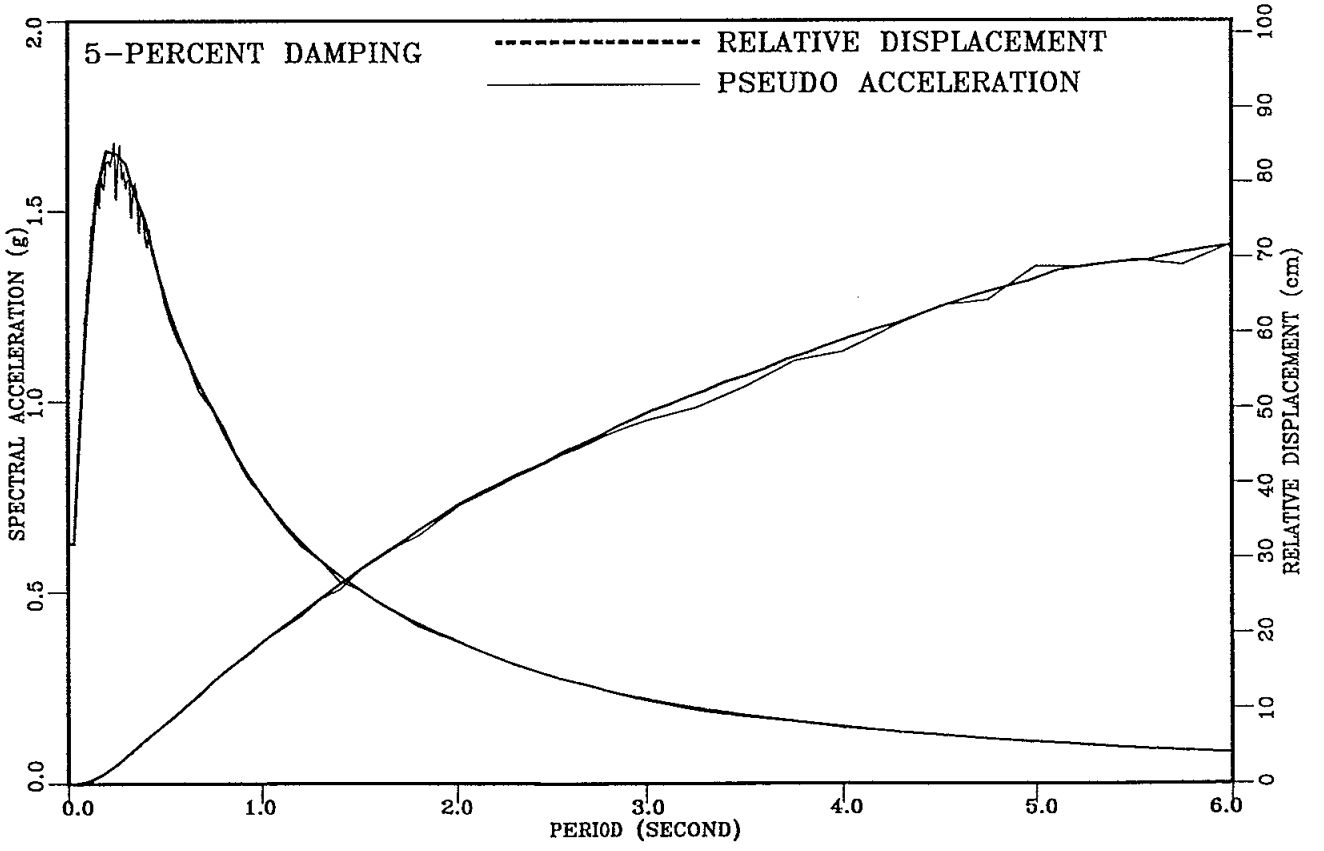

REFERENCE ROCK OUTCROP MOTION, SET4, FP COMPONENT, HAYWARD EVENT, WEST PICO CANYON

SFOBB East Span Seismic Safety Project

PLATE 3-12

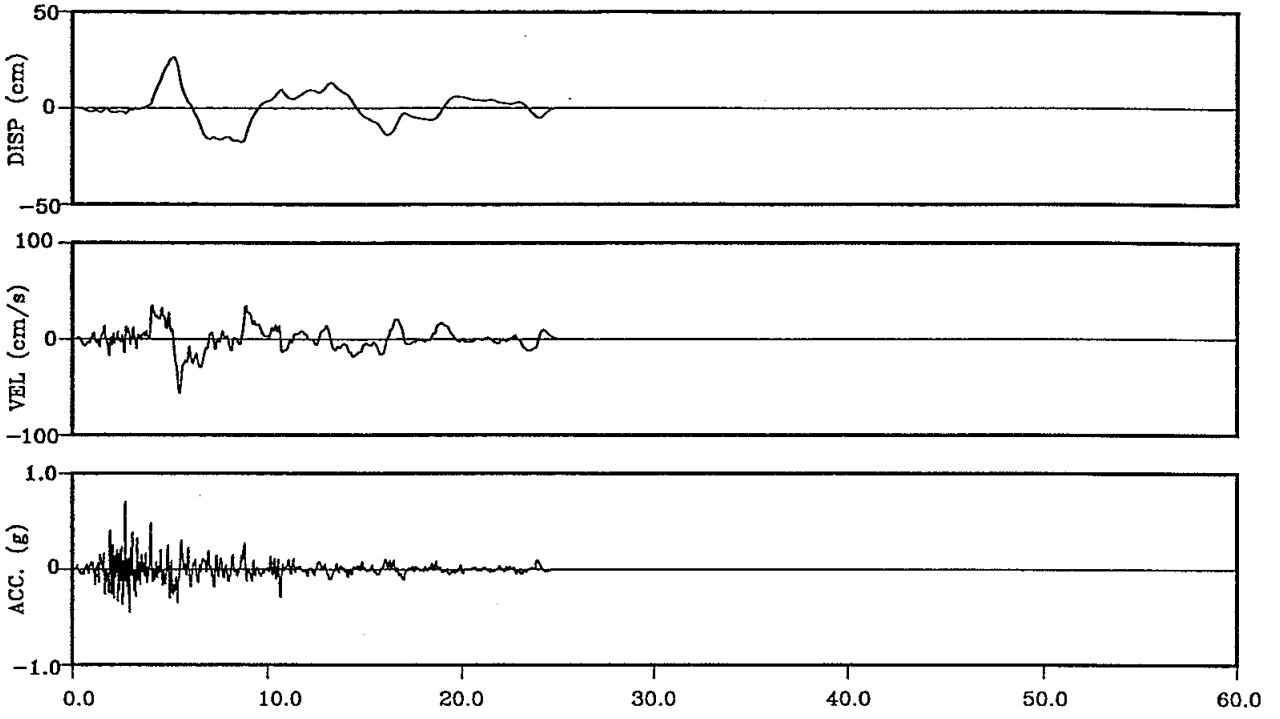

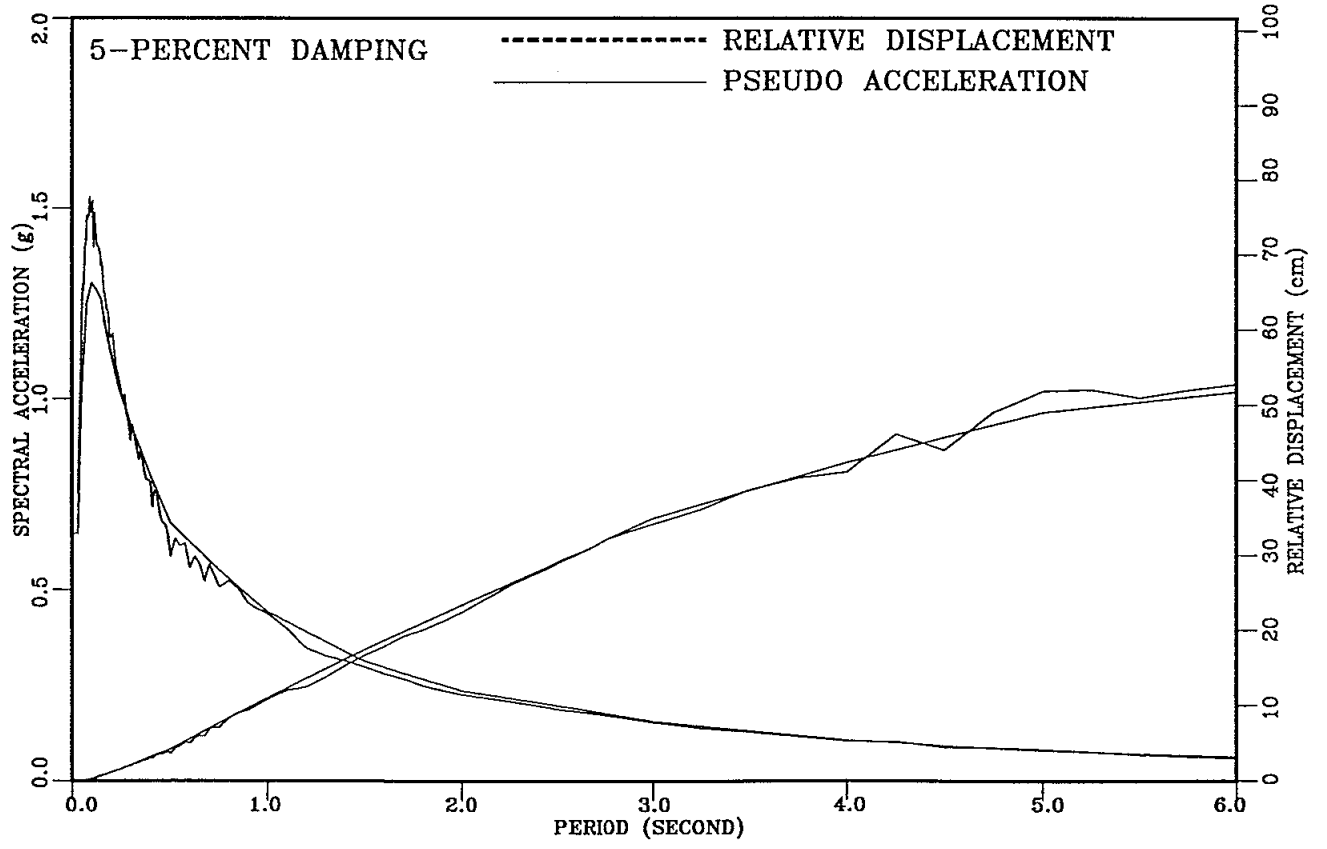

REFERENCE ROCK OUTCROP MOTION, SET4, VERT. COMPONENT, HAYWARD EVENT, WEST PICO CANYON

SFOBB East Span Seismic Safety Project

PLATE 3-13

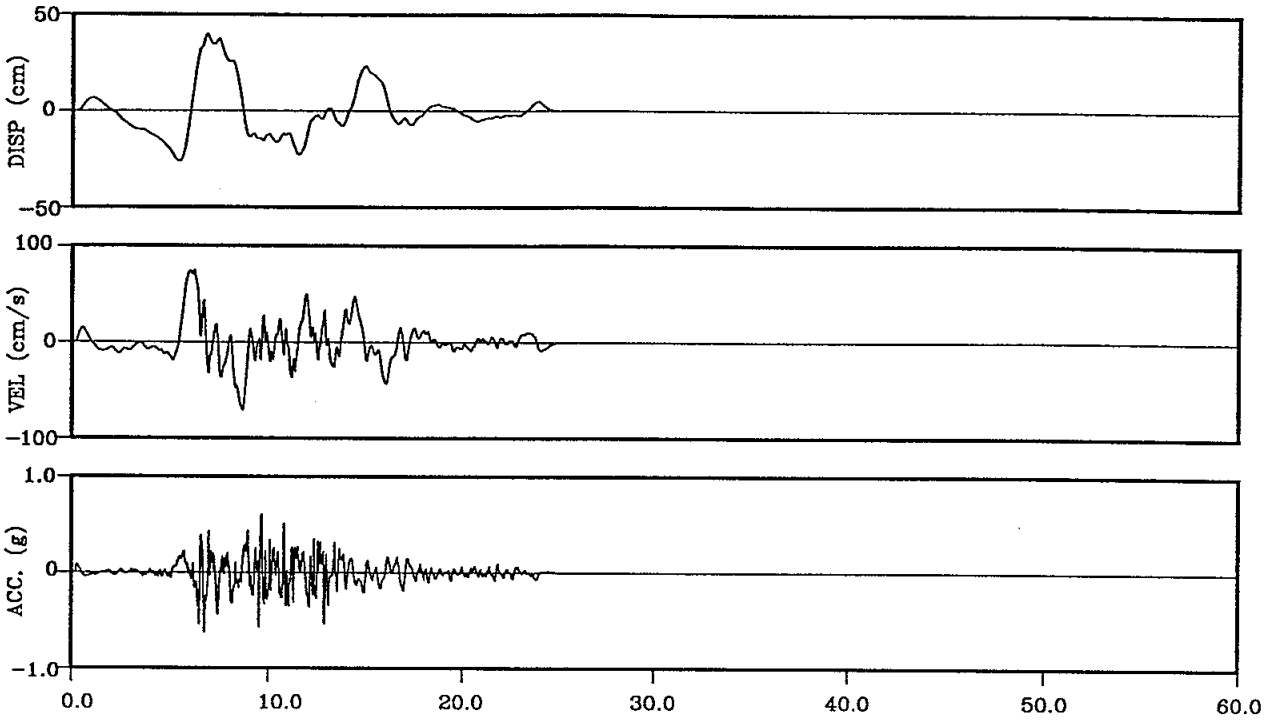

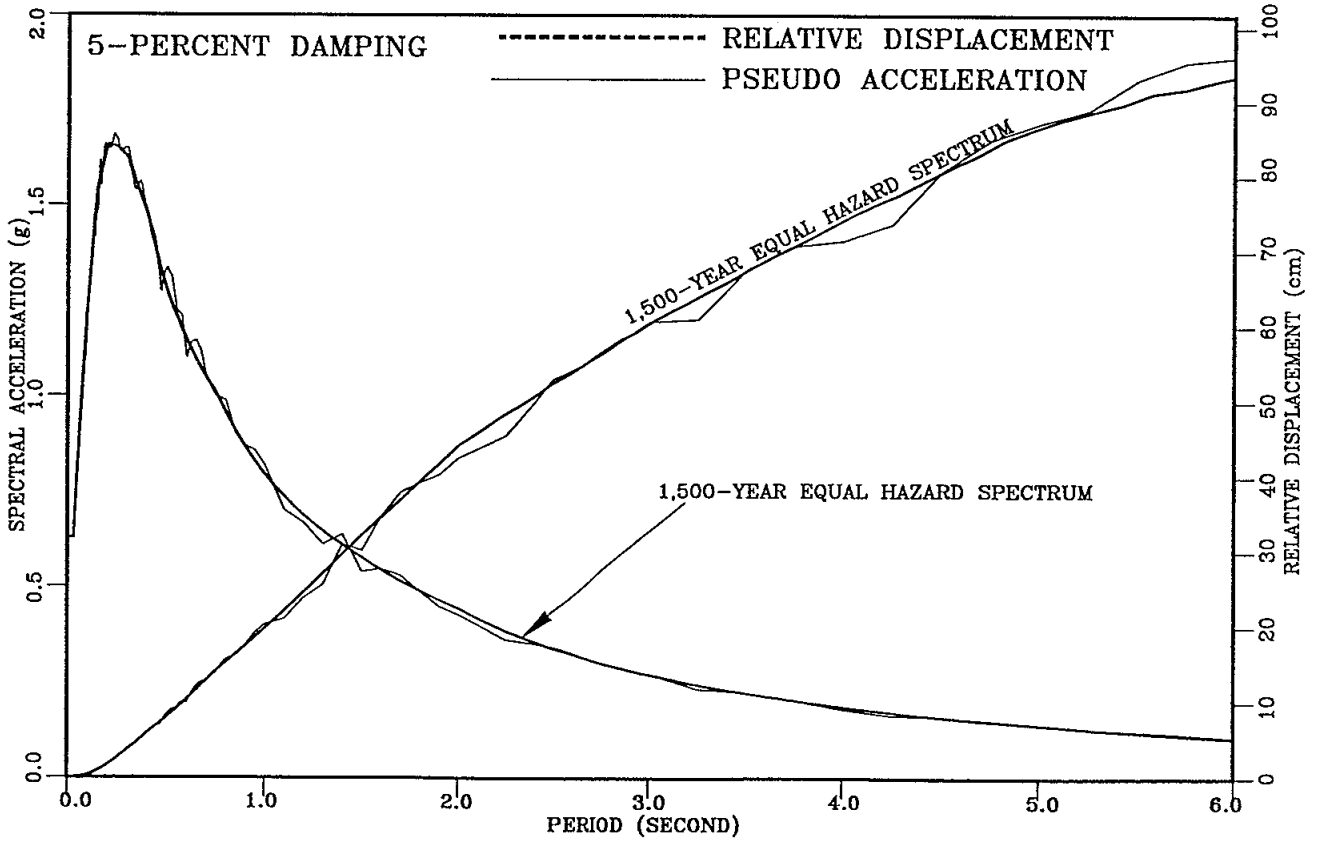

REFERENCE ROCK OUTCROP MOTION, SET5, FN COMPONENT, HAYWARD EVENT, LPGC RECORD

SFOBB East Span Seismic Safety Project

PLATE 3-14

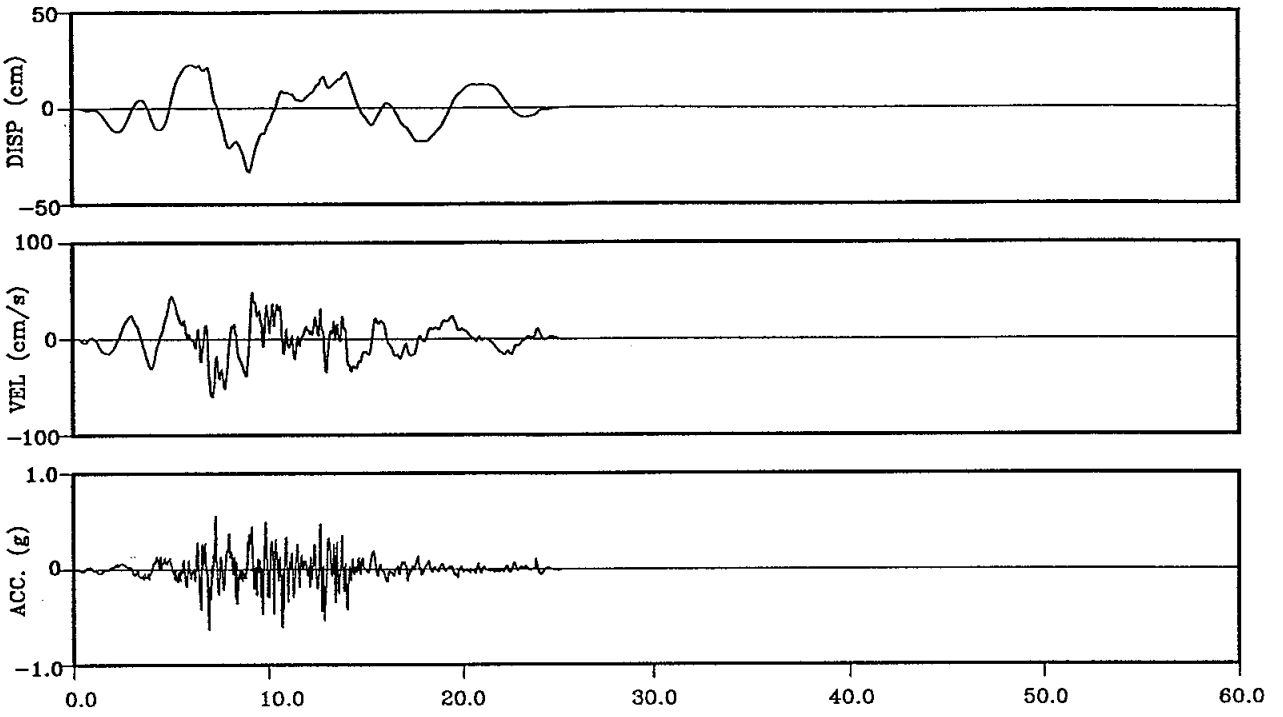

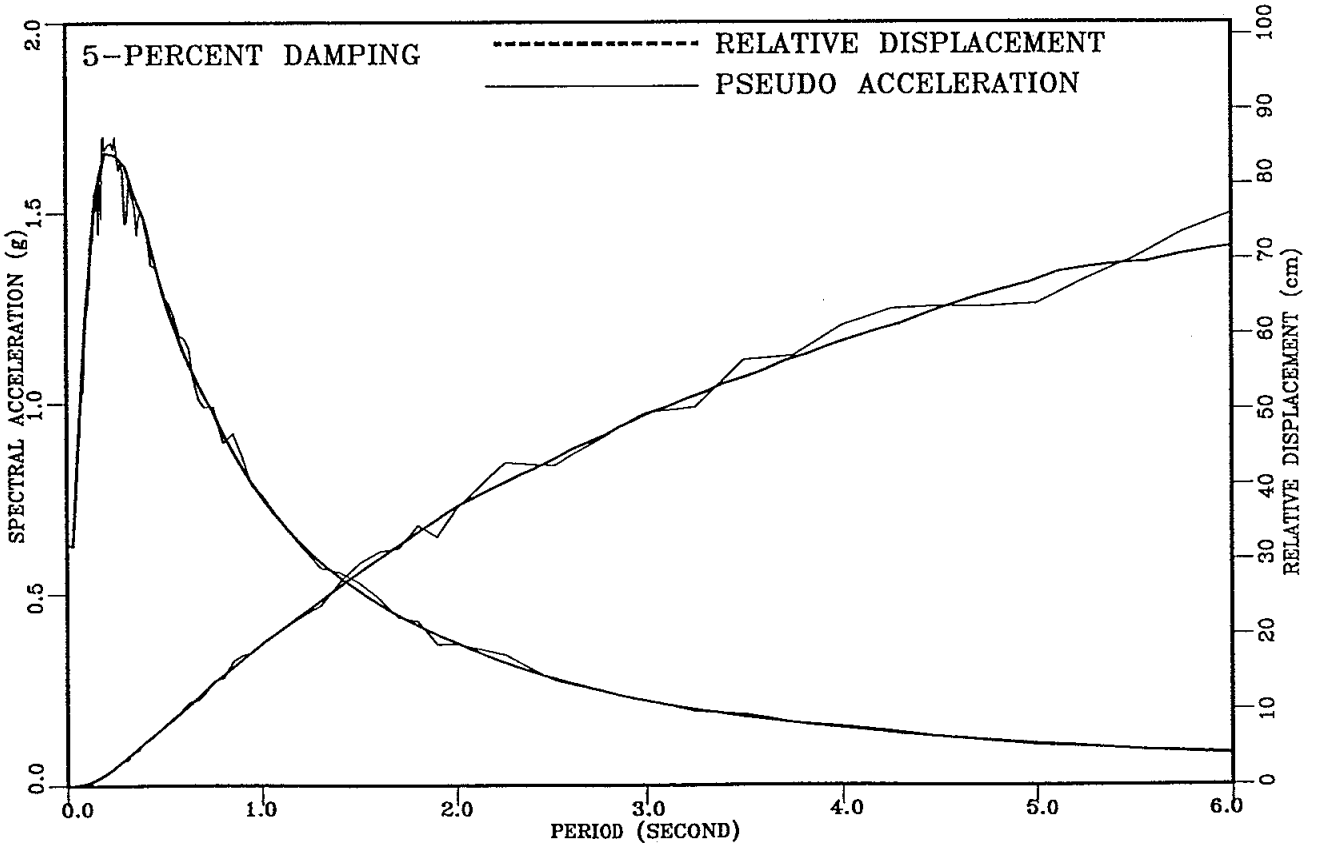

REFERENCE ROCK OUTCROP MOTION, SET5, FP COMPONENT, HAYWARD EVENT, LPGC RECORD

SFOBB East Span Seismic Safety Project

PLATE 3-15

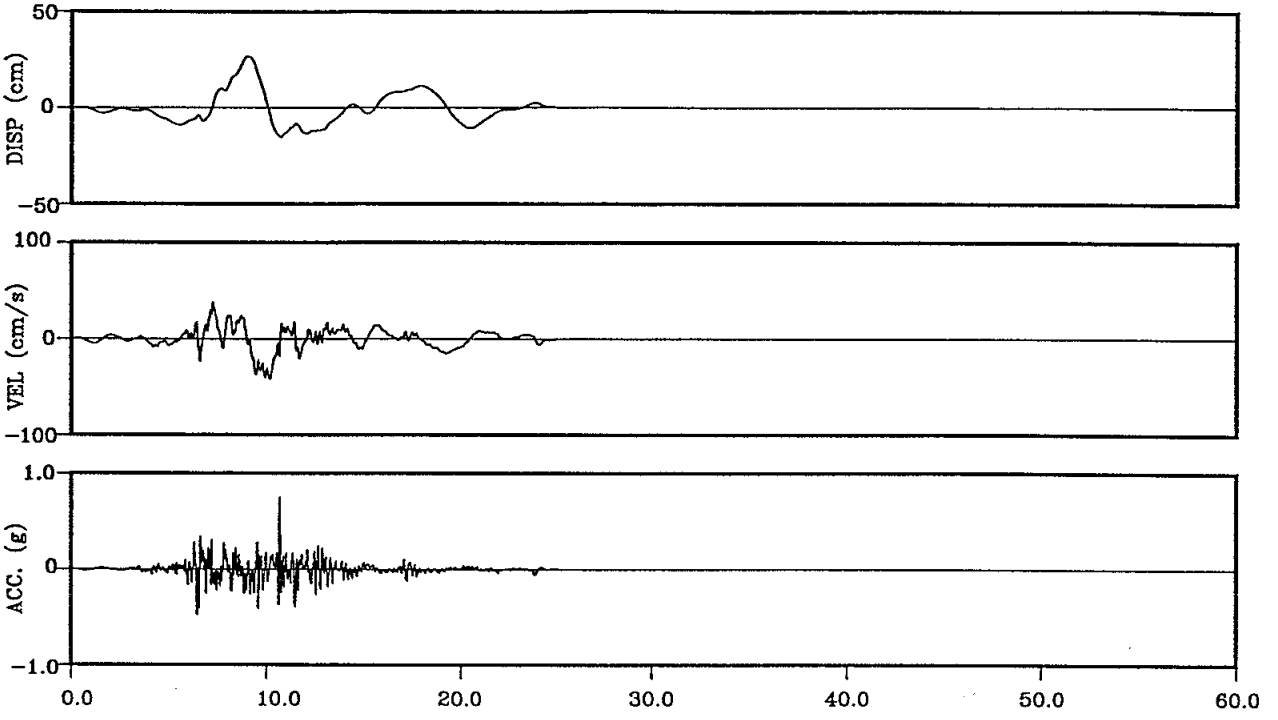

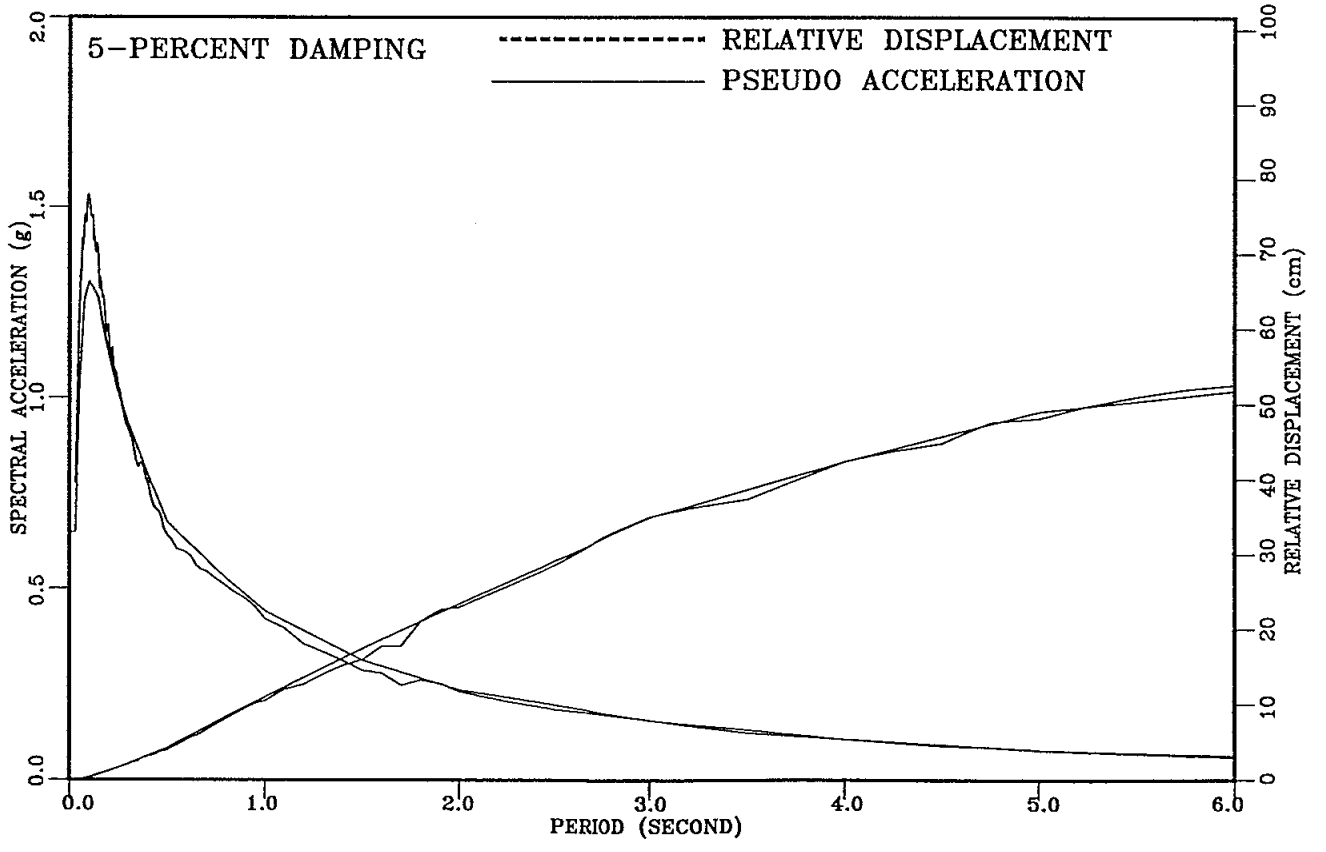

REFERENCE ROCK OUTCROP MOTION, SET5, VERT. COMPONENT, HAYWARD EVENT, LPGC RECORD

SFOBB East Span Seismic Safety Project

PLATE 3-16

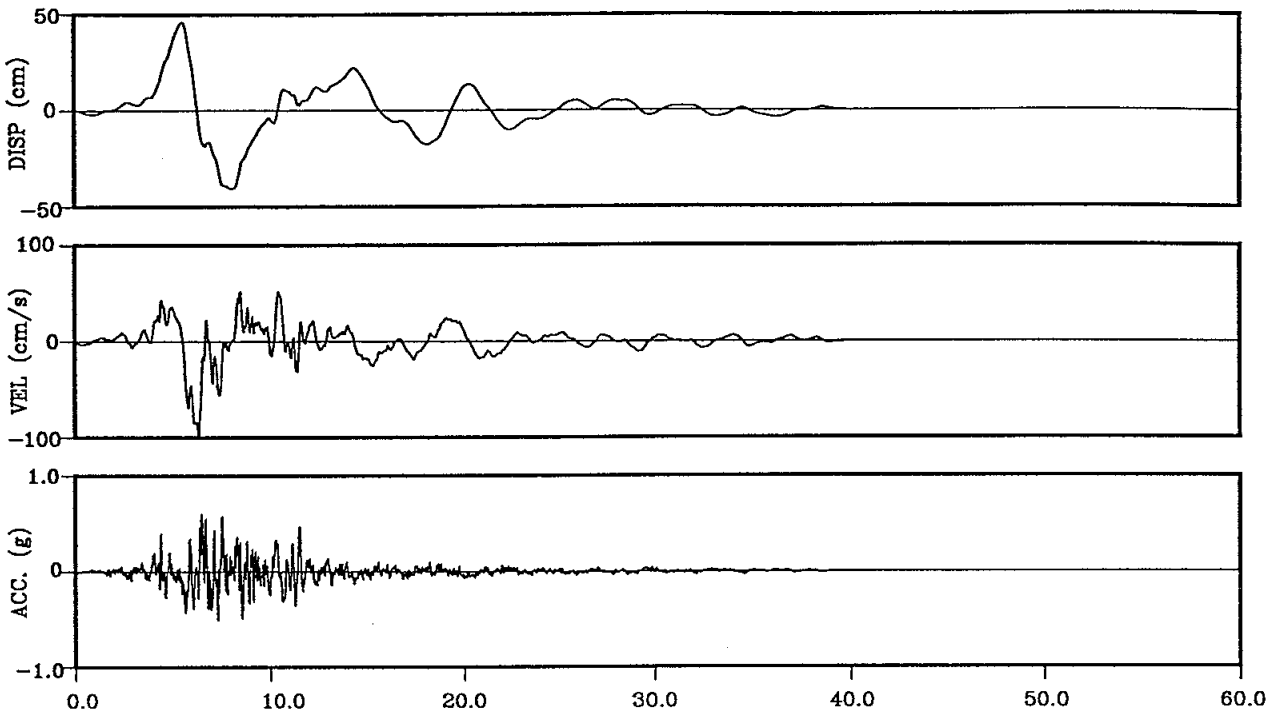

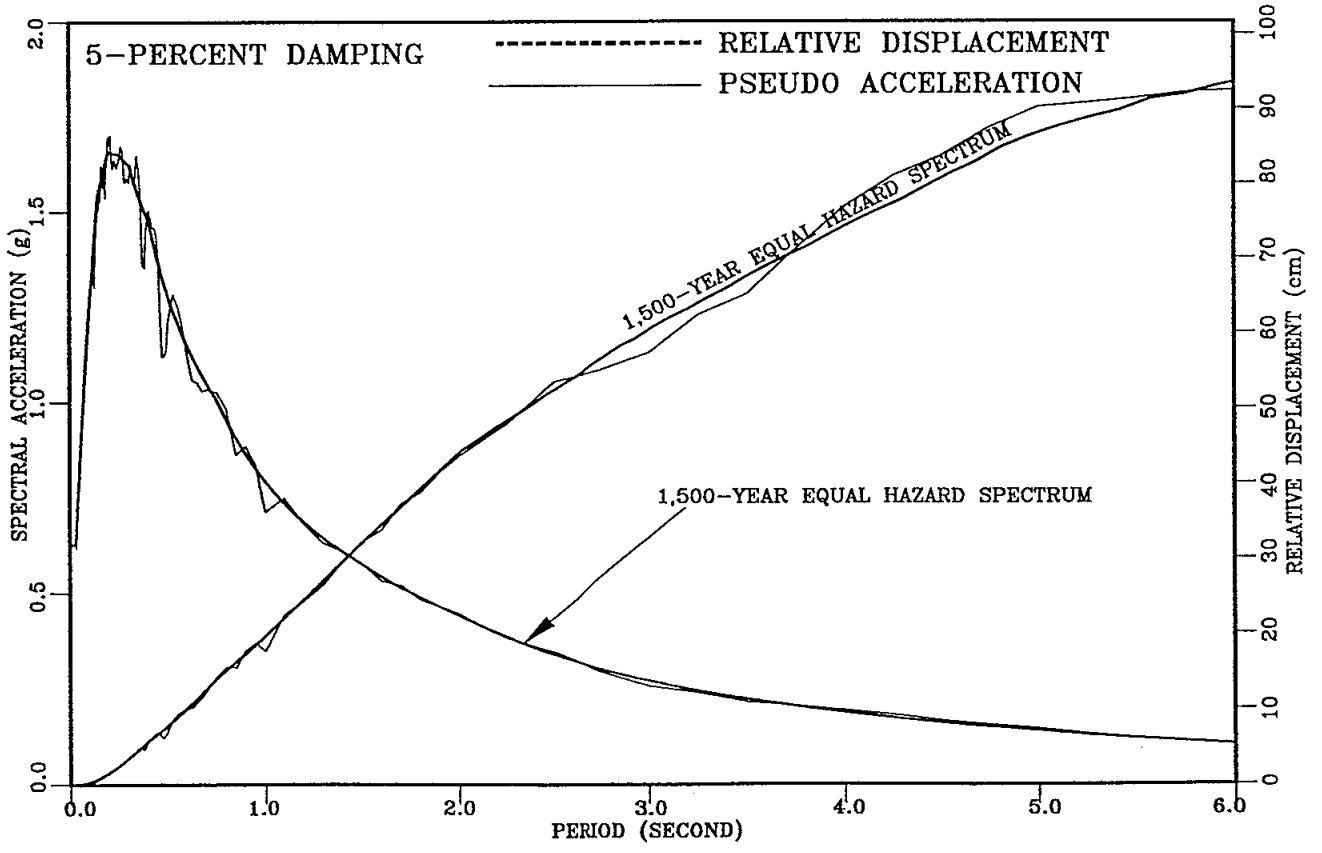

REFERENCE ROCK OUTCROP MOTION, SET6, FN COMPONENT, HAYWARD EVENT, SARATOGA RECORD

SFOBB East Span Seismic Safety Project

PLATE 3-17

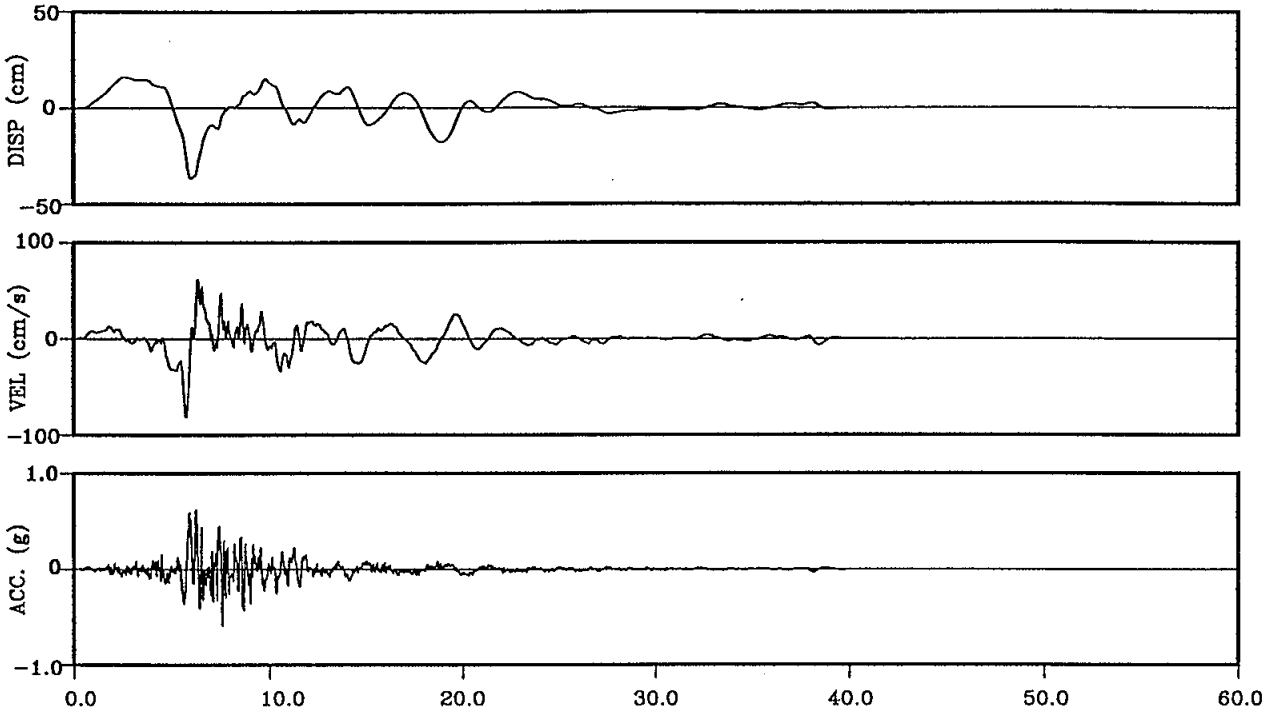

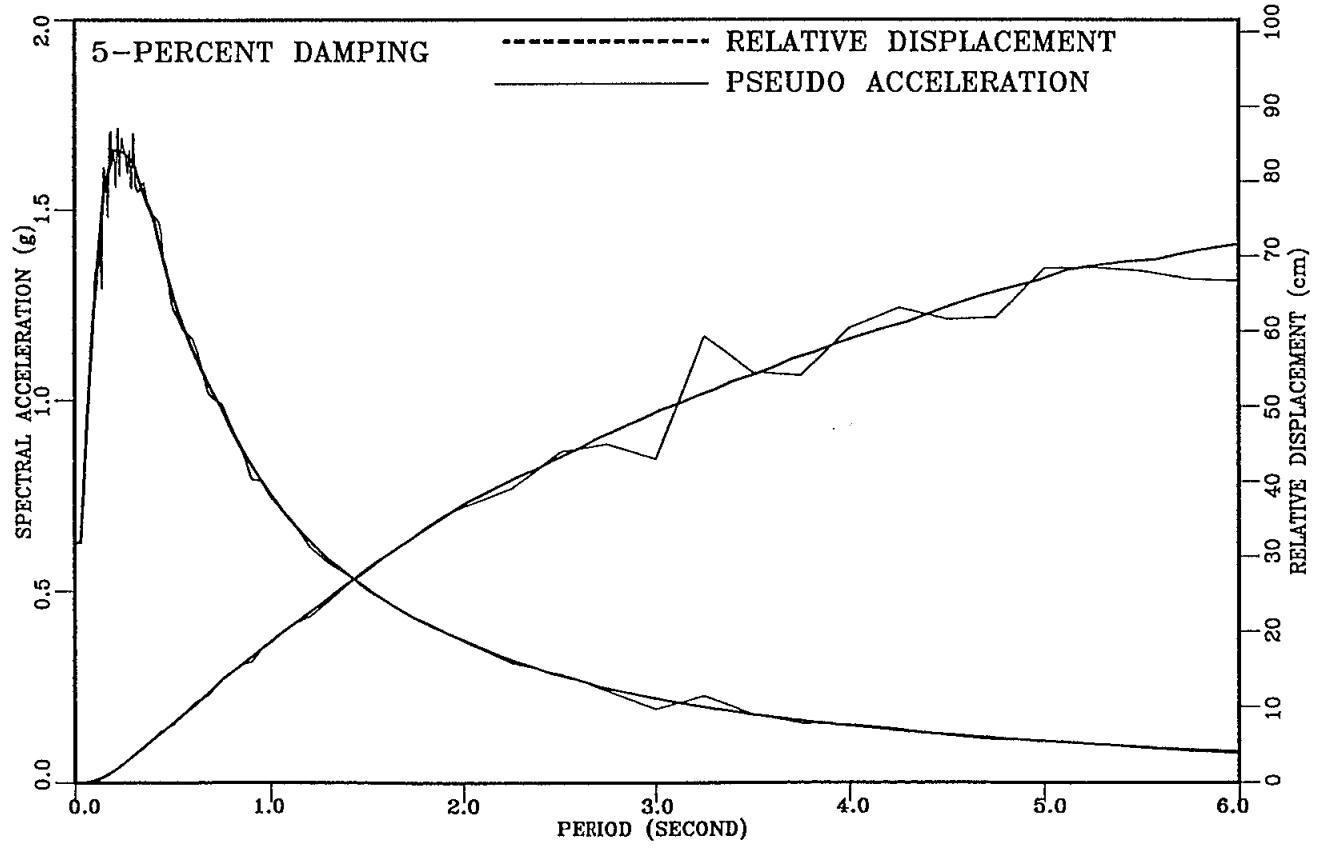

REFERENCE ROCK OUTCROP MOTION, SET6, FP COMPONENT, HAYWARD EVENT, SARATOGA RECORD

SFOBB East Span Seismic Safety Project

PLATE 3-18

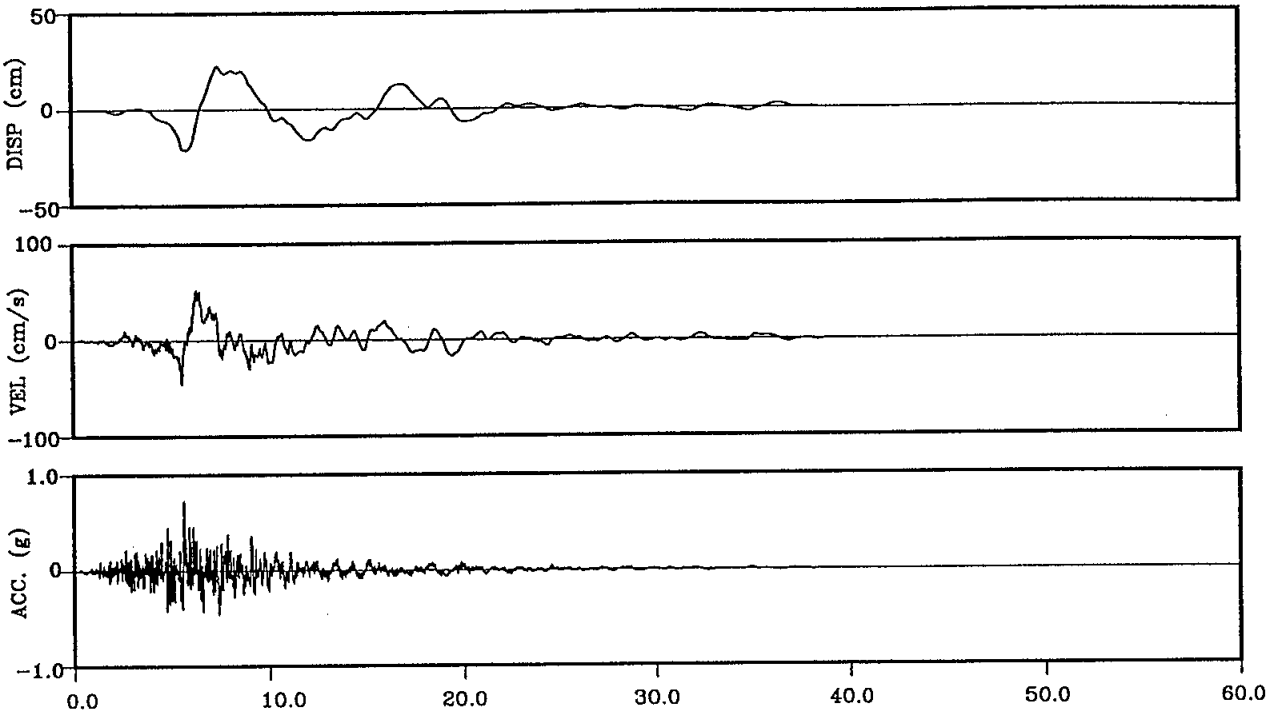

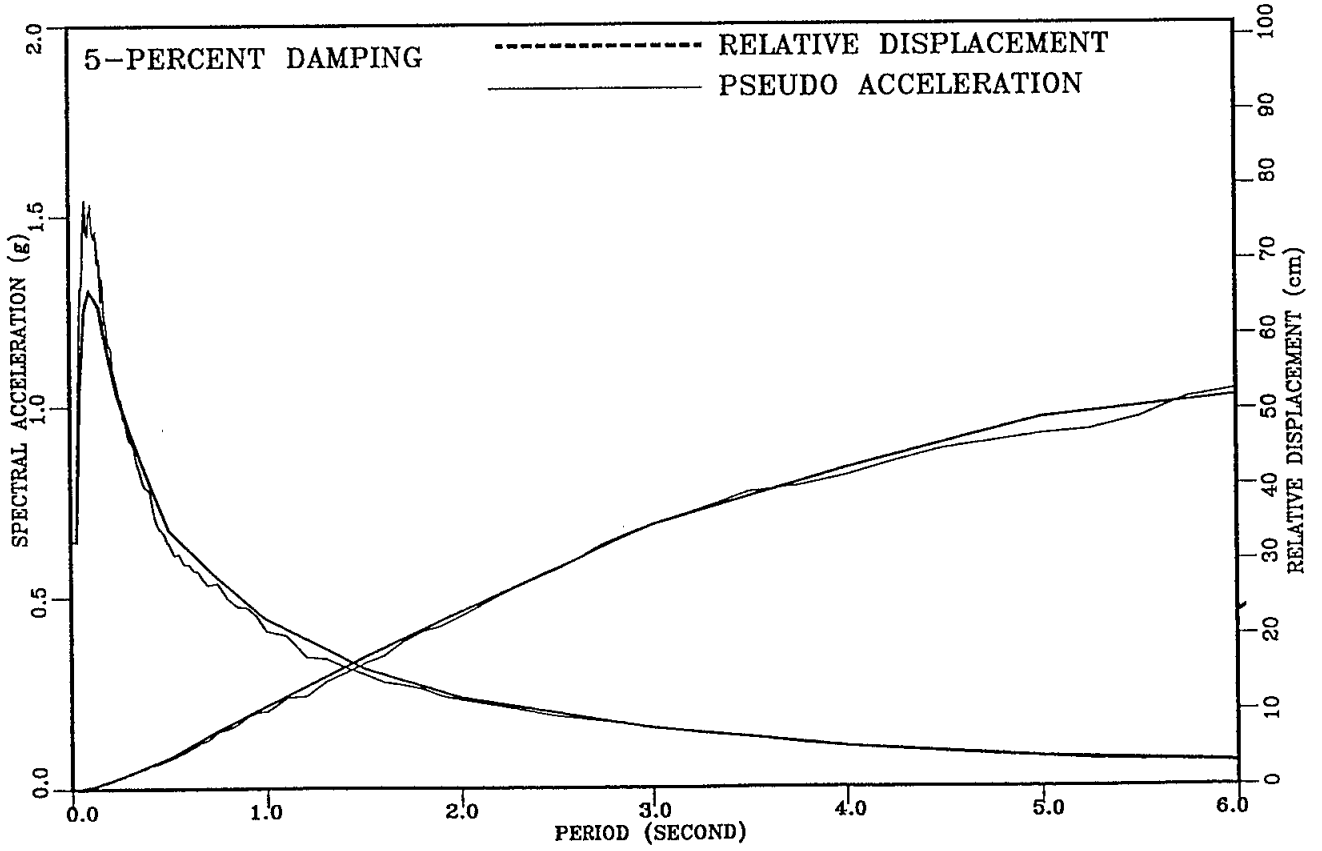

REFERENCE ROCK OUTCROP MOTION, SET6, VERT COMPONENT, HAYWARD EVENT, SARATOGA RECORD

SFOBB East Span Seismic Safety Project

PLATE 3-19

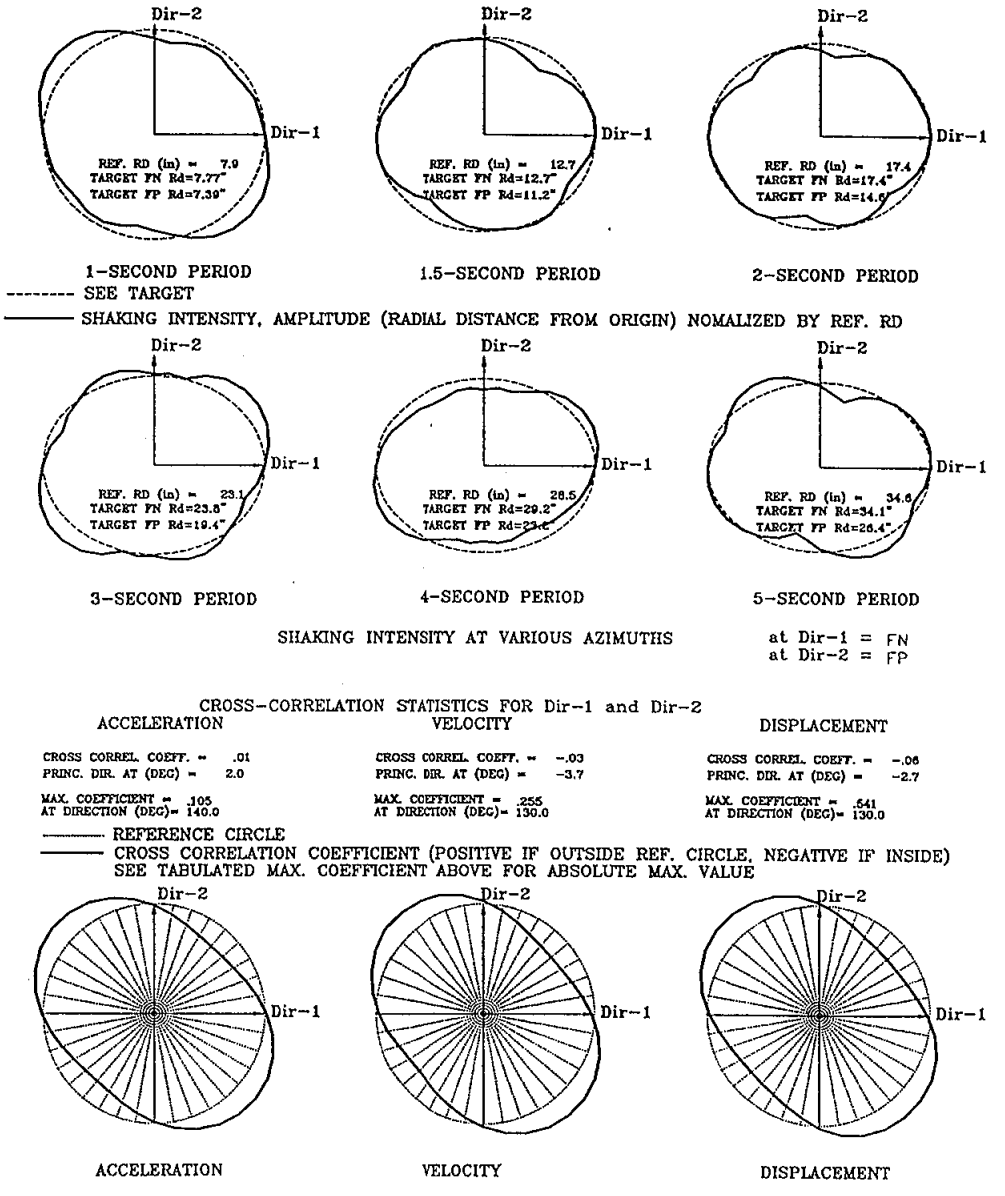

CROSS-CORRELATION OF HORIZONTAL COMPONENTS OF MOTION, SET1, SAN ANDREAS EVENT

SFOBB East Span Seismic Safety Project

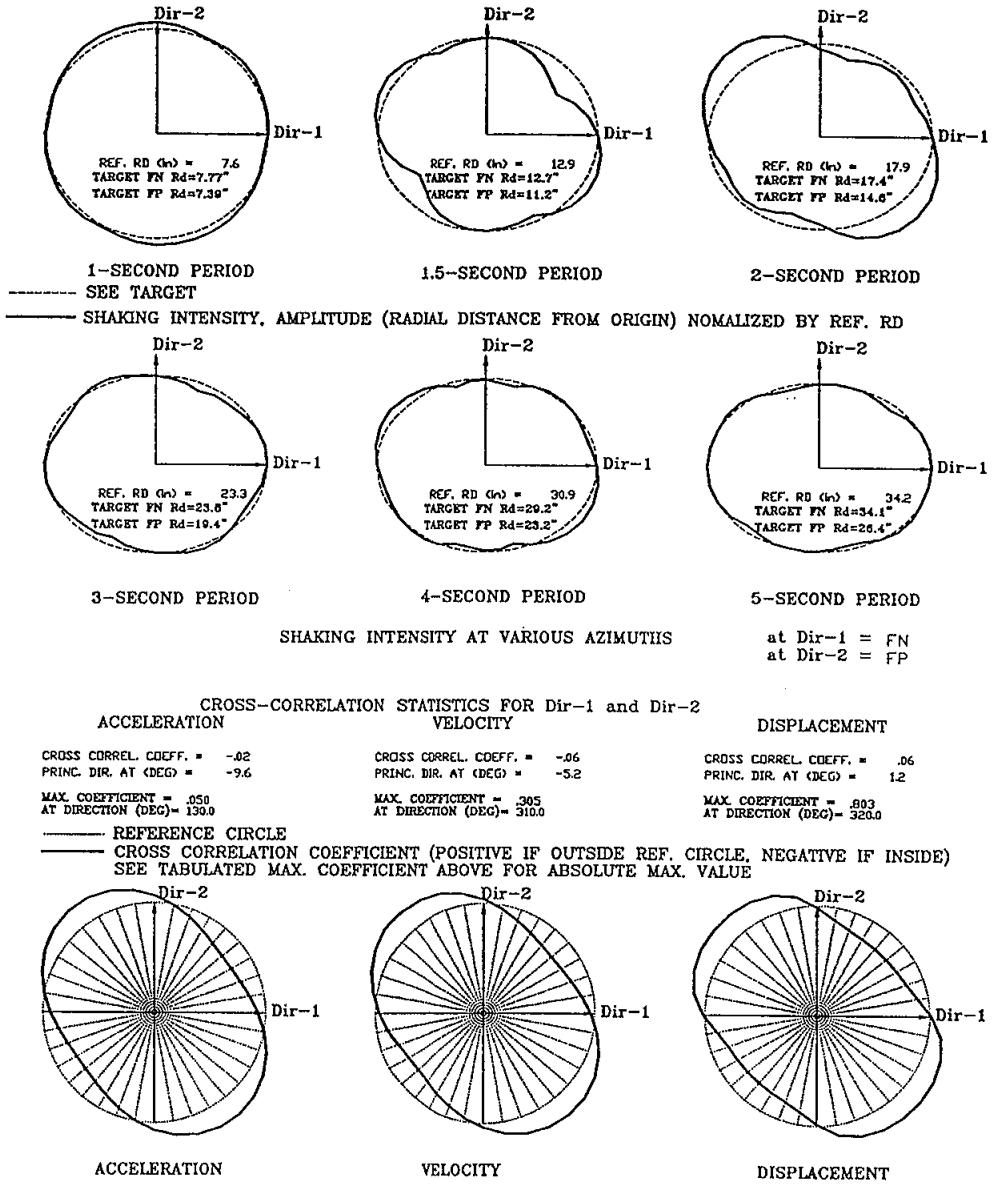

CROSS CORRELATION COEFFICIENT OF RECORDS UNDER ROTATION

CROSS-CORRELATION OF HORIZONTAL COMPONENTS OF MOTION, SET2, SAN ANDREAS EVENT

SFOBB East Span Seismic Safety Project

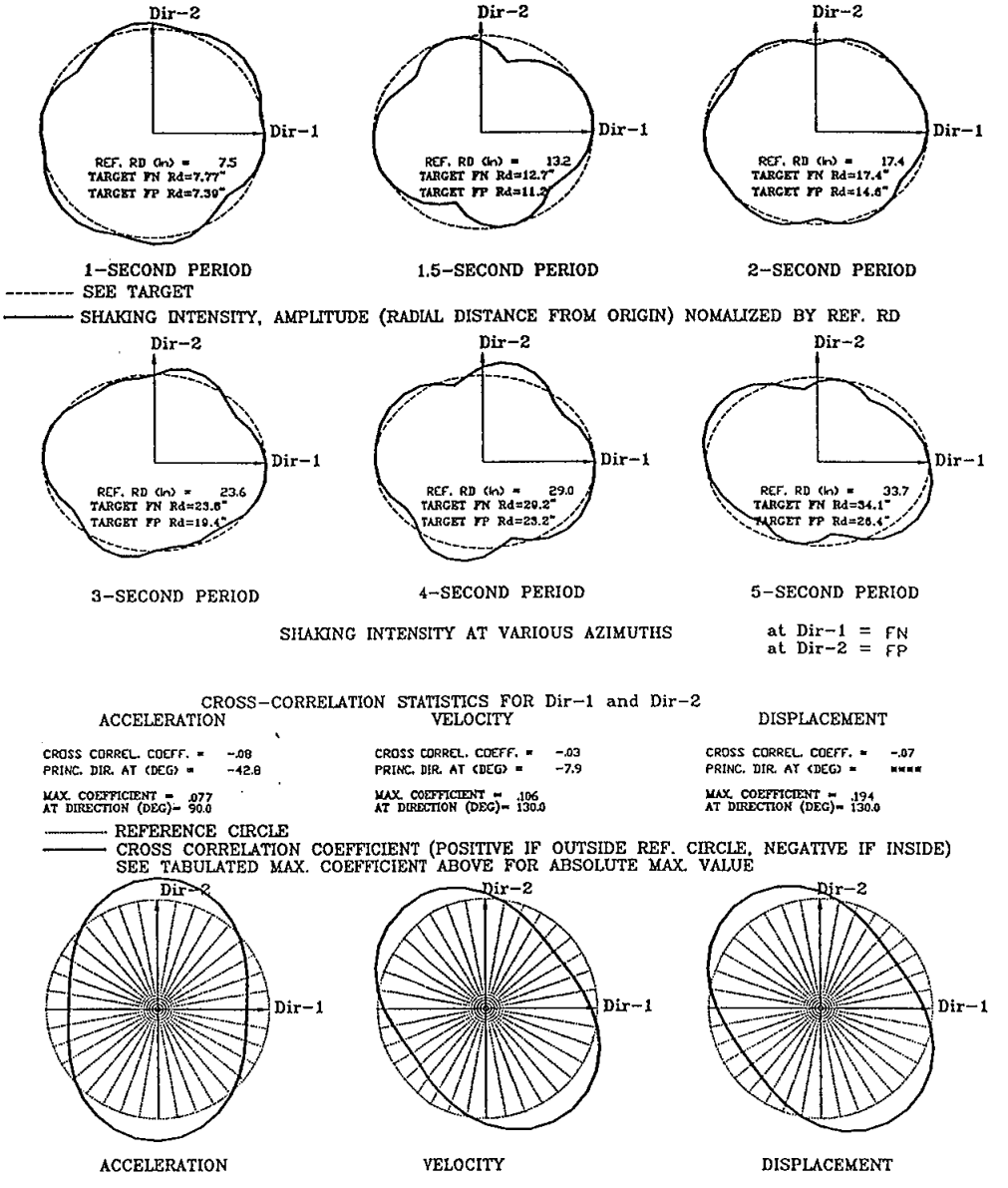

CROSS CORRELATION COEFFICIENT OF RECORDS UNDER ROTATION

CROSS-CORRELATION OF HORIZONTAL COMPONENTS OF MOTION, SET3, SAN ANDREAS EVENT

SFOBB East Span Seismic Safety Project

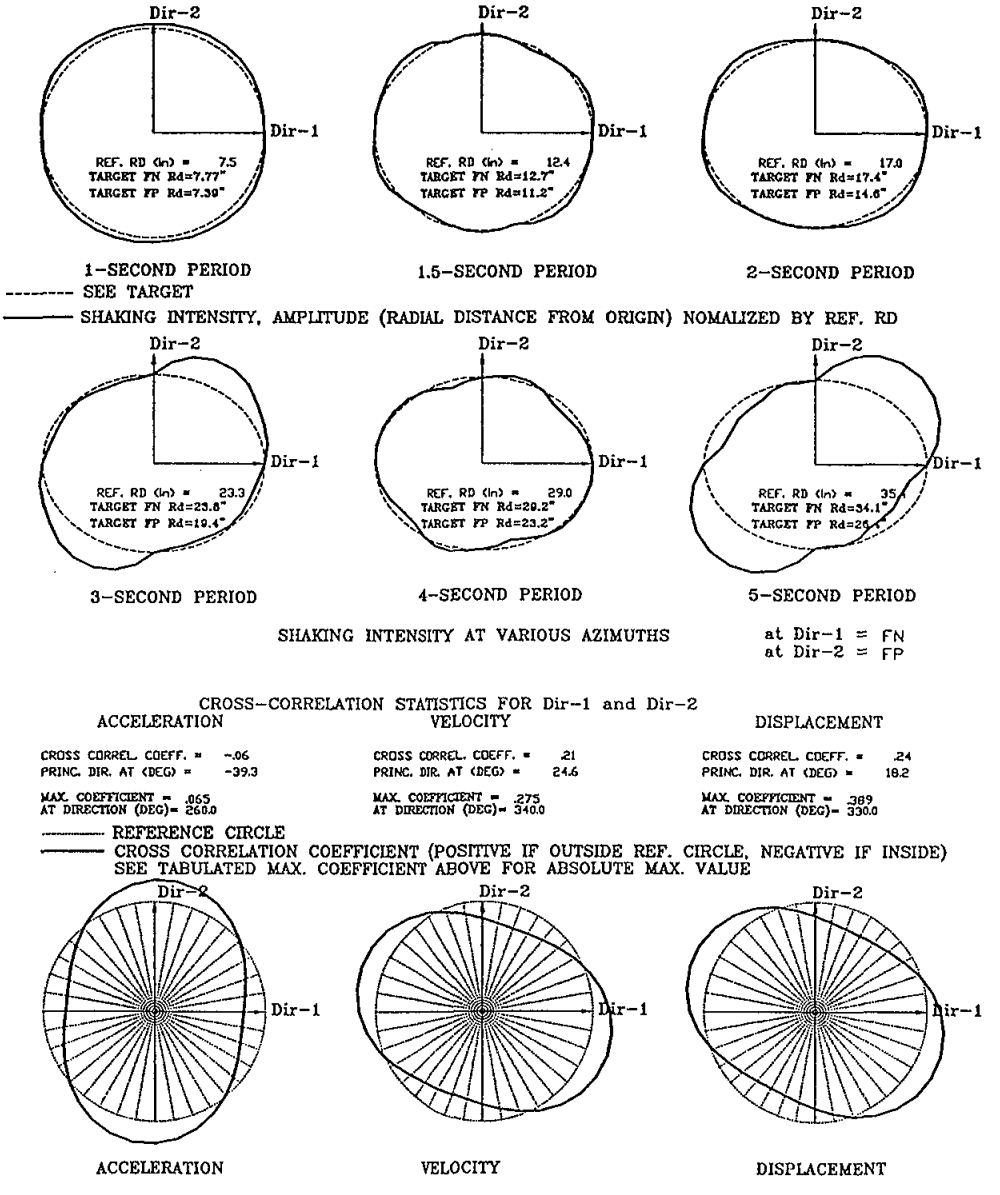

CROSS-CORRELATION OF HORIZONTAL COMPONENTS OF MOTION, SET4, HAYWARD EVENT

SFOBB East Span Seismic Safety Project

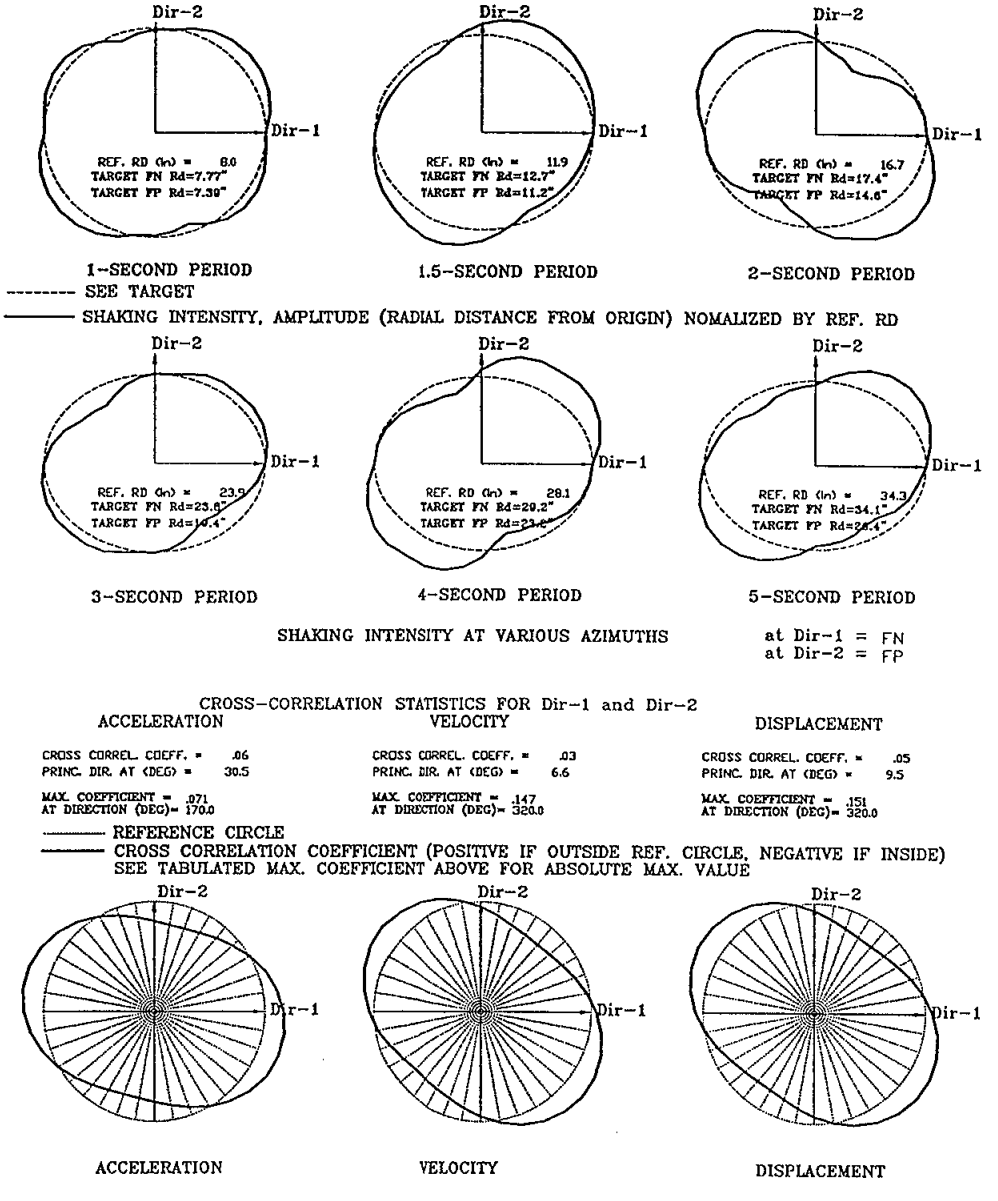

CROSS-CORRELATION OF HORIZONTAL COMPONENTS OF MOTION, SET5, HAYWARD EVENT

SFOBB East Span Seismic Safety Project

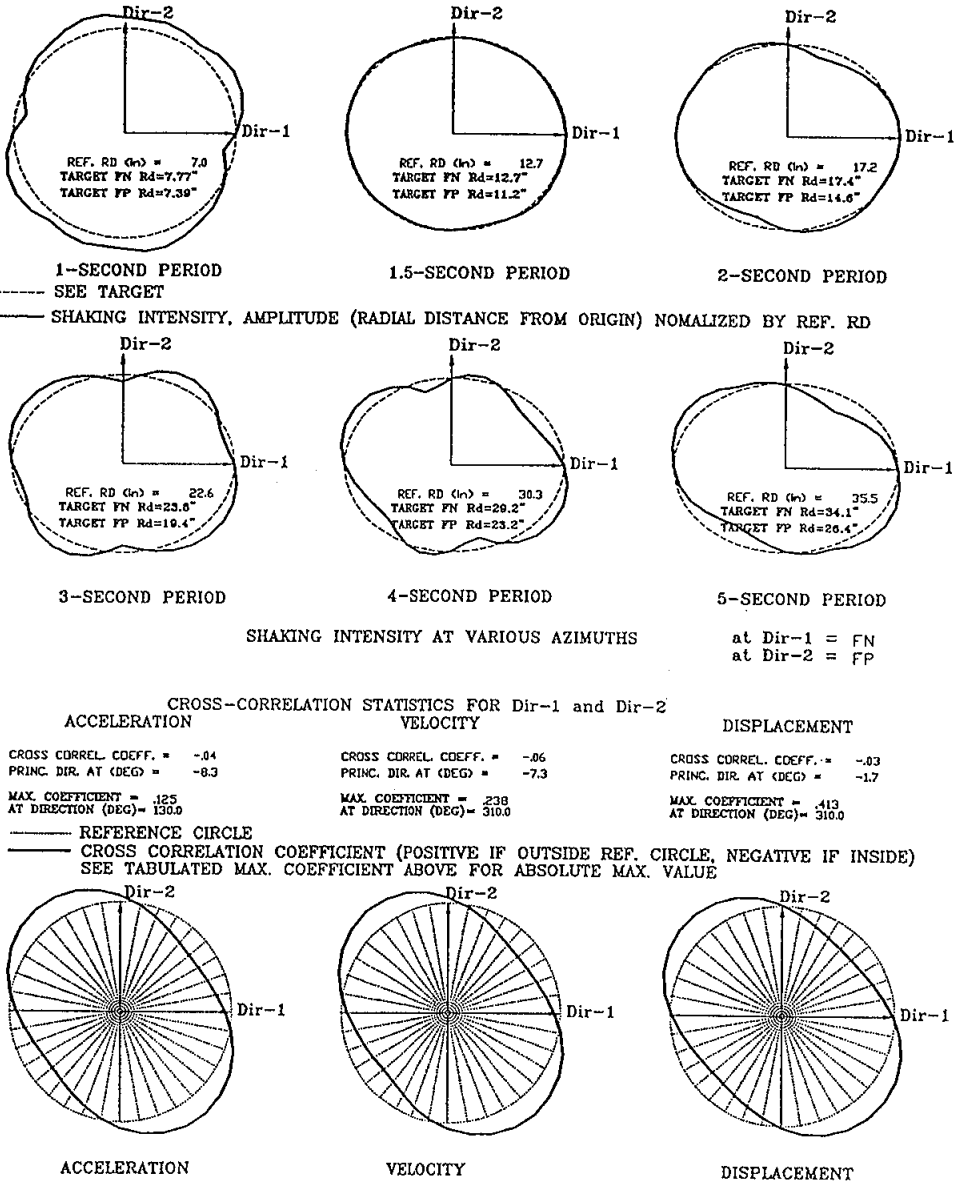

CROSS CORRELATION COEFFICIENT OF RECORDS UNDER ROTATION

CROSS-CORRELATION OF HORIZONTAL COMPONENTS OF MOTION, SET6, HAYWARD EVENT

SFOBB East Span Seismic Safety Project

SECTION 4.0
INCOHERENT MULTIPLE-SUPPORT ROCK MOTION TIME HISTORY

4.0 INCOHERENT MULTIPLE-SUPPORT ROCK MOTION TIME HISTORY

After development of the reference rock motions that are spectrum-compatible to the fault normal, fault parallel and vertical target rock, multiple-support rock motions are generated at all support points for the bridge structure to characterize the spatial variation of the rock motion. The spatial variation of the rock motion results from several effects: non-vertical wave propagation (wave passage effect), scattering and complex 3-D wave propagation (spatial coherency effect), and variable distance to the fault rupture (attenuation effect). The modeling of these effects is described below.

4.1 WAVE PASSAGE EFFECT

The wave passage effect is due to non-vertical wave propagation which produces systematic time shifts in the arrival of the seismic waves at the support locations. The wave-passage effect depends on the apparent velocity of the waves along the axis of the bridge. This requires information on both the apparent velocity of the waves in the direction of the wave propagation and the orientation of the structure with respect to the earthquake.

Studies of strong and weak motion array data have shown that the apparent velocity of S-waves is typically in the 2.0 to 3.5 km/s range (Abrahamson, 1992). This was found using data from several different arrays located in California, Taiwan, and Japan.

In other studies, numerical simulations have been used to estimate the horizontal wave speed. These numerical solutions typically lead to higher horizontal wave speeds than measured from array data. The discrepancy may be due to the use of simplified crustal models in the simulations. The array measurements of the wave speeds are more reliable than the numerical simulations and are the basis for the selection of the apparent wave velocity in this study.

Based on the array data measurements, an apparent wave speed of 2.5 km/s for S-waves is used. This velocity is selected because it is toward the lower end of the range of measured speeds. This leads to somewhat conservative estimates of the differential motions. The wave propagation is projected along the axis of the bridge. The apparent velocity along the bridge axis is given by

$$V_{bridge} = V / \sin(\theta) \qquad (4.1)$$

where V is the apparent velocity and θ is the angle between the line perpendicular to the bridge axis and the line connecting the closest point of the fault and the center of the bridge. For conservatism, a minimum value of 30 degrees is used. This minimum value accounts for waves arriving from other parts of the fault in addition to waves arriving from the closest point on the fault.

The wave passage effect is included by applying systematic time shifts to the coherency compatible time histories. Although the P, S, and surface wave will have different phase velocities, the S-wave phase velocity is applied to the entire time history. The rationale for this

approach is that the S-waves generally contain the strongest shaking. Therefore, for an engineering analysis, it is adequate to simply model the S-wave wave-passage effect. More complex wave propagation methods can be used if the differential motion caused by the P-wave and surface waves are considered to be important for the structural response.

4.2 SPATIAL COHERENCY EFFECT

The scattering and complex wave propagation result in variations in both Fourier amplitude and Fourier phase of the ground motions. The phase variations are explicitly included through the coherency function. Since the ground motions are modified to be spectrum compatible at each support location, amplitude variations are not specifically included, however, there are some variations in the spectral amplitudes of the final ground motion because the frequency domain method for spectral matching is not as tight as the time domain method.

The coherency of ground motion is parameterized by a coherency function. The coherency is a complex number. The absolute value of the complex coherency is called the lagged coherency because it is equivalent to lining up (lagging) the ground motion at the two locations so that the wave passage effect is removed. The lagged coherency does not restrict the alignment of the ground motions to be consistent from frequency to frequency; that is the apparent wave speeds can be different at each frequency. At high frequencies, the wave speed implied by the complex coherency becomes more random. However, in the application of the wave passage effect described earlier, a constant wave speed is used for all frequencies. To be consistent with this application, the coherency function needs to correspond to the coherency that would be computed by aligning the ground motion to a single wave speed. This coherency is called the plane-wave coherency.

Empirical models for the plane-wave coherency for the horizontal and vertical components developed by Abrahamson (unpublished) are given in Appendix F. The coherency functions are plotted in Plates 4-1a and 4-1b for the horizontal and vertical components, respectively.

When evaluating the coherency of the generated ground motions, the plane wave coherency is computed by taking the real part of the complex coherency before the wave passage effect is applied. As a result, the computed plane-wave coherency ranges from -1 to 1 and not 0 to 1 as is the case for the lagged coherency.

4.3 ATTENUATION

For sources close to the structure, the different distances to the various support locations can result in different ground motions due to attenuation of the ground motion. The attenuation is modeled by the attenuation of the 1-second period spectral acceleration from the Sadigh et al.(Geomatrix, 1995) rock attenuation relation since the bridge is most sensitive to the longer period motions. This 1-second period scale factor is applied to the entire record in the time domain.

4.4 GENERATION OF MULTIPLE SUPPORT GROUND MOTIONS

Multiple support time histories are generated for each support location for the Main Span, skyway, and Oakland Mole structures. These multiple support time histories were developed to be compatible with an empirical spatial coherency functions based on the procedure described by Abrahamson (1992). This procedure modifies the Fourier phase angles at each support location using a relation between the spatial coherency and the degree of randomness in the phase angle. The steps in developing the incoherent ground motions are listed below:

- Step 1: Generate coherency compatible time histories at each support location.
- Step 2: Modify the incoherent time histories to be compatible with the target spectrum using a frequency domain approach.
- Step 3: Apply a baseline correction to the incoherent time histories.
- Step 4: Apply the wave passage and attenuation effects

The reference rock motion is located at the Main (Middle) Pier of the bridge (with appropriate attenuation applied) to yield the most stable incoherent ground motions.

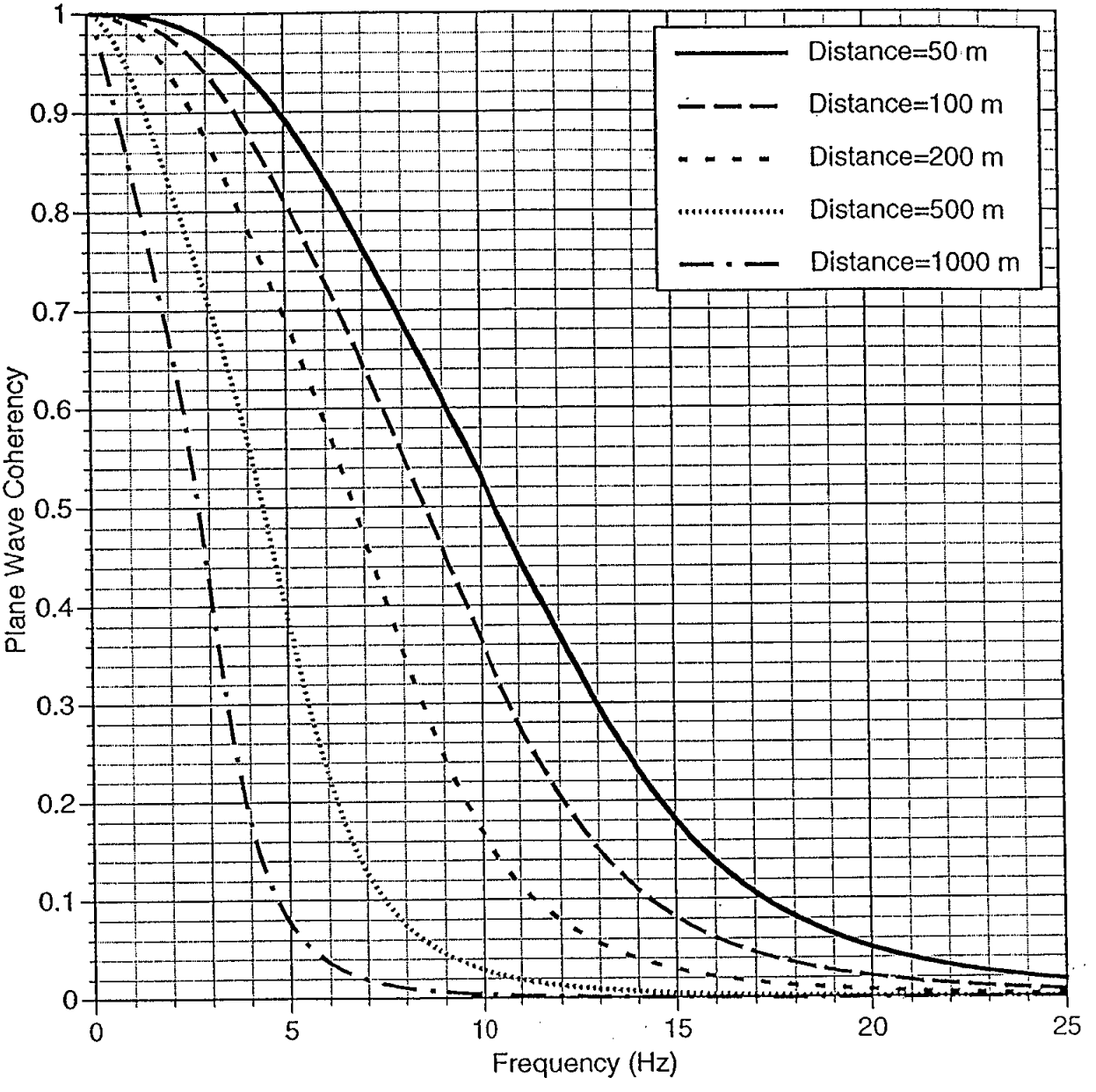

COHERENCY FUNCTIONS FOR HORIZONTAL COMPONENT MOTION
SFOBB East Span Seismic Safety Project

PLATE 4-1a

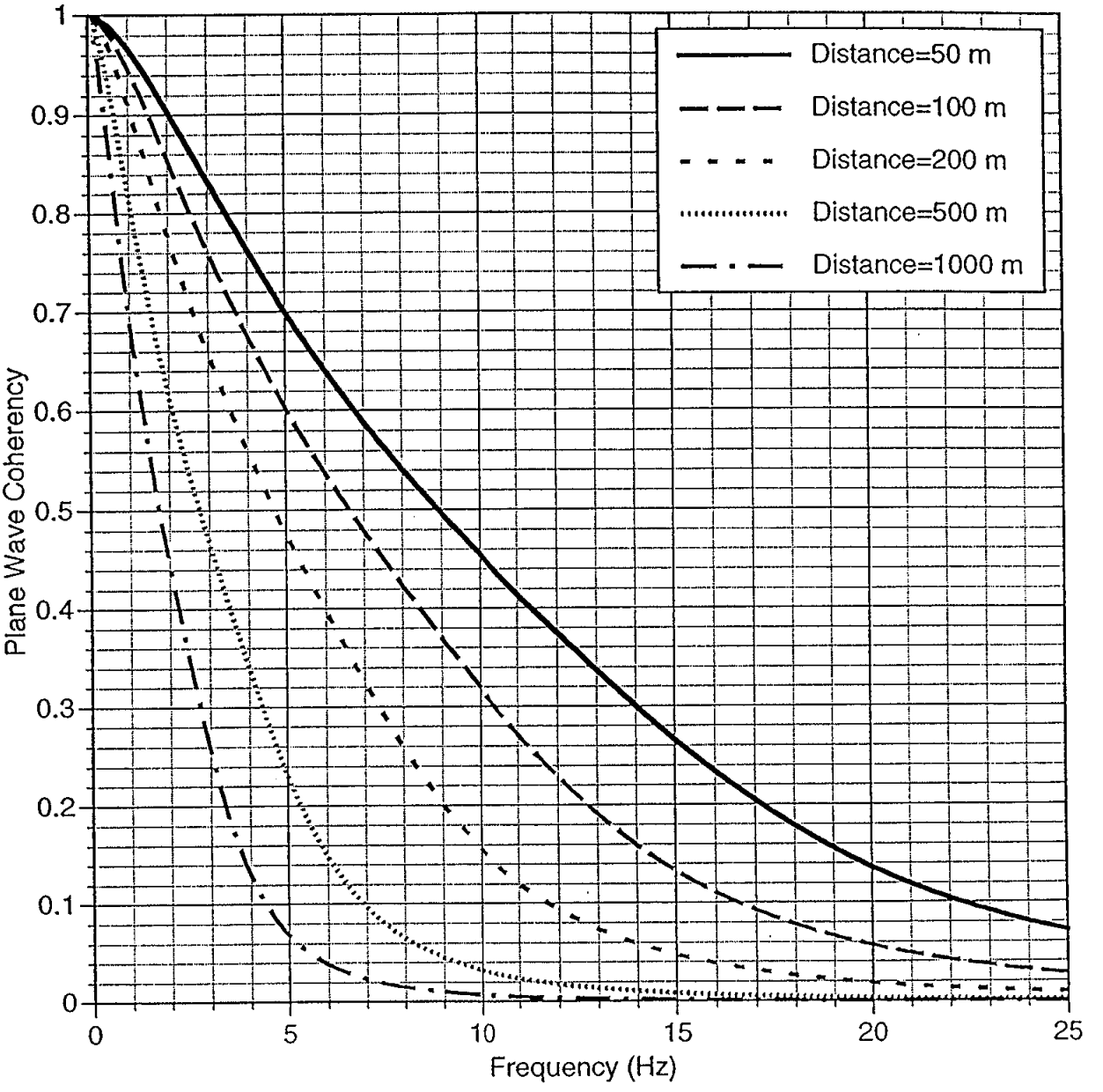

COHERENCY FUNCTIONS FOR VERTICAL COMPONENT MOTION
SFOBB East Span Seismic Safety Project

PLATE 4-1b

SECTION 5.0
FREE-FIELD SITE RESPONSE ANALYSES

5.0 FREE-FIELD SITE RESPONSE ANALYSES

5.1 GENERAL

This chapter describes the site response analyses performed at different locations along the bridge structure. Site response studies are pertinent to the marine piers and Oakland Mole area where bedrock is encountered at a great depth and the ground response is influenced by the deep deposits of soil sediments. The site response analyses were conducted only for the horizontal components of ground motion. Due to lack of proven methodology to analyze the propagation of vertical motions, no site response analysis was conducted for the vertical component, i.e., vertical rock motions were used directly.

The ground response analyses were performed to achieve two objectives: 1) development of ARS design criteria for the Skyway and Oakland Mole structures, and 2) computation of depth-varying ground motions at pier-specific locations in the total system where individual piles are modeled. For the purpose of development of ARS design criteria for the Skyway structure, soil stratigraphy and the engineering properties of the foundation sites along the Skyway alignment were grouped into four representative profiles. These representative profiles are designated as profiles A through D. Site response analyses conducted on these four representative profiles along with kinematic soil-pile interaction analyses using the six sets of reference rock motions guided much of development for the ARS design curves.

The Skyway design performed initially with ARS design criteria is finally checked against time history analyses using six sets of multiple-support motions. The geotechnical information collected during the marine investigations (both Phase I and Phase II) provided necessary data in sufficient detail so that subsoil profile could be developed at each pier location and pier-specific site response analyses could be performed. From the pier-specific site response analyses depth-varying free-field motions for each set of rock motion are extracted and used by the structural engineers to prescribe input motions along the length of the pile in the bridge model employing a total-system.

There are a total of 14 pier locations (Piers E3 through E16) in the proposed Skyway portion of the bridge. From the east end of the Main Suspension Bridge, Skyway Structure splits into two parallel bridges; eastbound and westbound. In terms of pier numbering, a letter 'E' or 'W' is attached at the end of pier number to differentiate the eastbound bridge from the westbound bridge. For example, Pier E3E denotes eastbound Pier 3 and Pier E3W denotes westbound Pier 3. Although eastbound and westbound Skyway Structures are independent, the ground motion analyses were not performed for eastbound and westbound piers separately because of minor variations in the subsoil conditions between them. In other words, the same site response analyses are applicable for both eastbound and westbound piers.

5.2 SUBSURFACE CONDITION

5.2.1 Yerba Buena Island

Yerba Buena Island (YBI) is composed mainly of Jurassic/Cretaceous-age Franciscan Formation. The alignment for the YBI structure and a portion of the suspension bridge is shown in Plate 5-1. The West and Main Piers of the suspension bridge are constructed in the Franciscan rock formation. The majority of the Franciscan Formation on the island is covered with unlithified sand and alluvial sand, along with localized areas of artificial fill. The field investigation program for the island was delayed for about one year because the required right-of-entry permits were not available. The right-of-entry permits were eventually granted in September, 1999, and the full site investigation was conducted and completed in January, 2000. Based on the investigation completed to date, rock outcrop can be found at the Northeastern Point of the island, while bedrock may be found within depths of 30 to 40 meters elsewhere. Plates 5-2a and 5-2b show the subsurface conditions on the island based on the available information. The YBI site characterization report describes the geologic condition on the island in details (Fugro-EMI, 2000, a).

5.2.2 Offshore Marine Area

Extensive offshore exploration has been conducted during Phases I, II and III of the geotechnical investigation works carried out by the Fugro-EMI joint venture. Plates 5-3 and 5-4 show the alignment of the bridge and the locations of soil borings conducted for the marine geotechnical investigations. In addition to the soil borings, cone penetration tests and an array of geophysical (2D and 3 D) measurements were also made. The following reports are the most relevant documents issued by Fugro-EMI J.V. describing the site conditions for the marine piers:

Fugro-EMI (1998), Subcontractor Report, Phase I Site Investigation
Fugro-EMI (2000, f), Subcontractor Report, Phase II Site Investigation
Fugro-EMI (2001, b), Final Marine Geotechnical Site Investigation
Fugro-EMI (2001, c), Final Marine Geophysical Survey

Five subsoil cross-sections offshore YBI were drawn along the proposed Skyway alignment and they are presented in Plates 5-5 through 5-9. As shown in these profiles, the subsoil in the marine area extending from Main Pier through Oakland Mole can be grouped into the following geologic units in the descending order of occurrence which is consistent with the characteristics of the bay area's geology.

Young Bay Mud (YBM): Young Bay Mud is a marine clay sediment that was deposited within last 11,000 years. This layer occurs over the entire length of the alignment with depths varying from approximately 8 to 25 meters along the Skyway alignment, with deeper deposits usually associated with paleo-channels (ancient river channel). Because of the meandering nature of the paleo-channels, the thickness of the deposit is found to vary in both, east-west and north-south directions. YBM consists of very soft to firm fat clay.

Merritt-Posey-San Antonio Formation (MPSA): This formation, consisting of layered deposit of sands and clays, underlies YBM, and occurs along portions of the N6 alignment. The thickness of the deposit varies along the alignment with maximum thickness of about 6.0 m. The deposit is completely absent within the paleo-channels. Although the elevation of top of the deposit varies due to erosion and channeling, the elevation of base of the deposit is less variable. MPSA consists of dense to very dense sand with layers of stiff to very stiff clay and sandy clay.

Old Bay Mud (OBM)/ Upper Alameda (UAM): These sediments consist of primarily thick deposits of stiff to hard clays and underlie the MPSA or YBM deposits. Within the limits of the skyway structure the thickness of this deposit is more or less constant, and is about 55 to 60 meters. The borings show that these two formations typically include multiple crustal layers with higher undrained shear strengths. The undrained shear strength of this formation increases from about 125 to 175 kPa at the top of the sequence to about 150 to 250 kPa to the base of the sequence. Due to the presence of crustal layers, the undrained shear strengths could locally increase by about 25 to 50 kPa. Although this formation primarily composed of stiff to hard marine clays, some sand layers were encountered. These dense to very dense sand layers were found below El. -55 to 60 meters.

Lower Alameda (LAA): This sediment consists of primarily alluvial deposits of dense to very dense granular materials. These sediments underlie the OBM/UAM formations and extend down to the Franciscan bedrock formation. Although the sediment consists primarily of granular deposits, layers of hard clay deposit were also encountered. The thickness of the deposit increases from west to east along the alignment. Towards the eastern end of the skyway, the thickness of this formation was found to be about 60 meters.

Franciscan Formation (FF): The bedrock contact can be found near elevation –110 m at the western end of Skyway. The bedrock descends toward east and can be found near elevation – 140 m at the eastern end of Skyway. The strata of the Franciscan Formation are composed predominately of graywacke sandstone with a few zones of interbedded, siltstone and claystone. The shear wave velocity of Franciscan Formation ranges from 1,500 to 3000 meters per second.

5.2.3 Oakland Mole Area

Most of the site investigation in this area was conducted on-land from the existing fills supplemented by offshore Seascout CPT soundings. The exploration consists of about 25 soil borings and 9 conventional CPT soundings conducted on-land and more than 40 tethered Seascout CPT soundings conducted in the tidal flat to the north of the existing mole. Plate 5-10 shows the alignment and boring locations. The findings from the Oakland Mole investigation are documented in a report submitted to Caltrans (Fugro-EMI, 2001, h).

Cross-sections showing soil conditions along the Oakland shore approach are presented in Plates 5-11a and 5-11b. Based on the site exploration, the subsurface at the Oakland Mole is underlain by the Young Bay Mud, typically about 15 meters thick in the general area. The existing mole was constructed by placing about 10 meters of fills above the Young Bay Mud in

1936. A large area immediately next to the shoreline appears to be covered by surficial beach sands. Merritt Sand can be found underneath the YBM outside the paleochannels and the thickness of this deposit varies along the alignment with maximum thickness of about 6.0 m. The deposit is completely absent within the paleochannels. YBM and Merritt Sand deposits are underlain by stiff Old Bay Mud (OBM).

5.3 SHEAR WAVE VELOCITY

Shear wave velocities within the soil sediments and the bedrock were measured in the marine and on-land borings using the suspension logging method. The measured data showed that the shear wave velocity increased with depth. The variation of shear wave velocity with depth at each pier location from pier E2 through E16 is plotted in Plate 5-12 through Plate 5-26. Based on these measured velocities, idealized shear wave velocity profiles were developed for each location for the purpose of site response analysis. The idealized profiles are also shown in these Plates. It may be mentioned here that at each pier location the subsoil information for eastbound and westbound piers were combined and one set of site response analysis was performed at each pier location using the combined profile. Given the amount of scatter in the measured data, it is not justifiable to further refine the shear wave velocity profile to distinguish between eastbound and westbound.

5.4 MODULUS REDUCTION AND DAMPING CURVES

Dynamic properties of Young and Old Bay Muds were evaluated from the results of resonant column (RC), torsional shear (TC) and cyclic simple shear (CSS) tests performed on soil samples collected during the marine investigation program. A total of 10 specimens were tested. For a detailed discussion of the test procedure and interpretation of test results, the reader is referred to Phase I Marine Geotechnical Characterization report (Fugro-EMI, 1998).

The variation of shear modulus, G, with shear strain is given by normalized plots of G/G_{max} with shear strain where G_{max} is the initial small strain shear modulus. In Plates 5-27 and 5-28, normalized shear modulus, G/G_{max}, is plotted against logarithm of shear strain for YBM and OBM, respectively. Also shown in the Plates are the modulus reduction curves proposed by Idriss (1990) for Bay Mud. The measured G/G_{max} curves compare favorably with those proposed by Idriss up to about 0.3 percent shear strain. For larger shear strains the measured values fall slightly below Idriss relationship. The measured values are also compared with those proposed by Pyke et al. (1995) for reference strain, γ_r of 0.2, 0.3 and 0.4 percent. The reference strain, γ_r, is given by

$$\gamma_r = \frac{\tau_{max}}{G_{max}} \qquad (5.1)$$

in which τ_{max} is the maximum shear stress. The measured data generally fall between modulus reduction curves for 0.2 and 0.4 percent reference strain. In fact, it matches reasonably well with the curve corresponding to 0.3 percent strain.

The damping ratio, D, versus shear strain plots for YBM and OBM are shown in Plates 5-29 and 5-30, respectively. The measured values of D for the YBM tend to plot above the relationship proposed by Idriss (1990) at small strains, but the measured values plot below the proposed relationship at large strains. A comparison with Pyke et al. relationship shows that the measured values for YBM plot above the 0.2 to 0.4 percent curves developed by Pyke et al.

5.5 SITE RESPONSE ANALYSIS

5.5.1 YBI Structure

Franciscan rock outcrop can be found at the northeastern point of the Yerba Buena Island. The alluvial sands found elsewhere on the island are very competent and are typically underlain by the bedrock at a shallow depth (less than 40 meters). The effects of shallow sand deposits on the ground motion would not be significant, and therefore, no site response analysis was conducted for YBI portion of the structures. The rock motions developed for YBI is used directly for the structural analysis.

5.5.2 Suspension Bridge

The signature self-anchored suspension bridge has three supports: West Pier (W2), Main Pier (E1), and East Pier (E2). West Pier and Main Pier are founded on rock, whereas the East Pier is founded in a sequence of sediments similar to the Skyway Structure. No site response study was conducted for the West Pier and Main Pier, as the rock motions developed at these supports are directly applicable for structural analysis. However, detailed site response studies have been conducted at East Pier (E2) because the geologic conditions in the vicinity of Pier E2 present extreme changes in geometry and soil properties.

Wave propagation phenomena near Pier E2 can be influenced by basin effects, and the traditional one-dimensional site response approach may not be applicable for the SV wave propagation. However, the one-dimensional wave propagation would still be applicable for the SH wave where the particle velocity is polarized in the out-of-plane direction. Therefore, the ground motion in the longitudinal direction along the bridge alignment, was studied with a two-dimensional site response approach using the computer program QUAD4M (Hudson et al., 1994) because the propagation can be viewed as a SV wave problem. One-dimensional site response was used to compute the transverse component using the program SHAKE (Idriss and Sun, 1992), as it is considered a SH wave problem.

To investigate potential basin edge effects using two-dimensional site response, calibration studies were first conducted to gain confidence on the analysis procedure by making comparison between SHAKE run and QUAD4M run on a horizontally layered soil deposit. The comparison was found to be satisfactory. The results of the comparison, reported in various meetings with the peer review members, are not presented here.

After performing the comparison studies, true 2-D wave propagation, specific to the site condition at Pier E2, was studied. The initial results were presented and discussed among the ground motion team consisting of Caltrans personnel, members of the Peer Review Committee, and consultant seismologists. The discussion on boundary effects led to extension of the lateral boundaries of the finite element mesh; the final mesh is shown in Plate 5-31. As shown in the Plate, the bottom of 2-D mesh is at elevation –107 meters where input rock motions are prescribed, while the reference datum for the Skyway Structure is at elevation –95 meter for one-dimensional site response analyses. To be consistent with Skyway site response studies, the input rock was de-convoluted before using in the 2-D site response studies in order to eliminate additional travel time required to reach elevation –95 meters from elevation –107 meters.

Some representative results from the final run are presented in the Plate 5-32. We also conducted parallel one-dimensional site response analysis at Pier E2 for comparison. From the 2-D versus 1-D comparison, the two-dimensional site response calculations show higher shaking at long-periods (above 2-seconds) especially for the surficial Young Bay Mud deposit in the vicinity of the Pier E2. However, the seismic analysis of Pier E2 would eventually be based on 2-D site response for the longitudinal component.

The transverse free-field motions at Pier E2 were computed with one dimensional site response approach using the program, SHAKE. Soil layering for the 1-D SHAKE analysis was arranged such a way to provide free-field motions at the same elevations as those obtained from the 2-D QUAD4M analyses. These two sets of motions (longitudinal from QUAD4M analysis and transverse from SHAKE analysis) were used as depth-varying input motions for the total system.

5.5.3 Skyway Structure

Site response analyses for the skyway structure were performed in two stages. In the first stage, site response analyses were performed for four idealized soil profiles, A, B, C, and D mentioned in Section 5.1; the purpose was to develop ARS design criteria that was used to develop 65 percent structural design. In the second stage, pier specific soil profiles were developed at each pier location of the skyway structure and site response analyses were performed for each profile. The purpose of the second stage of site response analysis is to develop multiple support motions for time history analysis. All the site response analyses were performed using the computer program, SHAKE.

5.5.3.1 Site Response Analyses for ARS Design Criteria

When response spectrum analysis is conducted for a bridge frame consisting of several bents, it is inherently assumed that all support points are excited with a same input motion which forms the basis for the ARS curve. As a result, a single representative soil profile is needed for each bridge frame, which could consist of multiple bents. For the development of ARS design curves for the Skyway portion, four representative soil conditions denoted as profiles A to D

were considered. Site response analyses were first conducted for these profiles, which are interpreted to be generally representative of the stratigraphic conditions in the following areas:

Profile A: Western 1/3rd of Skyway Alignment, outside (south) of recent paleo-channel

Profile B: Western 1/3rd of Skyway Alignment, within flank of recent paleo-channel

Profile C: Eastern 2/3rd of Skyway Alignment, outside (south) of recent paleo-channel

Profile D: Eastern 2/3rd of Skyway Alignment, within flank of recent paleo-channel

Plates 5-33 shows a plan view of the skyway portion of the structure delineating different representative profile locations. Plate 5-34 shows Profiles A through D which have been idealized to be representative of the general area.

Site response analyses were conducted using both equivalent linear (or iterative linear) and nonlinear analysis methods for these representative soil profiles. The equivalent linear analyses were conducted using the computer program SHAKE91 (Idriss and Sun, 1992), re-compiled to enable computation of FFT up to 16382 points in the input acceleration history. The nonlinear analyses were conducted using the computer program TESS (TAGAsoft, 1998). The simplified nonlinear soil model used in TESS is based on the generic modulus reduction curve incorporating hysteretic behavior and is described by Pyke et al. (1993,1995). A detailed discussion on ARS design criteria based on these analyses is presented in Section 7.

5.5.3.2 Pier Specific Site Response Analyses

In addition to the site response analyses performed for four subsoil conditions (Profiles A through D) to develop ARS design curves, site response analyses at pier-specific location were also performed. The results of pier-specific site response analysis were used for multiple-support time history analysis of the bridge. Although at most pier location, there was no significant variation between eastbound and westbound soil profile, some judgment was applied to combine the two profiles where they were at variance. The typical soil layering scheme at each pier location from E03 through E16 is shown in Plates 5-35 through 5-48. Also shown in these Plates are soil properties used in the analyses, pile configuration, and pile node locations used in the kinematic interaction analyses. Detailed discussion on kinematic interaction analysis is presented in Section 8.

It is expected that most of the soil-pile interaction would take place within 10 pile diameters (approximately 24 m) from the ground surface. With that in view, the soil profile was discretized in 3.0-meter layers from the ground surface down to a depth of 24 meters and thereafter the layer thickness was increased to 6.0 meters. The soil deposit below the depth of 24 meters in most part of the alignment consists of fat clay of OBM/UAM deposit. However, some sand layers occur as a part of UAM deposit. If these sand layers were found to be less than 1 pile diameter thick they were not included in the idealized soil profile. Such omission would not have any significant effect on the ground response.

In all the analyses, the input rock motion was applied to the soil column as 'outcropping motion' at an elevation of El -95 meters within the Lower Alameda (LAA) formation. The LAA formation was adopted as the transmitting boundary instead of the Franciscan rock formation. The average shear wave velocity in the LAA is in the order of 460 m/s (1500 fps) which corresponds with average shear wave velocity of 1500 fps for top 30 meters of typical rock sites. The average shear wave velocity at the surface of sites that were used in developing attenuation relationships for ground motion on rock is about 305 m/s (1000 fps).

A number of SHAKE runs were performed for the Skyway piers (pier E3 through E16) using six sets of fault-normal and fault parallel motions at each pier. For each run, ground motions at different depths were extracted. These depth-varying motions were also used in the kinematic interaction analyses as described in Section 8 of this report where comparison plots between depth-varying ground motions and kinematic motions are presented.

5.5.4 Oakland Mole

Site response analysis for the Oakland Mole was performed for the development of ARS design curve for the Oakland shore structure including pile-supported slab. It is not expected that multiple support time history analysis involving incoherent motions would be performed for this portion of the bridge. However, separate site response studies using representative soil profiles were conducted for East Bound and West Bound bridges because of difference in grading elevations. The mudline for the West Bound bridge is around elevation –3 meters and the grade elevation for the existing fill that can be found along the East Bound bridge is at elevation +13 meters. A detailed discussion on ARS design criteria for the Oakland Mole is presented in Section 8.

Separate two dimensional site response analyses were conducted to address seismic slope stability for the geotechnical fill option. The Caltrans personnel undertook the design of embankment fill while Fugro-EMI provided analyses for seismic performance. The main objective of the 2D site response analyses is to compute seismic coefficient time histories of a potential failure mass subjected for the six rock motions. The seismic coefficient time histories were then used in Newmark's sliding analyses (Newmark, 1965) to estimate the permanent displacement of the slope. Only the fault parallel component of the ground motion was used in assessment of the permanent displacement.

Earth Mechanics FUGRO

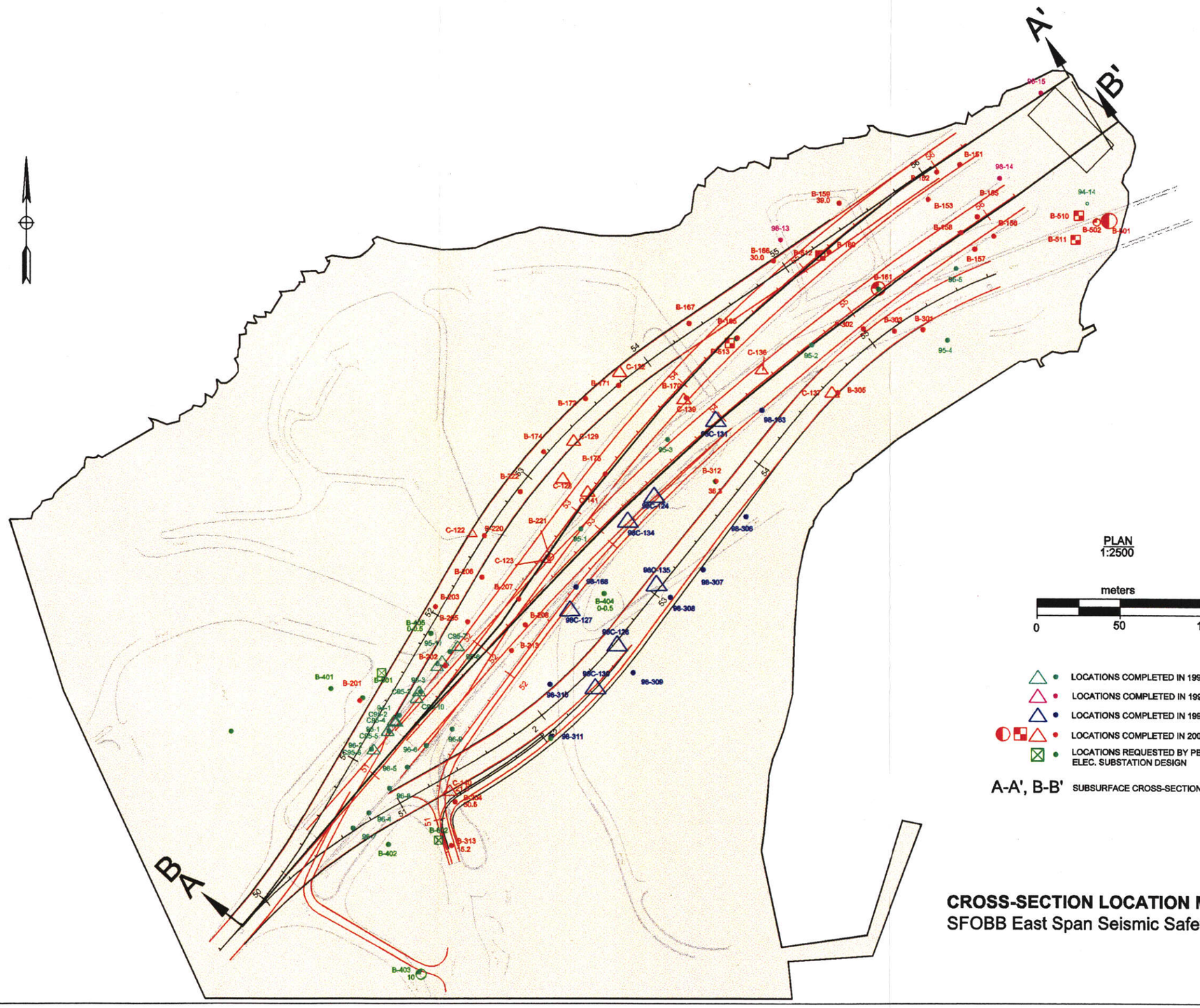

PLAN
1:2500

meters
0 50 100

- LOCATIONS COMPLETED IN 1994-1996 (PRE-EXISTING)
- LOCATIONS COMPLETED IN 1998 (PHASE 1)
- LOCATIONS COMPLETED IN 1998 (PHASE 2A)
- LOCATIONS COMPLETED IN 2000 (PHASE 2B)
- LOCATIONS REQUESTED BY PB FOR ROADWAY/ ELEC. SUBSTATION DESIGN

A-A', B-B' SUBSURFACE CROSS-SECTION LOCATION

CROSS-SECTION LOCATION MAP, YBI
SFOBB East Span Seismic Safety Project

PLATE 5-1

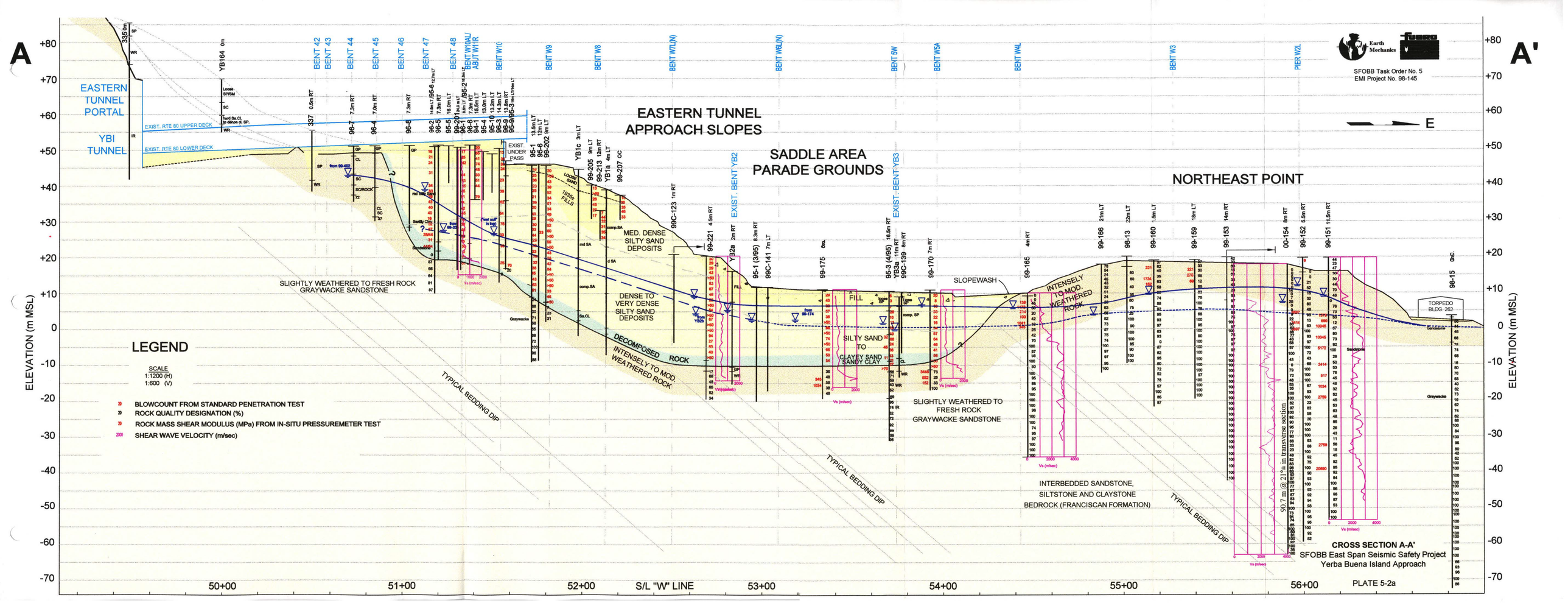
A
A'
EASTERN TUNNEL PORTAL
YBI TUNNEL
EXIST. RTE 80 UPPER DECK
EXIST. RTE 80 LOWER DECK
EASTERN TUNNEL APPROACH SLOPES
SADDLE AREA PARADE GROUNDS
NORTHEAST POINT
BENT 42
BENT 43
BENT 44
BENT 45
BENT 46
BENT 47
BENT 48
BENT W10
BENT W9
BENT W8
BENT W7L(N)
BENT W6L(N)
BENT W5W
BENT W5A
BENT W4L
BENT W3
PIER W2L
EXIST. BENT YB2
EXIST. BENT YB3
SLIGHTLY WEATHERED TO FRESH ROCK GRAYWACKE SANDSTONE
MED. DENSE SILTY SAND DEPOSITS
DENSE TO VERY DENSE SILTY SAND DEPOSITS
DECOMPOSED ROCK
INTENSELY TO MOD. WEATHERED ROCK
SLOPEWASH
FILL
SILTY SAND TO CLAYEY SAND SANDY CLAY
SLIGHTLY WEATHERED TO FRESH ROCK GRAYWACKE SANDSTONE
INTENSELY TO MOD. WEATHERED ROCK
INTERBEDDED SANDSTONE, SILTSTONE AND CLAYSTONE BEDROCK (FRANCISCAN FORMATION)
TYPICAL BEDDING DIP
TYPICAL BEDDING DIP
TYPICAL BEDDING DIP
90.7 m @ 21°± in transverse section
TORPEDO BLDG. 262
LEGEND
SCALE
1:1200 (H)
1:600 (V)
BLOWCOUNT FROM STANDARD PENETRATION TEST
ROCK QUALITY DESIGNATION (%)
ROCK MASS SHEAR MODULUS (MPa) FROM IN-SITU PRESSUREMETER TEST
SHEAR WAVE VELOCITY (m/sec)
ELEVATION (m MSL)
ELEVATION (m MSL)
+80
+70
+60
+50
+40
+30
+20
+10
0
-10
-20
-30
-40
-50
-60
-70
50+00
51+00
52+00
S/L "W" LINE
53+00
54+00
55+00
56+00
Earth Mechanics
SFOBB Task Order No. 5
EMI Project No. 98-145
E
CROSS SECTION A-A'
SFOBB East Span Seismic Safety Project
Yerba Buena Island Approach
PLATE 5-2a

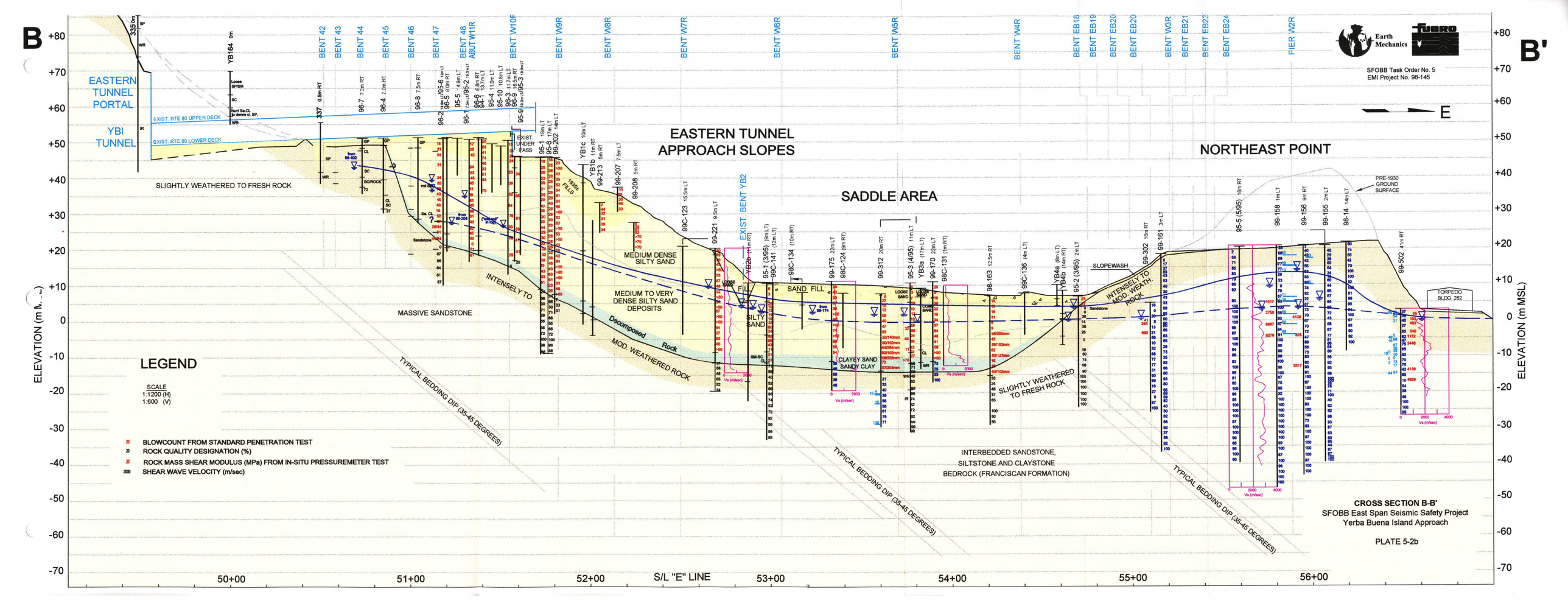

CROSS SECTION B-B'
SFOBB East Span Seismic Safety Project
Yerba Buena Island Approach

PLATE 5-2b

Earth Mechanics

FUGRO

SKYWAY

MATCHLINE

MAIN SPAN AREA

E1 (PYLON)

E2 (EAST PIER)

WEST PIER

A1

A1'A2

A2'A3

E3 E4 E5 E6 E7 E8 E9

98-9 98-8 98-7 98-6 98-3 98-10 98-20

98-50 98-40 98-28 98-29 98-41 98-30 98-31 98-32 98-19 98-27 98-25 98-26 98-82 98-81

48-90 48-89 48-88

94-4 94-7 94-3 94-11 94-12 96-5 96-4 96-3 96-2 96-1 95-19 95-18 94-9 95-20

N W E S

SCALE: 1:5000

0 100 m 200 m

LEGEND

- 1998 Phase 2 Boring Locations
- 1998 Phase 1 Boring Locations
- Pre-1998 Boring Locations
- San Francisco-Oakland Bay Bridge
- Proposed N6 (Revision 4) Alignment (Approximate)
- Bathymetry (meters), MSL
- Subsurface Cross-Section Locations

CROSS SECTION LOCATION MAP

SFOBB East Span Seismic Safety Project

PLATE 5-3

/bones/baymetric/maps/reptloc.aml, emirept1, 10/05/99 CBD, 98-42-0054

Earth Mechanics

FUGRO

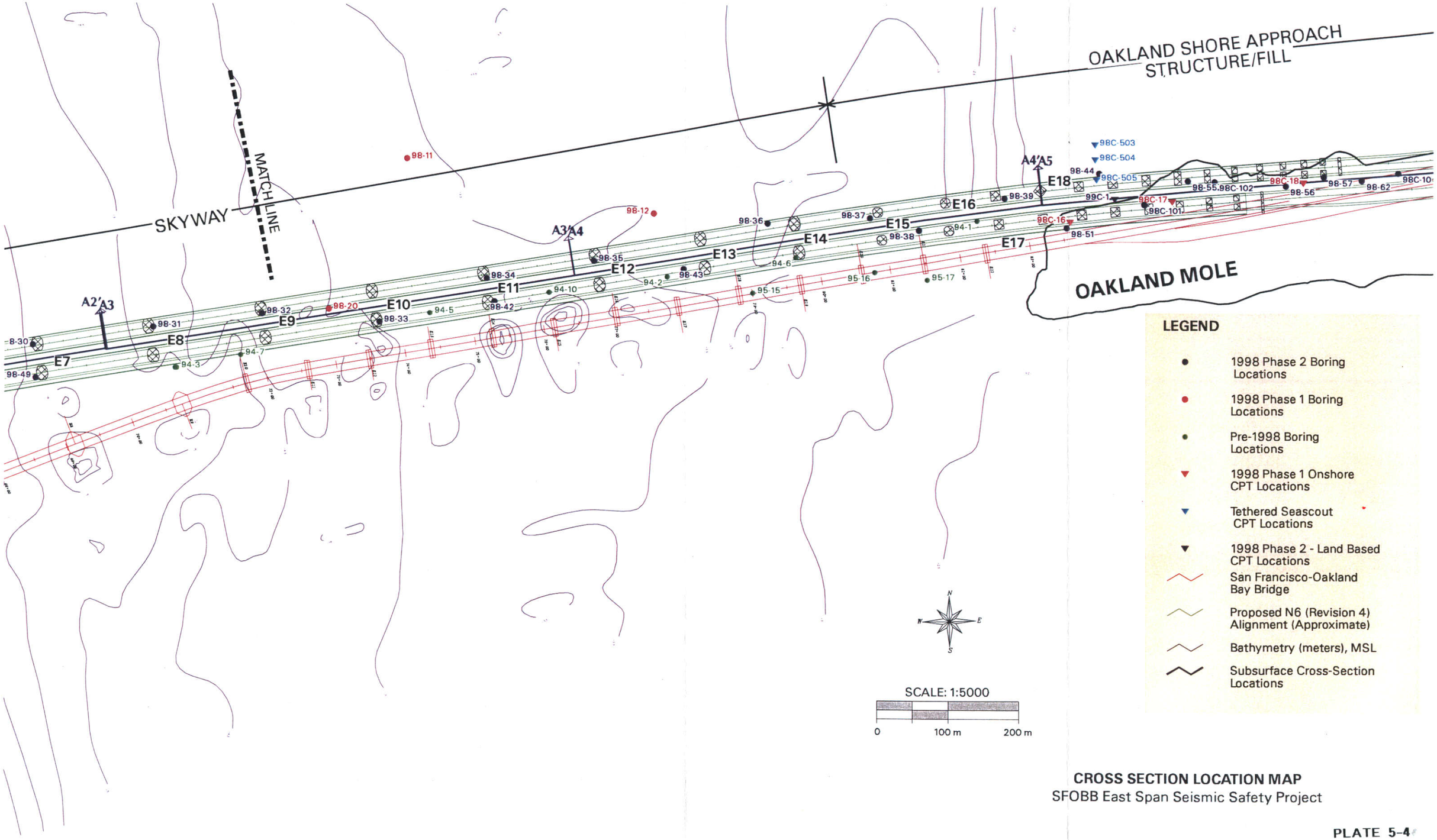

LEGEND

- 1998 Phase 2 Boring Locations
- 1998 Phase 1 Boring Locations
- Pre-1998 Boring Locations
- 1998 Phase 1 Onshore CPT Locations
- Tethered Seascout CPT Locations
- 1998 Phase 2 - Land Based CPT Locations
- San Francisco-Oakland Bay Bridge
- Proposed N6 (Revision 4) Alignment (Approximate)
- Bathymetry (meters), MSL
- Subsurface Cross-Section Locations

N
W
E
S

SCALE: 1:5000

0 100 m 200 m

/bones/baymetric/maps/reptloc.aml, emirept2, 10/05/99 CBD, 98-42-0054

CROSS SECTION LOCATION MAP

SFOBB East Span Seismic Safety Project

PLATE 5-4

Earth Mechanics

FUGRO

A1

S55W

98-21, 5 m North

98-2, 3 m South

B-B'

Main Pylon

98-24, 1 m South

98-5, 9 m South

98-6, 43 m North

E-E'

98-7, 37 m South

98-25, 24 m North

Pier E2

F-F'

S60W Inflection N55E

S68W Inflection N60E

98-27, 25 m South

Pier E3

A1'

N68E

Elevation, meters

0
-10
-20
-30
-40
-50
-60
-70
-80
-90
-100
-110
-120
-130
-140
-150
-160
-170

Elevation, feet

0
-50
-100
-150
-200
-250
-300
-350
-400
-450
-500
-550

MERRITT-POSEY-SAN ANTONIO SEQUENCE

VERY STIFF TO HARD CLAY WITH DENSE SAND LAYERS

YOUNG BAY MUD

DENSE TO VERY DENSE SAND WITH STIFF TO VERY STIFF CLAY LAYERS

VERY SOFT TO FIRM CLAY

OLD BAY MUD/UPPER ALAMEDA SEDIMENTS

UPPER ALAMEDA MARINE PALEOCHANNEL SAND

DENSE TO VERY DENSE SAND WITH HARD CLAY LAYERS

LOWER ALAMEDA ALLUVIAL SEDIMENTS

LAA-CLAY CAP

LAA-SAND

FRANCISCAN FORMATION BEDROCK

0 750 1500 2250
Velocity (m/s)

GENERAL NOTES:

1) Stratigraphic contacts are approximate and are interpreted from lithology in borings, CPT soundings, and geologic structure imaged by geophysical survey. Conditions vary both along and perpendicular to the alignment.

2) Strata descriptions are generalized. Individual logs of borings and CPT soundings should be consulted for details.

3) Refer to Key to Cross Sections (Plate 4.6) for details of data plotted on cross-sections. Note that lithologies for pre-1998 boring logs are in some instances modified from those shown on Caltrans' Log of Test Boring Sheets. Modifications were made based on subsequent laboratory results and extrapolation from adjacent 1998 borings.

4) The CPT lithologies for onshore CPT soundings are based on the empirical correlation between tip resistance and friction ratio (Robertson and Campanella, 1984) shown on Plate 4.6.

10m

0 20m

/bones/baymetric/strat/sectall.aml, /bones/baymetric/strat/colra1ps.map, 09/04/99 CBD

SUBSURFACE CROSS SECTION A1-A1'
With P- and S-Wave Velocity
SFOBB East Span Seismic Safety Project

PLATE 5-5

Earth Mechanics

FUGRO

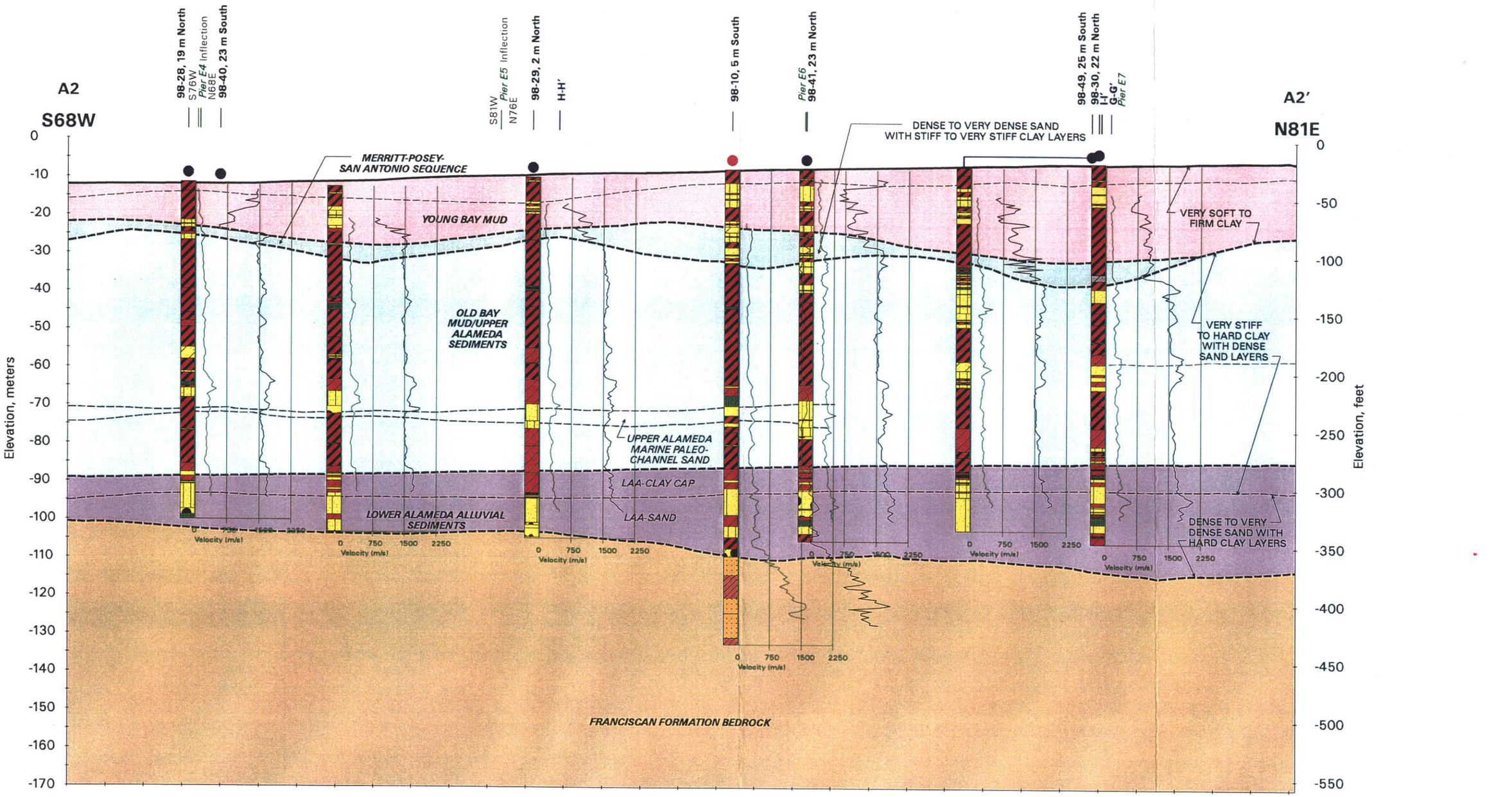

GENERAL NOTES:

1) Stratigraphic contacts are approximate and are interpreted from lithology in borings, CPT soundings, and geologic structure imaged by geophysical survey. Conditions vary both along and perpendicular to the alignment.

2) Strata descriptions are generalized. Individual logs of borings and CPT soundings should be consulted for details.

3) Refer to Key to Cross Sections (Plate 4.6) for details of data plotted on cross-sections. Note that lithologies for pre-1998 boring logs are in some instances modified from those shown on Caltrans' Log of Test Boring Sheets. Modifications were made based on subsequent laboratory results and extrapolation from adjacent 1998 borings.

4) The CPT lithologies for onshore CPT soundings are based on the empirical correlation between tip resistance and friction ratio (Robertson and Campanella, 1984) shown on Plate 4.6.

10m
0 20m

/bones/baymetric/strat/sectall.aml, /bones/baymetric/strat/colra2ps.map, 09/04/99 CBD

SUBSURFACE CROSS SECTION A2-A2′
With P- and S-Wave Velocity
SFOBB East Span Seismic Safety Project

PLATE 5-6

Earth Mechanics | FUGRO

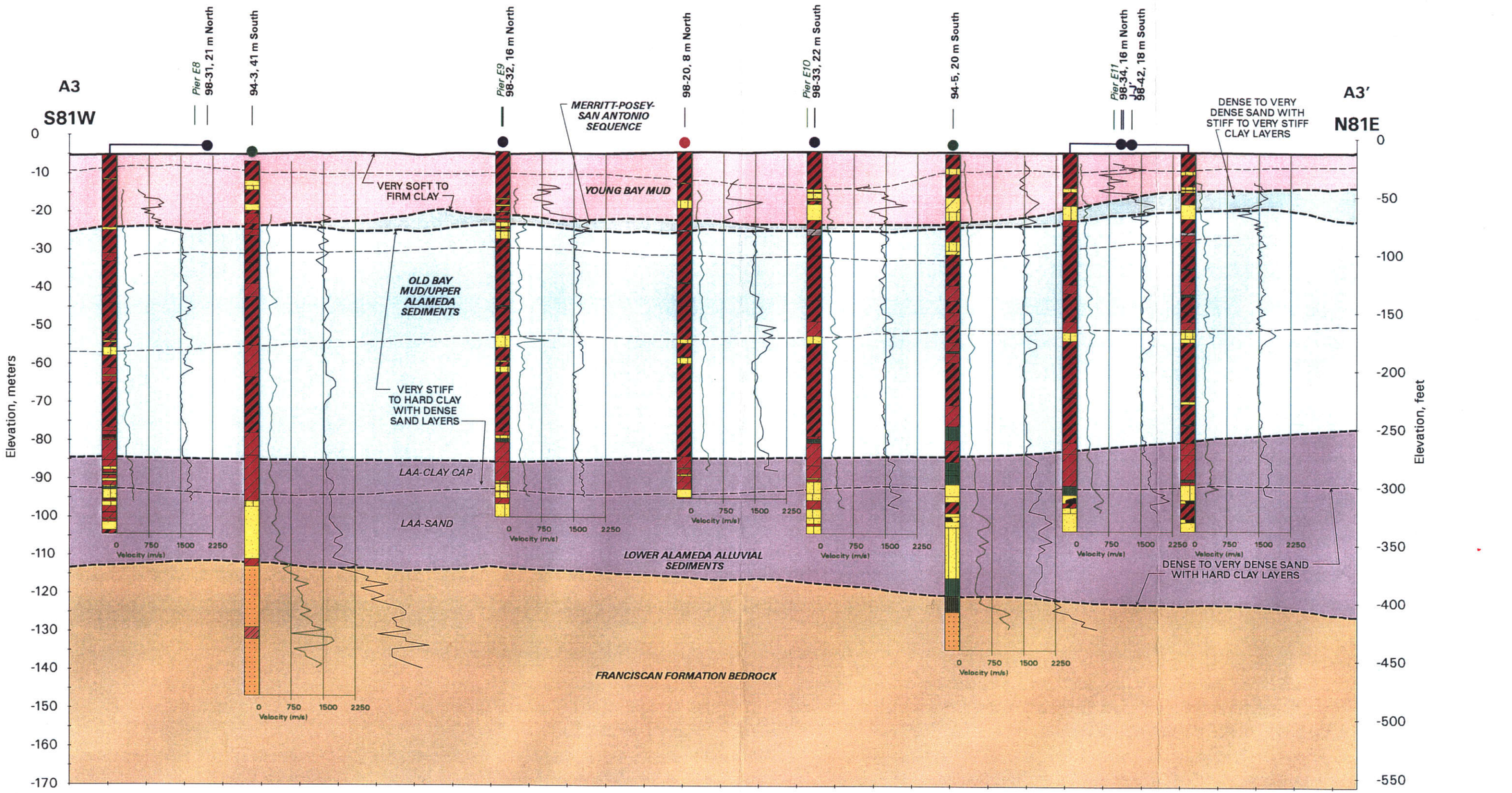

GENERAL NOTES:

1) Stratigraphic contacts are approximate and are interpreted from lithology in borings, CPT soundings, and geologic structure imaged by geophysical survey. Conditions vary both along and perpendicular to the alignment.

2) Strata descriptions are generalized. Individual logs of borings and CPT soundings should be consulted for details.

3) Refer to Key to Cross Sections (Plate 4.6) for details of data plotted on cross-sections. Note that lithologies for pre-1998 boring logs are in some instances modified from those shown on Caltrans' Log of Test Boring Sheets. Modifications were made based on subsequent laboratory results and extrapolation from adjacent 1998 borings.

4) The CPT lithologies for onshore CPT soundings are based on the empirical correlation between tip resistance and friction ratio (Robertson and Campanella, 1984) shown on Plate 4.6.

10m
0 20m

/bones/baymetric/strat/sectall.aml, /bones/baymetric/strat/colra3ps.map, 09/04/99 CBD

SUBSURFACE CROSS SECTION A3-A3'
With P- and S-Wave Velocity
SFOBB East Span Seismic Safety Project

PLATE 5-7

Earth Mechanics

FUGRO

A4

S81W

98-35, 16 m North
Pier E12

MERRITT-POSEY-SAN ANTONIO SEQUENCE

98-12, 69 m North

K-K'

Pier E13

98-36, 29 m North

Pier E14

DENSE TO VERY DENSE SAND WITH STIFF TO VERY STIFF CLAY LAYERS

98-37, 15 m North

Pier E15

98-38, 13 m South

S82W

Inflection

N81E

Pier E16

94-1, 11 m South

Pier E17

98-39, 16 m North

Pier E18

A4'

N82E

YOUNG BAY MUD

VERY SOFT TO FIRM CLAY

OLD BAY MUD/UPPER ALAMEDA SEDIMENTS

VERY STIFF TO HARD CLAY WITH DENSE SAND LAYERS

LAA-CLAY CAP

LOWER ALAMEDA ALLUVIAL SEDIMENTS

LAA-SAND

DENSE TO VERY DENSE SAND WITH HARD CLAY LAYERS

FRANCISCAN FORMATION BEDROCK

Velocity (m/s) 0 750 1500 2250

Elevation, meters

0 -10 -20 -30 -40 -50 -60 -70 -80 -90 -100 -110 -120 -130 -140 -150 -160 -170

Elevation, feet

0 -50 -100 -150 -200 -250 -300 -350 -400 -450 -500 -550

GENERAL NOTES:

1) Stratigraphic contacts are approximate and are interpreted from lithology in borings, CPT soundings, and geologic structure imaged by geophysical survey. Conditions vary both along and perpendicular to the alignment.

2) Strata descriptions are generalized. Individual logs of borings and CPT soundings should be consulted for details.

3) Refer to Key to Cross Sections (Plate 4.6) for details of data plotted on cross-sections. Note that lithologies for pre-1998 boring logs are in some instances modified from those shown on Caltrans' Log of Test Boring Sheets. Modifications were made based on subsequent laboratory results and extrapolation from adjacent 1998 borings.

4) The CPT lithologies for onshore CPT soundings are based on the empirical correlation between tip resistance and friction ratio (Robertson and Campanella, 1984) shown on Plate 4.6.

10m

0 20m

/bones/baymetric/strat/sectall.aml, /bones/baymetric/strat/colra4ps.map, 09/04/99 CBD

SUBSURFACE CROSS SECTION A4-A4'
With P- and S-Wave Velocity
SFOBB East Span Seismic Safety Project

PLATE 5-8

Earth Mechanics

FUGRO

A5

S85W

B-3, 20 m South

Pier E19

98-44, 37 m North

L-L'

Pier E20

98C-101, 13 m South

Pier E21

98C-17, 12 m South

Pier E22

S85W Inflection N85E

98C-102, 11 m North

Pier E23

MERRITT-POSEY SAN ANTONIO SEQUENCE

Pier E24

Pier E25

Pier E26

98C-18, 1 m South

Pier E27

98-52, 6 m North

Pier E29

98C-109, 47 m South

S85W Inflection N85E

98-59, 9 m North

S83W Inflection N85E

A5'

N83E

YOUNG BAY MUD

VERY SOFT TO FIRM CLAY

DENSE TO VERY DENSE SAND AND STIFF TO VERY STIFF CLAY LAYERS

OLD BAY MUD AND UPPER ALAMEDA SEDIMENTS

VERY STIFF TO HARD CLAY WITH DENSE SAND LAYERS

LOWER ALAMEDA ALLUVIAL SEDIMENTS

DENSE TO VERY DENSE SAND WITH HARD CLAY LAYERS

FRANCISCAN FORMATION

Tip Resistance (MPa) 20 10 0

Velocity (m/s) 0 750 1500 2250

Elevation, meters: 0, -10, -20, -30, -40, -50, -60, -70, -80, -90, -100, -110, -120, -130, -140, -150, -160, -170

Elevation, feet: 0, -50, -100, -150, -200, -250, -300, -350, -400, -450, -500, -550

GENERAL NOTES:

1) Stratigraphic contacts are approximate and are interpreted from lithology in borings, CPT soundings, and geologic structure imaged by geophysical survey. Conditions vary both along and perpendicular to the alignment.

2) Strata descriptions are generalized. Individual logs of borings and CPT soundings should be consulted for details.

3) Refer to Key to Cross Sections (Plate 4.6) for details of data plotted on cross-sections. Note that lithologies for pre-1998 boring logs are in some instances modified from those shown on Caltrans' Log of Test Boring Sheets. Modifications were made based on subsequent laboratory results and extrapolation from adjacent 1998 borings.

4) The CPT lithologies for onshore CPT soundings are based on the empirical correlation between tip resistance and friction ratio (Robertson and Campanella, 1984) shown on Plate 4.6.

10m

0 20m

/bones/baymetric/strat/sectall.aml, /bones/baymetric/strat/colra5ps.map, 09/04/99 CBD

SUBSURFACE CROSS SECTION A5-A5'
With P- and S-Wave Velocity
SFOBB East Span Seismic Safety Project

PLATE 5-9

Earth Mechanics FUGRO

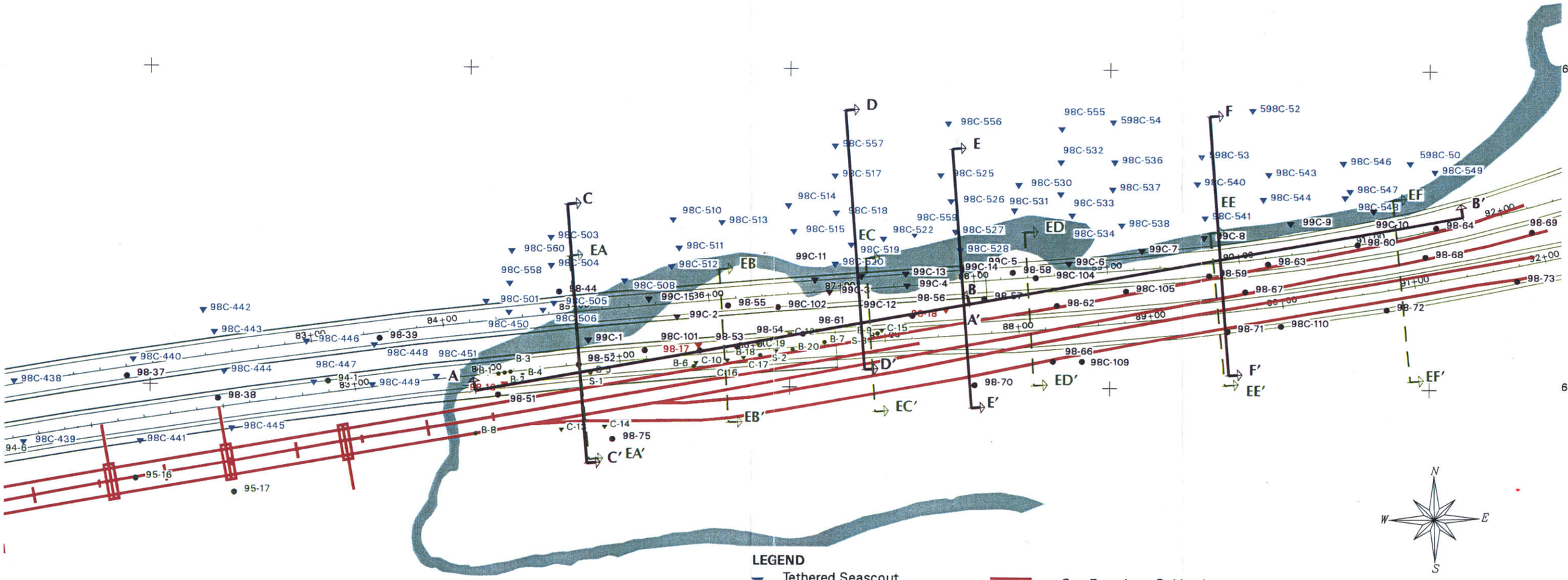

Scale: 1:3000

0 60m 120m

LEGEND

- Tethered Seascout CPT Locations
- 1998 Phase 2 - Land Based CPT Locations
- 1998 Phase 2 Boring Locations
- 1998 Phase 1 CPT Locations
- Pre-1998 Borings
- San Francisco-Oakland Bay Bridge
- Proposed N6 (Revision 4) Alignment (Approximate)
- Subsurface Cross-Section Locations
- Engineering Cross-Section Locations

CROSS-SECTION LOCATION MAP
Oakland Shore Approach
SFOBB East Span Seismic Safety Proje

PLATE 5-10

SFOBB Task Order No. 5
Project No. 98-42-0058

Earth Mechanics FUGRO

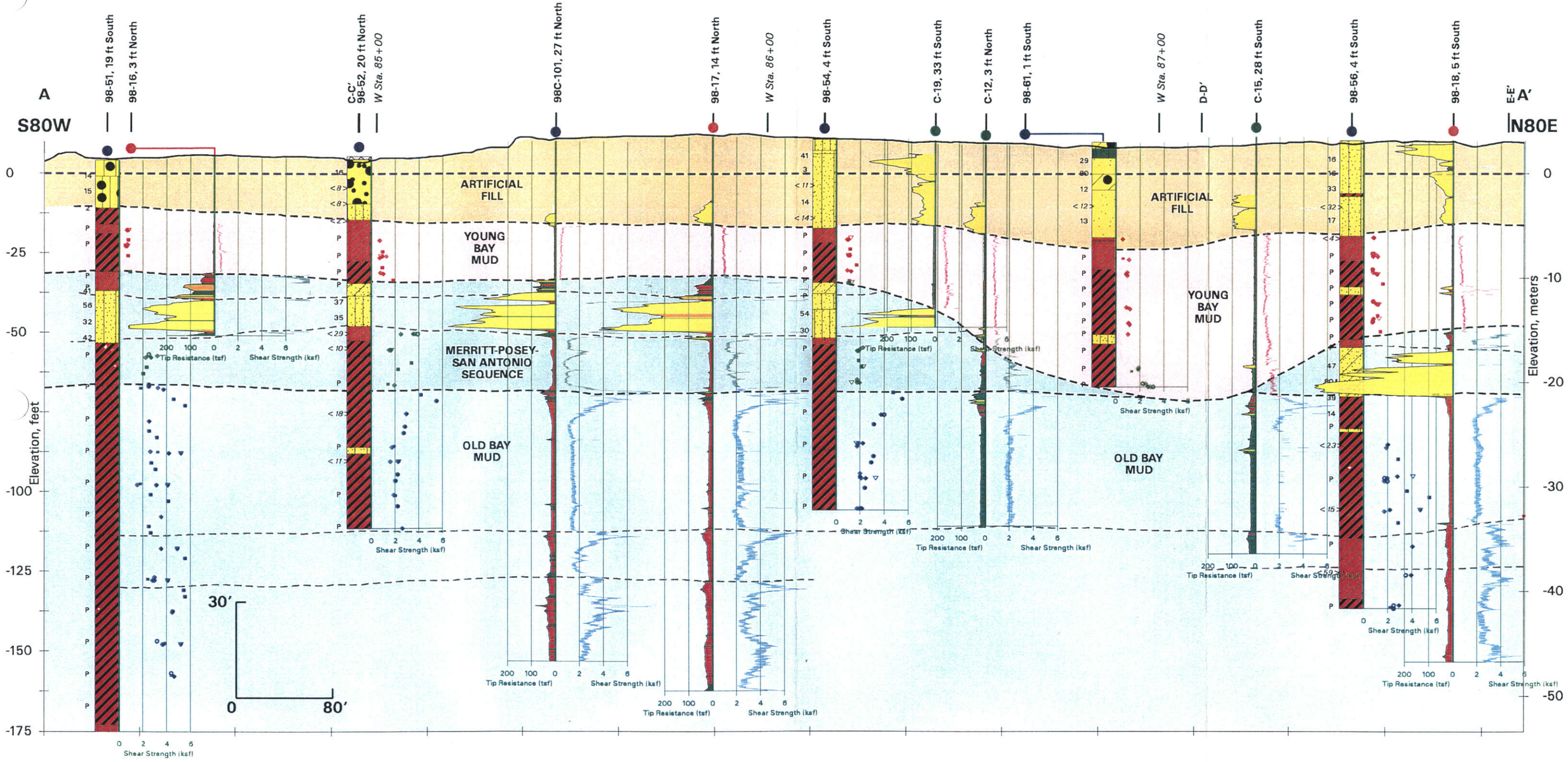

GENERAL NOTES:

1) Stratigraphic contacts are approximate and are interpreted from lithology in borings and CPT soundings. Conditions vary both along and perpendicular to the cross section.

2) Strata descriptions are generalized. Individual logs of borings and CPT soundings should be consulted for details.

3) Refer to Key to Cross Sections (Plate 4.6) for details of data plotted on cross-sections. Note that lithologies for pre-1998 boring and CPT logs are as shown on Caltrans' Log of Test Boring Sheets.

4) The CPT lithologies are based on the empirical correlation between tip resistance and friction ratio (Robertson and Campanella, 1984) shown on Plate 4.6.

UNDRAINED SHEAR STRENGTH LEGEND

- ▲ Unconsolidated Undrained (UU)
- △ Unconfined Compression (UC)
- ○ Pocket Penetrometer (PP)
- ◆ Torvane (TV)
- ◆ Miniature Vane (MV)
- ■ Remote Vane (RV)
- ▽ Fall Cone (FC)

SUBSURFACE CROSS SECTION A-A'
With Undrained Shear Strength
SFOBB East Span Seismic Safety Project

PLATE 5-11a

/bones/bay/explcovs/sectall.aml, fig5-11a.map, 03/20/99; 02/16/01 CBD

SFOBB Task Order No. 5
Project No. 98-42-0058

Earth Mechanics FUGRO

B

S80W

W Sta. 88+00

98-57, 7 ft North

98-58, 59 ft North

98C-104, 36 ft North

98-62, 41 ft South

W Sta. 89+00

98C-105, 36 ft South

98-59, 34 ft South

F-F'

W Sta. 90+00

98-67, 89 ft South

98-63, 31 ft South

98-60, 22 ft South

W Sta. 91+00

98-68, 81 ft South

98-64, 14 ft South

B'

N80E

ARTIFICIAL FILL

YOUNG BAY MUD

MERRITT-POSEY-SAN ANTONIO SEQUENCE

OLD BAY MUD

Elevation, feet

Elevation, meters

0
-25
-50
-100
-125
-150
-175

0
-10
-20
-30
-40
-50

Tip Resistance (tsf) Shear Strength (ksf)

Shear Strength (ksf)

30'

0 80'

GENERAL NOTES:

1) Stratigraphic contacts are approximate and are interpreted from lithology in borings and CPT soundings. Conditions vary both along and perpendicular to the cross section.

2) Strata descriptions are generalized. Individual logs of borings and CPT soundings should be consulted for details.

3) Refer to Key to Cross Sections (Plate 4.6) for details of data plotted on cross-sections. Note that lithologies for pre-1998 boring and CPT logs are as shown on Caltrans' Log of Test Boring Sheets.

4) The CPT lithologies are based on the empirical correlation between tip resistance and friction ratio (Robertson and Campanella, 1984) shown on Plate 4.6.

UNDRAINED SHEAR STRENGTH LEGEND

- ▲ Unconsolidated Undrained (UU)
- △ Unconfined Compression (UC)
- ○ Pocket Penetrometer (PP)
- ◆ Torvane (TV)
- ◆ Miniature Vane (MV)
- ■ Remote Vane (RV)
- ▽ Fall Cone (FC)

SUBSURFACE CROSS SECTION B-B'
With Undrained Shear Strength
SFOBB East Span Seismic Safety Project

PLATE 5-11b

/bones/bay/explcovs/sectall.aml, fig5-11b.map, 03/20/99; 02/16/01 CBD

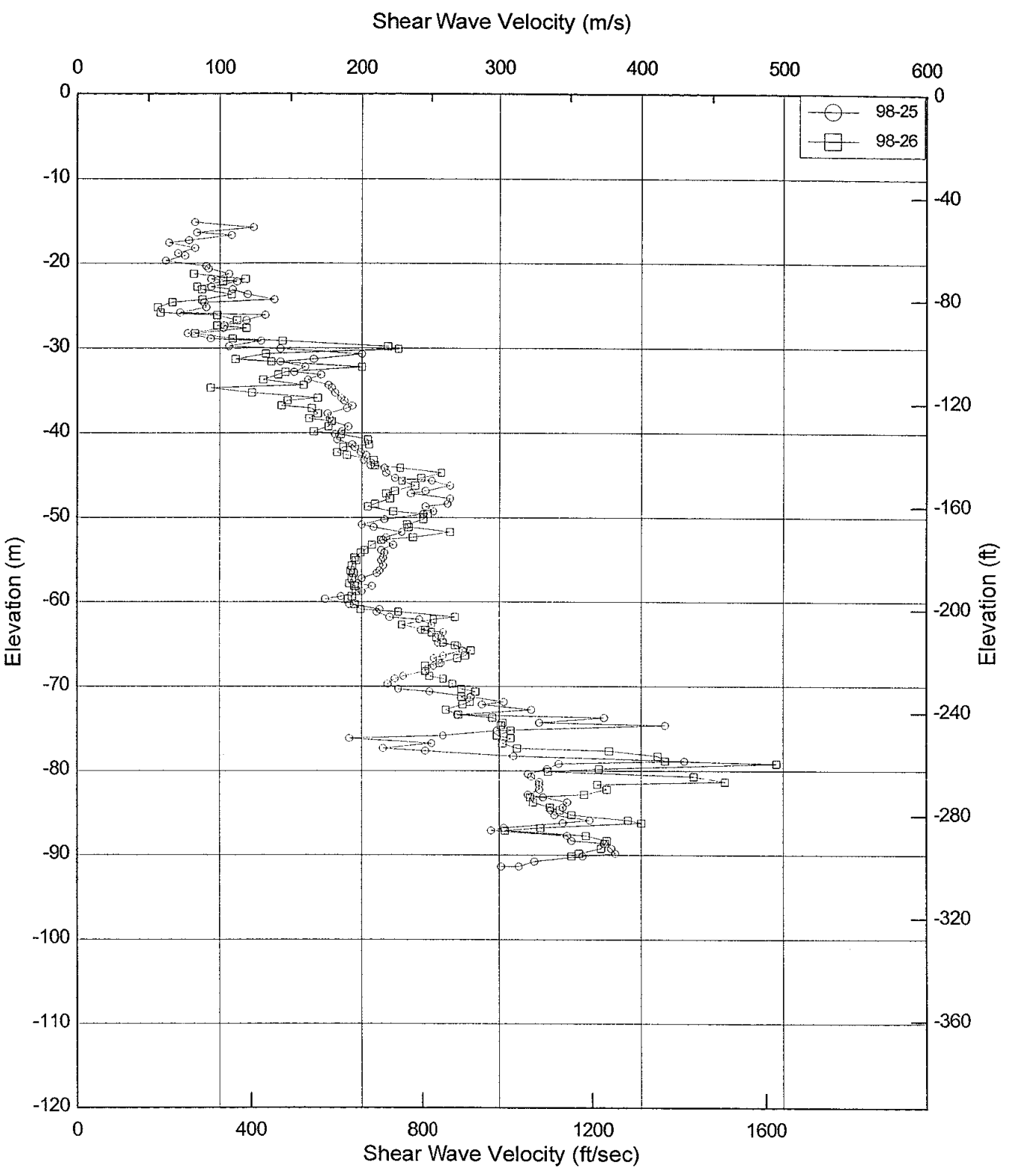

SHEAR WAVE VELOCITY PROFILE
Pier E02
SFOBB East Span Seismic Safety Project

PLATE 5-12

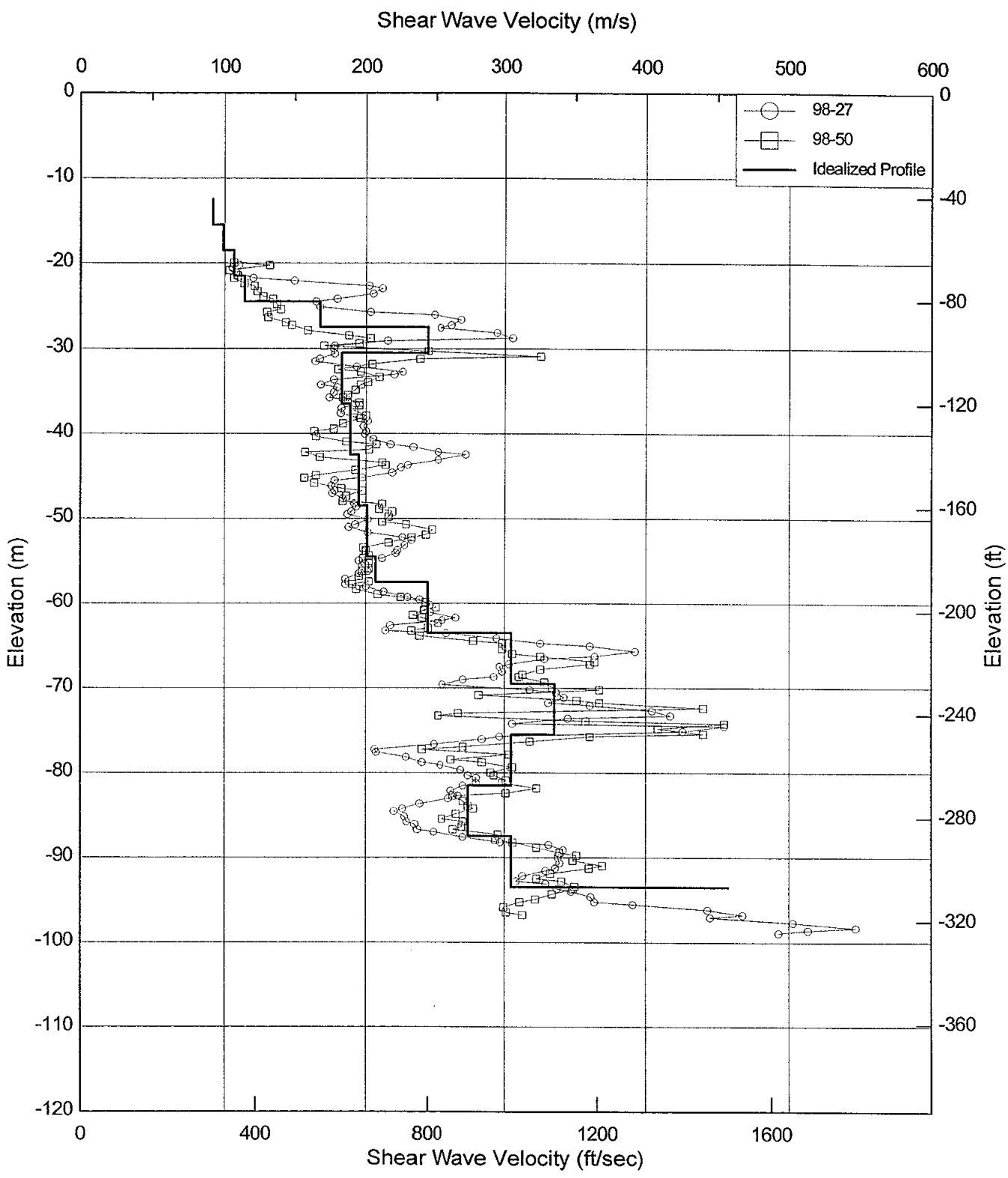

SHEAR WAVE VELOCITY PROFILE
Pier E03
SFOBB East Span Seismic Safety Project

PLATE 5-13

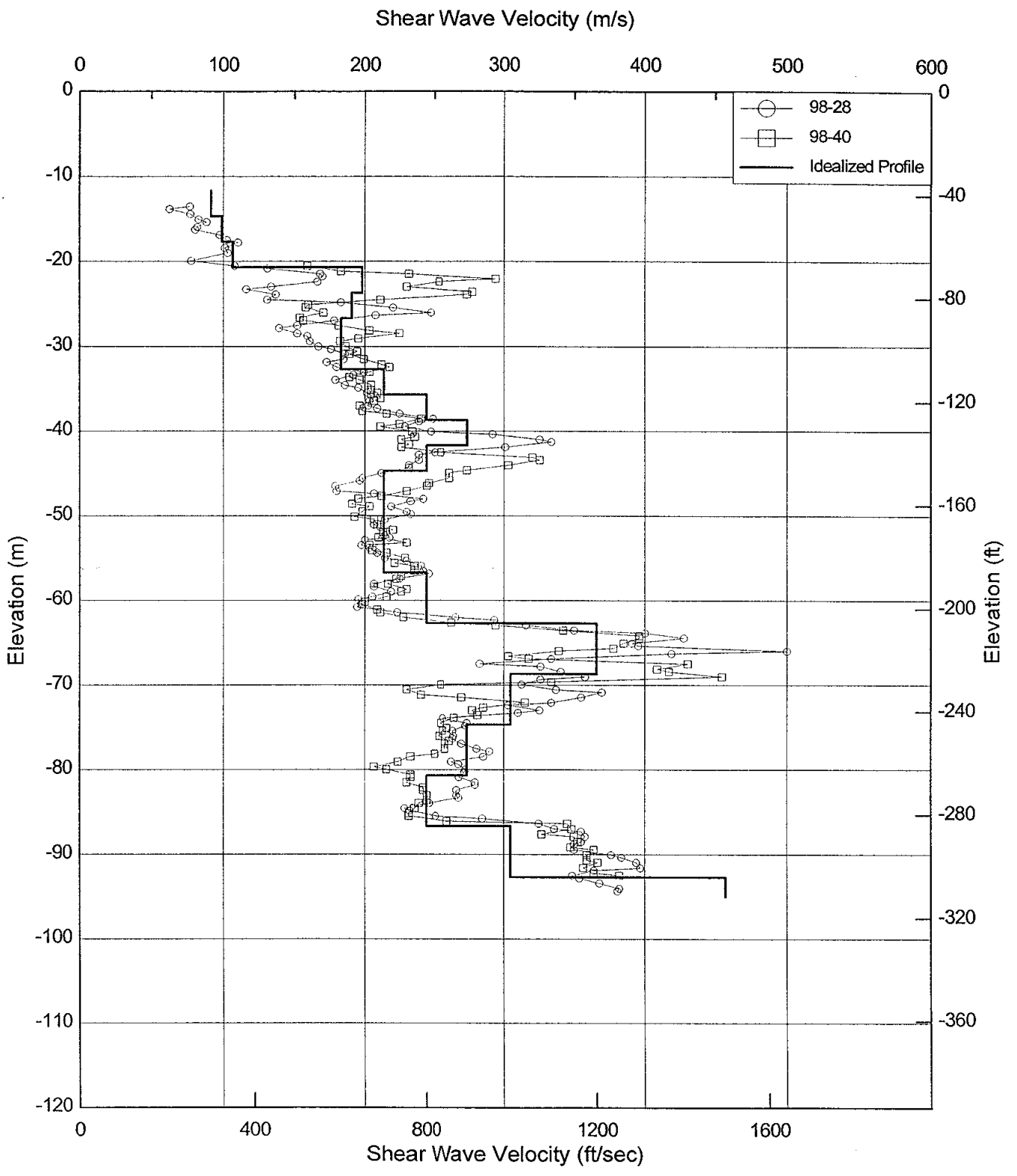

SHEAR WAVE VELOCITY PROFILE
Pier E04
SFOBB East Span Seismic Safety Project

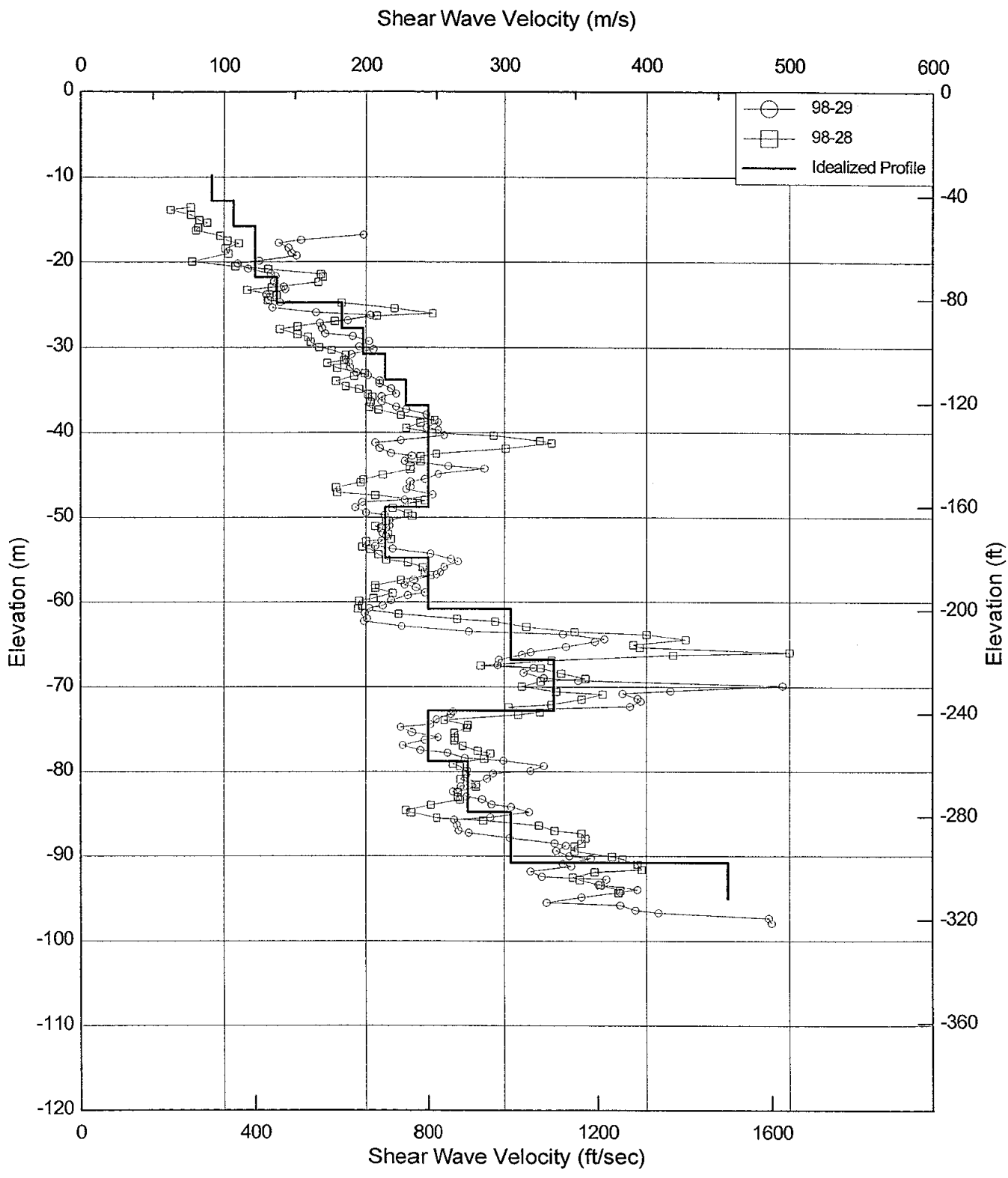

SHEAR WAVE VELOCITY PROFILE
Pier E05
SFOBB East Span Seismic Safety Project

PLATE 5-15

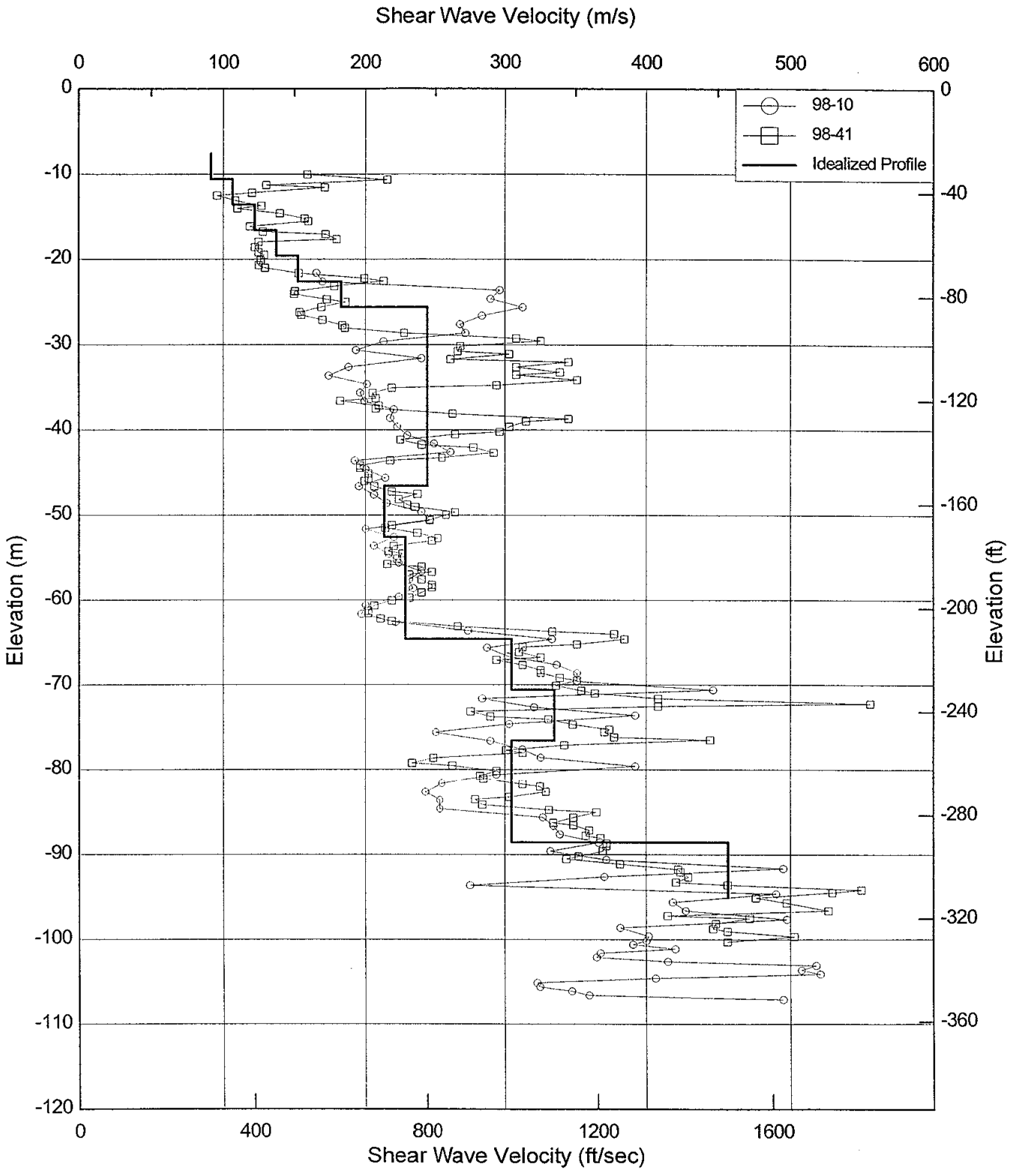

SHEAR WAVE VELOCITY PROFILE
Pier E06
SFOBB East Span Seismic Safety Project

PLATE 5-16

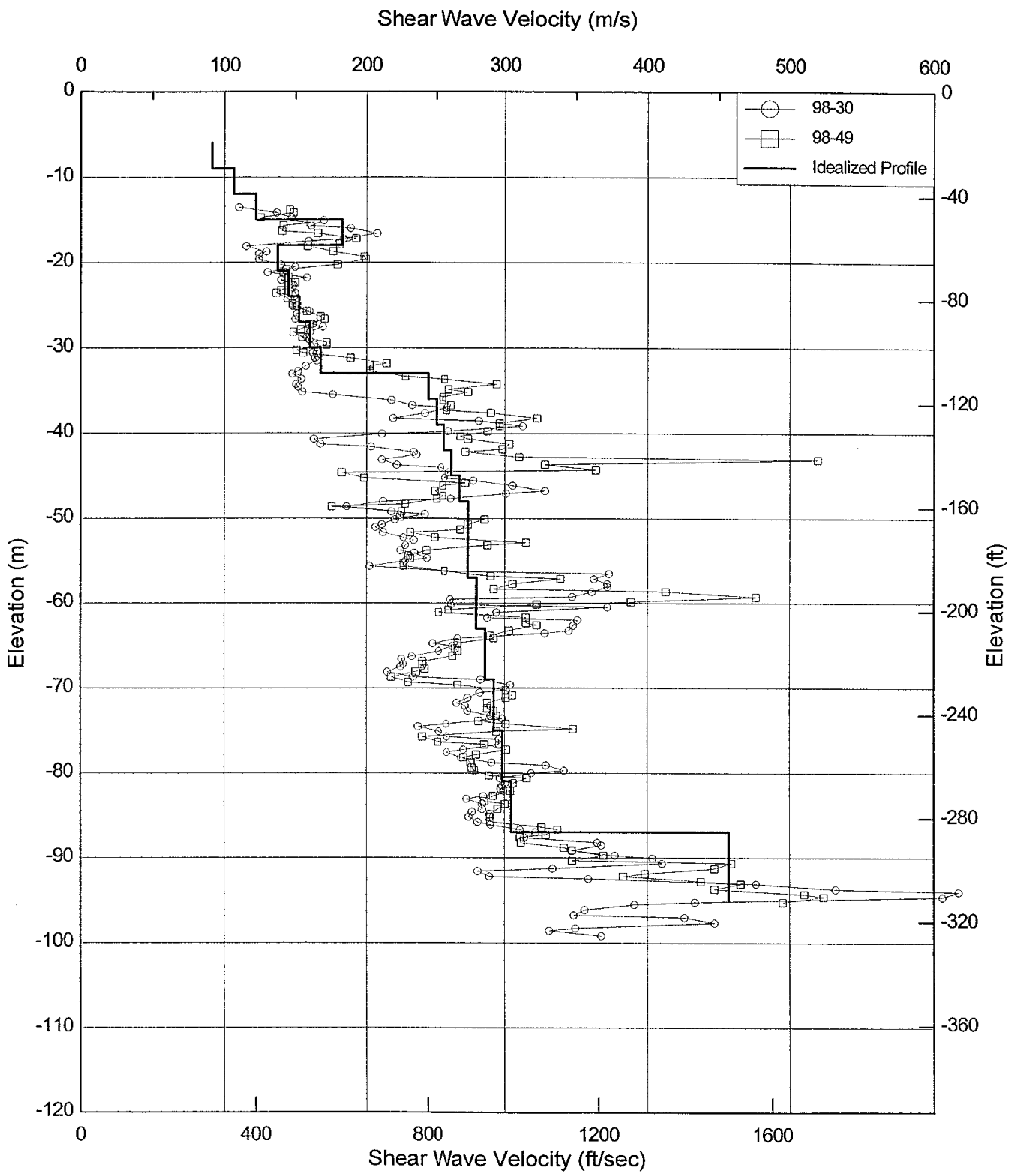

SHEAR WAVE VELOCITY PROFILE
Pier E07
SFOBB East Span Seismic Safety Project

PLATE 5-17

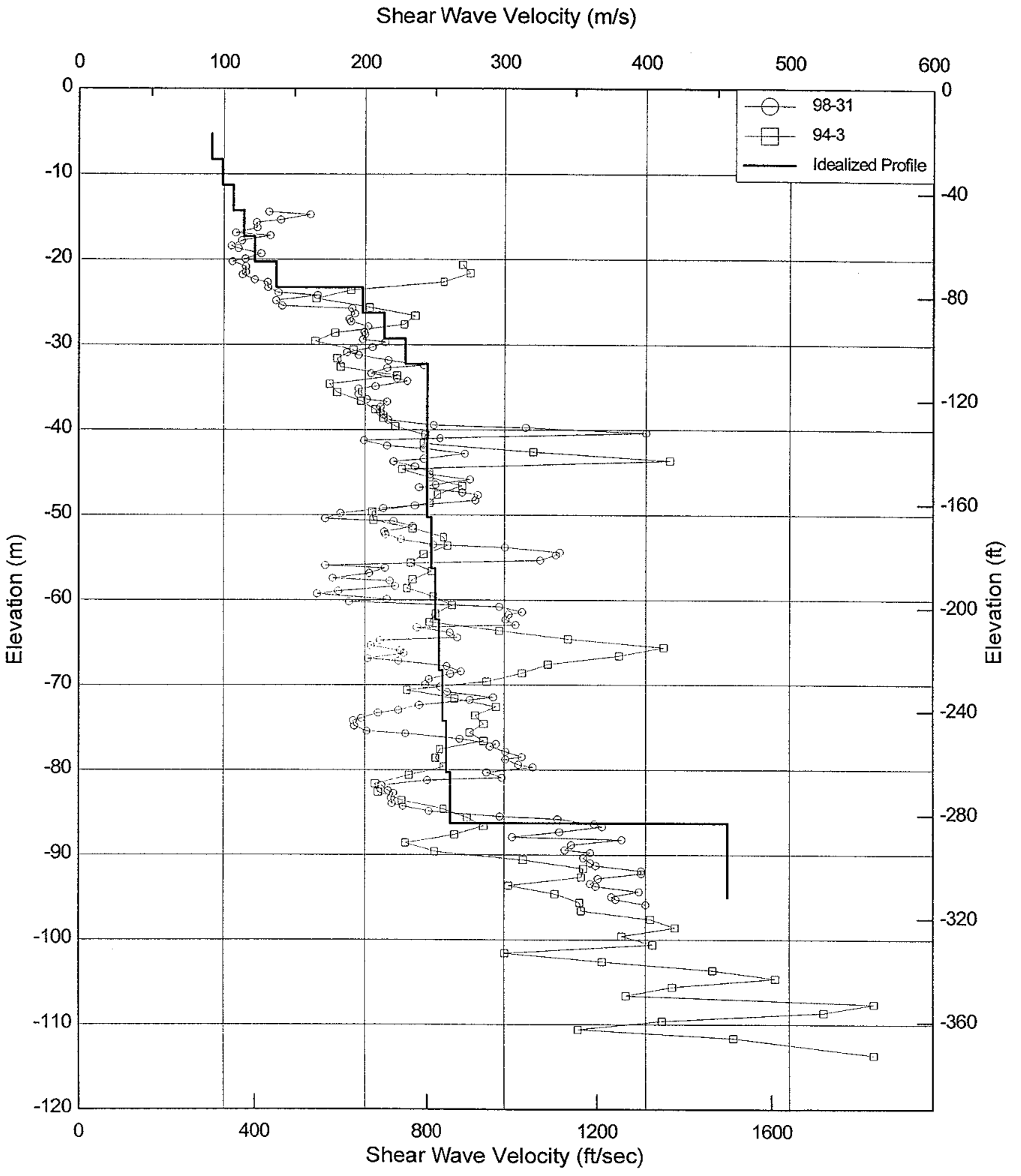

SHEAR WAVE VELOCITY PROFILE
Pier E08
SFOBB East Span Seismic Safety Project

PLATE 5-18

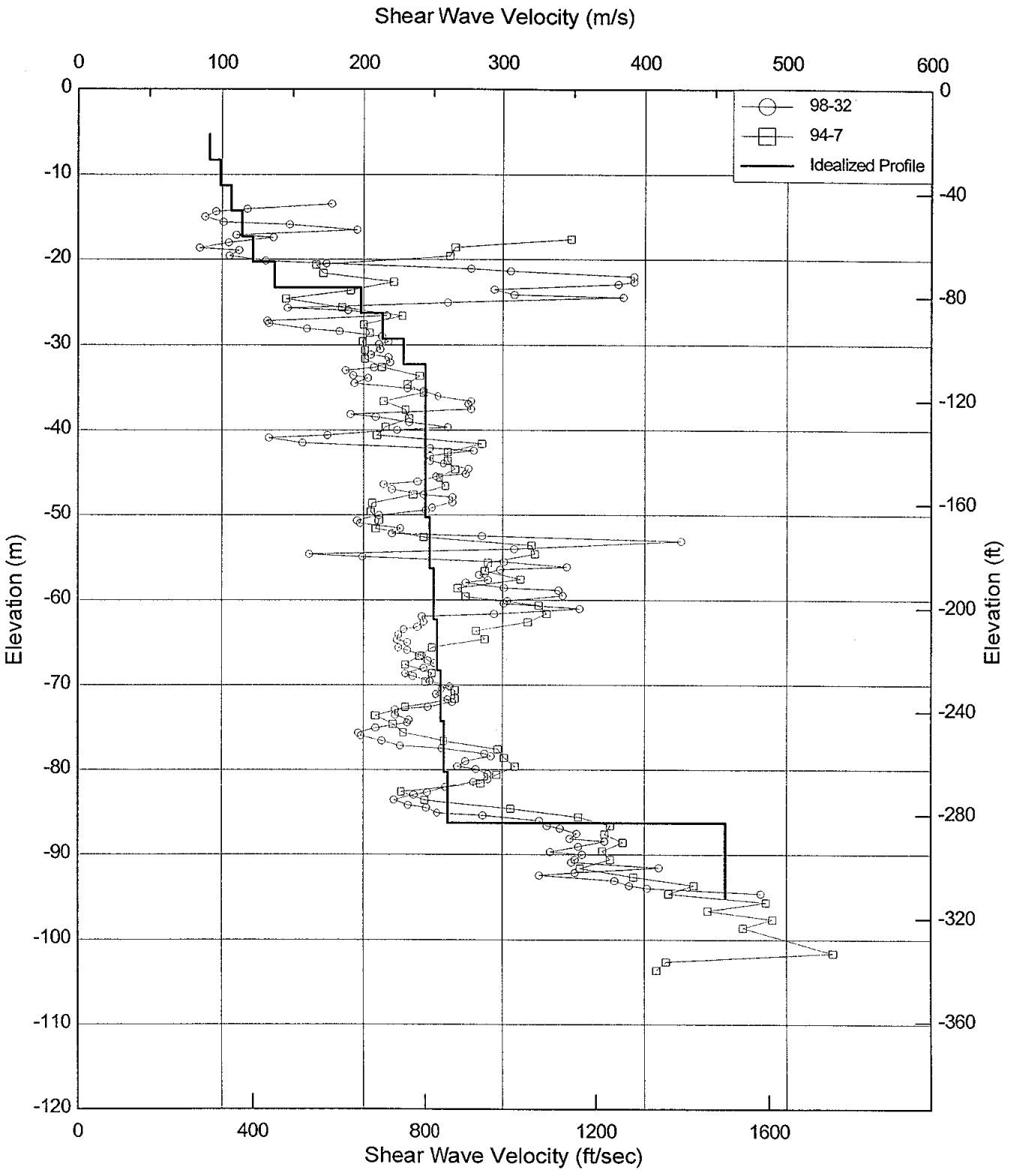

SHEAR WAVE VELOCITY PROFILE
Pier E09
SFOBB East Span Seismic Safety Project

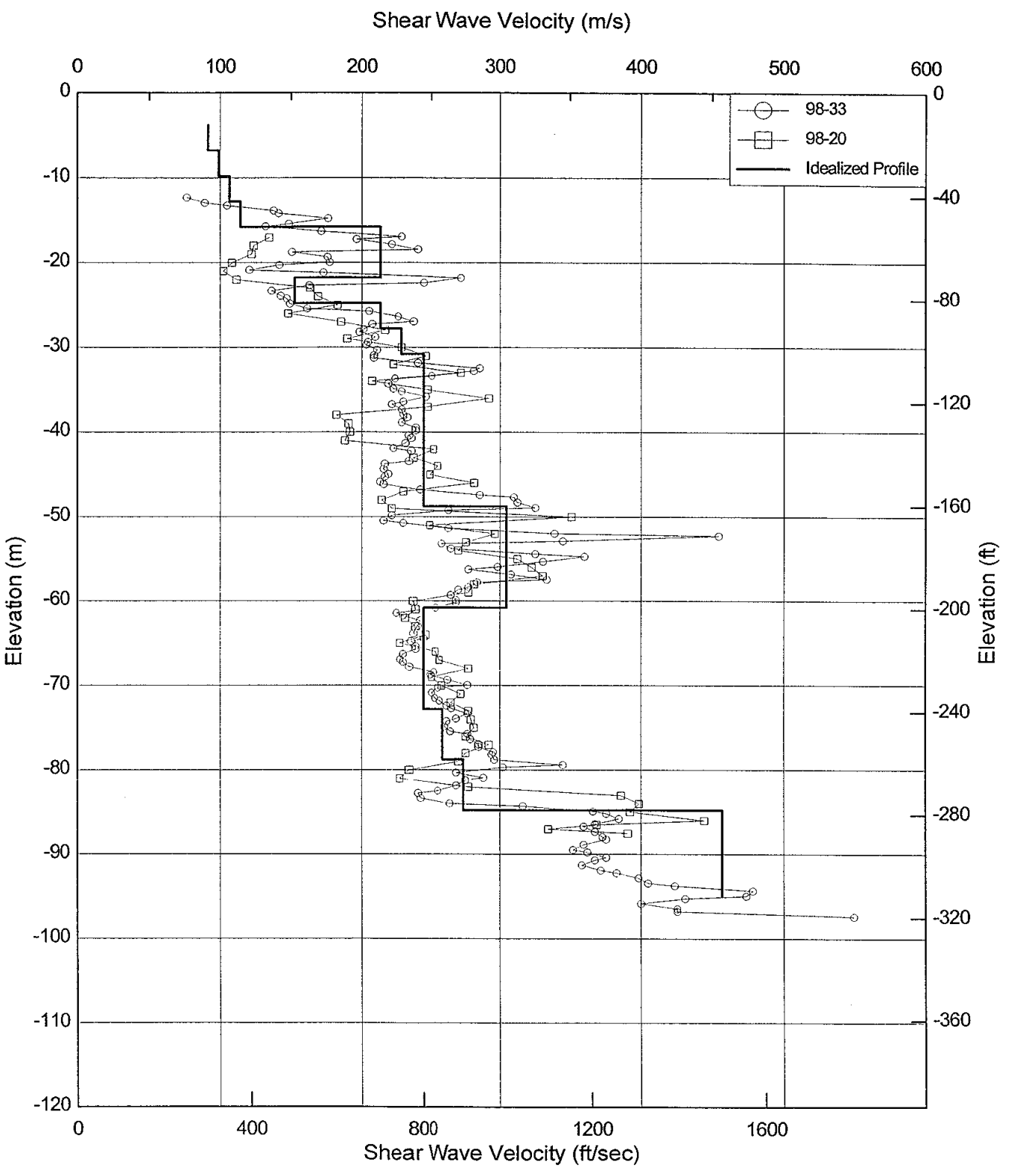

SHEAR WAVE VELOCITY PROFILE
Pier E10
SFOBB East Span Seismic Safety Project

PLATE 5-20

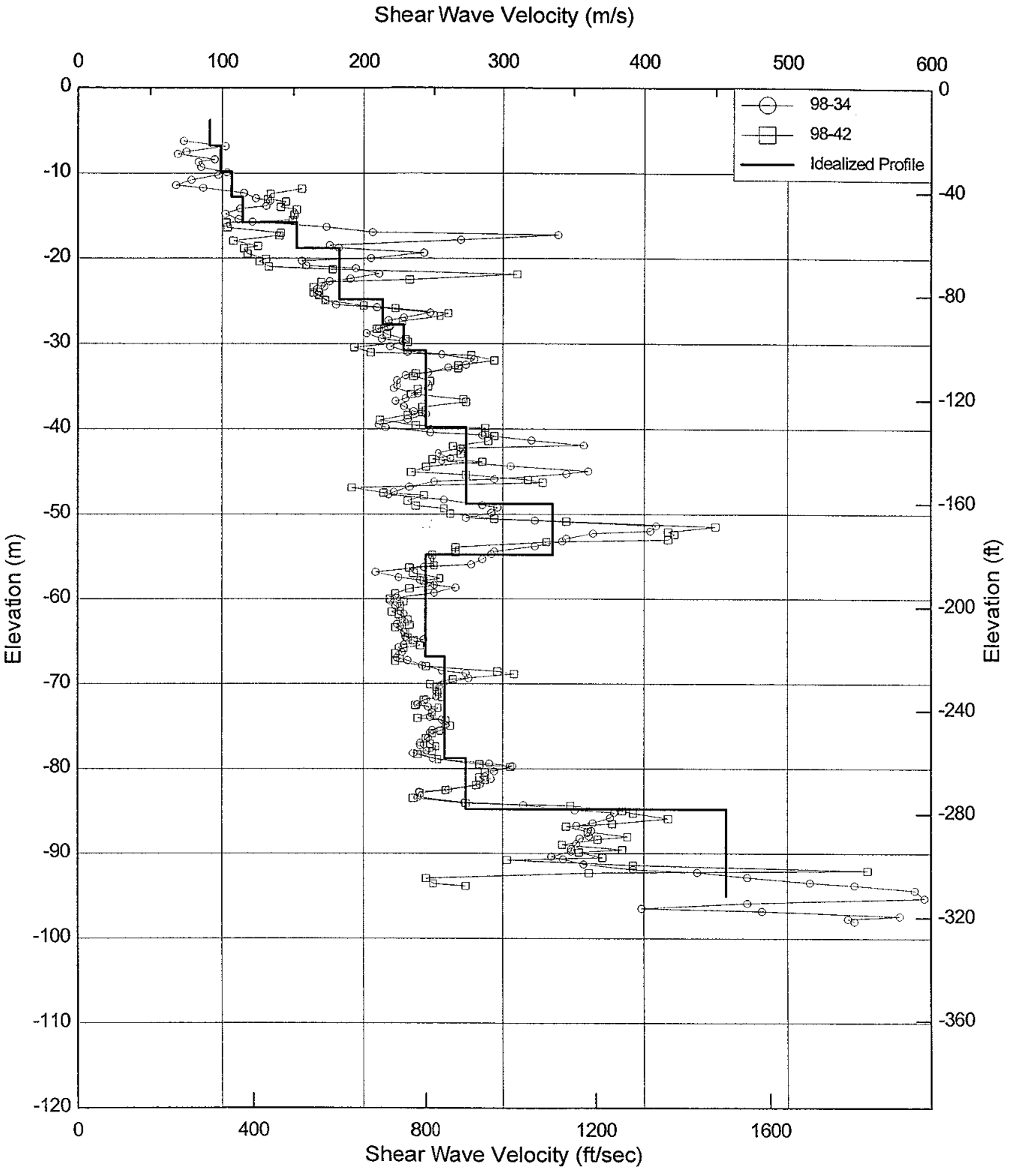

SHEAR WAVE VELOCITY PROFILE
Pier E11
SFOBB East Span Seismic Safety Project

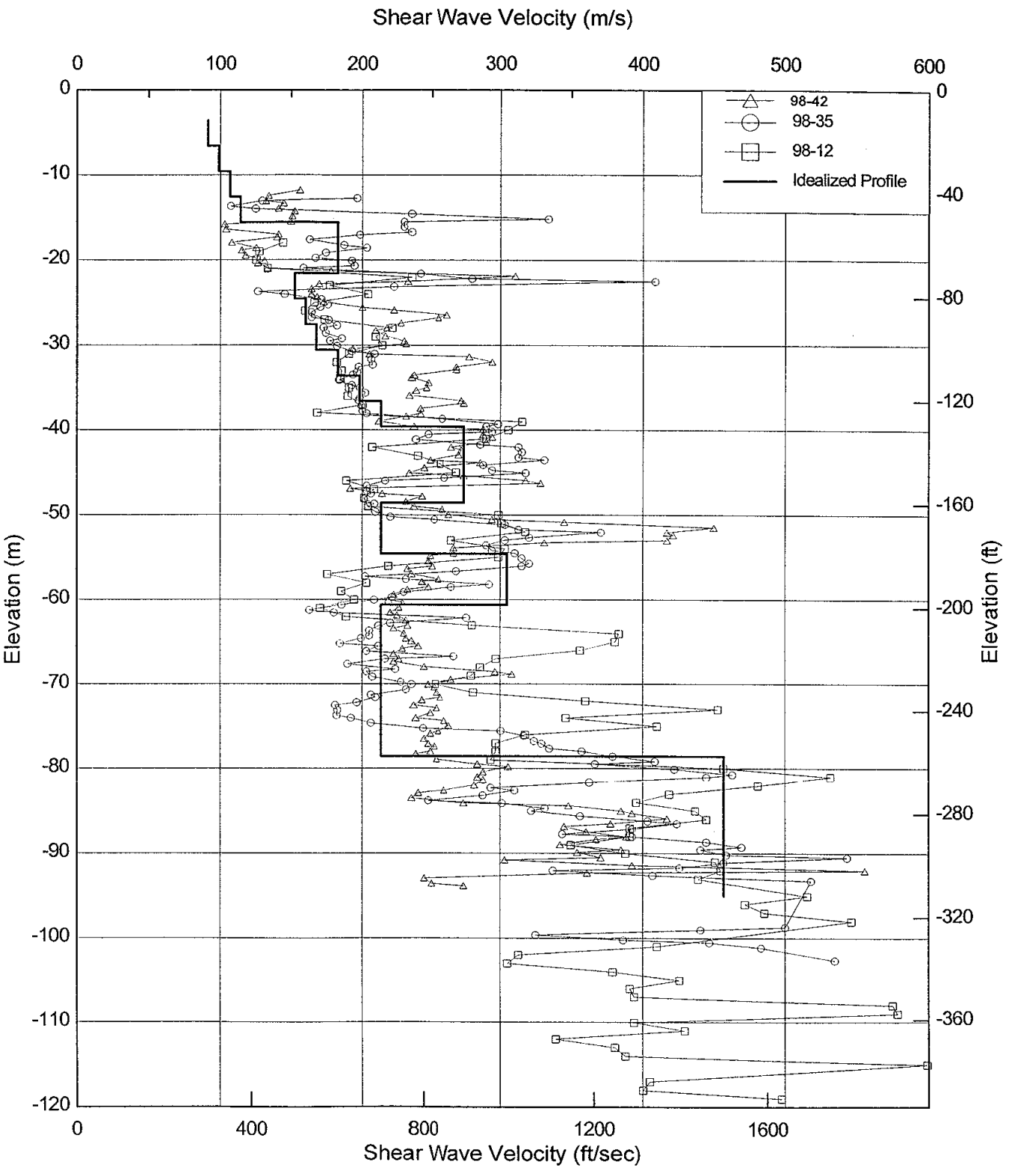

SHEAR WAVE VELOCITY PROFILE
Pier E12
SFOBB East Span Seismic Safety Project

PLATE 5-22

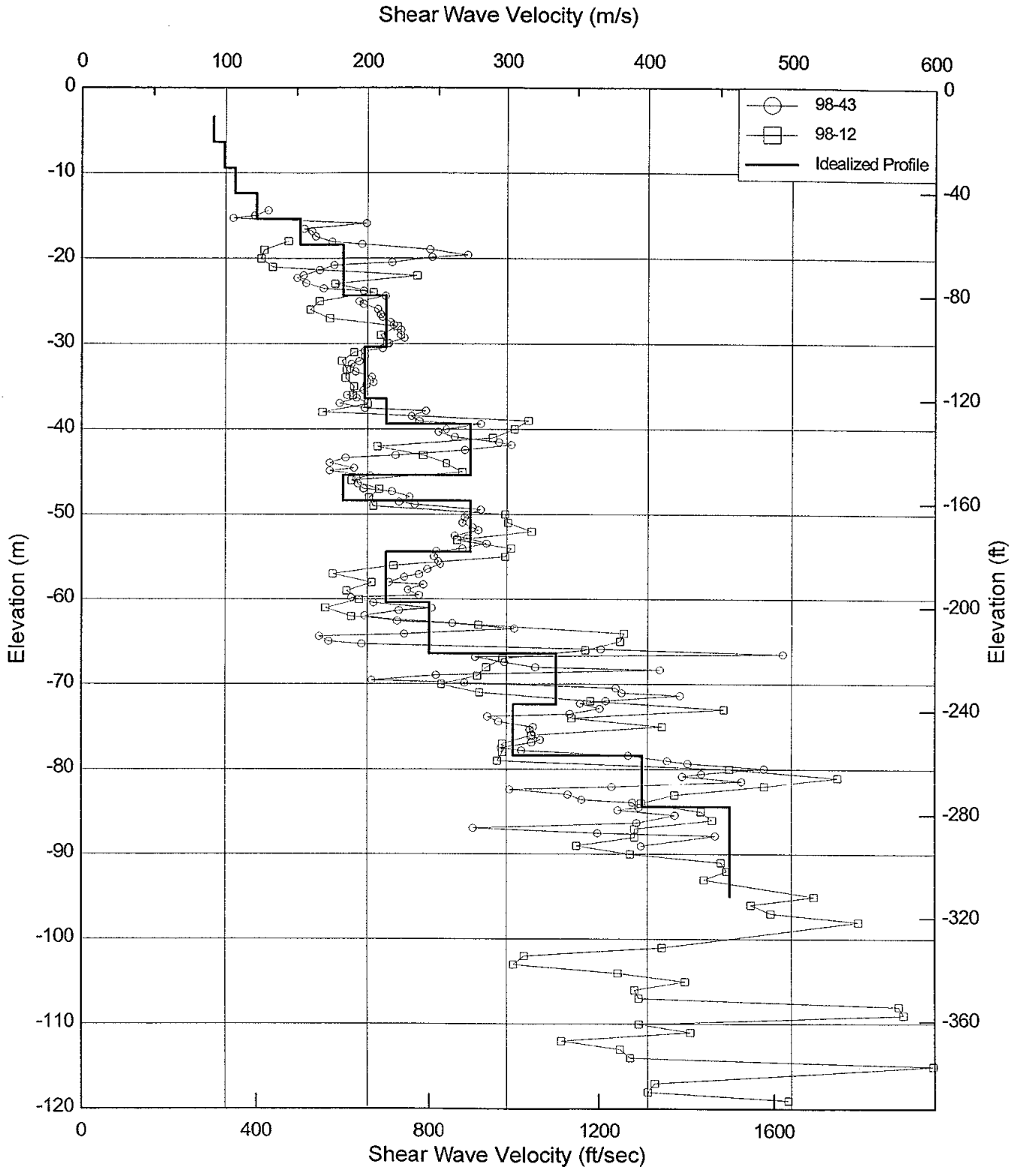

SHEAR WAVE VELOCITY PROFILE
Pier E13
SFOBB East Span Seismic Safety Project

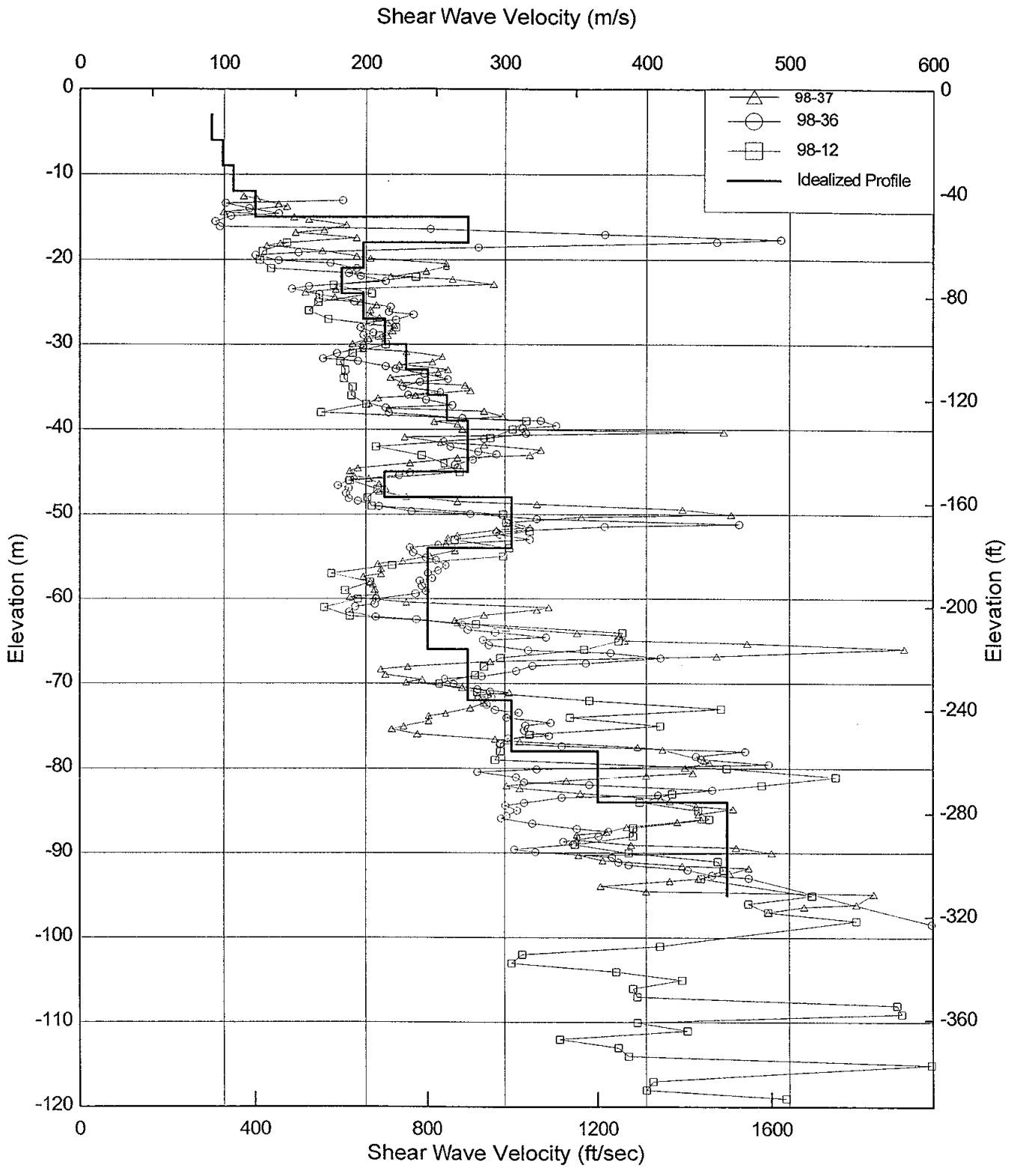

SHEAR WAVE VELOCITY PROFILE
Pier E14
SFOBB East Span Seismic Safety Project

PLATE 5-24

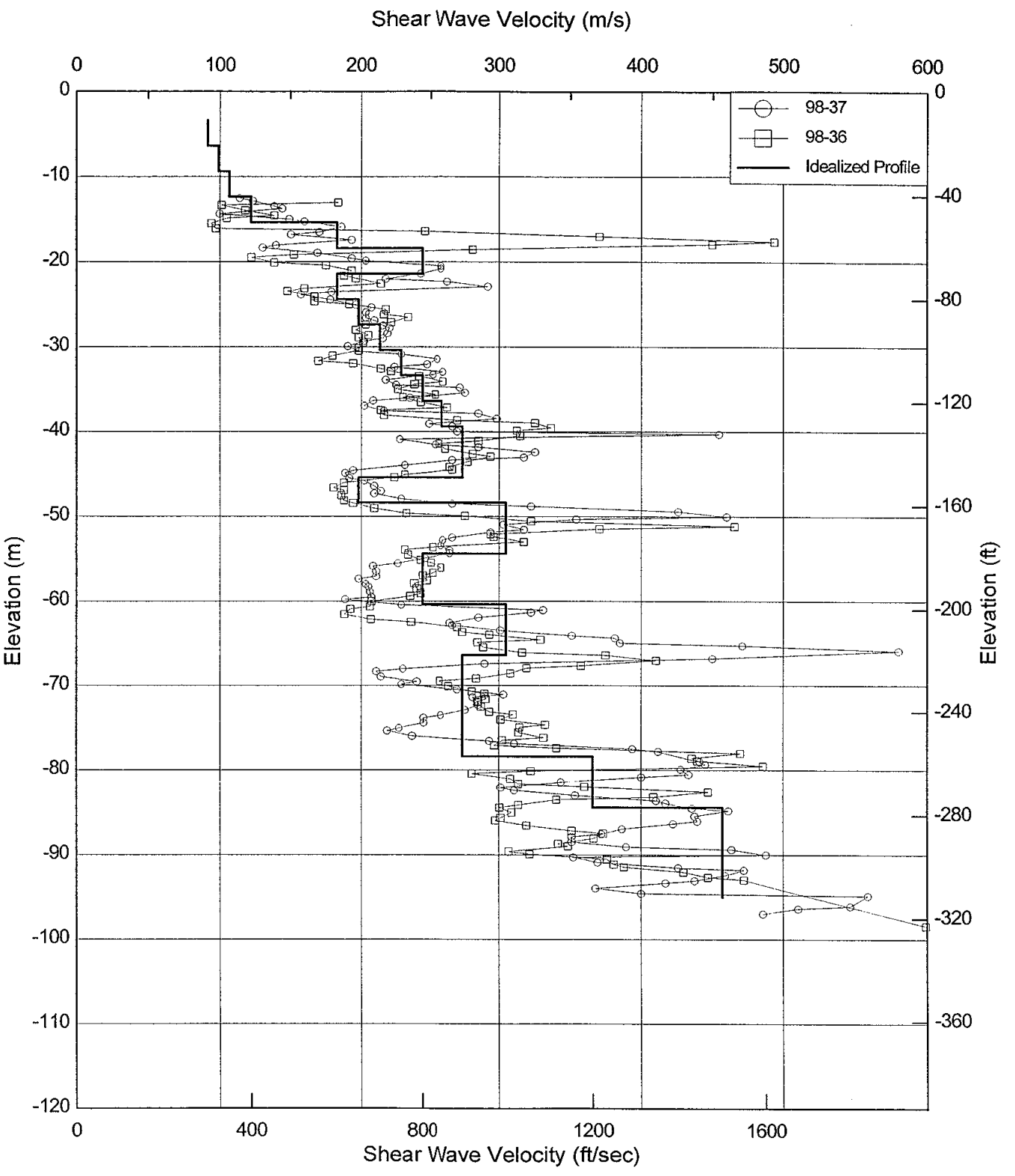

SHEAR WAVE VELOCITY PROFILE
Pier E15
SFOBB East Span Seismic Safety Project

PLATE 5-25

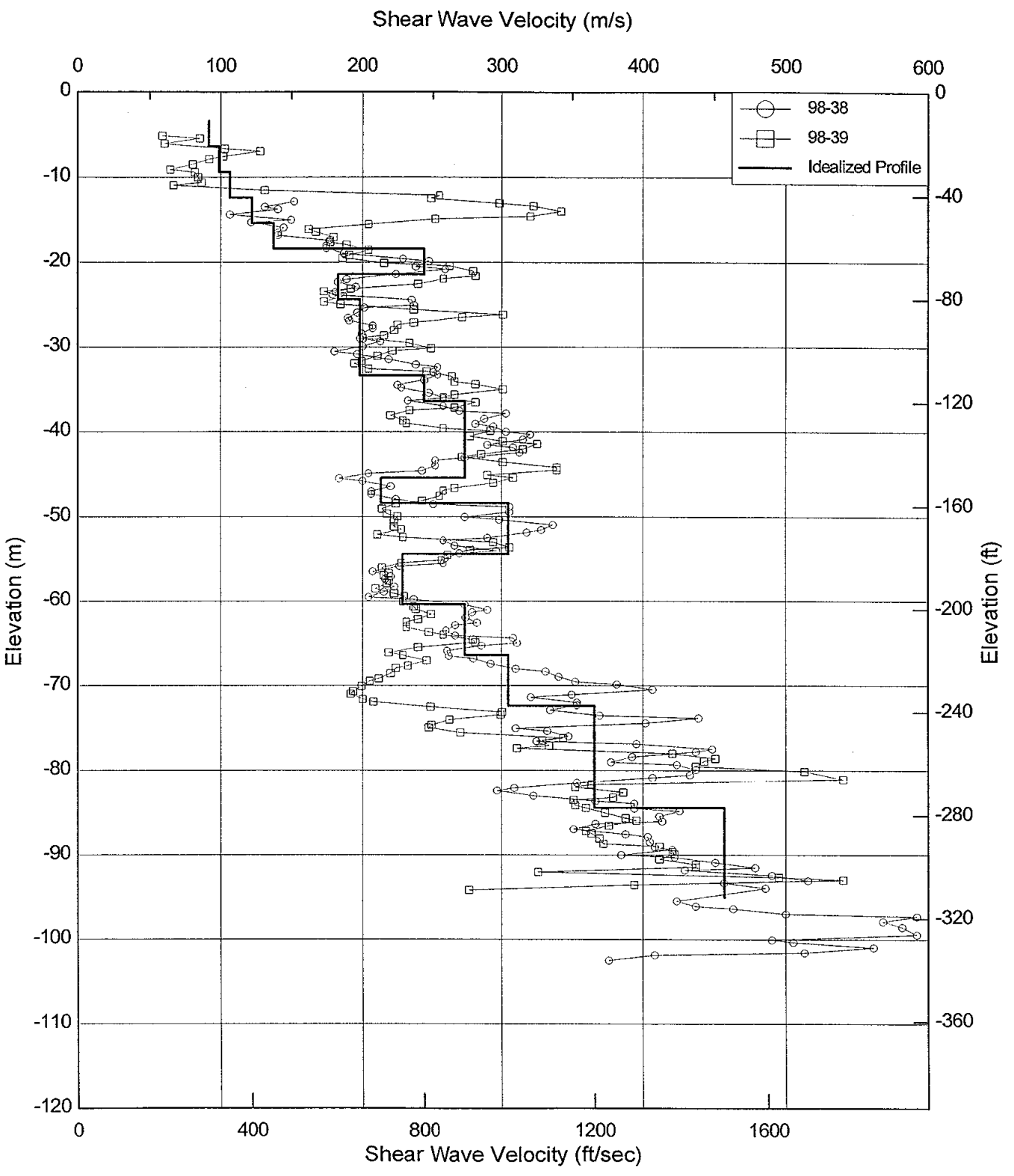

SHEAR WAVE VELOCITY PROFILE
Pier E16
SFOBB East Span Seismic Safety Project

PLATE 5-26

Earth Mechanics FUGRO

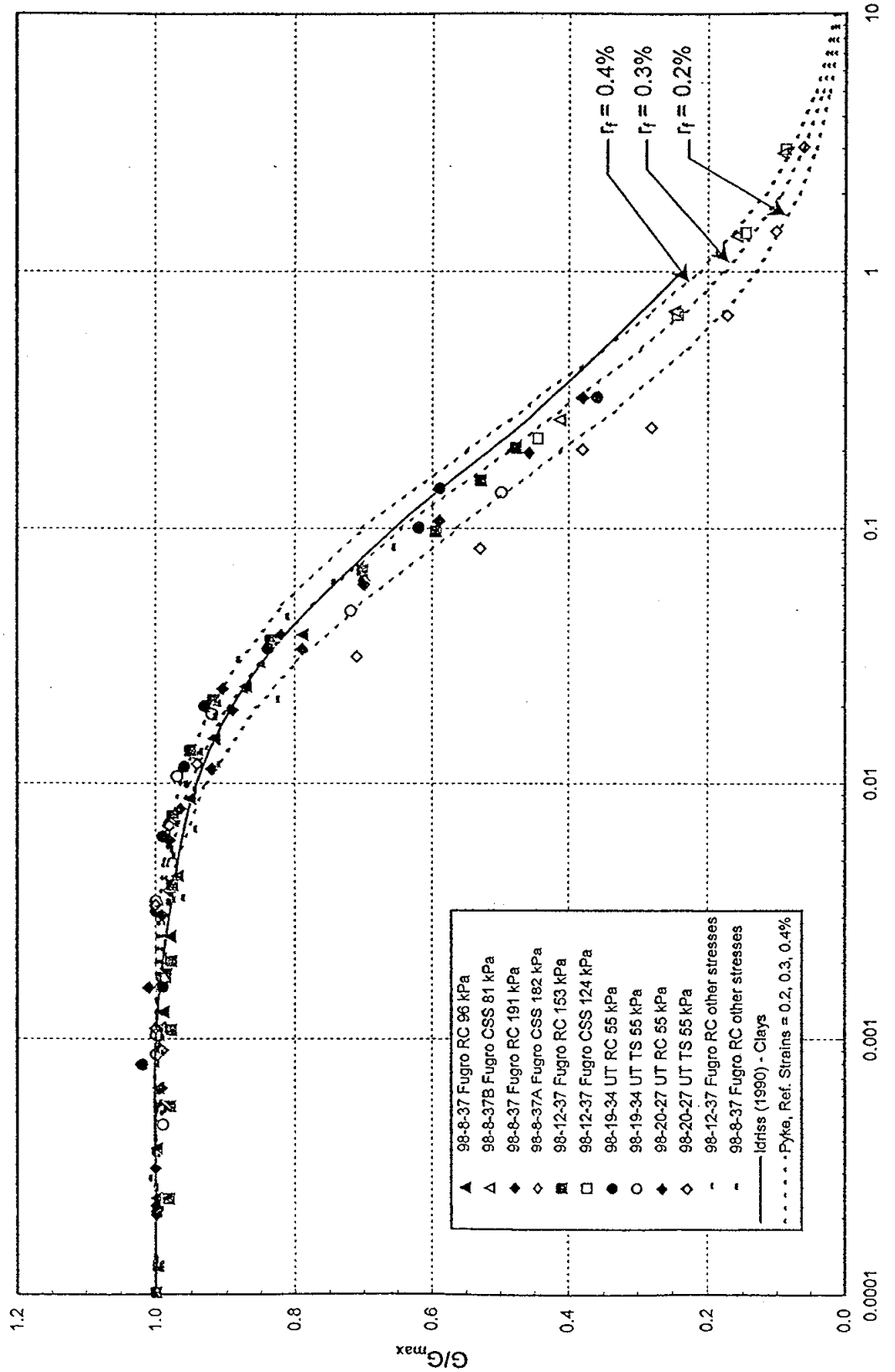

MODULUS REDUCTION Vs. SHEAR STRAIN FOR YOUNG BAY MUD

SFOBB East Span Seismic Safety Project

Earth Mechanics

FUGRO

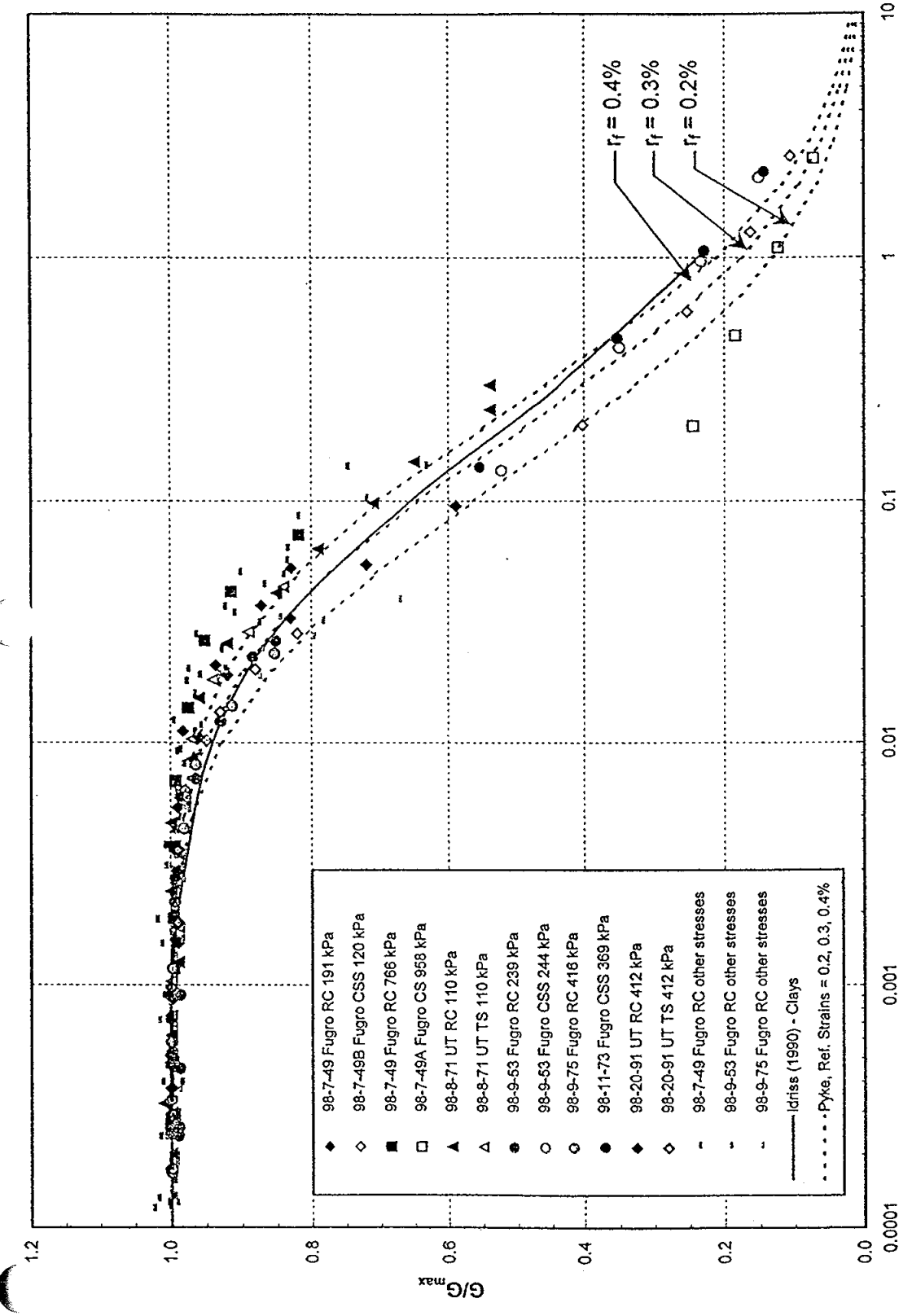

MODULUS REDUCTION Vs. SHEAR STRAIN FOR OLD BAY MUD

SFOBB East Span Seismic Safety Project

PLATE 5-28

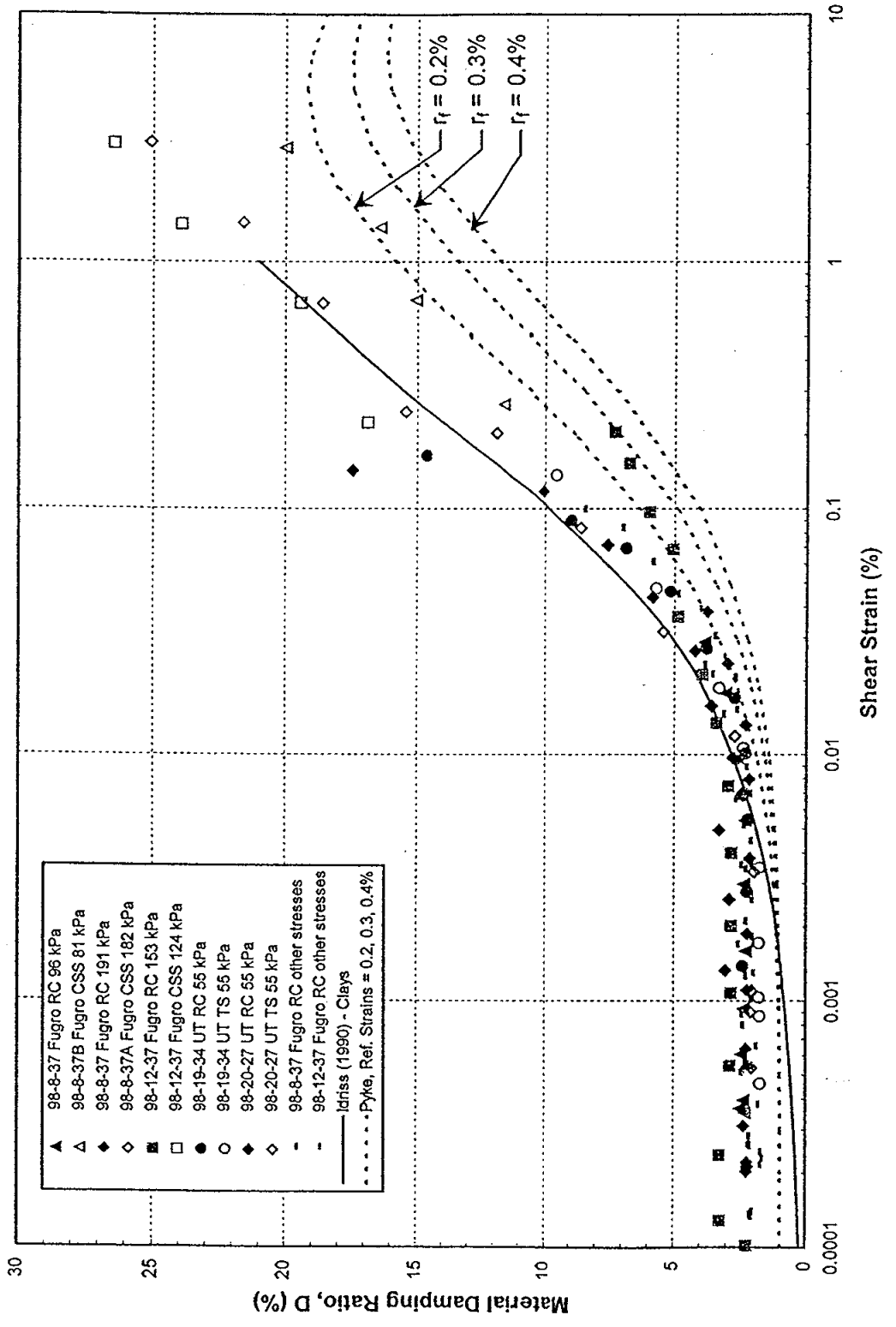

DAMPING RATIO Vs. SHEAR STRAIN FOR YOUNG BAY MUD

SFOBB East Span Seismic Safety Project

Earth Mechanics FUGRO

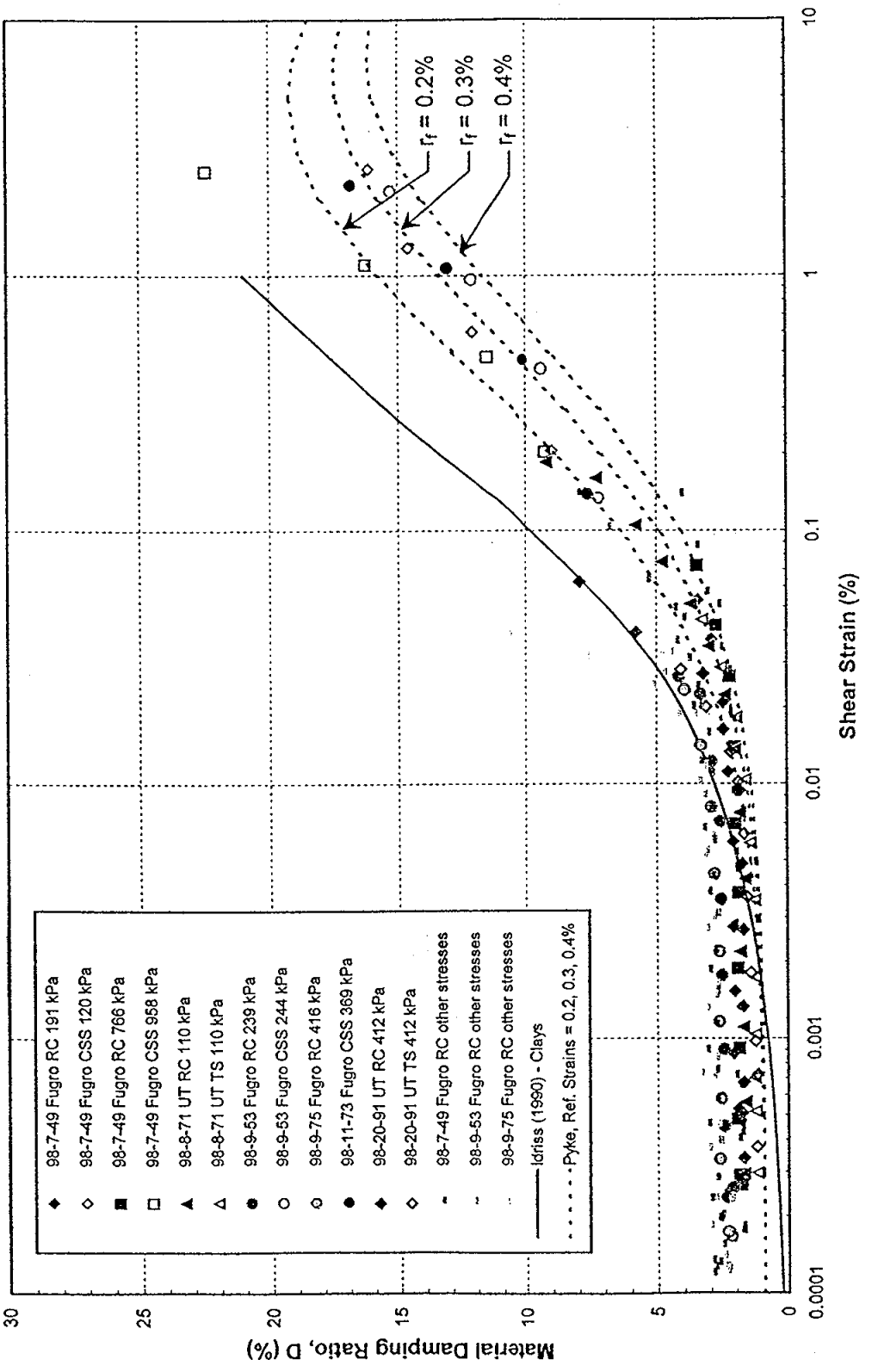

DAMPING RATIO Vs. SHEAR STRAIN FOR OLD BAY MUD

SFOBB East Span Seismic Safety Project

Earth Mechanics

FUGRO

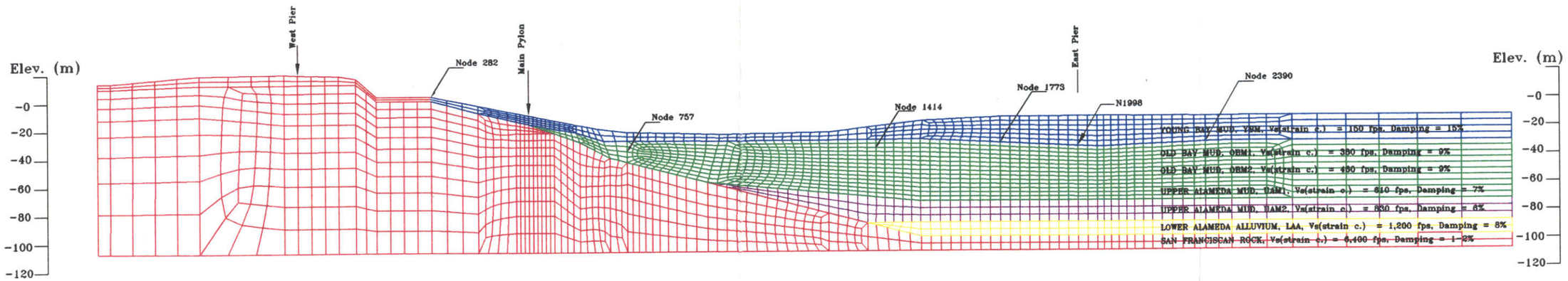

SUMMARY OF STRAIN COMPATIBLE PROPERTIES

YOUNG BAY MUD, YBM, Vs(strain c.) = 150 fps, Damping = 15%
OLD BAY MUD, OBM1, Vs(strain c.) = 380 fps, Damping = 9%
OLD BAY MUD, OBM2, Vs(strain c.) = 460 fps, Damping = 9%
UPPER ALAMEDA MUD, UAM1, Vs(strain c.) = 610 fps, Damping = 7%
UPPER ALAMEDA MUD, UAM2, Vs(strain c.) = 830 fps, Damping = 6%
LOWER ALAMEDA ALLUVIUM, LAA, Vs(strain c.) = 1,200 fps, Damping = 8%
SAN FRANCISCAN ROCK, Vs(strain c.) = 6,400 fps, Damping = 1-2%

HOR. SCALE:

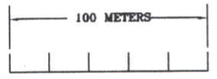

- Young Bay Mud
- Old Bay Mud
- Upper Alameda Formation
- Lower Alameda Formation
- Bedrock

2-D FINITE ELEMENT MESH FOR QUAD4M ANALYSIS AT MAIN SPAN LOCATION
SFOBB East Span Seismic Safety Project

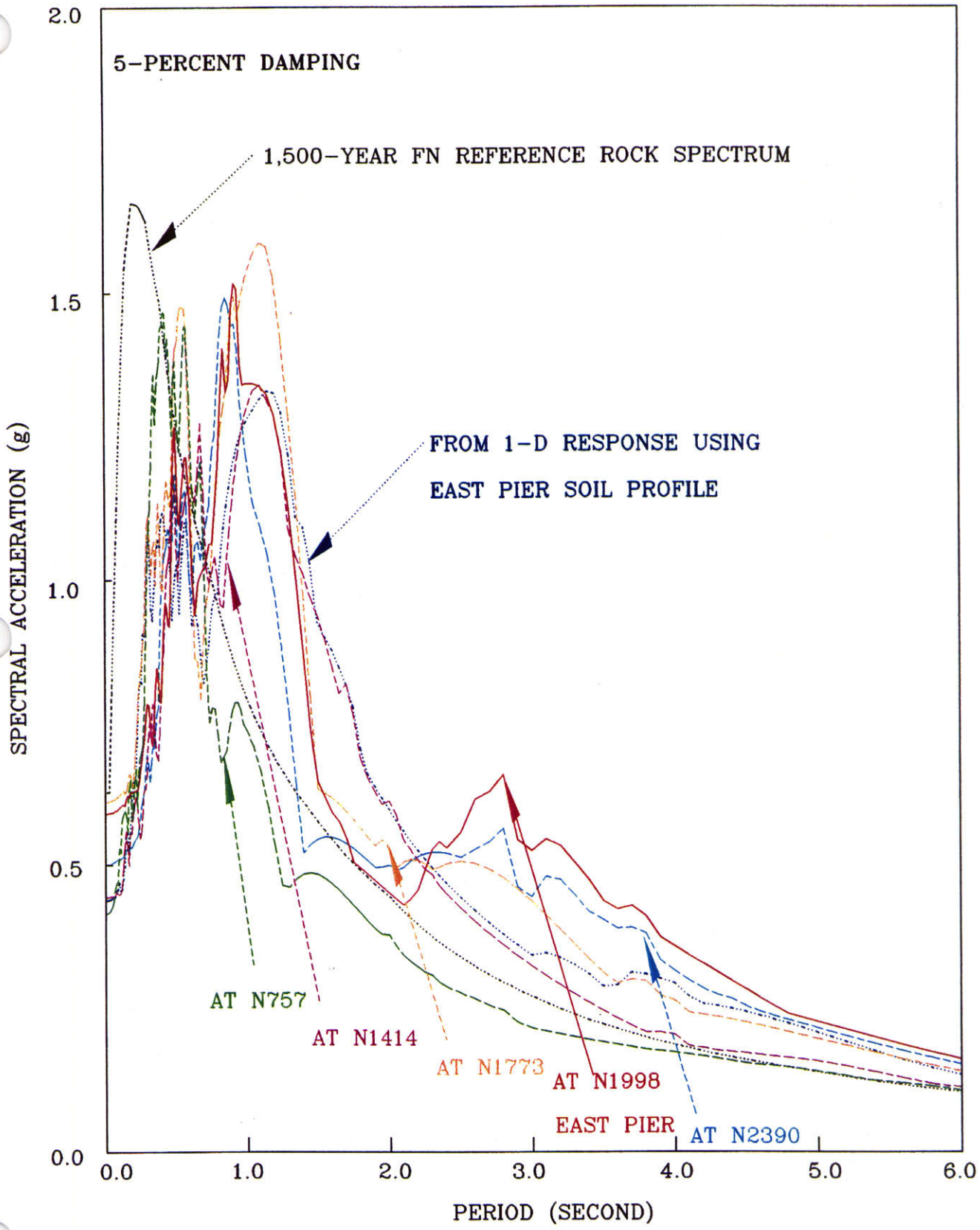

SELECTED RESULTS FROM QUAD4M ANALYSES
Set 1, Fault Normal Motion
SFOBB East Span Seismic Safety Project

PLATE 5-32

June 1998
Project No. 98-42-0035
SFOBB Task Order No. 3

Earth Mechanics

FUGRO

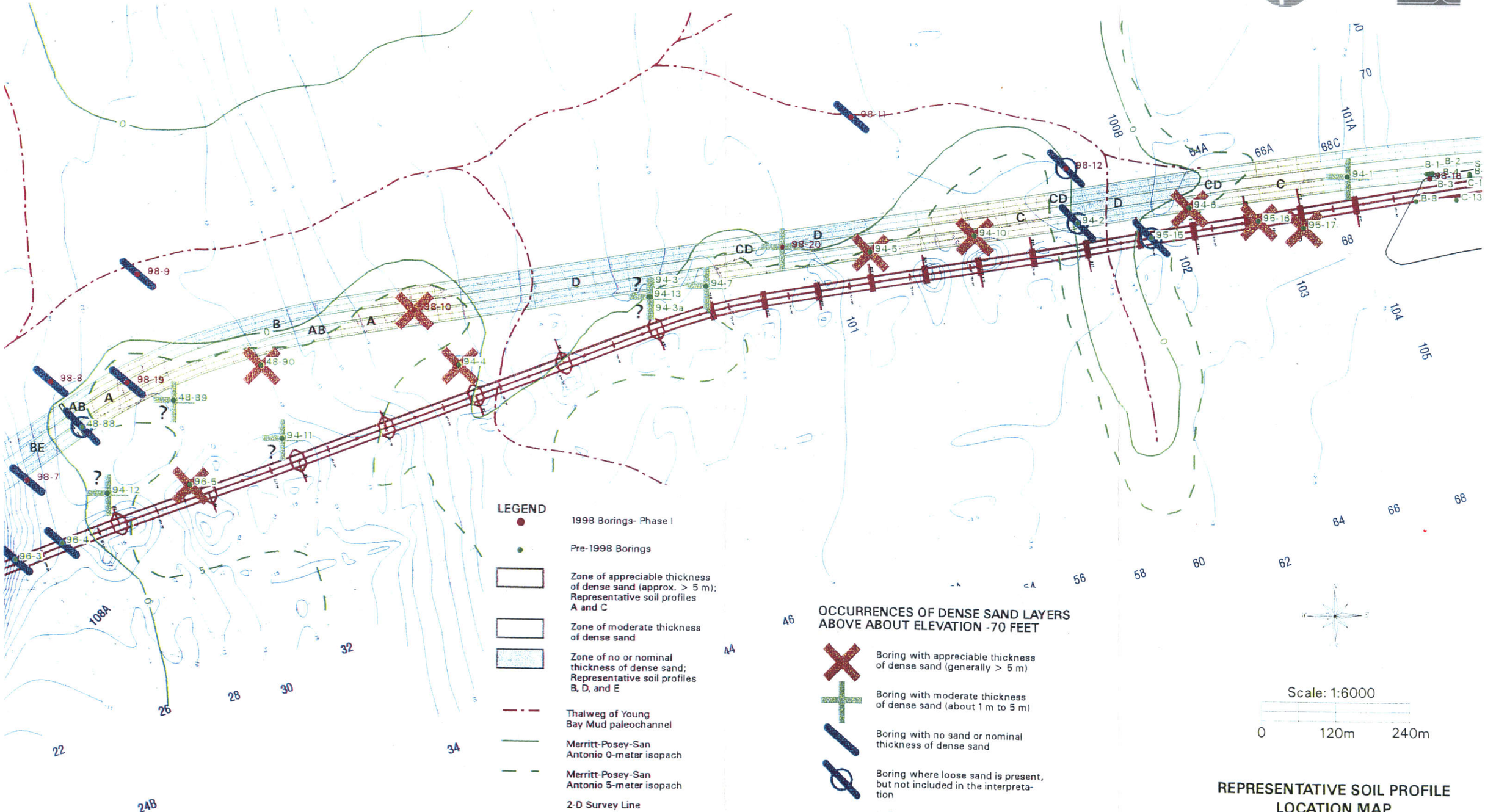

LEGEND

- 1998 Borings- Phase I
- Pre-1998 Borings
- Zone of appreciable thickness of dense sand (approx. > 5 m); Representative soil profiles A and C
- Zone of moderate thickness of dense sand
- Zone of no or nominal thickness of dense sand; Representative soil profiles B, D, and E
- Thalweg of Young Bay Mud paleochannel
- Merritt-Posey-San Antonio 0-meter isopach
- Merritt-Posey-San Antonio 5-meter isopach
- 2-D Survey Line
- Bathymetry (meters), re MSL
- Proposed N6 (Revision 2) Alignment (Approximate)
- San Francisco-Oakland Bay Bridge

OCCURRENCES OF DENSE SAND LAYERS ABOVE ABOUT ELEVATION -70 FEET

- Boring with appreciable thickness of dense sand (generally > 5 m)
- Boring with moderate thickness of dense sand (about 1 m to 5 m)
- Boring with no sand or nominal thickness of dense sand
- Boring where loose sand is present, but not included in the interpretation
- ? Indicates uncertain interpretation for pre-1998 borings

Scale: 1:6000

0 120m 240m

REPRESENTATIVE SOIL PROFILE LOCATION MAP

SFOBB East Span Seismic Safety Project

PLATE 5-33

Earth Mechanics | FUGRO

MAIN SPAN EAST PIER
Profile E

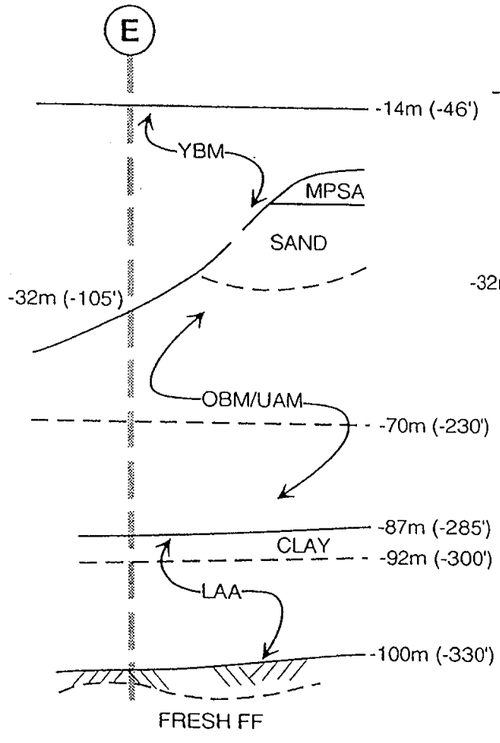

WESTERN 1/3RD OF SKYWAY (FRAME 1)
Profiles A and B

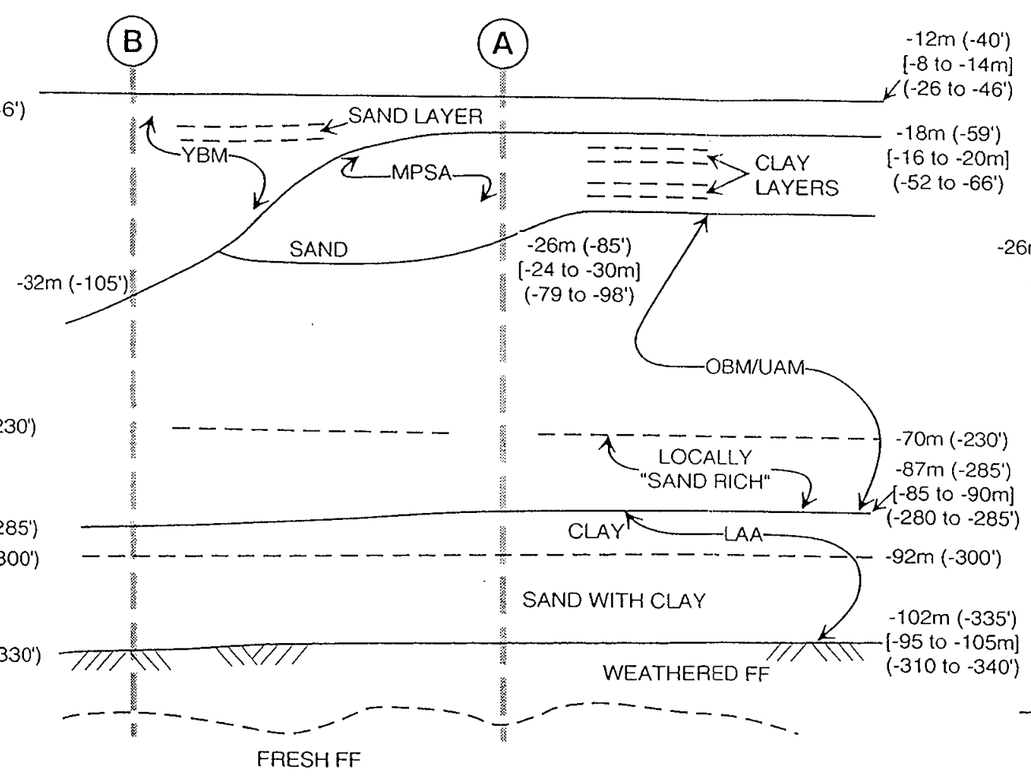

EASTERN 2/3RD OF SKYWAY (FRAMES 2-5)
Profiles C and D

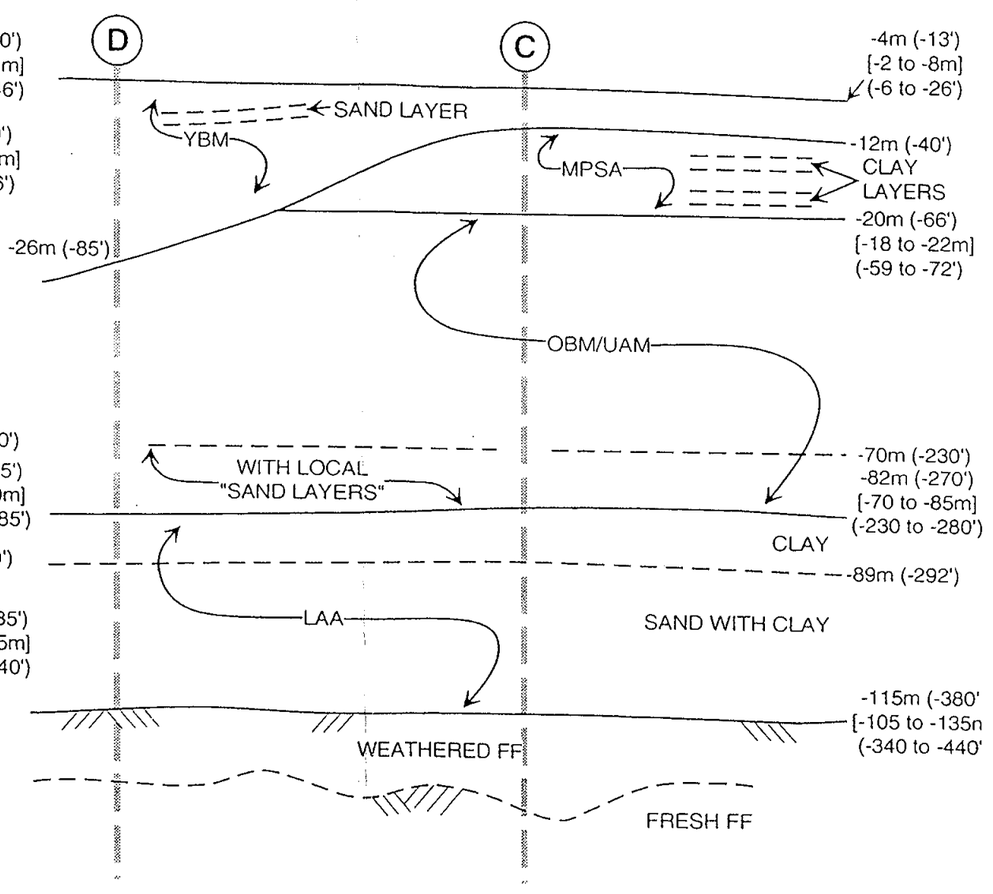

YBM = Young Bay Mud

MPSA = Merritt-Posey-San Antonio Formations (Also may be referred to as Merritt Sand)

OBM = Old Bay Mud

UAM = Upper Alameda (Primary Marine) Sediments

LAA = Lower Alameda (Primary Alluvial) Sediment

FF = Franciscan Formation

-82m (-270') = Typical Elevation

[-70 to -85m] (-230 to 440') = Typical Range of Elevation

Note:

Representative soil profiles are simplifications of subsurface variability along the alignment. Formation contacts and layering within formations are locally variable.

REPRESENTATIVE SOIL PROFILES
SFOBB East Span Seismic Safety Project

Pier No.	E03
EL. Bot. of Cap (m)	-3.5
EL. of Mudline (m)	-12.5

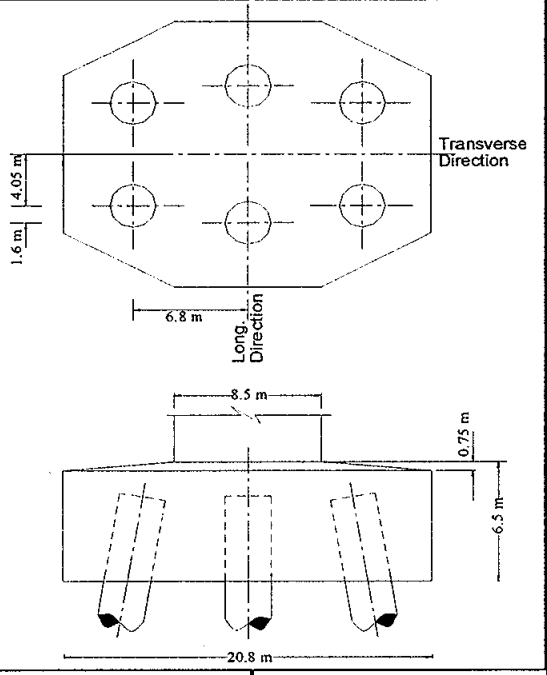

V_s (ft/sec)	γ (pcf)	Depth (m)	Elev (m)
From SHAKE Profile	From SHAKE Profile		-12.5
300	102	3.0	-15.5
325	102	6.0	-18.5
350	102	9.0	-21.5
375	102	12.0	-24.5
550	104	15.0	-27.5
800	128	18.0	-30.5
600	116	21.0	-33.5
600	116	24.0	-36.5
620	116	27.0	-39.5
620	116	30.0	-42.5
640	116	33.0	-45.5
640	116	36.0	-48.5
660	116	39.0	-51.5
660	116	42.0	-54.5
680	116	45.0	-57.5
800	122	51.0	-63.5
1000	122	57.0	-69.5
1100	122	63.0	-75.5
1000	122	69.0	-81.5
900	122	75.0	-87.5
1000	122	81.0	-93.5
1500	122	82.5	-95.0

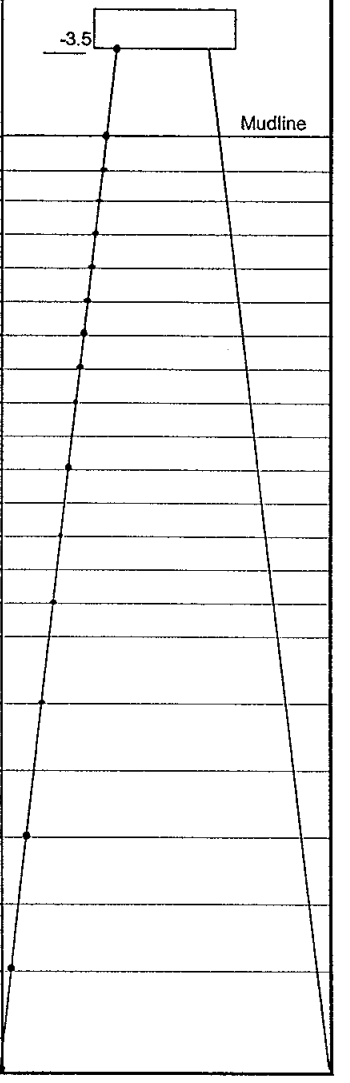

Pile Tip Elevation
Eastbound : El -100 m
Westbound : El -102 m

Conversions :
1pcf = 0.157 kN/m3
1ft/sec = 0.305 m/sec

- Location of Pile Node for Kinematic Analysis

PILE GROUP CONFIGURATION PIER E03

SFOBB East Span Seismic Safety Project

Pier No.	E04
EL. Bot. of Cap (m)	-3.5
EL. of Mudline (m)	-11.7

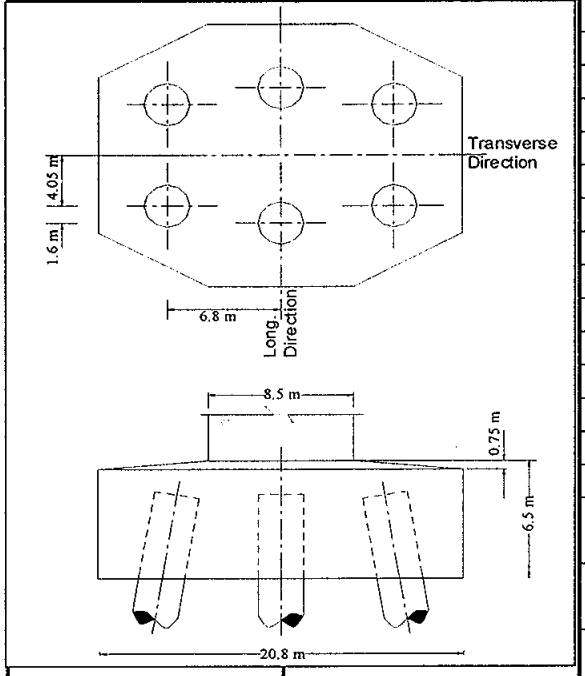

Pile Tip Elevation	**Conversions :**
Eastbound : El -97	1pcf = 0.157 kN/m3
Westbound : El -94	1ft/sec = 0.305 m/sec

V_s (ft/sec)	γ (pcf)	Depth (m)	Elev (m)
From SHAKE Profile	From SHAKE Profile		-11.7
300	102	3.0	-14.7
325	102	6.0	-17.7
350	102	9.0	-20.7
650	128	12.0	-23.7
625	128	15.0	-26.7
600	116	18.0	-29.7
600	116	21.0	-32.7
700	116	24.0	-35.7
800	116	27.0	-38.7
900	116	30.0	-41.7
800	116	33.0	-44.7
700	116	36.0	-47.7
700	116	39.0	-50.7
700	116	42.0	-53.7
700	116	45.0	-56.7
800	122	51.0	-62.7
1200	122	57.0	-68.7
1000	122	63.0	-74.7
900	122	69.0	-80.7
800	122	75.0	-86.7
1000	122	81.0	-92.7
1500	130	83.3	-95.0

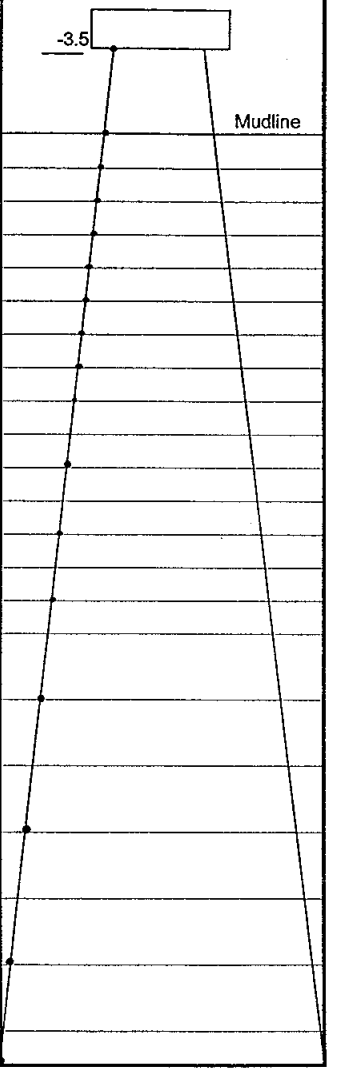

- Location of Pile Node for Kinematic Analysis

PILE GROUP CONFIGURATION PIER E04

SFOBB East Span Seismic Safety Project

Pier No.	E05
EL. Bot. of Cap (m)	-3.5
EL. of Mudline (m)	-9.8

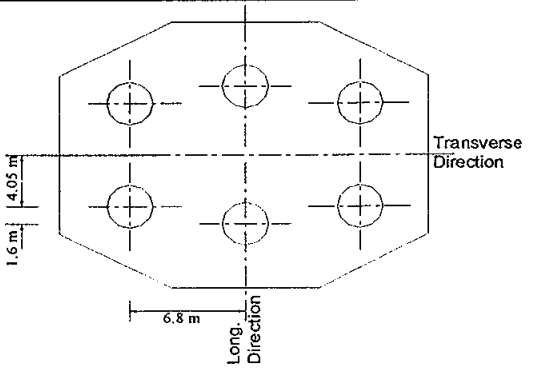

Pile Tip Elevation -20.8

Conversions:

Eastbound : El -98 m
Westbound : El -98 m

1pcf = 0.157 kN/m3
1ft/sec = 0.305 m/sec

V_s (ft/sec)	γ (pcf)	Depth (m)	Elev (m)
From SHAKE Profile	From SHAKE Profile		-9.8
300	102	3.0	-12.8
350	102	6.0	-15.8
400	102	9.0	-18.8
400	128	12.0	-21.8
450	128	15.0	-24.8
600	116	18.0	-27.8
650	116	21.0	-30.8
700	116	24.0	-33.8
750	116	27.0	-36.8
800	116	30.0	-39.8
800	116	33.0	-42.8
800	116	36.0	-45.8
800	116	39.0	-48.8
700	116	42.0	-51.8
700	116	45.0	-54.8
800	122	51.0	-60.8
1000	122	57.0	-66.8
1100	122	63.0	-72.8
800	122	69.0	-78.8
900	122	75.0	-84.8
1000	122	81.0	-90.8
1500	130	85.2	-95.0

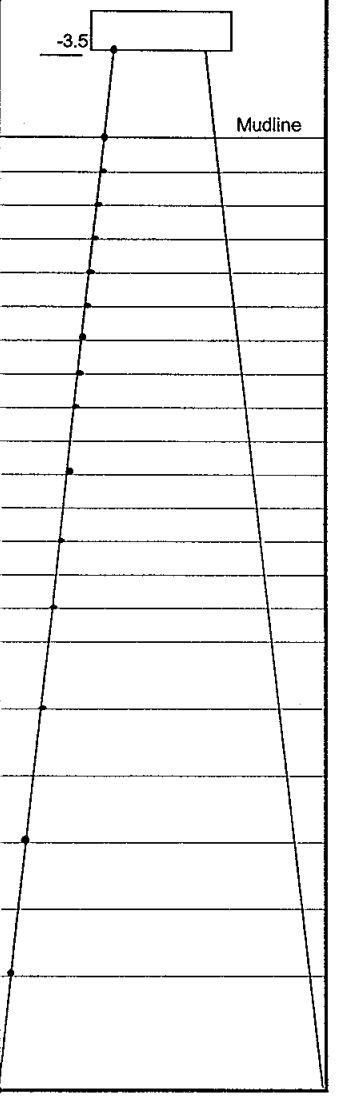

- Location of Pile Node for Kinematic Analysis

PILE GROUP CONFIGURATION PIER E05

SFOBB East Span Seismic Safety Project

Earth Mechanics FUGRO

Pier No.	E06
EL. Bot. of Cap (m)	-3.5
EL. of Mudline (m)	-7.6

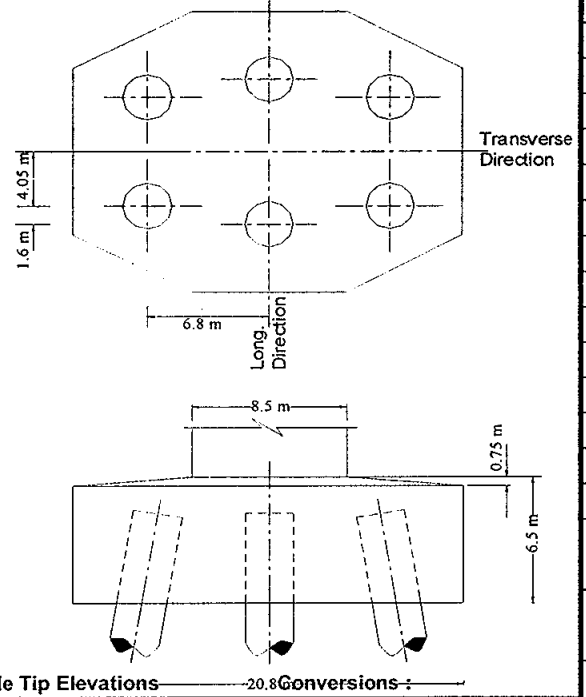

Pile Tip Elevations

Eastbound : El -96 m

Westbound : El -96 m

Conversions :

1pcf = 0.157 kN/m3

1ft/sec = 0.305 m/sec

v_s (ft/sec)	γ (pcf)	Depth (m)	Elev (m)
From SHAKE Profile	From SHAKE Profile		-3.5
			-7.6 Mudline
300	102	3.0	-10.6
350	102	6.0	-13.6
400	102	9.0	-16.6
450	128	12.0	-19.6
500	128	15.0	-22.6
600	116	18.0	-25.6
800	116	21.0	-28.6
800	116	24.0	-31.6
800	116	27.0	-34.6
800	116	30.0	-37.6
800	116	33.0	-40.6
800	116	36.0	-43.6
800	116	39.0	-46.6
700	116	42.0	-49.6
700	116	45.0	-52.6
750	122	51.0	-58.6
750	122	57.0	-64.6
1000	122	63.0	-70.6
1100	122	69.0	-76.6
1000	122	75.0	-82.6
1000	122	81.0	-88.6
1500	130	87.4	-95.0

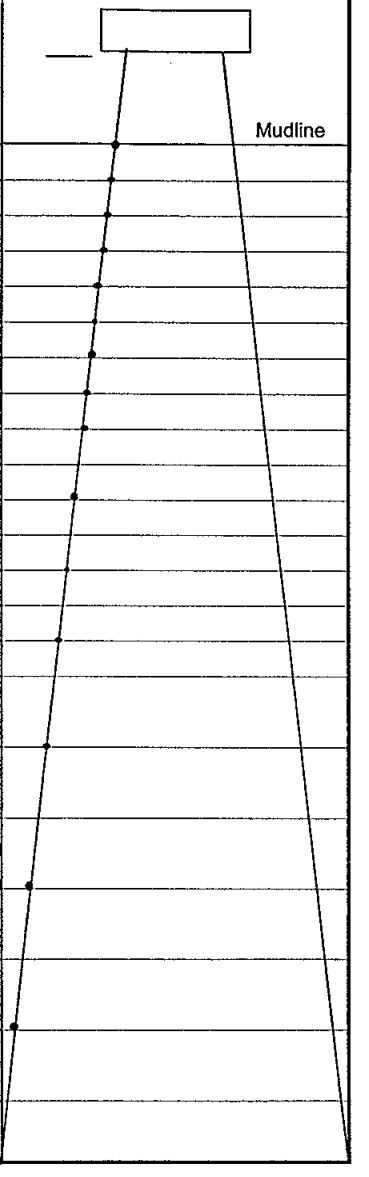

- Location of Pile Node for Kinematic Analysis

PILE GROUP CONFIGURATION PIER E06

SFOBB East Span Seismic Safety Project

Pier No.	E07
EL. Bot. of Cap (m)	-12.5
EL. of Mudline (m)	-6.0

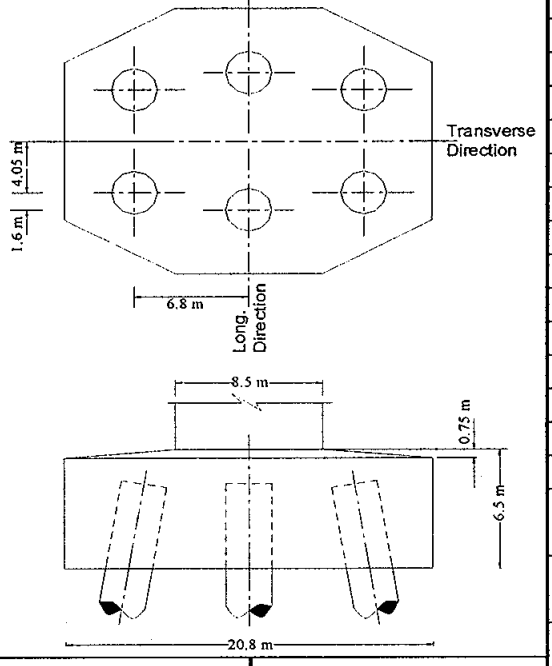

V_s (ft/sec)	γ (pcf)	Depth (m)	Elev (m)
From SHAKE Profile	From SHAKE Profile		
			-6.0
300	102	3.0	-9.0
350	109	6.0	-12.0
400	109	9.5	-15.5
600	130	12.5	-18.5
450	104	15.5	-21.5
475	104	18.5	-24.5
500	104	21.5	-27.5
525	104	24.5	-30.5
550	104	27.5	-33.5
800	125	30.5	-36.5
820	125	33.5	-39.5
840	125	36.5	-42.5
860	125	39.5	-45.5
880	125	42.5	-48.5
900	125	45.5	-51.5
900	122	51.5	-57.5
920	120	57.5	-63.5
940	118	63.5	-69.5
960	116	69.5	-75.5
98-	114	75.5	-81.5
1000	112	81.5	-87.5
1500	130	89.0	-95.0

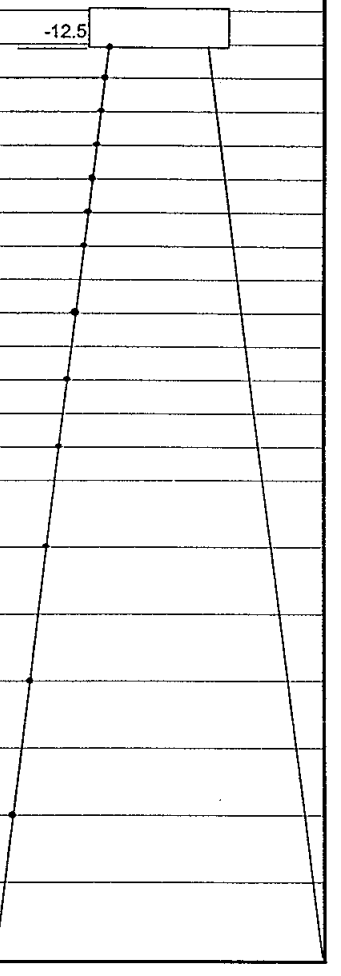

Pile Tip Elevations
Eastbound : El -93 m
Westbound : El -94 m

Conversions :
1pcf = 0.157 kN/m3
1ft/sec = 0.305 m/sec

• Location of Pile Node for Kinematic Analysis

PILE GROUP CONFIGURATION PIER E07

SFOBB East Span Seismic Safety Project

Pier No.	E08
EL. Bot. of Cap (m)	-11.3
EL. of Mudline (m)	-5.3

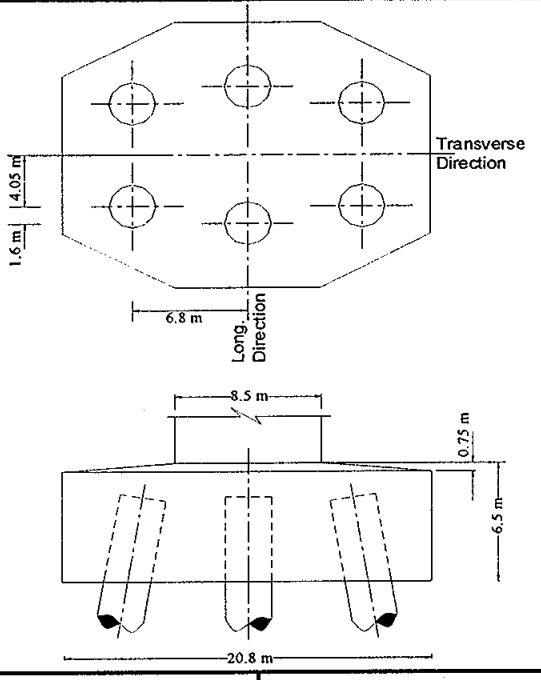

V_s (ft/sec)	γ (pcf)	Depth (m)	Elev (m)
From SHAKE Profile	From SHAKE Profile		-5.3
300	102	3.0	-8.3
325	102	6.0	-11.3
350	102	9.0	-14.3
375	102	12.0	-17.3
400	104	15.0	-20.3
450	104	18.0	-23.3
650	116	21.0	-26.3
700	116	24.0	-29.3
750	116	27.0	-32.3
800	116	30.0	-35.3
800	116	33.0	-38.3
800	116	36.0	-41.3
800	116	39.0	-44.3
800	116	42.0	-47.3
800	116	45.0	-50.3
810	116	51.0	-56.3
820	116	57.0	-62.3
830	116	63.0	-68.3
840	116	69.0	-74.3
850	114	75.0	-80.3
860	112	81.0	-86.3
1500	130	89.7	-95.0

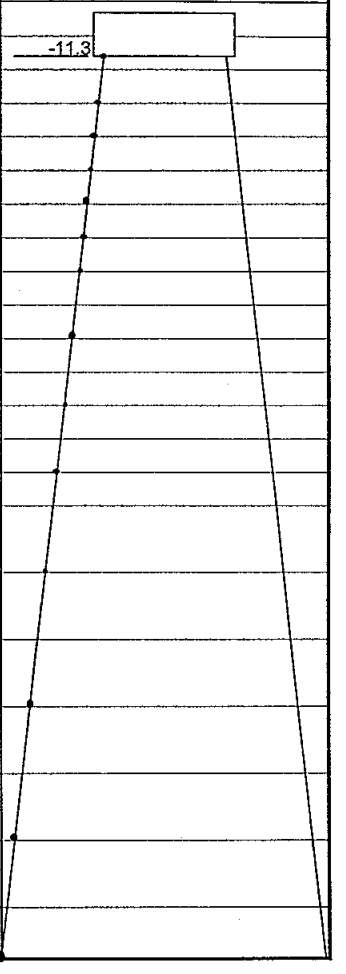

Pile Tip Elevations

Eastbound : El -97 m

Westbound : El -96 m

Conversions :

1pcf = 0.157 kN/m3

1ft/sec = 0.305 m/sec

- Location of Pile Node for Kinematic Analysis

Pier No.	E09
EL. Bot. of Cap (m)	-10.9
EL. of Mudline (m)	-4.0

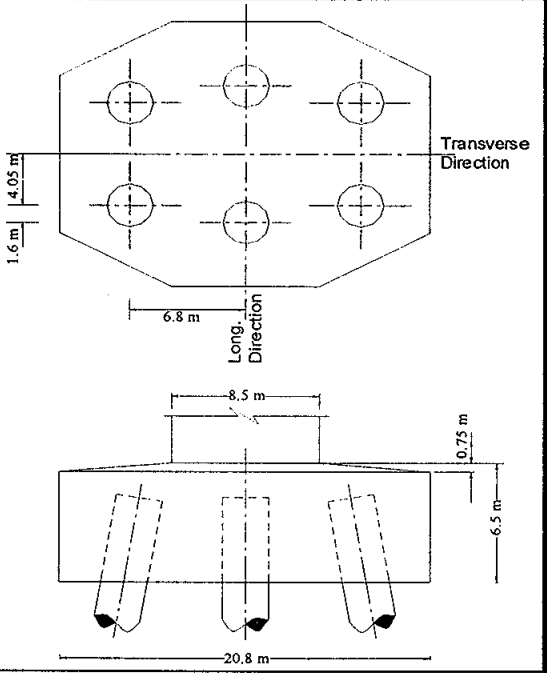

V_s (ft/sec)	γ (pcf)	Depth (m)	Elev (m)
From SHAKE Profile	From SHAKE Profile		-4.0
300	104	3.0	-7.0
325	104	6.0	-10.0
350	104	9.0	-13.0
375	104	12.0	-16.0
400	104	15.0	-19.0
450	104	18.0	-22.0
900	130	21.0	-25.0
700	116	24.0	-28.0
750	116	27.0	-31.0
800	116	30.0	-34.0
800	116	33.0	-37.0
800	116	36.0	-40.0
800	116	39.0	-43.0
800	116	42.0	-46.0
800	116	45.0	-49.0
1000	116	51.0	-55.0
1000	116	57.0	-61.0
800	116	63.0	-67.0
800	116	69.0	-73.0
850	116	75.0	-79.0
900	116	81.0	-85.0
1500	130	91.0	-95.0

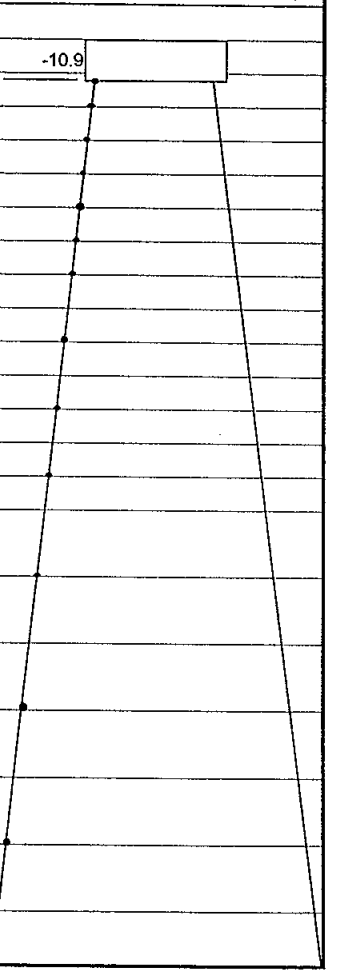

Pile Tip Elevations
Eastbound : El -96 m
Westbound : El -94 m

Conversions :
1pcf = 0.157 kN/m3
1ft/sec = 0.305 m/sec

- Location of Pile Node for Kinematic Analysis

PILE GROUP CONFIGURATION PIER E09

SFOBB East Span Seismic Safety Project

Pier No.	E10
EL. Bot. of Cap (m)	-11.75
EL. of Mudline (m)	-3.8

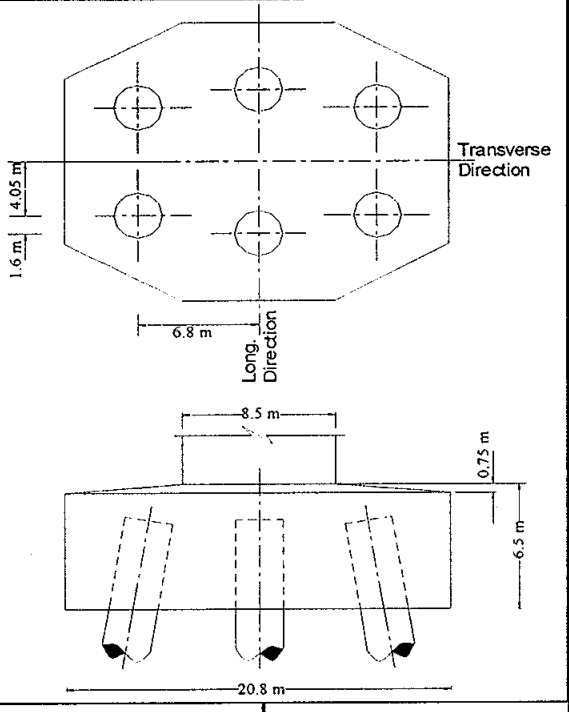

V_s (ft/sec)	γ (pcf)	Depth (m)	Elev (m)
From SHAKE Profile	From SHAKE Profile		
			-3.8 Mudline
300	102	3	-6.8
325	102	6	-9.8
350	102	9	-12.8
375	102	12	-15.8
700	128	15	-18.8
700	128	18	-21.8
500	116	21	-24.8
700	116	24	-27.8
750	116	27	-30.8
800	116	30	-33.8
800	116	33	-36.8
800	116	36	-39.8
800	116	39	-42.8
800	116	42	-45.8
800	116	45	-48.8
1000	116	51	-54.8
1000	116	57	-60.8
800	116	63	-66.8
800	116	69	-72.8
850	116	75	-78.8
900	116	81	-84.8
1500	130	91	-95

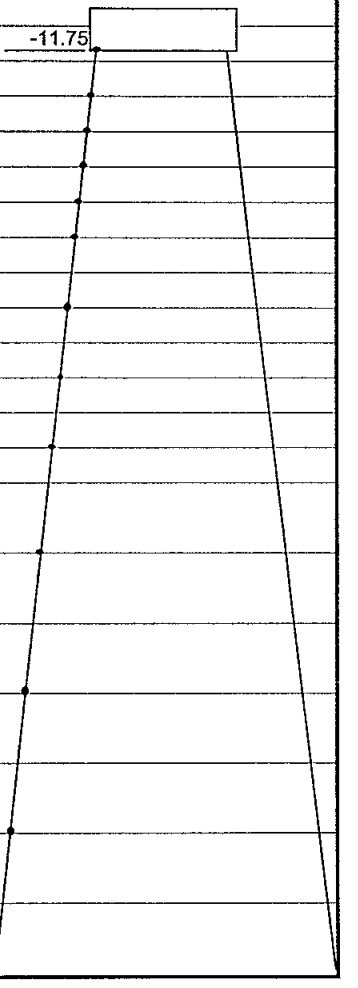

Pile Tip Elevations
Eastbound : El -95 m
Westbound : El -98 m

Conversions :
1pcf = 0.157 kN/m3
1ft/sec = 0.305 m/sec

- Location of Pile Node for Kinematic Analysis

PILE GROUP CONFIGURATION PIER E10

SFOBB East Span Seismic Safety Project

Pier No.	E11
EL. Bot. of Cap (m)	-9.6
EL. of Mudline (m)	-3.8

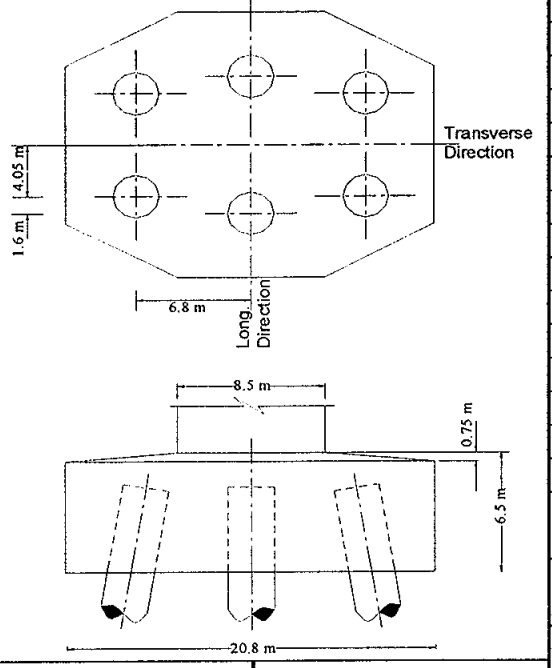

V_s (ft/sec)	γ (pcf)	Depth (m)	Elev (m)
From SHAKE Profile	From SHAKE Profile		
			-3.8
300	102	3	-6.8
325	102	6	-9.8
350	102	9	-12.8
375	102	12	-15.8
500	125	15	-18.8
600	125	18	-21.8
600	116	21	-24.8
700	116	24	-27.8
750	116	27	-30.8
800	116	30	-33.8
800	116	33	-36.8
800	116	36	-39.8
900	116	39	-42.8
900	116	42	-45.8
900	116	45	-48.8
1100	116	51	-54.8
800	116	57	-60.8
800	116	63	-66.8
850	116	69	-72.8
850	116	75	-78.8
900	116	81	-84.8
1500	130	91	-95

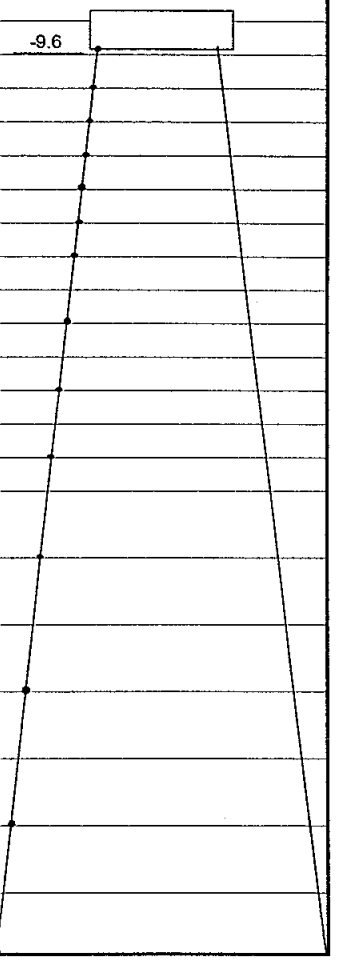

Pile Tip Elevations

Eastbound : El -95 m

Westbound : El -95 m

Conversions :

1pcf = 0.157 kN/m3

1ft/sec = 0.305 m/sec

- Location of Pile Node for Kinematic Analysis

PILE GROUP CONFIGURATION PIER E11

SFOBB East Span Seismic Safety Project

Pier No.	E12
EL. Bot. of Cap (m)	-12.6
EL. of Mudline (m)	-3.6

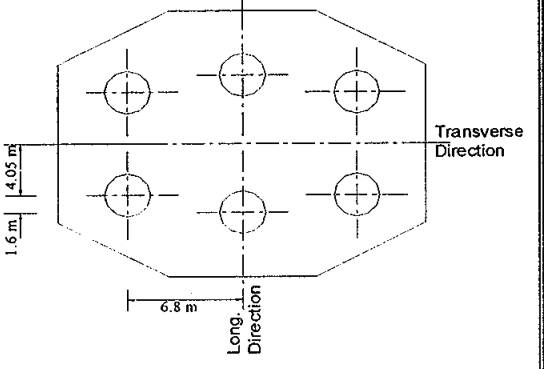

V_s (ft/sec)	γ (pcf)	Depth (m)	Elev (m)
From SHAKE Profile	From SHAKE Profile		-3.6
300.0	102	3.0	-6.6
325.0	102	6.0	-9.6
350.0	102	9.0	-12.6
375.0	102	12.0	-15.6
600.0	122	15.0	-18.6
600.0	122	18.0	-21.6
500.0	116	21.0	-24.6
525.0	116	24.0	-27.6
550.0	116	27.0	-30.6
600.0	116	30.0	-33.6
650.0	116	33.0	-36.6
700.0	116	36.0	-39.6
900.0	116	39.0	-42.6
900.0	116	42.0	-45.6
900.0	116	45.0	-48.6
1000	116	51.0	-54.6
800	116	57.0	-60.6
700	116	63.0	-66.6
700	116	69.0	-72.6
700	116	75.0	-78.6
1100	116	81.0	-84.6
1500	130	91.4	-95.0

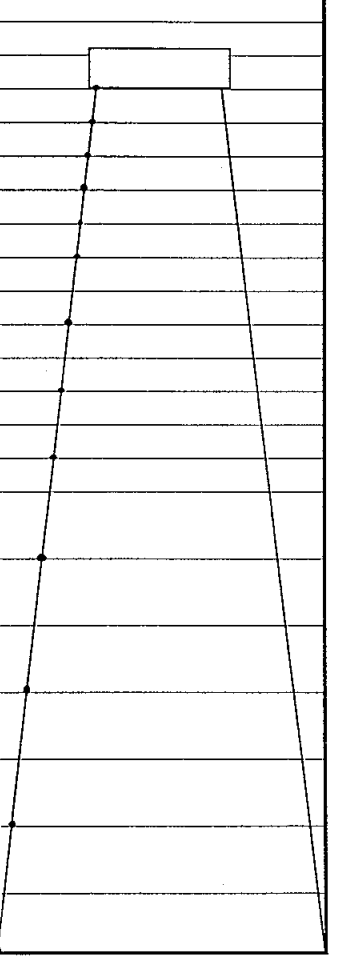

Pile Tip Elevations
Eastbound : El -97 m
Westbound : El -97 m

Conversions :
1pcf = 0.157 kN/m3
1ft/sec = 0.305 m/sec

- Location of Pile Node for Kinematic Analysis

PILE GROUP CONFIGURATION PIER E12
SFOBB East Span Seismic Safety Project

Pier No.	E13
EL. Bot. of Cap (m)	-14.5
EL. of Mudline (m)	-3.4

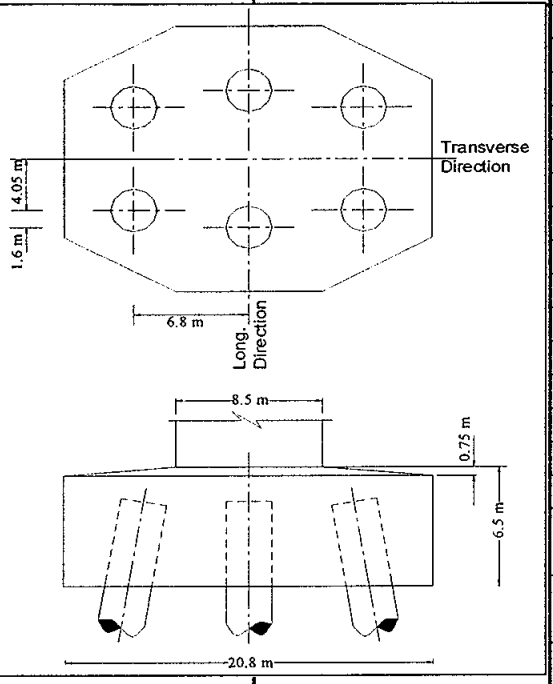

V_s (ft/sec)	γ (pcf)	Depth (m)	Elev (m)
From SHAKE Profile	From SHAKE Profile		-3.4
300	102	3.0	-6.4
325	102	6.0	-9.4
350	102	9.0	-12.4
400	102	12.0	-15.4
500	115	15.0	-18.4
600	115	18.0	-21.4
600	116	21.0	-24.4
700	116	24.0	-27.4
700	116	27.0	-30.4
650	116	30.0	-33.4
650	116	33.0	-36.4
700	116	36.0	-39.4
900	116	39.0	-42.4
900	116	42.0	-45.4
600	116	45.0	-48.4
900	116	51.0	-54.4
700	116	57.0	-60.4
800	116	63.0	-66.4
1100	116	69.0	-72.4
1000	116	75.0	-78.4
1300	116	81.0	-84.4
1500	130	91.6	-95.0

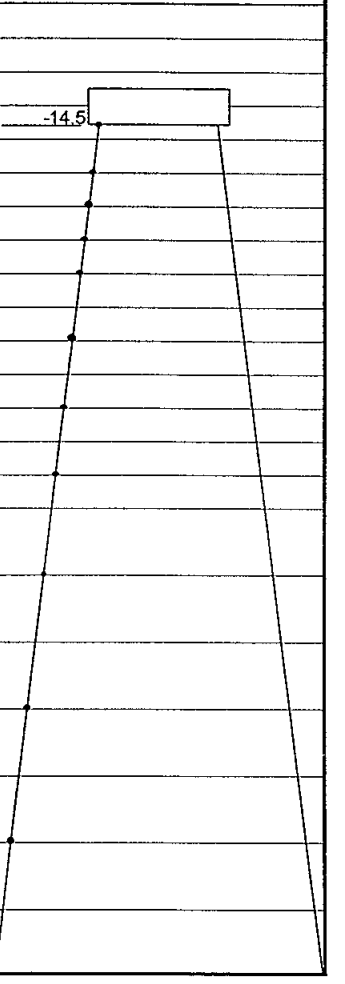

Pile Tip Elevations
Eastbound : El -91 m
Westbound : El -94 m

Conversions :
1pcf = 0.157 kN/m3
1ft/sec = 0.305 m/sec

• Location of Pile Node for Kinematic Analysis

PILE GROUP CONFIGURATION PIER E13

SFOBB East Span Seismic Safety Project

Pier No.	E14
EL. Bot. of Cap (m)	-16.0
EL. of Mudline (m)	-3.0

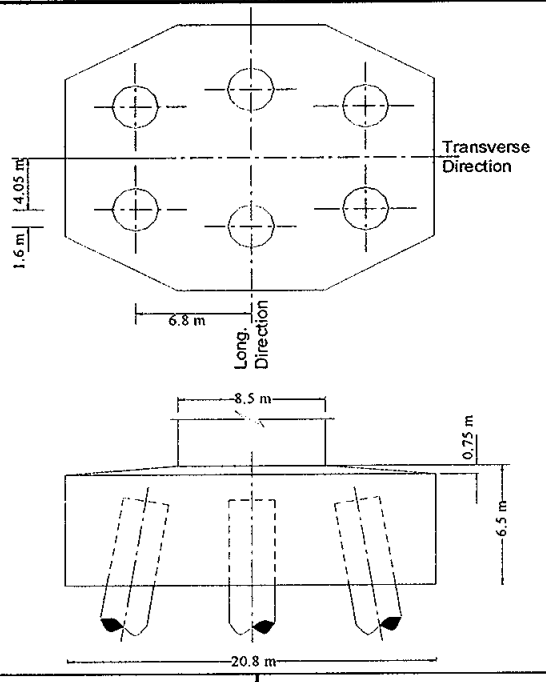

Pile Tip Elevation	Conversions :
Eastbound : El -95 m	1pcf = 0.157 kN/m3
Westbound : El -95 m	1ft/sec = 0.305 m/sec

V_s (ft/sec)	γ (pcf)	Depth (m)	Elev (m)
From SHAKE Profile	From SHAKE Profile		-3.0
300	102	3.0	-6.0
325	102	6.0	-9.0
350	102	9.0	-12.0
400	102	12.0	-15.0
900	122	15.0	-18.0
650	122	18.0	-21.0
600	116	21.0	-24.0
650	116	24.0	-27.0
700	116	27.0	-30.0
750	116	30.0	-33.0
800	116	33.0	-36.0
850	116	36.0	-39.0
900	116	39.0	-42.0
900	116	42.0	-45.0
700	116	45.0	-48.0
1000	116	51.0	-54.0
800	116	57.0	-60.0
800	116	63.0	-66.0
900	116	69.0	-72.0
1000	116	75.0	-78.0
1200	116	81.0	-84.0
1500	130	92.0	-95

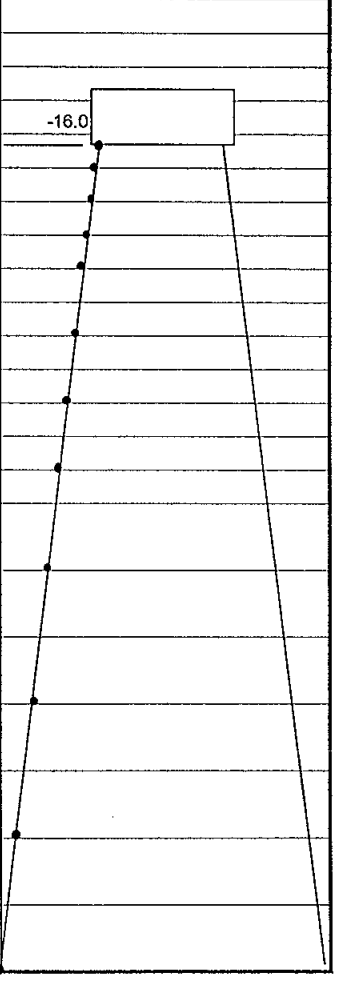

• Location of Pile Node for Kinematic Analysis

PILE GROUP CONFIGURATION PIER E14
SFOBB East Span Seismic Safety Project

Pier No.	E15
EL. Bot. of Cap (m)	-10.5
EL. of Mudline (m)	-3.4

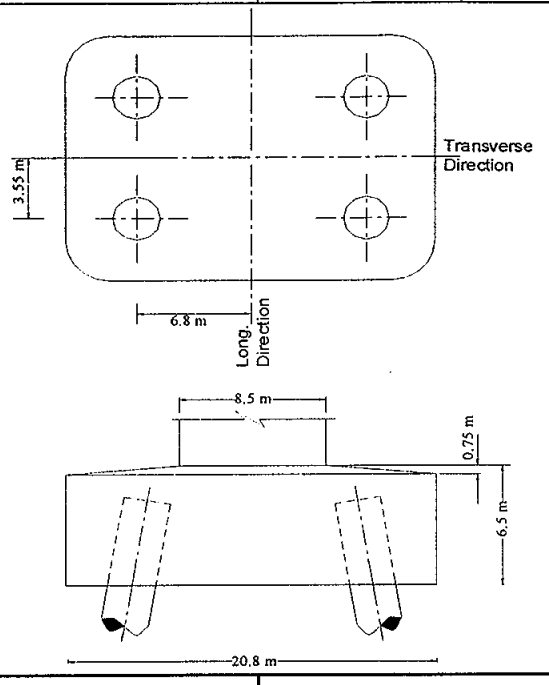

Pile Tip Elevation	Conversions :
Eastbound : El -93 m	1pcf = 0.157 kN/m3
Westbound : El -93 m	1ft/sec = 0.305 m/sec

V_s (ft/sec)	γ (pcf)	Depth (m)	Elev (m)
From SHAKE Profile	From SHAKE Profile		-3.4
300	102	3.0	-6.4
325	102	6.0	-9.4
350	102	9.0	-12.4
400	102	12.0	-15.4
600	122	15.0	-18.4
800	122	18.0	-21.4
600	116	21.0	-24.4
650	116	24.0	-27.4
700	116	27.0	-30.4
750	116	30.0	-33.4
800	116	33.0	-36.4
850	116	36.0	-39.4
900	116	39.0	-42.4
900	116	42.0	-45.4
650	116	45.0	-48.4
1000	116	51.0	-54.4
800	116	57.0	-60.4
1000	116	63.0	-66.4
900	116	69.0	-72.4
900	116	75.0	-78.4
1200	116	81.0	-84.4
1500	130	91.6	-95.0

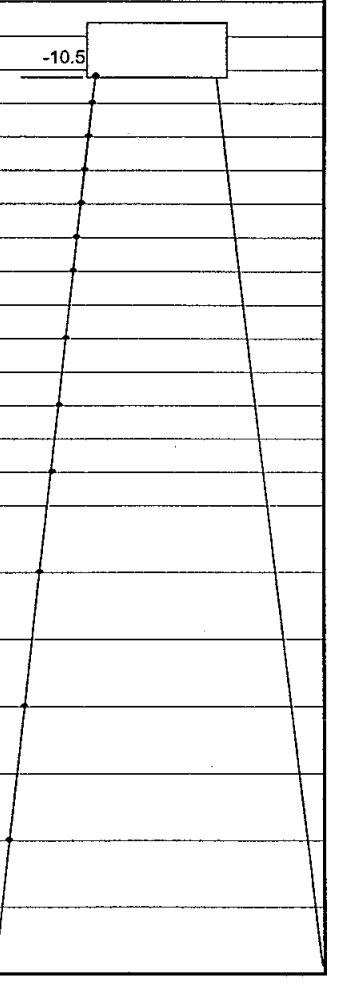

- Location of Pile Node for Kinematic Analysis

PILE GROUP CONFIGURATION PIER E15
SFOBB East Span Seismic Safety Project

Earth Mechanics FUGRO

Pier No.	E16
EL. Bot. of Cap (m)	-11.0
EL. of Mudline (m)	-3.4

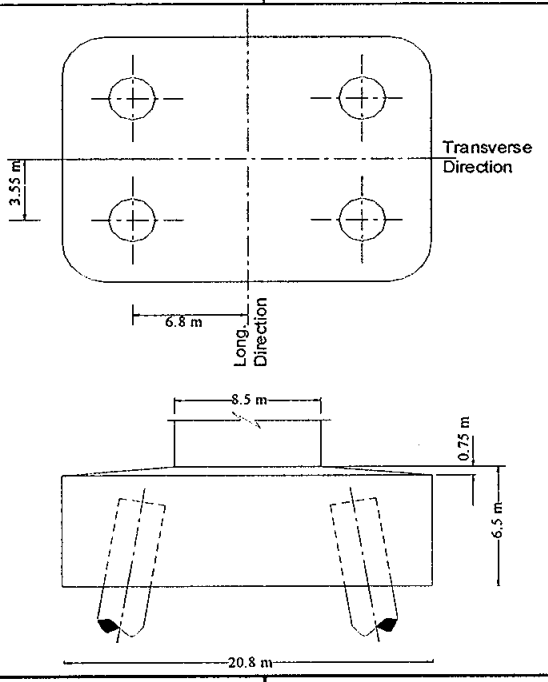

Pile Tip Elevation	Conversions :
Eastbound : El -94 m	1pcf = 0.157 kN/m3
Westbound : El -94 m	1ft/sec = 0.305 m/sec

V_s (ft/sec)	γ (pcf)	Depth (m)	Elev (m)
From SHAKE Profile	From SHAKE Profile		-3.4
300	109	3.0	-6.4
325	109	6.0	-9.4
350	109	9.0	-12.4
400	109	12.0	-15.4
450	109	15.0	-18.4
800	116	18.0	-21.4
600	116	21.0	-24.4
650	116	24.0	-27.4
650	116	27.0	-30.4
650	116	30.0	-33.4
800	116	33.0	-36.4
900	116	36.0	-39.4
900	116	39.0	-42.4
900	116	42.0	-45.4
700	116	45.0	-48.4
1000	116	51.0	-54.4
750	116	57.0	-60.4
900	125	63.0	-66.4
1000	125	69.0	-72.4
1200	125	75.0	-78.4
1200	125	81.0	-84.4
1500	130	91.6	-95.0

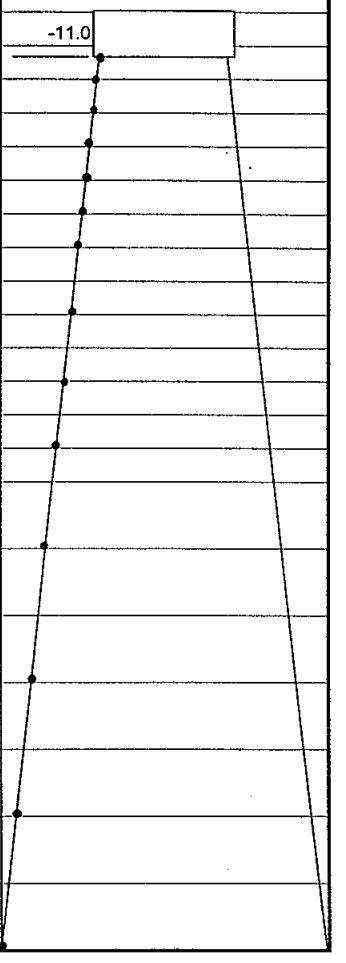

• Location of Pile Node for Kinematic Analysis

PILE GROUP CONFIGURATION PIER E16

SFOBB East Span Seismic Safety Project

SECTION 6.0
KINEMATIC SOIL-PILE INTERACTION

6.0 KINEMATIC SOIL-PILE INTERACTION

6.1 CONCEPT FOR SUBSTRUCTURING

Soil-structure interaction should be included when dealing with seismic response of bridges especially those located in poor site conditions. To evaluate dynamic response of a structure on deep foundation, it would be most desirable to create a complete analytical model of the total system including the superstructure, pile cap, and the soil-pile (foundation) system along the entire embedded pile length in a time history response analysis. Such model would account for depth varying nonlinear soil springs (p-y curves), depth varying ground motion, and inertial forces of the foundation system. However, such a model would be cumbersome and the analysis would involve a large number of degrees of freedom.

The solution for keeping model size small and reducing the number of degrees of freedom is to use the method of substructuring. The total structure can be divided into two substructures: a substructure for the foundation and a substructure for the superstructure, with a convenient interface between the two at the pile cap level. The procedure involves two steps: the first step is conducted in the foundation substructure and the second step is conducted in the bridge substructure. In the first step, the stiffness of the foundation system and the forces arising from the soil-pile interaction can be condensed at the pile cap level without prior knowledge of superstructure. Then the foundation stiffness and force vector can be used in the second step to analyze the seismic response of the bridge superstructure. As pile foundations are supported on multiple soil layers (soil springs) that are excited by depth-varying free-field motions of different characteristics, kinematic interaction analysis provides a rational means to develop appropriate response spectrum that retain the characteristics of the depth varying motion.

6.2 THEORETICAL BACKGROUND

For a single-degree-of-freedom lumped mass system as shown in Plate 6.1(a), the equation of motion can be given as

$$m\ddot{x} + c\dot{x} + kx = -m\ddot{x}_g \qquad (6.1)$$

where x_g is the absolute displacement of the support (ground) with respect to a fixed frame of reference, x is the relative displacement of the mass with respect to the ground, and m, c and k are mass, damping coefficient and stiffness coefficient, respectively. The response of this SDOF system to specified ground acceleration can be solved by Duhamel integral. The maximum value of the response is computed from the response spectrum of the ground motion (S_d), such that

$$x_{max} = \frac{1}{\omega}\left[\int_0^t \ddot{x}_g(\tau)\exp[-\xi\omega(t-\tau)]\sin\omega(t-\tau)d\tau\right]_{max} = \frac{1}{\omega}S_v(\zeta,T) = S_d(\zeta,T) \qquad (6.2)$$

where S_v is the spectral pseudo-velocity and S_d is the spectral relative displacement of the ground motion $\ddot{x}_g$. For the formulation of a multiple-degree-of-freedom (MDOF) lumped mass system subjected to base motion as shown in Plate 6.1(b), the solution can be obtained in a manner analogous to the SDOF system. The equations of motion for the MDOF system can be written in the matrix form as

$$[m]\{\ddot{x}\} + [c]\{\dot{x}\} + [k]\{x\} = -[m]\{1\}\ddot{x}_g(t) \tag{6.3}$$

Approximate response of the MDOF system is often obtained by carrying out the analysis for a few modes in the normal coordinate system and superimposing these responses. The transformation to normal coordinate system results in a set n uncoupled equations for n-degree of freedom system (e.g., Clough and Penzien, 1975). The equation for the nth mode can be written

$$M_n \ddot{X}_n + C_n \dot{X}_n + K_n X_n = \lambda_n \ddot{x}_g(t) \tag{6.4}$$

as

where $\lambda_n = \phi_n{}^T [m]\{1\}$, and ϕ_n is the nth mode shape. For each individual mode of the structure, the maximum response can be obtained from the response spectrum (S_d),

$$x_{n,max} = \phi_n \frac{\lambda_n}{M_n \omega_n} S_v(\xi_n, T_n) = \phi_n \frac{\lambda_n}{M_n} S_d(\xi_n, T_n) \tag{6.5}$$

where M_n, ξ_n and T_n are the modal mass, damping ratio and period of the nth mode, respectively. When a structure is supported at more than one points and has different ground motions applied at each as shown in Plate 6.1(c), the formulation of equations for this multiple-support system is expressed in terms of the total motions of the structure (including the support motion) as

$$[m]\{\ddot{x}^t\} + [c]\{\dot{x}^t\} + [k]\{x^t\} = -[k_g]\{x_g(t)\} \tag{6.6}$$

where $[k_g]$ is the stiffness matrix expressing the force developed in the active degrees of freedom by the motions of the support, and $\{x_g(t)\}$ is a time-varying vector representing multiple input motions. Now, the question arises as to which ground motion should be used to define the response spectrum (S_d) in the earthquake-response analysis. This situation is highly relevant to pile-foundation where each pile is supported on multiple soil layers (soil springs) and the characteristics of free-field motions of those soil layers could be significantly different from each others depending on the soil conditions. The following discussion provides a basis for developing a response spectrum for such a multiple-input multiple-degree-of-freedom system.

6.3 DEVELOPMENT OF KINEMATIC MOTION AND CONDENSED STIFFNESS MATRIX

A typical bridge problem can be considered as a multiple-input, multiple-degree-of-freedom (MDOF) system; it consists of superstructure (deck and column), pile-cap, and pile-foundation as shown in Plate 6.2. For the purpose of discussion, the damping term is ignored and the mass matrix is based on a lumped mass system. The equations of motion for this MDOF system due to multiple-input ground motion $\{x_g(t)\}$ are written as

$$\begin{bmatrix} [m_s] & & \\ & [m_c] & \\ & & [m_p] \end{bmatrix} \begin{Bmatrix} \{\ddot{x}_s\} \\ \{\ddot{x}_c\} \\ \{\ddot{x}_p\} \end{Bmatrix} + \begin{bmatrix} [K_{ss}] & [K_{sc}] & \\ [K_{cs}] & [K_{cc}] & [K_{cp}] \\ & [K_{pc}] & [K_{pp}] \end{bmatrix} \begin{Bmatrix} \{x_s\} \\ \{x_c\} \\ \{x_p\} \end{Bmatrix} = \begin{Bmatrix} 0 \\ 0 \\ [K_g]\{x_g\} \end{Bmatrix} \tag{6.7}$$

where the subscript "s", "c" and "p" denote the superstructure, pile-cap and the pile degrees of freedom, respectively. The mass and stiffness are represented by the matrices [m] and [K]. The vectors $\{x_s\}$, $\{x_c\}$ and $\{x_p\}$ represent displacement of the superstructure, pile-cap, and pile degrees of freedom relative to the earth inertia reference frame (i.e, total displacements), respectively. The displacement vector $\{x_g\}$ represents the depth-varying free-field motions which can be computed from an appropriate site response study, and $[K_g]$ is the soil stiffness surrounding the piles. The pile-cap node would have 6 degrees of freedom (three translation, and three rotation). It is assumed that mass of the pile is small and can be ignored, i.e, $[m_p]=0$. Typically this is the case because inertial forces of the piles are relatively small compared to the more massive superstructure, and therefore neglecting the foundation inertial effect does not normally cause significant error. Then the system of equations become:

$$\begin{bmatrix} [m_s] & & \\ & [m_c] & \\ & & [0] \end{bmatrix} \begin{Bmatrix} \{\ddot{x}_s\} \\ \{\ddot{x}_c\} \\ \{\ddot{x}_p\} \end{Bmatrix} + \begin{bmatrix} [K_{ss}] & [K_{sc}] & \\ [K_{cs}] & [K_{cc}] & [K_{cp}] \\ & [K_{pc}] & [K_{pp}] \end{bmatrix} \begin{Bmatrix} \{x_s\} \\ \{x_c\} \\ \{x_p\} \end{Bmatrix} = \begin{Bmatrix} 0 \\ 0 \\ [K_g]\{x_g\} \end{Bmatrix} \tag{6.8}$$

With the pile mass assumed to be zero, static condensation can be performed to eliminate the pile degrees of freedom. After eliminating the pile degrees of freedom, dynamic response analysis can be performed using the following set of equations involving the superstructure $\{x_s\}$ and the pile cap nodes $\{x_c\}$;

$$\begin{bmatrix} [m_s] & \\ & [m_c] \end{bmatrix} \begin{Bmatrix} \{\ddot{x}_s\} \\ \{\ddot{x}_c\} \end{Bmatrix} + \begin{bmatrix} [K_{ss}] & [K_{sc}] \\ [K_{cs}] & [K] \end{bmatrix} \begin{Bmatrix} \{x_s\} \\ \{x_c\} \end{Bmatrix} = \begin{Bmatrix} 0 \\ \{f\} \end{Bmatrix} \tag{6.9}$$

where [K] and {f} in the above equation are defined as

$$[K] = [K_{cc}] - [K_{cp}][K_{pp}]^{-1}[K_{pc}] \tag{6.10}$$

$$\{f\} = -[K_{cp}][K_{pp}]^{1}[K_g]\{x_g\} \tag{6.11}$$

It is noted that Equation 6.9 contains only the pile-cap and the superstructure degrees of freedom, and in fact the solutions to this set of equations are what the structural engineers are seeking in order to determine demands for the superstructure and the pile-cap. The transformation of the original problem into a substructured system consisting only of the superstructure and pile-cap is entirely based on classical static condensation (e.g., Cook, et al., 1989). The stiffness of the pile foundation system is now represented by the 6x6 condensed stiffness matrix [K], given by Equation 6.10 and the equivalent force applied at the pile-cap represented by the 6x1 forcing function {f}, given by Equation 6.11. Both the stiffness matrix [K] (which is constant with time) and the forcing function {f} (which is time dependent and related to the time histories of the depth-varying free-field input ground motion) can be pre-calculated without knowledge of the response of the superstructure or the pile cap. Instead of using the forcing function {f} explicitly on the right hand side of Equation 6.9, a 6x1 vector {X} is introduced, such that

$$\{f\} = [K]\{X\} \tag{6.12}$$

Then Equation 6.9 becomes

$$\begin{bmatrix} [m_s] & \\ & [m_c] \end{bmatrix} \begin{Bmatrix} \{\ddot{x}_s\} \\ \{\ddot{x}_c\} \end{Bmatrix} + \begin{bmatrix} [K_{ss}] & [K_{sc}] \\ [K_{cs}] & [K] \end{bmatrix} \begin{Bmatrix} \{x_s\} \\ \{x_c\} \end{Bmatrix} = \begin{Bmatrix} 0 \\ [K]\{X\} \end{Bmatrix} \tag{6.13}$$

It can be noted that loading from ground excitation is introduced into the overall structure as a right hand vector in a form of a displacement vector {X} times the foundation stiffness [K], and therefore {X} represent some form of rigid-base motion derived from the depth-varying free-field ground motion. This six-component motion {X} is termed kinematic motion. This kinematic motion {X}, calculated at a single point on the pile cap implicitly contains the statically condensed forces transmitted from the ground to the superstructure along the entire embedded pile length due to both the depth-varying shaking intensity in soil motion as well as the depth-varying soil stiffnesses. The kinematic motion is derived using a massless pile-group model, and therefore maintains the frequency contents of the original ground motion.

Generally, this type of analysis for a pile foundation subjected to ground excitation would involve all six degrees of freedom kinematic motion in order to form the complete force vector {f}. In many cases, when the kinematic motion is derived at the pile-cap, the axial pile stiffness would imply a very large rotational stiffness of the pile group leading to negligible pile-cap rotations, and therefore the rotational components can be neglected. By eliminating the

rotational components, the kinematic motion represents pure translational rigid-base motion compatible with most earthquake engineering analyses involving firm ground input motions. Thus, a Duhamel integral of the kinematic motion that has zero rotation (i.e., kinematic translations at pile-cap) could be used to define response spectra for bridge design as they represent equivalent ground shaking level felt by the superstructure.

6.4 TREATMENT OF MASS AND DAMPING

The substructuring approach using static condensation, as described above, provides rigorous solutions for massless piles. However, for piles with some limited mass, the method is only approximate and the error depends on the relative magnitude of the pile mass to the superstructure mass. The solution can be greatly improved by implementing a condensed mass to represent an inertia effect of the foundation substructure. This is to maintain the fundamental mode of vibration of the entire foundation system in the condensed substructure. One approach would be based on computation of eigenvalues for the soil-pile system representing the entire foundation. The condensed mass, [M], can be approximated by

$$[M] = \frac{1}{\omega^2}[K] \tag{6.14}$$

where [K] is the condensed stiffness matrix obtained from the substructuring approach and ω is an angular frequency. The numeric value for ω is often chosen as the fundamental frequency (1st mode) for each of the six axes (3 translation and 3 rotation) of the original foundation (before condensation). By doing so, the condensed model consisting of the 6x6 mass matrix [M] and the 6x6 stiffness matrix [K] would reproduce the same 6 fundamental modes of vibration as the original foundation prior to adding the superstructure. For practical application, [M] is assumed to be diagonal to simplify the computation.

In many cases, however, computation of natural frequencies and mode shapes for a large pile group can be very time consuming. A method similar to static condensation can be employed to reduce the number of degrees of freedom for a dynamic system which minimizes the expense of computing eigenvalues and eigenvectors. This condensation algorithm is known in the literature as Guyan reduction, mass condensation, dynamic condensation, or eigenvalue economization (Cosk et al., 1989). In the context of a pile foundation, free vibration characteristics of the pile-cap/pile system can be expressed as

$$\left(\begin{bmatrix} [K_{cc}] & [K_{cp}] \\ [K_{pc}] & [K_{pp}] \end{bmatrix} - \omega^2 \begin{bmatrix} [m_c] & \\ & [m_p] \end{bmatrix} \right) \begin{Bmatrix} \{x_c\} \\ \{x_p\} \end{Bmatrix} = \begin{Bmatrix} 0 \\ 0 \end{Bmatrix} \tag{6.15}$$

In order to obtain a relation between $\{x_c\}$ and $\{x_p\}$, all the masses are temporally ignored, and thus providing the following relationship:

$$\begin{Bmatrix} \{x_c\} \\ \{x_p\} \end{Bmatrix} = [T]\{x_c\} \tag{6.16}$$

where

$$[T] = \begin{bmatrix} [I] \\ -[K_{pp}]^{-1}[K_{pc}] \end{bmatrix} \tag{6.17}$$

and [I] is an identity matrix. Substituting Equation 6.16 into Equation 6.15 and pre-multiplying by $[T]^T$ yields a condensed eigen problem as follows

$$([K] - \omega^2[M])\{x_c\} = \{0\} \tag{6.18}$$

where the reduced stiffness and mass matrices are symmetric and are given by

$$[K] = [T]^T \begin{bmatrix} [K_{cc}] & [K_{cp}] \\ [K_{pc}] & [K_{pp}] \end{bmatrix} [T] = [K_{cc}] - [K_{cp}][K_{pp}]^{-1}[K_{pc}] \tag{6.19}$$

and

$$[M] = [T]^T \begin{bmatrix} [m_c] & \\ & [m_p] \end{bmatrix} [T] \tag{6.20}$$

It can be seen that [T] plays a similar role as Ritz vectors in the Raleigh-Ritz method, and the stiffness matrix [K] is the same matrix as produced by static condensation. Furthermore, it is noted the condensed mass [M] is banded and is a combination of both mass and stiffness coefficients. However, to simplify the modeling effort, only the diagonal coefficients of the mass matrix are used for bridge analyses.

If a damping matrix appears in the equation of motion, the same principle can be employed to obtain a condensed damping matrix [C] as

$$[C] = [T]^T \begin{bmatrix} [C_{cc}] & [C_{cp}] \\ [C_{pc}] & [C_{pp}] \end{bmatrix} [T] \tag{6.21}$$

where $[C_{cc}]$ and $[C_{pp}]$ are damping matrices arising from the pile-cap and the piles, respectively. However in typical seismic response analyses for bridges, damping coefficients are not explicitly used. Instead, global damping parameters such as those based on Raleigh damping coefficients are generally used.

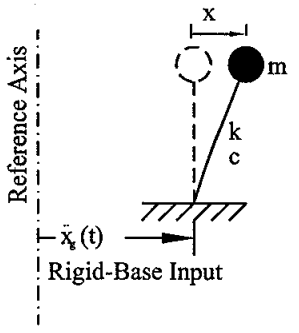

a. Single-Degree-of-Freedom System
Rigid Base Motion

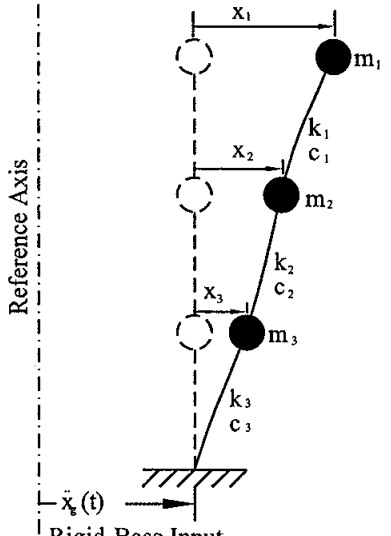

b. Multiple-Degree-of-Freedom System
Rigid Base Motion

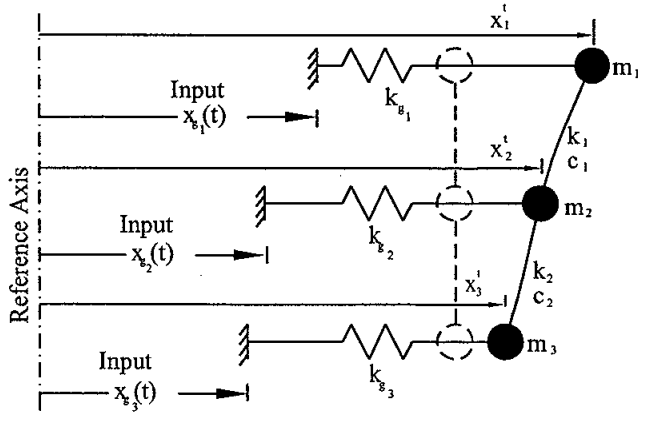

c. Multiple-Degree-of-Freedom System
Multiple Input Motion

SOIL-STRUCTURE INTERACTION:
RIGID-BASED SINGLE DEGREE OF FREEDOM
SFOBB East Span Seismic Safety Project

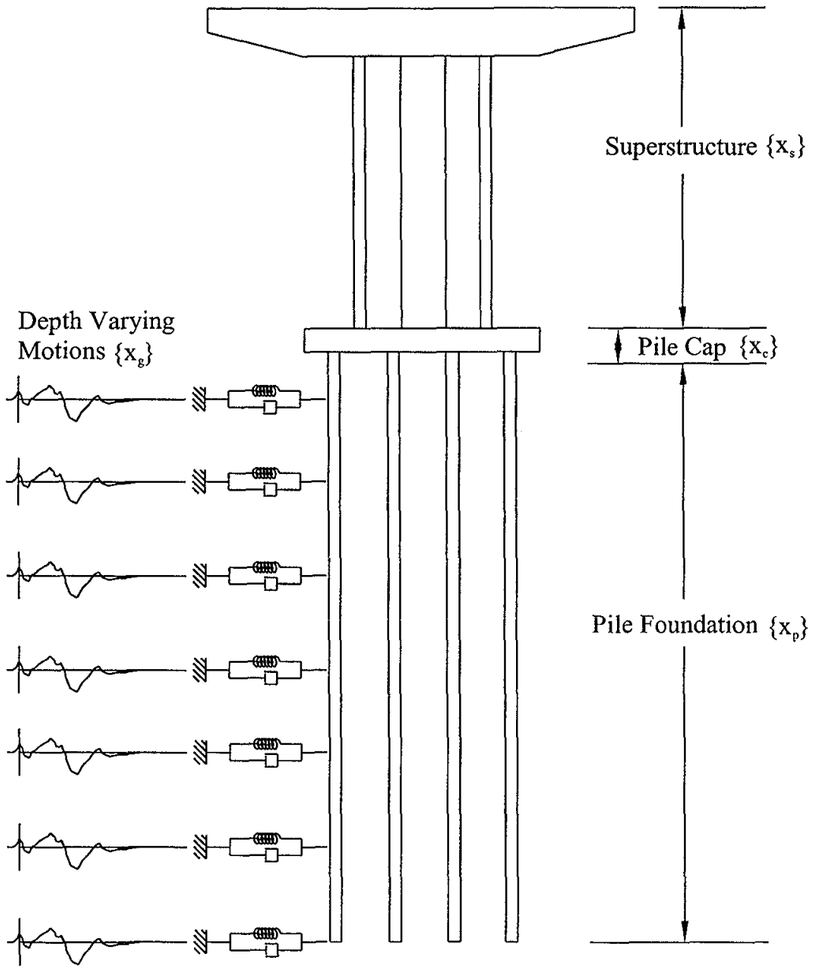

METHOD OF CONDENSATION

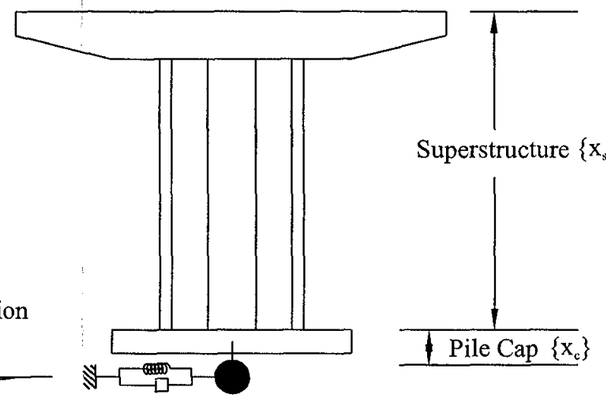

Condensed 6x6 Mass Matrix [M]
Condensed 6x6 Stiffness Matrix [K]
Condensed 6x6 Damping Matrix [C]

SOIL-STRUCTURE INTERACTION:
KINEMATIC MOTION AND CONDENSED MATRICES
SFOBB East Span Seismic Safety Project

SECTION 7.0
DEVELOPMENT OF ARS DESIGN CRITERIA

7.0 DEVELOPMENT OF ARS DESIGN CRITERIA

7.1 YBI STRUCTURE

As the bedrock is shallow on the Yerba Buena Island, the same bedrock motion would be expected at the foundation level. The reference rock ARS curve, without site response studies, can be used directly for response spectrum analyses of the YBI structures.

7.2 SUSPENSION BRIDGE

As the self-anchored suspension bridge would not be designed by the ARS design criteria, no specific ARS curve has been recommended for this structure. Time history analysis would form a basis for seismic loading.

7.3 SKYWAY STRUCTURE

7.3.1 Sensitivity Studies

One of the difficult tasks for defining appropriate loading condition for the superstructure is associated with uncertainty in soil parameters. Variation of shear wave velocity and changing of stress-stain relation of soils would affect the free-field site response analyses which in turn impact the resultant shaking level. To study these effects, some sensitivity analyses were conducted using one soil profile denoted as Profile S. This profile is a composite of soil profiles A, B, C, and D, and was constructed for various sensitivity studies without having to analyze all the profiles. Therefore, it does not represent any part of the bridge structure, and will not be used in the design. But it facilitates parametric studies to appreciate the level of standard deviation due to variation in soil properties. The data shown in Table 7-1 are used in the site response parametric studies. In general two parameters are examined in sensitivity studies: the effects of shear wave velocity of the soil column and the effects of velocity for the compliance base.

Table 7-1 Parameters Used for Sensitivity Study

Case	Shear Wave Velocity Profile	Shear Wave Velocity of Base
S2 (Benchmark)	Best Estimate	457 m/s (1500 ft/s)
S2E	Best Estimate	915 m/s (3000 ft/s)
S2W	Best Estimate	305 m/s (1000 ft/s)
S2N	25% Higher than Best Estimate	457 m/s (1500 ft/s)
S2S	25% Lower than Best Estimate	457 m/s (1500 ft/s)

The above mentioned study (also known as S-Matrix study in the meetings) provided standard deviation for the kinematic response spectrum. The standard deviation is period

dependent. The standard deviation was normalized with the arithmetic mean of response spectra from the S-Matrix study. These ratios can then be multiplied to the mean values of the best-estimated kinematic runs for each of Profiles A, B, C & D to develop their respective absolute standard deviations.

Other sensitivity analyses were conducted for variation in p-y stiffness. In one case, the stiffness was increased by 100 percent, and in other case, the stiffness was reduced by 50 percent. From this parametric study on p-y stiffness, it was concluded that the effect of p-y stiffness is very small and the influence can be neglected. The kinematic analyses were also conducted for both vertical and battered pile options. The battered piles ARS solutions result in between a 5 to 10 percent reduction in shaking from the vertical pile groups at short periods, but approaches the vertical pile ARS criteria at longer period.

There were some discussions on whether the sensitivity study of site response and kinematic soil-structure interaction analyses reflected a sufficient level of uncertainties. The seismologists, particularly, Norm Abrahamson and Walt Silva felt that the uncertainties inherently considered in the ground motion (standard deviation in rock motions) include some degree of uncertainties related to site effects. Also, the design based on ARS criteria would be checked against 6 sets of multiple-support motions which provides additional margin of safety in the design process. The basis adopted for design appeared to be sufficiently robust.

7.3.2 Other Considerations

Frame 1 of the Skyway structure is within soil profiles A and B, while Frames 2 to 6 are within soil profiles C and D. It would be appropriate to develop a set of ARS curves for Frame 1, and separate set of ARS curves for Frames 2 to 6. The following considerations are the major elements in developing the final ARS recommendations:

- To include uncertainty of soil parameters, the mean value from 6 best-estimated kinematic solutions of each profile is added with the one standard deviation as obtained from S-Matrix study. This presumably becomes the 84th percentile solution after accounting for variation in site response analyses.
- The shape of response spectra as obtained from kinematic soil-pile interaction studies contains multiple peaks and valleys. From past experience, this results in difficulty in decision process when the design ARS curves have pronounced multiple peaks and valleys. It was decided that the final ARS recommendations should be constrained by a well-behaved ARS curve shape in both spectral acceleration and displacement.
- At short period range (around 0.5 to 1 second period), the spectral value be the same between fault normal and fault parallel components.

Our recommended ARS curves as presented in Plates 7-1 and 7-2. Plate 7-1 shows the ARS curves for fault normal direction while the ARS curves for fault parallel are shown in Plate 7-2. The results are also presented in Tables 7-2 and 7-3. Shown in each of these Plates are ARS curves for profiles A/B and for profiles C/D. The curves for Profiles A/B are applicable to the western one-third of the Skyway, and the one for Profiles C/D are applicable to the eastern two-

third of the Skyway. The curves presented in these Plates correspond to 5 percent damping. Scaling factors for different levels of damping are presented in Table 7-4. Response spectra for different structural damping values can be obtained by multiplying the scaling factors with the 5-percent spectra. The ARS curves presented in Plates 7-1 and 7-2 were developed for vertical as well as battered pile configurations with a batter angle of 1:6 corresponding to the 30 percent design. Subsequently, in the 65 percent design, the batter angle was changed to 1:8 and 1:12. The ARS curves for these piles would be bounded by those for vertical piles and piles with a batter angle of 1:6.

7.4 Oakland Mole Structure

The bridge structure at the Oakland Mole (east of Pier 17 inclusive) would be supported on two pile types: 610-mm Prestressed Concrete (PCC) piles and 1800-mm Cast-In-Steel-Shell (CISS) piles. The soil influence controlling lateral pile behavior of small-diameter piles such as 610-mm PCC piles would be small (say up to 6 m of pile length). For such small-size piles with top embedded in the competent material of Oakland Mole fills, the kinematic response at the pile top typically corresponds to the lateral free-field ground motions close to the mudline. Therefore, mudline motions is used to represent effective loading for 610-mm PCC piles.

For the 1800-mm CISS piles, formal kinematic soil-pile interaction analyses were conducted for a typical westbound pier and eastbound pier. The soil conditions at the westbound pier is characterized by a marine profile representative of submerged mudline in the tidal flat area, while those at the eastbound pier is characterized by an on-land profile which includes the existing Mole fills above water. The resulting kinematic response at the pile top is found to be correspond to the free-field ground motion at 9 to 12 meters depth for the both subsoil profiles considered. The smooth ARS design spectra for the entire Oakland structure are shown in Plates 7-3 and 7-4 for fault normal and fault parallel directions, respectively.

7.5 Vertical ARS Spectra

A great deal of effort had been devoted to the vertical component ground motion or the vertical ARS spectrum, including collecting and studying downhole array strong motion data collected worldwide. These studies were conducted under the review of Dr. Idriss (member of SSPRP) and Dr. Penzien (member of the Ground Motion Ad Hoc Committee). Ultimately it was concluded that the vertical motion criteria be based on the soft rock spectrum based on compressional, P-wave velocity, to account for the wave passage effect as the motion is propagated upward in the soil mass. The resultant vertical spectrum closely resembles the soft rock target spectrum, except that the shaking is reduced (from 1.3 g to 0.75 g peak spectral acceleration) for periods lower than 0.4 seconds. The resultant vertical design spectrum is provided in table 7-2.

Table 7-2 ARS Curves for Skyway Structure for Vertical Piles at 5 % Damping

Period (sec)	Spectral Acceleration (g)					Relative Displacement (inch)				
	Fault Normal		Fault Parallel		Vertical	Fault Normal		Fault Parallel		Vertical
	Prof. A&B	Prof. C&D	Prof. A&B	Prof. C&D	All Prof.	Prof. A&B	Prof. C&D	Prof. A&B	Prof. C&D	All Prof.
0.030	0.745	0.580	0.745	0.580	0.385	0.007	0.005	0.007	0.005	0.003
0.035	0.745	0.580	0.745	0.580	0.399	0.009	0.007	0.009	0.007	0.005
0.040	0.745	0.580	0.745	0.580	0.413	0.012	0.009	0.012	0.009	0.006
0.045	0.747	0.580	0.747	0.580	0.427	0.015	0.011	0.015	0.011	0.008
0.050	0.750	0.580	0.750	0.580	0.441	0.018	0.014	0.018	0.014	0.011
0.055	0.752	0.582	0.752	0.582	0.455	0.022	0.017	0.022	0.017	0.013
0.060	0.755	0.584	0.755	0.584	0.469	0.027	0.021	0.027	0.021	0.017
0.065	0.765	0.589	0.765	0.589	0.483	0.032	0.024	0.032	0.024	0.020
0.070	0.775	0.594	0.775	0.594	0.497	0.037	0.029	0.037	0.029	0.024
0.075	0.782	0.596	0.782	0.596	0.510	0.043	0.033	0.043	0.033	0.028
0.080	0.790	0.597	0.790	0.597	0.524	0.049	0.037	0.049	0.037	0.033
0.085	0.795	0.598	0.798	0.598	0.538	0.056	0.042	0.056	0.042	0.038
0.090	0.800	0.600	0.806	0.600	0.552	0.063	0.048	0.064	0.048	0.044
0.095	0.814	0.606	0.816	0.606	0.566	0.072	0.054	0.072	0.054	0.050
0.100	0.827	0.612	0.827	0.612	0.580	0.081	0.060	0.081	0.060	0.057
0.105	0.840	0.621	0.840	0.621	0.593	0.091	0.067	0.091	0.067	0.064
0.110	0.852	0.630	0.852	0.630	0.606	0.101	0.075	0.101	0.075	0.072
0.115	0.864	0.640	0.864	0.640	0.619	0.112	0.083	0.112	0.083	0.080
0.120	0.877	0.649	0.877	0.649	0.632	0.124	0.091	0.124	0.091	0.089
0.125	0.889	0.658	0.889	0.658	0.645	0.136	0.101	0.136	0.101	0.099
0.130	0.901	0.667	0.901	0.667	0.658	0.149	0.110	0.149	0.110	0.109
0.135	0.914	0.677	0.914	0.677	0.671	0.163	0.121	0.163	0.121	0.120
0.140	0.926	0.686	0.926	0.686	0.684	0.178	0.132	0.178	0.132	0.131
0.145	0.939	0.695	0.939	0.695	0.697	0.193	0.143	0.193	0.143	0.143
0.150	0.951	0.704	0.951	0.704	0.710	0.209	0.155	0.209	0.155	0.156
0.155	0.963	0.714	0.963	0.714	0.714	0.227	0.168	0.227	0.168	0.168
0.160	0.976	0.723	0.976	0.723	0.718	0.244	0.181	0.244	0.181	0.180
0.165	0.988	0.732	0.988	0.732	0.722	0.263	0.195	0.263	0.195	0.192
0.170	1.000	0.741	1.000	0.741	0.726	0.283	0.210	0.283	0.210	0.205
0.175	1.013	0.750	1.013	0.750	0.730	0.304	0.225	0.304	0.225	0.219
0.180	1.025	0.760	1.025	0.760	0.734	0.325	0.241	0.325	0.241	0.233
0.185	1.038	0.769	1.038	0.769	0.738	0.348	0.258	0.348	0.258	0.247
0.190	1.050	0.778	1.050	0.778	0.742	0.371	0.275	0.371	0.275	0.262
0.195	1.062	0.787	1.062	0.787	0.746	0.395	0.293	0.395	0.293	0.278
0.200	1.075	0.797	1.075	0.797	0.750	0.421	0.312	0.421	0.312	0.294
0.210	1.132	0.822	1.132	0.822	0.748	0.488	0.355	0.488	0.355	0.323
0.220	1.189	0.847	1.189	0.847	0.746	0.563	0.401	0.563	0.401	0.353
0.230	1.246	0.873	1.246	0.873	0.744	0.645	0.452	0.645	0.452	0.385
0.240	1.303	0.898	1.302	0.898	0.742	0.734	0.506	0.734	0.506	0.418
0.250	1.359	0.923	1.359	0.923	0.740	0.832	0.565	0.832	0.565	0.453
0.260	1.416	0.949	1.416	0.949	0.738	0.937	0.628	0.937	0.628	0.488
0.270	1.473	0.974	1.473	0.974	0.736	1.051	0.695	1.051	0.695	0.525
0.280	1.530	0.999	1.530	0.999	0.734	1.174	0.767	1.174	0.767	0.563
0.290	1.587	1.025	1.587	1.025	0.732	1.307	0.843	1.307	0.843	0.603
0.300	1.644	1.050	1.644	1.050	0.730	1.448	0.925	1.448	0.925	0.643
0.310	1.680	1.090	1.683	1.090	0.728	1.580	1.025	1.583	1.025	0.685
0.320	1.715	1.130	1.721	1.130	0.726	1.719	1.133	1.725	1.133	0.728
0.330	1.751	1.170	1.759	1.170	0.724	1.866	1.247	1.875	1.247	0.772
0.340	1.787	1.210	1.797	1.210	0.722	2.022	1.369	2.034	1.369	0.817
0.350	1.822	1.250	1.836	1.250	0.720	2.185	1.499	2.201	1.499	0.863

Table 7-2 Cont'd

0.360	1.858	1.290	1.874	1.290	0.718	2.357	1.637	2.377	1.637	0.911
0.370	1.893	1.330	1.912	1.330	0.716	2.537	1.783	2.562	1.783	0.959
0.380	1.929	1.370	1.951	1.370	0.714	2.726	1.937	2.757	1.937	1.009
0.390	1.964	1.410	1.989	1.410	0.712	2.925	2.100	2.961	2.100	1.060
0.400	2.000	1.451	2.027	1.451	0.710	3.132	2.272	3.175	2.272	1.112
0.410	2.000	1.468	2.025	1.468	0.705	3.291	2.415	3.331	2.415	1.160
0.420	2.000	1.485	2.022	1.485	0.700	3.453	2.564	3.491	2.564	1.209
0.430	2.000	1.502	2.019	1.502	0.695	3.620	2.719	3.655	2.719	1.258
0.440	2.000	1.520	2.017	1.520	0.690	3.790	2.879	3.821	2.879	1.308
0.450	2.000	1.537	2.014	1.537	0.685	3.964	3.046	3.992	3.046	1.358
0.460	2.000	1.554	2.011	1.554	0.680	4.142	3.219	4.166	3.219	1.408
0.470	2.000	1.571	2.009	1.571	0.675	4.324	3.397	4.343	3.397	1.459
0.480	2.000	1.589	2.006	1.589	0.670	4.510	3.582	4.524	3.582	1.511
0.490	2.000	1.606	2.003	1.606	0.665	4.700	3.774	4.708	3.774	1.563
0.500	2.000	1.623	2.001	1.623	0.660	4.894	3.971	4.896	3.971	1.615
0.525	1.975	1.626	1.975	1.626	0.649	5.327	4.386	5.329	4.386	1.750
0.550	1.949	1.629	1.950	1.629	0.637	5.772	4.823	5.773	4.823	1.887
0.575	1.924	1.632	1.924	1.632	0.626	6.227	5.280	6.227	5.280	2.025
0.600	1.899	1.635	1.899	1.635	0.614	6.691	5.759	6.691	5.759	2.165
0.625	1.878	1.617	1.878	1.617	0.603	7.179	6.183	7.179	6.183	2.306
0.650	1.856	1.600	1.856	1.600	0.592	7.677	6.616	7.677	6.616	2.447
0.675	1.835	1.582	1.835	1.582	0.580	8.183	7.057	8.183	7.057	2.588
0.700	1.814	1.565	1.814	1.565	0.569	8.699	7.506	8.699	7.506	2.729
0.750	1.762	1.512	1.762	1.512	0.546	9.701	8.325	9.701	8.325	3.007
0.800	1.710	1.459	1.710	1.459	0.525	10.713	9.140	10.712	9.140	3.290
0.850	1.667	1.414	1.672	1.414	0.504	11.785	10.002	11.822	10.002	3.566
0.900	1.623	1.370	1.634	1.370	0.483	12.867	10.859	12.951	10.859	3.832
0.950	1.592	1.315	1.597	1.328	0.462	14.060	11.614	14.106	11.728	4.084
1.000	1.560	1.260	1.560	1.286	0.441	15.272	12.332	15.272	12.584	4.320
1.100	1.518	1.205	1.507	1.222	0.415	17.977	14.270	17.852	14.473	4.921
1.200	1.467	1.150	1.450	1.161	0.390	20.683	16.209	20.432	16.360	5.491
1.300	1.414	1.097	1.391	1.103	0.364	23.388	18.146	23.011	18.247	6.015
1.400	1.360	1.047	1.334	1.050	0.338	26.095	20.084	25.590	20.136	6.479
1.500	1.308	1.000	1.279	1.000	0.312	28.799	22.023	28.170	22.023	6.867
1.600	1.257	0.963	1.186	0.949	0.297	31.489	24.135	29.708	23.774	7.430
1.700	1.208	0.928	1.105	0.902	0.281	34.180	26.248	31.249	25.526	7.956
1.800	1.163	0.894	1.034	0.860	0.266	36.870	28.361	32.788	27.280	8.434
1.900	1.120	0.862	0.972	0.822	0.251	39.561	30.473	34.328	29.035	8.858
2.000	1.079	0.832	0.916	0.786	0.235	42.249	32.586	35.867	30.785	9.216
2.250	0.882	0.734	0.728	0.663	0.216	43.680	36.391	36.074	32.863	10.678
2.500	0.737	0.657	0.593	0.571	0.196	45.110	40.198	36.283	34.937	11.966
2.750	0.629	0.594	0.493	0.500	0.176	46.545	43.999	36.493	37.011	13.006
3.000	0.545	0.543	0.417	0.444	0.156	47.975	47.808	36.699	39.086	13.725
3.250	0.466	0.468	0.357	0.383	0.143	48.157	48.405	36.919	39.586	14.831
3.500	0.403	0.409	0.310	0.334	0.131	48.345	49.004	37.146	40.096	15.719
3.750	0.353	0.360	0.272	0.295	0.119	48.533	49.593	37.370	40.591	16.345
4.000	0.311	0.321	0.240	0.262	0.106	48.721	50.193	37.586	41.094	16.663
4.250	0.276	0.288	0.214	0.233	0.099	48.707	50.935	37.799	41.105	17.587
4.500	0.246	0.261	0.192	0.207	0.093	48.699	51.692	37.996	41.108	18.344
4.750	0.221	0.237	0.173	0.186	0.086	48.696	52.428	38.206	41.099	18.910
5.000	0.199	0.217	0.157	0.168	0.079	48.695	53.173	38.418	41.110	19.258
5.250	0.180	0.199	0.142	0.152	0.074	48.480	53.794	38.417	41.115	19.930
5.500	0.163	0.184	0.130	0.139	0.069	48.292	54.421	38.402	41.097	20.445
5.750	0.149	0.170	0.119	0.127	0.064	48.089	55.015	38.413	41.099	20.784
6.000	0.136	0.158	0.109	0.117	0.059	47.887	55.639	38.408	41.086	20.931

Table 7-3 ARS Curves for Skyway Structure for Battered Piles at 5% Damping

Period (sec)	Spectral Acceleration (g)					Relative Displacement (inch)				
	Fault Normal		Fault Parallel		Vertical	Fault Normal		Fault Parallel		Vertical
	Prof. A&B	Prof. C&D	Prof. A&B	Prof. C&D	All Prof.	Prof. A&B	Prof. C&D	Prof. A&B	Prof. C&D	All Prof.
0.030	0.747	0.497	0.747	0.497	0.385	0.007	0.004	0.007	0.004	0.003
0.035	0.747	0.507	0.747	0.507	0.399	0.009	0.006	0.009	0.006	0.005
0.040	0.747	0.497	0.747	0.497	0.413	0.012	0.008	0.012	0.008	0.006
0.045	0.747	0.503	0.747	0.503	0.427	0.015	0.010	0.015	0.010	0.008
0.050	0.747	0.497	0.747	0.497	0.441	0.018	0.012	0.018	0.012	0.011
0.055	0.747	0.510	0.747	0.510	0.455	0.022	0.015	0.022	0.015	0.013
0.060	0.747	0.512	0.747	0.512	0.469	0.026	0.018	0.026	0.018	0.017
0.065	0.754	0.527	0.754	0.527	0.483	0.031	0.022	0.031	0.022	0.020
0.070	0.761	0.532	0.761	0.532	0.497	0.036	0.026	0.036	0.026	0.024
0.075	0.768	0.550	0.768	0.552	0.510	0.042	0.030	0.042	0.030	0.028
0.080	0.776	0.559	0.776	0.562	0.524	0.049	0.035	0.049	0.035	0.033
0.085	0.787	0.576	0.787	0.578	0.538	0.056	0.041	0.056	0.041	0.038
0.090	0.798	0.586	0.798	0.587	0.552	0.063	0.046	0.063	0.047	0.044
0.095	0.814	0.602	0.814	0.603	0.566	0.072	0.053	0.072	0.053	0.050
0.100	0.830	0.613	0.830	0.613	0.580	0.081	0.060	0.081	0.060	0.057
0.105	0.840	0.673	0.840	0.673	0.593	0.091	0.073	0.091	0.073	0.064
0.110	0.851	0.720	0.851	0.720	0.606	0.101	0.085	0.101	0.085	0.072
0.115	0.861	0.757	0.861	0.757	0.619	0.111	0.098	0.111	0.098	0.080
0.120	0.871	0.785	0.871	0.785	0.632	0.123	0.111	0.123	0.111	0.089
0.125	0.881	0.807	0.881	0.807	0.645	0.135	0.123	0.135	0.123	0.099
0.130	0.892	0.822	0.892	0.822	0.658	0.147	0.136	0.147	0.136	0.109
0.135	0.902	0.834	0.902	0.834	0.671	0.161	0.149	0.161	0.149	0.120
0.140	0.912	0.841	0.912	0.841	0.684	0.175	0.161	0.175	0.161	0.131
0.145	0.922	0.846	0.922	0.846	0.697	0.190	0.174	0.190	0.174	0.143
0.150	0.932	0.848	0.932	0.848	0.710	0.205	0.187	0.205	0.187	0.156
0.155	0.953	0.848	0.953	0.848	0.714	0.224	0.199	0.224	0.199	0.168
0.160	0.973	0.847	0.973	0.847	0.718	0.244	0.212	0.244	0.212	0.180
0.165	0.993	0.844	0.993	0.844	0.722	0.265	0.225	0.265	0.225	0.192
0.170	1.013	0.840	1.013	0.840	0.726	0.287	0.238	0.287	0.238	0.205
0.175	1.033	0.835	1.033	0.835	0.730	0.310	0.250	0.310	0.250	0.219
0.180	1.053	0.829	1.053	0.829	0.734	0.334	0.263	0.334	0.263	0.233
0.185	1.074	0.823	1.074	0.823	0.738	0.360	0.276	0.360	0.276	0.247
0.190	1.094	0.816	1.094	0.816	0.742	0.386	0.288	0.386	0.288	0.262
0.195	1.114	0.808	1.114	0.808	0.746	0.415	0.301	0.415	0.301	0.278
0.200	1.134	0.801	1.134	0.801	0.750	0.444	0.314	0.444	0.314	0.294
0.210	1.180	0.865	1.180	0.866	0.748	0.509	0.373	0.509	0.374	0.323
0.220	1.226	0.914	1.226	0.917	0.746	0.581	0.433	0.581	0.434	0.353
0.230	1.272	0.952	1.272	0.955	0.744	0.659	0.493	0.659	0.495	0.385
0.240	1.318	0.980	1.318	0.985	0.742	0.743	0.553	0.743	0.555	0.418
0.250	1.364	1.001	1.364	1.006	0.740	0.834	0.612	0.834	0.615	0.453
0.260	1.410	1.016	1.410	1.021	0.738	0.933	0.672	0.933	0.676	0.488
0.270	1.456	1.026	1.456	1.032	0.736	1.039	0.732	1.039	0.736	0.525
0.280	1.502	1.032	1.502	1.038	0.734	1.153	0.792	1.153	0.797	0.563
0.290	1.548	1.035	1.548	1.041	0.732	1.274	0.852	1.274	0.857	0.603
0.300	1.594	1.035	1.594	1.041	0.730	1.404	0.911	1.404	0.917	0.643
0.310	1.621	1.096	1.621	1.101	0.728	1.524	1.031	1.524	1.036	0.685
0.320	1.647	1.148	1.647	1.152	0.726	1.651	1.151	1.651	1.155	0.728
0.330	1.674	1.192	1.674	1.194	0.724	1.784	1.270	1.784	1.273	0.772
0.340	1.700	1.228	1.700	1.230	0.722	1.924	1.390	1.924	1.392	0.817
0.350	1.727	1.259	1.727	1.260	0.720	2.071	1.509	2.071	1.510	0.863
0.360	1.754	1.284	1.754	1.284	0.718	2.224	1.629	2.224	1.629	0.911

Table 7-3 Cont'd

0.370	1.780	1.305	1.780	1.304	0.716	2.385	1.749	2.385	1.747	0.959
0.380	1.807	1.322	1.807	1.320	0.714	2.554	1.868	2.554	1.866	1.009
0.390	1.833	1.335	1.833	1.333	0.712	2.729	1.988	2.729	1.985	1.060
0.400	1.860	1.346	1.860	1.343	0.710	2.913	2.107	2.913	2.103	1.112
0.410	1.860	1.371	1.860	1.369	0.705	3.060	2.256	3.060	2.253	1.160
0.420	1.860	1.392	1.860	1.391	0.700	3.211	2.404	3.211	2.402	1.209
0.430	1.860	1.410	1.860	1.410	0.695	3.366	2.552	3.366	2.552	1.258
0.440	1.860	1.425	1.860	1.426	0.690	3.525	2.701	3.525	2.702	1.308
0.450	1.860	1.438	1.860	1.439	0.685	3.687	2.849	3.687	2.851	1.358
0.460	1.860	1.447	1.860	1.449	0.680	3.852	2.998	3.852	3.001	1.408
0.470	1.860	1.455	1.860	1.457	0.675	4.022	3.146	4.022	3.150	1.459
0.480	1.860	1.461	1.860	1.463	0.670	4.195	3.294	4.195	3.300	1.511
0.490	1.860	1.465	1.860	1.468	0.665	4.371	3.443	4.371	3.450	1.563
0.500	1.860	1.468	1.860	1.471	0.660	4.551	3.591	4.551	3.599	1.615
0.525	1.844	1.495	1.844	1.497	0.649	4.975	4.033	4.975	4.039	1.750
0.550	1.828	1.512	1.828	1.513	0.637	5.412	4.475	5.412	4.480	1.887
0.575	1.812	1.520	1.812	1.520	0.626	5.864	4.917	5.864	4.920	2.025
0.600	1.796	1.521	1.796	1.521	0.614	6.329	5.360	6.329	5.360	2.165
0.625	1.779	1.504	1.779	1.506	0.603	6.802	5.750	6.802	5.759	2.306
0.650	1.762	1.485	1.762	1.489	0.592	7.287	6.140	7.287	6.158	2.447
0.675	1.745	1.464	1.745	1.470	0.580	7.782	6.531	7.782	6.557	2.588
0.700	1.728	1.443	1.728	1.450	0.569	8.288	6.921	8.288	6.956	2.729
0.750	1.671	1.411	1.671	1.414	0.546	9.197	7.769	9.197	7.786	3.007
0.800	1.613	1.376	1.613	1.376	0.525	10.104	8.617	10.104	8.617	3.290
0.850	1.576	1.328	1.576	1.330	0.504	11.142	9.389	11.142	9.408	3.566
0.900	1.538	1.282	1.538	1.287	0.483	12.194	10.162	12.194	10.201	3.832
0.950	1.496	1.243	1.496	1.246	0.462	13.211	10.979	13.211	11.007	4.084
1.000	1.453	1.205	1.453	1.207	0.441	14.222	11.796	14.222	11.812	4.320
1.100	1.372	1.150	1.372	1.152	0.415	16.249	13.620	16.249	13.640	4.921
1.200	1.297	1.096	1.297	1.098	0.390	18.277	15.444	18.277	15.469	5.491
1.300	1.227	1.044	1.227	1.046	0.364	20.303	17.268	20.303	17.298	6.015
1.400	1.164	0.995	1.164	0.997	0.338	22.331	19.092	22.331	19.127	6.479
1.500	1.106	0.950	1.106	0.952	0.312	24.357	20.915	24.357	20.955	6.867
1.600	1.049	0.916	1.037	0.917	0.297	26.295	22.942	25.987	22.973	7.430
1.700	0.998	0.883	0.976	0.884	0.281	28.231	24.969	27.617	24.992	7.956
1.800	0.951	0.851	0.922	0.852	0.266	30.169	26.994	29.249	27.010	8.434
1.900	0.909	0.821	0.874	0.822	0.251	32.105	29.020	30.879	29.027	8.858
2.000	0.870	0.793	0.830	0.793	0.235	34.043	31.048	32.508	31.048	9.216
2.250	0.721	0.684	0.668	0.677	0.216	35.702	33.913	33.120	33.527	10.678
2.500	0.611	0.601	0.551	0.589	0.196	37.366	36.778	33.732	36.008	11.966
2.750	0.527	0.536	0.464	0.520	0.176	39.024	39.646	34.346	38.484	13.006
3.000	0.462	0.483	0.397	0.465	0.156	40.690	42.513	34.955	40.963	13.725
3.250	0.401	0.419	0.338	0.394	0.143	41.478	43.329	34.965	40.775	14.831
3.500	0.353	0.368	0.292	0.339	0.131	42.266	44.148	34.976	40.599	15.719
3.750	0.313	0.327	0.254	0.294	0.119	43.055	44.968	34.975	40.412	16.345
4.000	0.280	0.292	0.223	0.257	0.106	43.850	45.792	34.986	40.233	16.663
4.250	0.252	0.267	0.200	0.227	0.099	44.553	47.116	35.324	40.150	17.587
4.500	0.228	0.244	0.180	0.202	0.093	45.251	48.422	35.657	40.058	18.344
4.750	0.208	0.225	0.163	0.181	0.086	45.935	49.756	35.997	39.972	18.910
5.000	0.191	0.209	0.149	0.163	0.079	46.640	51.069	36.338	39.886	19.258
5.250	0.173	0.190	0.135	0.148	0.074	46.645	51.259	36.528	39.982	19.930
5.500	0.158	0.174	0.124	0.135	0.069	46.634	51.460	36.715	40.090	20.445
5.750	0.144	0.160	0.114	0.124	0.064	46.665	51.681	36.925	40.193	20.784
6.000	0.132	0.147	0.105	0.114	0.059	46.654	51.869	37.104	40.311	20.931

Table 7-4 Scaling Factors for Different Levels of Damping for Skyway ARS Curves

PERIOD (sec)	0% DAMPING	2% DAMPING	5% DAMPING	10% DAMPING	20% DAMPING
0.030	0.996	0.996	1.000	1.000	1.000
0.035	0.997	0.997	1.000	1.000	1.000
0.040	0.998	0.997	1.000	1.000	1.000
0.045	0.997	0.998	1.000	1.000	1.000
0.050	0.996	0.999	1.000	1.000	1.000
0.055	1.002	0.998	1.000	1.000	1.000
0.060	1.007	0.997	1.000	1.000	1.000
0.065	1.075	1.006	1.000	0.993	0.984
0.070	1.142	1.015	1.000	0.987	0.968
0.075	1.201	1.022	1.000	0.983	0.963
0.080	1.259	1.029	1.000	0.979	0.957
0.085	1.316	1.038	1.000	0.974	0.951
0.090	1.373	1.046	1.000	0.970	0.946
0.095	1.410	1.056	1.000	0.964	0.940
0.100	1.447	1.066	1.000	0.958	0.934
0.105	1.482	1.073	1.000	0.955	0.928
0.110	1.518	1.080	1.000	0.952	0.923
0.115	1.553	1.086	1.000	0.950	0.918
0.120	1.588	1.093	1.000	0.947	0.912
0.125	1.624	1.100	1.000	0.944	0.907
0.130	1.659	1.107	1.000	0.941	0.901
0.135	1.694	1.114	1.000	0.938	0.896
0.140	1.729	1.120	1.000	0.936	0.891
0.145	1.765	1.127	1.000	0.933	0.885
0.150	1.800	1.134	1.000	0.930	0.880
0.160	1.838	1.144	1.000	0.924	0.871
0.170	1.876	1.153	1.000	0.917	0.863
0.180	1.915	1.163	1.000	0.911	0.854
0.190	1.953	1.172	1.000	0.905	0.845
0.200	1.991	1.182	1.000	0.898	0.837
0.210	2.012	1.190	1.000	0.891	0.827
0.220	2.032	1.198	1.000	0.884	0.817
0.230	2.053	1.205	1.000	0.878	0.807
0.240	2.073	1.213	1.000	0.871	0.797
0.250	2.094	1.221	1.000	0.864	0.786
0.260	2.114	1.229	1.000	0.857	0.776
0.270	2.135	1.237	1.000	0.850	0.766
0.280	2.155	1.244	1.000	0.843	0.756
0.290	2.176	1.252	1.000	0.837	0.746
0.300	2.196	1.260	1.000	0.830	0.736
0.310	2.208	1.267	1.000	0.824	0.726
0.320	2.220	1.274	1.000	0.818	0.715
0.330	2.232	1.282	1.000	0.812	0.704
0.340	2.244	1.289	1.000	0.806	0.694
0.350	2.256	1.296	1.000	0.800	0.683
0.360	2.267	1.303	1.000	0.794	0.672
0.370	2.279	1.310	1.000	0.788	0.662
0.380	2.291	1.318	1.000	0.782	0.651
0.390	2.303	1.325	1.000	0.776	0.641

Table 7-4 Cont'd

0.400	2.315	1.332	1.000	0.770	0.630
0.410	2.319	1.336	1.000	0.770	0.629
0.420	2.323	1.339	1.000	0.770	0.628
0.430	2.327	1.343	1.000	0.770	0.627
0.440	2.331	1.346	1.000	0.771	0.626
0.450	2.335	1.350	1.000	0.771	0.625
0.460	2.334	1.353	1.000	0.771	0.624
0.470	2.333	1.355	1.000	0.771	0.624
0.480	2.331	1.358	1.000	0.772	0.623
0.490	2.330	1.360	1.000	0.772	0.622
0.500	2.329	1.363	1.000	0.772	0.622
0.525	2.313	1.358	1.000	0.774	0.624
0.550	2.298	1.353	1.000	0.776	0.626
0.575	2.282	1.347	1.000	0.777	0.628
0.600	2.266	1.342	1.000	0.779	0.630
0.625	2.253	1.339	1.000	0.781	0.633
0.650	2.239	1.336	1.000	0.782	0.635
0.675	2.226	1.332	1.000	0.784	0.637
0.700	2.212	1.329	1.000	0.786	0.639
0.750	2.192	1.324	1.000	0.789	0.644
0.800	2.172	1.318	1.000	0.792	0.648
0.850	2.148	1.313	1.000	0.794	0.652
0.900	2.124	1.308	1.000	0.797	0.656
0.950	2.106	1.304	1.000	0.799	0.659
1.000	2.087	1.299	1.000	0.802	0.662
1.100	2.057	1.292	1.000	0.805	0.668
1.200	2.027	1.285	1.000	0.808	0.674
1.300	1.996	1.279	1.000	0.811	0.680
1.400	1.966	1.272	1.000	0.815	0.686
1.500	1.936	1.265	1.000	0.818	0.692
1.600	1.918	1.260	1.000	0.821	0.696
1.700	1.899	1.255	1.000	0.824	0.700
1.800	1.881	1.250	1.000	0.828	0.705
1.900	1.862	1.245	1.000	0.831	0.709
2.000	1.844	1.240	1.000	0.834	0.713
2.250	1.809	1.232	1.000	0.839	0.721
2.500	1.773	1.223	1.000	0.844	0.729
2.750	1.738	1.215	1.000	0.849	0.736
3.000	1.702	1.206	1.000	0.853	0.744
3.250	1.678	1.200	1.000	0.857	0.750
3.500	1.654	1.194	1.000	0.860	0.755
3.750	1.630	1.187	1.000	0.864	0.761
4.000	1.606	1.181	1.000	0.867	0.766
4.250	1.586	1.177	1.000	0.870	0.770
4.500	1.565	1.172	1.000	0.873	0.775
4.750	1.545	1.168	1.000	0.875	0.779
5.000	1.524	1.163	1.000	0.878	0.783
5.250	1.508	1.159	1.000	0.880	0.787
5.500	1.492	1.155	1.000	0.882	0.790
5.750	1.476	1.151	1.000	0.885	0.794
6.000	1.460	1.147	1.000	0.887	0.797

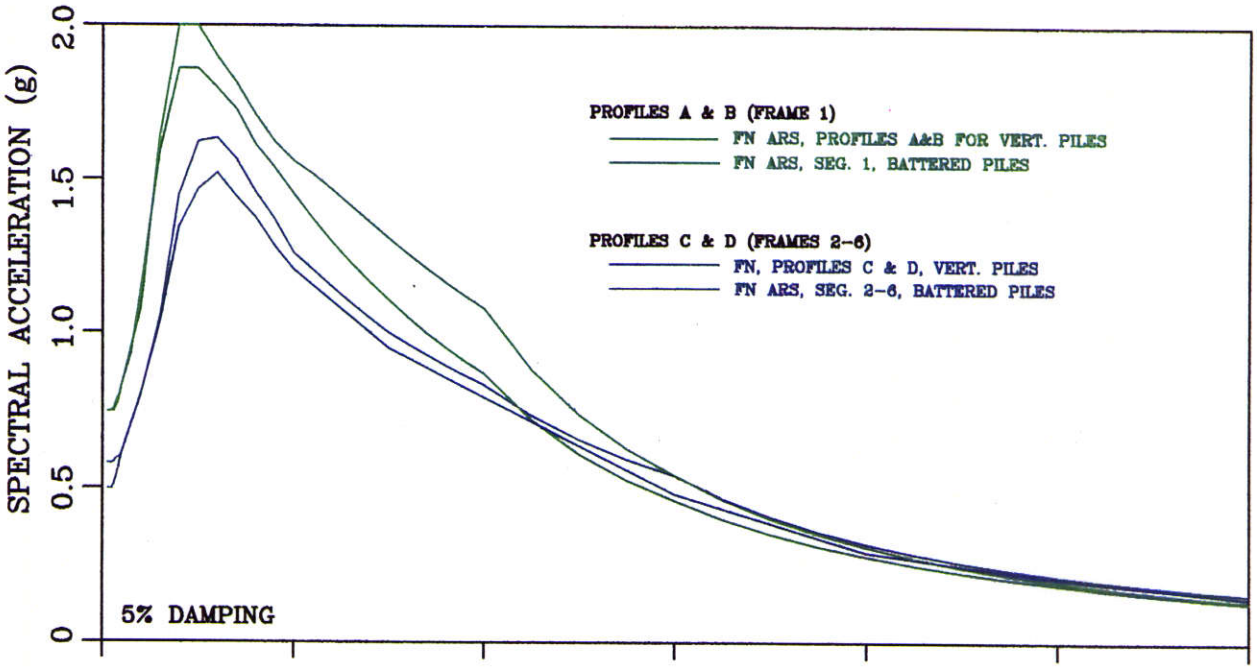

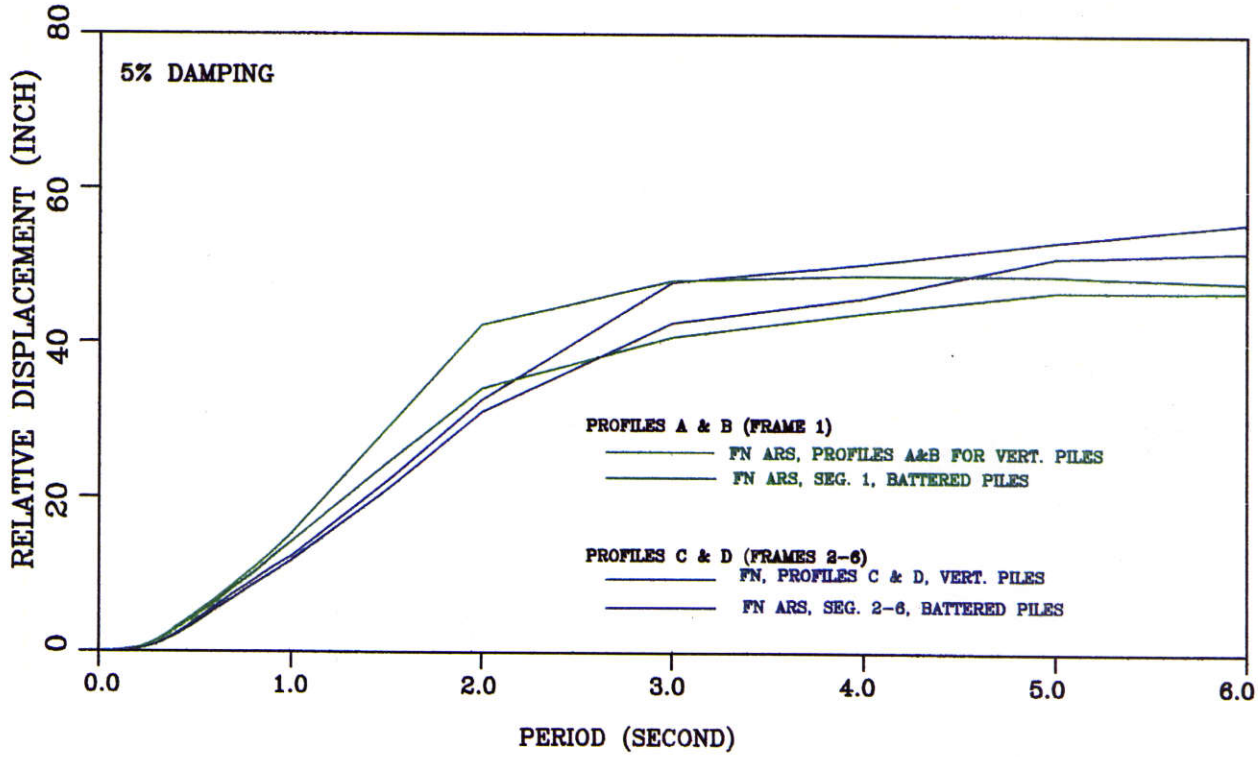

ARS DESIGN CURVES FOR SKYWAY STRUCTURE, FN
SFOBB East Span Seismic Safety Project

PLATE 7-1

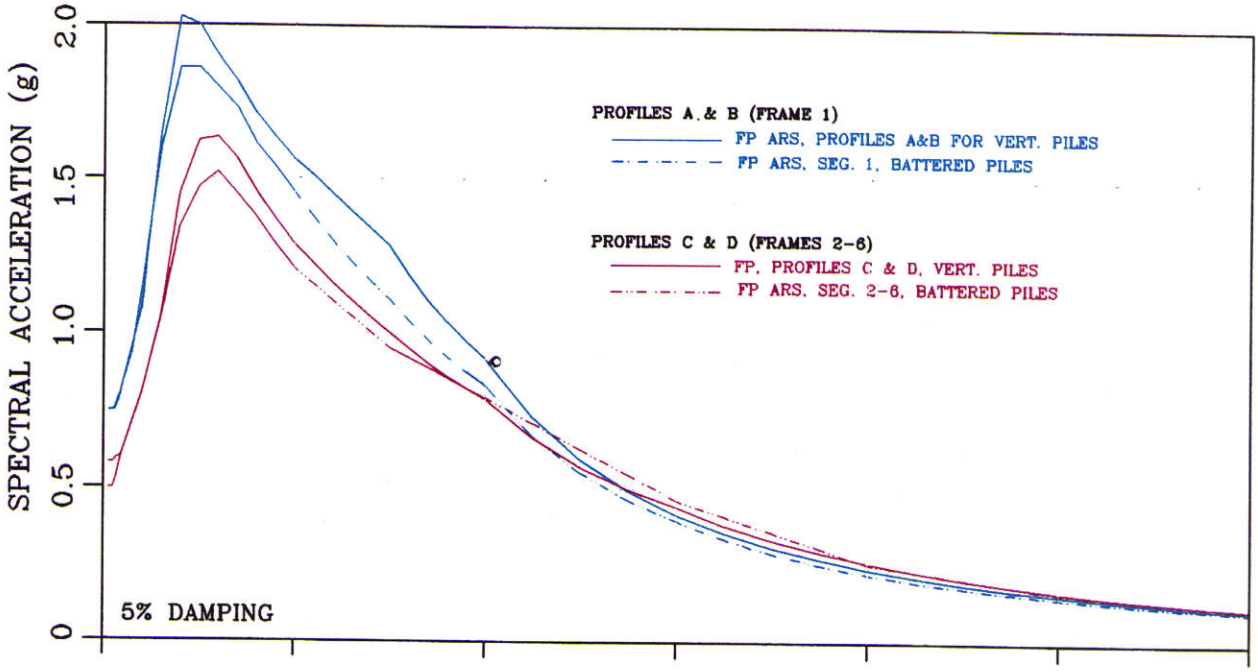

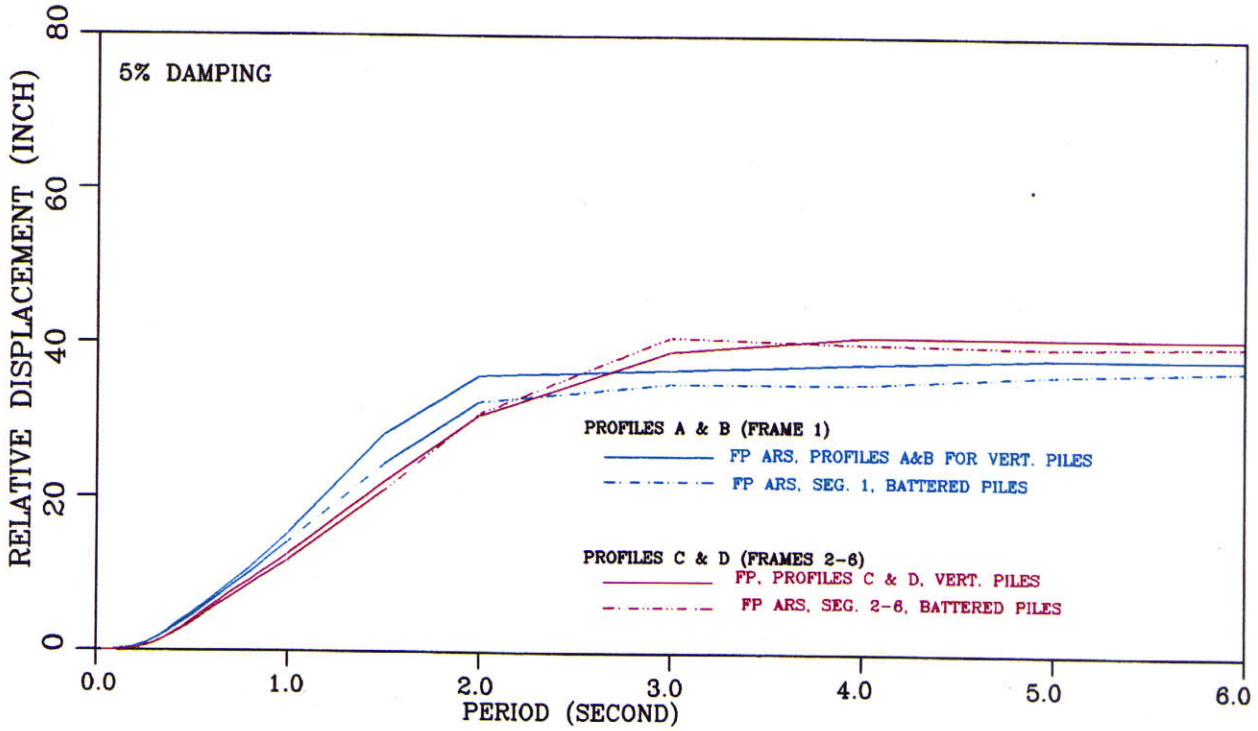

ARS DESIGN CURVES FOR SKYWAY STRUCTURE, FP
SFOBB East Span Seismic Safety Project

PLATE 7-2

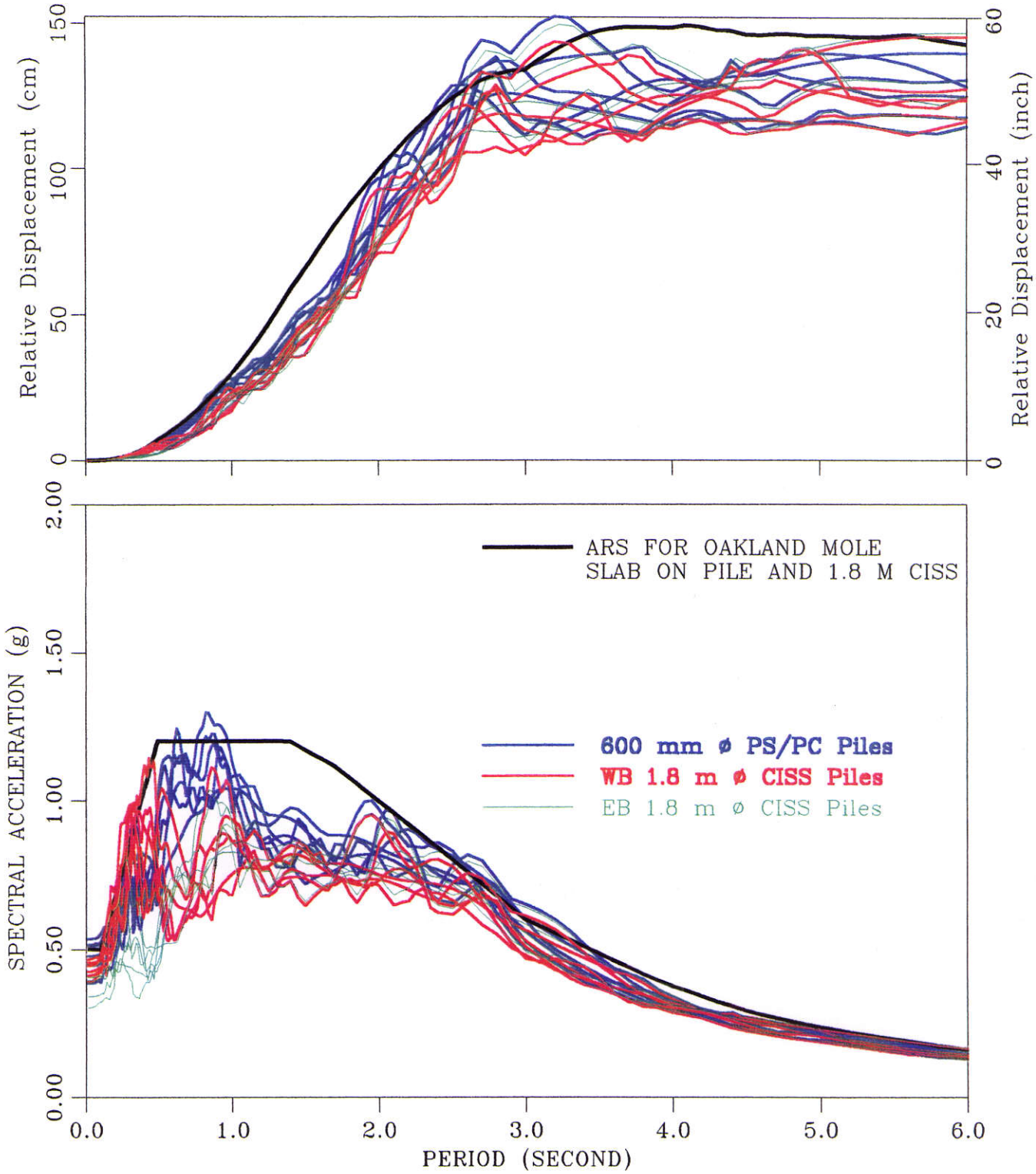

ARS DESIGN CURVES FOR OAKLAND MOLE, FN
SFOBB East Span Seismic Safety Project

PLATE 7-3

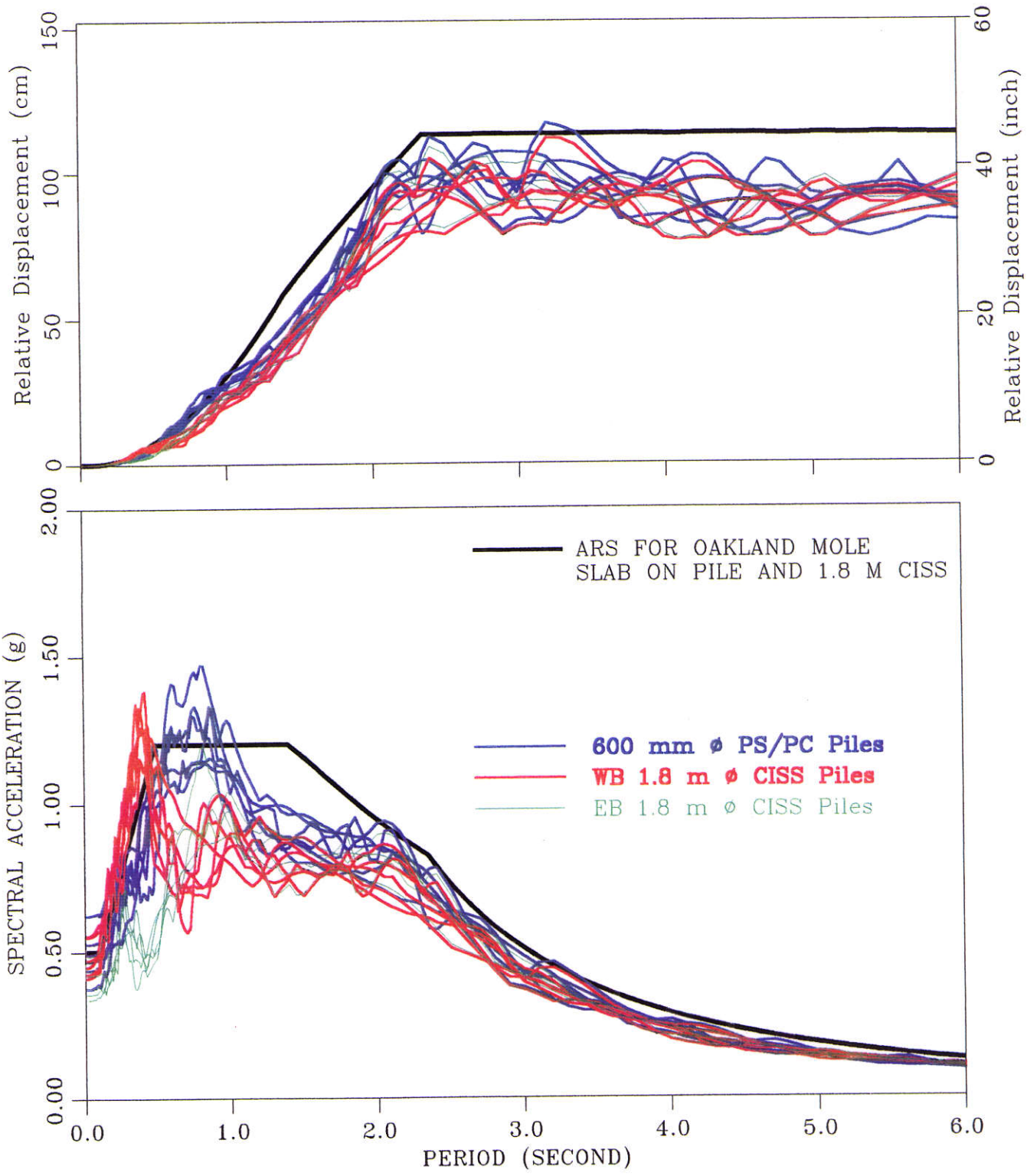

ARS DESIGN CURVES FOR OAKLAND MOLE, FP
SFOBB East Span Seismic Safety Project

PLATE 7-4

SECTION 8.0
MULTIPLE SUPPORT KINEMATIC MOTIONS

8.0 MULTIPLE SUPPORT KINEMATIC MOTIONS

8.1 ANALYTICAL PROCEDURE

Multiple support kinematic motions were computed for Pier E2 of the Main Bridge and the all piers for the Skyway Structure as these structures will be designed/checked with time history analyses. Multiple support time history analysis involving incoherent motions would not be performed for YBI and Oakland Mole structures. Therefore, the discussion presented in this section pertains to Pier E2 of Main Bridge and all the piers in the Skyway (Piers E03 through E16) portion only.

To perform kinematic analysis, it is necessary to construct a pile group model with appropriate soil springs attached to it at different depths. The depth varying free-field ground motions estimated from the site response analyses were applied to the model through the soil springs. Plate 8-1 shows schematic arrangement of a pile group model used for kinematic analysis. The lateral springs are estimated from p-y curves and the axial springs are estimated from t-z curves. The piles are discretized as shown in the Plate, and lumped soil springs were attached to the nodal points. Usually p-y and t-z curves are developed for unit length of a pile. The curves were lumped for each nodal location by multiplying the 'p' or 't' values with appropriate tributary length for the particular node.

8.2 SOIL SPRINGS AND PILE PROPERTIES

The p-y curves were developed according to the guidelines provided in API RP 2A (API, 1993). The detailed discussion on procedure for estimating p-y curves is presented in a report submitted by Fugro-EMI (Fugro-EMI, 2001, e).

The p-y curves or the lumped P-Y springs are nonlinear. However, the substructuring procedure described in the previous section can be implemented if the system is linear. Therefore it is necessary to linearize soil springs for the purpose of kinematic interaction analysis. The procedure for linearization of lateral and axial springs is explained here.

Linearization of Lateral Springs : Procedure for linearization is shown schematically in Plate 8-2. For a single pile, soil springs in terms of p-y curves were estimated at different depths and were lumped at nodal locations as mentioned earlier. The pile was assumed to have a fixed head condition (fixed against rotation respect to the pile cap). The pile was then pushed laterally at the pile top by 125 mm (5 inches). The pile top deformation of 125 mm is a representative displacement that is expected during the earthquake based on the preliminary analyses conducted using the response spectrum approach. The linear spring stiffness at each nodal location is estimated as the secant stiffness for the resulting pile displacement at that particular nodal location as shown in Plate 8-2. The linearized springs are used in the kinematic soil-structure interaction analysis. If the actual pile top displacement is judged to be significantly different from 125 mm from a refined global analysis, it may be required to linearize the springs at

different pile top displacement level that is consistent with the global behavior. However at this stage, the pile top displacement of 125 mm seems appropriate.

Linearization of Axial Spring : The axial t-z springs at each pier location was estimated based on API criteria (API, 1993). Detailed procedure for development of t-z curves has been presented in a report submitted by Fugro-EMI (Fugro-EMI, 2001, d). As in the case of lateral soil springs, axial soil springs (t- z curves) were lumped at nodal locations. To obtain the stiffness of the linearized lumped T-Z springs, secant modulus were calculated at 12 mm (0.5 inch) displacement.

Pile Data: The piles are 2.5-meter diameter steel pipe piles typically driven to the Lower Alameda Formation. The pile layouts are shown in Plates 8-3 and 8-4. Three different pile layouts are proposed as shown in these Plates; Pier E2 is founded on vertical piles, Piers E3 through E14 are founded on six battered piles, Piers E15 through E16 are supported on four battered piles. The upper section of the piles will be filled with reinforced concrete. The current design indicates that the wall thickness of the pipe piles will vary with depth. The sectional properties of the piles have been provided by TY Lin and are presented in Table 8-1.

8.3 TREATMENT OF VERTICAL MOTION

Well-calibrated site response techniques for vertical component motion are not currently available. The ground motion team has discussed the vertical propagation speed issue and has examined down-hole vertical strong motion data around the world. Available downhole strong motion array data were compiled and evaluated to guide vertical wave propagation for the SFOBB project. A conservative approach for vertical ground motion was adopted which takes no credit for the reduction in shaking amplitude with depth, but account for wave-passage effect with depth. Incorporating wave-passage effects tends to reduce vertical shaking intensity at a short period range. We have adopted the following propagation speeds for vertical wave-passage effects:

Depth	Vertical Propagation Speed
0 to 12 m	400 m/s
12 to 30 m	500 m/s
over 30 m	750 m/s

8.4 IMPLEMENTATION

The computer program to perform the kinematic soil-pile interaction analysis is named KIPS (Kinematic Interaction for Pile and Soil) written in MATLAB language. The program, based on finite element method employing static condensation, was developed in-house specifically to solve large pile group under seismic excitation. The abstract of the KIPS program is given in Plate 8-5. The program can handle battered piles as well as HP piles where moment of inertia in the strong axis can be different from the weak axis.

8.5 RESULTS OF KINEMATIC MOTIONS

The results of kinematic motion are presented in Plates 8-6 to 8-185. Each Plate contains the kinematic time histories of displacement, velocity, and acceleration. The acceleration and relative displacement spectra of the kinematic motion are compared with the free-field motions and with the reference 1,500-year return period rock spectra.

Table 8-1 Sectional Properties of Piles

Piers	Cut-off Elevation (m)	Bottom of Pile Cap (m)	Elevation (m)		Axial Stiffness (AE) (MN)	Flexural Stiffness (EI) (MN-m^2)
			From	To		
E2	-	-2.7	-2.7	-12.7	296100	187200
			-12.7	-13.9	290300	181800
			-13.9	-16.9	188600	94380
			-16.9	-22.0	220400	118800
			-22.0	-55.0	195900	101600
			Below -55.0		69400	52400
E3 thru E6	+2.25	-3.5	-3.5	-32.75	210000	88800
			-32.75	-47.75	202000	87800
			-47.75	-62.75	186000	81800
			Below -62.75		78400	58500
E7	-6.75	-12.5	-12.5	-41.75	210000	88800
			-41.75	-56.75	202000	87800
			-56.75	-71.75	186000	81800
			Below -71.75		78400	58500
E8	-5.55	-11.3	-11.3	-40.55	210000	88800
			-40.55	-55.55	202000	87800
			-55.55	-70.55	186000	81800
			Below -70.55		78400	58500
E9	-5.15	-10.9	-10.9	-40.15	210000	88800
			-40.15	-55.15	202000	87800
			-55.15	-70.15	186000	81800
			Below -70.15		78400	58500

Table 8-1 (Contd.)

Piers	Cut-off Elevation (m)	Bottom of Pile Cap (m)	Elevation (m)		Axial Stiffness (AE) (MN)	Flexural Stiffness (EI) (MN-m^2)
			From	To		
E10	-6.00	-11.75	-11.75	-41.00	210000	88800
			-41.00	-56.00	202000	87800
			-56.00	-71.00	186000	81800
			Below -71.00		78400	58500
E11	-3.85	-9.60	-9.60	-38.85	210000	88800
			-38.85	-53.85	202000	87800
			-53.85	-68.85	186000	81800
			Below -68.85		78400	58500
E12	-6.85	-12.60	-12.60	-41.85	210000	88800
			-41.85	-56.85	202000	87800
			-56.85	-71.85	186000	81800
			Below -71.85		78400	58500
E13	-8.75	-14.50	-14.50	-43.75	210000	88800
			-43.75	-58.75	202000	87800
			-58.75	-73.75	186000	81800
			Below -73.75		78400	58500
E14	-10.25	-16.00	-16.00	-45.25	210000	88800
			-45.25	-60.25	202000	87800
			-60.25	-75.25	186000	81800
			Below -75.25		78400	81800
E15	-4.75	-10.50	-10.5	-30.5	232000	99600
			-30.5	-50.5	202000	87800
			-50.5	-70.5	186000	81800
			Below -70.5		78400	58500
E16	-5.25	-11.0	-11.0	-30.75	232000	99600
			-30.75	-50.75	202000	87800
			-50.75	-70.75	186000	81800
			Below -70.75		78400	58500

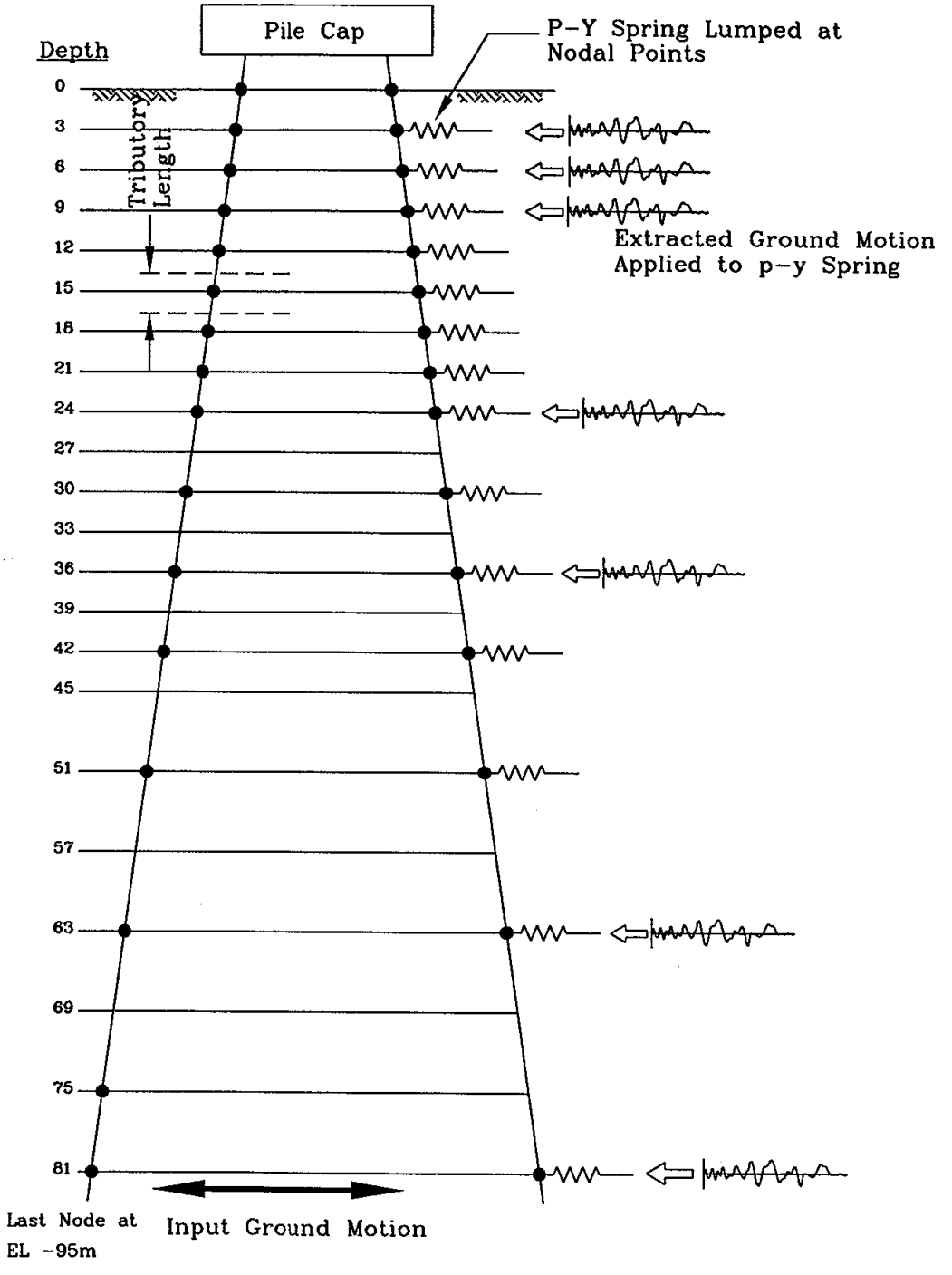

DISCRETIZATION SCHEME
SFOBB East Span Seismic Safety Project

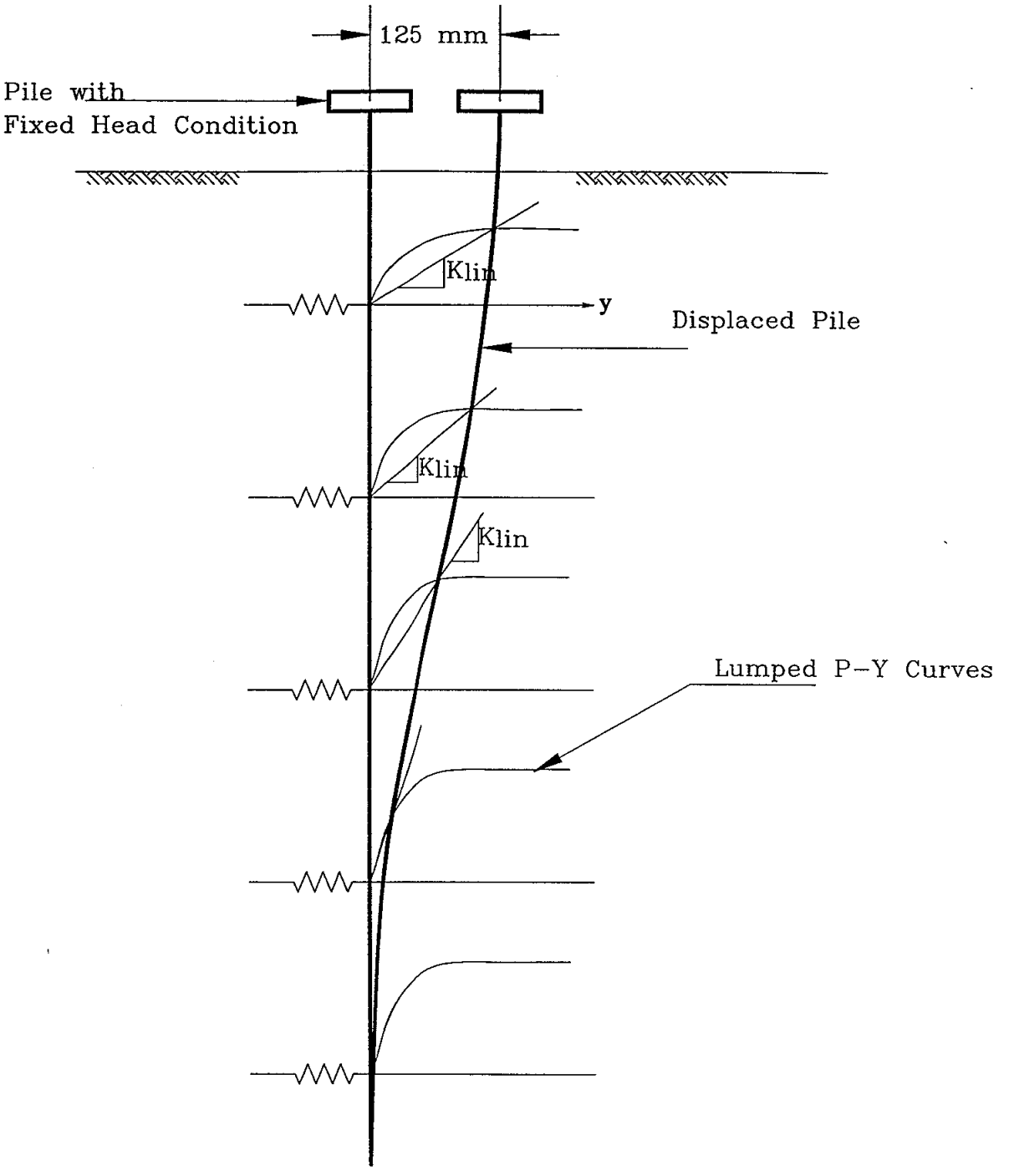

p-y LINEARIZATION PROCEDURE
SFOBB East Span Seismic Safety Project

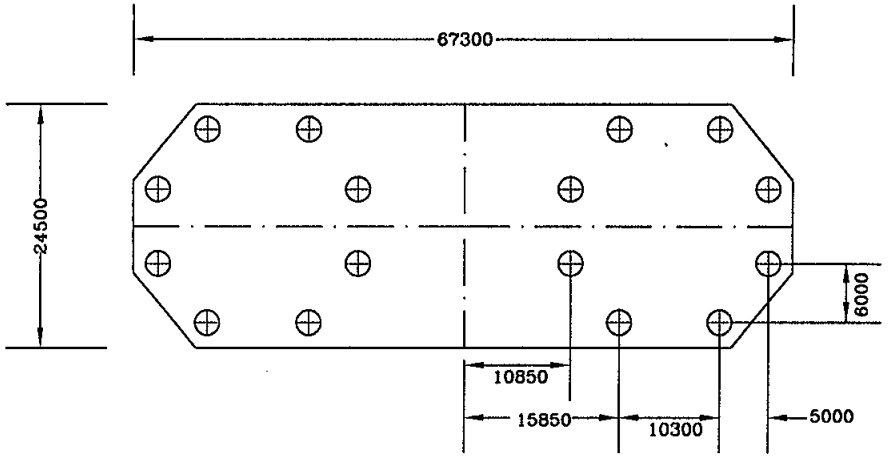

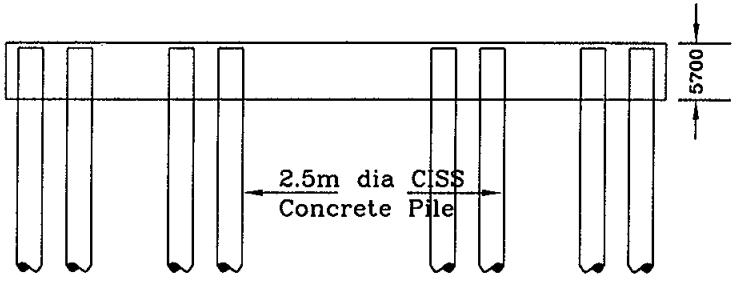

LAYOUT OF PIER E2

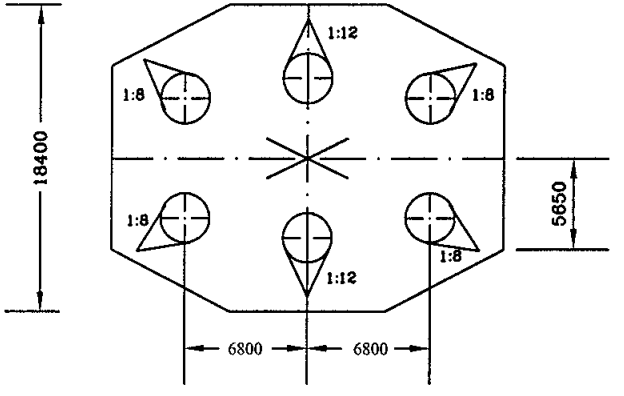

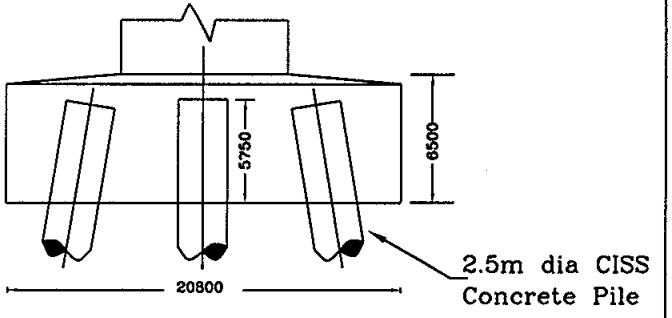

LAYOUT OF PIER E3 THRU E14
(EASTBOUND OR WESTBOUND)

PILE LAYOUT FOR PIERS E02 THROUGH E14
SFOBB East Span Seismic Safety Project

PLATE 8-3

SFOBB Task Order No. 5
EMI Project No. 98-145

Earth Mechanics
FUGRO

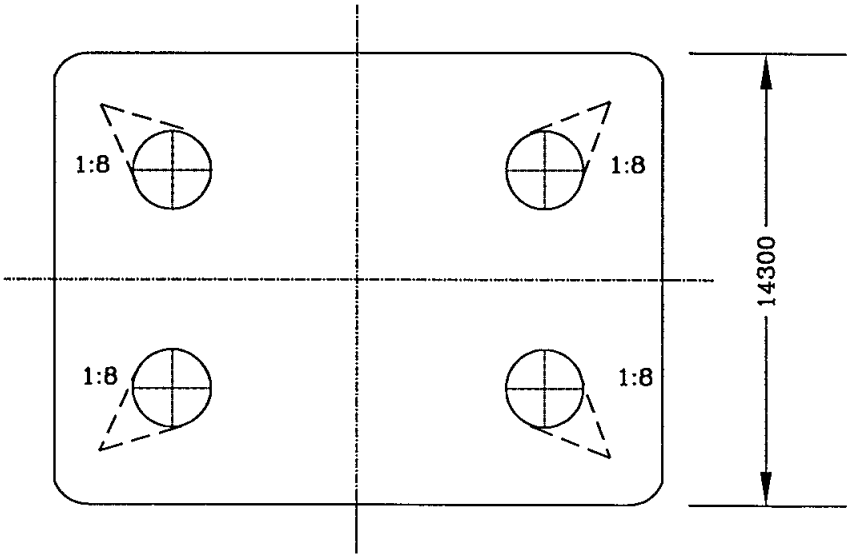

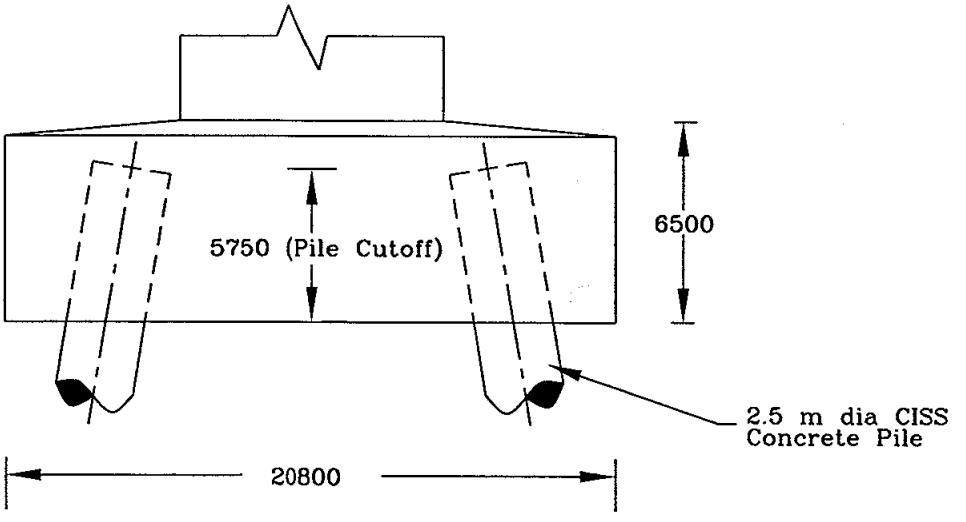

PILE LAYOUT FOR PIERS E15 AND E16
SFOBB East Span Seismic Safety Project

Earth Mechanics FUGRO

KIPS
Kinematic Interaction for Pile and Soil

Description: KIPS is a computer program for kinematic interaction of pile and soil to develop a foundation substructure model under three dimensional seismic loading. The foundation substructure model typically consists of stiffness and mass matrices and associated forcing function to fully characterize the soil-pile system. The objective of the program is to reduce the number of degrees-of-freedom for the foundation to be used in the global bridge model while maintaining mathematical rigor. This is achieved by taking full advantage of static condensation in stiffness matrix formulation, and using Guyan reduction techniques (also known as eigen economizeation) for mass matrix. Back substitution can also be performed using solutions from the global analysis to recover displacements along the individual piles.

Features: Easy data preparation including preprocessing of free-field ground motions and fully automated for postprocessing the results for graphic presentation. The program is written in Matlab® routine, and the increase in number of piles within the pile-group would not affect the memory requirement.

Project Experience: This substructuring techniques has been used successfully in the seismic retrofit projects or being employed in the new designs of the following toll bridges in California.

- Vincent Thomas Bridge
- San Diego - Coronado Bay Bridge
- Existing and New Carquinez Bridges
- Richmond - San Rafael Bridge
- New Benicia - Martinez Bridge
- New San Francisco - Oakland Bay Bridge

Reference:

(1) Cook, R.D., Malkus, D. S. and Plesha, M. E., Concepts and Applications of Finite Element Analysis, John Wiley & Sons, Third Edition, 1989.
(2) Clough, R. W. and Penzien, J., Dynamics of Structures, McGraw-Hill, First Edition, 1975
(3) Lam, P. I. and Law, H. K. "Application of Substructuring Techniques for Soil-Structure Interaction under Seismic Loading" NCEER Project 106-E-4.10, 1997

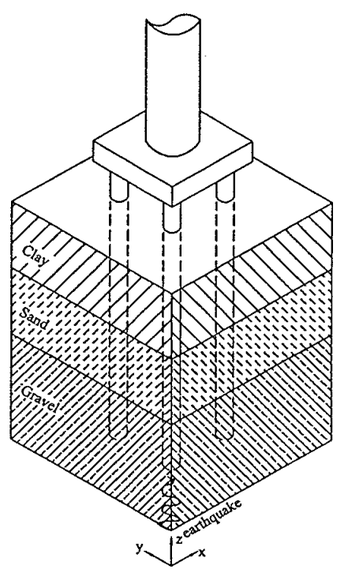

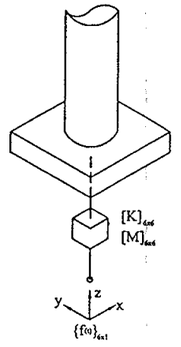

Foundation Substructure

For More Information Contact:

EARTH MECHANICS, INC (EMI)
17660 Newhope Street, Suite E
Fountain Valley, CA 92708
Tel (714) 751-3826

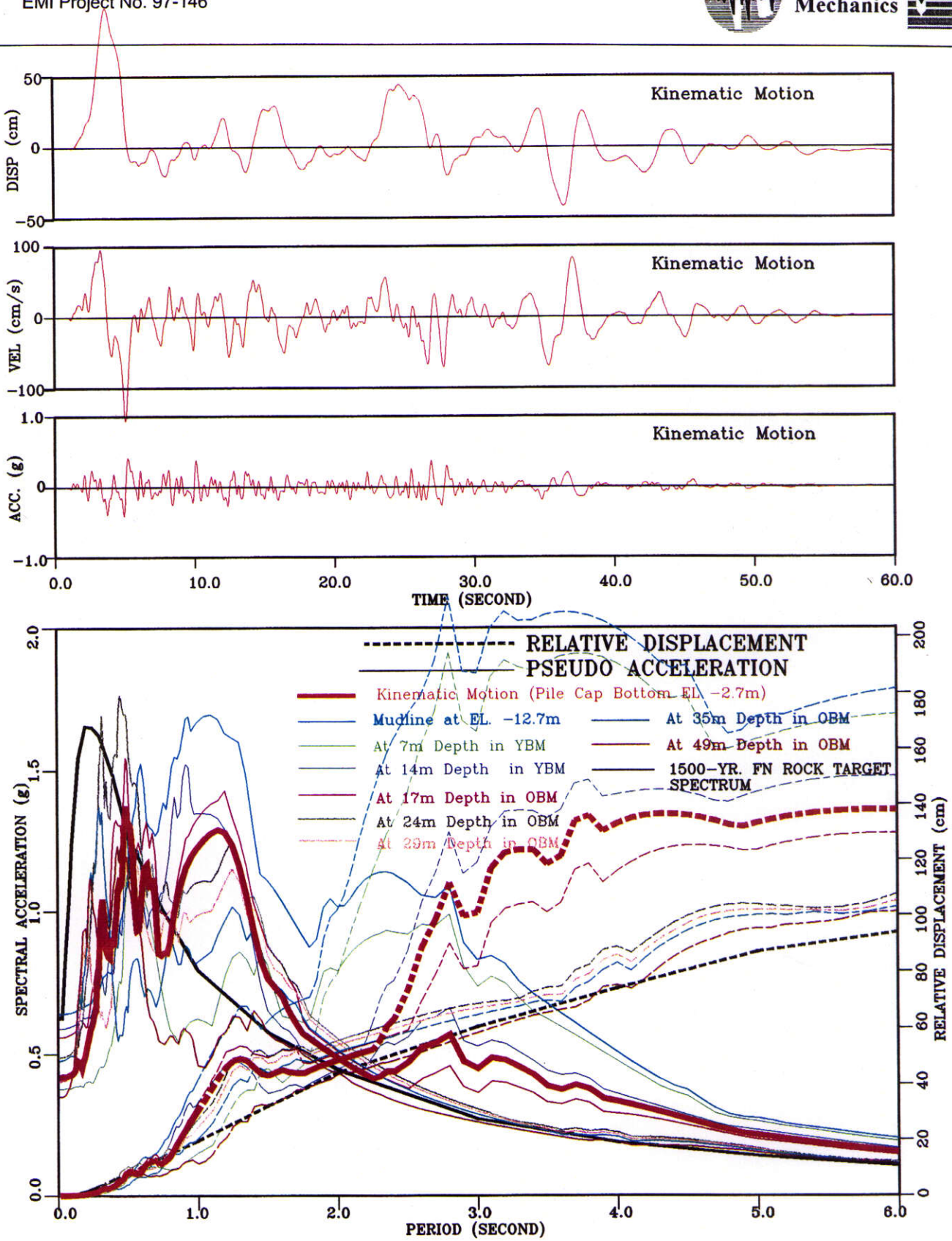

KINEMATIC AND DEPTH-VARYING FREE FIELD MOTIONS
PIER E02, INPUT ROCK MOTION SET 1, FAULT NORMAL COMPONENT
SFOBB East Span Seismic Safety Project

PLATE 8-6

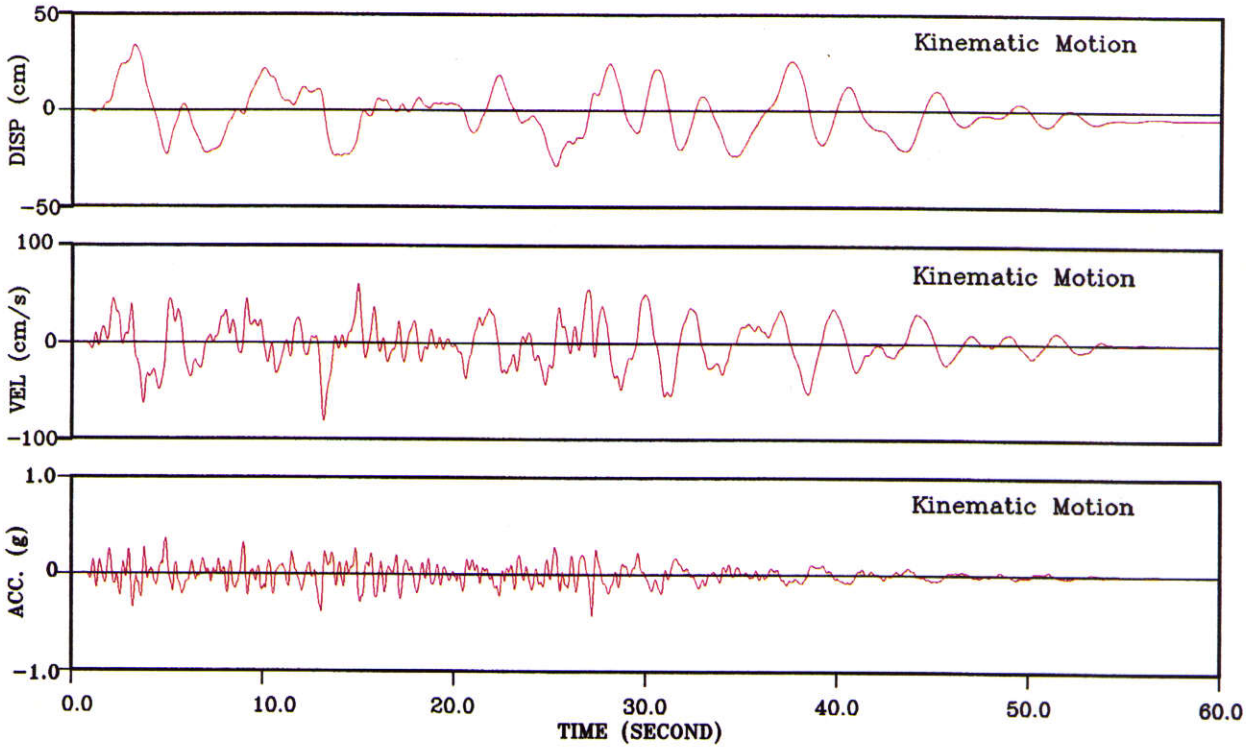

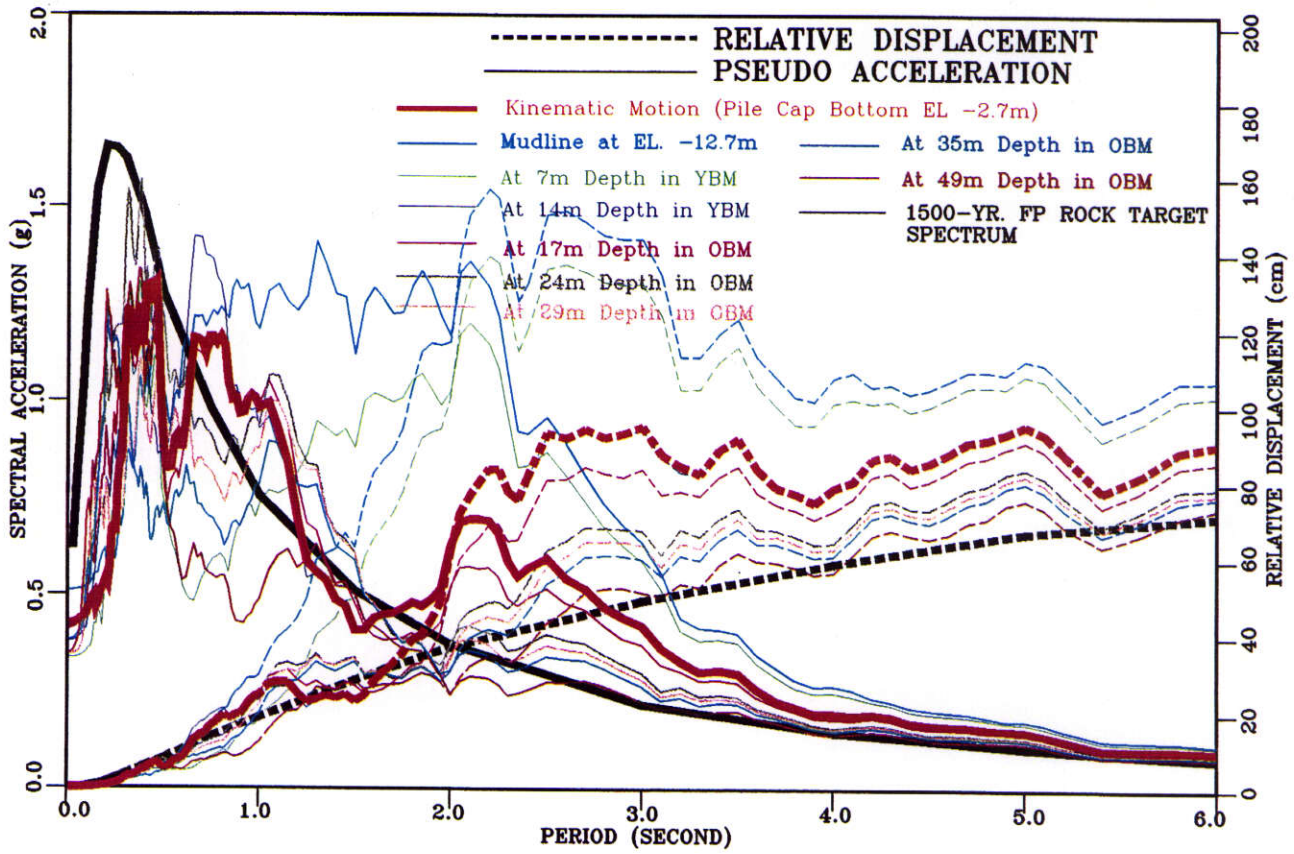

KINEMATIC AND DEPTH-VARYING FREE FIELD MOTIONS
PIER E02, INPUT ROCK MOTION SET 1, FAULT PARALLEL COMPONENT
SFOBB East Span Seismic Safety Project

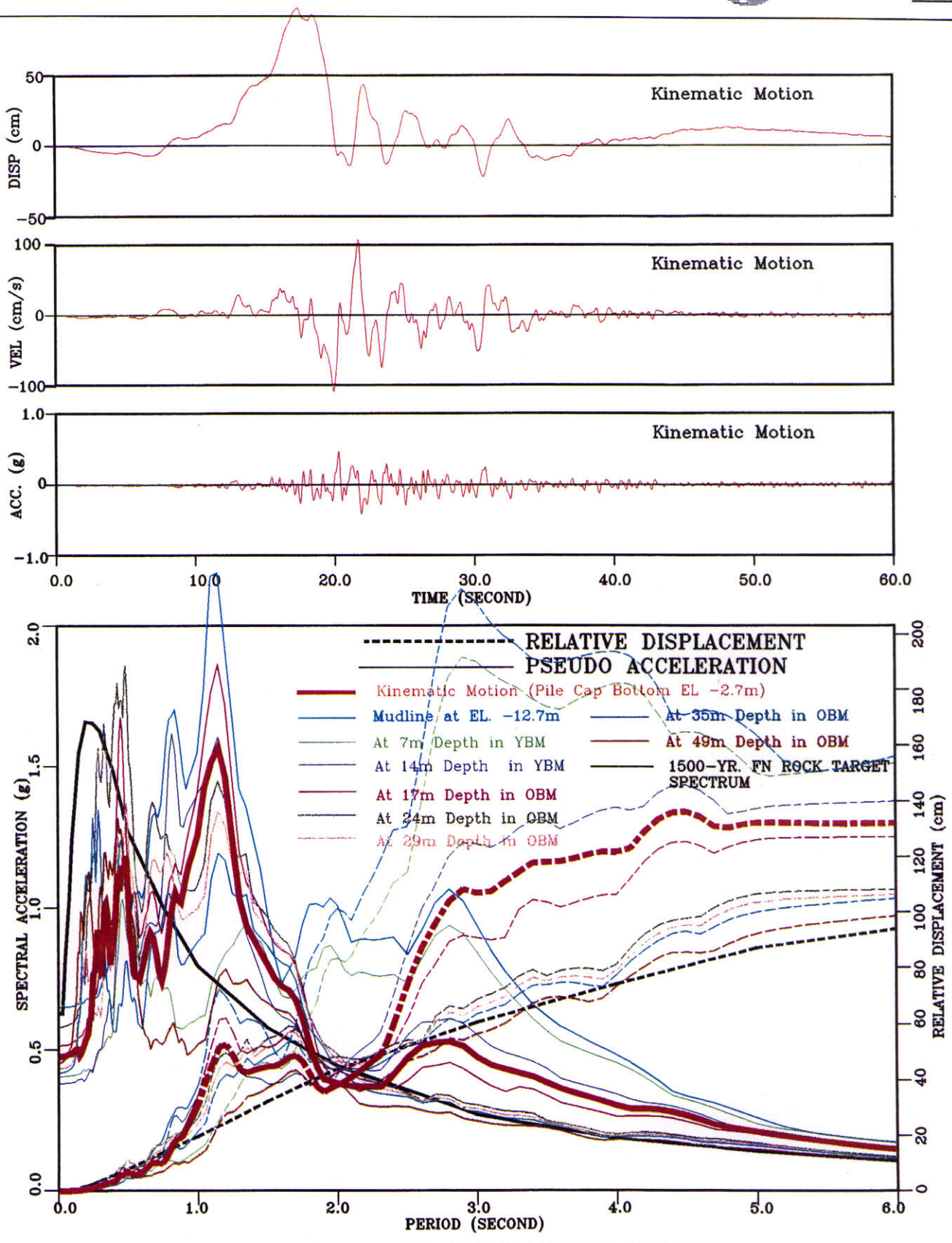

KINEMATIC AND DEPTH-VARYING FREE FIELD MOTIONS
PIER E02, INPUT ROCK MOTION SET 2, FAULT NORMAL COMPONENT
SFOBB East Span Seismic Safety Project

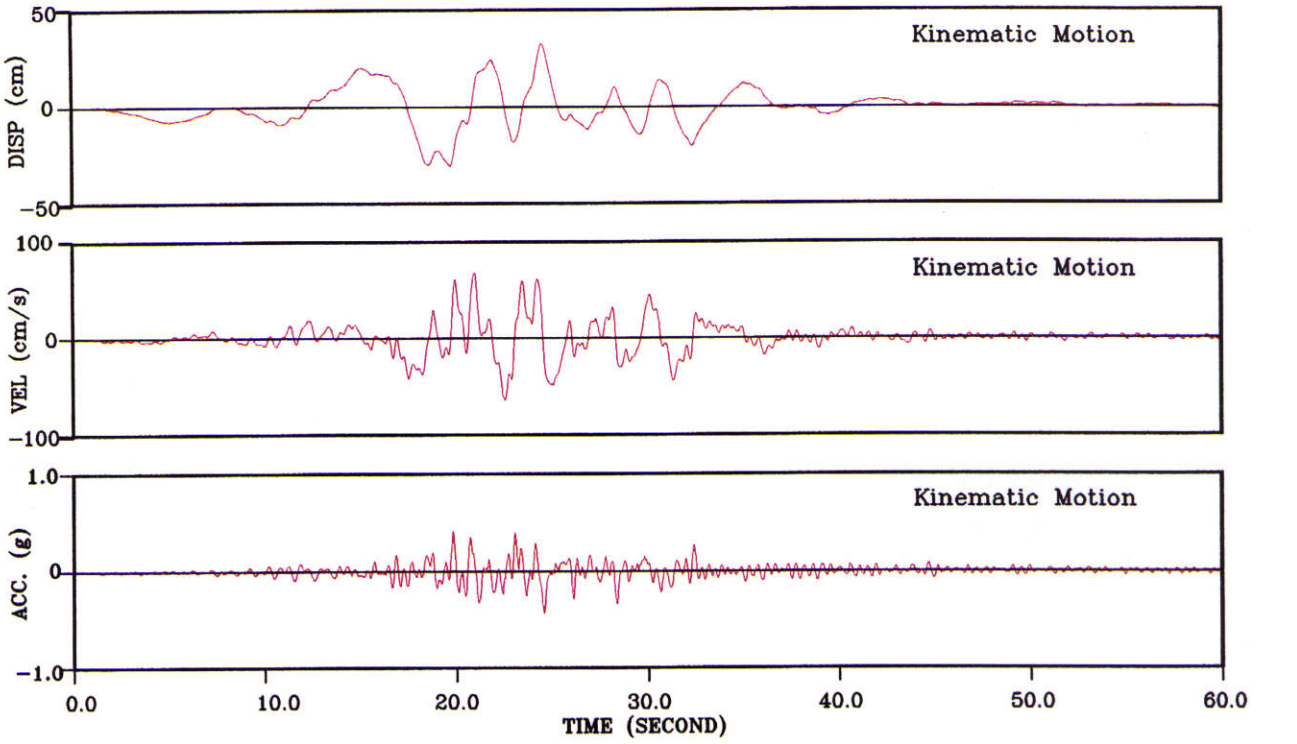

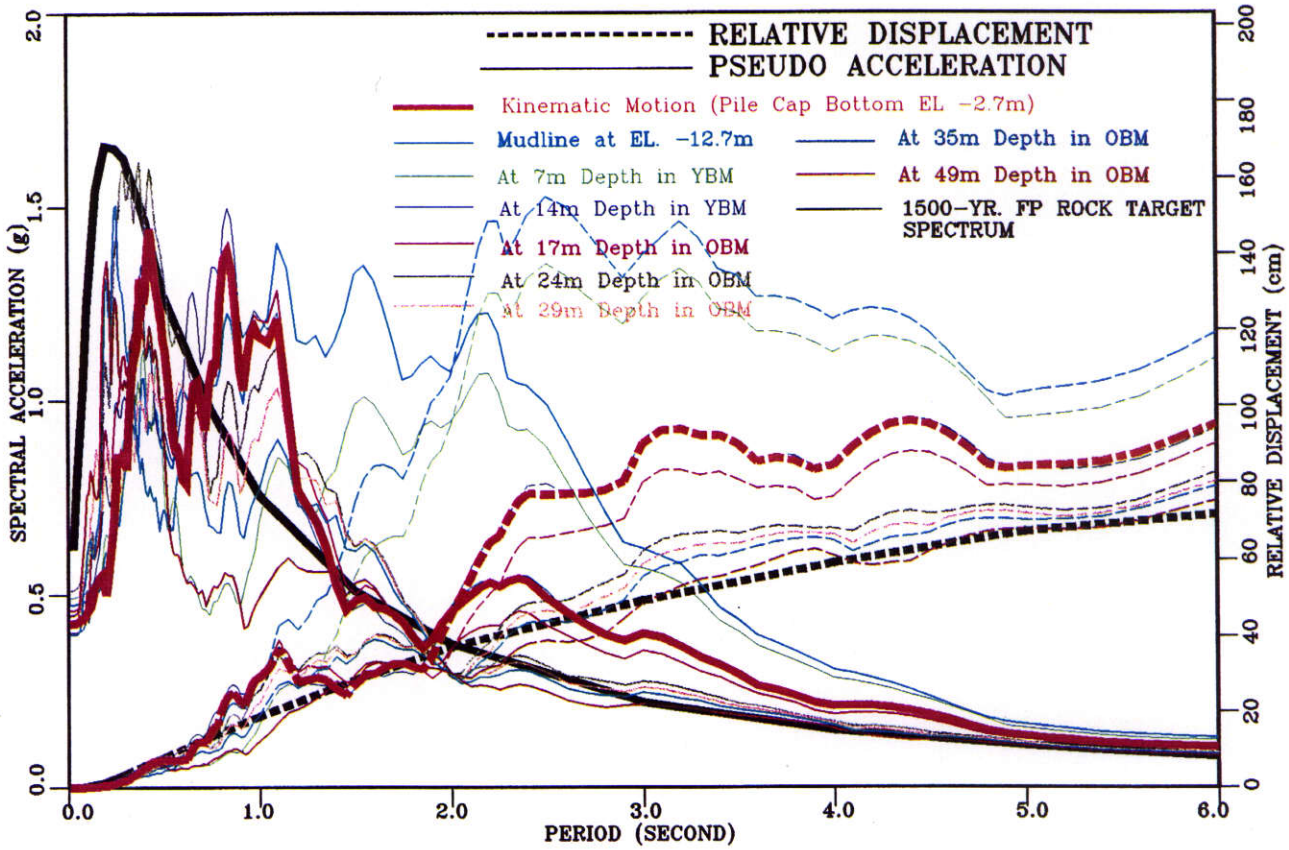

KINEMATIC AND DEPTH-VARYING FREE FIELD MOTIONS
PIER E02, INPUT ROCK MOTION SET 2, FAULT PARALLEL COMPONENT
SFOBB East Span Seismic Safety Project

PLATE 8-9

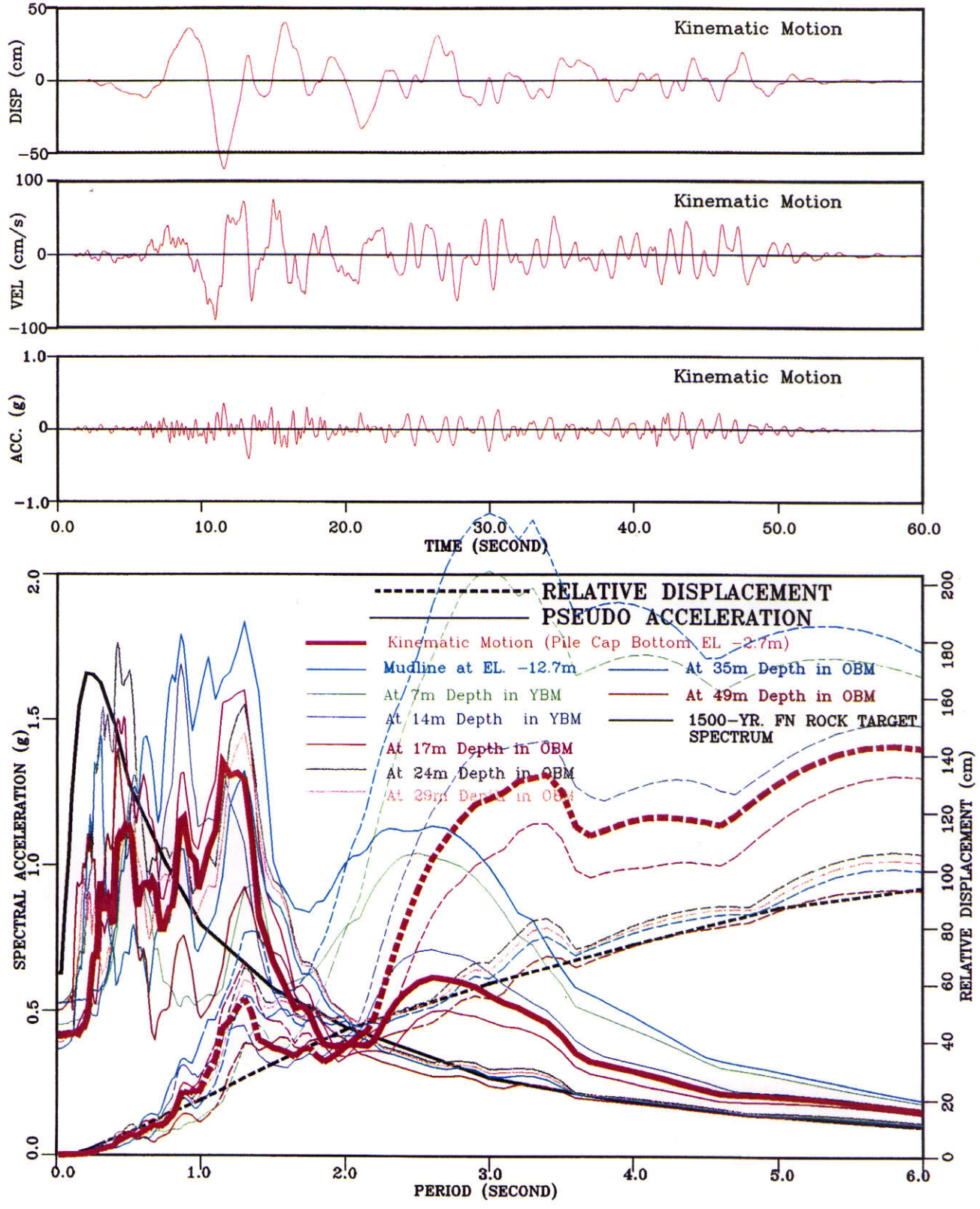

KINEMATIC AND DEPTH-VARYING FREE FIELD MOTIONS
PIER E02, INPUT ROCK MOTION SET 3, FAULT NORMAL COMPONENT
SFOBB East Span Seismic Safety Project

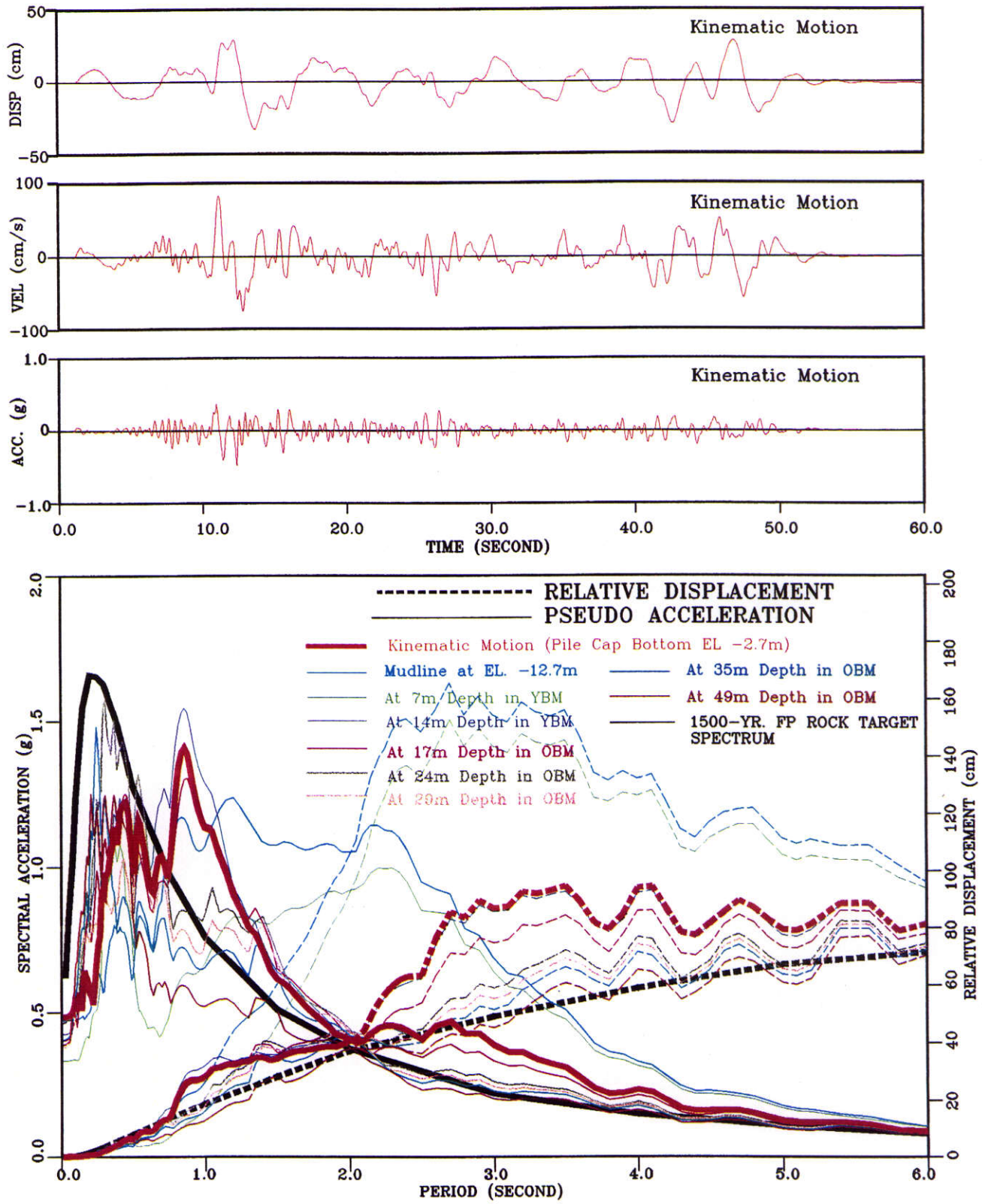

KINEMATIC AND DEPTH-VARYING FREE FIELD MOTIONS
PIER E02, INPUT ROCK MOTION SET 3, FAULT PARALLEL COMPONENT
SFOBB East Span Seismic Safety Project

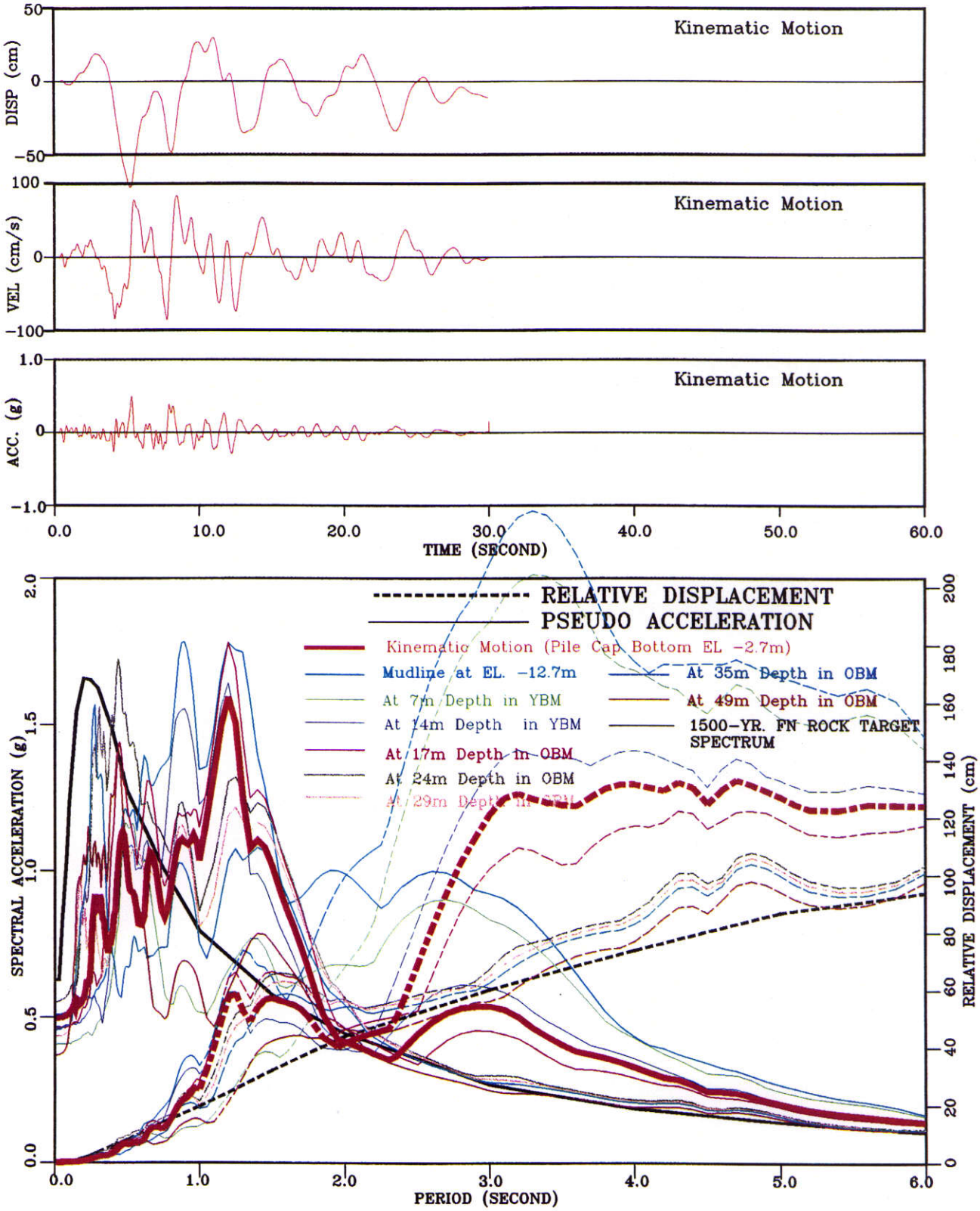

KINEMATIC AND DEPTH-VARYING FREE FIELD MOTIONS
PIER E02, INPUT ROCK MOTION SET 4, FAULT NORMAL COMPONENT
SFOBB East Span Seismic Safety Project

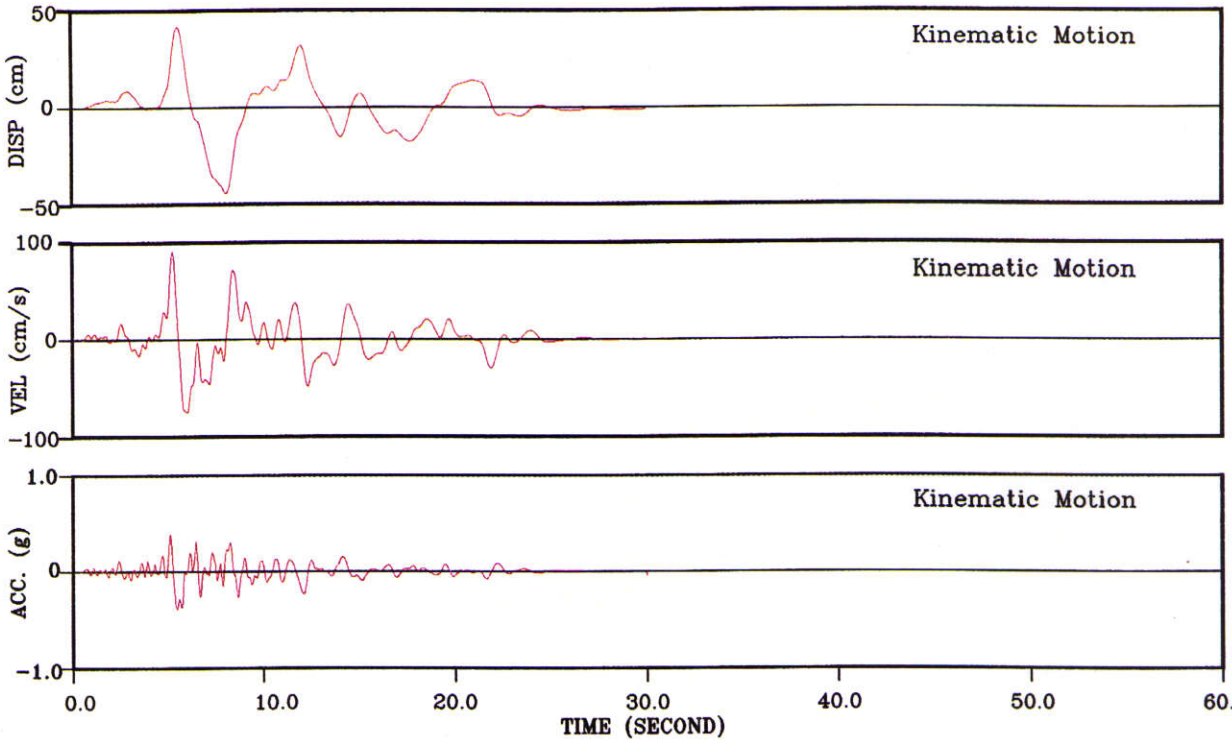

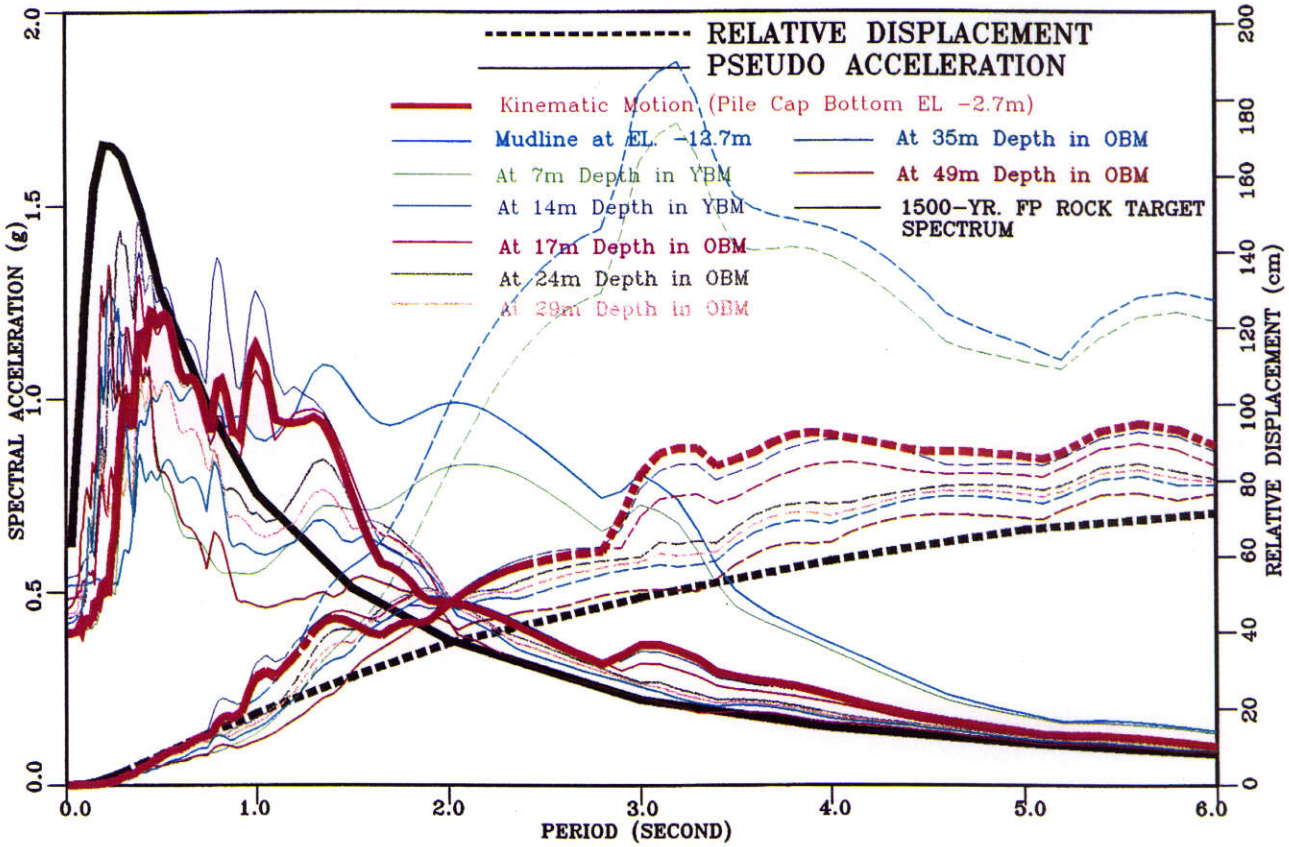

KINEMATIC AND DEPTH-VARYING FREE FIELD MOTIONS
PIER E02, INPUT ROCK MOTION SET 4, FAULT PARALLEL COMPONENT
SFOBB East Span Seismic Safety Project

PLATE 8-13

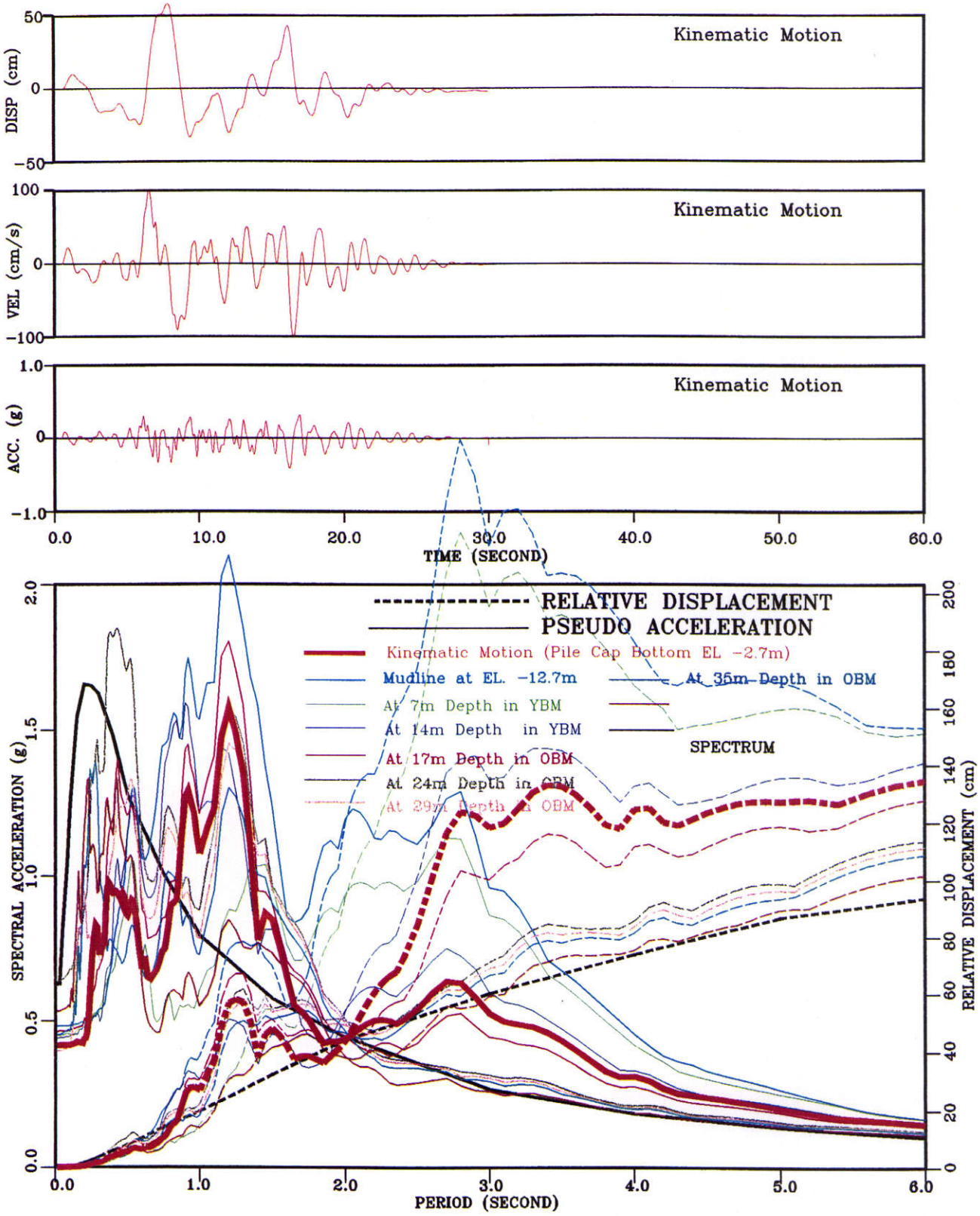

KINEMATIC AND DEPTH-VARYING FREE FIELD MOTIONS
PIER E02, INPUT ROCK MOTION SET 5, FAULT NORMAL COMPONENT
SFOBB East Span Seismic Safety Project

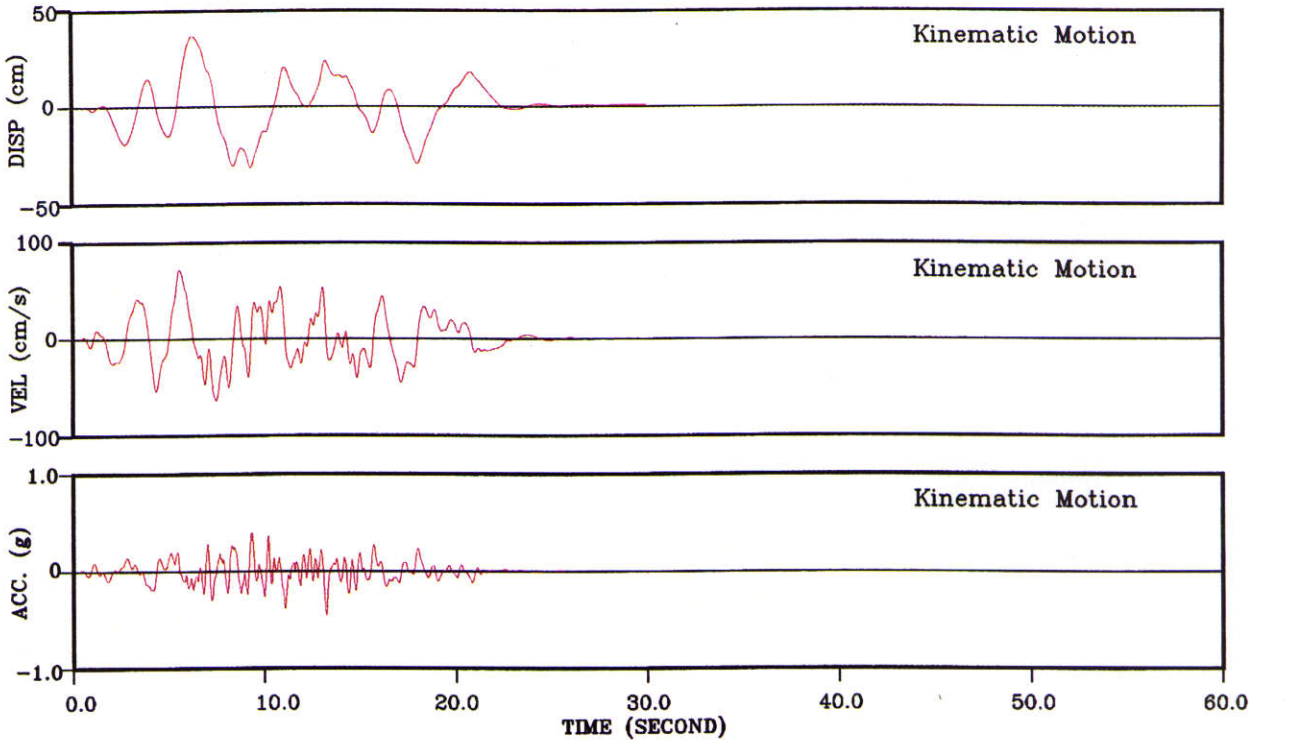

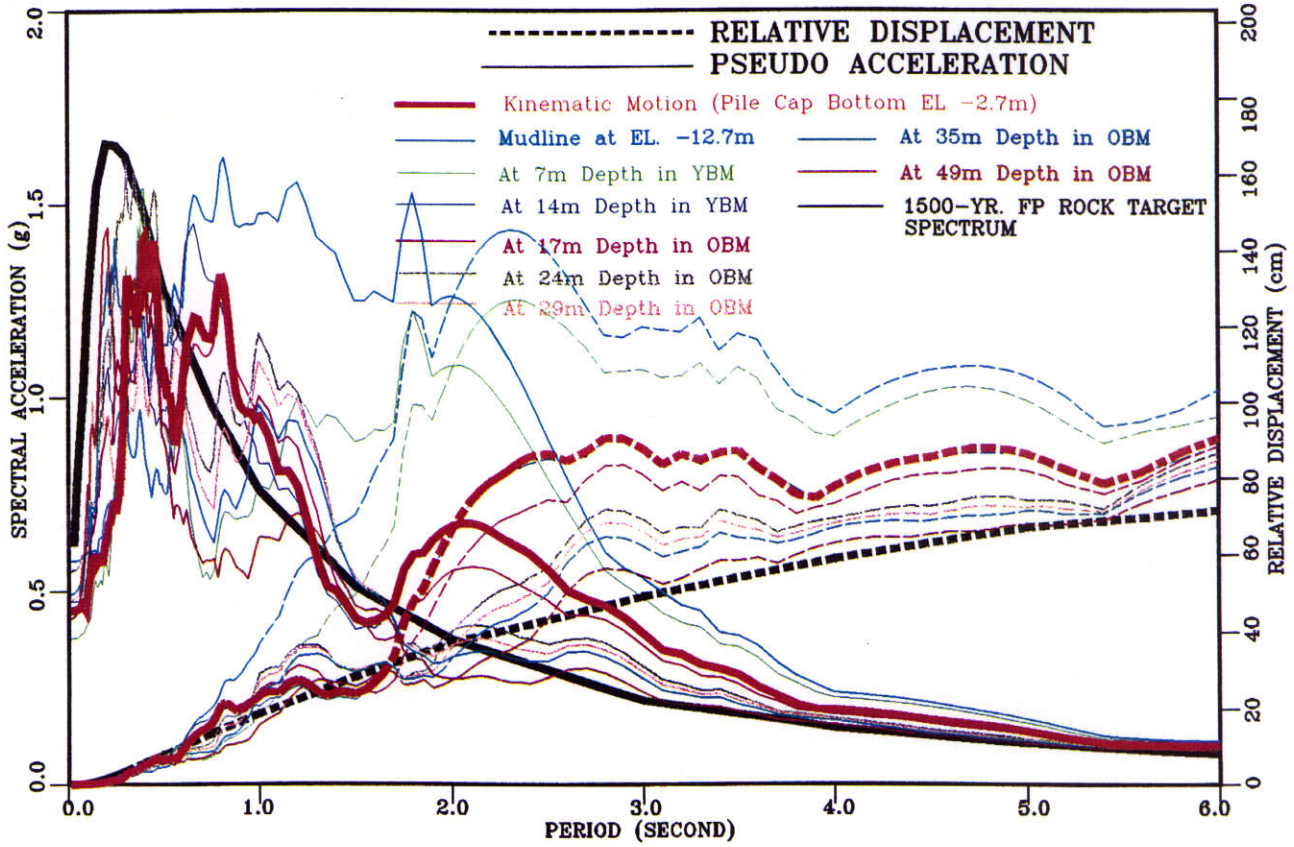

KINEMATIC AND DEPTH-VARYING FREE FIELD MOTIONS
PIER E02, INPUT ROCK MOTION SET 5, FAULT PARALLEL COMPONENT
SFOBB East Span Seismic Safety Project

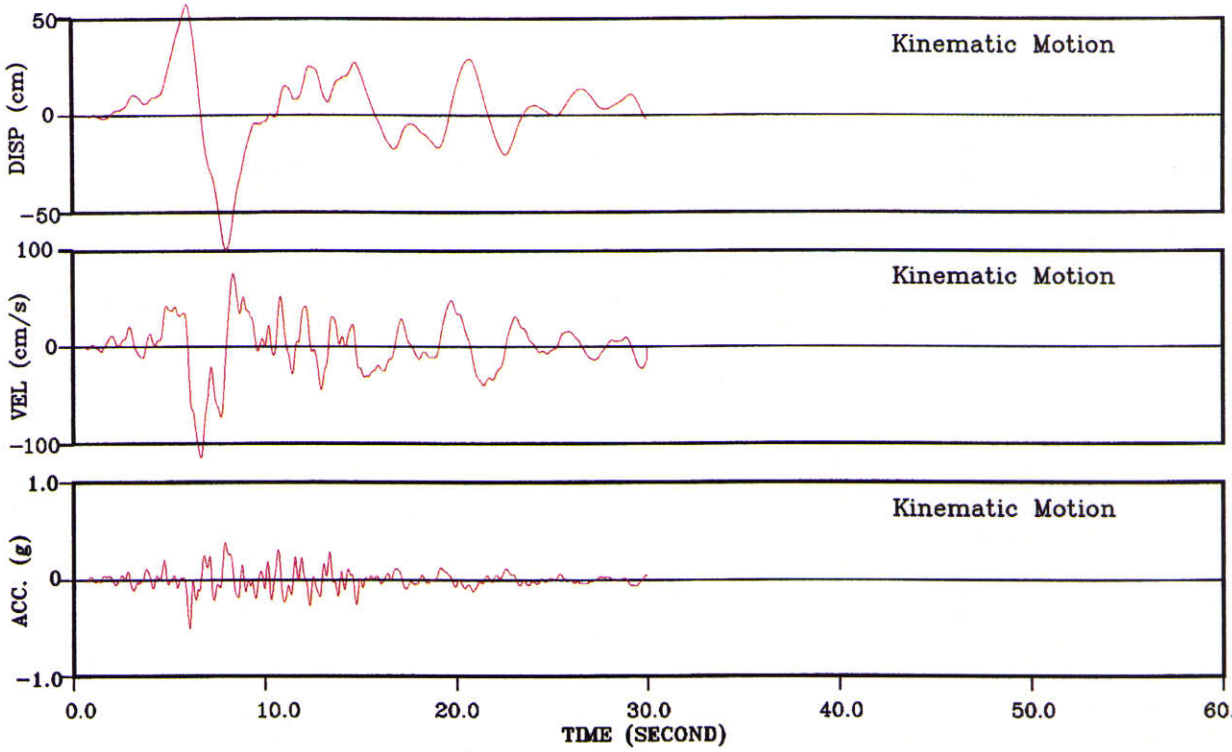

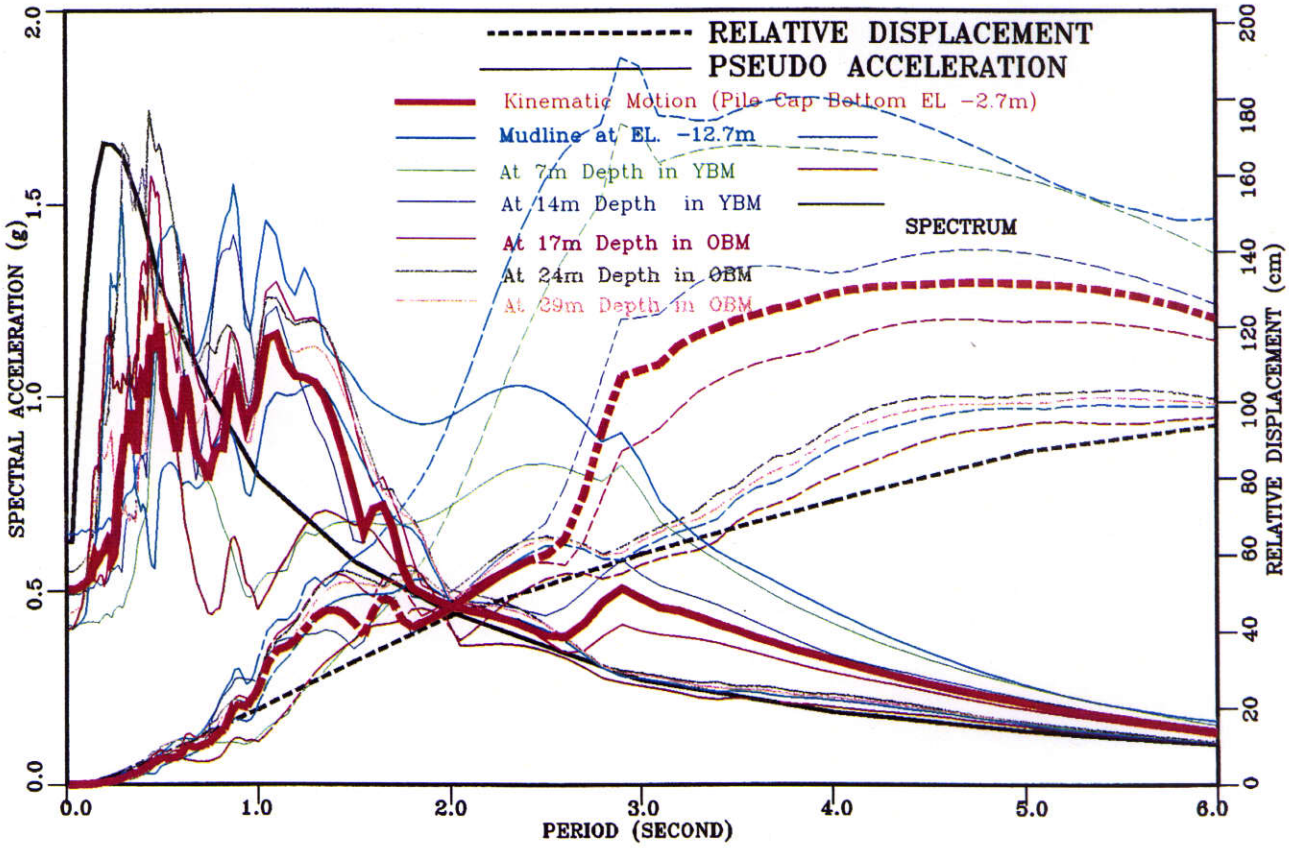

KINEMATIC AND DEPTH-VARYING FREE FIELD MOTIONS
PIER E02, INPUT ROCK MOTION SET 6, FAULT NORMAL COMPONENT
SFOBB East Span Seismic Safety Project

PLATE 8-16

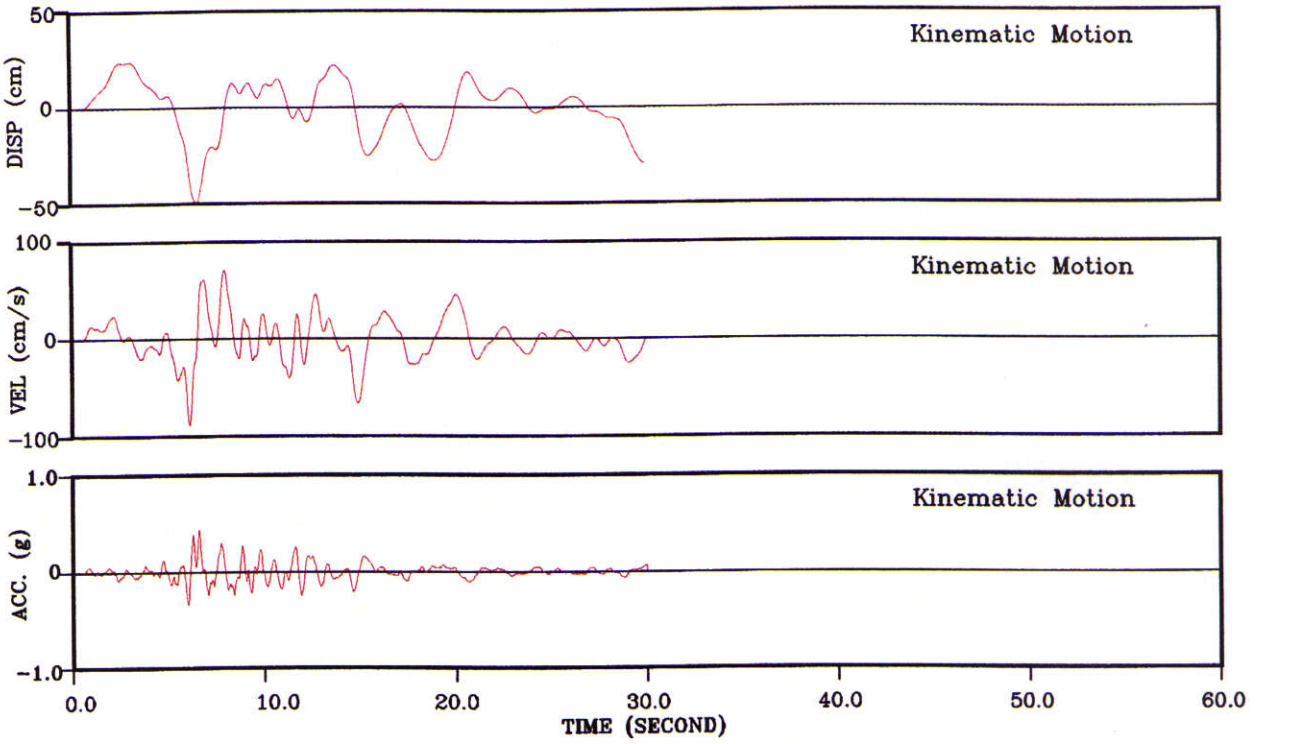

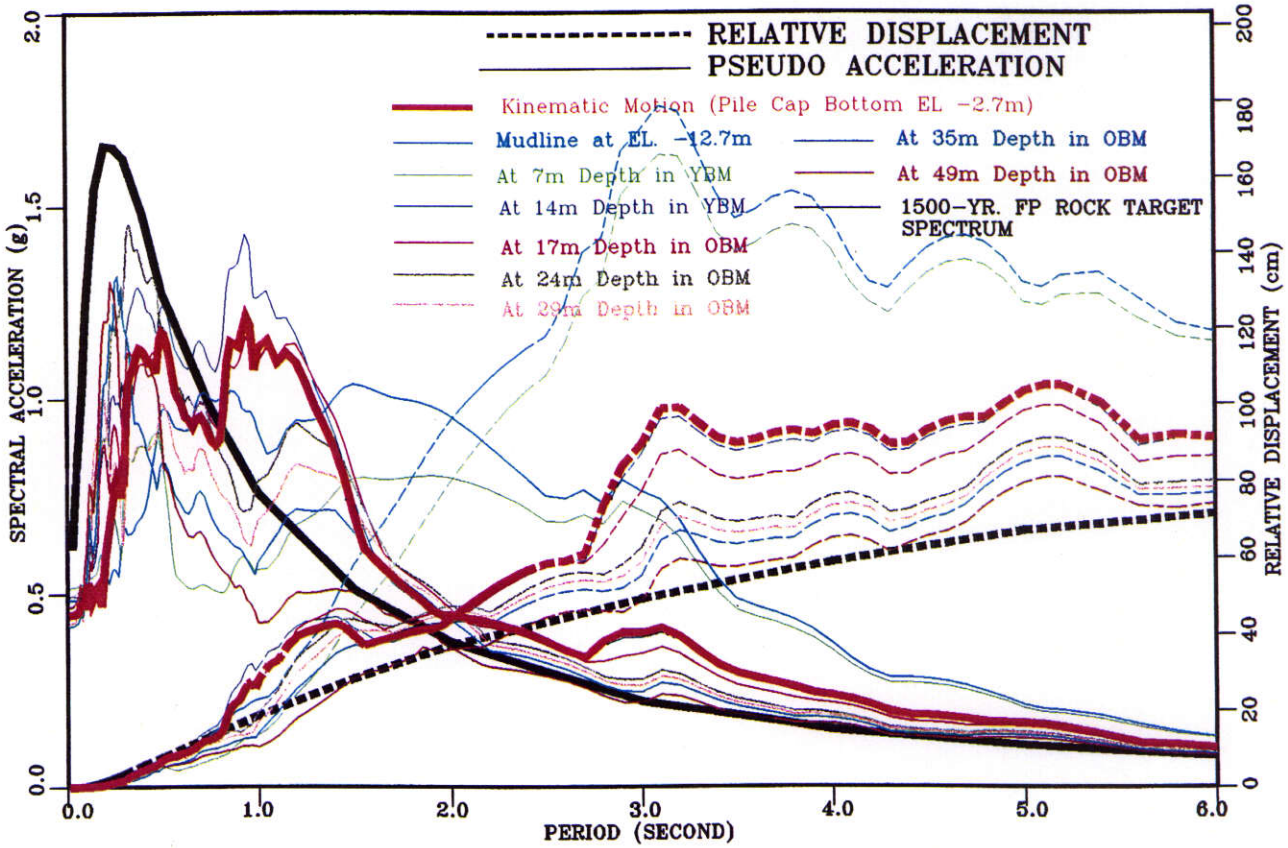

KINEMATIC AND DEPTH-VARYING FREE FIELD MOTIONS
PIER E02, INPUT ROCK MOTION SET 6, FAULT PARALLEL COMPONENT
SFOBB East Span Seismic Safety Project

PLATE 8-17

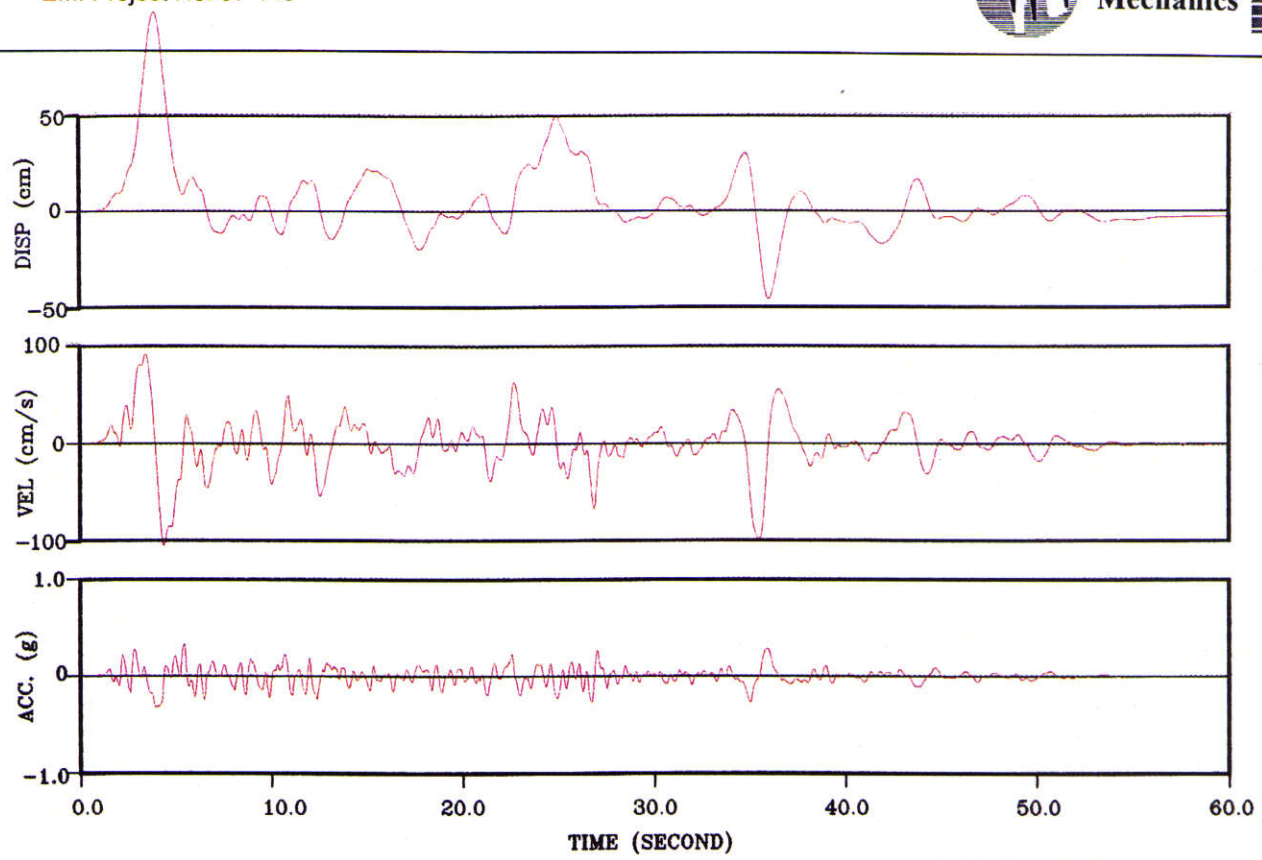

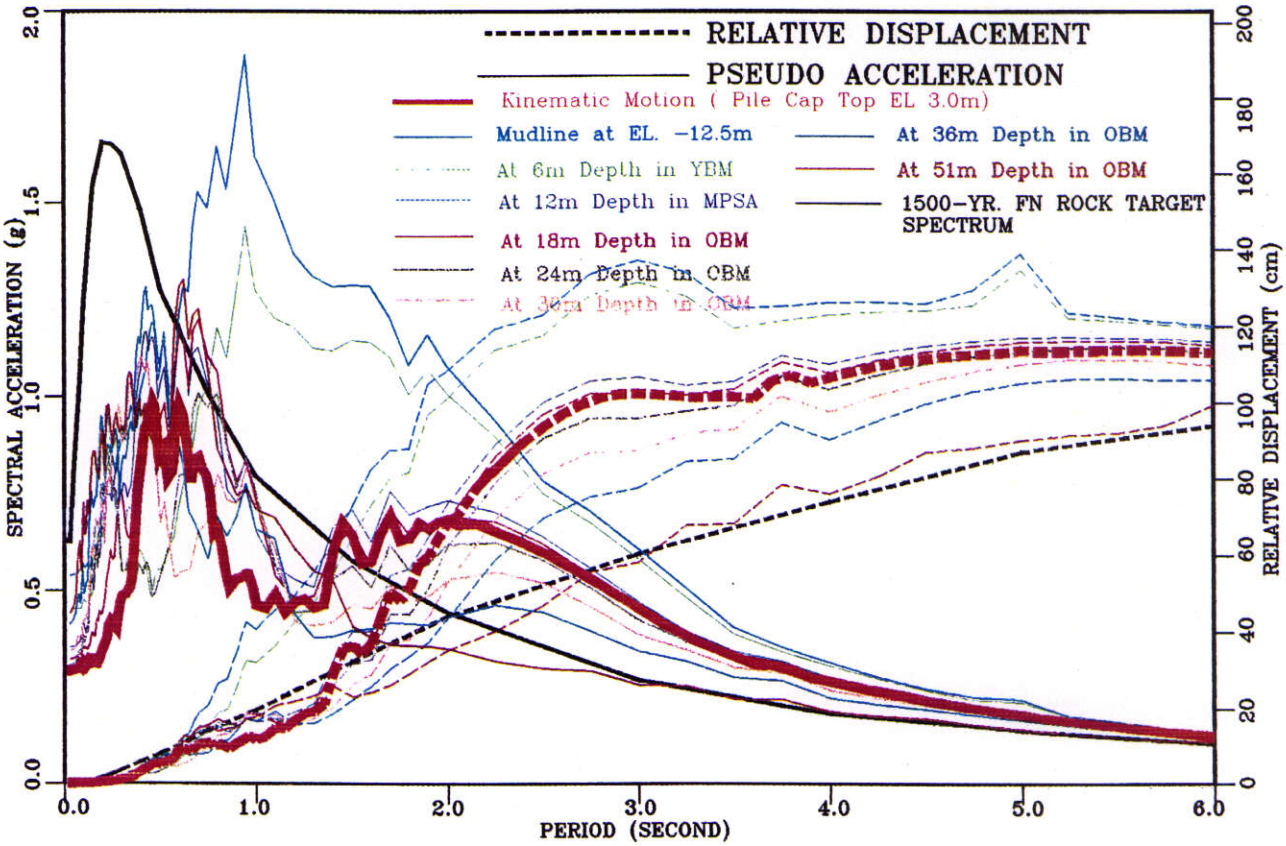

KINEMATIC AND DEPTH-VARYING FREE FIELD MOTIONS
PIER E03, INPUT ROCK MOTION SET 1, FAULT NORMAL COMPONENT
SFOBB East Span Seismic Safety Project

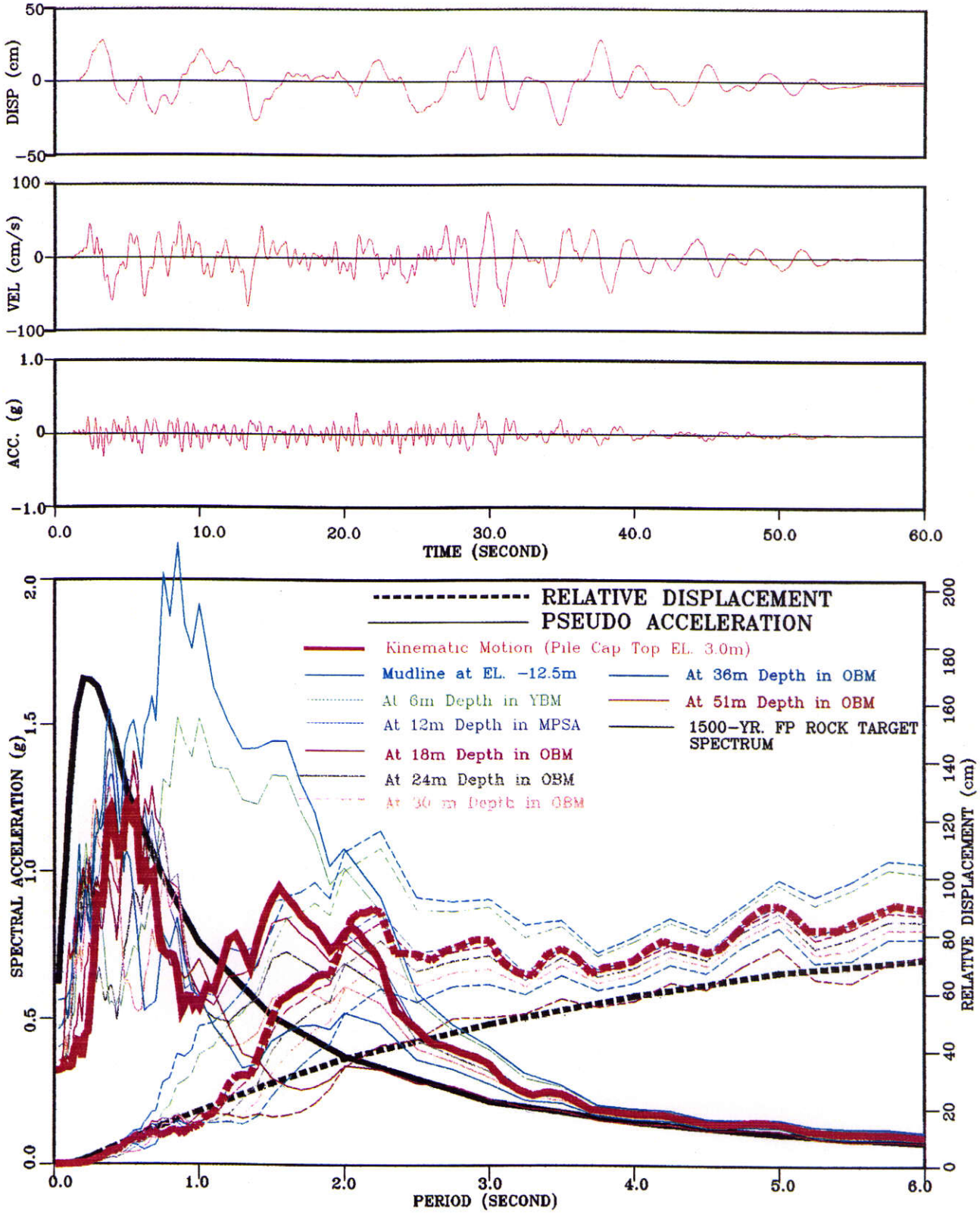

KINEMATIC AND DEPTH-VARYING FREE FIELD MOTIONS
PIER E03, INPUT ROCK MOTION SET 1, FAULT PARALLEL COMPONENT
SFOBB East Span Seismic Safety Project

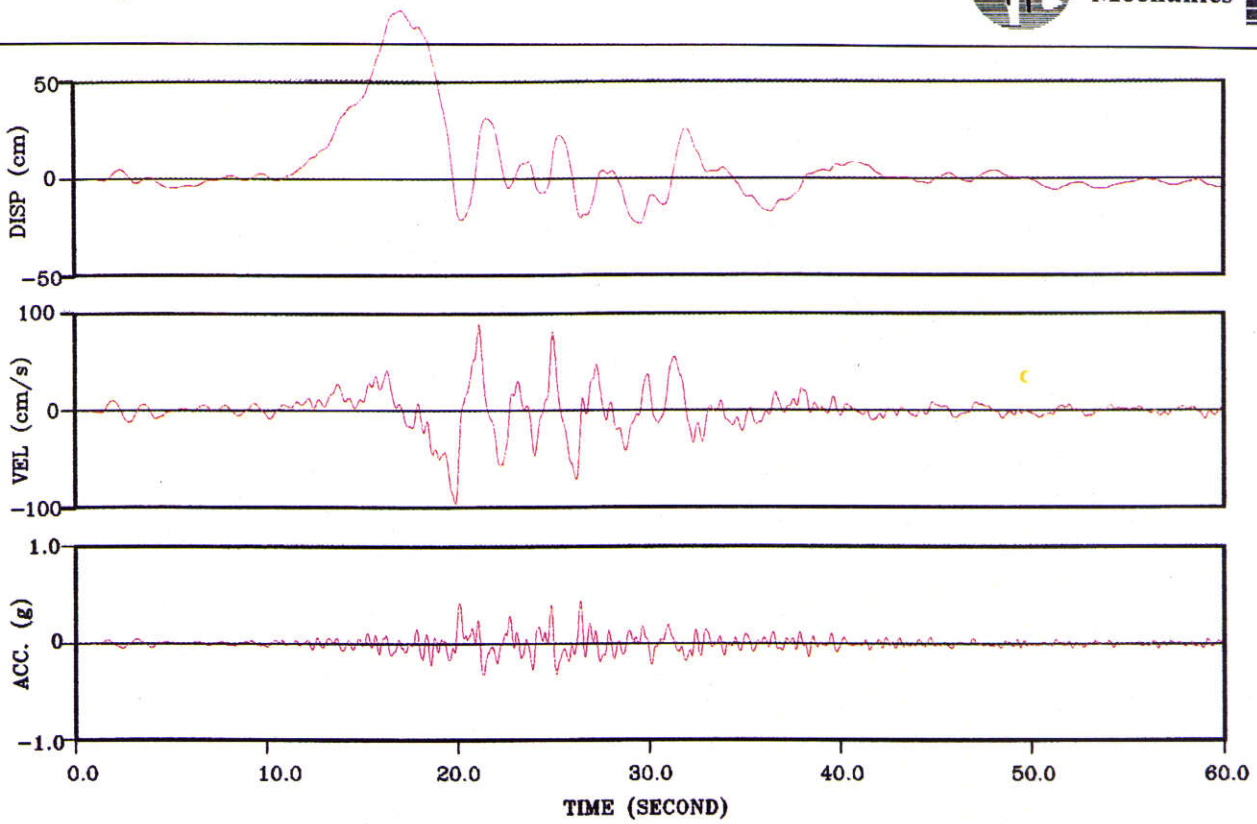

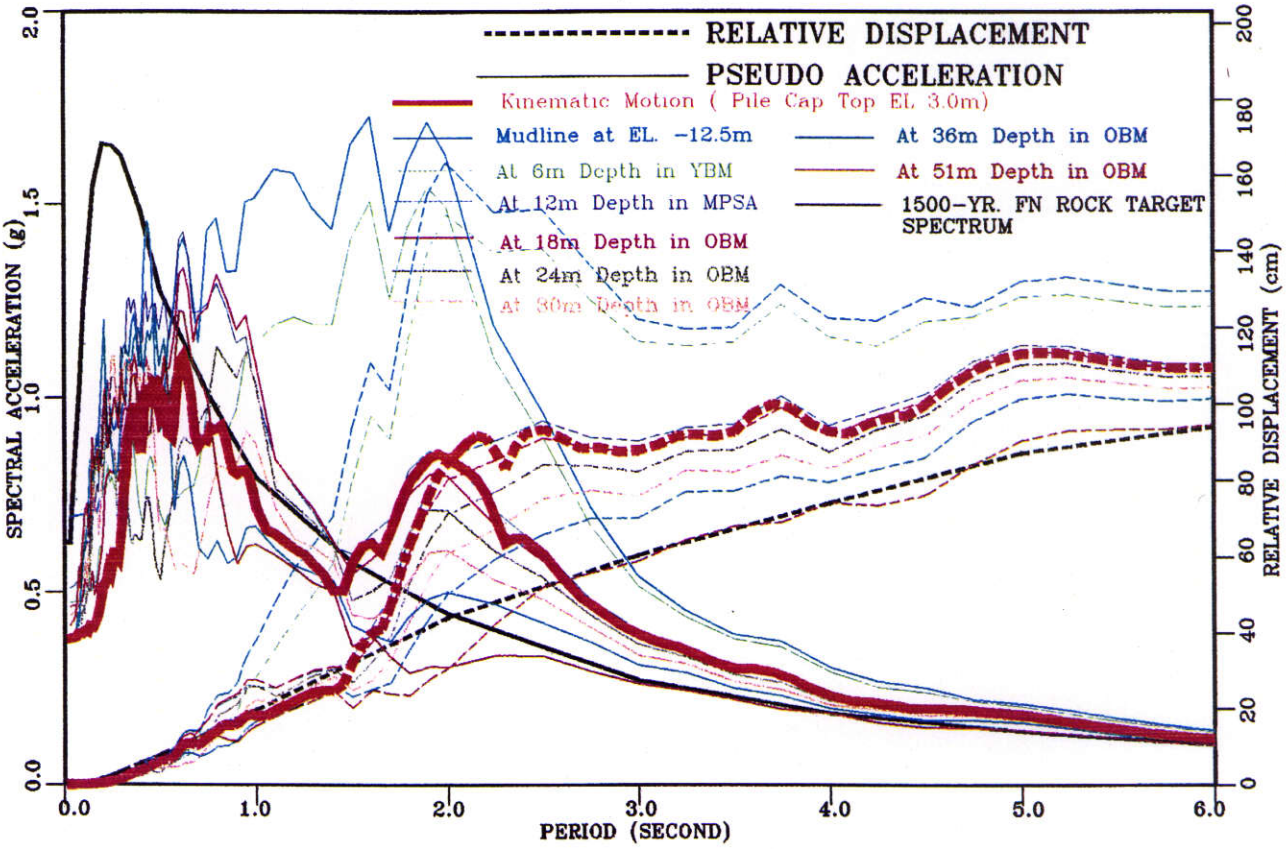

KINEMATIC AND DEPTH-VARYING FREE FIELD MOTIONS
PIER E03, INPUT ROCK MOTION SET 2, FAULT NORMAL COMPONENT
SFOBB East Span Seismic Safety Project

PLATE 8-20

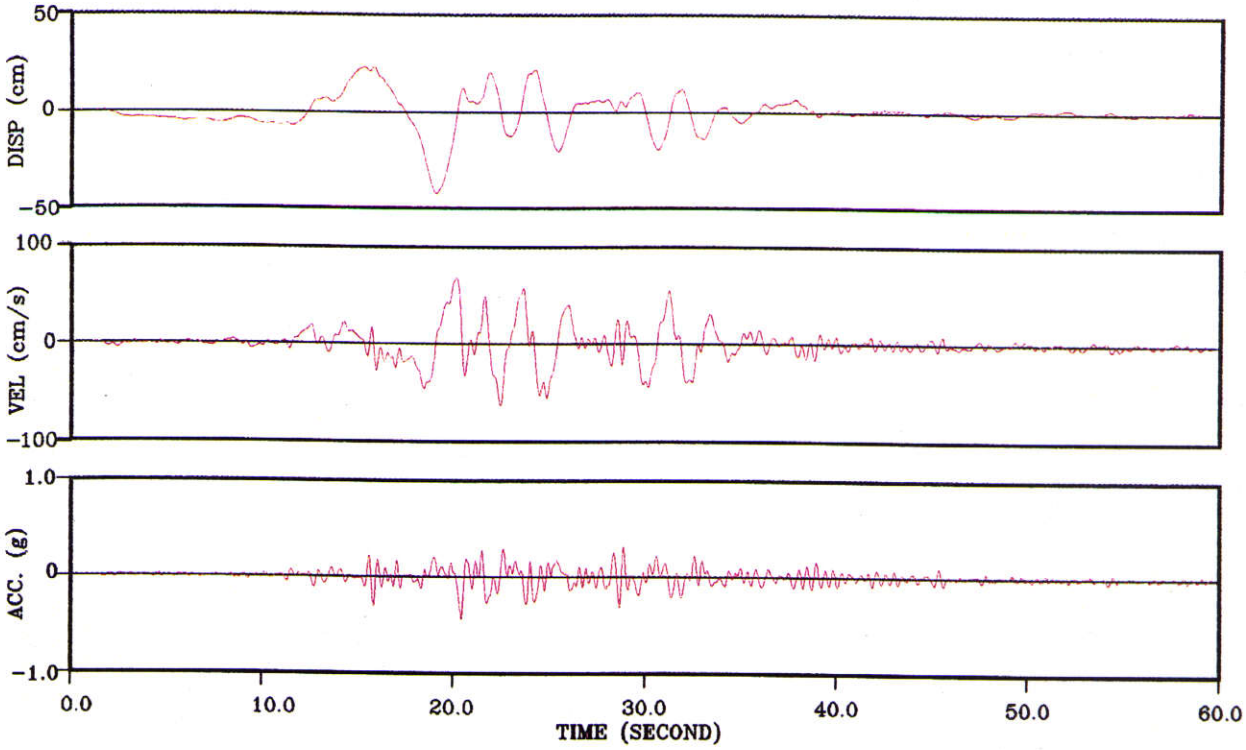

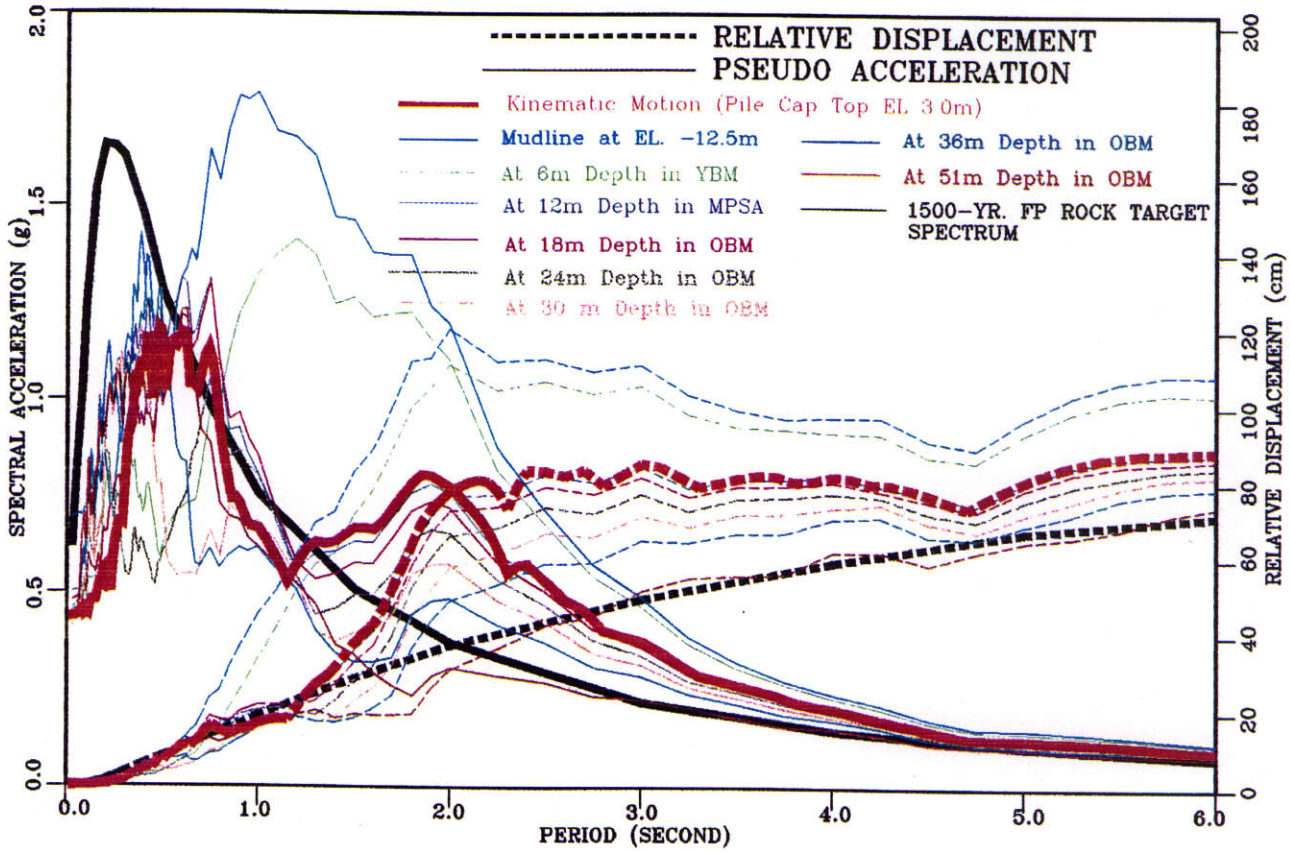

KINEMATIC AND DEPTH-VARYING FREE FIELD MOTIONS
PIER E03, INPUT ROCK MOTION SET 2, FAULT PARALLEL COMPONENT
SFOBB East Span Seismic Safety Project

PLATE 8-21

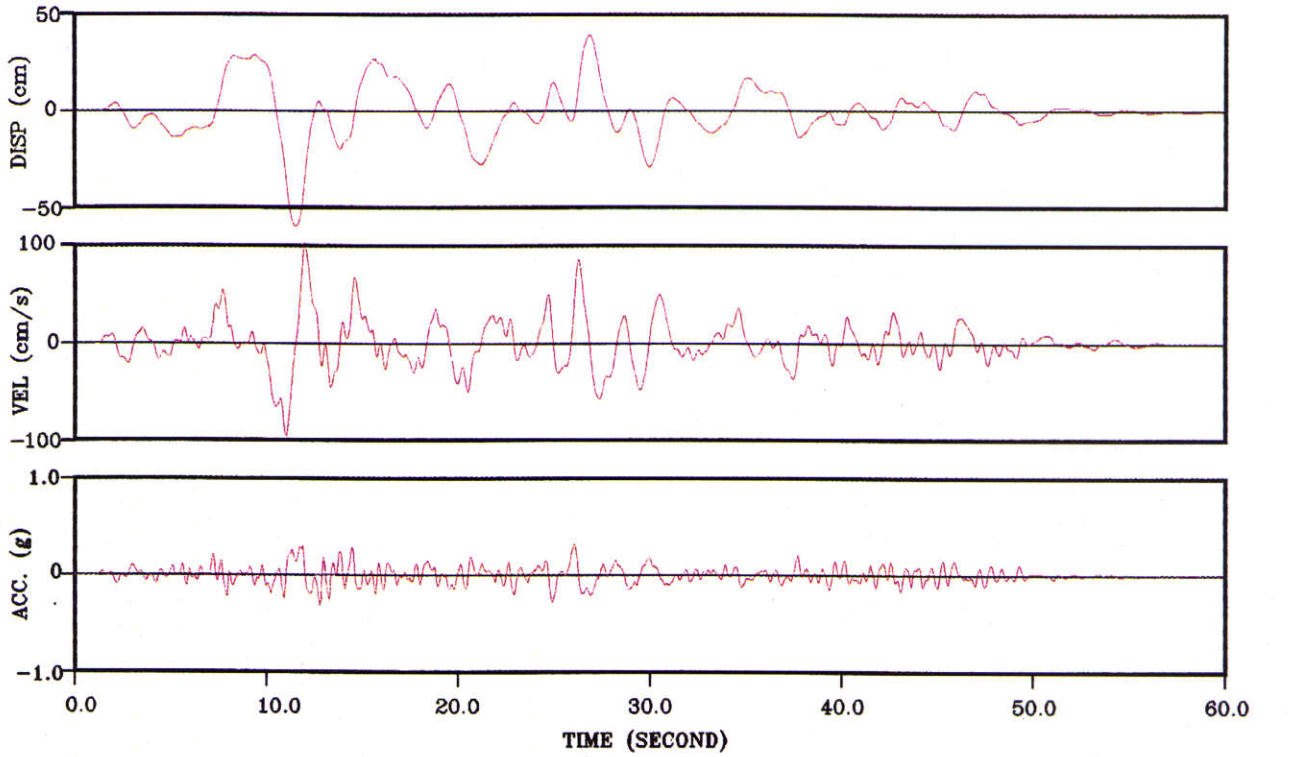

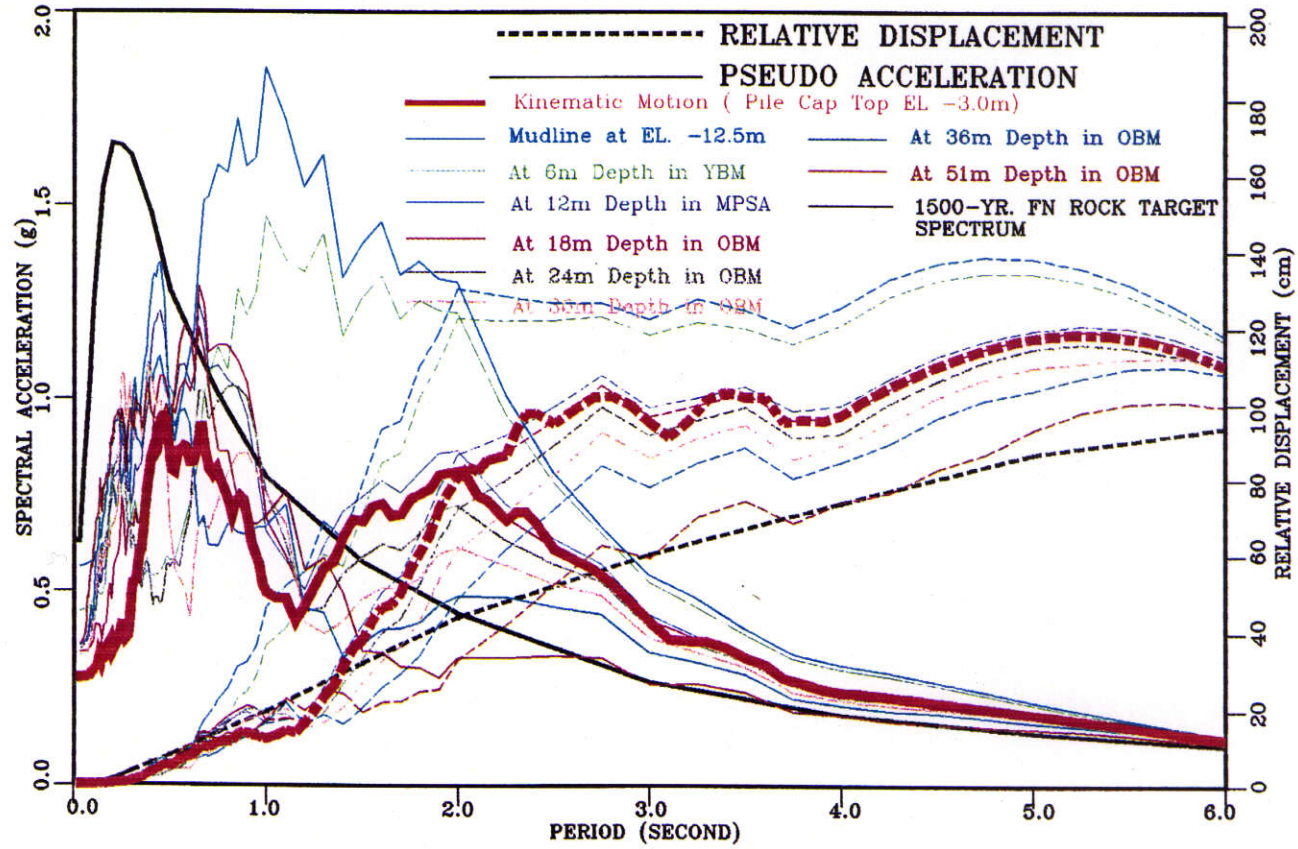

KINEMATIC AND DEPTH-VARYING FREE FIELD MOTIONS
PIER E03, INPUT ROCK MOTION SET 3, FAULT NORMAL COMPONENT
SFOBB East Span Seismic Safety Project

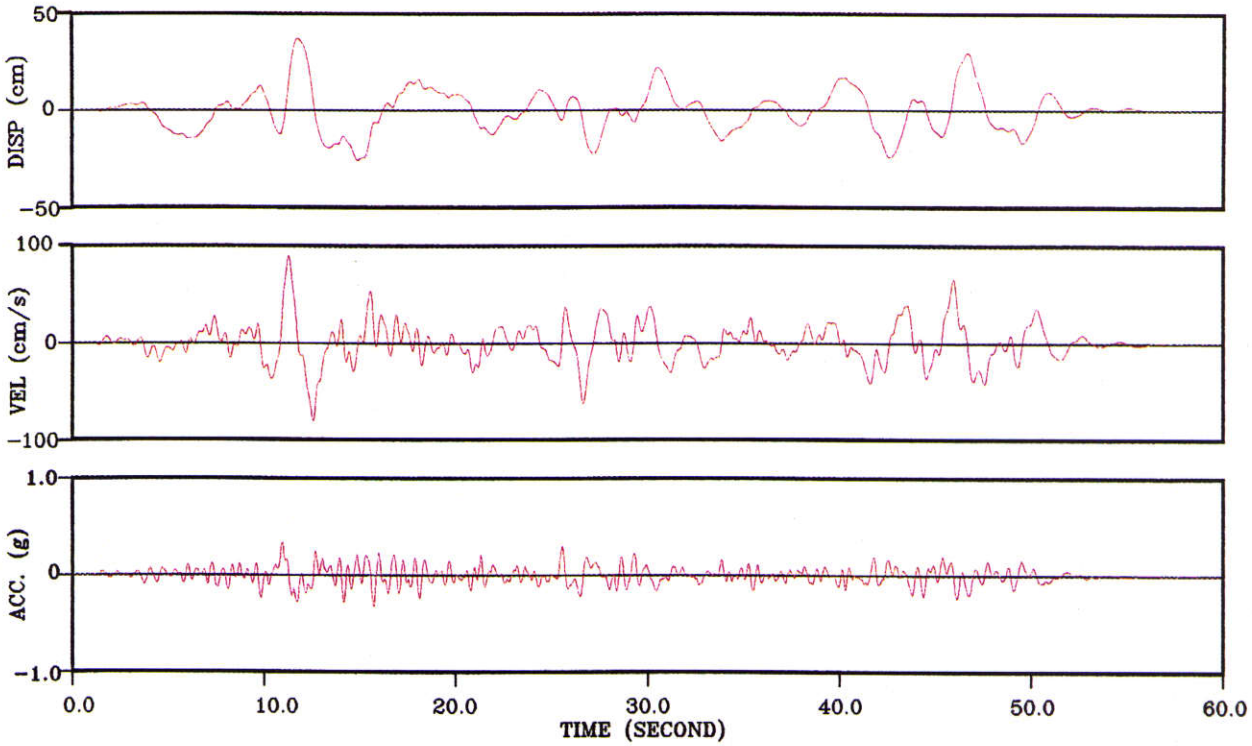

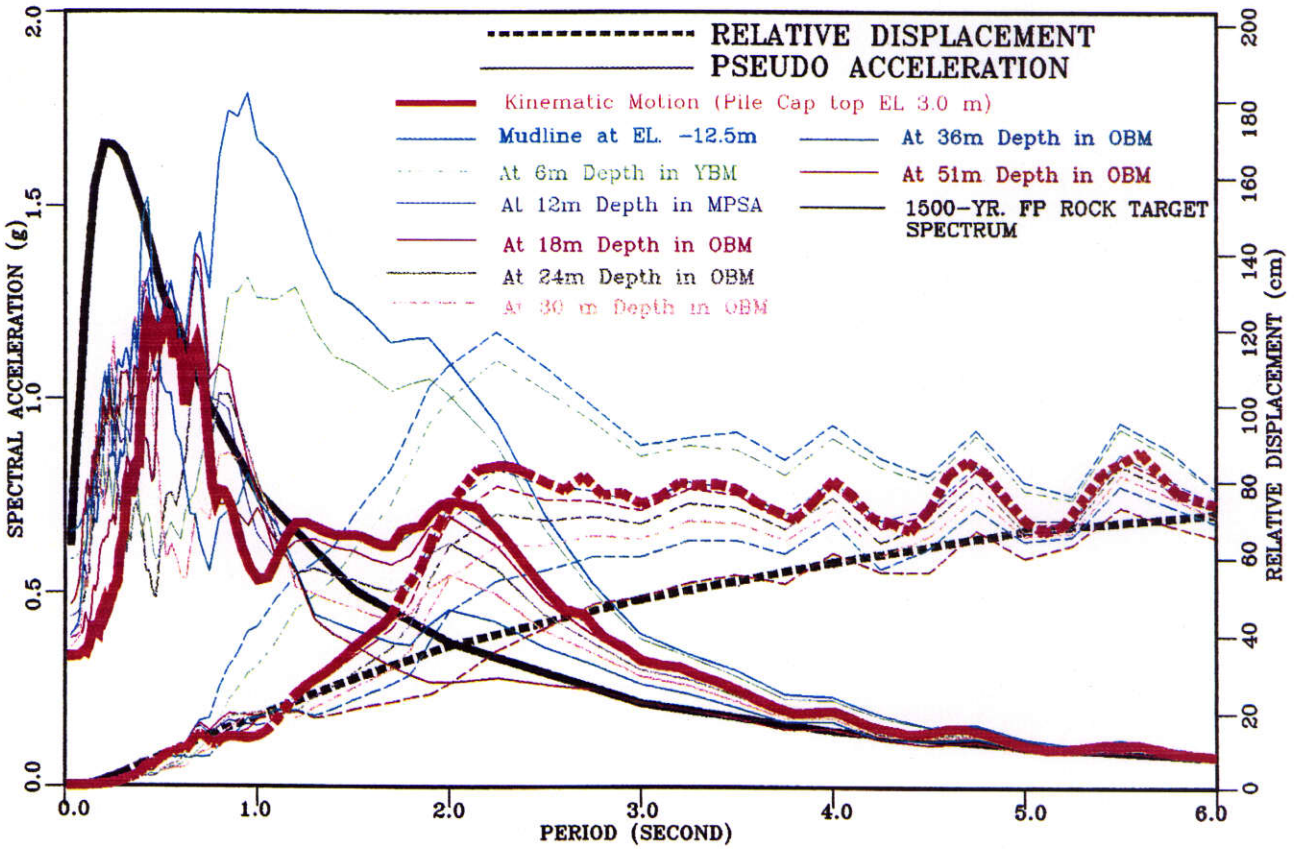

KINEMATIC AND DEPTH-VARYING FREE FIELD MOTIONS
PIER E03, INPUT ROCK MOTION SET 3, FAULT PARALLEL COMPONENT
SFOBB East Span Seismic Safety Project

PLATE 8-23

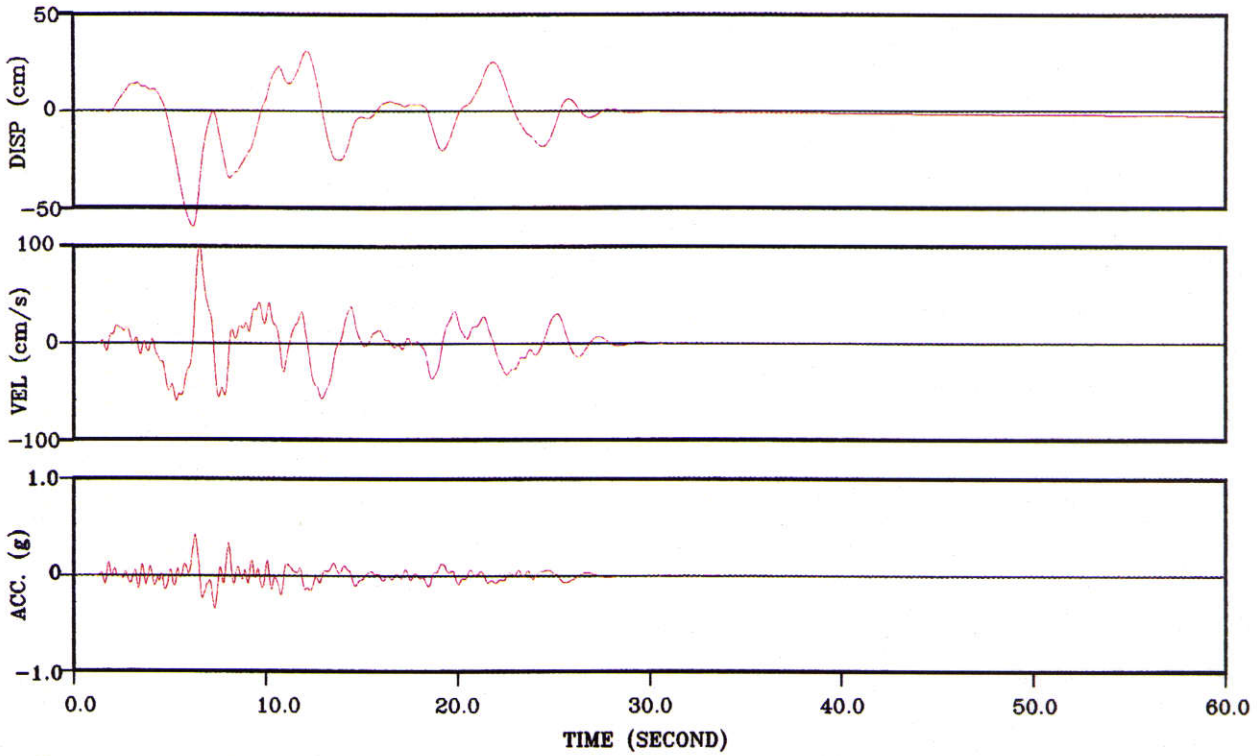

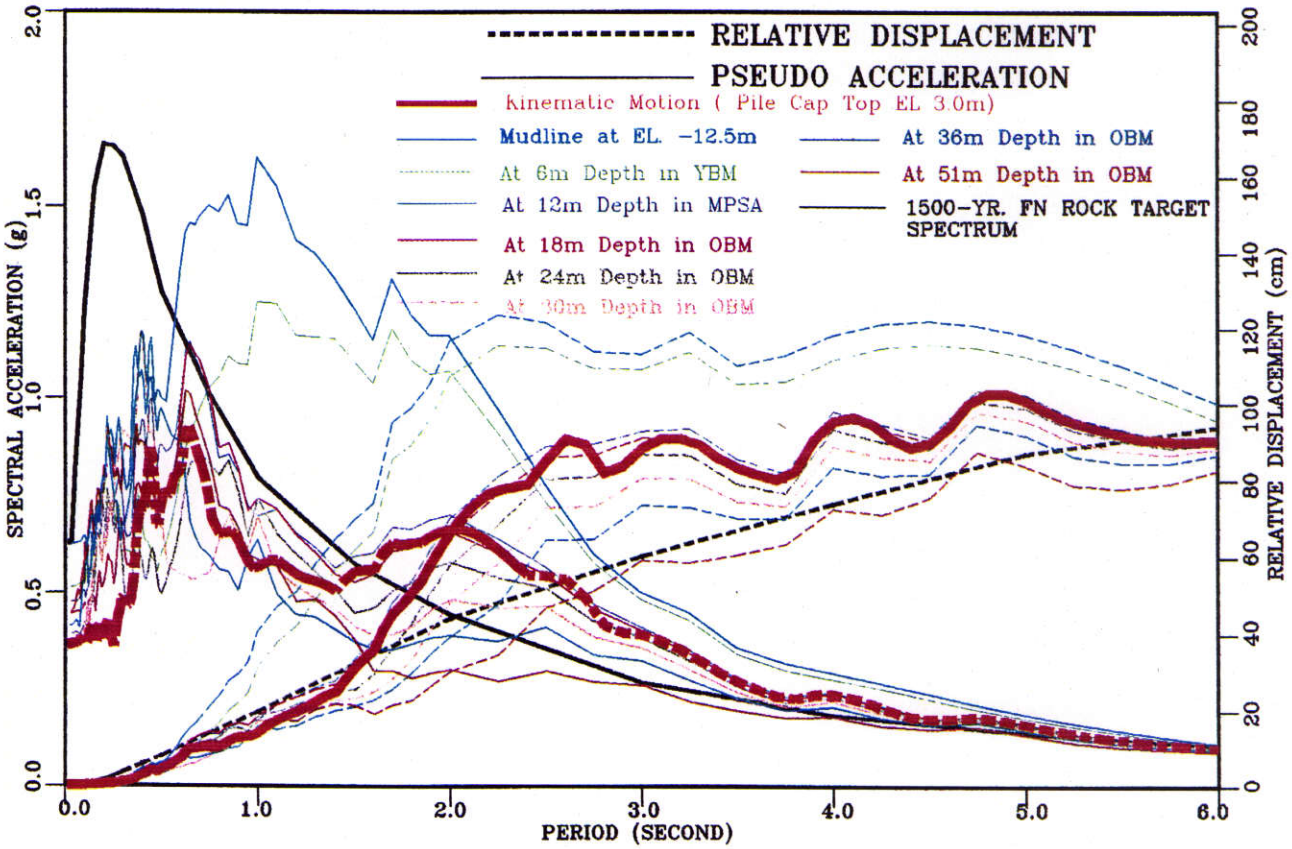

KINEMATIC AND DEPTH-VARYING FREE FIELD MOTIONS
PIER E03, INPUT ROCK MOTION SET 4, FAULT NORMAL COMPONENT
SFOBB East Span Seismic Safety Project

PLATE 8-24

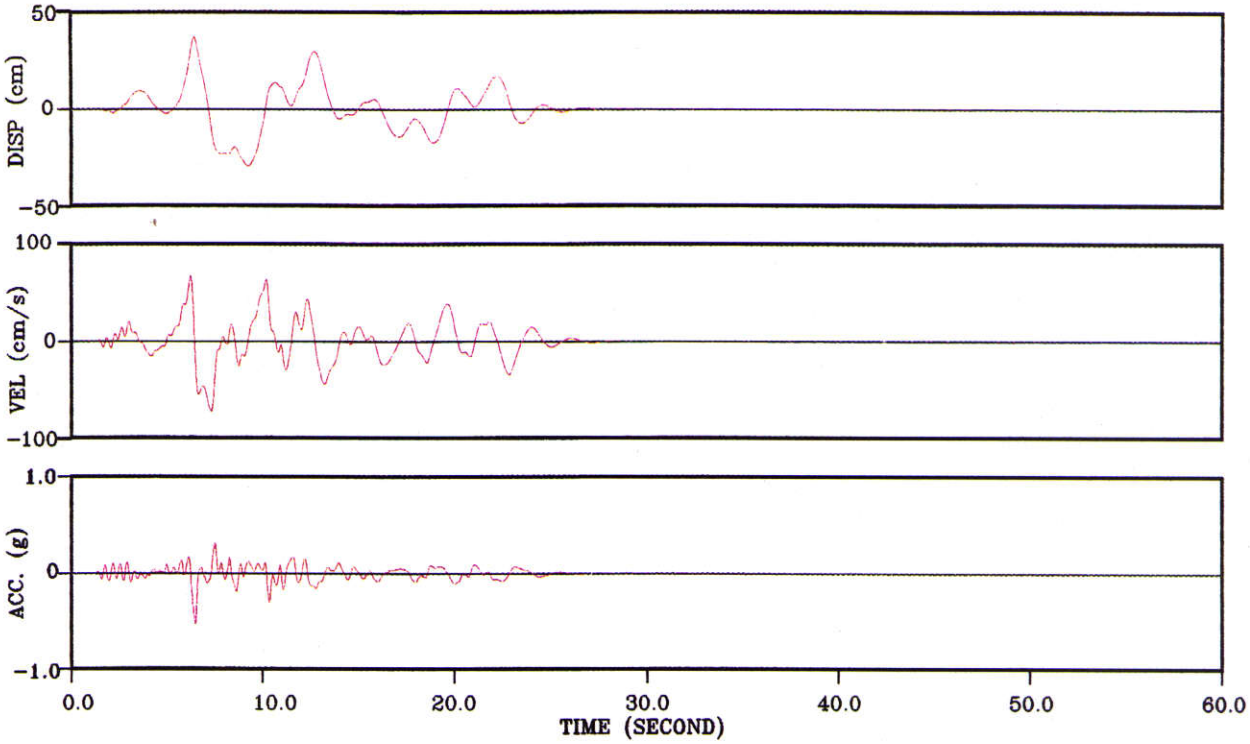

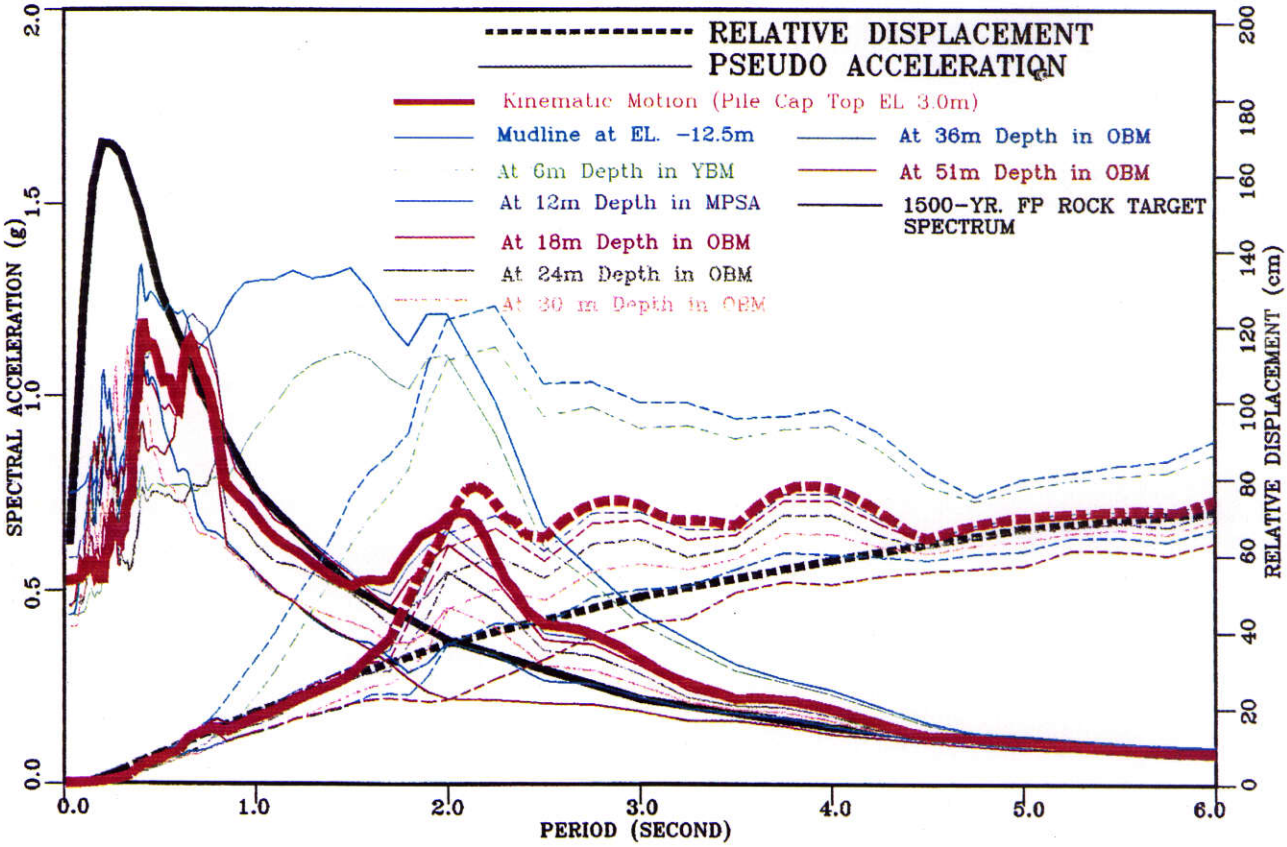

KINEMATIC AND DEPTH-VARYING FREE FIELD MOTIONS
PIER E03, INPUT ROCK MOTION SET 4, FAULT PARALLEL COMPONENT
SFOBB East Span Seismic Safety Project

PLATE 8-25

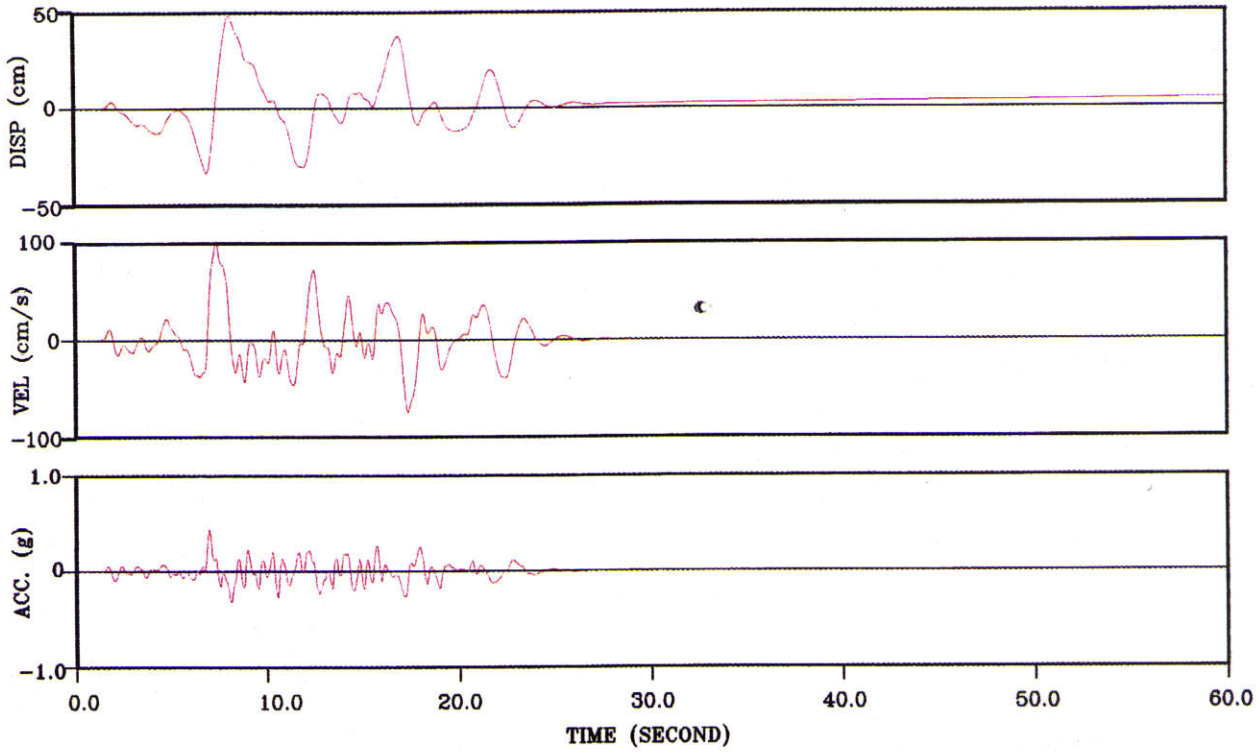

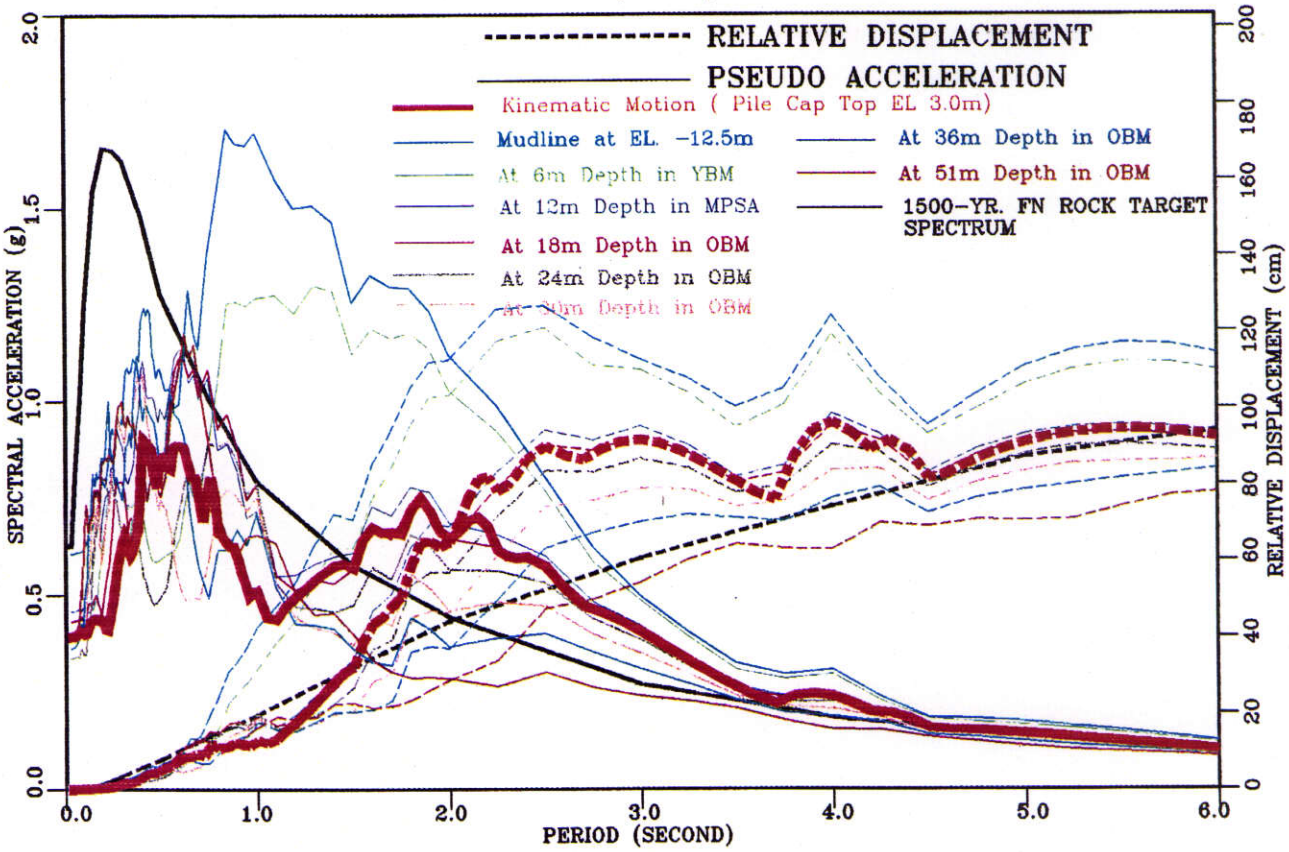

KINEMATIC AND DEPTH-VARYING FREE FIELD MOTIONS
PIER E03, INPUT ROCK MOTION SET 5, FAULT NORMAL COMPONENT
SFOBB East Span Seismic Safety Project

PLATE 8-26

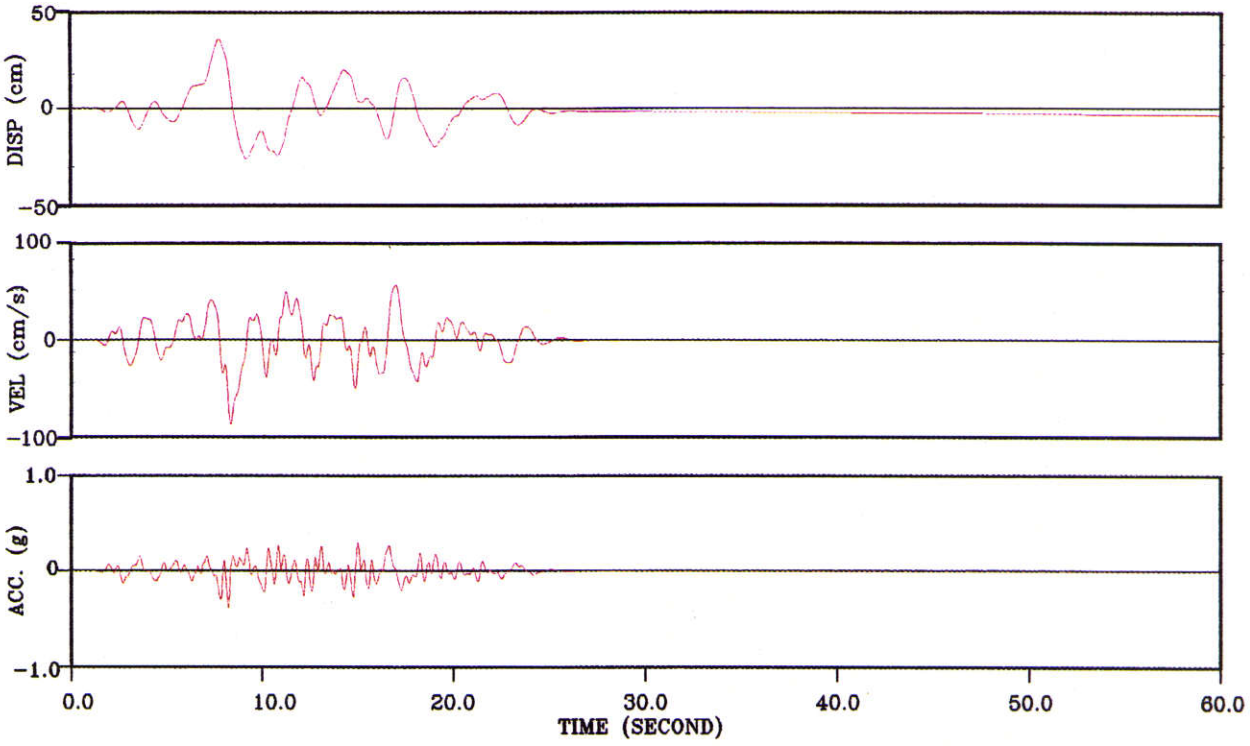

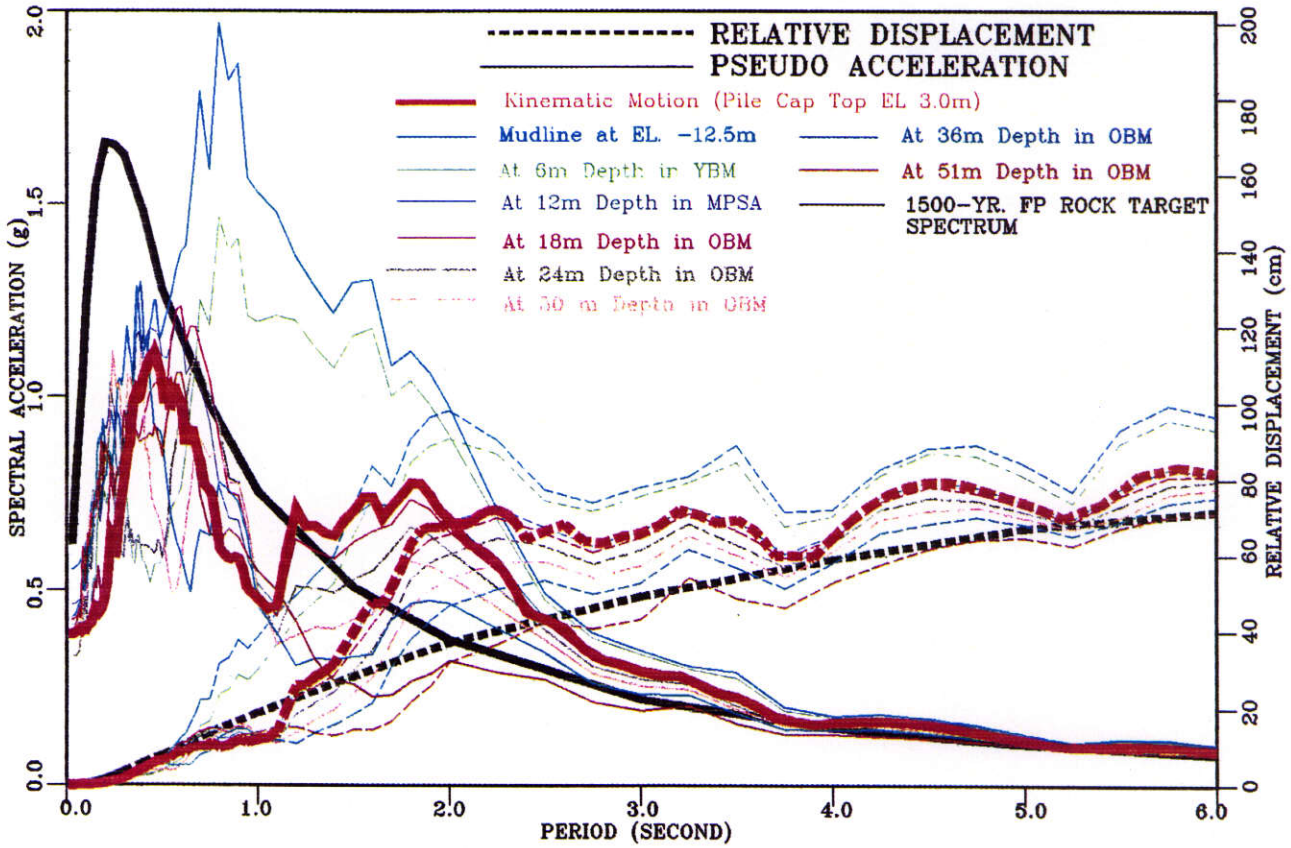

KINEMATIC AND DEPTH-VARYING FREE FIELD MOTIONS
PIER E03, INPUT ROCK MOTION SET 5, FAULT PARALLEL COMPONENT
SFOBB East Span Seismic Safety Project

PLATE 8-27

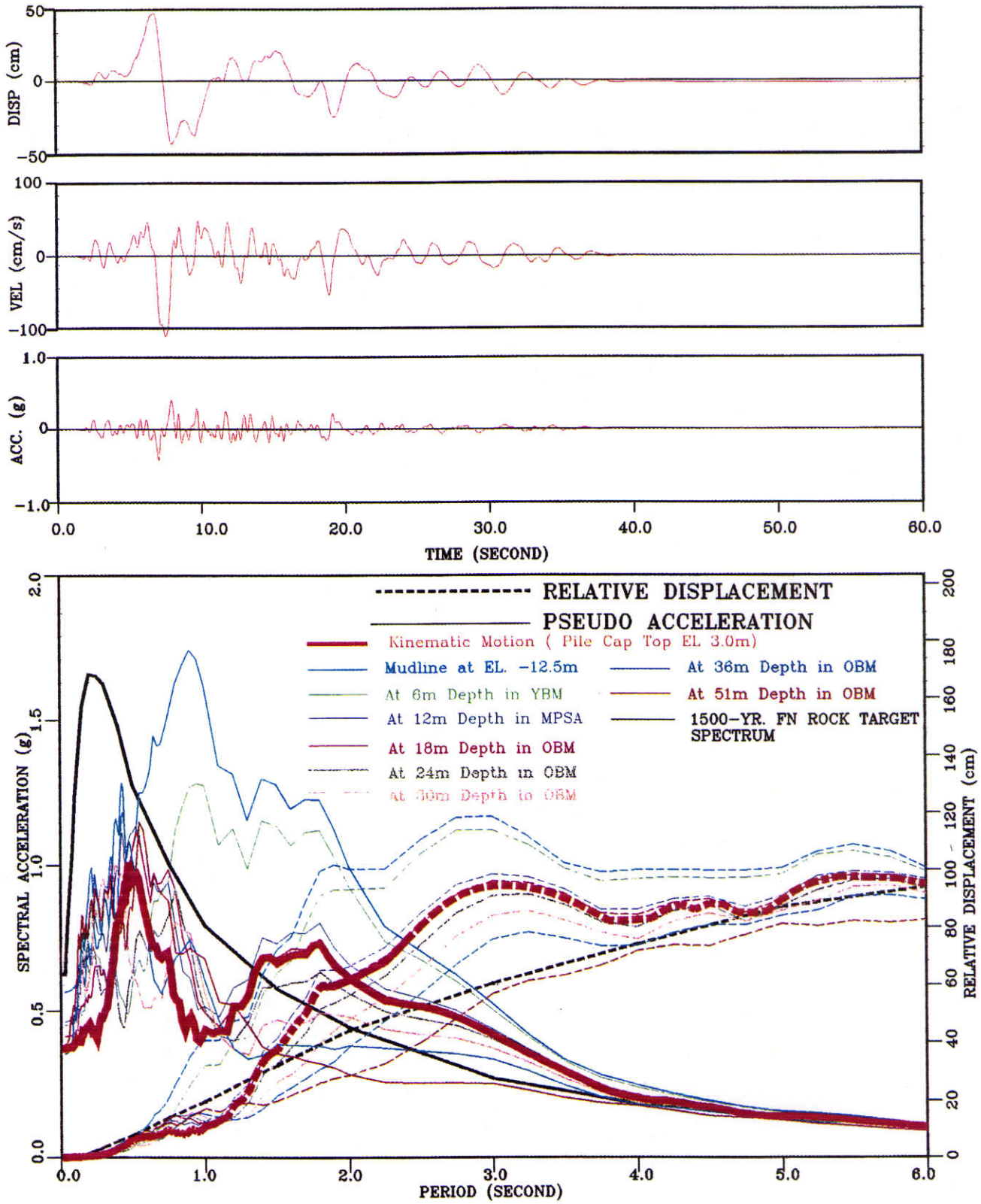

KINEMATIC AND DEPTH-VARYING FREE FIELD MOTIONS
PIER E03, INPUT ROCK MOTION SET 6, FAULT NORMAL COMPONENT
SFOBB East Span Seismic Safety Project

PLATE 8-28

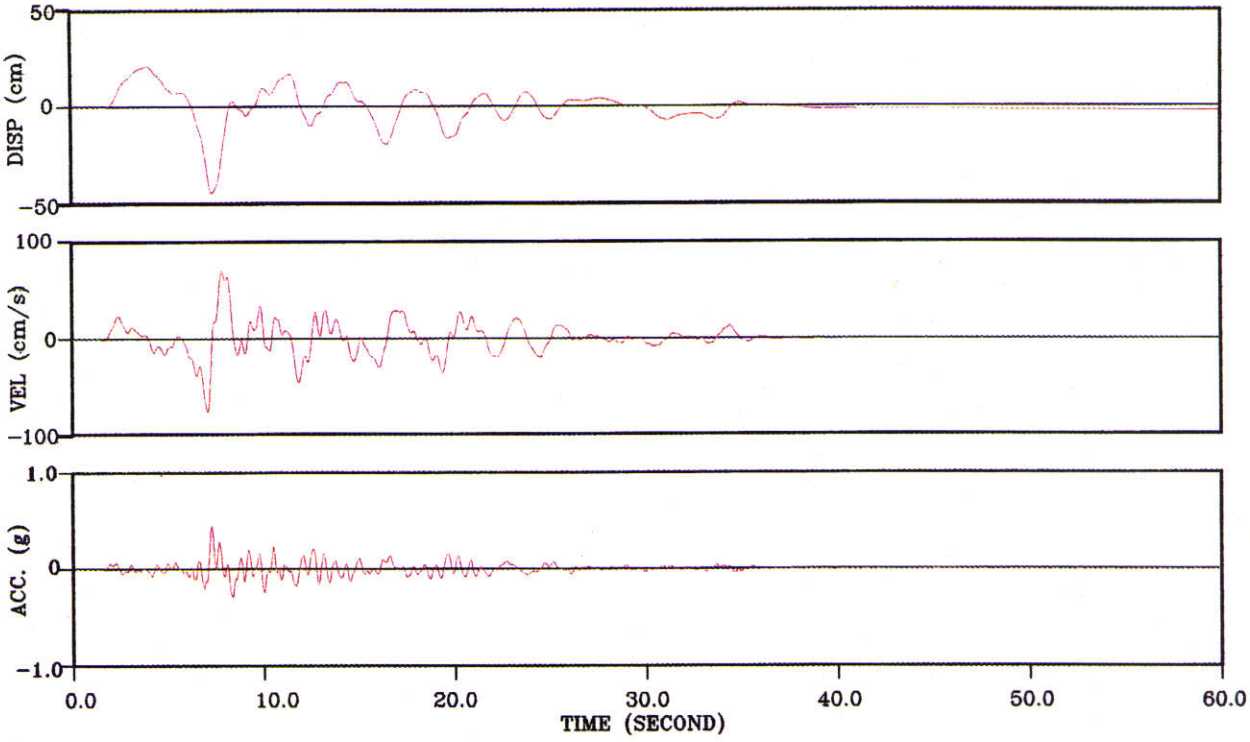

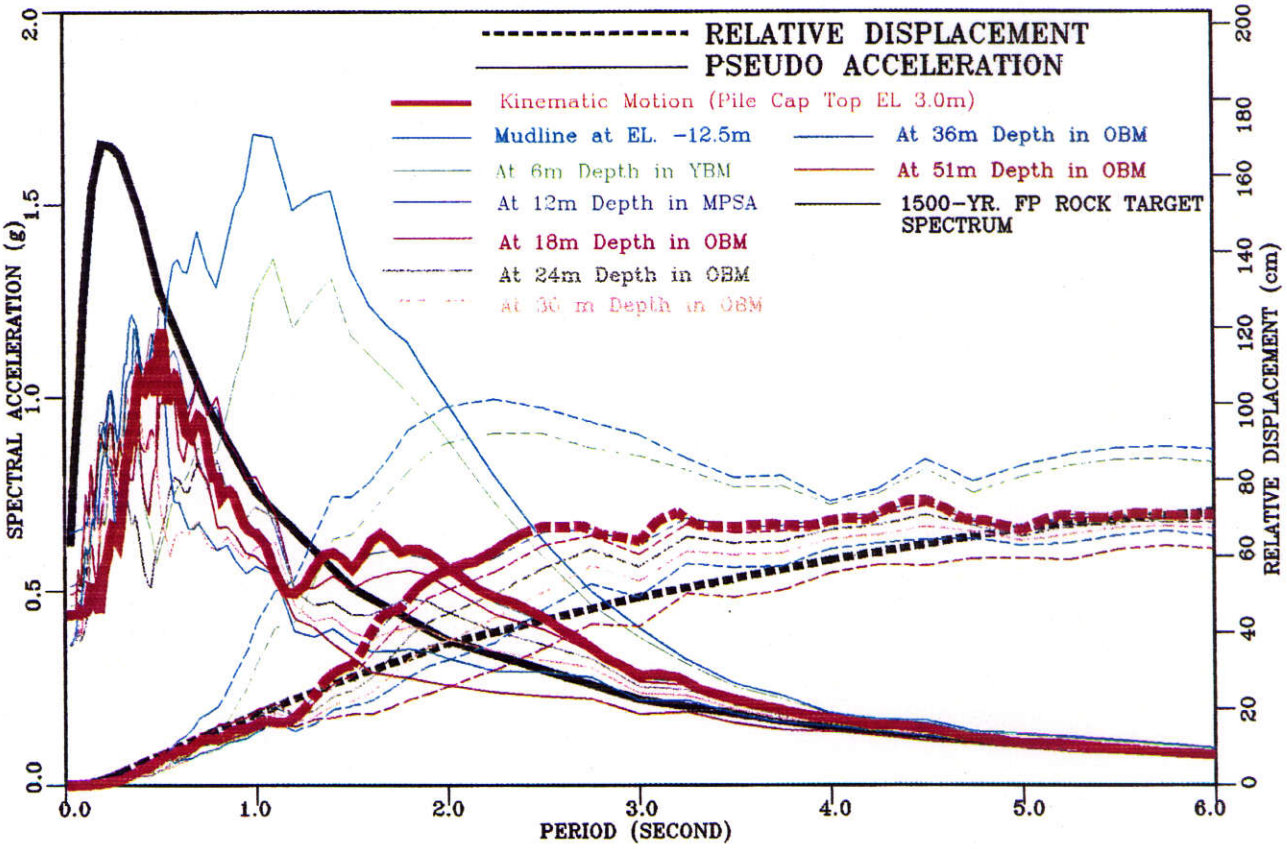

KINEMATIC AND DEPTH-VARYING FREE FIELD MOTIONS
PIER E03, INPUT ROCK MOTION SET 6, FAULT PARALLEL COMPONENT
SFOBB East Span Seismic Safety Project

PLATE 8-29

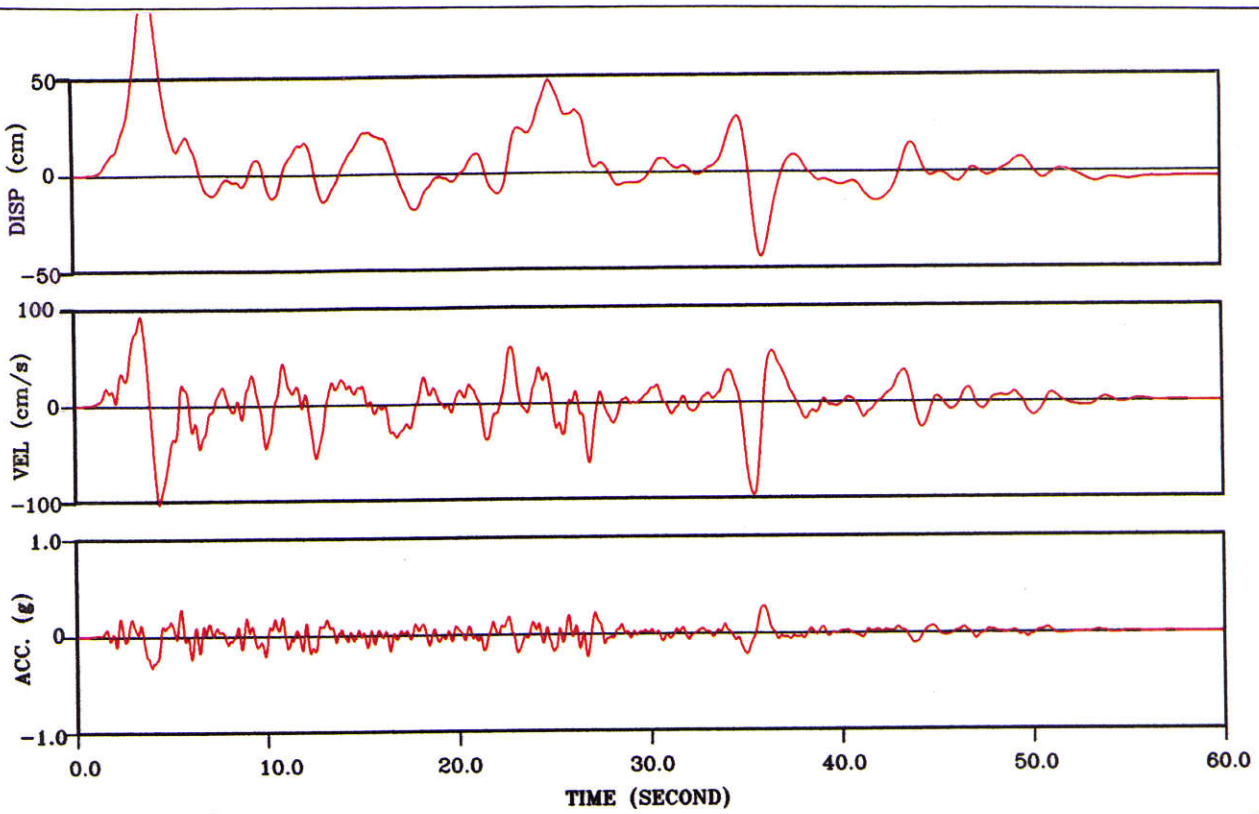

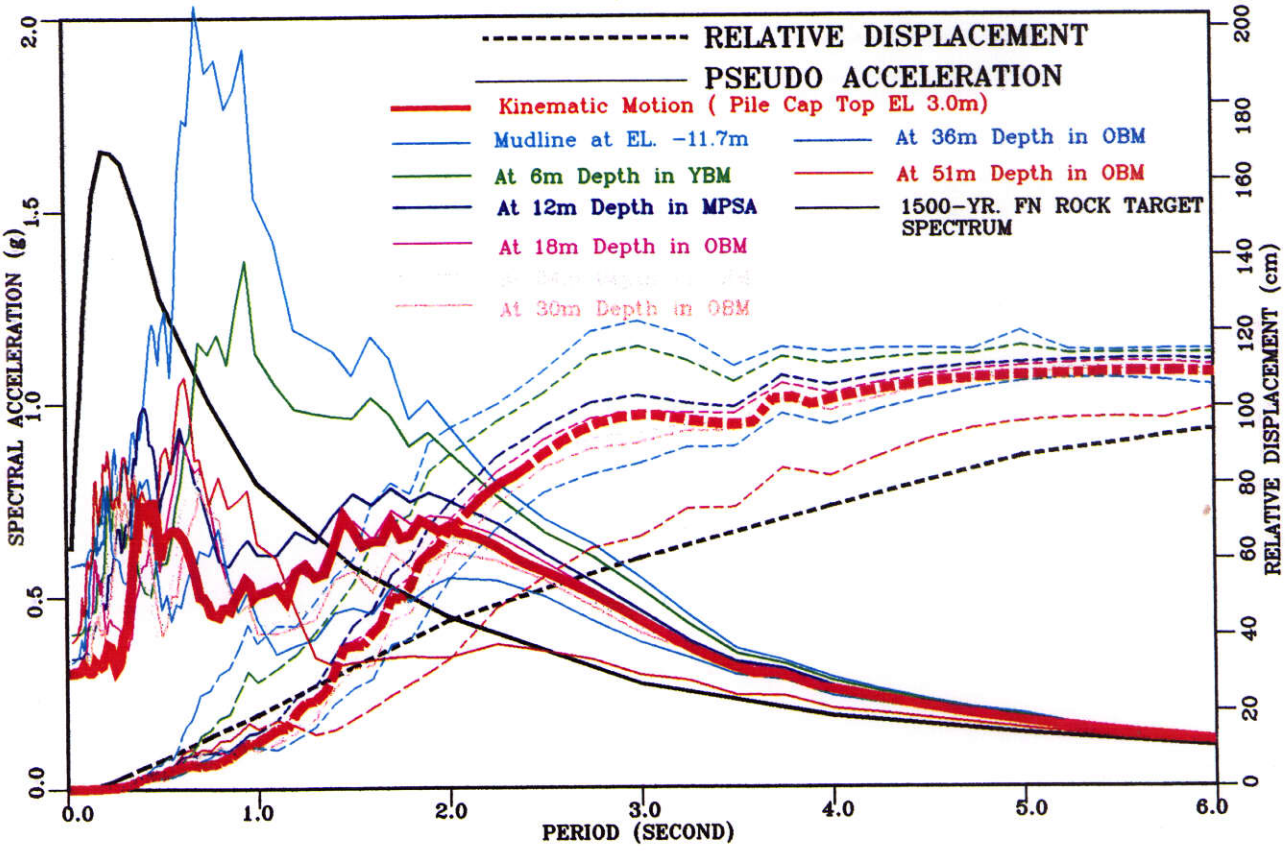

KINEMATIC AND DEPTH-VARYING FREE FIELD MOTIONS
PIER E04, INPUT ROCK MOTION SET 1, FAULT NORMAL COMPONENT
SFOBB East Span Seismic Safety Project

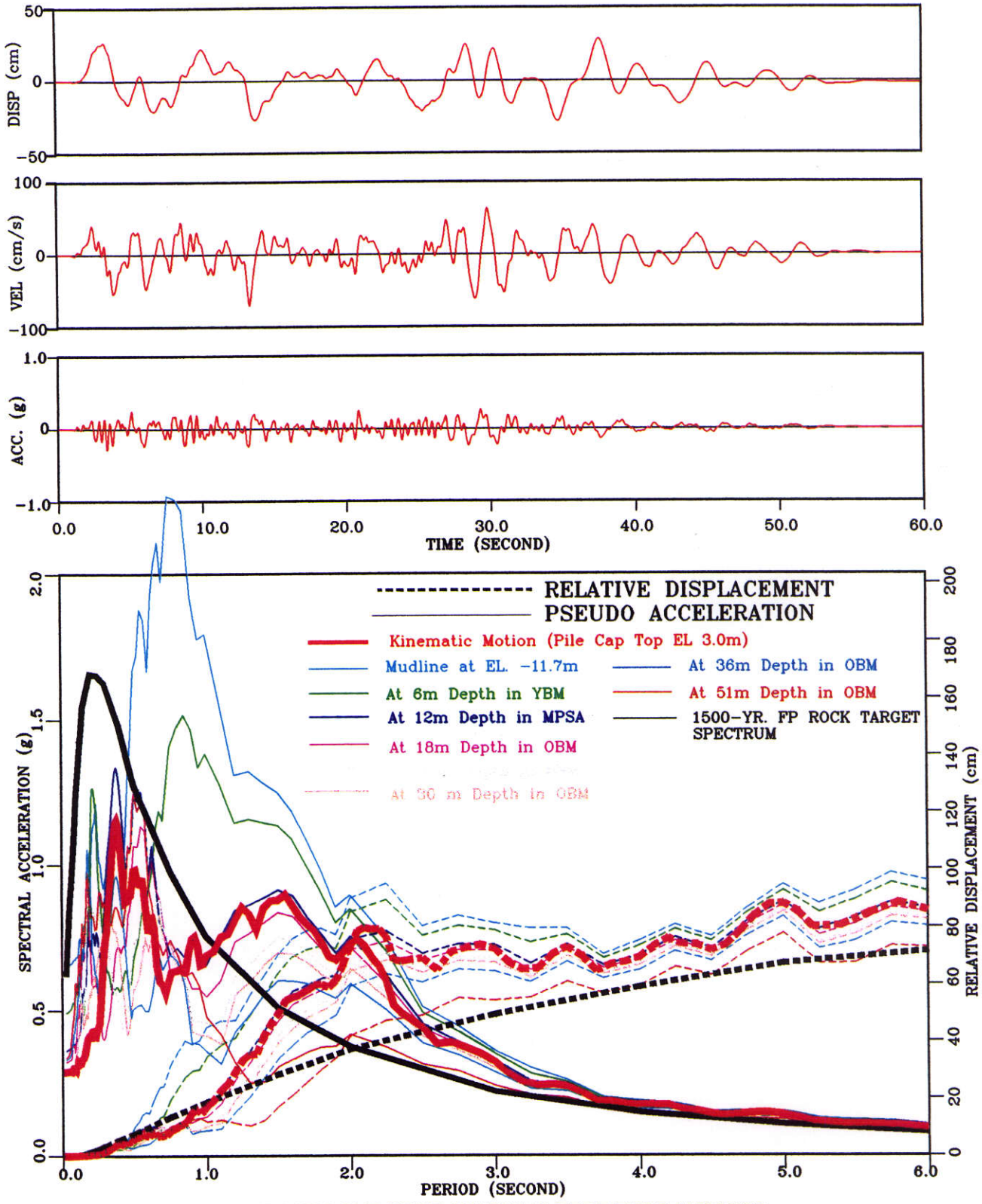

KINEMATIC AND DEPTH-VARYING FREE FIELD MOTIONS
PIER E04, INPUT ROCK MOTION SET 1, FAULT PARALLEL COMPONENT
SFOBB East Span Seismic Safety Project

PLATE 8-31

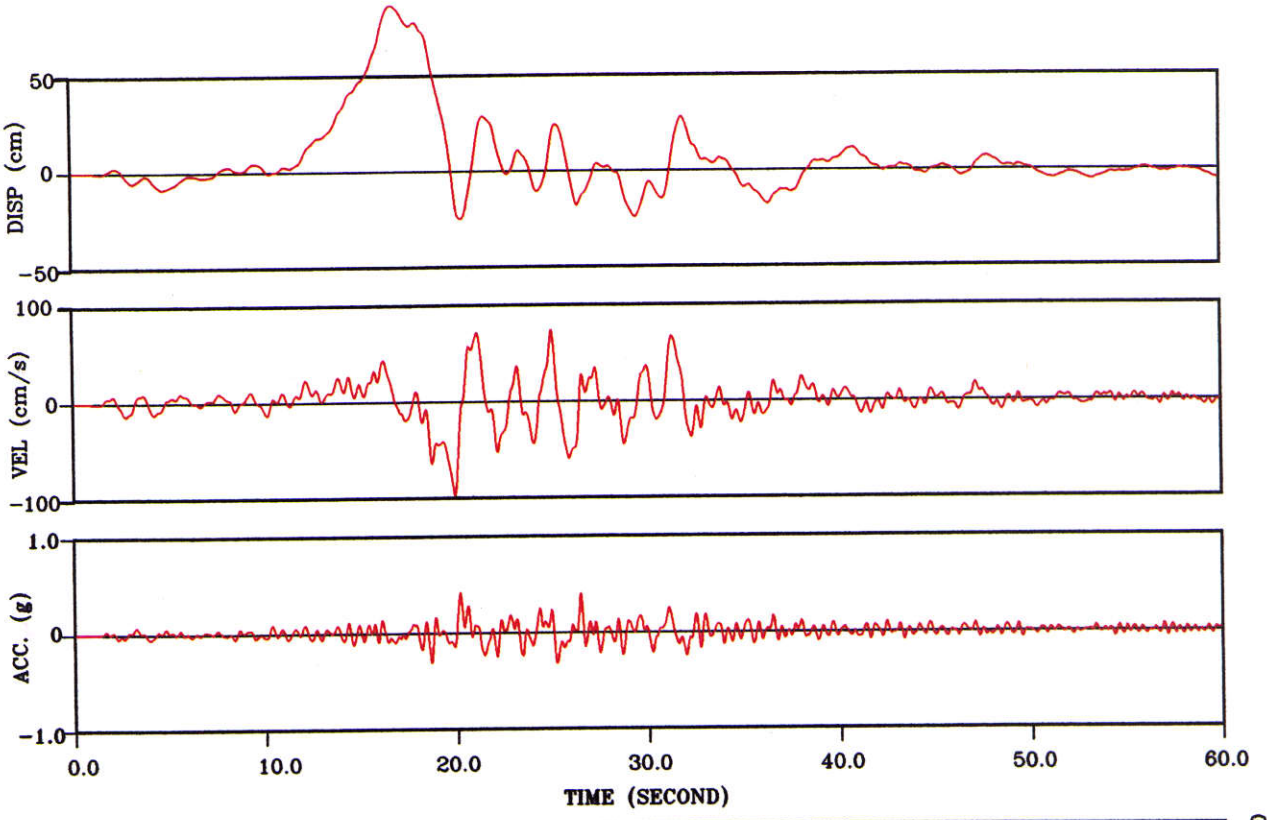

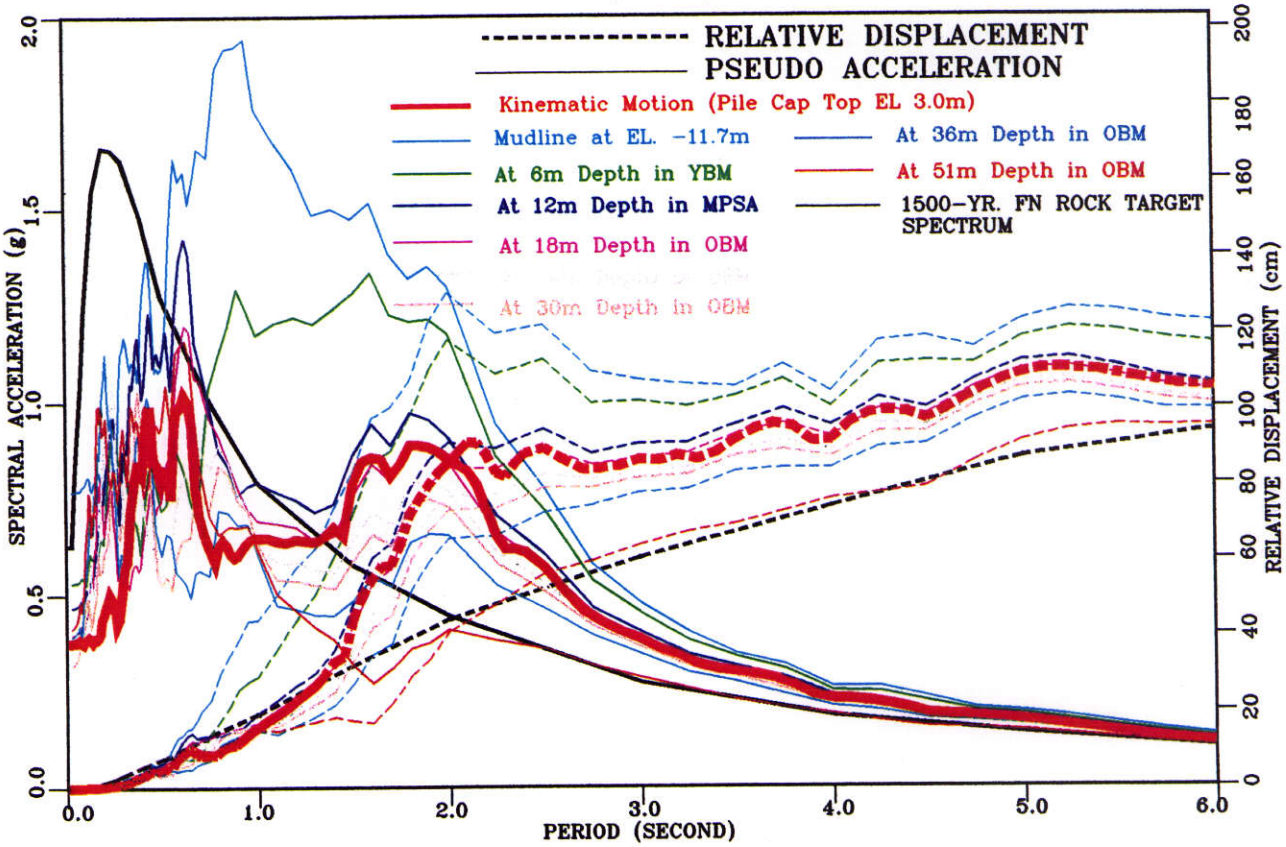

KINEMATIC AND DEPTH-VARYING FREE FIELD MOTIONS
PIER E04, INPUT ROCK MOTION SET 2, FAULT NORMAL COMPONENT
SFOBB East Span Seismic Safety Project

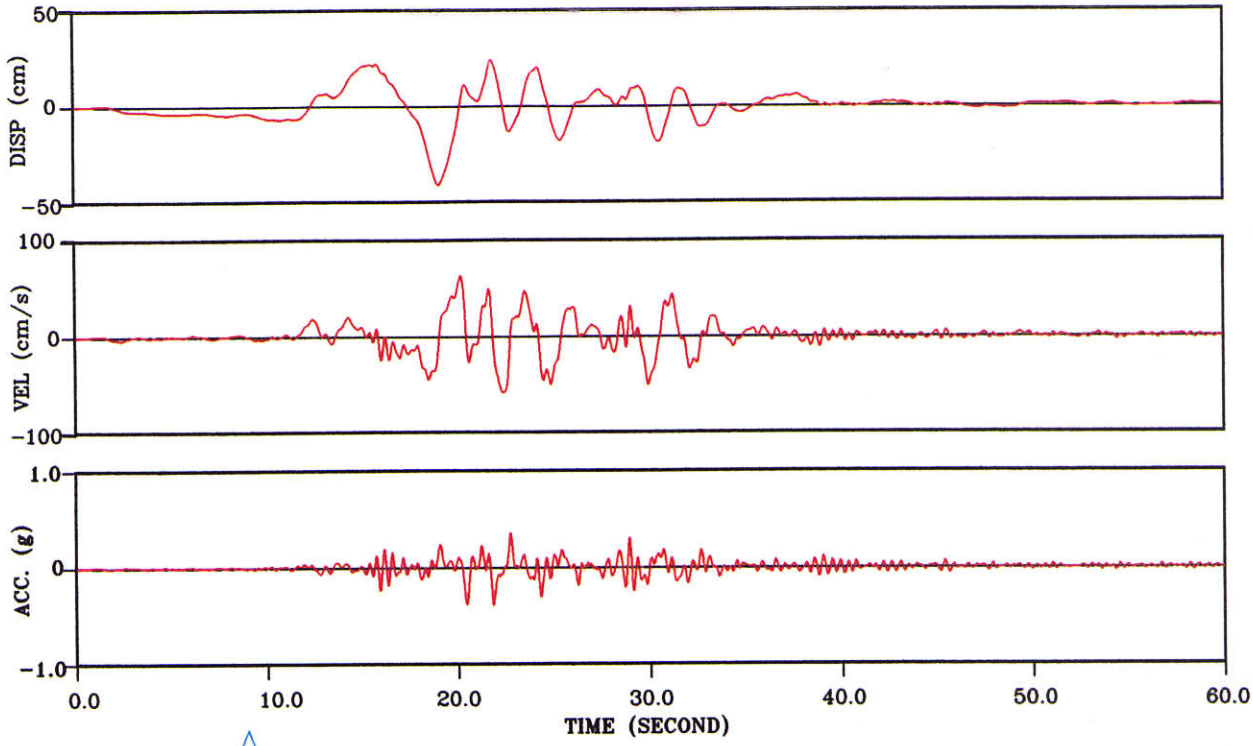

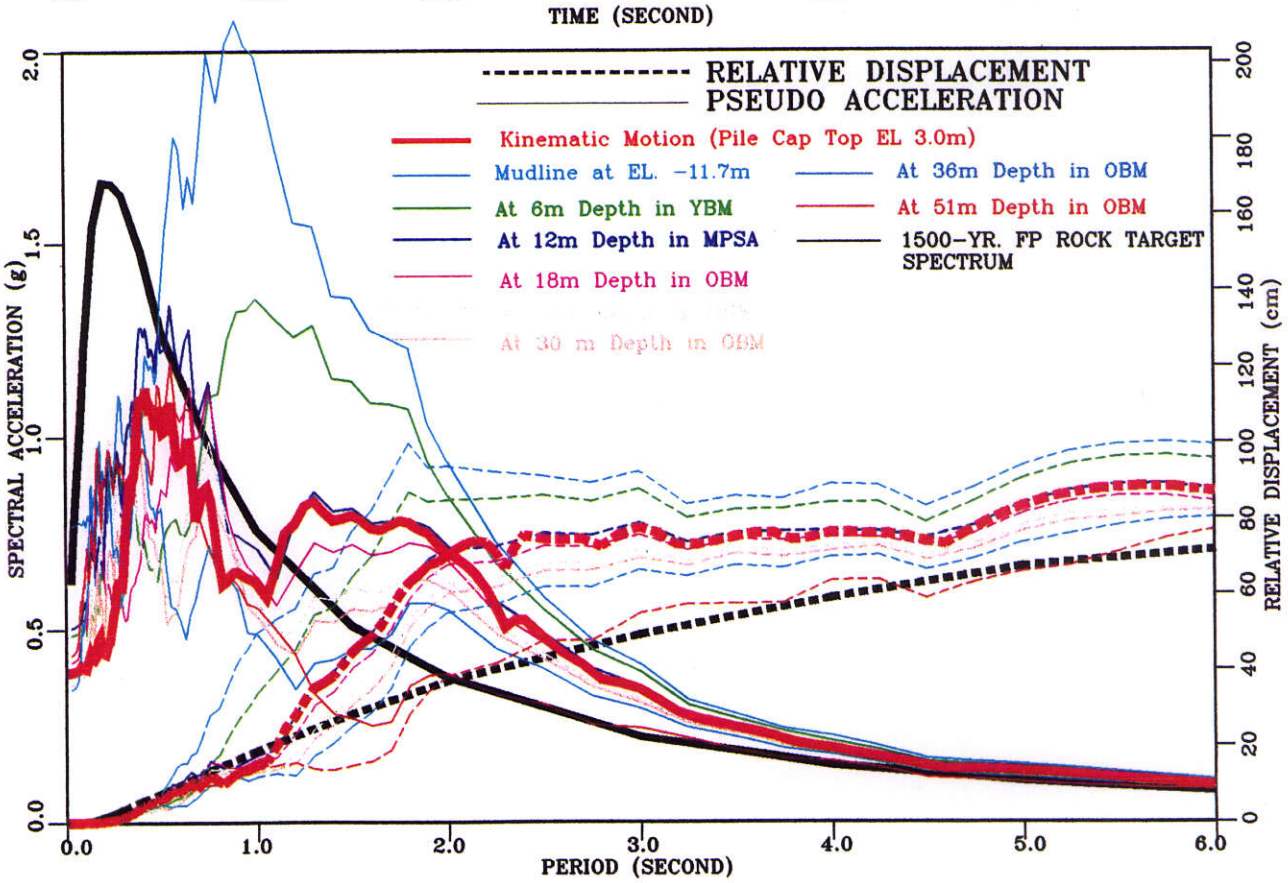

KINEMATIC AND DEPTH-VARYING FREE FIELD MOTIONS
PIER E04, INPUT ROCK MOTION SET 2, FAULT PARALLEL COMPONENT
SFOBB East Span Seismic Safety Project

PLATE 8-33

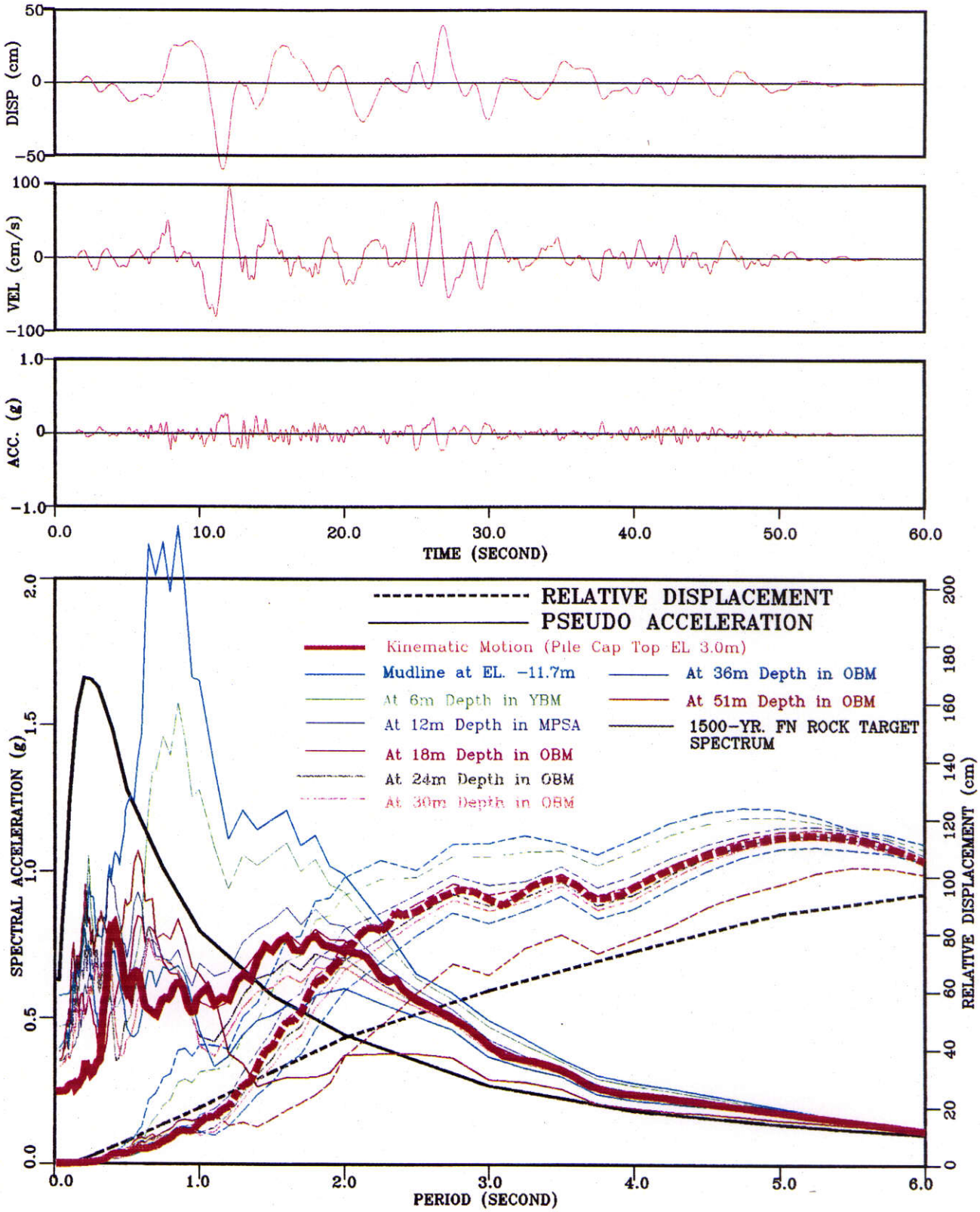

KINEMATIC AND DEPTH-VARYING FREE FIELD MOTIONS
PIER E04, INPUT ROCK MOTION SET 3, FAULT NORMAL COMPONENT
SFOBB East Span Seismic Safety Project

PLATE 8-34

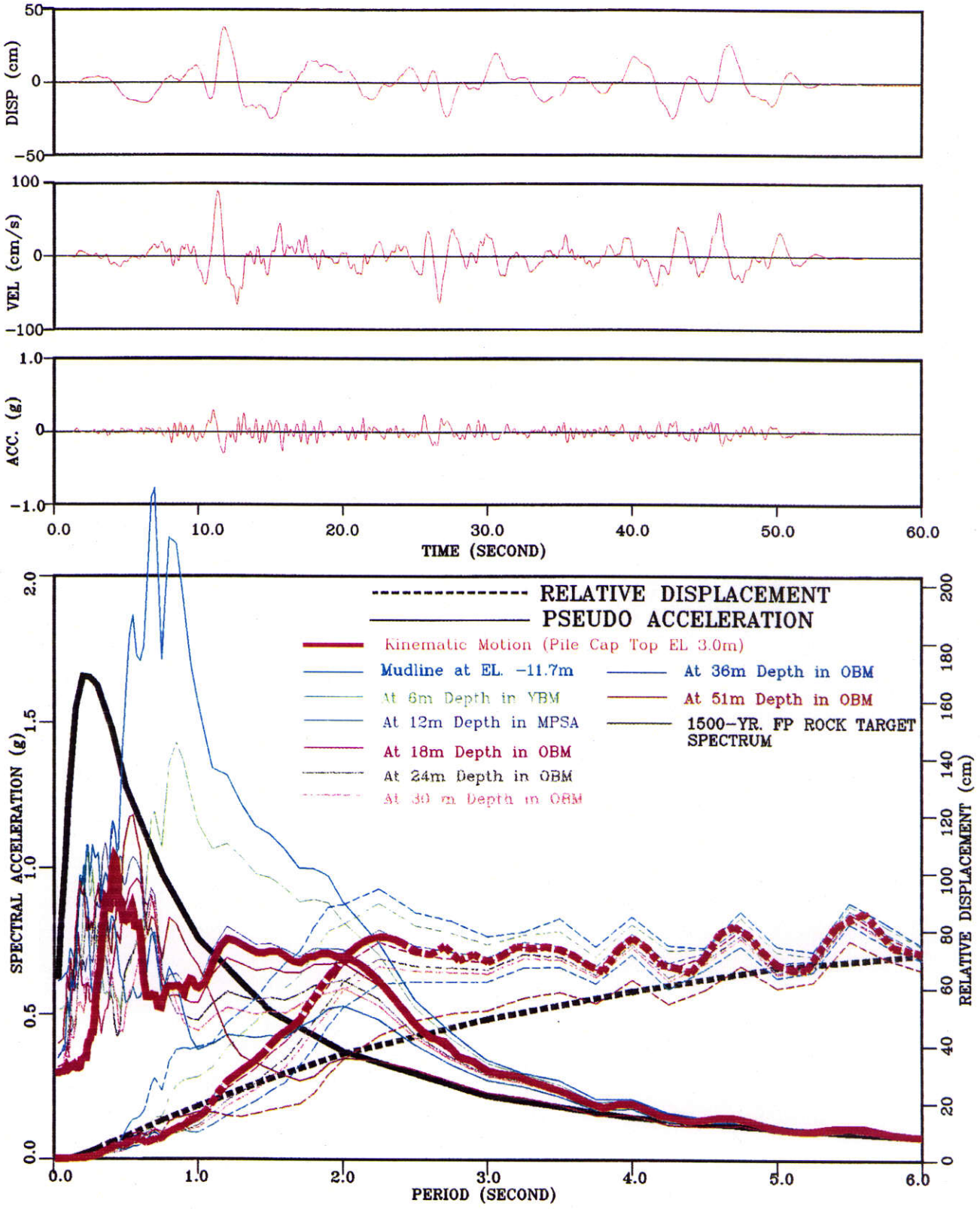

KINEMATIC AND DEPTH-VARYING FREE FIELD MOTIONS
PIER E04, INPUT ROCK MOTION SET 3, FAULT PARALLEL COMPONENT
SFOBB East Span Seismic Safety Project

PLATE 8-35

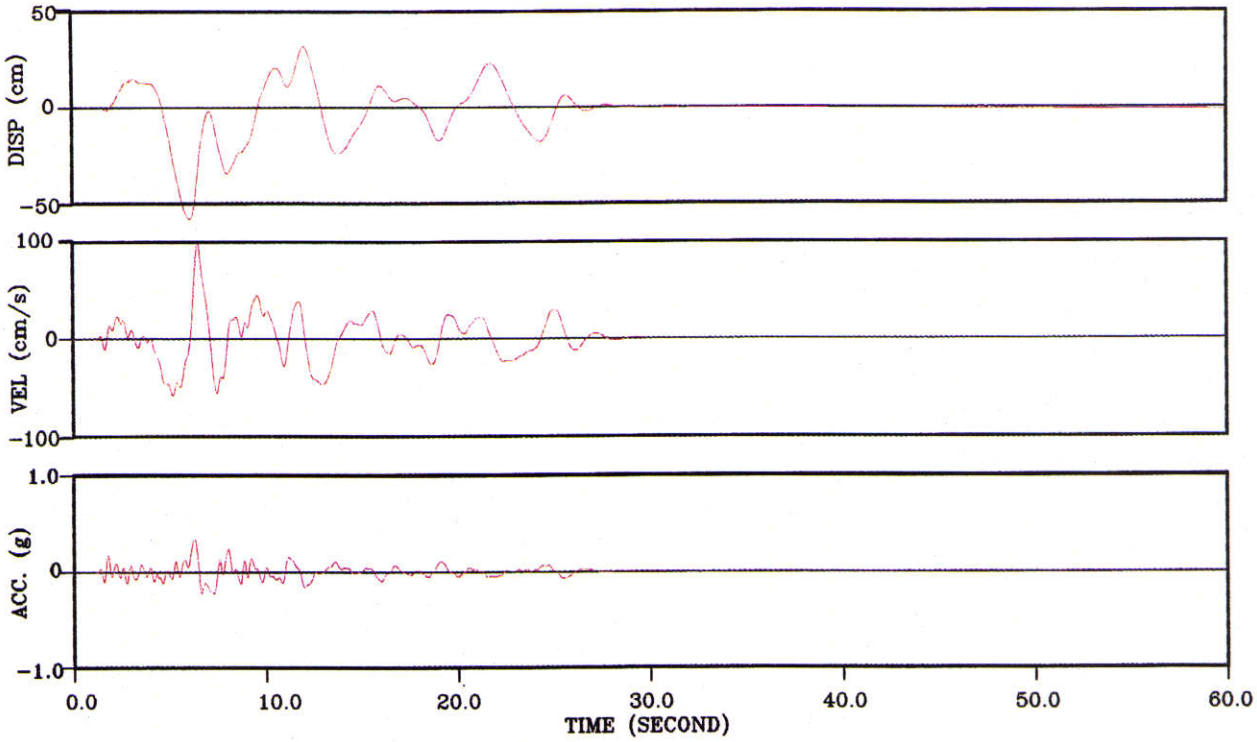

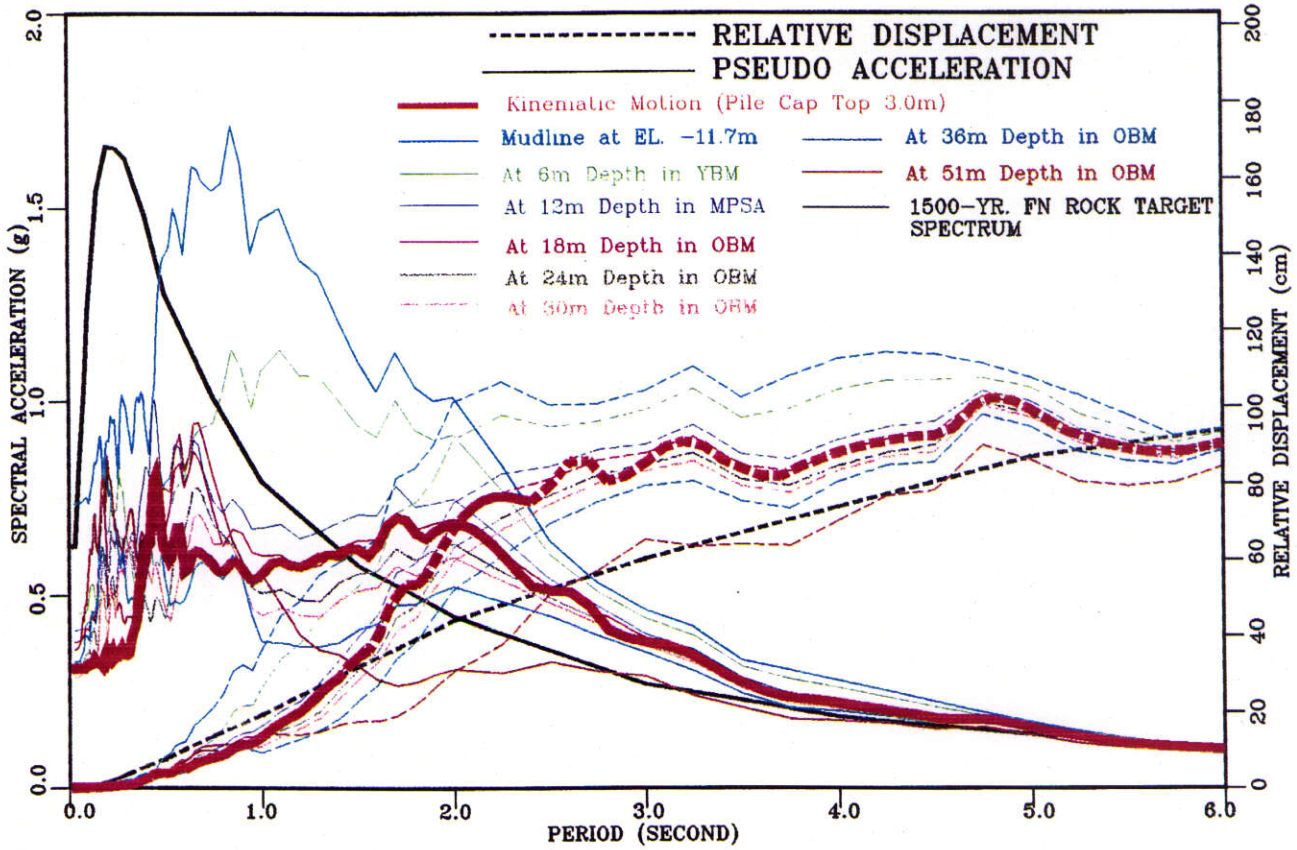

KINEMATIC AND DEPTH-VARYING FREE FIELD MOTIONS
PIER E04, INPUT ROCK MOTION SET 4, FAULT NORMAL COMPONENT
SFOBB East Span Seismic Safety Project

PLATE 8-36

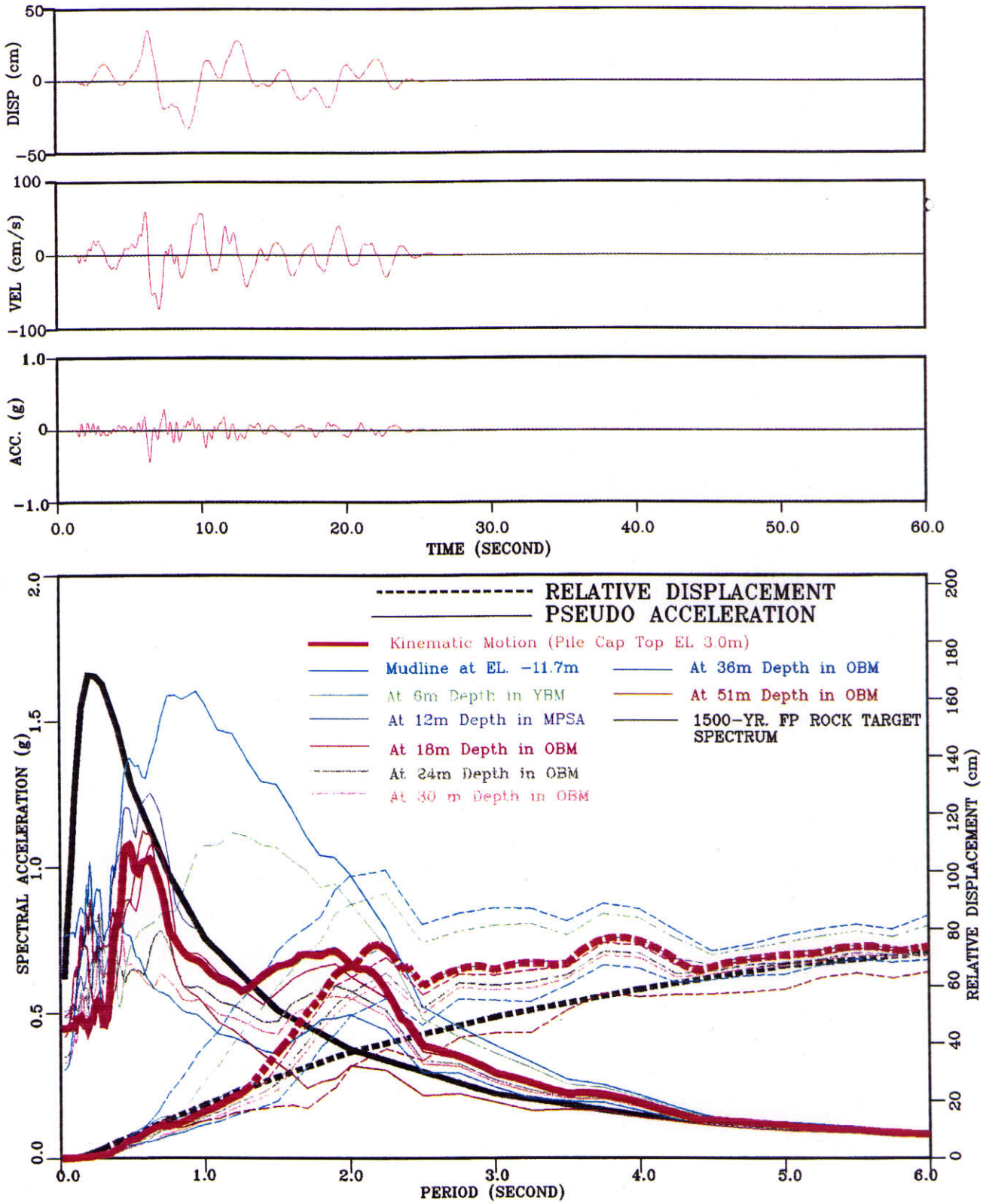

KINEMATIC AND DEPTH-VARYING FREE FIELD MOTIONS
PIER E04, INPUT ROCK MOTION SET 4, FAULT PARALLEL COMPONENT
SFOBB East Span Seismic Safety Project

PLATE 8-37

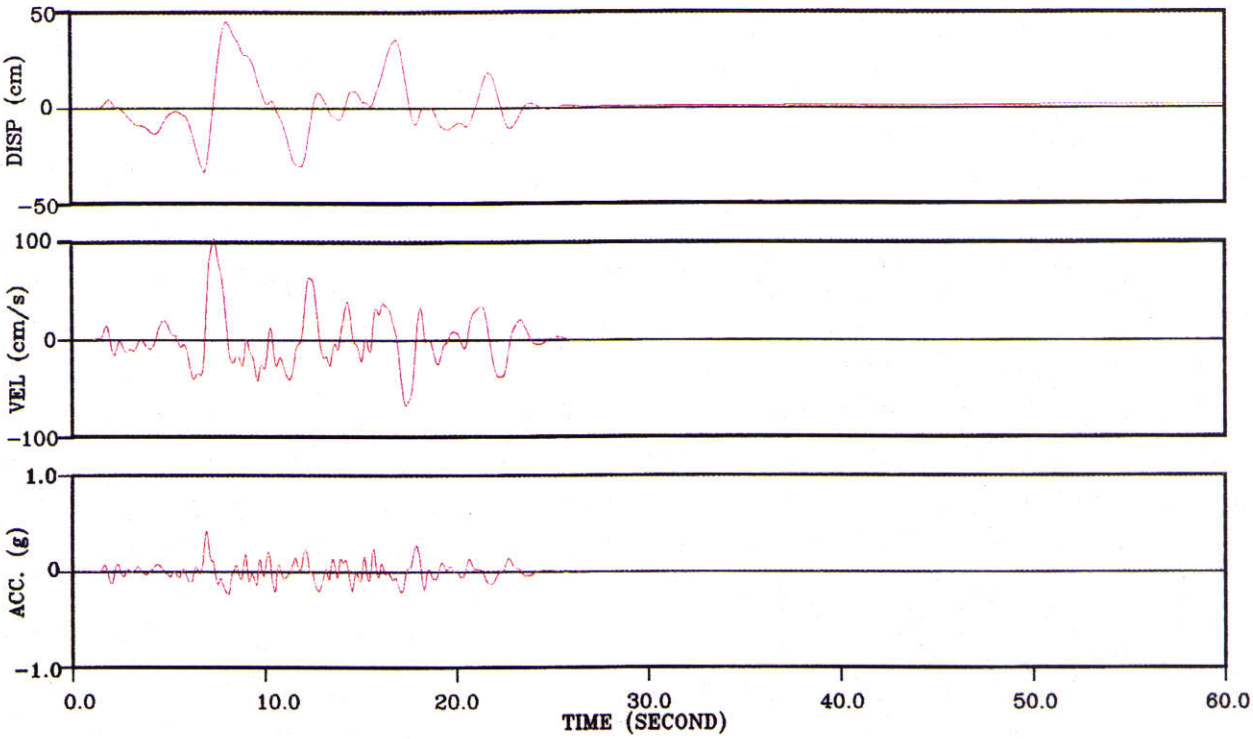

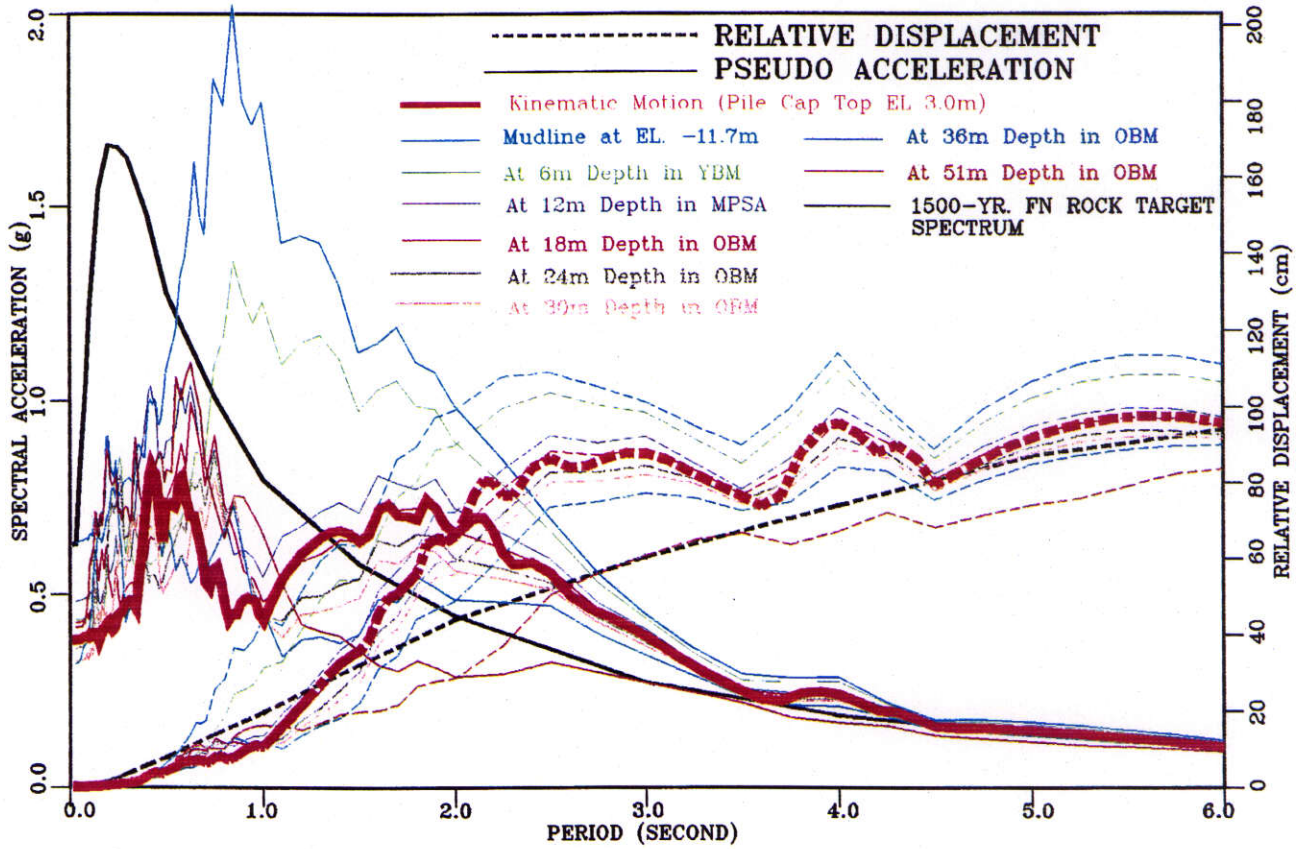

KINEMATIC AND DEPTH-VARYING FREE FIELD MOTIONS
PIER E04, INPUT ROCK MOTION SET 5, FAULT NORMAL COMPONENT
SFOBB East Span Seismic Safety Project

PLATE 8-38

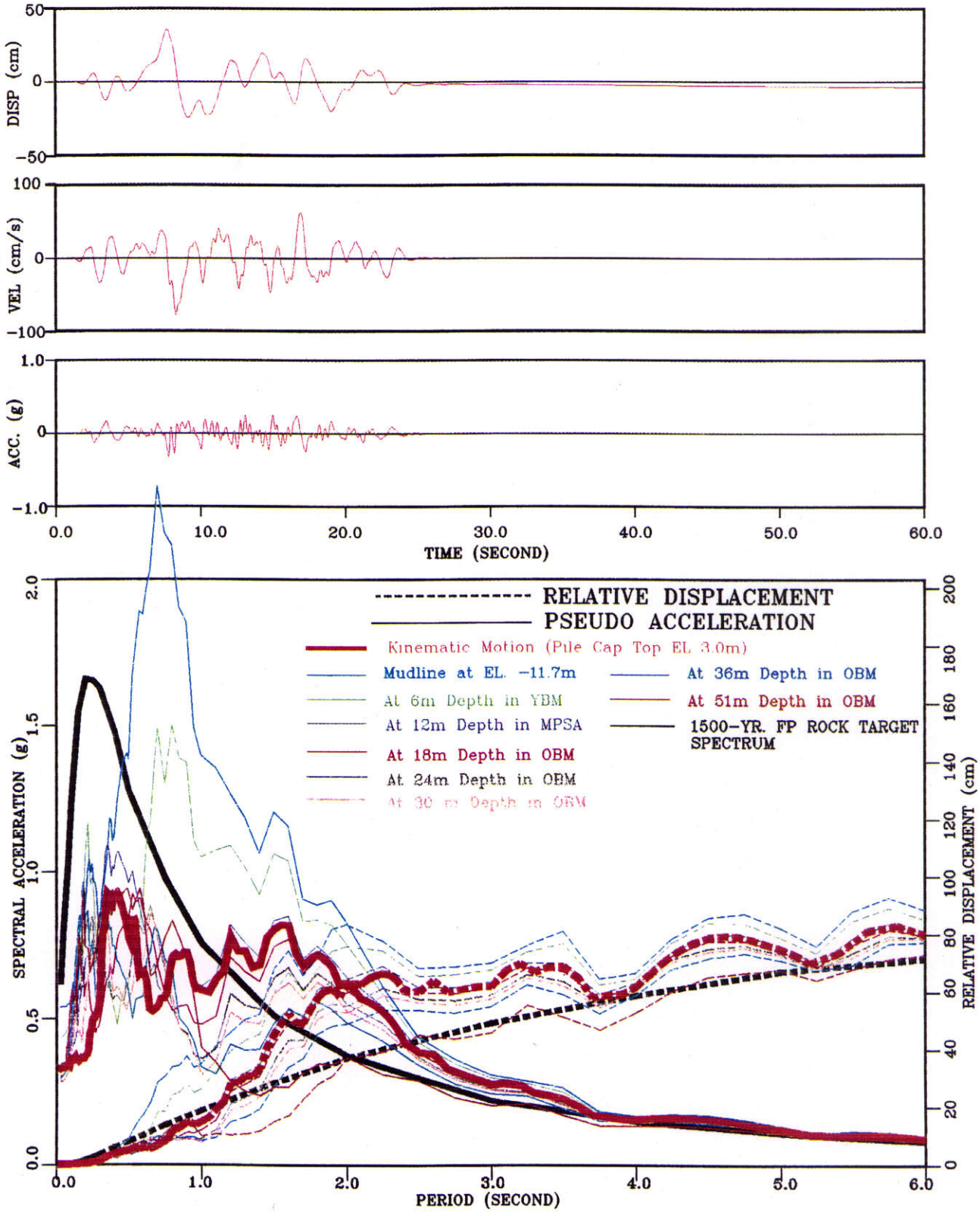

KINEMATIC AND DEPTH-VARYING FREE FIELD MOTIONS
PIER E04, INPUT ROCK MOTION SET 5, FAULT PARALLEL COMPONENT
SFOBB East Span Seismic Safety Project

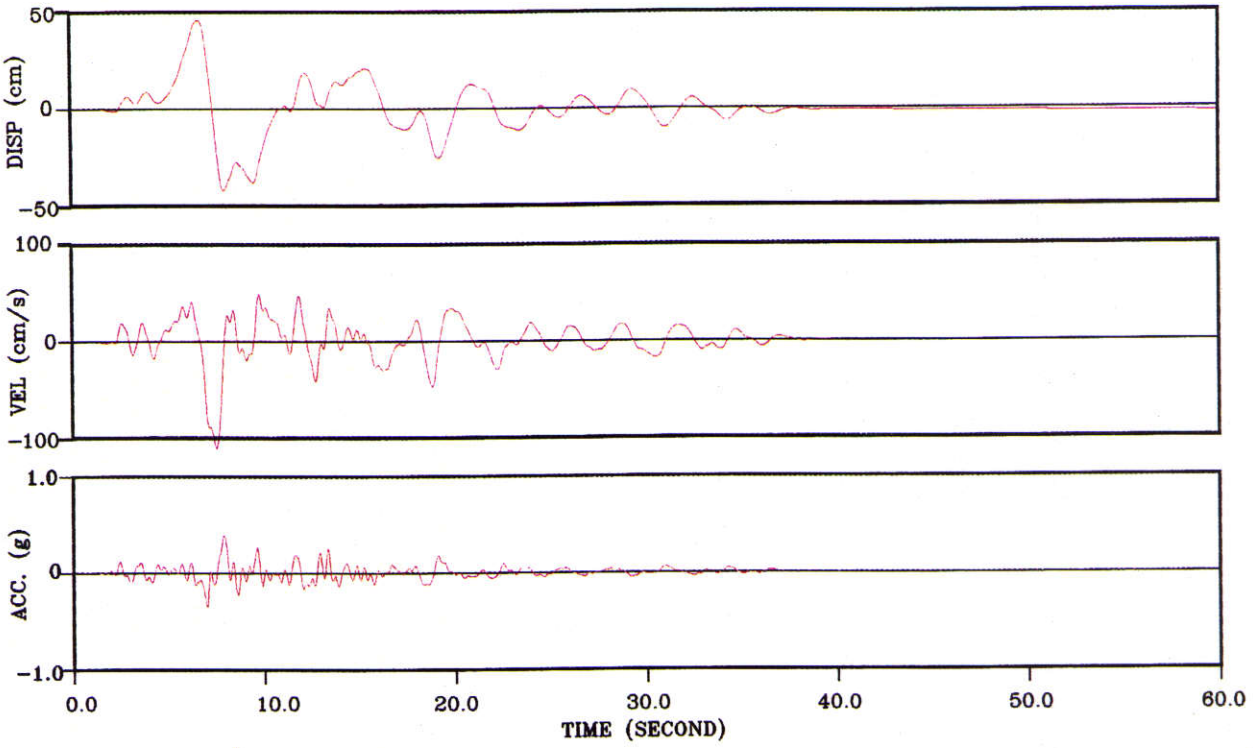

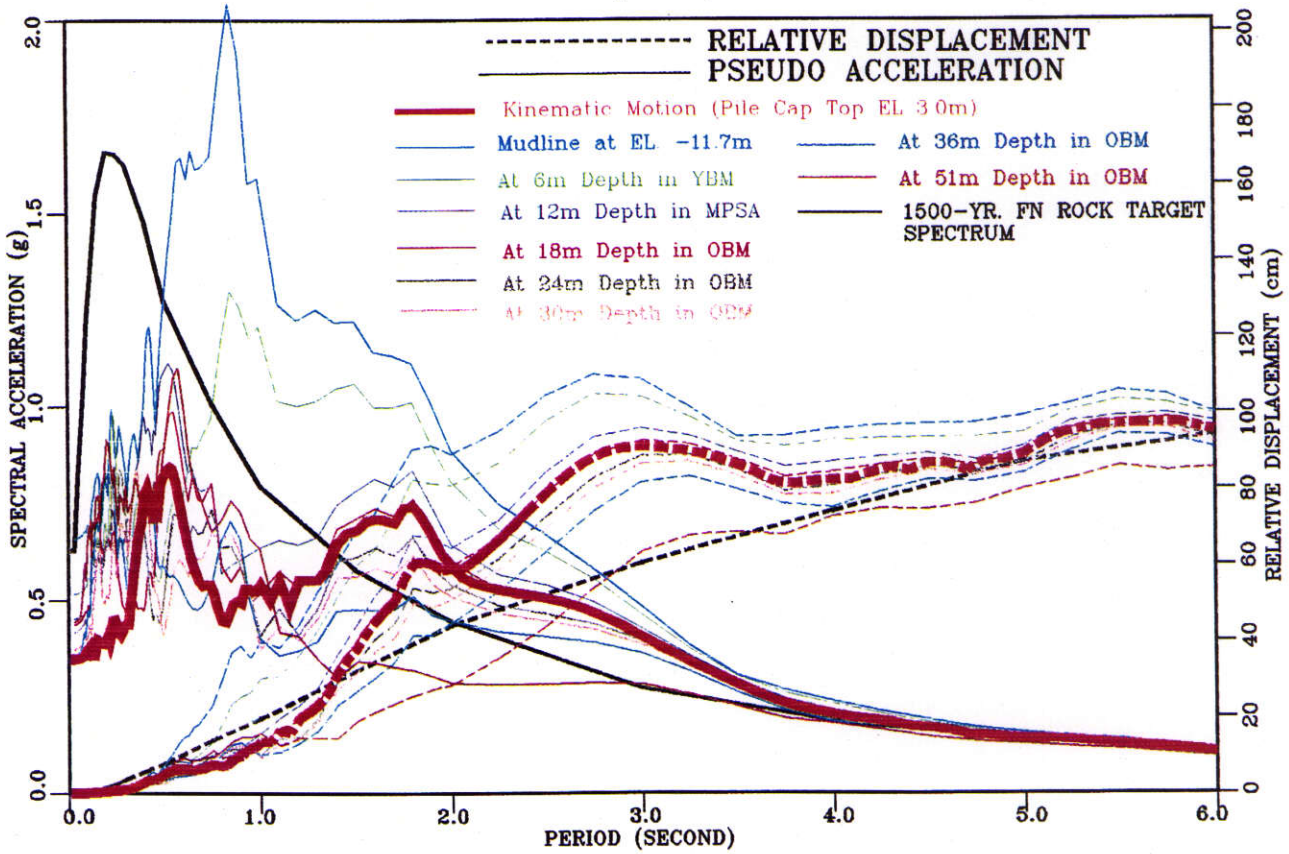

KINEMATIC AND DEPTH-VARYING FREE FIELD MOTIONS
PIER E04, INPUT ROCK MOTION SET 6, FAULT NORMAL COMPONENT
SFOBB East Span Seismic Safety Project

PLATE 8-40

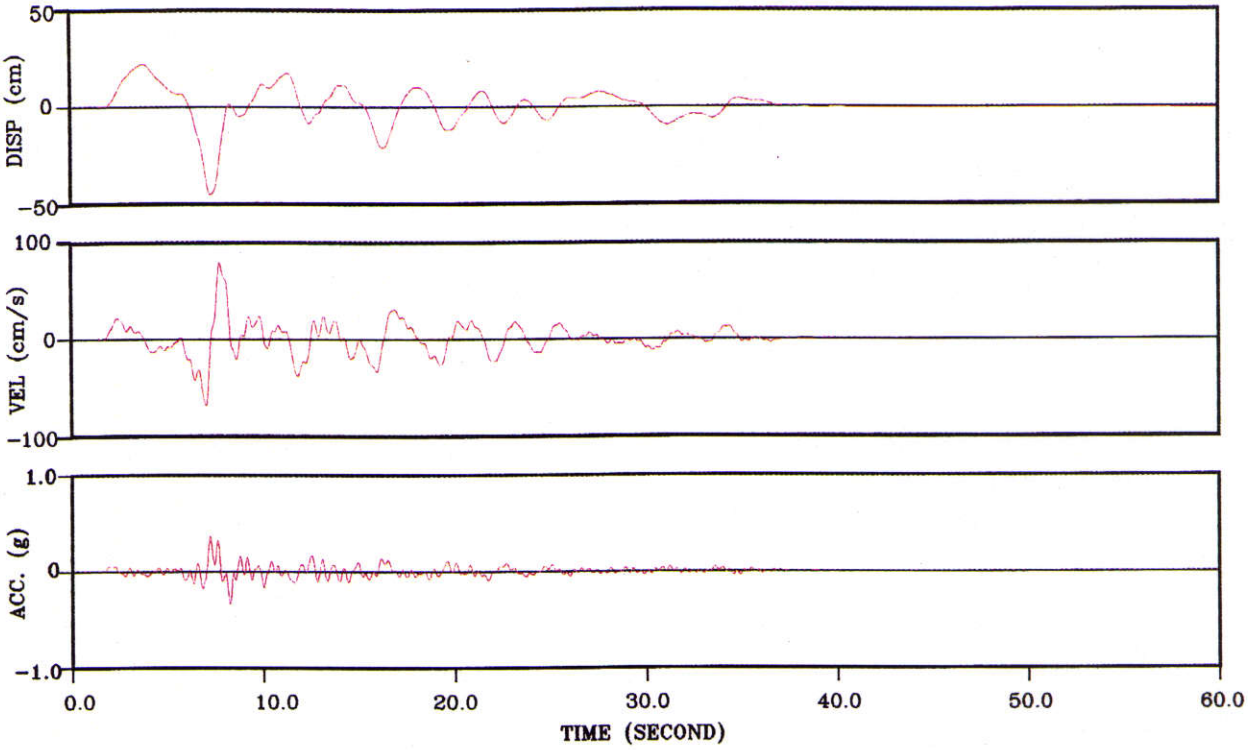

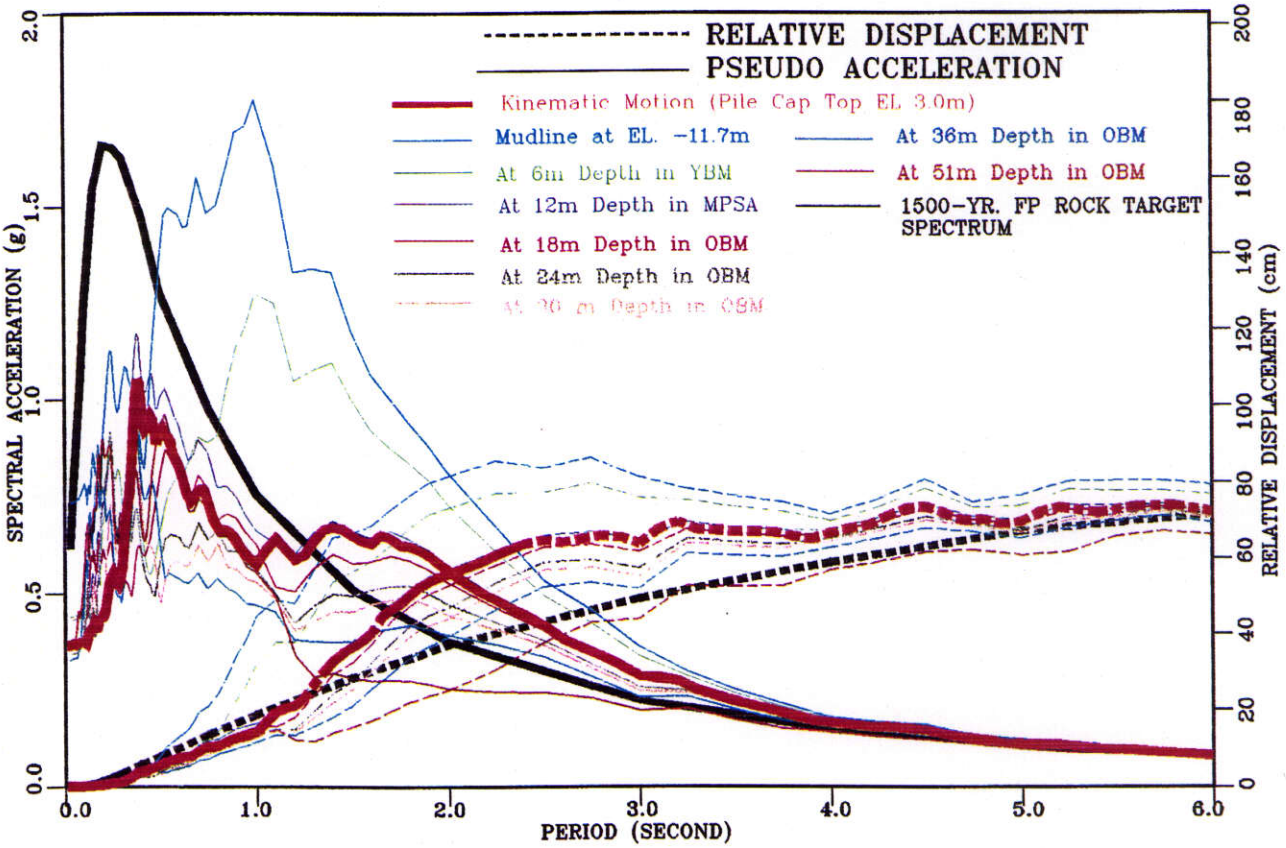

KINEMATIC AND DEPTH-VARYING FREE FIELD MOTIONS
PIER E04, INPUT ROCK MOTION SET 6, FAULT PARALLEL COMPONENT
SFOBB East Span Seismic Safety Project

PLATE 8-41

Earth Mechanics FUGRO

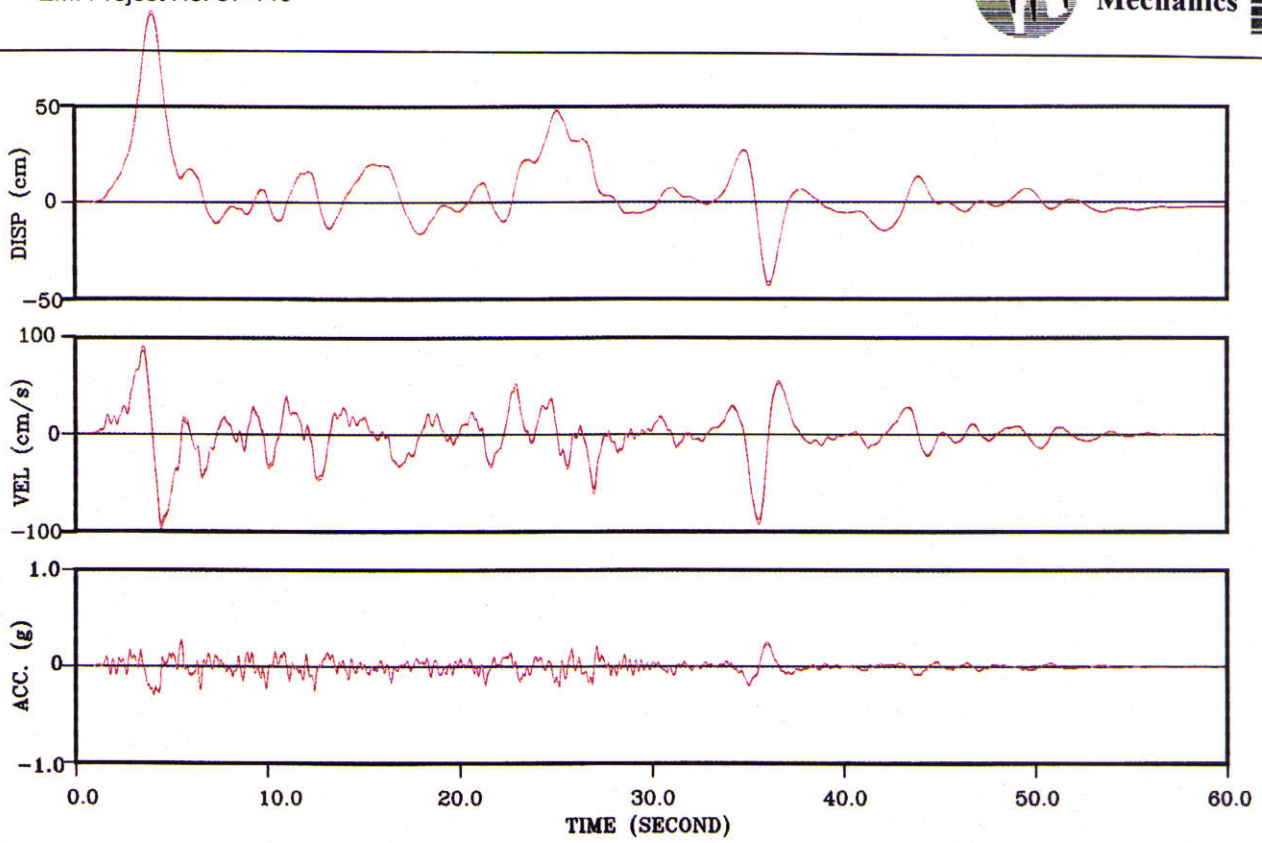

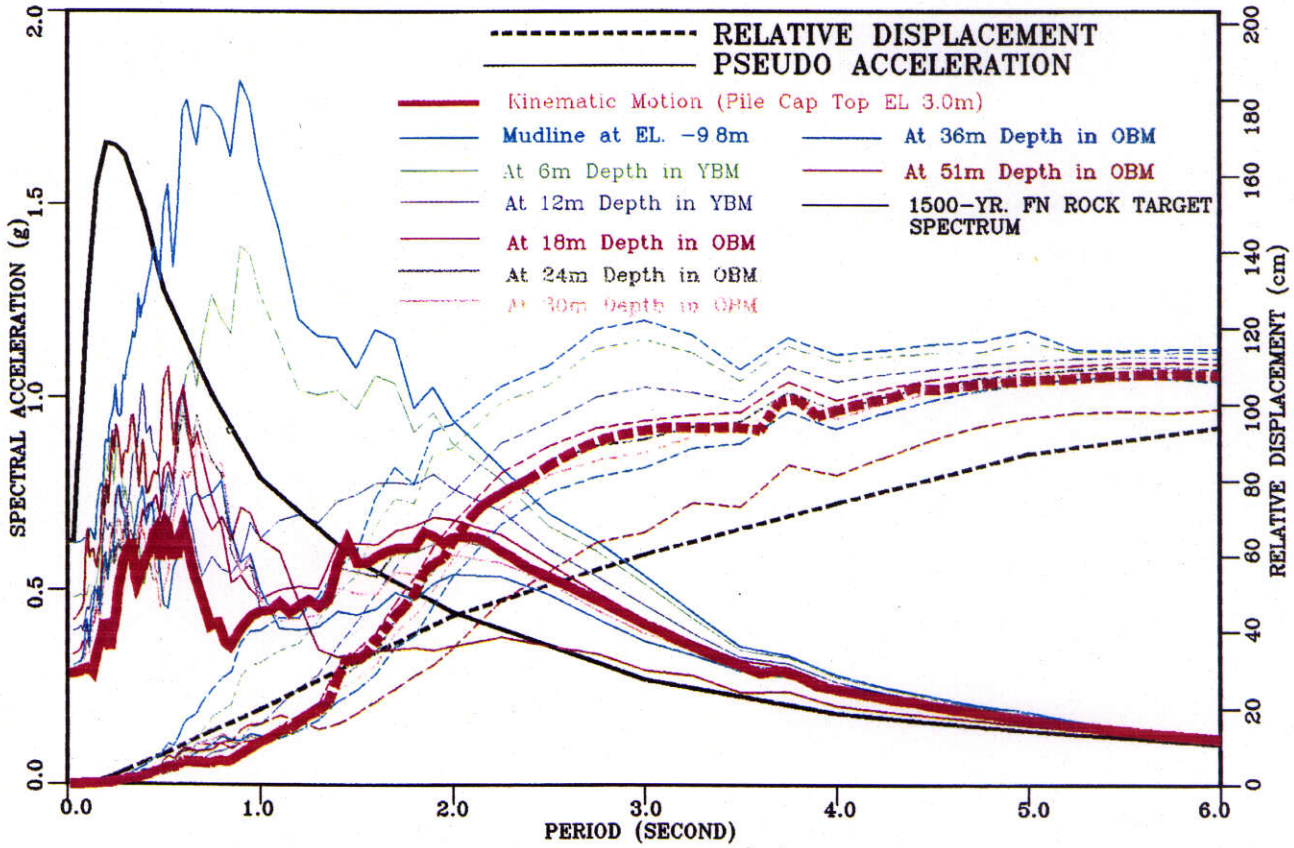

KINEMATIC AND DEPTH-VARYING FREE FIELD MOTIONS
PIER E05, INPUT ROCK MOTION SET 1, FAULT NORMAL COMPONENT
SFOBB East Span Seismic Safety Project

PLATE 8-42

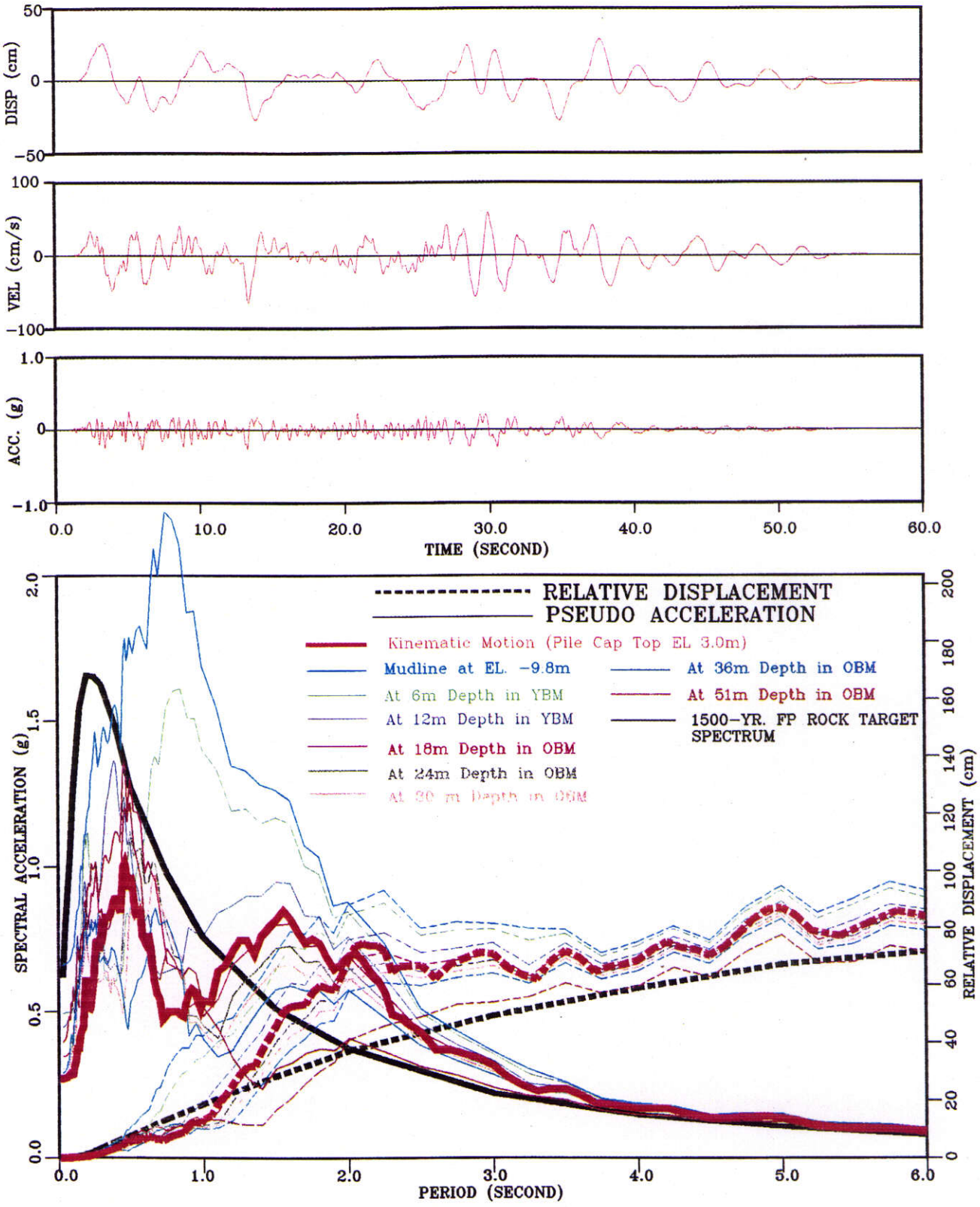

KINEMATIC AND DEPTH-VARYING FREE FIELD MOTIONS
PIER E05, INPUT ROCK MOTION SET 1, FAULT PARALLEL COMPONENT
SFOBB East Span Seismic Safety Project

PLATE 8-43

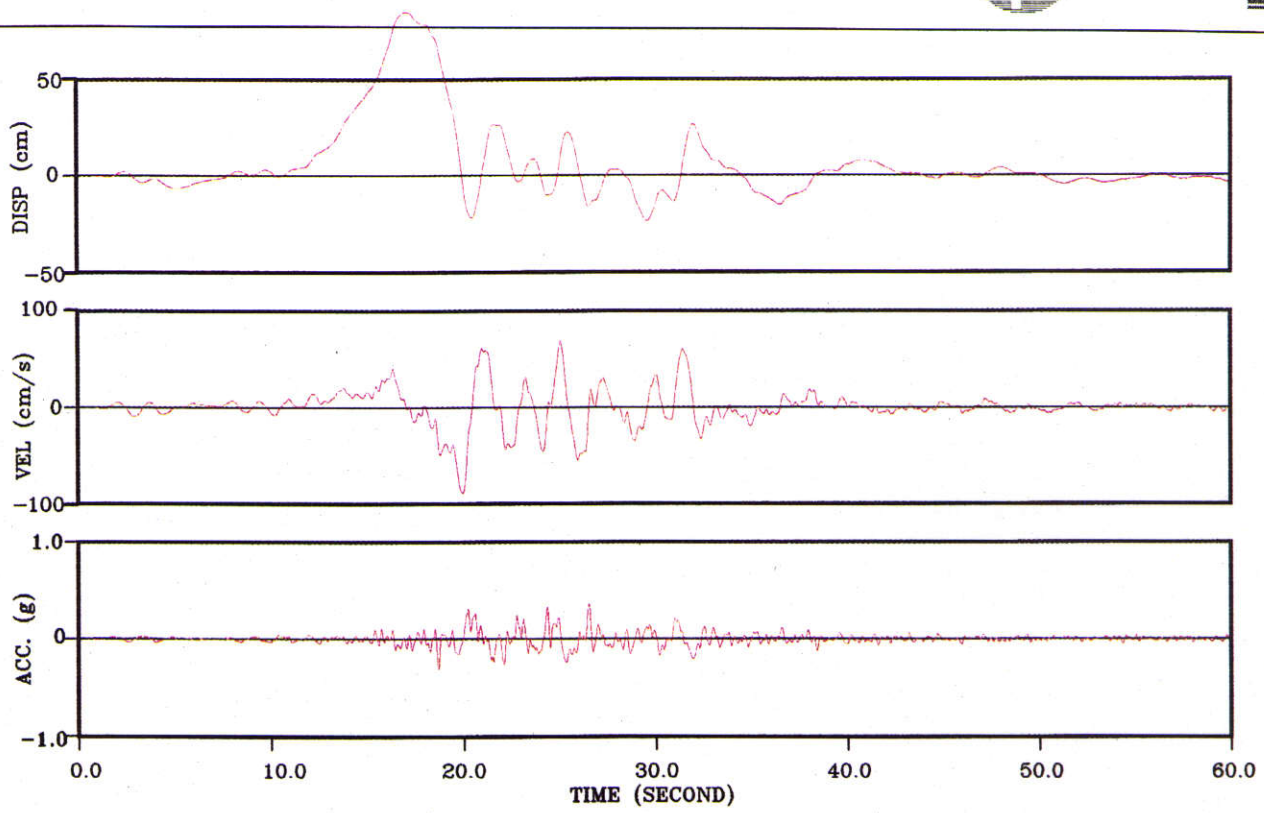

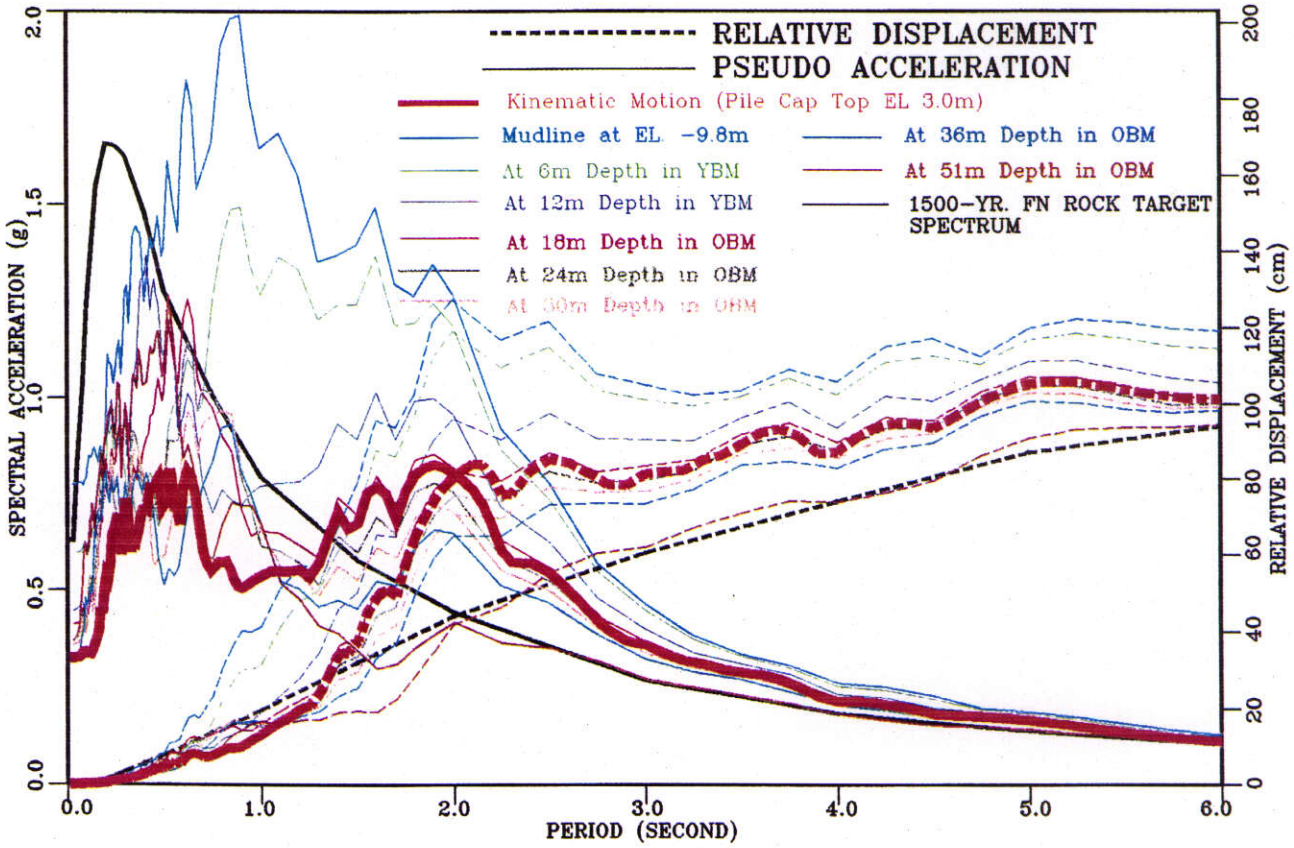

KINEMATIC AND DEPTH-VARYING FREE FIELD MOTIONS
PIER E05, INPUT ROCK MOTION SET 2, FAULT NORMAL COMPONENT
SFOBB East Span Seismic Safety Project

PLATE 8-44

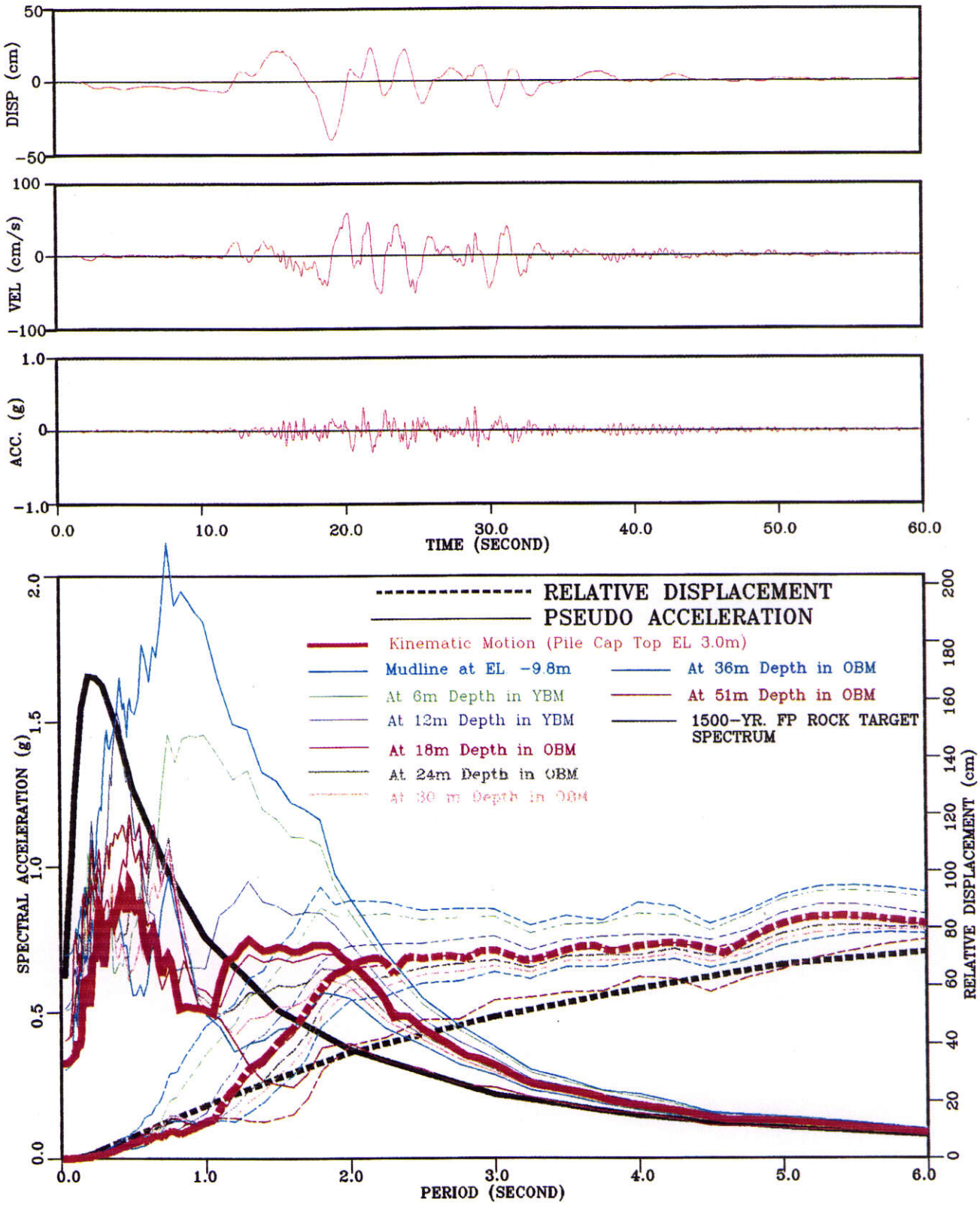

KINEMATIC AND DEPTH-VARYING FREE FIELD MOTIONS
PIER E05, INPUT ROCK MOTION SET 2, FAULT PARALLEL COMPONENT
SFOBB East Span Seismic Safety Project

PLATE 8-45

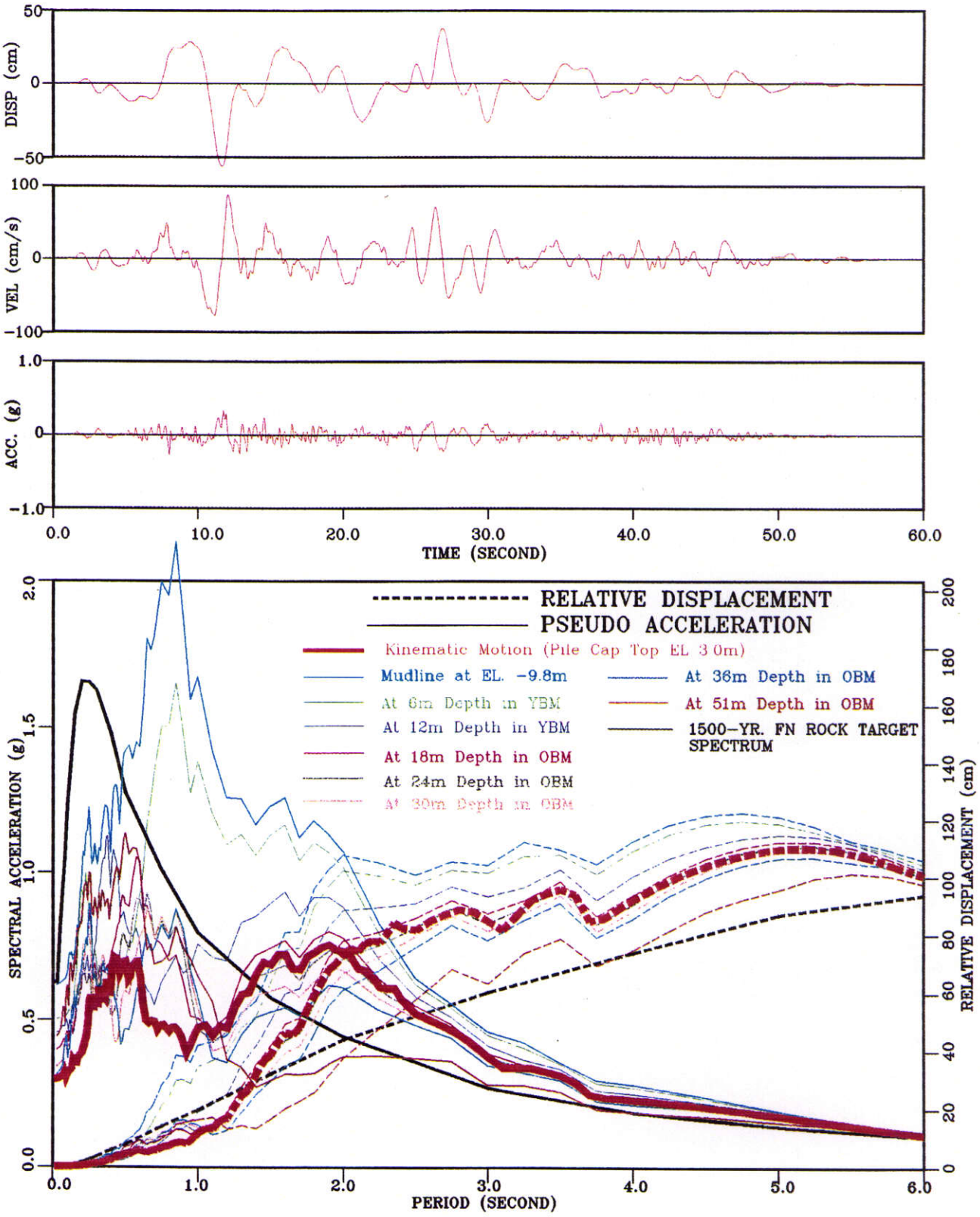

KINEMATIC AND DEPTH-VARYING FREE FIELD MOTIONS
PIER E05, INPUT ROCK MOTION SET 3, FAULT NORMAL COMPONENT
SFOBB East Span Seismic Safety Project

PLATE 8-46

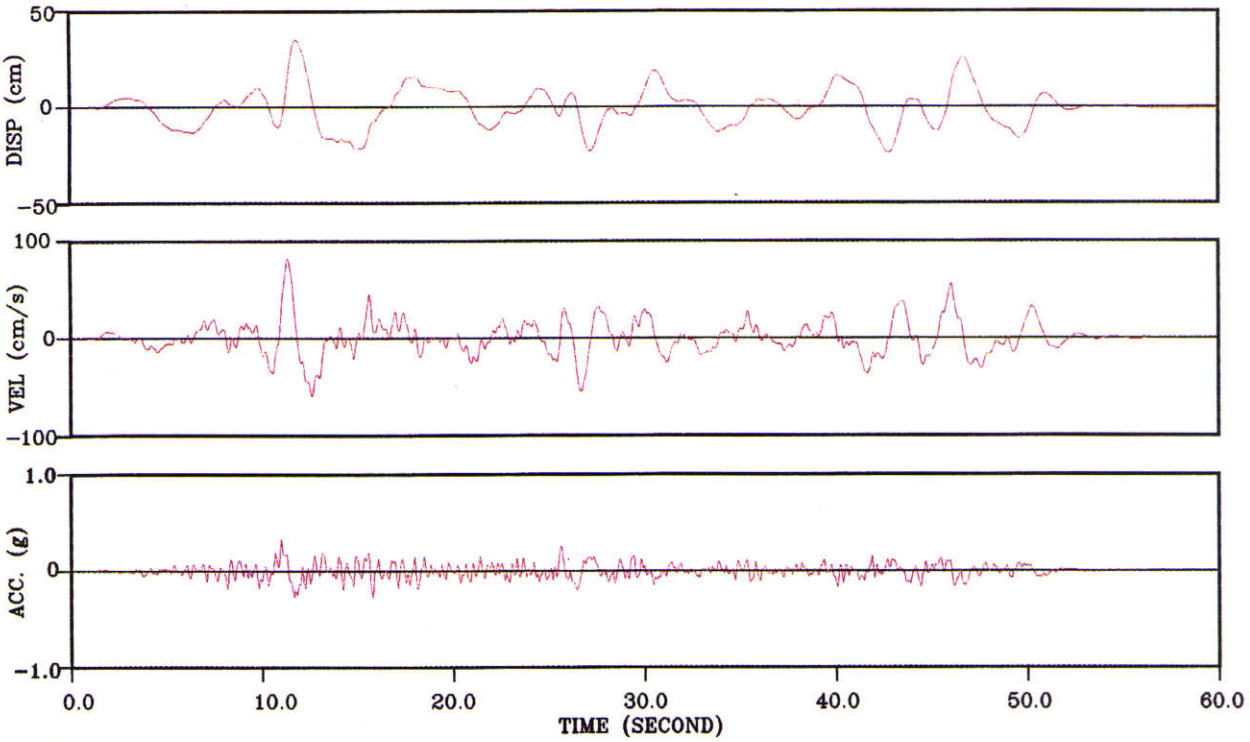

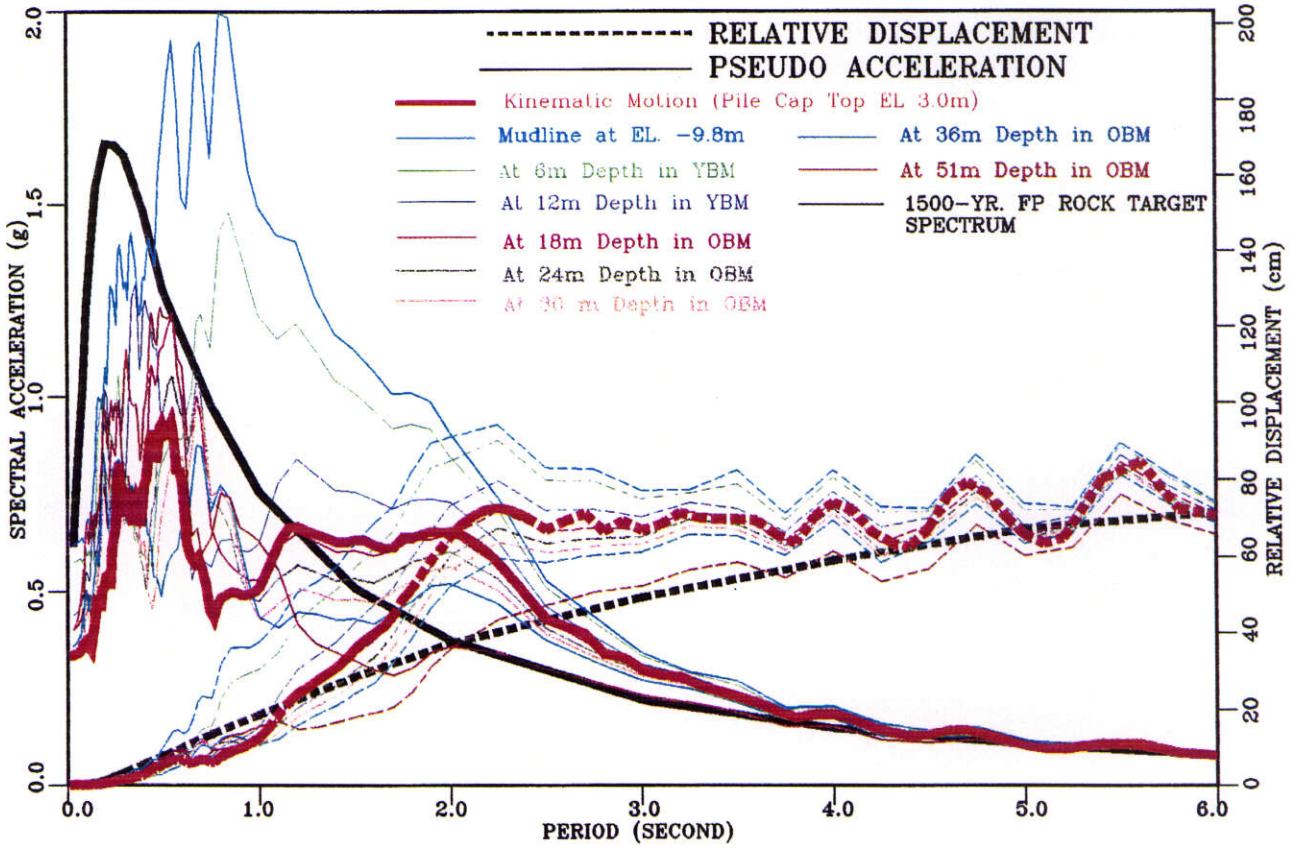

KINEMATIC AND DEPTH-VARYING FREE FIELD MOTIONS
PIER E05, INPUT ROCK MOTION SET 3, FAULT PARALLEL COMPONENT
SFOBB East Span Seismic Safety Project

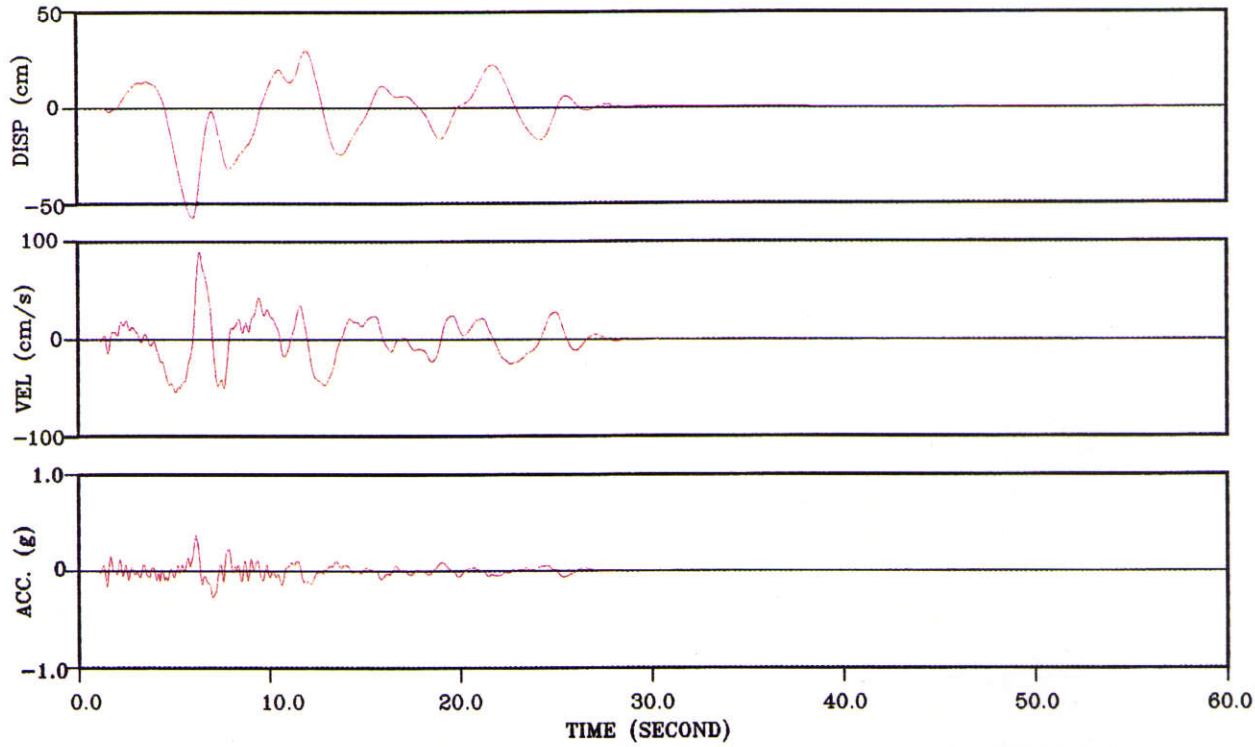

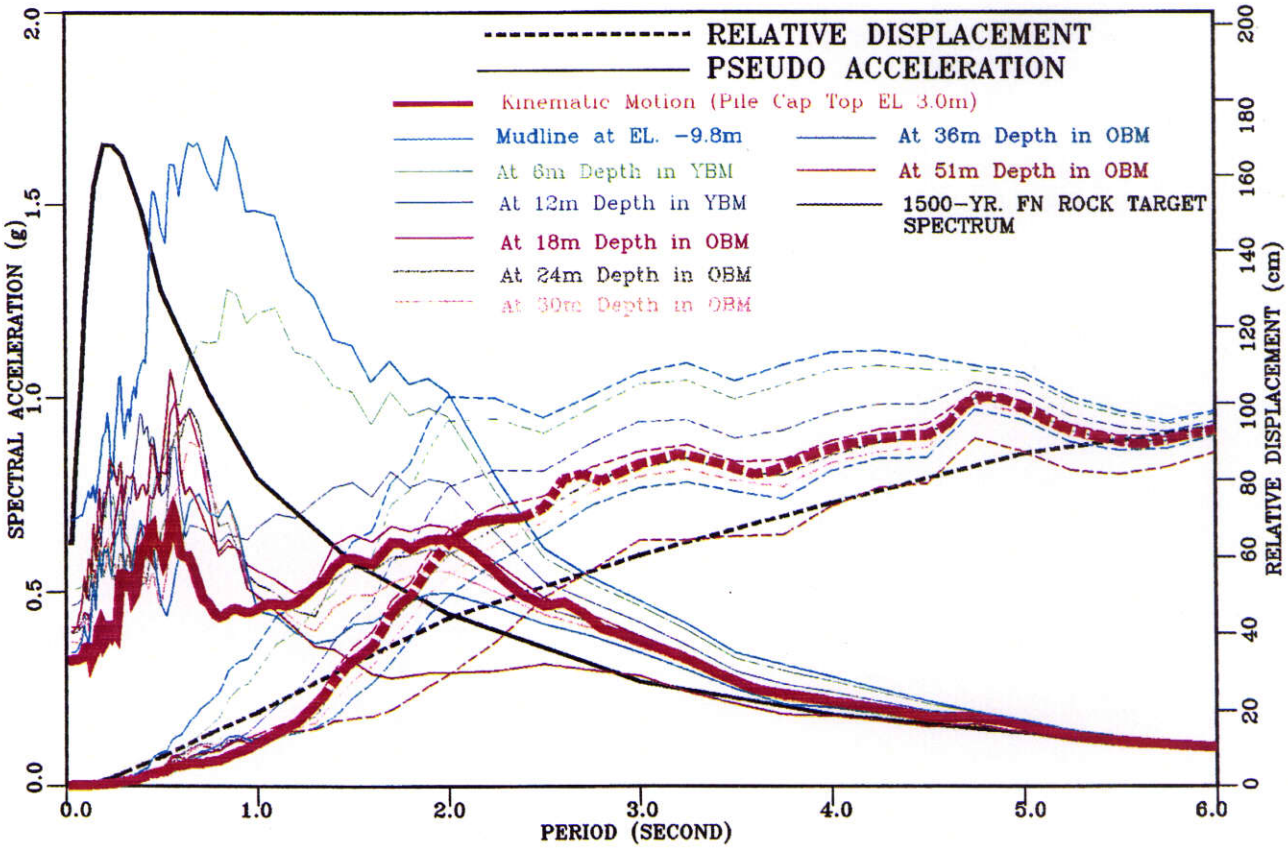

KINEMATIC AND DEPTH-VARYING FREE FIELD MOTIONS
PIER E05, INPUT ROCK MOTION SET 4, FAULT NORMAL COMPONENT
SFOBB East Span Seismic Safety Project

PLATE 8-48

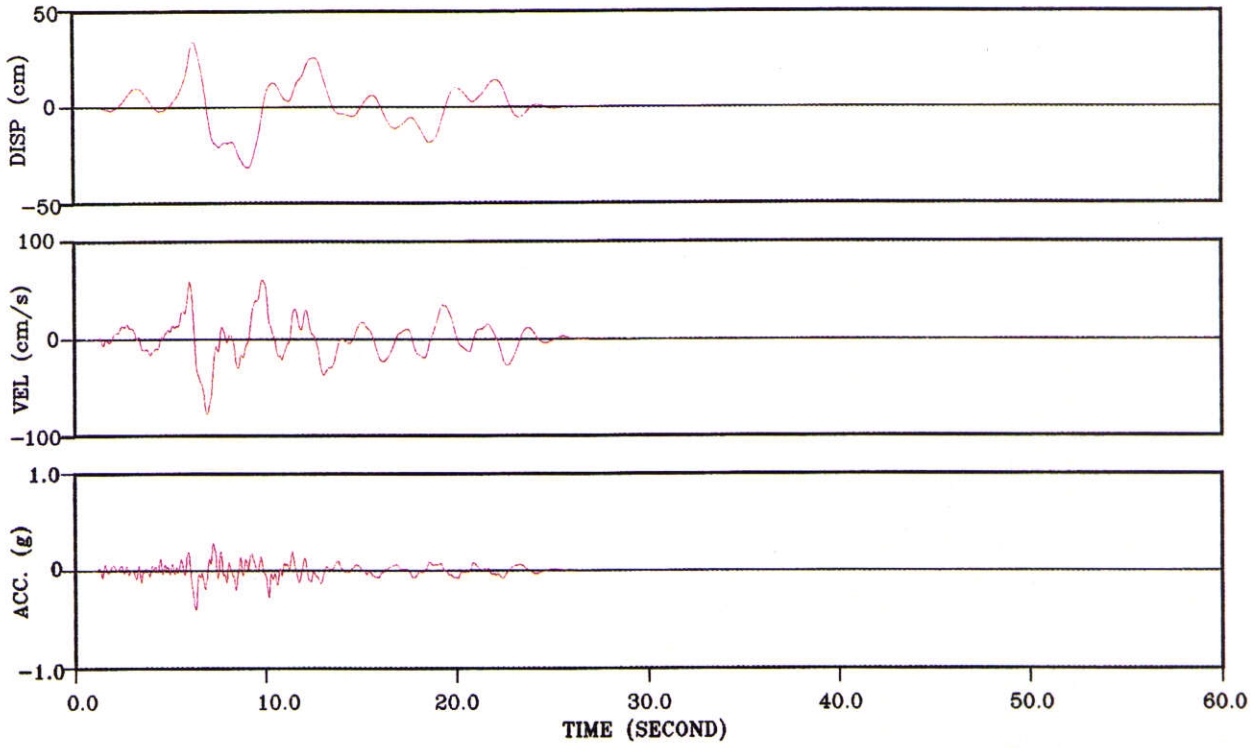

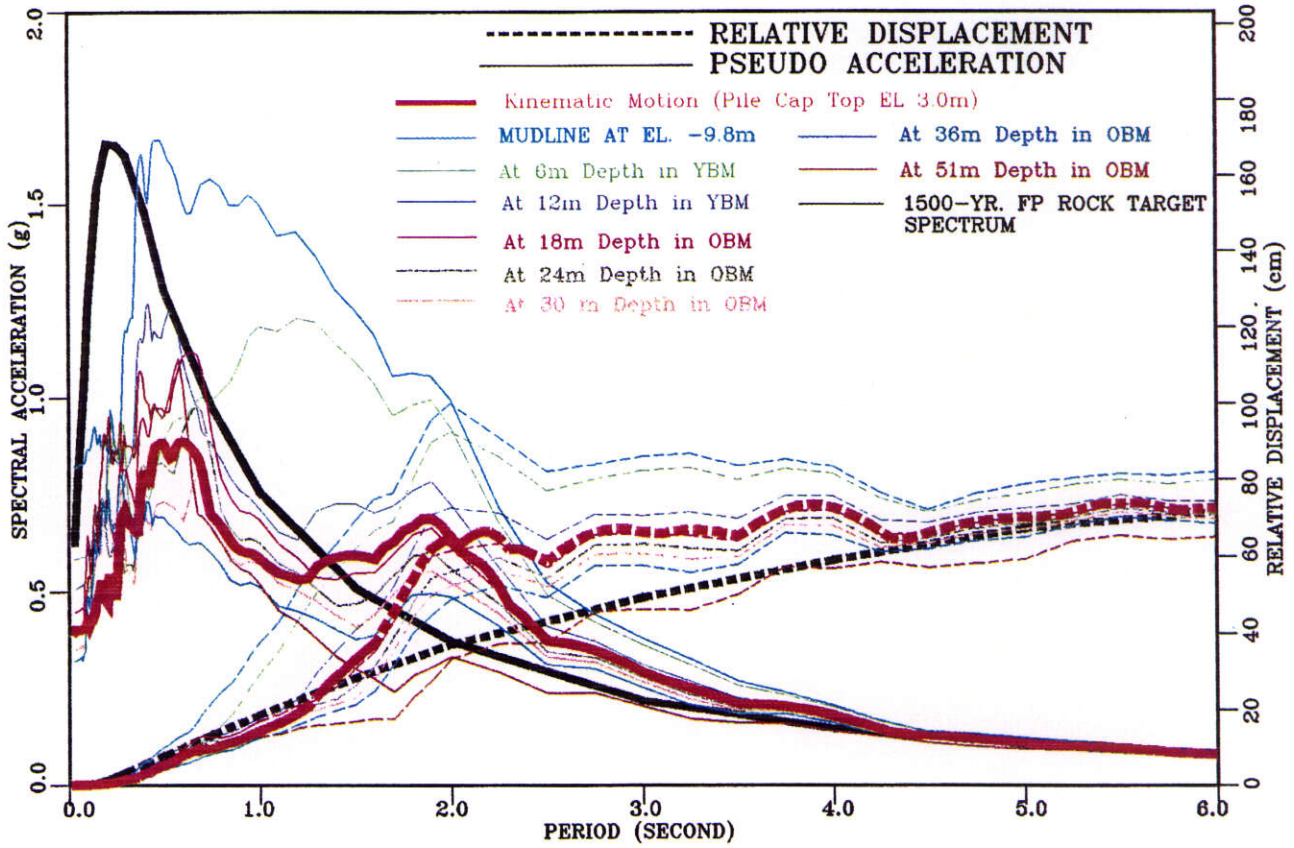

KINEMATIC AND DEPTH-VARYING FREE FIELD MOTIONS
PIER E05, INPUT ROCK MOTION SET 4, FAULT PARALLEL COMPONENT
SFOBB East Span Seismic Safety Project

PLATE 8-49

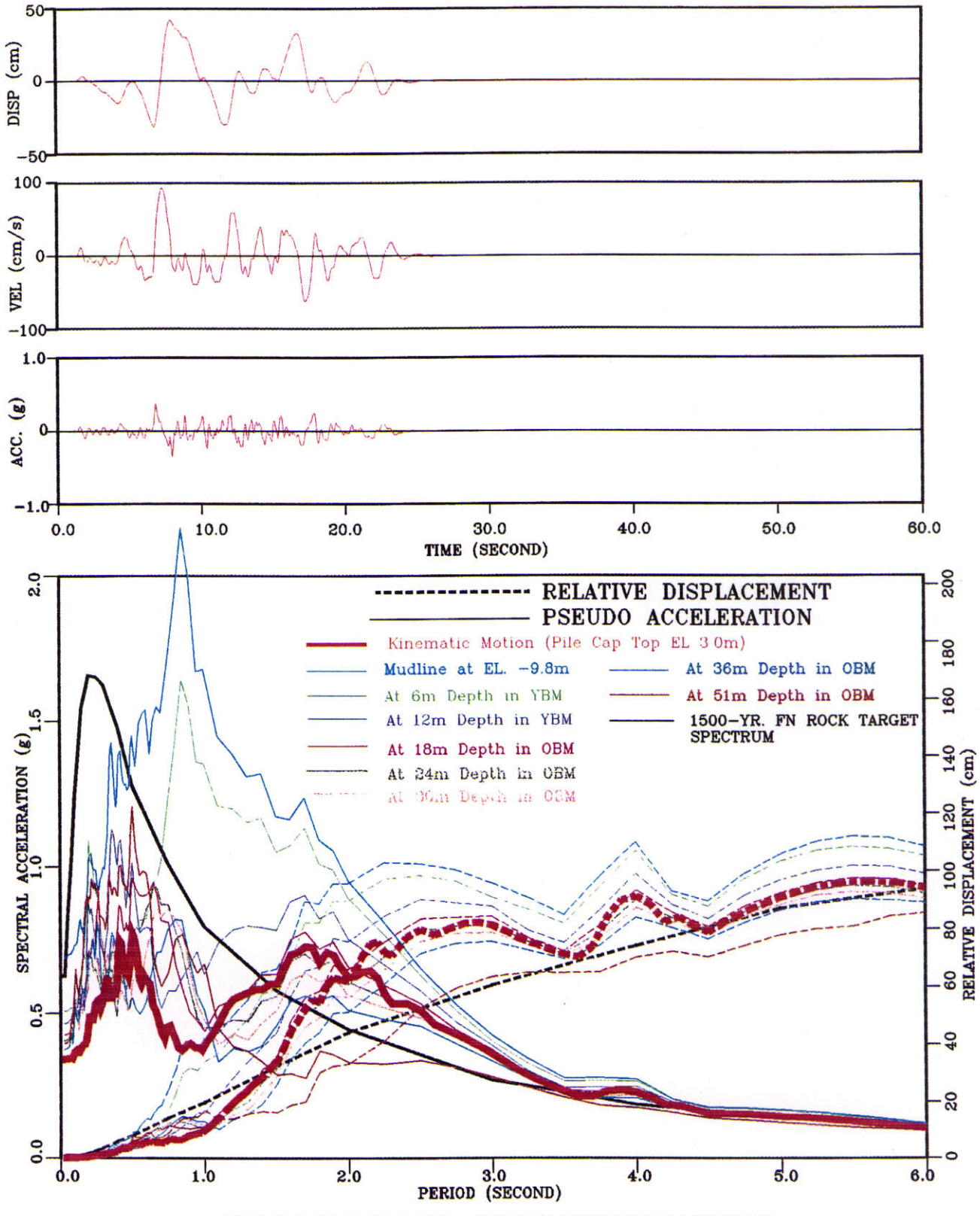

KINEMATIC AND DEPTH-VARYING FREE FIELD MOTIONS
PIER E05, INPUT ROCK MOTION SET 5, FAULT NORMAL COMPONENT
SFOBB East Span Seismic Safety Project

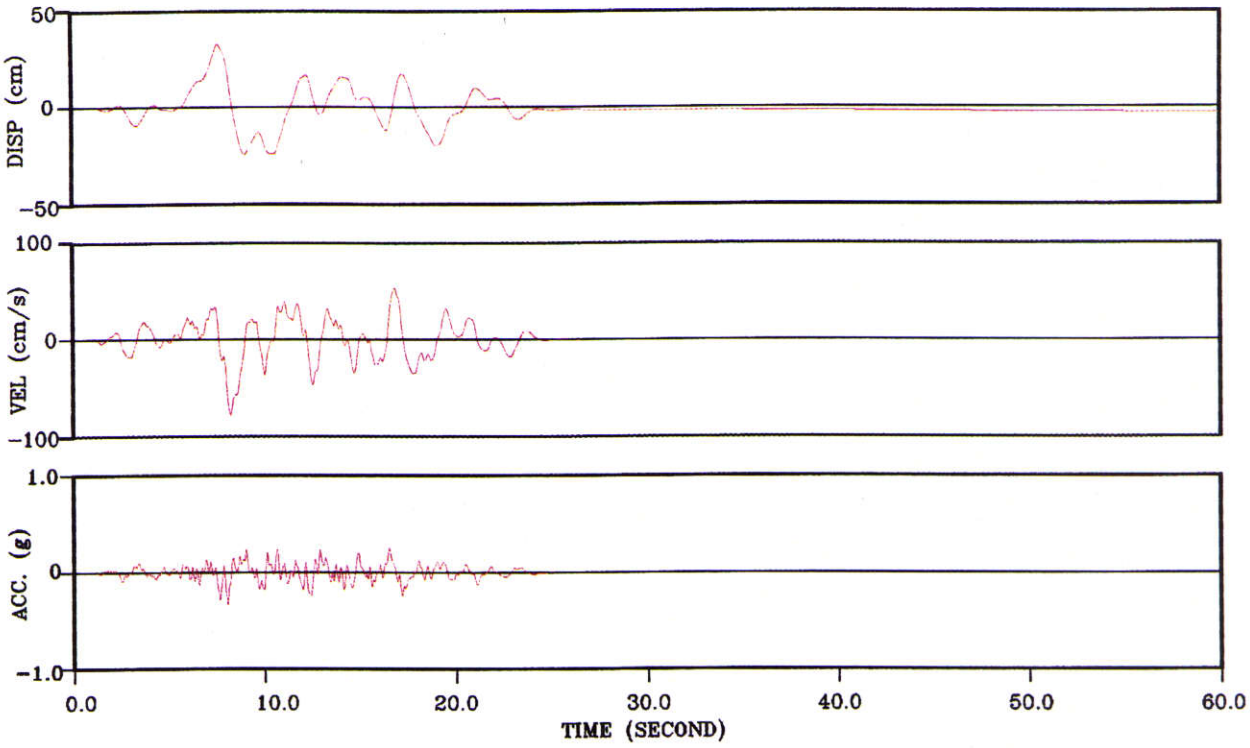

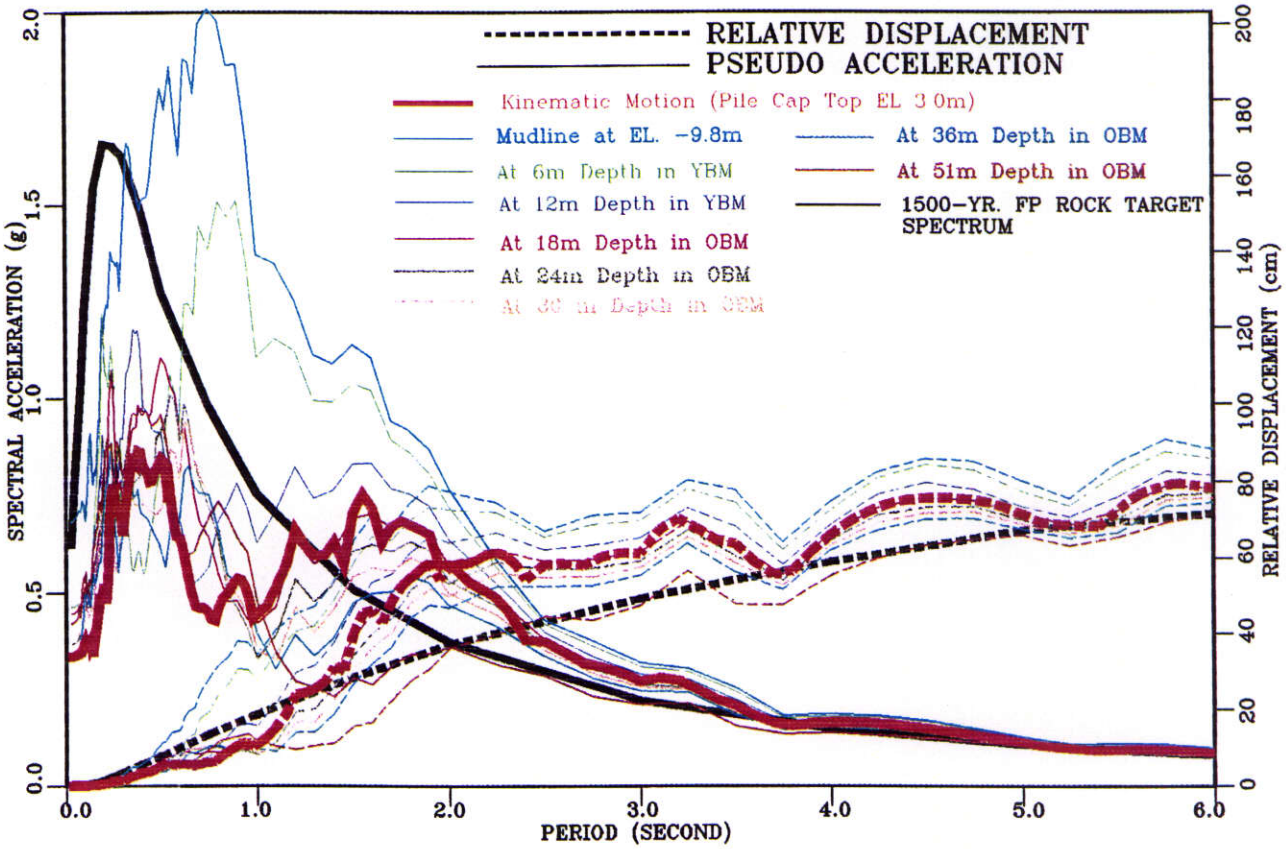

KINEMATIC AND DEPTH-VARYING FREE FIELD MOTIONS
PIER E05, INPUT ROCK MOTION SET 5, FAULT PARALLEL COMPONENT
SFOBB East Span Seismic Safety Project

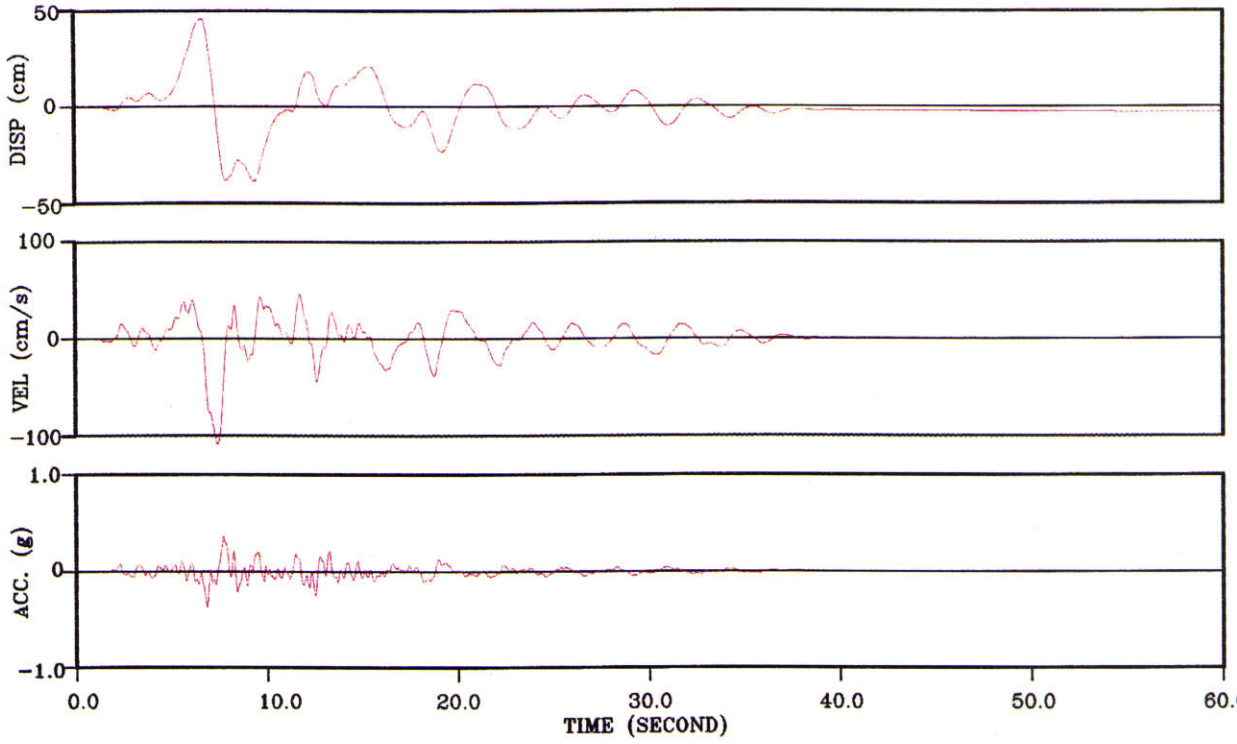

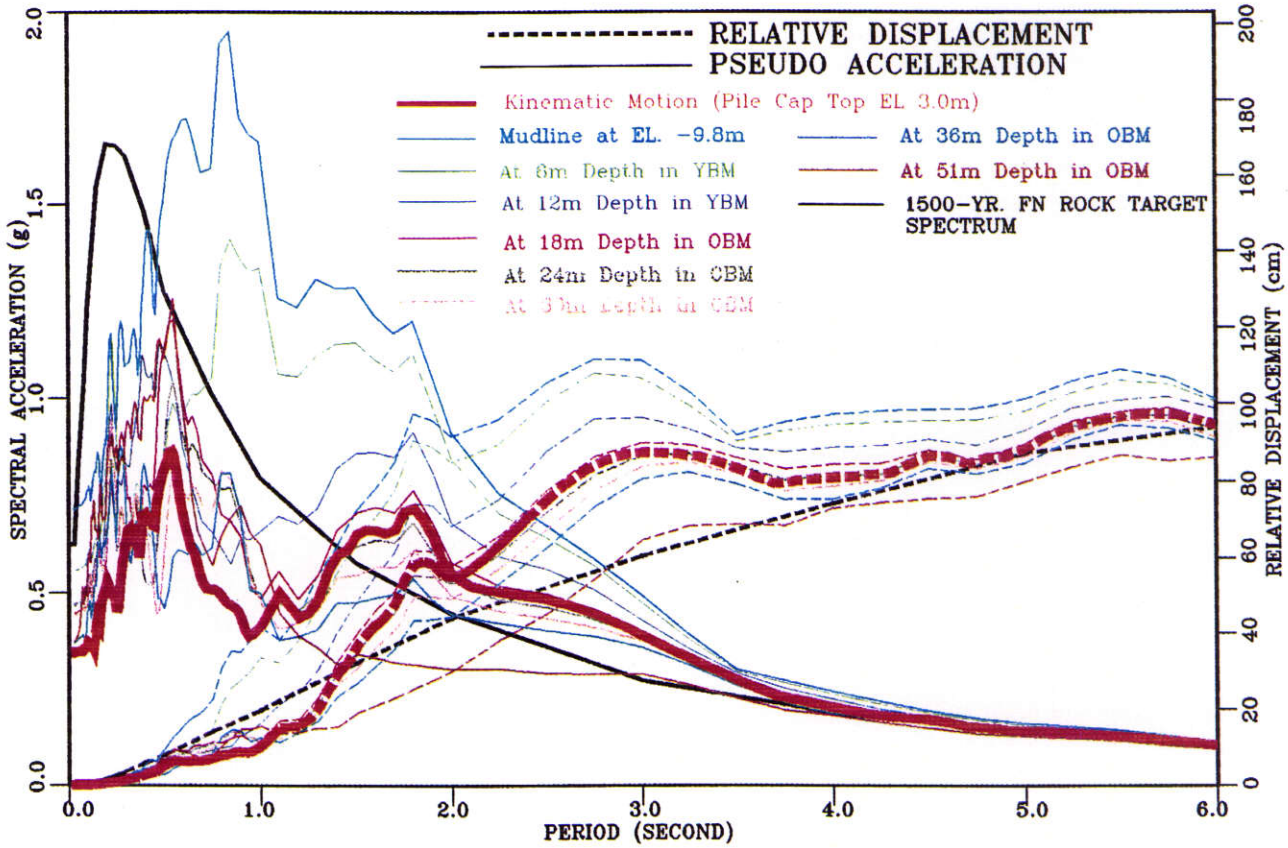

KINEMATIC AND DEPTH-VARYING FREE FIELD MOTIONS
PIER E05, INPUT ROCK MOTION SET 6, FAULT NORMAL COMPONENT
SFOBB East Span Seismic Safety Project

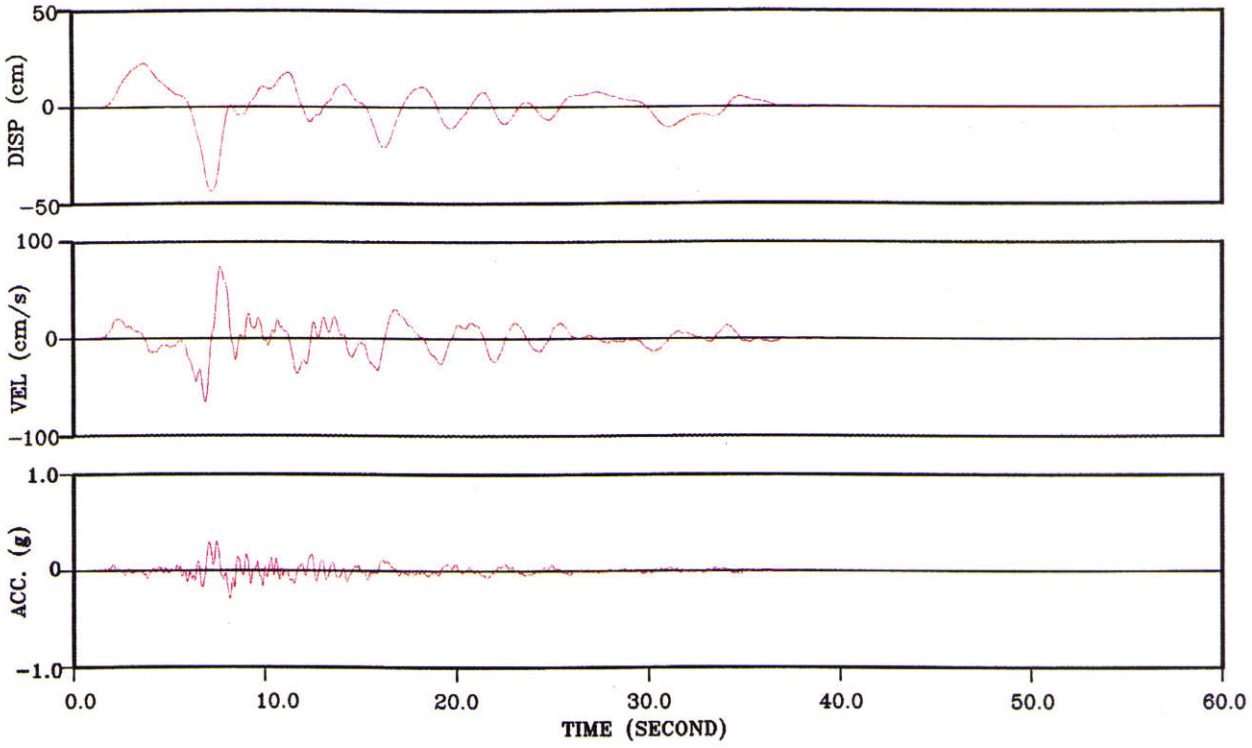

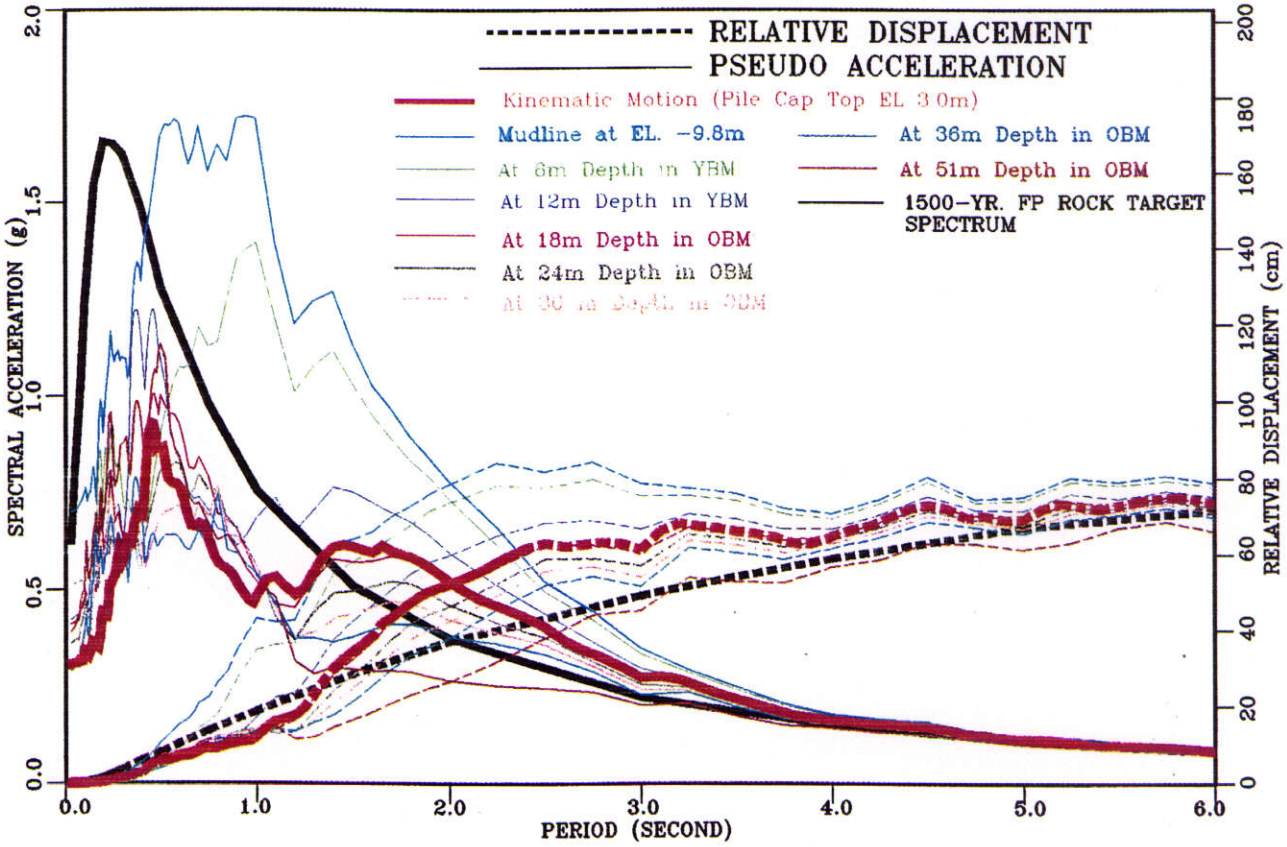

KINEMATIC AND DEPTH-VARYING FREE FIELD MOTIONS
PIER E05, INPUT ROCK MOTION SET 6, FAULT PARALLEL COMPONENT
SFOBB East Span Seismic Safety Project

PLATE 8-53

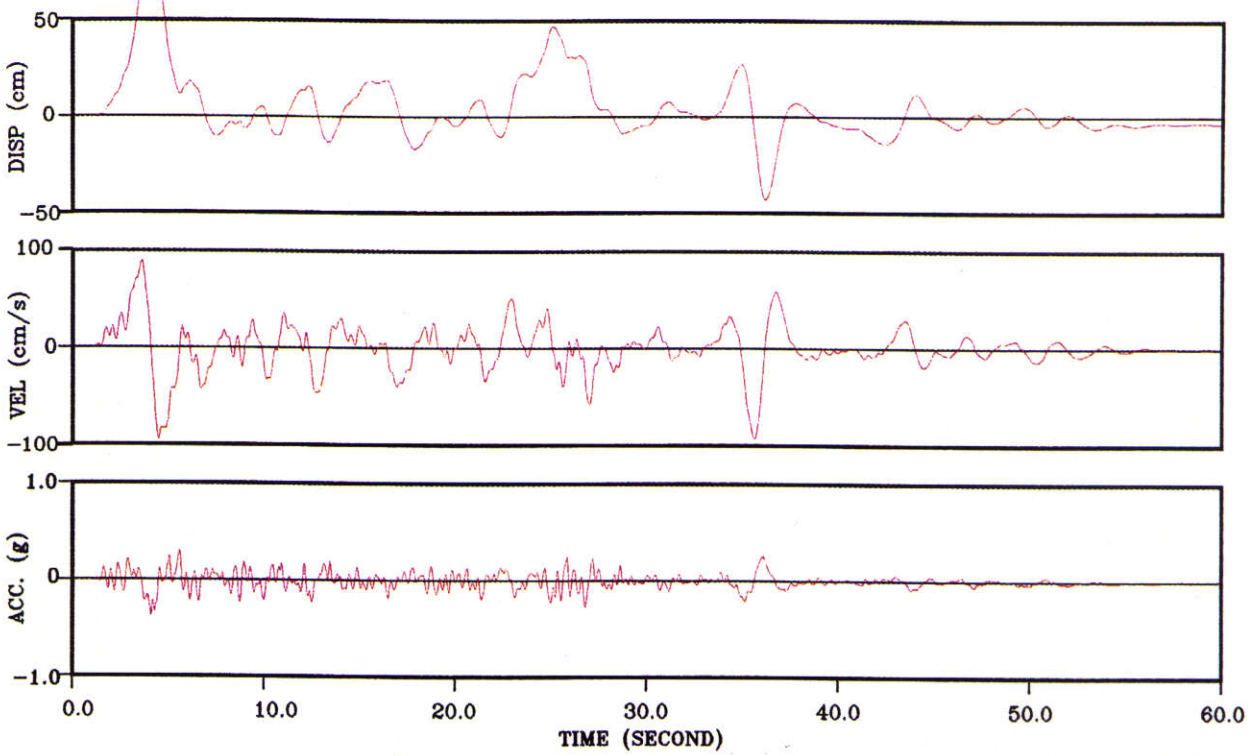

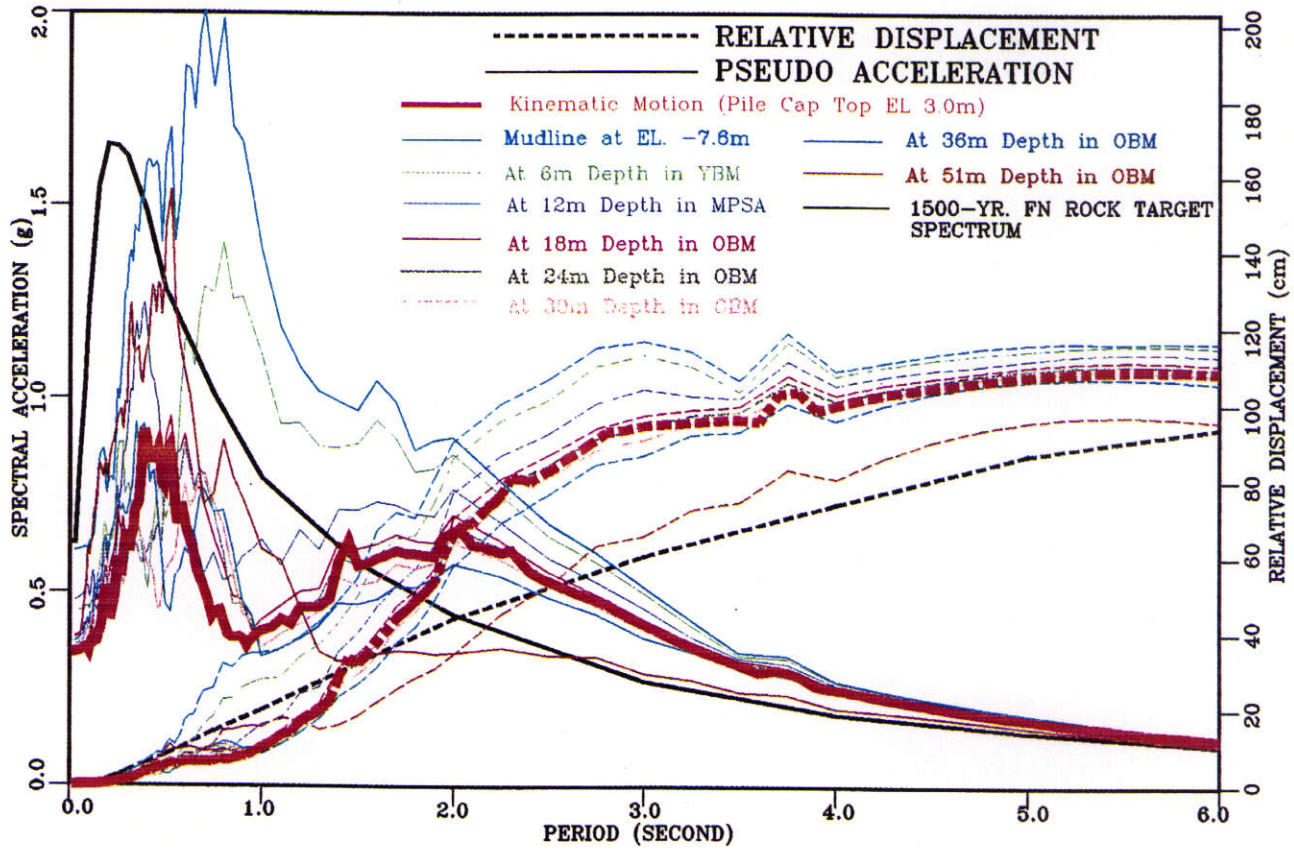

KINEMATIC AND DEPTH-VARYING FREE FIELD MOTIONS
PIER E06, INPUT ROCK MOTION SET 1, FAULT NORMAL COMPONENT
SFOBB East Span Seismic Safety Project

PLATE 8-54

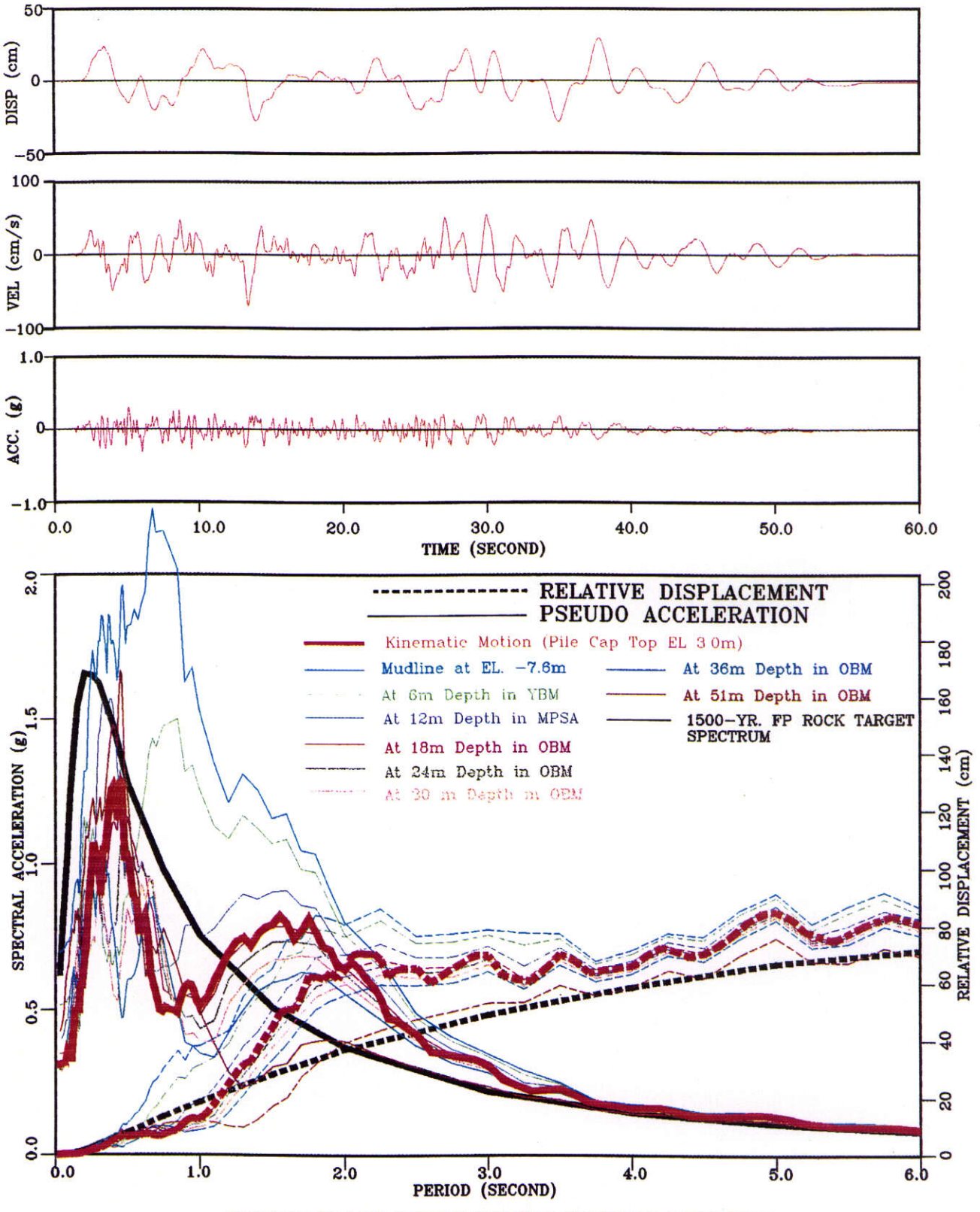

KINEMATIC AND DEPTH-VARYING FREE FIELD MOTIONS
PIER E06, INPUT ROCK MOTION SET 1, FAULT PARALLEL COMPONENT
SFOBB East Span Seismic Safety Project

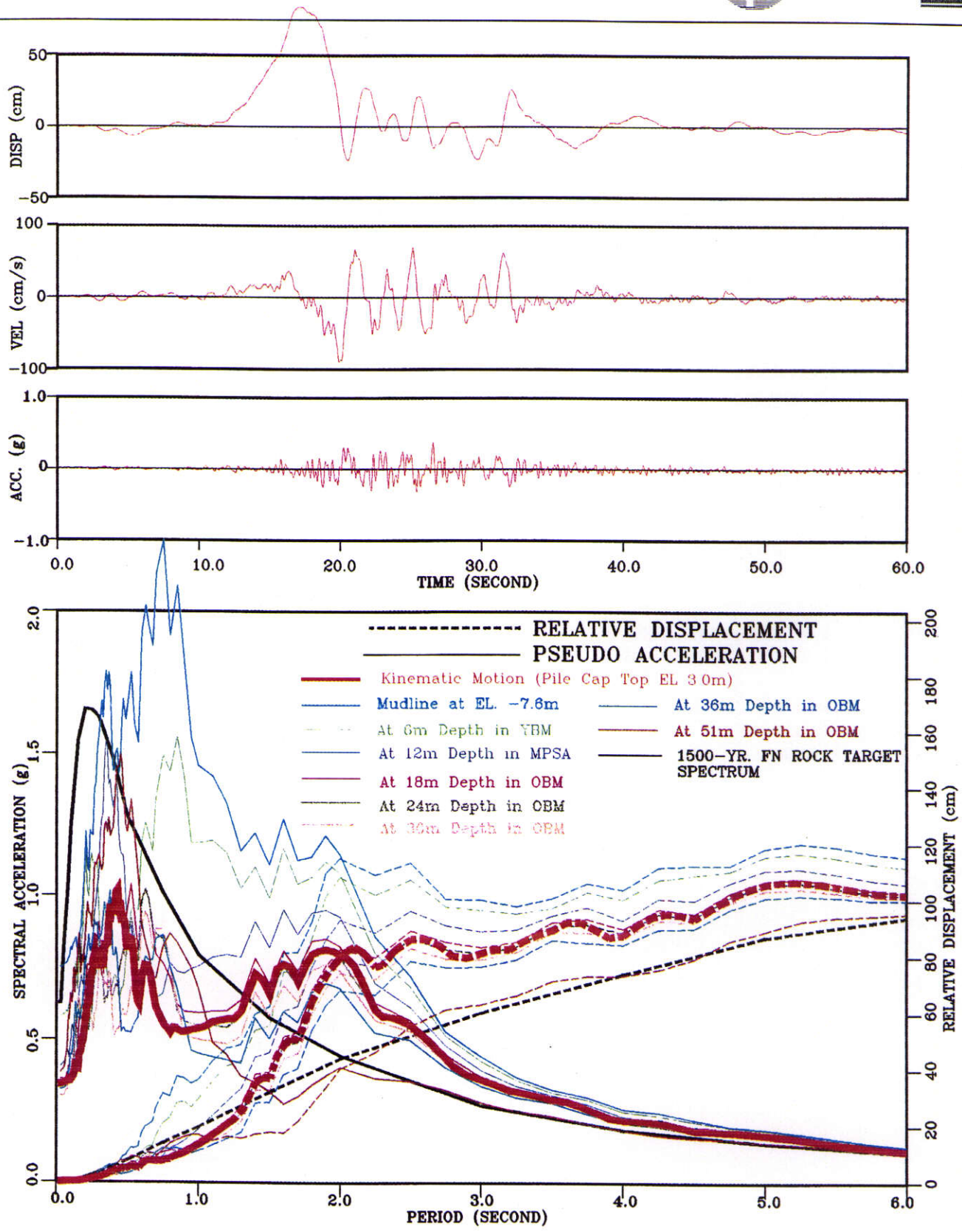

KINEMATIC AND DEPTH-VARYING FREE FIELD MOTIONS
PIER E06, INPUT ROCK MOTION SET 2, FAULT NORMAL COMPONENT
SFOBB East Span Seismic Safety Project

PLATE 8-56

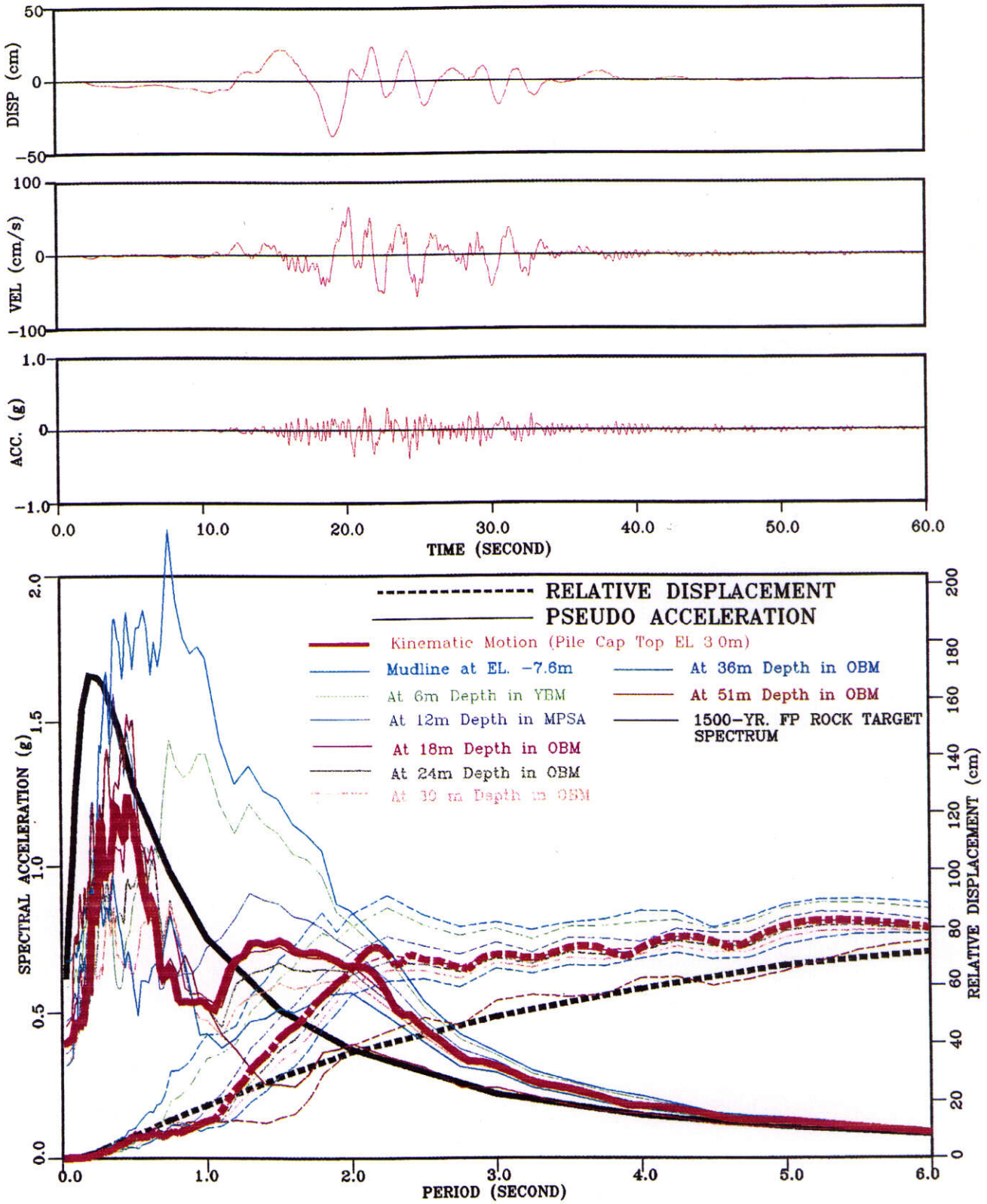

KINEMATIC AND DEPTH-VARYING FREE FIELD MOTIONS
PIER E06, INPUT ROCK MOTION SET 2, FAULT PARALLEL COMPONENT
SFOBB East Span Seismic Safety Project

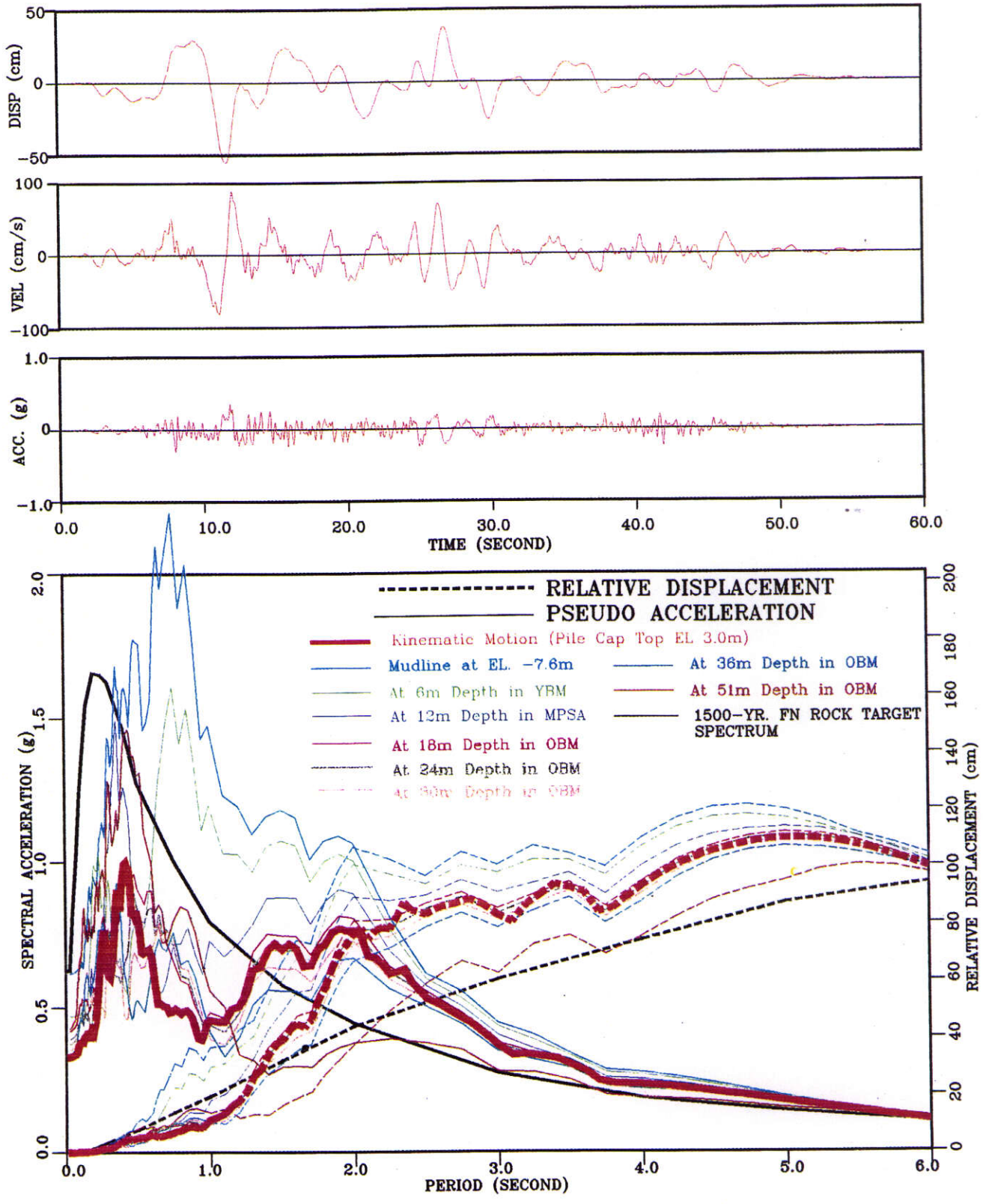

KINEMATIC AND DEPTH-VARYING FREE FIELD MOTIONS
PIER E06, INPUT ROCK MOTION SET 3, FAULT NORMAL COMPONENT
SFOBB East Span Seismic Safety Project

Earth Mechanics FUGRO

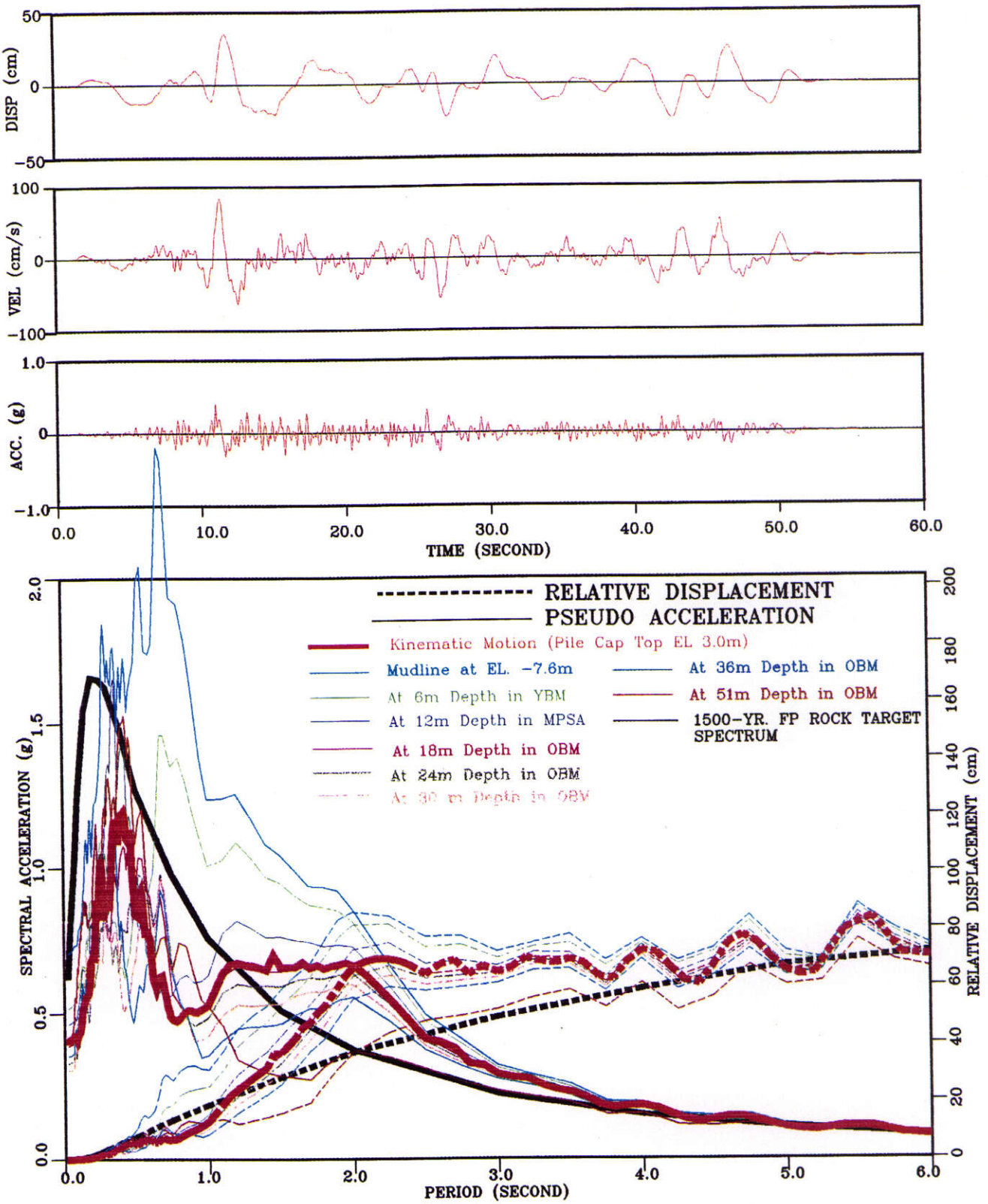

KINEMATIC AND DEPTH-VARYING FREE FIELD MOTIONS
PIER E06, INPUT ROCK MOTION SET 3, FAULT PARALLEL COMPONENT
SFOBB East Span Seismic Safety Project

PLATE 8-59

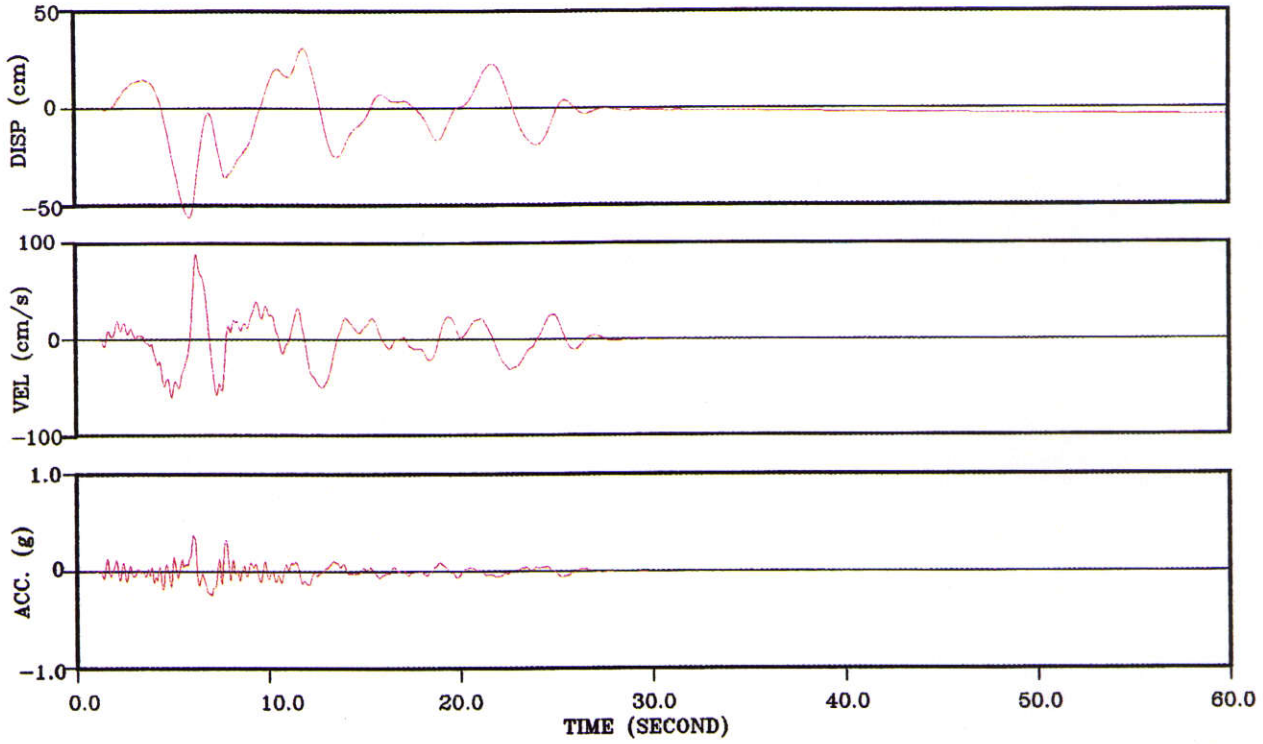

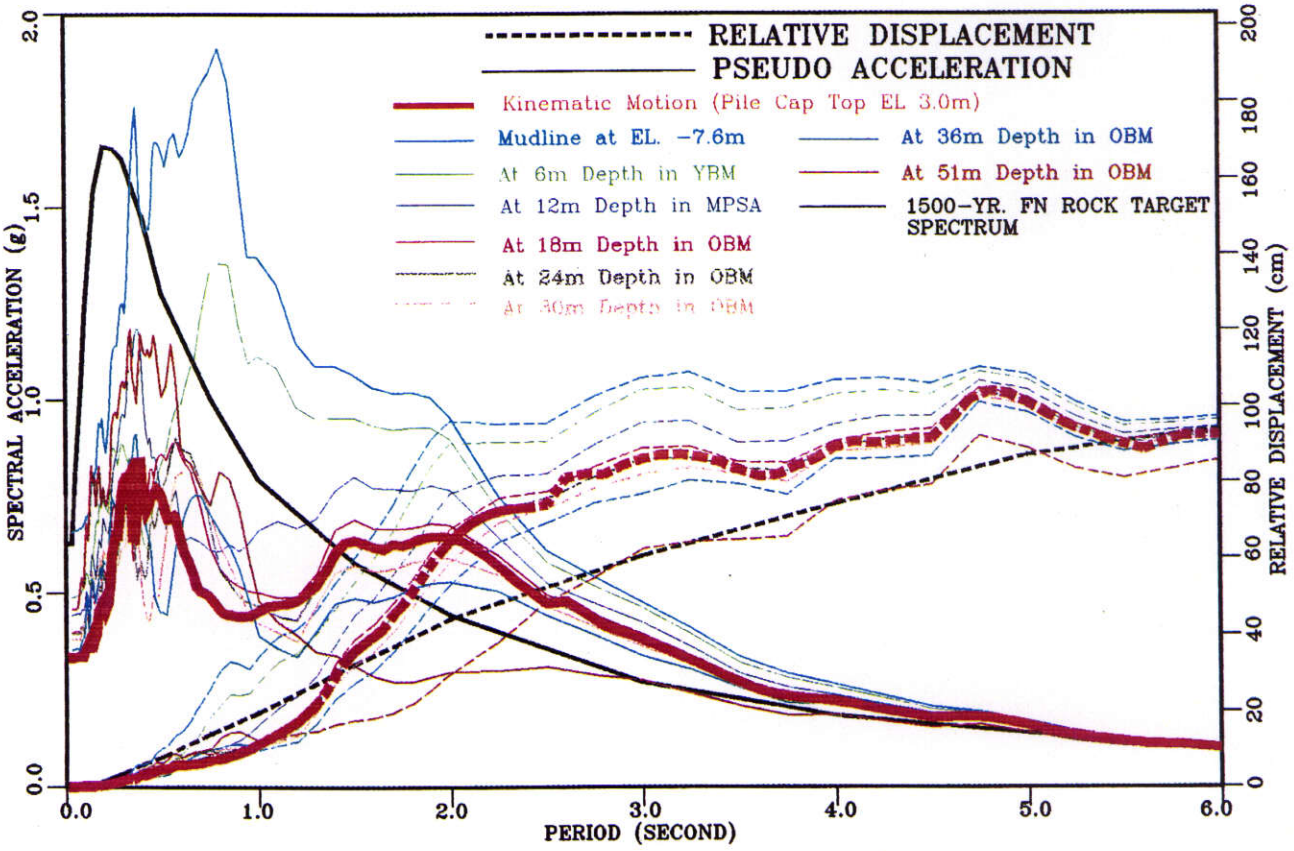

KINEMATIC AND DEPTH-VARYING FREE FIELD MOTIONS
PIER E06, INPUT ROCK MOTION SET 4, FAULT NORMAL COMPONENT
SFOBB East Span Seismic Safety Project

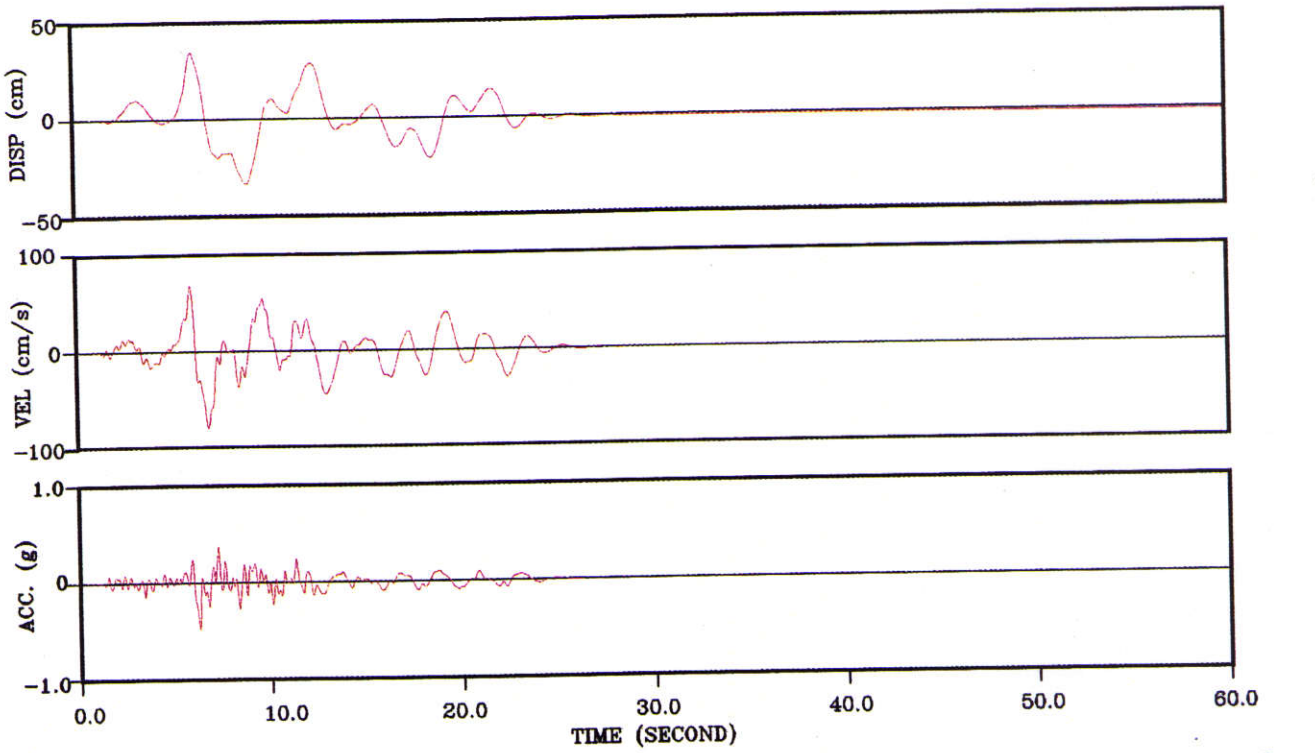

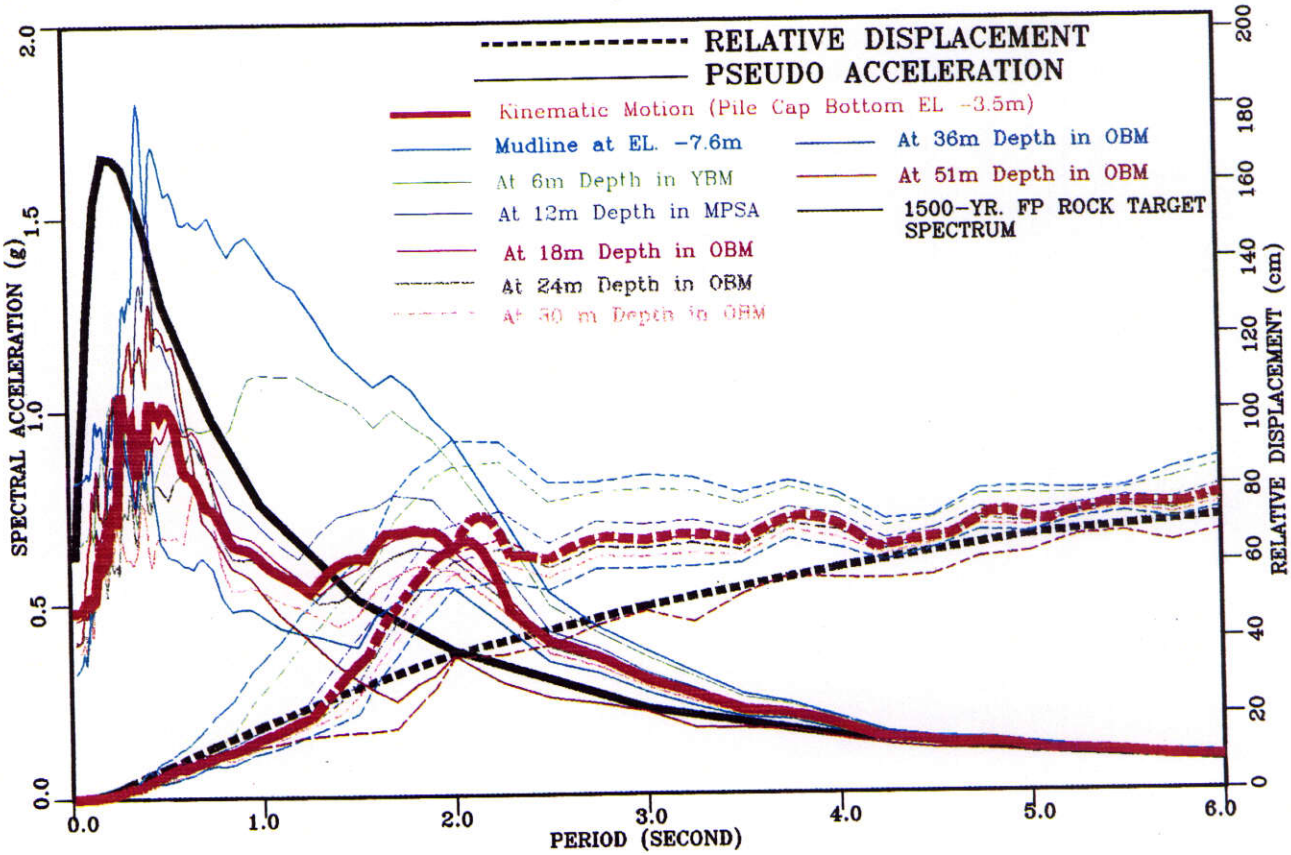

KINEMATIC AND DEPTH-VARYING FREE FIELD MOTIONS
PIER E06, INPUT ROCK MOTION SET 4, FAULT PARALLEL COMPONENT
SFOBB East Span Seismic Safety Project

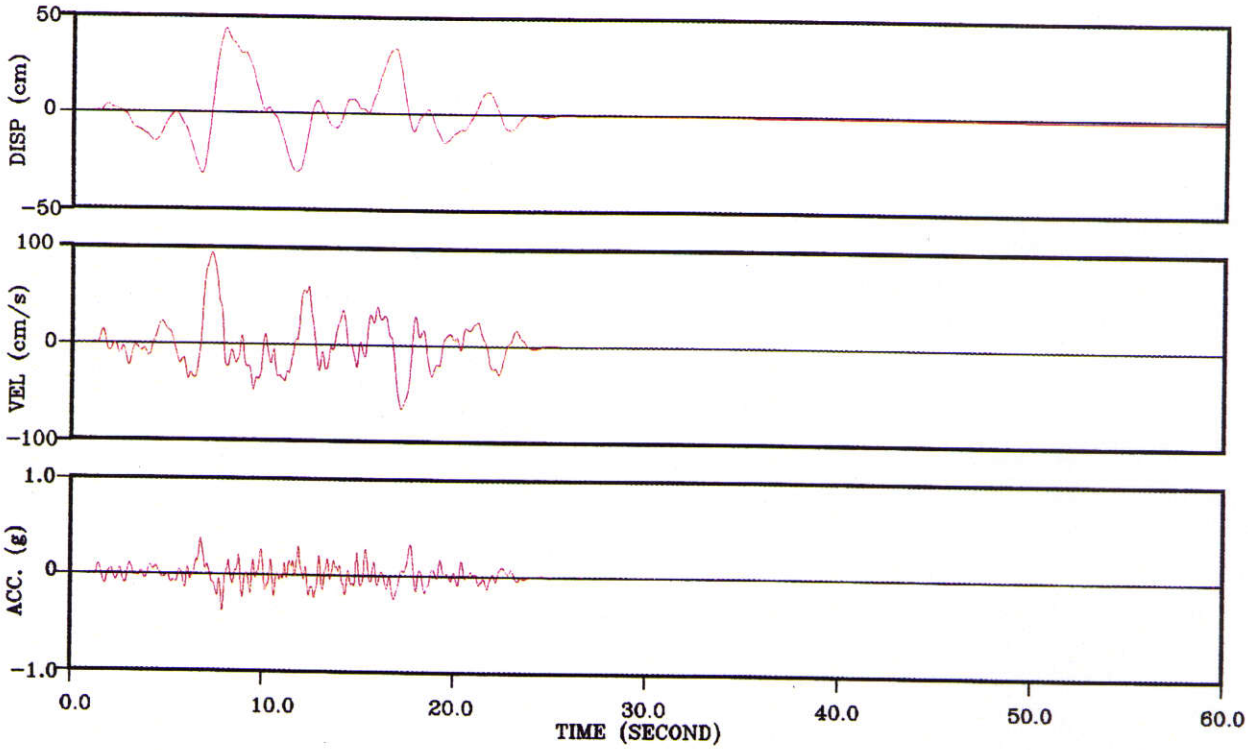

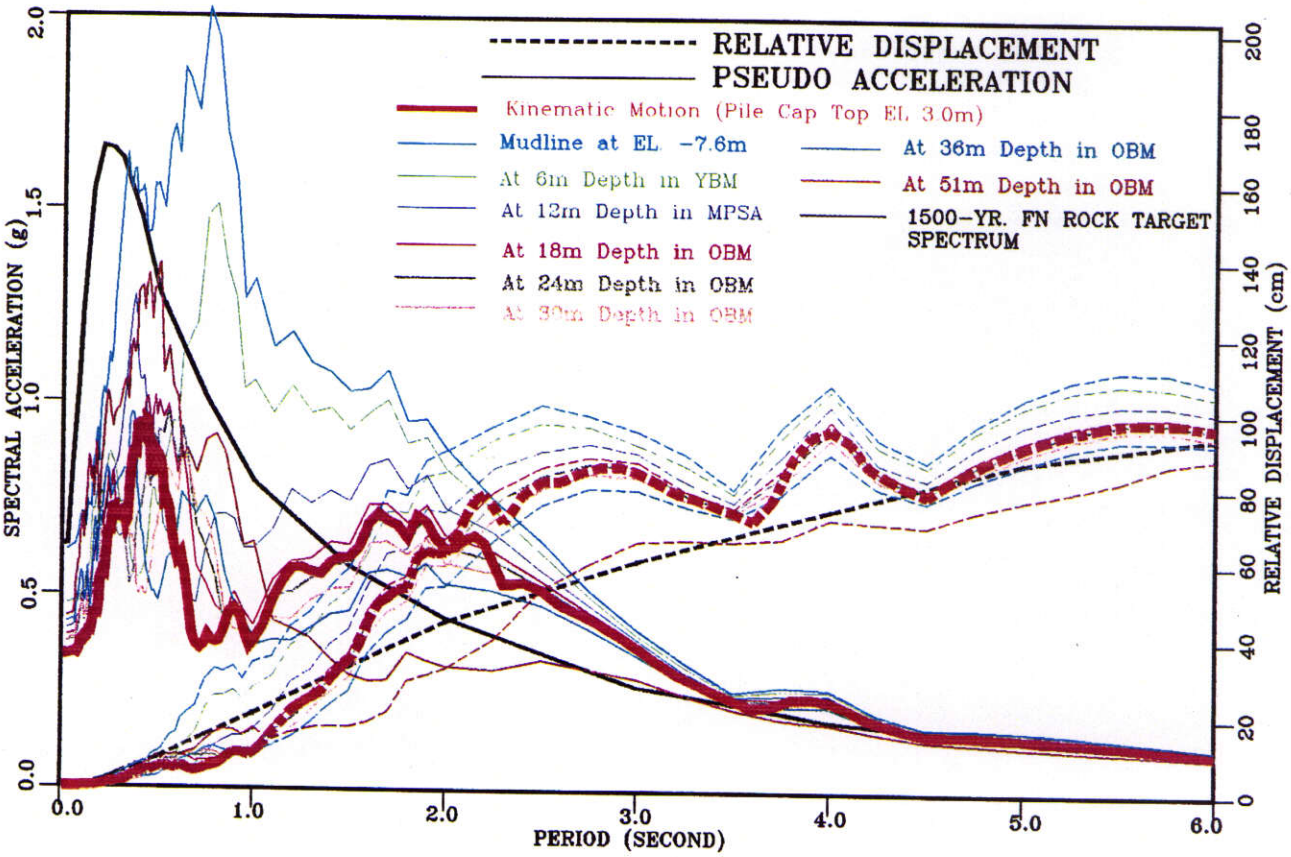

KINEMATIC AND DEPTH-VARYING FREE FIELD MOTIONS
PIER E06, INPUT ROCK MOTION SET 5, FAULT NORMAL COMPONENT
SFOBB East Span Seismic Safety Project

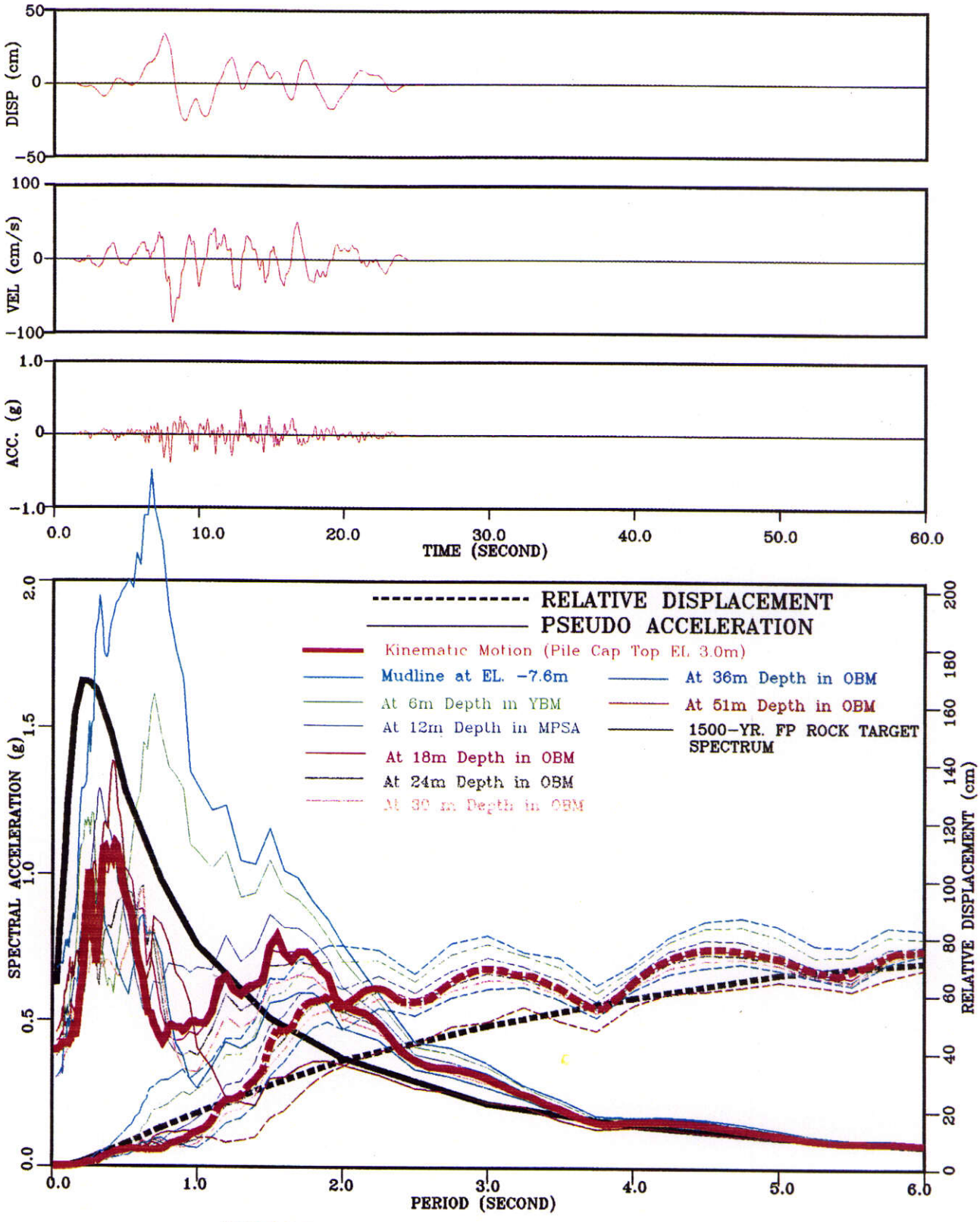

KINEMATIC AND DEPTH-VARYING FREE FIELD MOTIONS
PIER E06, INPUT ROCK MOTION SET 5, FAULT PARALLEL COMPONENT
SFOBB East Span Seismic Safety Project

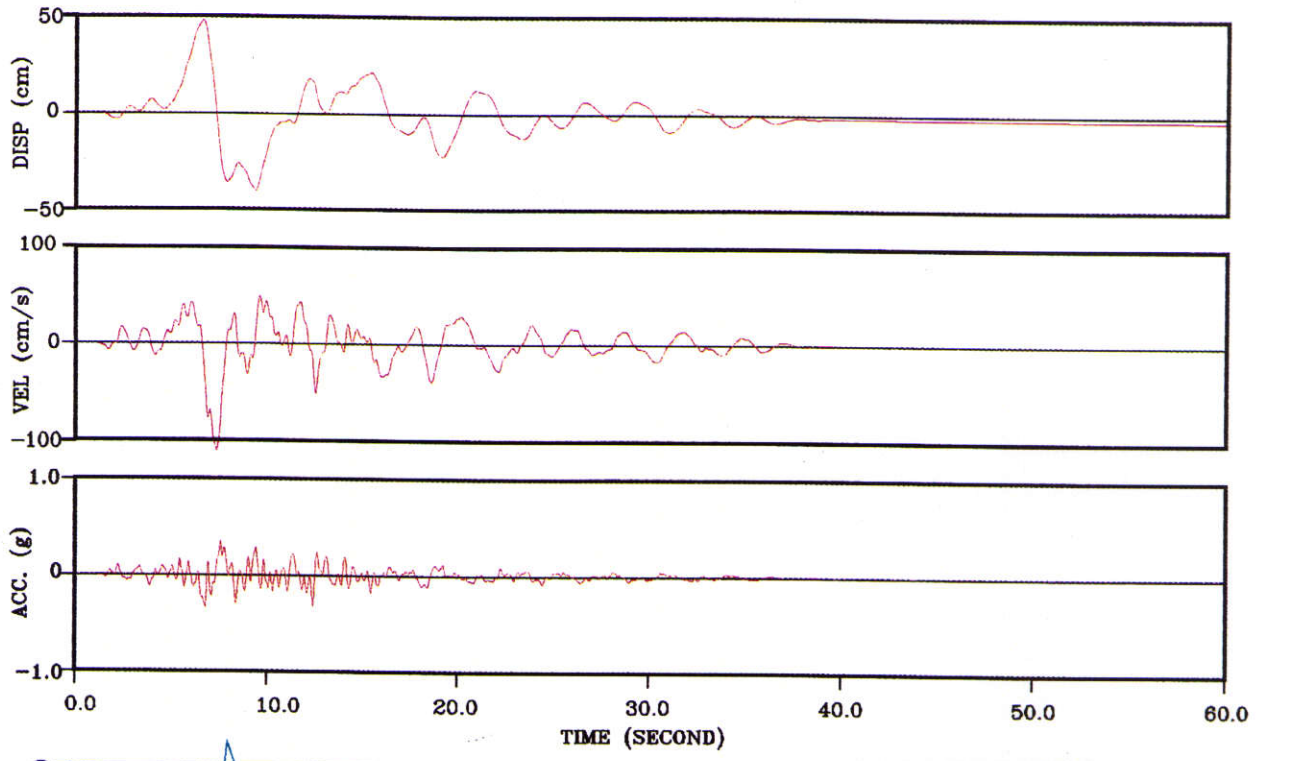

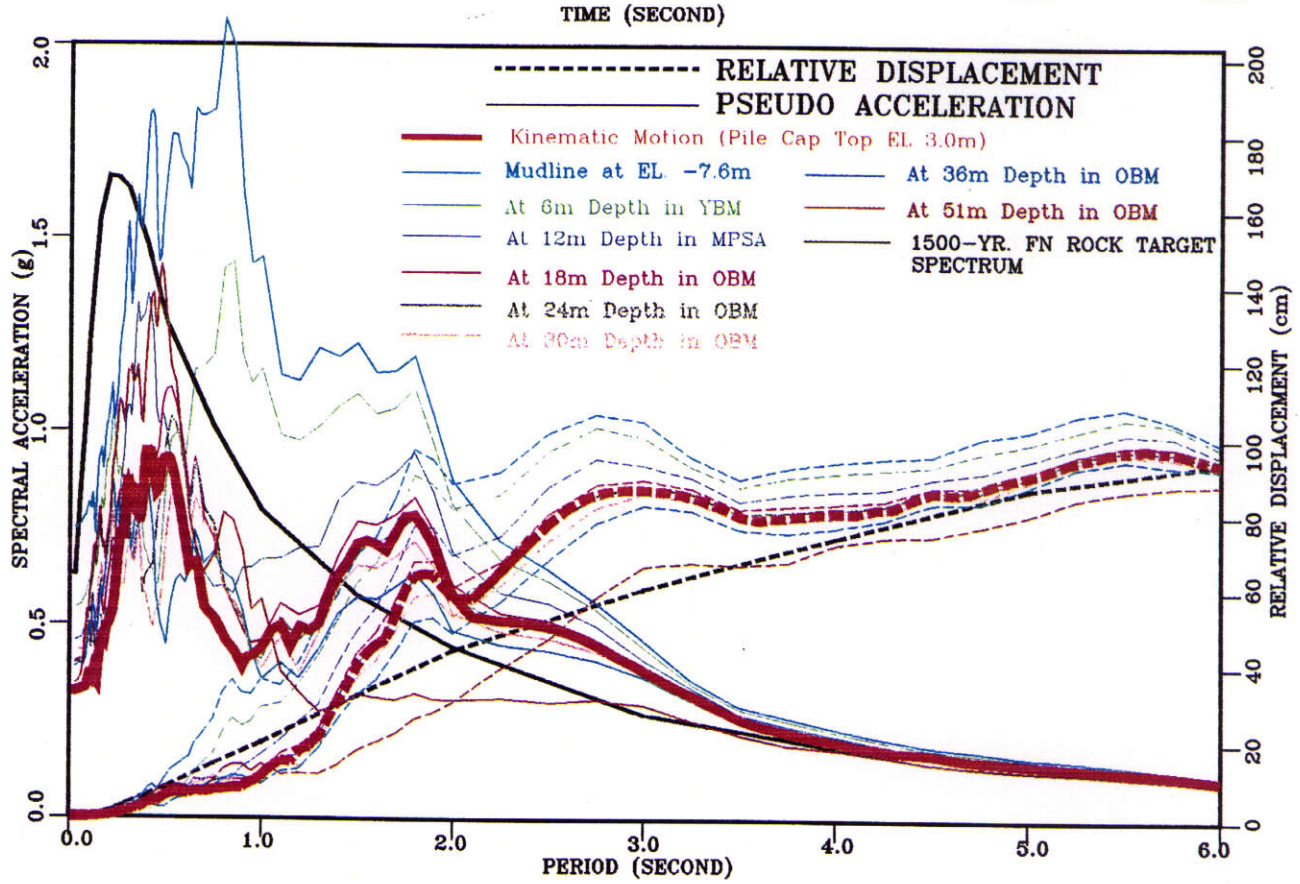

KINEMATIC AND DEPTH-VARYING FREE FIELD MOTIONS
PIER E06, INPUT ROCK MOTION SET 6, FAULT NORMAL COMPONENT
SFOBB East Span Seismic Safety Project

PLATE 8-64

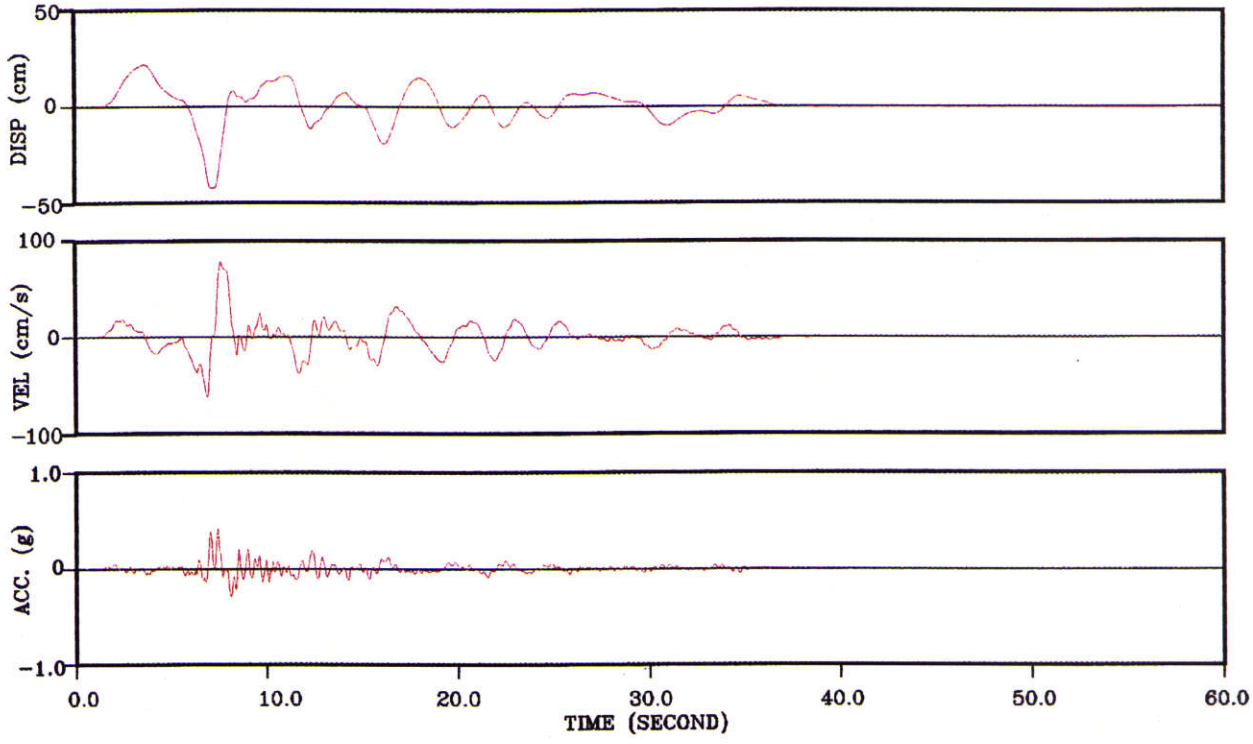

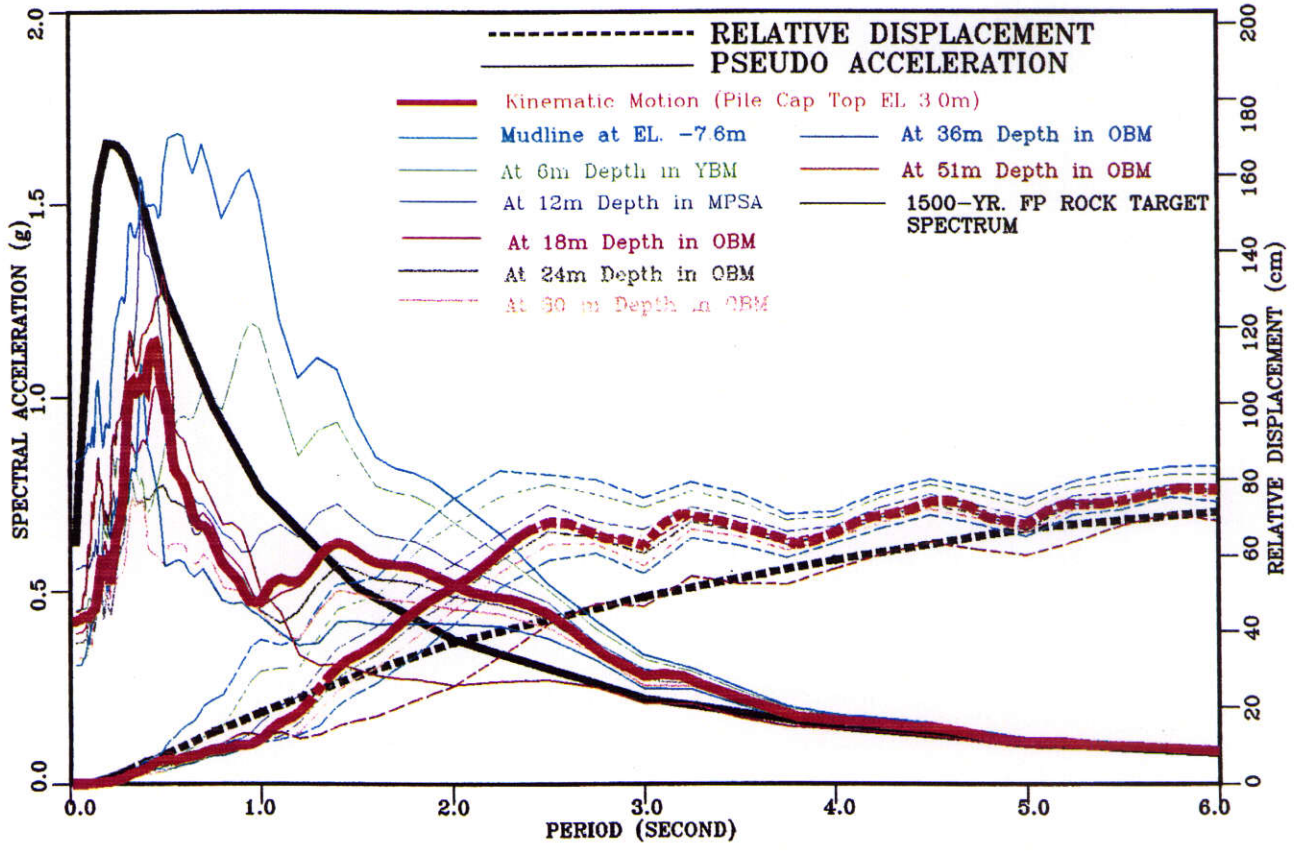

KINEMATIC AND DEPTH-VARYING FREE FIELD MOTIONS
PIER E06, INPUT ROCK MOTION SET 6, FAULT PARALLEL COMPONENT
SFOBB East Span Seismic Safety Project

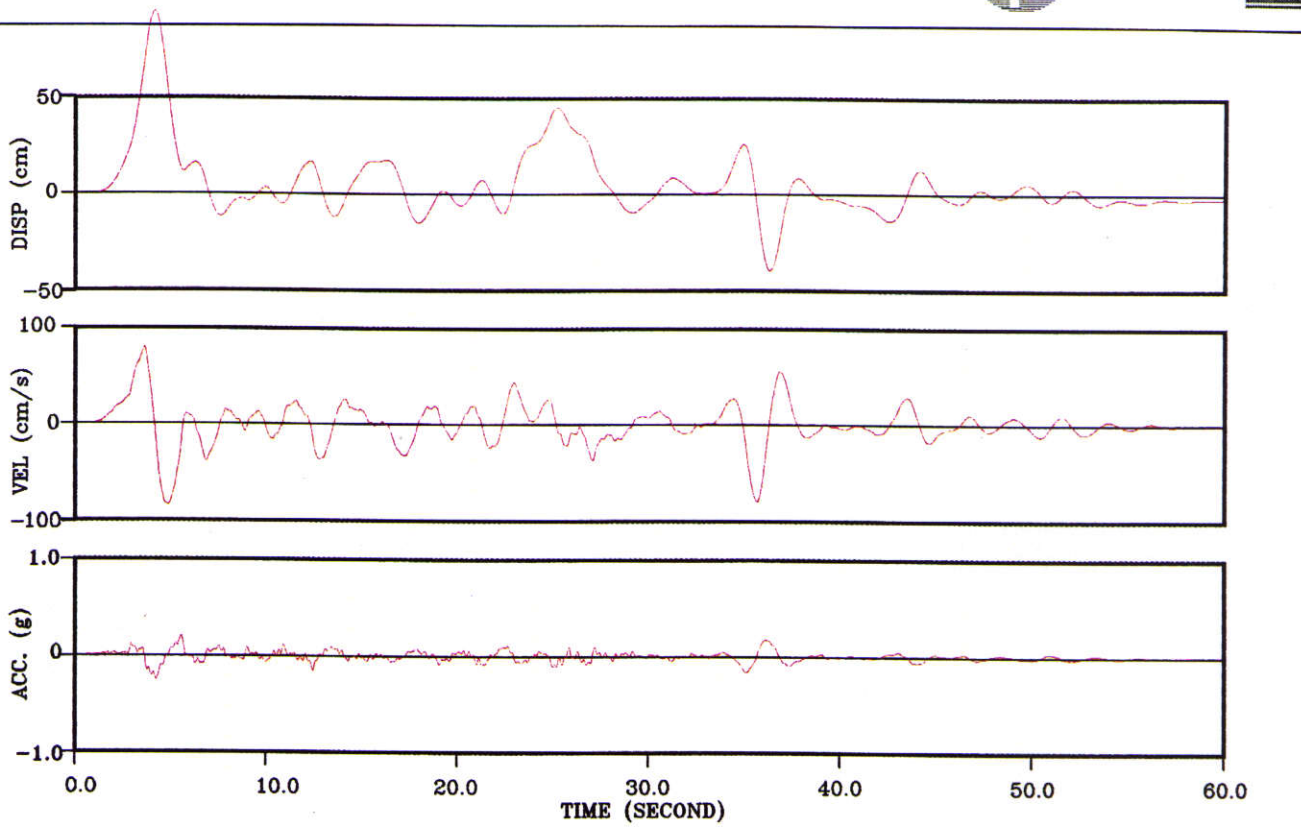

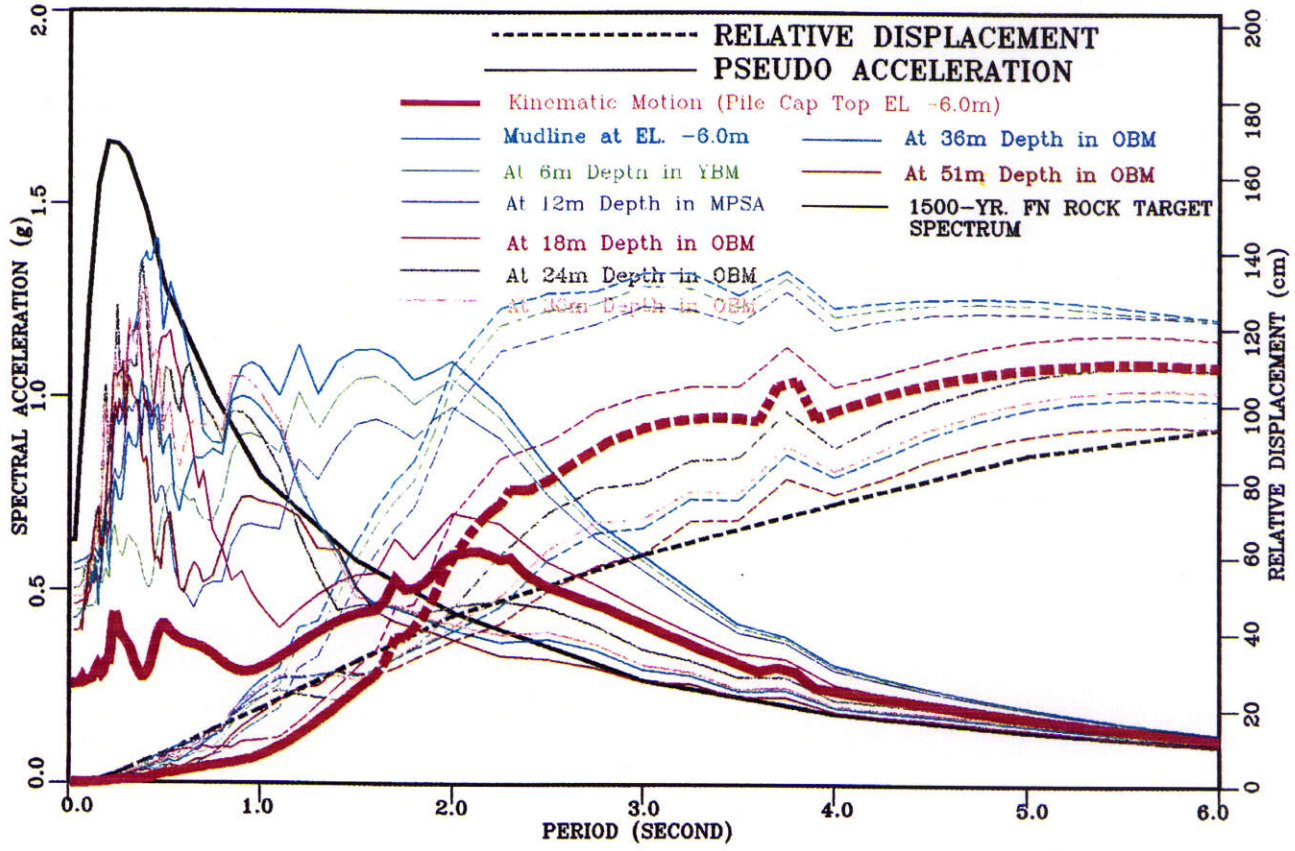

KINEMATIC AND DEPTH-VARYING FREE FIELD MOTIONS
PIER E07, INPUT ROCK MOTION SET 1, FAULT NORMAL COMPONENT
SFOBB East Span Seismic Safety Project

Earth Mechanics FUGRO

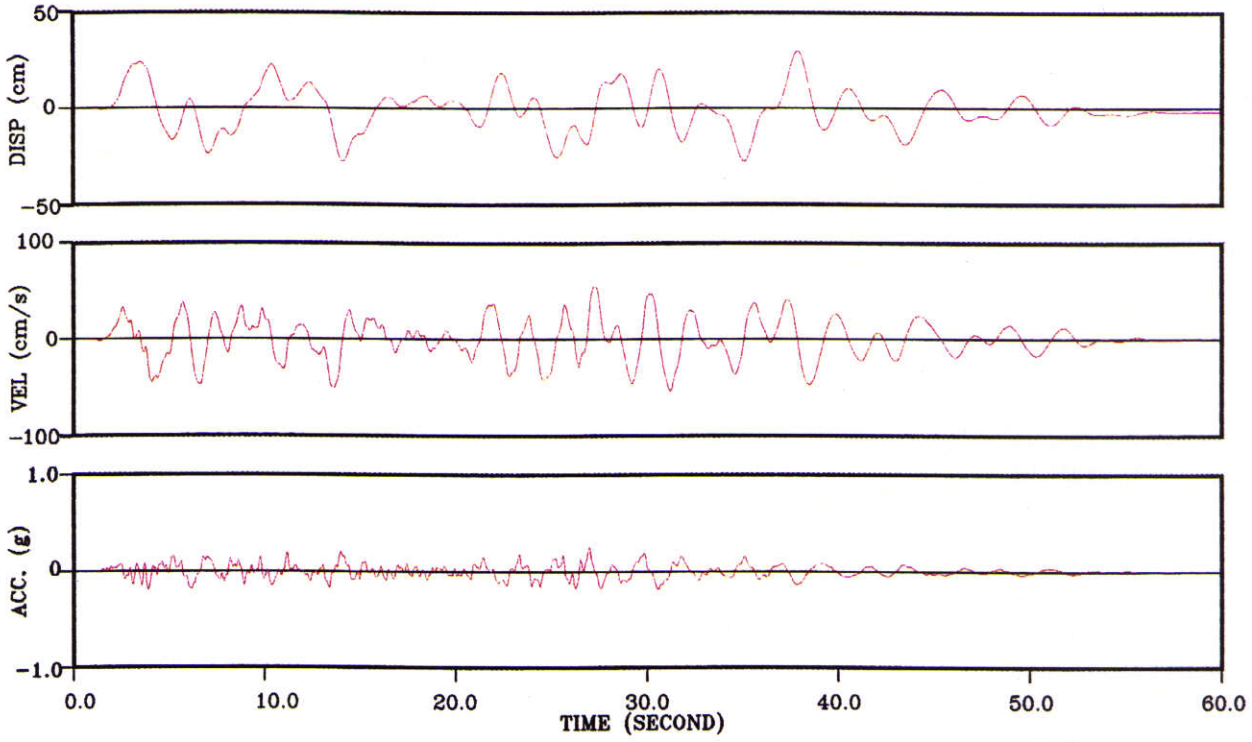

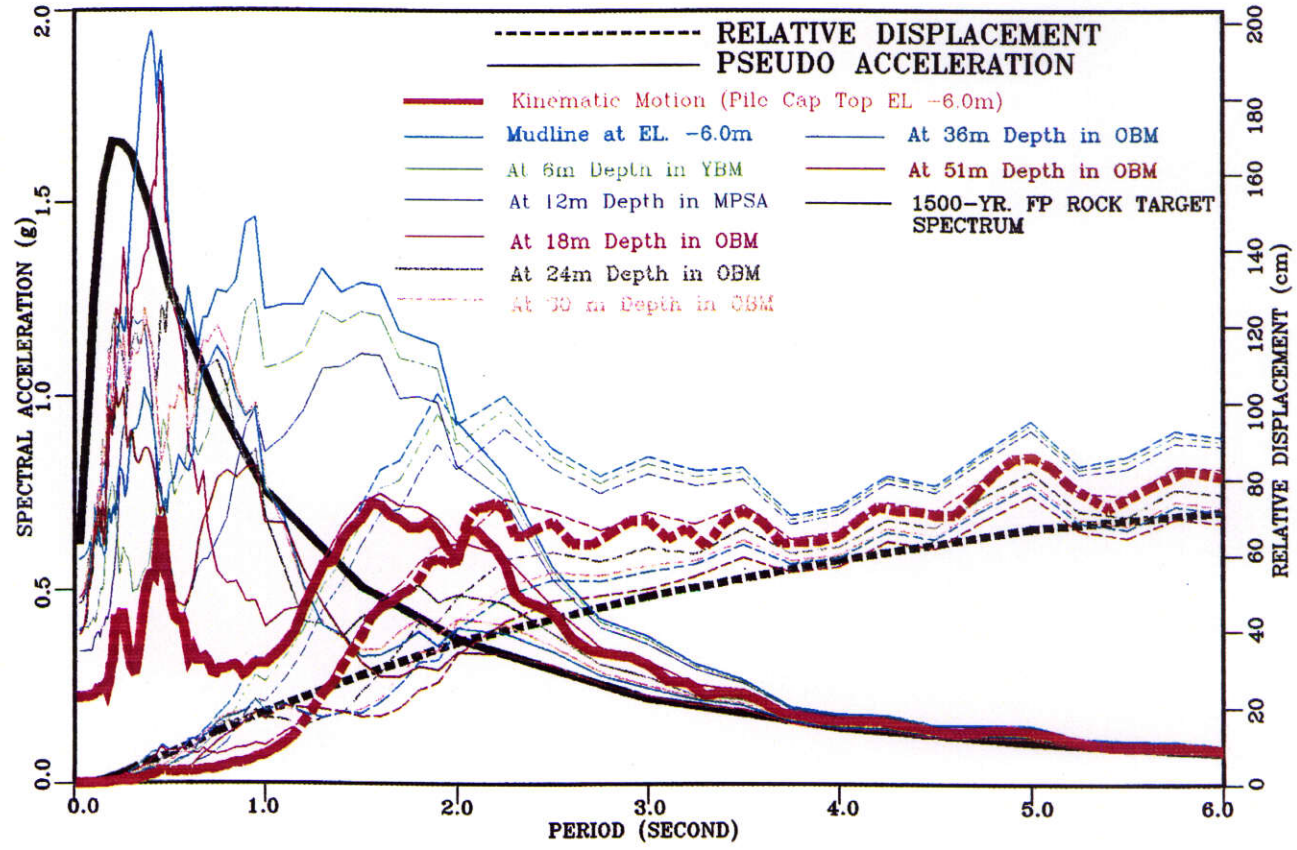

KINEMATIC AND DEPTH-VARYING FREE FIELD MOTIONS
PIER E07, INPUT ROCK MOTION SET 1, FAULT PARALLEL COMPONENT
SFOBB East Span Seismic Safety Project

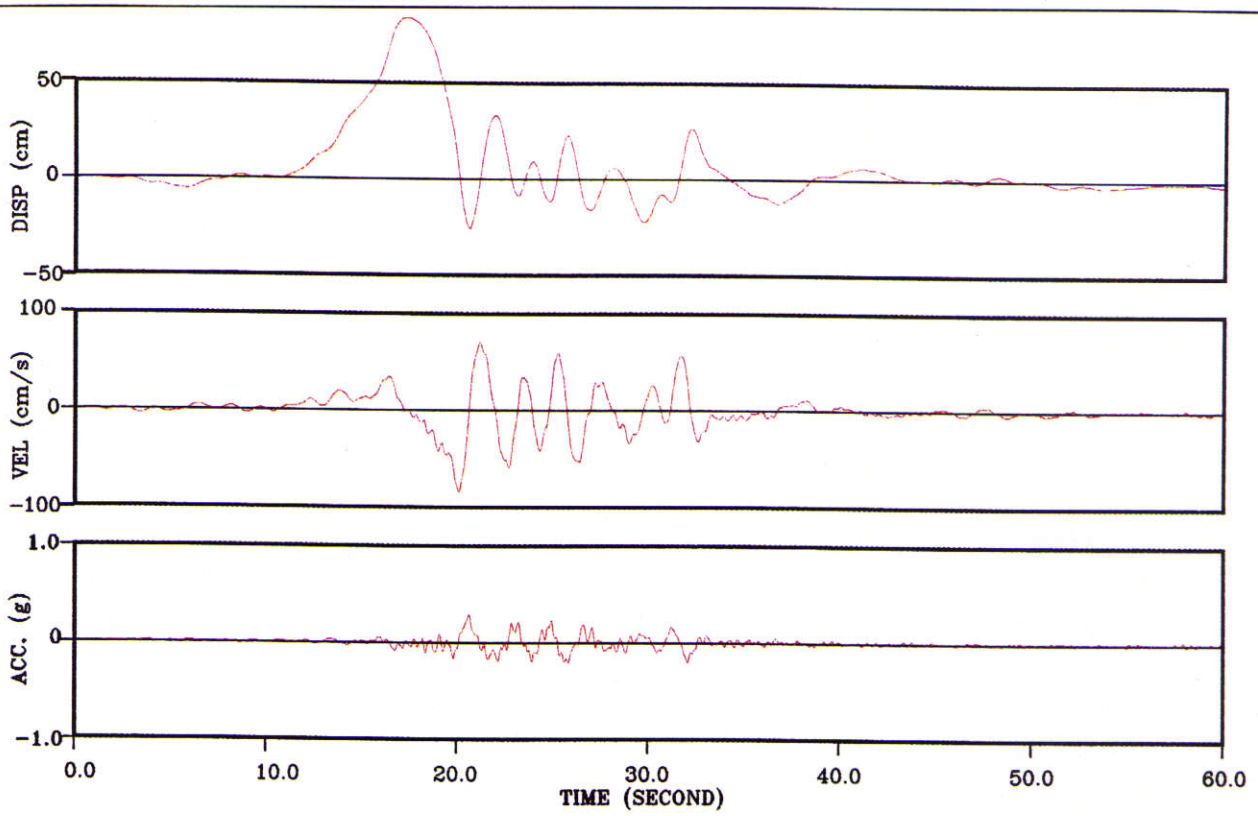

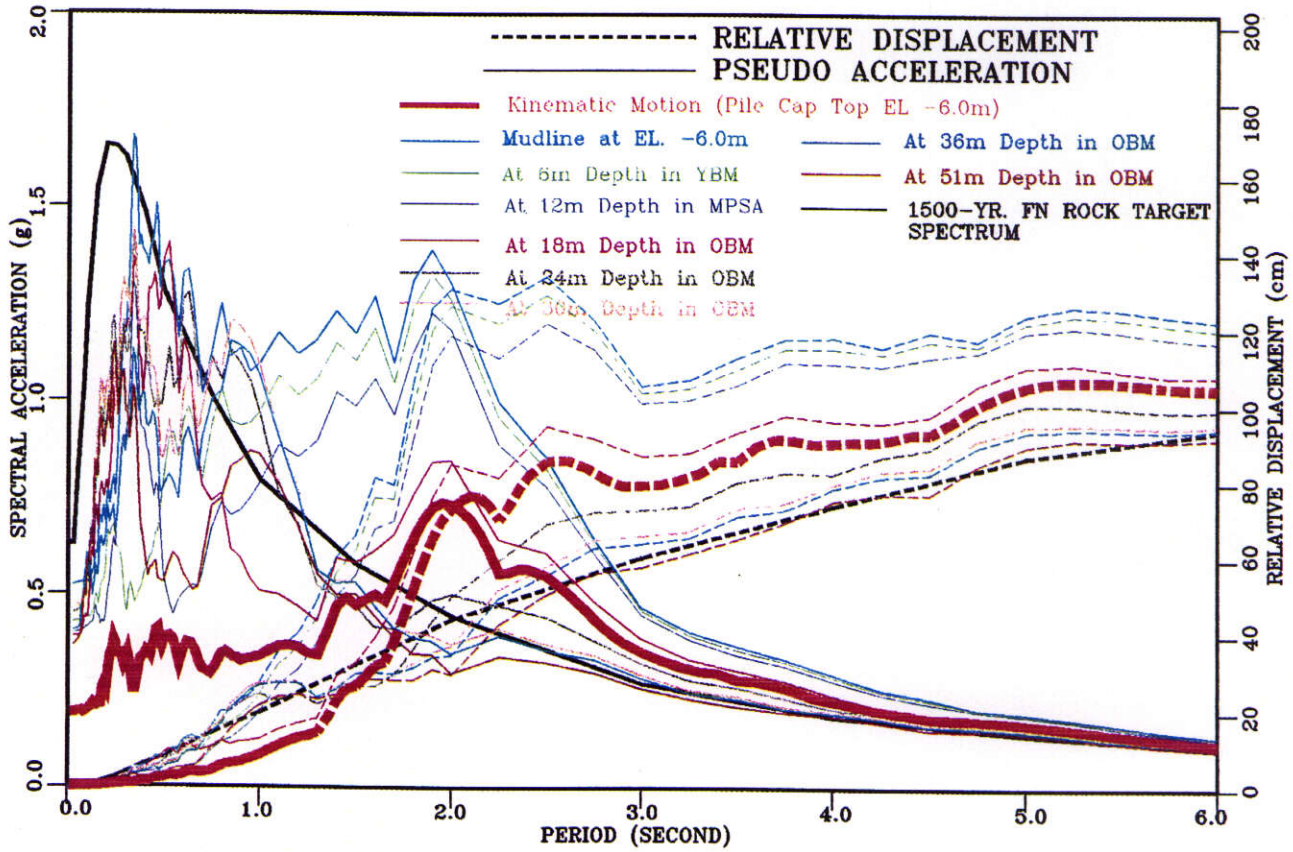

KINEMATIC AND DEPTH-VARYING FREE FIELD MOTIONS
PIER E07, INPUT ROCK MOTION SET 2, FAULT NORMAL COMPONENT
SFOBB East Span Seismic Safety Project

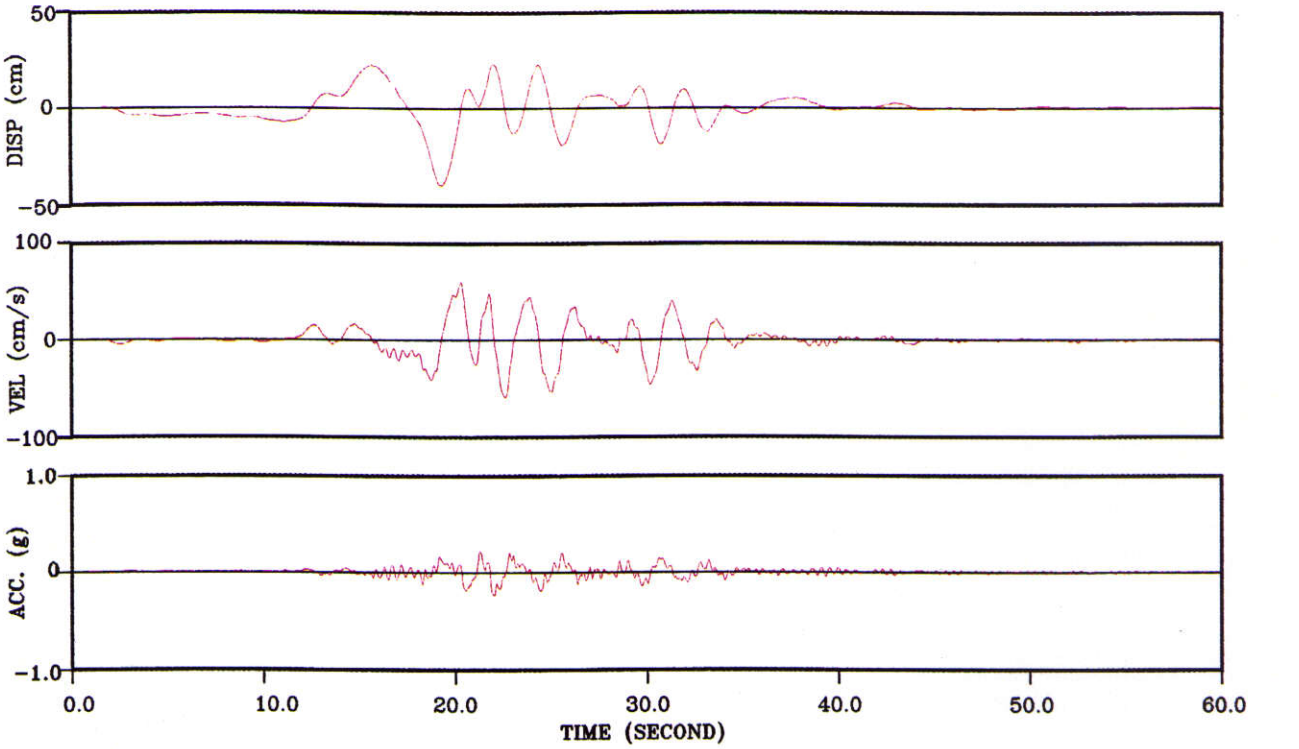

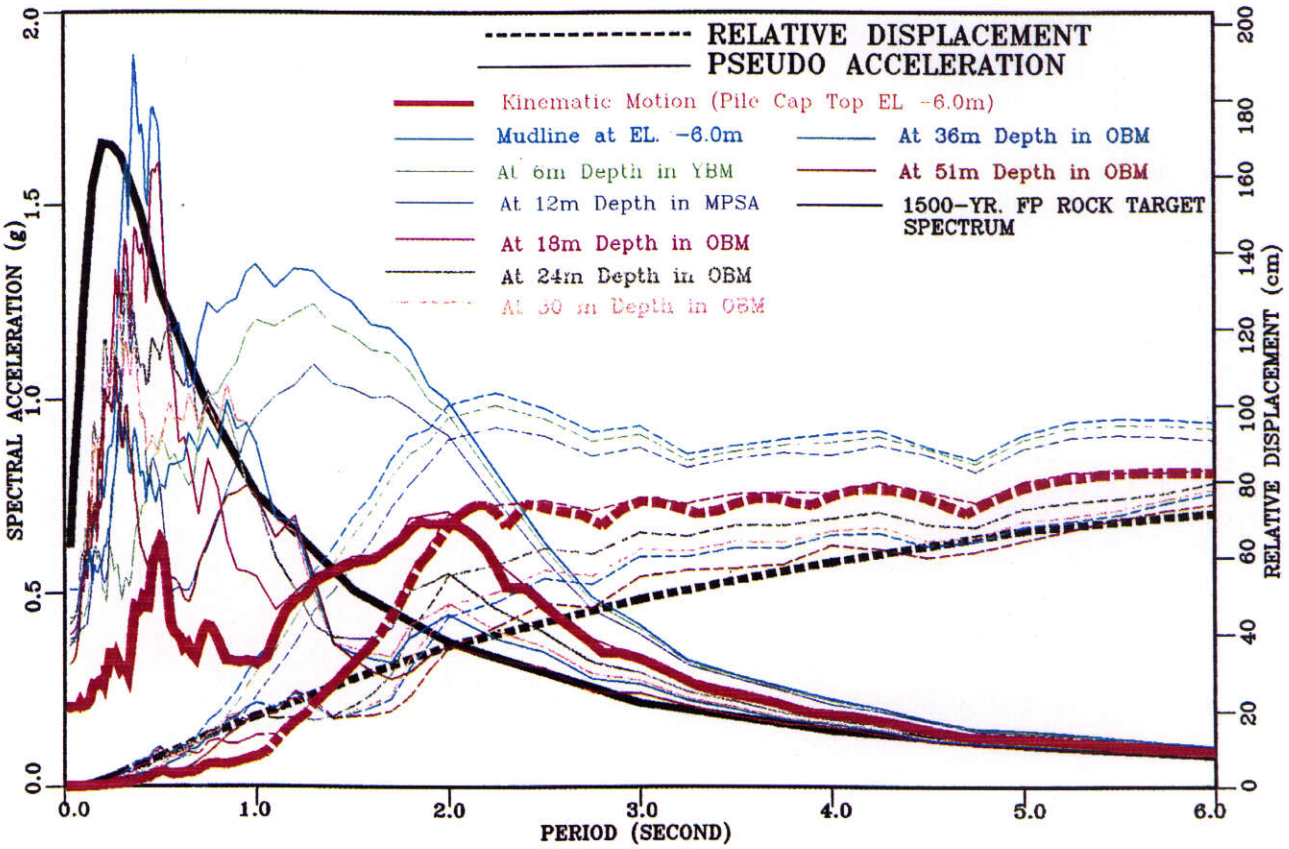

KINEMATIC AND DEPTH-VARYING FREE FIELD MOTIONS
PIER E07, INPUT ROCK MOTION SET 2, FAULT PARALLEL COMPONENT
SFOBB East Span Seismic Safety Project

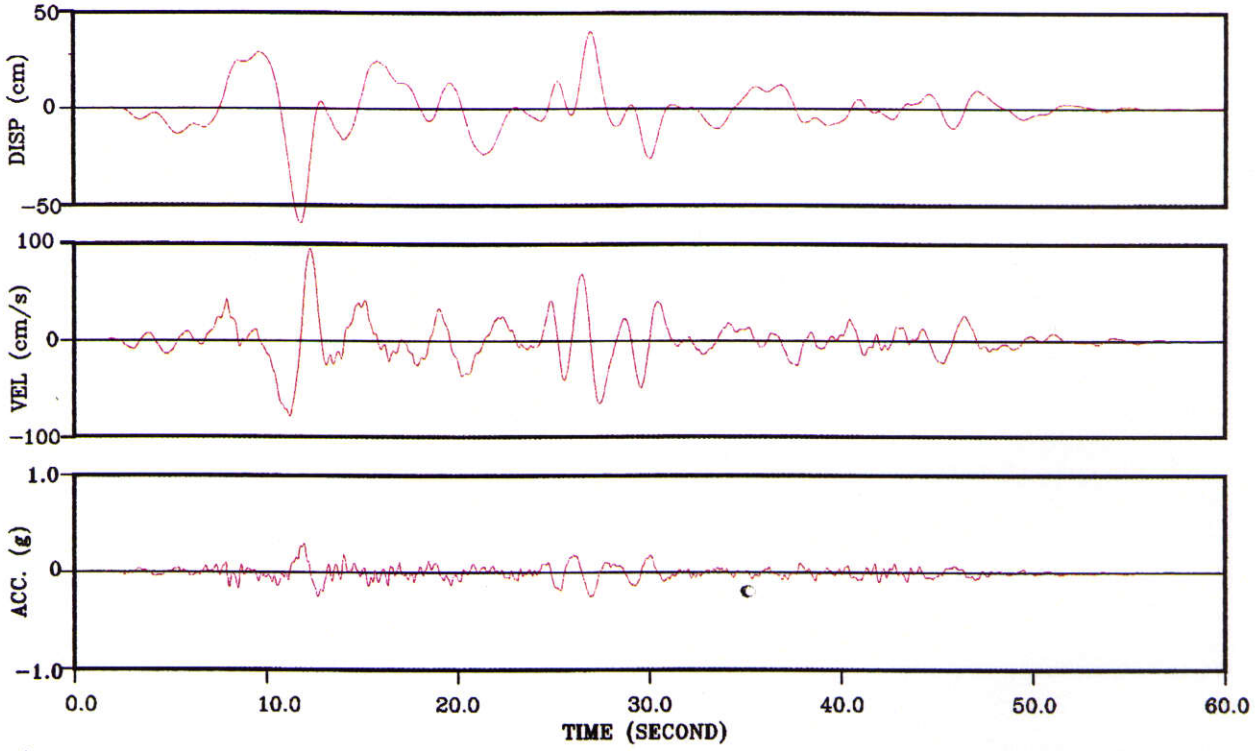

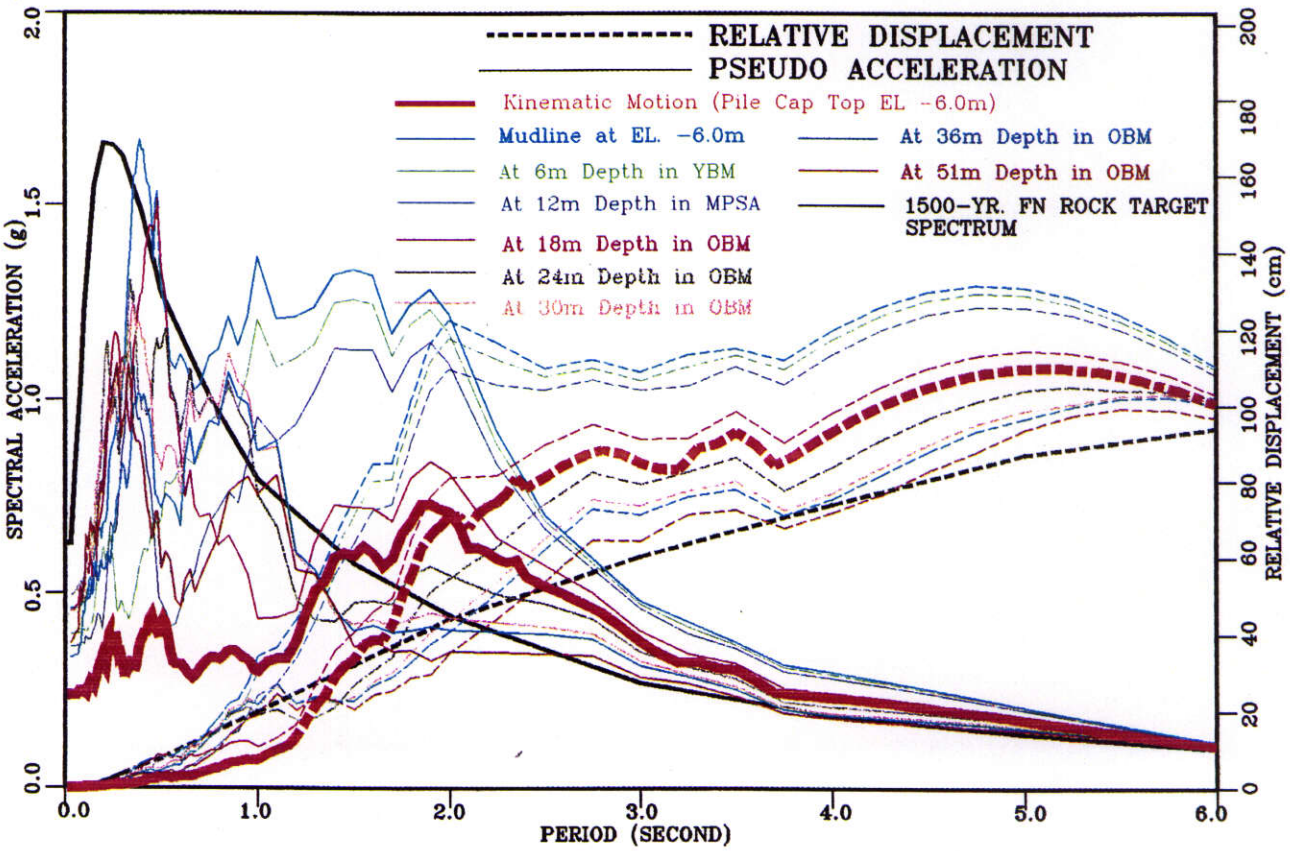

KINEMATIC AND DEPTH-VARYING FREE FIELD MOTIONS
PIER E07, INPUT ROCK MOTION SET 3, FAULT NORMAL COMPONENT
SFOBB East Span Seismic Safety Project

PLATE 8-70

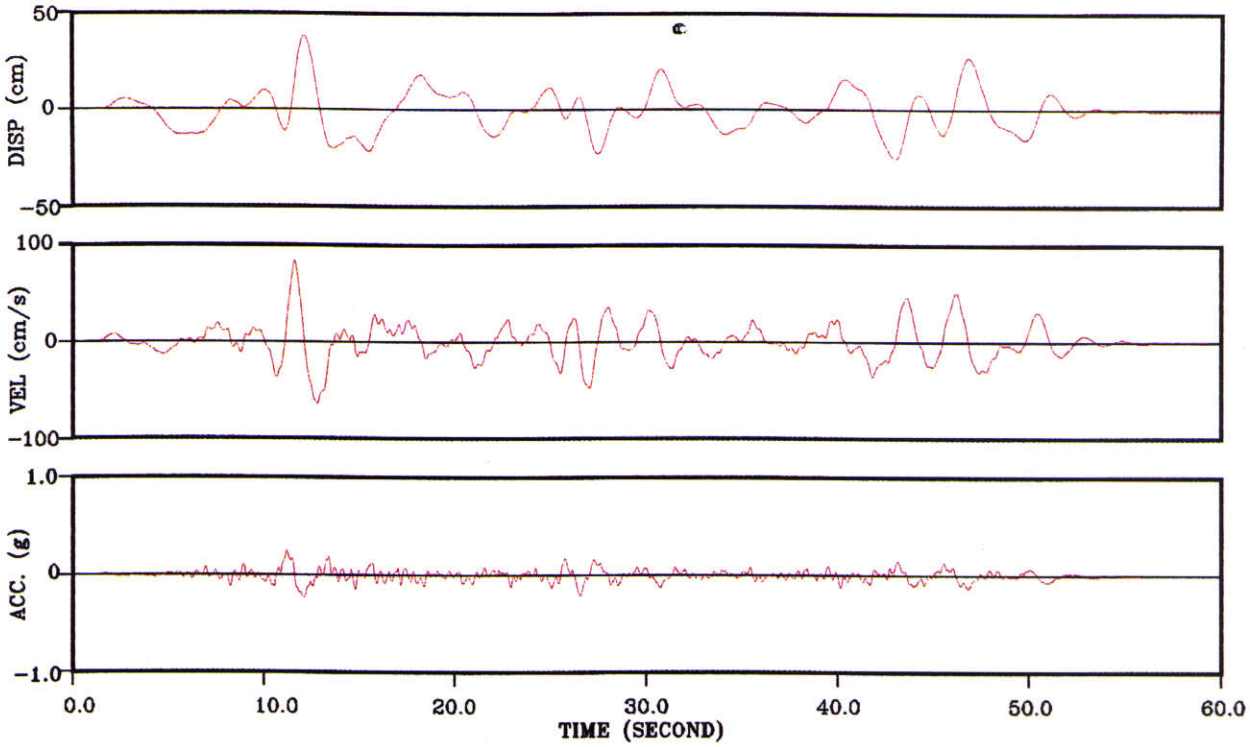

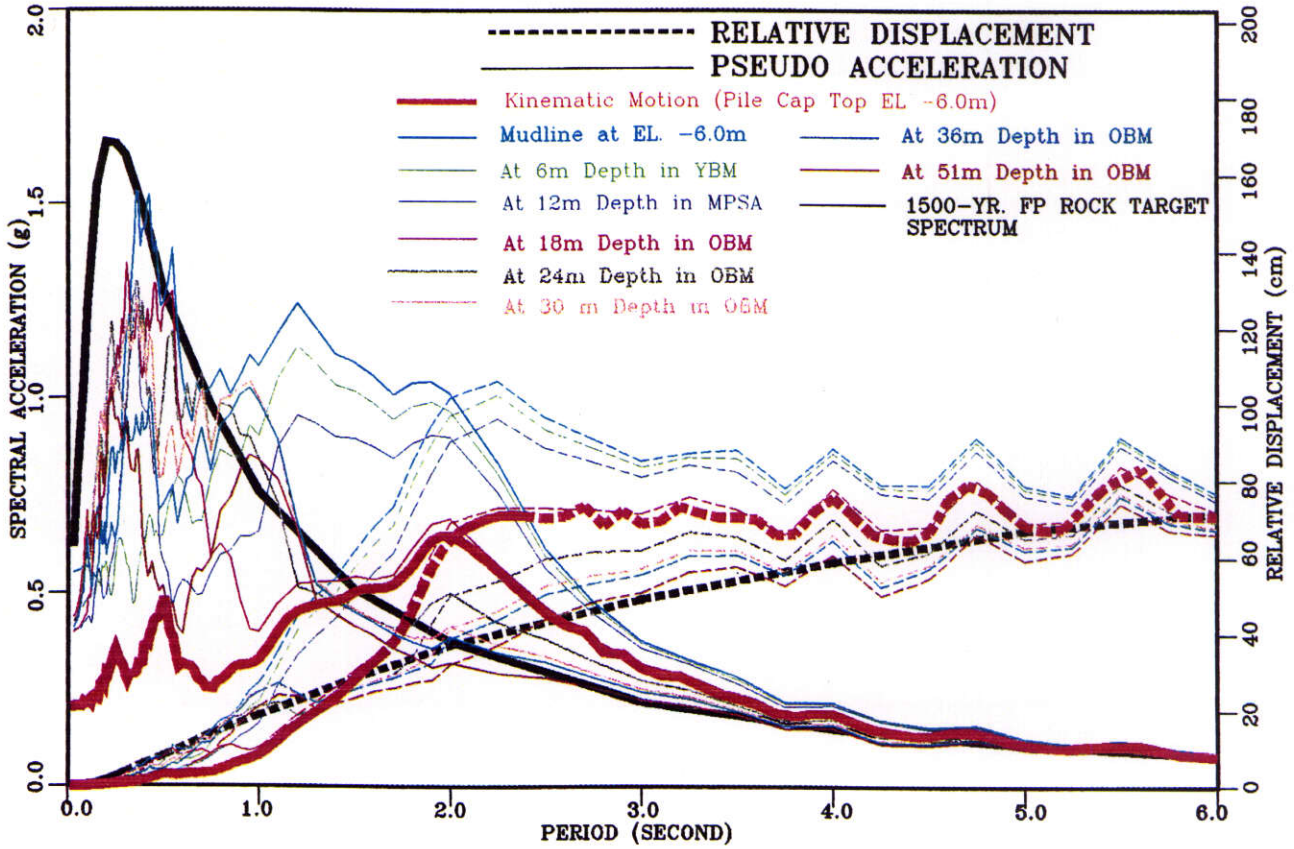

KINEMATIC AND DEPTH-VARYING FREE FIELD MOTIONS
PIER E07, INPUT ROCK MOTION SET 3, FAULT PARALLEL COMPONENT
SFOBB East Span Seismic Safety Project

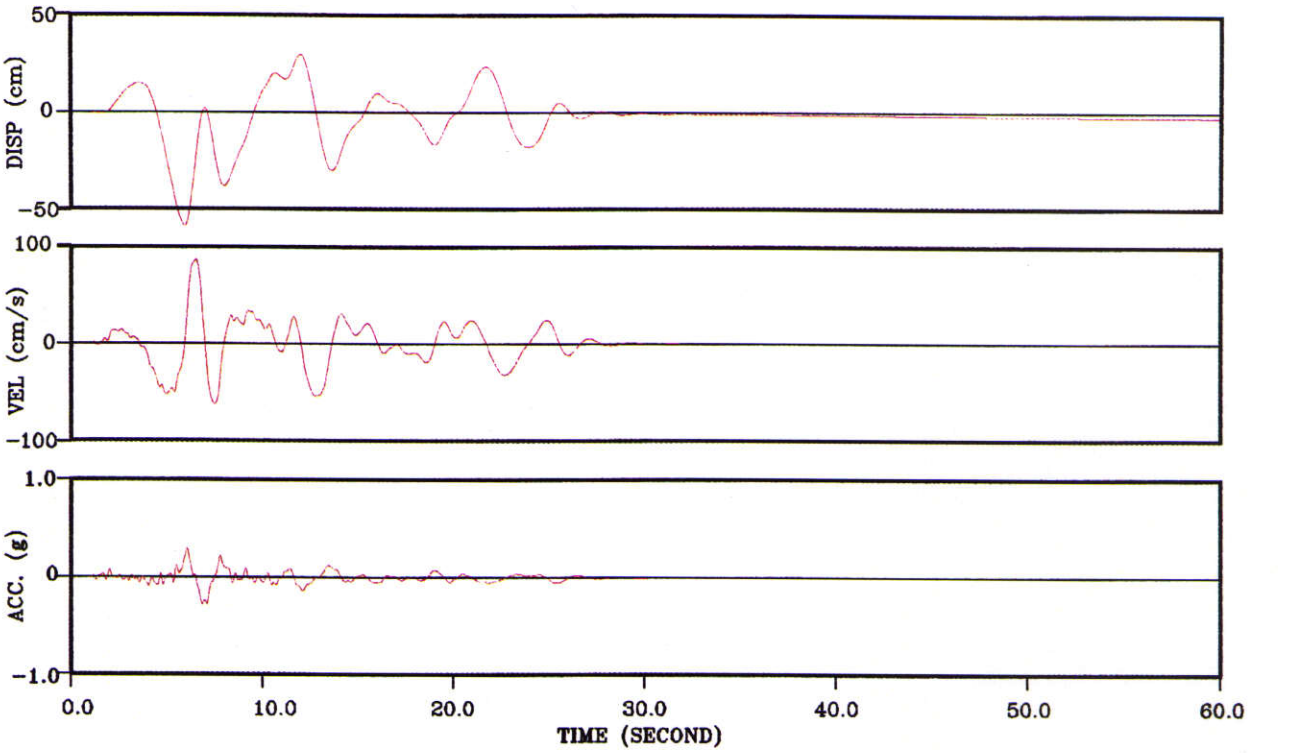

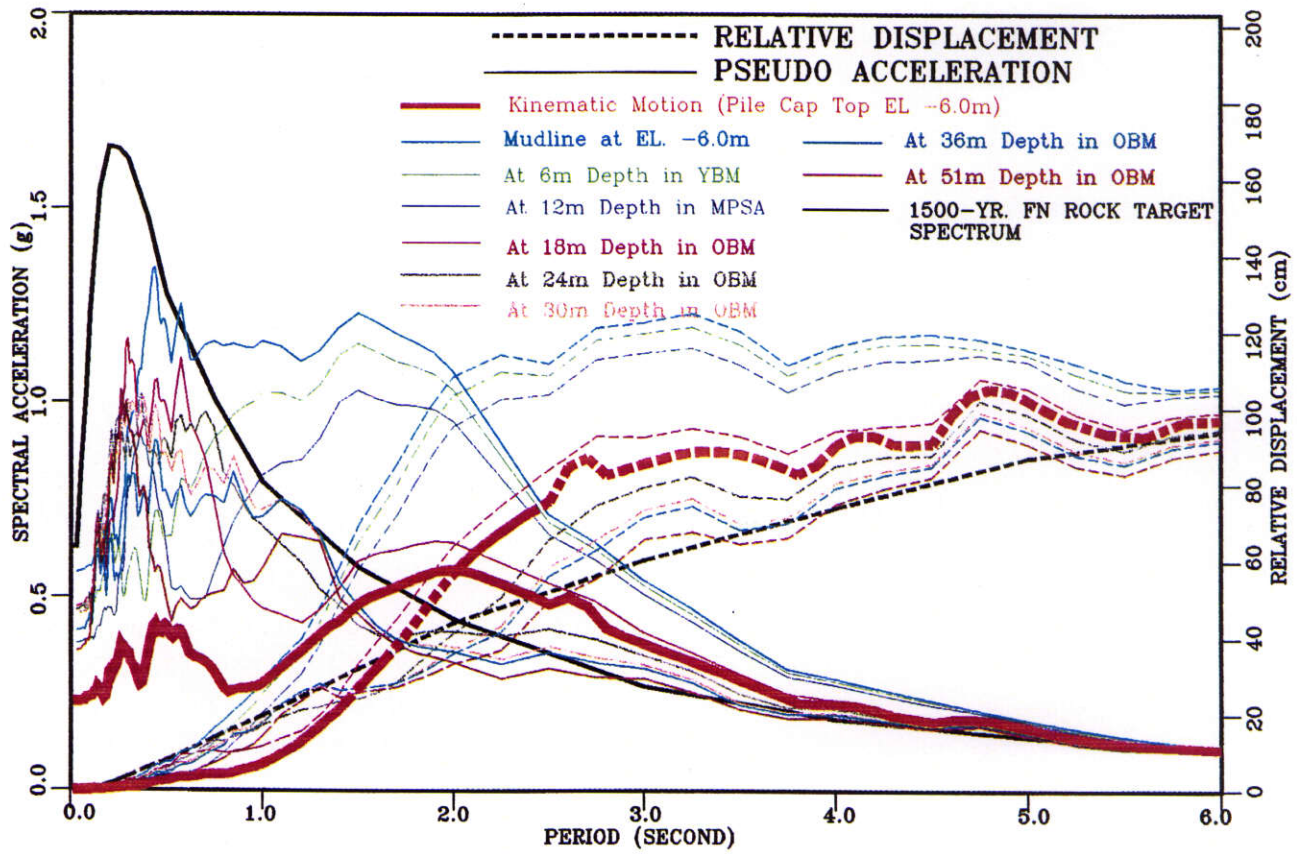

KINEMATIC AND DEPTH-VARYING FREE FIELD MOTIONS
PIER E07, INPUT ROCK MOTION SET 4, FAULT NORMAL COMPONENT
SFOBB East Span Seismic Safety Project

PLATE 8-72

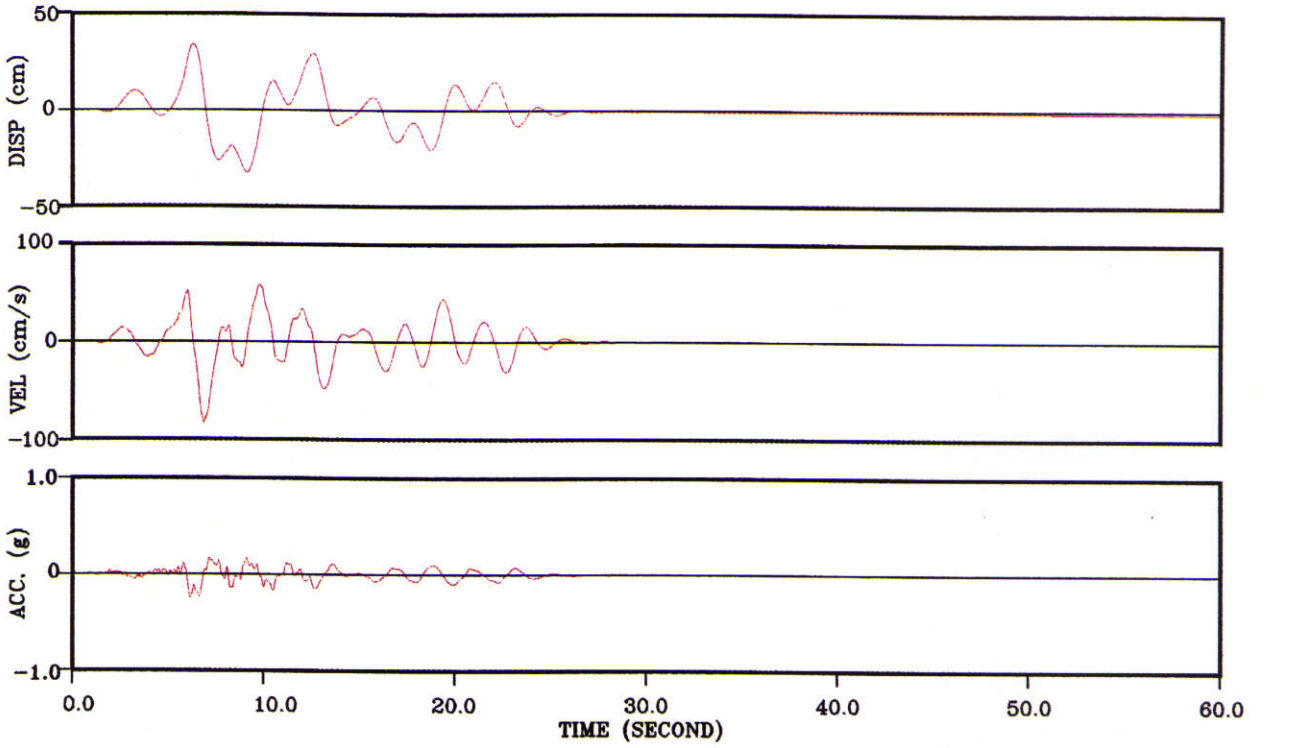

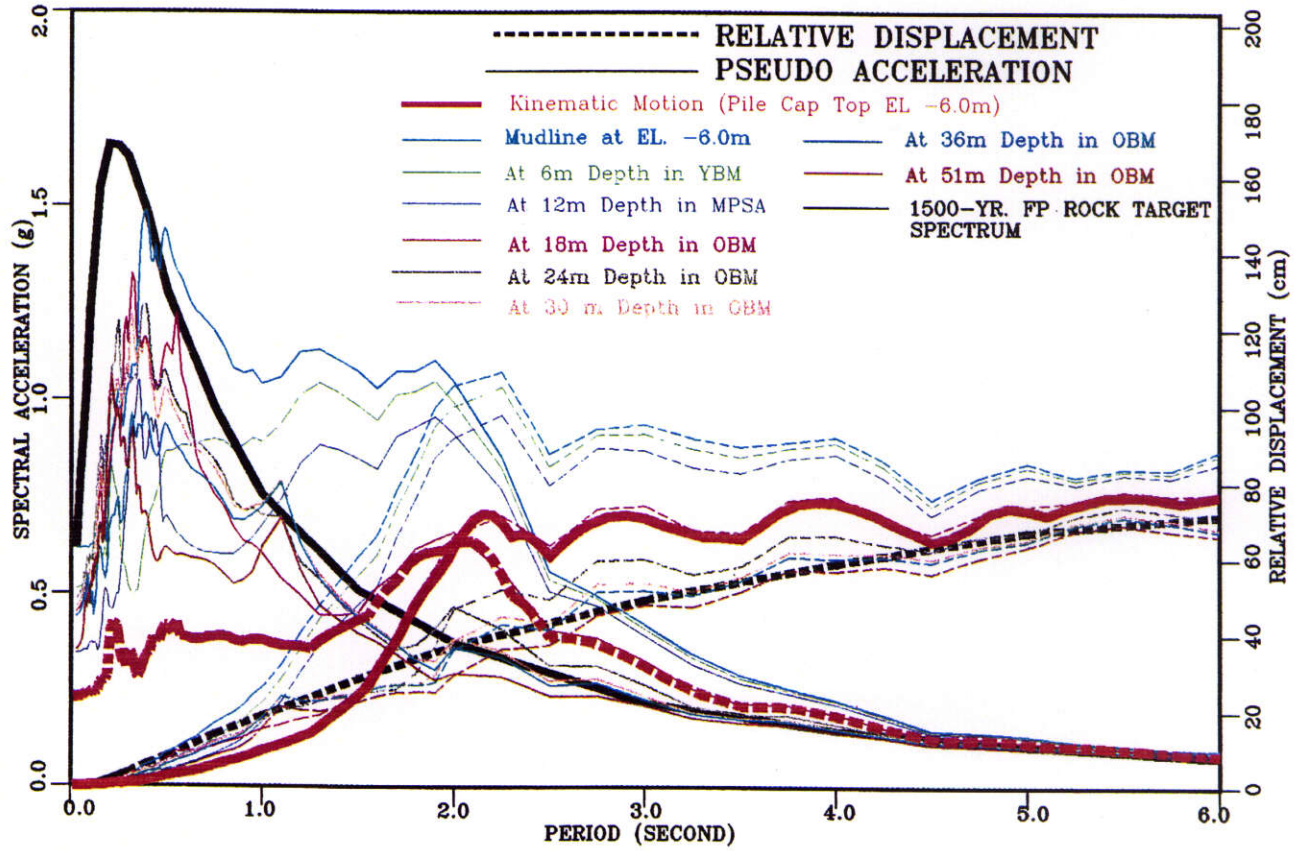

KINEMATIC AND DEPTH-VARYING FREE FIELD MOTIONS
PIER E07, INPUT ROCK MOTION SET 4, FAULT PARALLEL COMPONENT
SFOBB East Span Seismic Safety Project

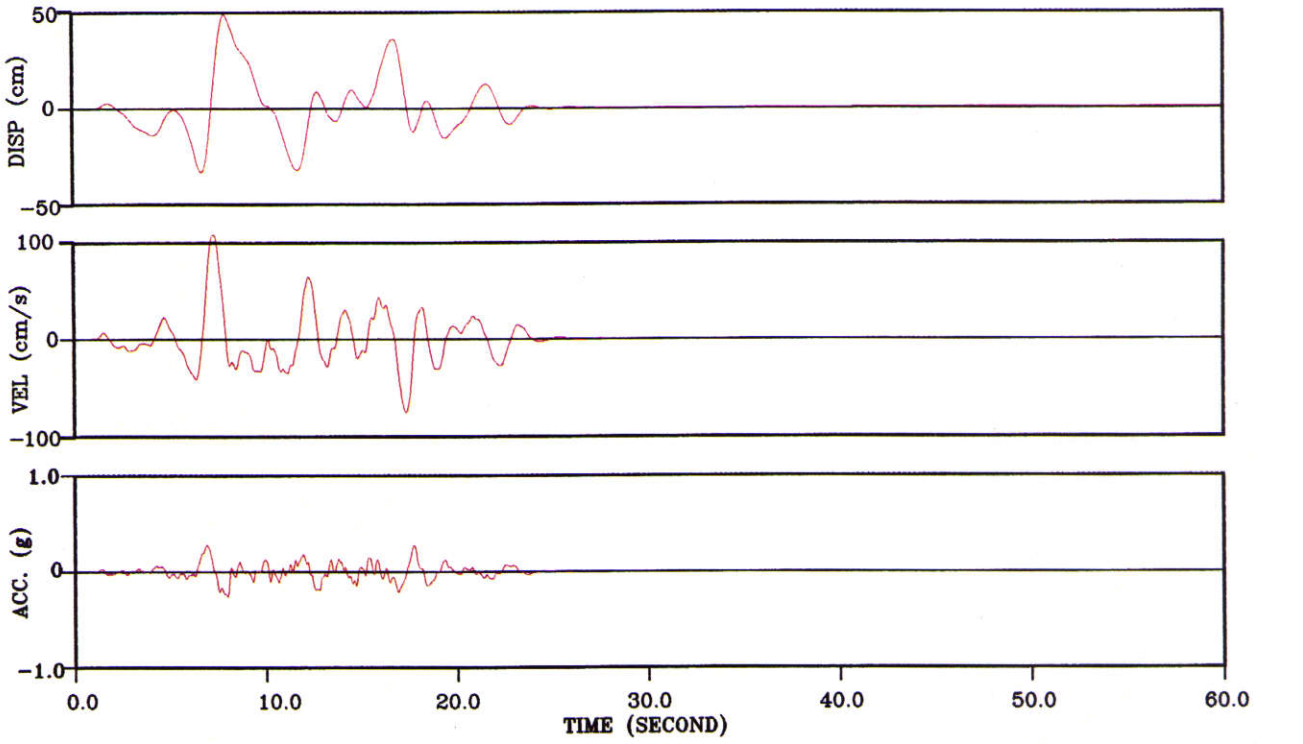

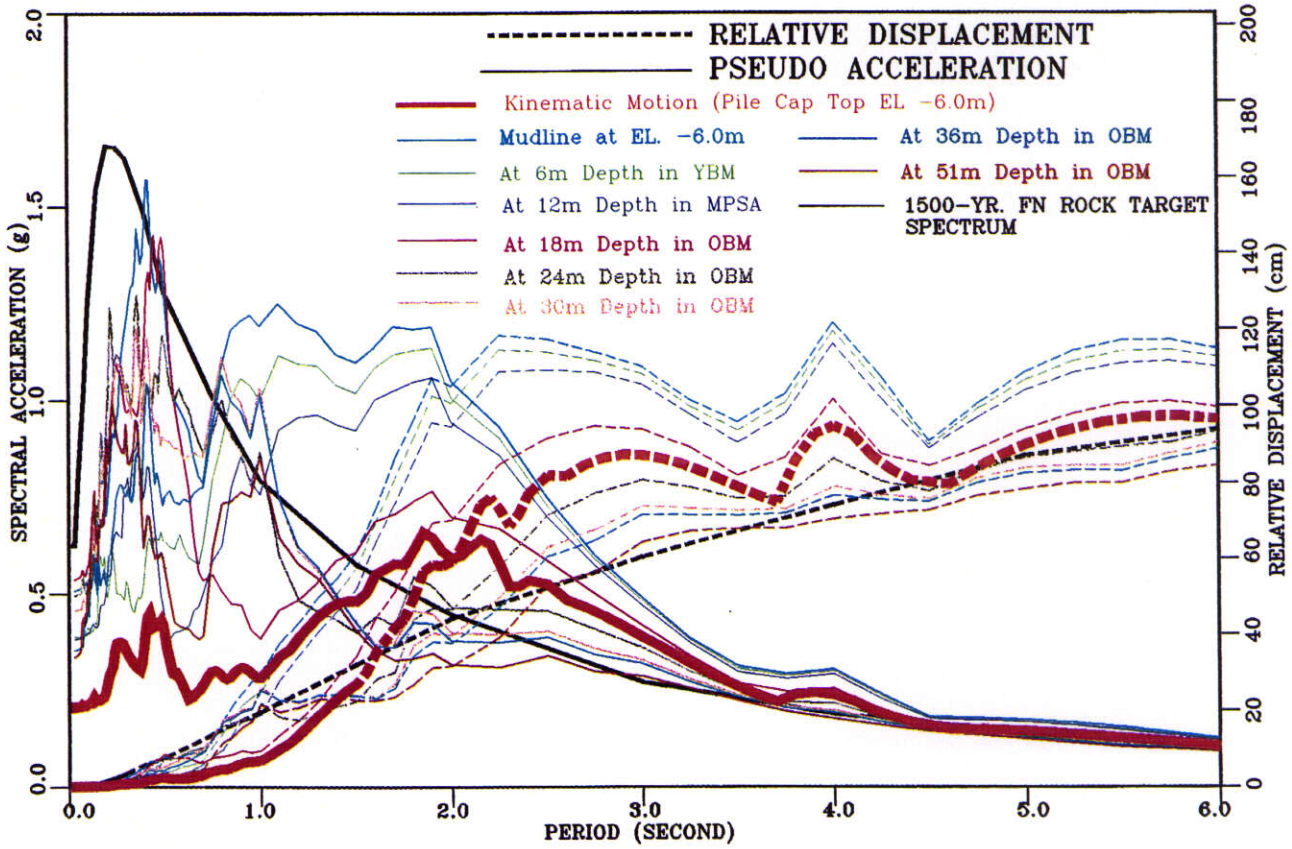

KINEMATIC AND DEPTH-VARYING FREE FIELD MOTIONS
PIER E07, INPUT ROCK MOTION SET 5, FAULT NORMAL COMPONENT
SFOBB East Span Seismic Safety Project

PLATE 8-74

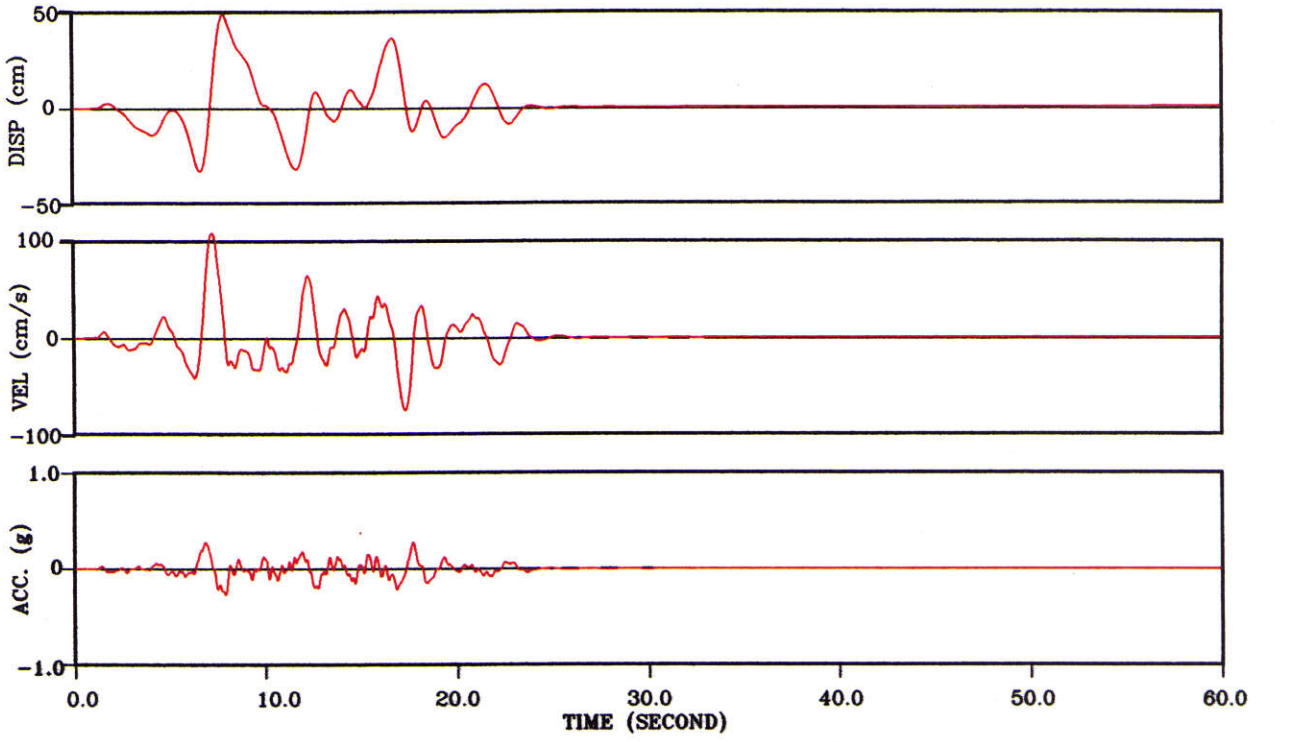

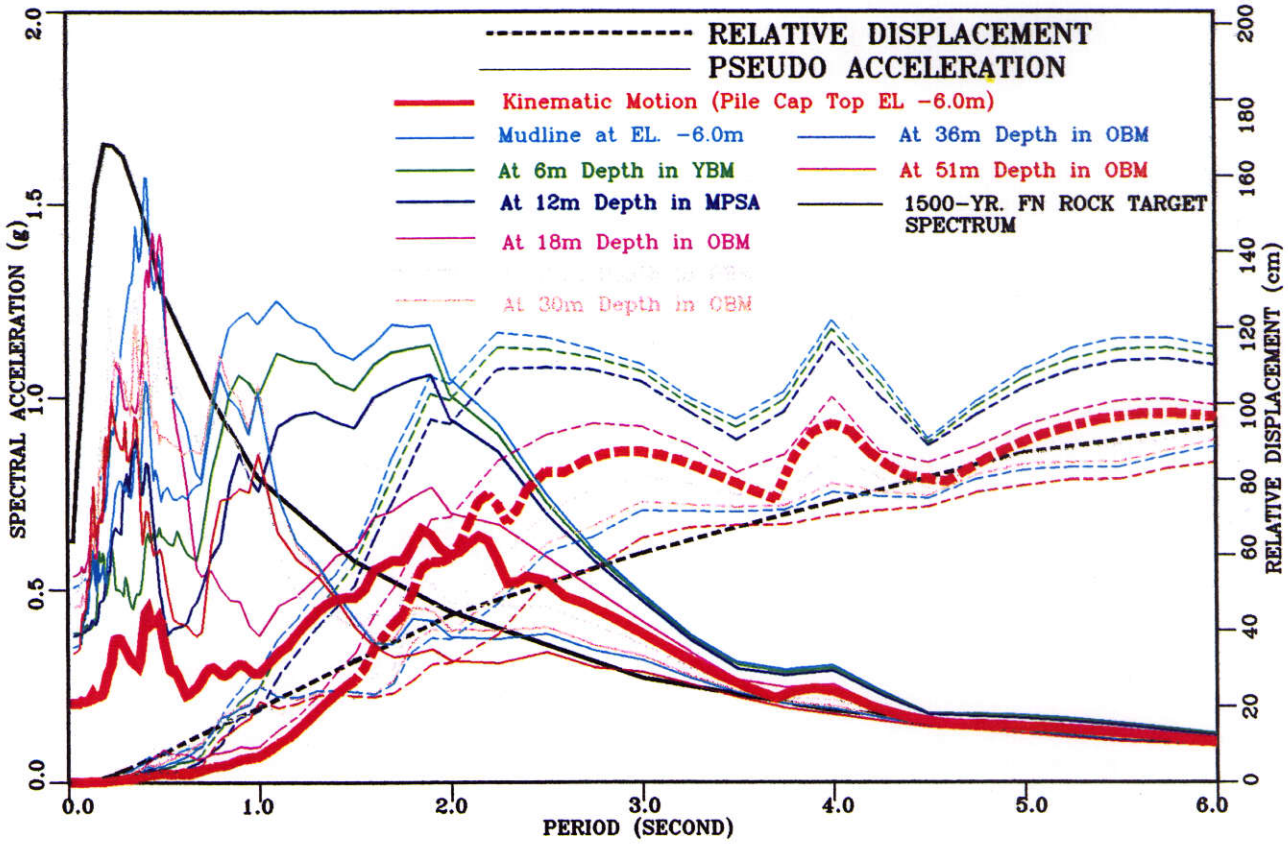

KINEMATIC AND DEPTH-VARYING FREE FIELD MOTIONS
PIER E07, INPUT ROCK MOTION SET 5, FAULT NORMAL COMPONENT
SFOBB East Span Seismic Safety Project

PLATE 8-75

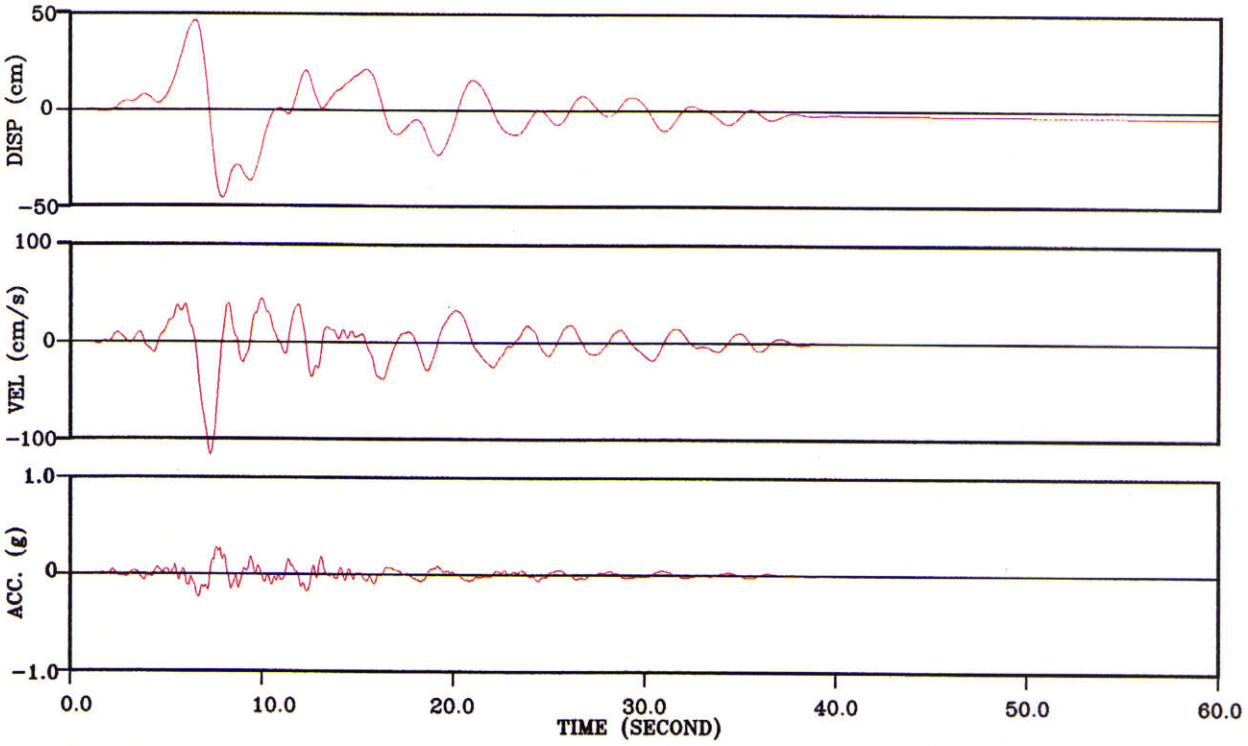

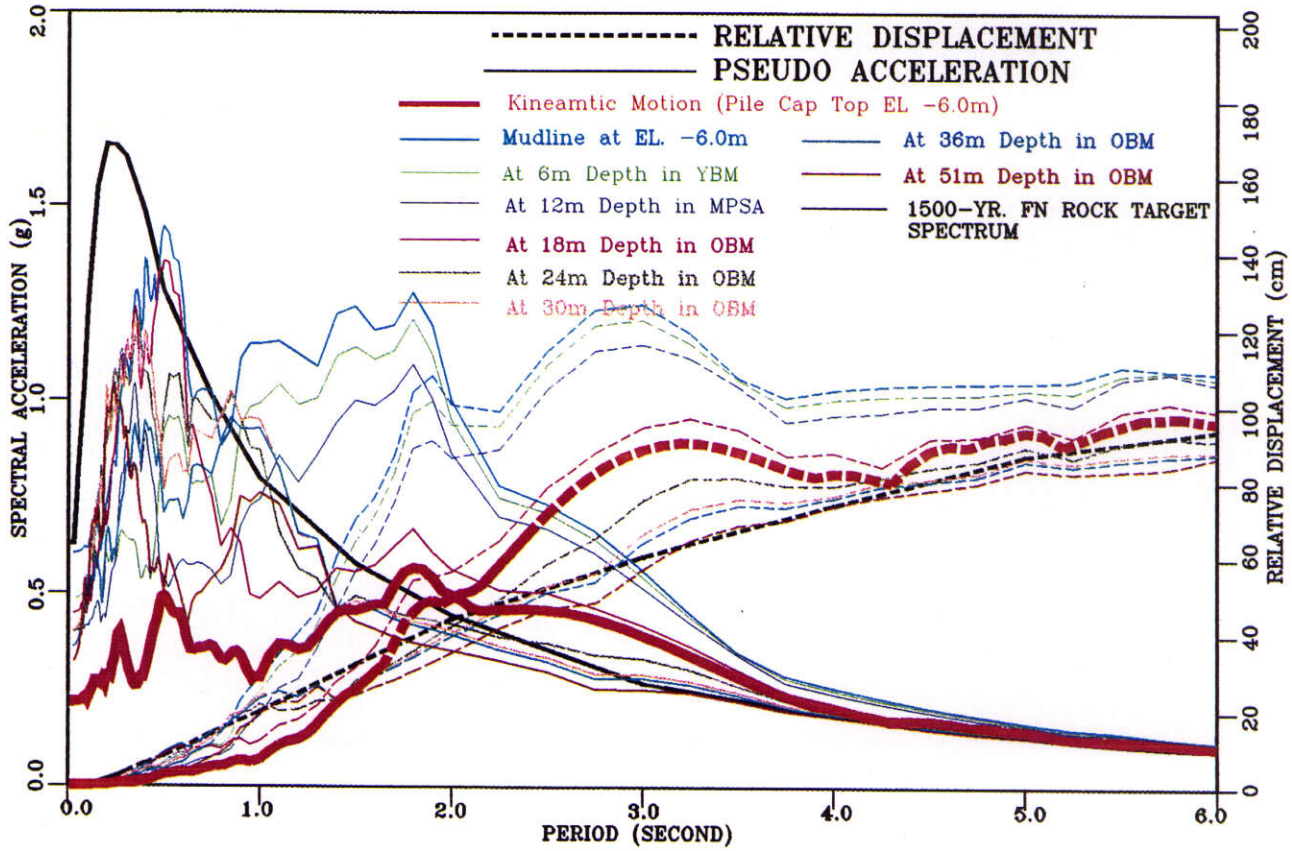

KINEMATIC AND DEPTH-VARYING FREE FIELD MOTIONS
PIER E07, INPUT ROCK MOTION SET 6, FAULT NORMAL COMPONENT
SFOBB East Span Seismic Safety Project

PLATE 8-76

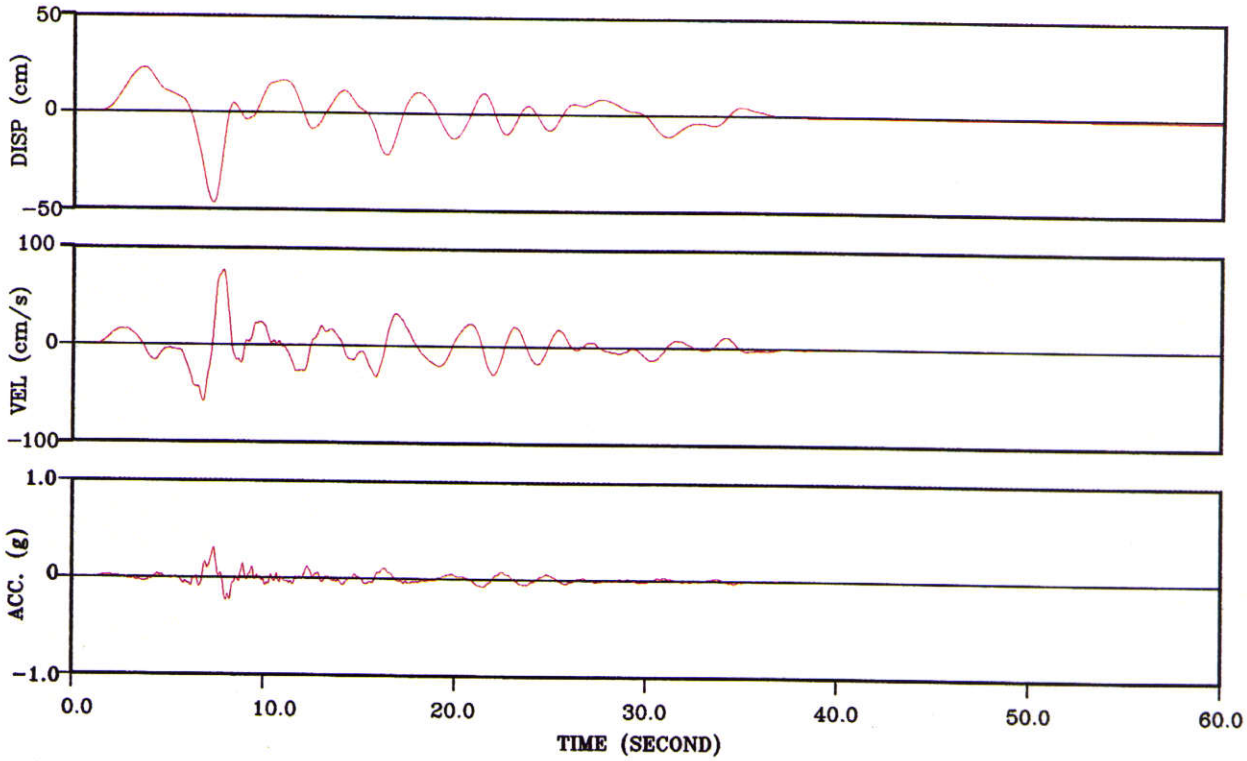

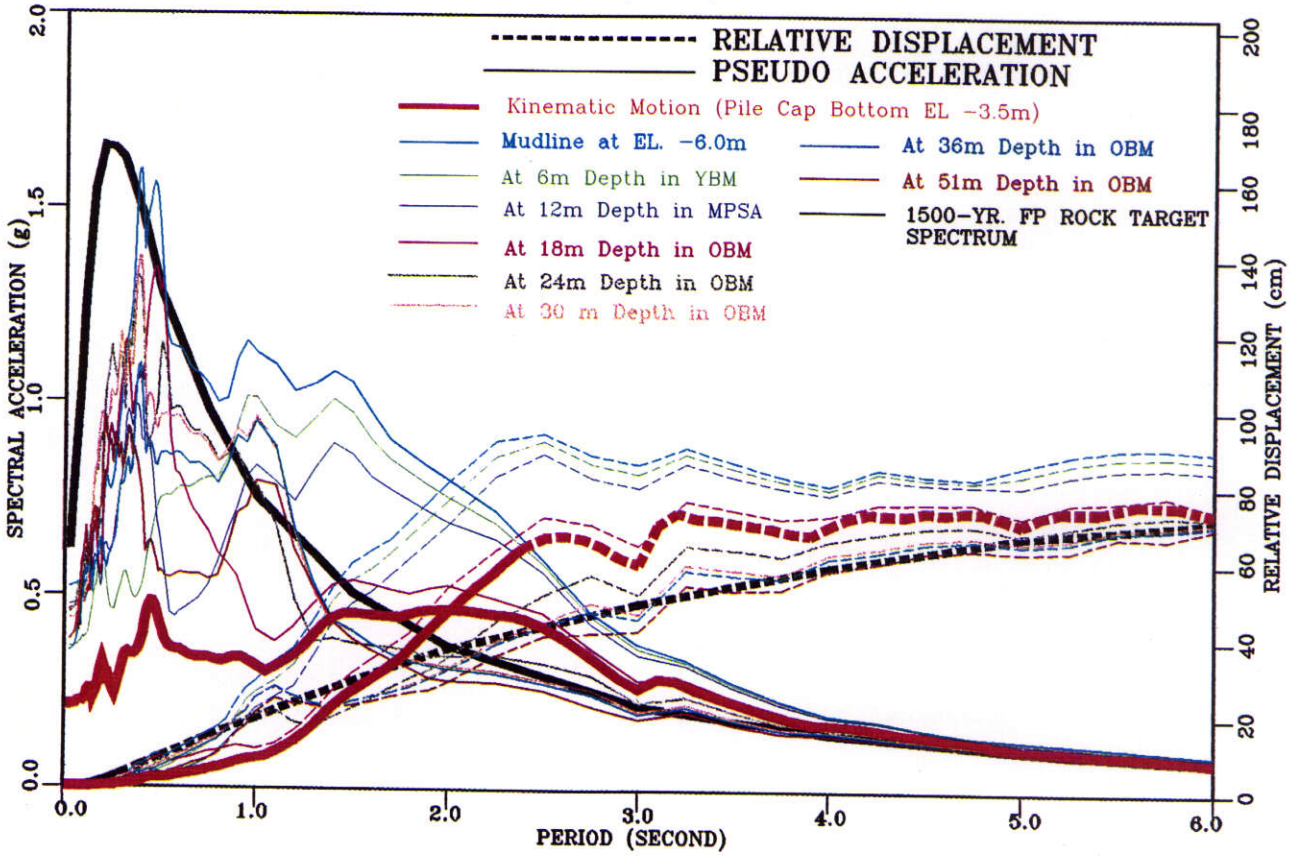

KINEMATIC AND DEPTH-VARYING FREE FIELD MOTIONS
PIER E07, INPUT ROCK MOTION SET 6, FAULT PARALLEL COMPONENT
SFOBB East Span Seismic Safety Project

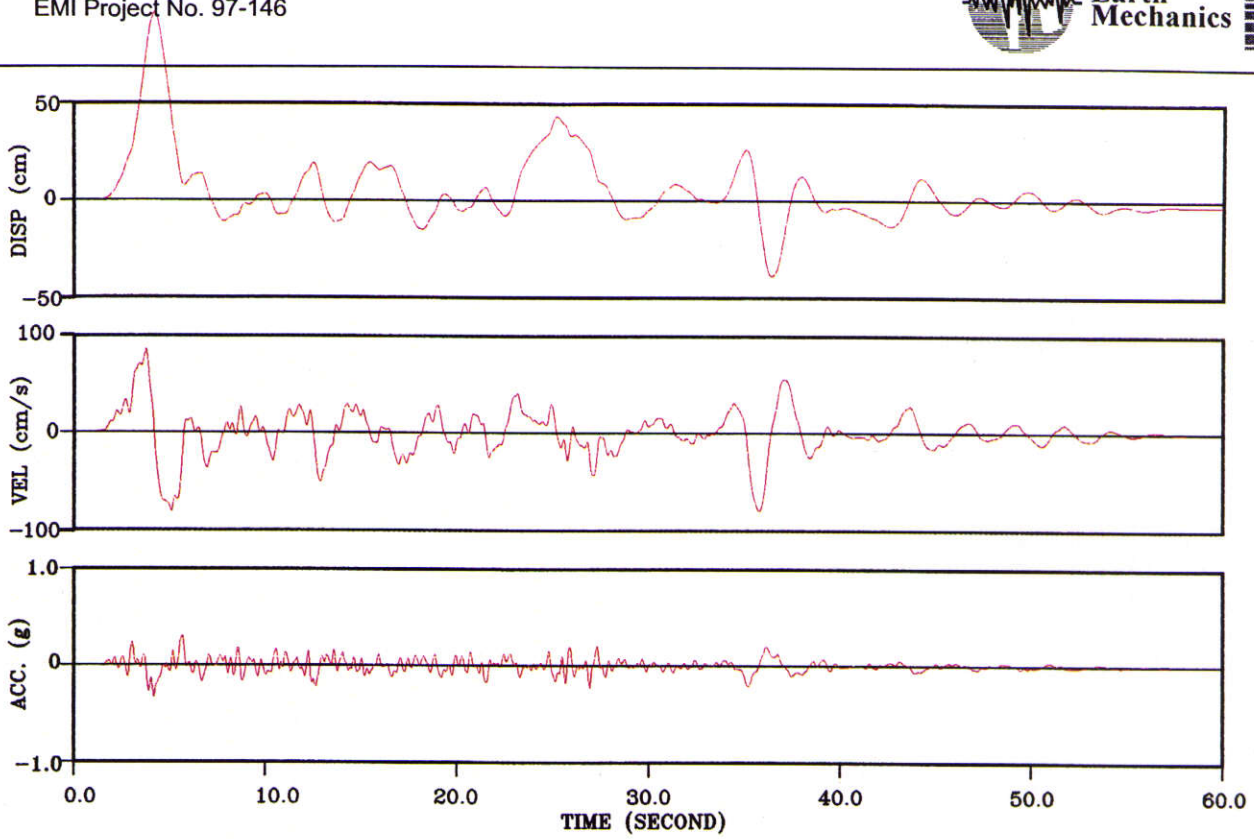

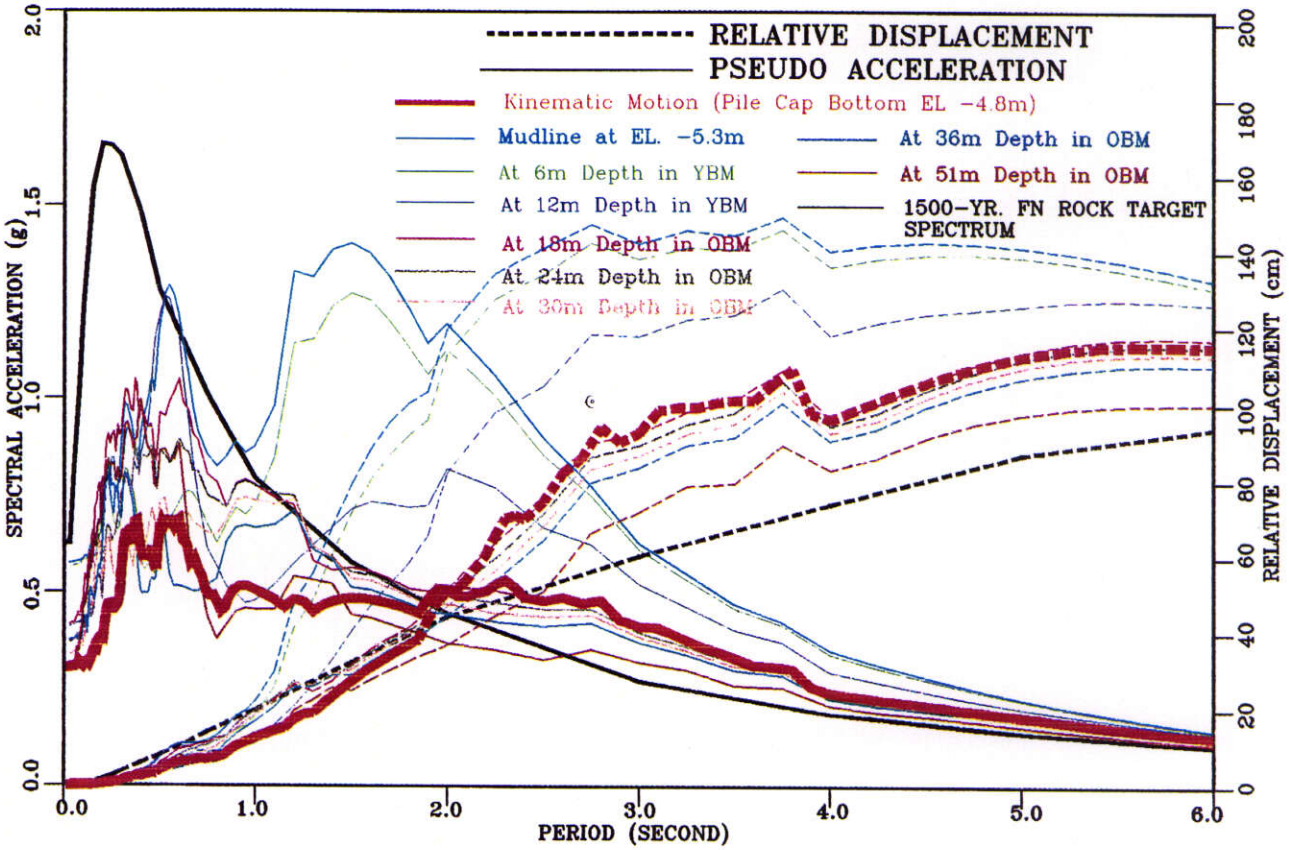

KINEMATIC AND DEPTH-VARYING FREE FIELD MOTIONS
PIER E08, INPUT ROCK MOTION SET 1, FAULT NORMAL COMPONENT
SFOBB East Span Seismic Safety Project

PLATE 8-78

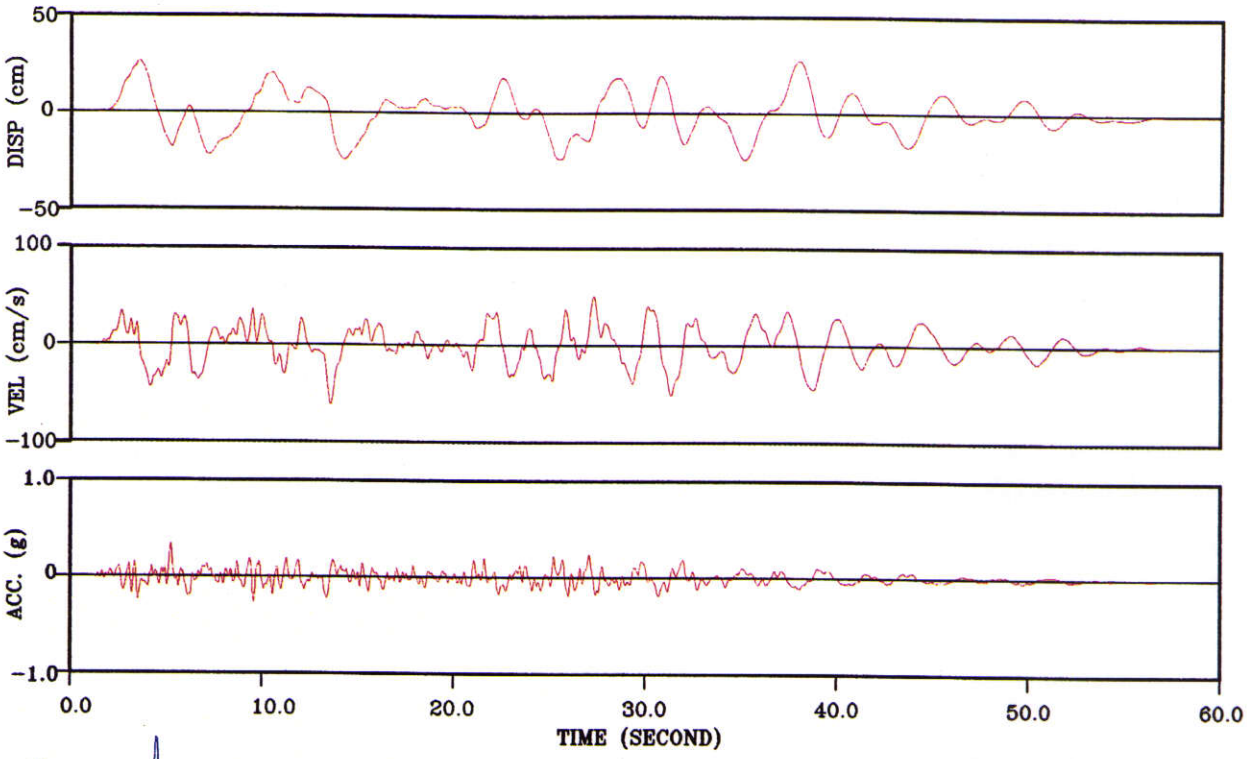

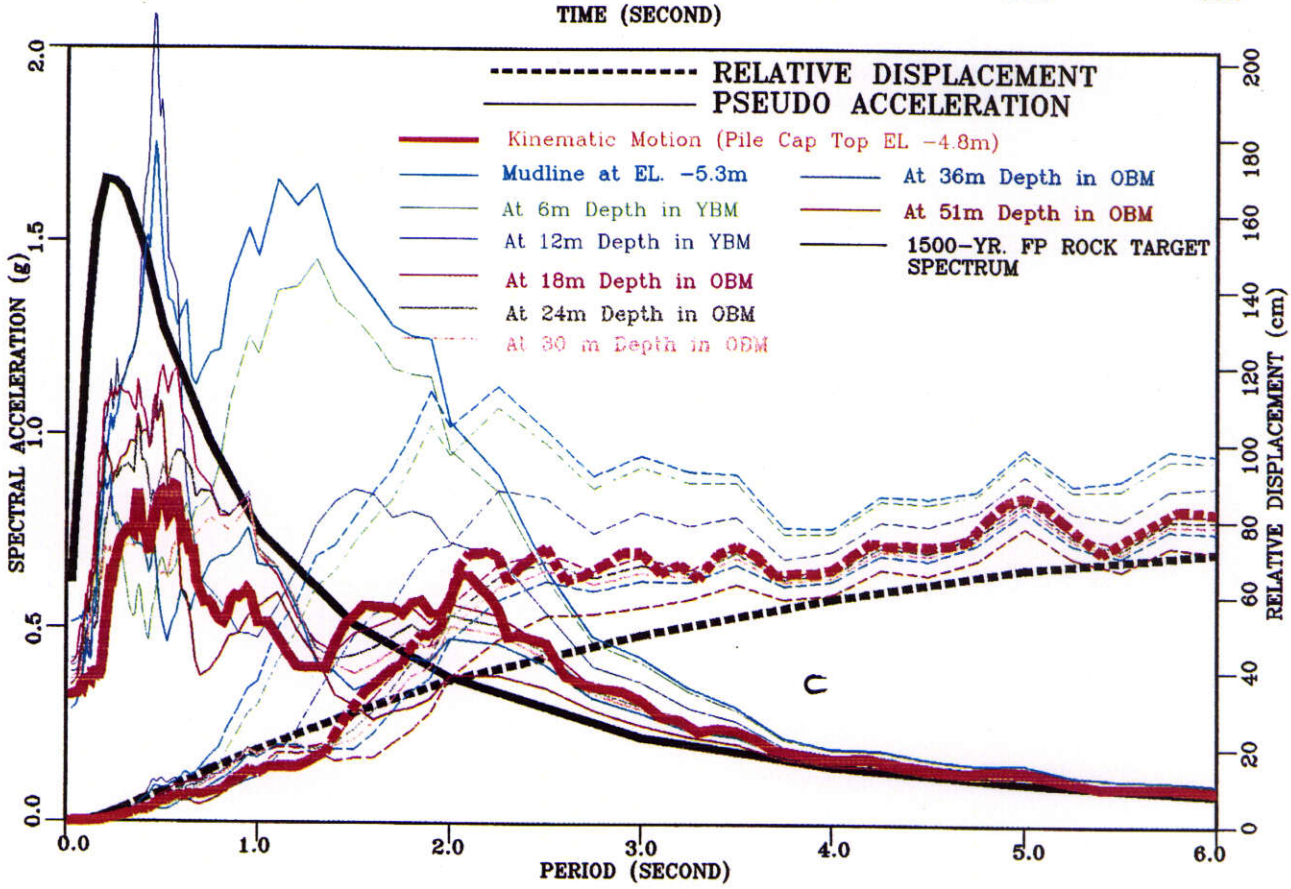

KINEMATIC AND DEPTH-VARYING FREE FIELD MOTIONS
PIER E08, INPUT ROCK MOTION SET 1, FAULT PARALLEL COMPONENT
SFOBB East Span Seismic Safety Project

PLATE 8-79

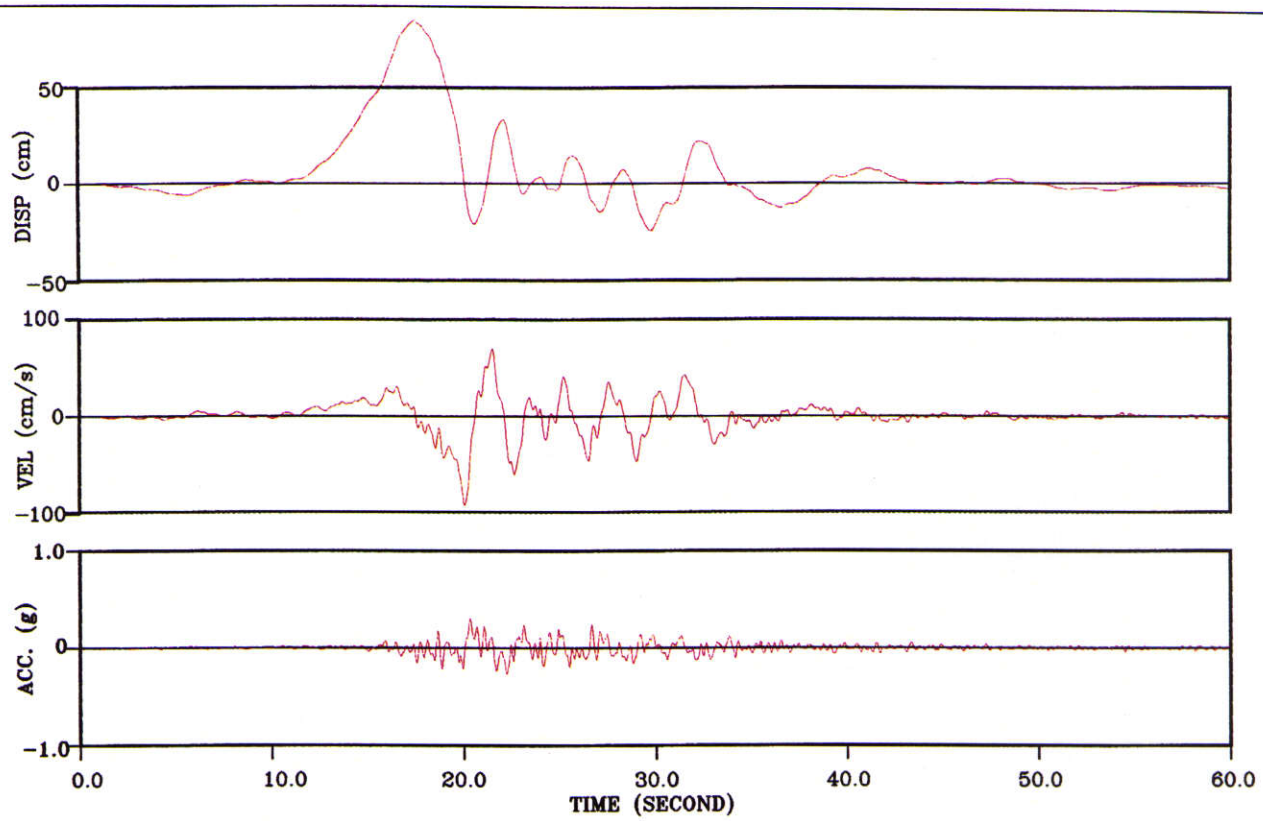

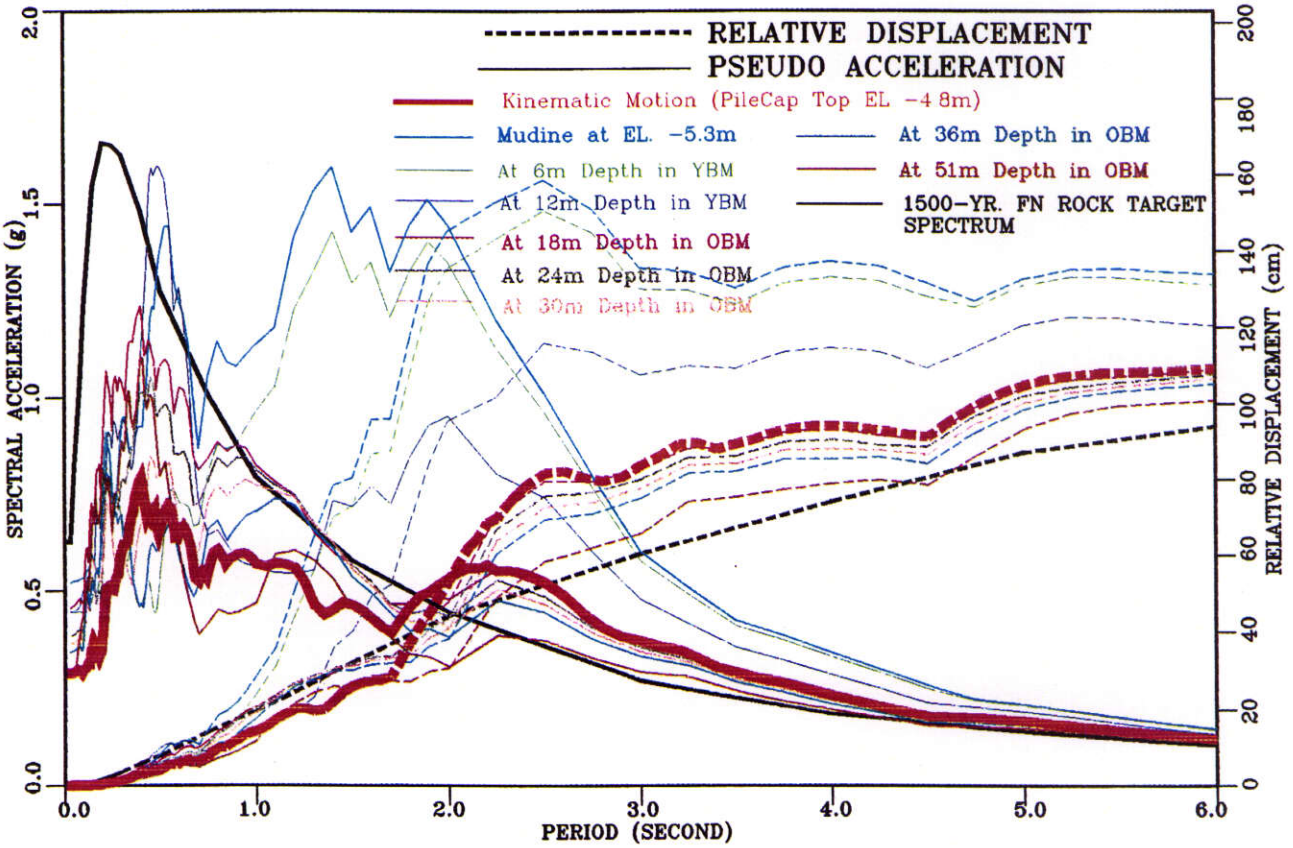

KINEMATIC AND DEPTH-VARYING FREE FIELD MOTIONS
PIER E08, INPUT ROCK MOTION SET 2, FAULT NORMAL COMPONENT
SFOBB East Span Seismic Safety Project

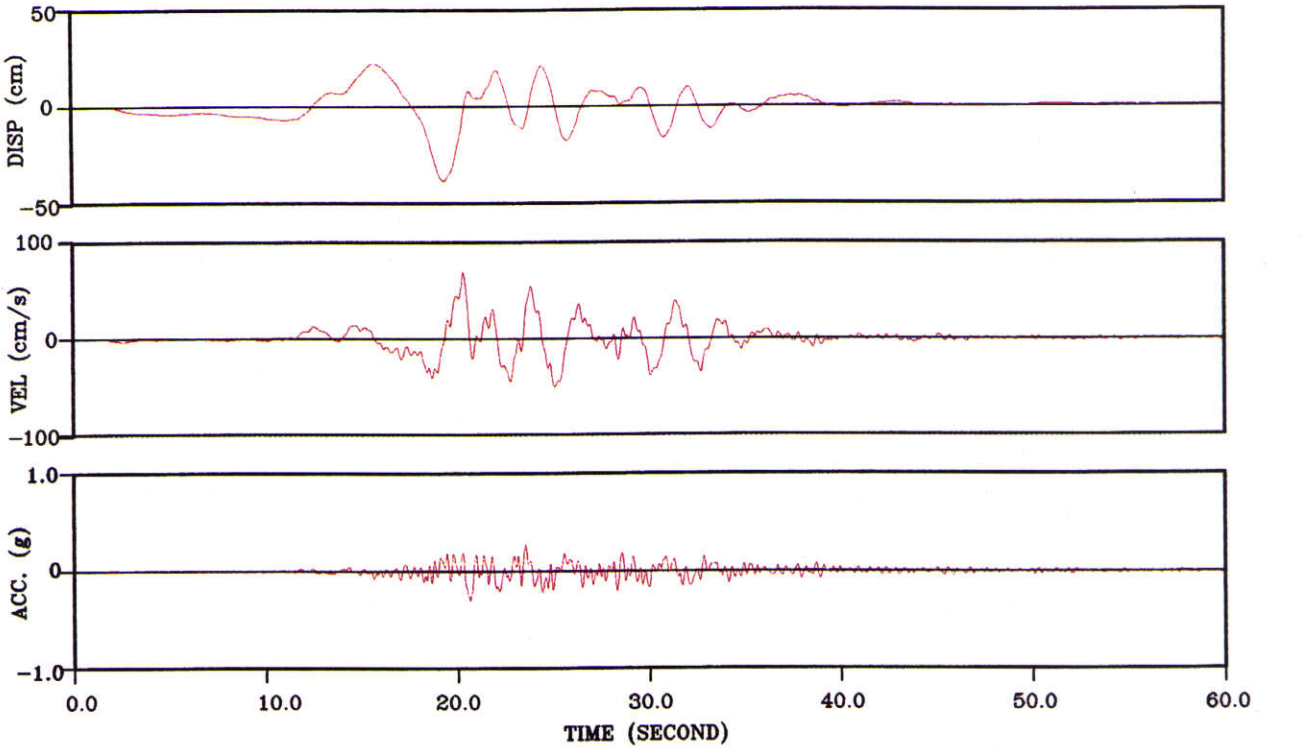

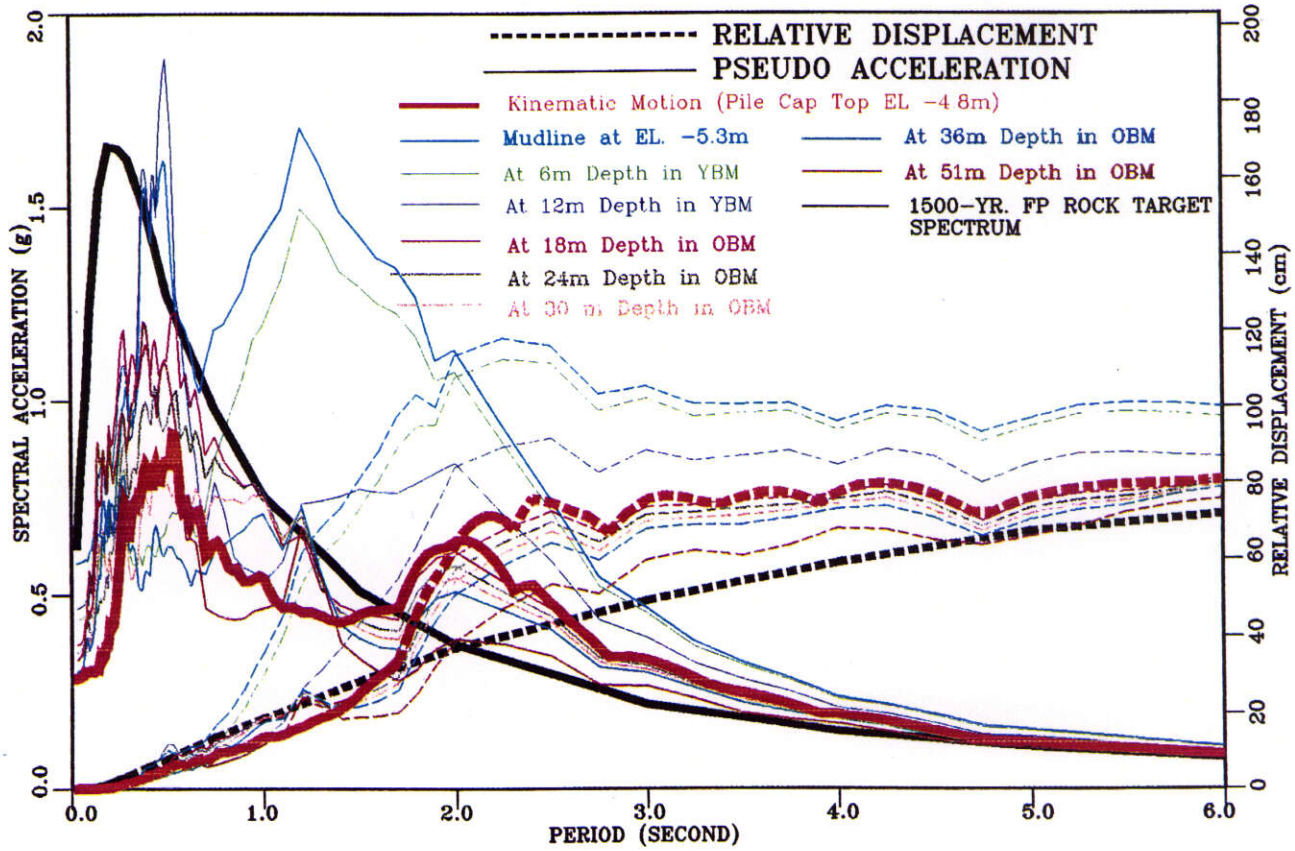

KINEMATIC AND DEPTH-VARYING FREE FIELD MOTIONS
PIER E08, INPUT ROCK MOTION SET 2, FAULT PARALLEL COMPONENT
SFOBB East Span Seismic Safety Project

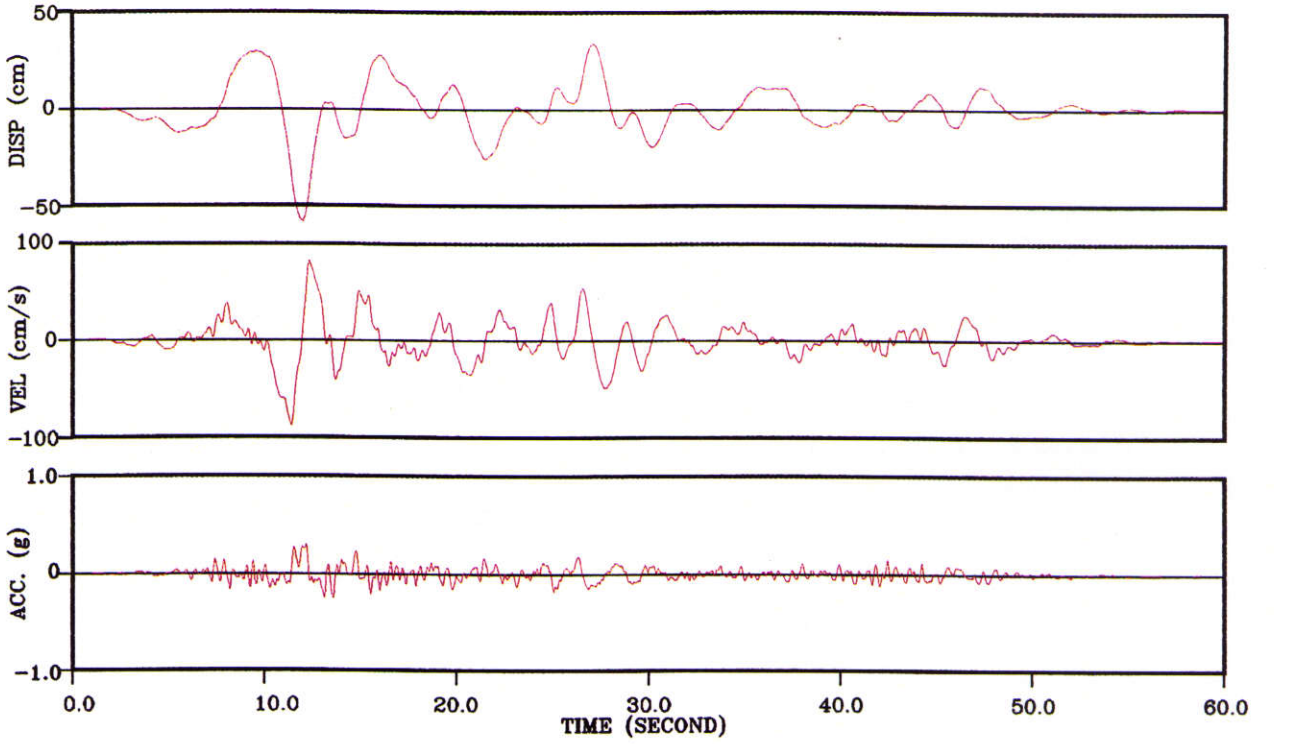

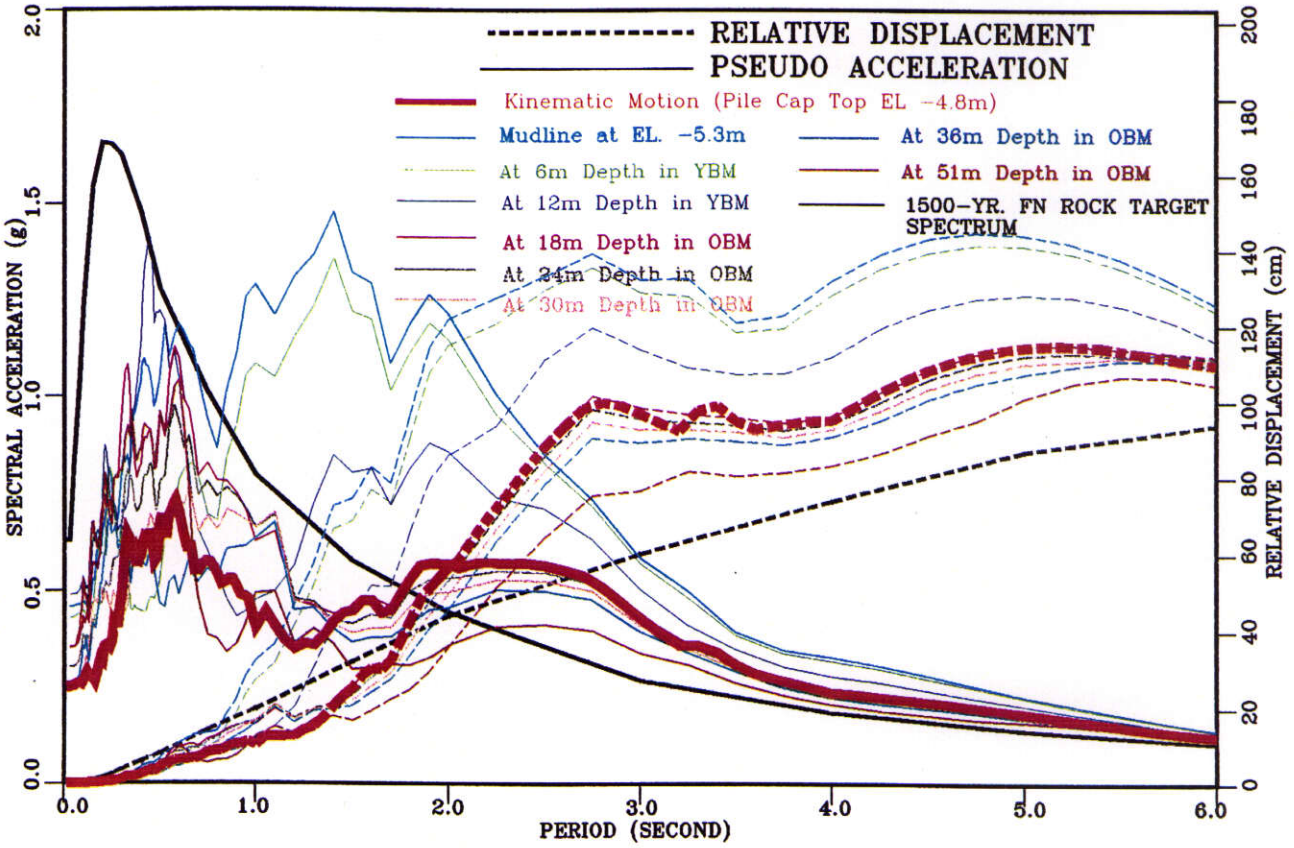

KINEMATIC AND DEPTH-VARYING FREE FIELD MOTIONS
PIER E08, INPUT ROCK MOTION SET 3, FAULT NORMAL COMPONENT
SFOBB East Span Seismic Safety Project

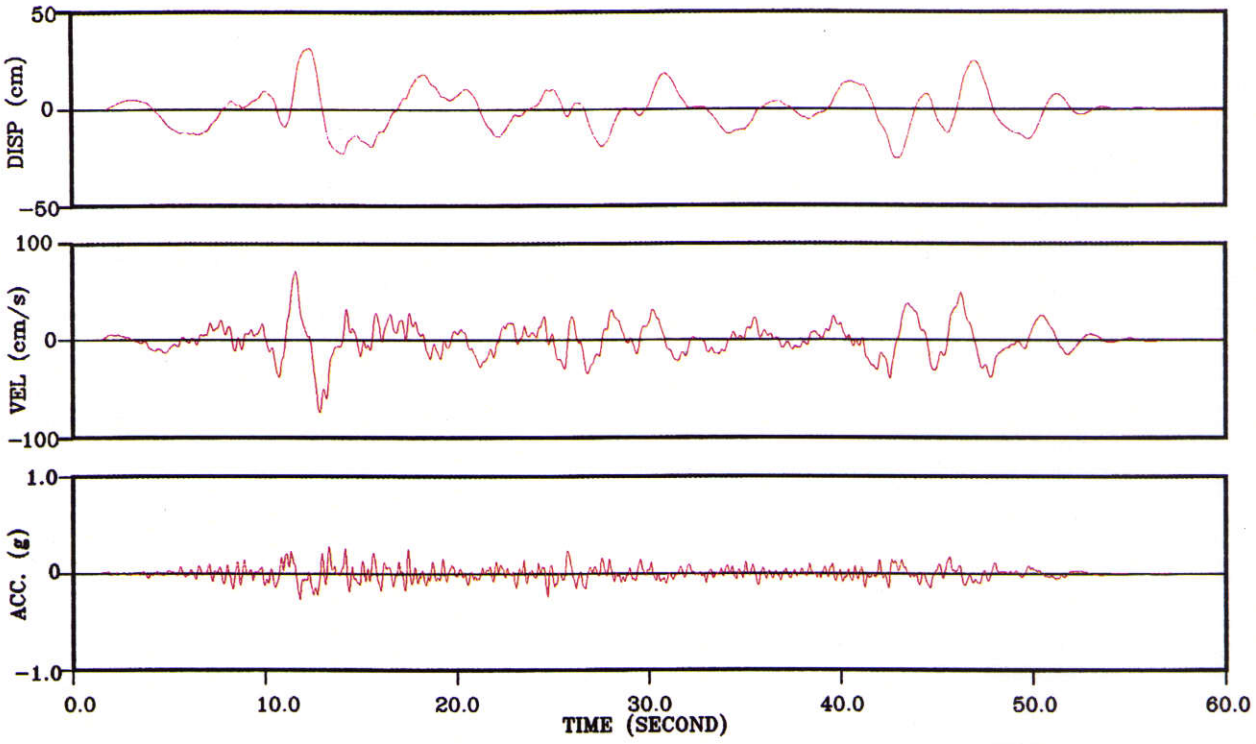

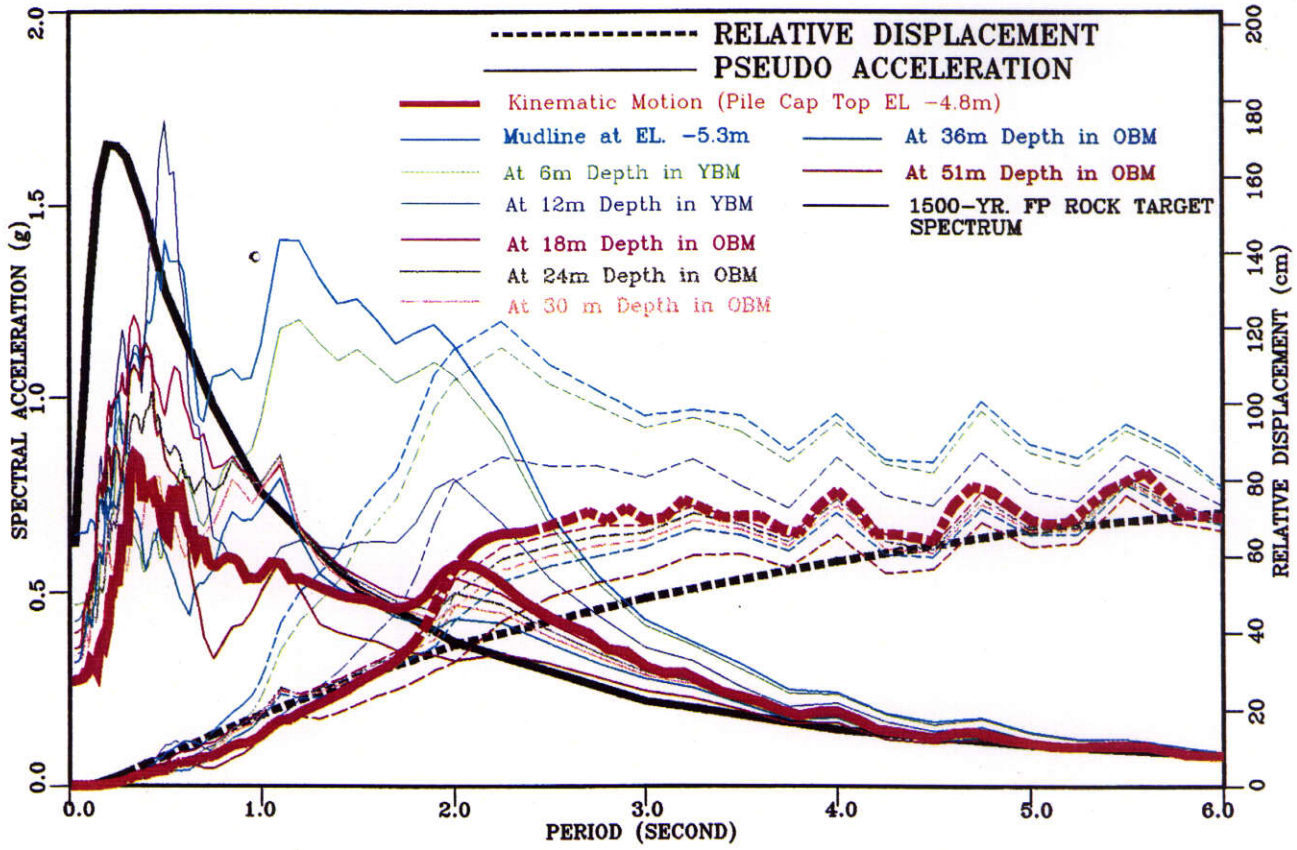

KINEMATIC AND DEPTH-VARYING FREE FIELD MOTIONS
PIER E08, INPUT ROCK MOTION SET 3, FAULT PARALLEL COMPONENT
SFOBB East Span Seismic Safety Project

PLATE 8-83

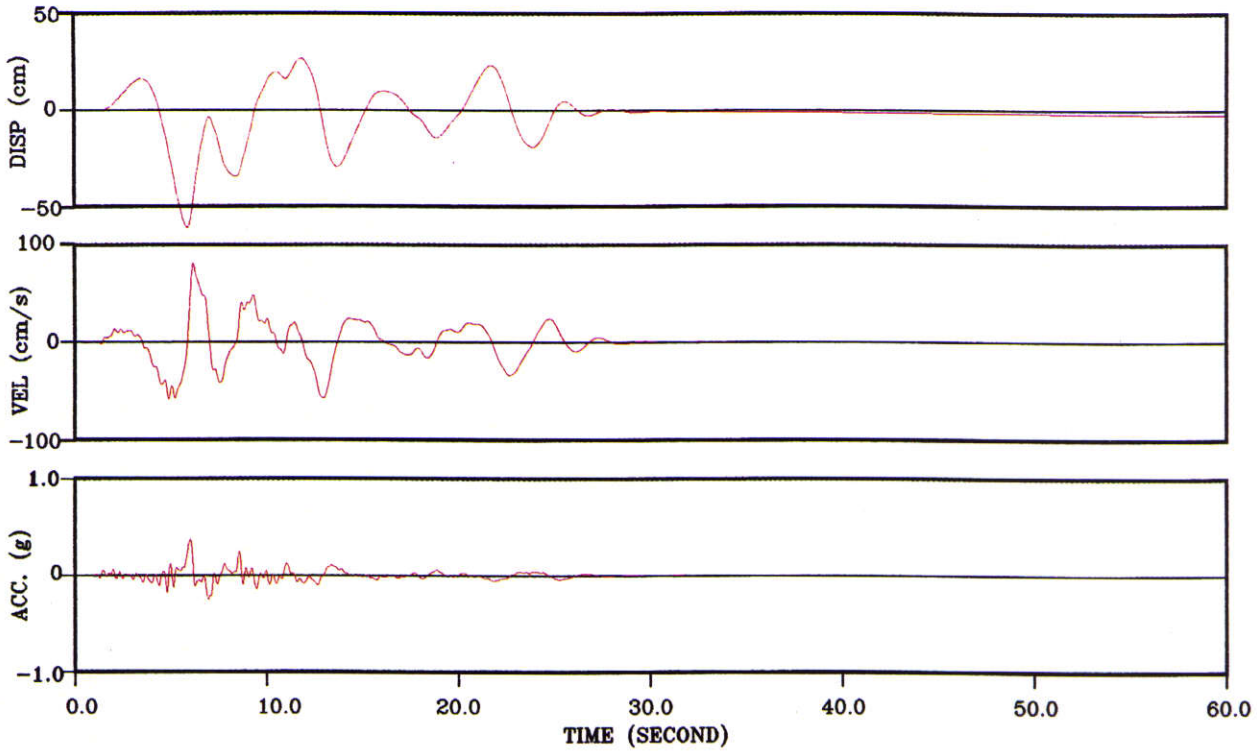

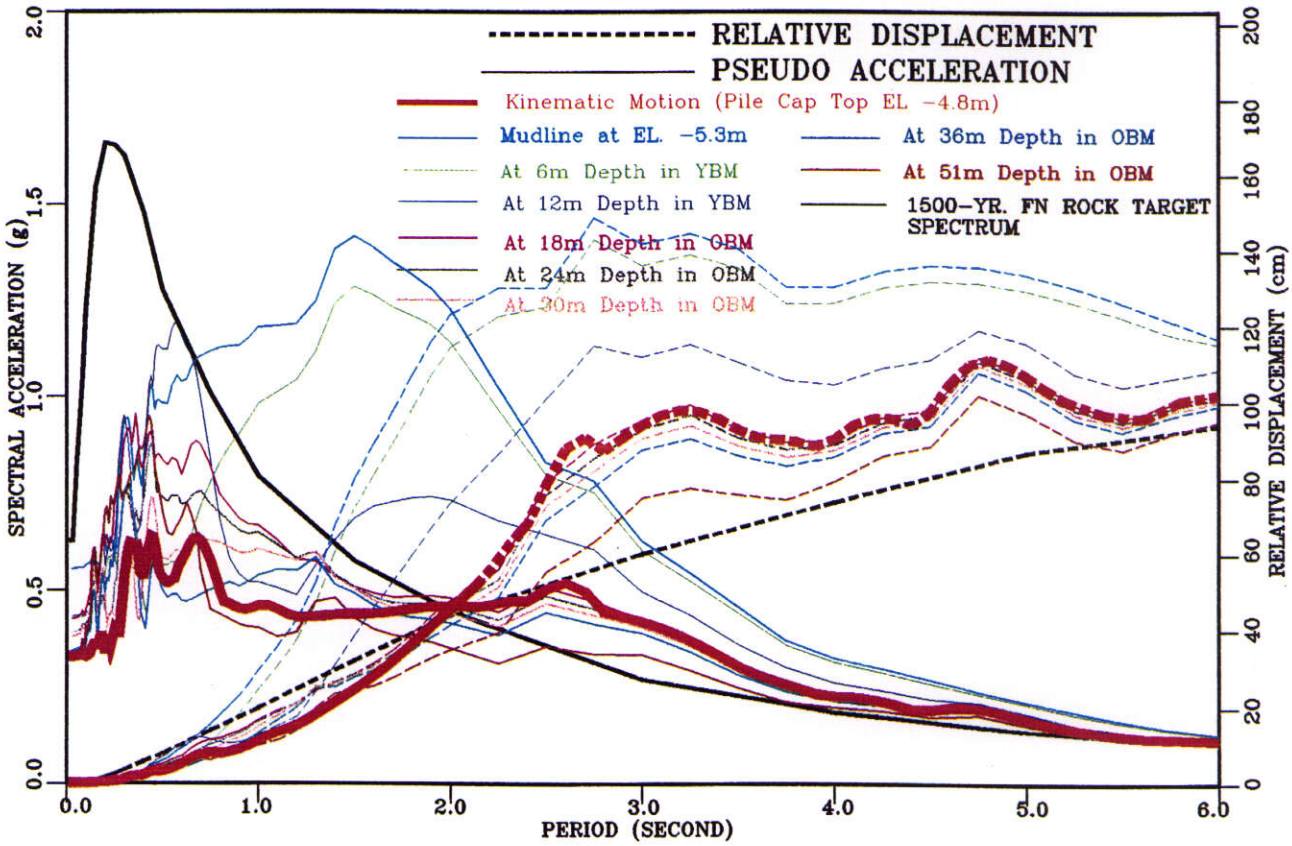

KINEMATIC AND DEPTH-VARYING FREE FIELD MOTIONS
PIER E08, INPUT ROCK MOTION SET 4, FAULT NORMAL COMPONENT
SFOBB East Span Seismic Safety Project

PLATE 8-84

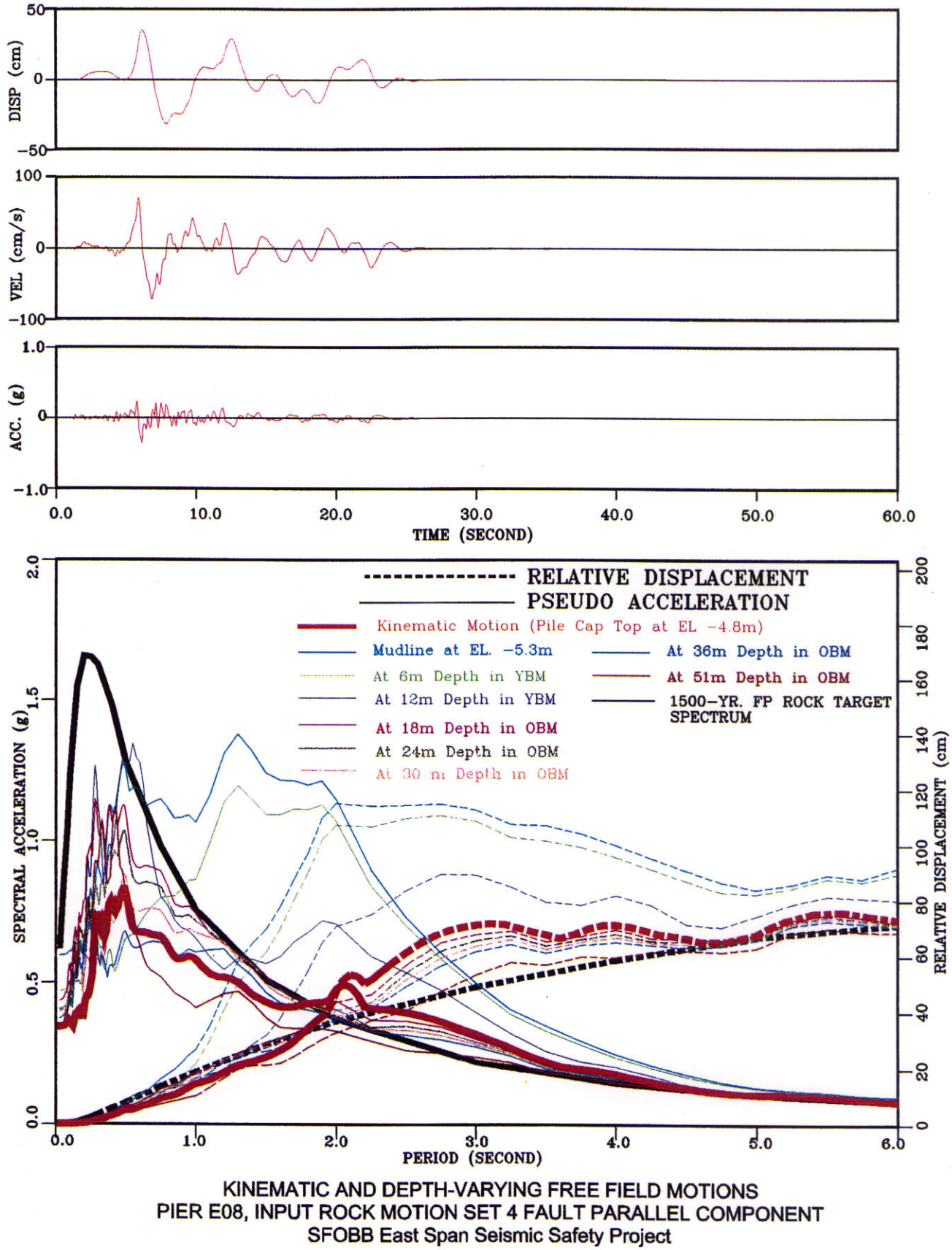

KINEMATIC AND DEPTH-VARYING FREE FIELD MOTIONS
PIER E08, INPUT ROCK MOTION SET 4 FAULT PARALLEL COMPONENT
SFOBB East Span Seismic Safety Project

PLATE 8-85

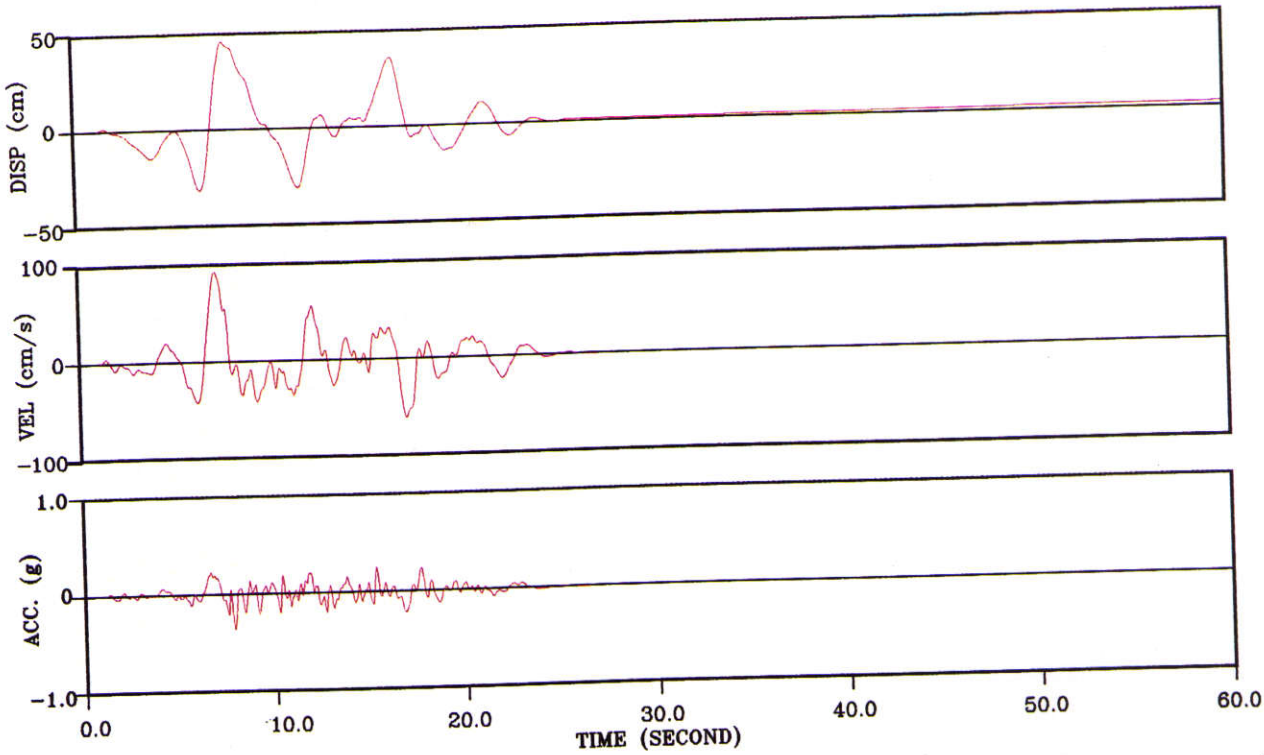

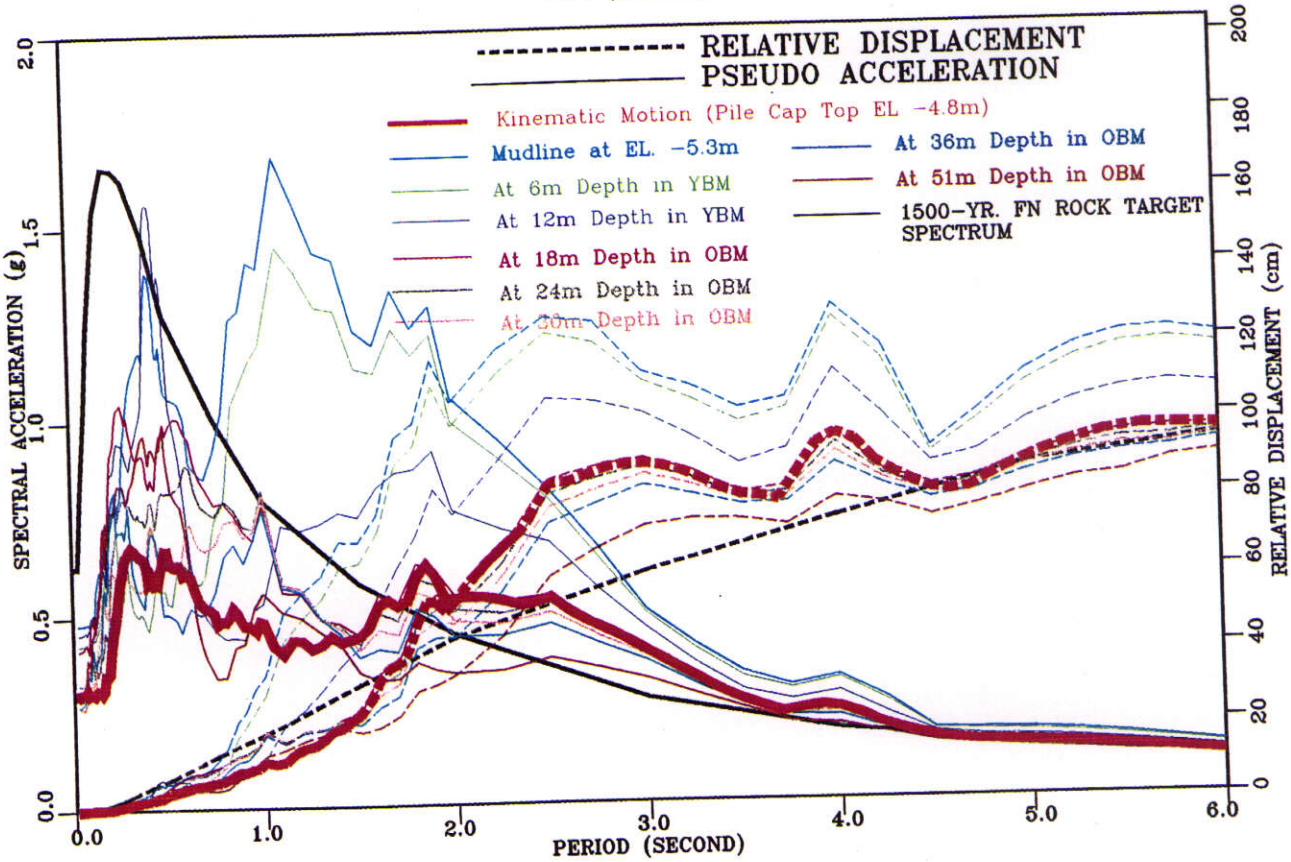

KINEMATIC AND DEPTH-VARYING FREE FIELD MOTIONS
PIER E08, INPUT ROCK MOTION SET 5, FAULT NORMAL COMPONENT
SFOBB East Span Seismic Safety Project

PLATE 8-86

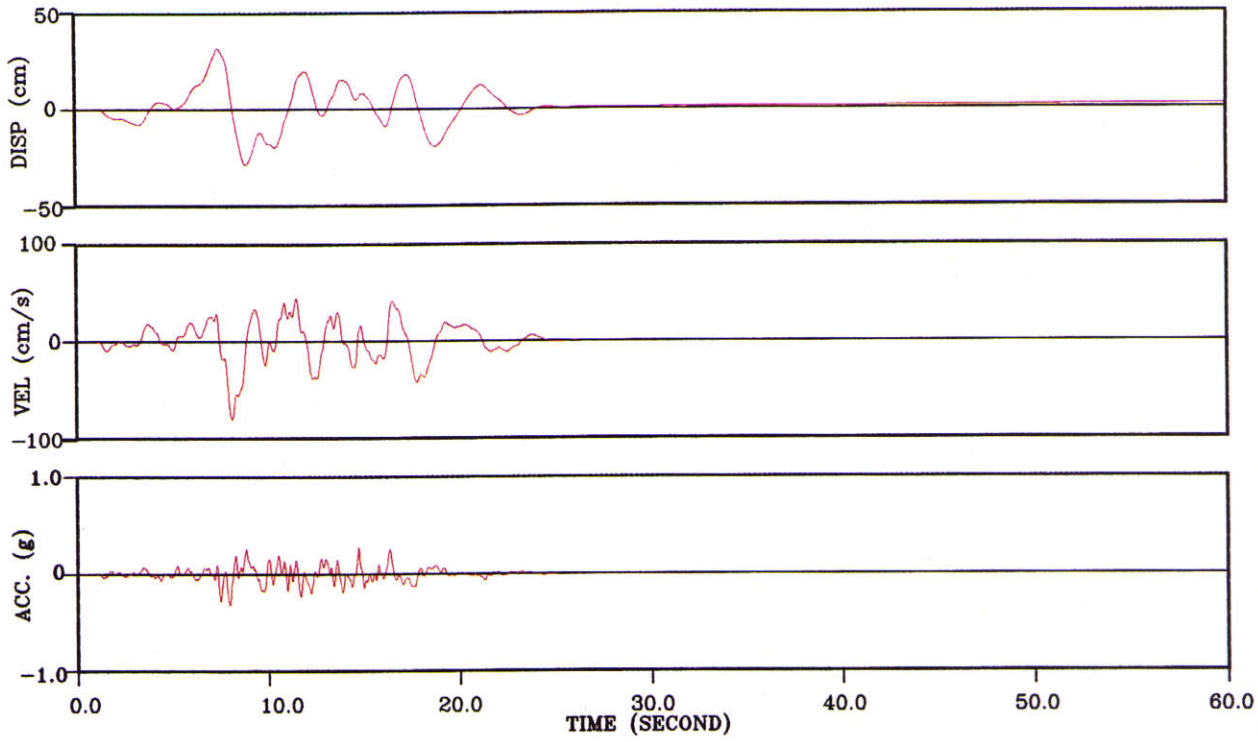

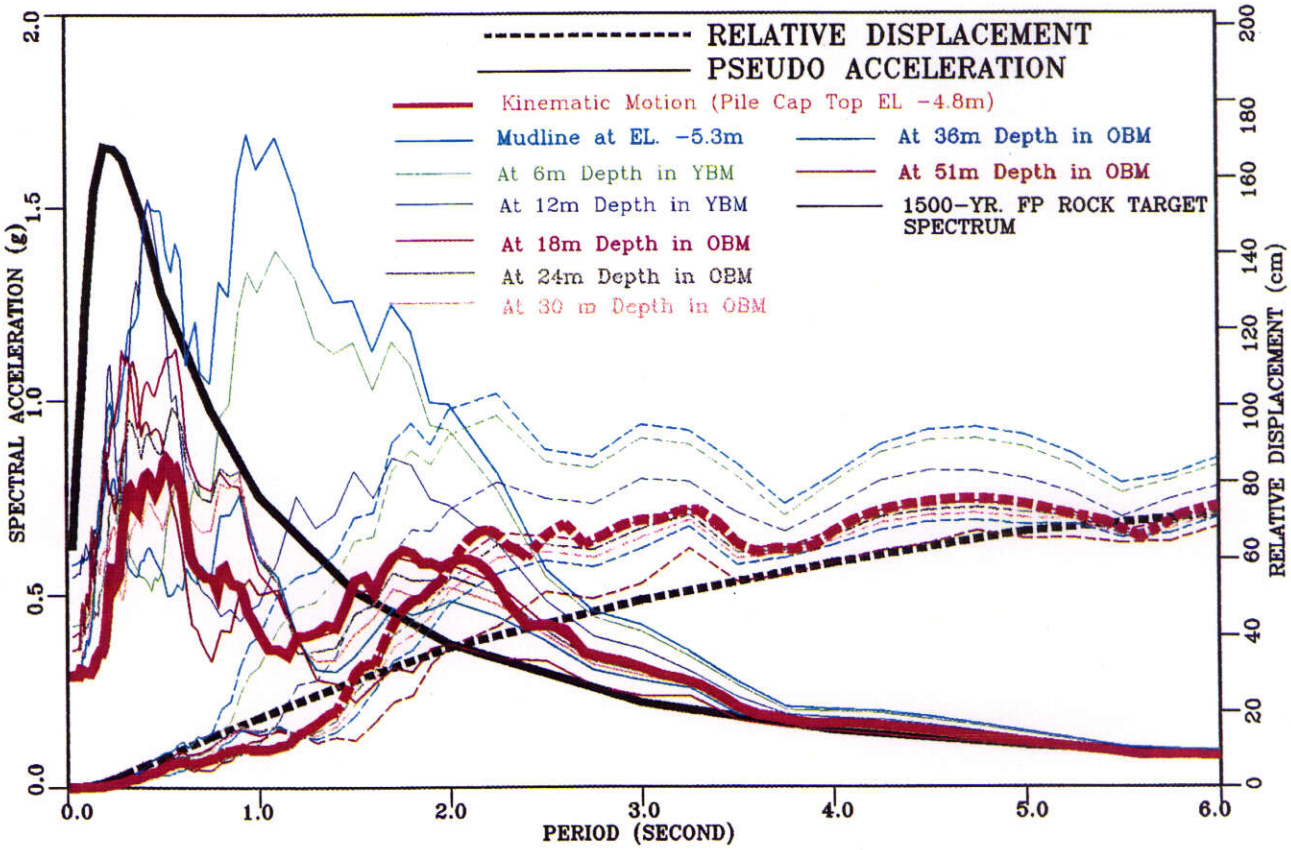

KINEMATIC AND DEPTH-VARYING FREE FIELD MOTIONS
PIER E08, INPUT ROCK MOTION SET 5, FAULT PARALLEL COMPONENT
SFOBB East Span Seismic Safety Project

Earth Mechanics

FUGRO

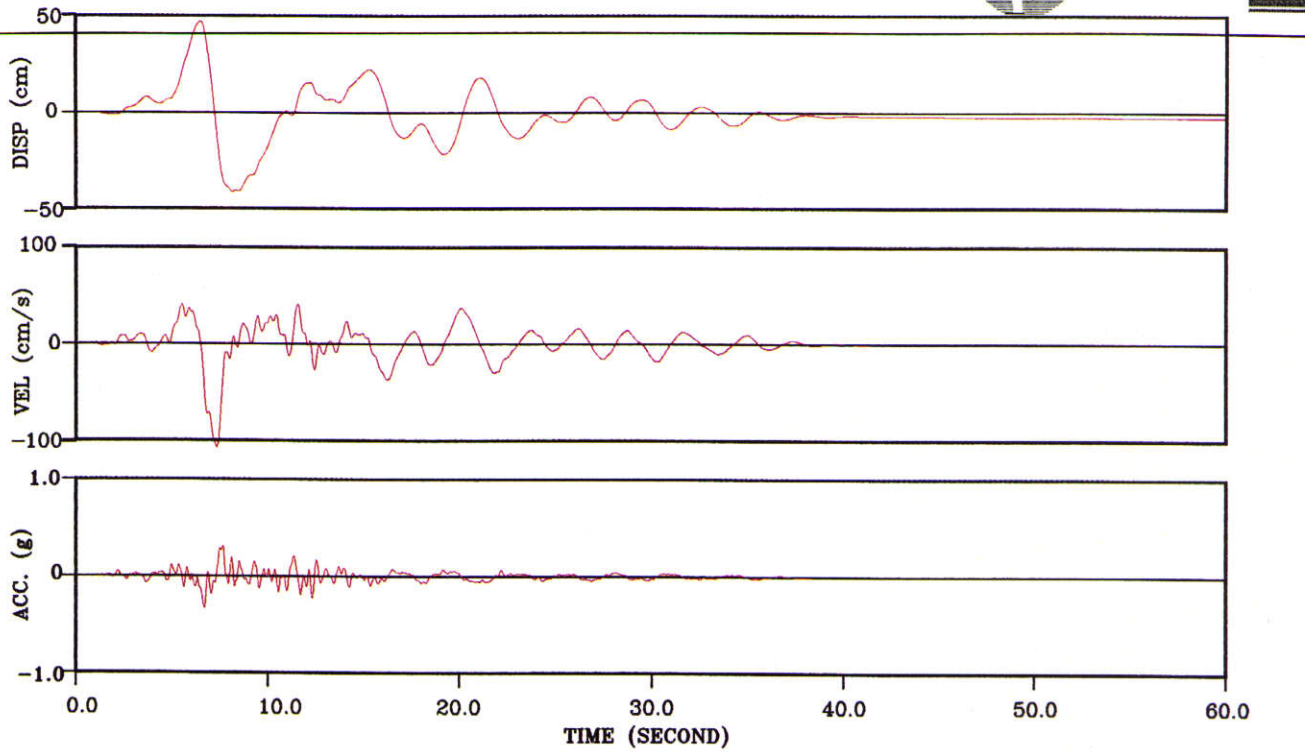

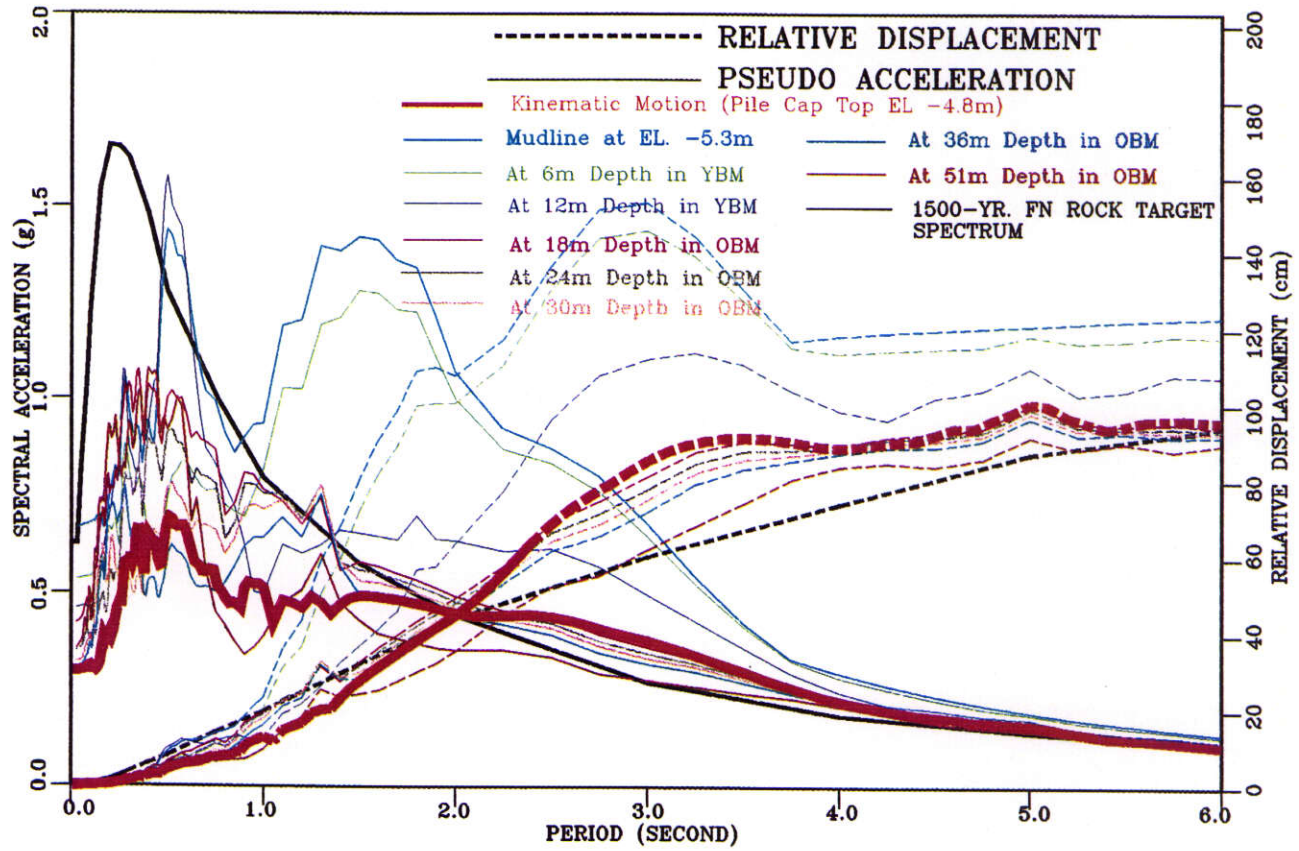

KINEMATIC AND DEPTH-VARYING FREE FIELD MOTIONS
PIER E08, INPUT ROCK MOTION SET 6, FAULT NORMAL COMPONENT
SFOBB East Span Seismic Safety Project

PLATE 8-88

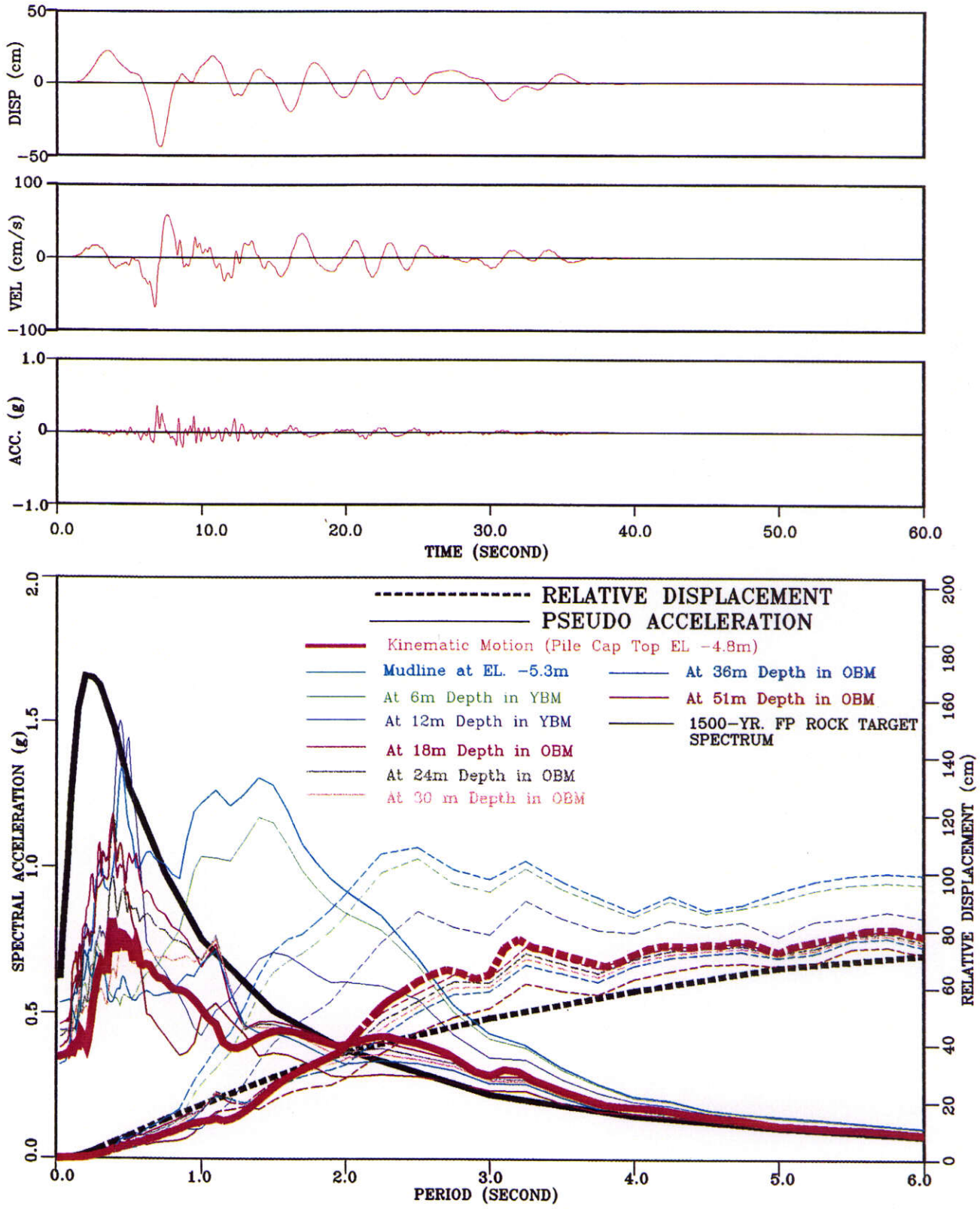

KINEMATIC AND DEPTH-VARYING FREE FIELD MOTIONS
PIER E08, INPUT ROCK MOTION SET 6, FAULT PARALLEL COMPONENT
SFOBB East Span Seismic Safety Project

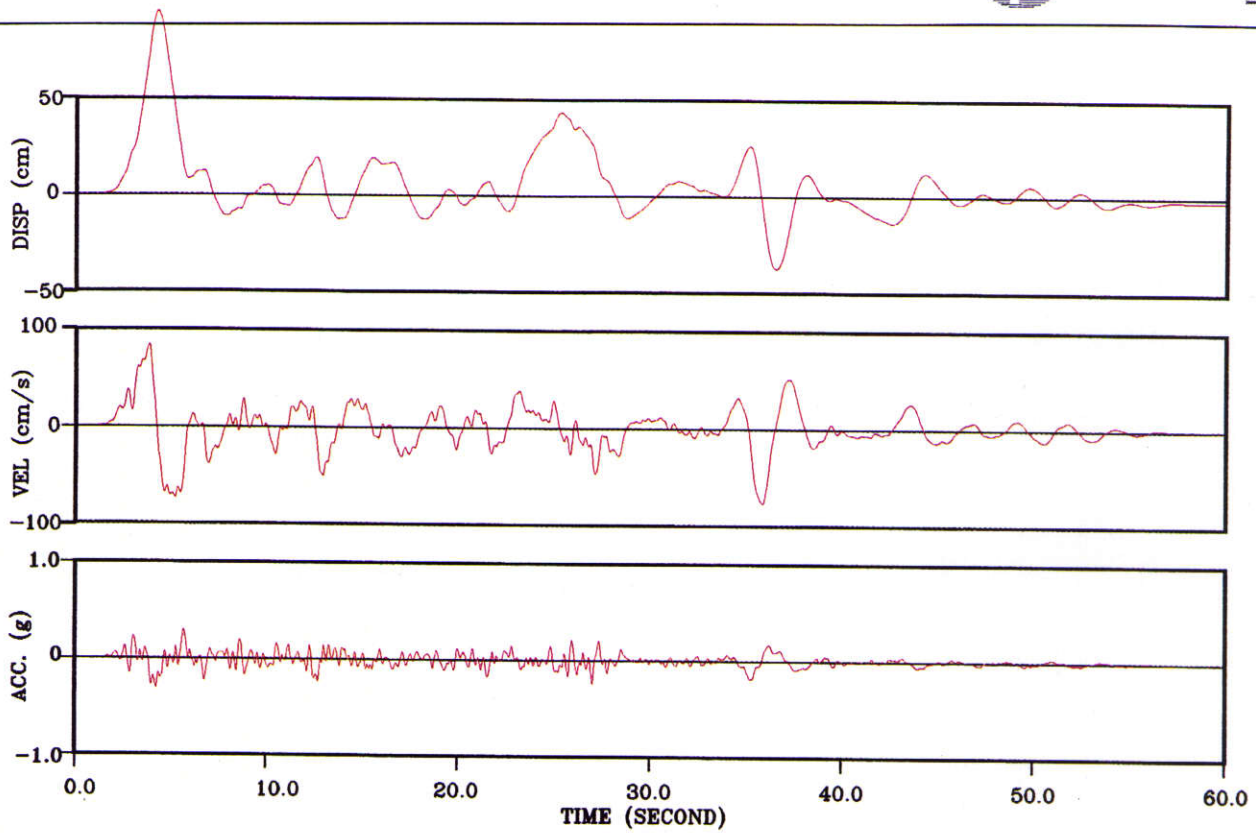

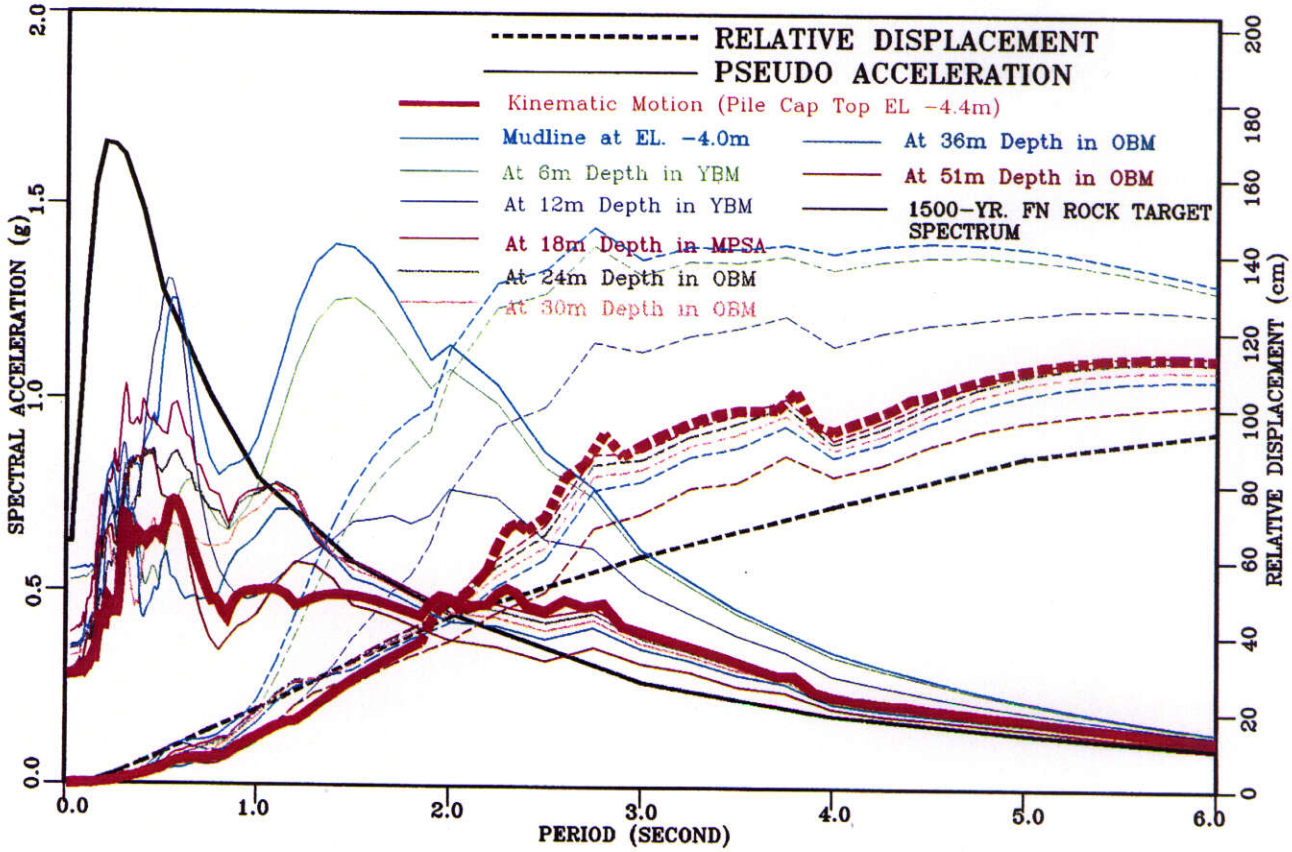

KINEMATIC AND DEPTH-VARYING FREE FIELD MOTIONS
PIER E09, INPUT ROCK MOTION SET 1, FAULT NORMAL COMPONENT
SFOBB East Span Seismic Safety Project

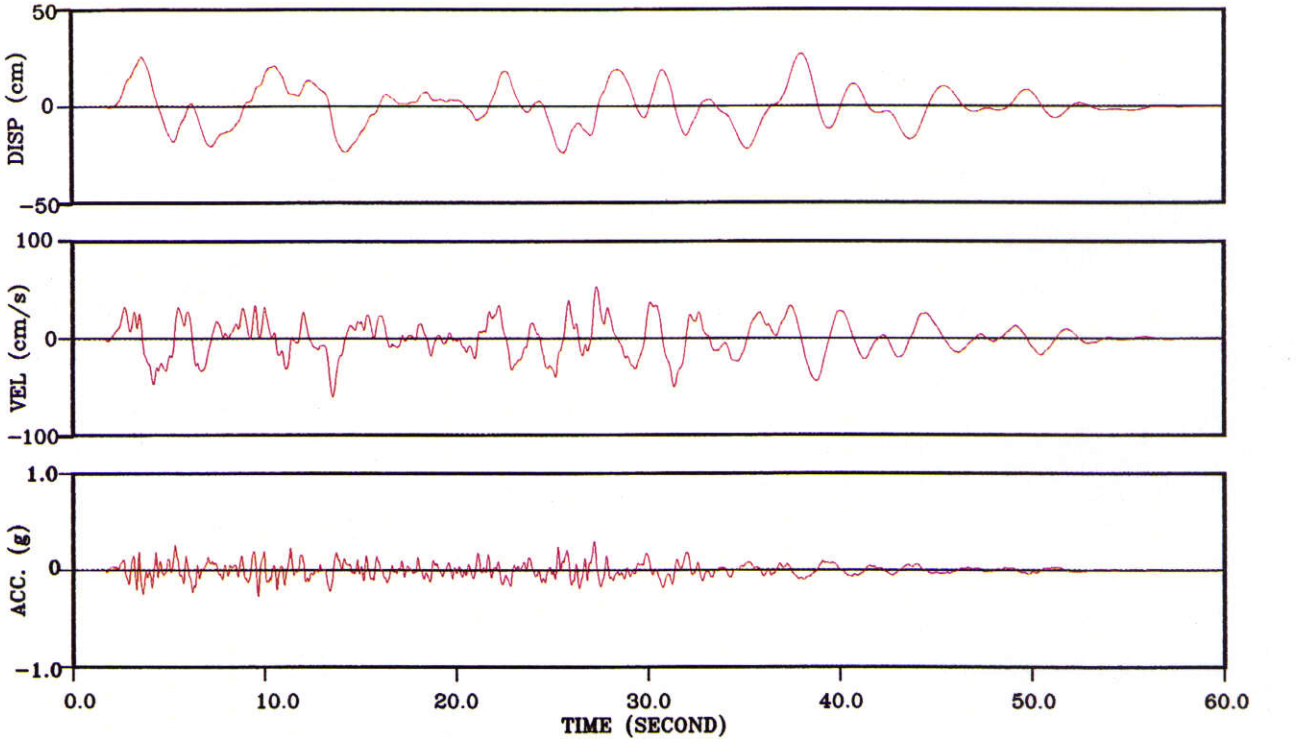

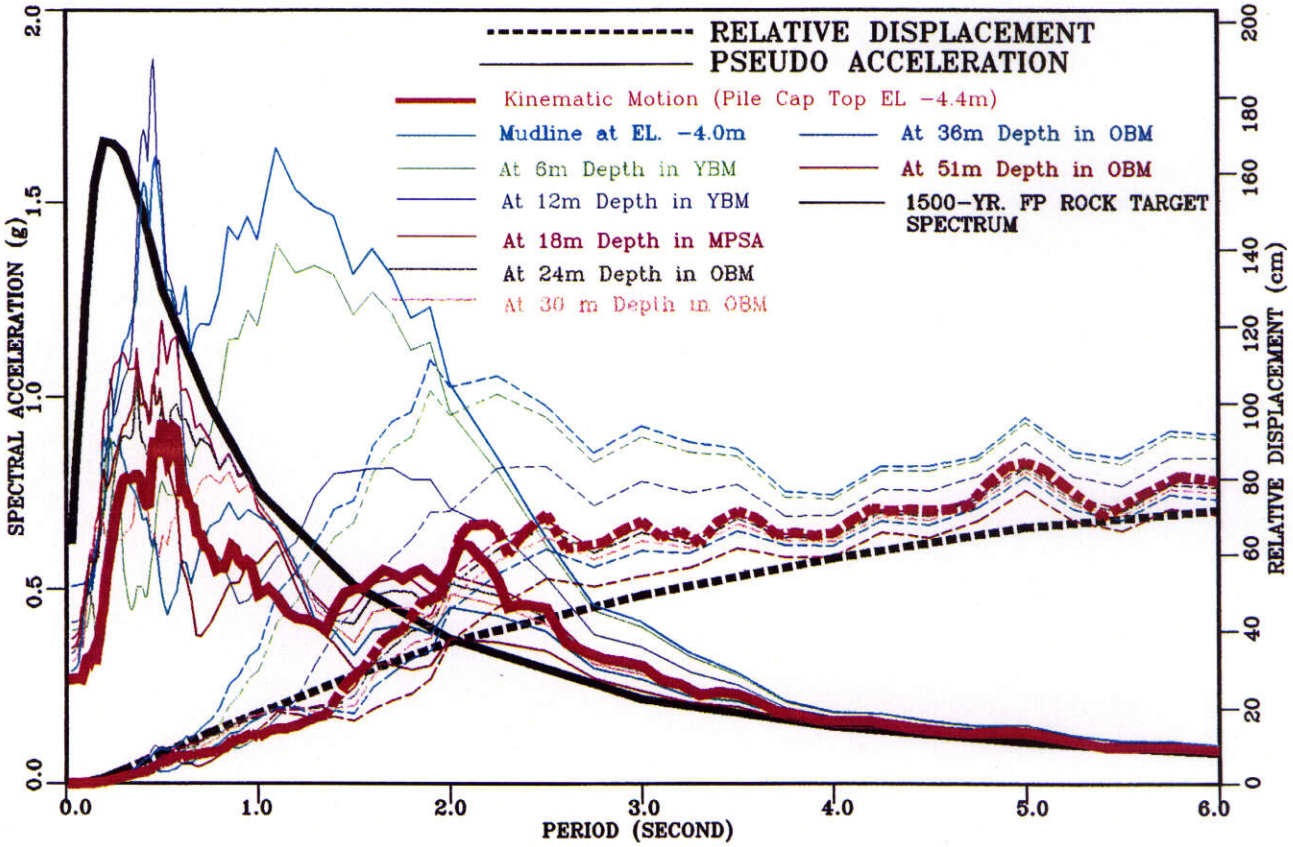

KINEMATIC AND DEPTH-VARYING FREE FIELD MOTIONS
PIER E09, INPUT ROCK MOTION SET 1, FAULT PRALLEL COMPONENT
SFOBB East Span Seismic Safety Project

Earth Mechanics FUGRO

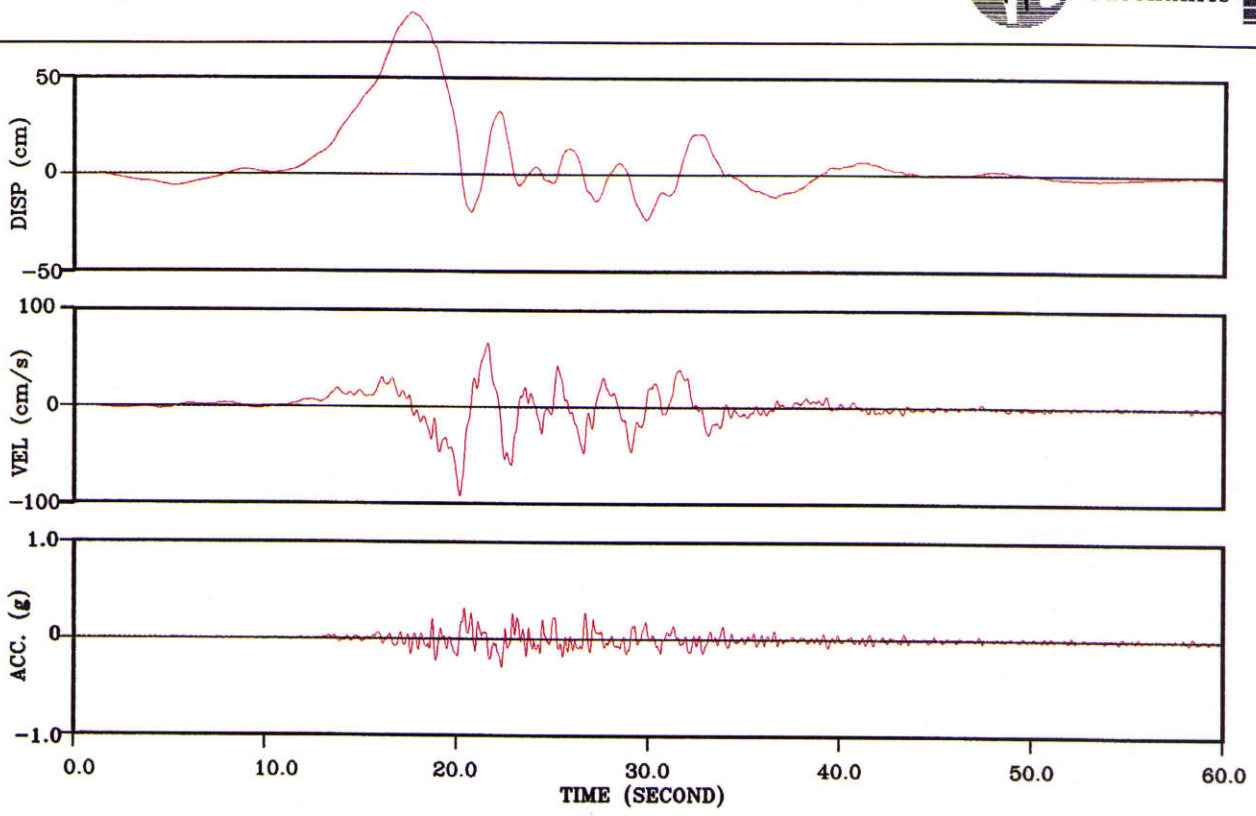

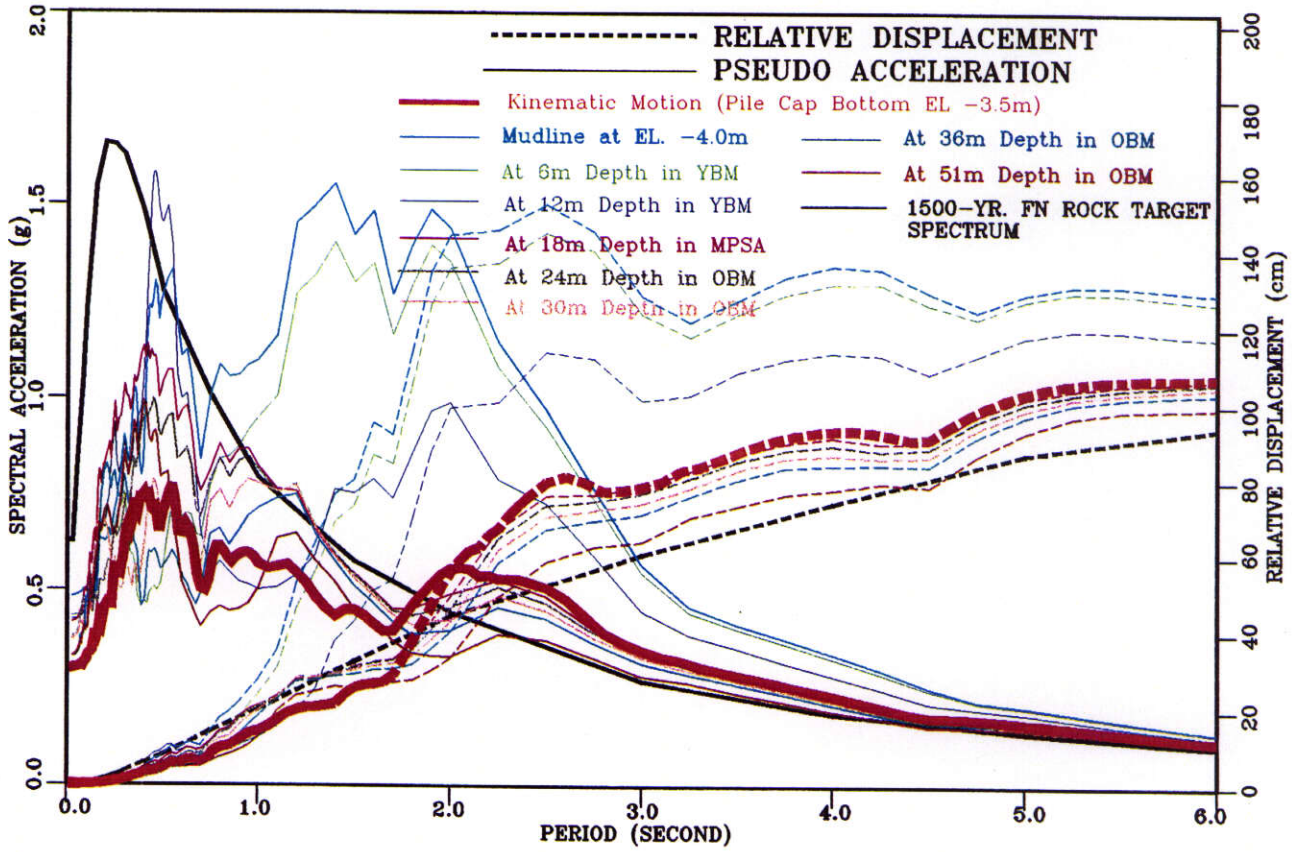

KINEMATIC AND DEPTH-VARYING FREE FIELD MOTIONS
PIER E09, INPUT ROCK MOTION SET 2, FAULT NORMAL COMPONENT
SFOBB East Span Seismic Safety Project

PLATE 8-92

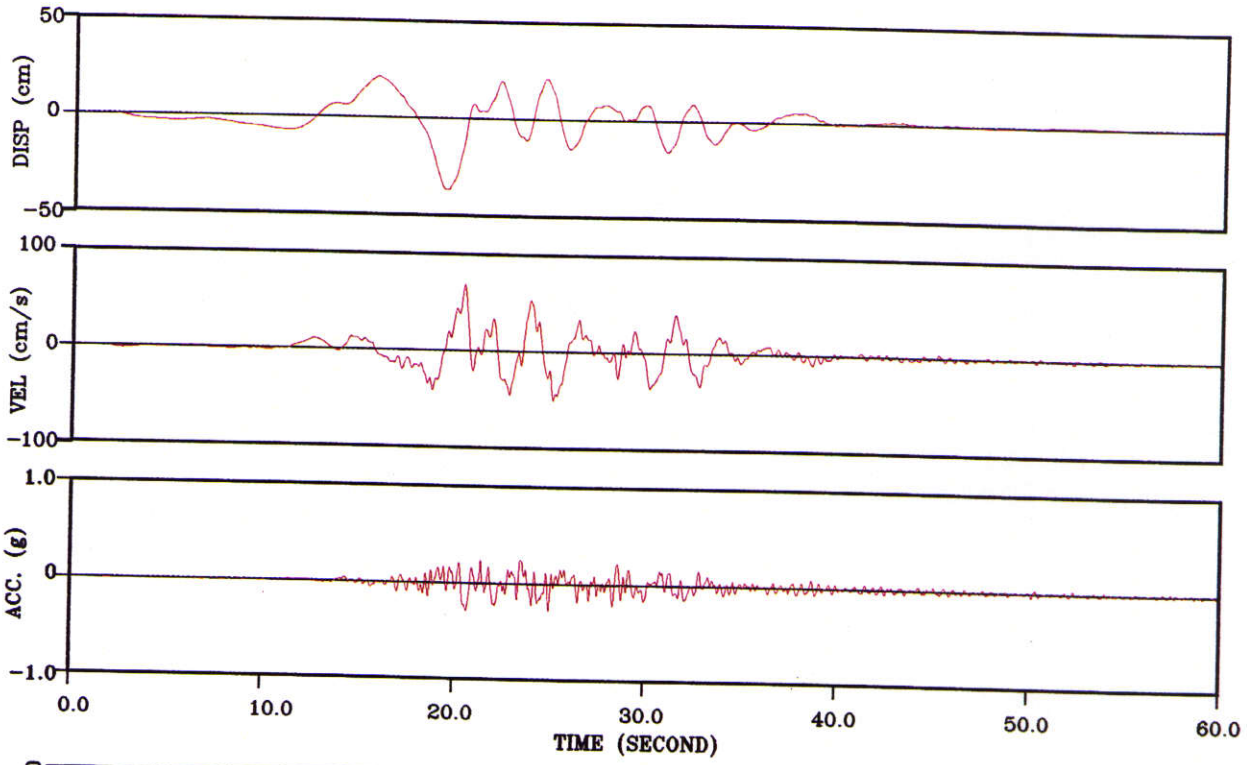

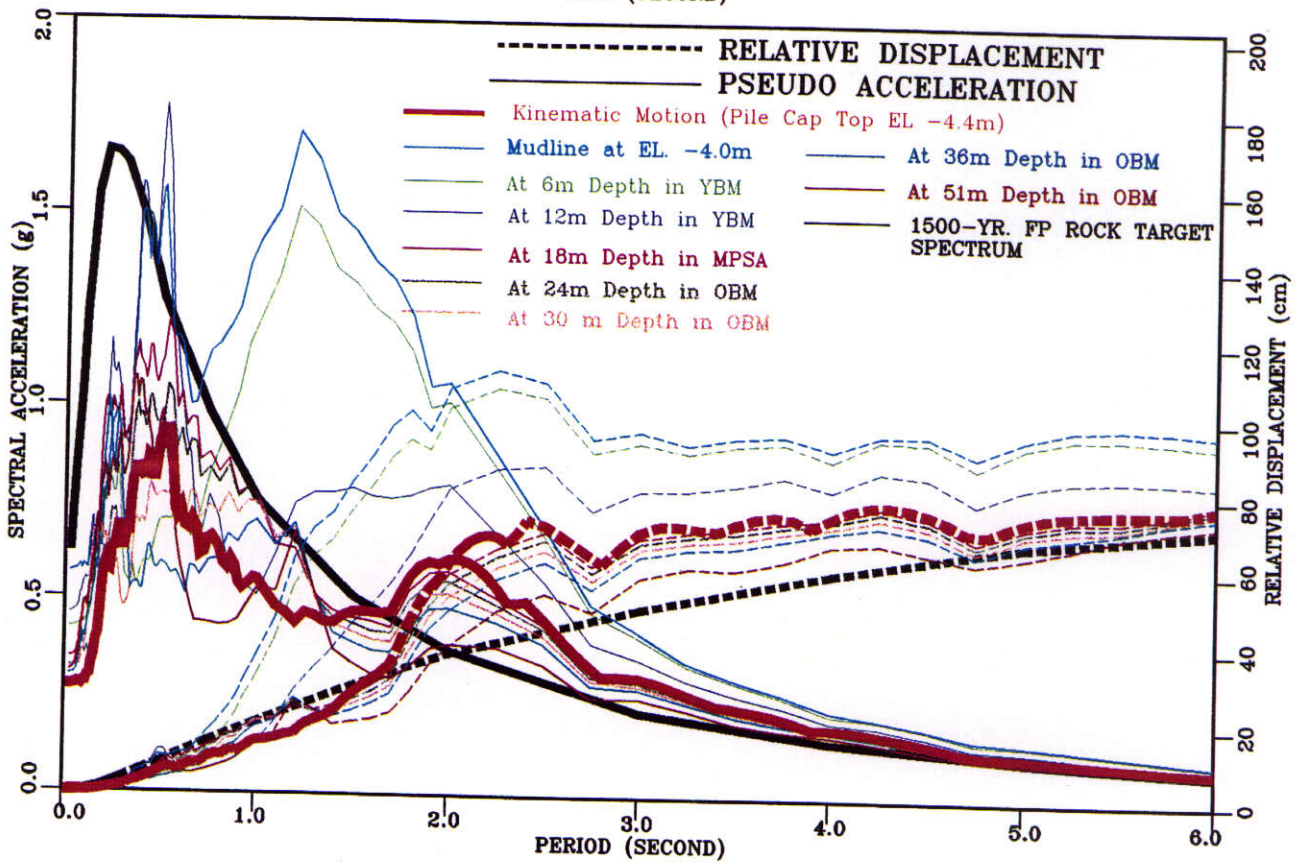

KINEMATIC AND DEPTH-VARYING FREE FIELD MOTIONS
PIER E09, INPUT ROCK MOTION SET 2, FAULT PARALLEL COMPONENT
SFOBB East Span Seismic Safety Project

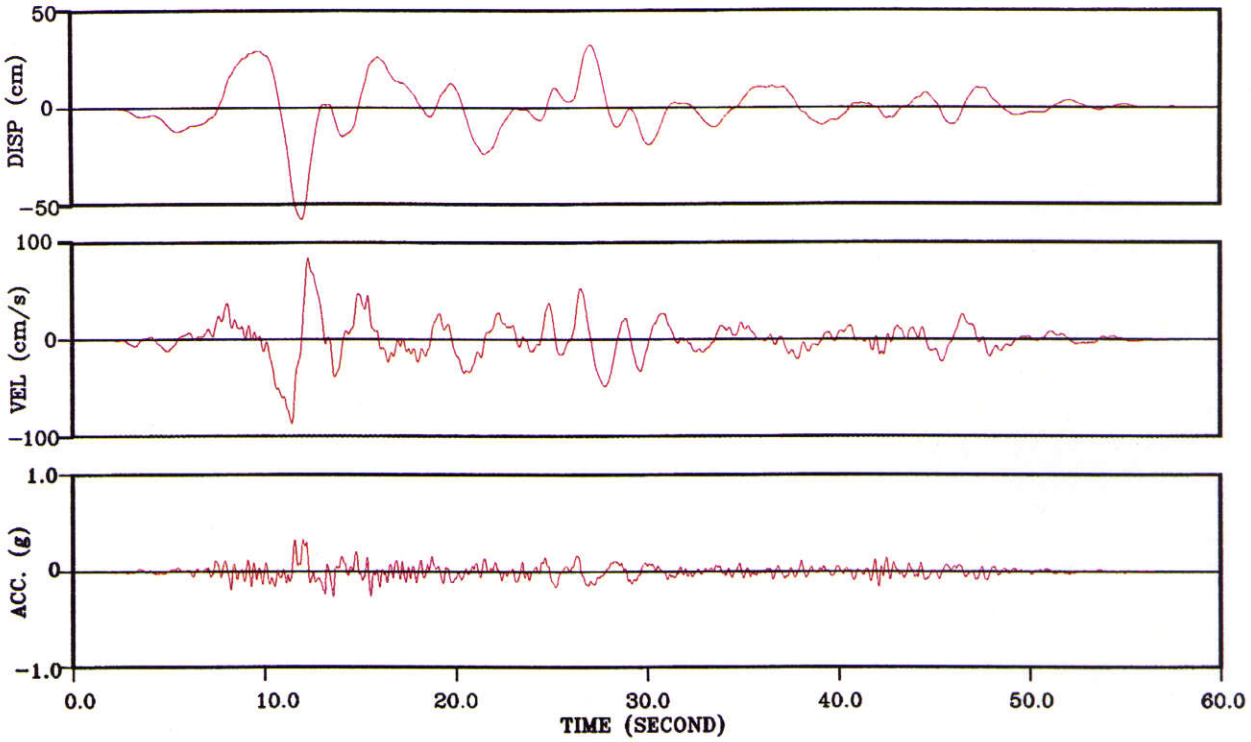

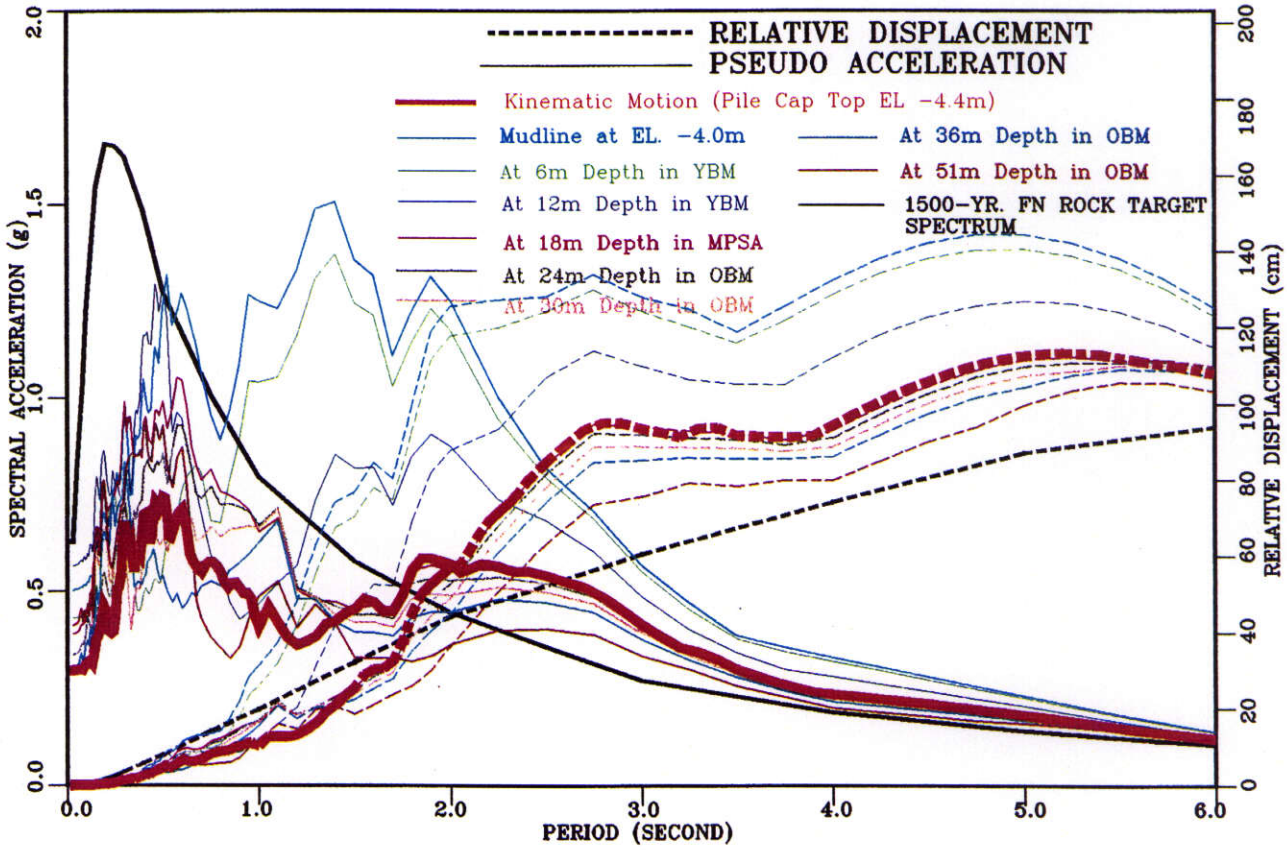

KINEMATIC AND DEPTH-VARYING FREE FIELD MOTIONS
PIER E09, INPUT ROCK MOTION SET 3, FAULT NORMAL COMPONENT
SFOBB East Span Seismic Safety Project

PLATE 8-94

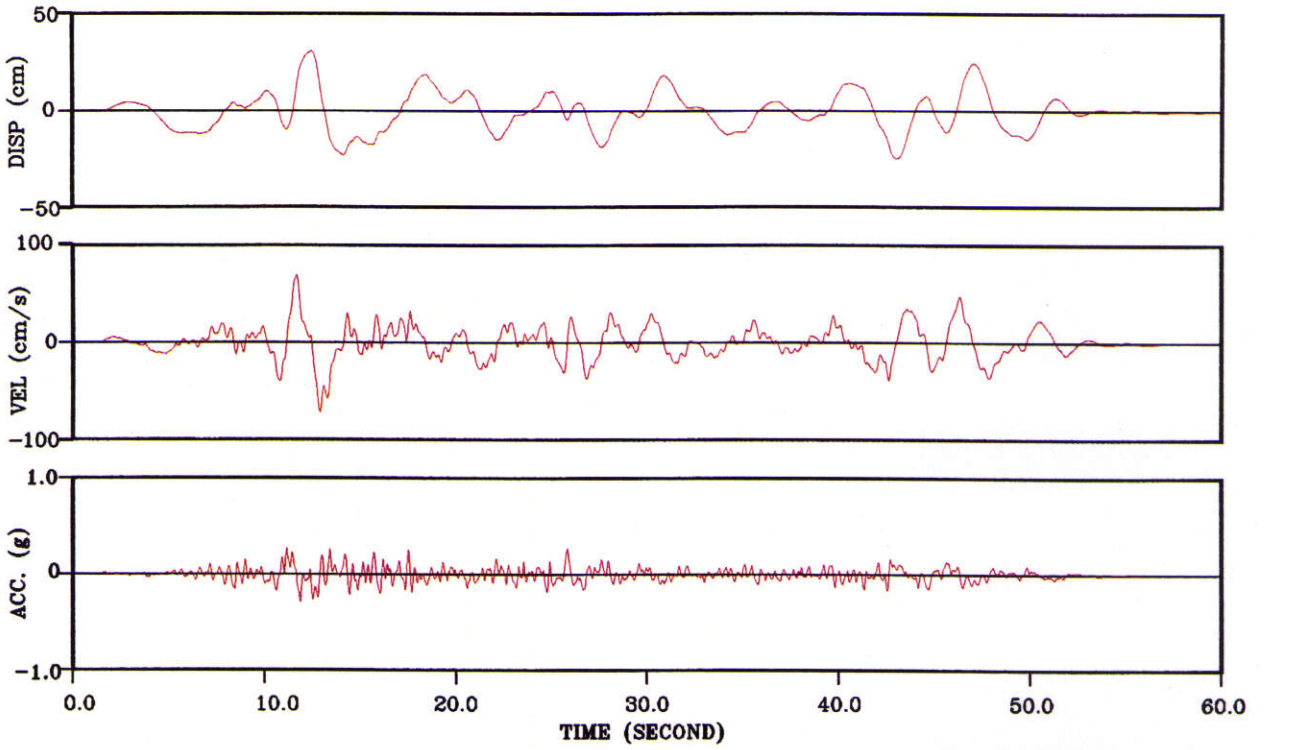

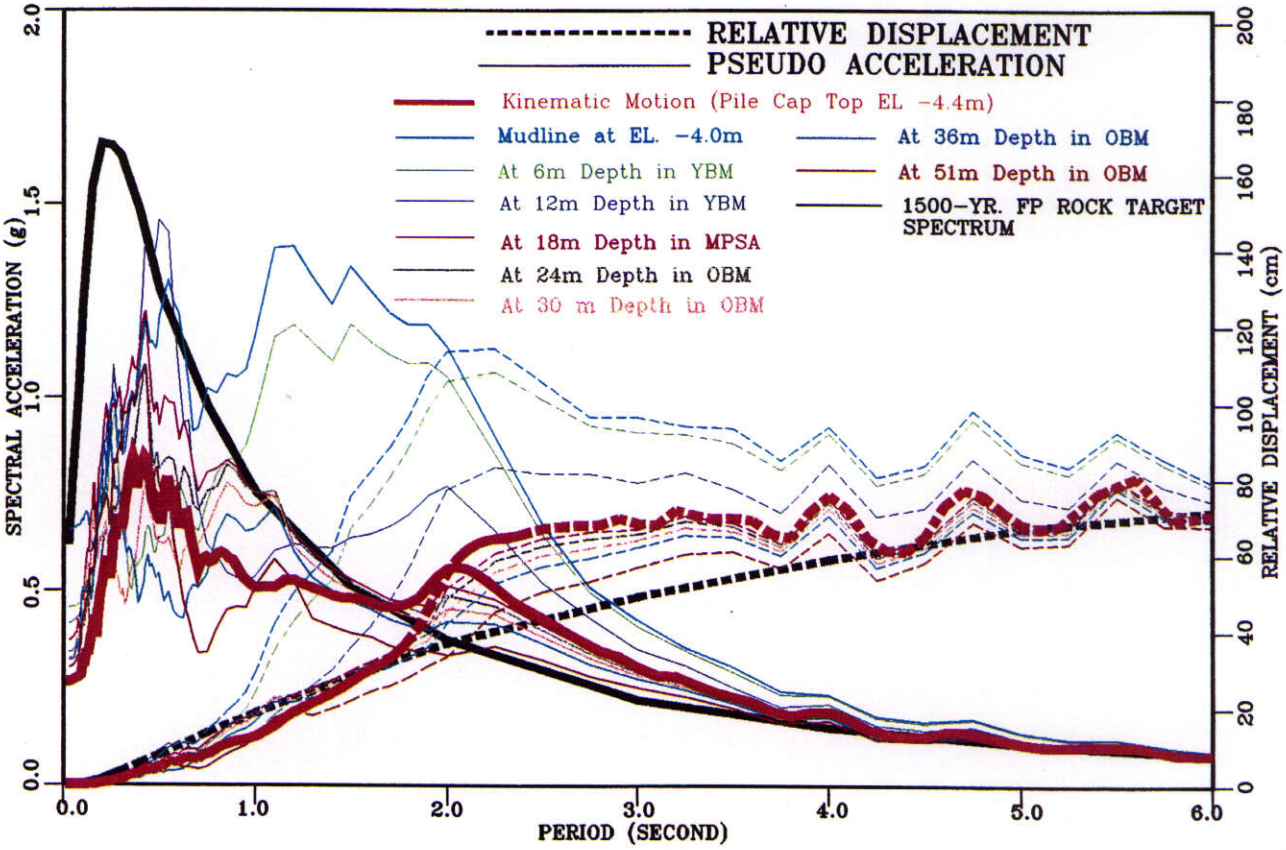

KINEMATIC AND DEPTH-VARYING FREE FIELD MOTIONS
PIER E09, INPUT ROCK MOTION SET 3, FAULT PARALLEL COMPONENT
SFOBB East Span Seismic Safety Project

PLATE 8-95

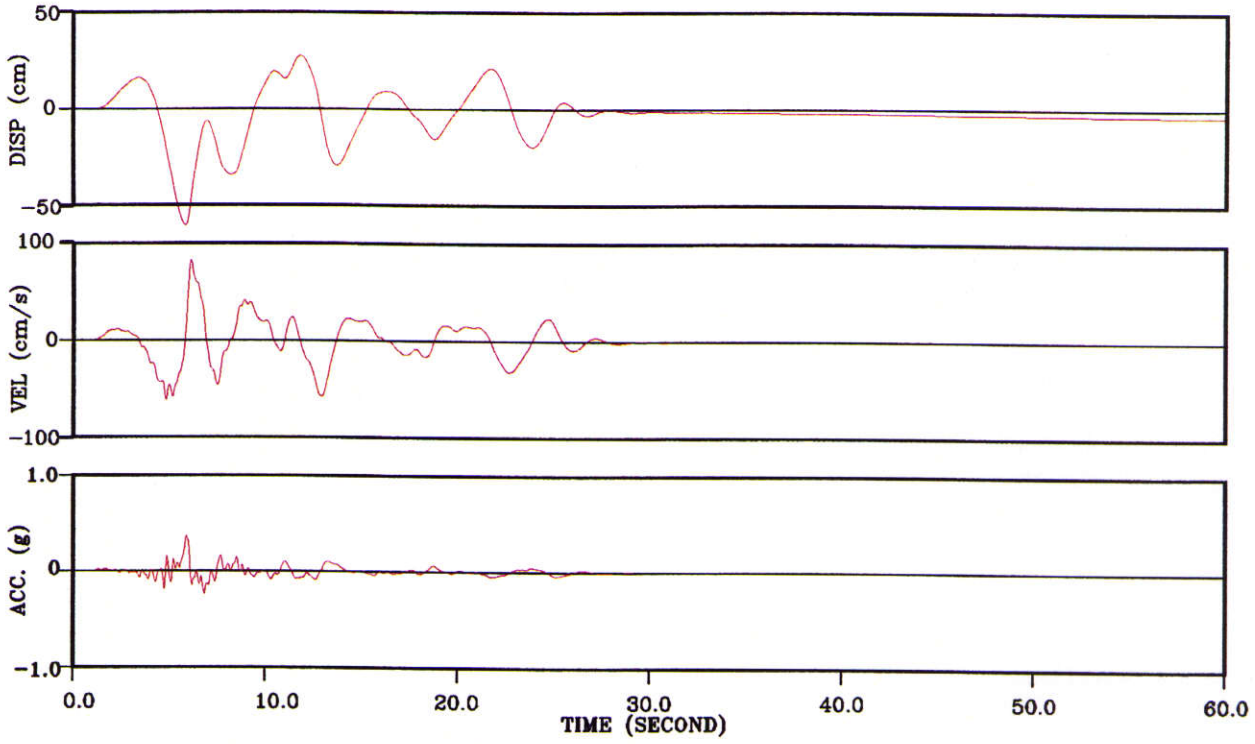

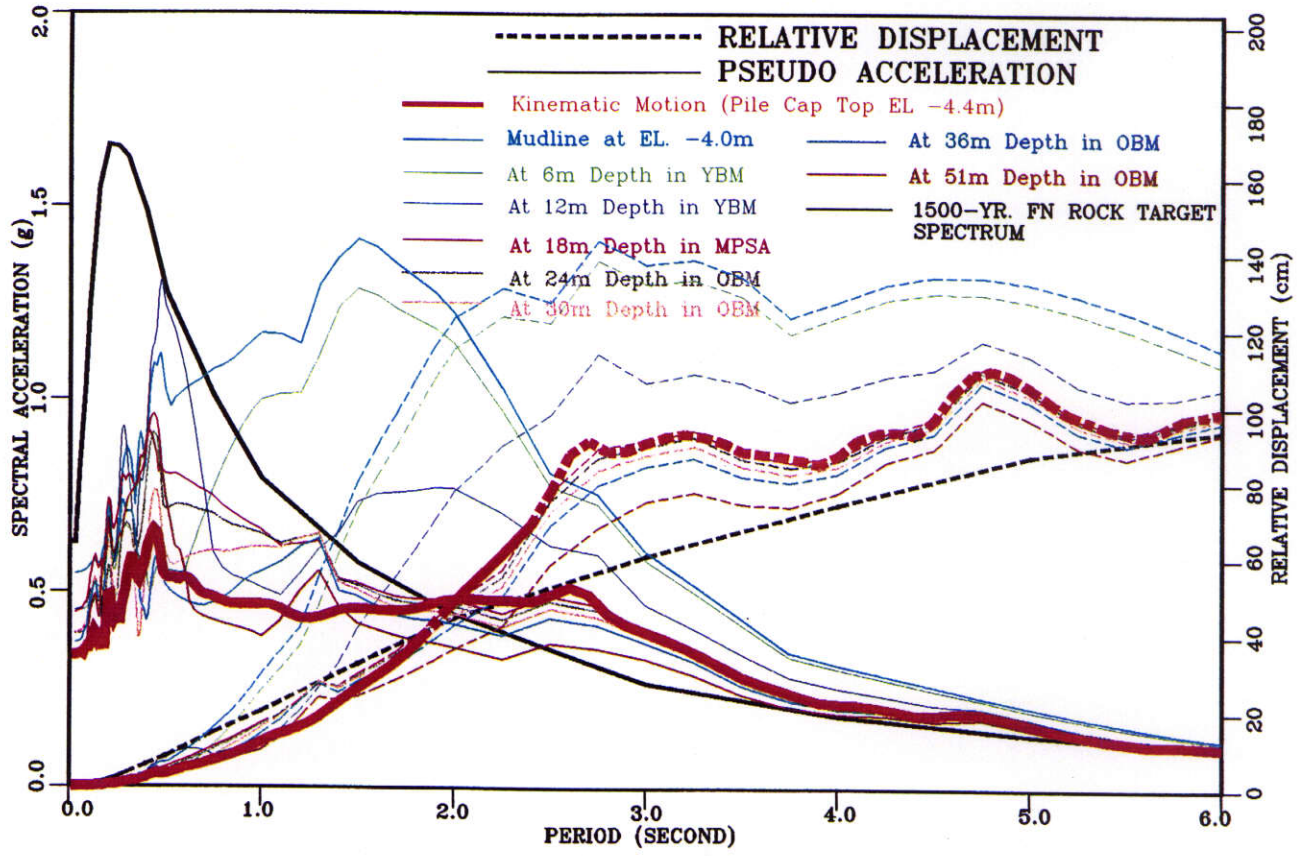

KINEMATIC AND DEPTH-VARYING FREE FIELD MOTIONS
PIER E09, INPUT ROCK MOTION SET 4, FAULT NORMAL COMPONENT
SFOBB East Span Seismic Safety Project

PLATE 8-96

Earth Mechanics FUGRO

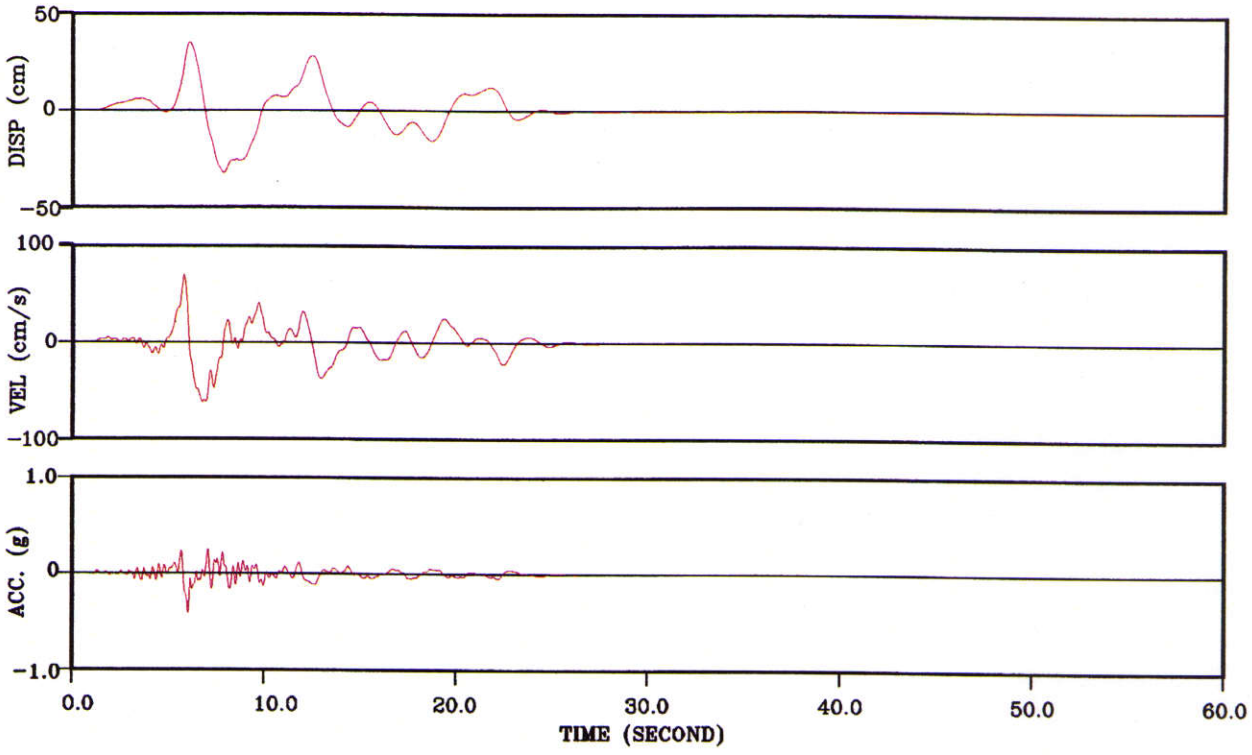

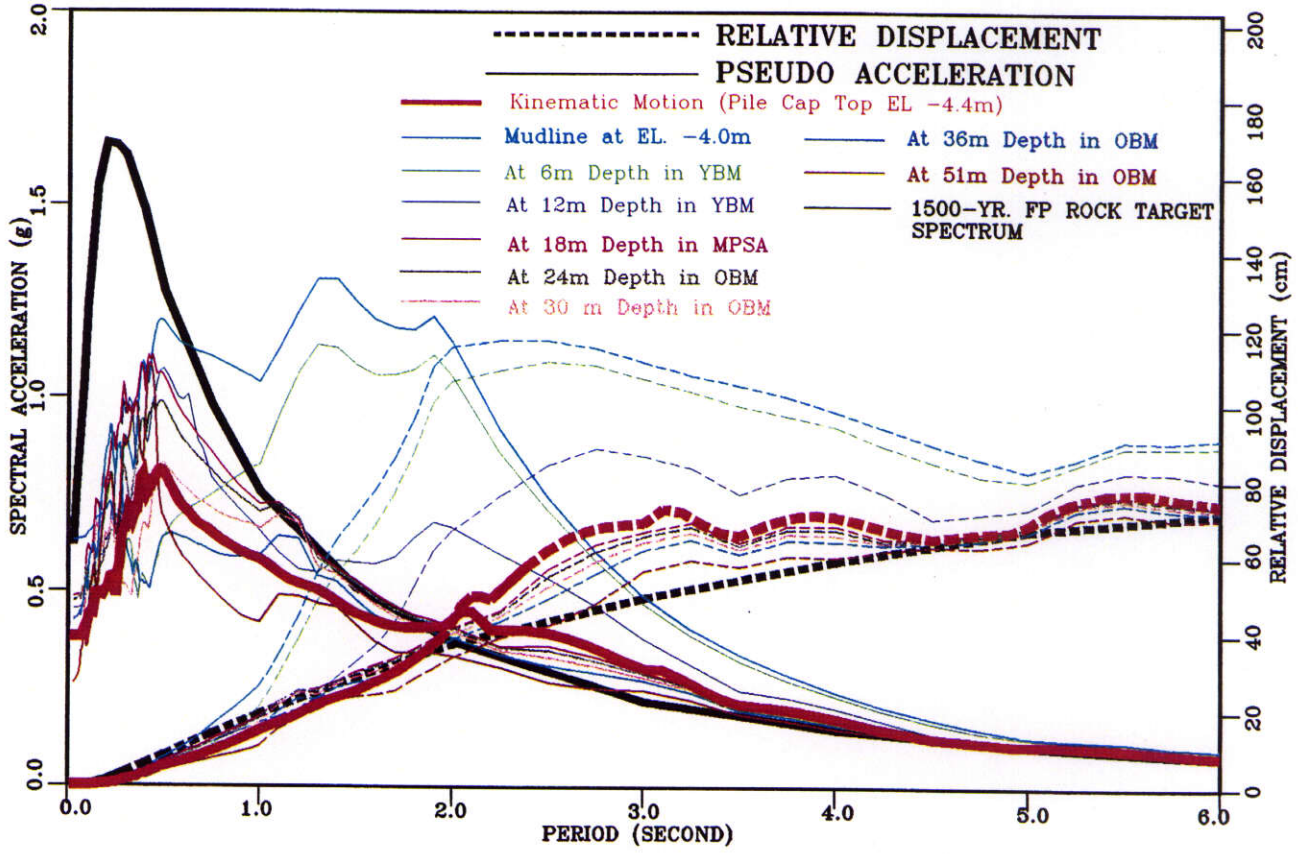

KINEMATIC AND DEPTH-VARYING FREE FIELD MOTIONS
PIER E09, INPUT ROCK MOTION SET 4, FAULT PARALLEL COMPONENT
SFOBB East Span Seismic Safety Project

PLATE 8-97

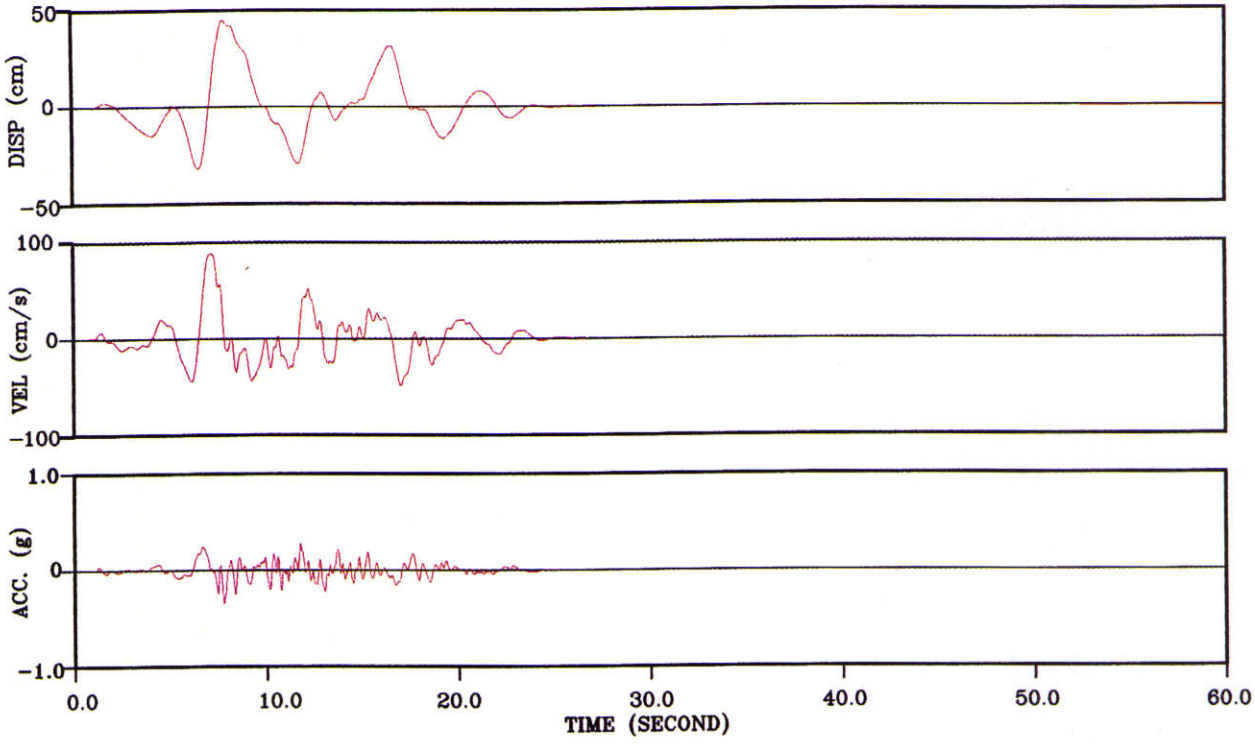

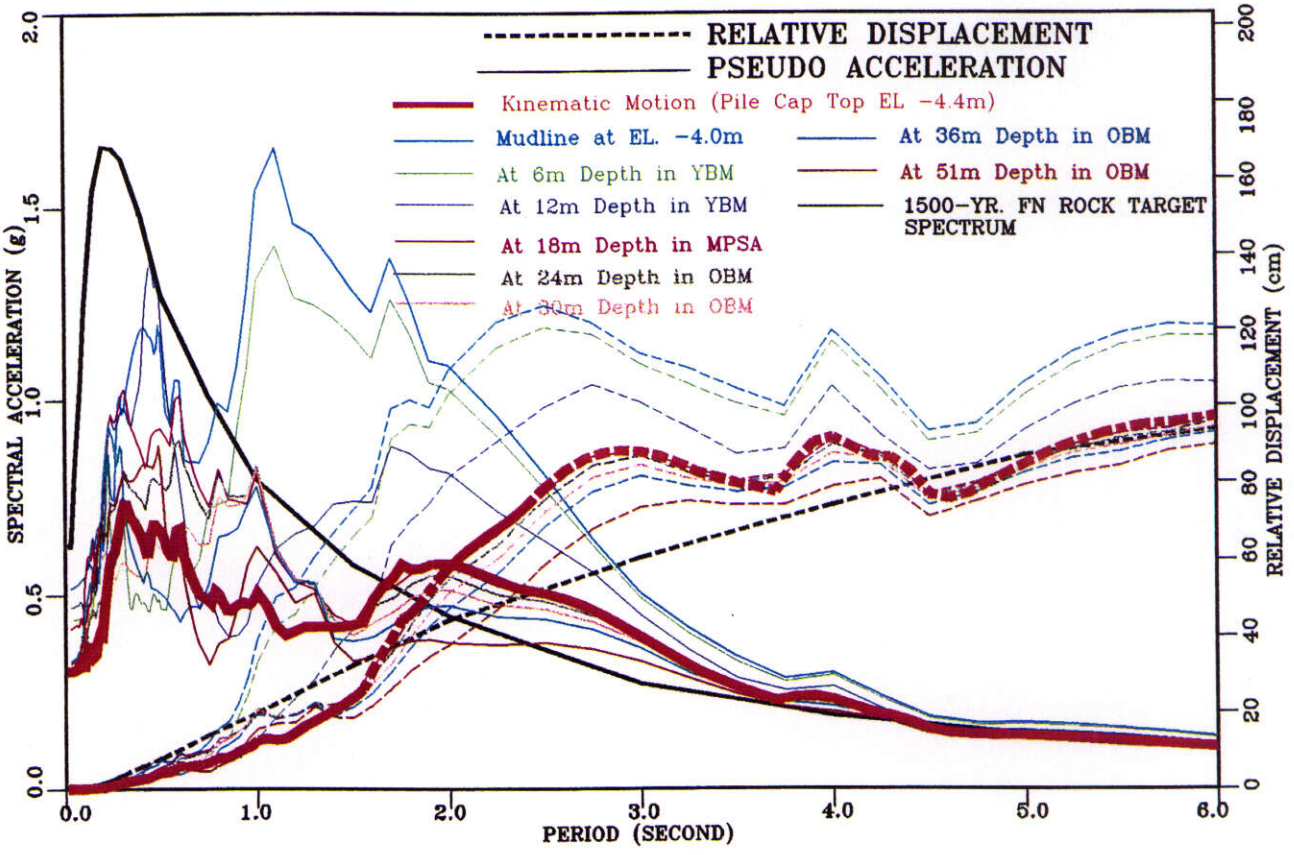

KINEMATIC AND DEPTH-VARYING FREE FIELD MOTIONS
PIER E09, INPUT ROCK MOTION SET 5, FAULT NORMAL COMPONENT
SFOBB East Span Seismic Safety Project

PLATE 8-98

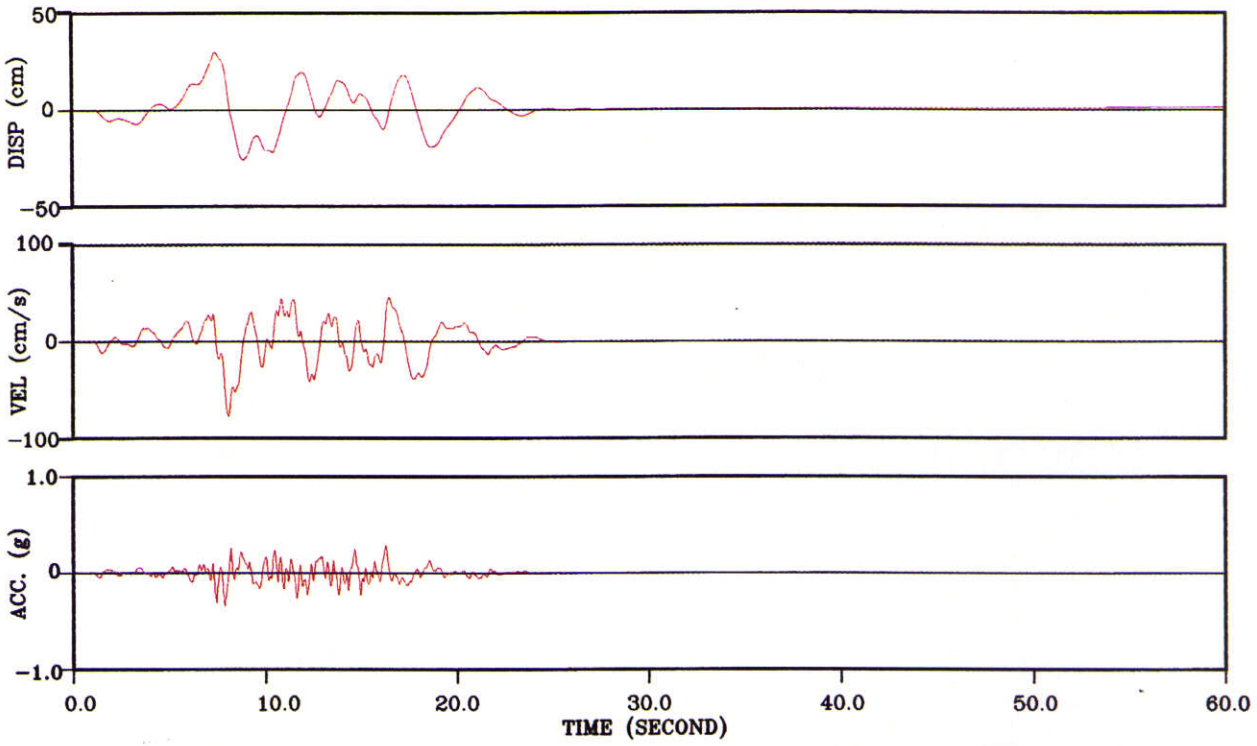

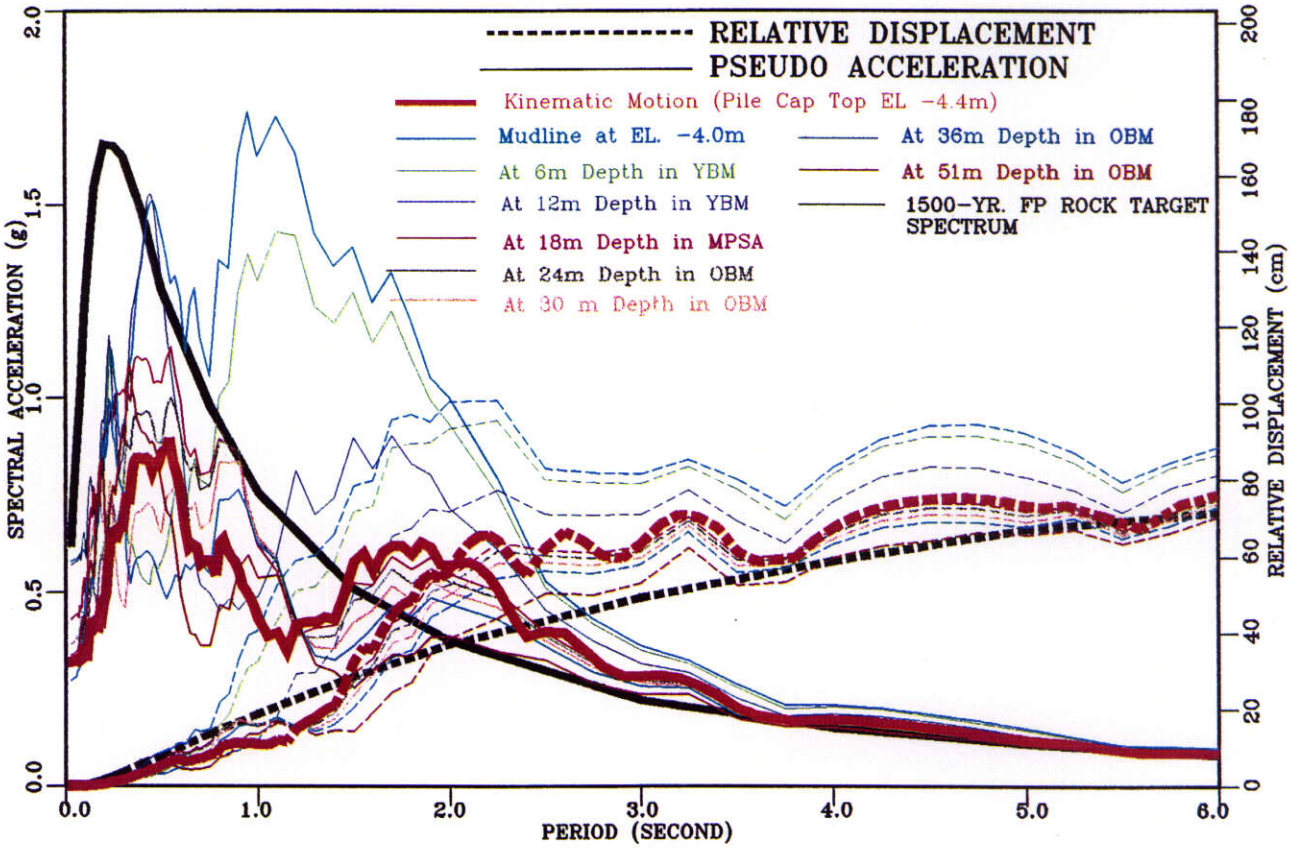

KINEMATIC AND DEPTH-VARYING FREE FIELD MOTIONS
PIER E09, INPUT ROCK MOTION SET 5, FAULT PARALLEL COMPONENT
SFOBB East Span Seismic Safety Project

PLATE 8-99

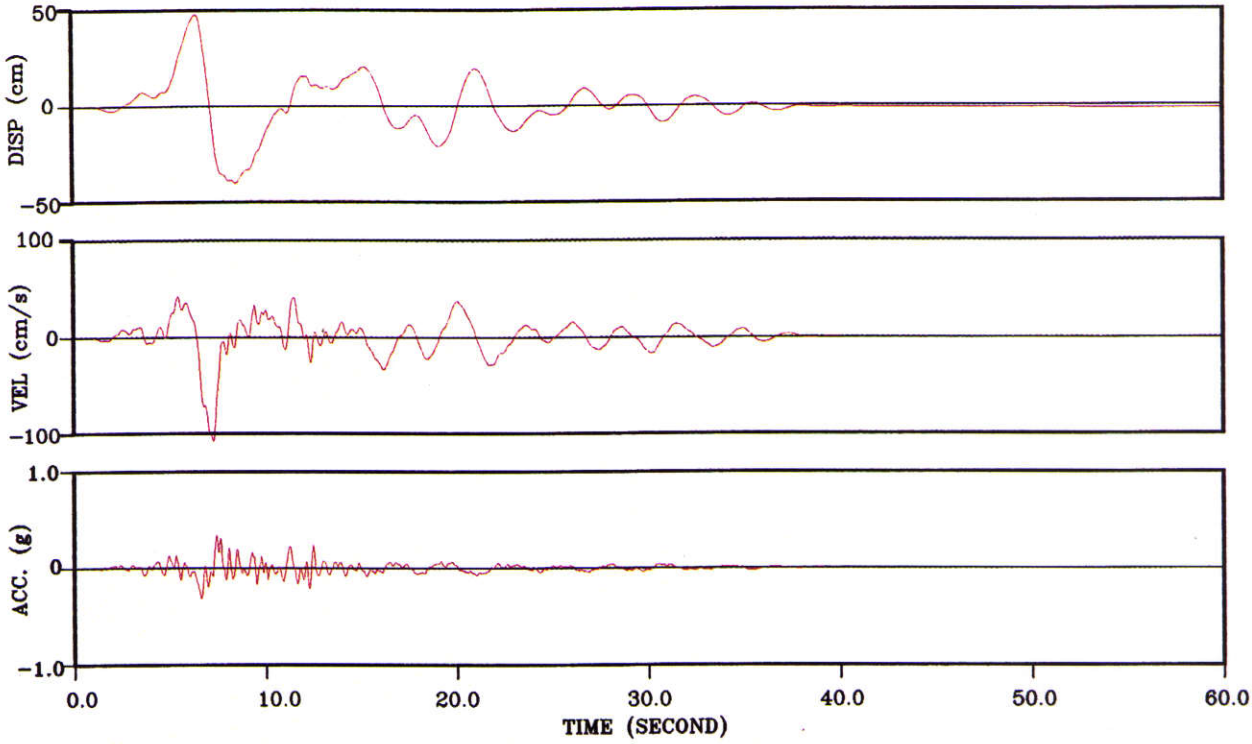

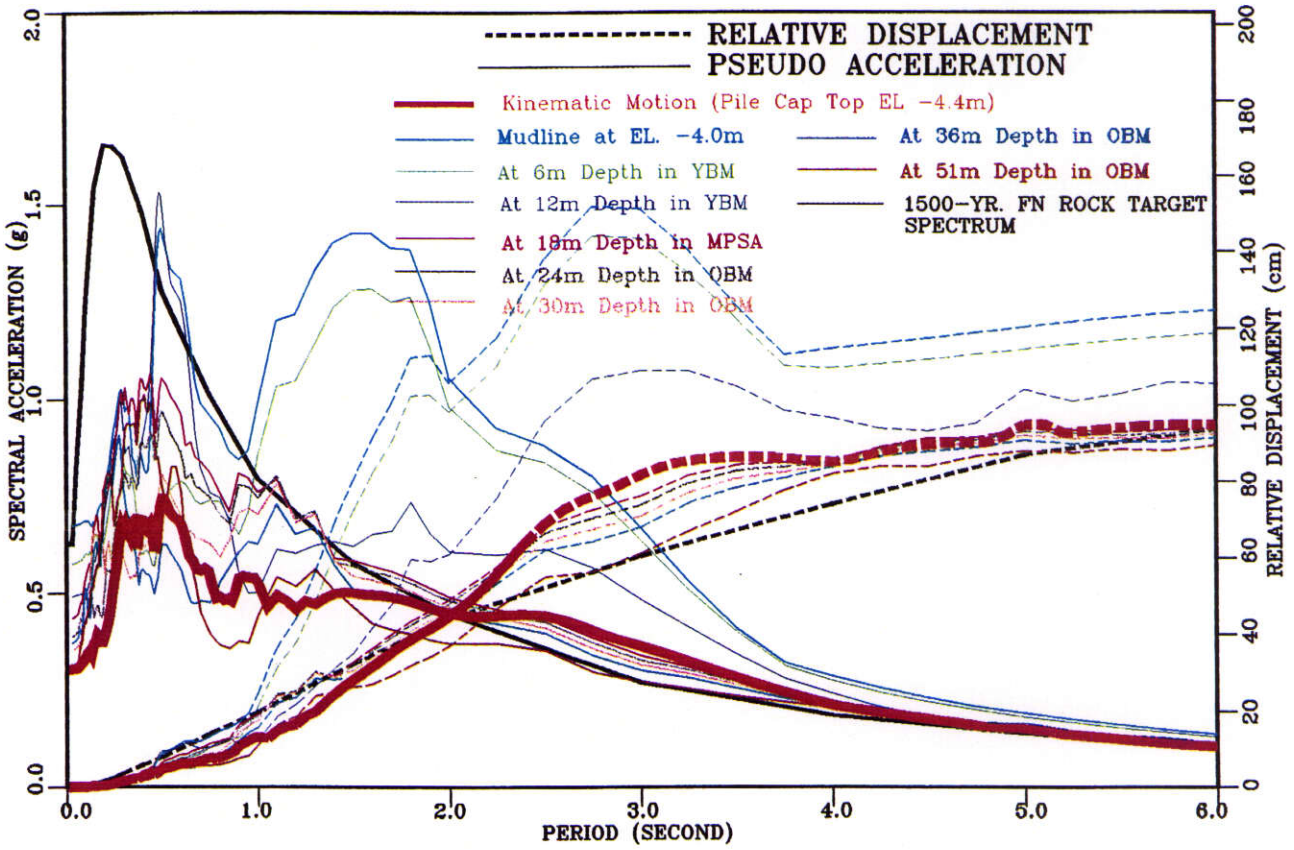

KINEMATIC AND DEPTH-VARYING FREE FIELD MOTIONS
PIER E09, INPUT ROCK MOTION SET 6, FAULT NORMAL COMPONENT
SFOBB East Span Seismic Safety Project

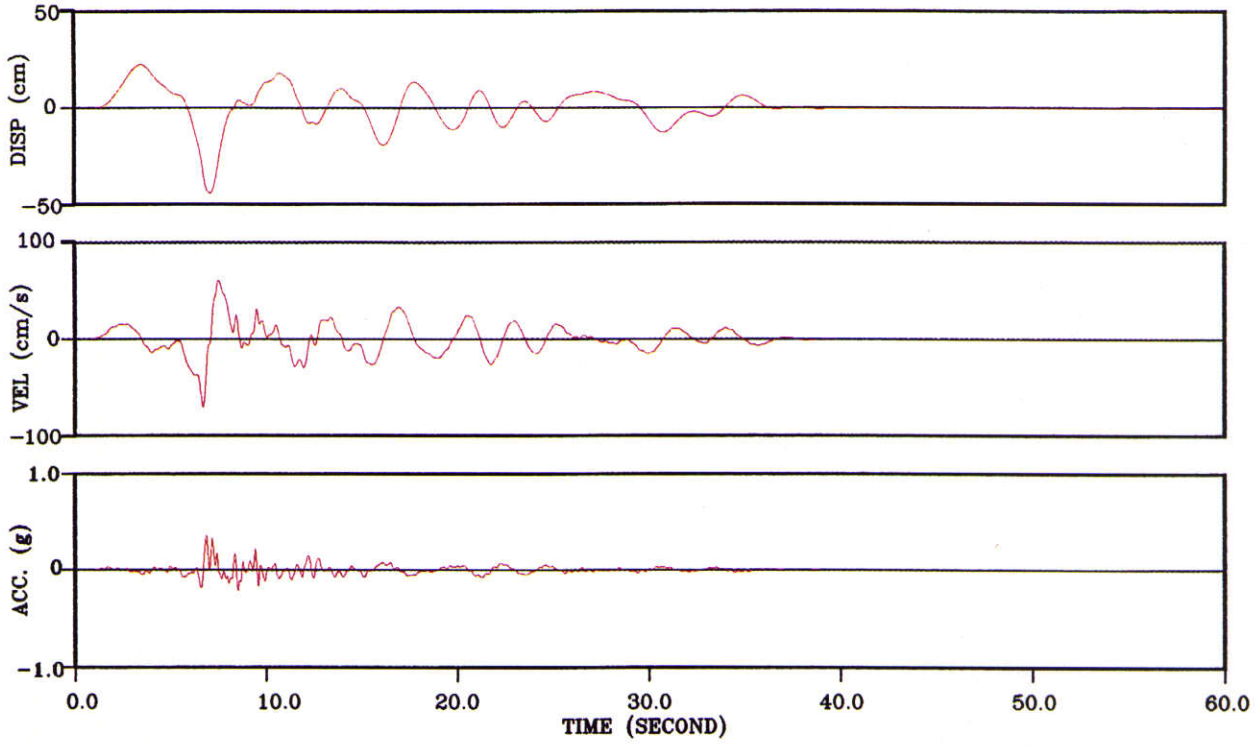

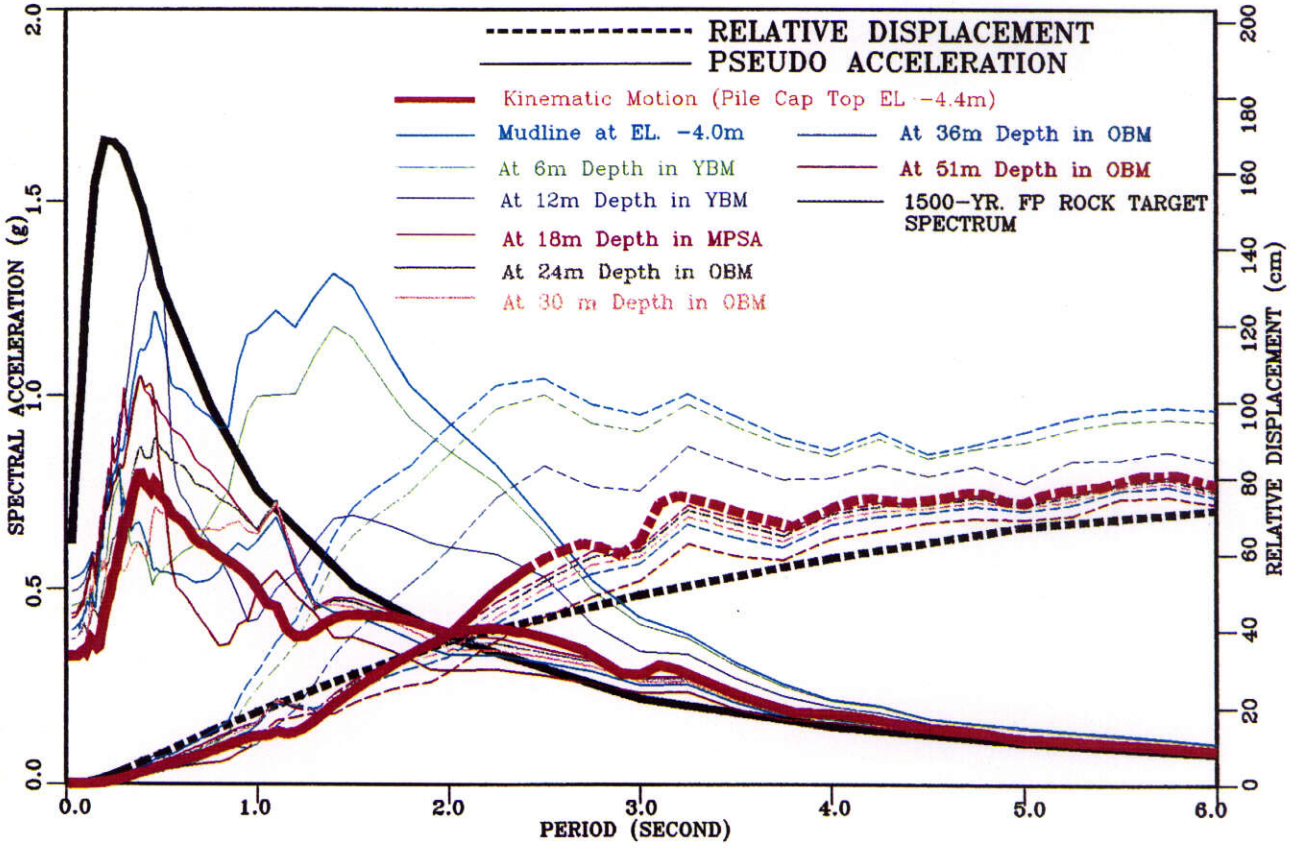

KINEMATIC AND DEPTH-VARYING FREE FIELD MOTIONS
PIER E09, INPUT ROCK MOTION SET 6, FAULT PARALLEL COMPONENT
SFOBB East Span Seismic Safety Project

PLATE 8-101

Earth Mechanics FUGRO

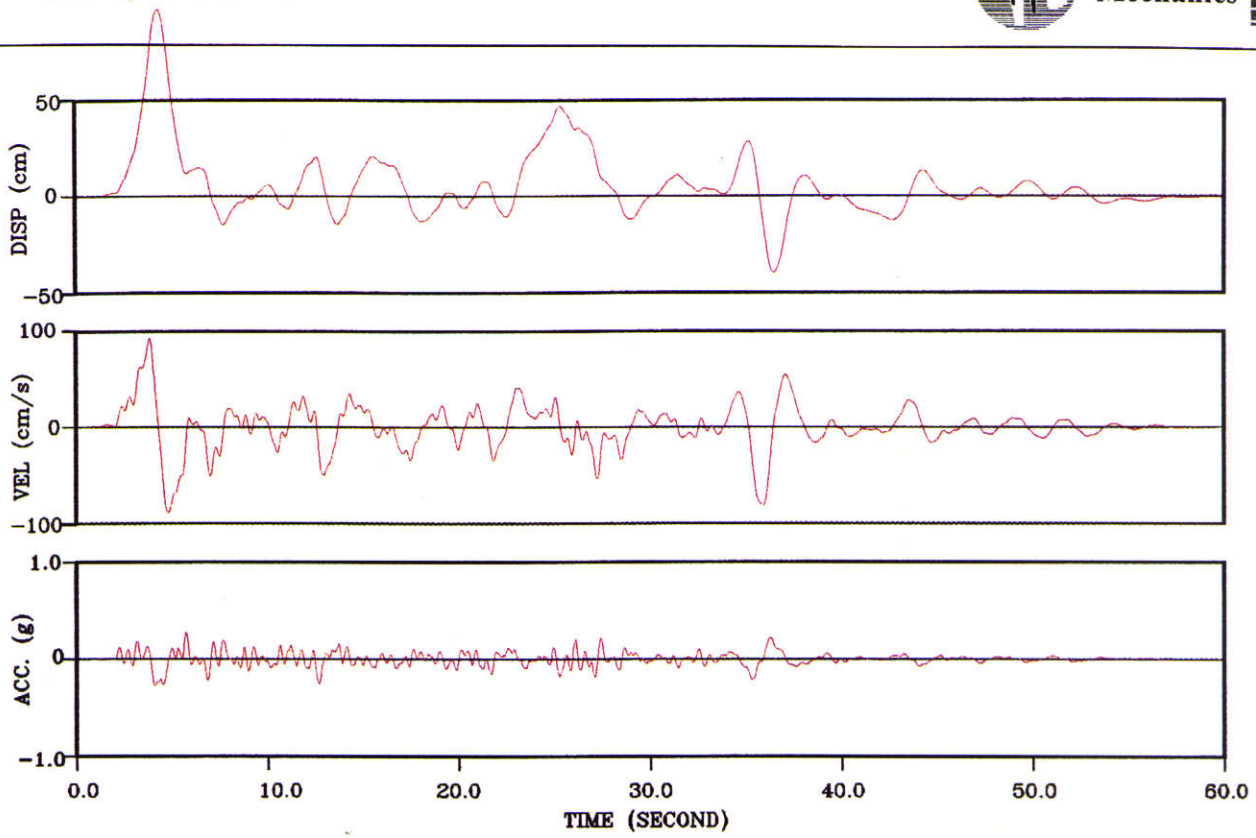

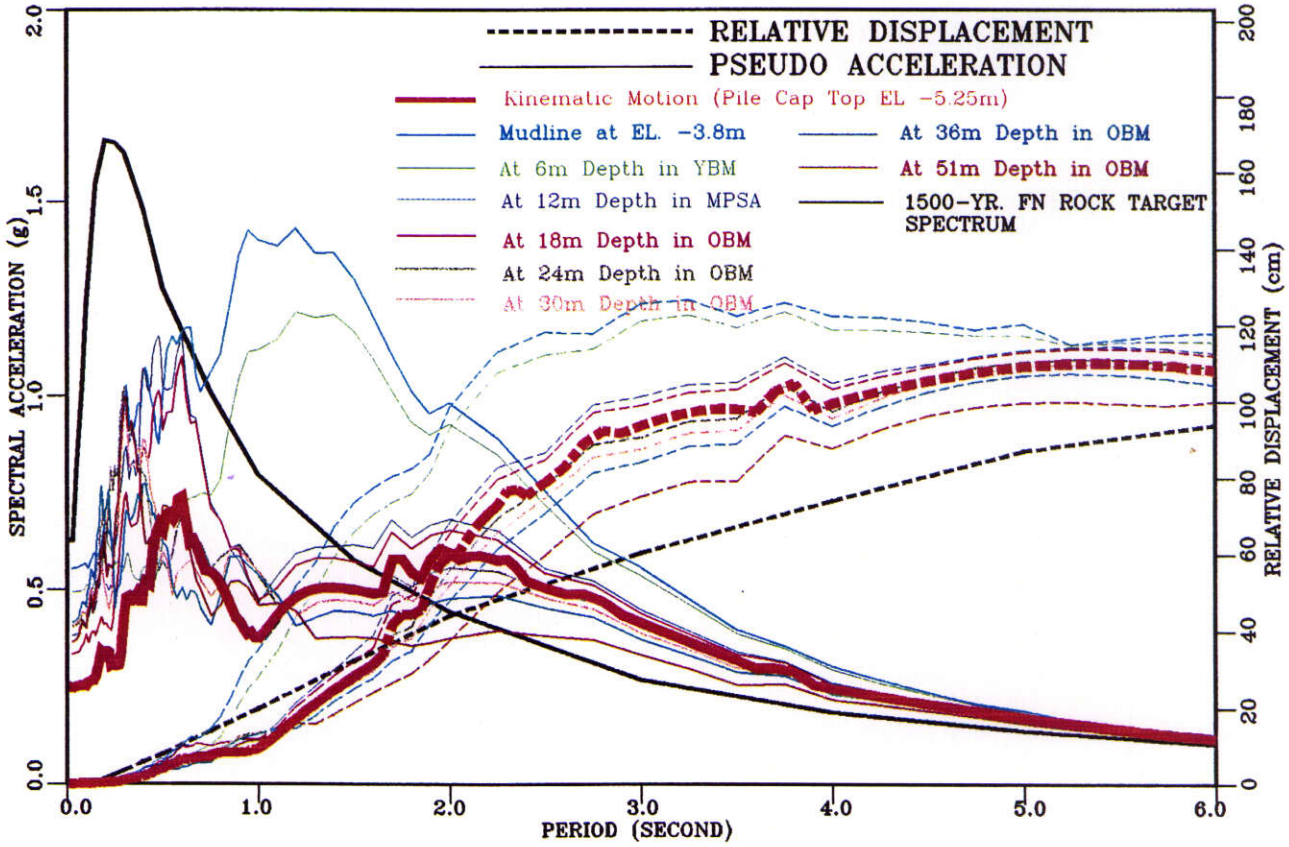

KINEMATIC AND DEPTH-VARYING FREE FIELD MOTIONS
PIER E10, INPUT ROCK MOTION SET 1, FAULT NORMAL COMPONENT
SFOBB East Span Seismic Safety Project

PLATE 8-102

Earth Mechanics FUGRO

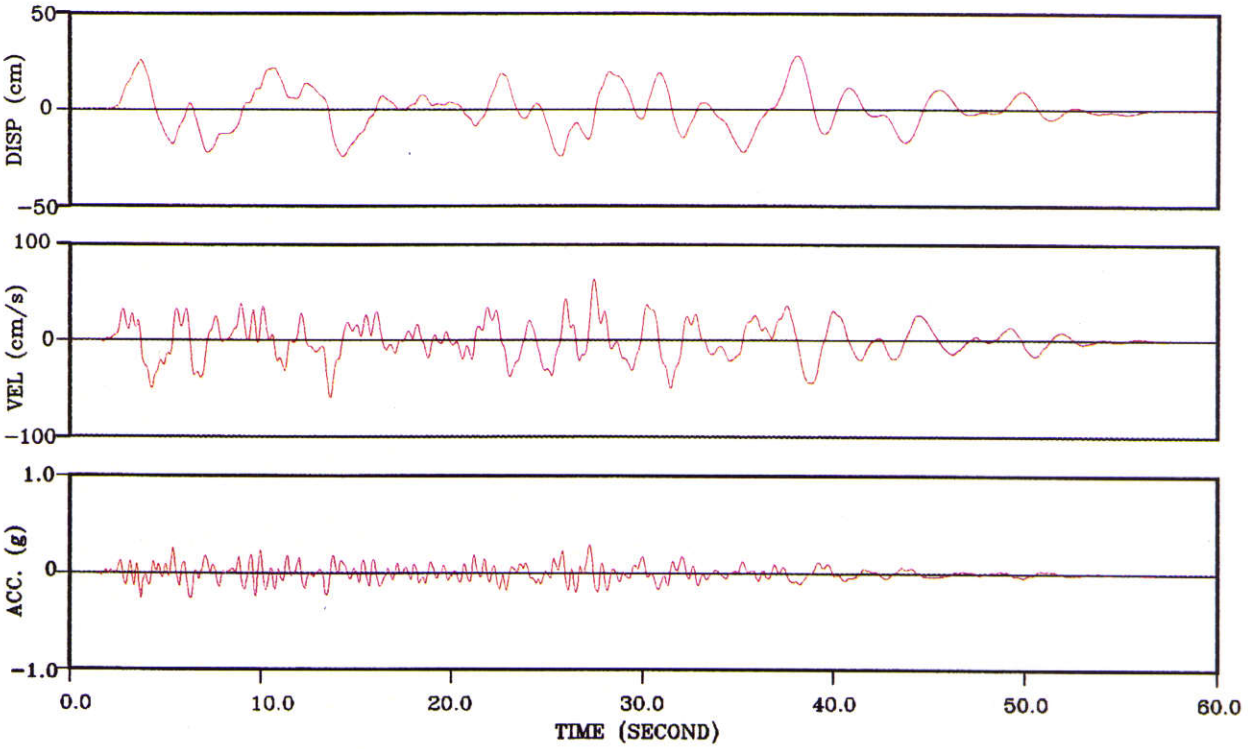

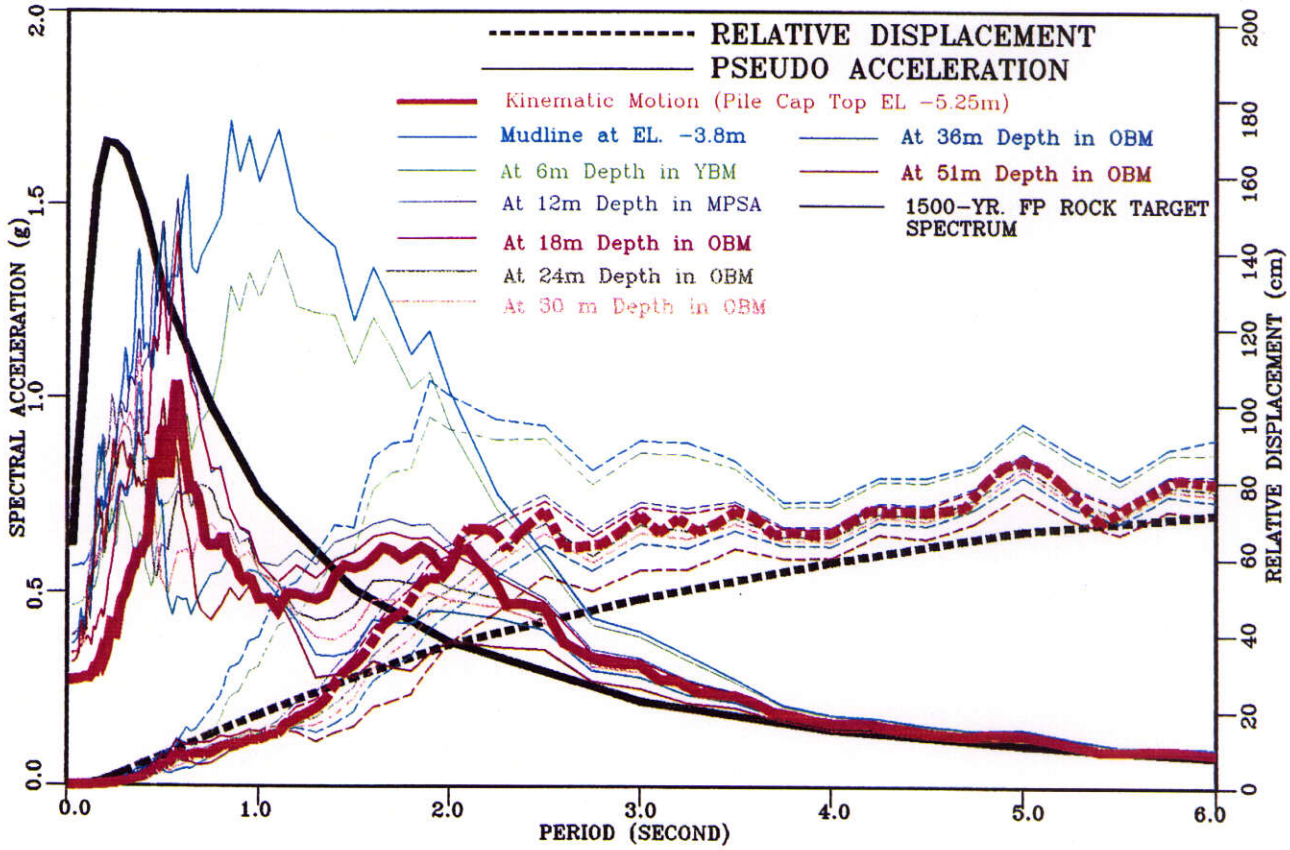

KINEMATIC AND DEPTH-VARYING FREE FIELD MOTIONS
PIER E10, INPUT ROCK MOTION SET 1, FAULT PARALLEL COMPONENT
SFOBB East Span Seismic Safety Project

Earth Mechanics FUGRO

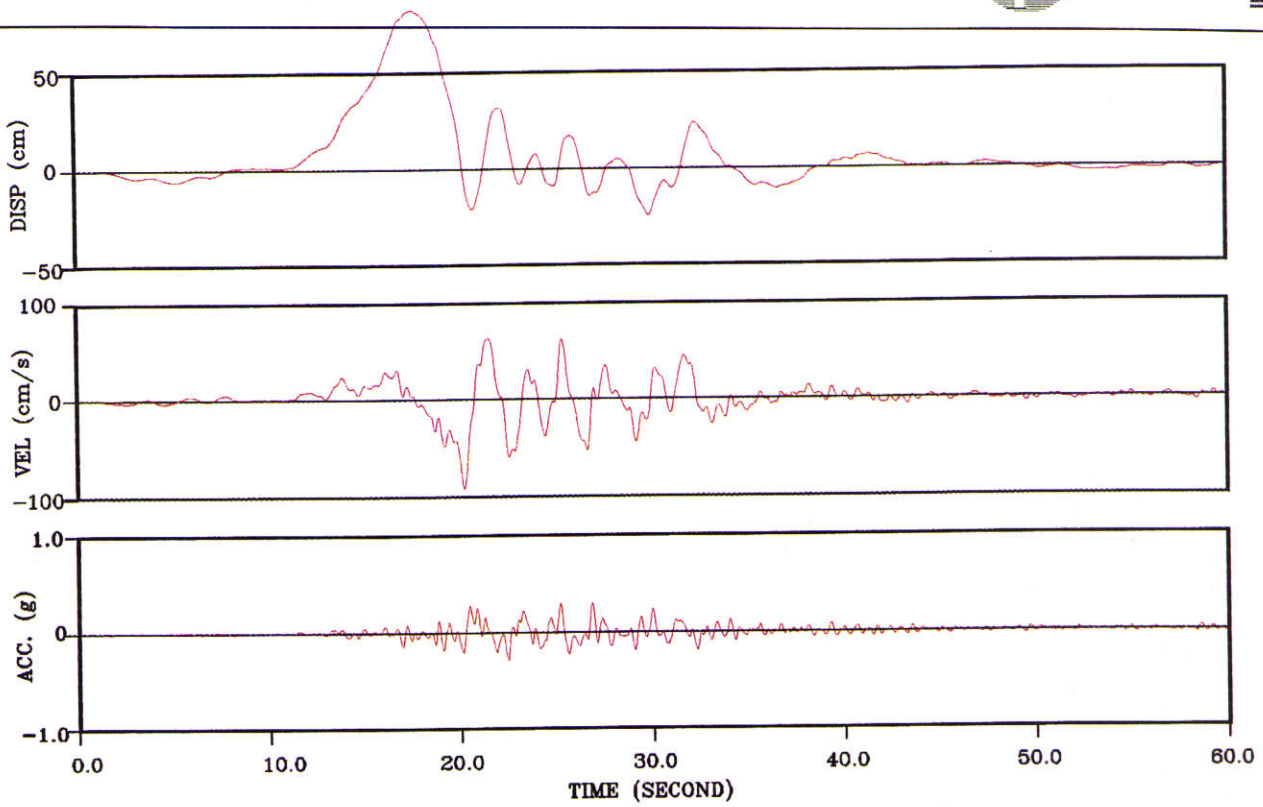

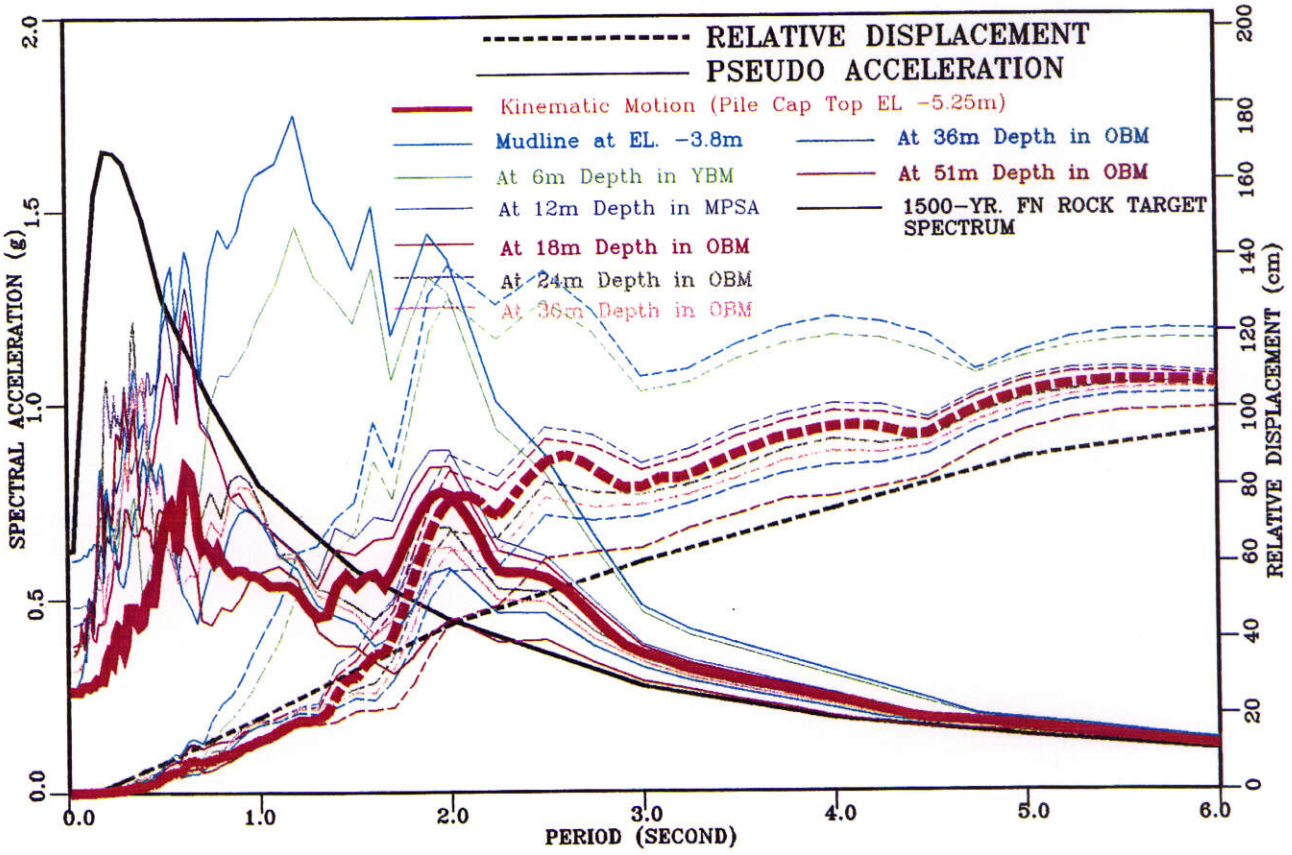

KINEMATIC AND DEPTH-VARYING FREE FIELD MOTIONS
PIER E10, INPUT ROCK MOTION SET 2, FAULT NORMAL COMPONENT
SFOBB East Span Seismic Safety Project

PLATE 8-104

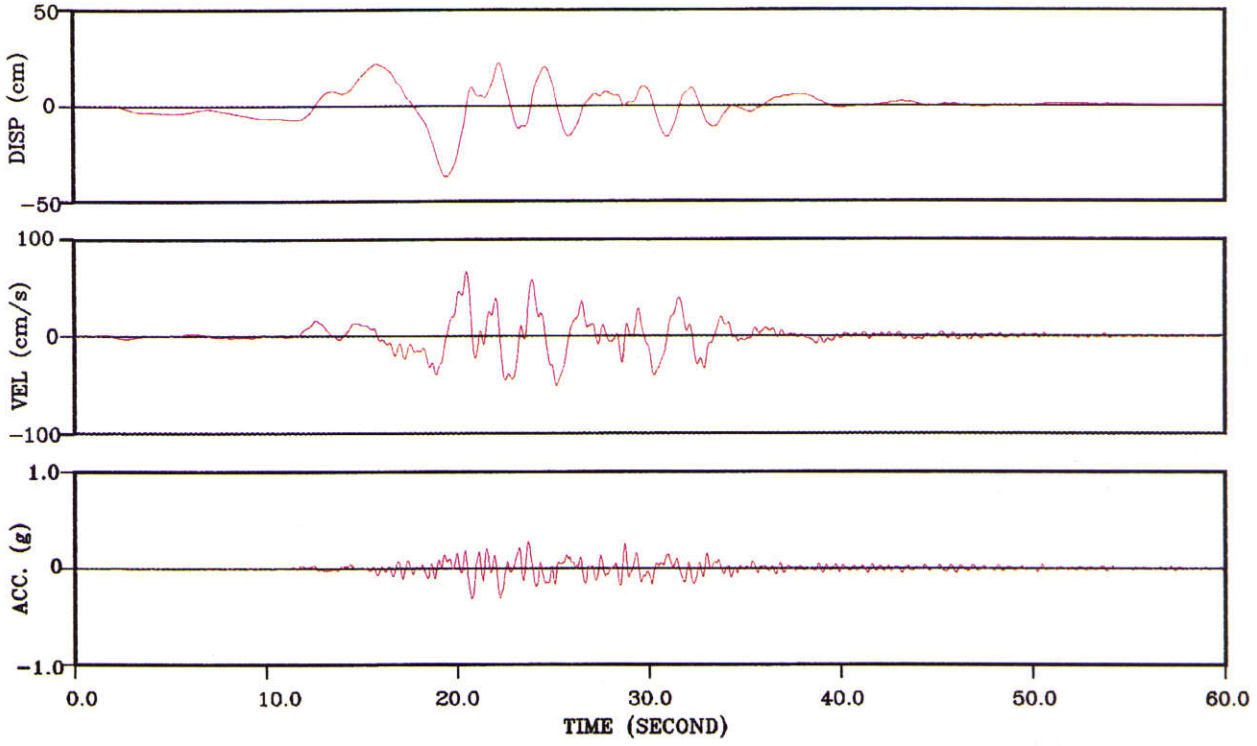

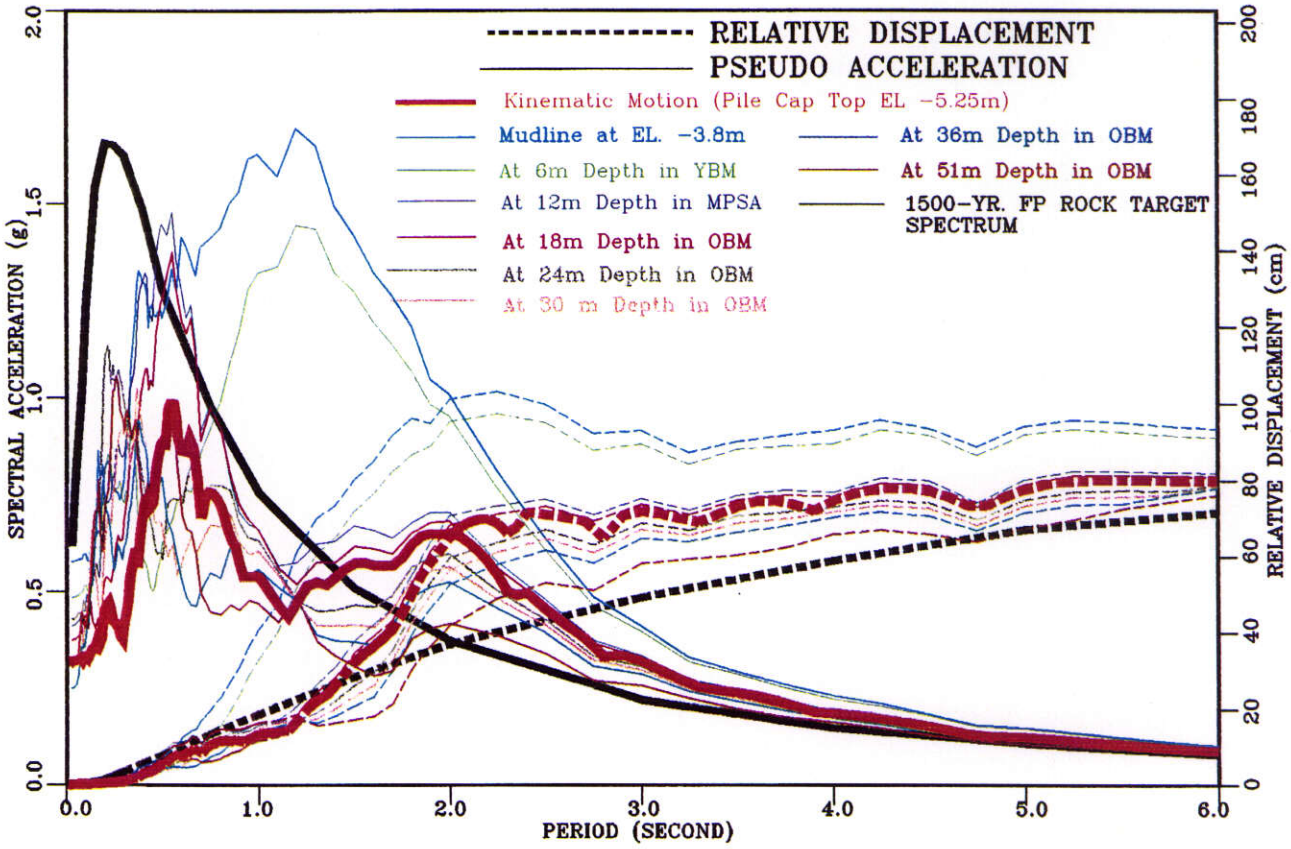

KINEMATIC AND DEPTH-VARYING FREE FIELD MOTIONS
PIER E10, INPUT ROCK MOTION SET 2, FAULT PARALLEL COMPONENT
SFOBB East Span Seismic Safety Project

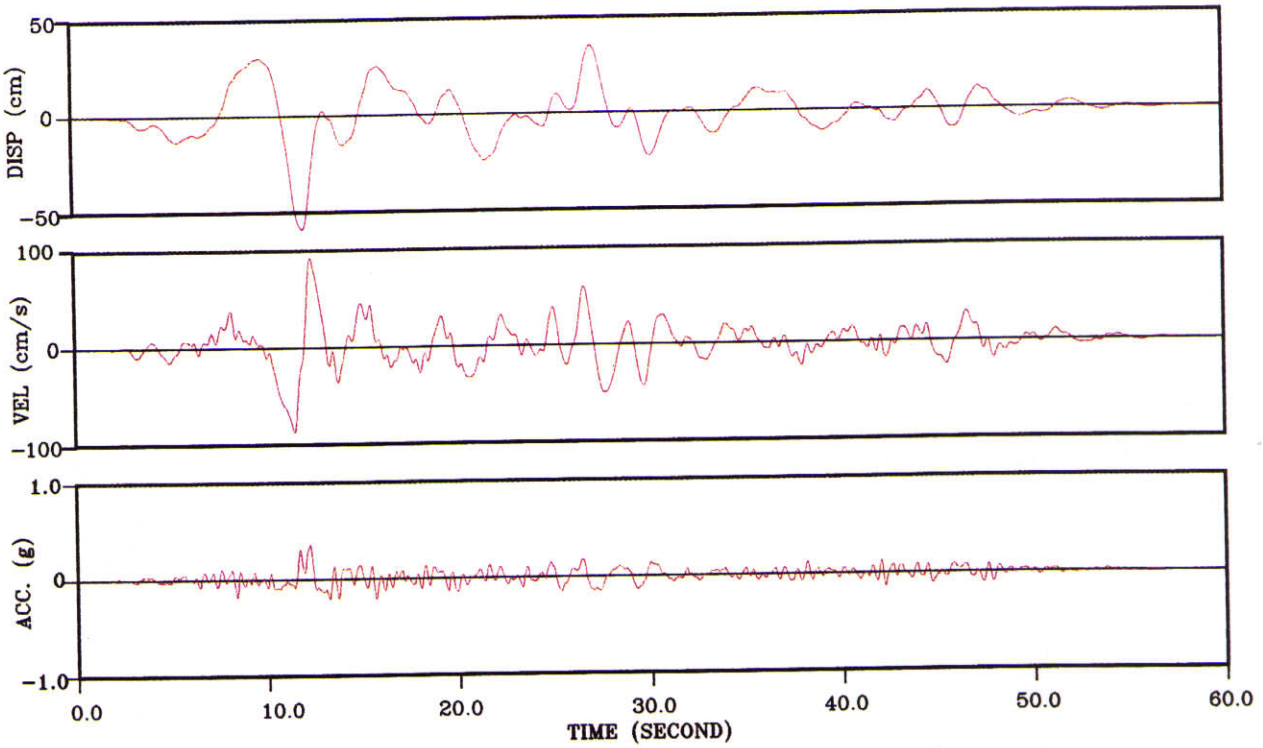

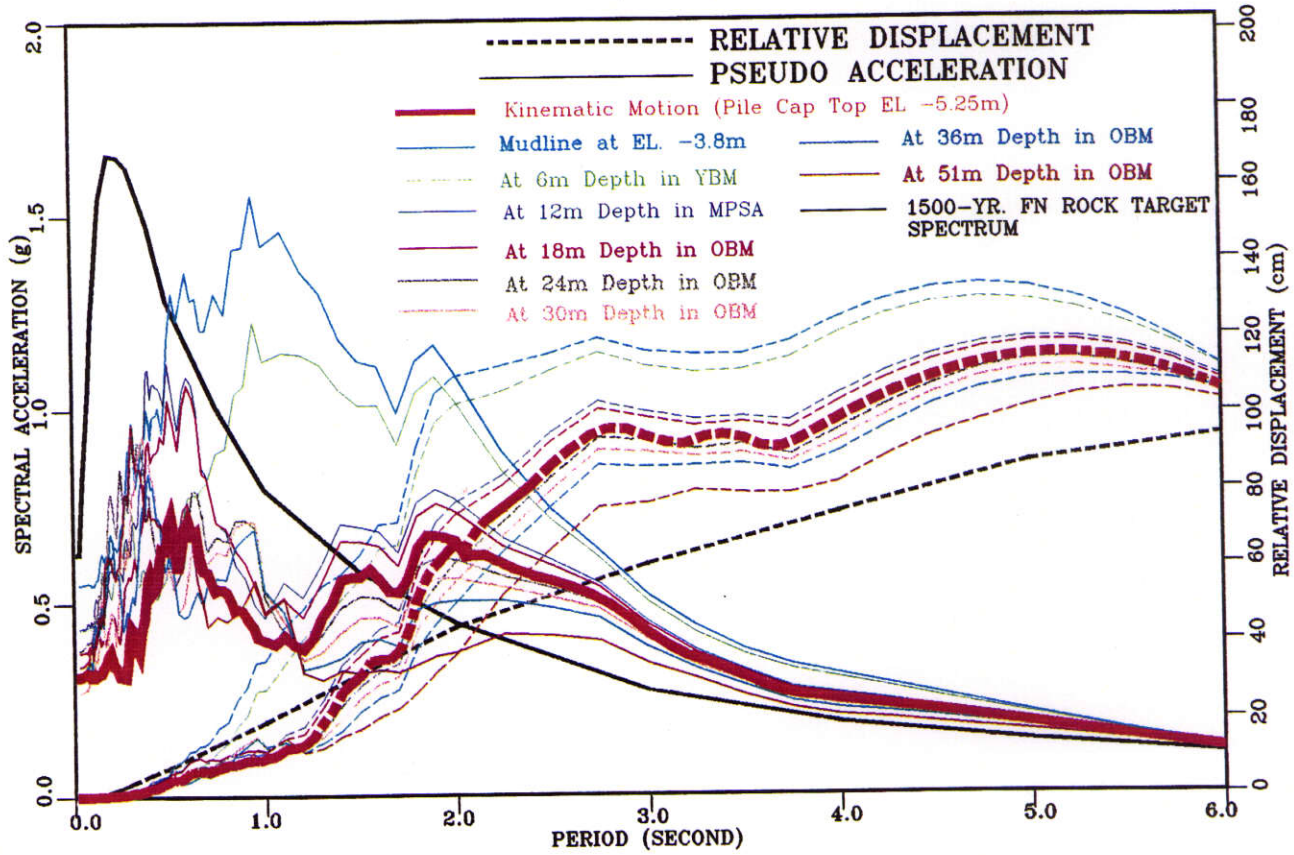

KINEMATIC AND DEPTH-VARYING FREE FIELD MOTIONS
PIER E10, INPUT ROCK MOTION SET 3, FAULT NORMAL COMPONENT
SFOBB East Span Seismic Safety Project

PLATE 8-106

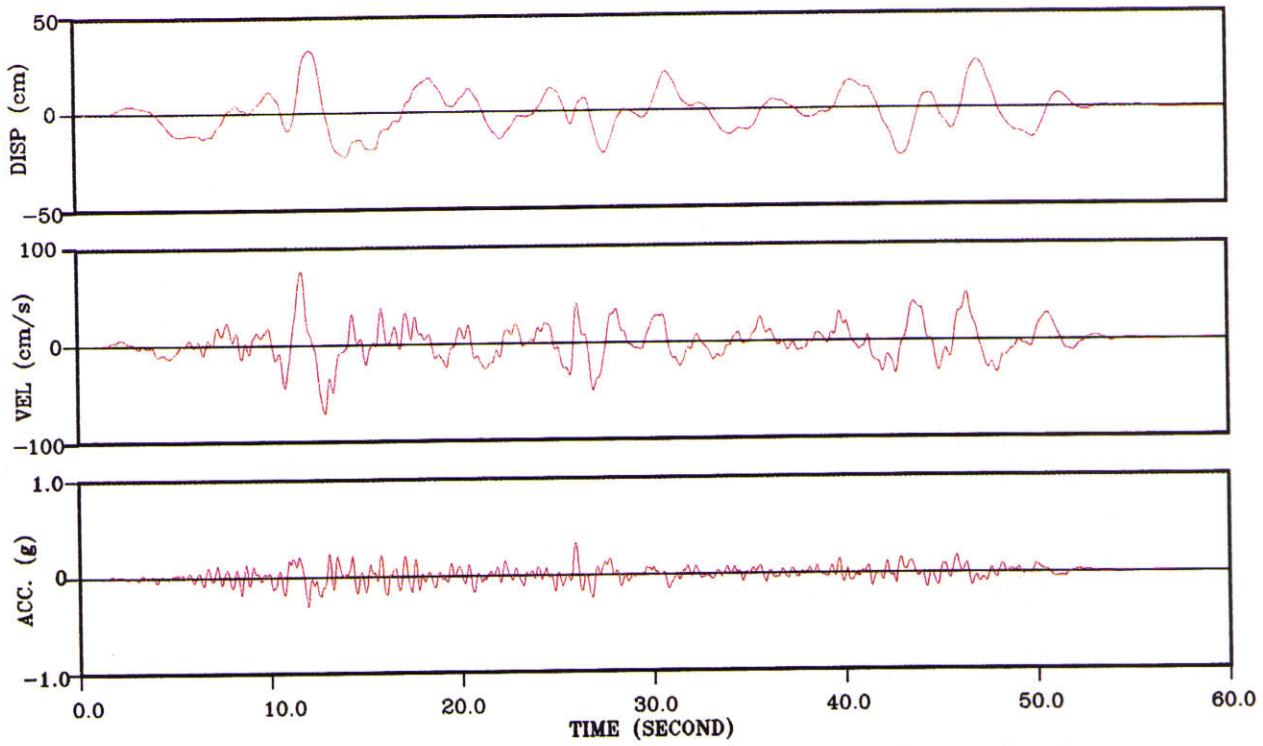

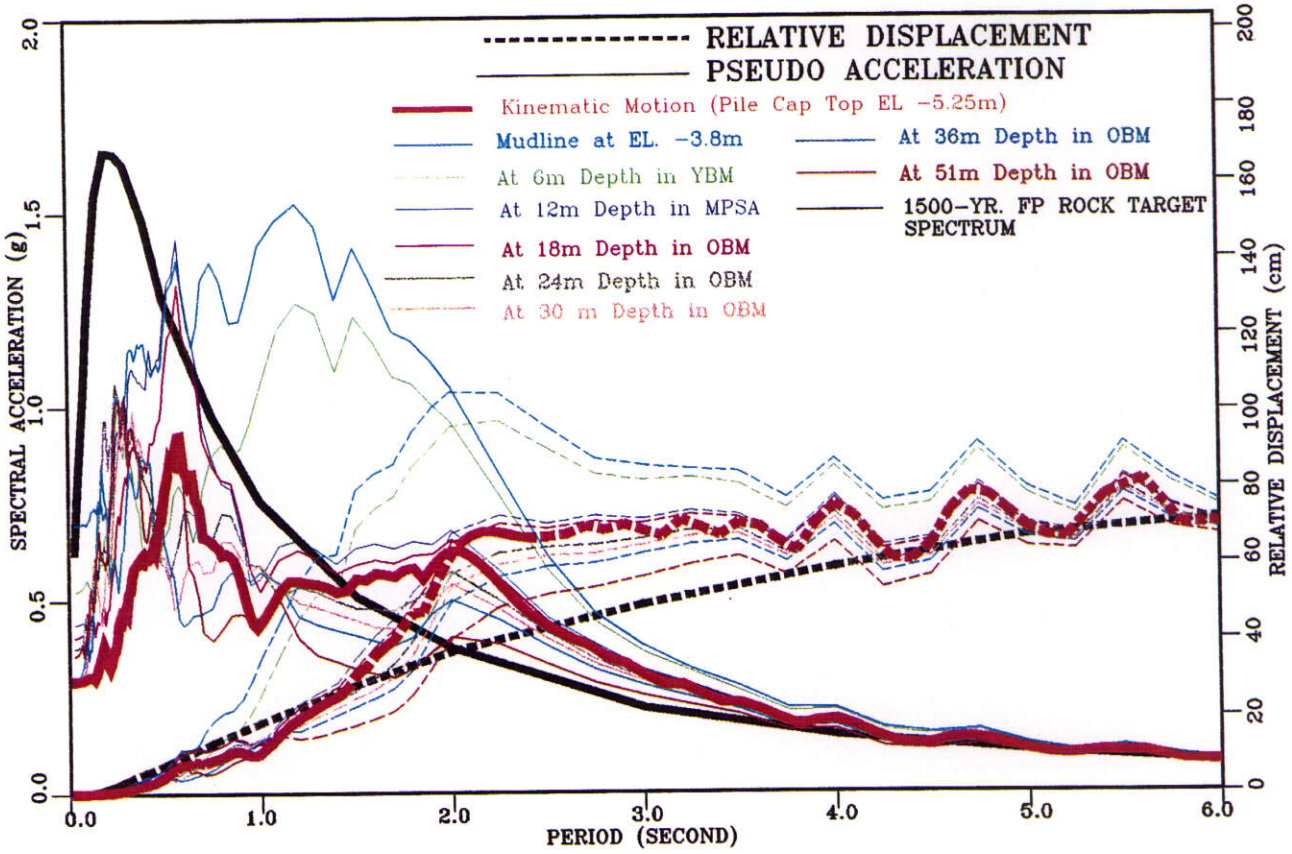

KINEMATIC AND DEPTH-VARYING FREE FIELD MOTIONS
PIER E10, INPUT ROCK MOTION SET 3, FAULT PARALLEL COMPONENT
SFOBB East Span Seismic Safety Project

PLATE 8-107

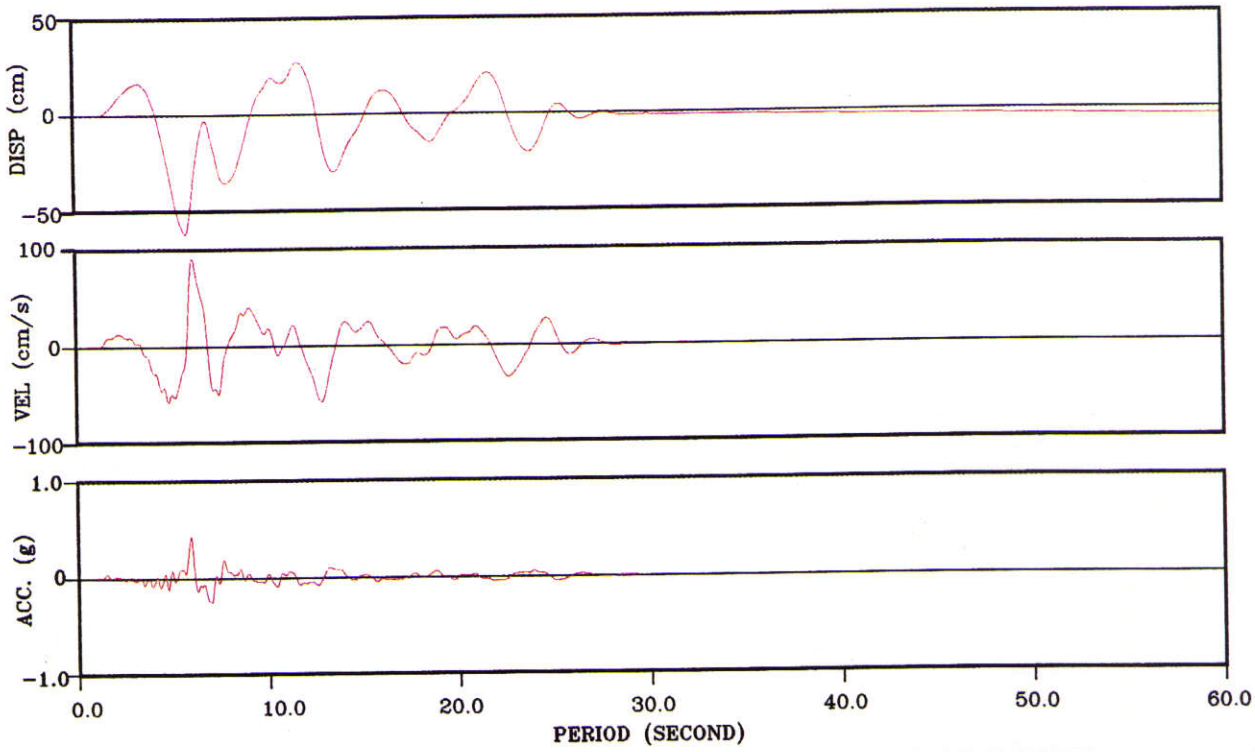

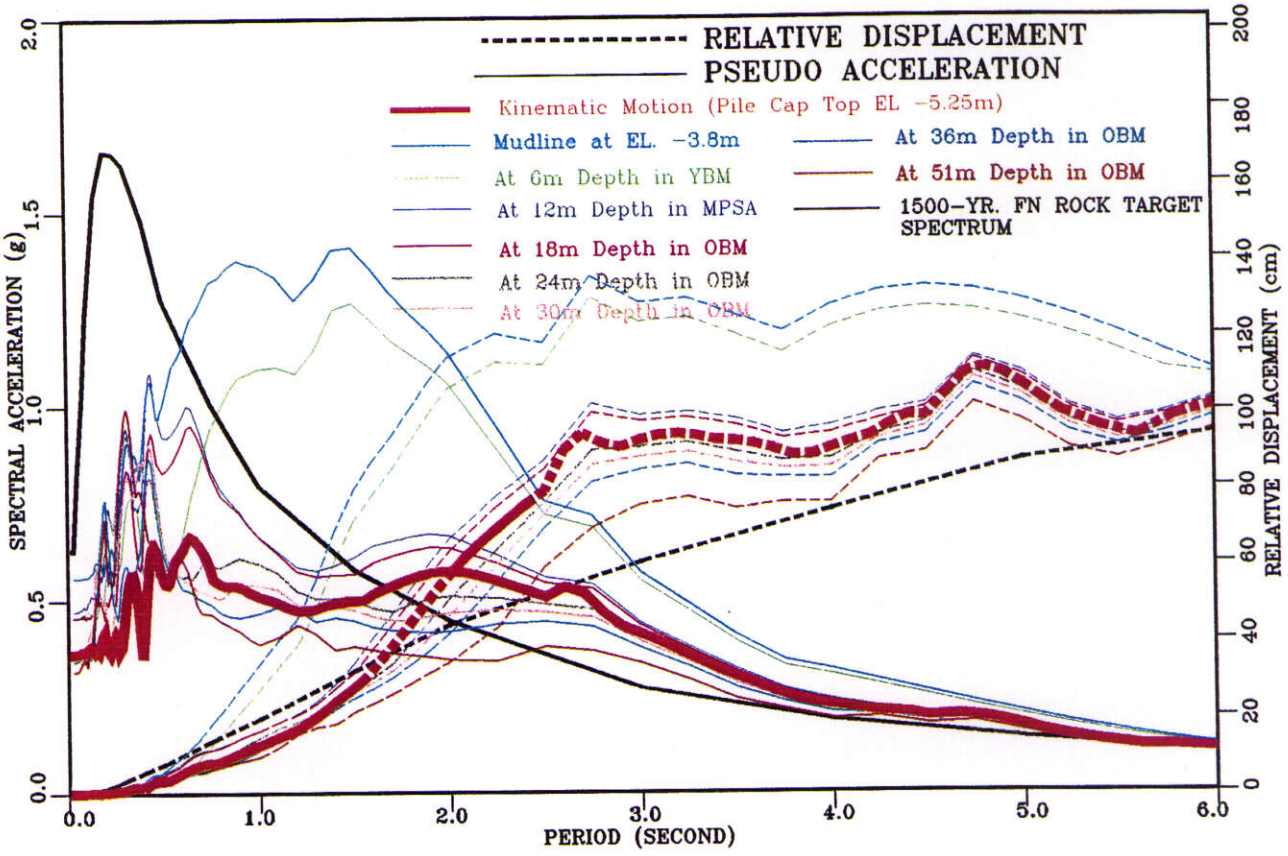

KINEMATIC AND DEPTH-VARYING FREE FIELD MOTIONS
PIER E10, INPUT ROCK MOTION SET 4, FAULT NORMAL COMPONENT
SFOBB East Span Seismic Safety Project

PLATE 8-108

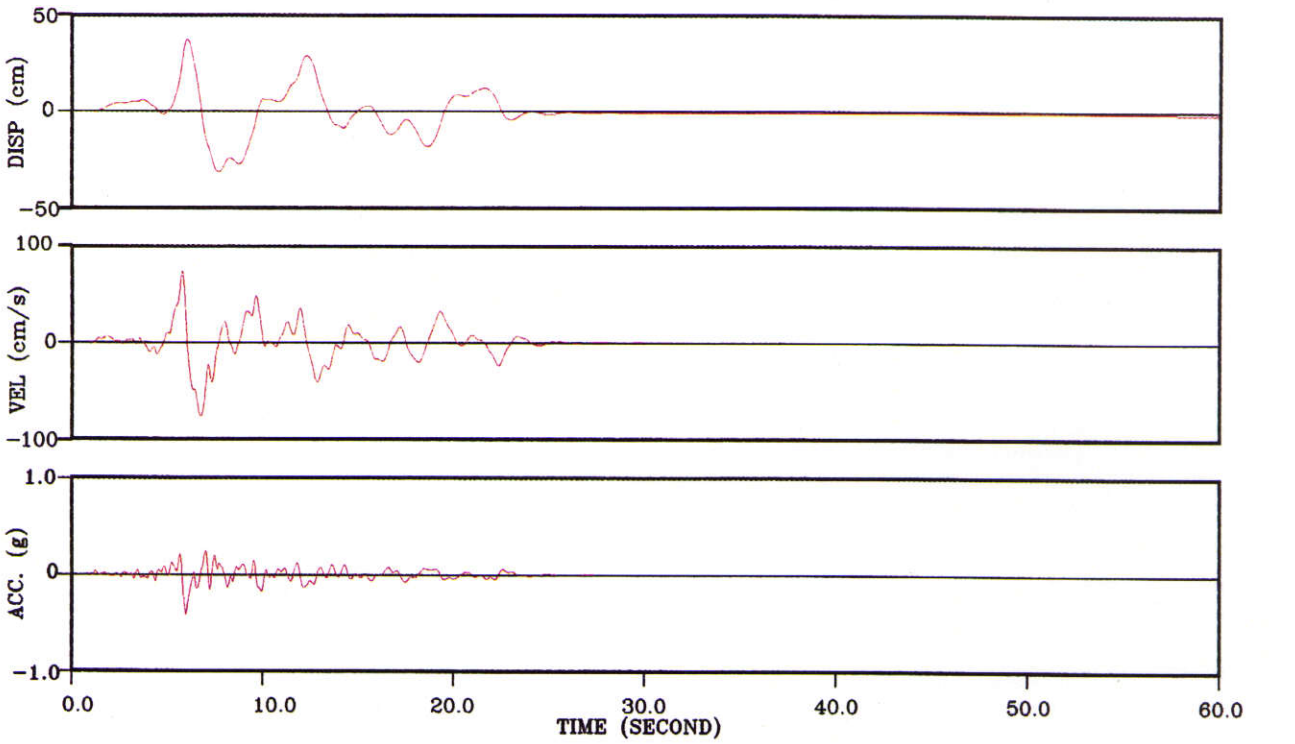

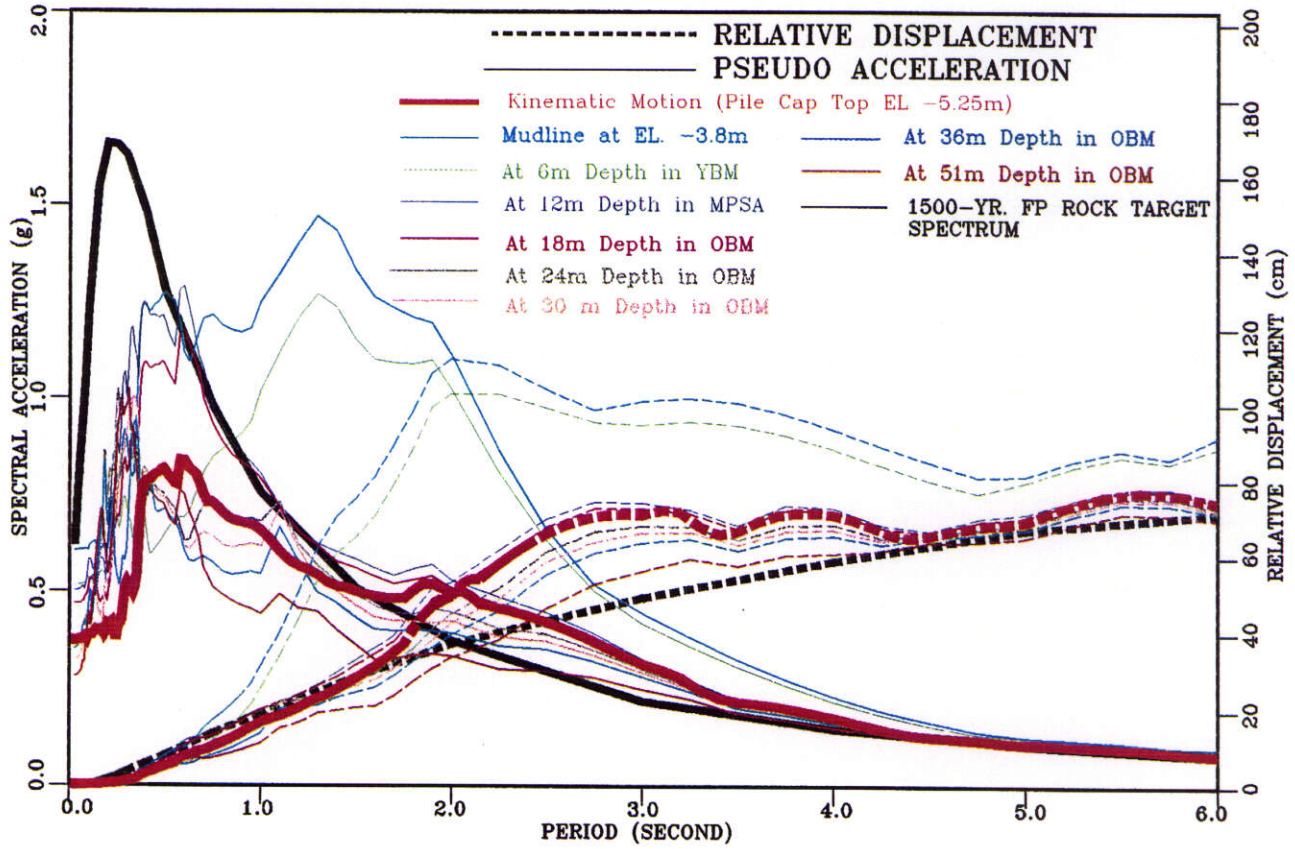

KINEMATIC AND DEPTH-VARYING FREE FIELD MOTIONS
PIER E10, INPUT ROCK MOTION SET 4, FAULT PARALLEL COMPONENT
SFOBB East Span Seismic Safety Project

PLATE 8-109

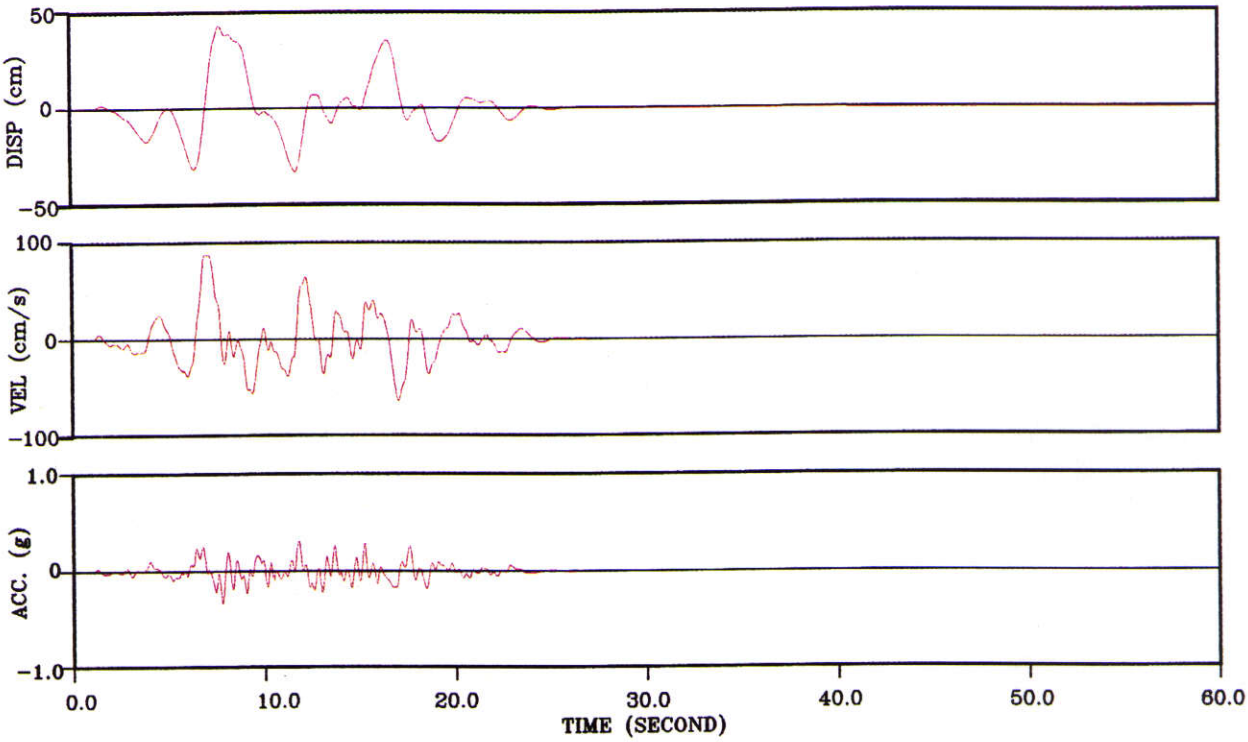

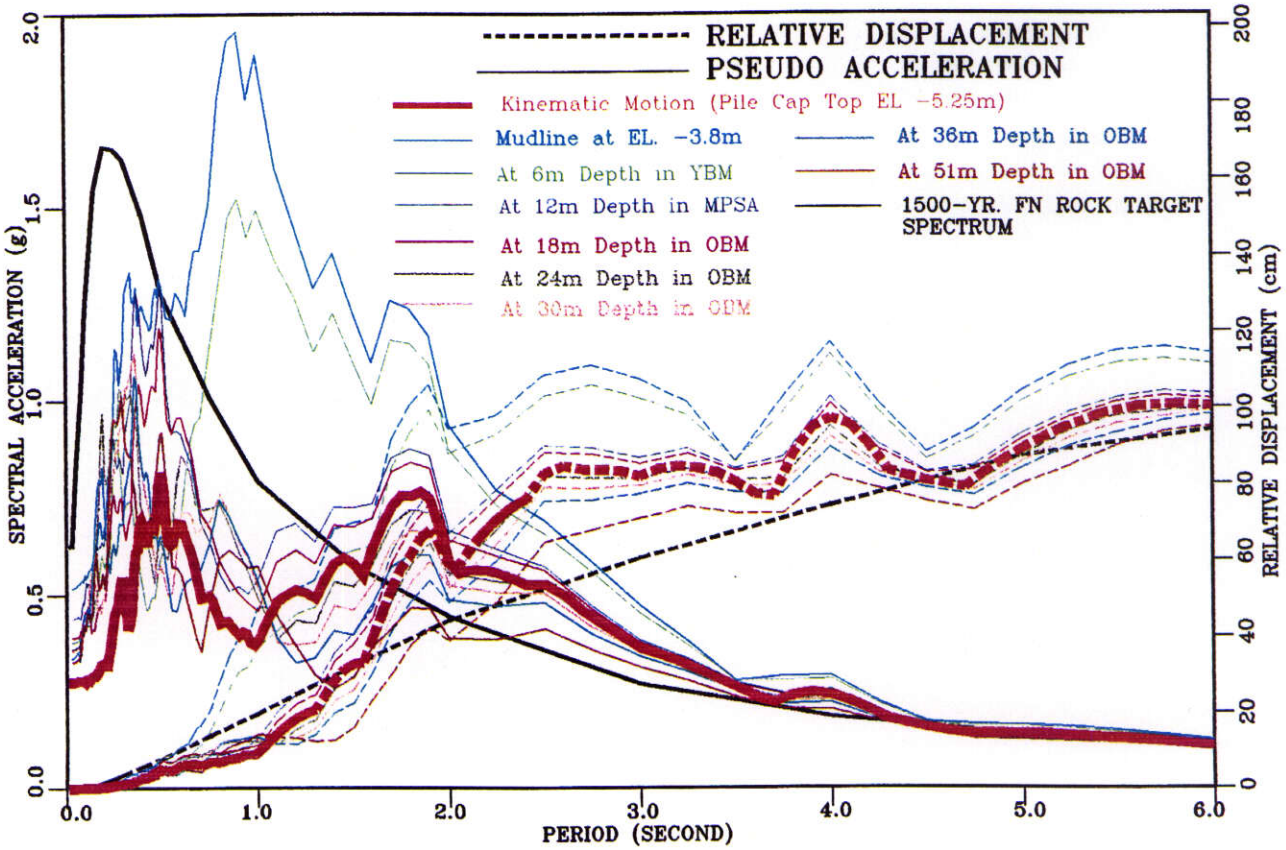

KINEMATIC AND DEPTH-VARYING FREE FIELD MOTIONS
PIER E10, INPUT ROCK MOTION SET 5, FAULT NORMAL COMPONENT
SFOBB East Span Seismic Safety Project

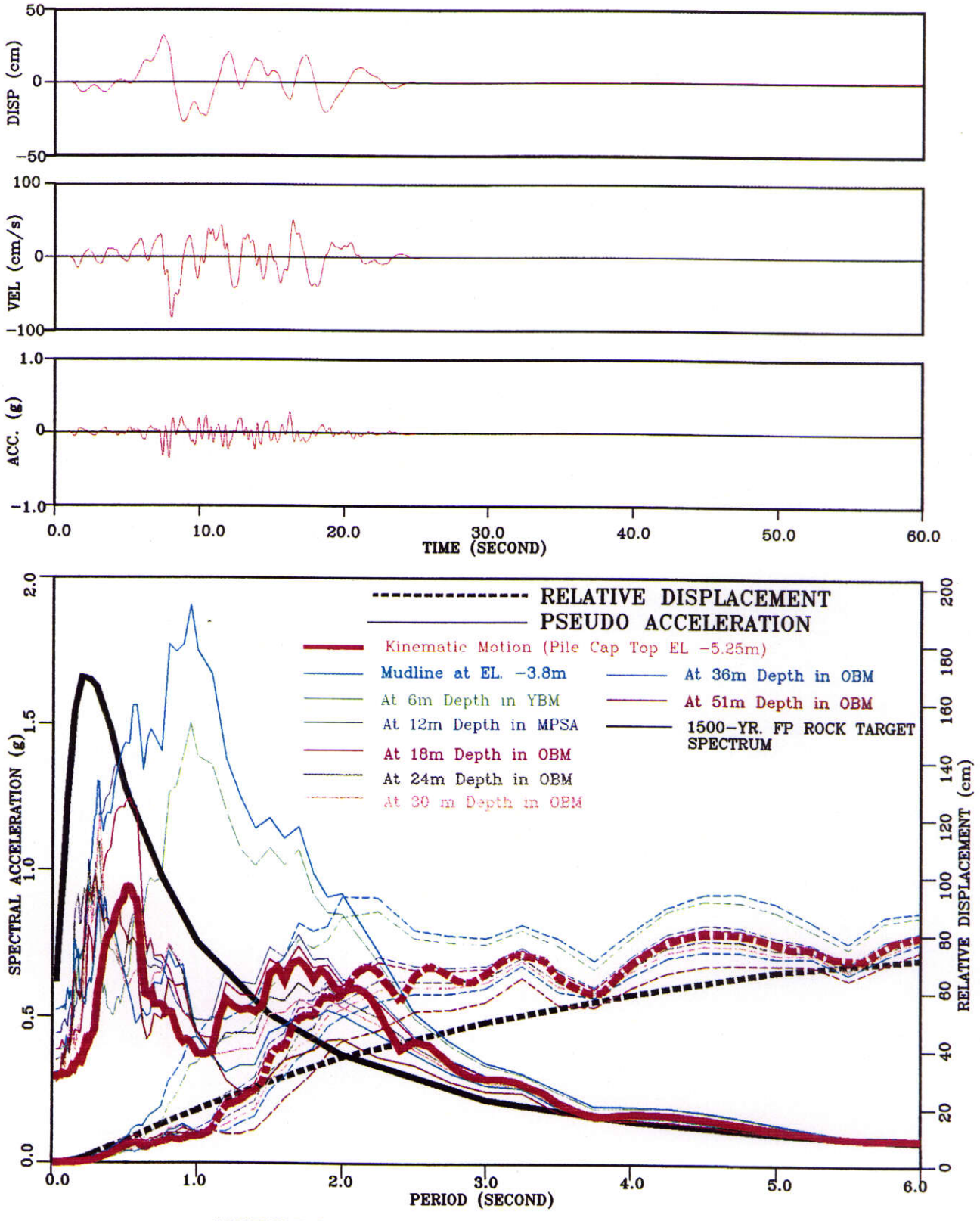

KINEMATIC AND DEPTH-VARYING FREE FIELD MOTIONS
PIER E10, INPUT ROCK MOTION SET 5, FAULT PARALLEL COMPONENT
SFOBB East Span Seismic Safety Project

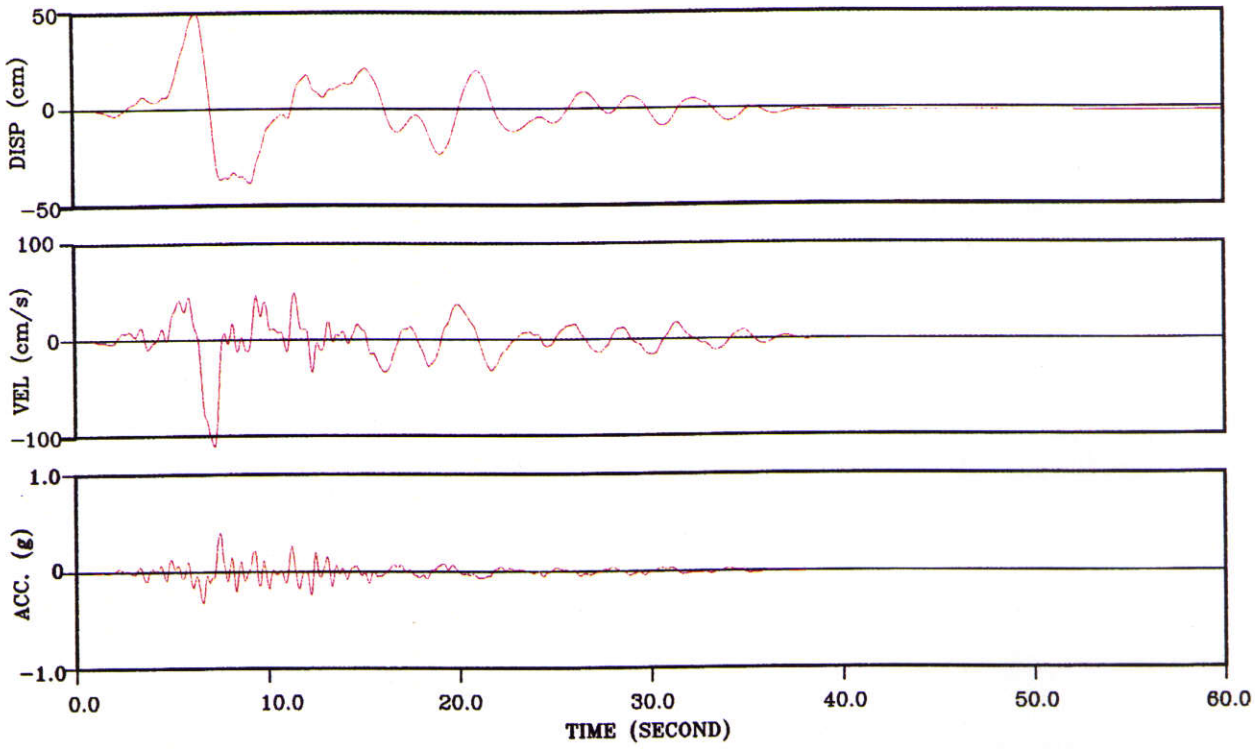

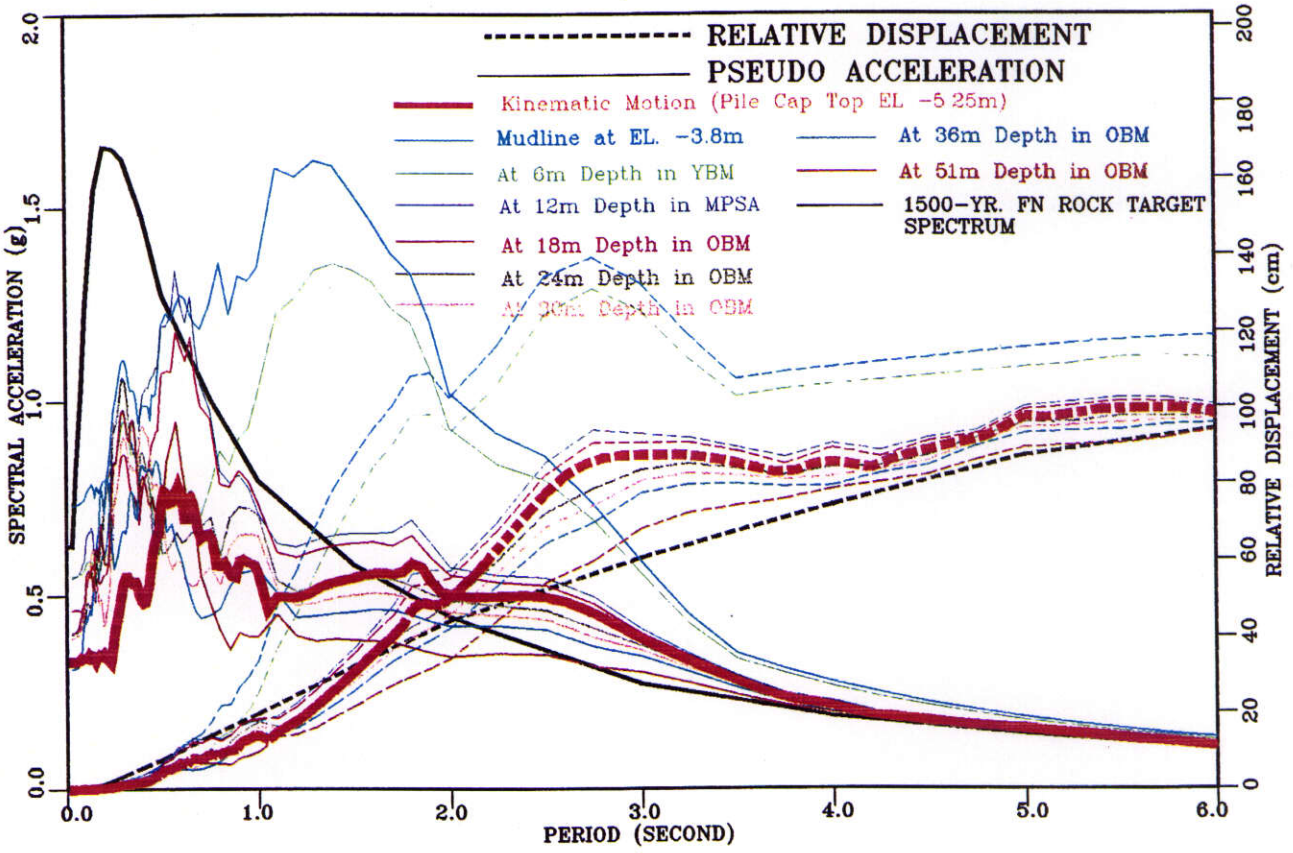

KINEMATIC AND DEPTH-VARYING FREE FIELD MOTIONS
PIER E10, INPUT ROCK MOTION SET 6, FAULT NORMAL COMPONENT
SFOBB East Span Seismic Safety Project

PLATE 8-112

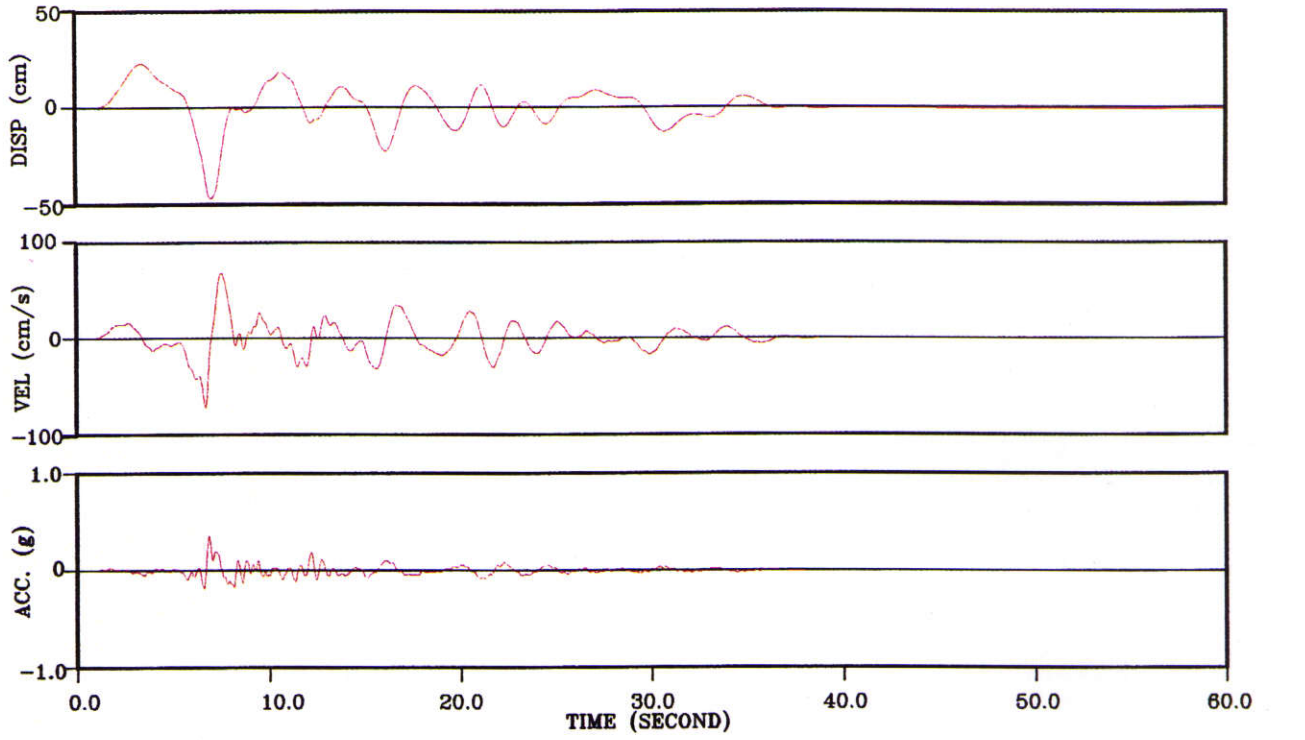

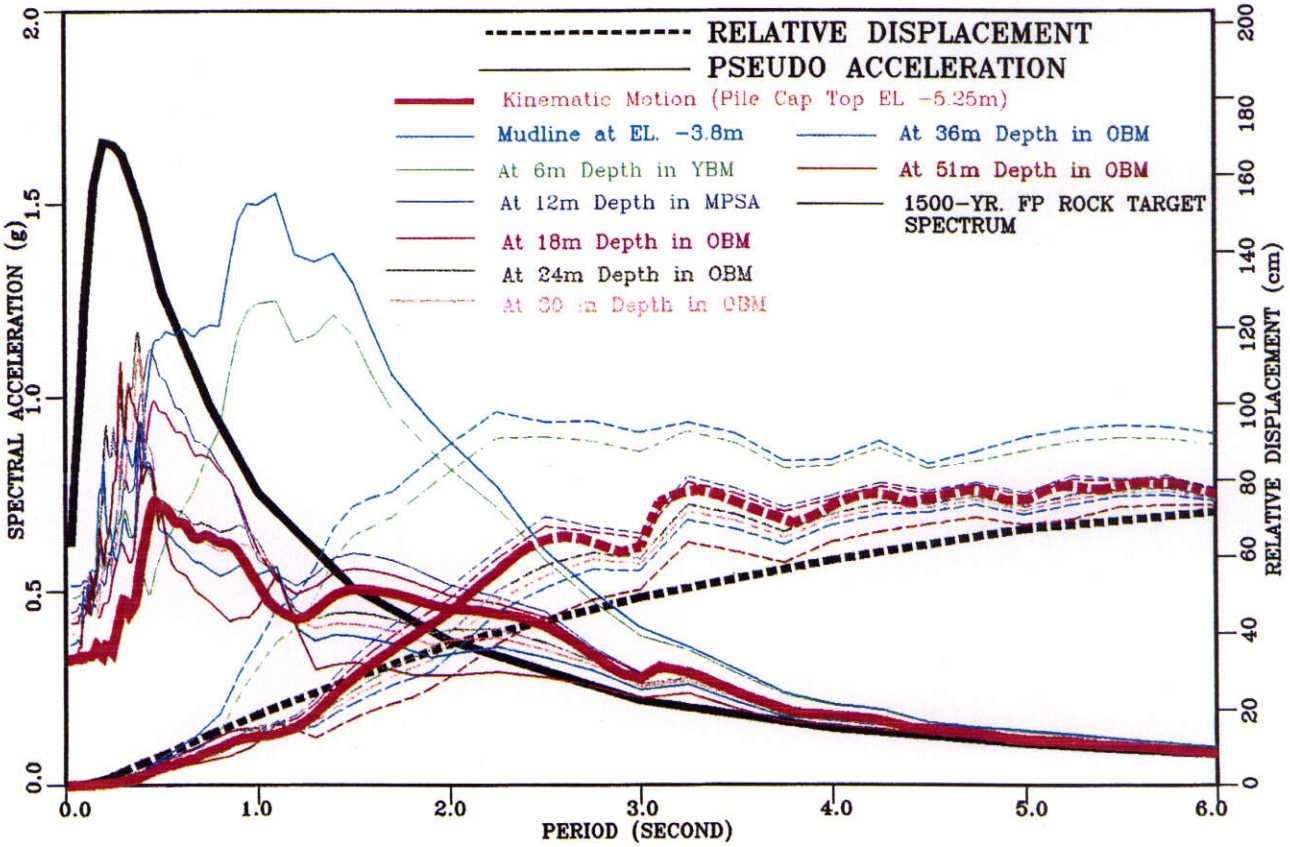

KINEMATIC AND DEPTH-VARYING FREE FIELD MOTIONS
PIER E10, INPUT ROCK MOTION SET 6, FAULT PARALLEL COMPONENT
SFOBB East Span Seismic Safety Project

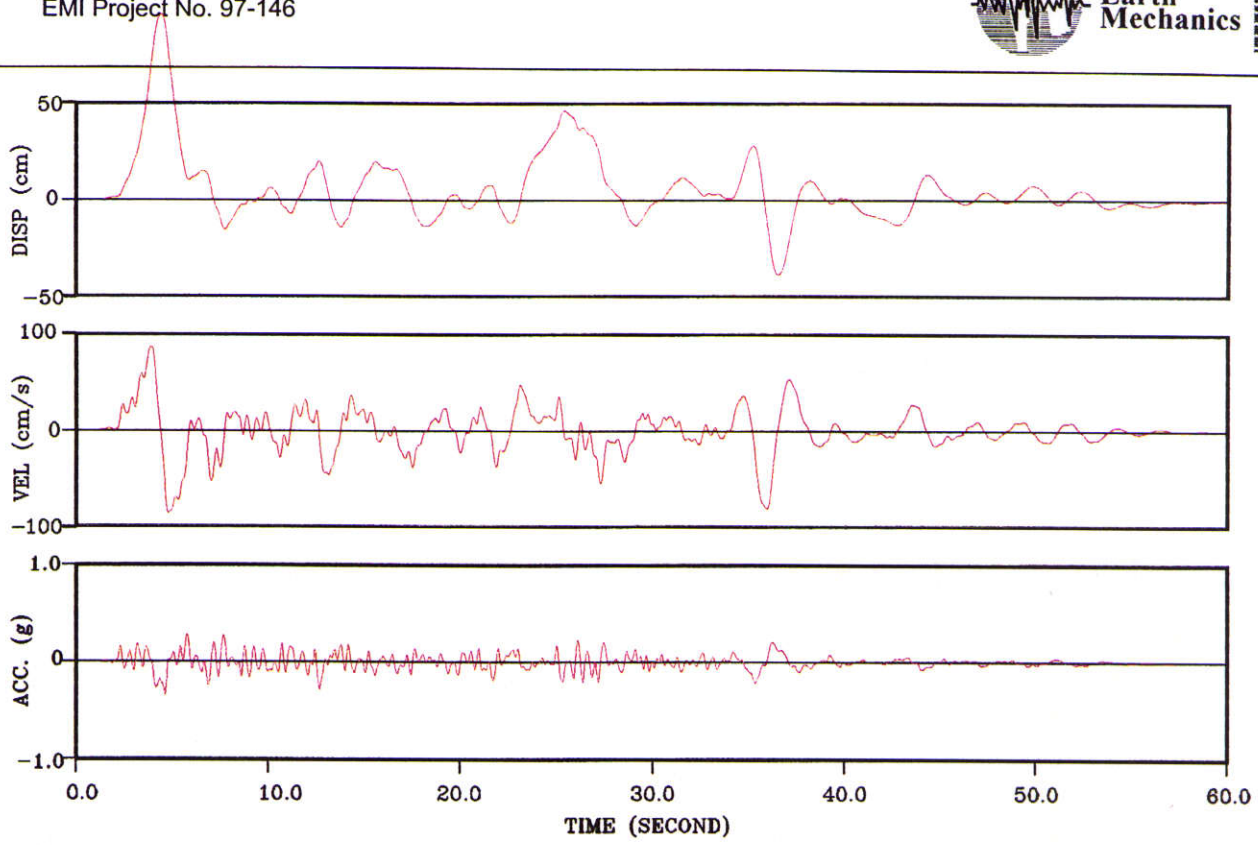

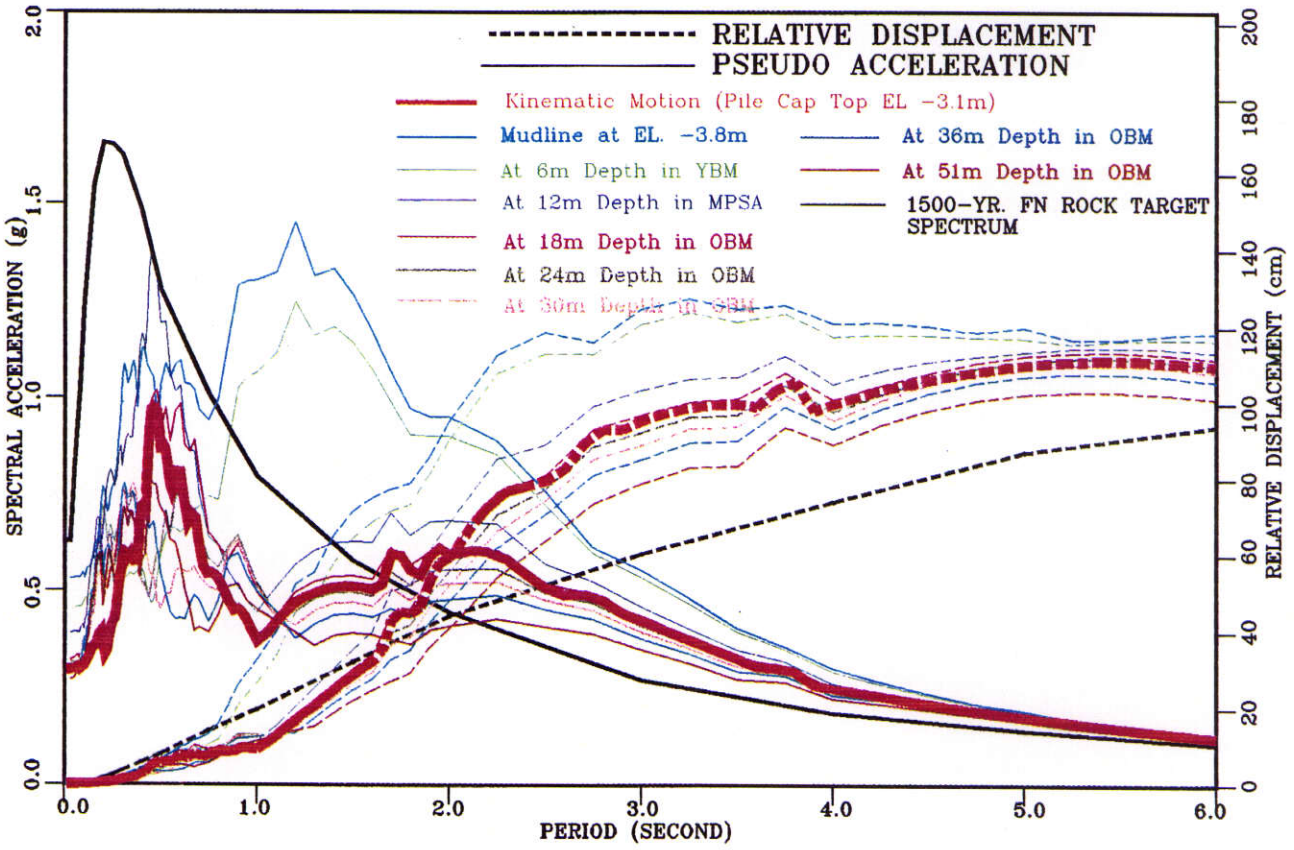

KINEMATIC AND DEPTH-VARYING FREE FIELD MOTIONS
PIER E11, INPUT ROCK MOTION SET 1, FAULT NORMAL COMPONENT
SFOBB East Span Seismic Safety Project

PLATE 8-114

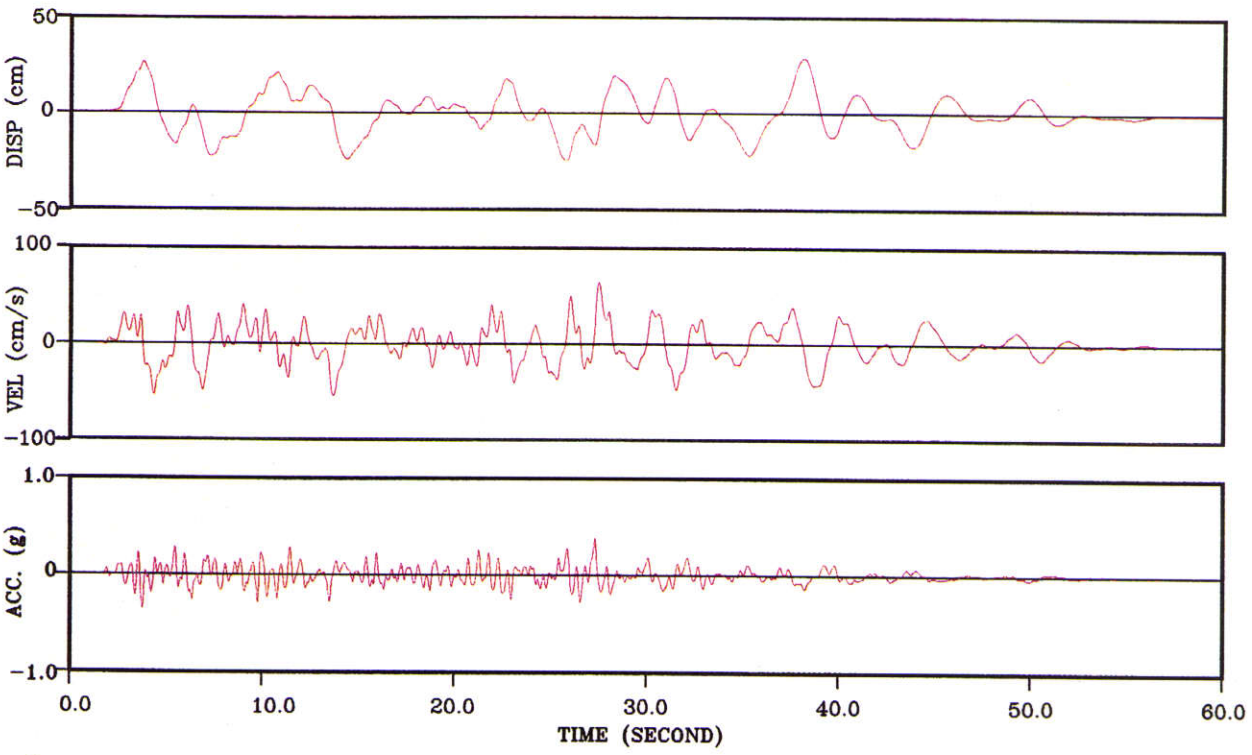

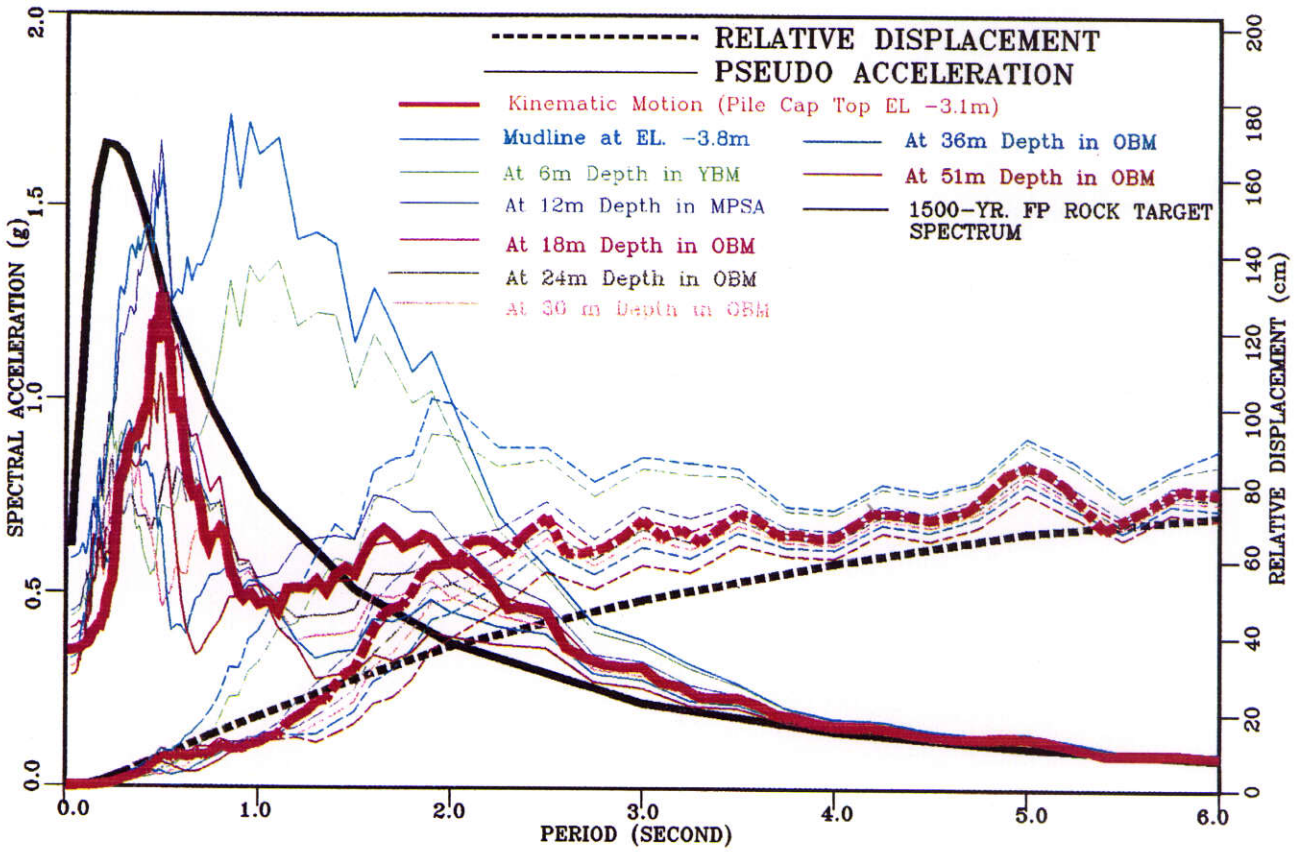

KINEMATIC AND DEPTH-VARYING FREE FIELD MOTIONS
PIER E11, INPUT ROCK MOTION SET 1, FAULT PARALLEL COMPONENT
SFOBB East Span Seismic Safety Project

Earth Mechanics FUGRO

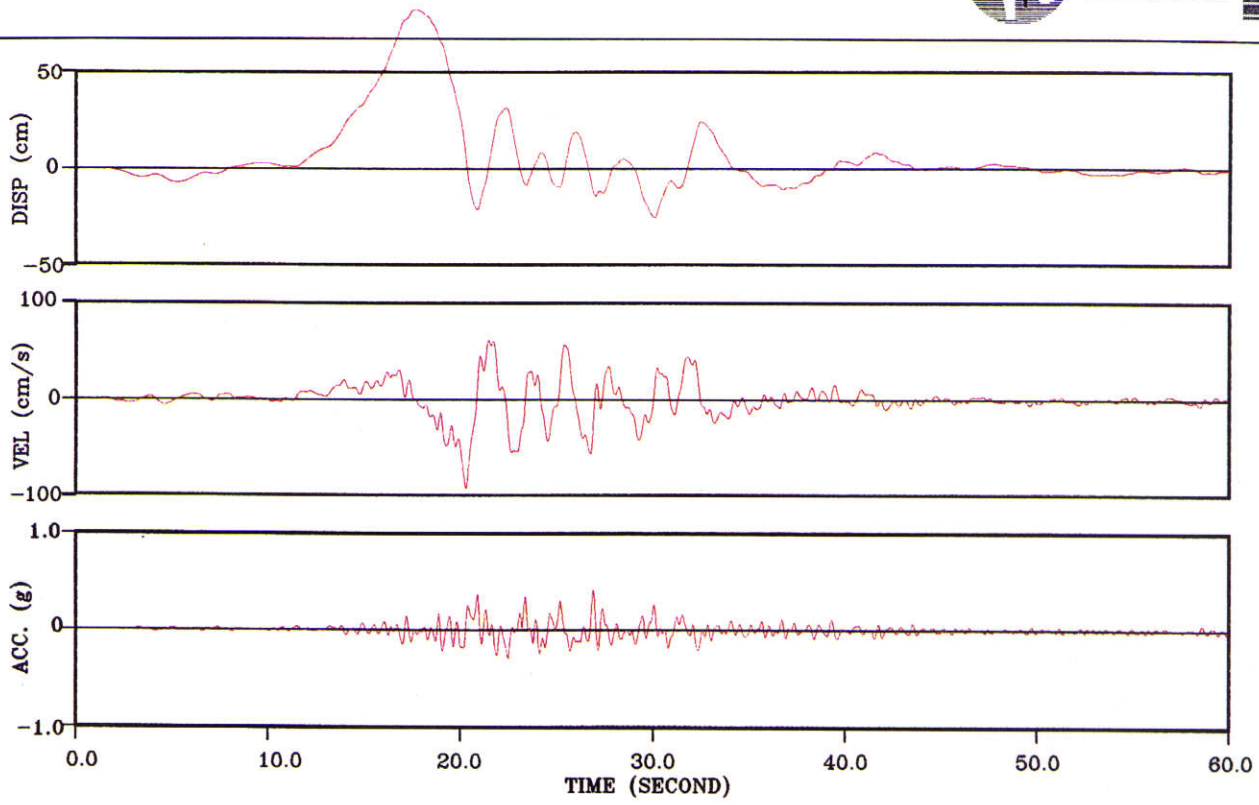

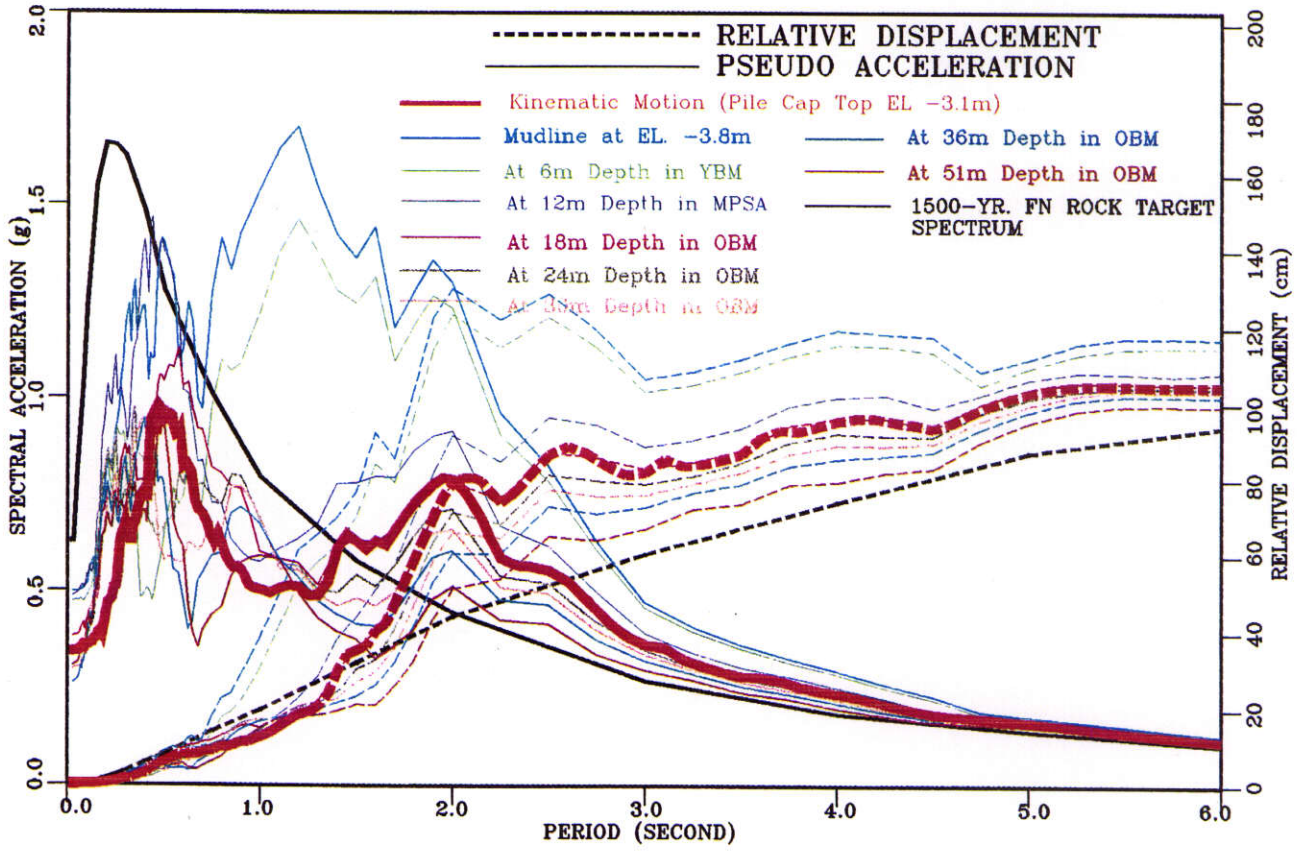

KINEMATIC AND DEPTH-VARYING FREE FIELD MOTIONS
PIER E11, INPUT ROCK MOTION SET 2, FAULT NORMAL COMPONENT
SFOBB East Span Seismic Safety Project

PLATE 8-116

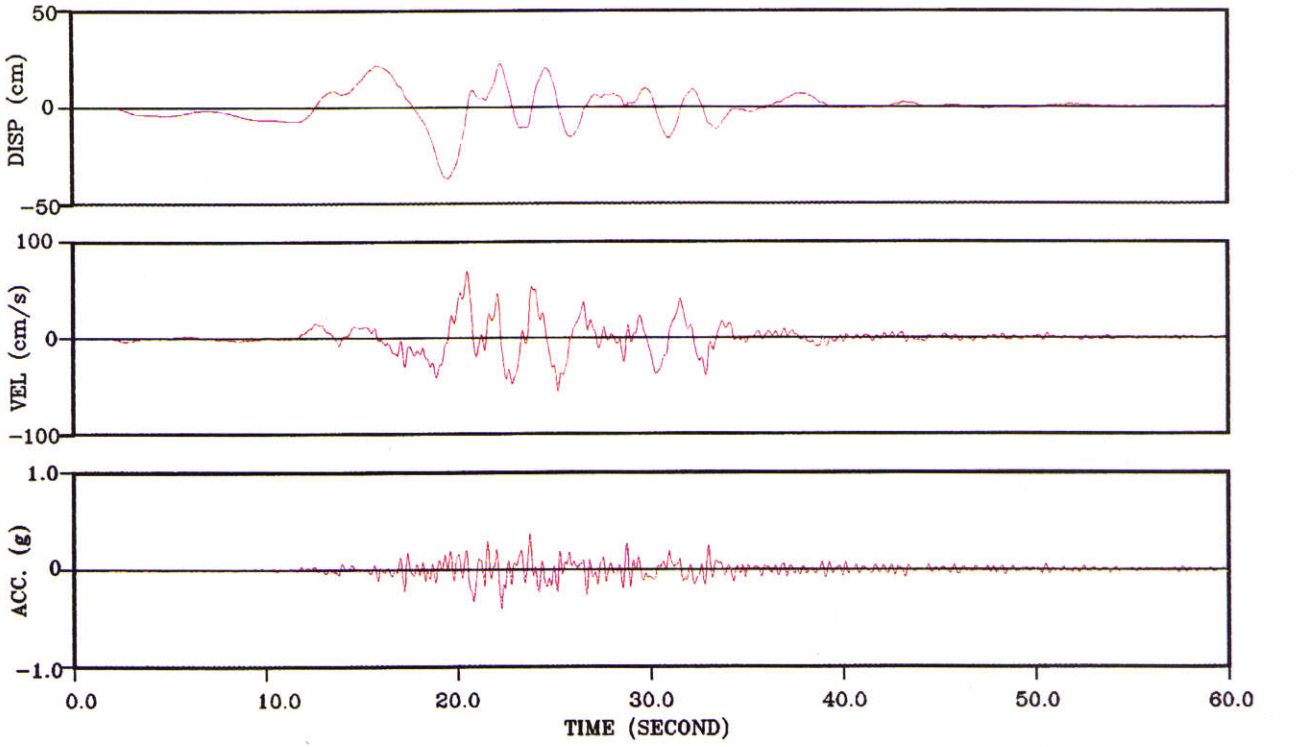

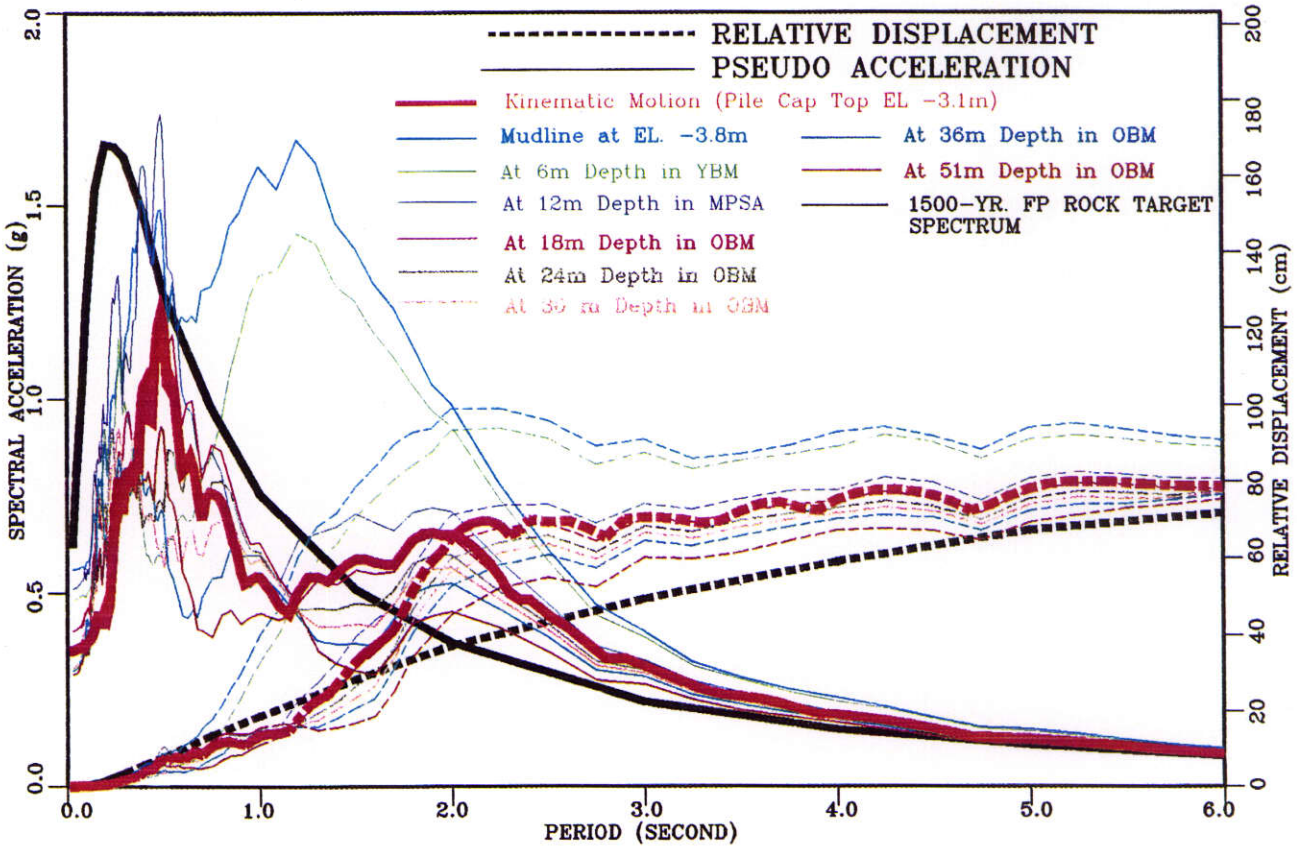

KINEMATIC AND DEPTH-VARYING FREE FIELD MOTIONS
PIER E11, INPUT ROCK MOTION SET 2, FAULT PARALLEL COMPONENT
SFOBB East Span Seismic Safety Project

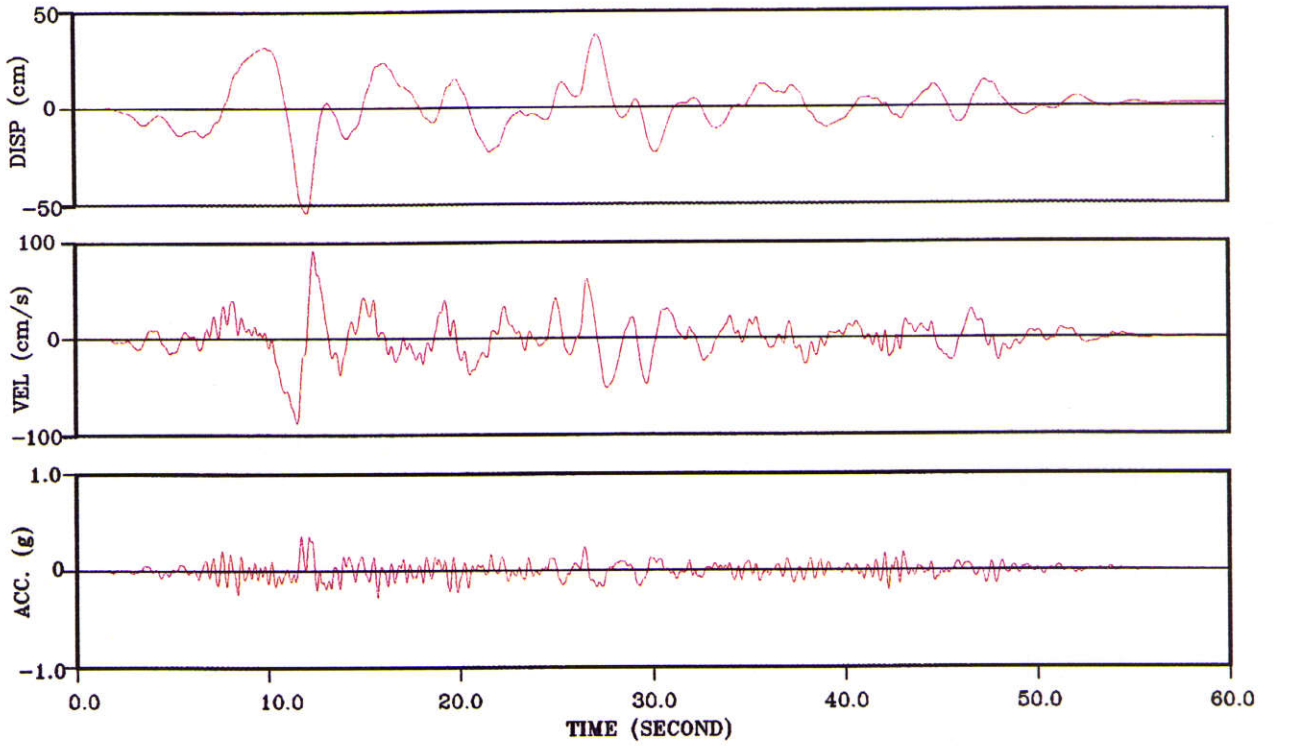

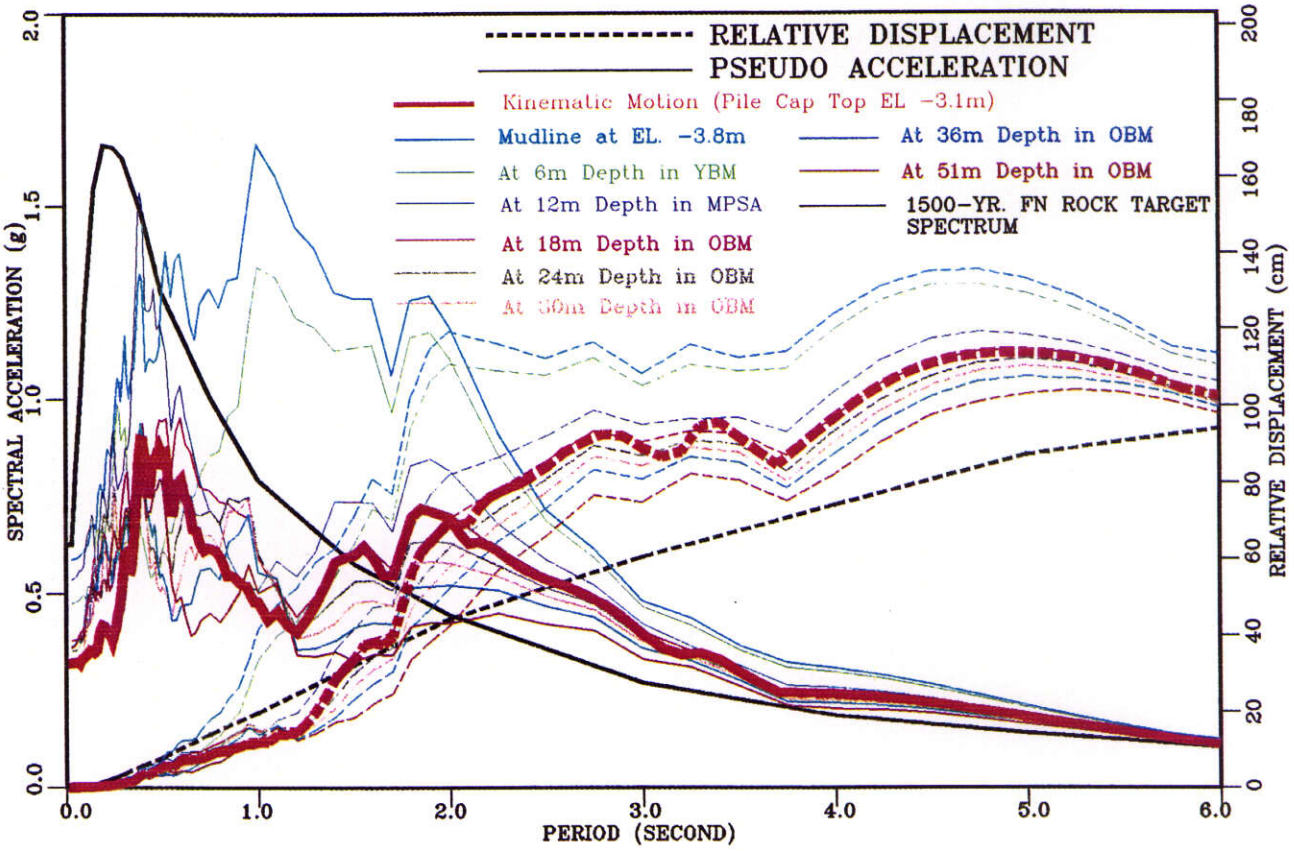

KINEMATIC AND DEPTH-VARYING FREE FIELD MOTIONS
PIER E11, INPUT ROCK MOTION SET 3, FAULT NORMAL COMPONENT
SFOBB East Span Seismic Safety Project

PLATE 8-118

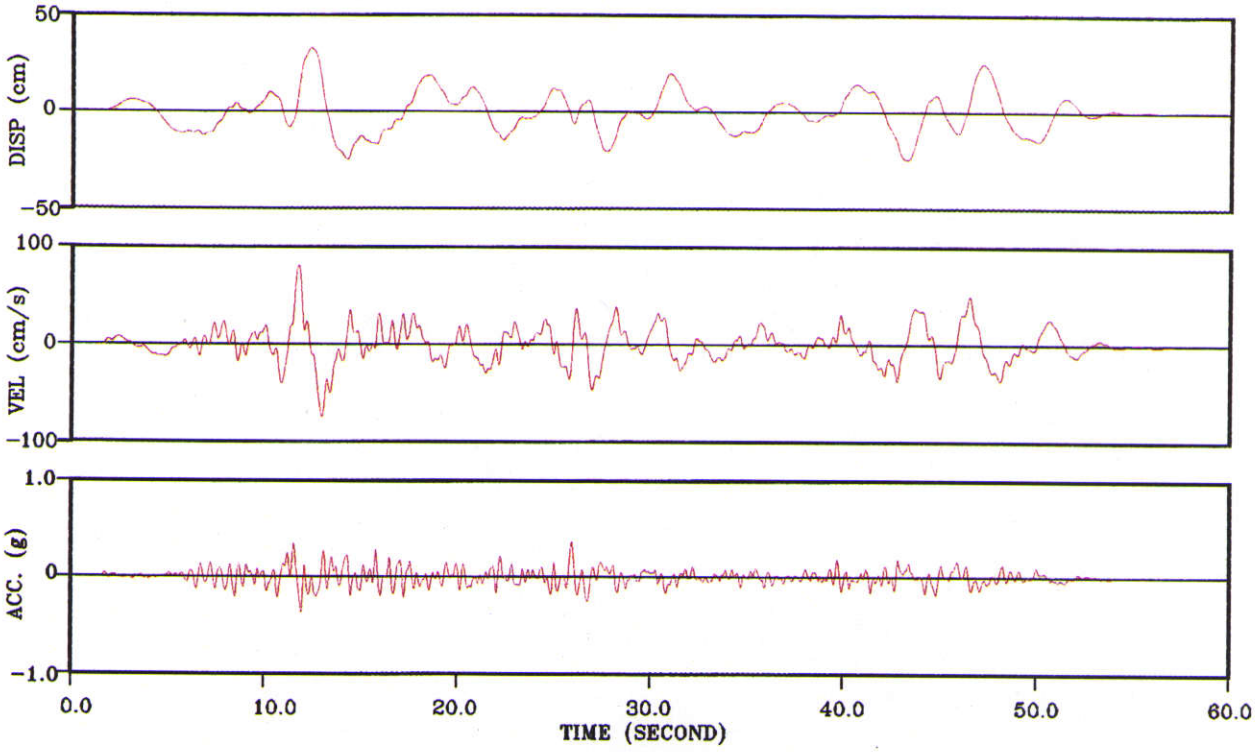

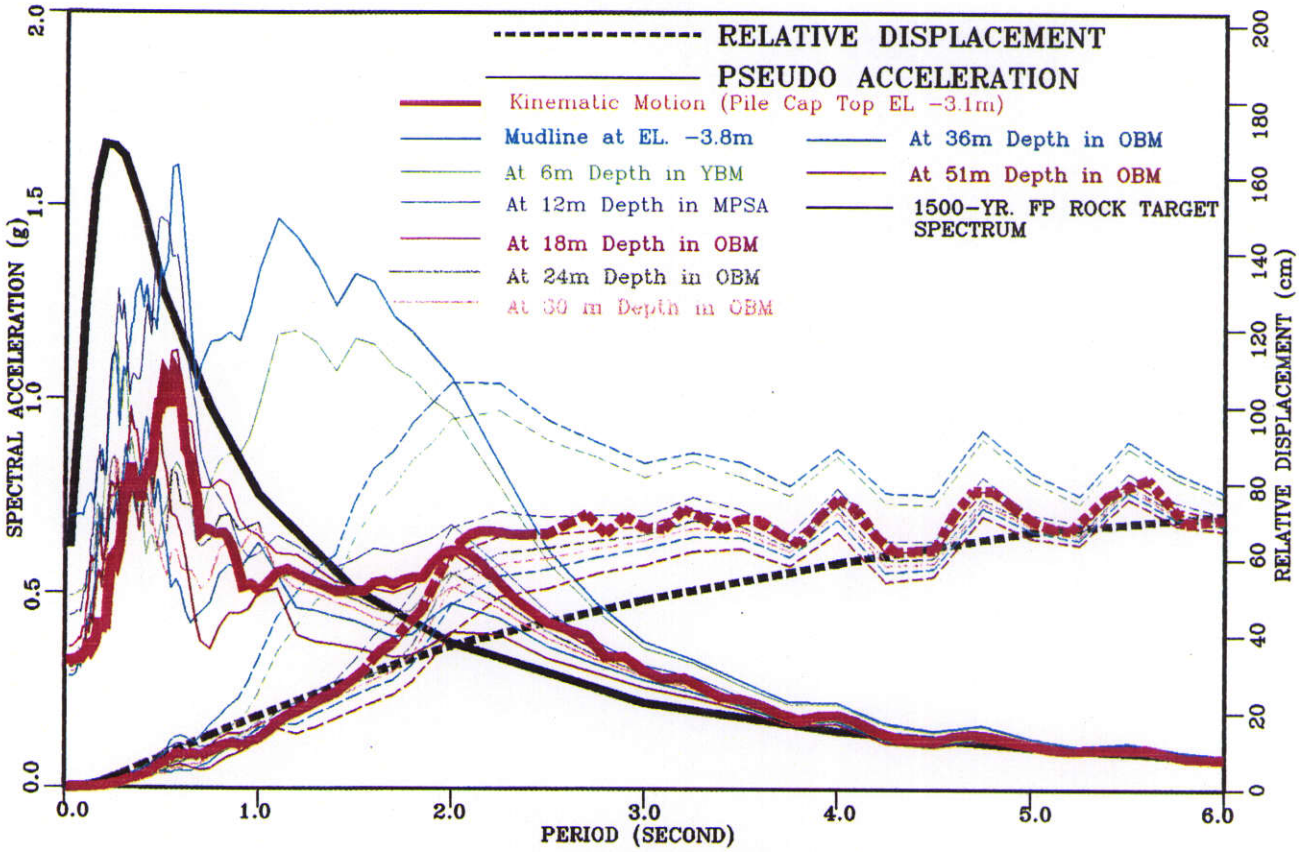

KINEMATIC AND DEPTH-VARYING FREE FIELD MOTIONS
PIER E11, INPUT ROCK MOTION SET 3, FAULT PARALLEL COMPONENT
SFOBB East Span Seismic Safety Project

PLATE 8-119

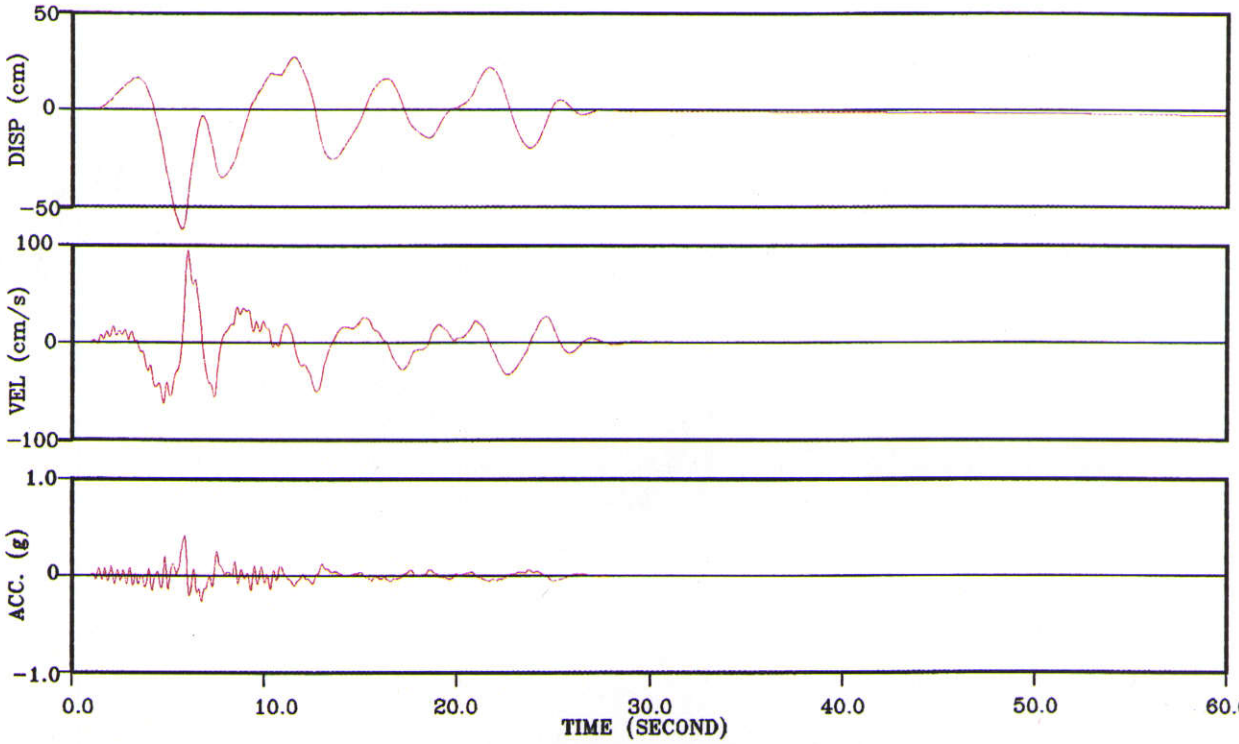

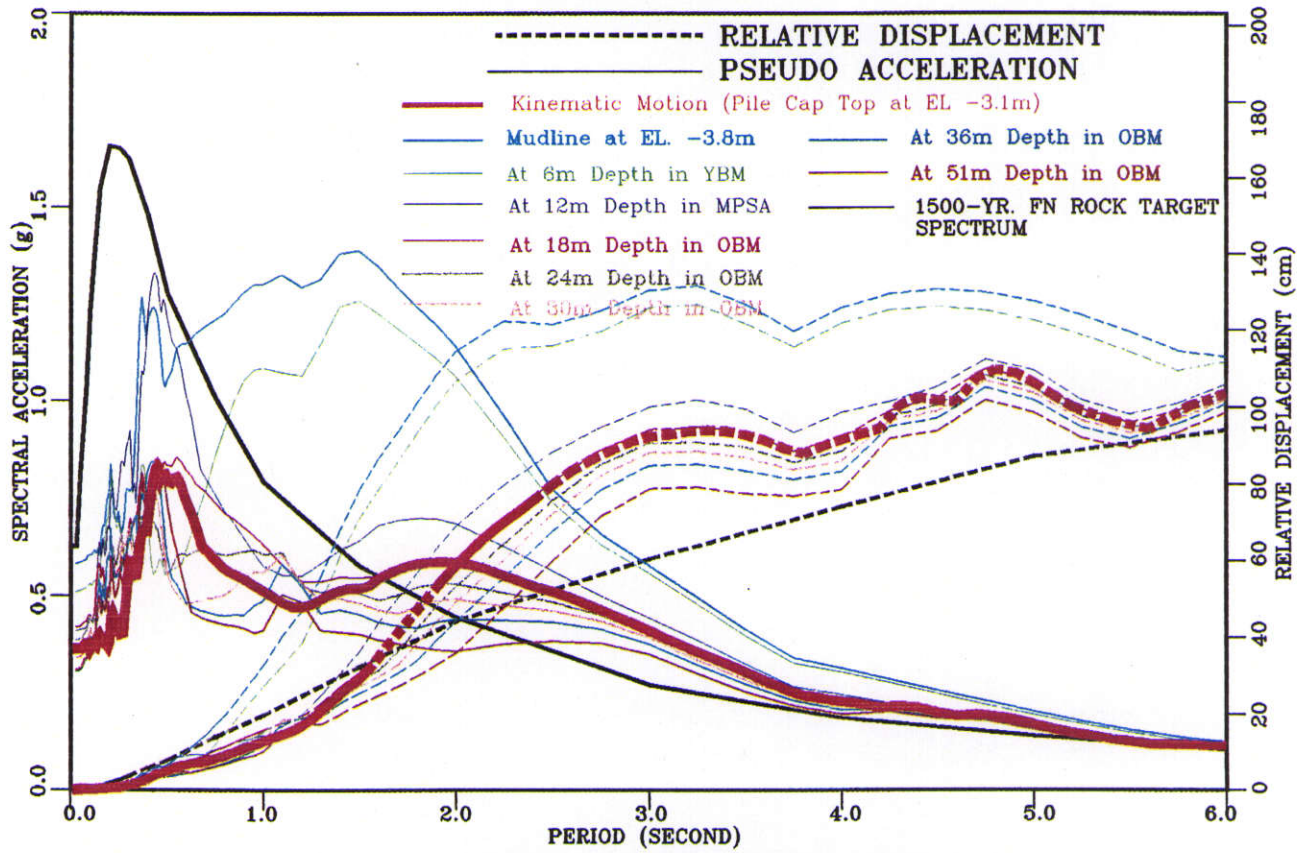

KINEMATIC AND DEPTH-VARYING FREE FIELD MOTIONS
PIER E11, INPUT ROCK MOTION SET 4, FAULT NORMAL COMPONENT
SFOBB East Span Seismic Safety Project

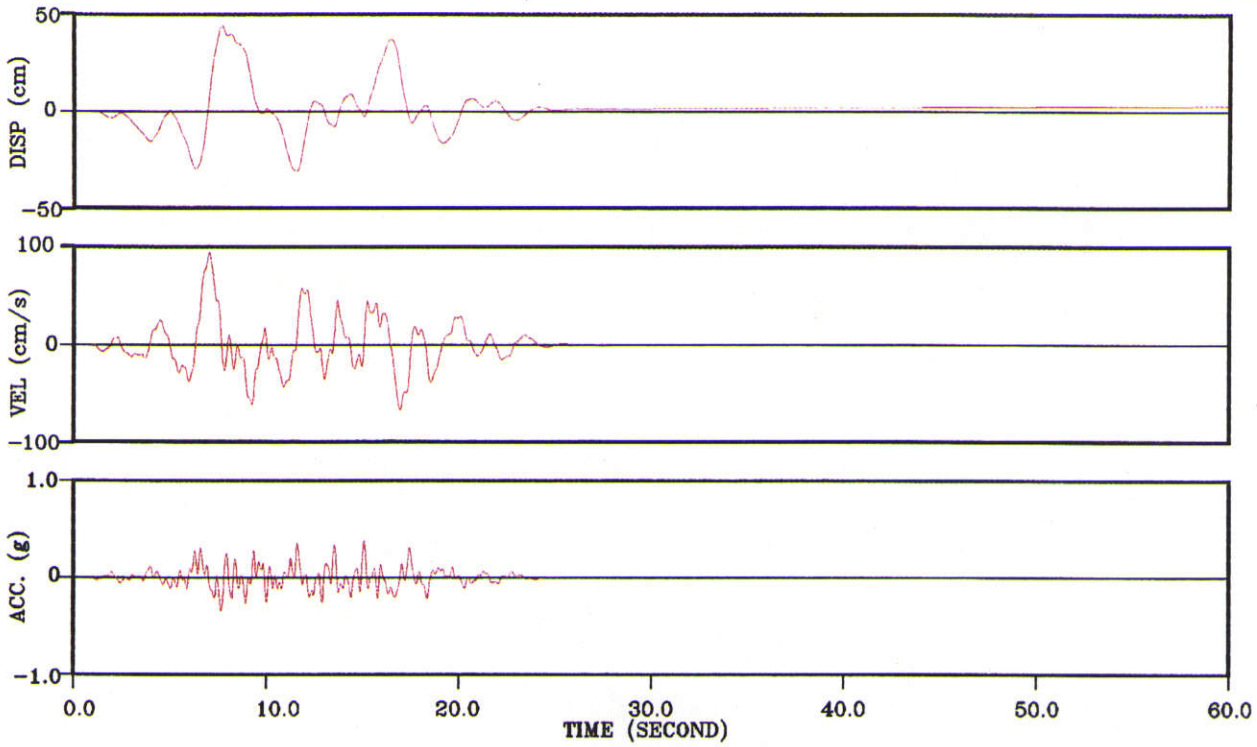

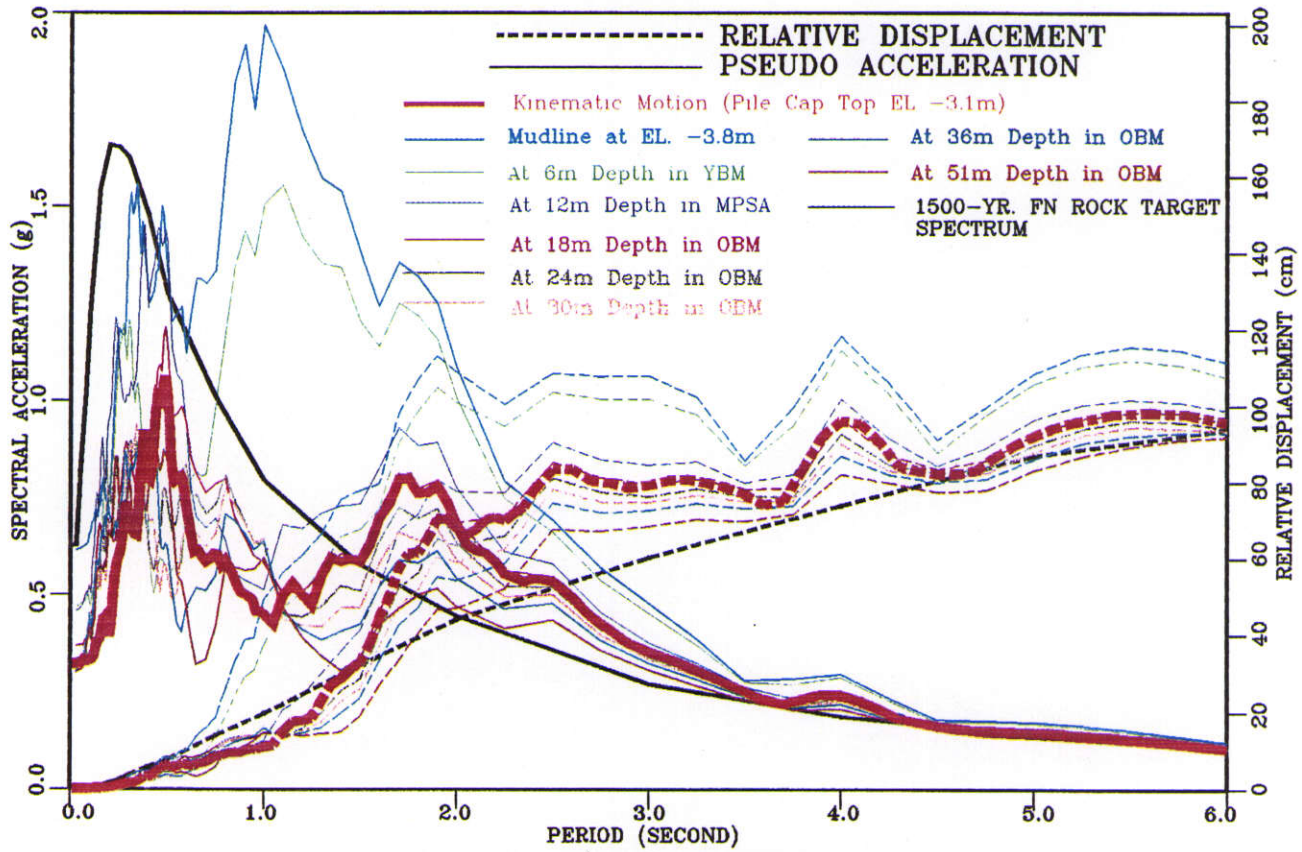

KINEMATIC AND DEPTH-VARYING FREE FIELD MOTIONS
PIER E11, INPUT ROCK MOTION SET 5, FAULT NORMAL COMPONENT
SFOBB East Span Seismic Safety Project

PLATE 8-122

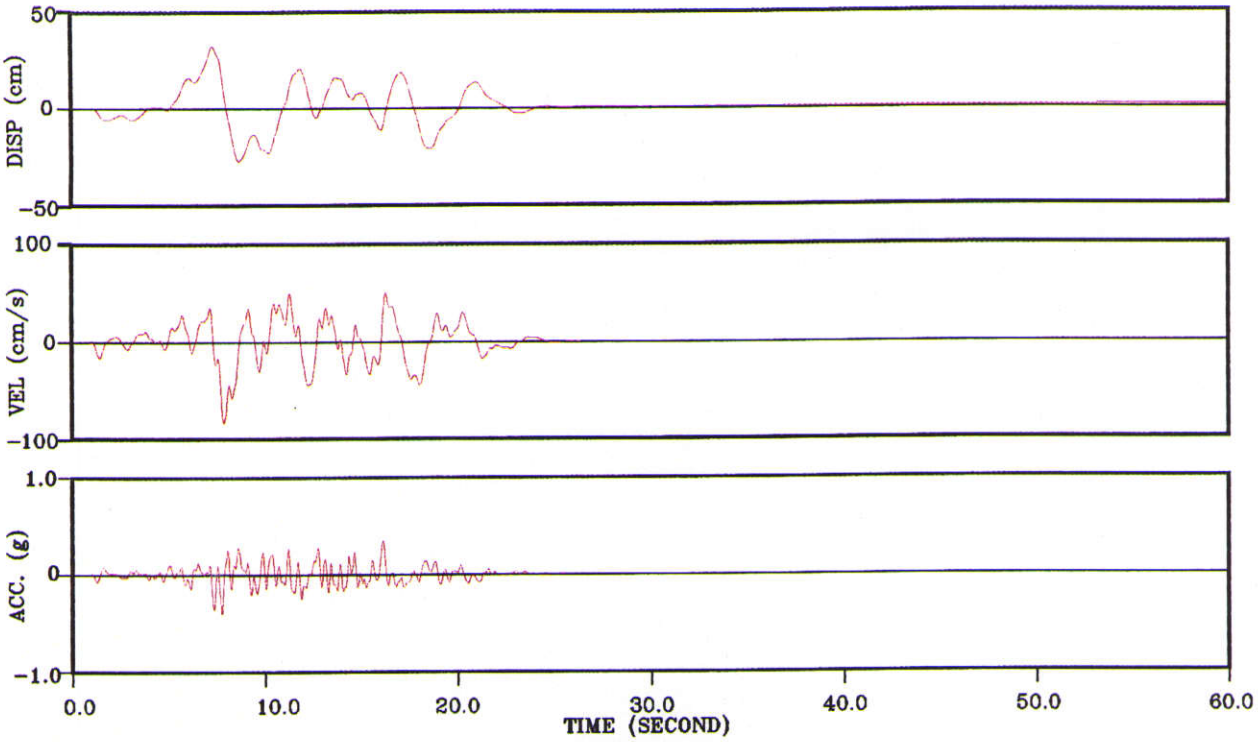

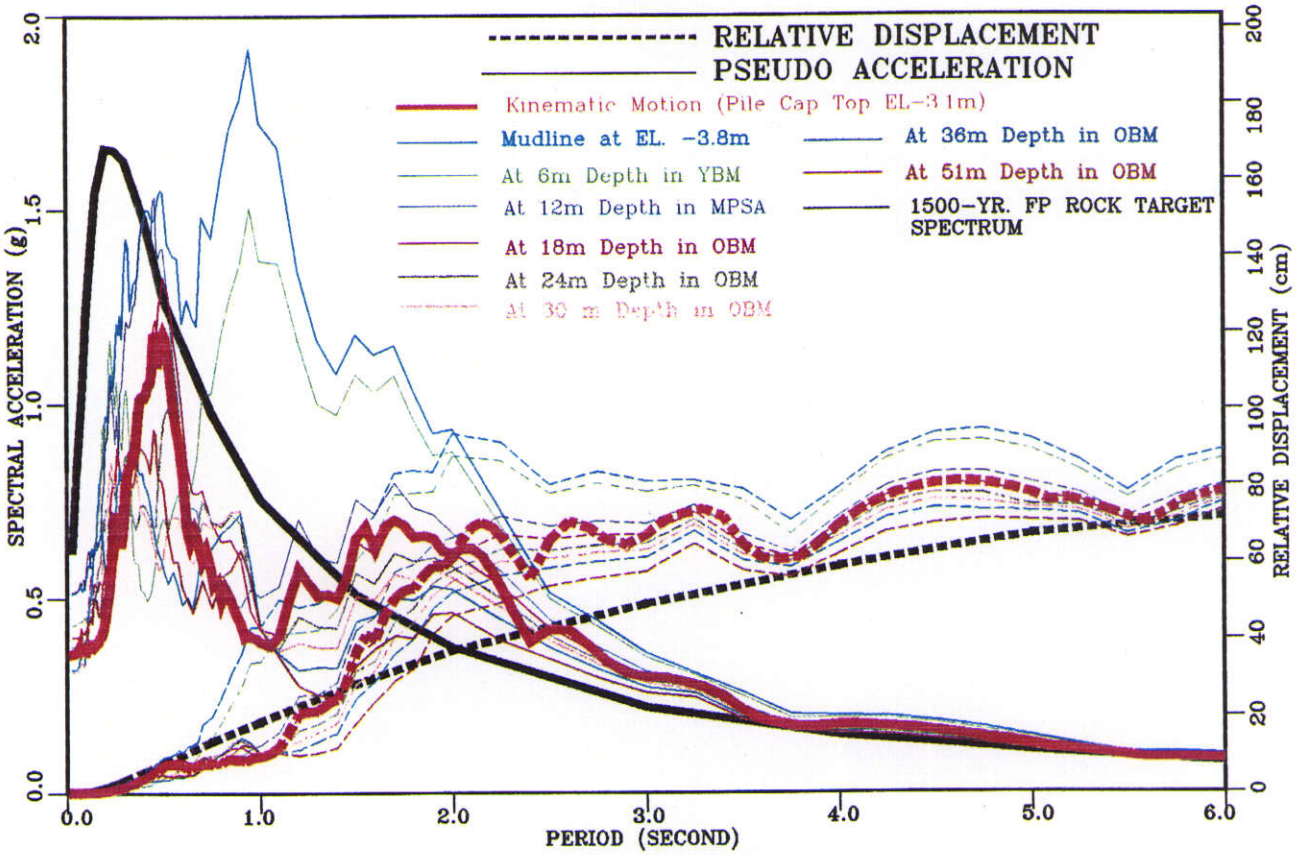

KINEMATIC AND DEPTH-VARYING FREE FIELD MOTIONS
PIER E11, INPUT ROCK MOTION SET 5 FAULT PARALLEL COMPONENT
SFOBB East Span Seismic Safety Project

PLATE 8-123

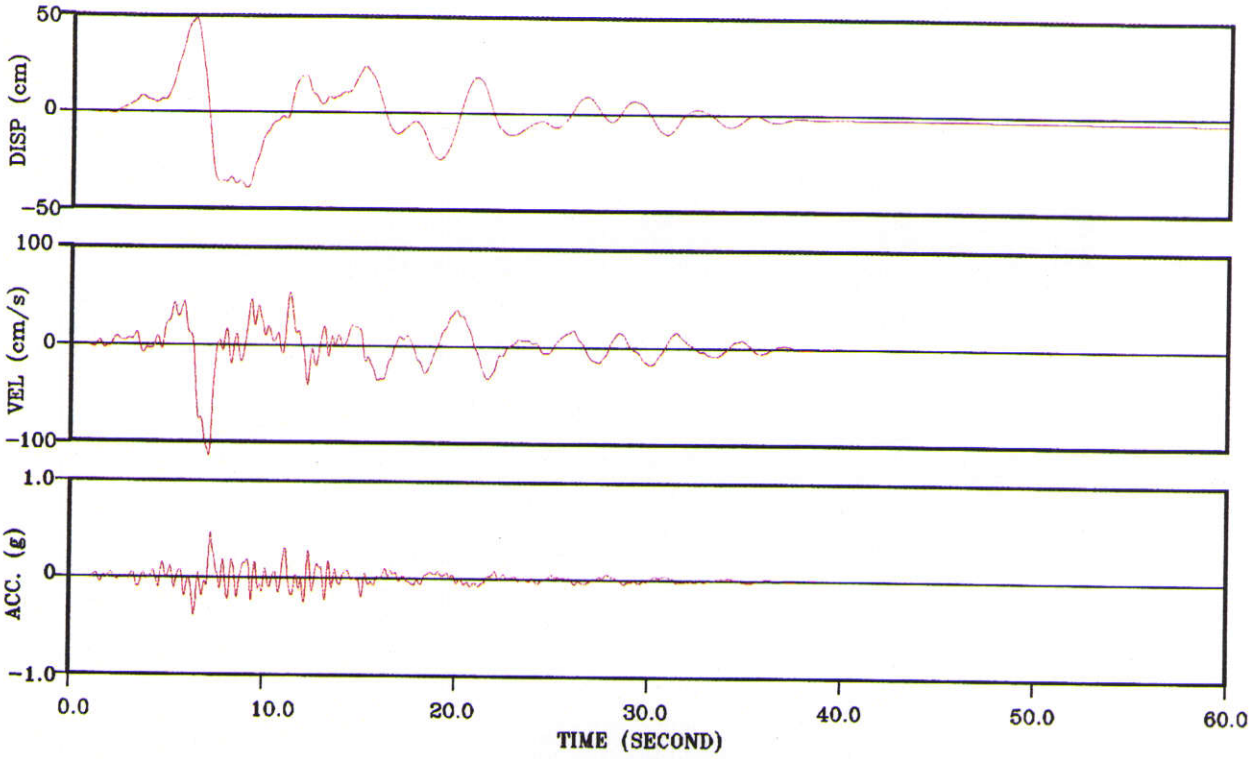

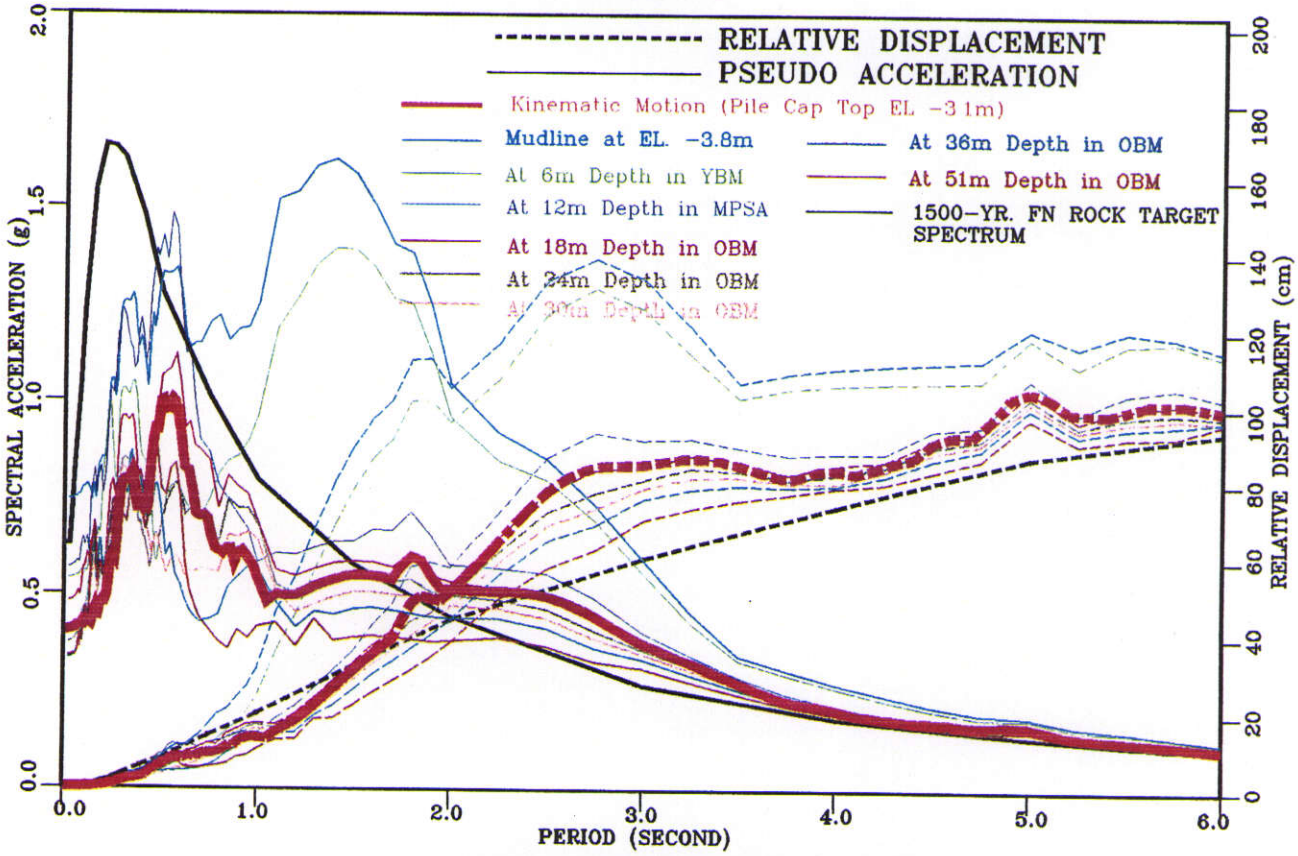

KINEMATIC AND DEPTH-VARYING FREE FIELD MOTIONS
PIER E11, INPUT ROCK MOTION SET 6, FAULT NORMAL COMPONENT
SFOBB East Span Seismic Safety Project

Earth Mechanics FUGRO

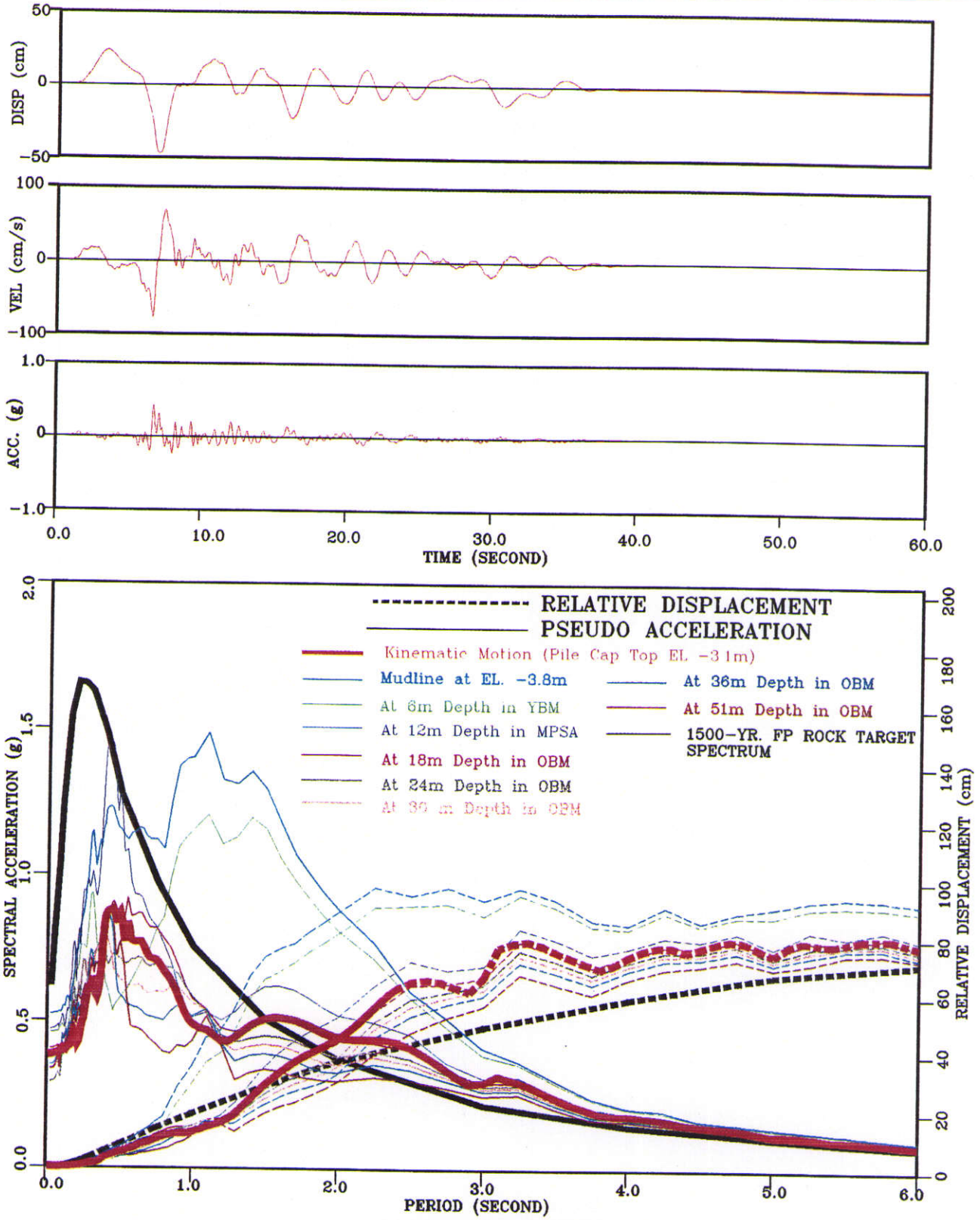

KINEMATIC AND DEPTH-VARYING FREE FIELD MOTIONS
PIER E11, INPUT ROCK MOTION SET 6, FAULT PARALLEL COMPONENT
SFOBB East Span Seismic Safety Project

PLATE 8-125

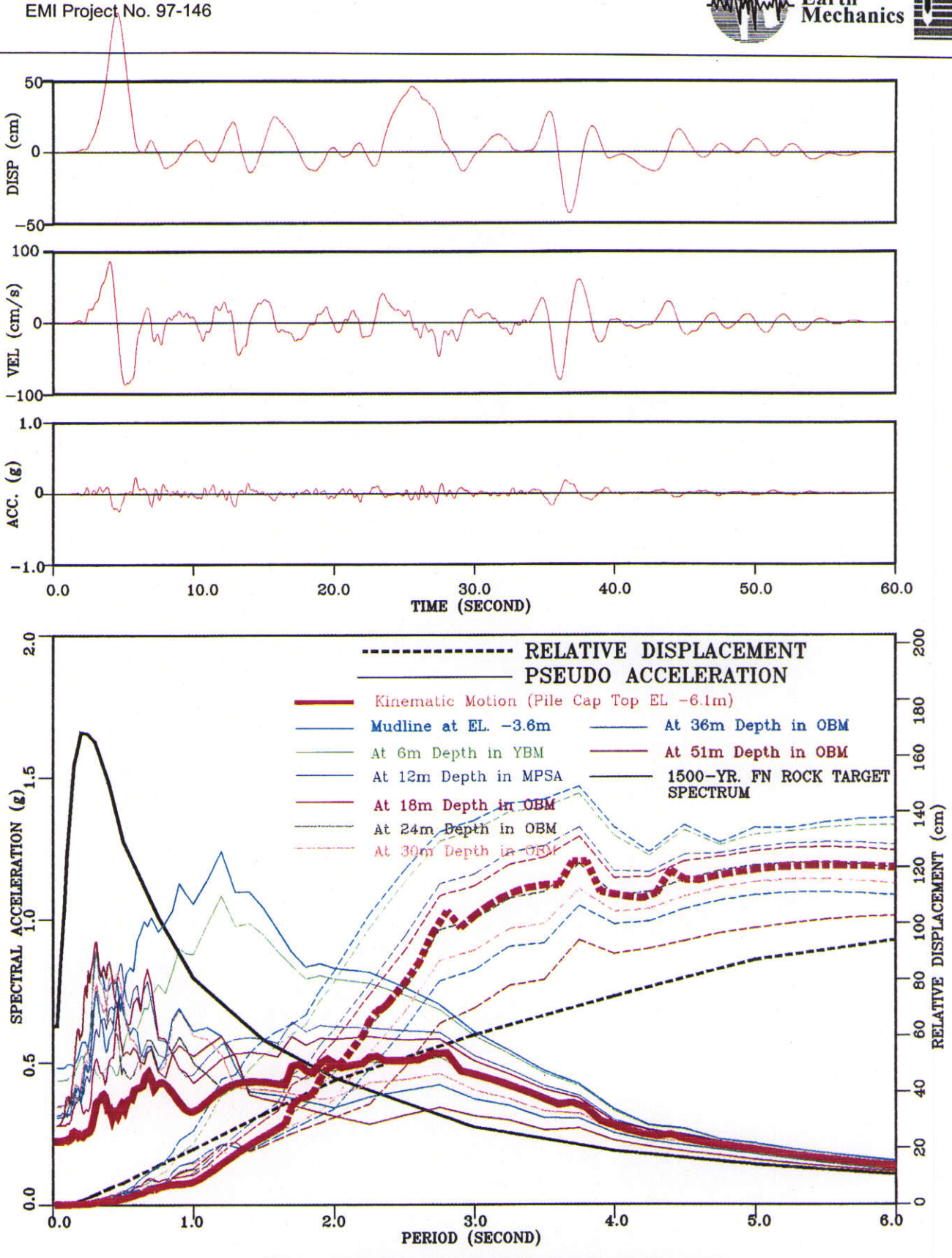

KINEMATIC AND DEPTH-VARYING FREE FIELD MOTIONS
PIER E12, INPUT ROCK MOTION SET 1, FAULT NORMAL COMPONENT
SFOBB East Span Seismic Safety Project

PLATE 8-126

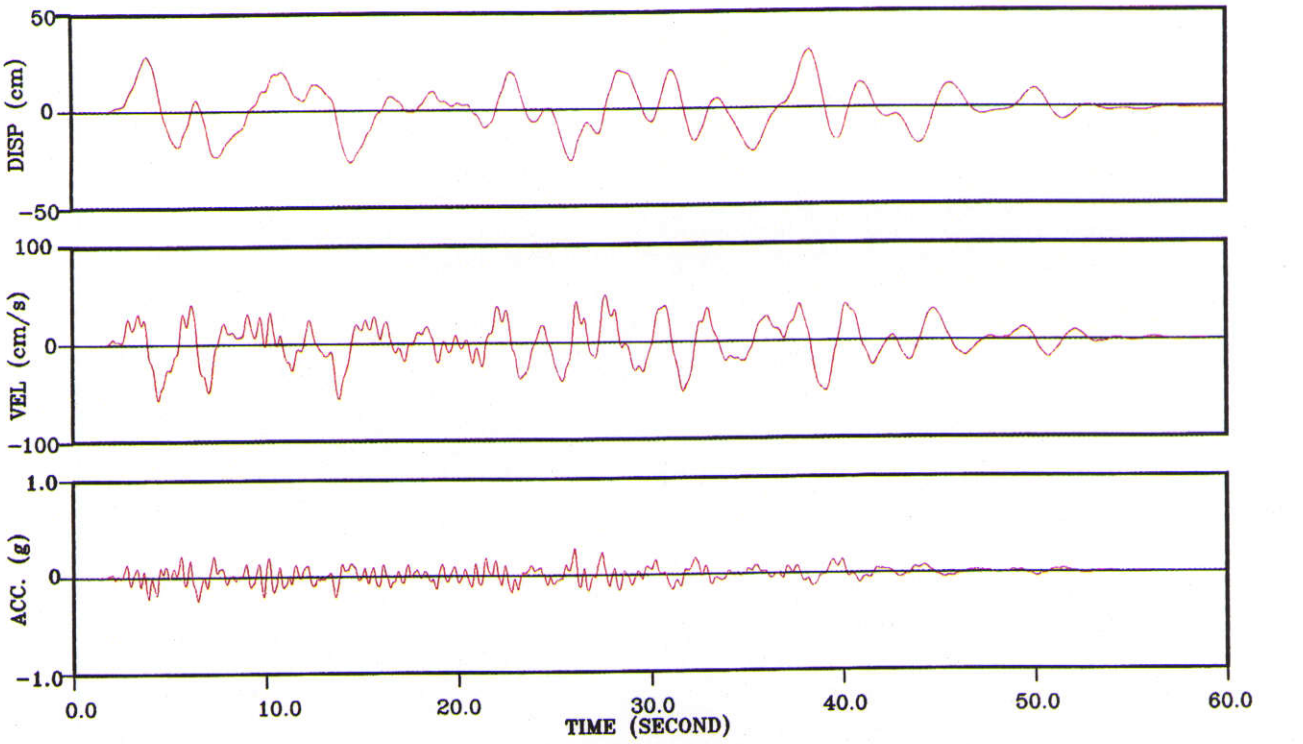

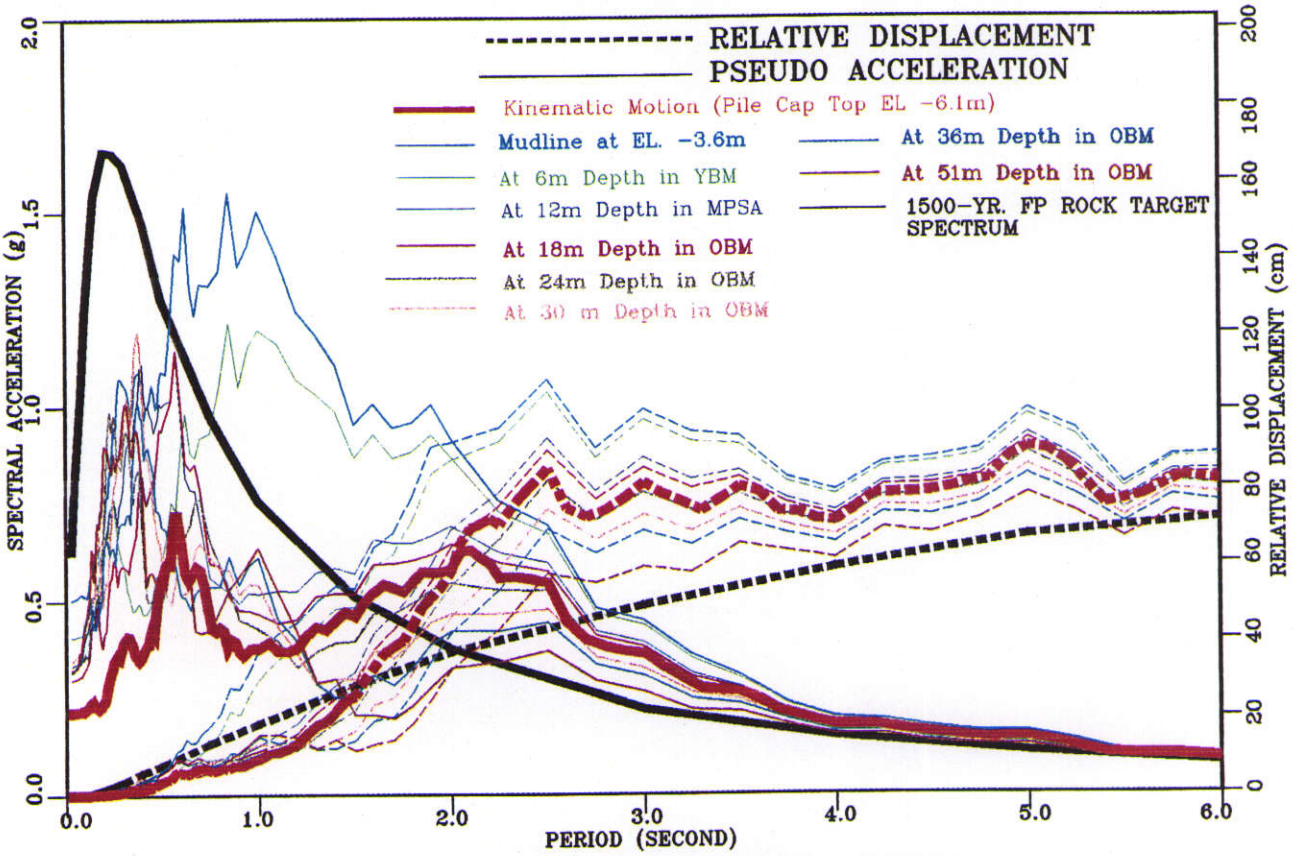

KINEMATIC AND DEPTH-VARYING FREE FIELD MOTIONS
PIER E12, INPUT ROCK MOTION SET 1, FAULT PARALLEL COMPONENT
SFOBB East Span Seismic Safety Project

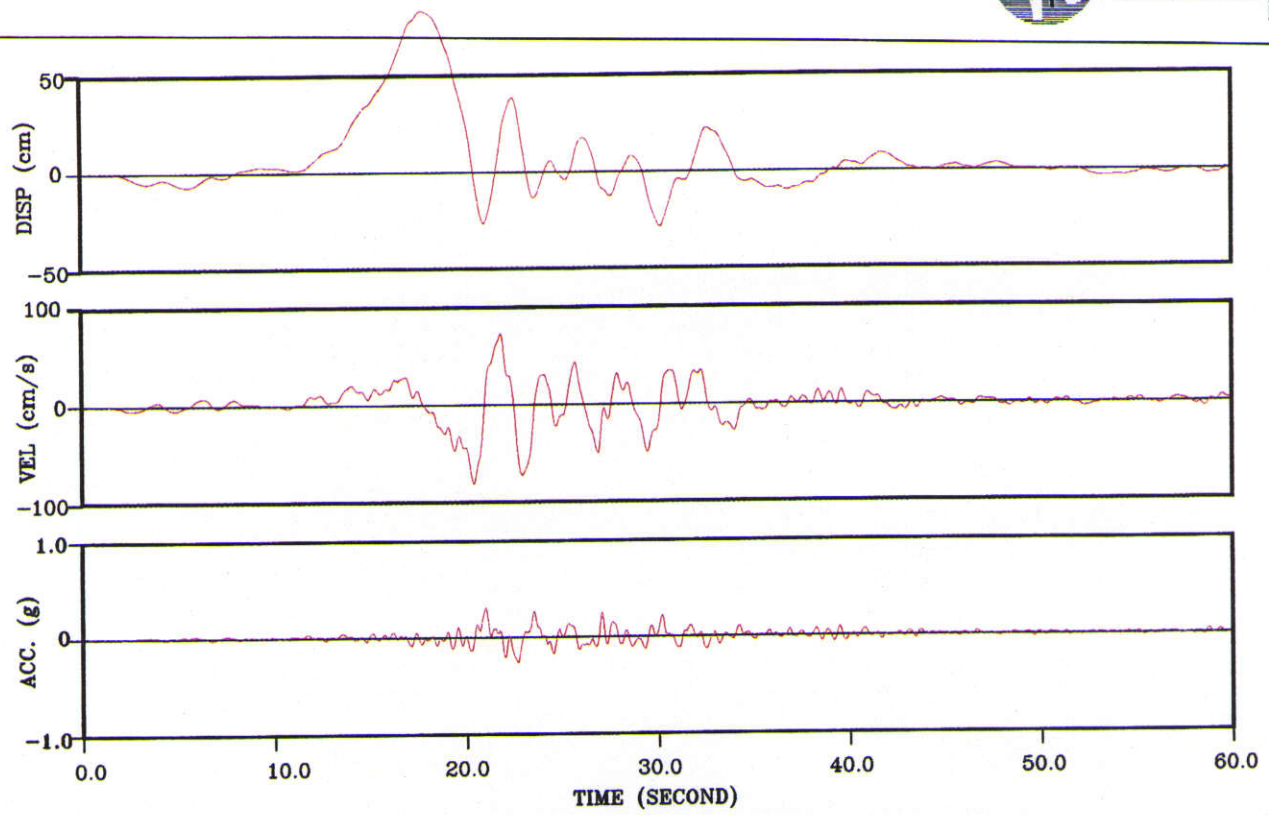

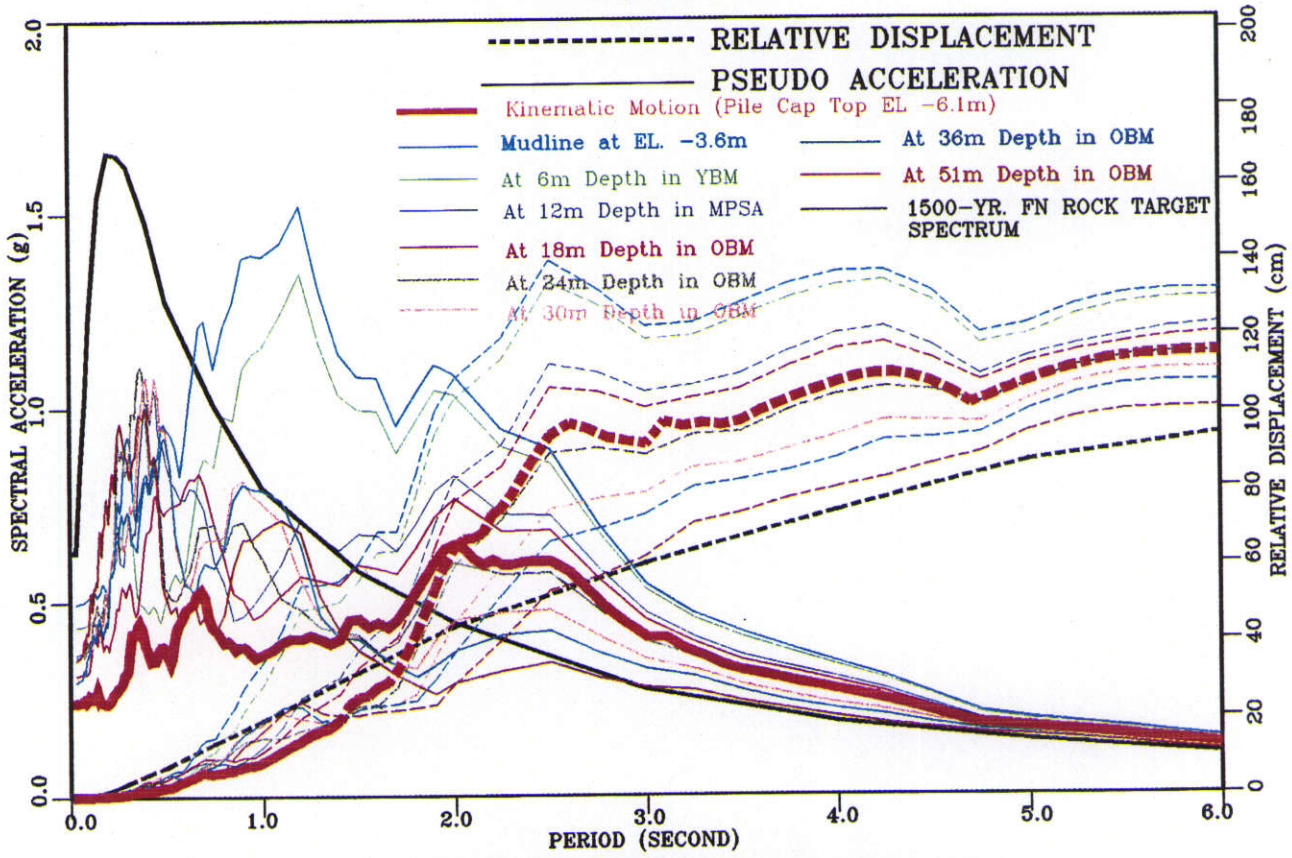

KINEMATIC AND DEPTH-VARYING FREE FIELD MOTIONS
PIER E12, INPUT ROCK MOTION SET 2, FAULT NORMAL COMPONENT
SFOBB East Span Seismic Safety Project

PLATE 8-128

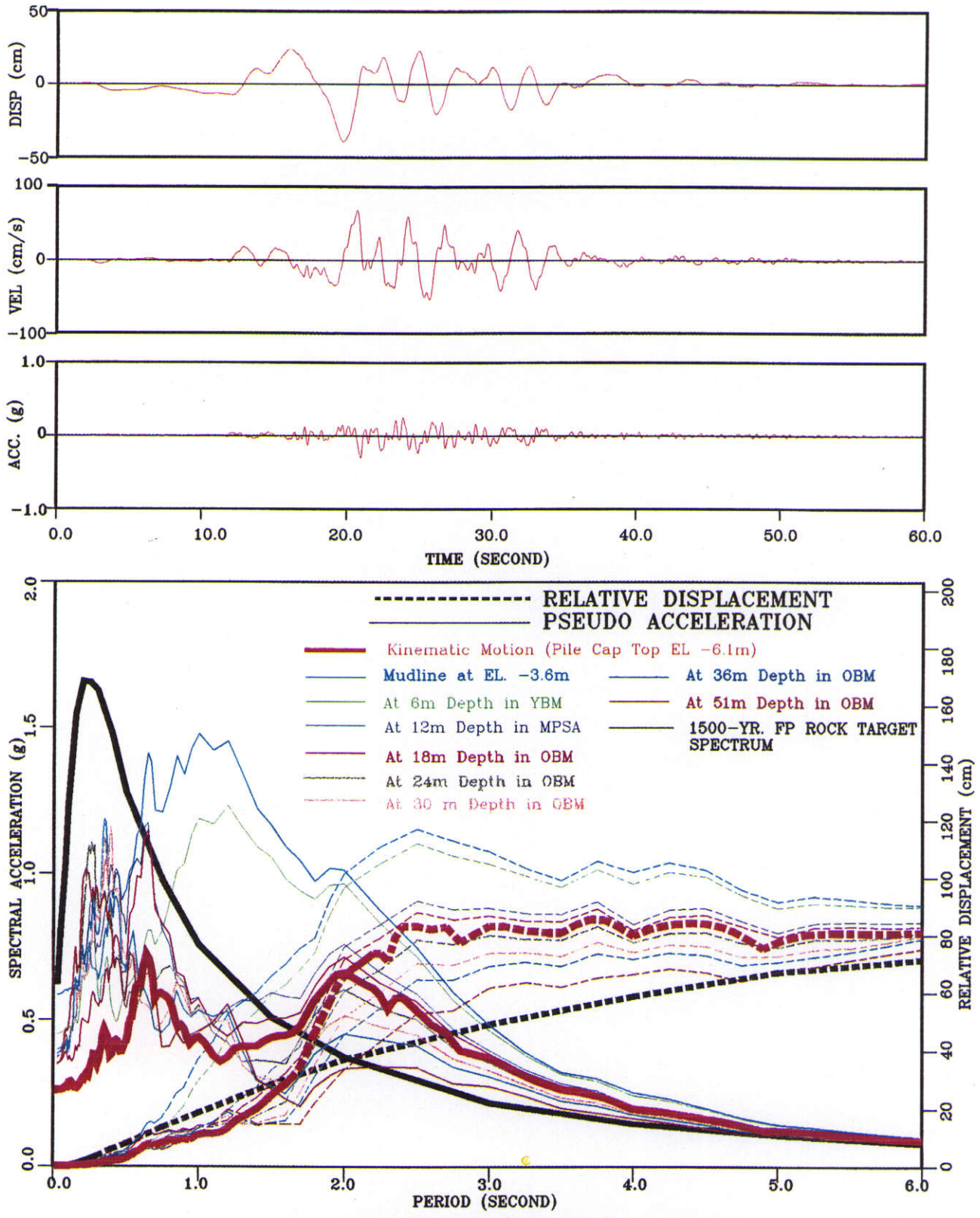

KINEMATIC AND DEPTH-VARYING FREE FIELD MOTIONS
PIER E12, INPUT ROCK MOTION SET 2, FAULT PARALLEL COMPONENT
SFOBB East Span Seismic Safety Project

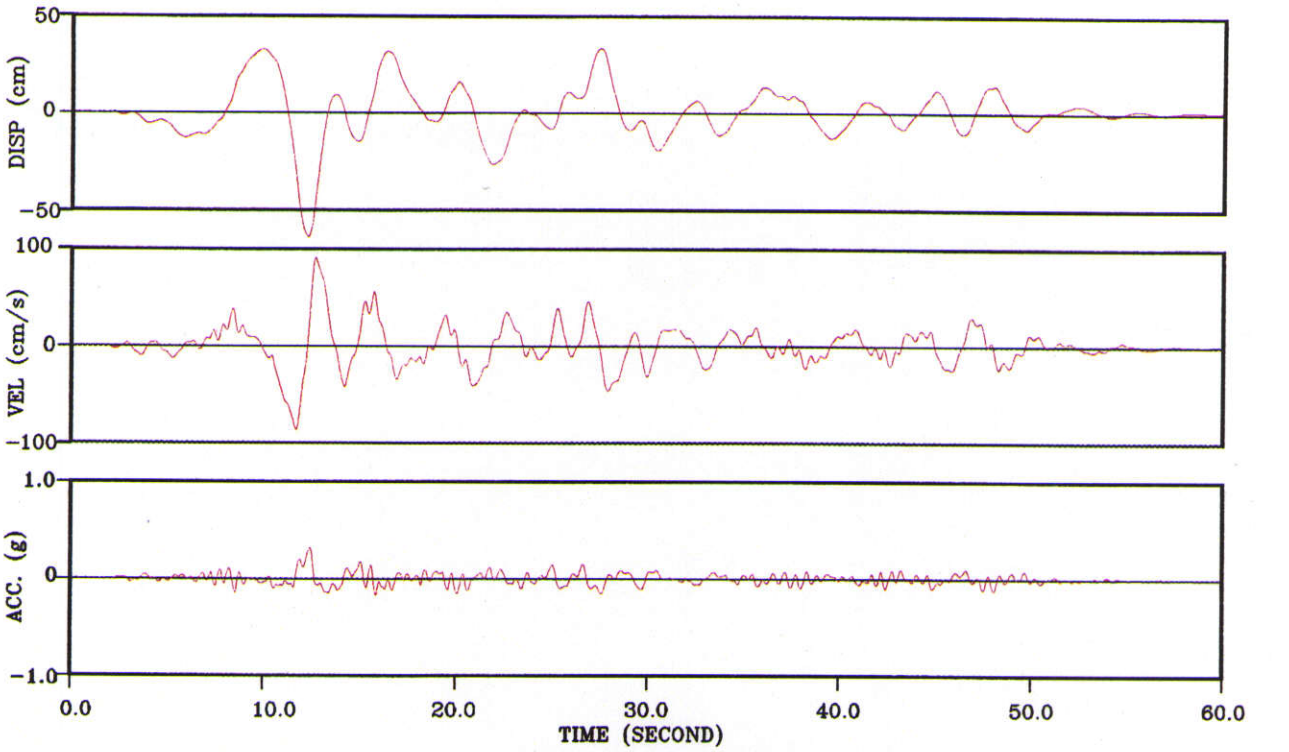

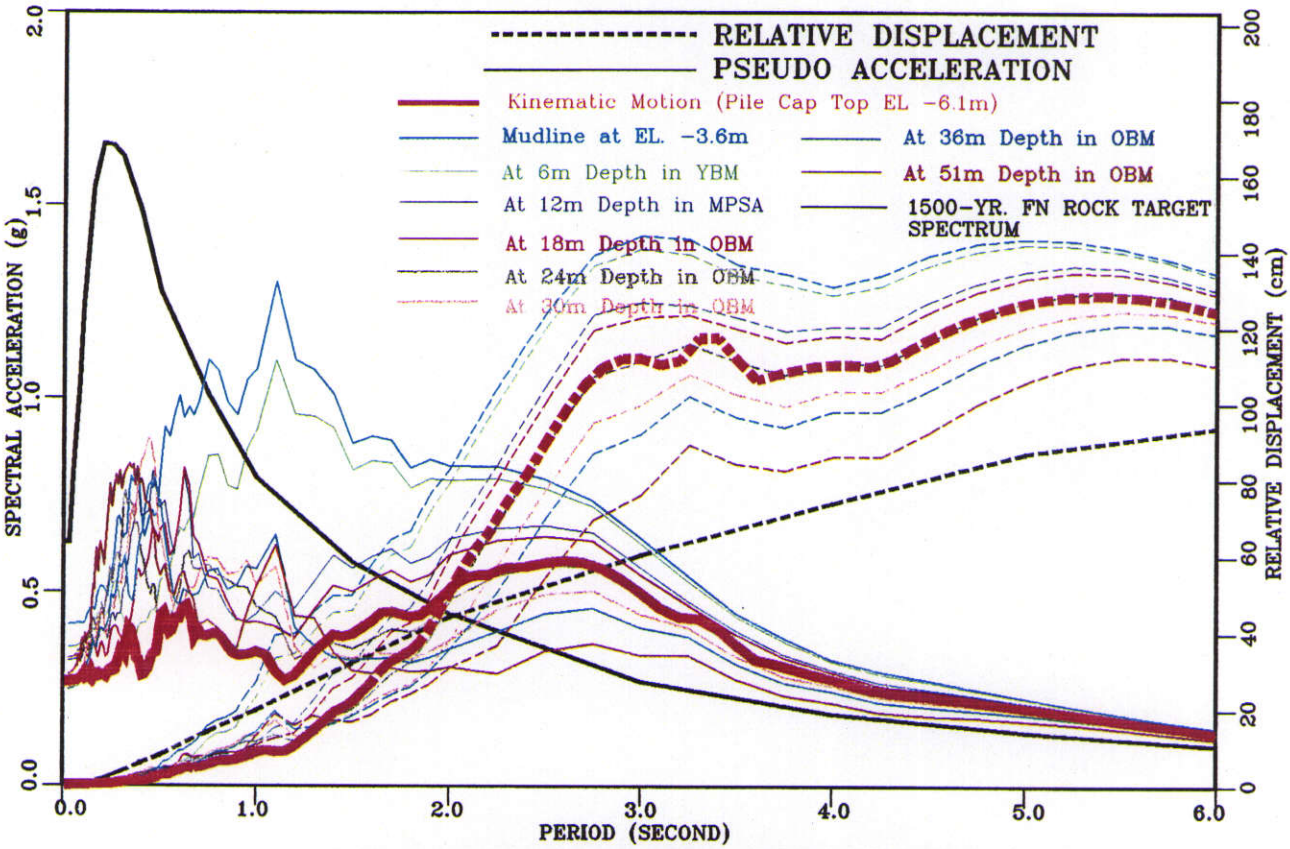

KINEMATIC AND DEPTH-VARYING FREE FIELD MOTIONS
PIER E12, INPUT ROCK MOTION SET 3, FAULT NORMAL COMPONENT
SFOBB East Span Seismic Safety Project

PLATE 8-130

Earth Mechanics FUGRO

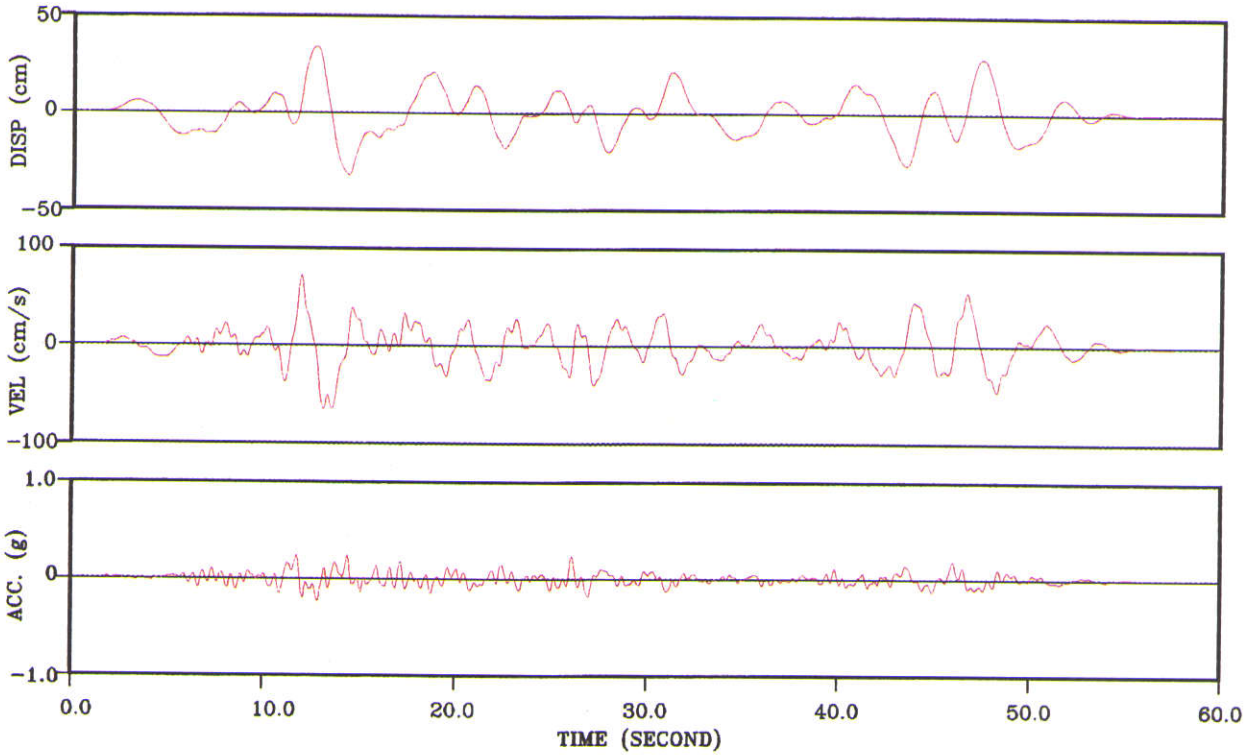

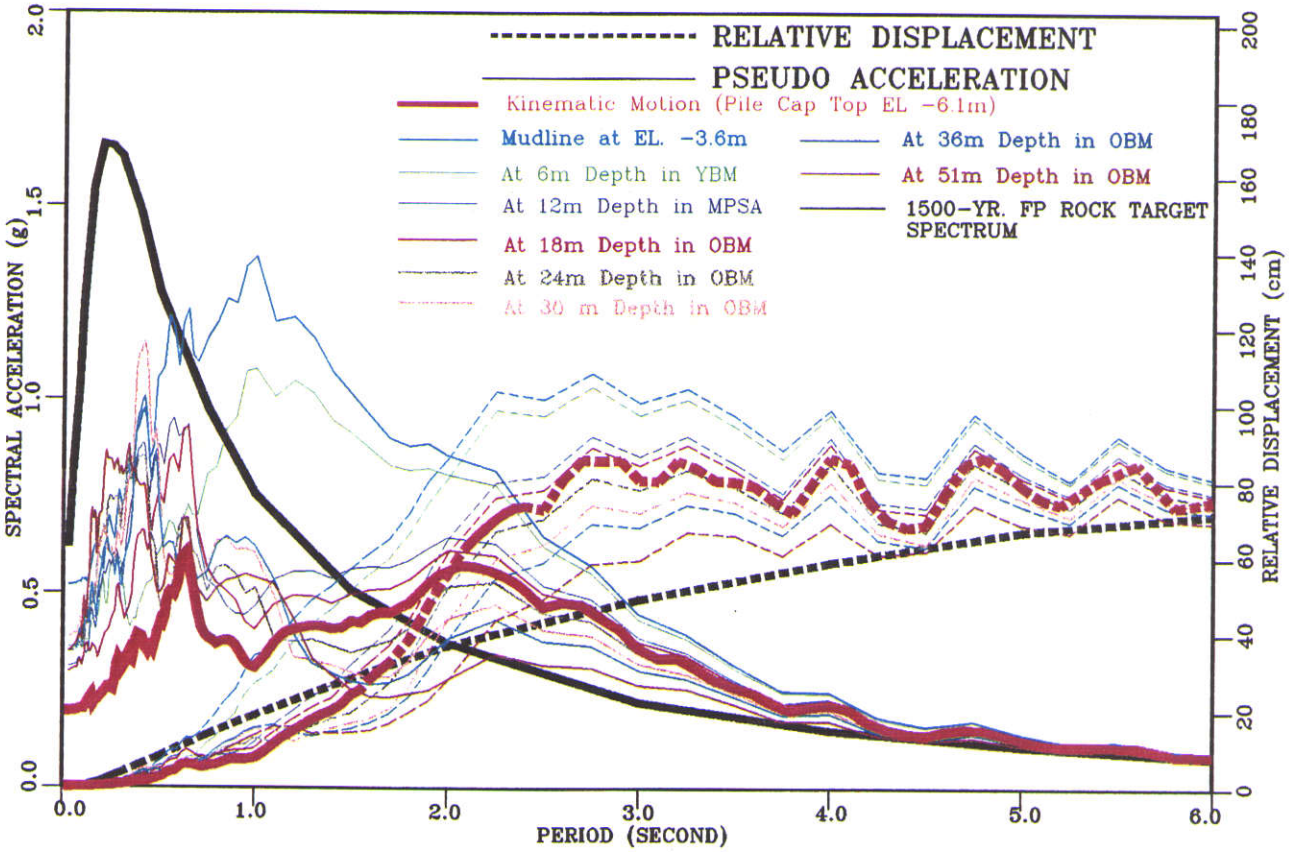

KINEMATIC AND DEPTH-VARYING FREE FIELD MOTIONS
PIER E12, INPUT ROCK MOTION SET 3, FAULT PARALLEL COMPONENT
SFOBB East Span Seismic Safety Project

PLATE 8-131

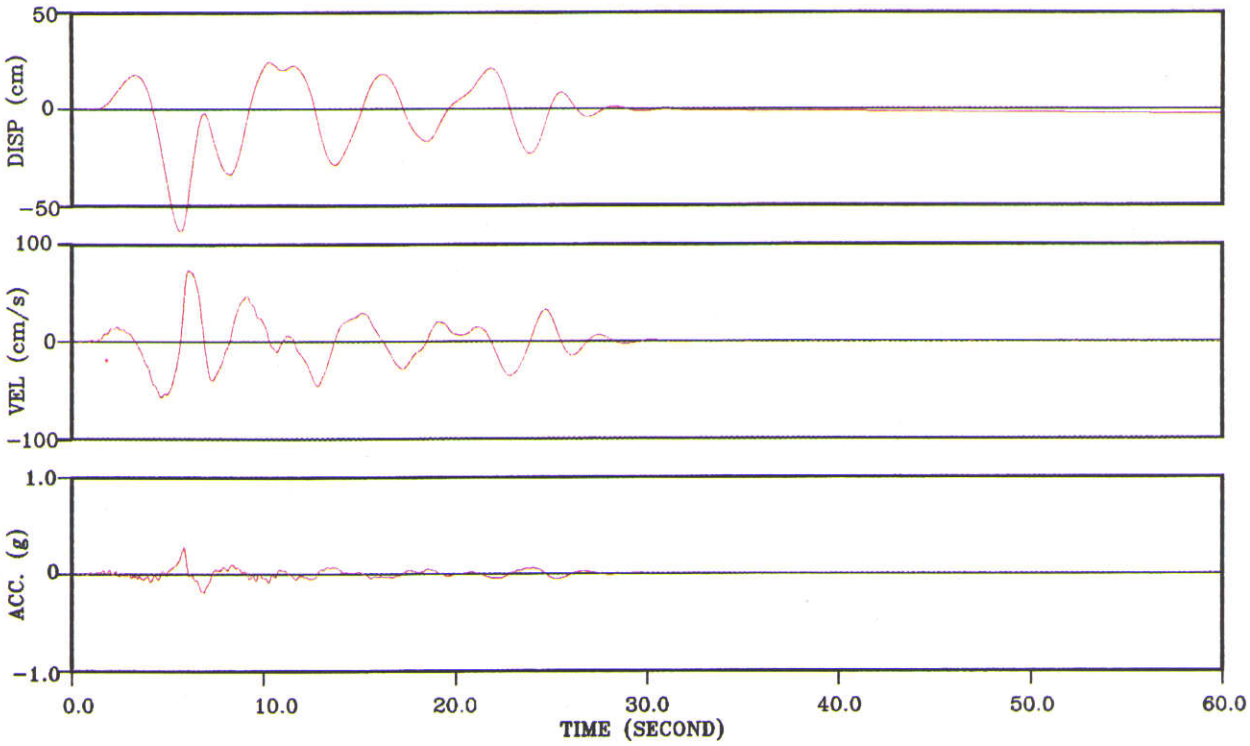

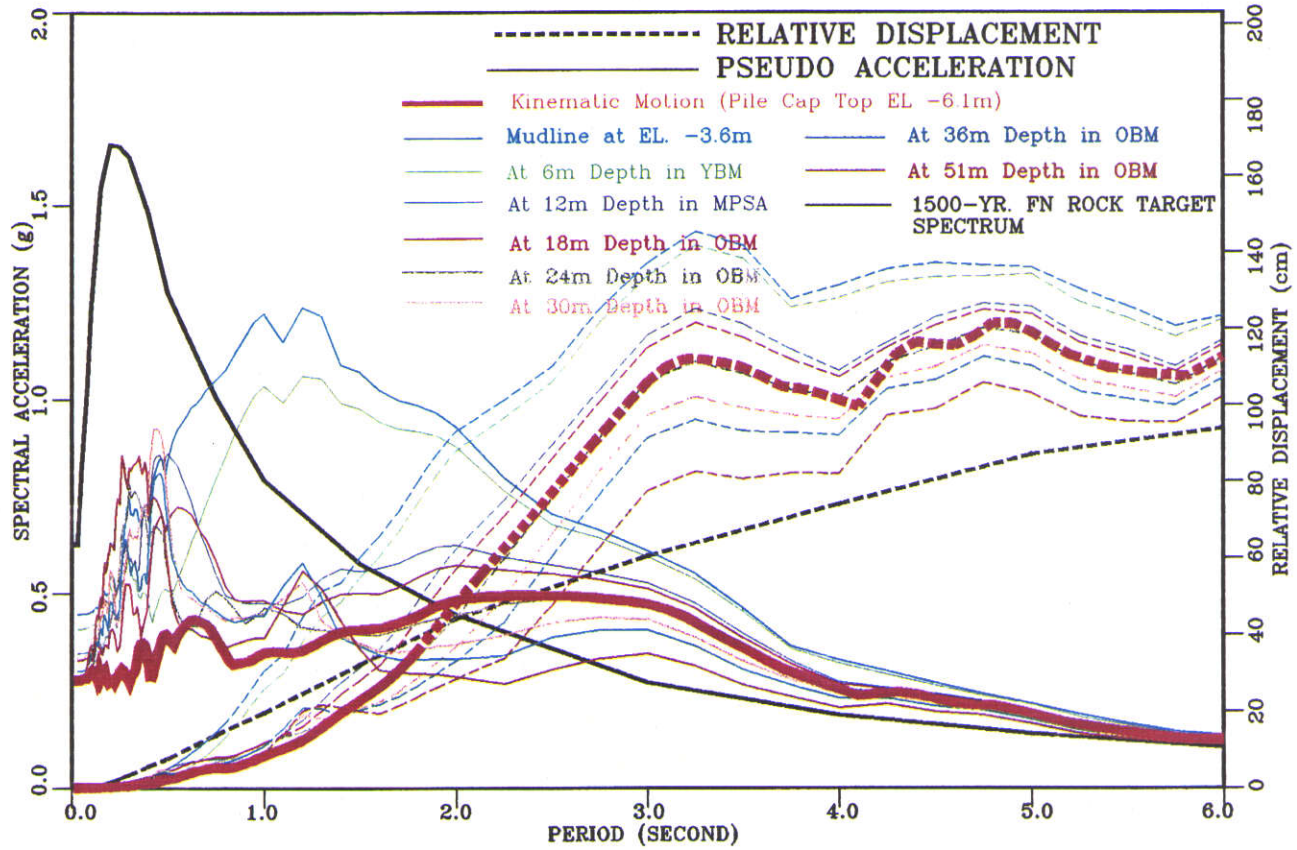

KINEMATIC AND DEPTH-VARYING FREE FIELD MOTIONS
PIER E12, INPUT ROCK MOTION SET 4, FAULT NORMAL COMPONENT
SFOBB East Span Seismic Safety Project

PLATE 8-132

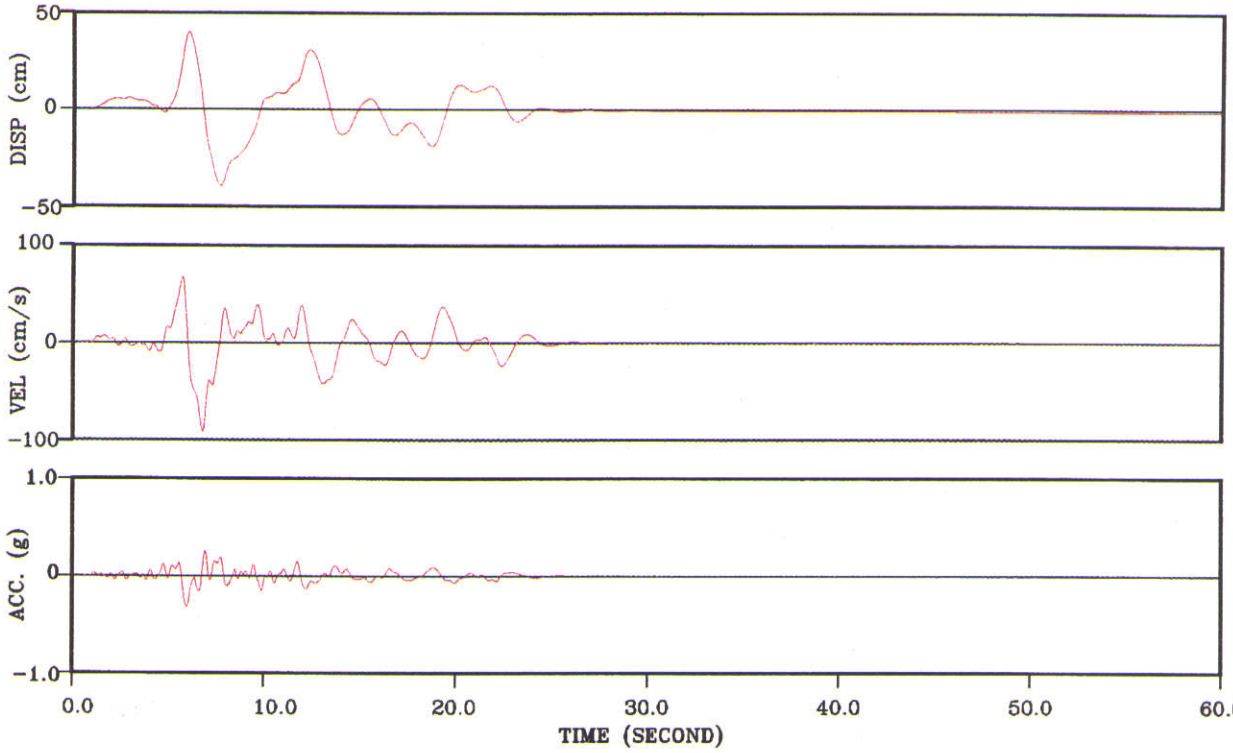

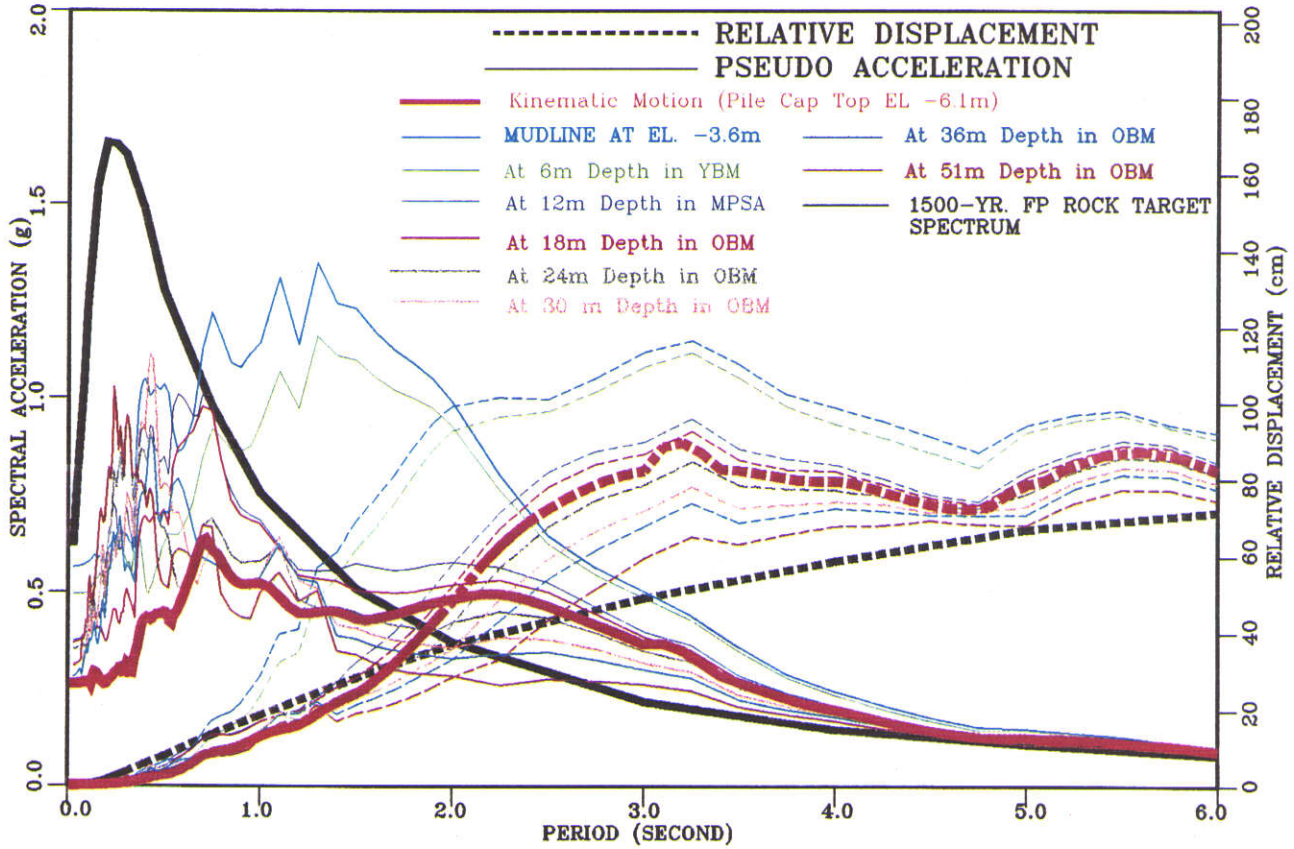

KINEMATIC AND DEPTH-VARYING FREE FIELD MOTIONS
PIER E12, INPUT ROCK MOTION SET 4, FAULT PARALLEL COMPONENT
SFOBB East Span Seismic Safety Project

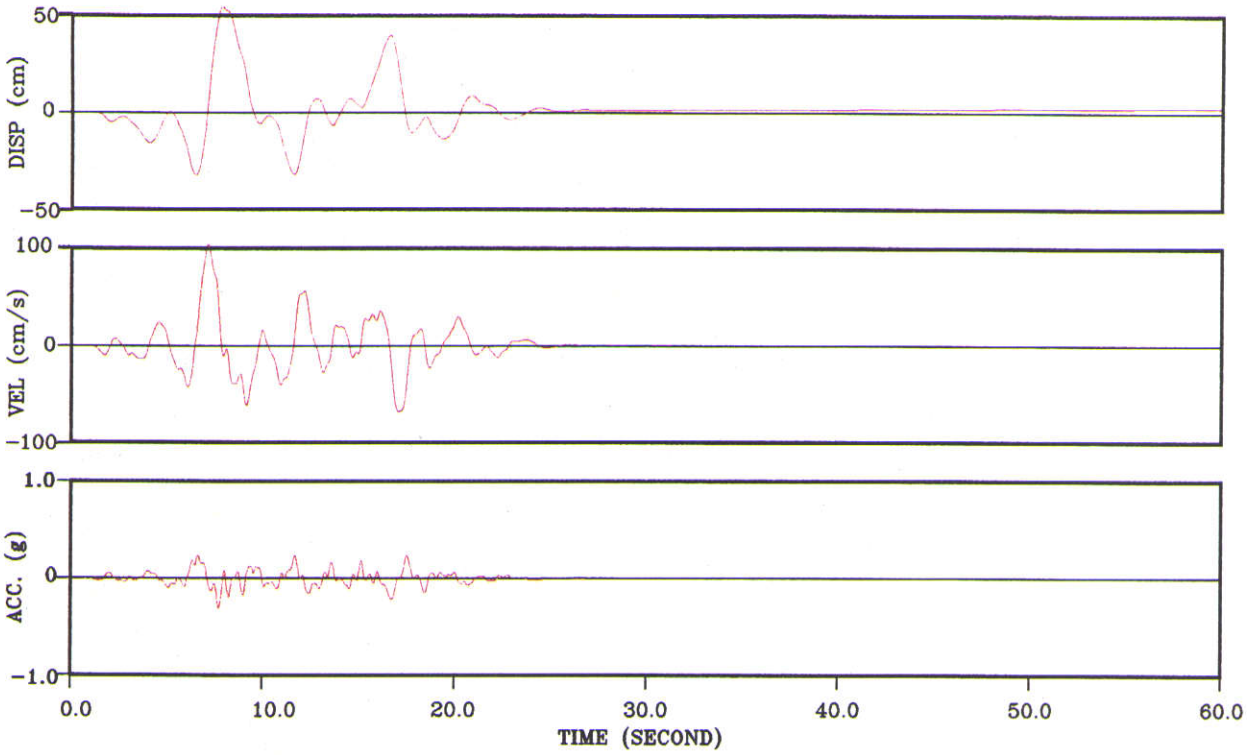

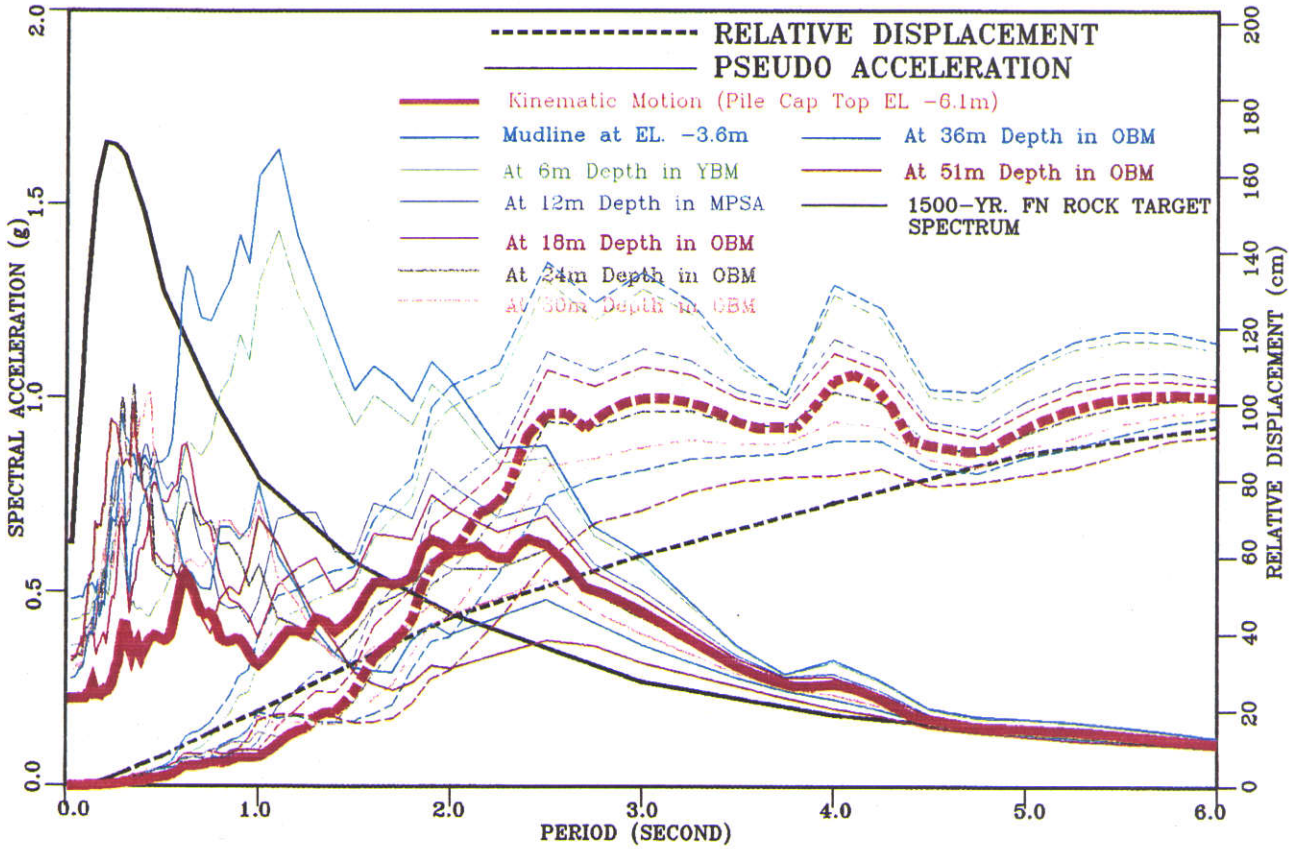

KINEMATIC AND DEPTH-VARYING FREE FIELD MOTIONS
PIER E12, INPUT ROCK MOTION SET 5, FAULT NORMAL COMPONENT
SFOBB East Span Seismic Safety Project

PLATE 8-134

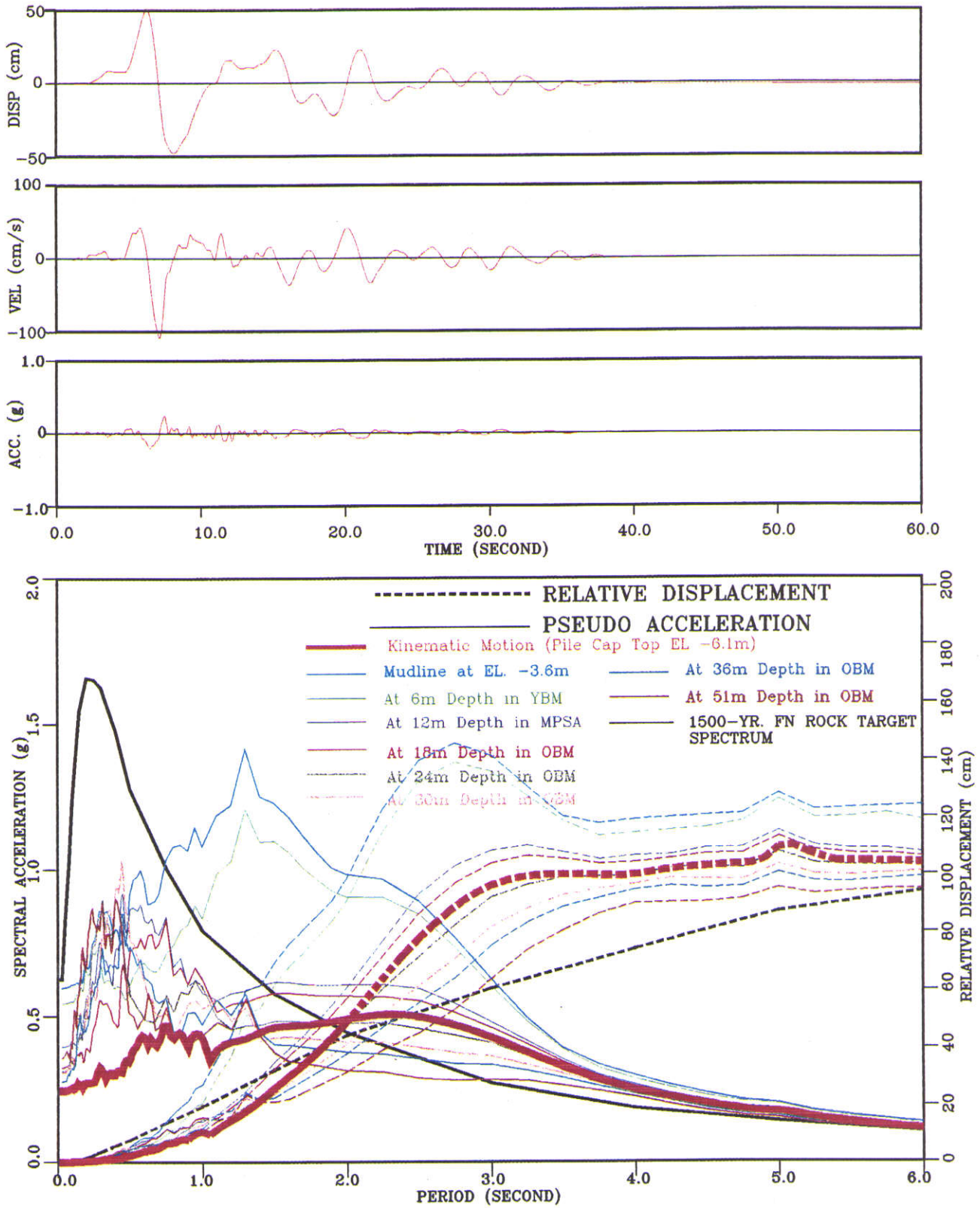

KINEMATIC AND DEPTH-VARYING FREE FIELD MOTIONS
PIER E12, INPUT ROCK MOTION SET 6, FAULT NORMAL COMPONENT
SFOBB East Span Seismic Safety Project

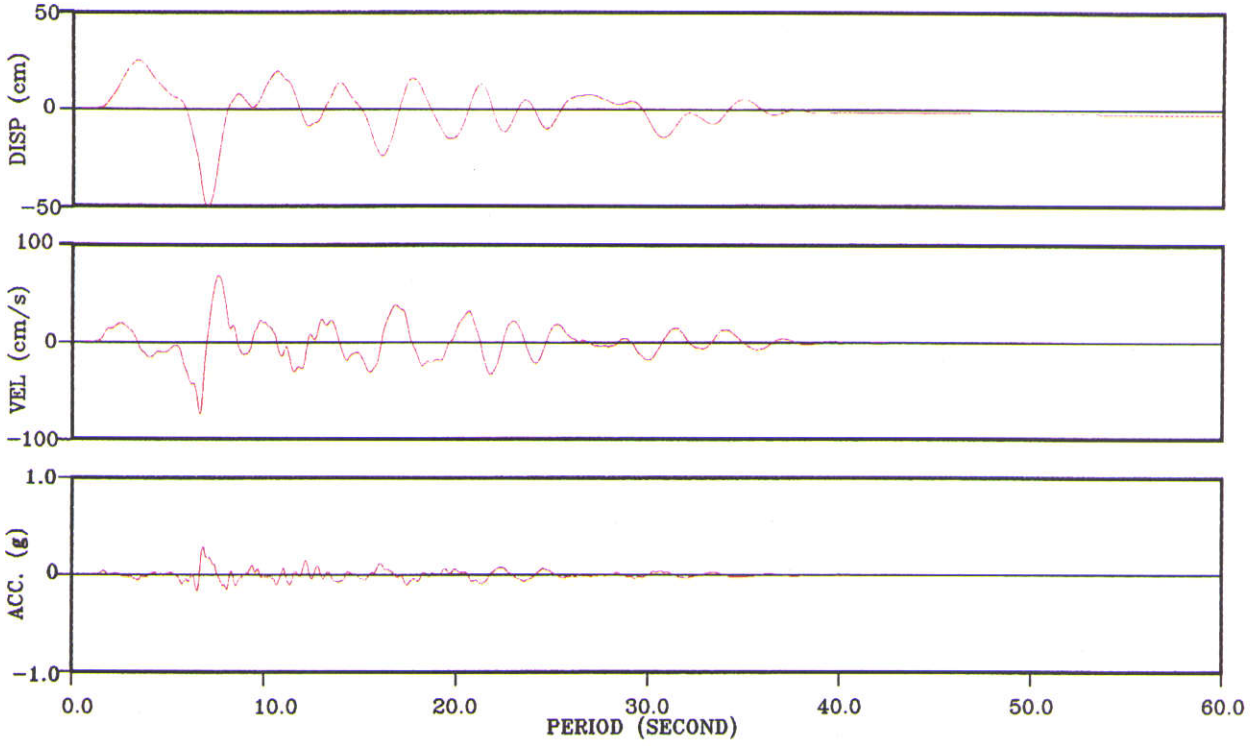

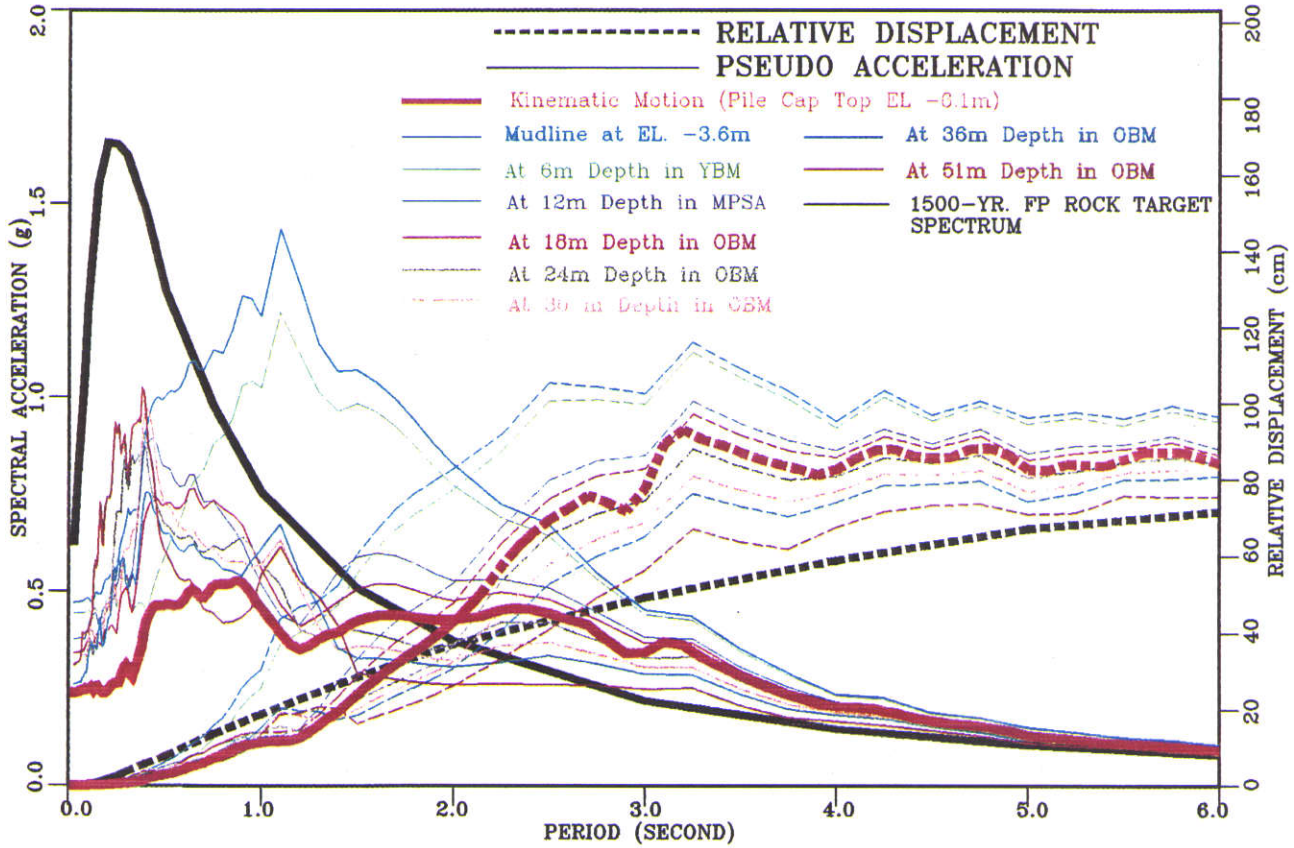

KINEMATIC AND DEPTH-VARYING FREE FIELD MOTIONS
PIER E12, INPUT ROCK MOTION SET 6, FAULT PARALLEL COMPONENT
SFOBB East Span Seismic Safety Project

PLATE 8-137

Earth Mechanics FUGRO

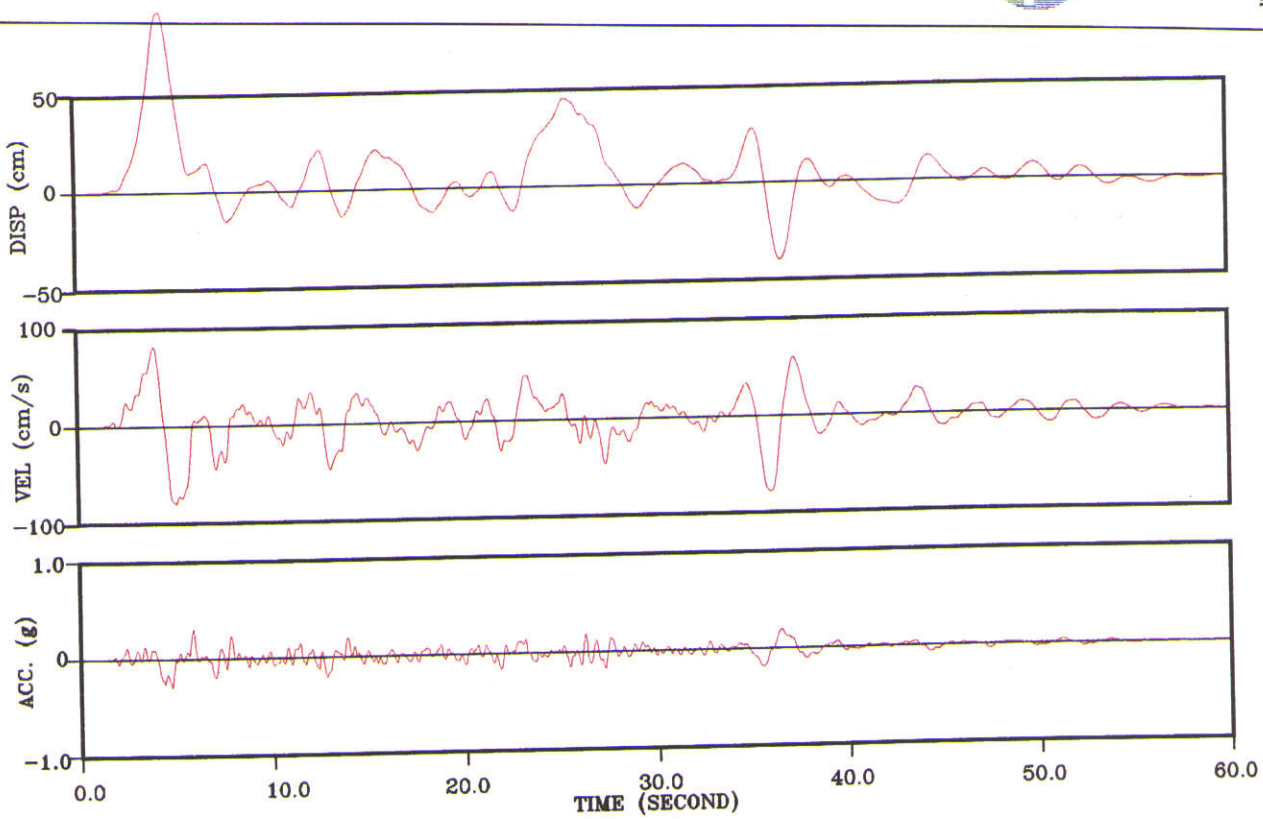

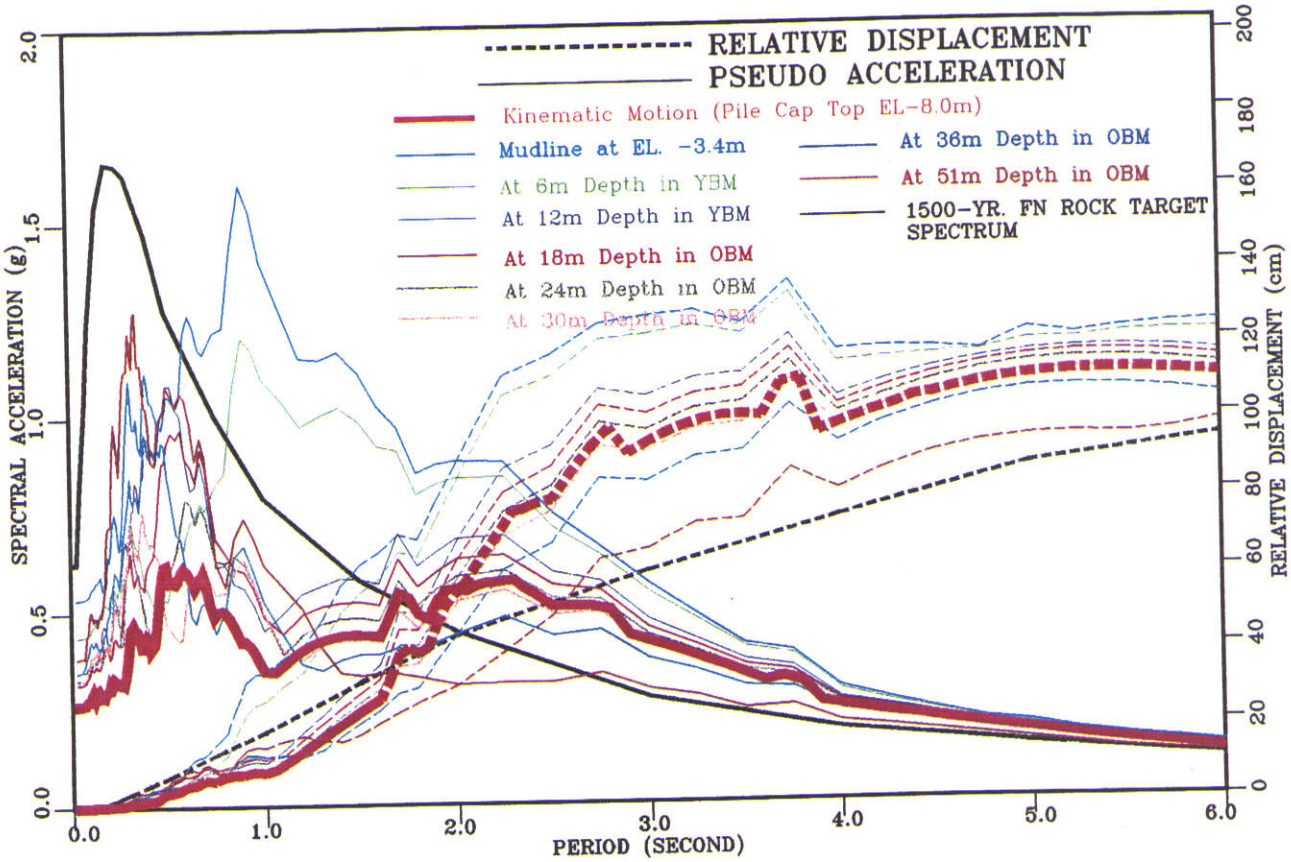

KINEMATIC AND DEPTH-VARYING FREE FIELD MOTIONS
PIER E13, INPUT ROCK MOTION SET 1, FAULT NORMAL COMPONENT
SFOBB East Span Seismic Safety Project

PLATE 8-138

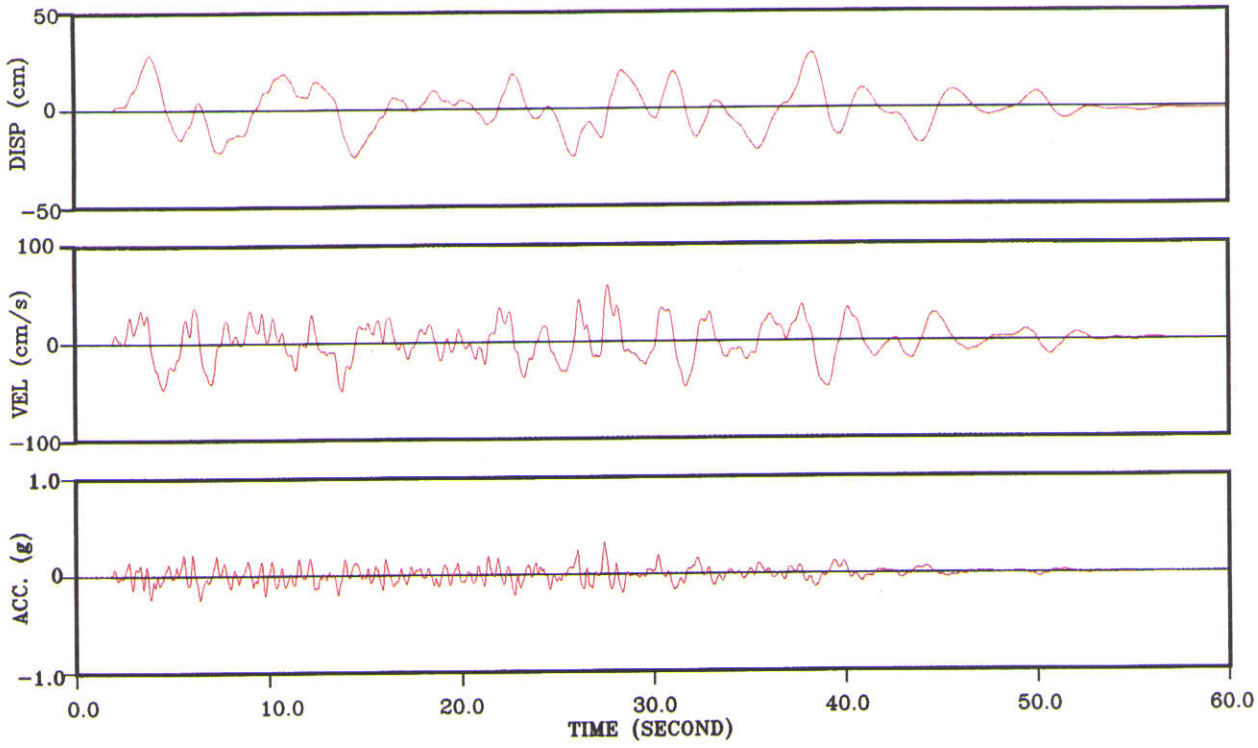

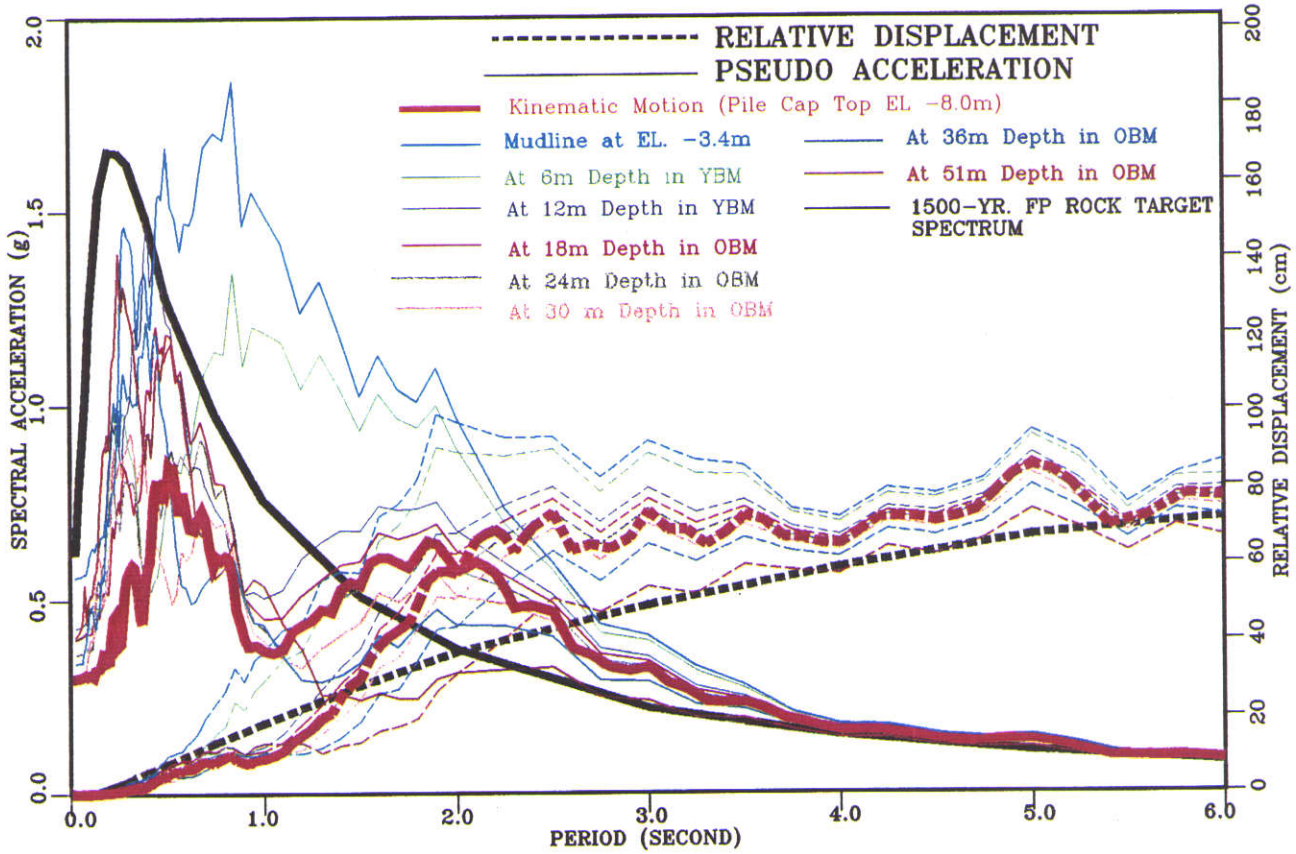

KINEMATIC AND DEPTH-VARYING FREE FIELD MOTIONS
PIER E13, INPUT ROCK MOTION SET 1, FAULT PARALLEL COMPONENT
SFOBB East Span Seismic Safety Project

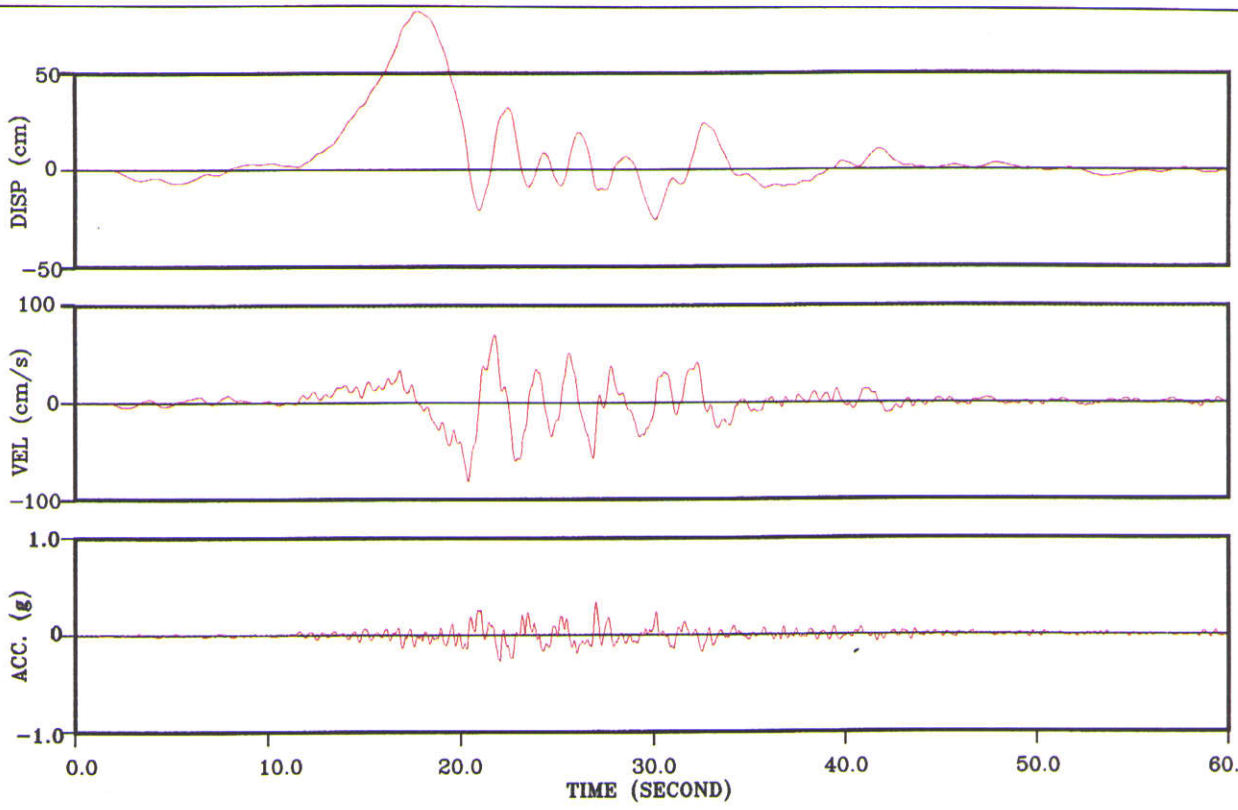

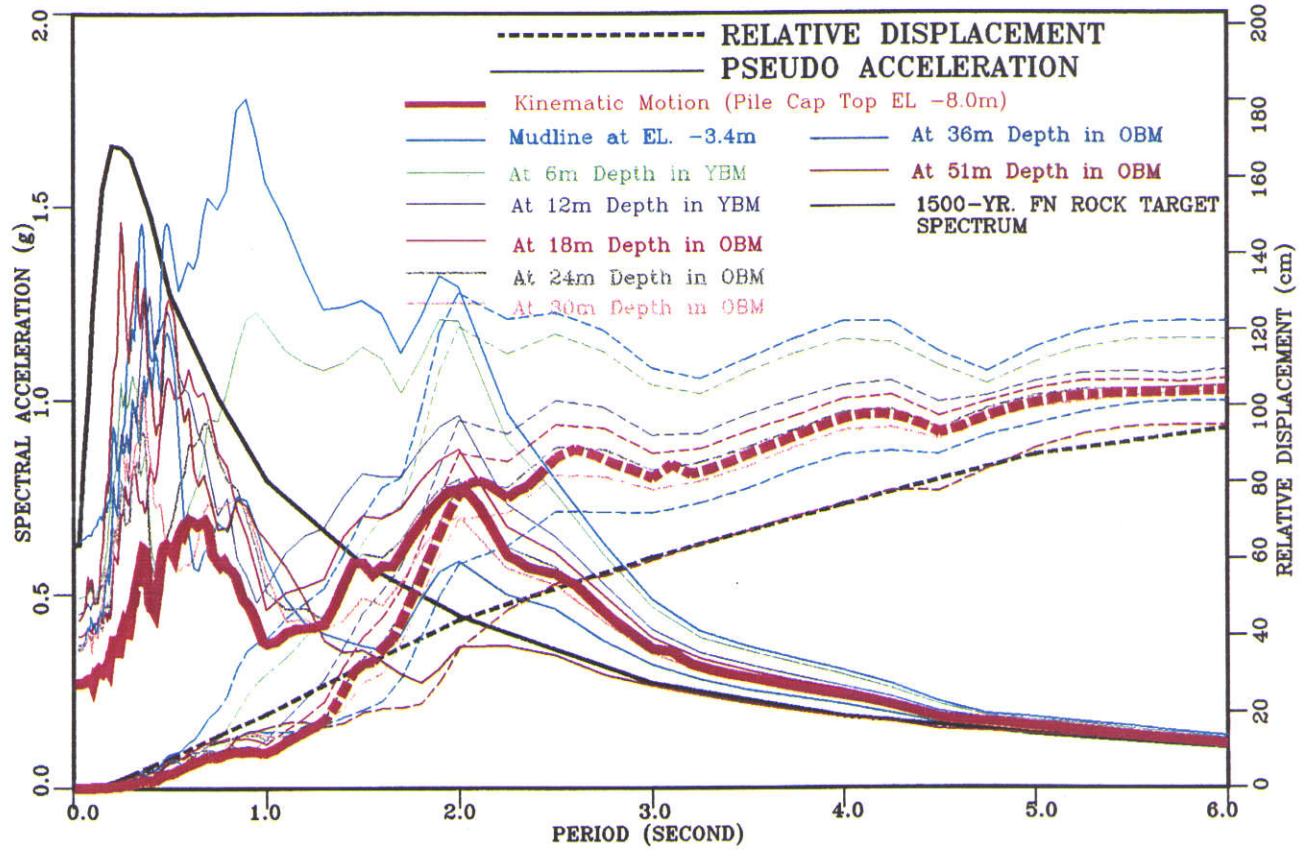

KINEMATIC AND DEPTH-VARYING FREE FIELD MOTIONS
PIER E13, INPUT ROCK MOTION SET 2, FAULT NORMAL COMPONENT
SFOBB East Span Seismic Safety Project

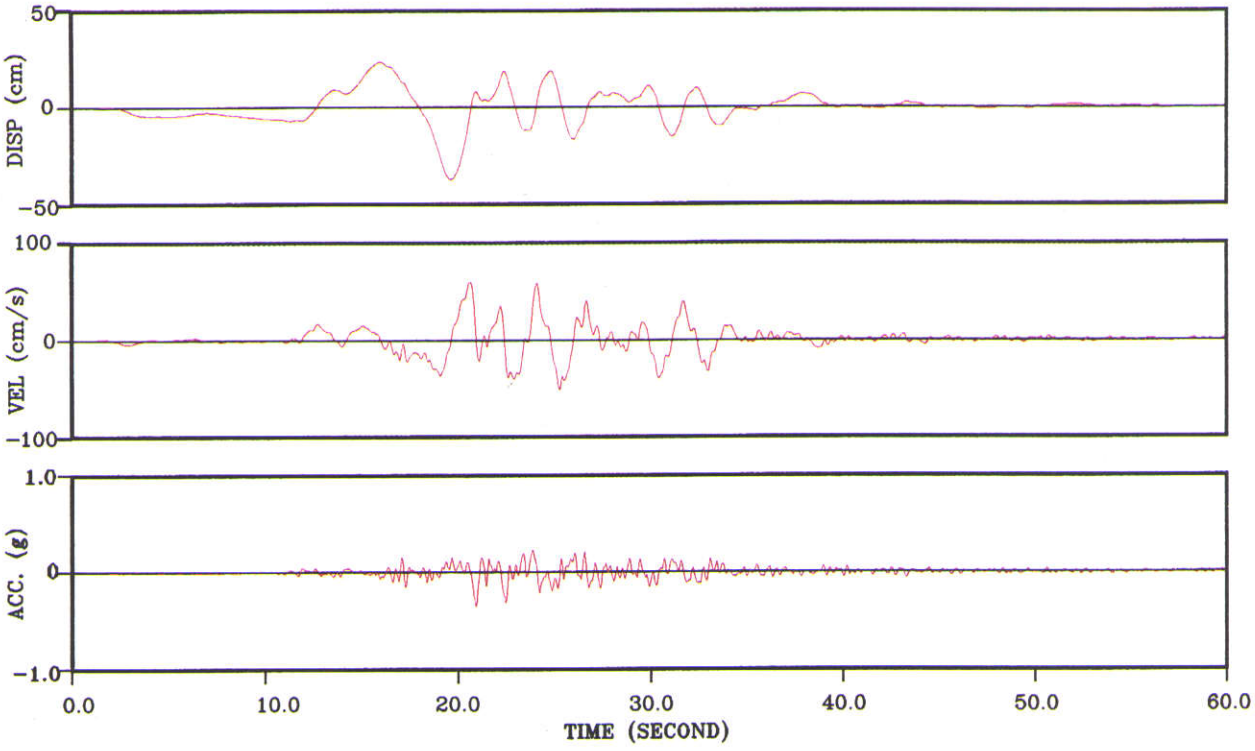

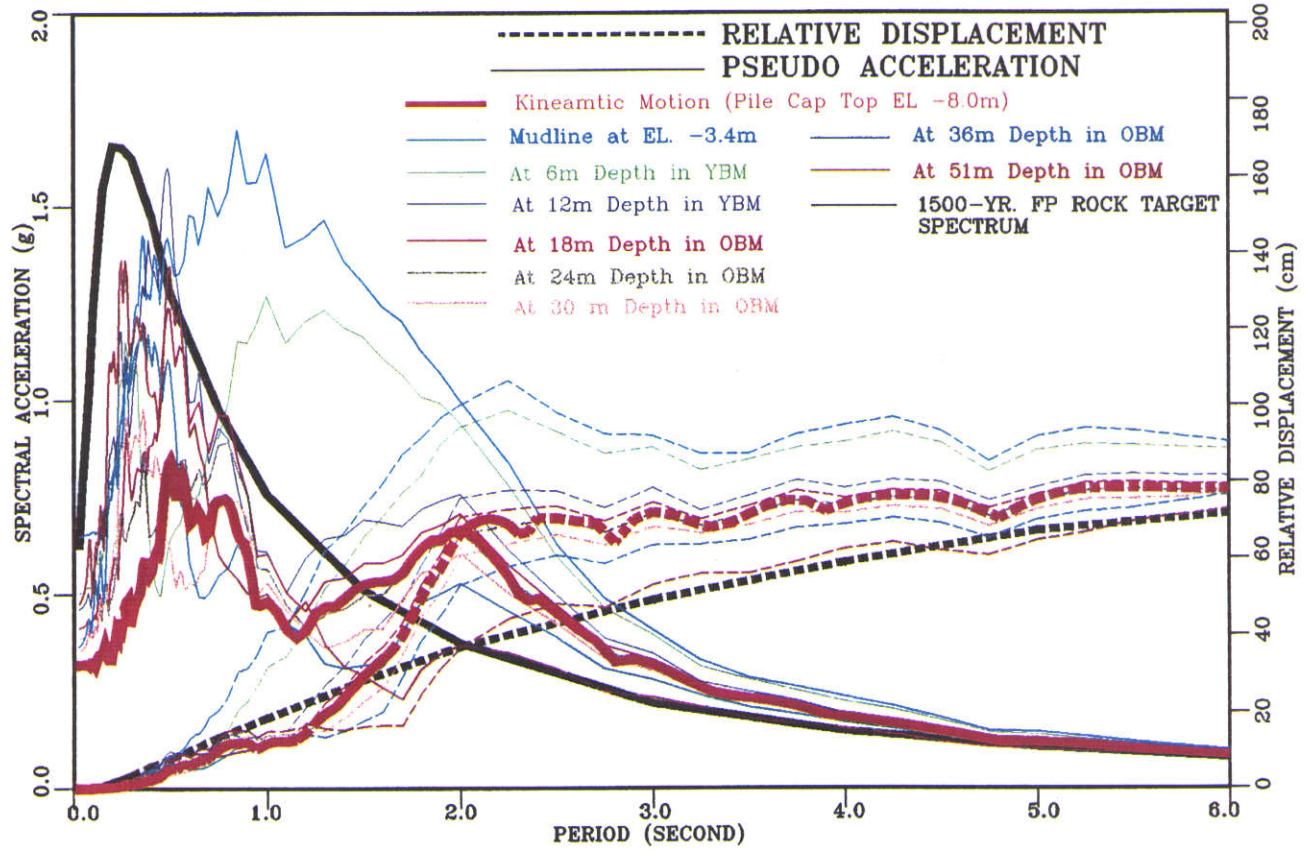

KINEMATIC AND DEPTH-VARYING FREE FIELD MOTIONS
PIER E13, INPUT ROCK MOTION SET 2, FAULT PARALLEL COMPONENT
SFOBB East Span Seismic Safety Project

PLATE 8-141

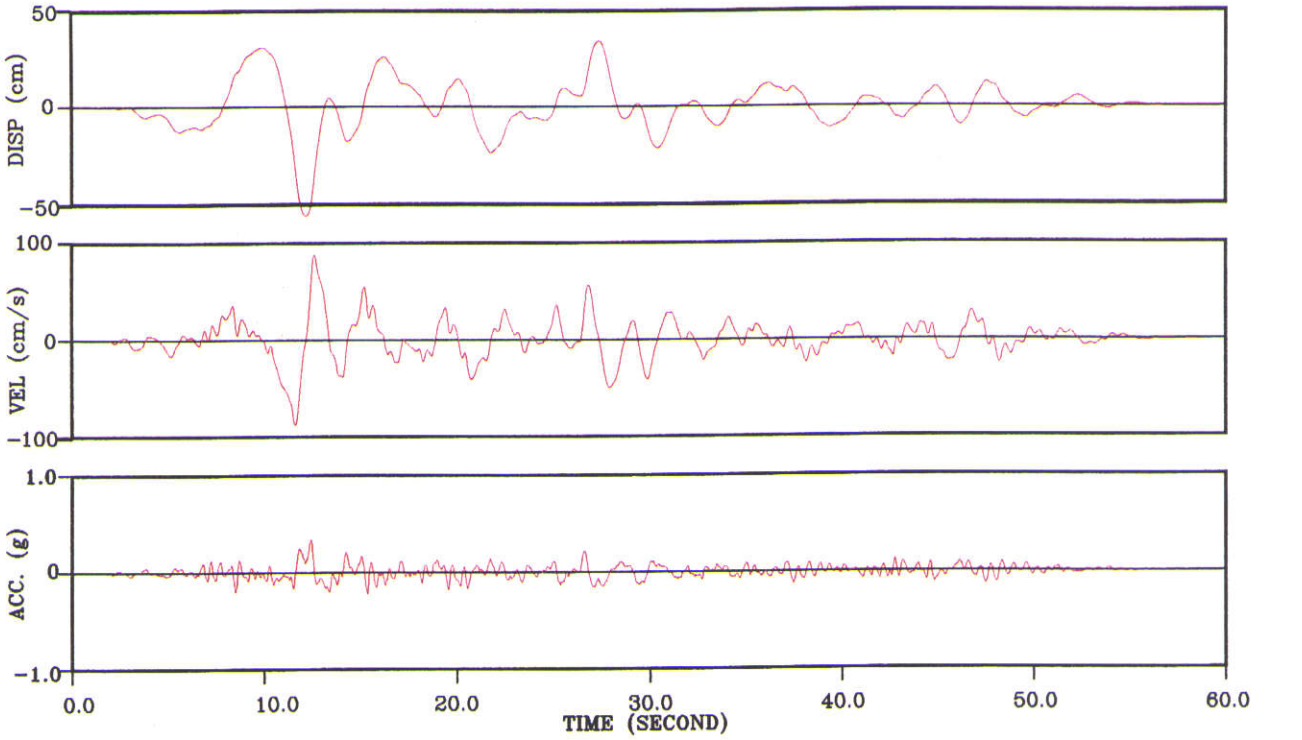

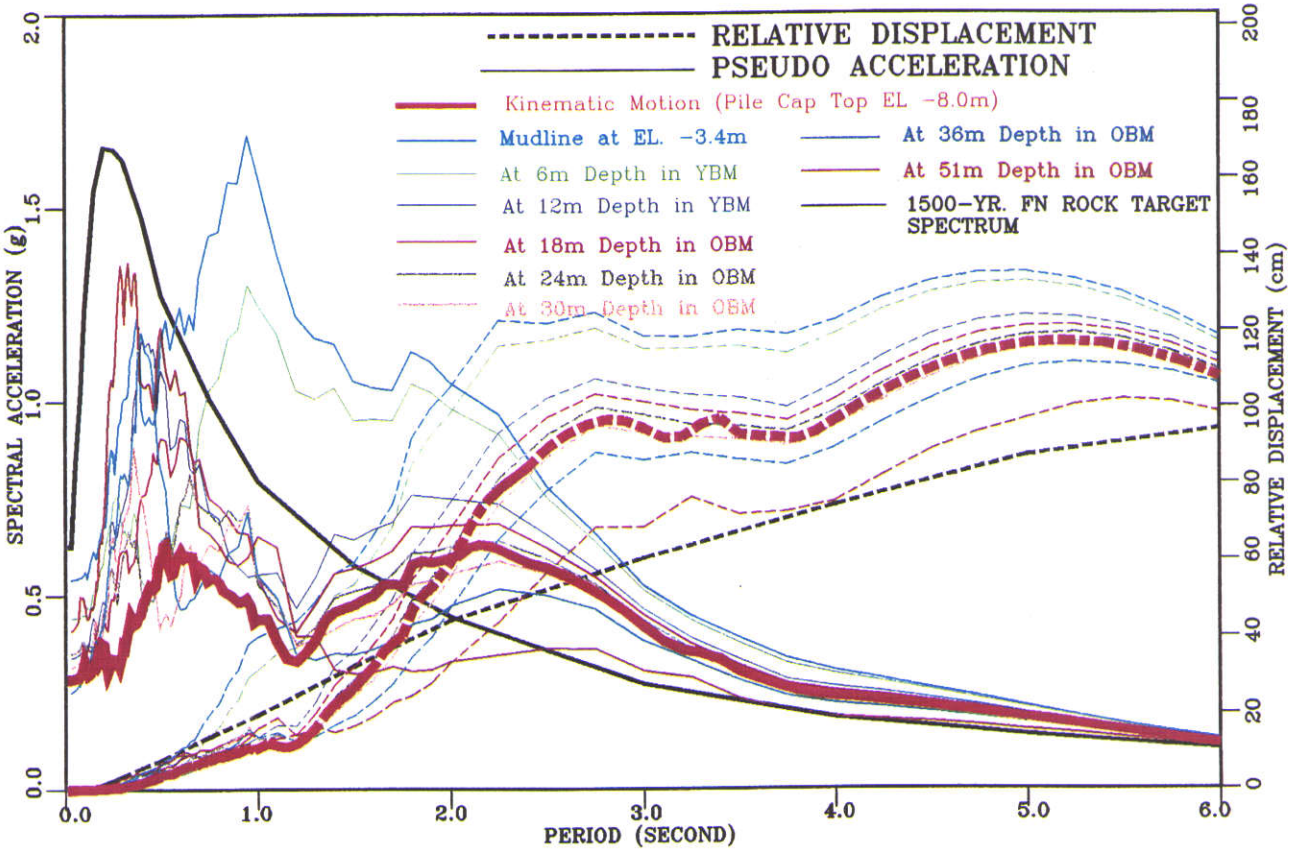

KINEMATIC AND DEPTH-VARYING FREE FIELD MOTIONS
PIER E13, INPUT ROCK MOTION SET 3, FAULT NORMAL COMPONENT
SFOBB East Span Seismic Safety Project

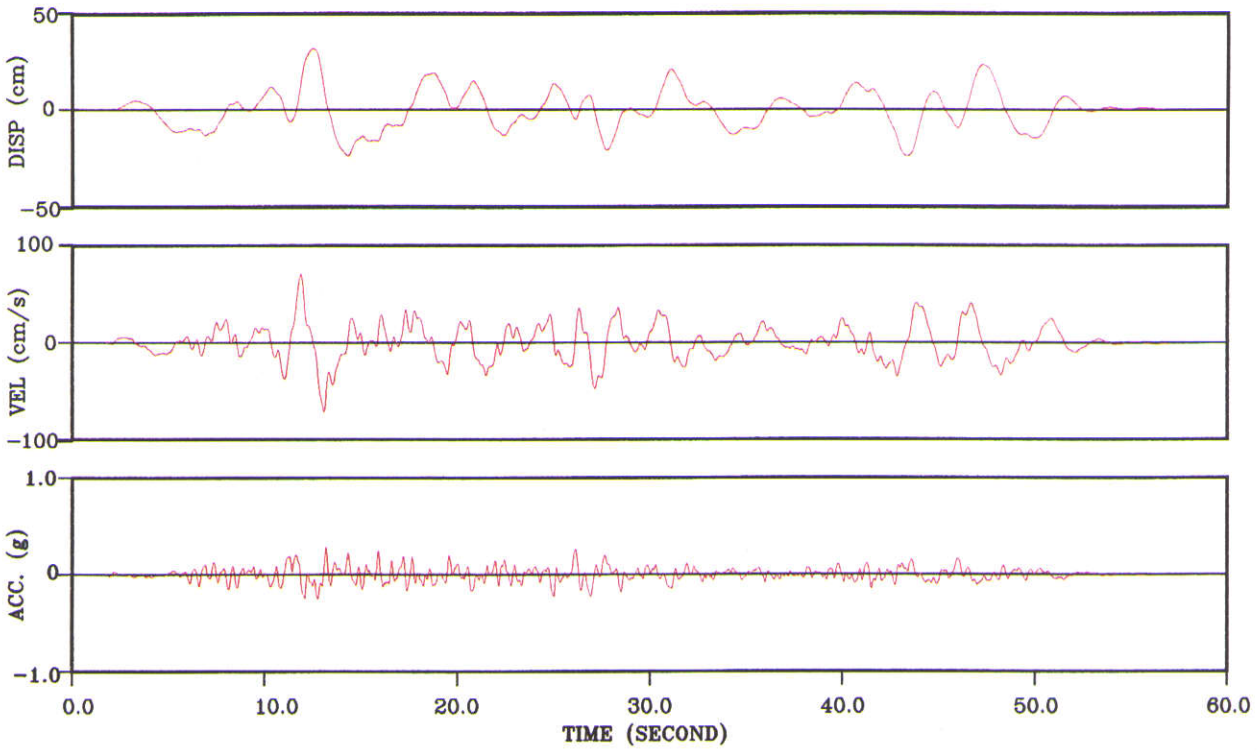

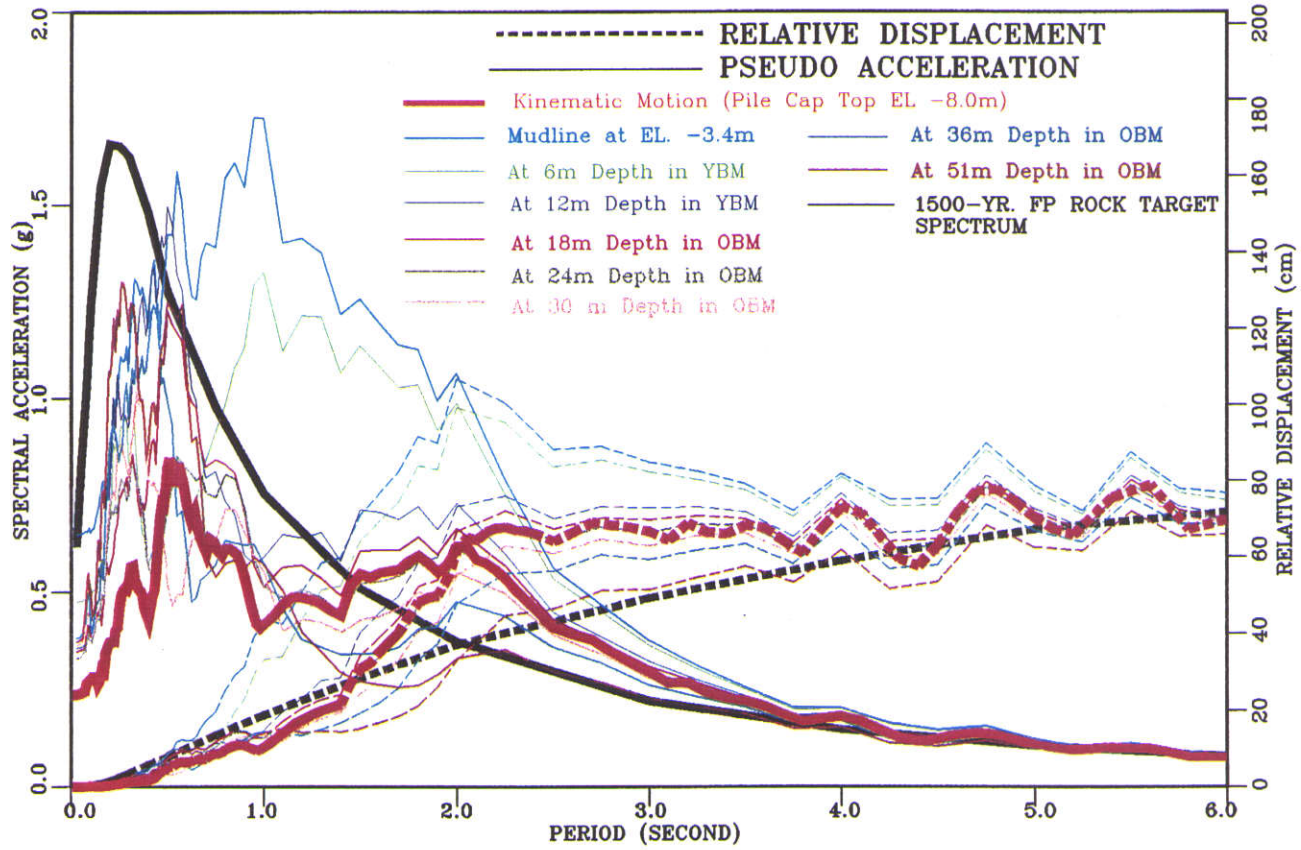

KINEMATIC AND DEPTH-VARYING FREE FIELD MOTIONS
PIER E13, INPUT ROCK MOTION SET 3, FAULT PARALLEL COMPONENT
SFOBB East Span Seismic Safety Project

PLATE 8-143

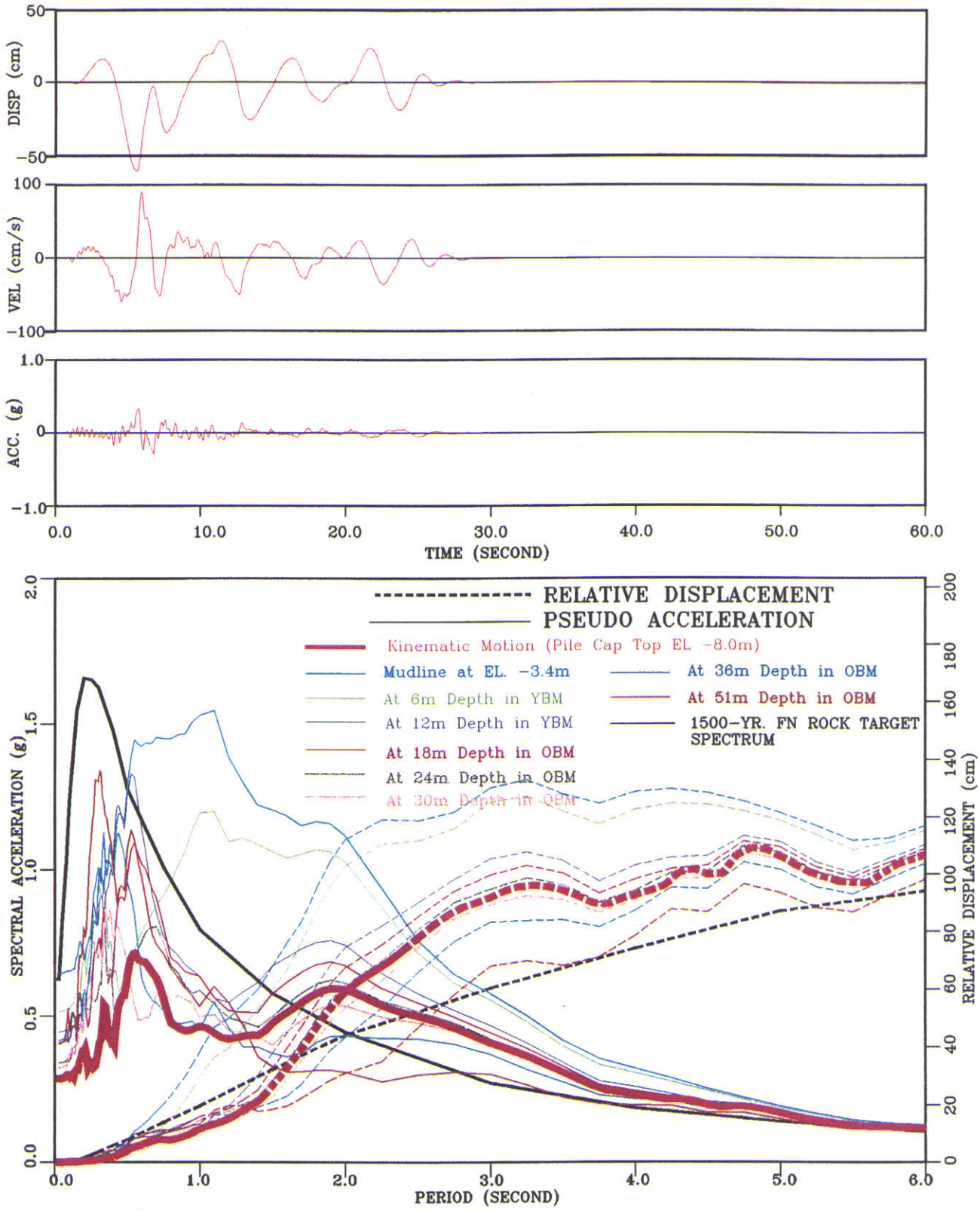

KINEMATIC AND DEPTH-VARYING FREE FIELD MOTIONS
PIER E13, INPUT ROCK MOTION SET 4, FAULT NORMAL COMPONENT
SFOBB East Span Seismic Safety Project

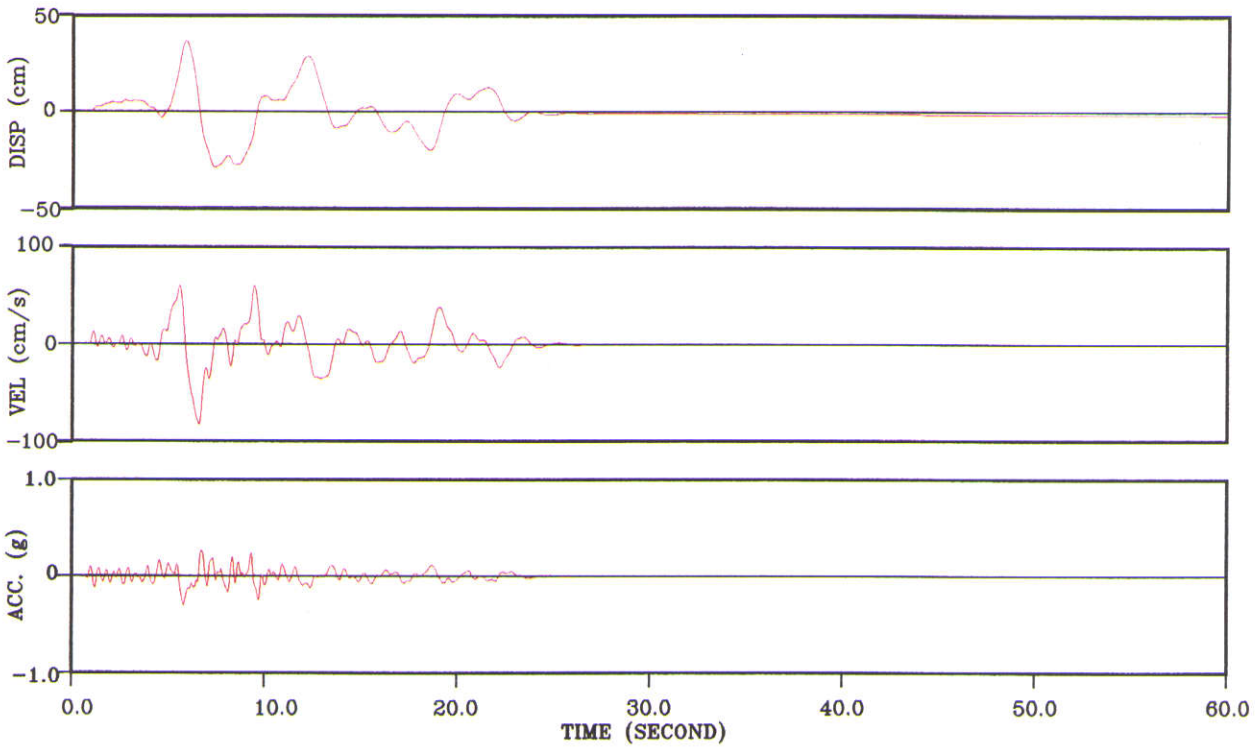

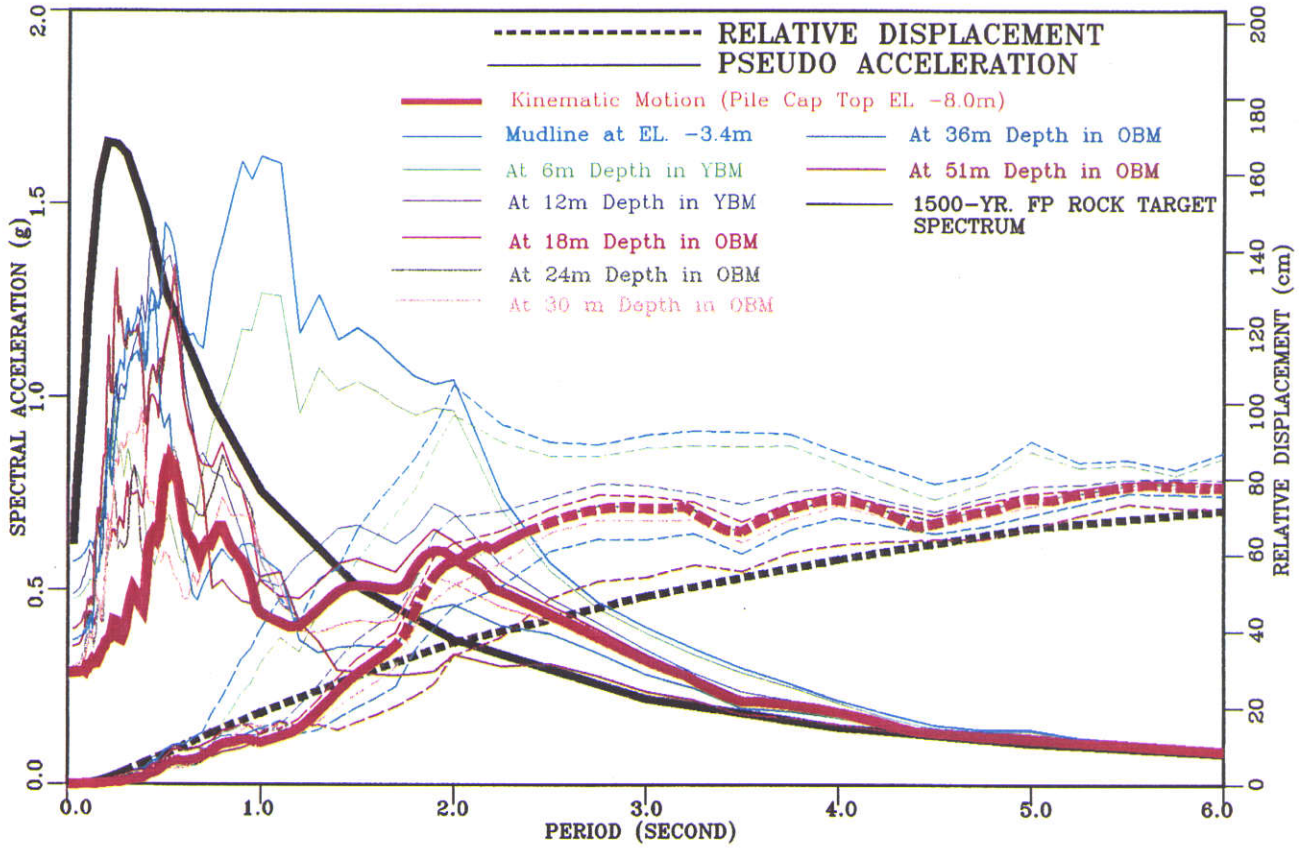

KINEMATIC AND DEPTH-VARYING FREE FIELD MOTIONS
PIER E13, INPUT ROCK MOTION SET 4, FAULT PARALLEL COMPONENT
SFOBB East Span Seismic Safety Project

PLATE 8-145

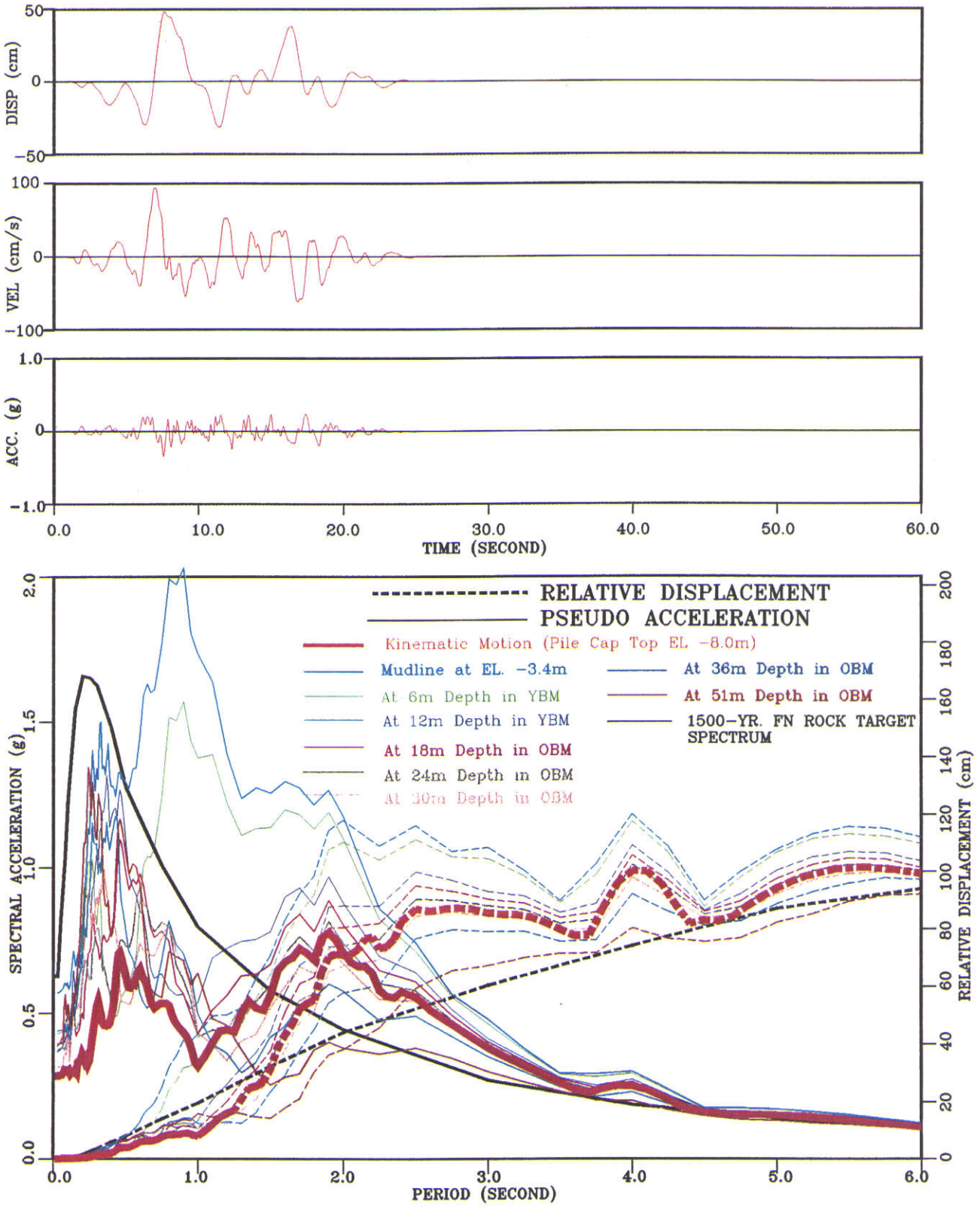

KINEMATIC AND DEPTH-VARYING FREE FIELD MOTIONS
PIER E13, INPUT ROCK MOTION SET 5, FAULT NORMAL COMPONENT
SFOBB East Span Seismic Safety Project

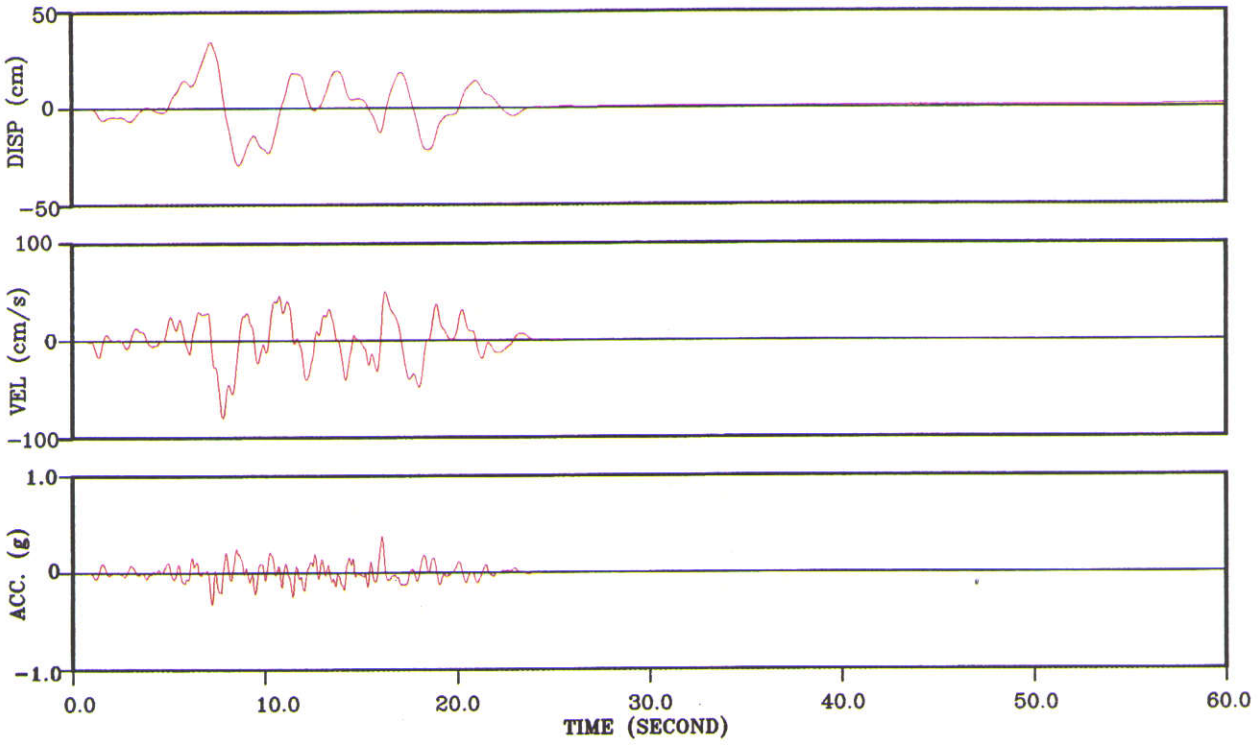

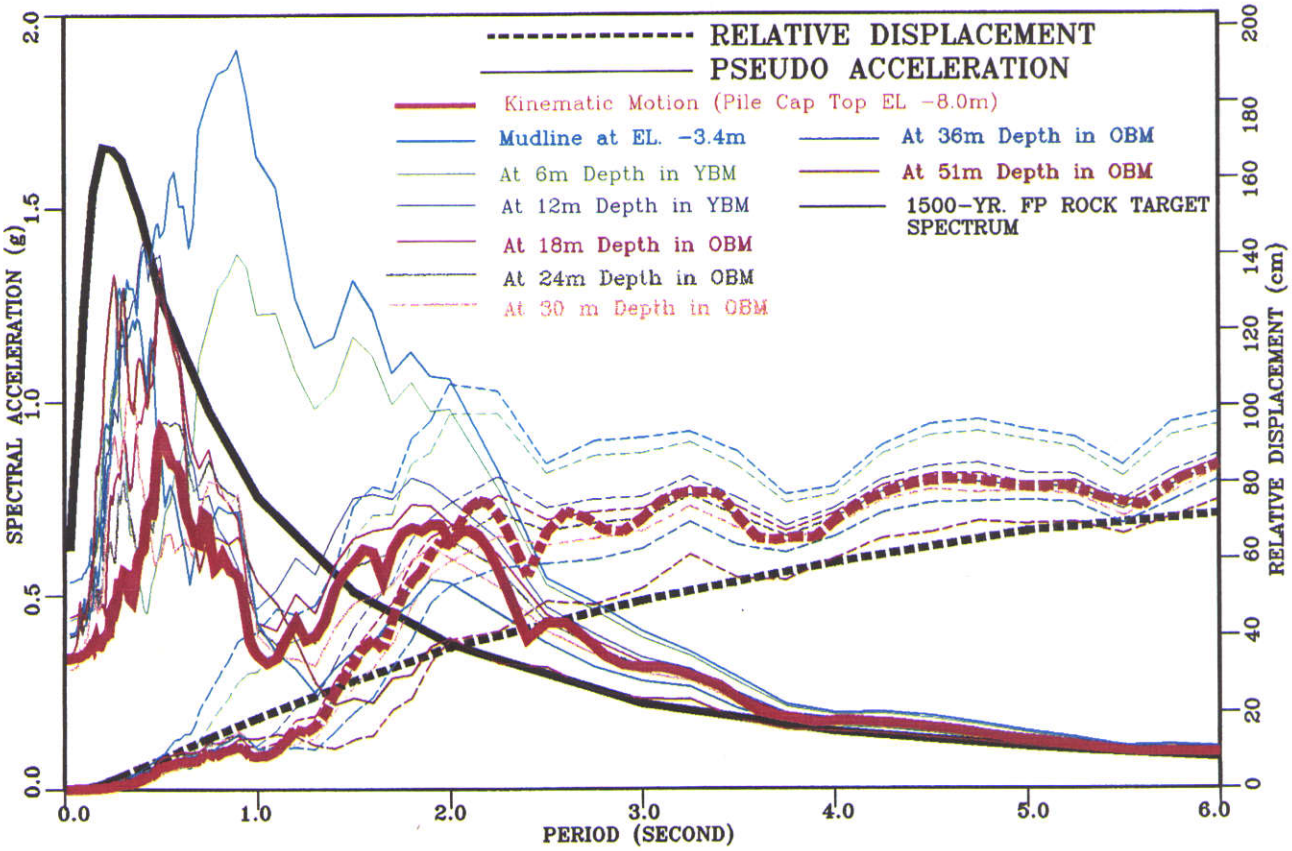

KINEMATIC AND DEPTH-VARYING FREE FIELD MOTIONS
PIER E13, INPUT ROCK MOTION SET 5, FAULT PARALLEL COMPONENT
SFOBB East Span Seismic Safety Project

PLATE 8-147

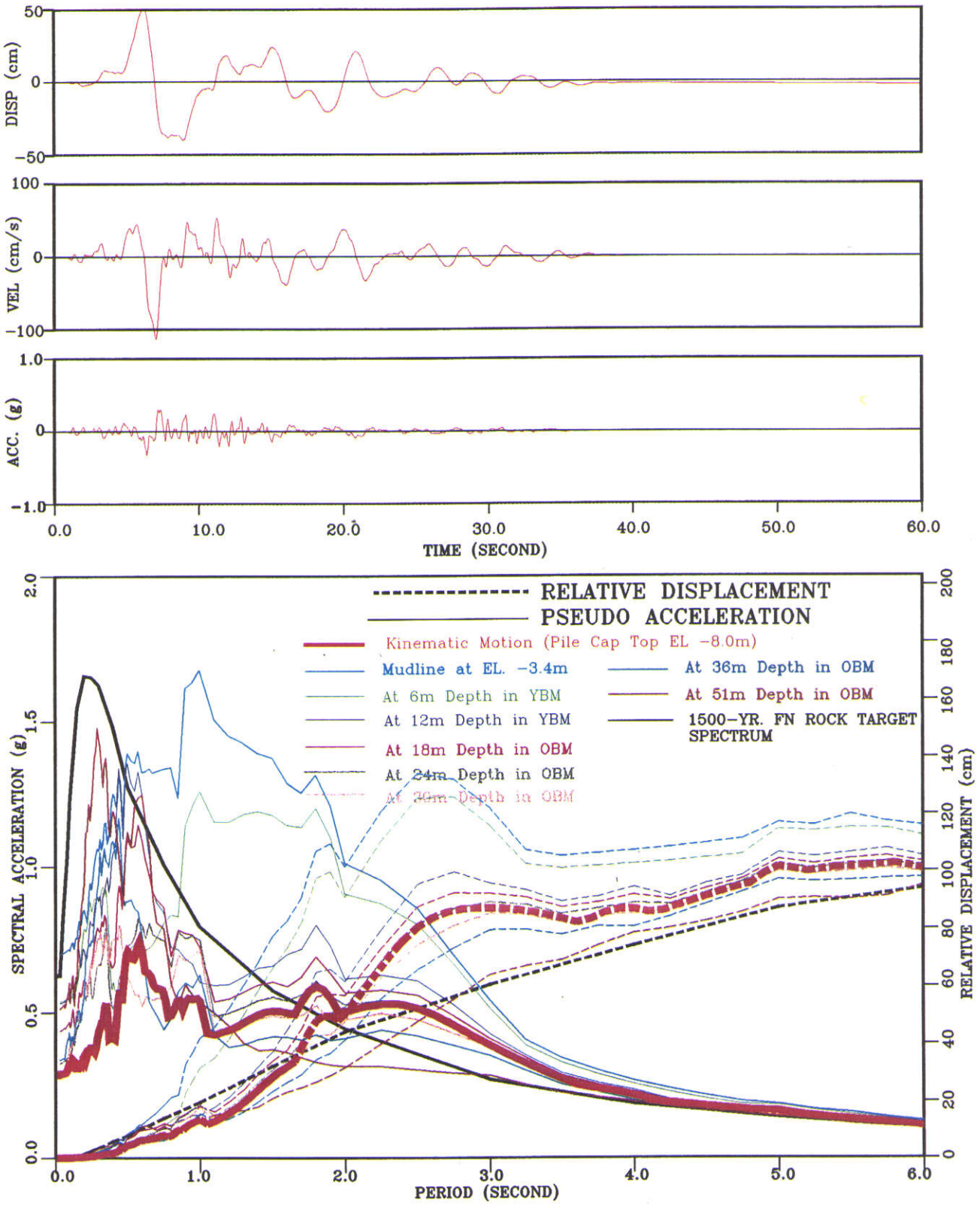

KINEMATIC AND DEPTH-VARYING FREE FIELD MOTIONS
PIER E13, INPUT ROCK MOTION SET 6, FAULT NORMAL COMPONENT
SFOBB East Span Seismic Safety Project

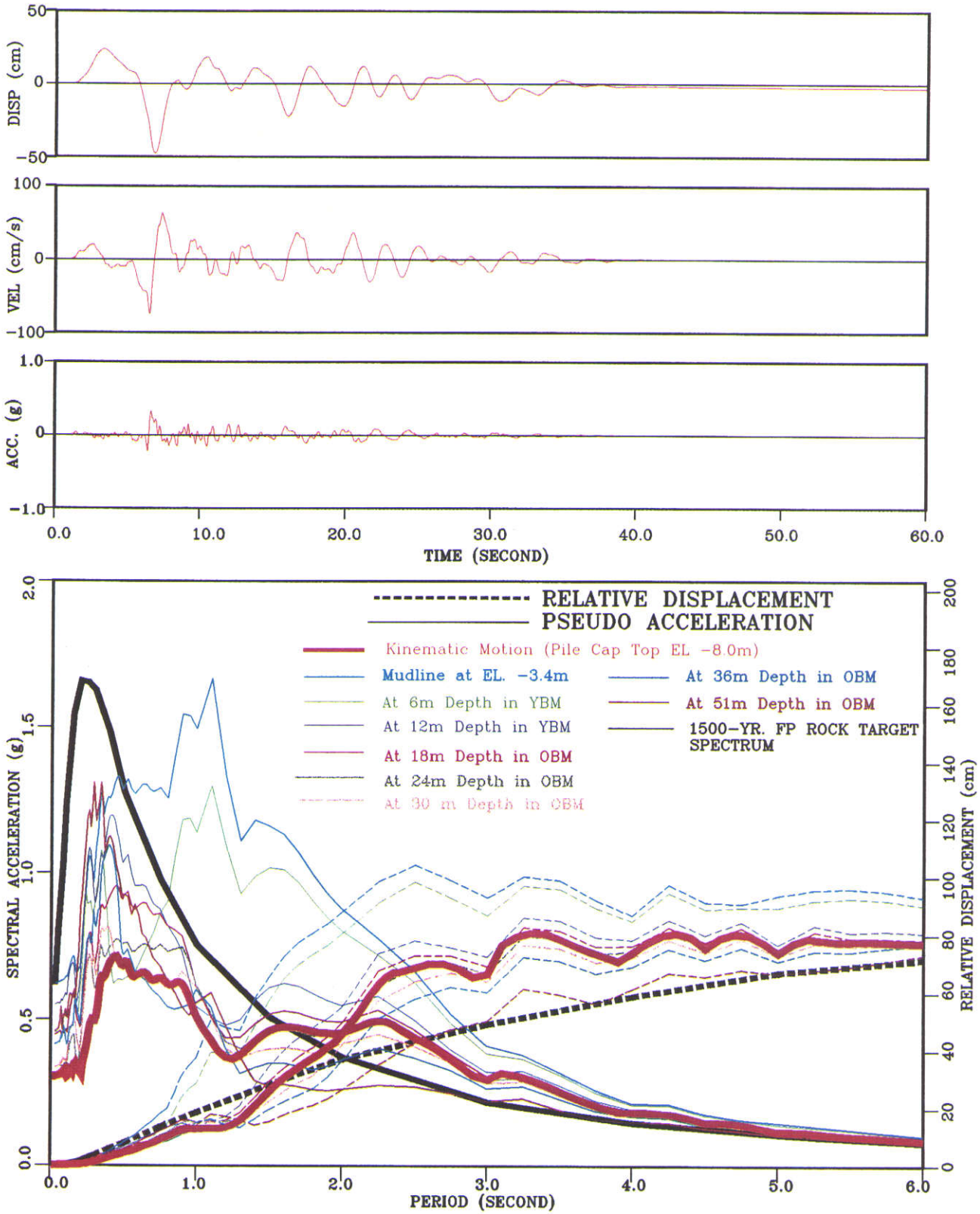

KINEMATIC AND DEPTH-VARYING FREE FIELD MOTIONS
PIER E13, INPUT ROCK MOTION SET 6, FAULT PARALLEL COMPONENT
SFOBB East Span Seismic Safety Project

Earth Mechanics FUGRO

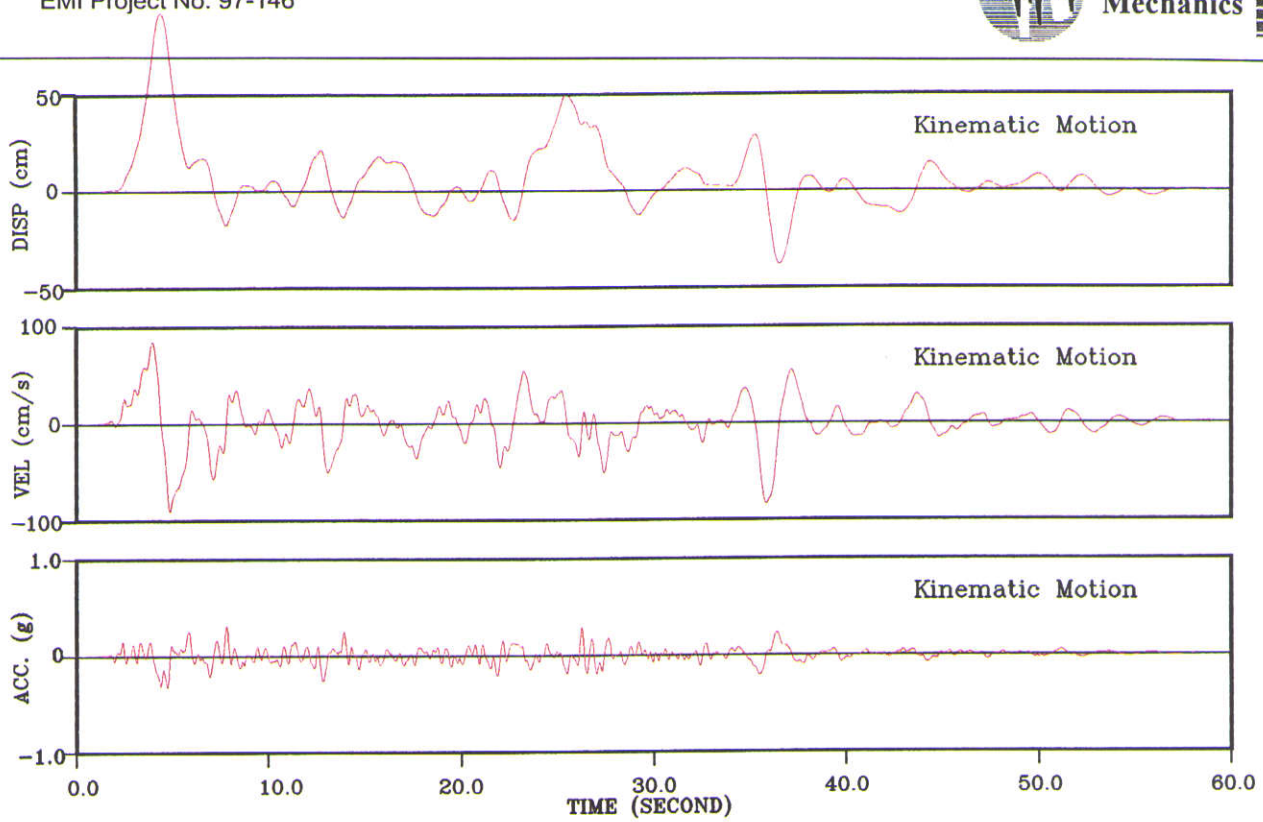

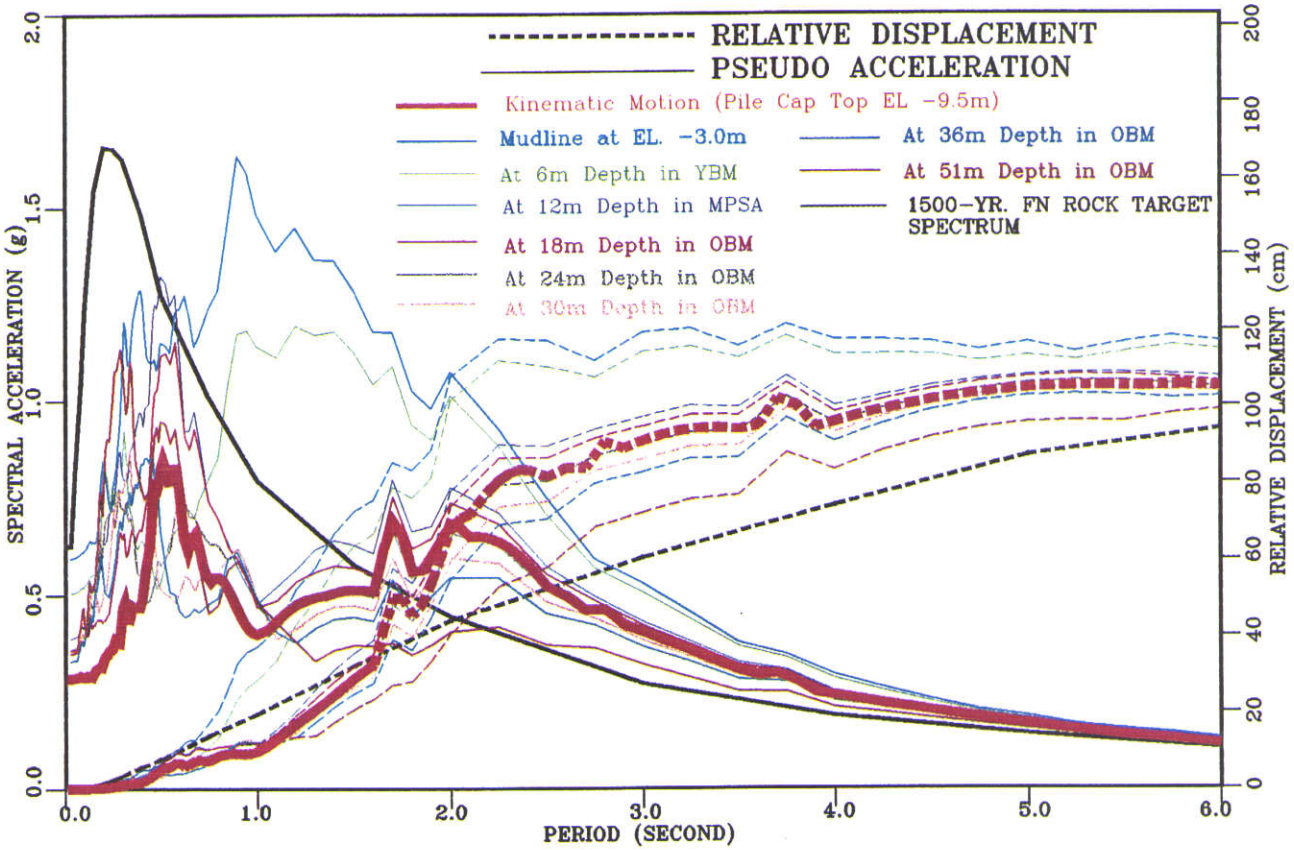

KINEMATIC AND DEPTH-VARYING FREE FIELD MOTIONS
PIER E14, INPUT ROCK MOTION SET 1, FAULT NORMAL COMPONENT
SFOBB East Span Seismic Safety Project

PLATE 8-150

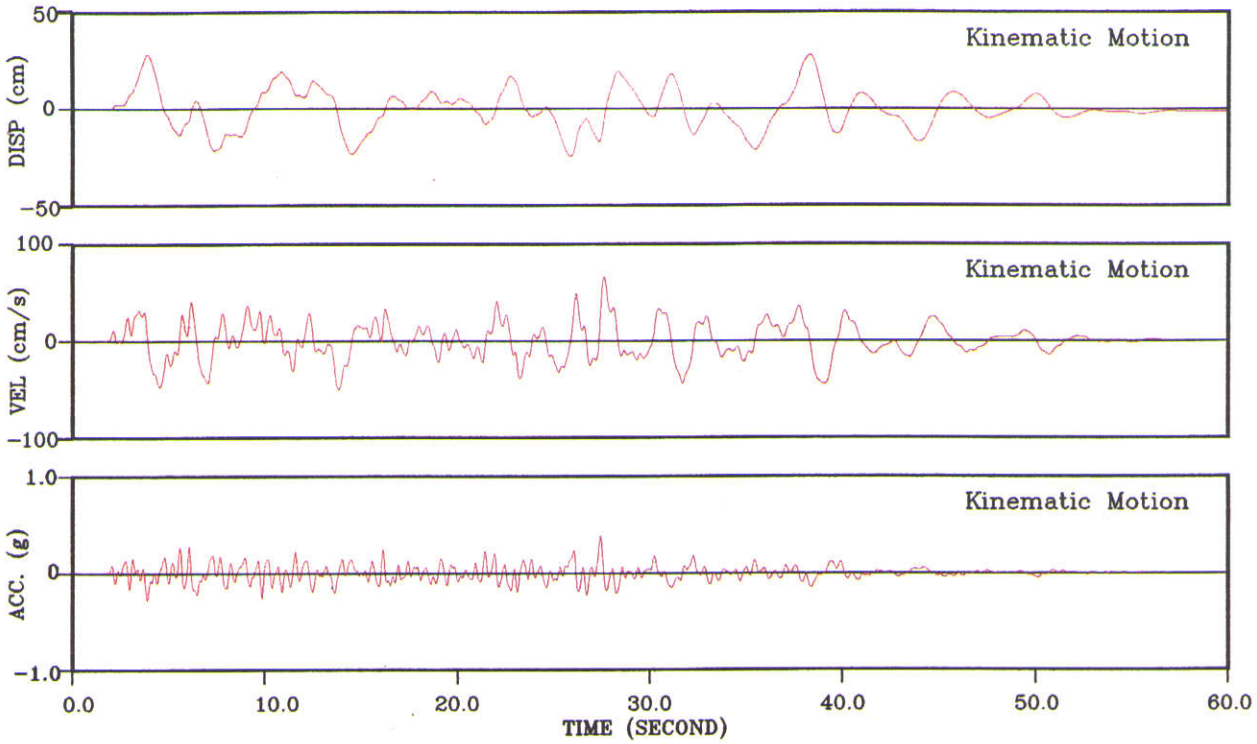

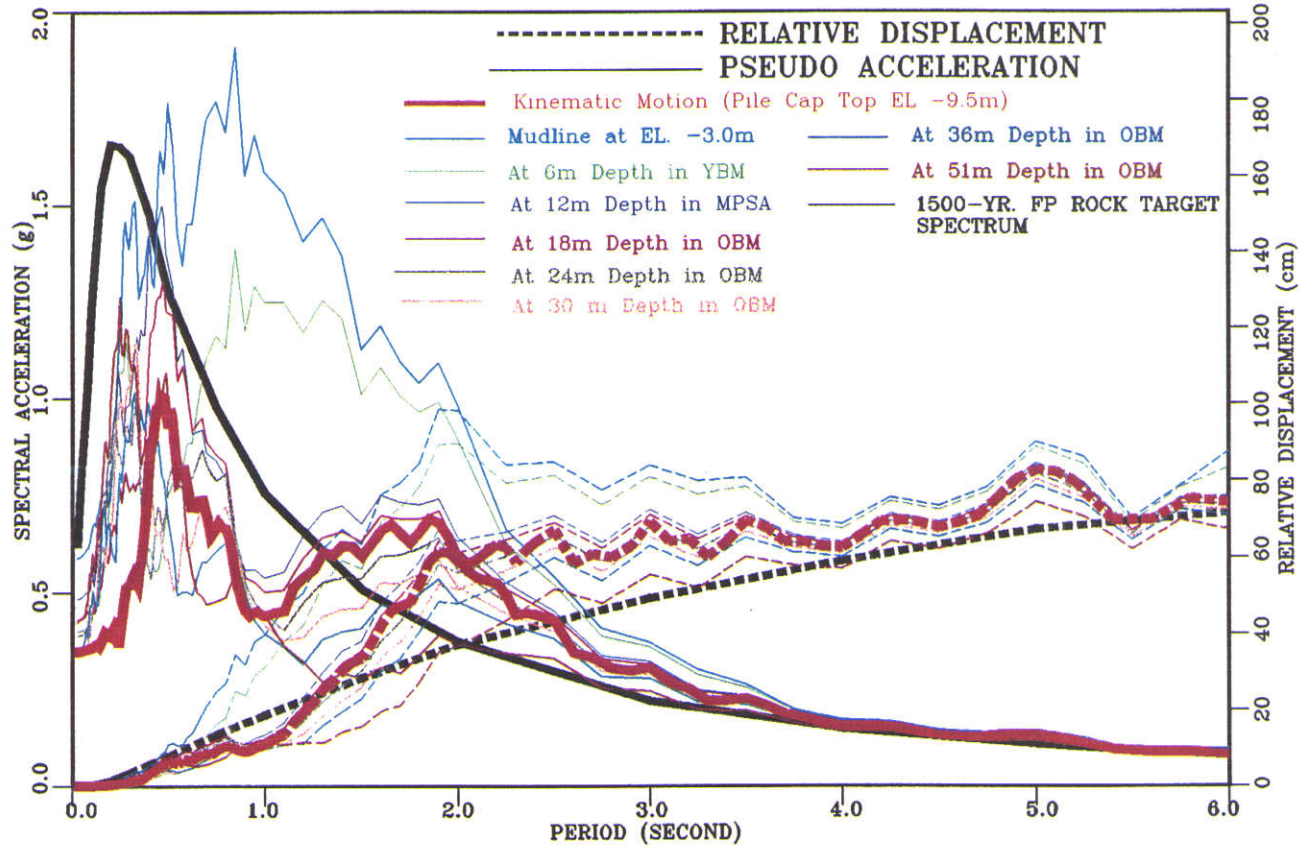

KINEMATIC AND DEPTH-VARYING FREE FIELD MOTIONS
PIER E14, INPUT ROCK MOTION SET 1, FAULT PARALLEL COMPONENT
SFOBB East Span Seismic Safety Project

PLATE 8-151

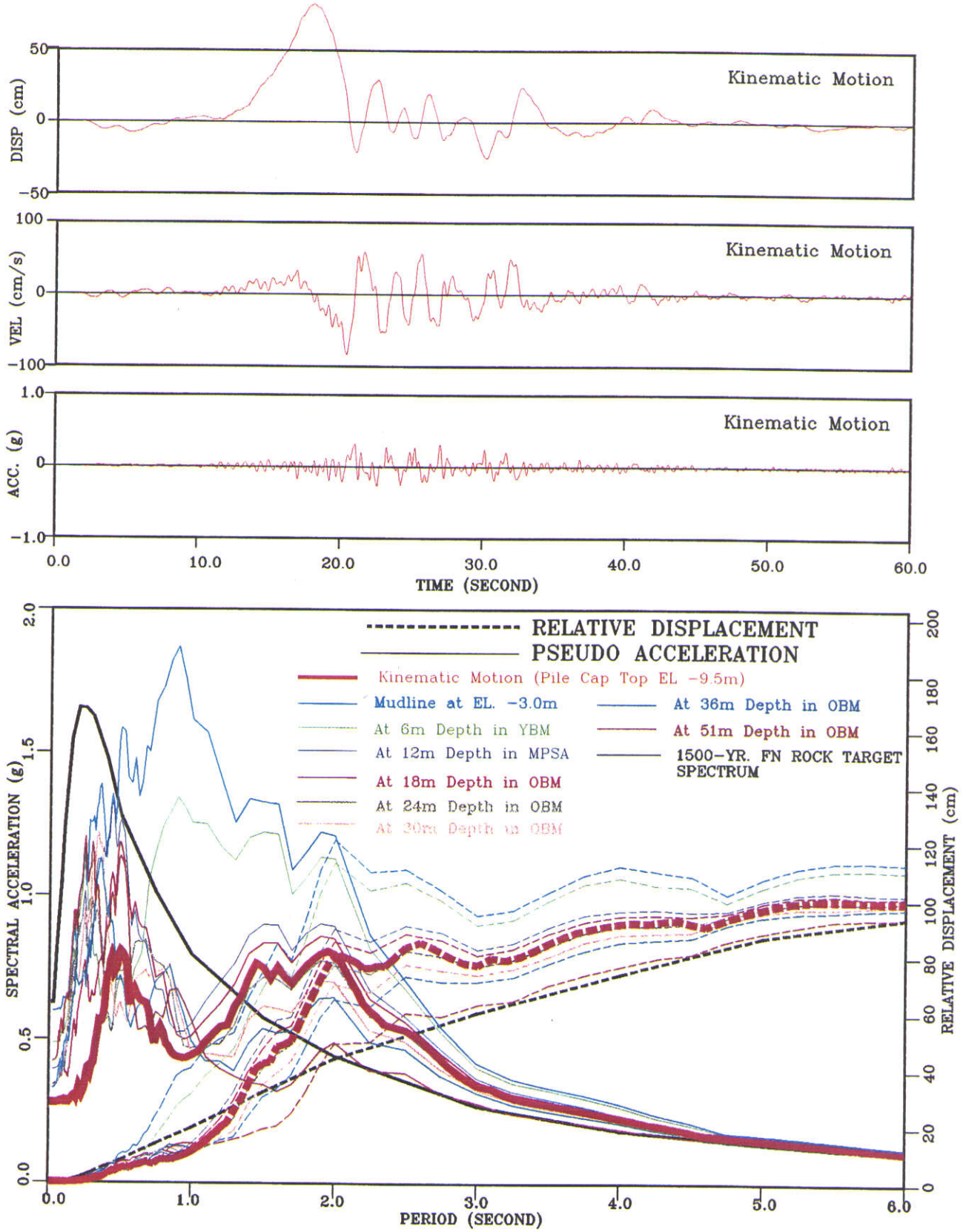

KINEMATIC AND DEPTH-VARYING FREE FIELD MOTIONS
PIER E14, INPUT ROCK MOTION SET 2, FAULT NORMAL COMPONENT
SFOBB East Span Seismic Safety Project

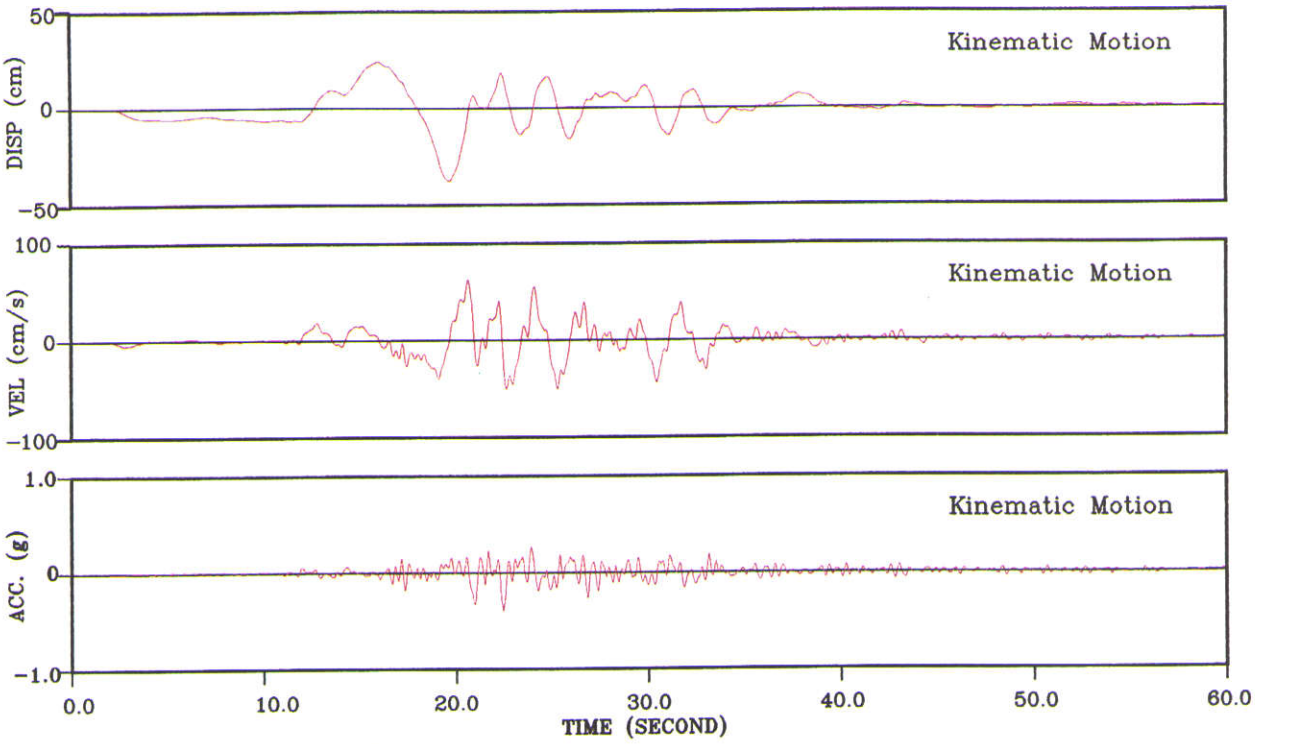

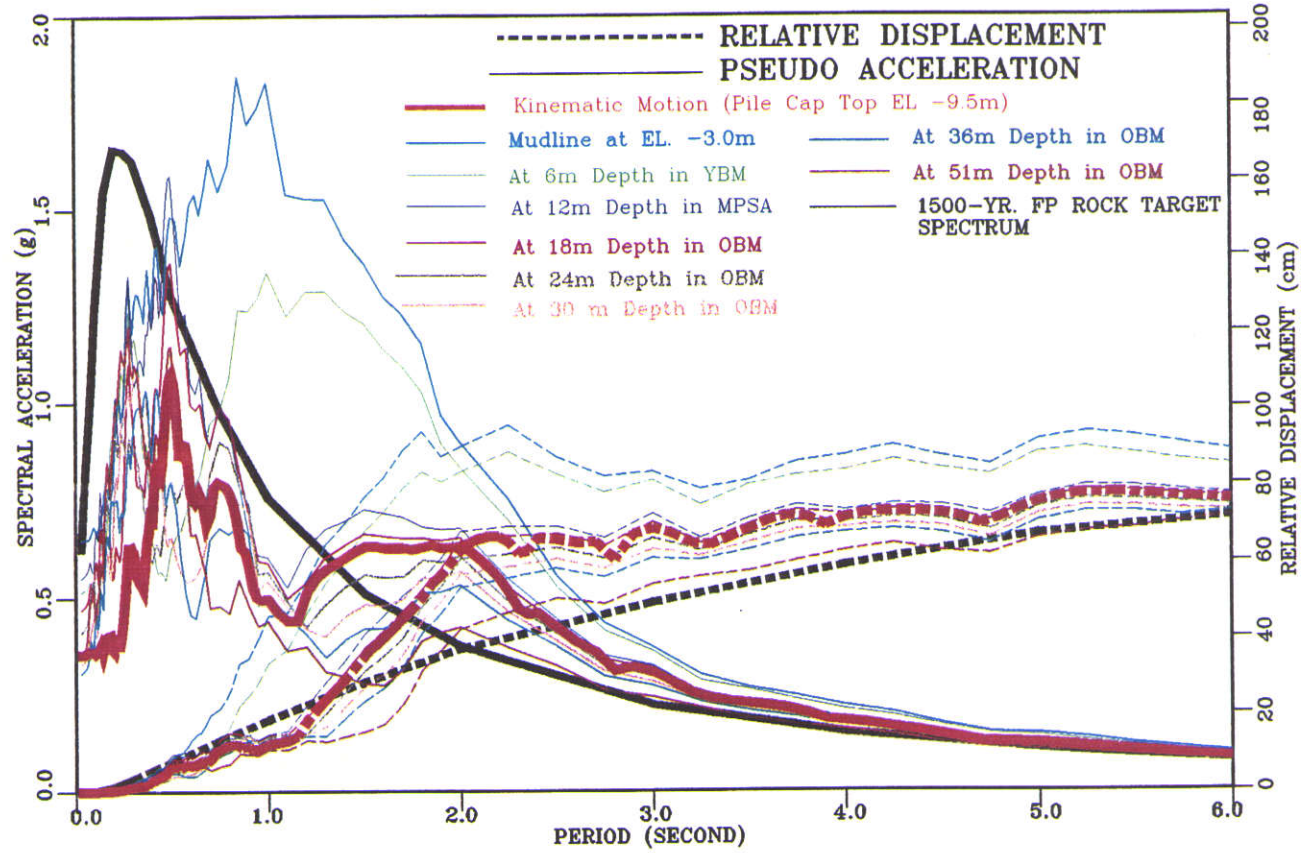

KINEMATIC AND DEPTH-VARYING FREE FIELD MOTIONS
PIER E14, INPUT ROCK MOTION SET 2, FAULT PARALLEL COMPONENT
SFOBB East Span Seismic Safety Project

PLATE 8-153

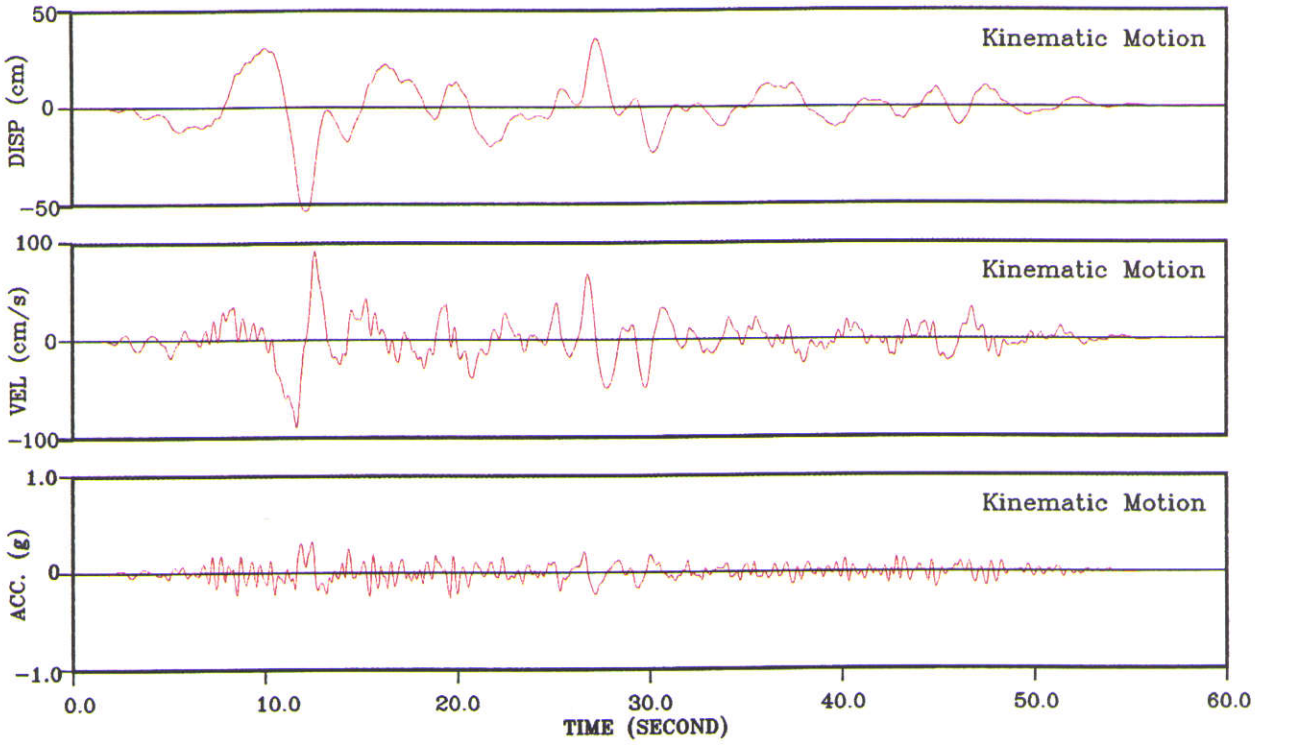

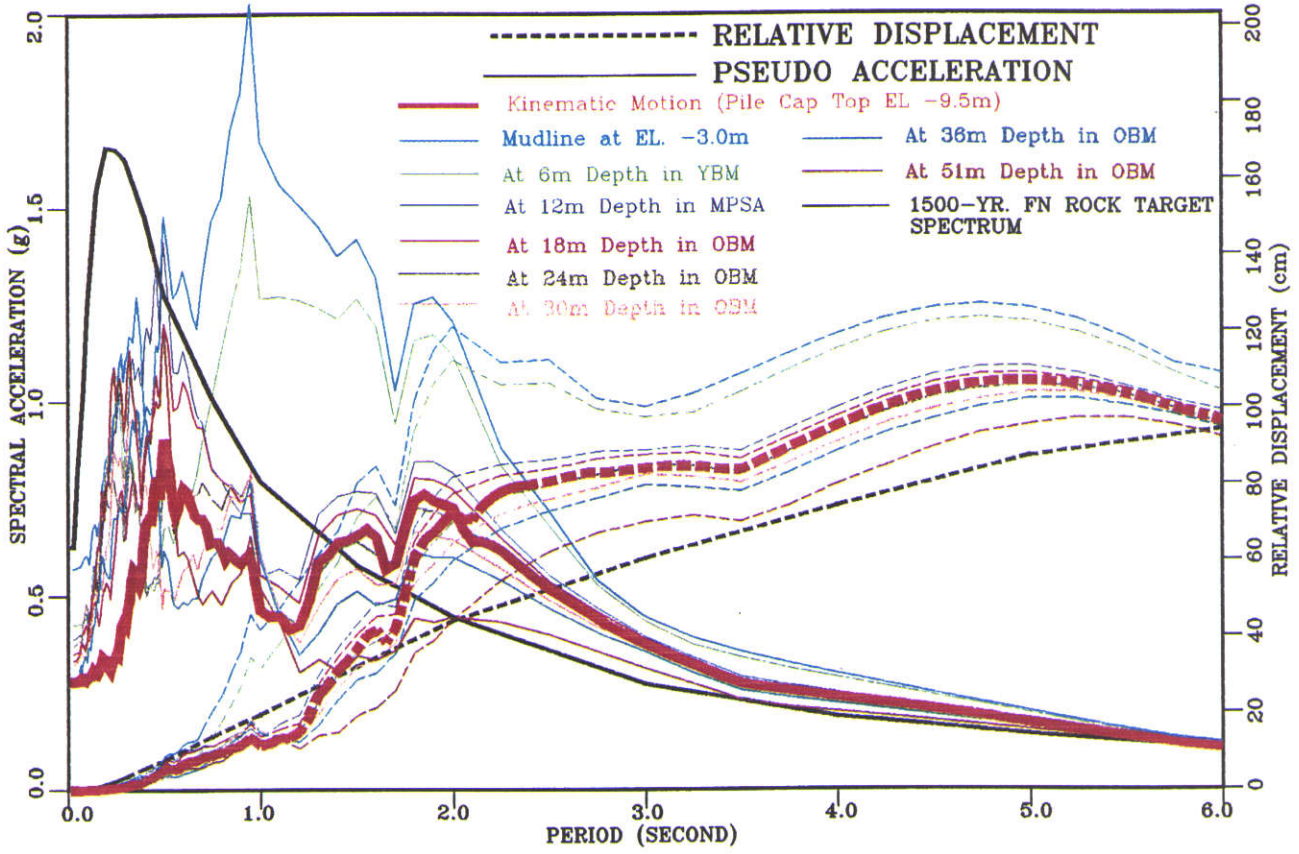

KINEMATIC AND DEPTH-VARYING FREE FIELD MOTIONS
PIER E14, INPUT ROCK MOTION SET 3, FAULT NORMAL COMPONENT
SFOBB East Span Seismic Safety Project

PLATE 8-154

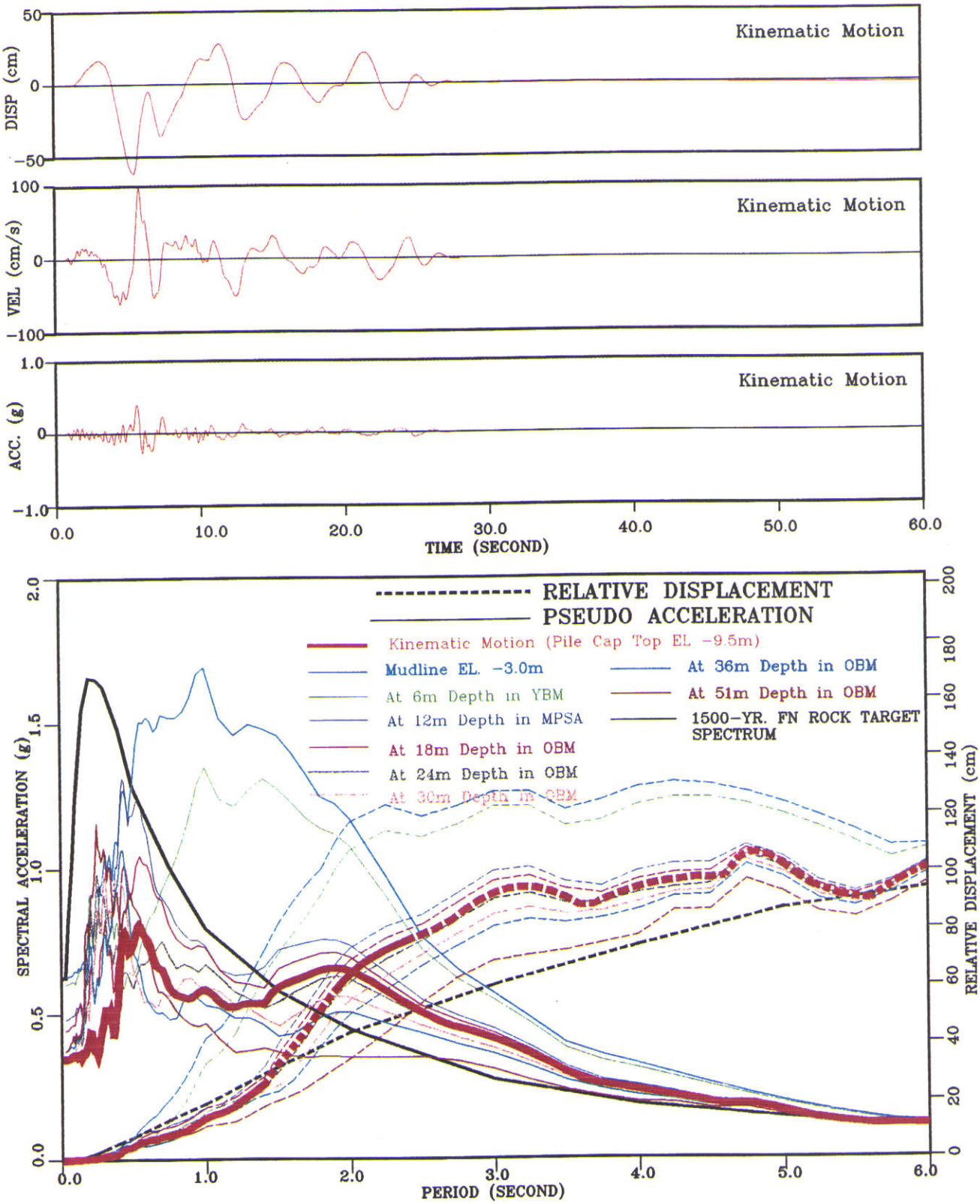

KINEMATIC AND DEPTH-VARYING FREE FIELD MOTIONS
PIER E14, INPUT ROCK MOTION SET 4, FAULT NORMAL COMPONENT
SFOBB East Span Seismic Safety Project

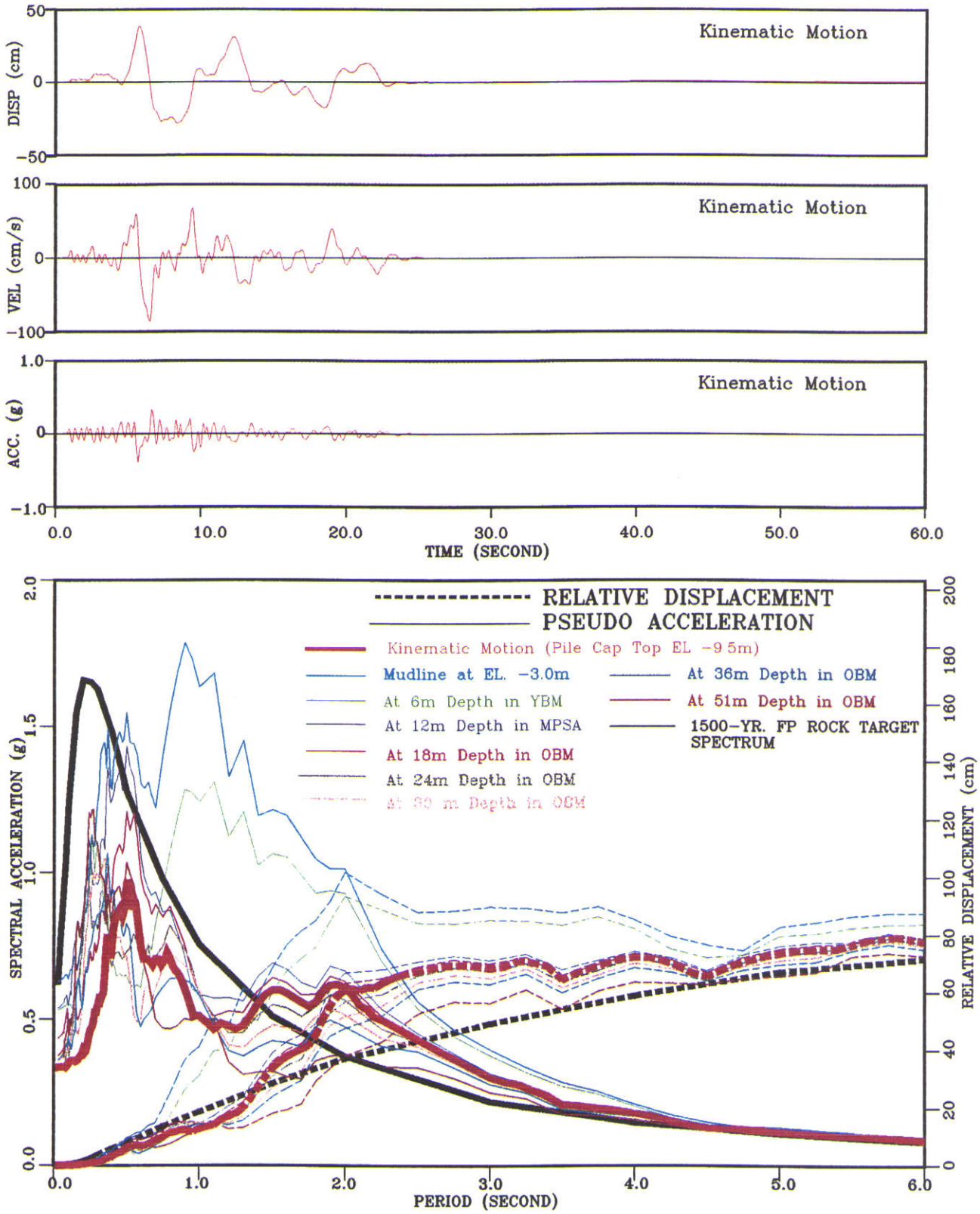

KINEMATIC AND DEPTH-VARYING FREE FIELD MOTIONS
PIER E14, INPUT ROCK MOTION SET 4, FAULT PARALLEL COMPONENT
SFOBB East Span Seismic Safety Project

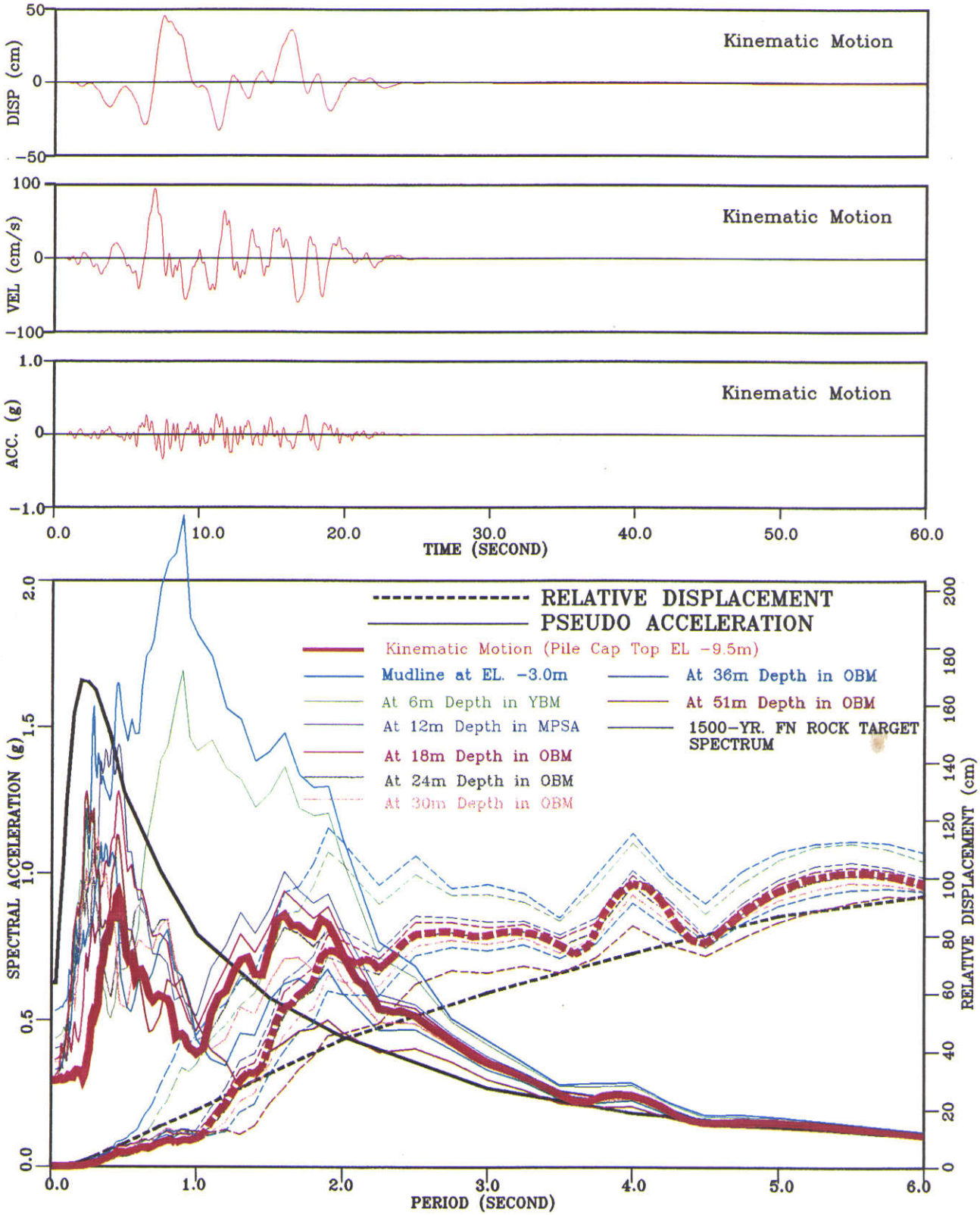

KINEMATIC AND DEPTH-VARYING FREE FIELD MOTIONS
PIER E14, INPUT ROCK MOTION SET 5, FAULT NORMAL COMPONENT
SFOBB East Span Seismic Safety Project

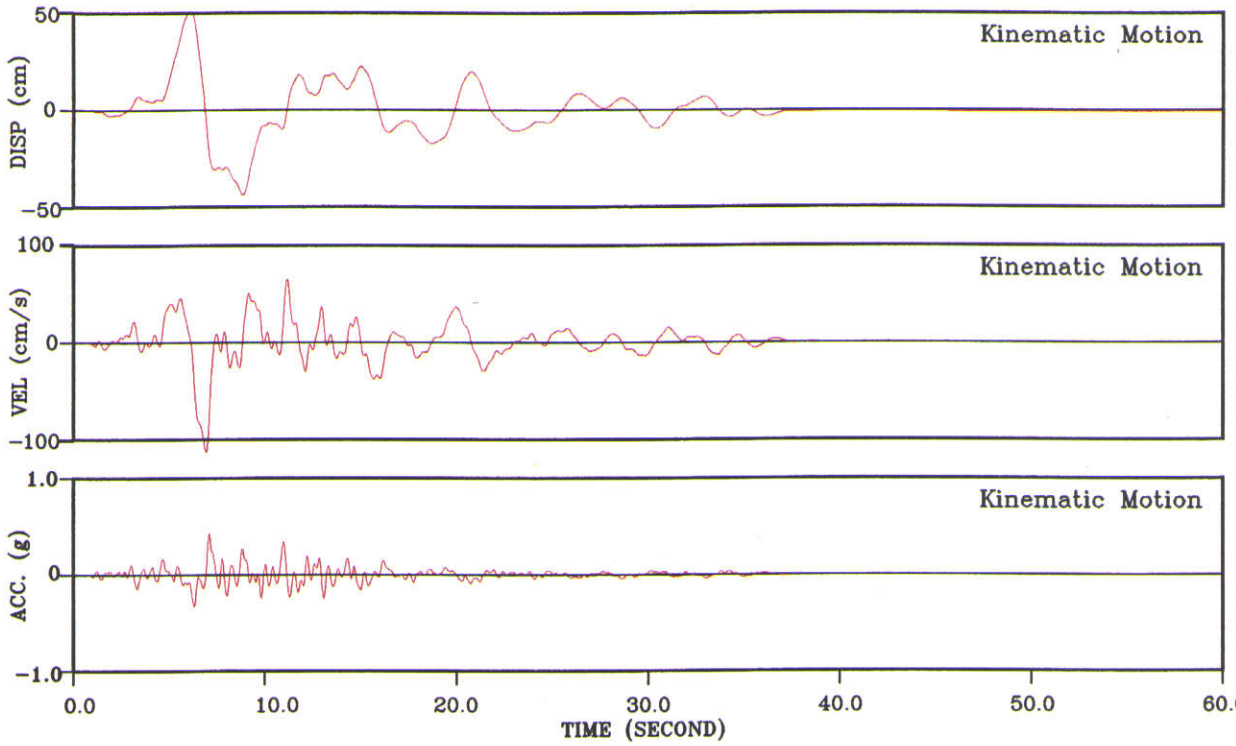

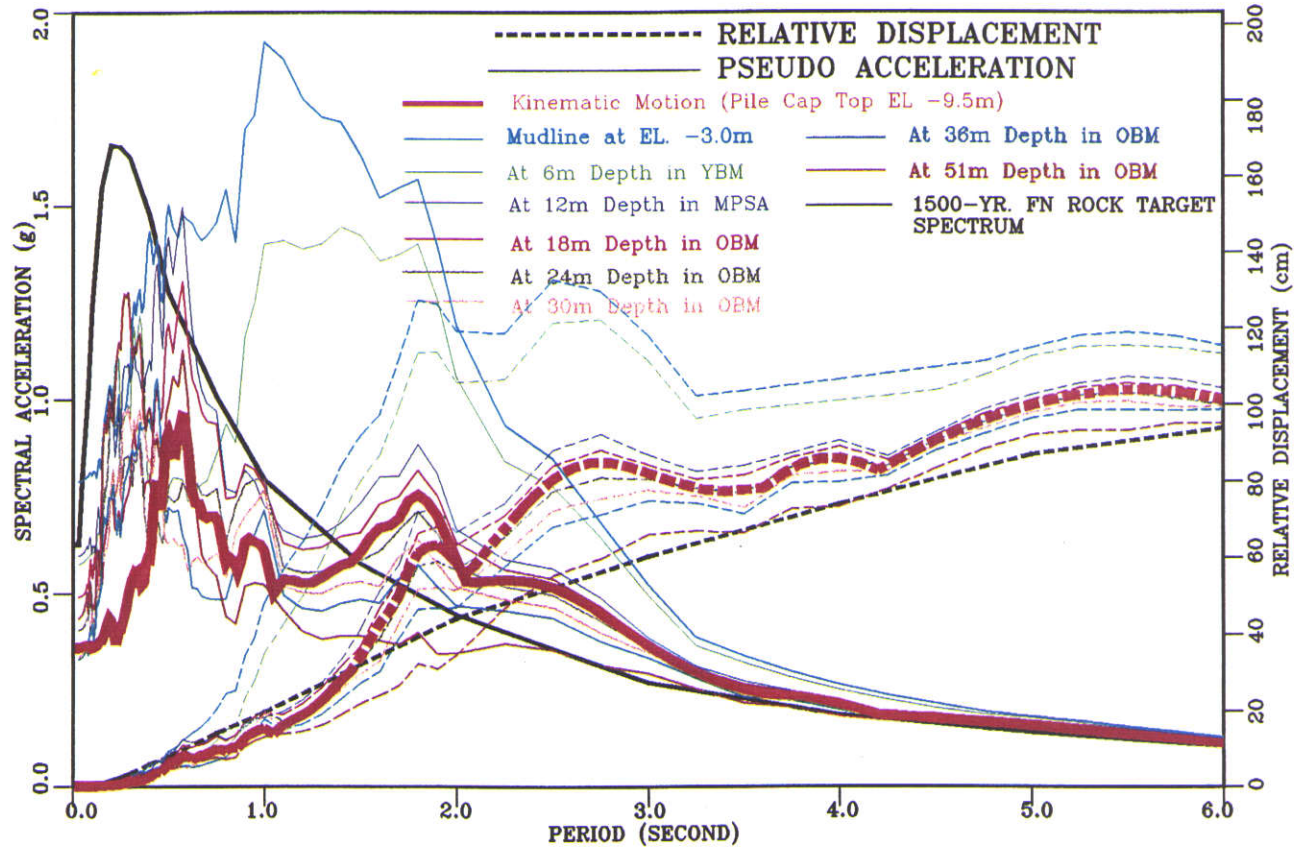

KINEMATIC AND DEPTH-VARYING FREE FIELD MOTIONS
PIER E14, INPUT ROCK MOTION SET 6, FAULT NORMAL COMPONENT
SFOBB East Span Seismic Safety Project

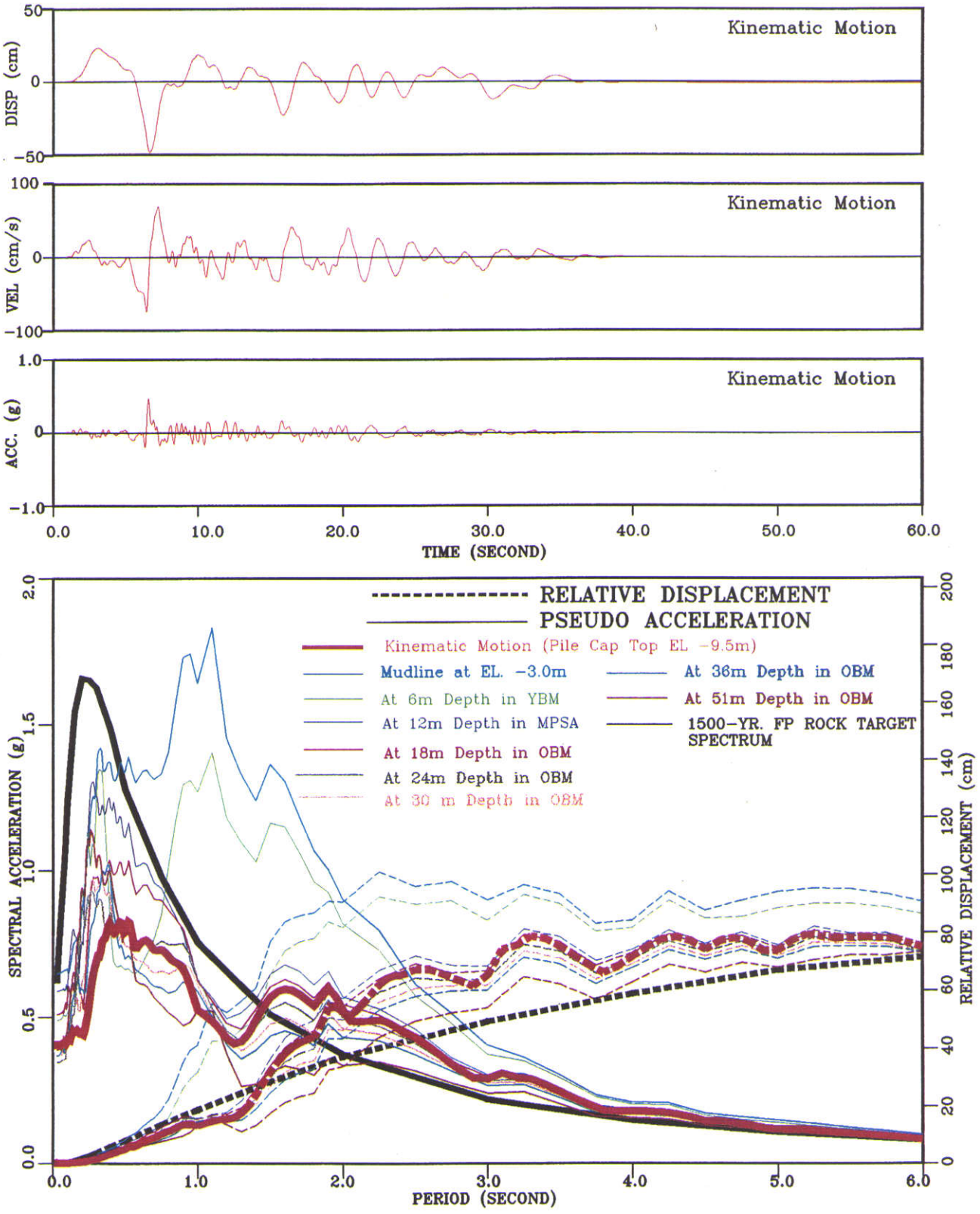

KINEMATIC AND DEPTH-VARYING FREE FIELD MOTIONS
PIER E14, INPUT ROCK MOTION SET 6, FAULT PARALLEL COMPONENT
SFOBB East Span Seismic Safety Project

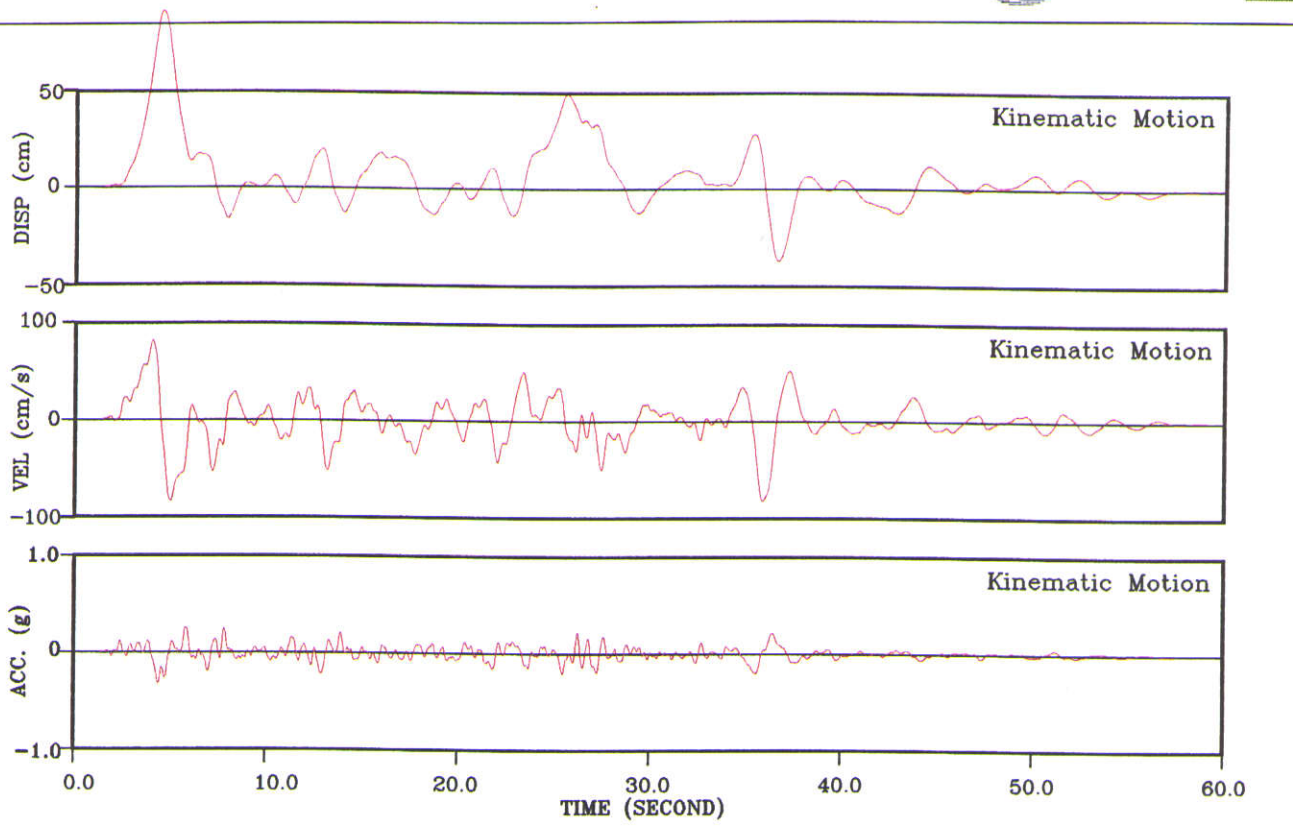

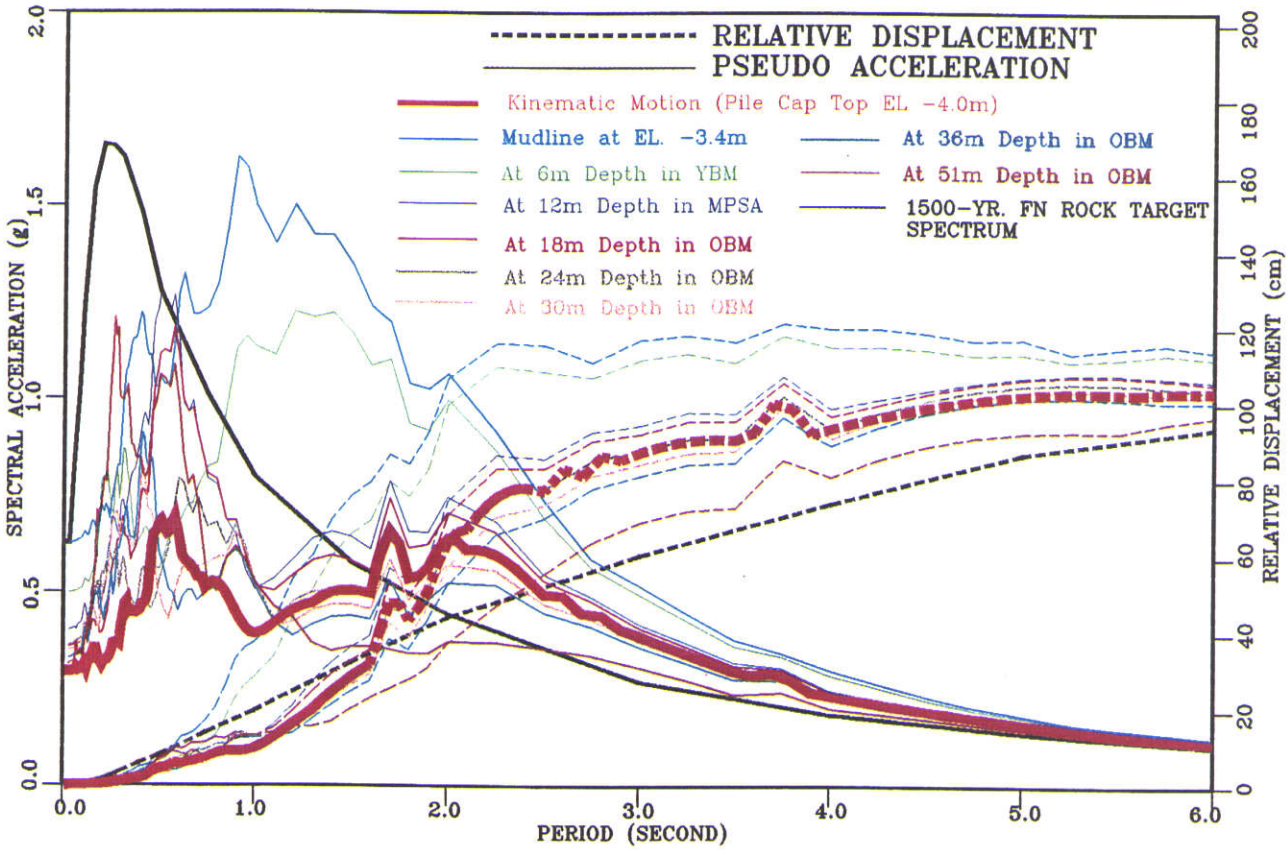

KINEMATIC AND DEPTH-VARYING FREE FIELD MOTIONS
PIER E15, INPUT ROCK MOTION SET 1, FAULT NORMAL COMPONENT
SFOBB East Span Seismic Safety Project

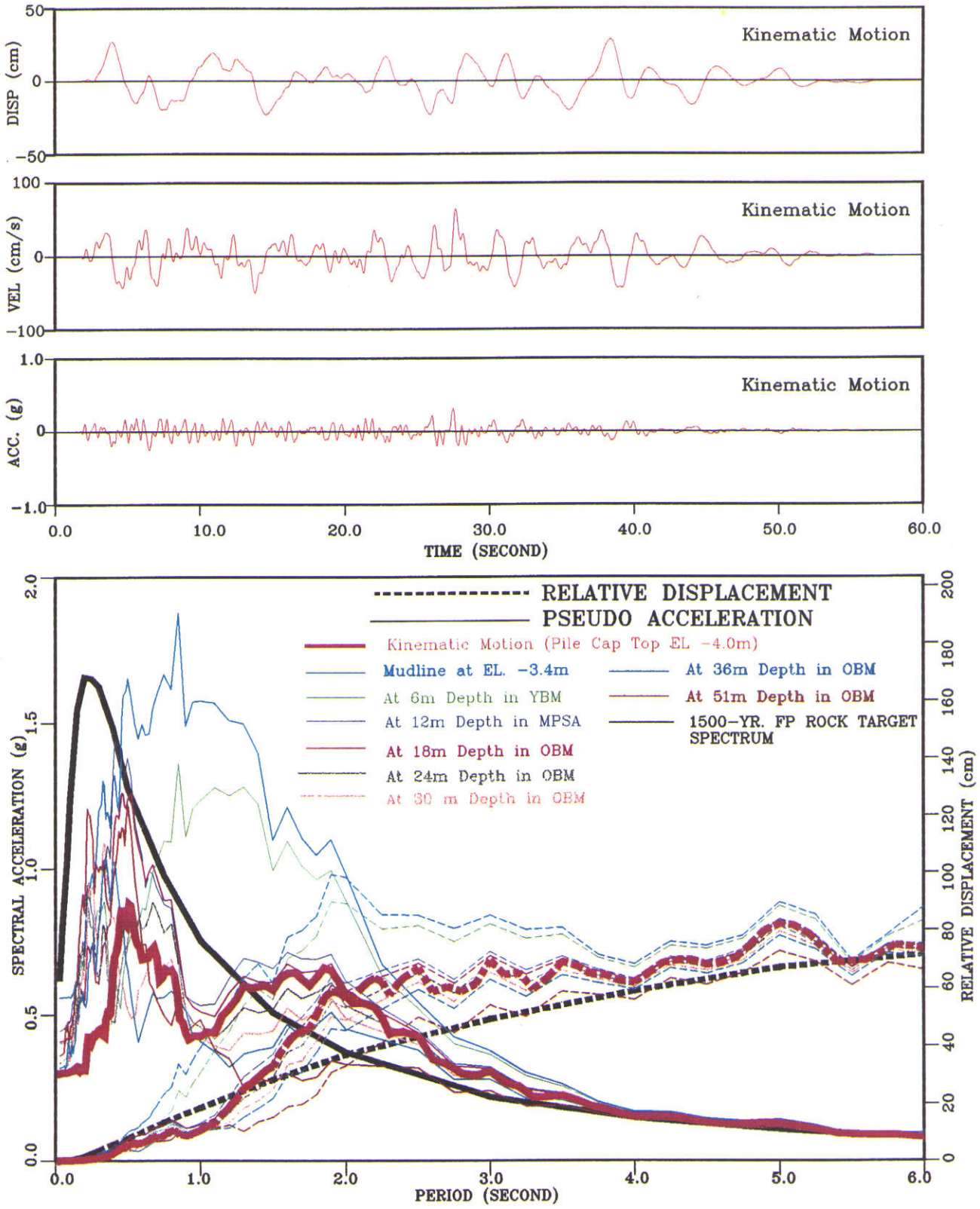

KINEMATIC AND DEPTH-VARYING FREE FIELD MOTIONS
PIER E15, INPUT ROCK MOTION SET 1, FAULT PARALLEL COMPONENT
SFOBB East Span Seismic Safety Project

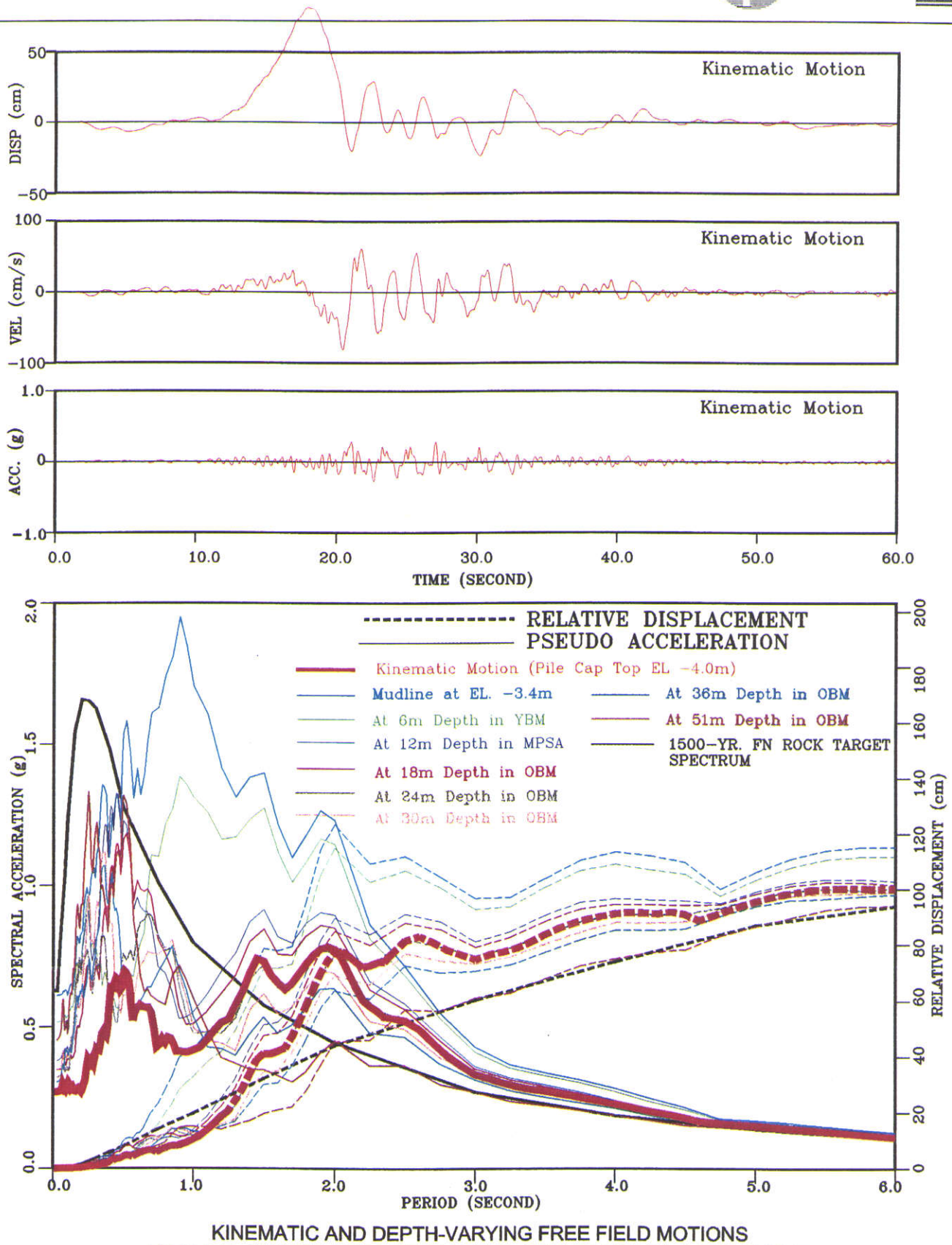

KINEMATIC AND DEPTH-VARYING FREE FIELD MOTIONS
PIER E15, INPUT ROCK MOTION SET 2, FAULT NORMAL COMPONENT
SFOBB East Span Seismic Safety Project

PLATE 8-164

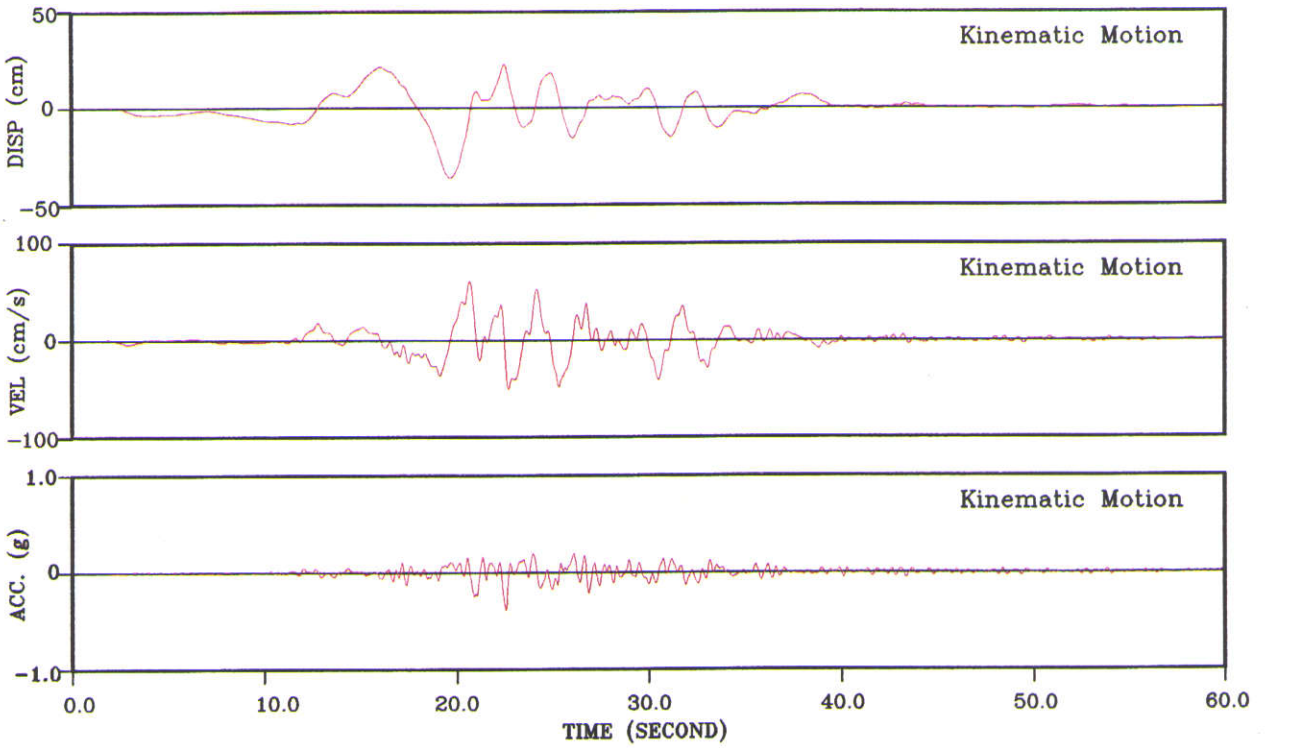

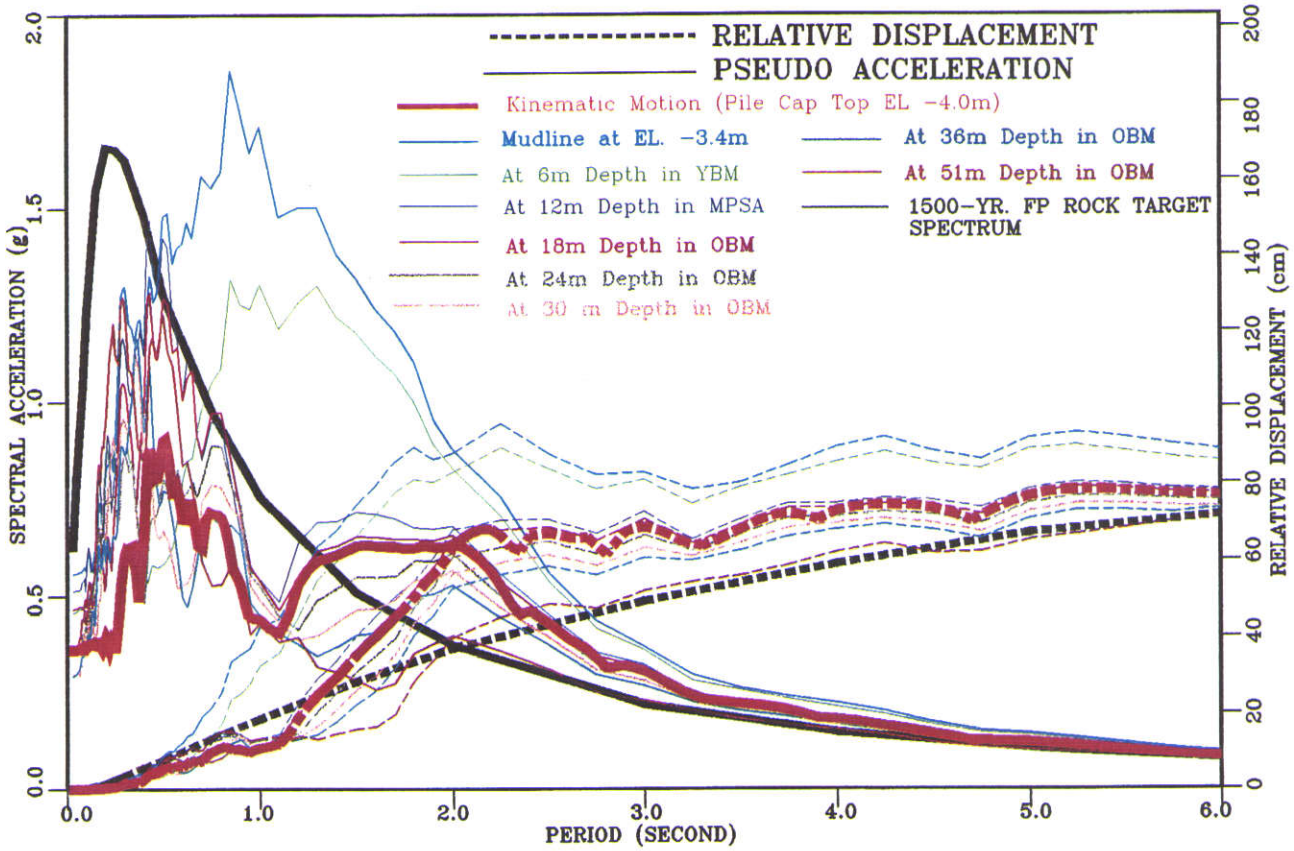

KINEMATIC AND DEPTH-VARYING FREE FIELD MOTIONS
PIER E15, INPUT ROCK MOTION SET 2, FAULT PARALLEL COMPONENT
SFOBB East Span Seismic Safety Project

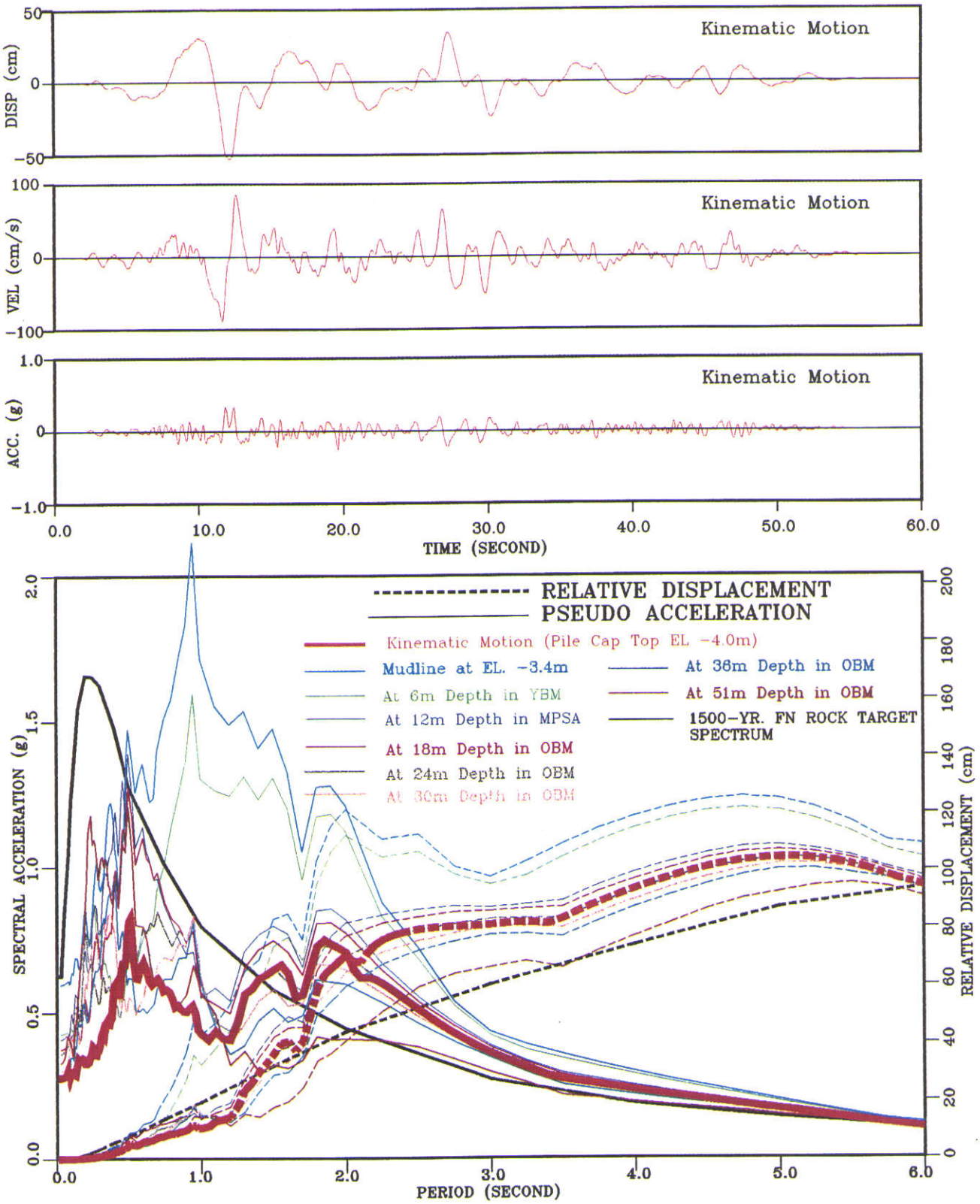

KINEMATIC AND DEPTH-VARYING FREE FIELD MOTIONS
PIER E15, INPUT ROCK MOTION SET 3, FAULT NORMAL COMPONENT
SFOBB East Span Seismic Safety Project

PLATE 8-166

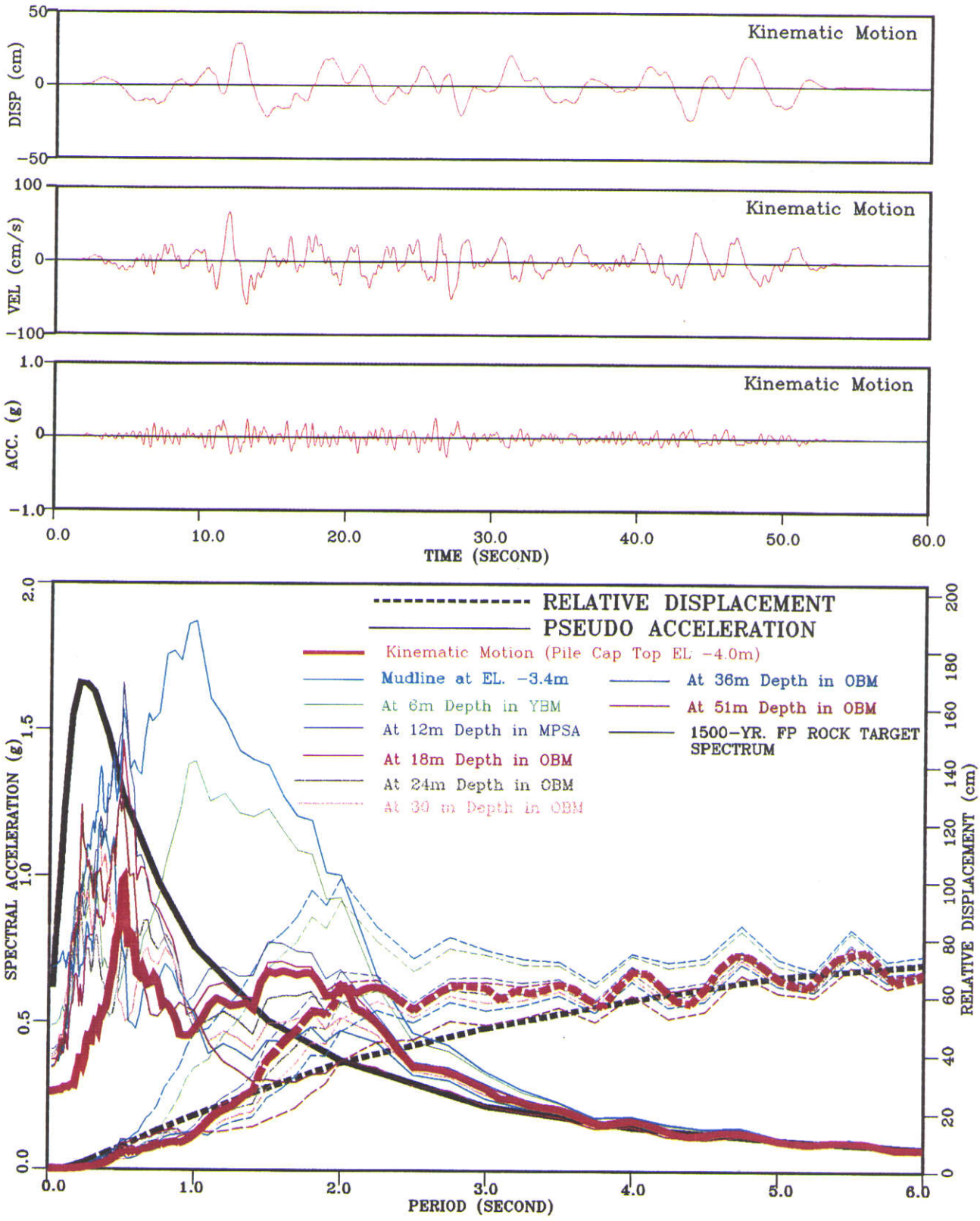

KINEMATIC AND DEPTH-VARYING FREE FIELD MOTIONS
PIER E15, INPUT ROCK MOTION SET 3, FAULT PARALLEL COMPONENT
SFOBB East Span Seismic Safety Project

PLATE 8-167

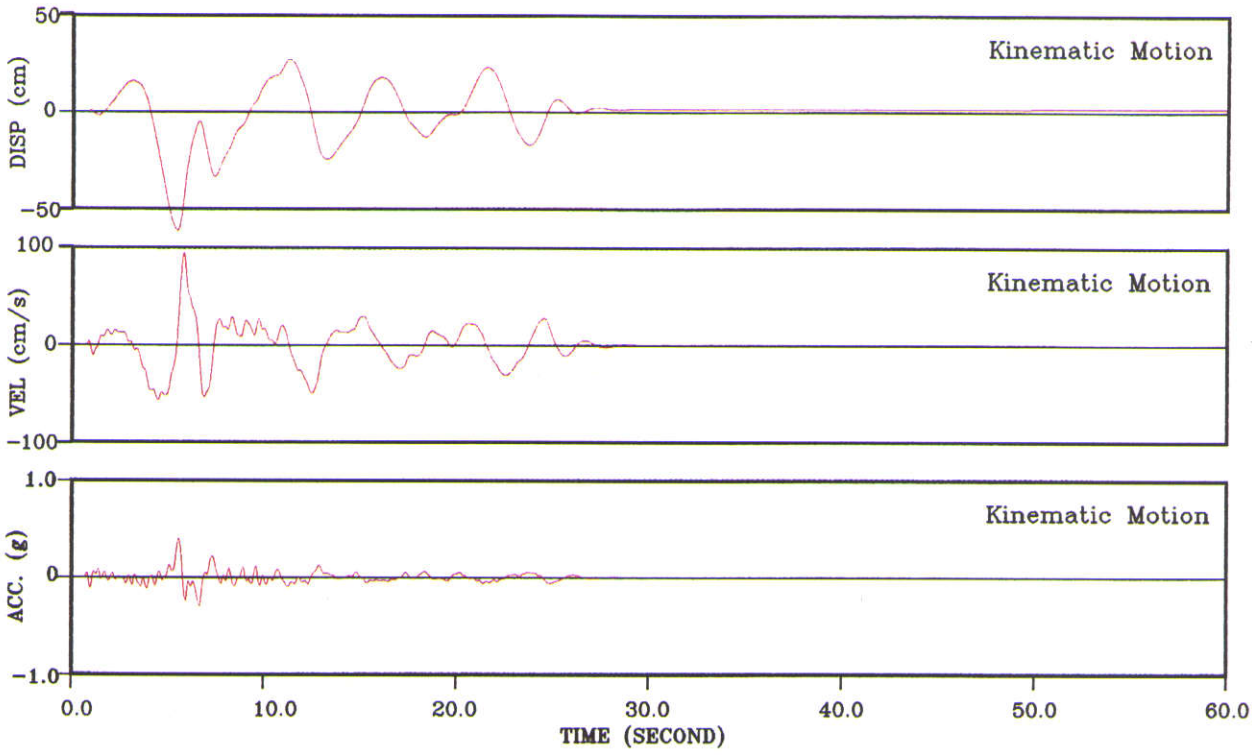

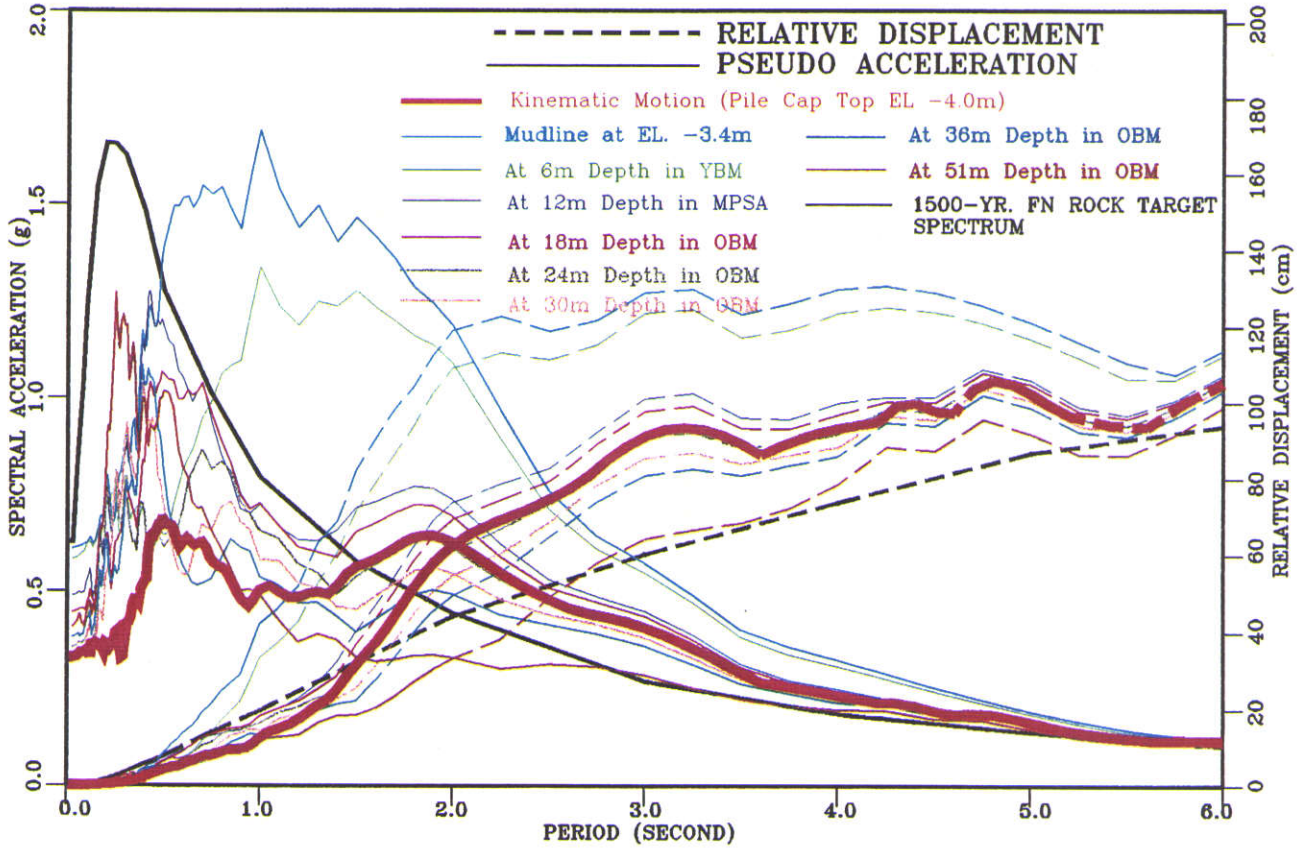

KINEMATIC AND DEPTH-VARYING FREE FIELD MOTIONS
PIER E15, INPUT ROCK MOTION SET 4, FAULT NORMAL COMPONENT
SFOBB East Span Seismic Safety Project

PLATE 8-168

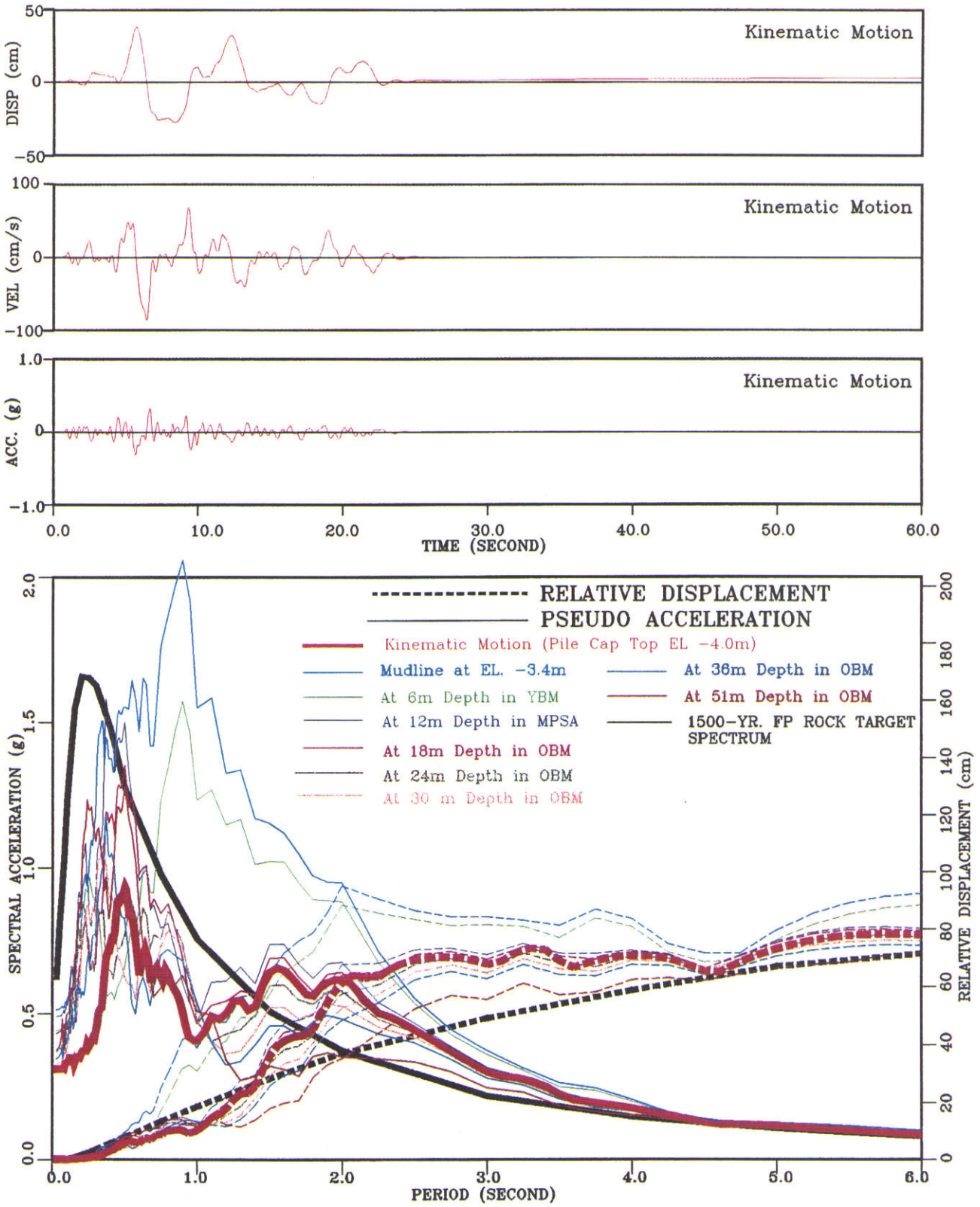

KINEMATIC AND DEPTH-VARYING FREE FIELD MOTIONS
PIER E15, INPUT ROCK MOTION SET 4, FAULT PARALLEL COMPONENT
SFOBB East Span Seismic Safety Project

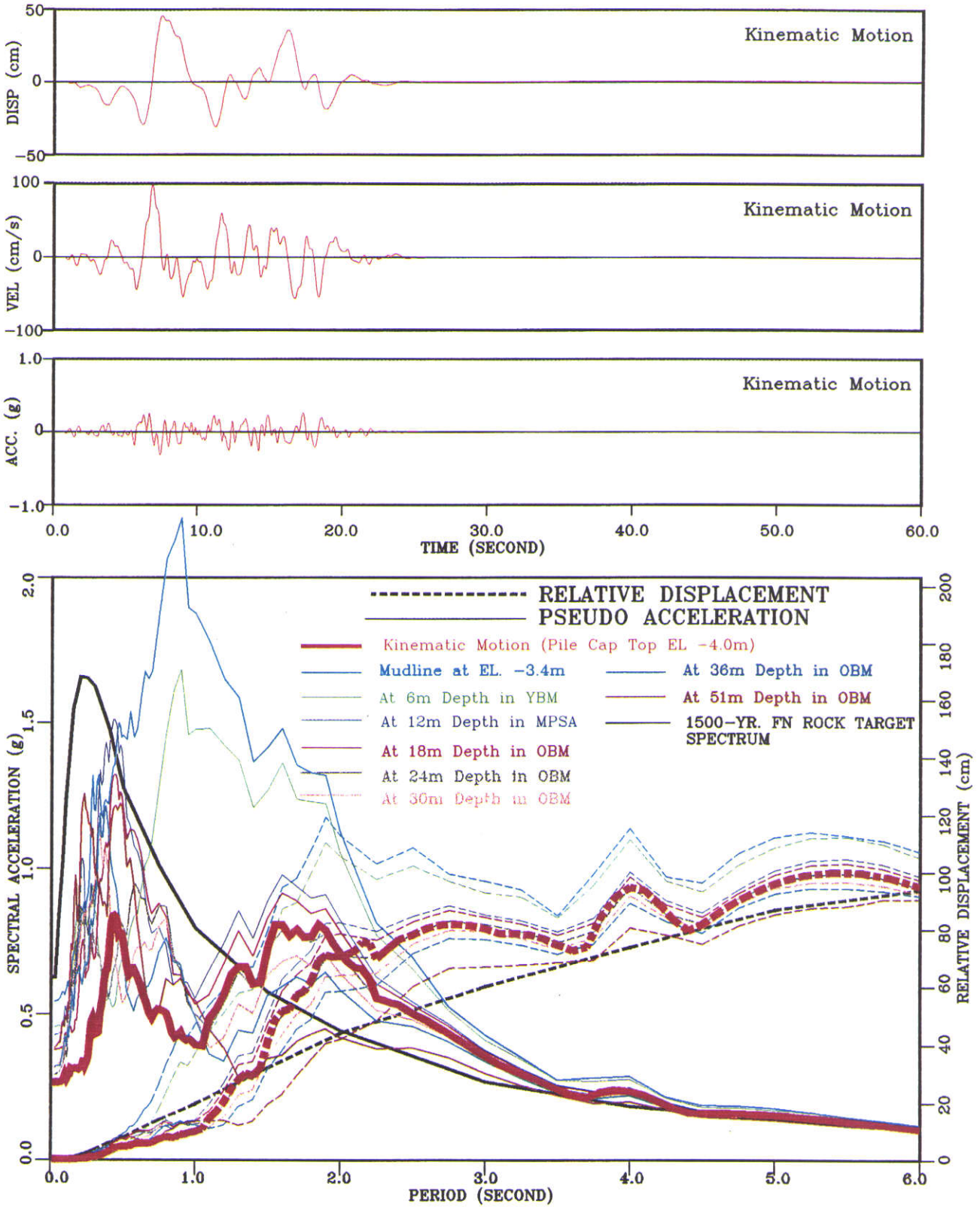

KINEMATIC AND DEPTH-VARYING FREE FIELD MOTIONS
PIER E15, INPUT ROCK MOTION SET 5, FAULT NORMAL COMPONENT
SFOBB East Span Seismic Safety Project

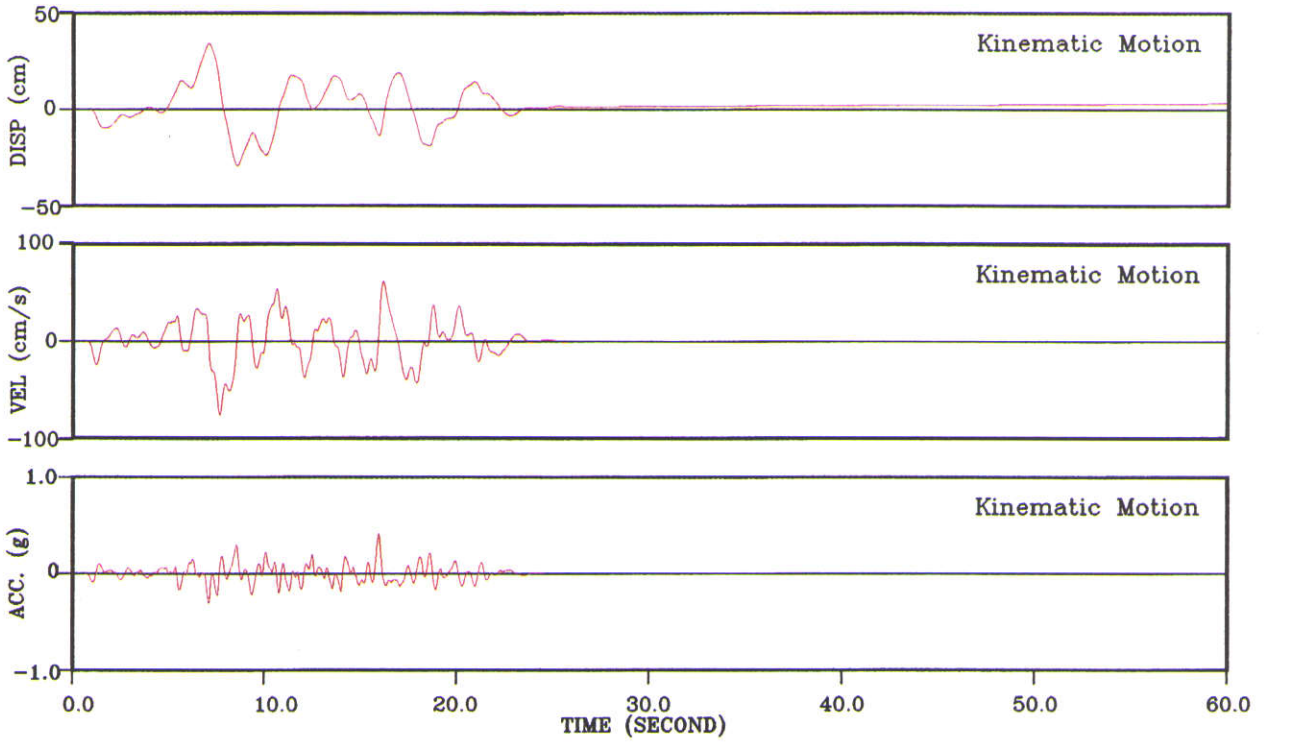

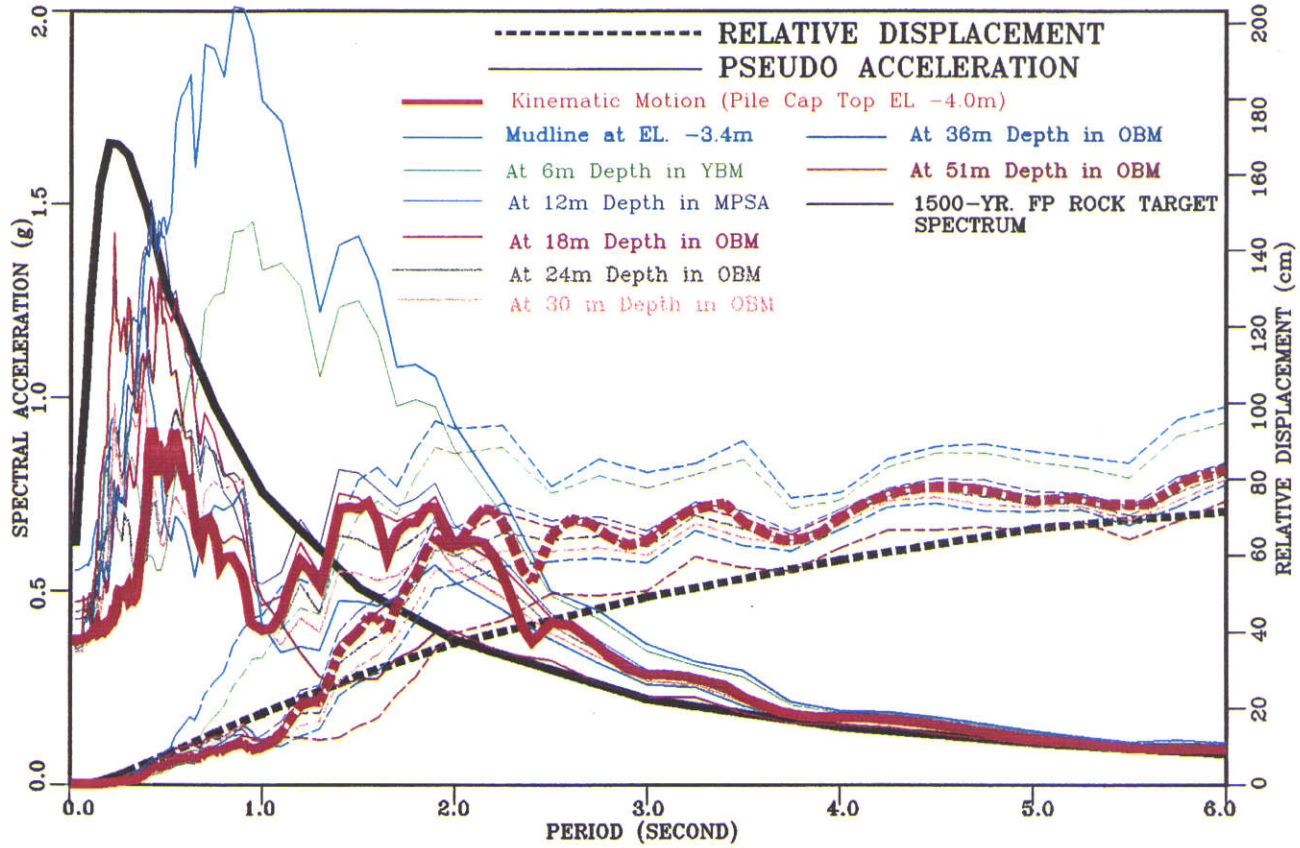

KINEMATIC AND DEPTH-VARYING FREE FIELD MOTIONS
PIER E15, INPUT ROCK MOTION SET 5, FAULT PARALLEL COMPONENT
SFOBB East Span Seismic Safety Project

PLATE 8-171

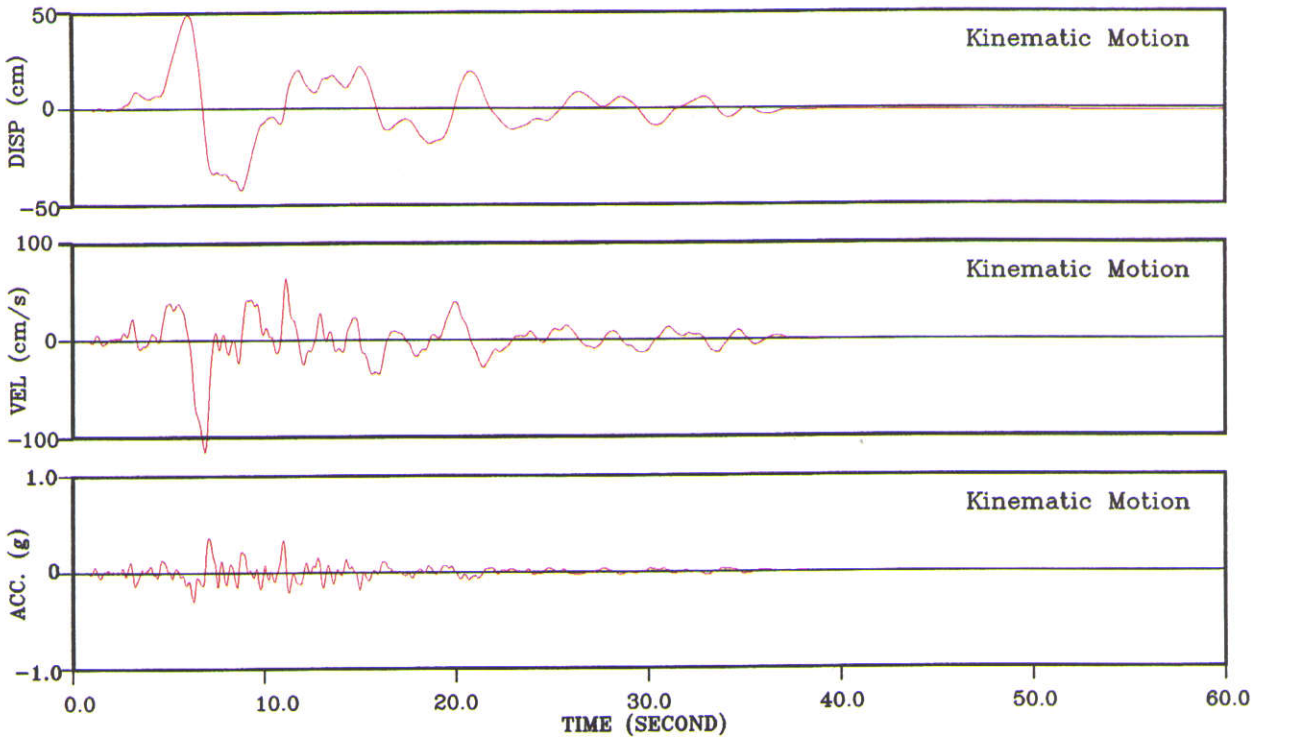

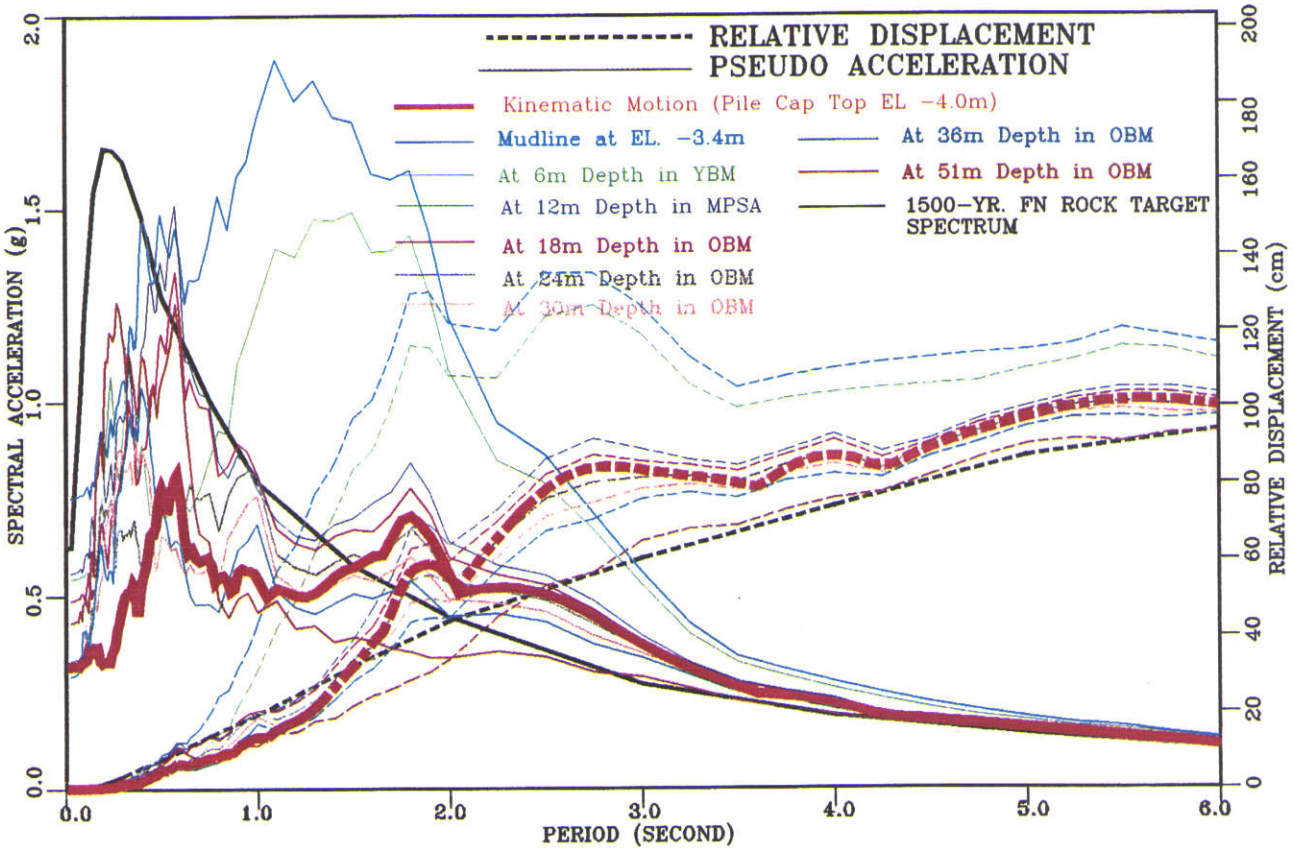

KINEMATIC AND DEPTH-VARYING FREE FIELD MOTIONS
PIER E15, INPUT ROCK MOTION SET 6, FAULT NORMAL COMPONENT
SFOBB East Span Seismic Safety Project

PLATE 8-172

Earth Mechanics FUGRO

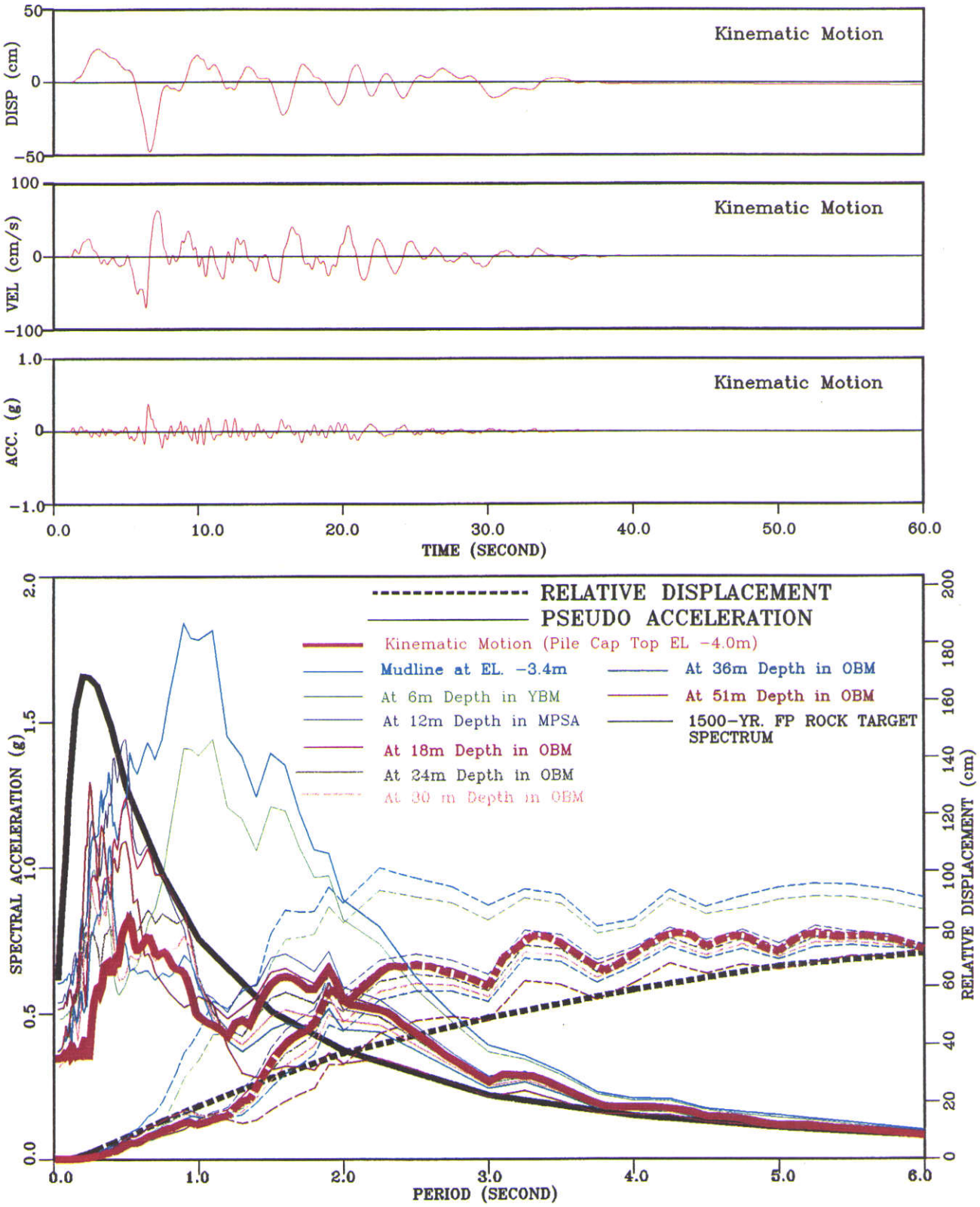

KINEMATIC AND DEPTH-VARYING FREE FIELD MOTIONS
PIER E15, INPUT ROCK MOTION SET 6, FAULT PARALLEL COMPONENT
SFOBB East Span Seismic Safety Project

PLATE 8-173

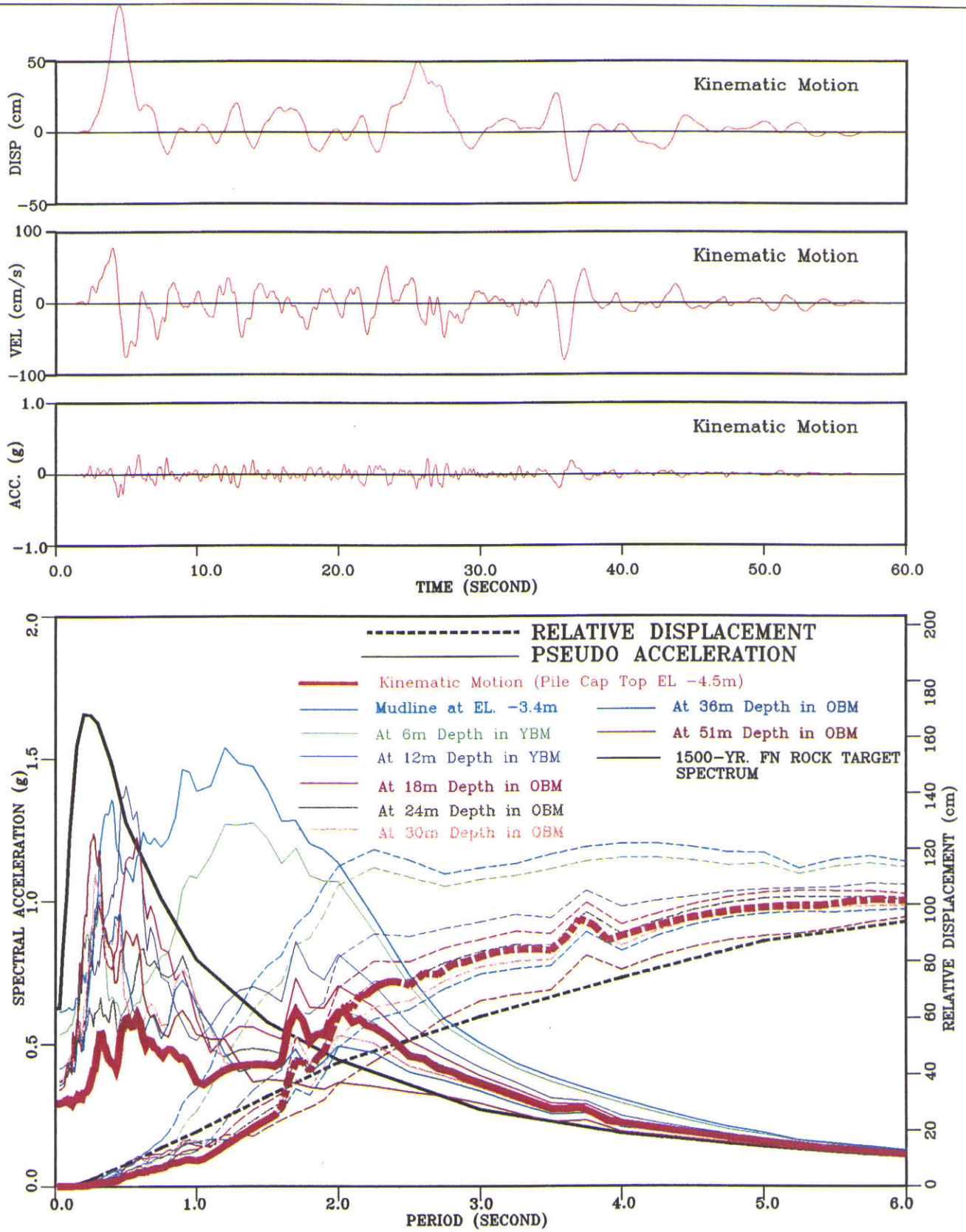

KINEMATIC AND DEPTH-VARYING FREE FIELD MOTIONS
PIER E16, INPUT ROCK MOTION SET 1, FAULT NORMAL COMPONENT
SFOBB East Span Seismic Safety Project

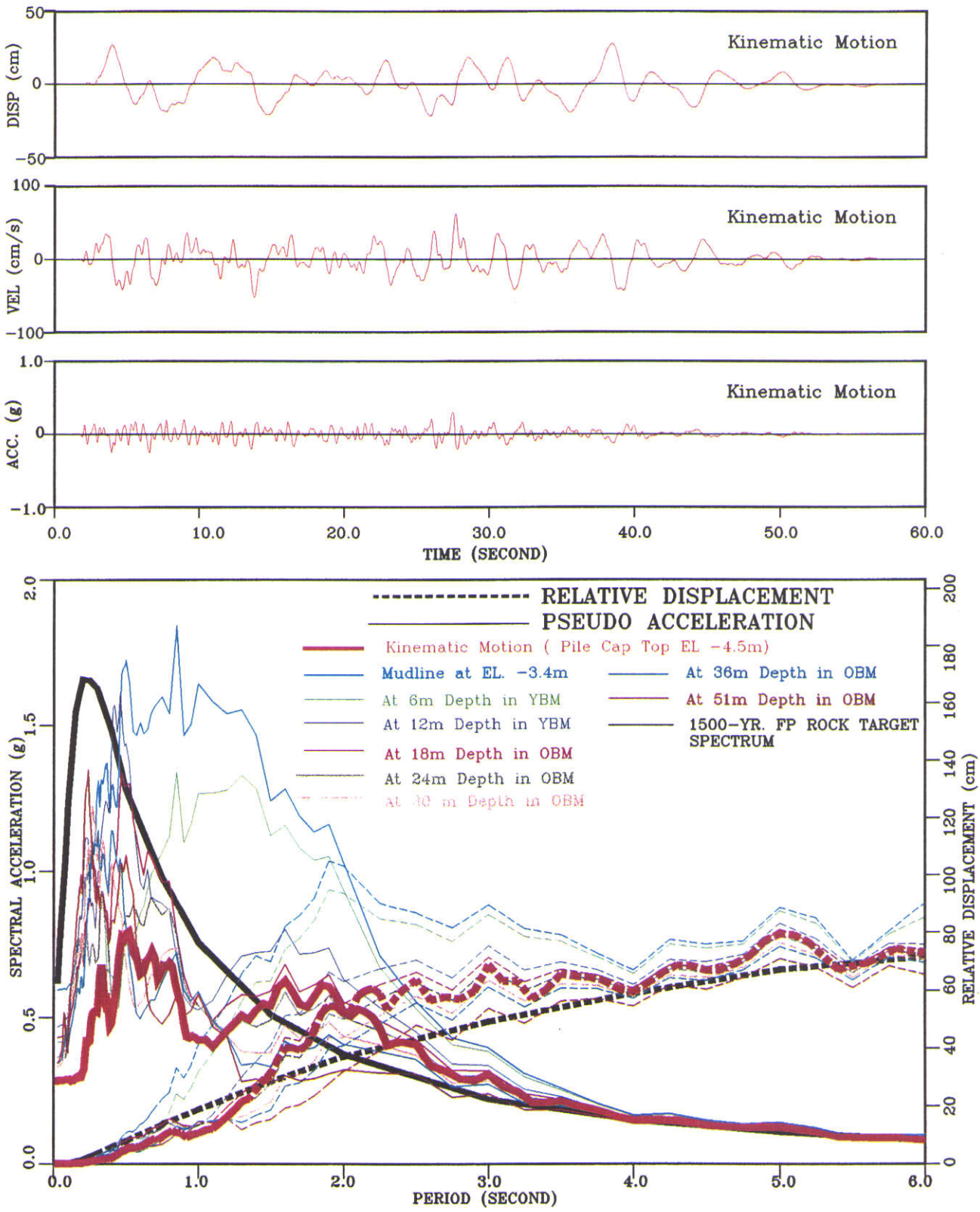

KINEMATIC AND DEPTH-VARYING FREE FIELD MOTIONS
PIER E16, INPUT ROCK MOTION SET 1, FAULT PARALLEL COMPONENT
SFOBB East Span Seismic Safety Project

PLATE 8-175

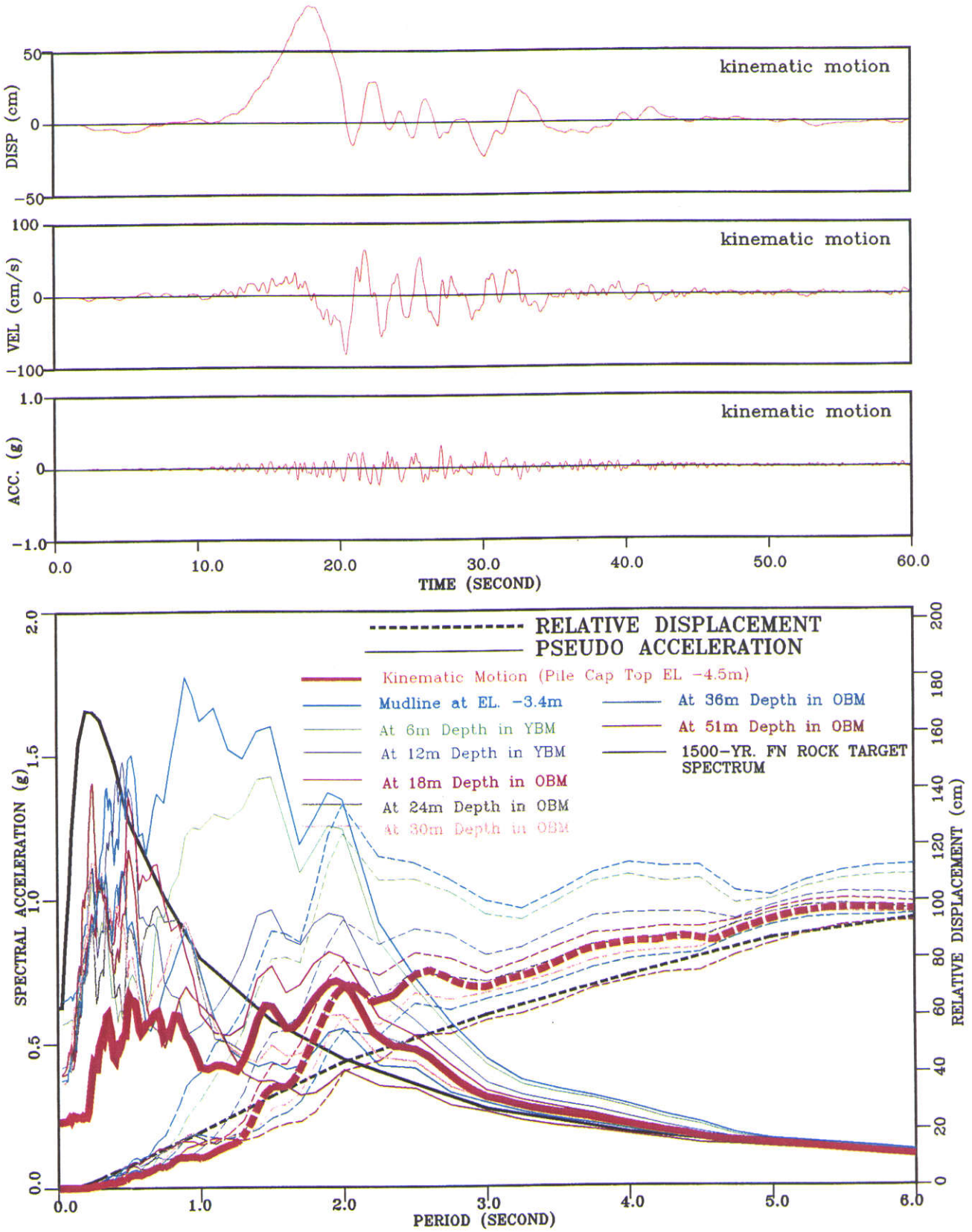

KINEMATIC AND DEPTH-VARYING FREE FIELD MOTIONS
PIER E16, INPUT ROCK MOTION SET 2, FAULT NORMALCOMPONENT
SFOBB East Span Seismic Safety Project

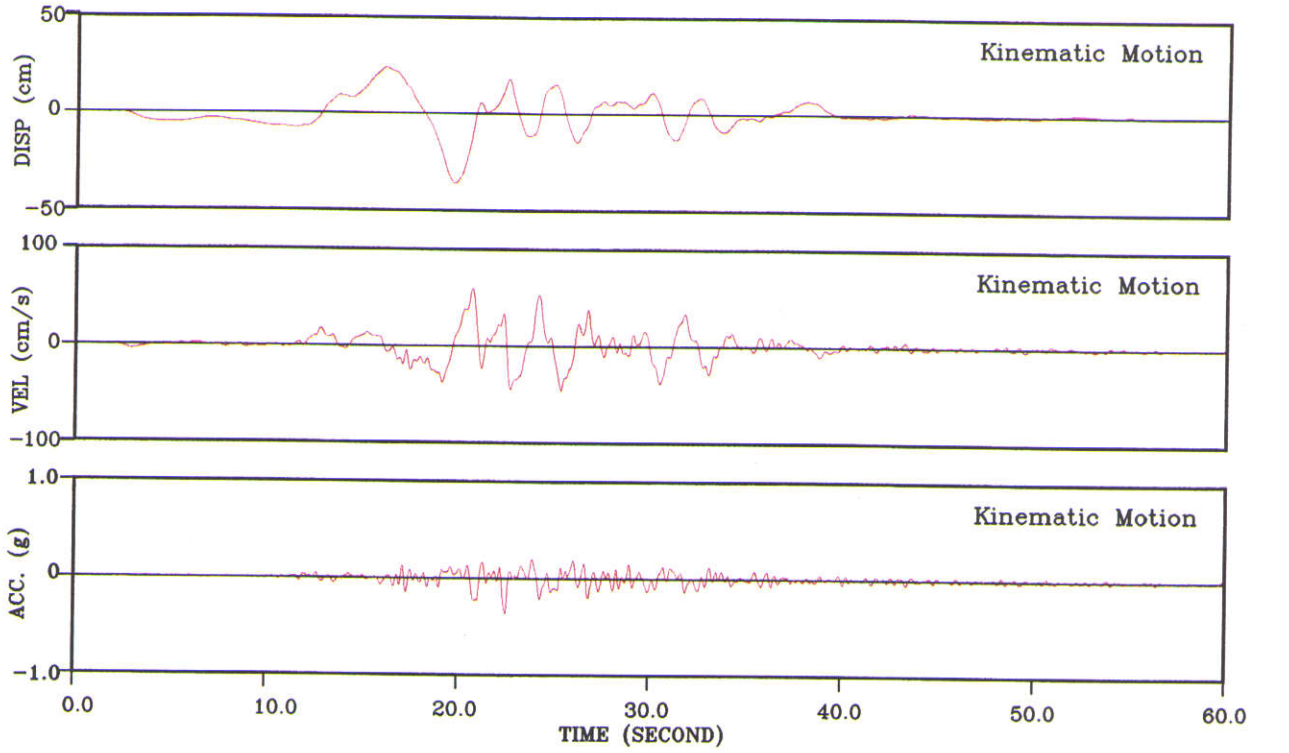

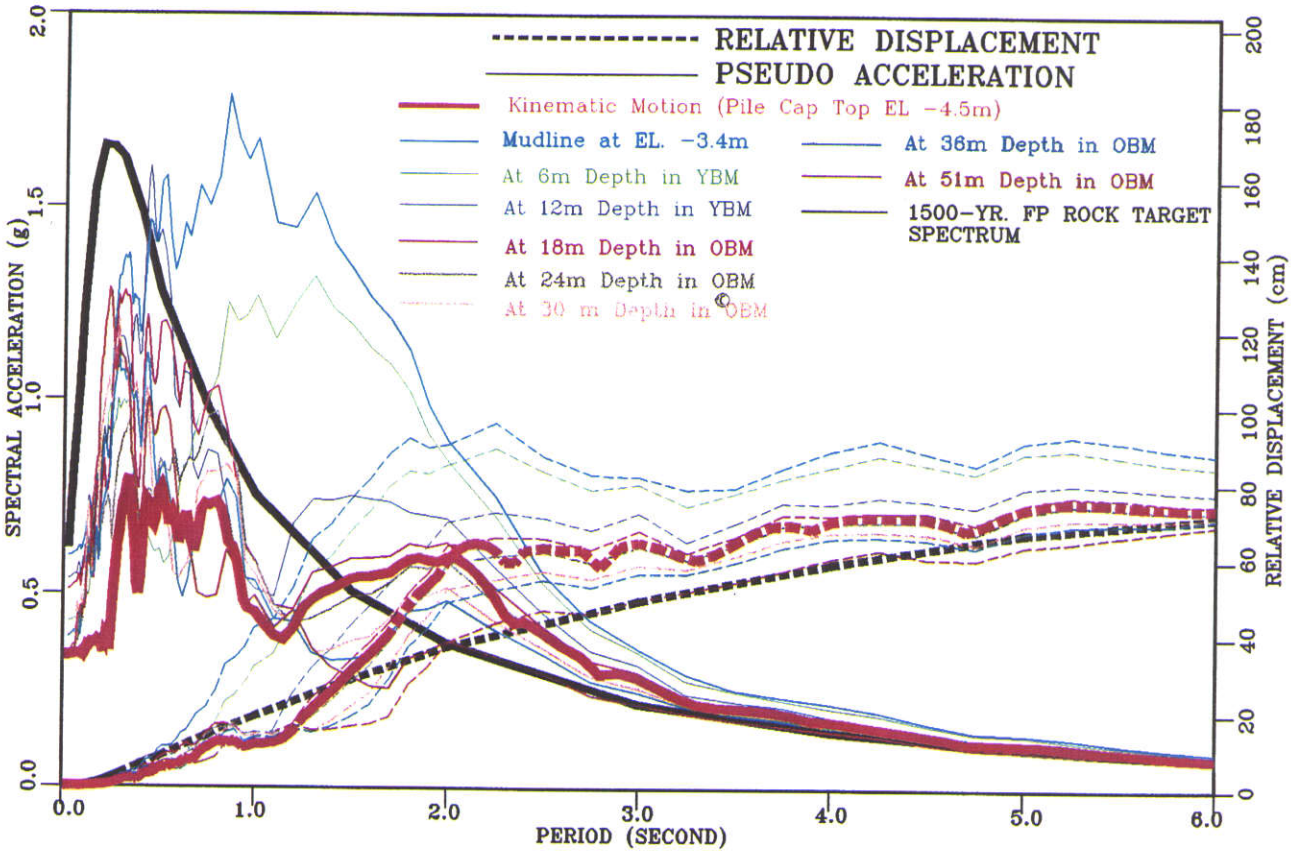

KINEMATIC AND DEPTH-VARYING FREE FIELD MOTIONS
PIER E16, INPUT ROCK MOTION SET 2, FAULT PARALLEL COMPONENT
SFOBB East Span Seismic Safety Project

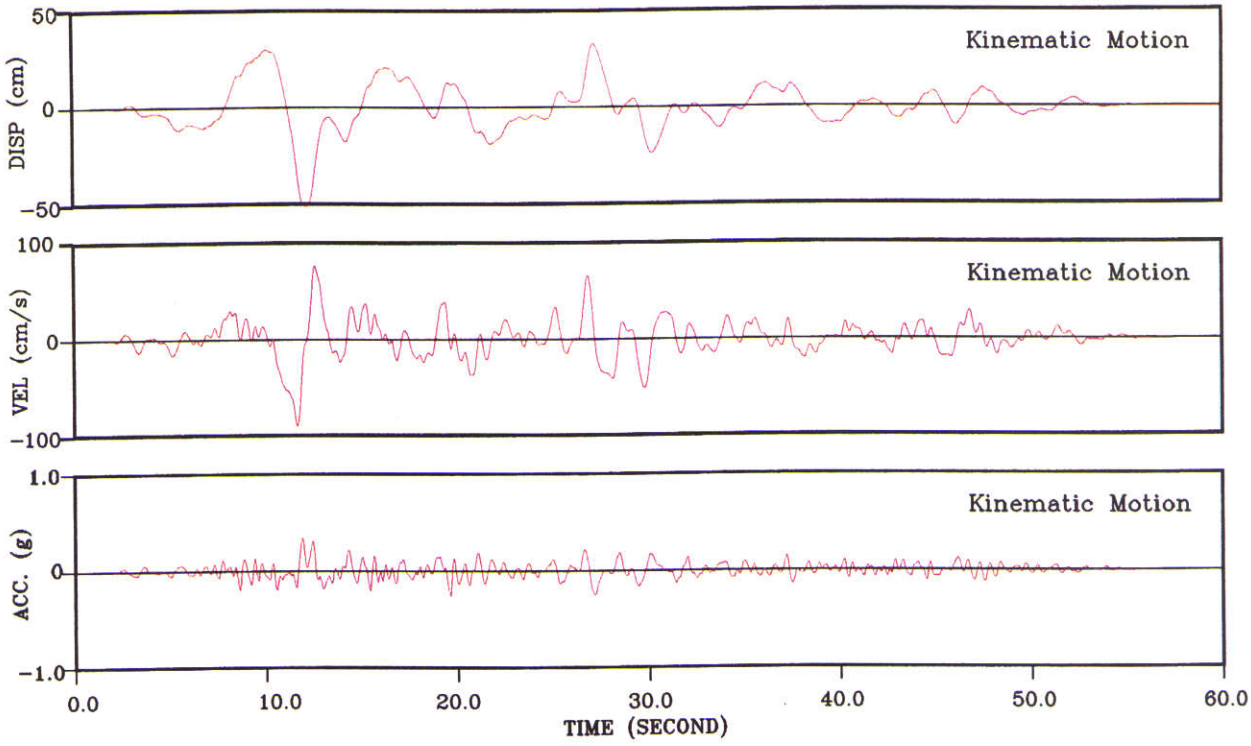

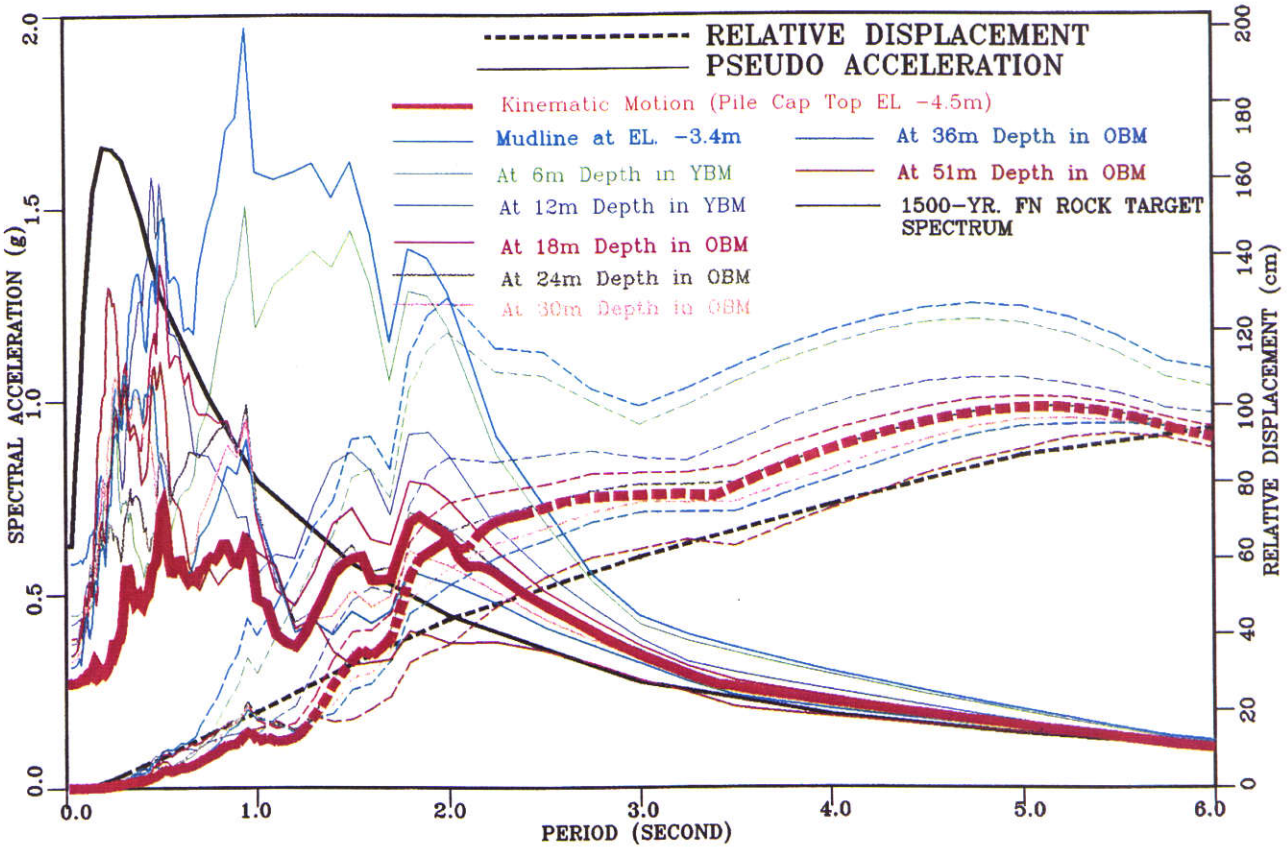

KINEMATIC AND DEPTH-VARYING FREE FIELD MOTIONS
PIER E16, INPUT ROCK MOTION SET 3, FAULT NORMAL COMPONENT
SFOBB East Span Seismic Safety Project

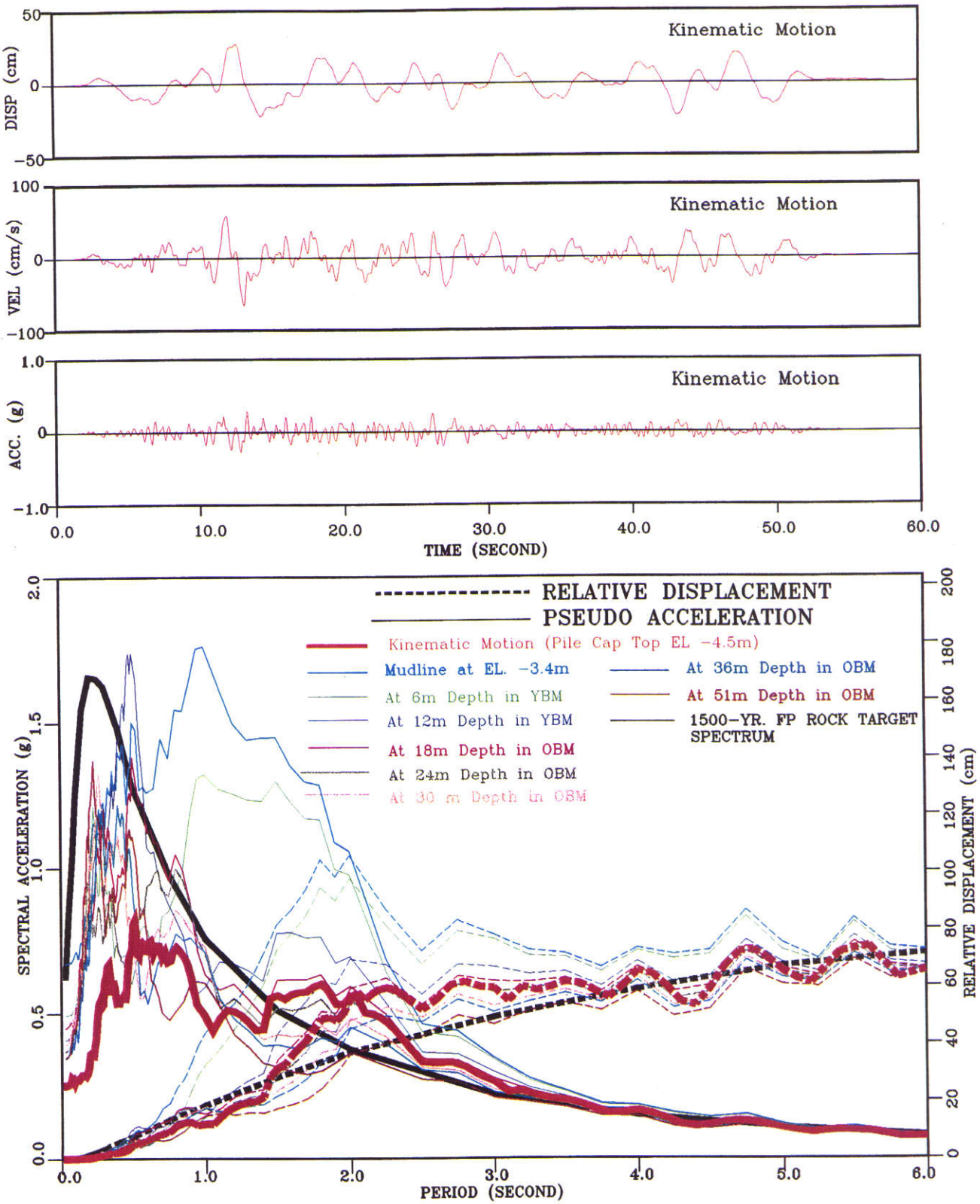

KINEMATIC AND DEPTH-VARYING FREE FIELD MOTIONS
PIER E16, INPUT ROCK MOTION SET 3, FAULT PARALLEL COMPONENT
SFOBB East Span Seismic Safety Project

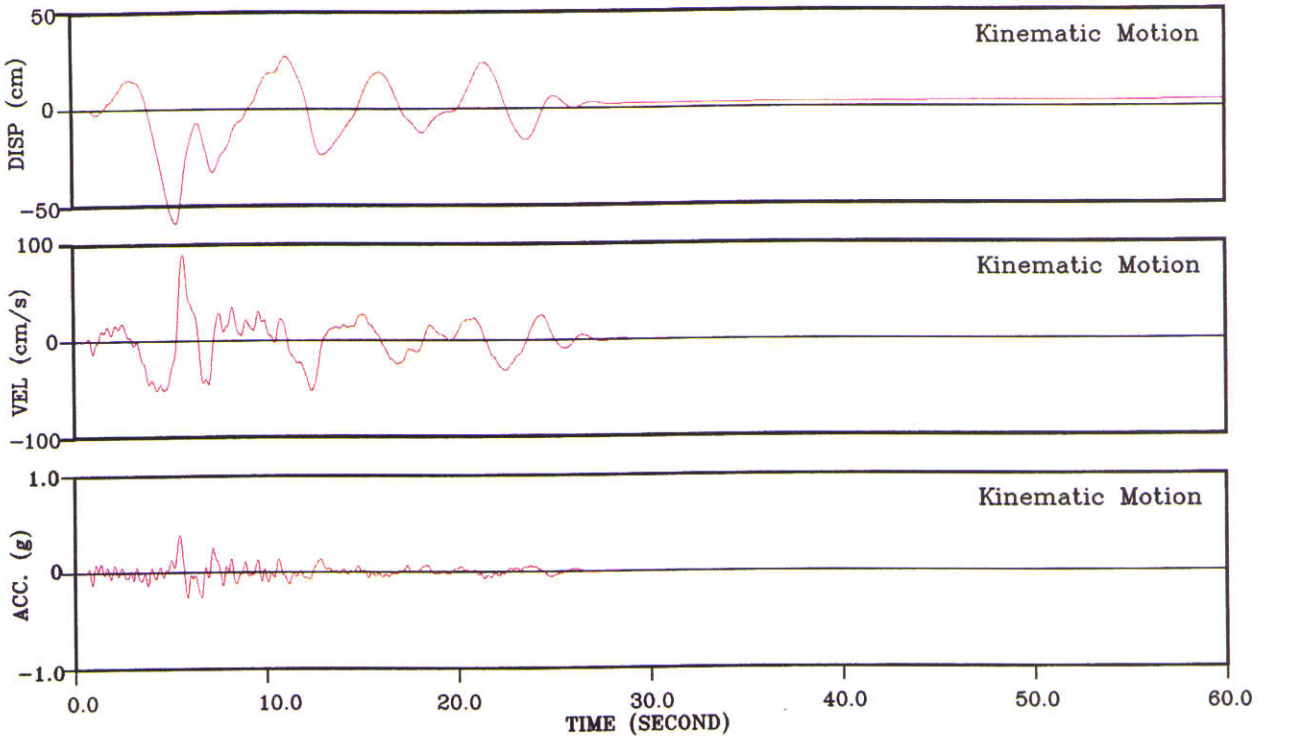

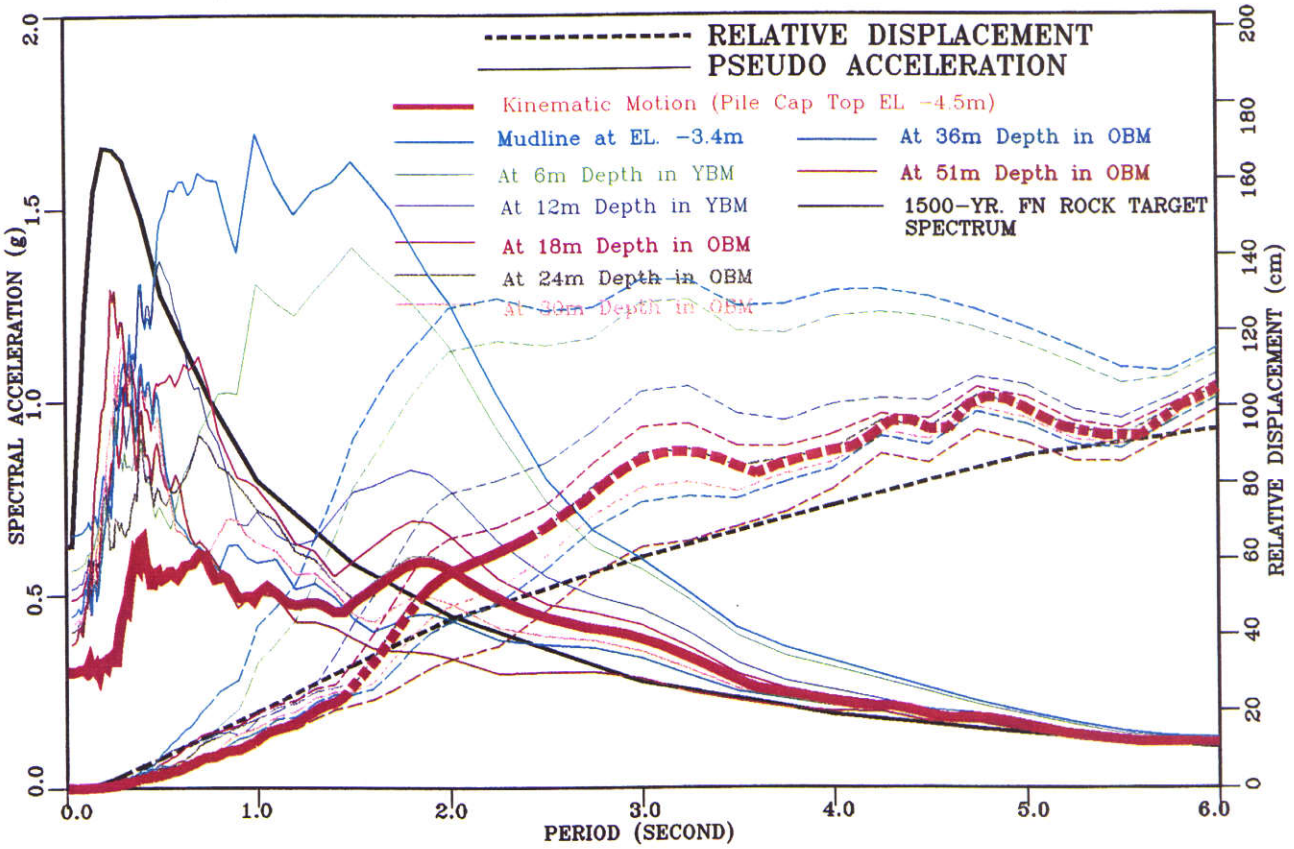

KINEMATIC AND DEPTH-VARYING FREE FIELD MOTIONS
PIER E16, INPUT ROCK MOTION SET 4, FAULT NORMAL COMPONENT
SFOBB East Span Seismic Safety Project

PLATE 8-180

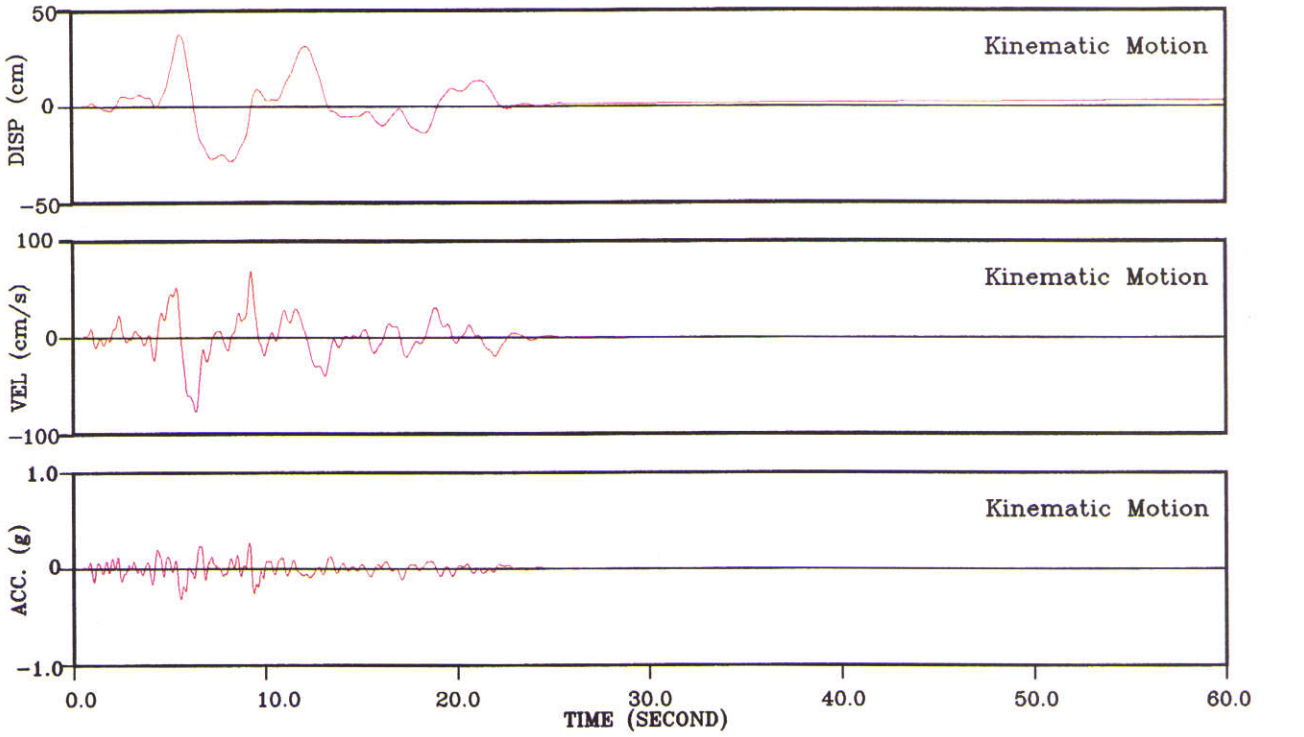

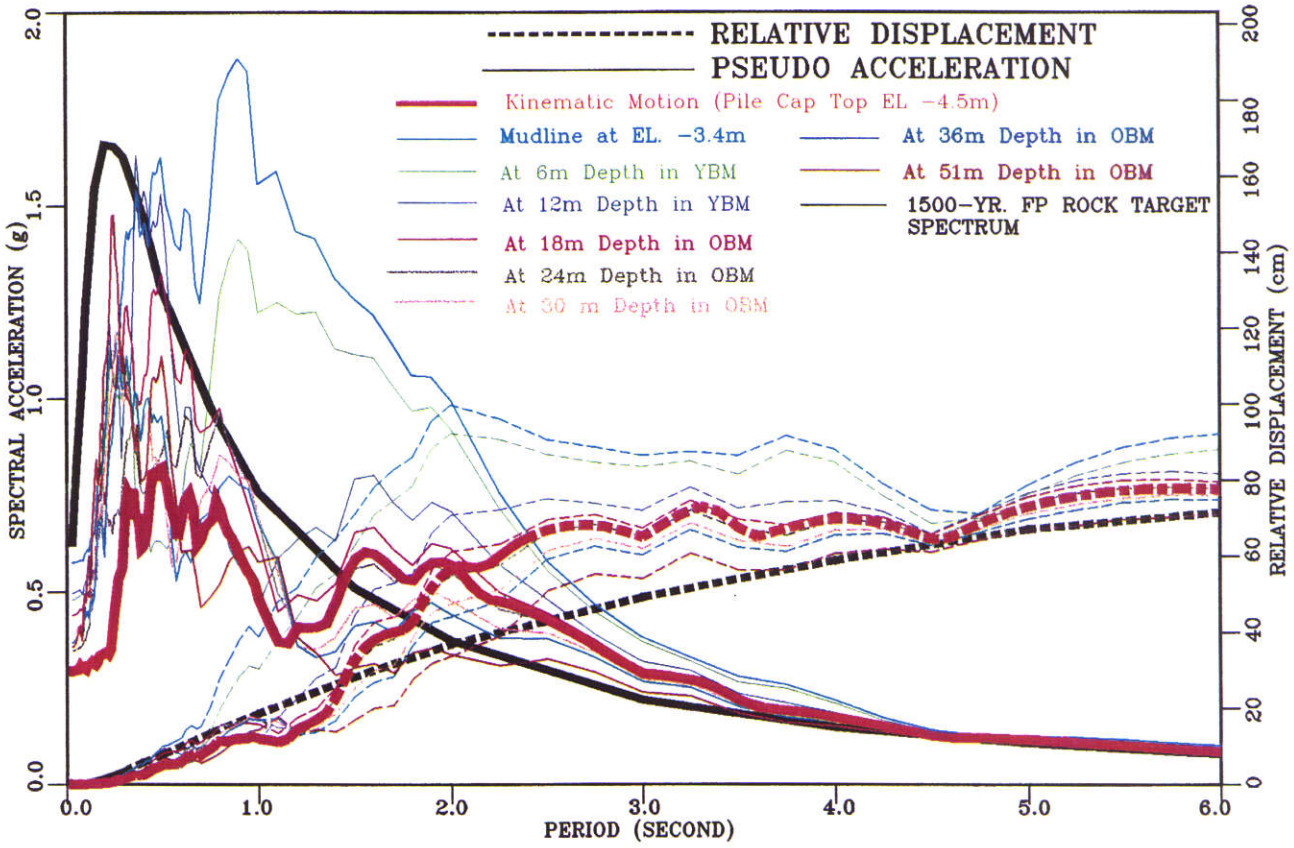

KINEMATIC AND DEPTH-VARYING FREE FIELD MOTIONS
PIER E16, INPUT ROCK MOTION SET 4, FAULT PARALLEL COMPONENT
SFOBB East Span Seismic Safety Project

PLATE 8-181

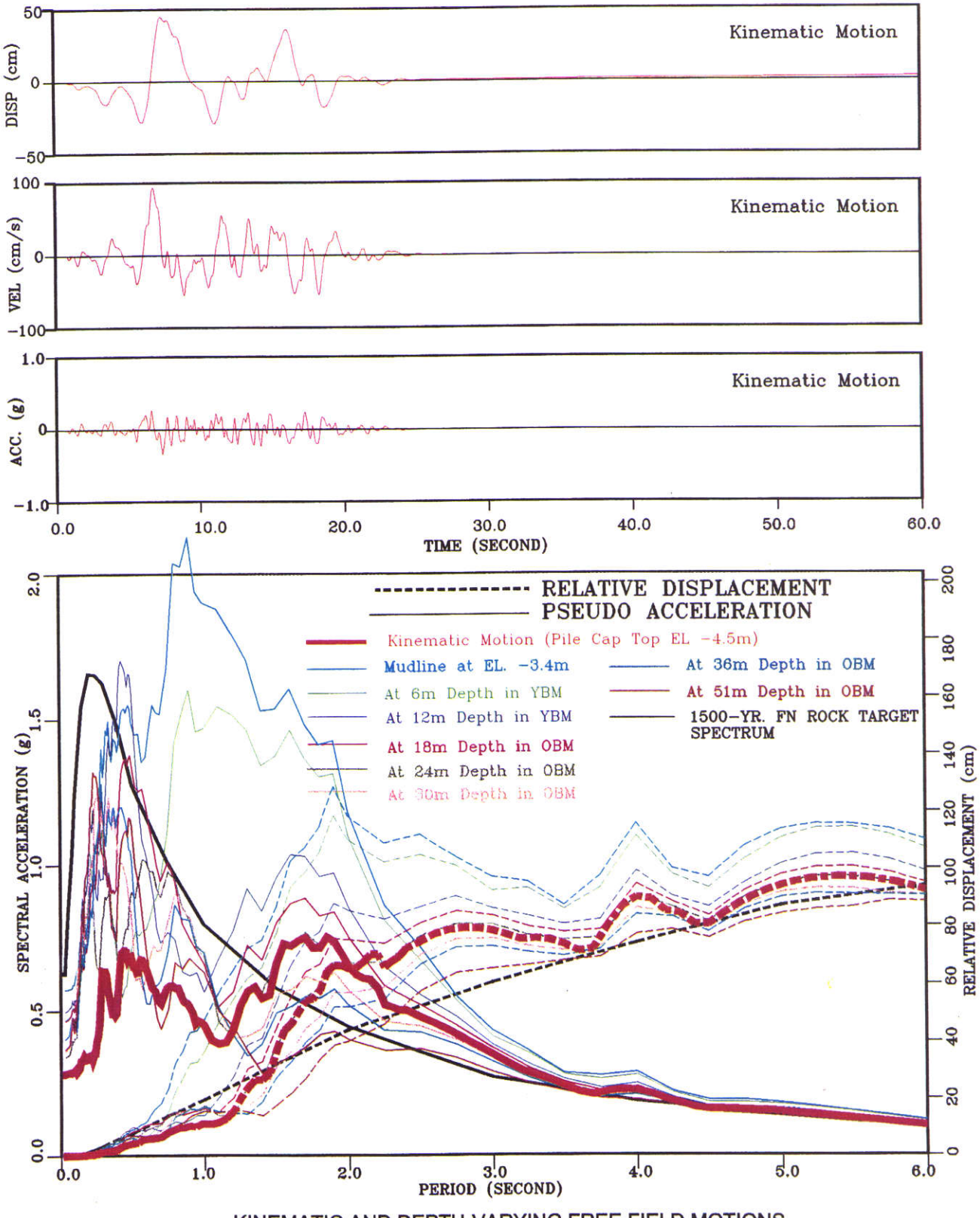

KINEMATIC AND DEPTH-VARYING FREE FIELD MOTIONS
PIER E16, INPUT ROCK MOTION SET 5, FAULT NORMAL COMPONENT
SFOBB East Span Seismic Safety Project

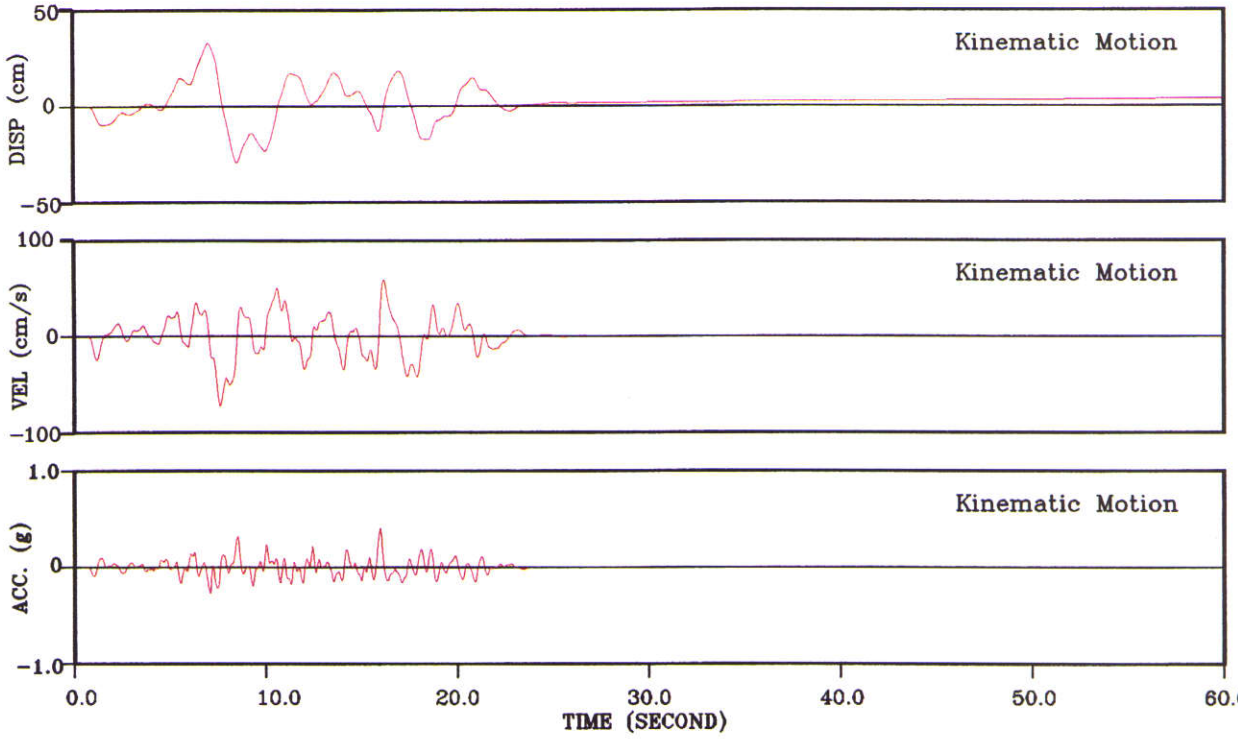

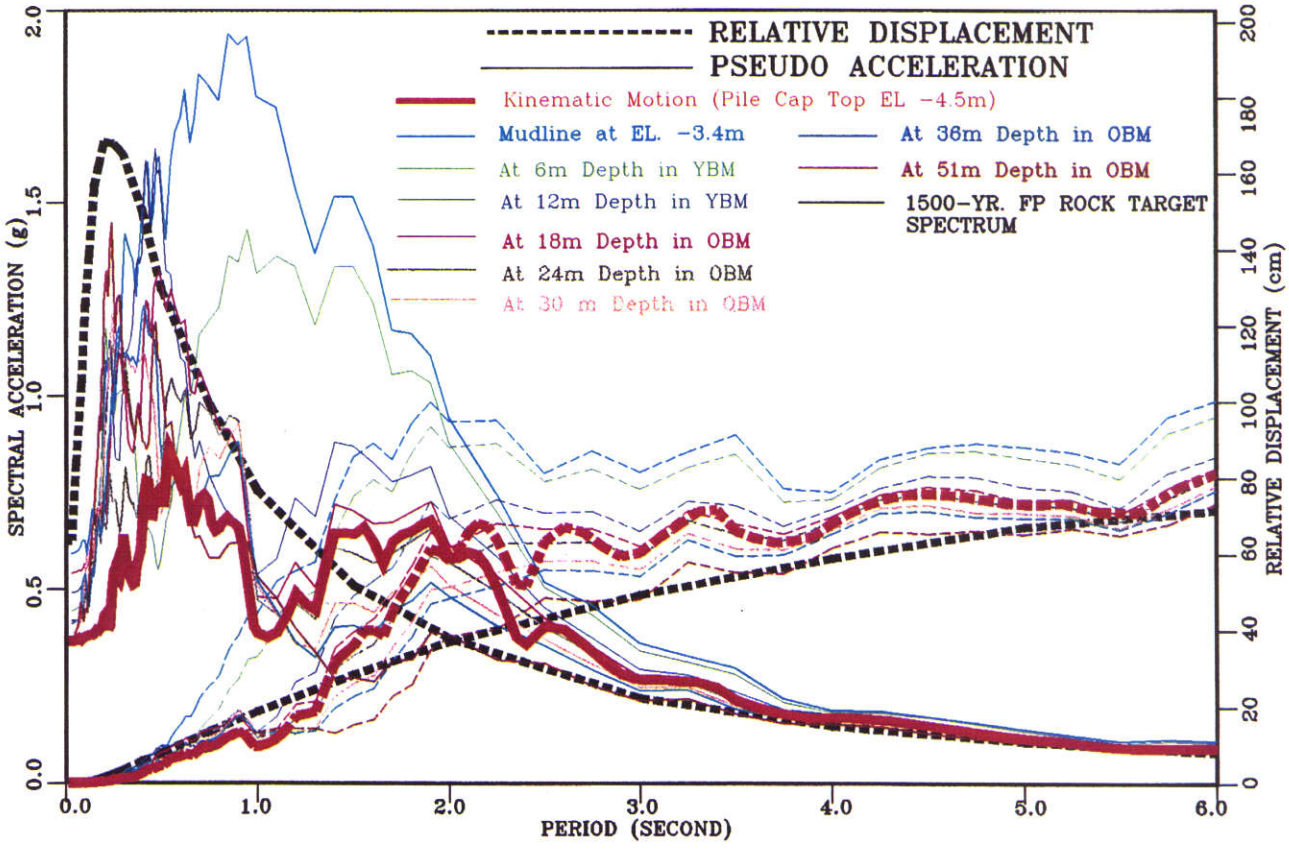

KINEMATIC AND DEPTH-VARYING FREE FIELD MOTIONS
PIER E16, INPUT ROCK MOTION SET51, FAULT PARALLEL COMPONENT
SFOBB East Span Seismic Safety Project

PLATE 8-183

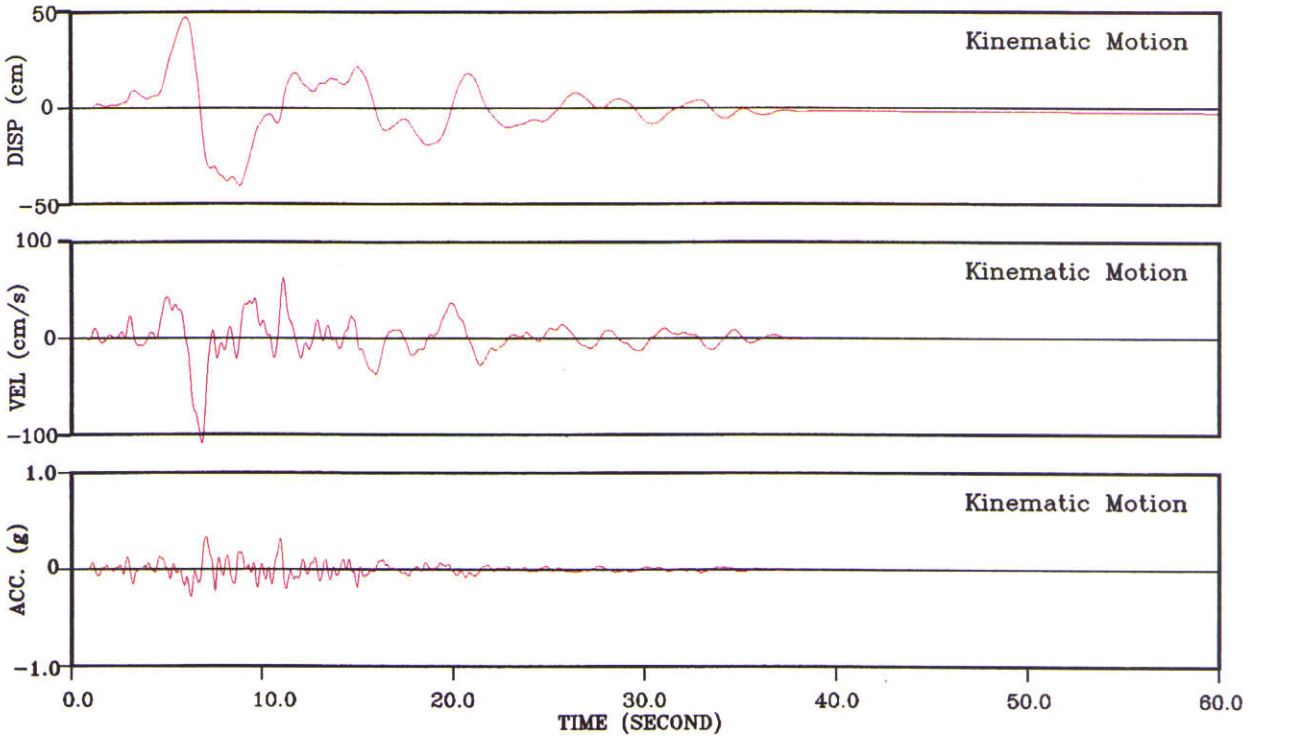

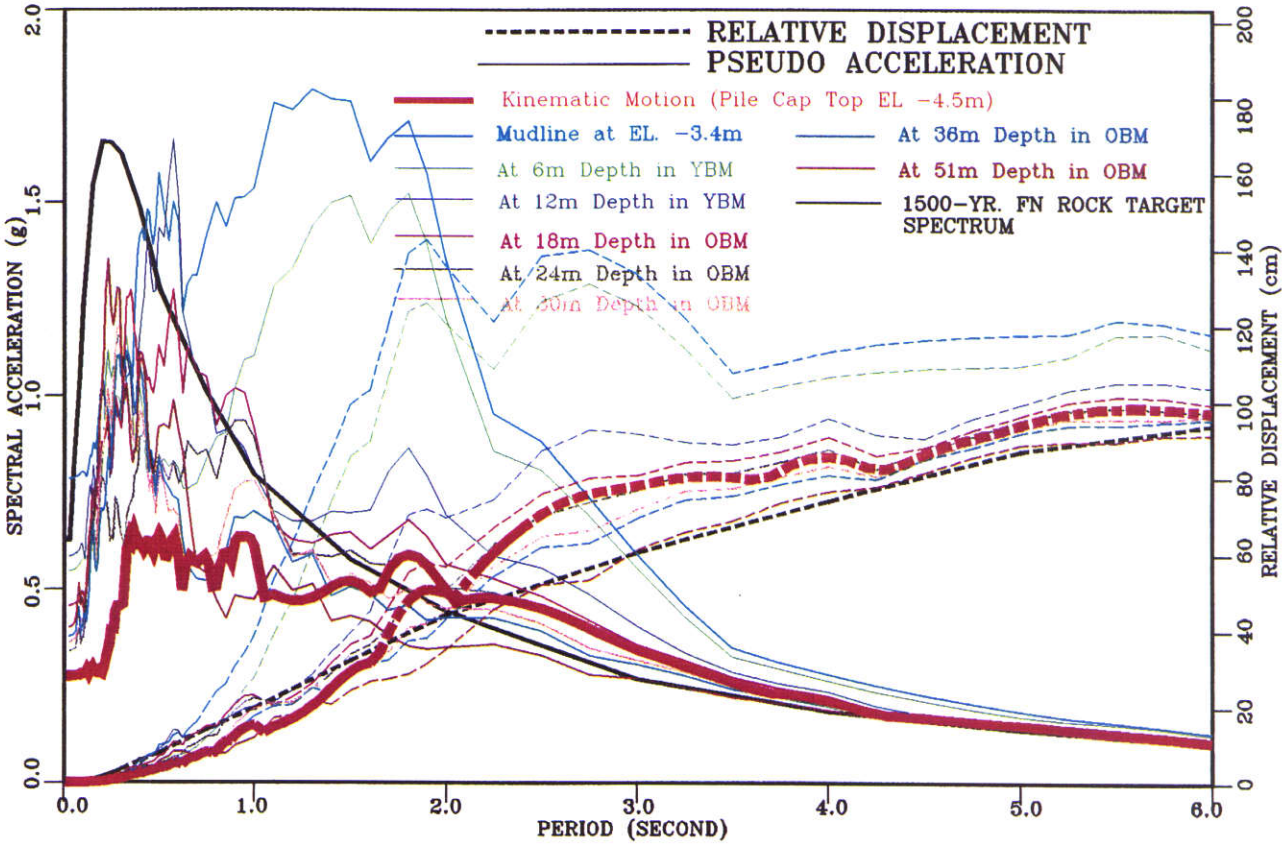

KINEMATIC AND DEPTH-VARYING FREE FIELD MOTIONS
PIER E16, INPUT ROCK MOTION SET 6, FAULT NORMAL COMPONENT
SFOBB East Span Seismic Safety Project

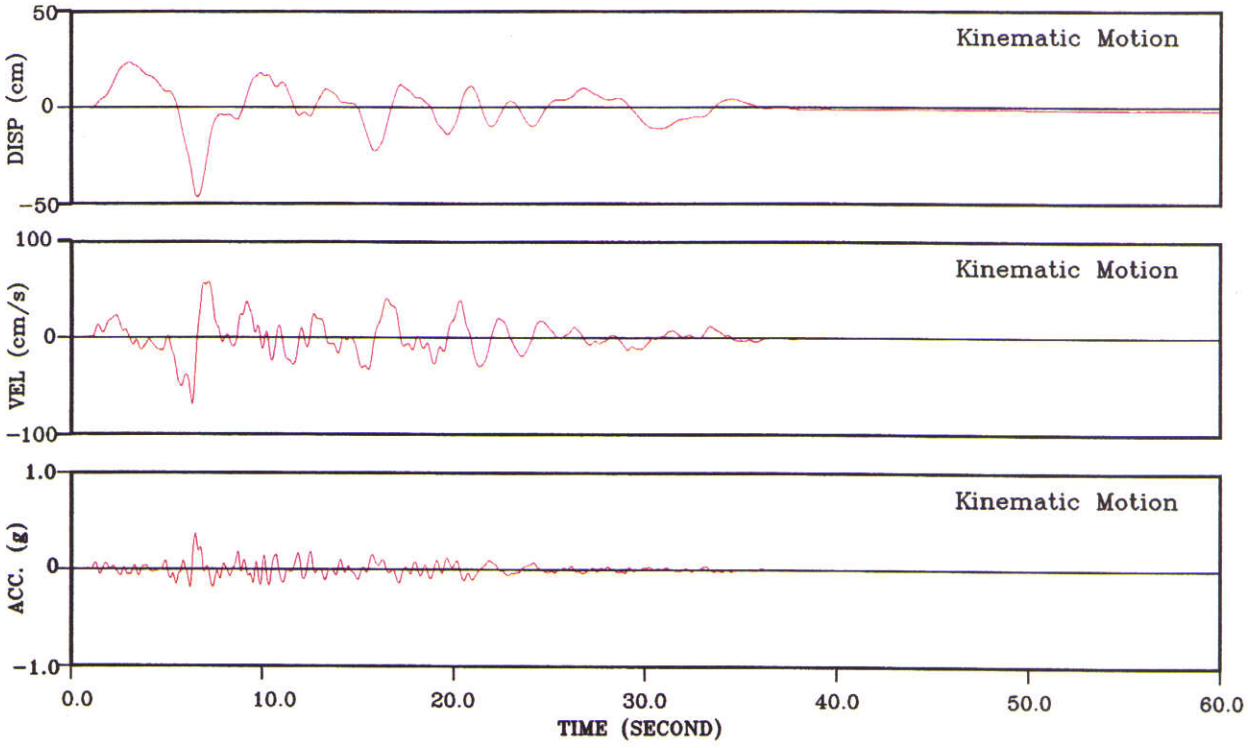

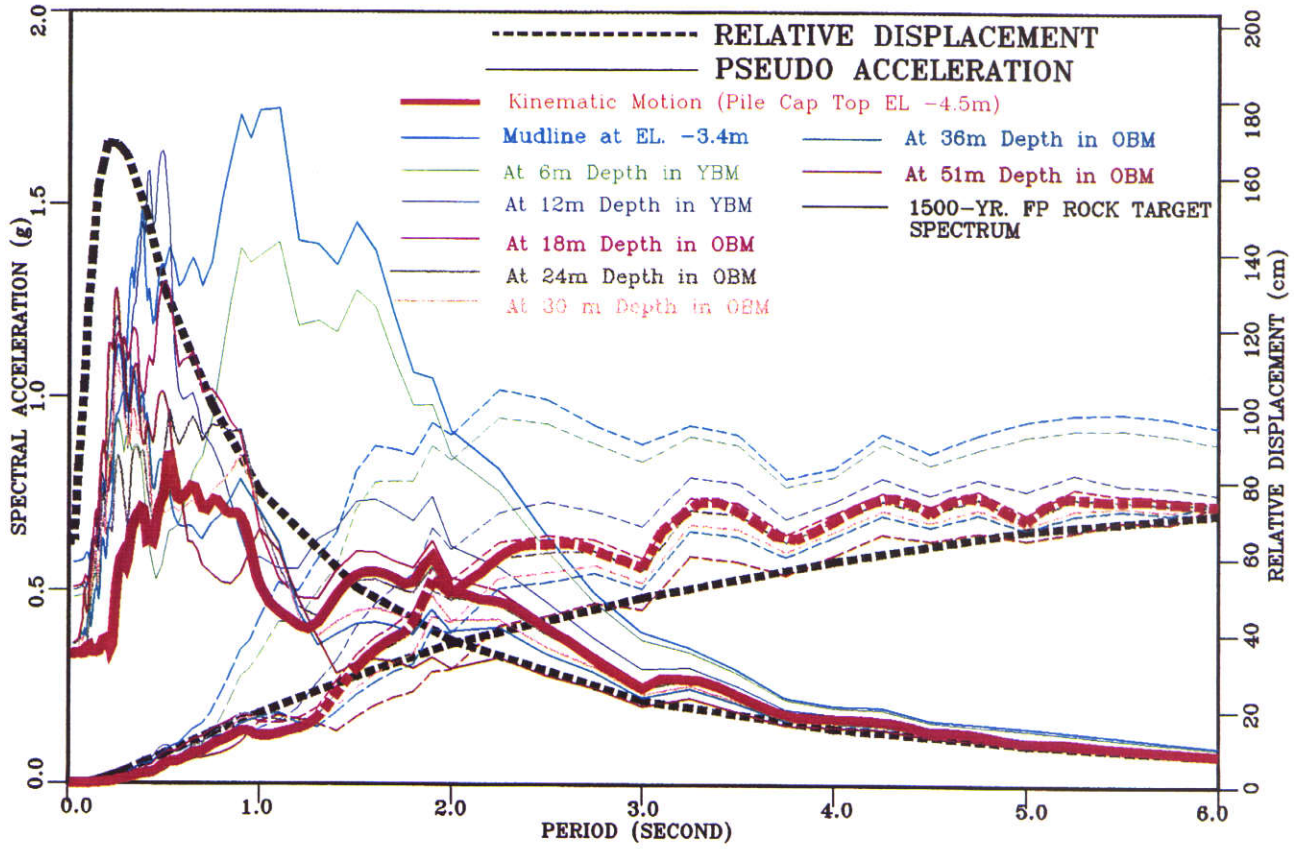

KINEMATIC AND DEPTH-VARYING FREE FIELD MOTIONS
PIER E16, INPUT ROCK MOTION SET 6, FAULT PARALLEL COMPONENT
SFOBB East Span Seismic Safety Project

SECTION 9.0
SUMMARY AND CONCLUSIONS

9.0 SUMMARY AND CONCLUSIONS

This report summarizes all the issues relating to ground motion for design of the San Francisco-Oakland Bay Bridge East Span Replacement Project. The following provides the major conclusions:

1. A 1,500-year return period has been adopted for the Safety Evaluation Earthquake (SEE) corresponding to a probability of 10 percent exceedance over the 150-year service life of the new Bay Bridge structure.

2. A deterministic earthquake corresponding to a Magnitude 6.5 event on the Hayward Fault at about 10 Km from the eastern end of the bridge has been adopted for Functional Evaluation Earthquake (FEE) which roughly corresponds to a 92-year return period. These shaking criteria also serve as the appropriate design level for design of temporary structures for safety level performance goal.

3. Six sets of multiple-support motions are developed for SEE design with 3 sets corresponding to the San Andreas event and 3 sets corresponding to the Hayward Event. The six sets of motion incorporate a wide range of seismological features (near fault displacement and velocity pulse characteristics) into the input motion for a robust design.

4. The self-anchor suspension bridge is designed by time history analyses. The Skyway structure is initially designed by ARS criteria and is later verified by multiple-support time history analyses. The YBI and Oakland Mole structures are designed by ARS criteria. Incoherent time history analysis is not conducted at YBI and Oakland Mole structures.

5. As West Pier and Main Pier of the suspension bridge are to be constructed in rock, the rock motions can be used directly at these locations. The supports for the YBI structure are founded in rock or near bedrock, the reference rock spectra are adopted for design.

6. East Pier of the suspension bridge is found in sediment, and geology in the vicinity of the foundation is rather complex. Two-dimensional site response analyses were conducted to obtain the free-field motions. As the suspension bridge would be designed by time history approach rather the response spectrum approach, the depth-varying free-field motions form a basis for seismic loading.

7. Site response and kinematic soil-structure interaction analyses have been conducted to develop the ARS criteria for the Skyway structures and Oakland Mole structure for the horizontal components. These ARS criteria are site and structure specific, incorporating state-of-the-art seismic design principles. Rock outcrop spectrum is adopted as the ARS criteria for the vertical component.

8. Pier-specific ground motions have been provided at Skyway structure for conducting multiple-support time history analyses in order to check the ARS design approach. The pier-specific time histories are provided in terms of free-field motions and kinematic motions.

SECTION 10.0
REFERENCES

10.0 REFERENCES

Abrahamson, N. A. (1992), Generation of spatially incoherent strong motion time histories, Proc. Tenth World Conf. Earthquake Engineering, Madrid, Spain, 845-850

Abrahamson, N. A. and Silva, W. J. (1997), Empirical Response Spectra Attenuation Relations for Shallow Crustal Earthquakes, Seismological Research Letters, Volume 68, No. 1, January/February

American Petroleum Institute (1993), Recommended Practice for Planning, Designing and Constructing Fixed Off-Shore Platforms – Working Stress Design, 2A-WSD, 20th ed., July

Applied Technology Council, ATC-32 (1996), Improved Seismic Design Criteria for California Bridges, Provisional Recommendations

Caltrans (1996), Seismic Hazard Map Based on Maximum Credible Earthquakes, July

Clough, R. W. and Penzien, J (1975), Dynamics of Structures, McGraw-Hill

Cook, R. D, Malkus, D.S., and Plesha, M.E. (1989), Concepts and Application of Finite Element Analysis, John Wiley & Sons

Cornell, C.A. (1968), Engineering Seismic Risk Analysis, Bulletin of the Seismological Society of America, 58, 1583-1606

Fugro-Earth Mechanics (1998), Subcontractor Reports, Phase I Site Characterization, San Francisco-Oakland Bay Bridge East Span Seismic Safety Project, Volumes 1 through 4, FWI Job No. 98-42-0035, prepared for California Department of Transportation, June 1998

Fugro-Earth Mechanics (2000, a), Draft Yerba Buena Island Geotechnical Site Characterization Report, San Francisco-Oakland Bay Bridge East Span Seismic Safety Project, prepared for California Department of Transportation, March 1

Fugro-Earth Mechanics (2000, b), Draft Geotechnical Foundation Report for Structural Alternative Oakland Shore Approach, San Francisco-Oakland Bay Bridge East Span Seismic Safety Project, prepared for California Department of Transportation, July 31

Fugro-Earth Mechanics (2001, a), Skyway Submittal, Geotechnical Summary Report, San Francisco-Oakland Bay Bridge East Span Seismic Safety Project, FWI Job No. 98-42-0035, prepared for California Department of Transportation, March 5

Fugro-Earth Mechanics (2001, b), Final Marine Geotechnical Site Characterization, San Francisco-Oakland Bay Bridge East Span Seismic Safety Project, Volumes 1A & 1B, Volumes 2A through 2H, FWI Job No. 98-42-0054, prepared for California Department of Transportation, March 5

Fugro-Earth Mechanics (2001, c), Final Marine Geophysical Survey, San Francisco-Oakland Bay Bridge East Span Seismic Safety Project, FWI Job No. 98-42-0054, prepared for California Department of Transportation, March 5

Fugro-Earth Mechanics (2001, d), Axial Pile Design and Drivability, Main Span-East Pier & Skyway Structures, San Francisco-Oakland Bay Bridge East Span Seismic Safety Project, FWI Job No. 98-42-0054, prepared for California Department of Transportation, March 5

Fugro-Earth Mechanics (2001, e), Lateral Pile Design for Main Span Pier E2 and Skyway Structure, San Francisco - Oakland Bay Bridge East Span Seismic Safety Project, prepared for California Department of Transportation, February, 28

Fugro-Earth Mechanics (2001, f), Subcontractor Reports, Phase II Site Characterization, San Francisco-Oakland Bay Bridge East Span Seismic Safety Project, Volumes 1 through 3, FWI Job No. 98-42-0054, prepared for California Department of Transportation, March 5

Fugro-Earth Mechanics (2001, g), Pile Installation Demonstration Project (PIDP) Geotechnical Report, SFOBB East Span Seismic Safety Project, FWI Job No. 98-42-0061, prepared for California Department of Transportation, March 5

Fugro-Earth Mechanics (2001, h), Final Oakland Shore Approach Geotechnical Site Characterization Report, San Francisco-Oakland Bay Bridge East Span Seismic Safety Project, Volumes 1 through 4, FWI Job No. 98-42-0058, prepared for California Department of Transportation, March 5

Fugro-Earth Mechanics (2001, i), Draft Geotechnical Foundation Report for the Yerba Buena Island Approach and Main Tower, San Francisco-Oakland Bay Bridge East Span Seismic Safety Project, prepared for California Department of Transportation

Gazetas, G, Fan, K, Tazoh, T., Shimizu, K., Kavvadas, M., and Makris, N. (1992), Seismic Pile-Group-Structure Interaction, ASCE Geotechnical Special Publication No. 34, Piles Under Dynamic Loads, Edited by Shamsher Prakash

Geomatrix Consultants (1992), Seismic Ground Motion Coherency Study for West Span San Francisco Bay Bridge, Report prepared for CALTRANS Division of Structures, Sacramento, California, Geomatrix Consultant, San Francisco

Geomatrix Consultants (1995), Adjustments to rock response spectra for CALTRANS toll bridges in northern California, Report prepared for Business, Transportation, and Housing Agency (CALTRANS) Division of Structures, Sacramento, California, Geomatrix Consultant, San Francisco

Hudson, M., Idriss, I. M., and Beikae, M. (1994), User's Manual for QUAD4M, De-partment of Civil and Environmental Engineering, University of California, Davis

Idriss, I. M., Dobry, R., and Singh, R. D. (1978), Nonlinear Behavior of Soft Clays, Journal of Geotechnical Engineering, ASCE, Vol.104, No.11, December

Idriss, I. M. (1990), Response of Soft Soil Sites during Earthquakes, Proceeding Memorial Symposium to Honor Professor H. B. Seed, CA

Idriss, I. M. (1991), Selection of earthquake ground motions at rock sites: Report Prepared for the Structures Division, Building and Fire Research Laboratory, National Institute of Standards and Technology, Department of Civil Engineering, University of California, Davis, September

Idriss, I. M., and Sun, J. I. (1992), User's Manual for SHAKE91, University of California, Davis, November

Kaul, M. K. (1978), Spectrum-Consistent Time-History Generation, ASCE Journal of Engineering Mechanics, EM4, 781-788

Kramer, S. L. (1996), Geotechnical Earthquake Engineering, Prentice Hall

Lam, I. P. and Law, H (2000), Soil Structure Interaction of Bridges for Seismic Analysis, Multidisciplinary Center for Earthquake Engineering Research, Technical Report MCEER-00-0008, September

Lam, I. P, Martin, G. R. and Imbsen, R (1991), Modeling Bridge Foundations for Seismic Design and Retrofitting, Transportation Research Record 1290

Lanzo, G., Vucetic, M., and Doroudian, M. (1997), Reduction of Shear Modulus at Small Strains in Simple Shear, Journal of Geotechnical and GeoEnviromental Engineering, ASCE, Vol.123, No.11, November

Lilhanand, K. and Tseng, W.S. (1987), Generation of Synthetic Time Histories Compatible with Multiple-Damping Response Spectra, SMIRT-9, Lausanne, K2/10

Lilhanand, K. and Tseng, W.S. (1988), Development and Application of Realistic Earthquake Time Histories Compatible with Multiple-Damping Response Spectra, Ninth World Conference on Earthquake Engineering, Tokyo, Japan, Vol II, 819-824

Matlock, H. (1970), Correlation for Design of Laterally Loaded Piles in Soft Clay, 2nd Annual Offshore Technology Conference, Paper No 1204, May

Mualchin, L. (1996), A Technical Report to Accompany the Caltrans California

Mylonakis, G., Nikolaou, A., and Gazetas, G. (1997), Soil-Pile-Bridge Seismic Interaction: Kinematic and Inertial Effects. Part I: Soft Soil, Earthquake Engineering and Structural Dynamics, Vol. 26, pp. 337-359

Newmark, N. M and Hall, W.J. (1973), Procedure and Criteria for Earthquake-Resistant Design, Report NUREG/CR-0098, Nuclear Regulatory Commission, Washington, DC

Newmark, N. M (1965), Effects of Earthquakes on Dams and Embankments. Fifth Rankine Lecture, Geotecnique, Vol. 15, pp 139-160

Pender, M. J. (1993), Aseismic Pile Foundation Design and Analysis, Bulletin of the New Zealand National Society for Earthquake Engineering, Vol 26, No. 1, 49-160

Petersen, M., Bryant W., Cramer C., Cao T., Reichle M., Frankel, J. Lienkaemper, McCrory P., Schwartz D. (1996), Probabilistic Seismic Hazard Assessment for the State of California, California Department of Conservation, Division of Mines and Geology, Open-File Report 96-08, U.S. Geologic Survey Open-file Report 96-706

Pyke, R. M., et al. (1993), Modeling of Dynamic Soil Properties, Appendix 7.A, Guidelines for Determining Design Basis Ground Motions, Report No. TR-102293, Electric Power Research Institute, November

Pyke, R. M., et al. (1995),Development of Generic Modulus Reduction and Damping Curves, submitted to EERI Spectra

Seed, H. B. and Idriss, I. M. (1976), Ground Motions and Soil Liquefaction During Earthquakes, EERI Monograph

Seed, R. B.Dickenson, S. E., Reimer, M. F., Bray, J. D., Sitar, N., Mitchell, J. K., Idriss, I.M., Kayen, R.E., Kropp, A., Harder, L. F. and Power, M. S (1990), Preliminary Report on the Principal Geotechnical Aspects of the October 17, 1989 Loma Prieta Earthquake, Report UCB/EERC 90/05, University of California, Berkeley

Reese, L., Cox, W., and Koop, R. (1974), Analysis of Laterally Load Piles in Sand, 6th Annual Offshore Technology Conference, Paper No. 2080, May

Reiter, L (1990), Earthquake Hazard Analysis; Issues and Insights, Columbia University Press, NY

Sommerville, P. G., Smith, N. F., Graves, R. W. and Abrahamson, N. A. (1997), Modification of Empirical Strong Motion Attenuation Relations to Include the Amplitude and Duration Effects of Rupture Directivity, Seismological Research Letters, Volume 68, No. 1, January/February

Stokoe, K. H. (1993), Dynamic Properties of Undisturbed Soil Samples from Treasure Island, California, Appendix 8.B.1, Guidelines for Determining Design Basis Ground Motions, Report No. TR-102293, Electric Power Research Institute, November

TAGAsoft Limited (1998), TESS Users' Manual, August

Vucetic, M., Lanzo, G., and Doroudian, M. (1997), Damping at Small Strains in Cyclic Simple Shear Test, Journal of Geotechnical and GeoEnviromental Engineering, ASCE, Vol.123, No.11, November

Wells, D. L., and Coppersmith, K. J. (1992), Analysis of Empirical Relationships among Magnitude, rupture length, rupture area, and surface displacement, Seismological Research Letters, Vol. 63, p. 73

Wells, D. L., and Coppersmith, K. J. (1994), New Empirical Relationships among Magnitude, rupture length, rupture width, rupture area, and surface displacement, BSSA, Vol. 84, p. 974-1,002

Working Group on Northern California Earthquake Potential (1996), Database of Potential Sources for Earthquakes Larger Than Magnitude 6 in Northern California: U.S. Geologic Survey Open-File Report 96-705, 40p

Youngs and Coppersmith (1985), Implication of Fault Slip Rate and Earthquake Recurrence Models to Probabilistic Seismic Hazard Estimates, Bulletin of the Seismological Society of America, 75: 939-964

APPENDIX A
PROBABILISTIC SEISMIC HAZARD ASSESSMENT MATHEMATICAL DETAILS

APPENDIX A
PROBABILISTIC SEISMIC HAZARD ASSESSMENT

INTRODUCTION

To help understand some of the concepts used in probabilistic seismic hazard analysis, it is useful to first think of probabilistic hazard analysis as a statistical evaluation of the ground motions at a site from an artificial catalog of future earthquakes. The seismic source characterization is the model use to develop the occurrence of earthquake in the future. This model could be used to predict the occurrence of earthquakes during the next 1,000,000 years, for example. For each earthquake in this large catalog, the ground motion at the site is predicted using attenuation relations. Since there is variability in the attenuation (the scatter in ground motion data represented by the standard deviation of the attenuation relation) sometimes the ground motion will be high and sometimes the ground motion will be low even for the same magnitude and distance to the site. In the end, we have a large artificial data set of peak ground motions that occur at the site in the next 1,000,000 years. We then compute how often different levels of ground motion occur in this artificial data set.

For example, if a peak acceleration of 0.2g occurs 10,000 times in our 1,000,000 year data set, then 0.2g occurs about every 100 years. Similarly if 1.0g occurs only 500 times in our 1,000,000 year data set, then 1.0g occurs about every 2000 years. If we plot these return periods, then we build up a hazard curve. The shape of the hazard curve results from the random variations in the locations and magnitudes of the earthquakes in our artificial catalog and from the random variations in the ground motion attenuation.

Of course, the models and assumptions that we used to build up the artificial data set may be wrong. If we used a different seismic source characterization model or a different ground motion attenuation relation, we would arrive at a different catalog of ground motions and potentially different return periods for the various levels of shaking. If we repeated the process for a different model, we would arrive at a different hazard curve. Therefore, different models of the seismic sources and attenuation relations lead to different hazard curves (as opposed to the shape of the hazard curve).

The term "aleatory uncertainty" is used to describe the random variations which lead to the shape of an individual hazard curve. The term "epistemic uncertainty" is used to describe the scientific uncertainty in our model of the occurrence of earthquakes and ground motion which leads to alternative hazard curves.

The example of using the seismic source characterization to develop a 1,000,000 year catalog is useful for an initial conceptual understanding of seismic hazard analysis; however, it is not what is we are doing. That is, we are not trying to predict what will happen over the next 1,000,000 years, but rather we are estimating the probabilities that a level of ground motion will occur in the next year (or 150 years). If the earthquake process is stationary (e.g. earthquake rates do not change with time) then the two approaches give the same answer. There is often a misunderstanding of hazard analysis for low annual probabilities. For example, if we are discussing the 10^{-4} yr ground motion level (return period of 10,000 years), someone may comment that we don't know what will happen 10,000 years from now. However, a 10^{-4} annual probability is just that, the 1 in 10,000 chance that the ground motion occurs next year. It does not imply that the models are applicable to the next 10,000 years.

The mathematical formulation of the hazard analysis is given below.

MATHEMATICAL FORMULATION

The probabilistic seismic hazard analysis follows the standard approach first developed by Cornell (1968). The main change from the original work is that more parameters are randomized (a more complete description of the aleatory variables) and epistemic uncertainty is considered. In particular, the aleatory variability in the ground motion was not considered in the original work. The ground motion aleatory variability has a large effect on the hazard and can not be ignored.

The basic methodology involves computing how often a specified level of ground motion will be exceeded at the site. The hazard analysis computes the annual number of events that produce a ground motion parameter, A, that exceeds a specified level, "a". This number of events per year, ν, is also called the "annual frequency of exceedance". The inverse of ν is called the "return period".

The calculation of the annual frequency of exceedance, ν, involves the rate of earthquakes of various magnitudes, the rupture dimension of the earthquakes, the location of the earthquakes relative to the site, and the attenuation of the ground motion from the earthquake rupture to the site.

The annual rate of events from the ith source that produce ground motions that exceed "a" at the site is the product of the probability that the ground motion exceeds the test value given that an earthquake has ocurred on the ith source and the annual rate of events with magnitude greater than m_{min} on the ith source.

$$\nu_i(A>a) = N_i(m_{min})P_i(A>a|E_i(m \geq m_{min}) \qquad \text{(A-1)}$$

where $N_i(m_{min})$ is the annual number of events with magnitude greater than m_{min} on the ith source and $E_i(m_{min})$ indicates that an event with magnitude $\geq m_{min}$ has occurred on the ith source

For multiple seismic sources, the total annual rate of events with ground motions that exceed z at the site is just the sum of the annual rate of events from the individual sources (assuming that the sources are independent).

$$\nu(A>a) = \sum_{i=1}^{N_{source}} \nu_i(A>a) \qquad \text{(A-2)}$$

Hazard for Fault Sources

Fault sources are modeled by multiple-planes which allows changing the strike of the fault. For planar sources (e.g. known faults), we need to consider the finite dimension and location of the rupture in order to compute the closest distance. Specifically, we need to randomize the rupture length, rupture width, rupture location along strike, rupture location down dip, and hypocenter location along the rupture length (for strike-slip faults). (Since rupture width and length are correlated, it is easier to consider the rupture area and rupture width and then back calculate the rupture length.)

The general form of the conditional probability for the ith fault is given by:

$$P_i(A>a \mid E_i(m \geq m_{min}) = \int_{RA=0}^{\infty} \int_{RW=0}^{\infty} \int_{Ex=0}^{1} \int_{Ey=0}^{1} \int_{x=0}^{1} \int_{m=M_{min}}^{M_{max_i}} f_{m_i}(m)\, f_{RA_i}(m) f_{RW_i}(m)\, f_{Ex}(Ex)\; f_{Ey}(Ey$$

$$f_{x_i}(x)\; P_i(A>a \mid m,r(Ex,Ey,RA,RW),x)\; dm\, dx\, dEy\, dEx\; dRW\, dRA$$

where $f_{RW}(m)$, $f_{RA}(m)$, $f_{Ex}(Ex)$, $f_{Ey}(Ey)$, $f_x(x)$, and $f_m(m)$ are probability density functions for the rupture width, rupture area, rupture location along strike, rupture location down dip, hypocenter location in the rupture plane, and magnitude, respectively. The models used for these probability density functions are described later.

For the fault normal component (FN), the probability of exceeding the ground motion "a" for a given magnitude, m, and closest distance, r, and hypocenter location, x, is given by

$$P(A > a|m,r,x) \;=\; 1 - \Phi\left(\frac{\ln(a) - \ln(Sa_{FN}(m,r,x))}{\sigma(m)}\right)$$

Where $Sa(m,r,x)$ and $\sigma(m)$ are the median and standard deviation of the ground motion from the attenuation relations for the fault normal component as described in appendix B, and $\Phi()$ is the normal probability integral given by

$$\Phi(z) \;=\; \int_{-\infty}^{z} \frac{1}{\sqrt{2\pi}} e^{-u^2/2}\, du$$

Probability of Exceedance

The annual rate of events given in Eq (A-2) is not probability; it can exceed 1. To convert the annual rate of events to a probability, we consider the probability that the ground motion exceeds test level "a" at least once during a specified time interval.

At this step, a common assumption is that the occurrence of earthquakes is a Poisson process. That is, there is no memory of past earthquakes, so the chance of an earthquake occurring in a given year does not depend on how long it has been since the last earthquake. (Non-Poisson models are discussed later.) If the occurrence of earthquakes is a Poisson process then the occurrence of peak ground motions is also a Poisson process. For a Poisson process, the probability of an event (e.g. ground motion exceeding z) occurring n times in time interval t is given by

$$p_n(t) = \exp(-\nu t)\,(\nu t)^n/n! \qquad \text{(A-6)}$$

The probability that at least one event occurs (e.g. $n \geq 1$) is 1 minus the probability that no events occur:

$$P(n \geq 1, t) = 1 - p_o(t) = 1 - \exp(-\nu t) \qquad \text{(A-7)}$$

So the probability of at least one occurrence of ground motion level z in t years is given by

$$P(A>a,t) = 1 - \exp(-\nu(A>a)t) \qquad \text{(A-8)}$$

For t=1 year, this probability is the annual hazard.

Aleatory and Epistemic Uncertainty

The basic part of the hazard calculation is computing the integrals in Eq (A-3). All of the aleatory variables are inside of the hazard integral. The randomness of the seismic source variables is characterized by the probability density functions which are discussed below. The randomness of the attenuation relation is accounted for in the probability of exceeding the ground motion, "a", for a given magnitude and closest distance.

Epistemic (scientific) uncertainty is considered by using alternative models and/or parameter values for the probability density functions, attenuation relation, and activity rate. For each alternative model, we recalculate the hazard and compute alternative hazard curves. Epistemic uncertainty is typically handled using a logic tree approach for specifying the alternative models for the density function, attenuation relation, and activity rates.

Activity Rate

There are two approaches to estimating the fault activity rate: historical seismicity and geologic (and geodetic) information.

If historical seismicity catalogs are used to estimate the activity rate, then the estimate of $N(m^L)$ is usually based on fitting the truncated exponential model (discussed below) to the historical data. Maximum likelihood procedures are generally preferred over least-squares for estimating the activity rate and the b-value.

When using geologic information on slip-rates of faults, the activity rate is computed by balancing the energy build-up estimated from geologic evidence with the total energy release of earthquakes. Knowing the dimension of the fault, the slip-rate, and the rigidity of the fault, we can balance the long term seismic moment so that the fault is in equilibrium. (e.g. Youngs and Coppersmith, 1985).

The seismic energy release is balanced by requiring the build up of seismic moment to be equal to the release of seismic moment in earthquakes. The build up of seismic moment is computed from the long term slip-rate. The seismic moment, Mo (in dyne cm), is given by

$$Mo = \mu A D \tag{A-9}$$

where μ is the rigidity of the crust, A is the area of the fault (in cm^2), and D is the average displacement (slip) on the fault surface (in cm). The annual rate of build up of seismic moment is given by

$$Mo = \mu A S \tag{A-10}$$

where S is the slip-rate in cm/year. The seismic moment released during an earthquake is given by

$$\log_{10} Mo = 1.5 M + 16.05 \tag{A-11}$$

where M is the moment magnitude of the earthquake.

To balance the moment build up and the moment release, the annual moment rate from the slip-rate is set equal to the sum of the moment released in all of the earthquakes that are expected to occur each year.

$$\mu AS = N(m^L) \int_{m=M^L}^{m^U} f_m(m)\ 10^{(1.5m + 16.05)} dm \tag{A-12}$$

Given the slip-rate, fault area, and magnitude density function, the activity rate, $N(m^L)$ is given by:

$$N(m^L) = \frac{\mu A S}{\int_{m=M^L}^{m^U} f_m(m)\, 10^{(1.5m + 16.05)} dm}$$

Magnitude Density Distribution

The magnitude density distribution describes the relative number of large magnitude and moderate magnitude events that occur on the seismic source. Two alternative magnitude density functions are considered: the truncated exponential model and the characteristic model.

The truncated exponential model is the standard Gutenberg-Richter model that is truncated at the minimum and maximum magnitudes and renormalized so that it integrates to unity. The density function for the truncated exponential model is given by

$$f_m(m) = \frac{\beta \exp(-\beta(m-m^L))}{1-\beta \exp(-\beta(m^U-m^L))} \qquad \text{(A-14)}$$

where β is ln(10) times the b-value. Regional estimates of the b-value are usually used with this model.

The characteristic model assumes that more of the seismic energy is released in large magnitude events than for the truncated exponential model. That is, there are fewer small

magnitude events for every large magnitude event for the characteristic model than for the truncated exponential model. There are different models for the characteristic model. Two commonly used models are the characteristic model as defined by Youngs and Coppersmith (1985) and the "maximum magnitude" characteristic model. In this paper, we will call these two models the characteristic model and maximum magnitude model, respectively.

The density function for the generalized form of the Youngs and Coppersmith characteristic model is given by

$$f_m(m) = \begin{cases} \dfrac{\beta \exp(-\beta(m-m^L))}{1-\beta \exp(-\beta(m^U-\Delta m_2-m^L))} \dfrac{1}{1+c} & \text{for } m < m^U-\Delta m_2 \\ \dfrac{\beta \exp(-\beta(m^U-\Delta m_1-\Delta m_2-m^L))}{1-\beta \exp(-\beta(m^U-\Delta m_2-m^L))} \dfrac{1}{1+c} & \text{for } m \geq m^U-\Delta m_2 \end{cases} \quad \text{(A-15)}$$

where

$$c = \frac{\beta \exp(-\beta(m^U-\Delta m_1-\Delta m_2-m^L))}{1-\beta \exp(-\beta(m^U-\Delta m_2-m^L))} \Delta m_2 \quad \text{(A-16)}$$

The density function for this model is shown in Figure A-1. In the Youngs and Coppersmith model, Δm_1=1.0 and Δm_2=0.5.

Comparing the examples of the truncated exponential and characteristic density functions shown in Figure A-1, we see that the density functions themselves are similar at small magnitudes. However, when the geologic moment-rate is used to set the annual rate of events, $N(m^L)$, then there is a large impact on $N(m^L)$ depending on the selection of the magnitude density function. Figure A-2 shows the comparison of the magnitude

recurrence relation for the truncated exponential and characteristic models (using the Youngs and Coppersmith value for Δm_1 and Δm_2) when they are constrained to have the same total moment rate. The characteristic model has many fewer moderate magnitude events than the truncated exponential model (about a factor of 10 difference).

Recent studies have found that the characteristic model does a better job of matching observed seismicity than the truncated exponential (Geomatrix, 1992, Woodward-Clyde, 1994) when the total moment rate is constrained by the geologic slip-rate.

Rupture Dimension Density Functions

For the rupture area and rupture width, the density function are determined from regression models which give the rupture area and rupture width as a function of magnitude. For this project, the Wells and Coppersmith (1994) empirical models for rupture area and rupture width are used:

$$\log_{10}(RA) = -3.49 + 0.91\,M \pm 0.24 \qquad \text{(A-17)}$$

$$\log_{10}(W) = -1.01 + 0.32\,M \pm 0.15 \qquad \text{(A-18)}$$

The density functions, $f_{RA}(m)$ and $f_{RW}(m)$ are log normal distributions centered about the median values given by Eq. (A-15) and (A-16). These distributions are truncated at $\pm 2\sigma$ in the hazard calculations.

Rupture Location Density Functions

The center of the rupture location is parameterized in terms of the normalized fault length and fault width. Ex is the fraction of the fault length (measure along strike) and Ey is the

fraction of the fault width (measured down dip). The location of the center of the rupture plane is assumed to be uniformly distributed over the fault plane. The resulting density functions for $f_{Ex}(E_x)$ and $f_{Ey}(E_y)$ are unity.

Hypocenter Location Density Function

For a given rupture dimension (length and width) and rupture location, the location of the hypocenter along strike is parameterized in terms of the normalized rupture length. The location of the hypocenter is assumed to be uniformly distributed over the rupture plane. The resulting density function for $f_x(x)$ is unity. In the hazard analysis, a total of 10 hypocenter locations evenly spaced along the rupture length are used for each magnitude, ruputure location, and rupture dimension.

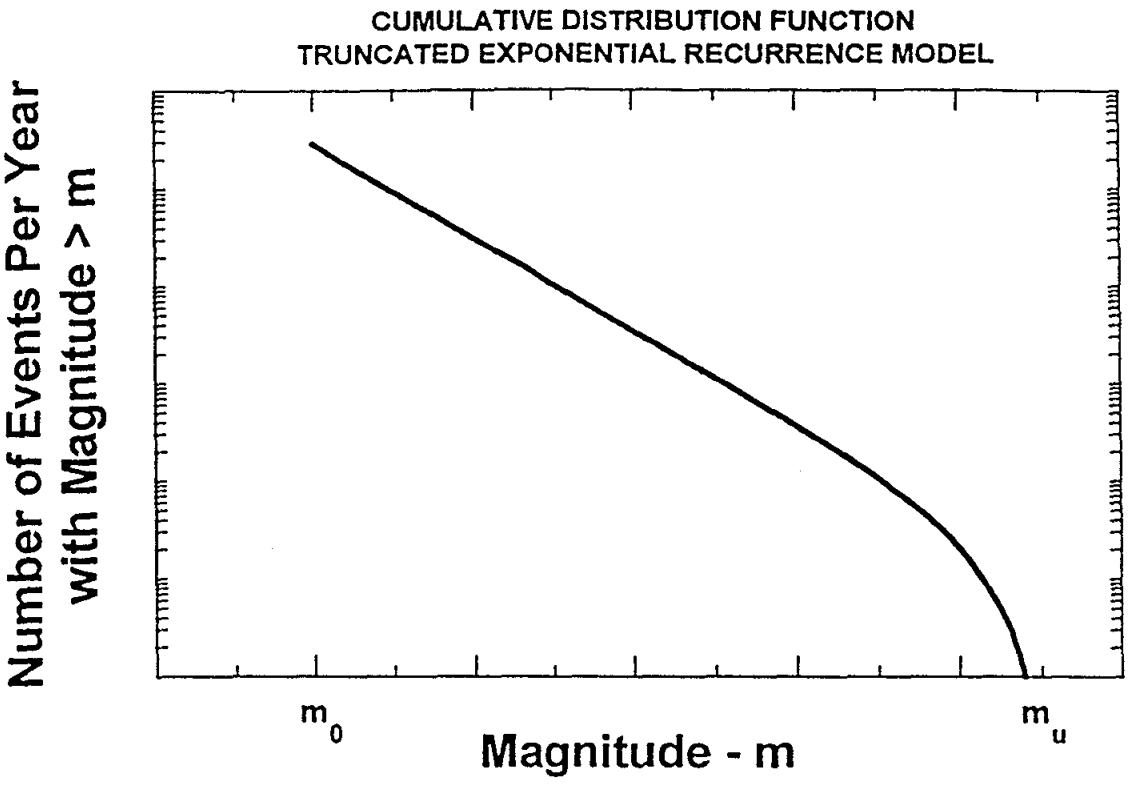

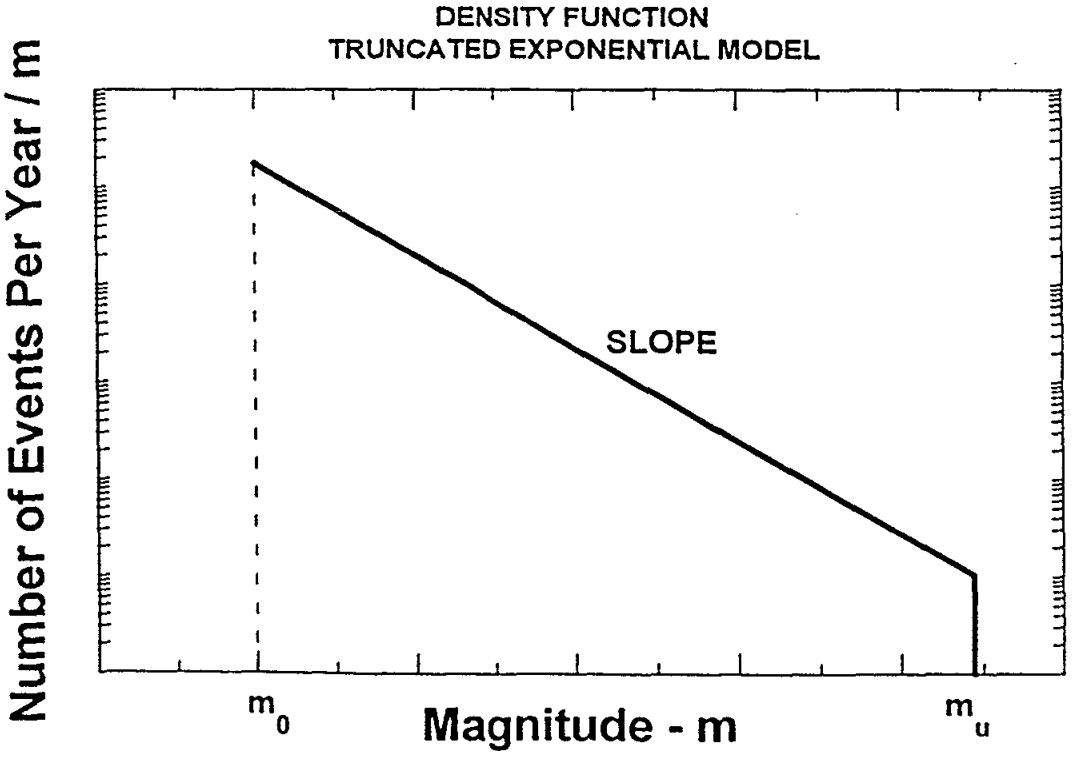

FIGURE A–1. CUMULATIVE DISTRIBUTION AND DENSITY FUNCTIONS FOR TRUNCATED EXPONENTIAL RECURRENCE MODEL

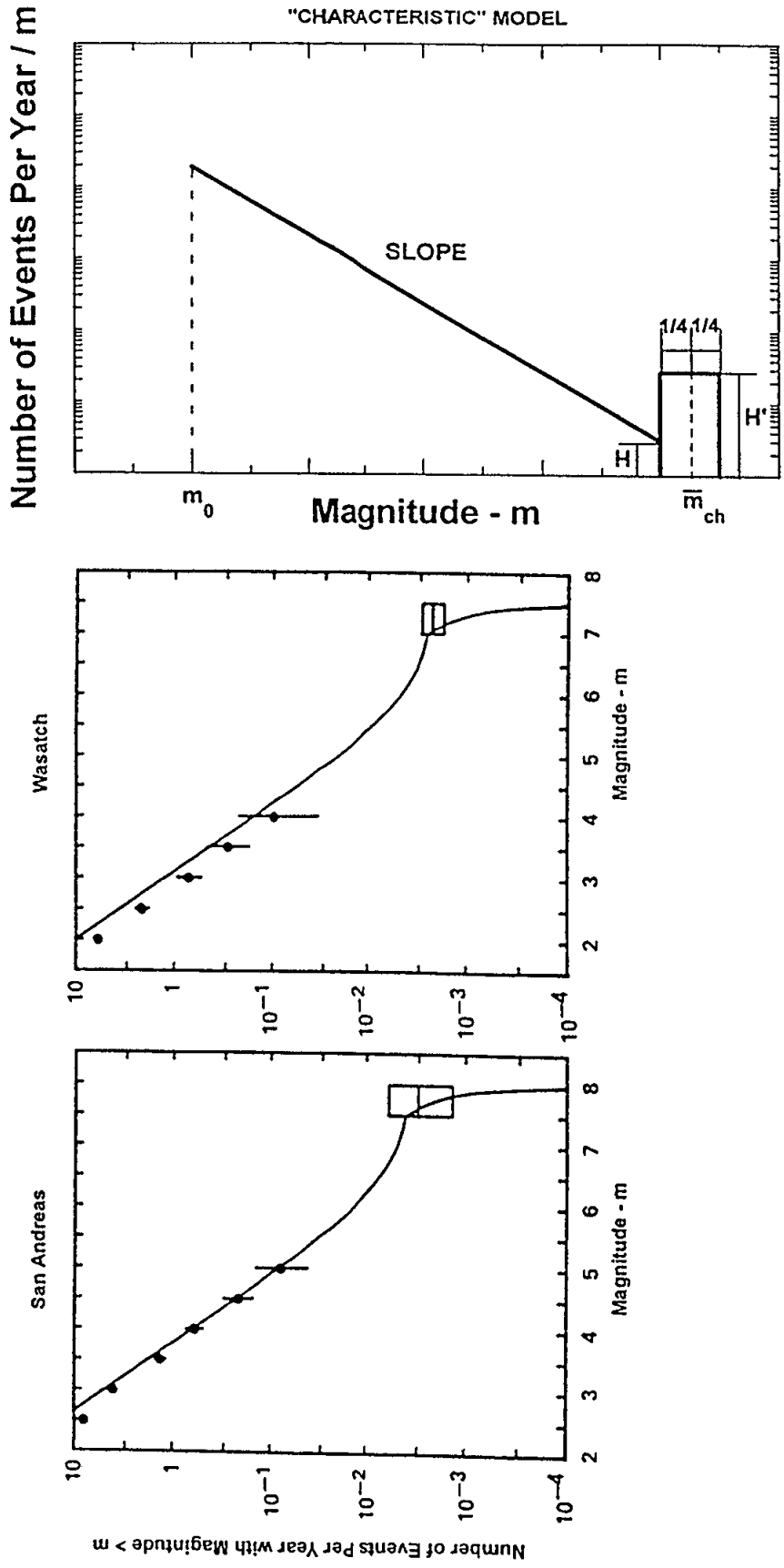

FIGURE A–2. DENSITY FUNCTIONS FOR CHARACTERISTIC RECURRENCE MODEL

APPENDIX B
ATTENUATION RELATIONS

Appendix B Attenuation Relations

The response spectral attenuation relations used in this study are listed in this appendix.. The following variables are used in all of the models:

M =	moment magnitude
R_{rup} =	closest distance to the rupture plane (km)
F_1 =	fault type: 0 for strike-slip, 0.5 for reverse/oblique, 1.0 for reverse
HW =	Hanging wall flag (for dipping fault): 1 for sites on the hanging wall side but not off the end of the rupture, 0 otherwise

For the horizontal component, all of the models are for the average of the two horizontal components. All of the models that are presented are for 5% damping.

Sadigh et al. (1997)

$$\text{Ln Sa(g)} = c_1 + c_2M + c_3(8.5\text{-}M)^{2.5} + c_4 \text{Ln}(R_{rup}+\exp(c_5+c_6M)) + c_7 \text{Ln}(R_{rup}+2) + c_8F_1 \quad \text{(B-1)}$$

This functional form is used to develop models for both the vertical and horizontal components for rock sites. The coefficients for the horizontal component at rock sites are listed in Tables B-1a and B-1b and the coefficients for the vertical component at rock sties are listed in Tables B-1c and B-1d.

Idriss (1991,1994,1995)

The Idriss (1991) model provides attenuation equations for horizontal peak acceleration and response spectral values on rock. The standard deviations of the response spectral values were updated in Idriss (1994). The peak acceleration was updated in Idriss (1995) to reflect the new data from the 1992 Landers and 1994 Northridge earthquakes. These updates are used to modify the Idriss (1991) model.

The Idriss (1991) model is given by:

$$\text{Ln } Sa_{91}(g) = \alpha_o + \exp(\alpha_1+\alpha_2M) + [\beta_o - \exp(\beta_1+\beta_2M)] \text{Ln}(R_{rup}+c) + F_1\phi \quad \text{(B-2)}$$

The 1991 model is based on data up through the 1989 Loma Prieta earthquake. The peak acceleration model was updated to include the data through the 1994 Northridge earthquake (Idriss, 1995) for rock sites. The same functional form is used for the 1995 model. The coefficients for the horizontal component for rock sites are listed in Tables B-2a and B-2b.

The spectral accelerations can be estimated by using the 1991 spectral shape scaled by the 1995 peak acceleration:

$$Sa_{95}(T) = (Sa_{91}(T) / pga_{91}) \; pga_{95} \quad \text{(B-3)}$$

In addition to modifying the peak acceleration, the standard errors were also revised to reflect the larger variations in ground motions observed in earthquakes recordings since Loma Prieta (Idriss, 1994). The updated standard errors are listed in Table B-2a and B-2b.

Abrahamson and Silva (1997)

The Abrahamson and Silva model was developed using data up through the 1994 Northridge earthquake. The general functional form is given by:

$$\ln Sa(g) = f_1(m,R_{rup}) + F\, f_3(m) + HW\, f_4(m,R_{rup}) + S\, f_5(\widehat{pga}_{rock}) \qquad \text{(B-4)}$$

where S is a dummy variable for the site class (0 for rock or shallow soil, 1 for deep soil).

The basic attenuation for strike-slip and normal events at rock sites is given by:

$$f_1(m,r) = \begin{cases} a_1 + a_2(m-m_1) + a_{12}(8.5-m)^n + [a_3+a_{13}(m-m_1)] \ln(R) & \text{for } m \le m_1 \\ a_1 + a_4(m-m_1) + a_{12}(8.5-m)^n + [a_3+a_{13}(m-m_1)] \ln(R) & \text{for } m > m_1 \end{cases} \qquad \text{(B-5)}$$

where

$$R = \sqrt{R_{rup}^2 + c_4^2} \qquad \text{(B-6)}$$

The style-of-faulting factor is allowed to be magnitude and period dependent:

$$f_3(m) = \begin{cases} a_5 & \text{for } m \le 5.8 \\ a_5 + \dfrac{(a_6-a_5)}{m_1-5.8}(m-5.8) & \text{for } 5.8 < m < m_1 \\ a_6 & \text{for } m \ge m_1 \end{cases} \qquad \text{(B-7)}$$

The hanging wall effect for dipping faults is magnitude and distance dependence and is modeled as separable in magnitude and distance so that

$$f_4(m,r) = f_{HW}(m)\, f_{HW}(R_{rup}) \qquad \text{(B-8)}$$

where

$$f_{hw}(m) = \begin{cases} 0 & \text{for } m \le 5.5 \\ m-5.5 & \text{for } 5.5 < m < 6.5 \\ 1 & \text{for } m \ge 6.5 \end{cases} \qquad \text{(B-9)}$$

and

$$f_{hw}(R_{rup}) = \begin{cases} 0 & R_{rup}<4 \\ a_9(R_{rup}-4)/4 & 4 < R_{rup} < 8 \\ a_9 & 8 < R_{rup} < 18 \\ a_9(1-(R_{rup}-18)/7) & 18 < R_{rup} < 25 \\ 0 & 25 < R_{rup} \end{cases} \quad \text{(B-10)}$$

The standard error is allowed to be magnitude dependent and is modeled as follows:

$$\sigma(m) = \begin{cases} b_1 & \text{for } m \leq 5.0 \\ b_1 - b_2(m-5) & \text{for } 5.0 < m < 7.0 \\ b_1 - 2b_2 & \text{for } m \geq 7.0 \end{cases} \quad \text{(B-12)}$$

The coefficients for this model are listed in Tables B-3a, B-3b, and B-3c.

Directivity Effects Model

The empirical attenuation relations discussed above were developed for the average horizonal component without regard to the direction of rupture. Somerville et al (1997) developed an empirically based model quantifying the effects of rupture directivity on horizontal response spectra that can be used to scale the average horizontal component from attenuation relations. There are two effects of rupture directivity on long period response spectral values that are modeled by Somerville. First, there is an increase in the average horizontal component for cases of rupture coming toward the site and there is a decrease in the average horizontal motion for rupture running away from the site. Second, there is a systematic difference in the two horizontal components of motion when they are oriented parallel and perpendicular to the strike of the fault. At long periods, the fault normal component is larger than the fault parallel component. This increase in the fault normal component has also been studied by Geomatrix (1995).

In this project the a modified form of the Somerville et al. (1997) model has been used to characterize the two parts of the directivity effect.

Somerville et al (1997) Model

Somerville et al (1997) provides scale factors to account for directivity effects for the horizontal components. The Somerville et al model for the difference in the two horizontal components (fault normal and fault parallel) for strike-slip earthquakes is given by

$$\ln (FN/Ave\ H) = \cos(2\phi)\ [C_1 + C_2 \ln(R_{rup}+1) + C_3 (M-6)] \quad \text{(B-13)}$$

for M>6 and $\phi < 45$; it is zero otherwise. The coefficients for these models are listed in Table B-4b. This model is used without modification in this study.

Somerville et al also provides a model for the effect of rupture direction on the average horizontal component. This model was modified for use on this project as described below.

Modifications of the Somerville et al (1997) model

There are several aspects of the empirical model for the average horizontal component scale factors developed by Somerville et al that needed to be modified to make the model applicable to a probabilistic hazard analysis.

(A) Distance dependence

As published, the model is independent of distance. The data set used in the analysis includes recordings at distances of 0 to 50 km. A distance dependent taper function was applied to the model that reduces the effect to zero for distances greater than 60km.

$$T_d(r) = \begin{cases} 1 & \text{for } r < 30 \text{ km} \\ 1 - (r-30)/30 & \text{for } 30 \text{ km} < r < 60 \text{ km} \\ 0 & \text{for } r > 60 \text{ km} \end{cases} \qquad \text{(B-14)}$$

(B) Magnitude dependence

As published, the model is applicable to magnitudes greater than 6.5. A magnitude taper was applied that reduces the effect to zero for magnitudes less than 6.0.

$$T_m(m) = \begin{cases} 1 & \text{for } m \geq 6.5 \\ 1 - (m-6.5)/0.5 & \text{for } 6 \leq m < 6.5 \\ 0 & \text{for } m < 6 \end{cases} \qquad \text{(B-15)}$$

(C) Saturation With x cos(θ)

The empirical model uses a form that increases a constant rate as x increases from 0 to 1. There is little empirical data with x cos(θ) values greater than 0.6, particularly for rupture distances less than 20 km. The short distance data suggest that there may be a saturation of the directivity effect as a function of x cos(θ).The extrapolation of the model to larger x cos(θ) values is not well constrained. To evaluate this extrapolation, three separate groups applied their seismological numerical modeling methods to generate synthetic time histories for a range of x cos(θ) values. The numerical modeling results indicated that the directivity effect saturates for x cos(θ) > 0.4, As a result, the functional form of the directivity model was changed to include saturation with x cos(θ). The coefficients of the model were based on the empirical data, and not on the synthetics.

Based on the trends in the numerical simulations, the form of the directivity function is modified to reach a maximum at x cos(θ) =0.4. The model was developed for a spectral

period of 3 seconds because this is an important period for the bridge. The slope is greater than the Somerville model, but it flattens out at a lower level . The hazard calculation is sensitive to the model values at large x cos(θ) (greater than 0.9) so this change results in a reduction of the ground motion.

The T=3 second value is used to guide the adjustment of the model at all periods. The resulting model is given by

$$y_{Dir}(x,\theta,T) = \begin{cases} C_1(T) + 1.88\, C_2(T)\, x \cos(\theta) & \text{for } x\cos(\theta) \le 0.4 \\ C_1(T) + 0.75\, C_2(T) & \text{for } x\cos(\theta) > 0.4 \end{cases} \quad \text{(B-15)}$$

where $C_1(T) + C_2(T)$ are from Somerville et al and are listed in Table A-4a.

(D) Reduction of the Standard Deviation

Including the directivity effect should results in a reduction of the standard deviation of the attenuation relation. The standard deviation of the data < 20 km including the directivity was compared to the standard deviation of the published model. At T=3 seconds, there is a reduction of about 0.05 natural log units. The period dependence of the reduction is approximated by the period dependence of the slope of the directivity effect. To account for the reduction in the standard deviation due to including the directivity effect as part of the model, the standard deviations for the published attenuation relations were modified for use in the hazard analysis using the following relation:

$$\sigma'(M,T) = \sigma(M,T) - 0.05\, C_2(T)/1.333 \quad \text{(B-16)}$$

where $C_2(T)$ is given in Table B-4a.

Final Directivity Model

The following model is used for the average horizontal component for strike-slip faults

$$\ln Sa_{dir}(M,r,x,\theta,T) = \ln Sa(M,r) + y_{Dir}(x,\theta,T)\, T_d(r)\, T_m(m) \qquad \text{(B-16)}$$

where Sa(M,r) is an empirical attenuation relation without directivity.

Table B-1a. Sadigh et al. (1997) Coefficients for M ≥ 6.5
Rock, Average Horizontal

period	c1	c2	c3	c4	c5	c6	c7	c8	sigma M<7	sigma M≥7
0.000	-1.274	1.1	0.000	-2.100	-0.48451	0.524	0.000	0.18	1.39-0.14M	0.38
0.050	-0.740	1.1	0.006	-2.128	-0.48451	0.524	-0.082	0.18	1.39-0.14M	0.38
0.070	-0.540	1.1	0.006	-2.128	-0.48451	0.524	-0.082	0.18	1.40-0.14M	0.39
0.090	-0.438	1.1	0.006	-2.140	-0.48451	0.524	-0.052	0.18	1.40-0.14M	0.39
0.100	-0.375	1.1	0.006	-2.148	-0.48451	0.524	-0.041	0.18	1.41-0.14M	0.40
0.120	-0.302	1.1	0.005	-2.162	-0.48451	0.524	-0.014	0.18	1.41-0.14M	0.40
0.140	-0.343	1.1	0.004	-2.144	-0.48451	0.524	0.000	0.18	1.42-0.14M	0.41
0.150	-0.365	1.1	0.002	-2.130	-0.48451	0.524	0.000	0.18	1.42-0.14M	0.41
0.170	-0.411	1.1	0.000	-2.110	-0.48451	0.524	0.000	0.18	1.42-0.14M	0.41
0.200	-0.497	1.1	-0.004	-2.080	-0.48451	0.524	0.000	0.18	1.43-0.14M	0.42
0.240	-0.590	1.1	-0.011	-2.053	-0.48451	0.524	0.000	0.18	1.44-0.14M	0.43
0.300	-0.707	1.1	-0.017	-2.028	-0.48451	0.524	0.000	0.18	1.45-0.14M	0.44
0.400	-0.948	1.1	-0.028	-1.990	-0.48451	0.524	0.000	0.18	1.48-0.14M	0.47
0.500	-1.238	1.1	-0.040	-1.945	-0.48451	0.524	0.000	0.18	1.50-0.14M	0.49
0.750	-1.858	1.1	-0.050	-1.865	-0.48451	0.524	0.000	0.18	1.52-0.14M	0.51
1.000	-2.355	1.1	-0.055	-1.800	-0.48451	0.524	0.000	0.18	1.53-0.14M	0.52
1.500	-3.057	1.1	-0.065	-1.725	-0.48451	0.524	0.000	0.18	1.53-0.14M	0.52
2.000	-3.595	1.1	-0.070	-1.670	-0.48451	0.524	0.000	0.18	1.53-0.14M	0.52
3.000	-4.350	1.1	-0.080	-1.615	-0.48451	0.524	0.000	0.18	1.53-0.14M	0.52
4.000	-4.880	1.1	-0.100	-1.570	-0.48451	0.524	0.000	0.18	1.53-0.14M	0.52
5.000	-5.364	1.1	-0.100	-1.540	-0.48451	0.524	0.000	0.18	1.53-0.14M	0.52
7.500	-6.180	1.1	-0.110	-1.510	-0.48451	0.524	0.000	0.18	1.53-0.14M	0.52

Table B-1b. Sadigh et al. (1997) Coefficients for M < 6.5
Rock, Average Horizontal

period	c1	c2	c3	c4	c5	c6	c7	c8	sigma
0.000	-0.624	1.0	0.000	-2.100	1.29649	0.25	0.000	0.18	1.39-0.14M
0.050	-0.090	1.0	0.006	-2.128	1.29649	0.25	-0.082	0.18	1.39-0.14M
0.070	0.110	1.0	0.006	-2.128	1.29649	0.25	-0.082	0.18	1.40-0.14M
0.090	0.212	1.0	0.006	-2.140	1.29649	0.25	-0.052	0.18	1.40-0.14M
0.100	0.275	1.0	0.006	-2.148	1.29649	0.25	-0.041	0.18	1.41-0.14M
0.120	0.348	1.0	0.005	-2.162	1.29649	0.25	-0.014	0.18	1.41-0.14M
0.140	0.307	1.0	0.004	-2.144	1.29649	0.25	0.000	0.18	1.42-0.14M
0.150	0.285	1.0	0.002	-2.130	1.29649	0.25	0.000	0.18	1.42-0.14M
0.170	0.239	1.0	0.000	-2.110	1.29649	0.25	0.000	0.18	1.42-0.14M
0.200	0.153	1.0	-0.004	-2.080	1.29649	0.25	0.000	0.18	1.43-0.14M
0.240	0.060	1.0	-0.011	-2.053	1.29649	0.25	0.000	0.18	1.44-0.14M
0.300	-0.057	1.0	-0.017	-2.028	1.29649	0.25	0.000	0.18	1.45-0.14M
0.400	-0.298	1.0	-0.028	-1.990	1.29649	0.25	0.000	0.18	1.48-0.14M
0.500	-0.588	1.0	-0.040	-1.945	1.29649	0.25	0.000	0.18	1.50-0.14M
0.750	-1.208	1.0	-0.050	-1.865	1.29649	0.25	0.000	0.18	1.52-0.14M
1.000	-1.705	1.0	-0.055	-1.800	1.29649	0.25	0.000	0.18	1.53-0.14M
1.500	-2.407	1.0	-0.065	-1.725	1.29649	0.25	0.000	0.18	1.53-0.14M
2.000	-2.945	1.0	-0.070	-1.670	1.29649	0.25	0.000	0.18	1.53-0.14M
3.000	-3.700	1.0	-0.080	-1.615	1.29649	0.25	0.000	0.18	1.53-0.14M
4.000	-4.230	1.0	-0.100	-1.570	1.29649	0.25	0.000	0.18	1.53-0.14M
5.000	-4.714	1.0	-0.100	-1.540	1.29649	0.25	0.000	0.18	1.53-0.14M
7.500	-5.530	1.0	-0.110	-1.510	1.29649	0.25	0.000	0.18	1.53-0.14M

Table B-1c. Sadigh et al. (1993) Coefficients (M≥6.5)
Vertical

period	c1	c3	c4	c5	c6	c7	c8	sigma
0.00	-1.0800	0.00000	-2.300	-0.3524	0.478	0	0.095	0.48
0.04	-0.3121	0.00000	-2.450	-0.3524	0.478	0	0.095	0.57
0.05	-0.1459	0.00000	-2.450	-0.3524	0.478	0	0.095	0.57
0.07	0.0396	0.00000	-2.450	-0.3524	0.478	0	0.095	0.57
0.09	0.0218	-0.00330	-2.420	-0.3524	0.478	0	0.095	0.57
0.10	-0.0248	-0.00468	-2.400	-0.3524	0.478	0	0.095	0.57
0.12	-0.0965	-0.00707	-2.380	-0.3524	0.478	0	0.095	0.57
0.14	-0.2687	-0.00909	-2.333	-0.3524	0.478	0	0.095	0.57
0.15	-0.3976	-0.01000	-2.300	-0.3524	0.478	0	0.095	0.57
0.17	-0.6378	-0.01462	-2.241	-0.3524	0.478	0	0.095	0.57
0.20	-0.9505	-0.02061	-2.164	-0.3524	0.478	0	0.095	0.57
0.24	-1.3178	-0.02734	-2.077	-0.3524	0.478	0	0.095	0.57
0.30	-1.7893	-0.03558	-1.971	-0.3524	0.478	0	0.095	0.57
0.40	-2.4157	-0.04619	-1.835	-0.3524	0.478	0	0.095	0.57
0.50	-2.9248	-0.05442	-1.729	-0.3524	0.478	0	0.095	0.57
0.75	-3.8562	-0.06939	-1.536	-0.3524	0.478	0	0.095	0.57
1.00	-4.5318	-0.08000	-1.400	-0.3524	0.478	0	0.095	0.57
1.50	-4.9118	-0.08554	-1.400	-0.3524	0.478	0	0.095	0.57
2.00	-5.2219	-0.08946	-1.400	-0.3524	0.478	0	0.095	0.57
2.50	-5.4667	-0.09251	-1.400	-0.3524	0.478	0	0.095	0.57
3.00	-5.6864	-0.09500	-1.400	-0.3524	0.478	0	0.095	0.57

Table B-1d. Sadigh et al. (1993) Coefficients (M<6.5)

Vertical

period	c1	c3	c4	c5	c6	c7	c8	sigma (M>6)	sigma (M≤6)
0	-0.624	0.000	-2.100	1.276	0.228	0.000	0.095	0.68	3.08 - 0.40M
0.05	-0.090	0.006	-2.128	1.276	0.228	-0.082	0.095	0.75	2.91 - 0.36M
0.07	0.110	0.006	-2.128	1.276	0.228	-0.082	0.095	0.75	2.91 - 0.36M
0.09	0.212	0.006	-2.140	1.276	0.228	-0.052	0.095	0.75	2.91 - 0.36M
0.1	0.275	0.006	-2.148	1.276	0.228	-0.041	0.095	0.75	2.91 - 0.36M
0.12	0.348	0.005	-2.162	1.276	0.228	-0.014	0.095	0.75	2.91 - 0.36M
0.14	0.307	0.004	-2.144	1.276	0.228	0.000	0.095	0.75	2.91 - 0.36M
0.15	0.285	0.002	-2.130	1.276	0.228	0.000	0.095	0.75	2.91 - 0.36M
0.17	0.239	0.000	-2.110	1.276	0.228	0.000	0.095	0.75	2.91 - 0.36M
0.2	0.153	-0.004	-2.080	1.276	0.228	0.000	0.095	0.75	2.91 - 0.36M
0.24	0.060	-0.011	-2.053	1.276	0.228	0.000	0.095	0.75	2.91 - 0.36M
0.3	-0.057	-0.017	-2.028	1.276	0.228	0.000	0.095	0.75	2.91 - 0.36M
0.4	-0.298	-0.028	-1.990	1.276	0.228	0.000	0.095	0.75	2.91 - 0.36M
0.5	-0.588	-0.040	-1.945	1.276	0.228	0.000	0.095	0.75	2.91 - 0.36M
0.75	-1.208	-0.050	-1.865	1.276	0.228	0.000	0.095	0.75	2.91 - 0.36M
1	-1.705	-0.055	-1.800	1.276	0.228	0.000	0.095	0.75	2.91 - 0.36M
1.5	-2.407	-0.065	-1.725	1.276	0.228	0.000	0.095	0.75	2.91 - 0.36M
2	-2.945	-0.070	-1.670	1.276	0.228	0.000	0.095	0.75	2.91 - 0.36M
2.5				1.276	0.228	0.000	0.095	0.75	2.91 - 0.36M
3	-3.700	-0.080	-1.615	1.276	0.228	0.000	0.095	0.75	2.91 - 0.36M

Table B-2a. Idriss (1991;1994,1995) Coefficients for M ≥ 6.0
Rock, Average Horizontal

period	a0	a1	a2	b0	b1	b2	c	ϕ	Sigma M<7.25	Sigma M≥7.25
PGA 94	0	2.763	-0.262	0.000	2.215	-0.288	10	0.28	1.29 - 0.12M	0.42
PGA 91	-0.050	3.477	-0.284	0.000	2.475	-0.286	20	0.20		
0.030	-0.050	3.477	-0.284	0.000	2.475	-0.286	20	0.20	1.29 - 0.12M	0.42
0.050	-0.278	3.426	-0.269	0.066	2.475	-0.286	20	0.20	1.29 - 0.12M	0.42
0.075	-0.308	3.359	-0.252	0.070	2.475	-0.286	20	0.20	1.29 - 0.12M	0.42
0.100	-0.318	3.327	-0.243	0.072	2.475	-0.286	20	0.20	1.32 - 0.12M	0.45
0.110	-0.328	3.289	-0.236	0.073	2.475	-0.286	20	0.20	1.33 - 0.12M	0.46
0.130	-0.338	3.233	-0.225	0.075	2.475	-0.286	20	0.20	1.34 - 0.12M	0.47
0.150	-0.348	3.185	-0.216	0.076	2.475	-0.286	20	0.20	1.35 - 0.12M	0.48
0.200	-0.358	3.100	-0.201	0.078	2.475	-0.286	20	0.20	1.37 - 0.12M	0.50
0.250	-0.429	3.034	-0.190	0.080	2.475	-0.286	20	0.20	1.38 - 0.12M	0.51
0.300	-0.486	2.982	-0.182	0.082	2.475	-0.286	20	0.20	1.39 - 0.12M	0.52
0.350	-0.535	2.943	-0.177	0.087	2.475	-0.286	20	0.20	1.40 - 0.12M	0.53
0.400	-0.577	2.906	-0.173	0.092	2.475	-0.286	20	0.20	1.41 - 0.12M	0.54
0.500	-0.648	2.850	-0.169	0.099	2.475	-0.286	20	0.20	1.42 - 0.12M	0.55
0.600	-0.705	2.803	-0.166	0.105	2.475	-0.286	20	0.20	1.43 - 0.12M	0.56
0.700	-0.754	2.765	-0.165	0.111	2.475	-0.286	20	0.20	1.44 - 0.12M	0.57
0.800	-0.796	2.728	-0.164	0.115	2.475	-0.286	20	0.20	1.45 - 0.12M	0.58
0.900	-0.834	2.694	-0.163	0.119	2.475	-0.286	20	0.20	1.46 - 0.12M	0.59
1.000	-0.867	2.662	-0.162	0.123	2.475	-0.286	20	0.20	1.47 - 0.12M	0.60
1.500	-0.970	2.536	-0.160	0.136	2.475	-0.286	20	0.20	1.47 - 0.12M	0.60
2.000	-1.046	2.447	-0.160	0.146	2.475	-0.286	20	0.20	1.47 - 0.12M	0.60
3.000	-1.143	2.295	-0.159	0.160	2.475	-0.286	20	0.20	1.47 - 0.12M	0.60
4.000	-1.177	2.169	-0.159	0.169	2.475	-0.286	20	0.20	1.47 - 0.12M	0.60
5.000	-1.214	2.042	-0.157	0.177	2.475	-0.286	20	0.20	1.47 - 0.12M	0.60

Table B-2b. Idriss (1991;1994,1995) Coefficients for M < 6.0
Rock, Average Horizontal

period	a0	a1	a2	b0	b1	b2	c	f	Sigma
PGA 94	0	1.127	0.011	0.000	1.126	-0.106	10	0.28	1.29 - 0.12M
PGA 91	-0.150	2.261	-0.083	0.000	1.602	-0.142	20	0.20	
0.030	-0.150	2.261	-0.083	0.000	1.602	-0.142	20	0.20	1.29 - 0.12M
0.050	-0.278	2.365	-0.092	0.066	1.602	-0.142	20	0.20	1.29 - 0.12M
0.075	-0.308	2.334	-0.081	0.070	1.602	-0.142	20	0.20	1.29 - 0.12M
0.100	-0.318	2.319	-0.075	0.072	1.602	-0.142	20	0.20	1.32 - 0.12M
0.110	-0.328	2.294	-0.070	0.073	1.602	-0.142	20	0.20	1.33 - 0.12M
0.130	-0.338	2.255	-0.062	0.075	1.602	-0.142	20	0.20	1.34 - 0.12M
0.150	-0.348	2.219	-0.055	0.076	1.602	-0.142	20	0.20	1.35 - 0.12M
0.200	-0.358	2.146	-0.042	0.078	1.602	-0.142	20	0.20	1.37 - 0.12M
0.250	-0.429	2.073	-0.030	0.080	1.602	-0.142	20	0.20	1.38 - 0.12M
0.300	-0.486	2.010	-0.020	0.082	1.602	-0.142	20	0.20	1.39 - 0.12M
0.350	-0.535	1.977	-0.016	0.087	1.602	-0.142	20	0.20	1.40 - 0.12M
0.400	-0.577	1.921	-0.009	0.092	1.602	-0.142	20	0.20	1.41 - 0.12M
0.500	-0.648	1.818	0.003	0.099	1.602	-0.142	20	0.20	1.42 - 0.12M
0.600	-0.705	1.704	0.017	0.105	1.602	-0.142	20	0.20	1.43 - 0.12M
0.700	-0.754	1.644	0.022	0.111	1.602	-0.142	20	0.20	1.44 - 0.12M
0.800	-0.796	1.593	0.025	0.115	1.602	-0.142	20	0.20	1.45 - 0.12M
0.900	-0.834	1.482	0.039	0.119	1.602	-0.142	20	0.20	1.46 - 0.12M
1.000	-0.867	1.432	0.043	0.123	1.602	-0.142	20	0.20	1.47 - 0.12M
1.500	-0.970	1.072	0.084	0.136	1.602	-0.142	20	0.20	1.47 - 0.12M
2.000	-1.046	0.762	0.121	0.146	1.602	-0.142	20	0.20	1.47 - 0.12M
3.000	-1.143	0.194	0.191	0.160	1.602	-0.142	20	0.20	1.47 - 0.12M
4.000	-1.177	-0.466	0.280	0.169	1.602	-0.142	20	0.20	1.47 - 0.12M
5.000	-1.214	-1.361	0.410	0.177	1.602	-0.142	20	0.20	1.47 - 0.12M

Table B-3a. Abrahamson and Silva (1997) Coefficients
Average Horizontal Component

period	c4	a1	a2	a3	a4	a5	a6	a9	a10	a11	a12	a13
5.0	3.50	-1.460	0.512	-0.7250	-0.144	0.400	-0.200	0.000	0.664	0.040	-0.2150	0.17
4.0	3.50	-1.130	0.512	-0.7250	-0.144	0.400	-0.200	0.039	0.640	0.040	-0.1956	0.17
3.0	3.50	-0.690	0.512	-0.7250	-0.144	0.400	-0.156	0.089	0.630	0.040	-0.1726	0.17
2.0	3.50	-0.150	0.512	-0.7250	-0.144	0.400	-0.094	0.160	0.610	0.040	-0.1400	0.17
1.5	3.55	0.260	0.512	-0.7721	-0.144	0.438	-0.049	0.210	0.600	0.040	-0.1200	0.17
1.0	3.70	0.828	0.512	-0.8383	-0.144	0.490	0.013	0.281	0.423	0.000	-0.1020	0.17
0.85	3.81	1.020	0.512	-0.8648	-0.144	0.512	0.038	0.309	0.370	-0.028	-0.0927	0.17
0.75	3.90	1.160	0.512	-0.8852	-0.144	0.528	0.057	0.331	0.320	-0.050	-0.0862	0.17
0.60	4.12	1.428	0.512	-0.9218	-0.144	0.557	0.091	0.370	0.194	-0.089	-0.0740	0.17
0.50	4.30	1.615	0.512	-0.9515	-0.144	0.581	0.119	0.370	0.085	-0.121	-0.0635	0.17
0.46	4.38	1.717	0.512	-0.9652	-0.144	0.592	0.132	0.370	0.020	-0.136	-0.0594	0.17
0.40	4.52	1.860	0.512	-0.9880	-0.144	0.610	0.154	0.370	-0.065	-0.160	-0.0518	0.17
0.36	4.62	1.955	0.512	-1.0052	-0.144	0.610	0.170	0.370	-0.123	-0.173	-0.0460	0.17
0.30	4.80	2.114	0.512	-1.0350	-0.144	0.610	0.198	0.370	-0.219	-0.195	-0.0360	0.17
0.24	4.97	2.293	0.512	-1.0790	-0.144	0.610	0.232	0.370	-0.350	-0.223	-0.0238	0.17
0.20	5.10	2.406	0.512	-1.1150	-0.144	0.610	0.260	0.370	-0.445	-0.245	-0.0138	0.17
0.17	5.20	2.430	0.512	-1.1350	-0.144	0.610	0.260	0.370	-0.522	-0.265	-0.0040	0.17
0.15	5.27	2.407	0.512	-1.1450	-0.144	0.610	0.260	0.370	-0.577	-0.280	0.0050	0.17
0.12	5.39	2.272	0.512	-1.1450	-0.144	0.610	0.260	0.370	-0.591	-0.280	0.0180	0.17
0.10	5.50	2.160	0.512	-1.1450	-0.144	0.610	0.260	0.370	-0.598	-0.280	0.0280	0.17
0.09	5.54	2.100	0.512	-1.1450	-0.144	0.610	0.260	0.370	-0.609	-0.280	0.0300	0.17
0.075	5.58	2.037	0.512	-1.1450	-0.144	0.610	0.260	0.370	-0.628	-0.280	0.0300	0.17
0.06	5.60	1.940	0.512	-1.1450	-0.144	0.610	0.260	0.370	-0.665	-0.280	0.0300	0.17
0.05	5.60	1.870	0.512	-1.1450	-0.144	0.610	0.260	0.370	-0.620	-0.267	0.0280	0.17
0.04	5.60	1.780	0.512	-1.1450	-0.144	0.610	0.260	0.370	-0.555	-0.251	0.0245	0.17
0.03	5.60	1.690	0.512	-1.1450	-0.144	0.610	0.260	0.370	-0.470	-0.230	0.0143	0.17

0.02	5.60	1.640	0.512	-1.1450	-0.144	0.610	0.260	0.370	-0.417	-0.230	0.0000	0.17
0.00	5.60	1.640	0.512	-1.1450	-0.144	0.610	0.260	0.370	-0.417	-0.230	0.0000	0.17

For all Periods:

m1 = 6.4, c5 = 0.03, n=2.0

Table B-3b. Abrahamson and Silva (1997) Coefficients
Vertical Component

period	c4	a1	a2	a3	a4	a5	a6	a9	a10	a11	a12	a13
0.010	6.00	1.642	0.909	-1.252	0.275	0.390	-0.050	0.63	-0.140	-0.22	0.00	0.06
0.030	6.00	2.100	0.909	-1.317	0.275	0.432	-0.050	0.63	-0.140	-0.22	0.00	0.06
0.050	6.00	2.620	0.909	-1.370	0.275	0.496	-0.050	0.63	-0.140	-0.22	0.00	0.06
0.075	6.00	2.750	0.909	-1.370	0.275	0.545	-0.050	0.63	-0.129	-0.22	0.00	0.06
0.100	6.00	2.700	0.909	-1.370	0.275	0.580	-0.050	0.63	-0.114	-0.22	0.00	0.06
0.120	6.00	2.480	0.909	-1.299	0.275	0.580	-0.017	0.63	-0.104	-0.22	0.00	0.06
0.150	6.00	2.170	0.909	-1.211	0.275	0.580	0.024	0.63	-0.093	-0.22	0.00	0.06
0.170	5.72	1.960	0.909	-1.162	0.275	0.580	0.047	0.60	-0.087	-0.22	0.00	0.06
0.200	5.34	1.688	0.909	-1.099	0.275	0.580	0.076	0.57	-0.078	-0.22	0.00	0.06
0.240	4.93	1.362	0.909	-1.027	0.275	0.580	0.109	0.53	-0.069	-0.22	0.00	0.06
0.300	4.42	0.973	0.909	-0.940	0.275	0.580	0.150	0.49	-0.057	-0.22	0.00	0.06
0.400	3.77	0.591	0.909	-0.878	0.275	0.539	0.150	0.43	-0.043	-0.22	-0.01	0.06
0.500	3.26	0.282	0.909	-0.829	0.275	0.471	0.150	0.38	-0.031	-0.22	-0.01	0.06
0.750	2.50	-0.253	0.909	-0.749	0.275	0.348	0.150	0.30	-0.010	-0.22	-0.01	0.06
1.000	2.50	-0.531	0.909	-0.740	0.275	0.260	0.150	0.24	0.004	-0.22	-0.01	0.06
1.500	2.50	-0.966	0.909	-0.729	0.275	0.260	0.058	0.24	0.025	-0.22	-0.02	0.06
2.000	2.50	-1.294	0.909	-0.720	0.275	0.260	-0.008	0.24	0.040	-0.22	-0.02	0.06
3.000	2.50	-1.745	0.909	-0.720	0.275	0.260	-0.100	0.24	0.040	-0.22	-0.04	0.06
4.000	2.50	-2.151	0.909	-0.720	0.275	0.260	-0.100	0.24	0.040	-0.22	-0.05	0.06
5.000	2.50	-2.447	0.909	-0.720	0.275	0.260	-0.100	0.24	0.040	-0.22	-0.06	0.06

For all Periods:

m1 = 6.4, c5 = 0.3, n=3.0

Table B-3c. Coefficients for the Standard Errors for the Abrahamson and Silva (1997) Attenuation Relation.

Period (Sec)	Horizontal		Vertical	
	b1	b2	b1	b2
0.010	0.700	0.135	0.760	0.085
0.030	0.700	0.135	0.760	0.085
0.050	0.713	0.135	0.760	0.085
0.075	0.728	0.135	0.760	0.085
0.100	0.739	0.135	0.760	0.085
0.120	0.746	0.135	0.740	0.075
0.150	0.754	0.135	0.720	0.063
0.170	0.759	0.135	0.700	0.056
0.200	0.765	0.135	0.690	0.050
0.240	0.772	0.135	0.690	0.050
0.300	0.780	0.135	0.690	0.050
0.400	0.791	0.135	0.690	0.050
0.500	0.799	0.130	0.690	0.050
0.750	0.814	0.123	0.690	0.050
1.000	0.825	0.118	0.690	0.050
1.500	0.840	0.110	0.690	0.050
2.000	0.851	0.105	0.690	0.050
3.000	0.866	0.097	0.720	0.050
4.000	0.877	0.092	0.750	0.050
5.000	0.885	0.087	0.780	0.050

Table B-4a. Model Coefficients for the modified Somerville et al. (1997) Directivity Effects for the Average Horizontal Component

Period (sec)	C1	C2
0.60	0.000	0.000
0.75	-0.084	0.185
1.00	-0.192	0.423
1.50	-0.344	0.759
2.00	-0.452	0.998
3.00	-0.605	1.333
4.00	-0.713	1.571
5.00	-0.797	1.757

Table B-4b. Model Coefficients for Somerville et al. (1997) Directivity effects for the Fault Normal / Average Horizontal Component

Period (sec)	C1	C2	C3
0.60	0.000	0.000	0.000
0.75	0.061	-0.0155	0.000
1.00	0.104	-0.0255	0.000
1.50	0.164	-0.0490	0.034
2.00	0.207	-0.0613	0.059
3.00	0.353	-0.1007	0.093
4.00	0.456	-0.1282	0.118
5.00	0.450	-0.1269	0.137

APPENDIX C
NON-STATIONARY SPECTRAL MATCHING PROGRAM RSPMATCH

Appendix C

Non-Stationary Spectral Matching Program RSPMATCH

Introduction

Various methods have been developed to modify a reference time history so that its response spectrum is compatible with a specified target spectrum. A review of spectral matching methods is given by Preumont (1984). A commonly used method adjusts the Fourier amplitude spectrum based on the ratio of the target response spectrum to the time history response spectrum while keeping the Fourier phase of the reference time history fixed. While this approach is straight-forward, it has two drawbacks. First, it generally does not have good convergence properties, particularly for multiple damping spectra. Second, it can alter the non-stationary character of the time history if the shape of the Fourier amplitude spectrum is changed significantly.

An alternative approach for spectral matching adjusts the time history in the time domain by adding wavelets to the reference time history. A formal optimization procedure for this type of time domain spectral matching was first proposed by Kaul (1978) and was extended to simultaneously match spectra at multiple damping values by Lilhanand and Tseng (1987, 1988). While this procedure is more complicated than the frequency domain approach, it has good convergence properties and in most cases preserves the non-stationary character of the reference time history.

The computer program, RSPMATCH, implements the Lilhanand and Tseng algorithm with some modifications that help preserve the non-stationary

character of the reference ground motion for a wider range of time histories. The methodology of this method is described in this appendix.

Methodology

Usually, response spectra studies are only concerned with the maximum response of the oscillator; however, for the time domain methods, the time and polarity of the peak response must also be considered. I will refer to the *response* to indicate the oscillator time history, not just its maximum value.

Let a(t) be the reference time history and Q_i be the target spectral value for frequency ω_i and damping β_i. Also let R_i be the absolute value of the peak response, t_i be the time of the peak response, and P_i be the polarity of the peak response ($P_i = 1$ if the maximum response is positive and $P_i = -1$ if the maximum response is negative). The difference between the target spectrum and the computed spectrum is given by

$$\Delta R_i = (Q_i - R_i)\, P_i \qquad \text{(C-1)}$$

where ΔR_i is the spectral misfit which includes the polarity of the response.

Assuming that the time of the peak response of a(t) will not be perturbed by adding a small adjustment to a(t), the basic method is to determine an adjustment time history, $\delta a(t)$, such that the response of $\delta a(t)$ at time t_i is equal to ΔR_i for all i. Let

$$\delta a(t) = \sum_{j=1}^{N} b_j\, f_j(t) \qquad \text{(C-2)}$$

where $f_j(t)$ is a set of adjustment functions, b_j is the set of coefficients to be determined, and N is the number of spectral points (frequency and damping pairs) to match. A restriction on $f_j(t)$ is that $f_j(t) = 0$ for $t<0$. The acceleration response of $\delta a(t)$ for frequency ω_i and damping β_i at time t_i is given by

$$\delta R_i = \int_0^\infty \delta a(\tau)\, h_i(t_i-\tau)\, d\tau \qquad \text{(C-3)}$$

where $h_i(t)$ is the acceleration impulse response of the oscillator for frequency ω_i and damping β_i. Substituting Eq. (C-2) into Eq. (C-3) gives

$$\delta R_i = \sum_{j=1}^{N} b_j \int_0^\infty f_j(\tau)\, h_i(t_i-\tau)\, d\tau\,. \qquad \text{(C-4)}$$

The acceleration impulse response is given by

$$h_i(t) = \frac{-\omega_i}{\sqrt{1-\beta_i^2}} \exp(-\omega_i\beta_i t)\, [\, (2\beta_i^2-1)\, \sin(\omega_i' t) - 2\beta_i\sqrt{1-\beta_i^2}\, \cos(\omega_i' t)\,] \qquad \text{(C-5)}$$

where

$$\omega_i' = \omega_i \sqrt{1-\beta_i^2} \qquad \text{(C-6)}$$

and $h_i(t) = 0$ for $t<0$.

Next let c_{ij} be the response at time t_i for the ith frequency and damping resulting from the motion $f_j(t)$:

$$c_{ij} = \int_0^{t_i} f_j(\tau)\, h_i(t_i-\tau)\, d\tau \qquad \text{(C-7)}$$

(the upper limit of the integral is t_i because $h_i(t) = 0$ for $t<0$). Substituting Eq. (C-7) into Eq. (C-4) gives

$$\delta R_i = \sum_{j=1}^{N} b_j\, c_{ij} \qquad \text{(C-8)}$$

If the response of the adjustment time history, δR_i, is equal to the spectral misfit, ΔR_i, then

$$\Delta R_i = \sum_{j=1}^{N} b_j\, c_{ij} \qquad \text{(C-9)}$$

Given the spectral misfits, ΔR_i, and the response coefficients c_{ij}, Eq. (C-9) can be solved for the coefficients b_j. In matrix notation, the solution is simply

$$\mathbf{b} = \mathbf{C}^{-1}\, \delta\mathbf{R} \qquad \text{(C-10)}$$

Given, the b_j, the adjustment time history, $\delta a(t)$, can be computed by Eq. (C-2). The adjusted time history for the first iteration is given by

$$a_1(t) = a_o(t) + \gamma\, \delta a(t) \qquad \text{(C-11)}$$

where γ is a relaxation parameter (between 0 and 1) to damp the adjustments. The algorithm is repeated using the adjusted time history until the desired spectral match is achieved.

Selection of the adjustment function

The key to the non-stationarity of the method is the selection of the adjustment function $f_j(t)$. The selection of the form of the adjustment function, $f_j(t)$, is where the seismological considerations enter the problem. What sort of adjustments can be made and yet still yield realistic seismograms? In considering the forms of $f_j(t)$, we need to also consider the numerical stability of the algorithm.

For the method to work efficiently, the timing of $f_j(t)$ should be such that the response of $f_j(t)$ is in phase with the peak response of a(t). For numerical speed, $f_j(t)$ should be chosen so that the elements of **C** given by the integral in Eq. (C-7) can be computed analytically. For numerical stability, the off-diagonal terms of **C** should be as small as possible.

As mentioned earlier, in the frequency domain approach, only the Fourier amplitude spectrum is modified. This is equivalent to using

$$f_j(t) = \cos(\omega_j' t + \theta_j) \qquad \text{(C-12)}$$

where θ_j is the Fourier phase of the reference time history (Figures C-1 and C-2, lower plots). The adjustments are computed from the ratio of the computed response to the target response which is equivalent to using $\mathbf{b}=\delta\mathbf{R}$. The poor convergence of this method results from the simplified estimation of **b** which

ignores the cross-terms in the **C** matrix (e.g. it is equivalent to assuming that **C** is the identity matrix). In addition, the timing of f_j may not be in phase with the peak response of a(t).

In the Lilhanand and Tseng algorithm, $f_j(t)$ is given by

$$f_j(t) = h_j(t_j - t) \tag{13}$$

which is just the oscillator impulse response in reverse time order. Since h(t)=0 for t<0, this form is one-sided as shown in Figures C-1 and C-2 (middle plot). This is called adjustment function model 1 in Appendix D. There are several numerical aspects that make this function attractive. First, it leads to a symmetric C matrix. Second, the abrupt stop insures that the response will peak at time t_i and not resonate to larger values at greater values of t for all damping values. At high frequencies, the f_i has a short duration, but at short frequencies f_i has a long duration.

From a seismological point of view, this form of the adjustment function has some undesirable features, particularly at long periods. The adjustment is emergent and stops abruptly. This is contrary to the behavior of strong motion time histories that generally have a sharp initiation and gradual decay. Forcing the long period adjustment early in the time history can lead to unrealistic ground motions if the long period response peaks early in the record as can be the case for near-fault recordings (dist < 5 km).

As an alternative, a tapered cosine wave can be used for the adjustment function:

$$f_j(t) = \cos\{\omega_j(t-t_j+\Delta t_j)\} \exp\{-|t-t_j+\Delta t_j| \alpha_j\} \qquad \text{(C-14)}$$

where Δt is the time delay between the maximum of $f_j(t)$ and a peak in the response of $f_j(t)$. This function is shown in the top plot of Figures C-1 and C-2. This is called adjustment function model 6 in Appendix D. The α term controls the time duration of $f_j(t)$. The frequency dependence of α can be estimated from the reference time history which helps to preserve the non-stationary character of the reference time history. That is, if the reference time history has a short duration at a particular frequency, the α should be selected such that the adjustment function at that frequency will also have a short duration. The model for a(f) used here is given by

$$\alpha(f) = \begin{cases} a_1 & \text{for } f < f_1 \\ a_1 + (a_2-a_1)\dfrac{(f-f_1)}{(f_2-f_1)} & \text{for } f_1 < f < f_2 \\ a_2 & \text{for } f > f_2 \end{cases}$$

The values of a(f) used in this project are shown in Figure C-3.

Numerical Aspects

Conceptually, the time domain spectral matching method appears straight-forward; however, there are some numerical difficulties. The C matrix in Eq. (C-10) is singular or near-singular for a large number of closely spaced frequencies and multiple damping values. The numerical problem is to find a way to handle this near-singular matrix.

Lilhanand and Tseng subdivided the target spectrum into several smaller subsets that each have about 20 to 30 frequency and damping pairs (Lilhanand, personal communication). Each subset should sample the entire frequency range rather than using low frequency, moderate frequency, high frequency, subgroups. For example, if 4 subsets are used, the first subset contains the 1st, 5th, 9th, ... frequencies. For each subset, the C matrix can be inverted numerically. The inverse of C is computed using singular value decomposition. For numerical stability, the eigenvectors corresponding to the small eigenvalues are removed.

Since the elements of C are computed analytically, the time step of the reference time history should be small enough so that the numerical calculation of the response is close to the analytical calculation. For most cases, this condition can be met using 200 samples/sec. In this project, all the time histories were interpolated to 200 samples/sec for the spectral matching.

Specifying the Target Spectrum

The method makes narrow band modifications to the time series. Therefore, it is important to use a fine enough frequency sampling to ensure that the response spectrum at frequencies not matched will remain smooth. Based on the bandwidth of the oscillator response, about 50 frequencies per decade (equally spaced on the log frequency axis) is sufficient. In this project, 200 frequencies are used between 0.1 Hz and 34 Hz.

References

Kaul, M. K. (1978). Spectrum-consistent time-history generation (1978). ASCE J. Eng. Mech., EM4, 781-788.

Lilhanand, K. and W. S. Tseng (1987). Generation of synthetic time histories compatible with multiple-damping response spectra, SMiRT-9, Lausanne, K2/10.

Lilhanand, K. and W. S. Tseng (1988). Development and application of realistic earthquake time histories compatible with multiple damping response spectra, Ninth World Conf. Earth. Engin., Tokyo, Japan, Vol II, 819-824.

Preumont, A. (1984). The generation of spectrum compatible accelerograms for the design of nuclear power plants, Earth. Engin. Struct. Dyn., **12**, 481-497.

APPENDIX D
SPECTRAL MATCHING EXAMPLE

Appendix D

Spectral Matching Example

A complete example of the spectral matching procedure for developing the reference rock time histories is provided in this appendix. The spectral match for the fault normal component of motion from the San Andreas set 3 (Landers composite time history) is presented here.

The initial starting time history from the Landers composite acceleration strong ground motion record is shown in Figure D-1. The spectral matching procedure is an iterative process. A baseline correction is applied after each spectral matching step to the modified time history. The first step in the spectral matching procedure is to match the starting time history to the 5% and 2% spectral damping target spectra simultaneously, which helps keep the power spectrum of the modified time history broadband. Once a satisfactory fit is obtained for the 5% and 2% spectral damping target spectra, a final spectral match is performed to the 5% spectral damping target spectra. The input parameters and period ranges for the individual steps spectral matching procedure are listed in Table D-1. The spectral match and corresponding modified time histories are shown in Figures D-2 through D-9. Figures D-2 through D-5 show the results for the multiple damping spectral matching and the figures D-6 through D-9 show the results for the final spectral match to the 5% spectral damping target spectrum.

Table D.1 Input parameters used in the spectral matching procedure.

Step	Number of Iterations	Mode 1	Period Range (sec)	Target Spectra
1	3	6	0.01-1.0	5% and 2% damping
2	5	6	0.01-2.0	5% and 2% damping
3	3	6	0.01-3.0	5% and 2% damping
4	5	1	0.01-5.0	5% and 2% damping
5	5	6	0.01-1.0	5% damping
6	5	6	0.01-2.0	5% damping
7	5	6	0.01-7.0	5% damping
8	3	6	0.01-8.0	5% damping

Appendix D

Spectral Matching Example

A complete example of the spectral matching procedure for developing the reference rock time histories is provided in this appendix. The spectral match for the fault normal component of motion from the San Andreas set 3 (Landers composite time history) is presented here.

The initial starting time history from the Landers composite acceleration strong ground motion record is shown in Figure D-1. The spectral matching procedure is an iterative process. A baseline correction is applied after each spectral matching step to the modified time history. The first step in the spectral matching procedure is to match the starting time history to the 5% and 2% spectral damping target spectra simultaneously, which helps keep the power spectrum of the modified time history broadband. Once a satisfactory fit is obtained for the 5% and 2% spectral damping target spectra, a final spectral match is performed to the 5% spectral damping target spectra. The input parameters and period ranges for the individual steps spectral matching procedure are listed in Table D-1. The spectral match and corresponding modified time histories are shown in Figures D-2 through D-9. Figures D-2 through D-5 show the results for the multiple damping spectral matching and the figures D-6 through D-9 show the results for the final spectral match to the 5% spectral damping target spectrum.

Table D.1 Input parameters used in the spectral matching procedure.

Step	Number of Iterations	Mode 1	Period Range (sec)	Target Spectra
1	3	6	0.01-1.0	5% and 2% damping
2	5	6	0.01-2.0	5% and 2% damping
3	3	6	0.01-3.0	5% and 2% damping
4	5	1	0.01-5.0	5% and 2% damping
5	5	6	0.01-1.0	5% damping
6	5	6	0.01-2.0	5% damping
7	5	6	0.01-7.0	5% damping
8	3	6	0.01-8.0	5% damping

Appendix D

Spectral Matching Example

A complete example of the spectral matching procedure for developing the reference rock time histories is provided in this appendix. The spectral match for the fault normal component of motion from the San Andreas set 3 (Landers composite time history) is presented here.

The initial starting time history from the Landers composite acceleration strong ground motion record is shown in Figure D-1. The spectral matching procedure is an iterative process. A baseline correction is applied after each spectral matching step to the modified time history. The first step in the spectral matching procedure is to match the starting time history to the 5% and 2% spectral damping target spectra simultaneously, which helps keep the power spectrum of the modified time history broadband. Once a satisfactory fit is obtained for the 5% and 2% spectral damping target spectra, a final spectral match is performed to the 5% spectral damping target spectra. The input parameters and period ranges for the individual steps spectral matching procedure are listed in Table D-1. The spectral match and corresponding modified time histories are shown in Figures D-2 through D-9. Figures D-2 through D-5 show the results for the multiple damping spectral matching and the figures D-6 through D-9 show the results for the final spectral match to the 5% spectral damping target spectrum.

Table D.1 Input parameters used in the spectral matching procedure.

Step	Number of Iterations	Mode 1	Period Range (sec)	Target Spectra
1	3	6	0.01-1.0	5% and 2% damping
2	5	6	0.01-2.0	5% and 2% damping
3	3	6	0.01-3.0	5% and 2% damping
4	5	1	0.01-5.0	5% and 2% damping
5	5	6	0.01-1.0	5% damping
6	5	6	0.01-2.0	5% damping
7	5	6	0.01-7.0	5% damping
8	3	6	0.01-8.0	5% damping

Appendix D

Spectral Matching Example

A complete example of the spectral matching procedure for developing the reference rock time histories is provided in this appendix. The spectral match for the fault normal component of motion from the San Andreas set 3 (Landers composite time history) is presented here.

The initial starting time history from the Landers composite acceleration strong ground motion record is shown in Figure D-1. The spectral matching procedure is an iterative process. A baseline correction is applied after each spectral matching step to the modified time history. The first step in the spectral matching procedure is to match the starting time history to the 5% and 2% spectral damping target spectra simultaneously, which helps keep the power spectrum of the modified time history broadband. Once a satisfactory fit is obtained for the 5% and 2% spectral damping target spectra, a final spectral match is performed to the 5% spectral damping target spectra. The input parameters and period ranges for the individual steps spectral matching procedure are listed in Table D-1. The spectral match and corresponding modified time histories are shown in Figures D-2 through D-9. Figures D-2 through D-5 show the results for the multiple damping spectral matching and the figures D-6 through D-9 show the results for the final spectral match to the 5% spectral damping target spectrum.

Table D.1 Input parameters used in the spectral matching procedure.

Step	Number of Iterations	Mode 1	Period Range (sec)	Target Spectra
1	3	6	0.01-1.0	5% and 2% damping
2	5	6	0.01-2.0	5% and 2% damping
3	3	6	0.01-3.0	5% and 2% damping
4	5	1	0.01-5.0	5% and 2% damping
5	5	6	0.01-1.0	5% damping
6	5	6	0.01-2.0	5% damping
7	5	6	0.01-7.0	5% damping
8	3	6	0.01-8.0	5% damping

Appendix D

Spectral Matching Example

A complete example of the spectral matching procedure for developing the reference rock time histories is provided in this appendix. The spectral match for the fault normal component of motion from the San Andreas set 3 (Landers composite time history) is presented here.

The initial starting time history from the Landers composite acceleration strong ground motion record is shown in Figure D-1. The spectral matching procedure is an iterative process. A baseline correction is applied after each spectral matching step to the modified time history. The first step in the spectral matching procedure is to match the starting time history to the 5% and 2% spectral damping target spectra simultaneously, which helps keep the power spectrum of the modified time history broadband. Once a satisfactory fit is obtained for the 5% and 2% spectral damping target spectra, a final spectral match is performed to the 5% spectral damping target spectra. The input parameters and period ranges for the individual steps spectral matching procedure are listed in Table D-1. The spectral match and corresponding modified time histories are shown in Figures D-2 through D-9. Figures D-2 through D-5 show the results for the multiple damping spectral matching and the figures D-6 through D-9 show the results for the final spectral match to the 5% spectral damping target spectrum.

Table D.1 Input parameters used in the spectral matching procedure.

Step	Number of Iterations	Mode 1	Period Range (sec)	Target Spectra
1	3	6	0.01-1.0	5% and 2% damping
2	5	6	0.01-2.0	5% and 2% damping
3	3	6	0.01-3.0	5% and 2% damping
4	5	1	0.01-5.0	5% and 2% damping
5	5	6	0.01-1.0	5% damping
6	5	6	0.01-2.0	5% damping
7	5	6	0.01-7.0	5% damping
8	3	6	0.01-8.0	5% damping

Appendix D

Spectral Matching Example

A complete example of the spectral matching procedure for developing the reference rock time histories is provided in this appendix. The spectral match for the fault normal component of motion from the San Andreas set 3 (Landers composite time history) is presented here.

The initial starting time history from the Landers composite acceleration strong ground motion record is shown in Figure D-1. The spectral matching procedure is an iterative process. A baseline correction is applied after each spectral matching step to the modified time history. The first step in the spectral matching procedure is to match the starting time history to the 5% and 2% spectral damping target spectra simultaneously, which helps keep the power spectrum of the modified time history broadband. Once a satisfactory fit is obtained for the 5% and 2% spectral damping target spectra, a final spectral match is performed to the 5% spectral damping target spectra. The input parameters and period ranges for the individual steps spectral matching procedure are listed in Table D-1. The spectral match and corresponding modified time histories are shown in Figures D-2 through D-9. Figures D-2 through D-5 show the results for the multiple damping spectral matching and the figures D-6 through D-9 show the results for the final spectral match to the 5% spectral damping target spectrum.

Table D.1 Input parameters used in the spectral matching procedure.

Step	Number of Iterations	Mode 1	Period Range (sec)	Target Spectra
1	3	6	0.01-1.0	5% and 2% damping
2	5	6	0.01-2.0	5% and 2% damping
3	3	6	0.01-3.0	5% and 2% damping
4	5	1	0.01-5.0	5% and 2% damping
5	5	6	0.01-1.0	5% damping
6	5	6	0.01-2.0	5% damping
7	5	6	0.01-7.0	5% damping
8	3	6	0.01-8.0	5% damping

Appendix D

Spectral Matching Example

A complete example of the spectral matching procedure for developing the reference rock time histories is provided in this appendix. The spectral match for the fault normal component of motion from the San Andreas set 3 (Landers composite time history) is presented here.

The initial starting time history from the Landers composite acceleration strong ground motion record is shown in Figure D-1. The spectral matching procedure is an iterative process. A baseline correction is applied after each spectral matching step to the modified time history. The first step in the spectral matching procedure is to match the starting time history to the 5% and 2% spectral damping target spectra simultaneously, which helps keep the power spectrum of the modified time history broadband. Once a satisfactory fit is obtained for the 5% and 2% spectral damping target spectra, a final spectral match is performed to the 5% spectral damping target spectra. The input parameters and period ranges for the individual steps spectral matching procedure are listed in Table D-1. The spectral match and corresponding modified time histories are shown in Figures D-2 through D-9. Figures D-2 through D-5 show the results for the multiple damping spectral matching and the figures D-6 through D-9 show the results for the final spectral match to the 5% spectral damping target spectrum.

Table D.1 Input parameters used in the spectral matching procedure.

Step	Number of Iterations	Mode 1	Period Range (sec)	Target Spectra
1	3	6	0.01-1.0	5% and 2% damping
2	5	6	0.01-2.0	5% and 2% damping
3	3	6	0.01-3.0	5% and 2% damping
4	5	1	0.01-5.0	5% and 2% damping
5	5	6	0.01-1.0	5% damping
6	5	6	0.01-2.0	5% damping
7	5	6	0.01-7.0	5% damping
8	3	6	0.01-8.0	5% damping

Appendix D

Spectral Matching Example

A complete example of the spectral matching procedure for developing the reference rock time histories is provided in this appendix. The spectral match for the fault normal component of motion from the San Andreas set 3 (Landers composite time history) is presented here.

The initial starting time history from the Landers composite acceleration strong ground motion record is shown in Figure D-1. The spectral matching procedure is an iterative process. A baseline correction is applied after each spectral matching step to the modified time history. The first step in the spectral matching procedure is to match the starting time history to the 5% and 2% spectral damping target spectra simultaneously, which helps keep the power spectrum of the modified time history broadband. Once a satisfactory fit is obtained for the 5% and 2% spectral damping target spectra, a final spectral match is performed to the 5% spectral damping target spectra. The input parameters and period ranges for the individual steps spectral matching procedure are listed in Table D-1. The spectral match and corresponding modified time histories are shown in Figures D-2 through D-9. Figures D-2 through D-5 show the results for the multiple damping spectral matching and the figures D-6 through D-9 show the results for the final spectral match to the 5% spectral damping target spectrum.

Table D.1 Input parameters used in the spectral matching procedure.

Step	Number of Iterations	Mode 1	Period Range (sec)	Target Spectra
1	3	6	0.01-1.0	5% and 2% damping
2	5	6	0.01-2.0	5% and 2% damping
3	3	6	0.01-3.0	5% and 2% damping
4	5	1	0.01-5.0	5% and 2% damping
5	5	6	0.01-1.0	5% damping
6	5	6	0.01-2.0	5% damping
7	5	6	0.01-7.0	5% damping
8	3	6	0.01-8.0	5% damping

Appendix D

Spectral Matching Example

A complete example of the spectral matching procedure for developing the reference rock time histories is provided in this appendix. The spectral match for the fault normal component of motion from the San Andreas set 3 (Landers composite time history) is presented here.

The initial starting time history from the Landers composite acceleration strong ground motion record is shown in Figure D-1. The spectral matching procedure is an iterative process. A baseline correction is applied after each spectral matching step to the modified time history. The first step in the spectral matching procedure is to match the starting time history to the 5% and 2% spectral damping target spectra simultaneously, which helps keep the power spectrum of the modified time history broadband. Once a satisfactory fit is obtained for the 5% and 2% spectral damping target spectra, a final spectral match is performed to the 5% spectral damping target spectra. The input parameters and period ranges for the individual steps spectral matching procedure are listed in Table D-1. The spectral match and corresponding modified time histories are shown in Figures D-2 through D-9. Figures D-2 through D-5 show the results for the multiple damping spectral matching and the figures D-6 through D-9 show the results for the final spectral match to the 5% spectral damping target spectrum.

Table D.1 Input parameters used in the spectral matching procedure.

Step	Number of Iterations	Mode 1	Period Range (sec)	Target Spectra
1	3	6	0.01-1.0	5% and 2% damping
2	5	6	0.01-2.0	5% and 2% damping
3	3	6	0.01-3.0	5% and 2% damping
4	5	1	0.01-5.0	5% and 2% damping
5	5	6	0.01-1.0	5% damping
6	5	6	0.01-2.0	5% damping
7	5	6	0.01-7.0	5% damping
8	3	6	0.01-8.0	5% damping

Appendix D

Spectral Matching Example

A complete example of the spectral matching procedure for developing the reference rock time histories is provided in this appendix. The spectral match for the fault normal component of motion from the San Andreas set 3 (Landers composite time history) is presented here.

The initial starting time history from the Landers composite acceleration strong ground motion record is shown in Figure D-1. The spectral matching procedure is an iterative process. A baseline correction is applied after each spectral matching step to the modified time history. The first step in the spectral matching procedure is to match the starting time history to the 5% and 2% spectral damping target spectra simultaneously, which helps keep the power spectrum of the modified time history broadband. Once a satisfactory fit is obtained for the 5% and 2% spectral damping target spectra, a final spectral match is performed to the 5% spectral damping target spectra. The input parameters and period ranges for the individual steps spectral matching procedure are listed in Table D-1. The spectral match and corresponding modified time histories are shown in Figures D-2 through D-9. Figures D-2 through D-5 show the results for the multiple damping spectral matching and the figures D-6 through D-9 show the results for the final spectral match to the 5% spectral damping target spectrum.

Table D.1 Input parameters used in the spectral matching procedure.

Step	Number of Iterations	Mode	Period Range (sec)	Target Spectra
1	3	6	0.01-1.0	5% and 2% damping
2	5	6	0.01-2.0	5% and 2% damping
3	3	6	0.01-3.0	5% and 2% damping
4	5	1	0.01-5.0	5% and 2% damping
5	5	6	0.01-1.0	5% damping
6	5	6	0.01-2.0	5% damping
7	5	6	0.01-7.0	5% damping
8	3	6	0.01-8.0	5% damping

Appendix D

Spectral Matching Example

A complete example of the spectral matching procedure for developing the reference rock time histories is provided in this appendix. The spectral match for the fault normal component of motion from the San Andreas set 3 (Landers composite time history) is presented here.

The initial starting time history from the Landers composite acceleration strong ground motion record is shown in Figure D-1. The spectral matching procedure is an iterative process. A baseline correction is applied after each spectral matching step to the modified time history. The first step in the spectral matching procedure is to match the starting time history to the 5% and 2% spectral damping target spectra simultaneously, which helps keep the power spectrum of the modified time history broadband. Once a satisfactory fit is obtained for the 5% and 2% spectral damping target spectra, a final spectral match is performed to the 5% spectral damping target spectra. The input parameters and period ranges for the individual steps spectral matching procedure are listed in Table D-1. The spectral match and corresponding modified time histories are shown in Figures D-2 through D-9. Figures D-2 through D-5 show the results for the multiple damping spectral matching and the figures D-6 through D-9 show the results for the final spectral match to the 5% spectral damping target spectrum.

Table D.1 Input parameters used in the spectral matching procedure.

Step	Number of Iterations	Mode 1	Period Range (sec)	Target Spectra
1	3	6	0.01-1.0	5% and 2% damping
2	5	6	0.01-2.0	5% and 2% damping
3	3	6	0.01-3.0	5% and 2% damping
4	5	1	0.01-5.0	5% and 2% damping
5	5	6	0.01-1.0	5% damping
6	5	6	0.01-2.0	5% damping
7	5	6	0.01-7.0	5% damping
8	3	6	0.01-8.0	5% damping

Appendix D

Spectral Matching Example

A complete example of the spectral matching procedure for developing the reference rock time histories is provided in this appendix. The spectral match for the fault normal component of motion from the San Andreas set 3 (Landers composite time history) is presented here.

The initial starting time history from the Landers composite acceleration strong ground motion record is shown in Figure D-1. The spectral matching procedure is an iterative process. A baseline correction is applied after each spectral matching step to the modified time history. The first step in the spectral matching procedure is to match the starting time history to the 5% and 2% spectral damping target spectra simultaneously, which helps keep the power spectrum of the modified time history broadband. Once a satisfactory fit is obtained for the 5% and 2% spectral damping target spectra, a final spectral match is performed to the 5% spectral damping target spectra. The input parameters and period ranges for the individual steps spectral matching procedure are listed in Table D-1. The spectral match and corresponding modified time histories are shown in Figures D-2 through D-9. Figures D-2 through D-5 show the results for the multiple damping spectral matching and the figures D-6 through D-9 show the results for the final spectral match to the 5% spectral damping target spectrum.

Table D.1 Input parameters used in the spectral matching procedure.

Step	Number of Iterations	Mode 1	Period Range (sec)	Target Spectra
1	3	6	0.01-1.0	5% and 2% damping
2	5	6	0.01-2.0	5% and 2% damping
3	3	6	0.01-3.0	5% and 2% damping
4	5	1	0.01-5.0	5% and 2% damping
5	5	6	0.01-1.0	5% damping
6	5	6	0.01-2.0	5% damping
7	5	6	0.01-7.0	5% damping
8	3	6	0.01-8.0	5% damping

Appendix D

Spectral Matching Example

A complete example of the spectral matching procedure for developing the reference rock time histories is provided in this appendix. The spectral match for the fault normal component of motion from the San Andreas set 3 (Landers composite time history) is presented here.

The initial starting time history from the Landers composite acceleration strong ground motion record is shown in Figure D-1. The spectral matching procedure is an iterative process. A baseline correction is applied after each spectral matching step to the modified time history. The first step in the spectral matching procedure is to match the starting time history to the 5% and 2% spectral damping target spectra simultaneously, which helps keep the power spectrum of the modified time history broadband. Once a satisfactory fit is obtained for the 5% and 2% spectral damping target spectra, a final spectral match is performed to the 5% spectral damping target spectra. The input parameters and period ranges for the individual steps spectral matching procedure are listed in Table D-1. The spectral match and corresponding modified time histories are shown in Figures D-2 through D-9. Figures D-2 through D-5 show the results for the multiple damping spectral matching and the figures D-6 through D-9 show the results for the final spectral match to the 5% spectral damping target spectrum.

Table D.1 Input parameters used in the spectral matching procedure.

Step	Number of Iterations	Mode 1	Period Range (sec)	Target Spectra
1	3	6	0.01-1.0	5% and 2% damping
2	5	6	0.01-2.0	5% and 2% damping
3	3	6	0.01-3.0	5% and 2% damping
4	5	1	0.01-5.0	5% and 2% damping
5	5	6	0.01-1.0	5% damping
6	5	6	0.01-2.0	5% damping
7	5	6	0.01-7.0	5% damping
8	3	6	0.01-8.0	5% damping

Appendix D

Spectral Matching Example

A complete example of the spectral matching procedure for developing the reference rock time histories is provided in this appendix. The spectral match for the fault normal component of motion from the San Andreas set 3 (Landers composite time history) is presented here.

The initial starting time history from the Landers composite acceleration strong ground motion record is shown in Figure D-1. The spectral matching procedure is an iterative process. A baseline correction is applied after each spectral matching step to the modified time history. The first step in the spectral matching procedure is to match the starting time history to the 5% and 2% spectral damping target spectra simultaneously, which helps keep the power spectrum of the modified time history broadband. Once a satisfactory fit is obtained for the 5% and 2% spectral damping target spectra, a final spectral match is performed to the 5% spectral damping target spectra. The input parameters and period ranges for the individual steps spectral matching procedure are listed in Table D-1. The spectral match and corresponding modified time histories are shown in Figures D-2 through D-9. Figures D-2 through D-5 show the results for the multiple damping spectral matching and the figures D-6 through D-9 show the results for the final spectral match to the 5% spectral damping target spectrum.

Table D.1 Input parameters used in the spectral matching procedure.

Step	Number of Iterations	Mode 1	Period Range (sec)	Target Spectra
1	3	6	0.01-1.0	5% and 2% damping
2	5	6	0.01-2.0	5% and 2% damping
3	3	6	0.01-3.0	5% and 2% damping
4	5	1	0.01-5.0	5% and 2% damping
5	5	6	0.01-1.0	5% damping
6	5	6	0.01-2.0	5% damping
7	5	6	0.01-7.0	5% damping
8	3	6	0.01-8.0	5% damping

Appendix D

Spectral Matching Example

A complete example of the spectral matching procedure for developing the reference rock time histories is provided in this appendix. The spectral match for the fault normal component of motion from the San Andreas set 3 (Landers composite time history) is presented here.

The initial starting time history from the Landers composite acceleration strong ground motion record is shown in Figure D-1. The spectral matching procedure is an iterative process. A baseline correction is applied after each spectral matching step to the modified time history. The first step in the spectral matching procedure is to match the starting time history to the 5% and 2% spectral damping target spectra simultaneously, which helps keep the power spectrum of the modified time history broadband. Once a satisfactory fit is obtained for the 5% and 2% spectral damping target spectra, a final spectral match is performed to the 5% spectral damping target spectra. The input parameters and period ranges for the individual steps spectral matching procedure are listed in Table D-1. The spectral match and corresponding modified time histories are shown in Figures D-2 through D-9. Figures D-2 through D-5 show the results for the multiple damping spectral matching and the figures D-6 through D-9 show the results for the final spectral match to the 5% spectral damping target spectrum.

Table D.1 Input parameters used in the spectral matching procedure.

Step	Number of Iterations	Mode 1	Period Range (sec)	Target Spectra
1	3	6	0.01-1.0	5% and 2% damping
2	5	6	0.01-2.0	5% and 2% damping
3	3	6	0.01-3.0	5% and 2% damping
4	5	1	0.01-5.0	5% and 2% damping
5	5	6	0.01-1.0	5% damping
6	5	6	0.01-2.0	5% damping
7	5	6	0.01-7.0	5% damping
8	3	6	0.01-8.0	5% damping

Appendix D

Spectral Matching Example

A complete example of the spectral matching procedure for developing the reference rock time histories is provided in this appendix. The spectral match for the fault normal component of motion from the San Andreas set 3 (Landers composite time history) is presented here.

The initial starting time history from the Landers composite acceleration strong ground motion record is shown in Figure D-1. The spectral matching procedure is an iterative process. A baseline correction is applied after each spectral matching step to the modified time history. The first step in the spectral matching procedure is to match the starting time history to the 5% and 2% spectral damping target spectra simultaneously, which helps keep the power spectrum of the modified time history broadband. Once a satisfactory fit is obtained for the 5% and 2% spectral damping target spectra, a final spectral match is performed to the 5% spectral damping target spectra. The input parameters and period ranges for the individual steps spectral matching procedure are listed in Table D-1. The spectral match and corresponding modified time histories are shown in Figures D-2 through D-9. Figures D-2 through D-5 show the results for the multiple damping spectral matching and the figures D-6 through D-9 show the results for the final spectral match to the 5% spectral damping target spectrum.

Table D.1 Input parameters used in the spectral matching procedure.

Step	Number of Iterations	Mode 1	Period Range (sec)	Target Spectra
1	3	6	0.01-1.0	5% and 2% damping
2	5	6	0.01-2.0	5% and 2% damping
3	3	6	0.01-3.0	5% and 2% damping
4	5	1	0.01-5.0	5% and 2% damping
5	5	6	0.01-1.0	5% damping
6	5	6	0.01-2.0	5% damping
7	5	6	0.01-7.0	5% damping
8	3	6	0.01-8.0	5% damping

Appendix D

Spectral Matching Example

A complete example of the spectral matching procedure for developing the reference rock time histories is provided in this appendix. The spectral match for the fault normal component of motion from the San Andreas set 3 (Landers composite time history) is presented here.

The initial starting time history from the Landers composite acceleration strong ground motion record is shown in Figure D-1. The spectral matching procedure is an iterative process. A baseline correction is applied after each spectral matching step to the modified time history. The first step in the spectral matching procedure is to match the starting time history to the 5% and 2% spectral damping target spectra simultaneously, which helps keep the power spectrum of the modified time history broadband. Once a satisfactory fit is obtained for the 5% and 2% spectral damping target spectra, a final spectral match is performed to the 5% spectral damping target spectra. The input parameters and period ranges for the individual steps spectral matching procedure are listed in Table D-1. The spectral match and corresponding modified time histories are shown in Figures D-2 through D-9. Figures D-2 through D-5 show the results for the multiple damping spectral matching and the figures D-6 through D-9 show the results for the final spectral match to the 5% spectral damping target spectrum.

Table D.1 Input parameters used in the spectral matching procedure.

Step	Number of Iterations	Mode 1	Period Range (sec)	Target Spectra
1	3	6	0.01-1.0	5% and 2% damping
2	5	6	0.01-2.0	5% and 2% damping
3	3	6	0.01-3.0	5% and 2% damping
4	5	1	0.01-5.0	5% and 2% damping
5	5	6	0.01-1.0	5% damping
6	5	6	0.01-2.0	5% damping
7	5	6	0.01-7.0	5% damping
8	3	6	0.01-8.0	5% damping

Appendix D

Spectral Matching Example

A complete example of the spectral matching procedure for developing the reference rock time histories is provided in this appendix. The spectral match for the fault normal component of motion from the San Andreas set 3 (Landers composite time history) is presented here.

The initial starting time history from the Landers composite acceleration strong ground motion record is shown in Figure D-1. The spectral matching procedure is an iterative process. A baseline correction is applied after each spectral matching step to the modified time history. The first step in the spectral matching procedure is to match the starting time history to the 5% and 2% spectral damping target spectra simultaneously, which helps keep the power spectrum of the modified time history broadband. Once a satisfactory fit is obtained for the 5% and 2% spectral damping target spectra, a final spectral match is performed to the 5% spectral damping target spectra. The input parameters and period ranges for the individual steps spectral matching procedure are listed in Table D-1. The spectral match and corresponding modified time histories are shown in Figures D-2 through D-9. Figures D-2 through D-5 show the results for the multiple damping spectral matching and the figures D-6 through D-9 show the results for the final spectral match to the 5% spectral damping target spectrum.

Table D.1 Input parameters used in the spectral matching procedure.

Step	Number of Iterations	Mode 1	Period Range (sec)	Target Spectra
1	3	6	0.01-1.0	5% and 2% damping
2	5	6	0.01-2.0	5% and 2% damping
3	3	6	0.01-3.0	5% and 2% damping
4	5	1	0.01-5.0	5% and 2% damping
5	5	6	0.01-1.0	5% damping
6	5	6	0.01-2.0	5% damping
7	5	6	0.01-7.0	5% damping
8	3	6	0.01-8.0	5% damping

Appendix D

Spectral Matching Example

A complete example of the spectral matching procedure for developing the reference rock time histories is provided in this appendix. The spectral match for the fault normal component of motion from the San Andreas set 3 (Landers composite time history) is presented here.

The initial starting time history from the Landers composite acceleration strong ground motion record is shown in Figure D-1. The spectral matching procedure is an iterative process. A baseline correction is applied after each spectral matching step to the modified time history. The first step in the spectral matching procedure is to match the starting time history to the 5% and 2% spectral damping target spectra simultaneously, which helps keep the power spectrum of the modified time history broadband. Once a satisfactory fit is obtained for the 5% and 2% spectral damping target spectra, a final spectral match is performed to the 5% spectral damping target spectra. The input parameters and period ranges for the individual steps spectral matching procedure are listed in Table D-1. The spectral match and corresponding modified time histories are shown in Figures D-2 through D-9. Figures D-2 through D-5 show the results for the multiple damping spectral matching and the figures D-6 through D-9 show the results for the final spectral match to the 5% spectral damping target spectrum.

Table D.1 Input parameters used in the spectral matching procedure.

Step	Number of Iterations	Mode 1	Period Range (sec)	Target Spectra
1	3	6	0.01-1.0	5% and 2% damping
2	5	6	0.01-2.0	5% and 2% damping
3	3	6	0.01-3.0	5% and 2% damping
4	5	1	0.01-5.0	5% and 2% damping
5	5	6	0.01-1.0	5% damping
6	5	6	0.01-2.0	5% damping
7	5	6	0.01-7.0	5% damping
8	3	6	0.01-8.0	5% damping

Appendix D

Spectral Matching Example

A complete example of the spectral matching procedure for developing the reference rock time histories is provided in this appendix. The spectral match for the fault normal component of motion from the San Andreas set 3 (Landers composite time history) is presented here.

The initial starting time history from the Landers composite acceleration strong ground motion record is shown in Figure D-1. The spectral matching procedure is an iterative process. A baseline correction is applied after each spectral matching step to the modified time history. The first step in the spectral matching procedure is to match the starting time history to the 5% and 2% spectral damping target spectra simultaneously, which helps keep the power spectrum of the modified time history broadband. Once a satisfactory fit is obtained for the 5% and 2% spectral damping target spectra, a final spectral match is performed to the 5% spectral damping target spectra. The input parameters and period ranges for the individual steps spectral matching procedure are listed in Table D-1. The spectral match and corresponding modified time histories are shown in Figures D-2 through D-9. Figures D-2 through D-5 show the results for the multiple damping spectral matching and the figures D-6 through D-9 show the results for the final spectral match to the 5% spectral damping target spectrum.

Table D.1 Input parameters used in the spectral matching procedure.

Step	Number of Iterations	Mode 1	Period Range (sec)	Target Spectra
1	3	6	0.01-1.0	5% and 2% damping
2	5	6	0.01-2.0	5% and 2% damping
3	3	6	0.01-3.0	5% and 2% damping
4	5	1	0.01-5.0	5% and 2% damping
5	5	6	0.01-1.0	5% damping
6	5	6	0.01-2.0	5% damping
7	5	6	0.01-7.0	5% damping
8	3	6	0.01-8.0	5% damping

APPENDIX E
CHARACTERISTICS OF INITIAL STARTUP MOTIONS & SEE REFERENCE MOTIONS

Figure E-1 Set1 Initial Fault Normal Time History.

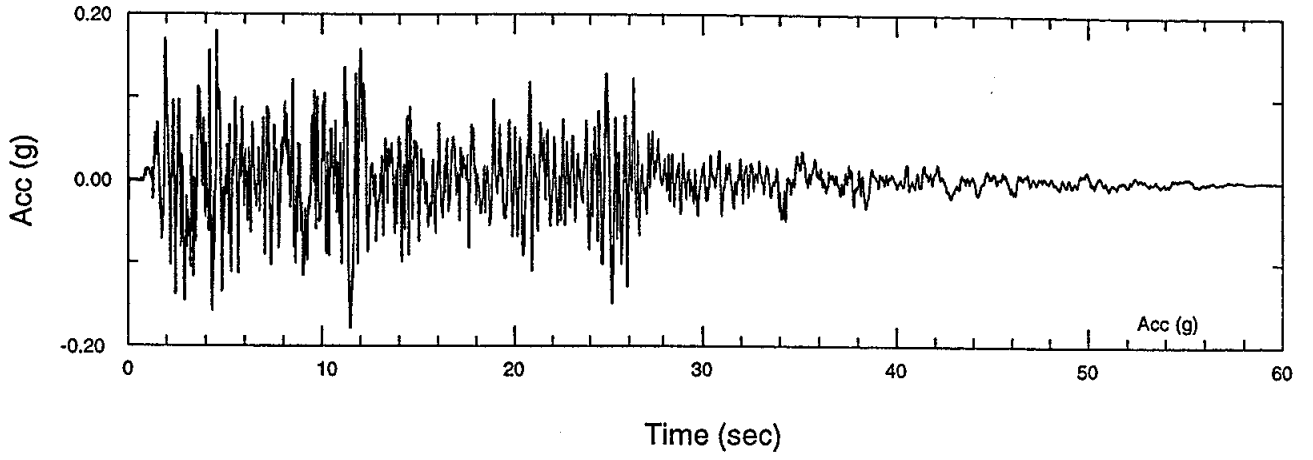

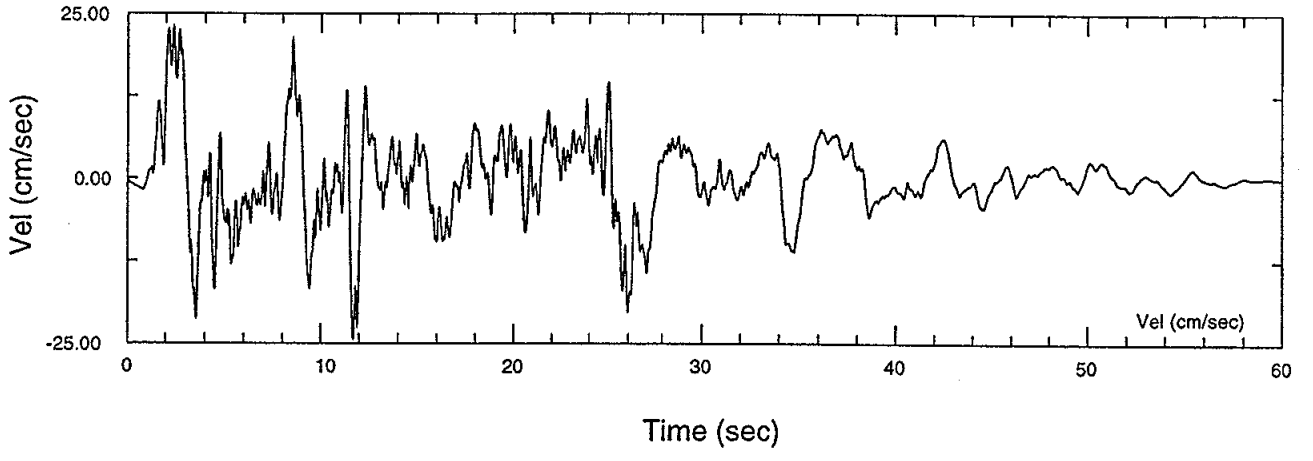

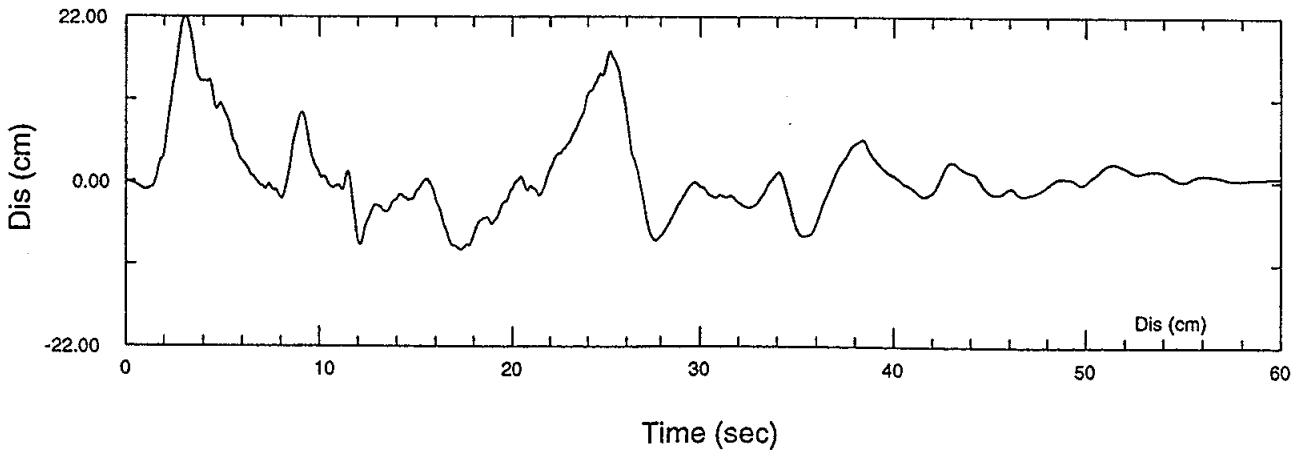

AP

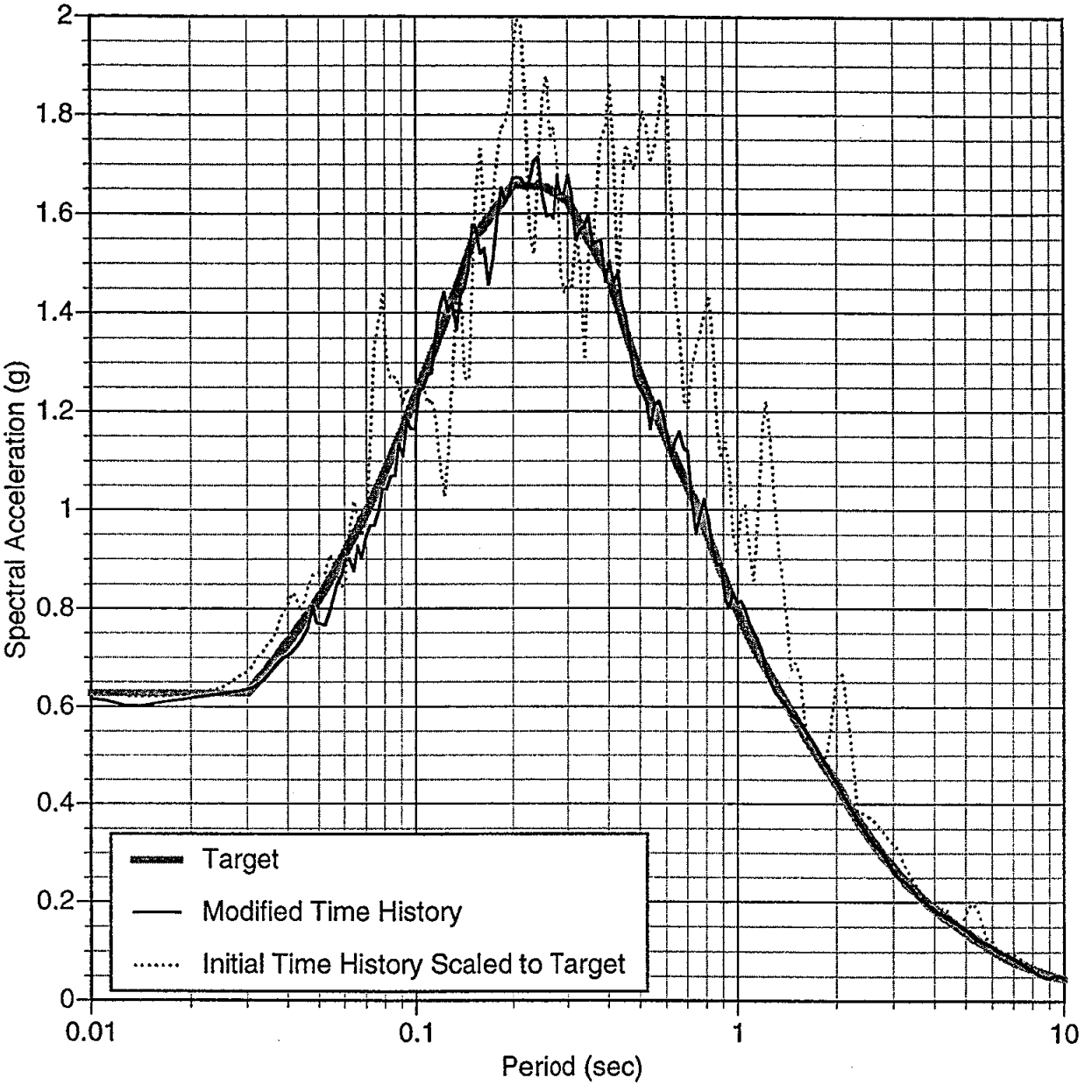

Figure E-2 Set1 5% damped response spectra for the modified Fault Normal component and initial time history scaled to the target PGA.

File: G3:Data1:East_BBridge_RefMotions:Report_Figures:Set1:Set1_rsp.dg

Figure E-3 Set1 Spectrum Compatible Fault Normal Reference Time History.

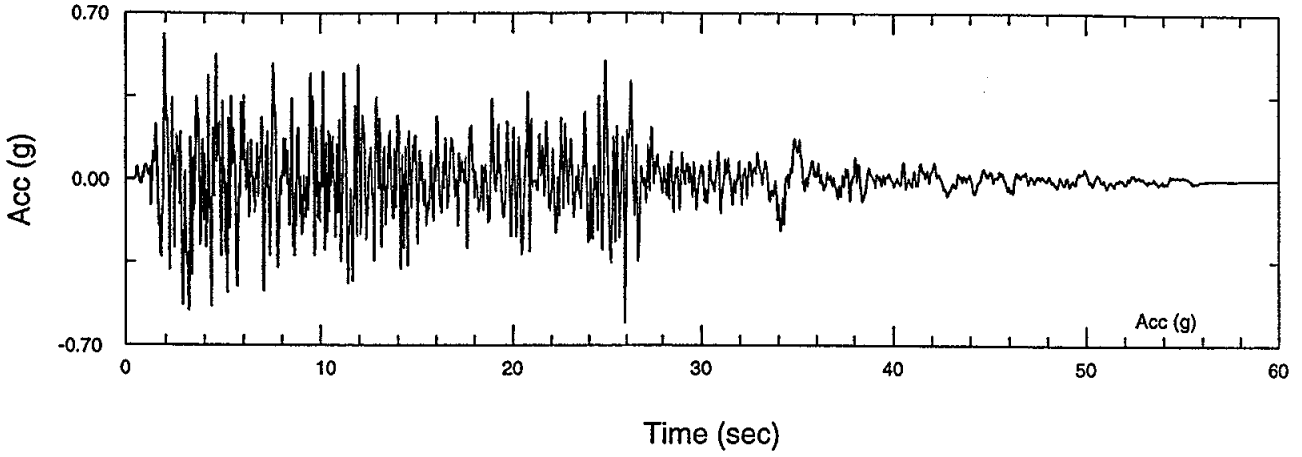

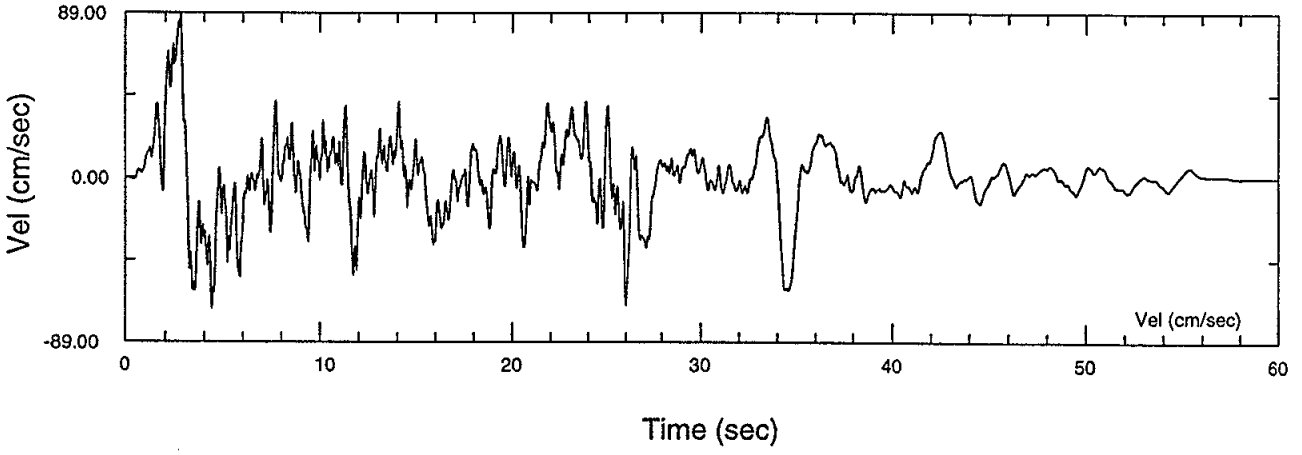

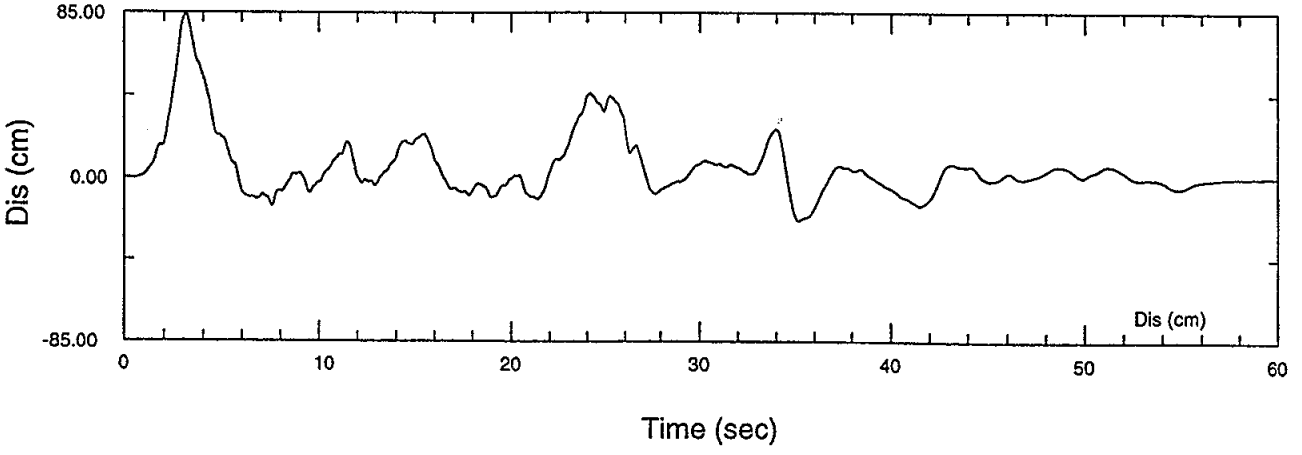

Figure E-4 Set1 Initial Fault Parallel Time History.

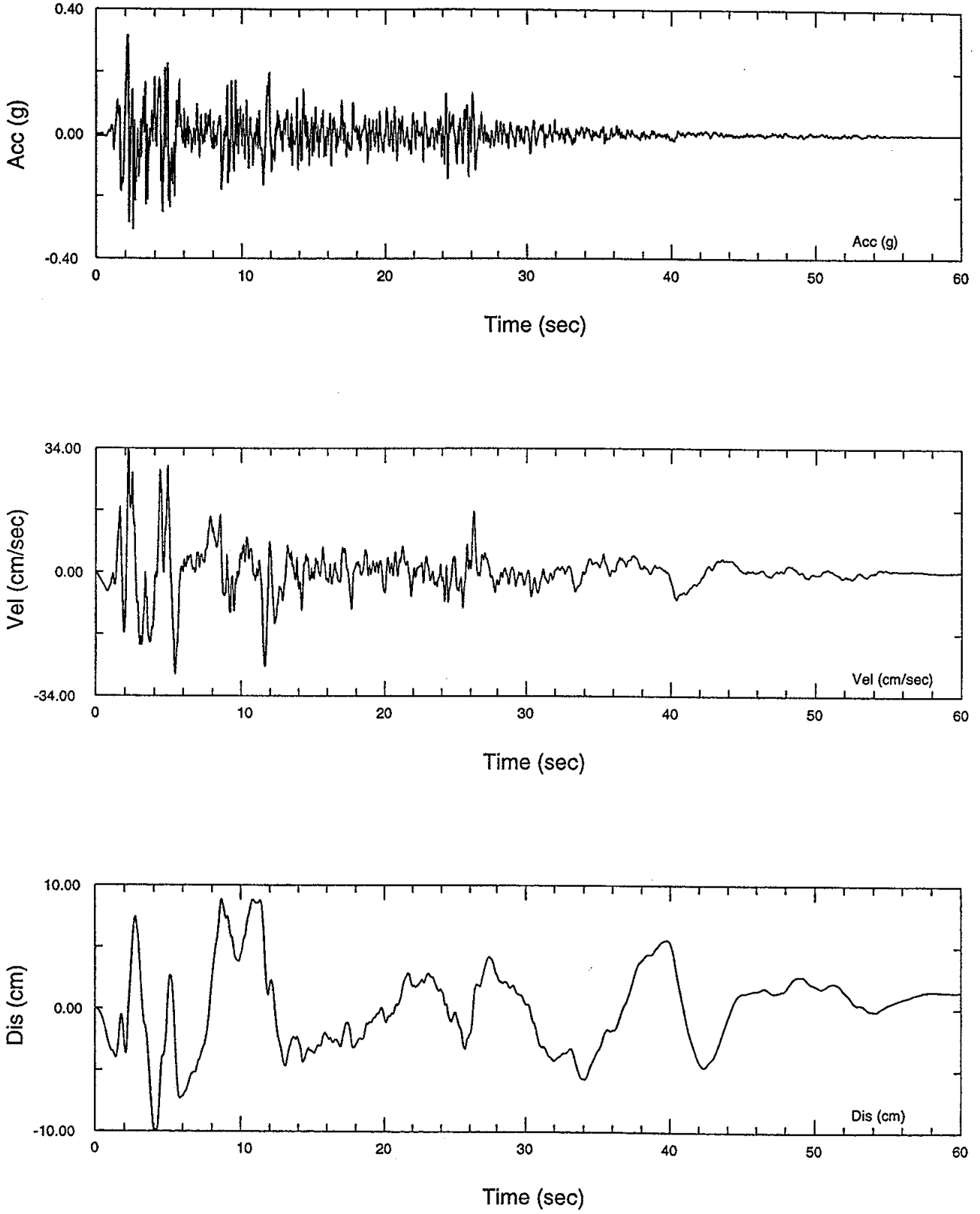

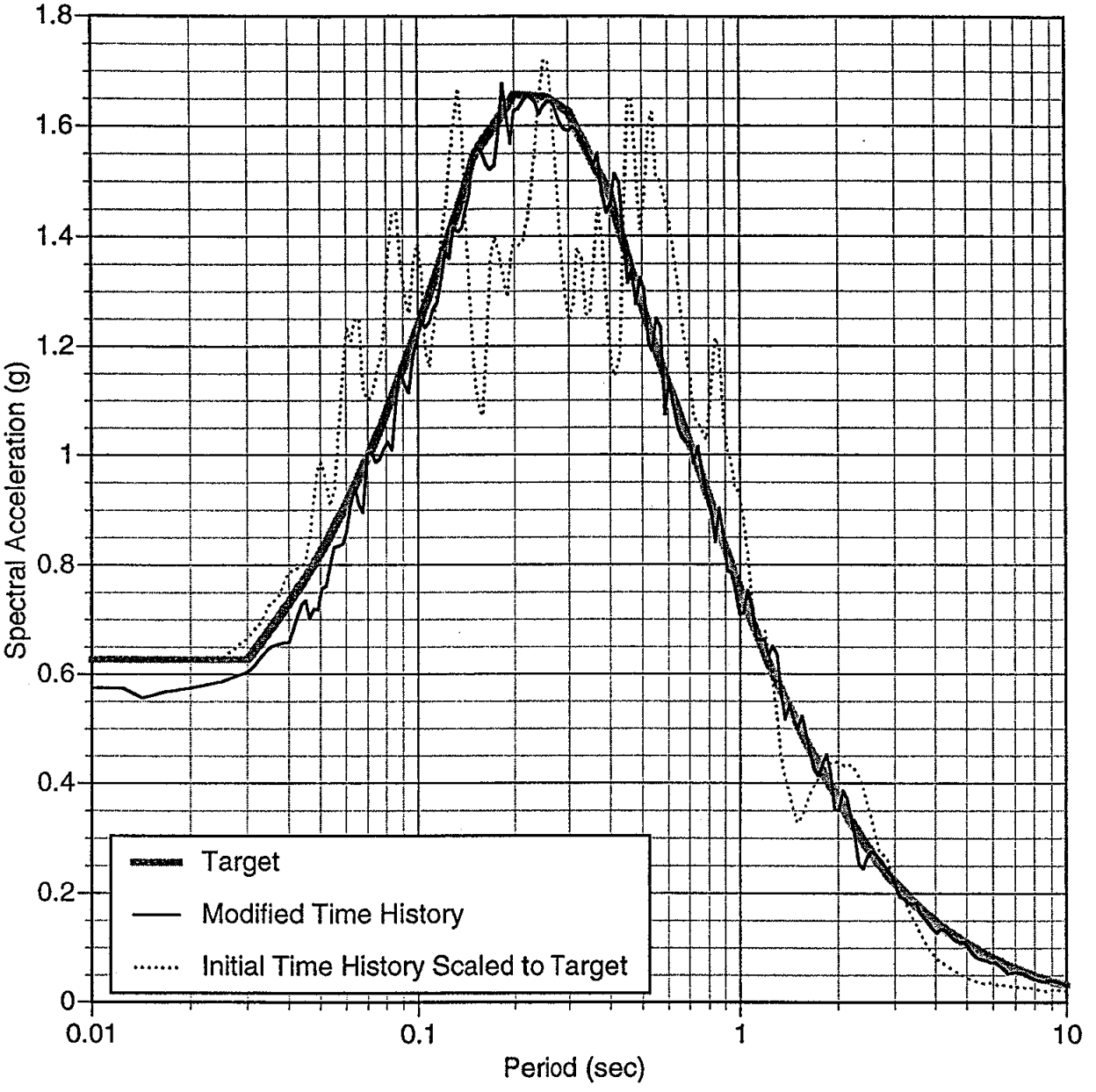

Figure E-5 Set1 5% damped response spectra for the modified Fault Parallel component and initial time history scaled to the target PGA.

File: G3:Data1:East_BBridge_RefMotions:Report_Figures:Set1:Set1_rsp.dg

Figure E-6 Set1 Spectrum Compatible Fault Parallel Reference Time History.

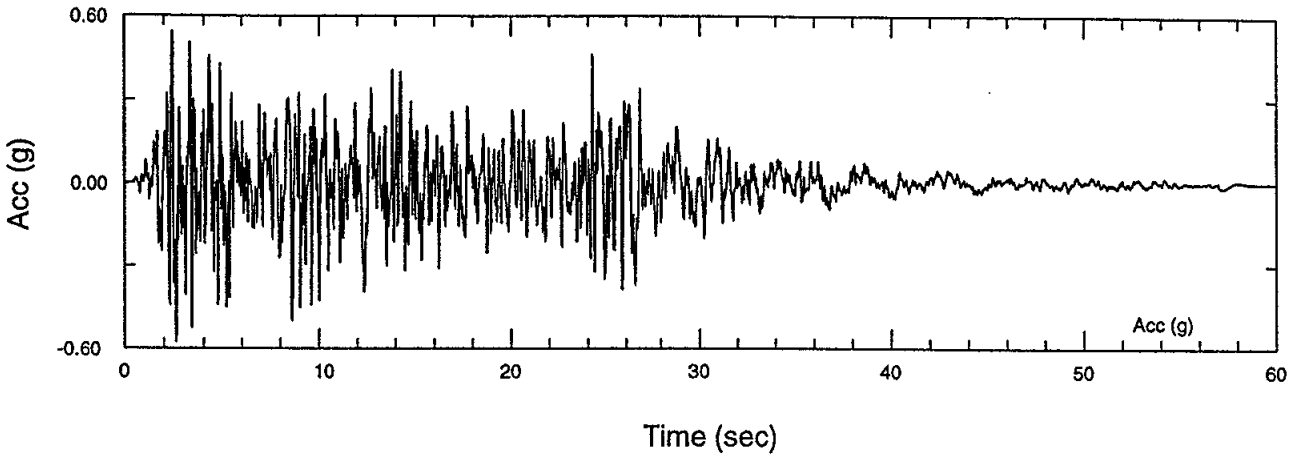

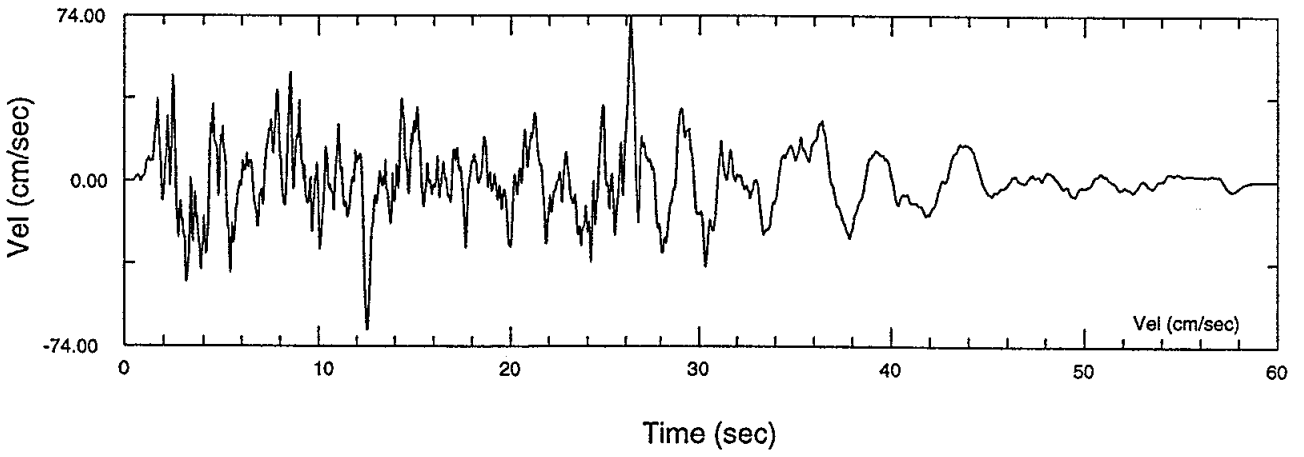

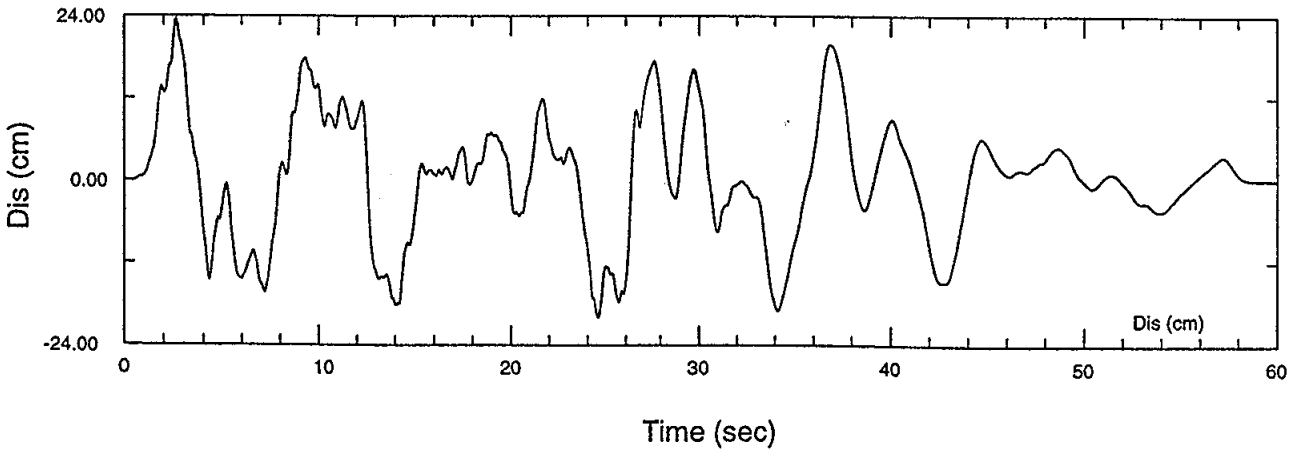

Figure E-7Set1 Initial Vertical Time History.

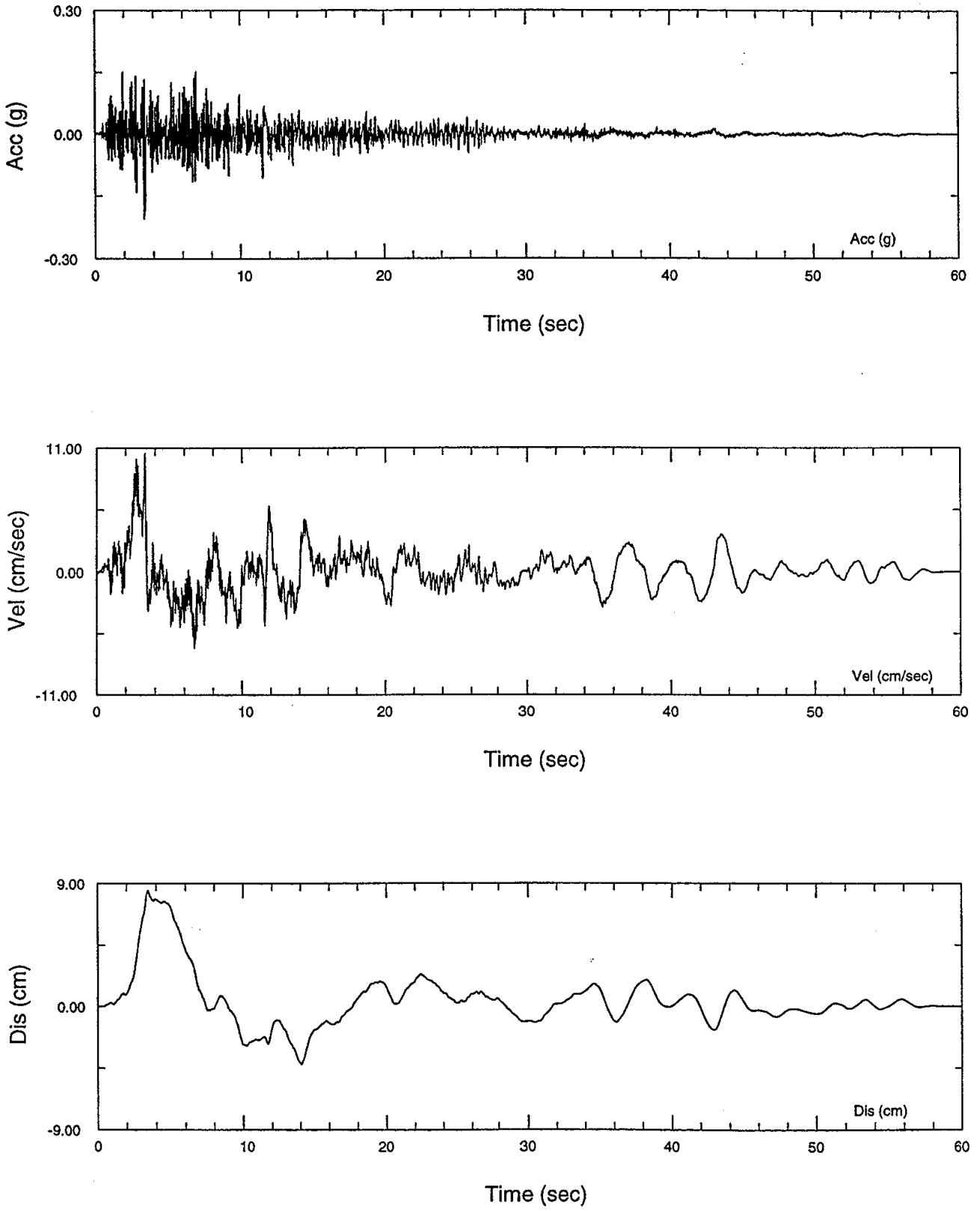

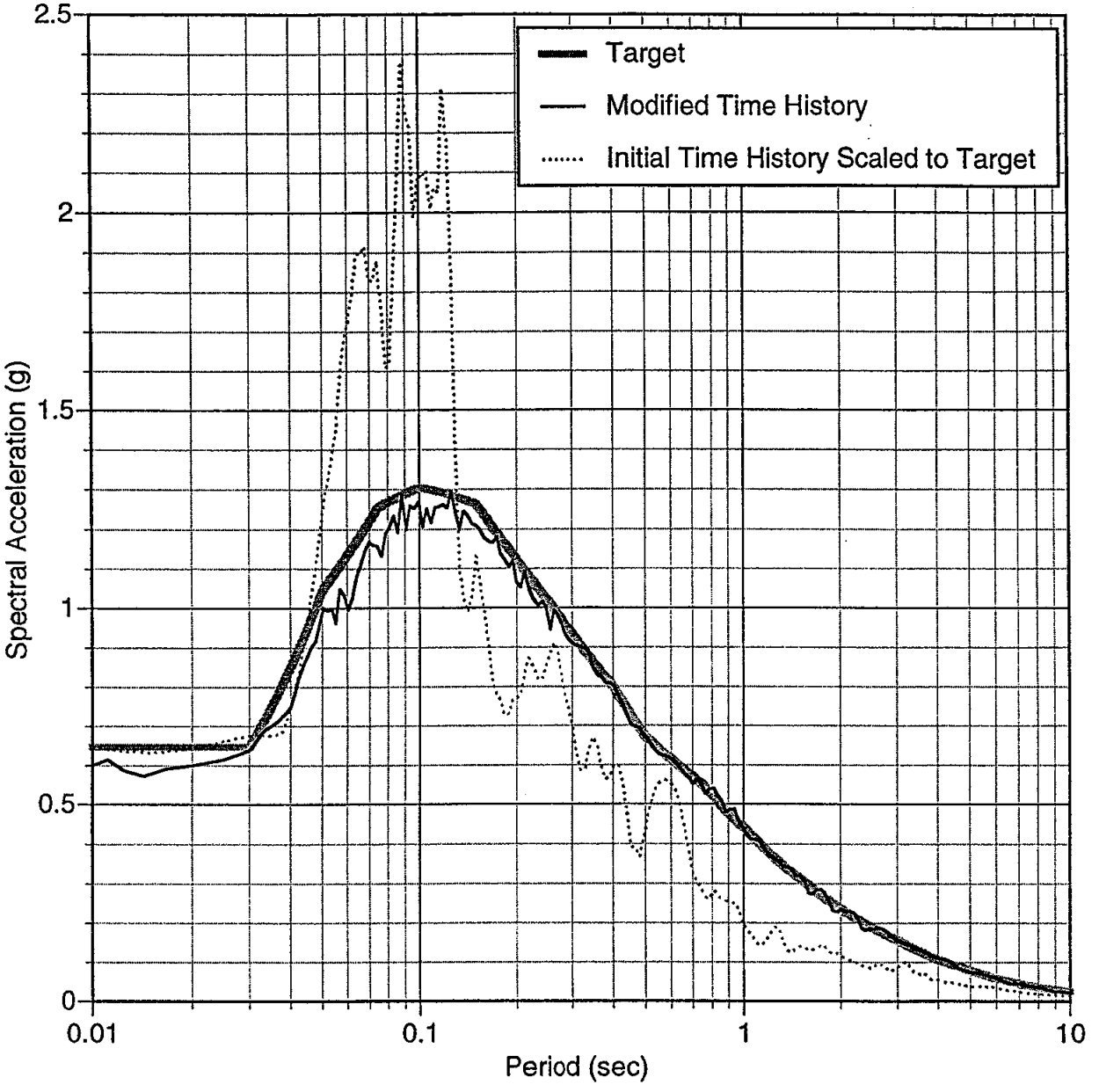

Figure E-8Set1 5% damped response spectra for the modified Vertical component and initial time history scaled to the target PGA.

...e: G3:Data1:East_BBridge_RefMotions:Report_Figures:Set1:Set1_rsp.dg

Figure E-9 Set1 Spectrum Compatible Vertical Reference Time History.

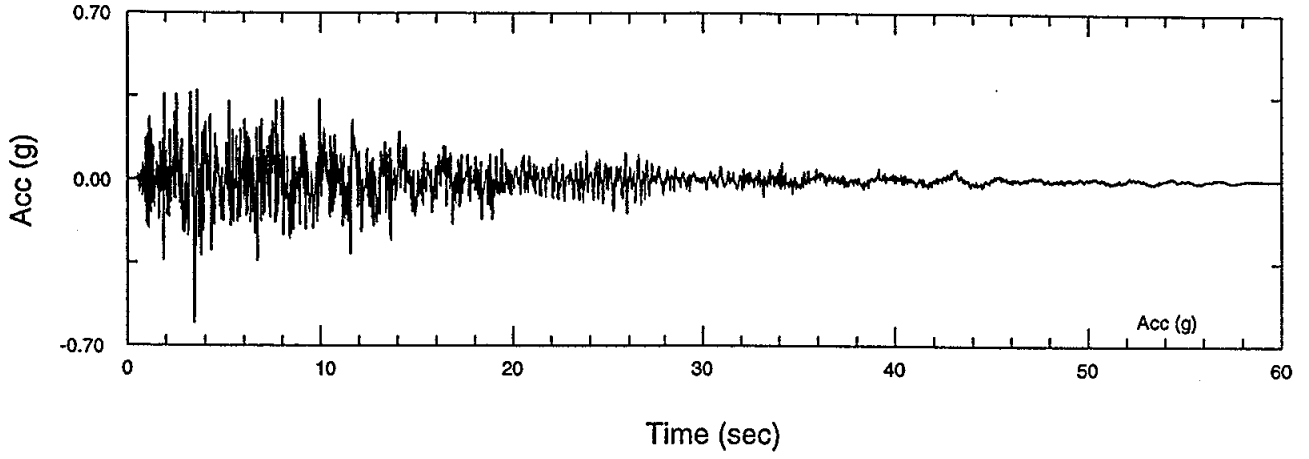

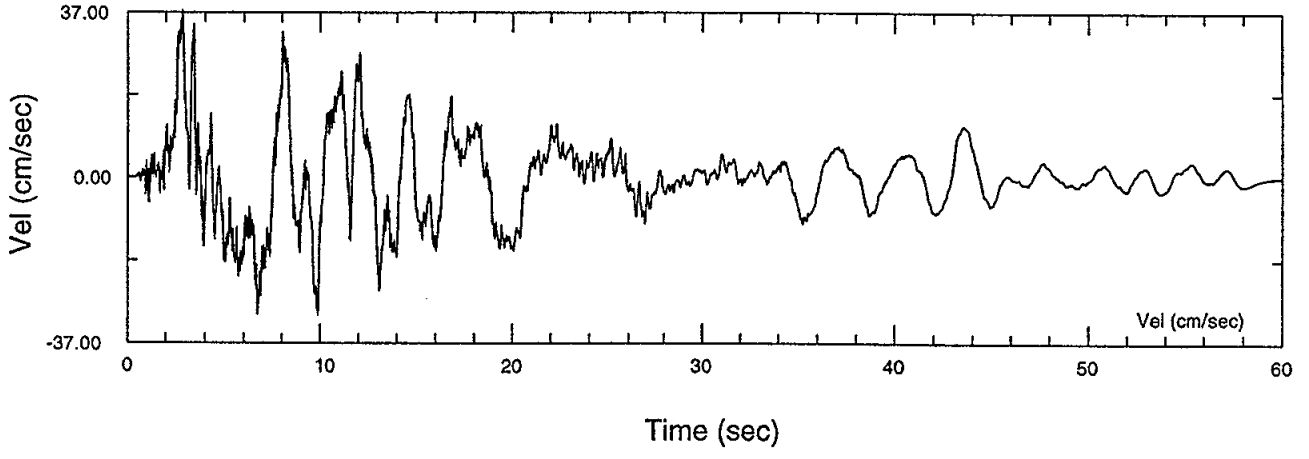

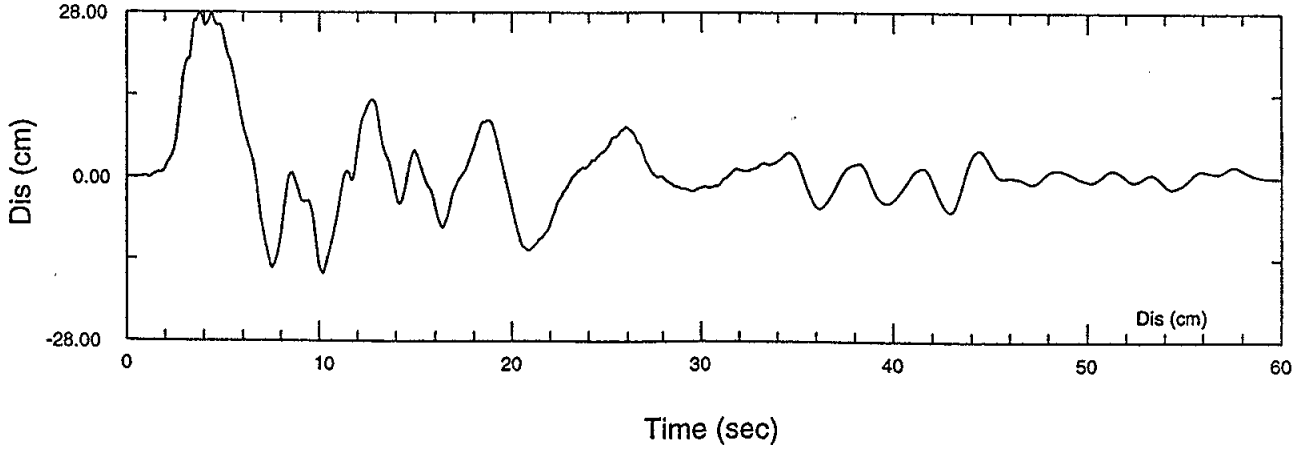

Figure E10 Set2 Initial Fault Normal Time History.

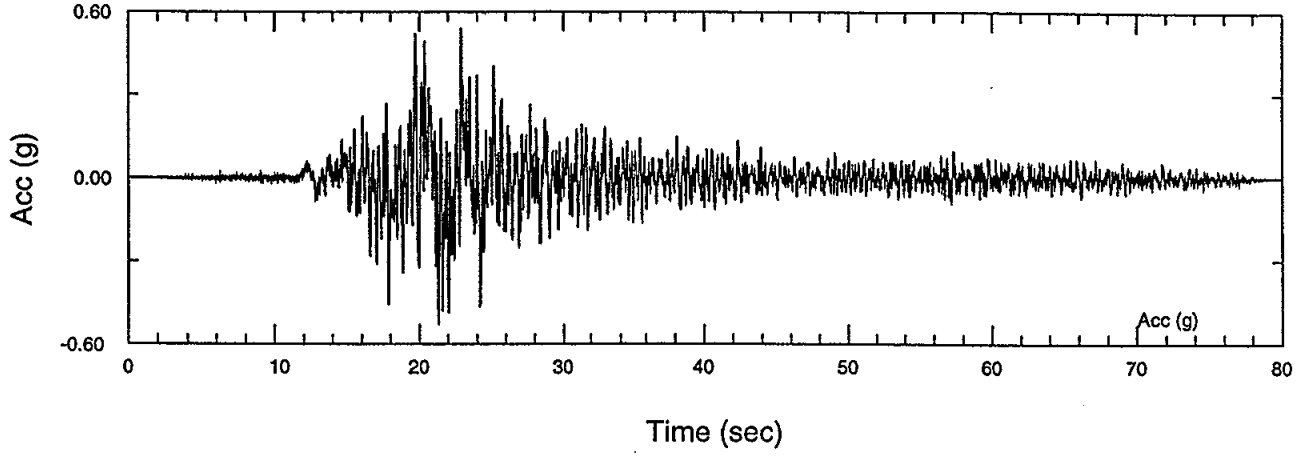

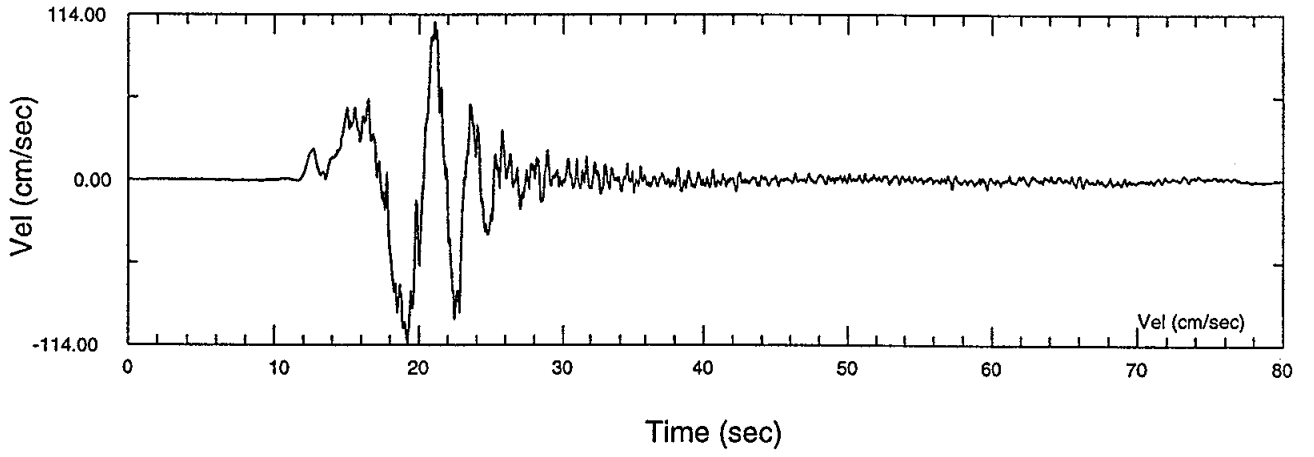

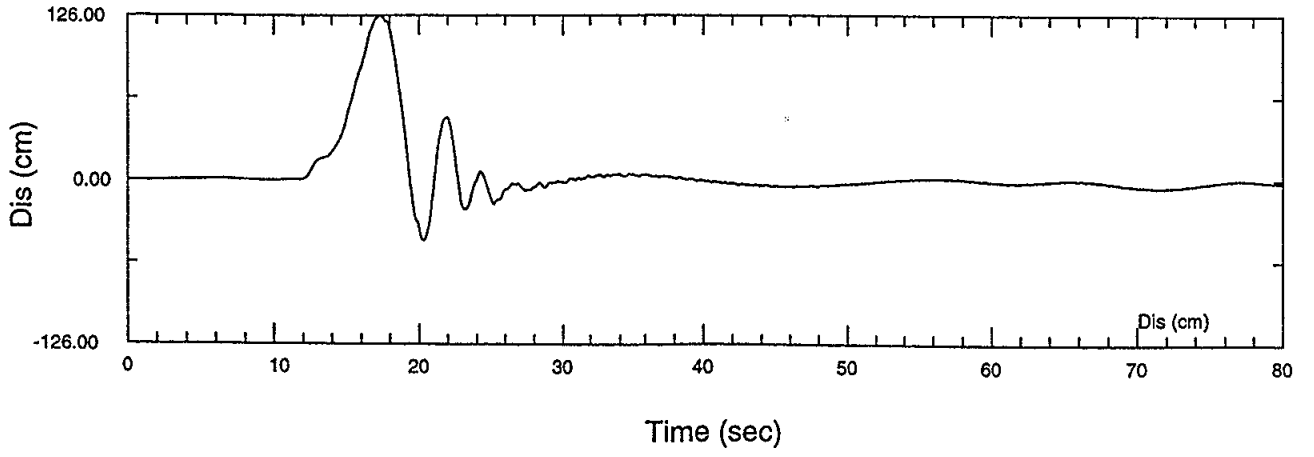

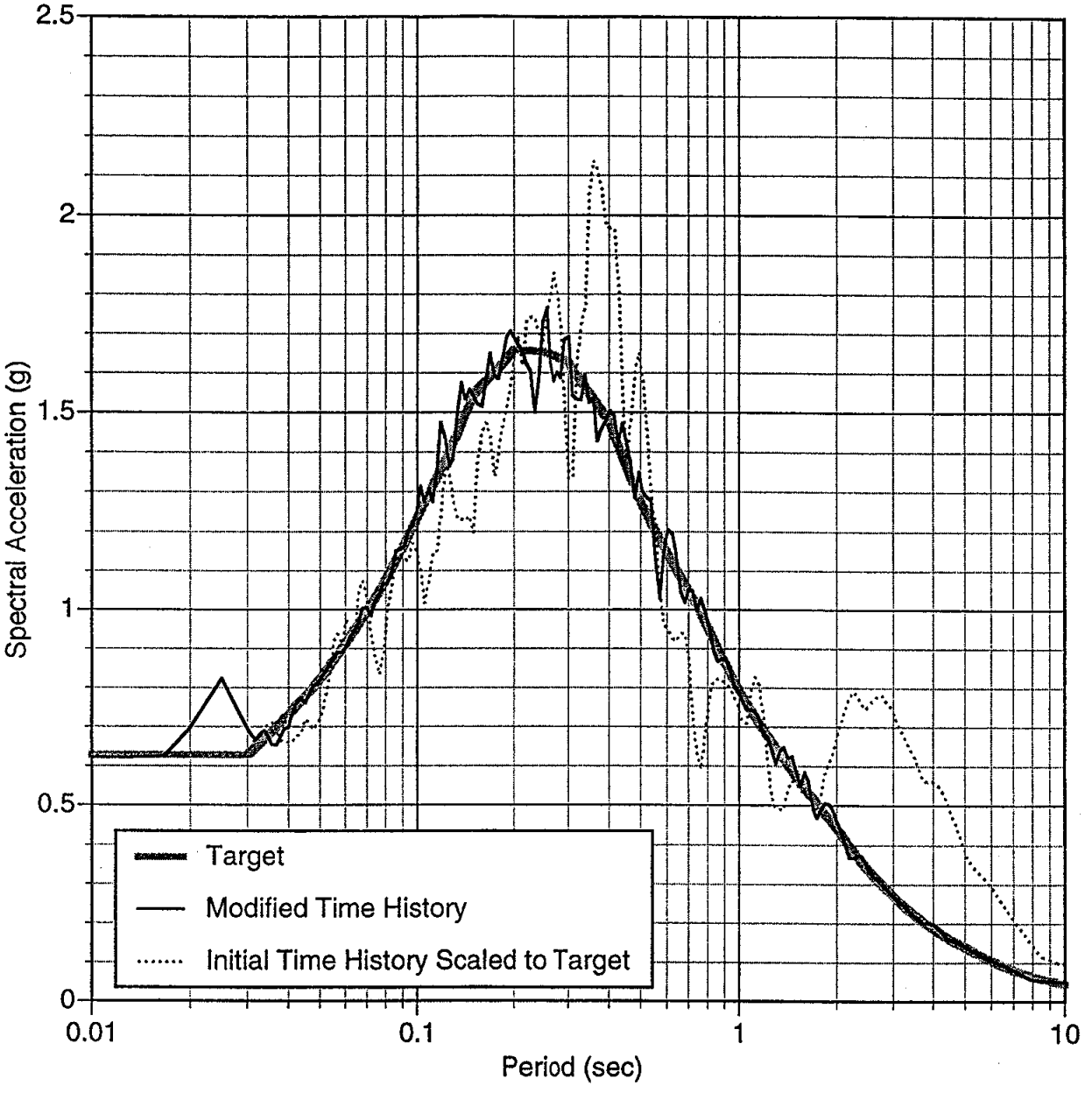

Figure E 11 Set2 5% damped response spectra for the modified Fault Normal component and initial time history scaled to the target PGA.

File: G3:Data1:East_BBridge_RefMotions:Report_Figures:Set2:Set2_rsp.dg

Figure E12 Set2 Spectrum Compatible Fault Normal Reference Time History.

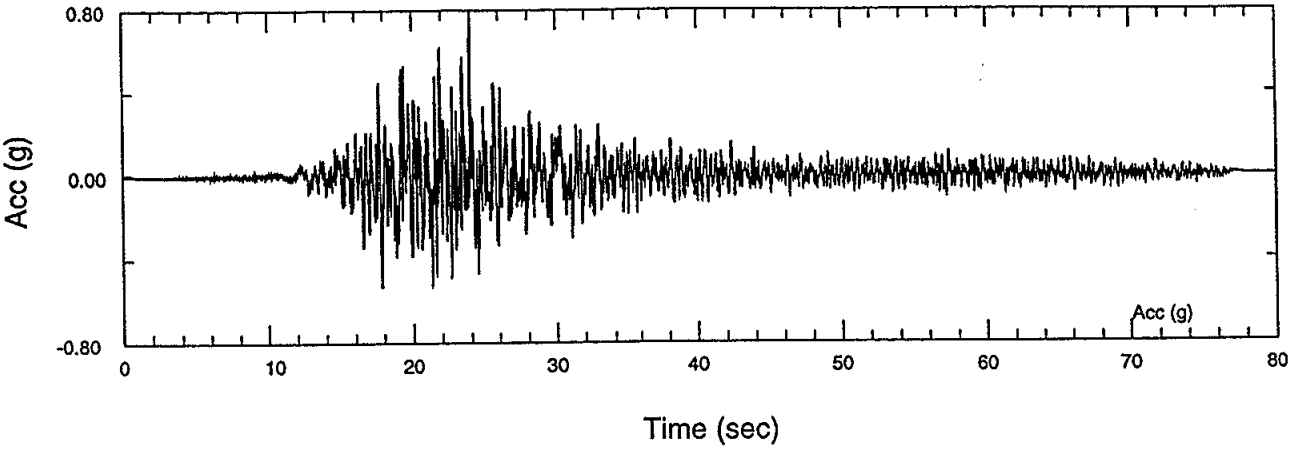

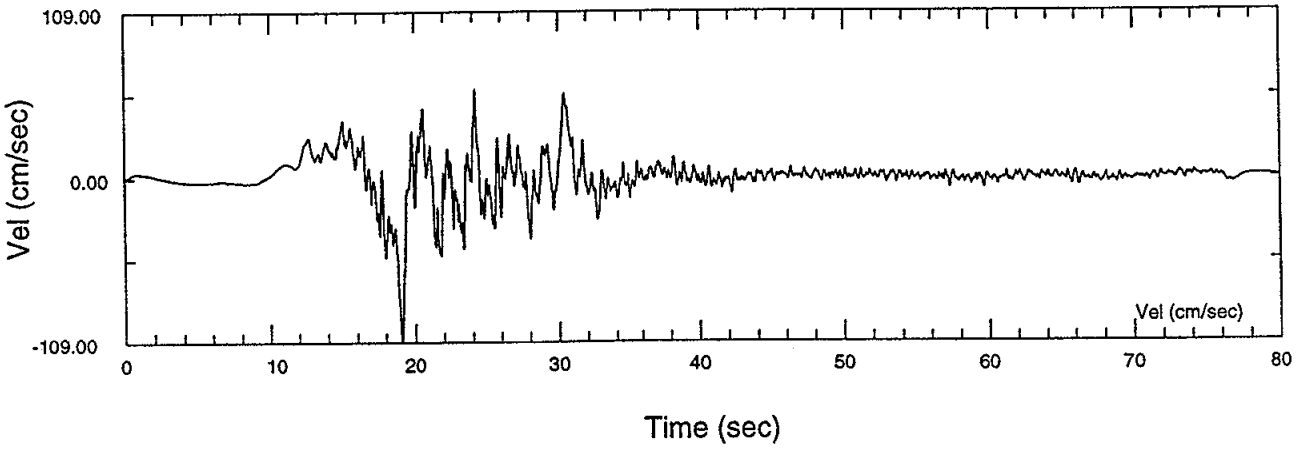

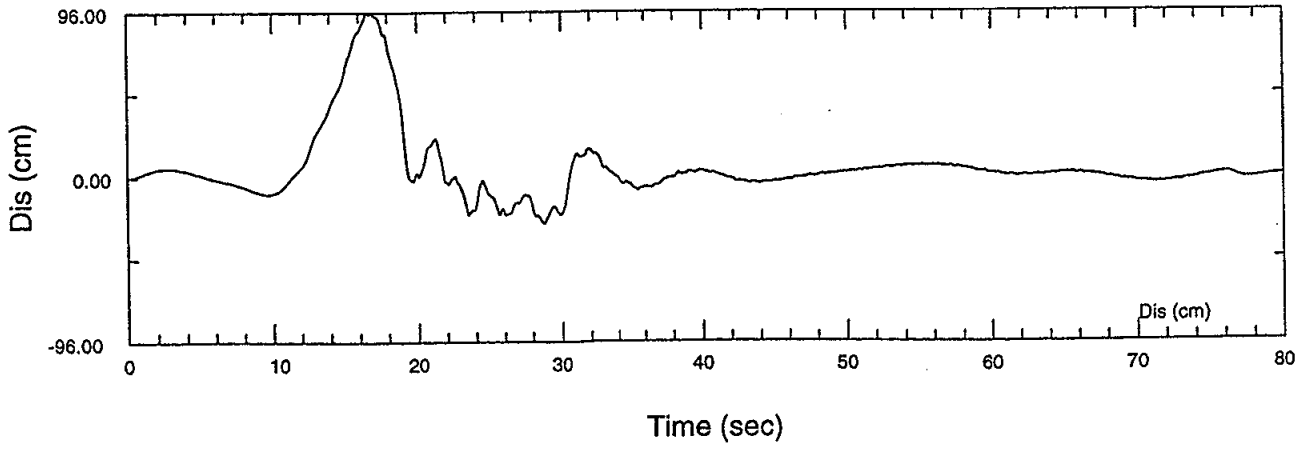

Figure E13 Set2 Initial Fault Parallel Time History.

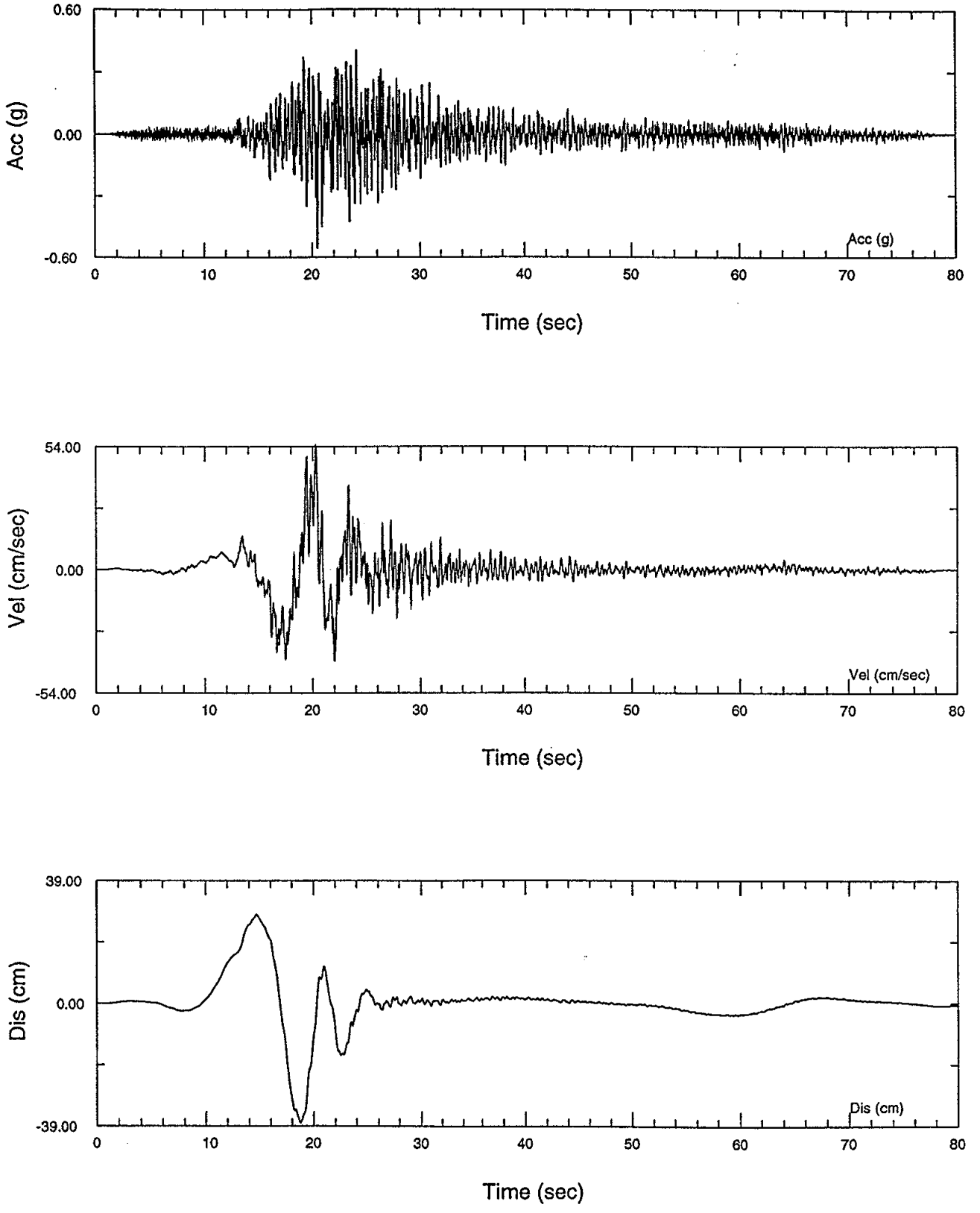

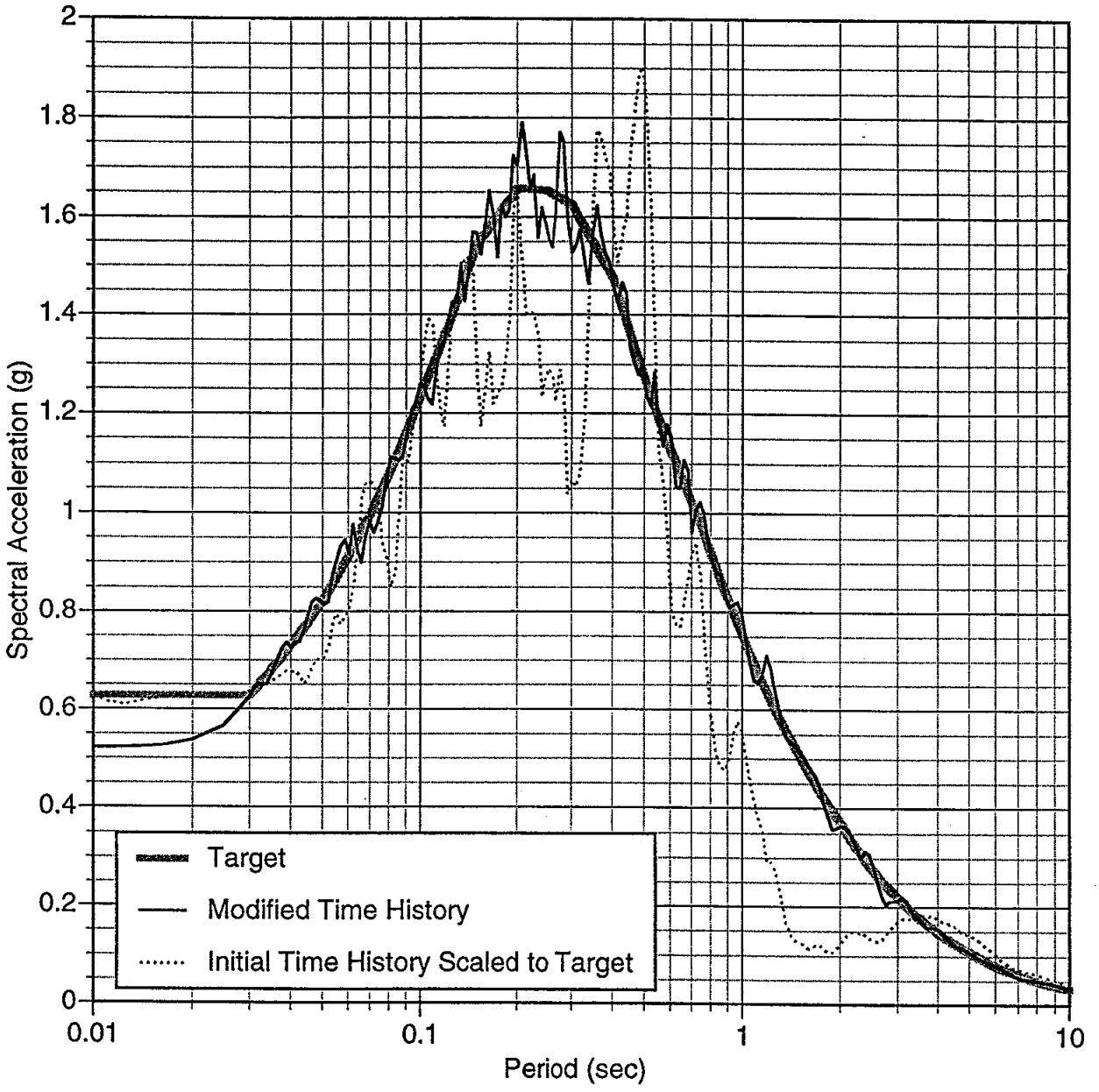

Figure E1.4Set2 5% damped response spectra for the modified Fault Parallel component and initial time history scaled to the target PGA.

File: G3:Data1:East_BBridge_RefMotions:Report_Figures:Set2:Set2_rsp.dg

Figure E15 Set2 Spectrum Compatible Fault Parallel Reference Time History.

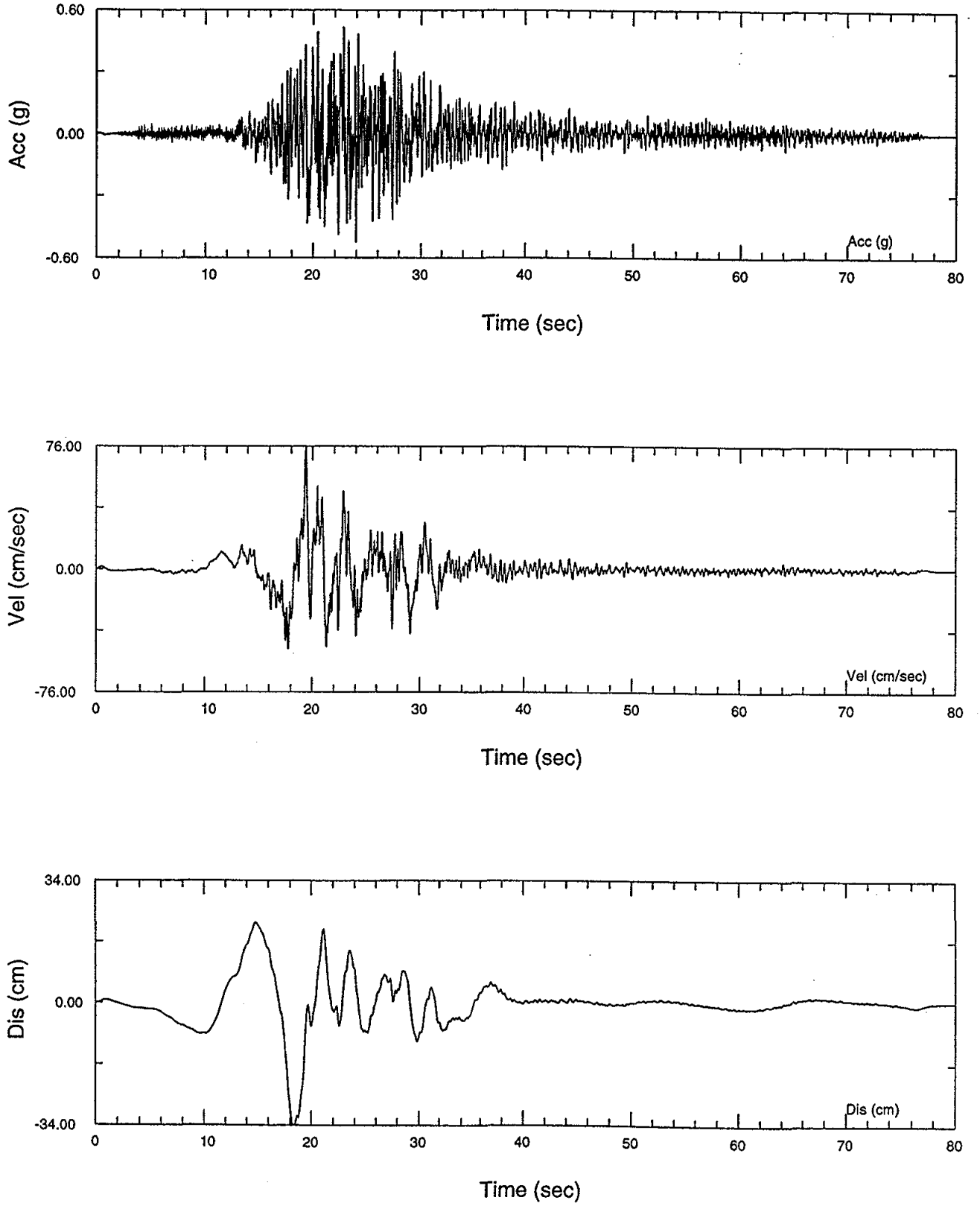

Figure E16 Set2 Initial Vertical Time History.

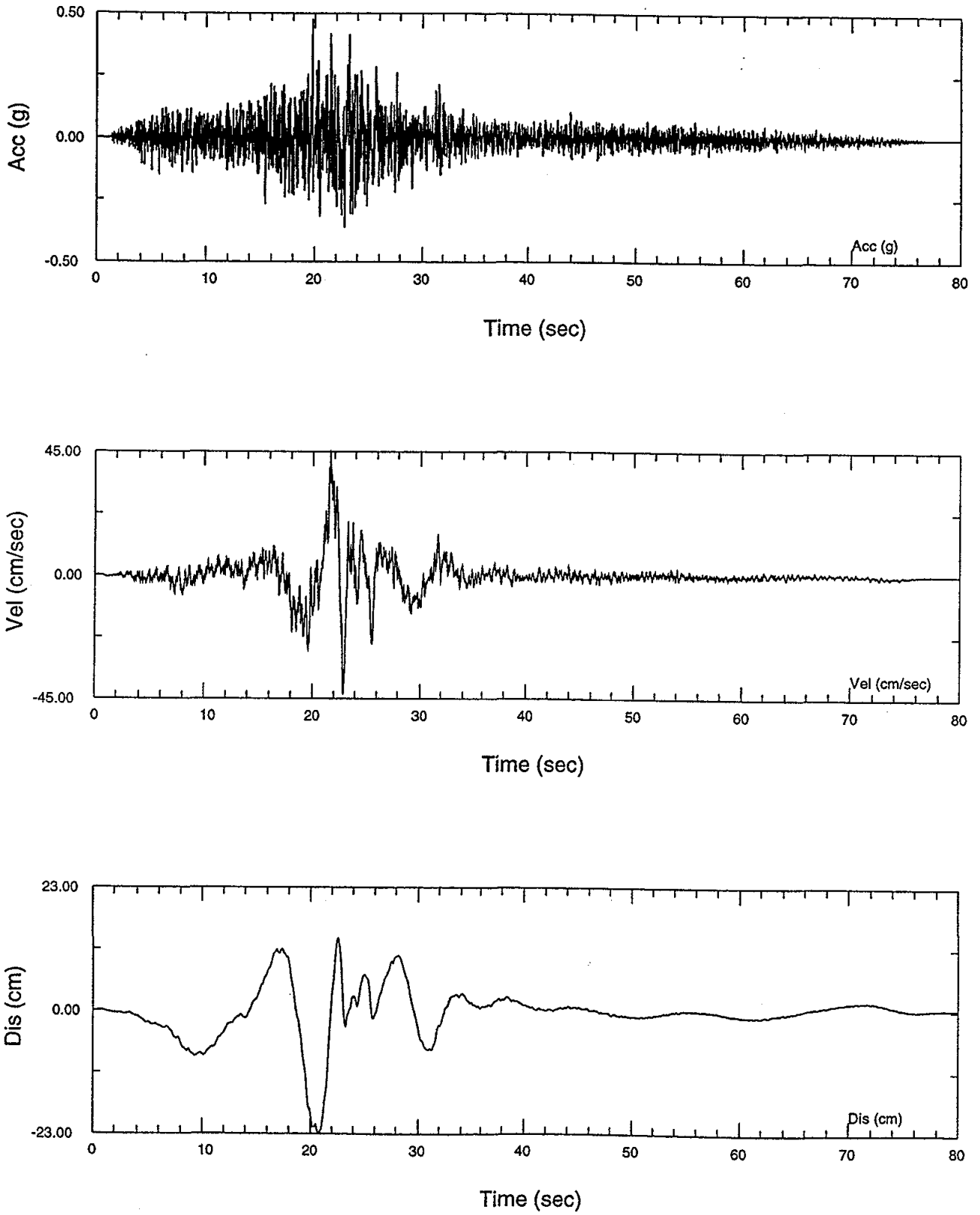

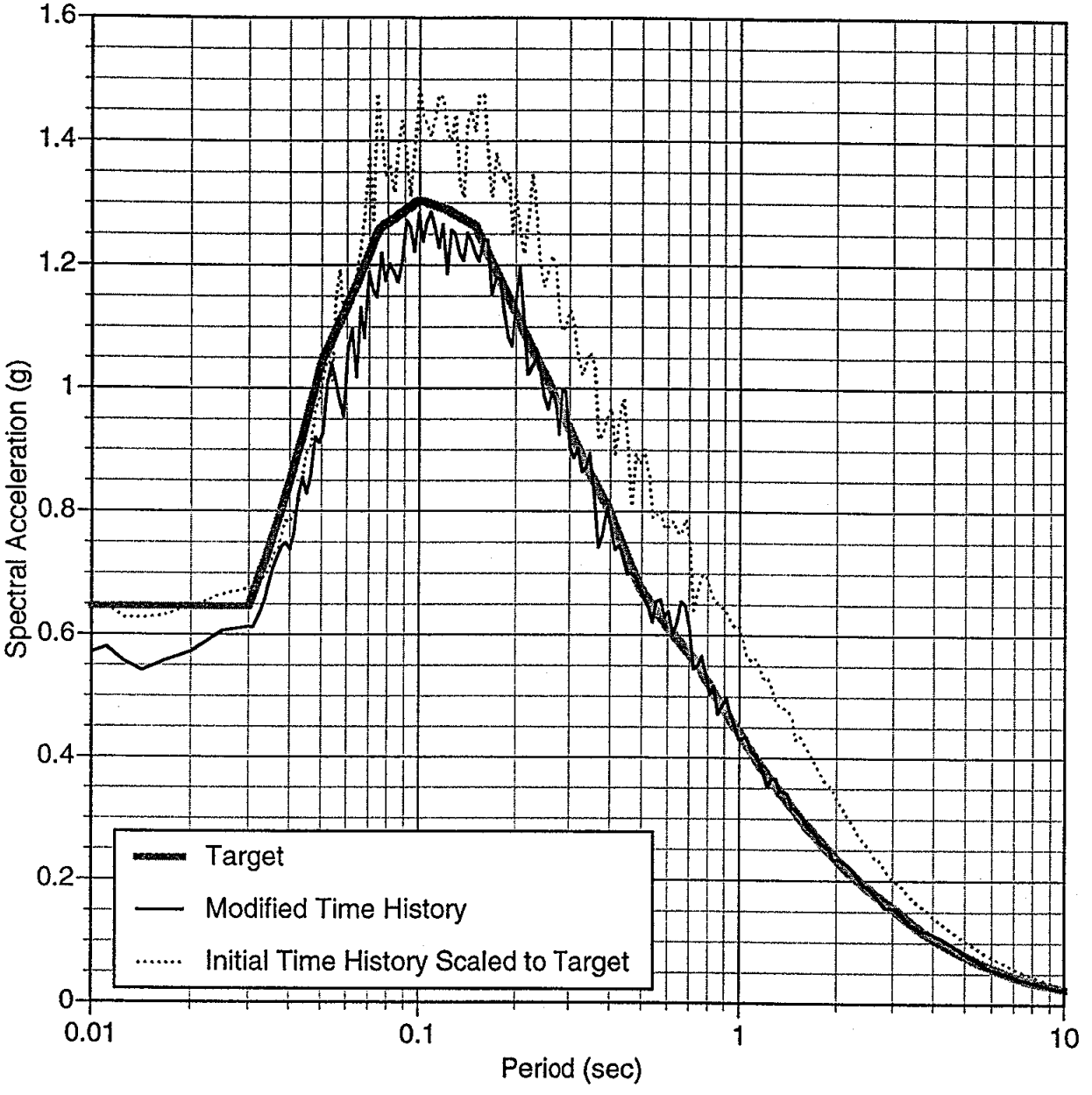

Figure E17 Set2 5% damped response spectra for the modified Vertical component and initial time history scaled to the target PGA.

...d: G3:Data1:East_BBridge_RefMotions:Report_Figures:Set2:Set2_rsp.dg

Figure E18. Set2 Spectrum Compatible Vertical Reference Time History.

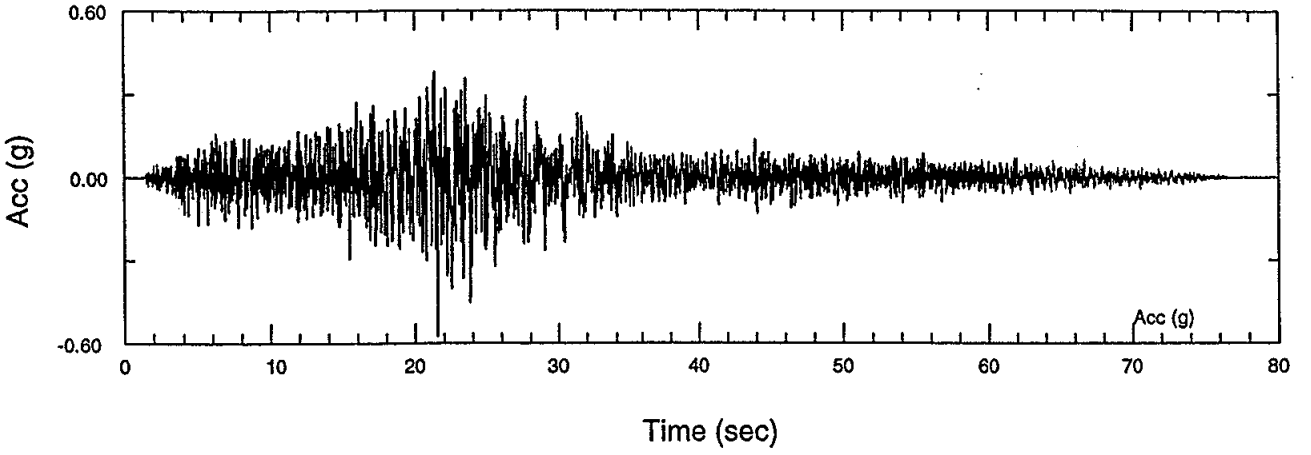

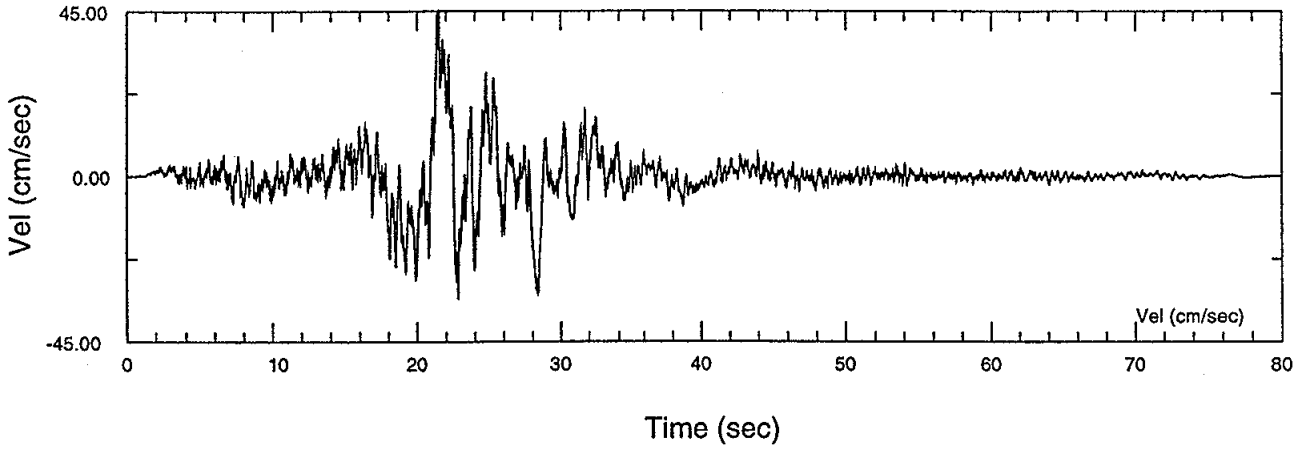

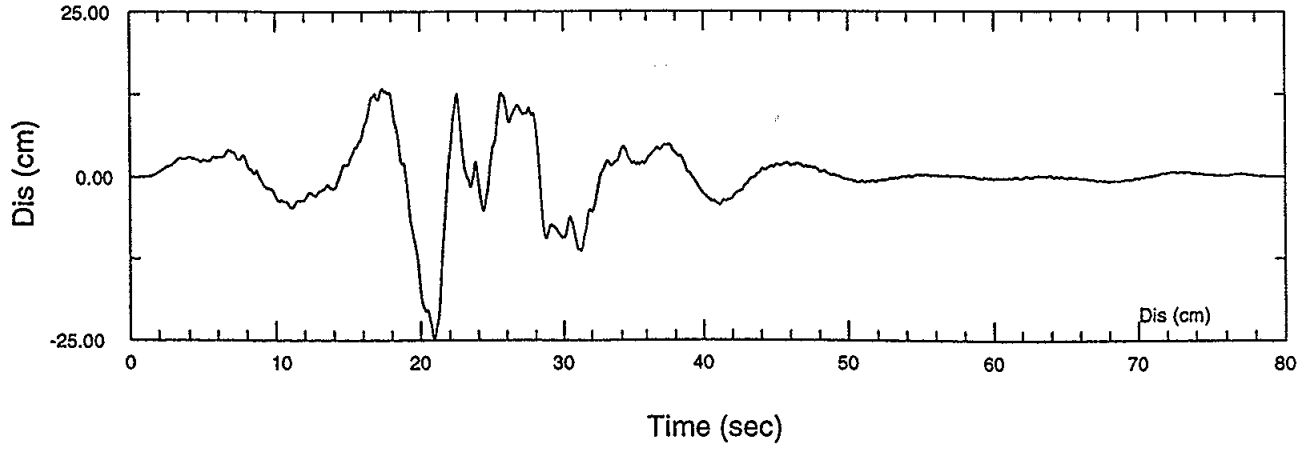

Figure E19 Set3 Initial Fault Normal Time History.

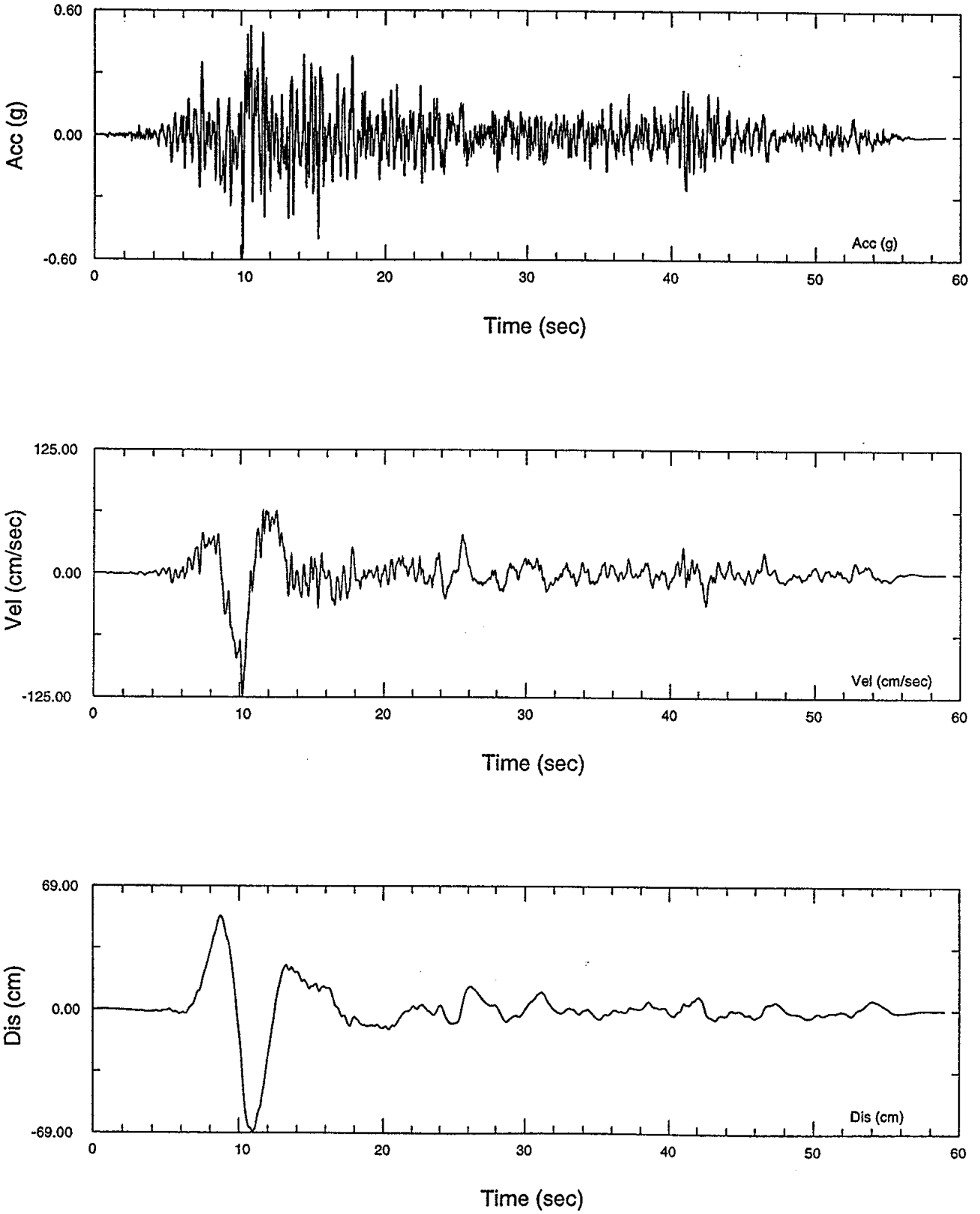

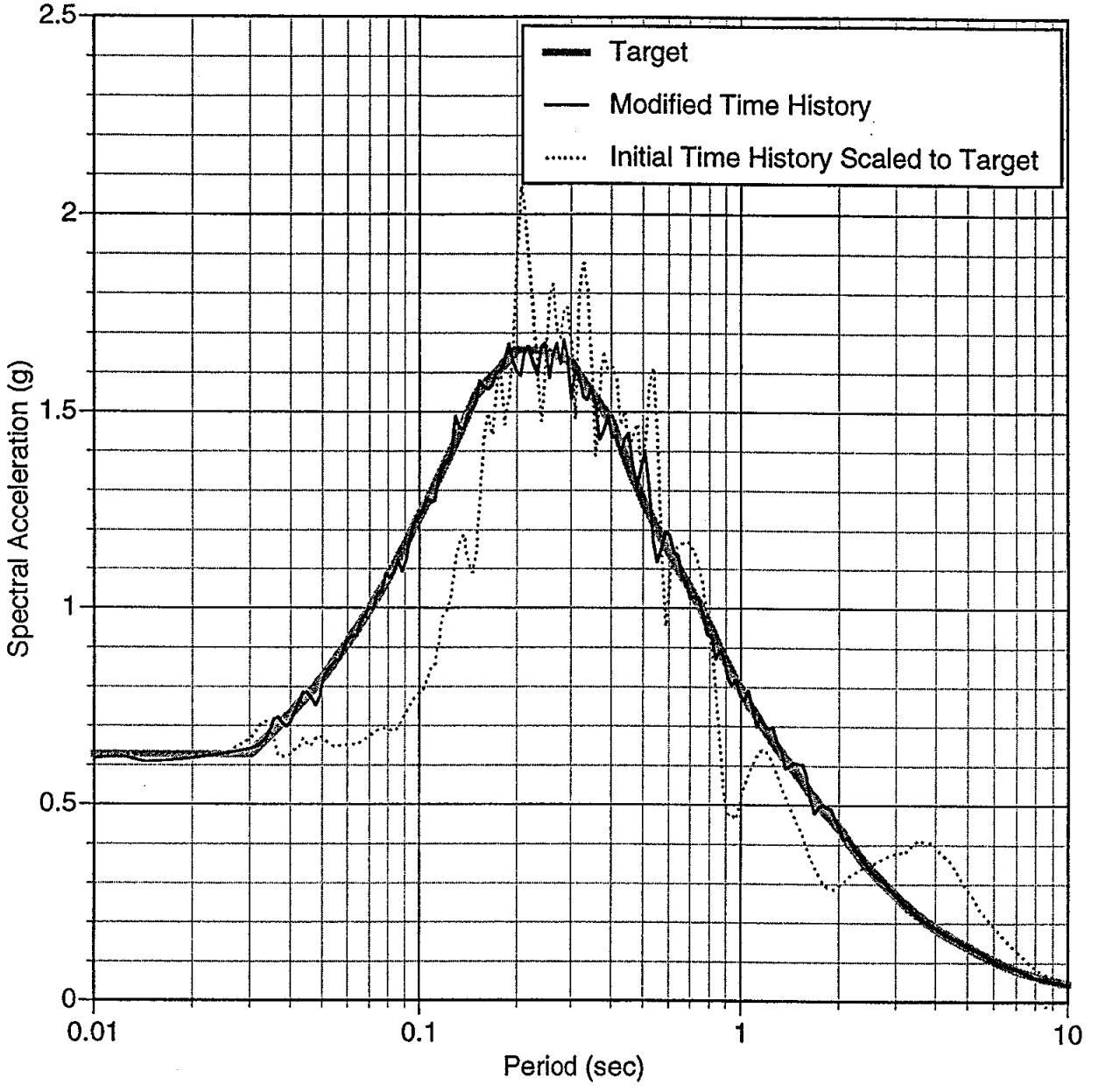

Figure E20 Set3 5% damped response spectra for the modified Fault Normal component and initial time history scaled to the target PGA.

File: G3:Data1:East_BBridge_RefMotions:Report_Figures:Set3:Set3_rsp.dg

Figure E2.1Set3 Spectrum Compatible Fault Normal Reference Time History.

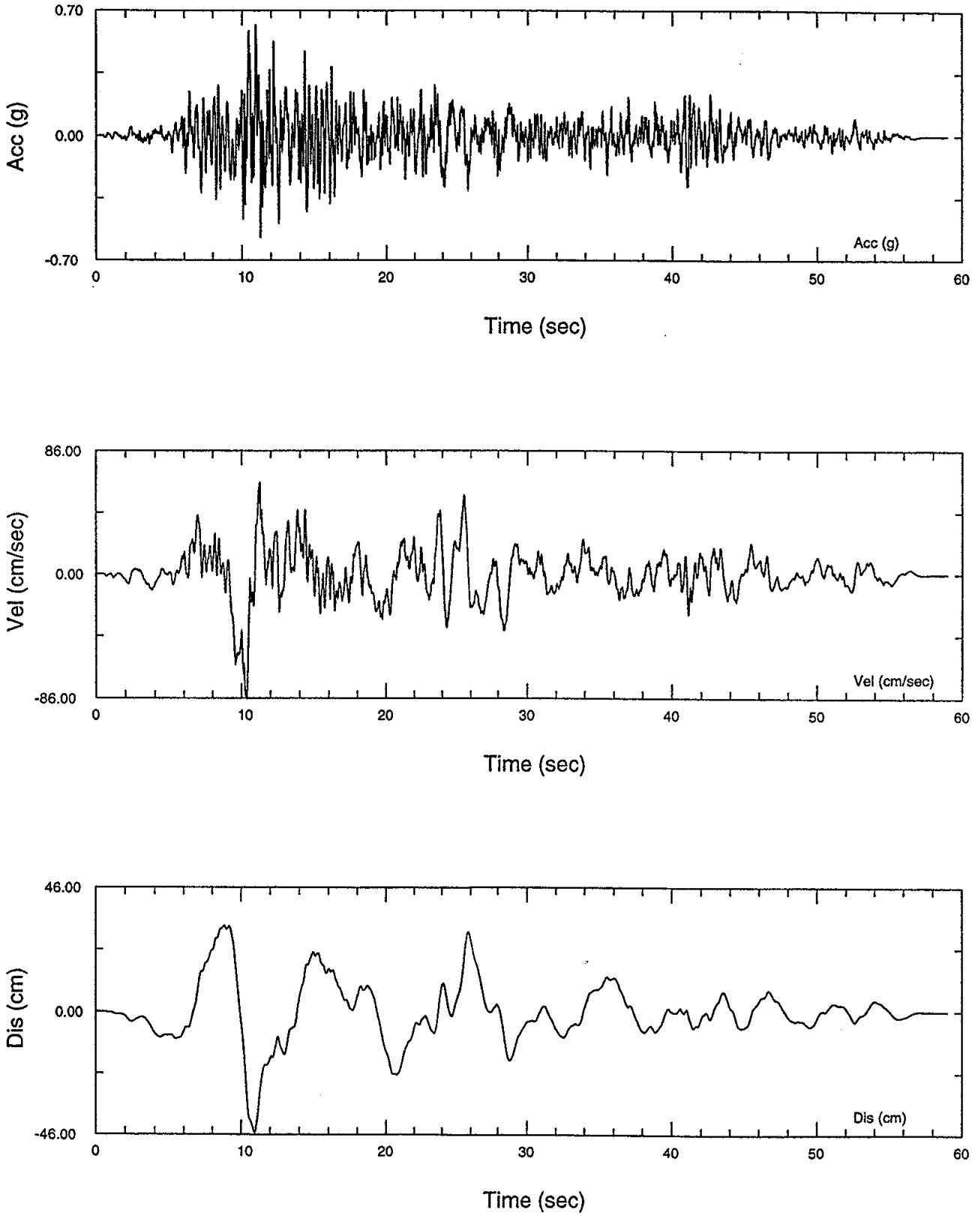

Figure E22 Set3 Initial Fault Parallel Time History.

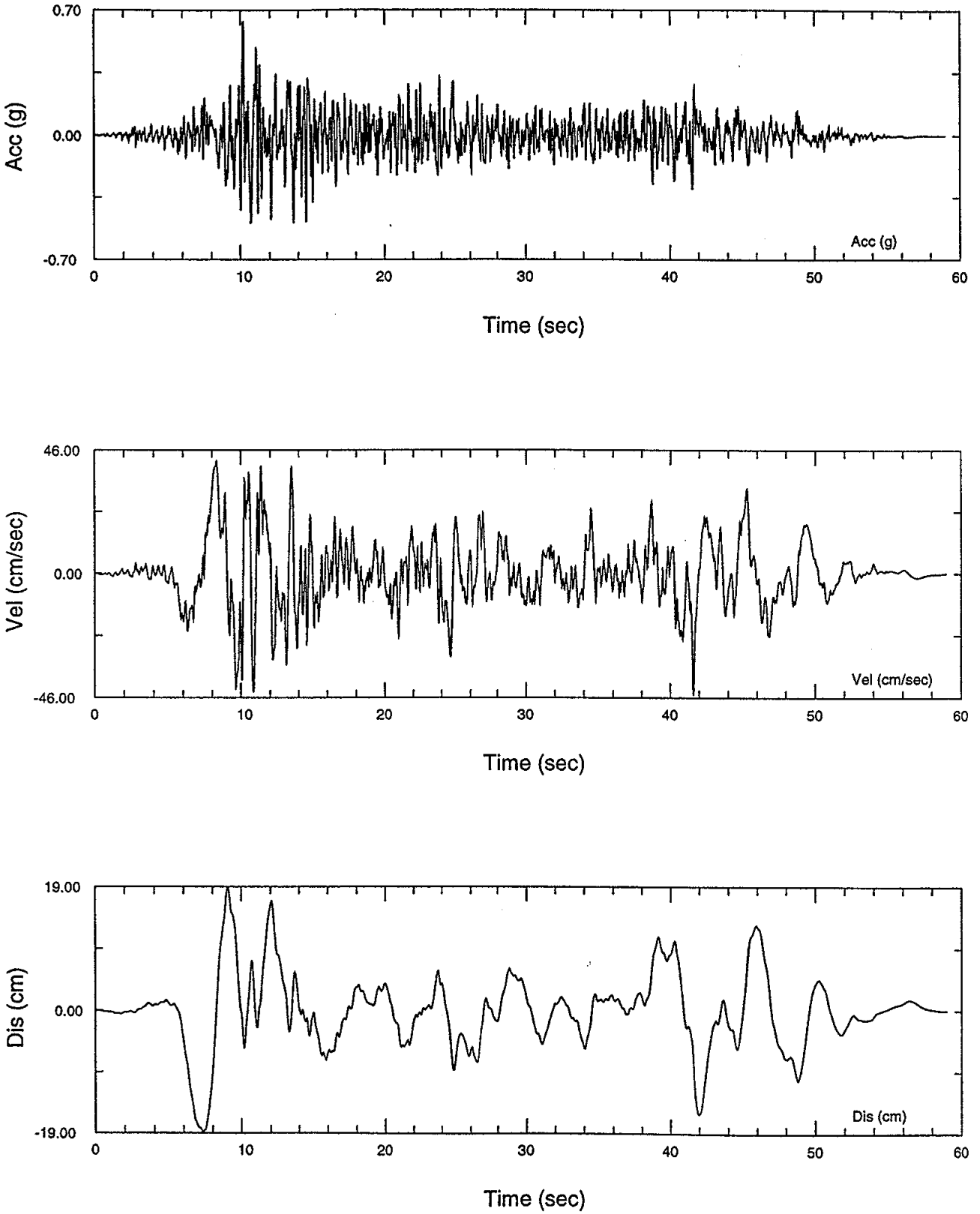

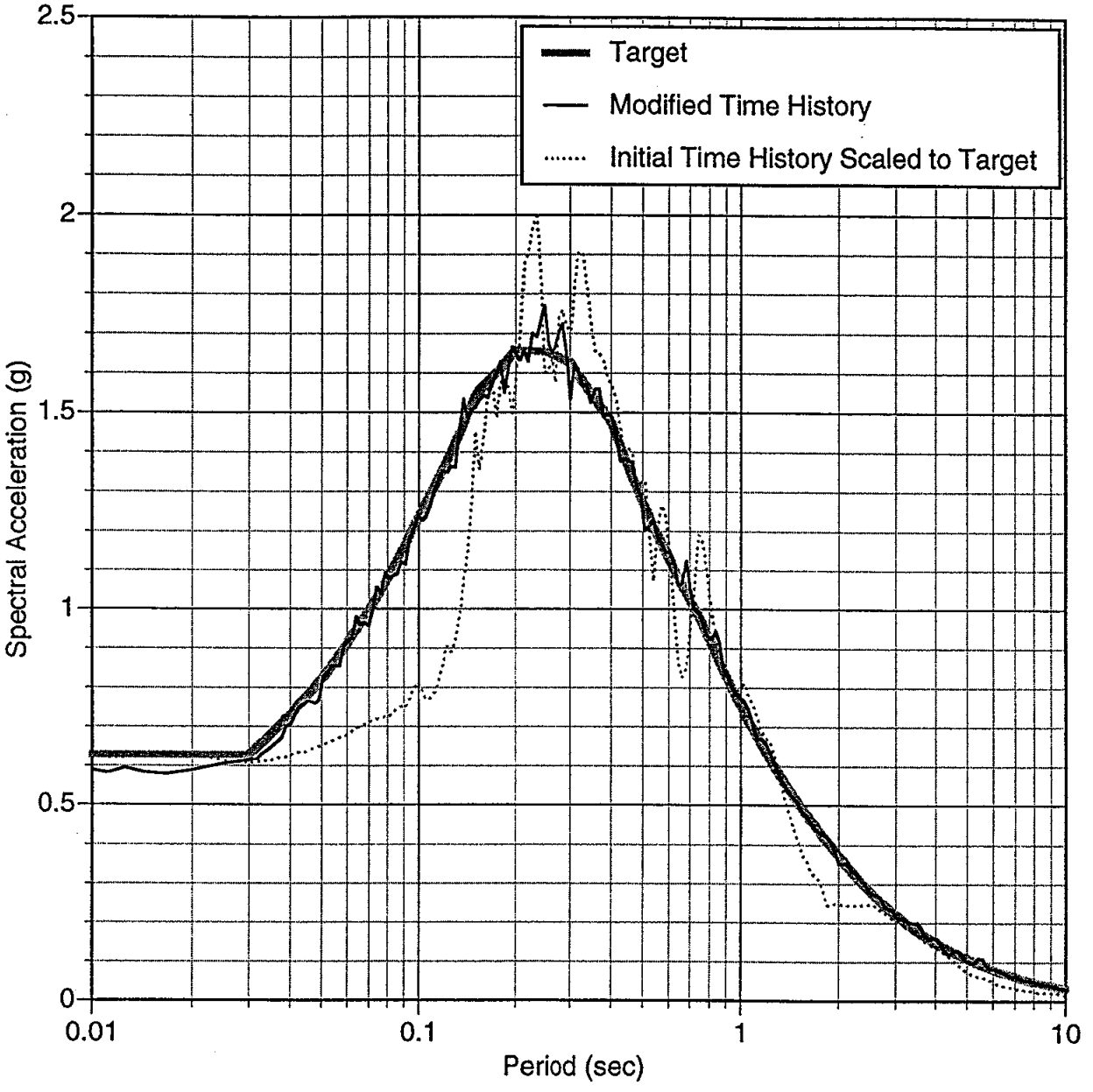

Figure E2.3Set3 5% damped response spectra for the modified Fault Parallel component and initial time history scaled to the target PGA.

File: G3:Data1:East_BBridge_RefMotions:Report_Figures:Set3:Set3_rsp.dg

Figure E24 Set3 Spectrum Compatible Fault Parallel Time History.

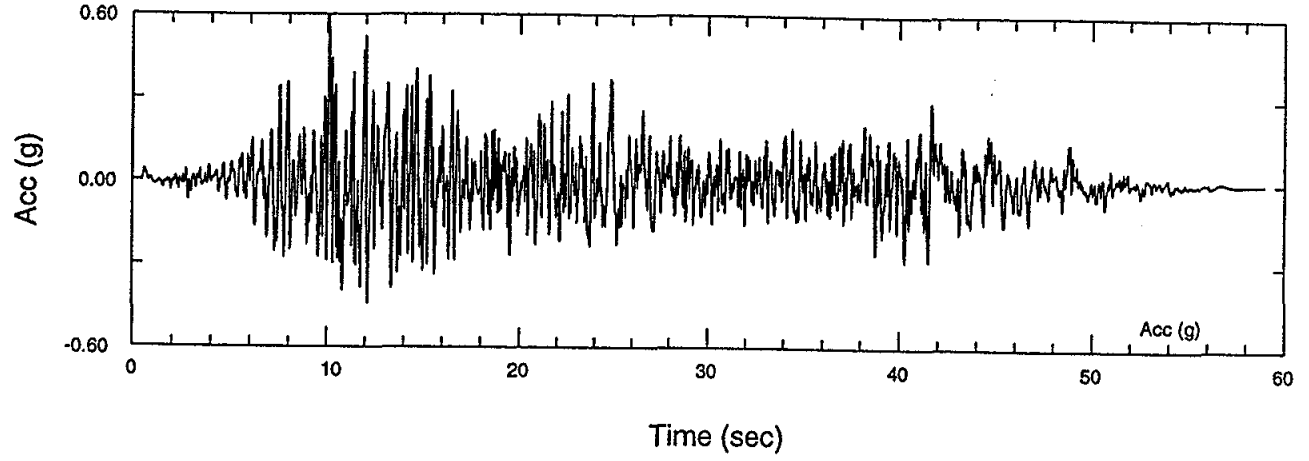

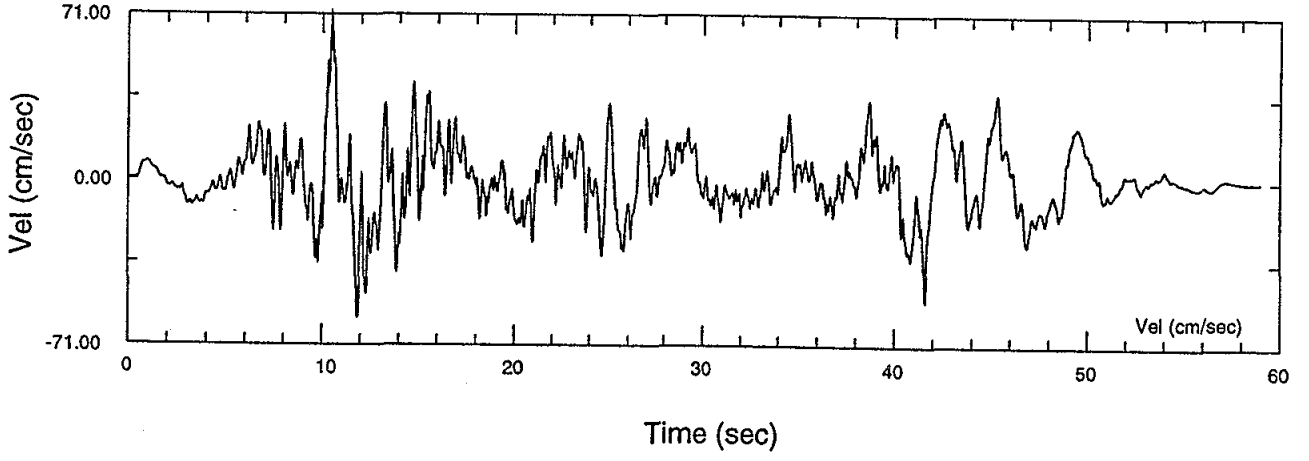

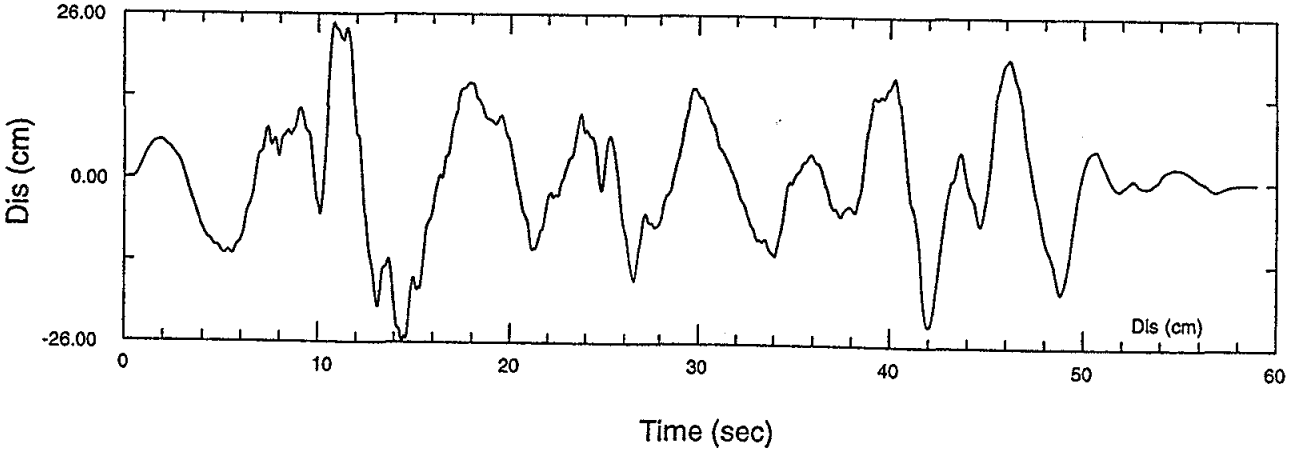

Figure E25 Set3 Initial Vertical Time History.

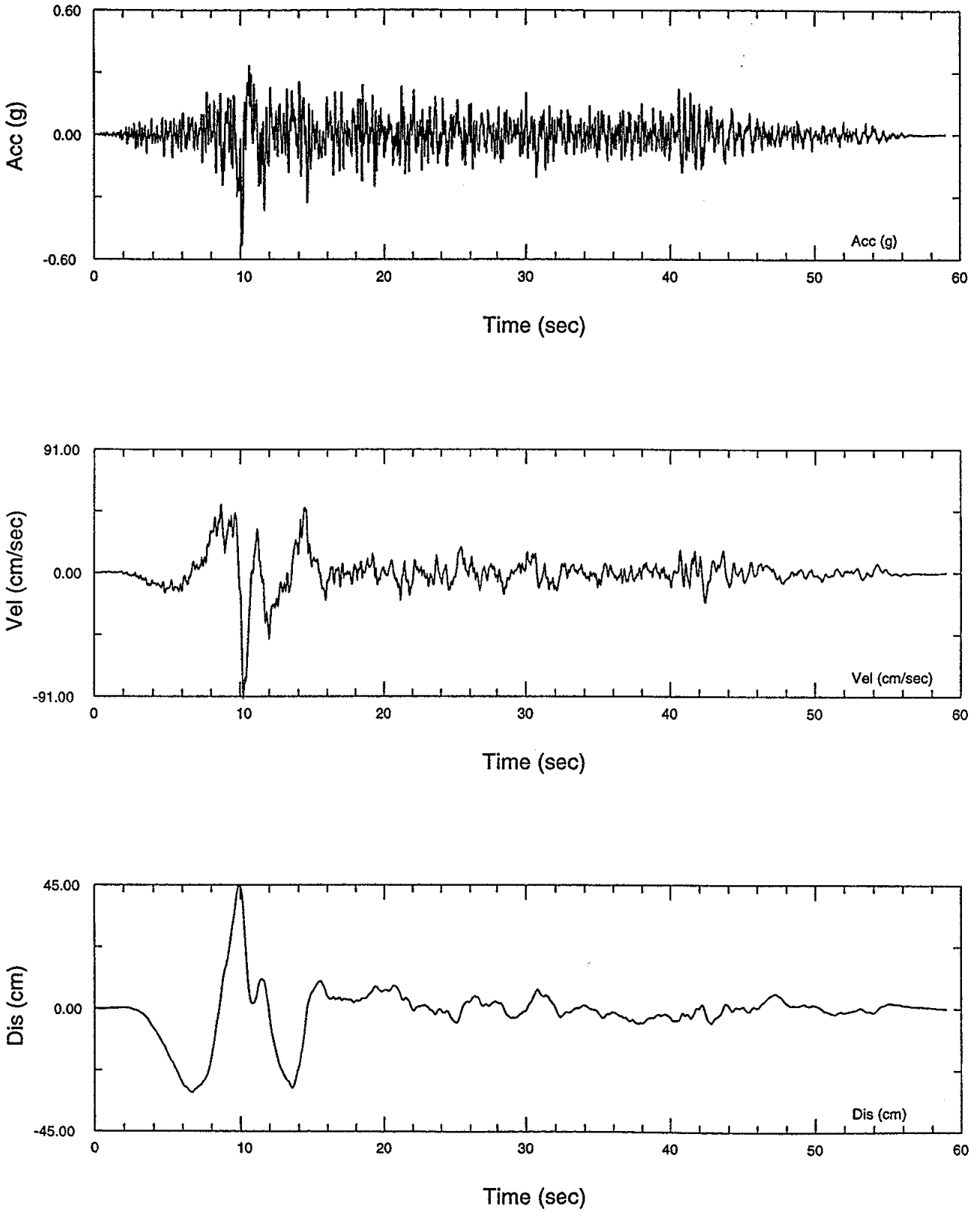

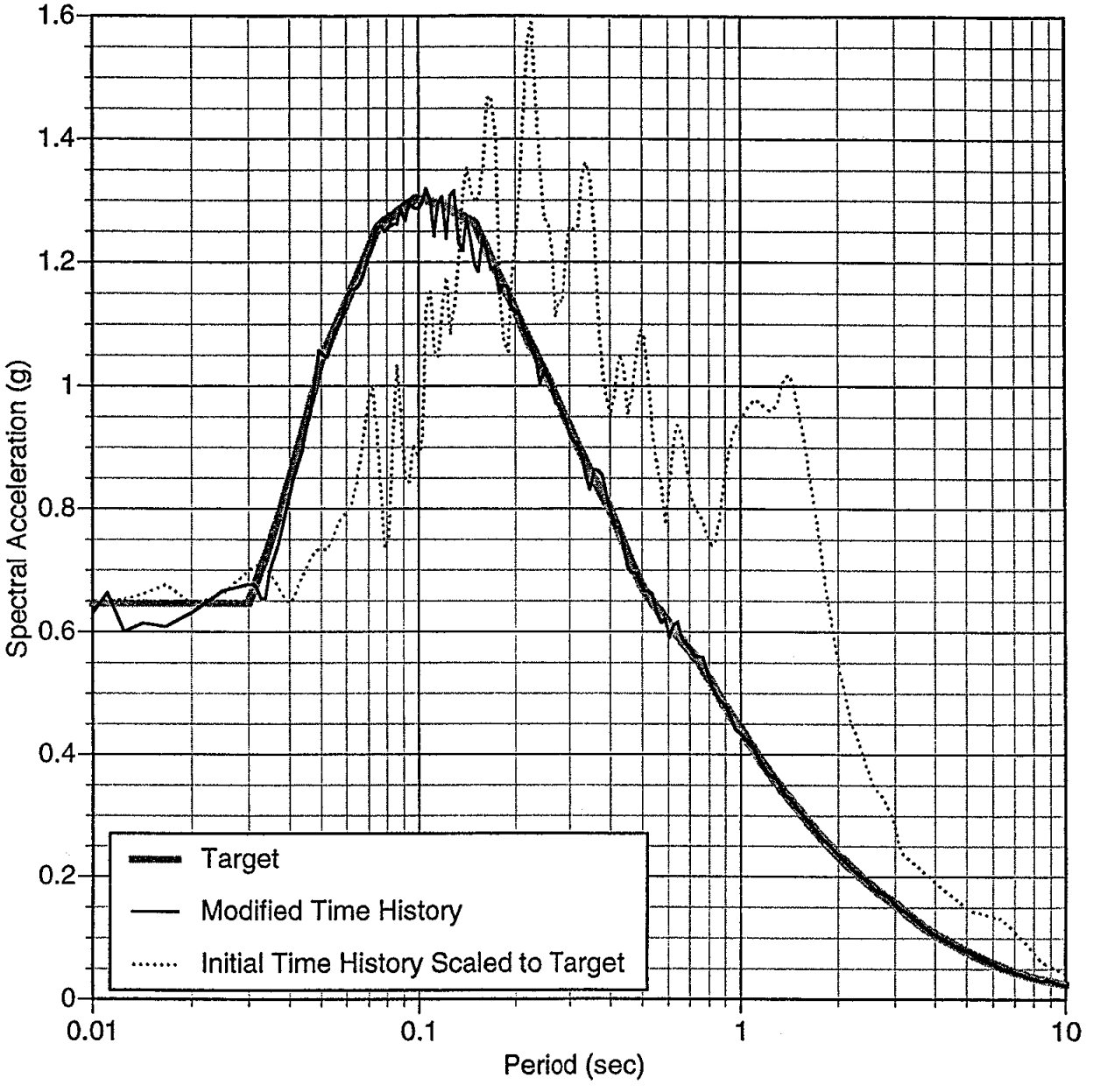

Figure E2.6 Set3 5% damped response spectra for the modified Vertical component and initial time history scaled to the target PGA.

File: G3:Data1:East_SBridge_RefMotions:Report_Figures:Set3:Set3_rsp.dg

Figure E27 Set3 Spectrum Compatible Vertical Time History.

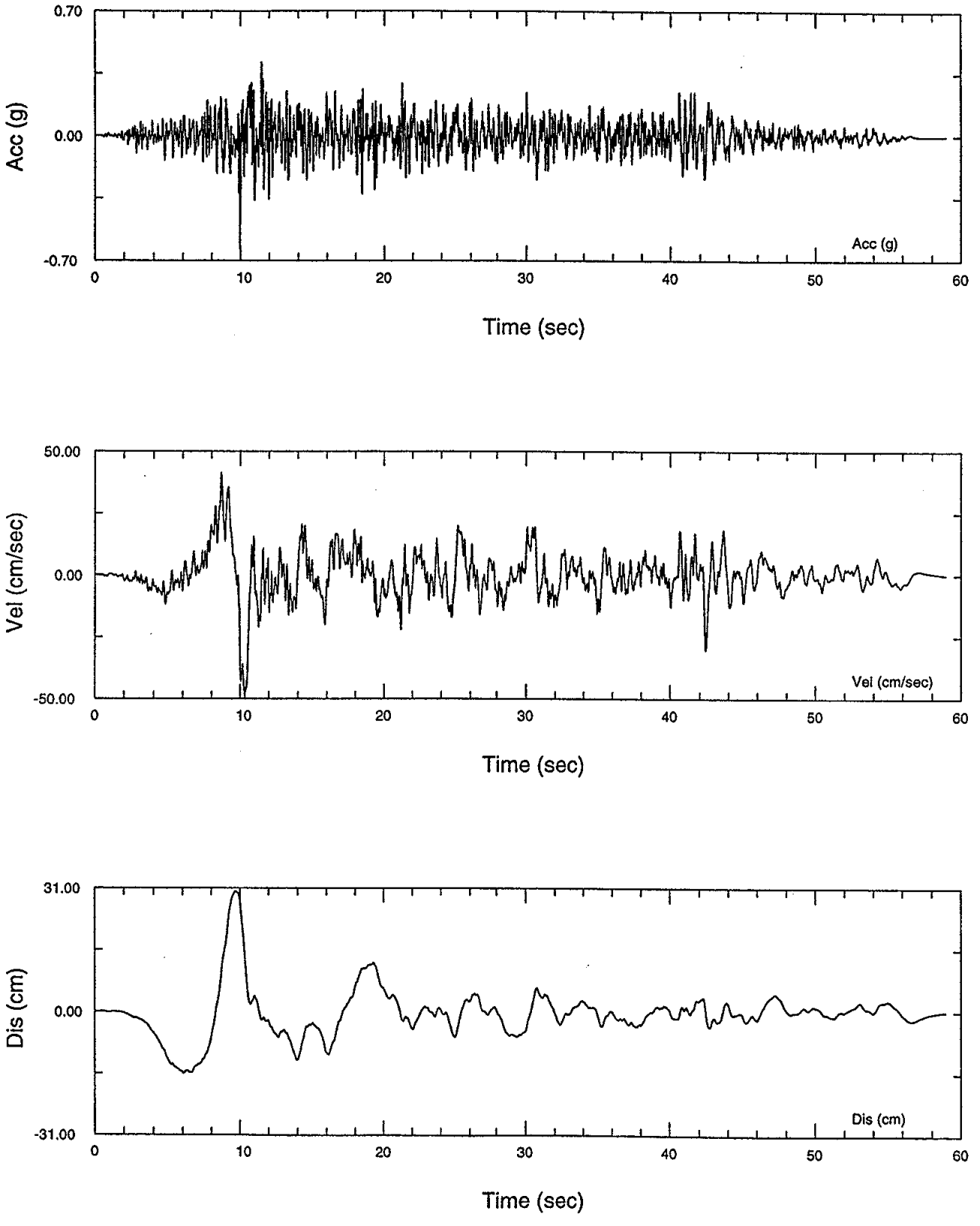

Figure E28 Set4 Initial Fault Normal Time History.

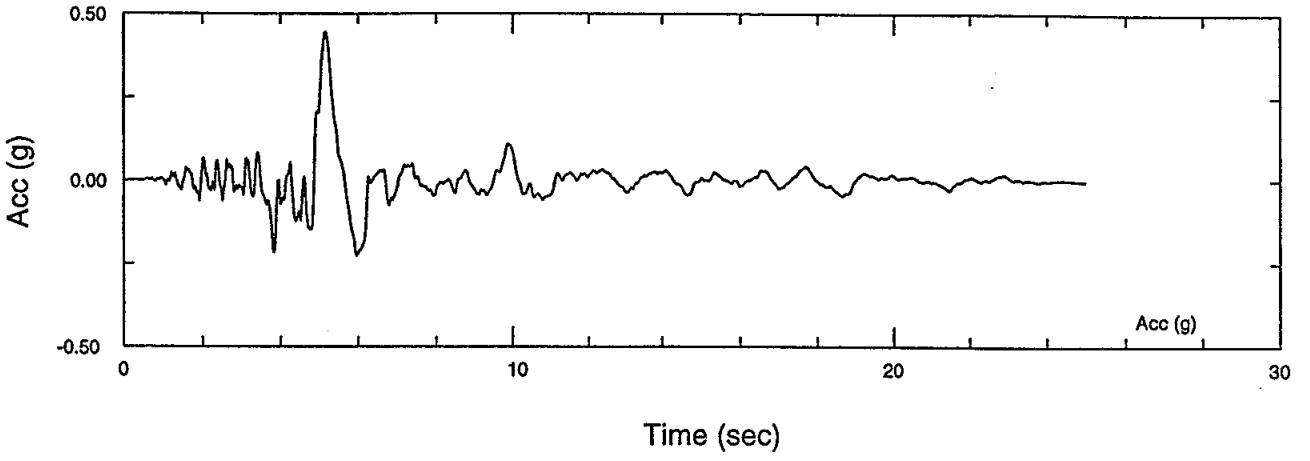

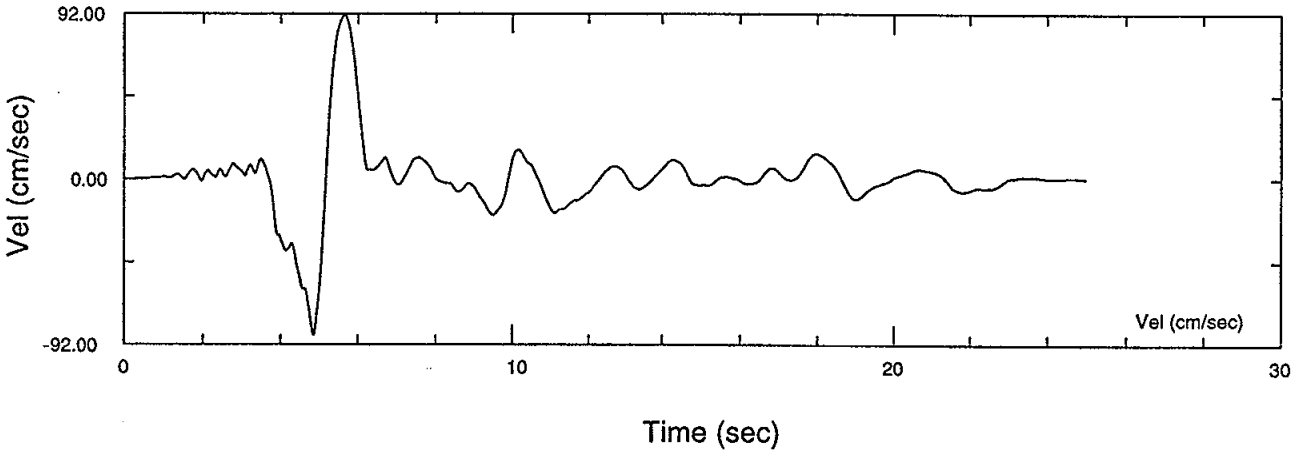

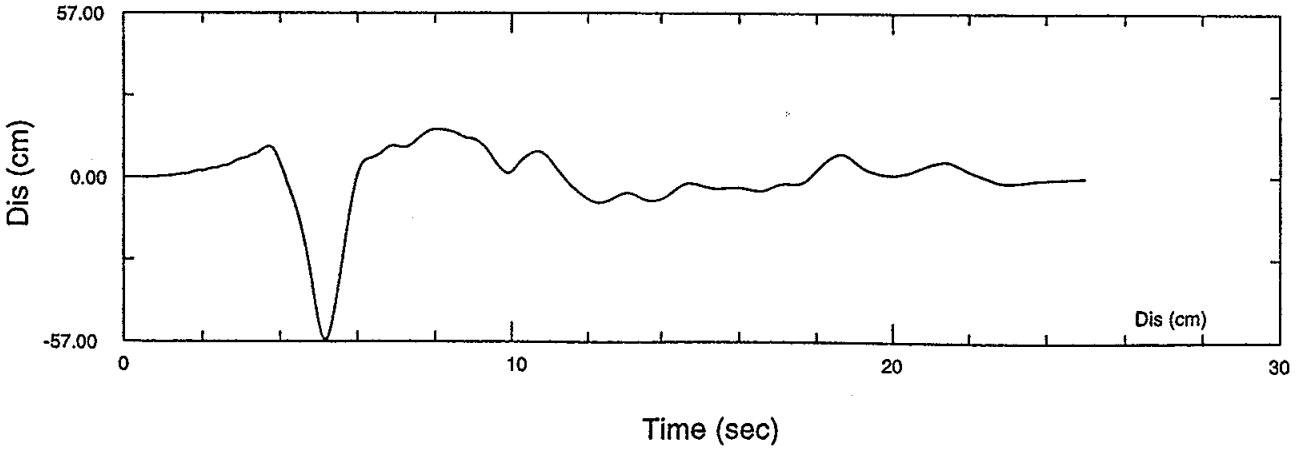

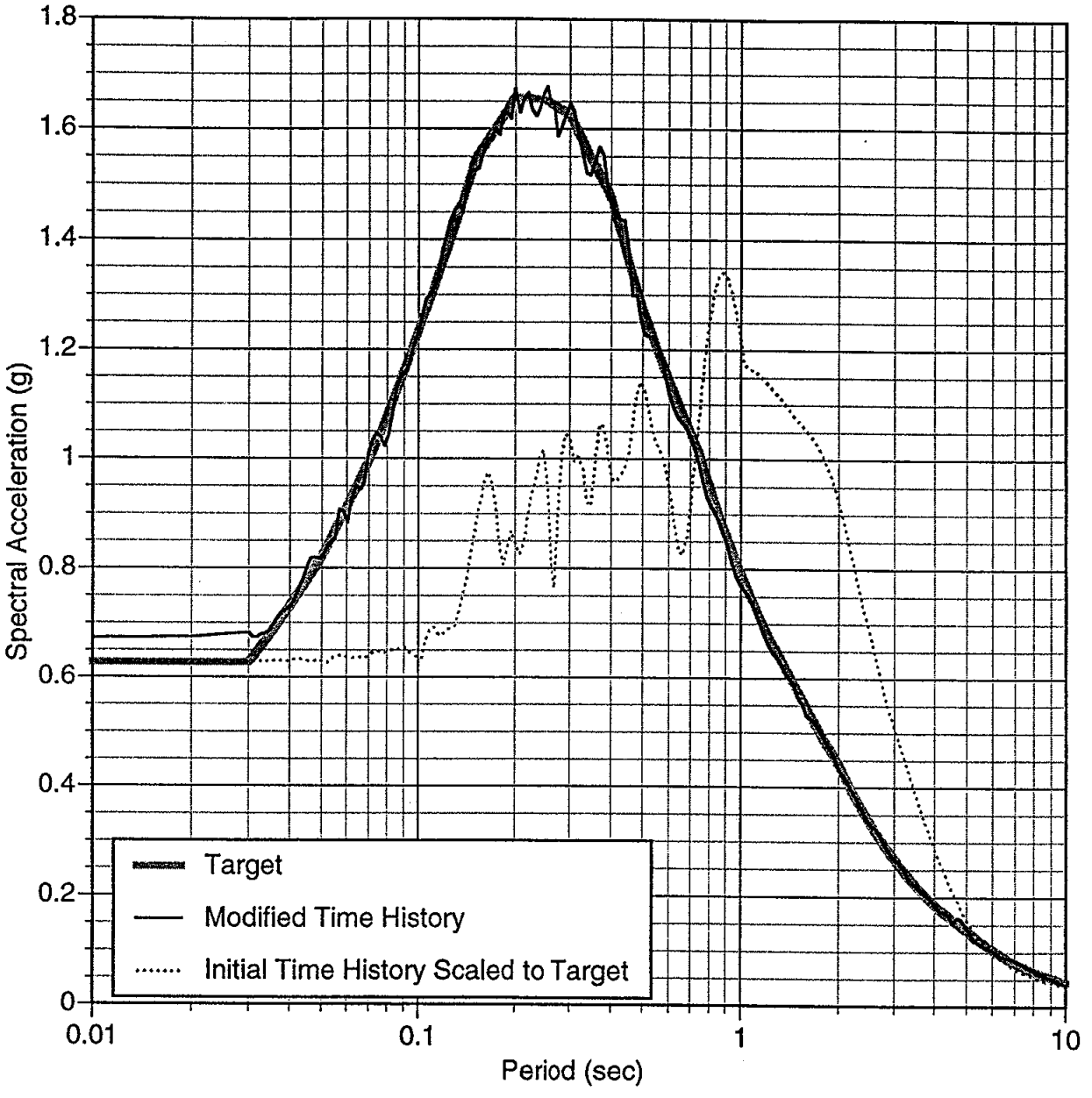

Figure E29 Set4 5% damped response spectra for the modified Fault Normal component and initial time history scaled to the target PGA.

File: G3:Data1:East_SBridge_RefMotions:Report_Figures:Set4:Set4_rsp.dg

Figure E30 Set4 Spectrum Compatible Fault Normal Reference Time History.

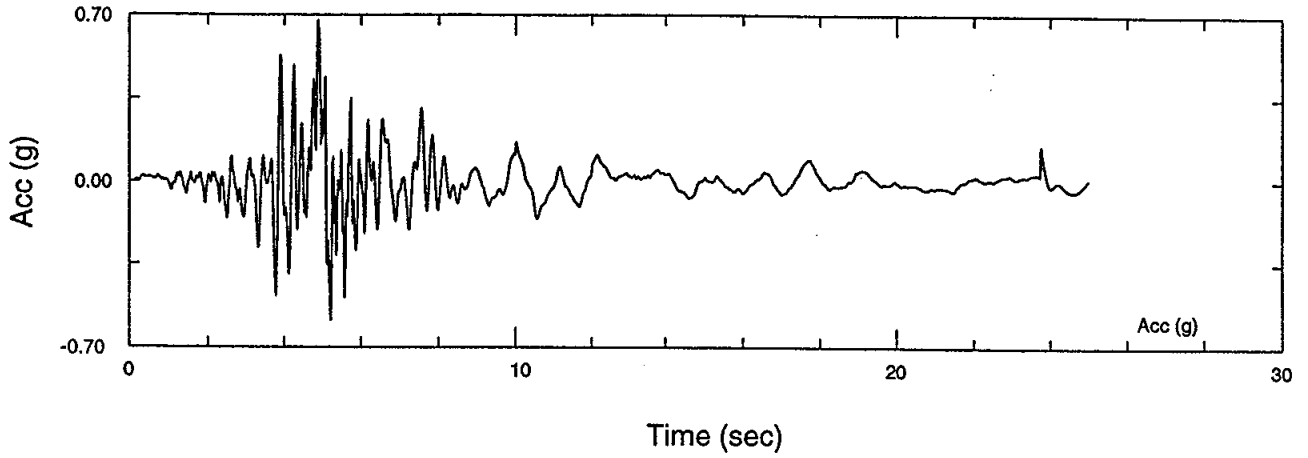

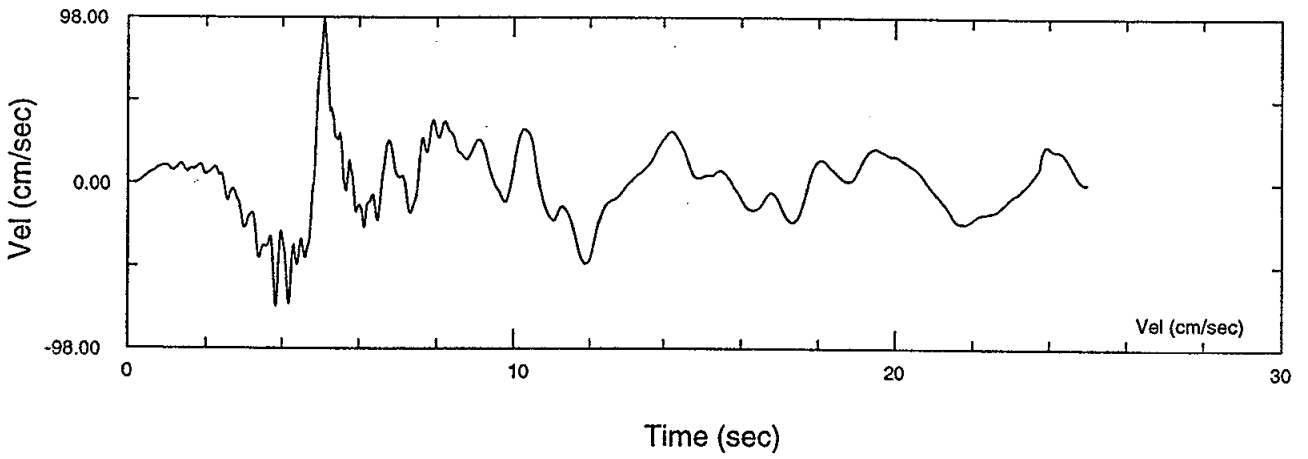

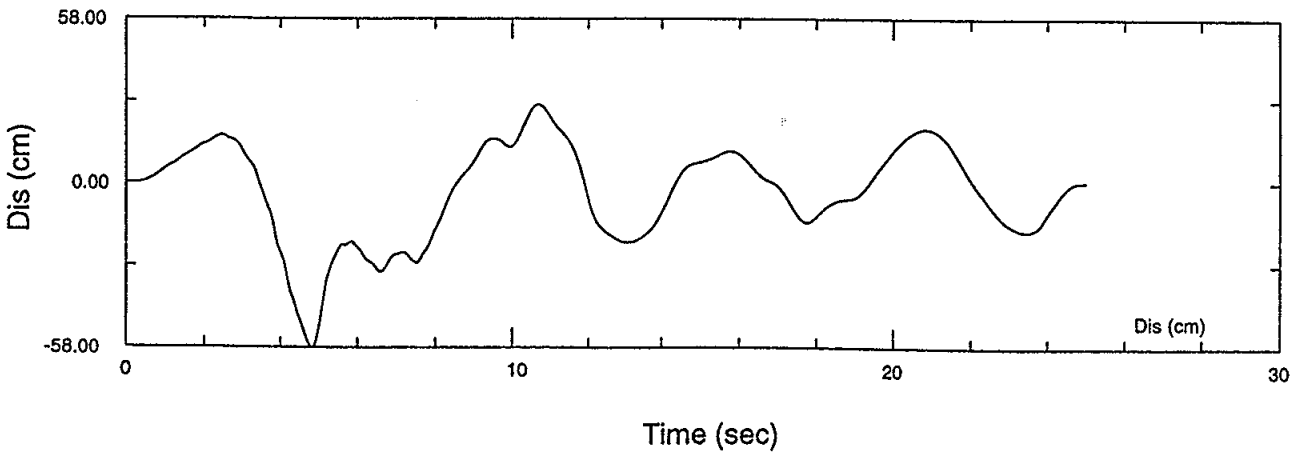

Figure E31. Set4 Initial Fault Parallel Time History.

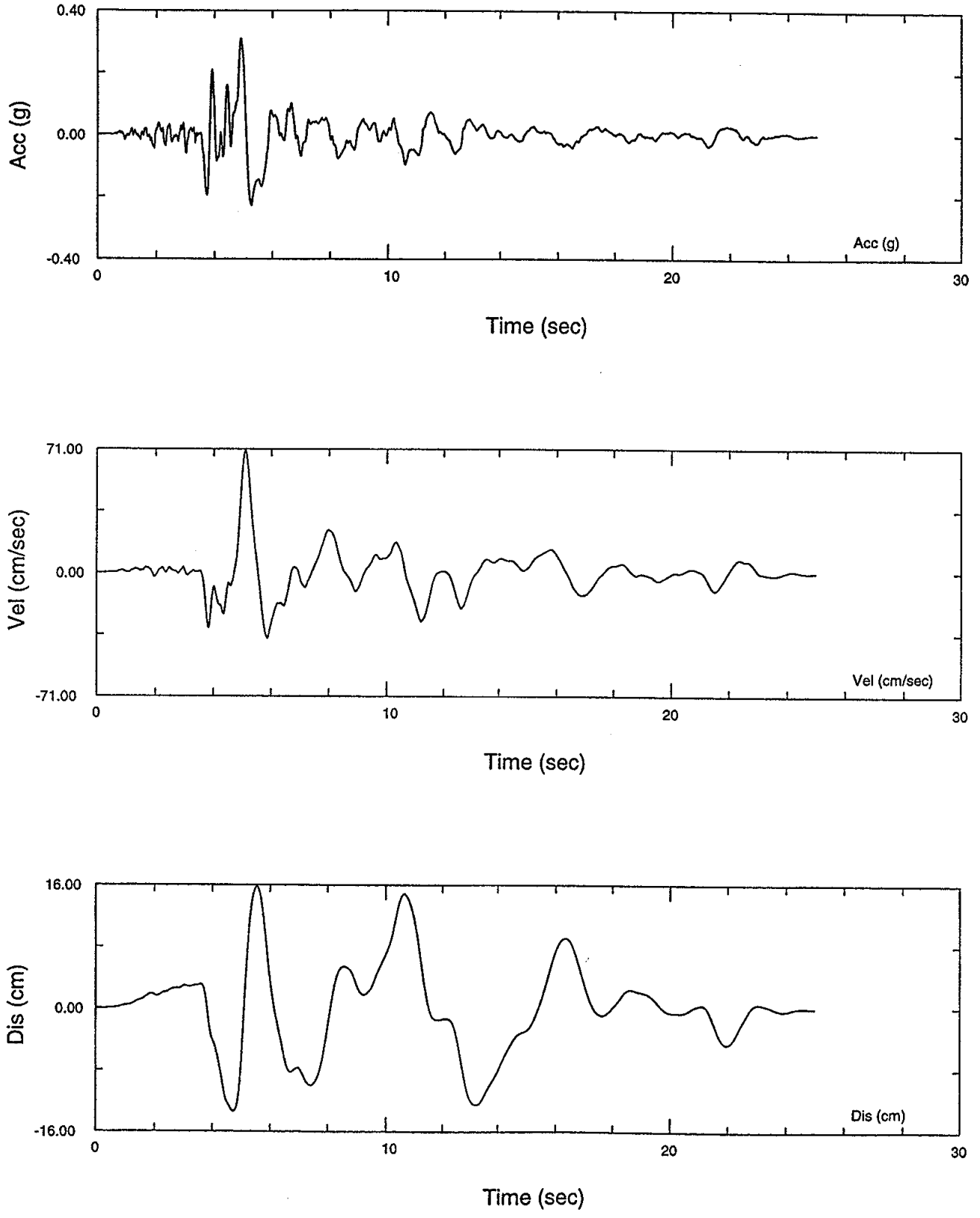

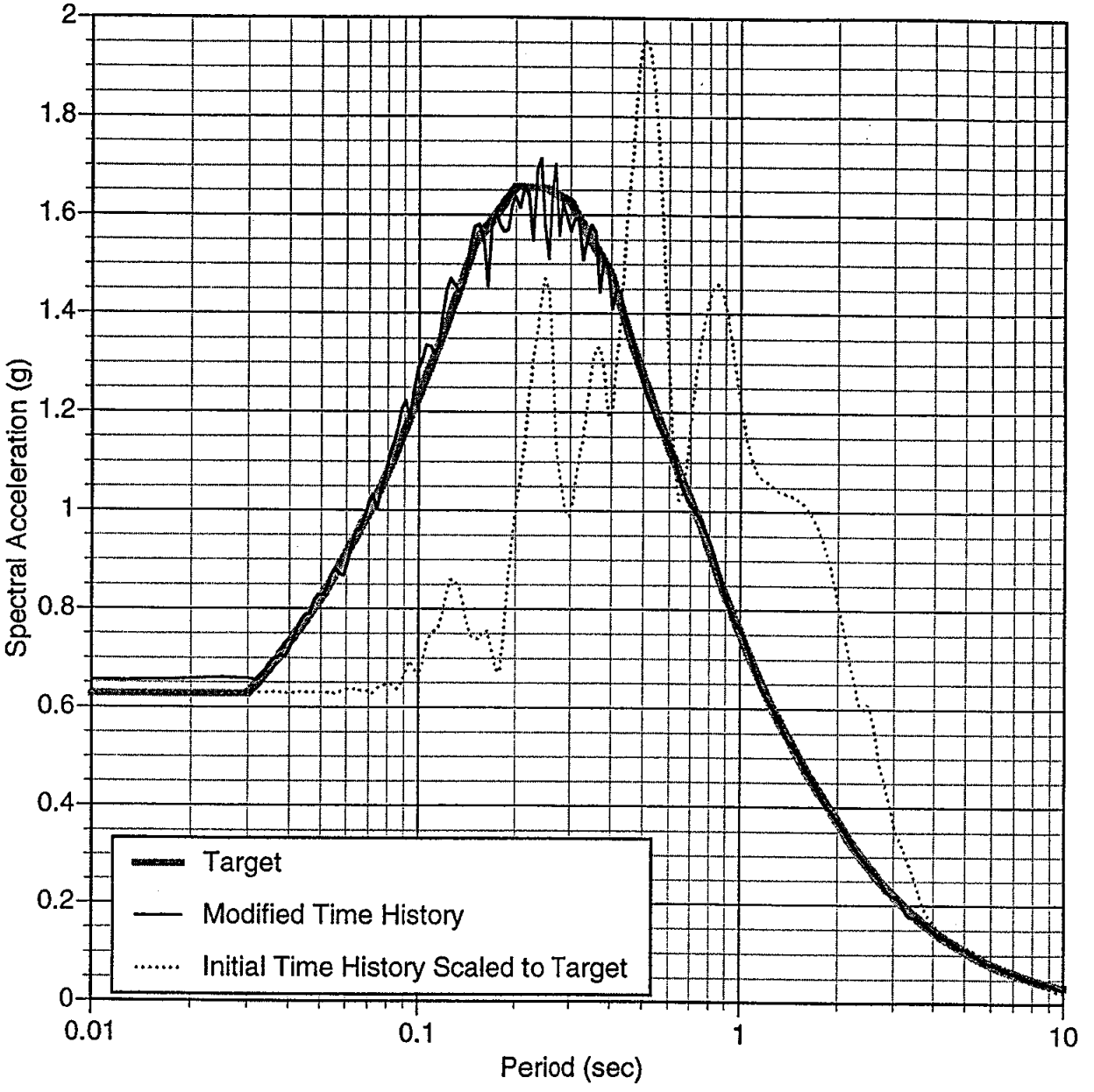

Figure E32Set4 5% damped response spectra for the modified Fault Parallel component and initial time history scaled to the target PGA.

File: G3:Data1:East_BBridge_RefMotions:Report_Figures:Set4:Set4_rsp.dg

Figure E33Set4 Spectrum Compatible Fault Parallel Reference Time History.

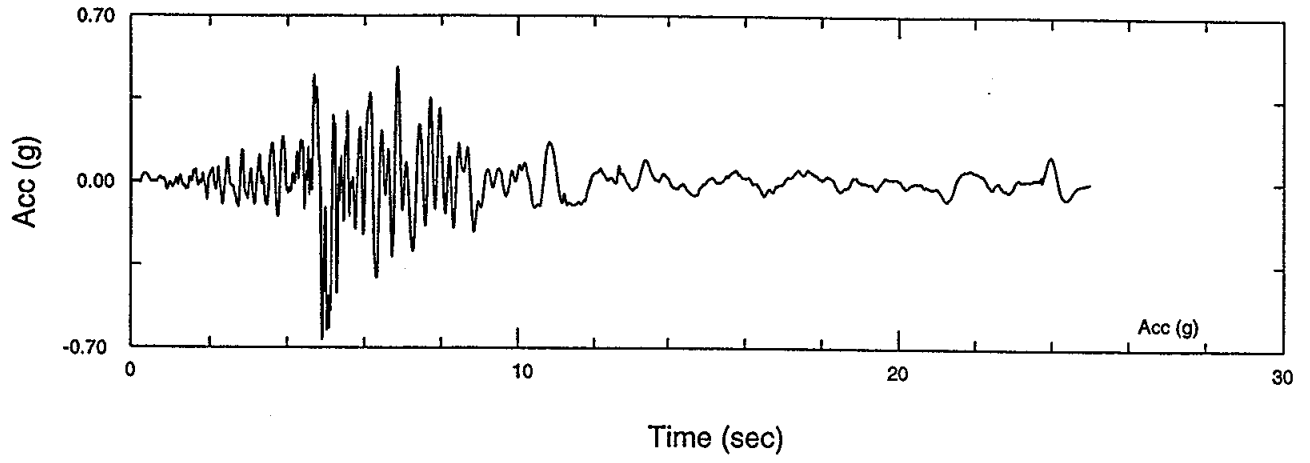

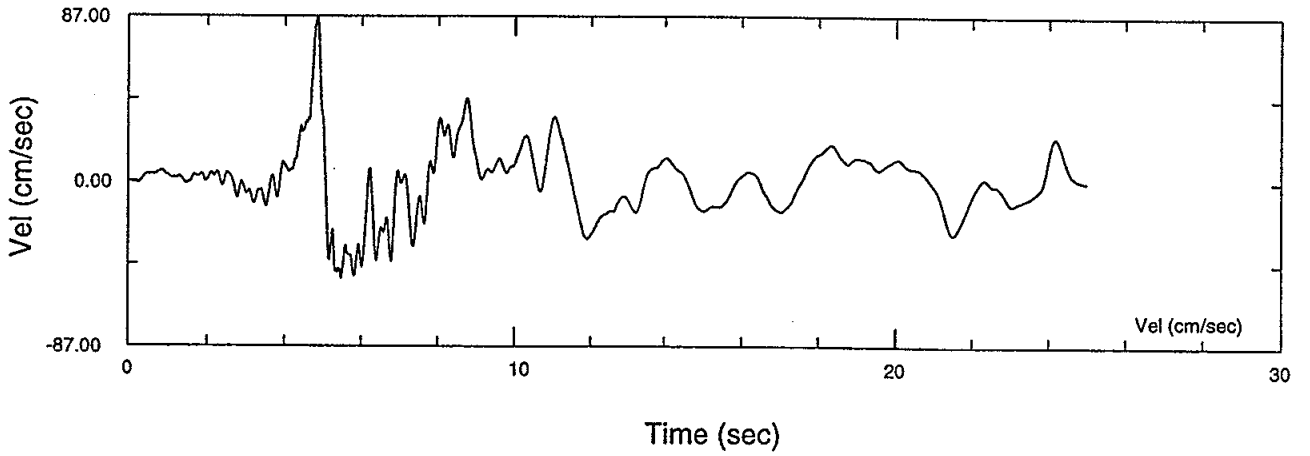

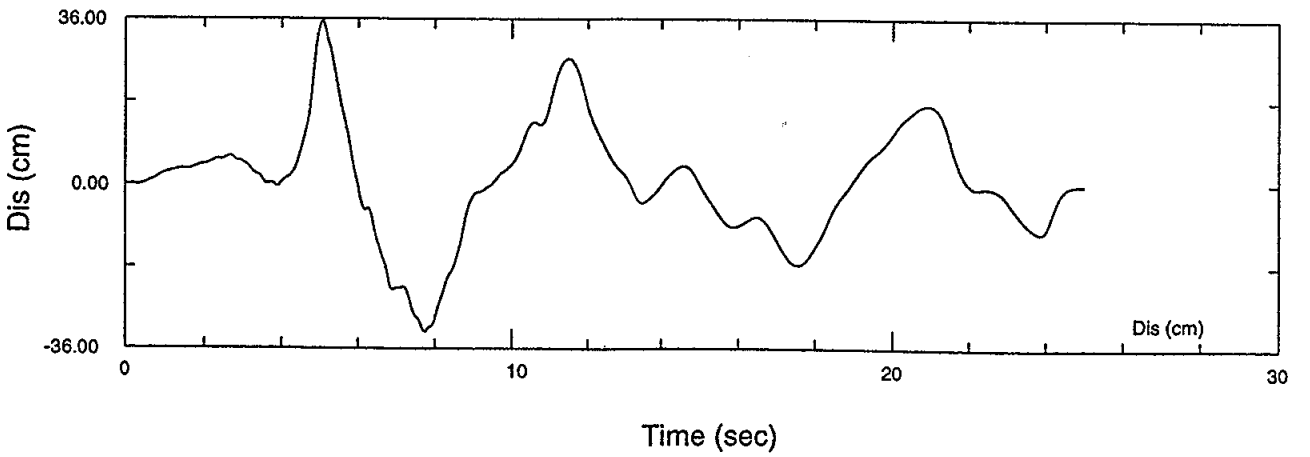

Figure E34Set4 Initial Vertical Time History.

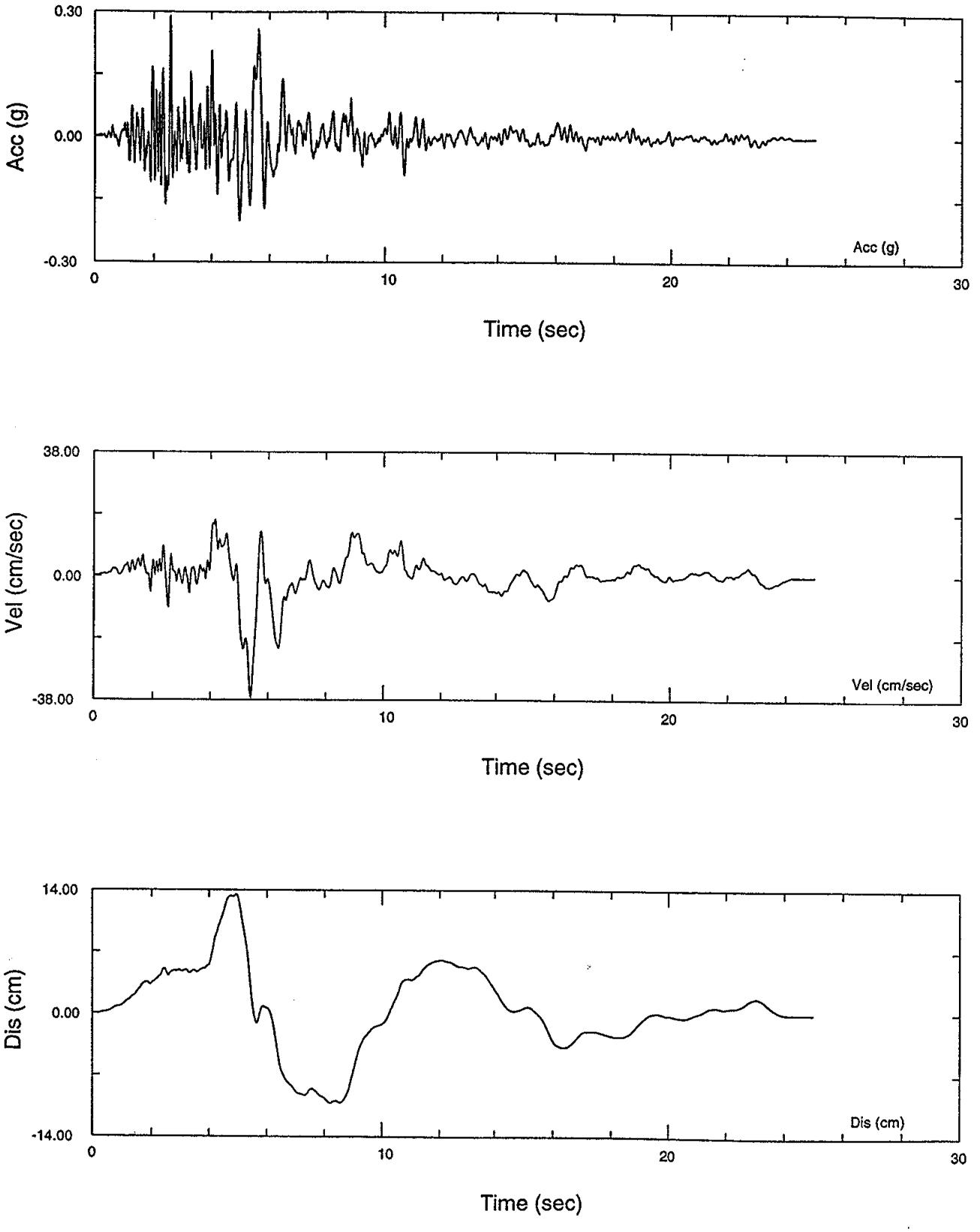

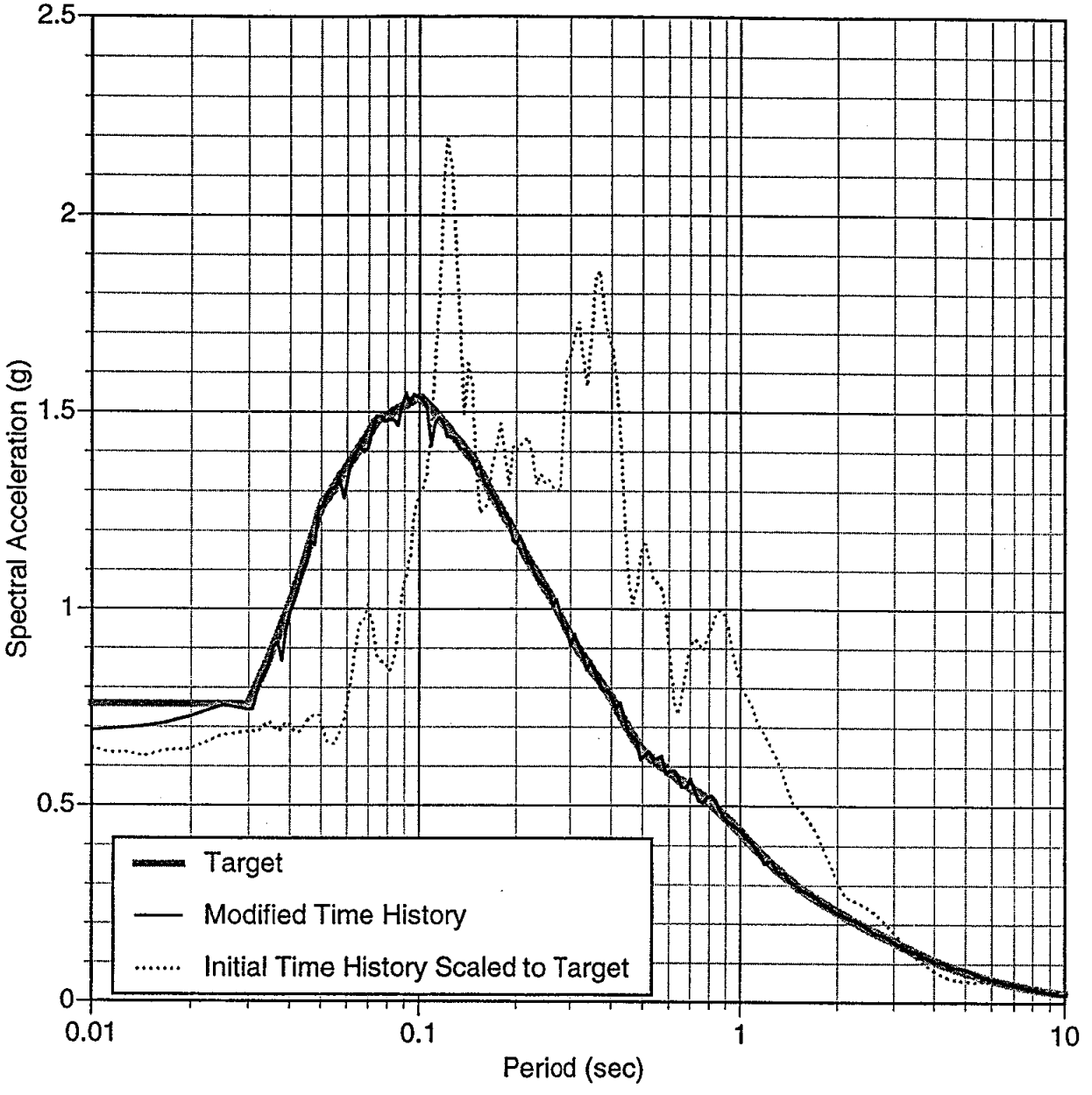

Figure E35Set4 5% damped response spectra for the modified Vertical component and initial time history scaled to the target PGA.

G3:Data1:East_BBridge_RefMotions:Report_Figures:Set4:Set4_rsp.dg

Figure E36 Set4 Spectrum Compatible Vertical Reference Time History.

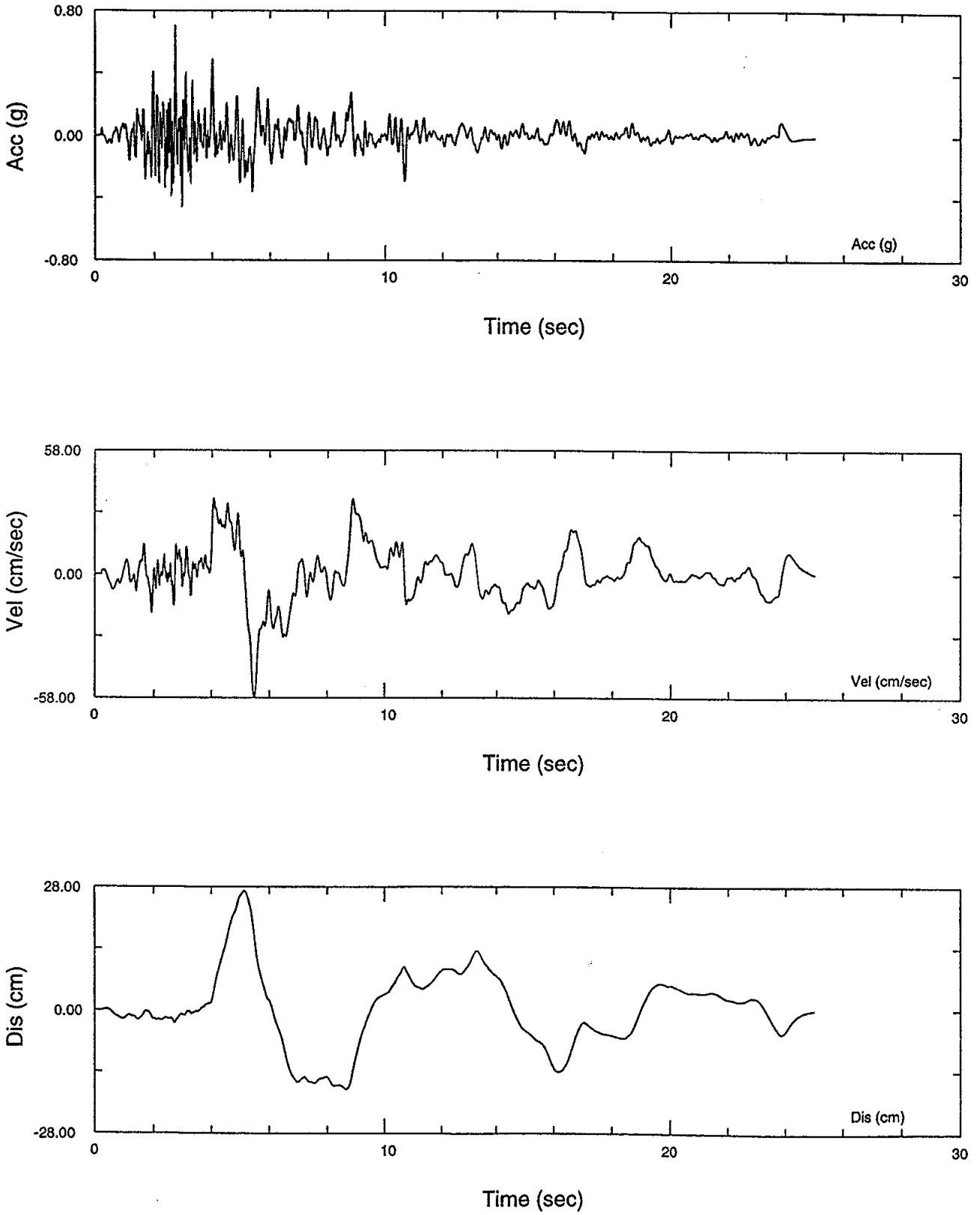

Figure E37 Set5 Initial Fault Normal Time History.

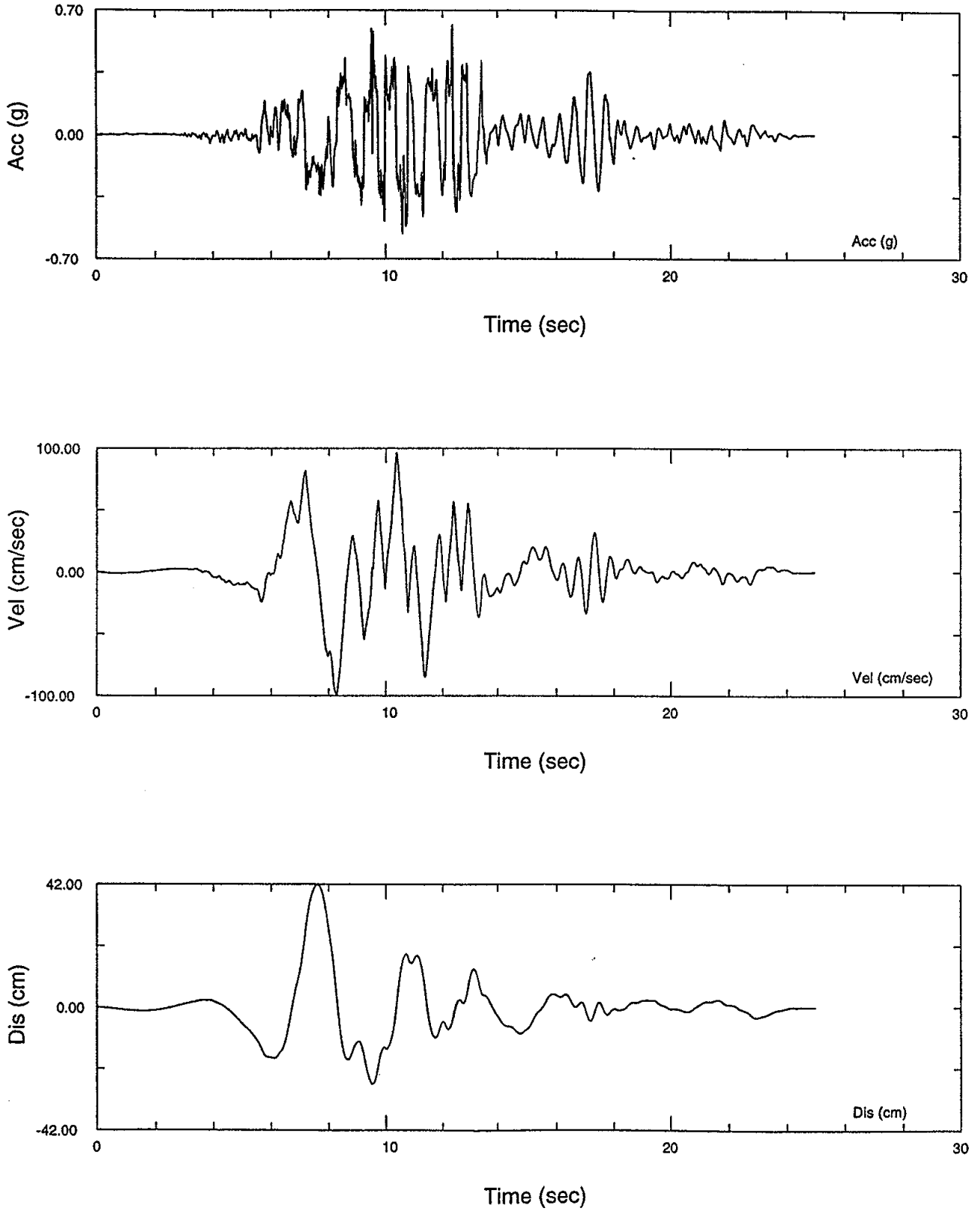

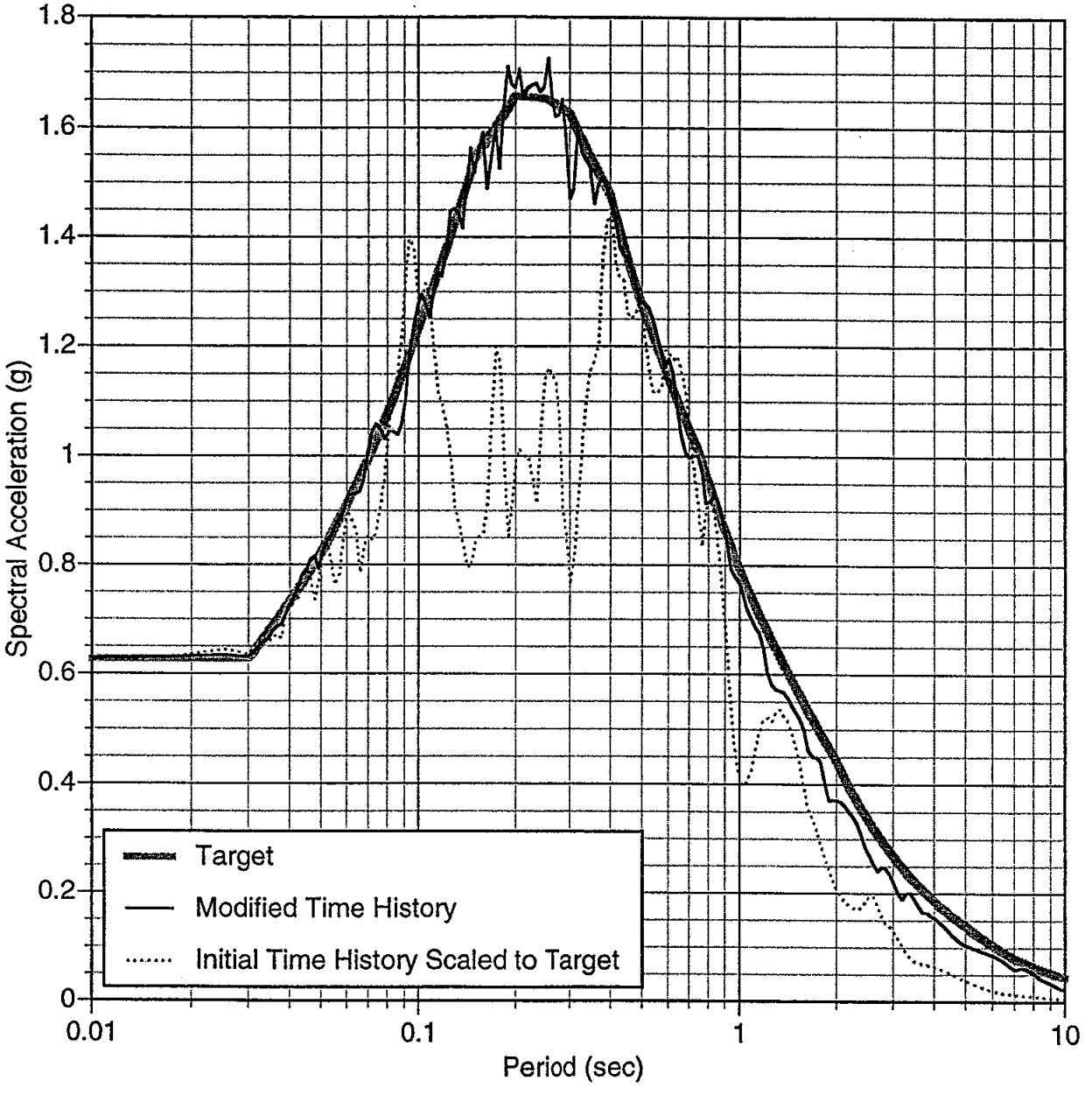

Figure E38Set5 5% damped response spectra for the modified Fault Normal component and initial time history scaled to the target PGA.

File: G3:Data1:East_SBridge_RefMotions:Report_Figures:Set5:Set5_rsp.dg

Figure E39 Set5 Spectrum Compatible Fault Normal Reference Time History.

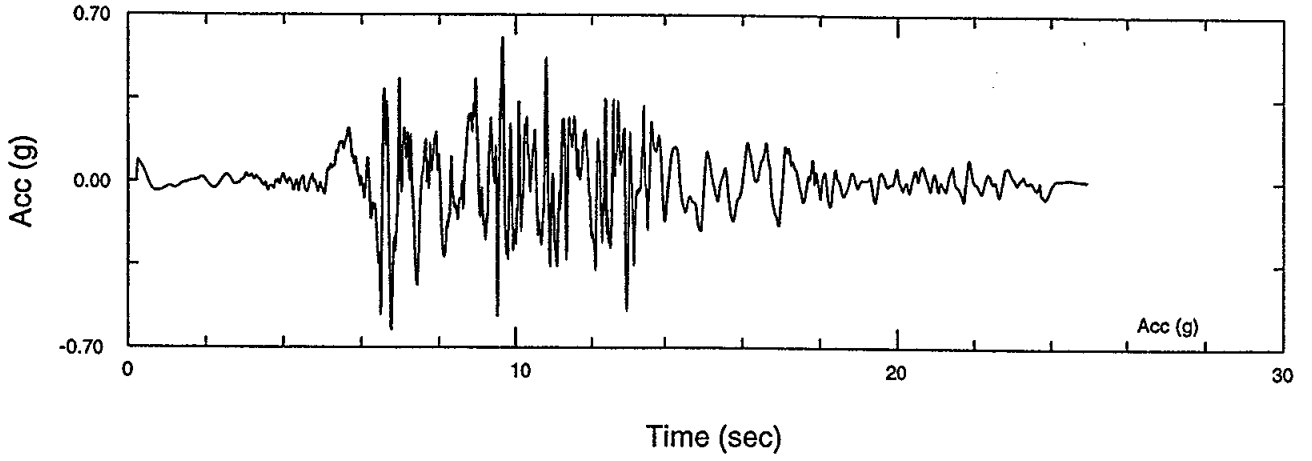

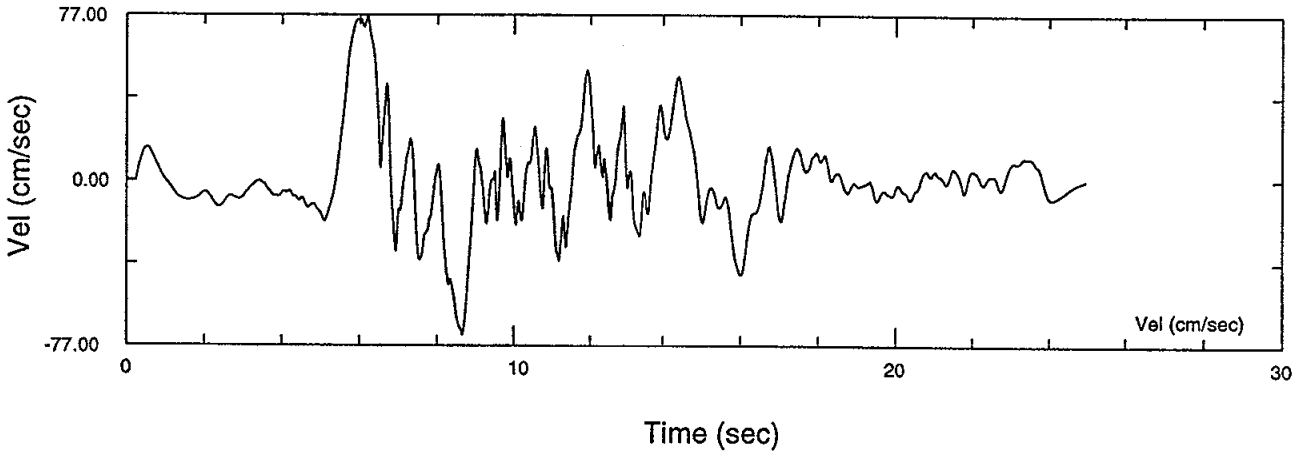

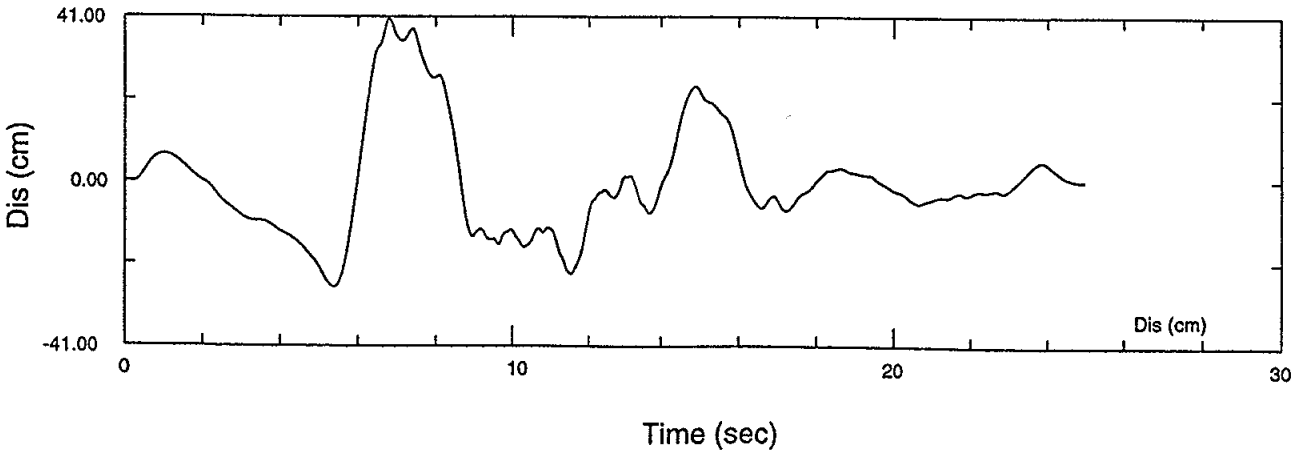

Figure E40Set5 Initial Fault Parallel Time History.

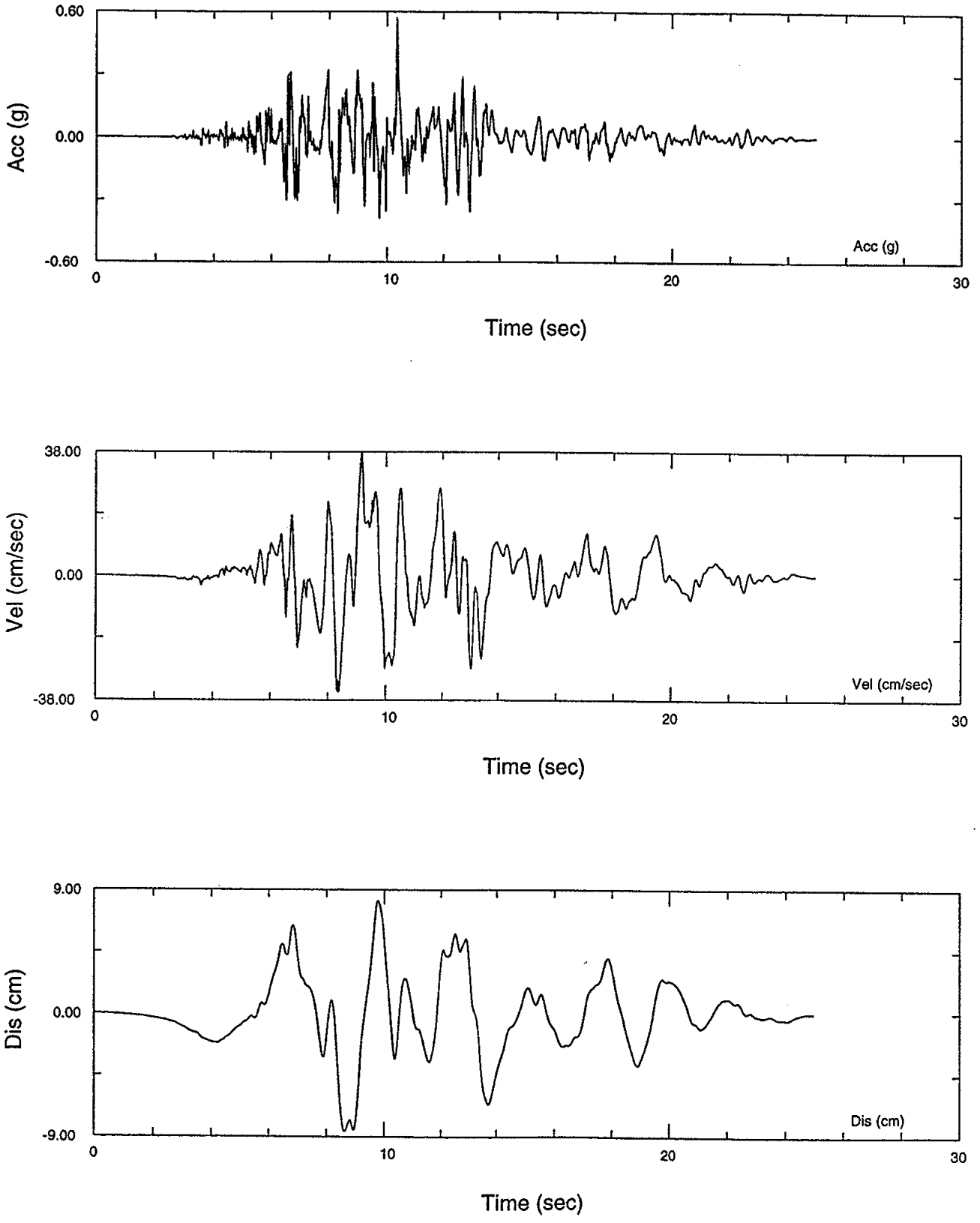

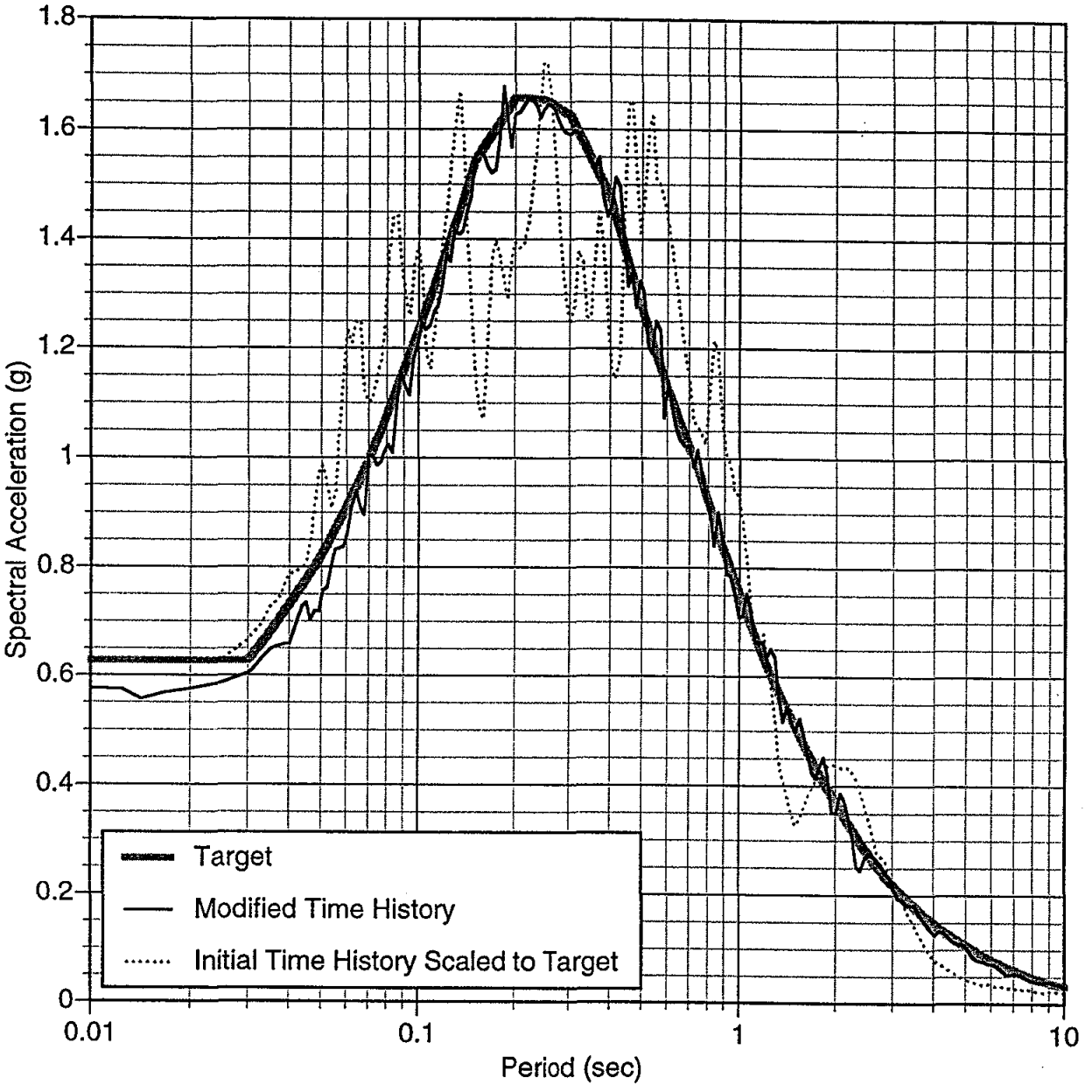

Figure E41Set5 5% damped response spectra for the modified Fault Parallel component and initial time history scaled to the target PGA.

File: G3:Data1:East_BBridge_RefMotions:Report_Figures:Set5:Set5_rsp.dg

Figure E42 Set5 Spectrum Compatible Fault Parallel Reference Time History.

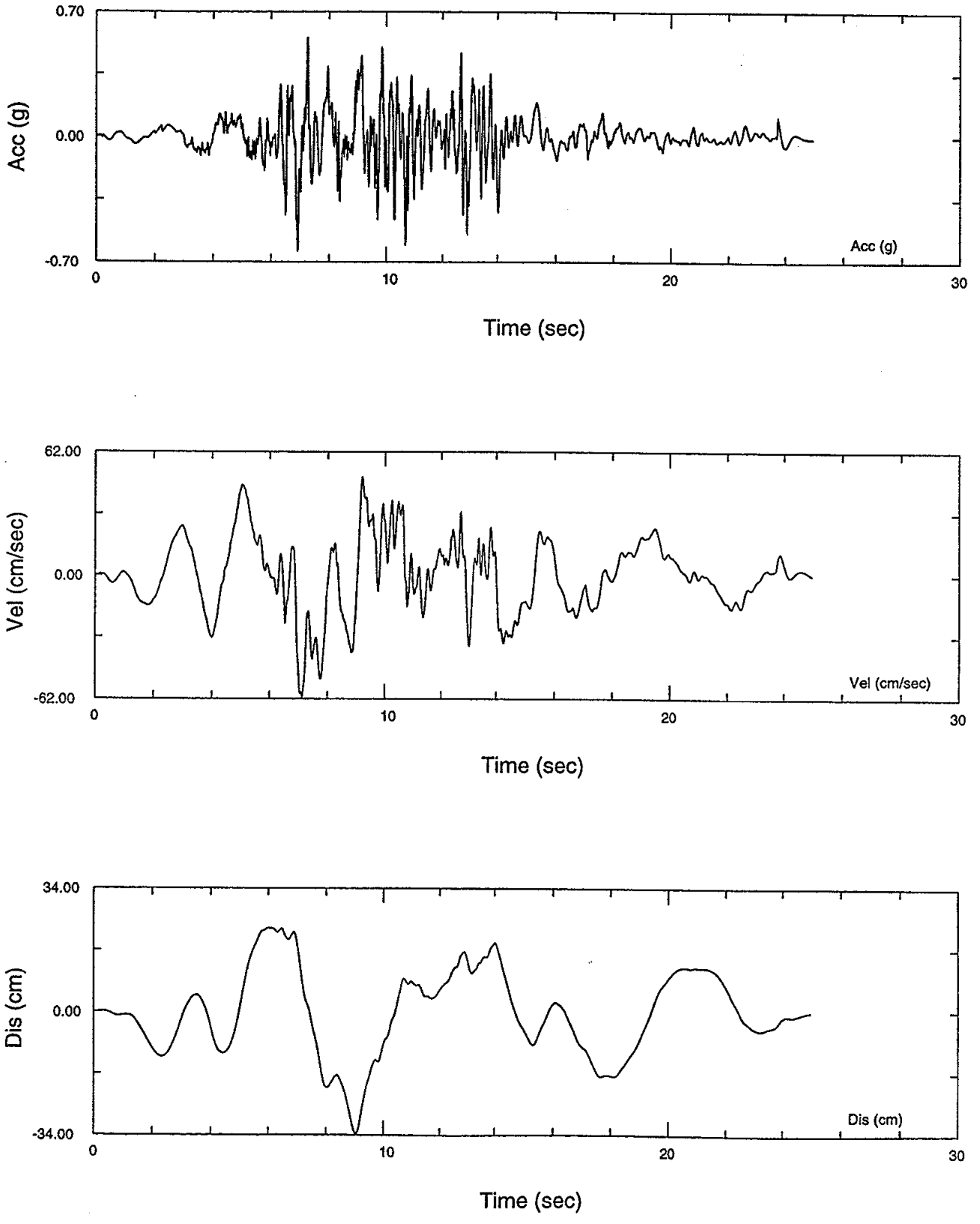

Figure E43Set5 Initial Vertical Time History.

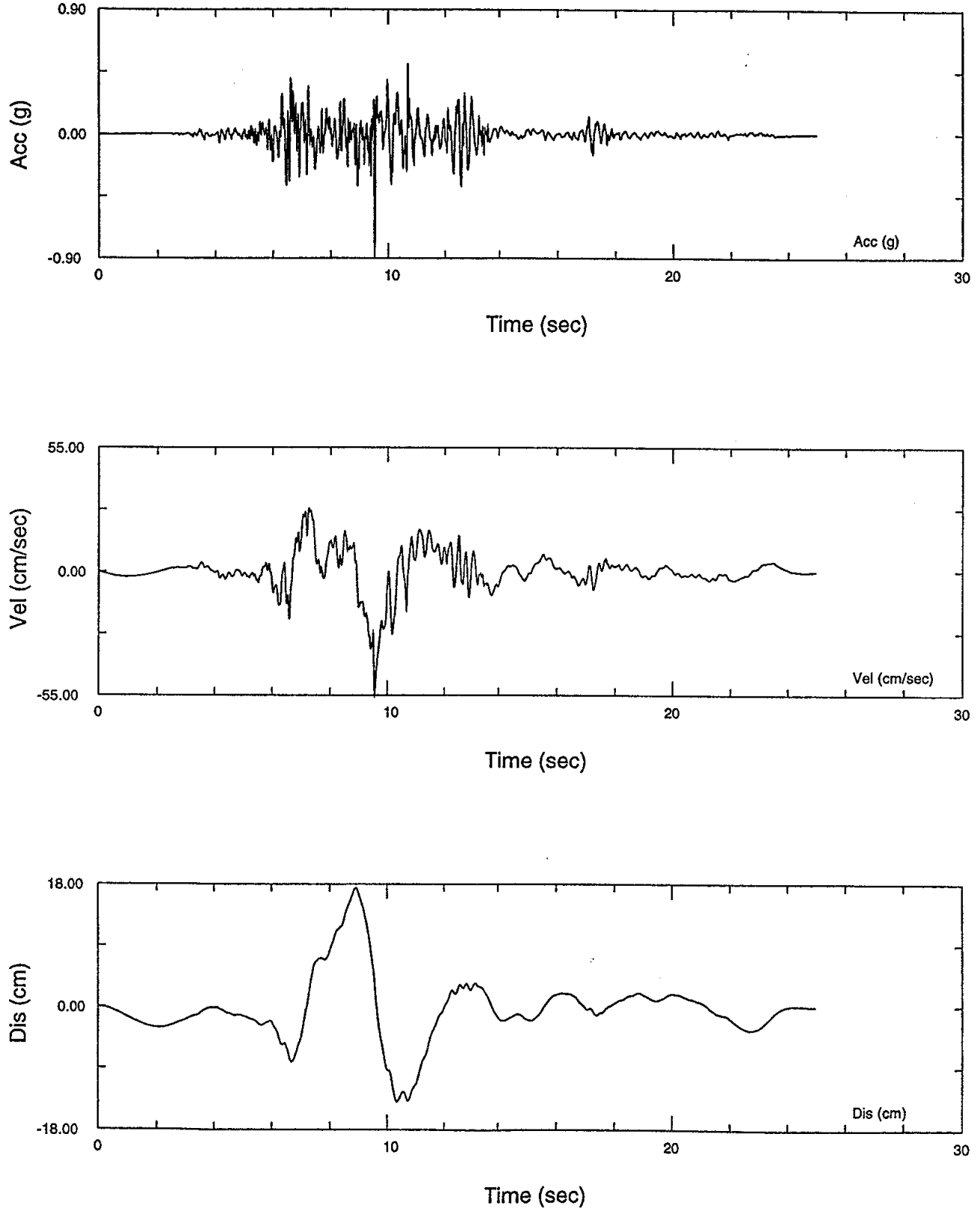

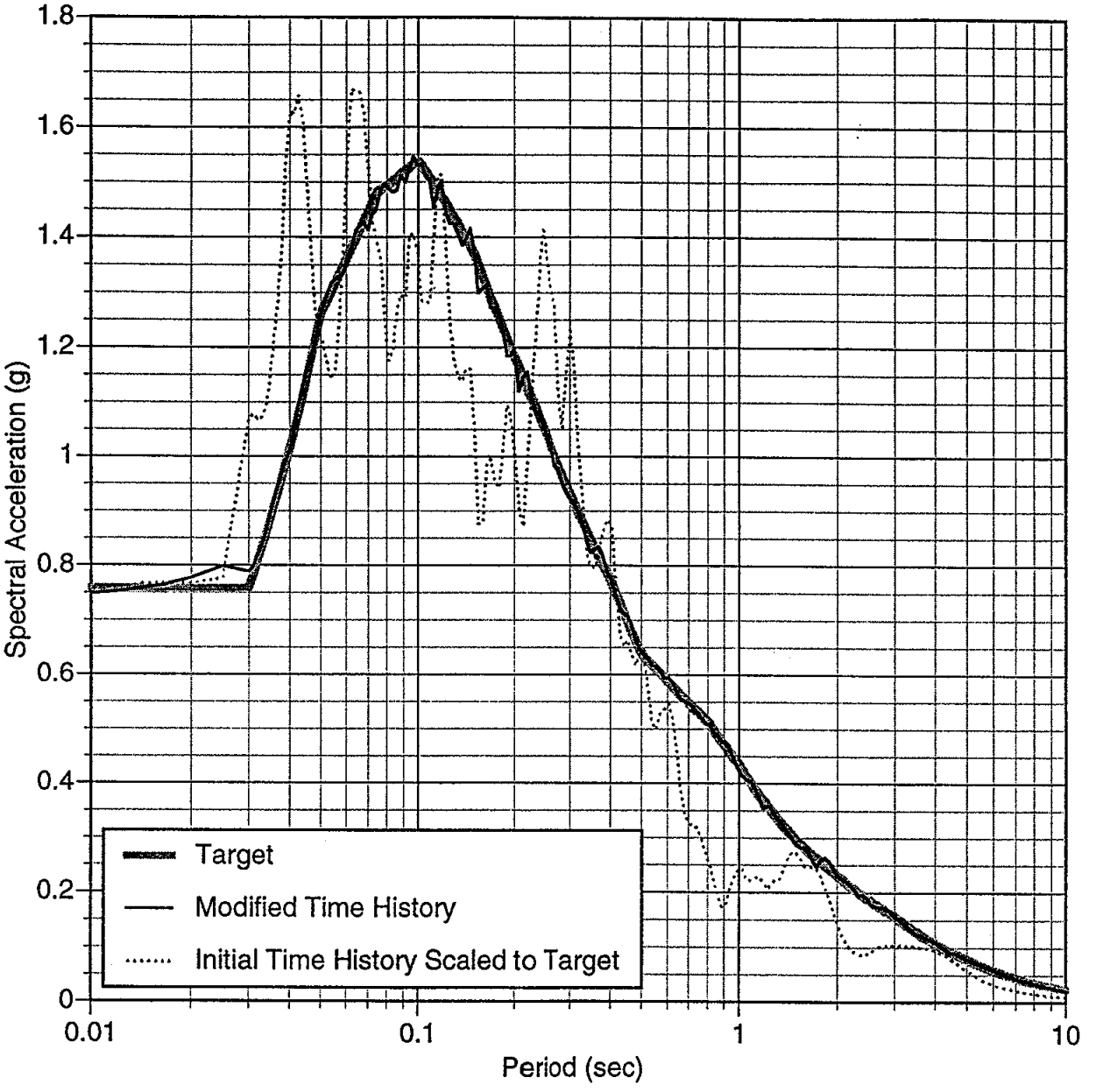

Figure E44Set5 5% damped response spectra for the modified Vertical component and initial time history scaled to the target PGA.

File: G3:Data1:East_BBridge_RefMotions:Report_Figures:Set5:Set5_rsp.dg

Figure E45 Set5 Spectrum Compatible Vertical Reference Time History.

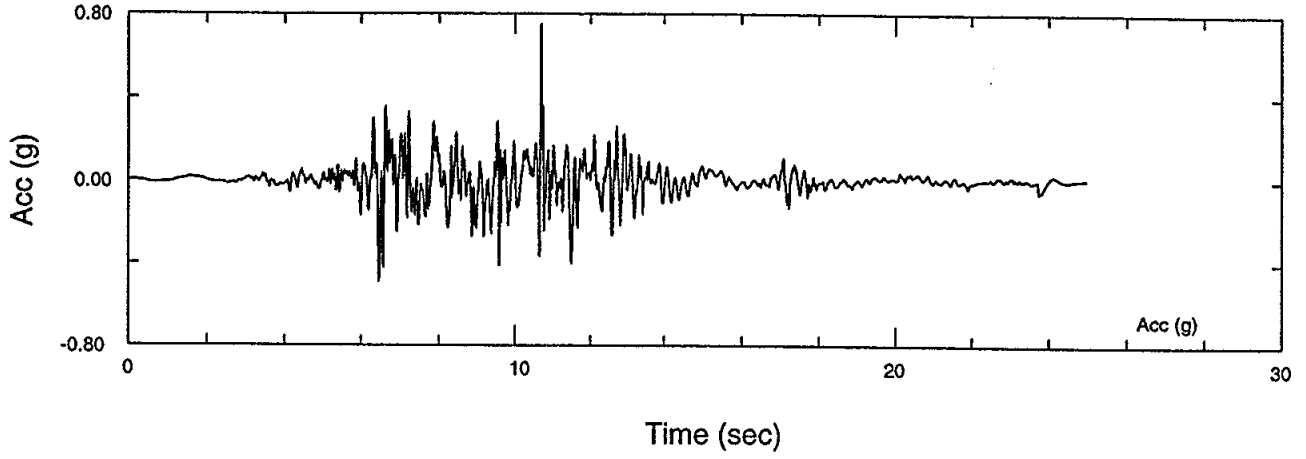

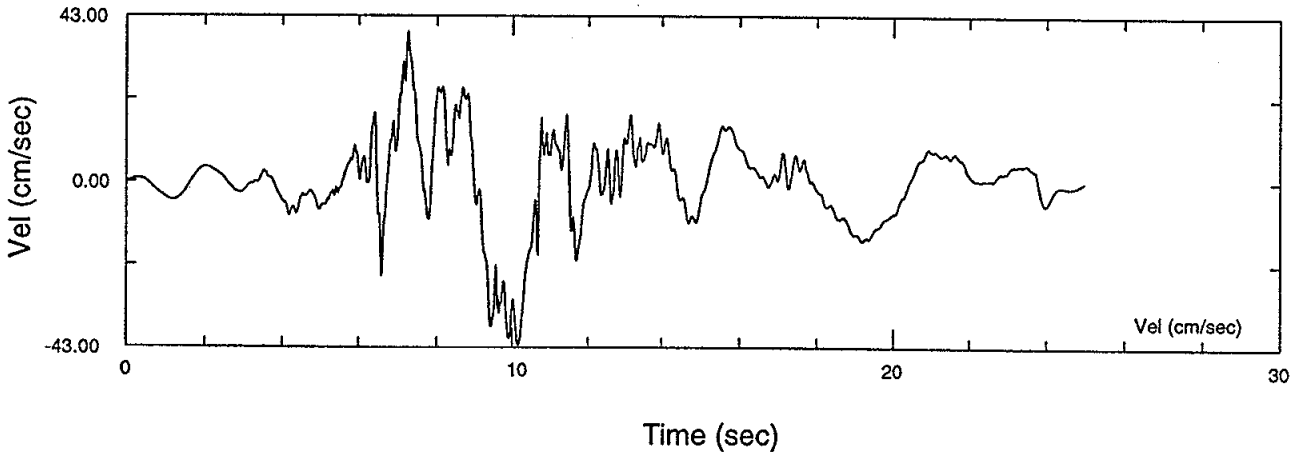

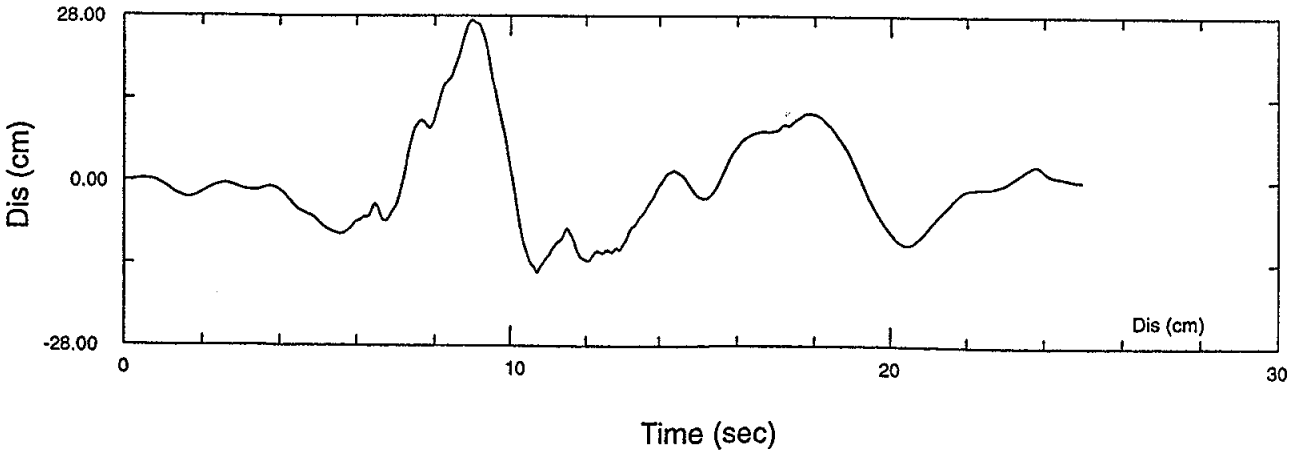

Figure E46 Set6 Initial Fault Normal Time History.

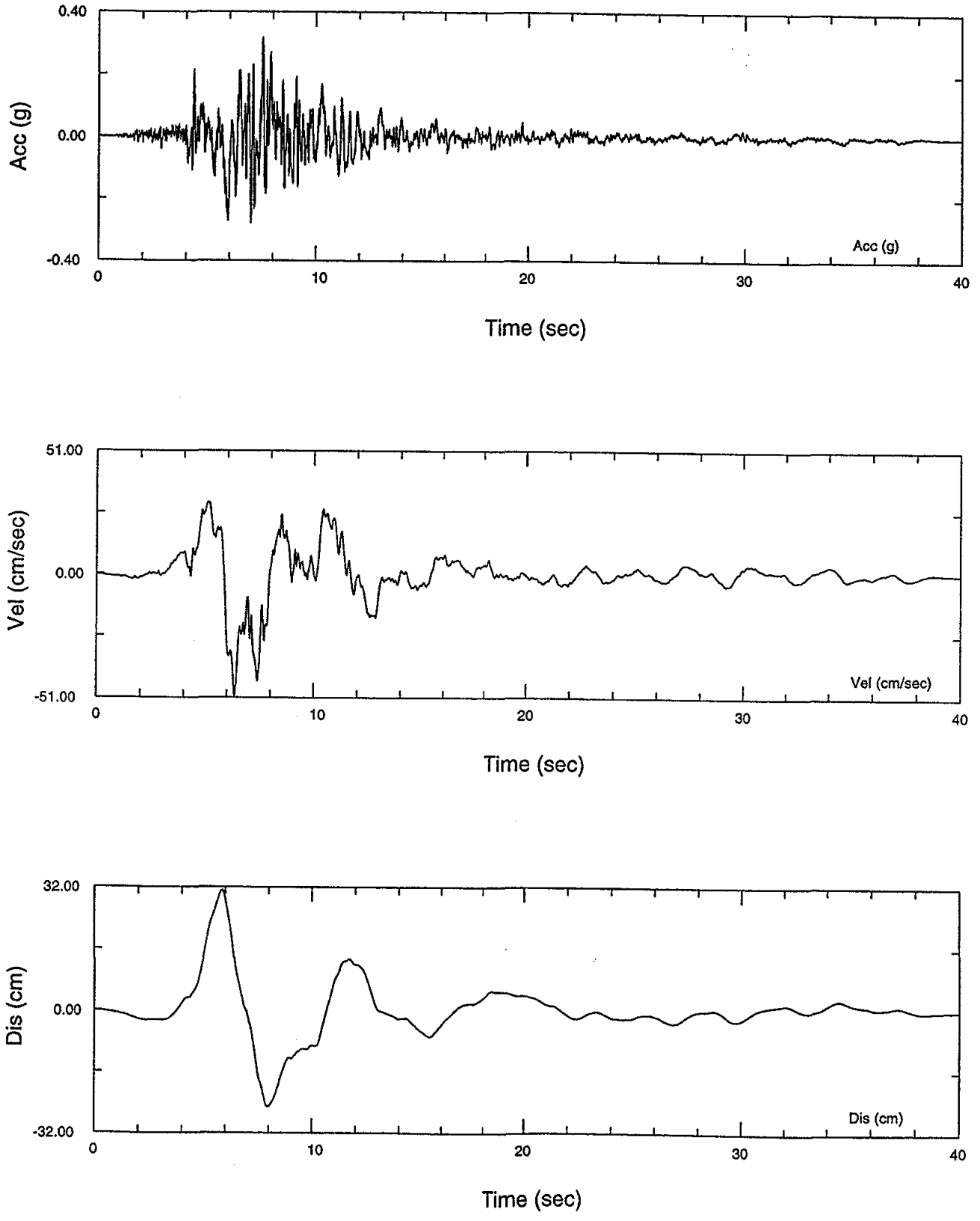

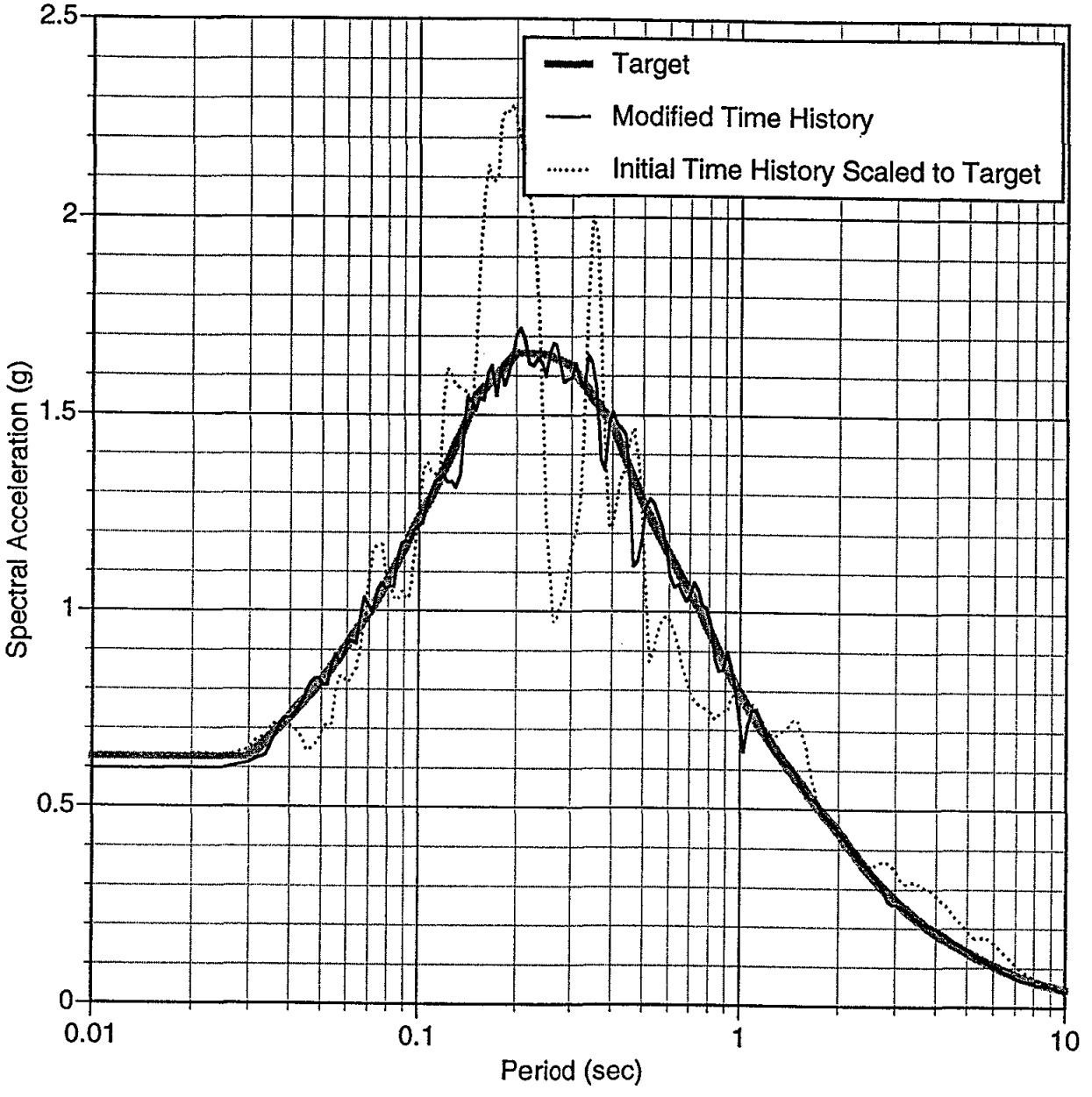

Figure E47Set6 5% damped response spectra for the modified Fault Normal component and initial time history scaled to the target PGA.

File: G3:Data1:East_BBridge_RefMotions:Report_Figures:Set6:Set6_rsp.dg

Figure E48 Set6 Spectrum Compatible Fault Normal Reference Time History.

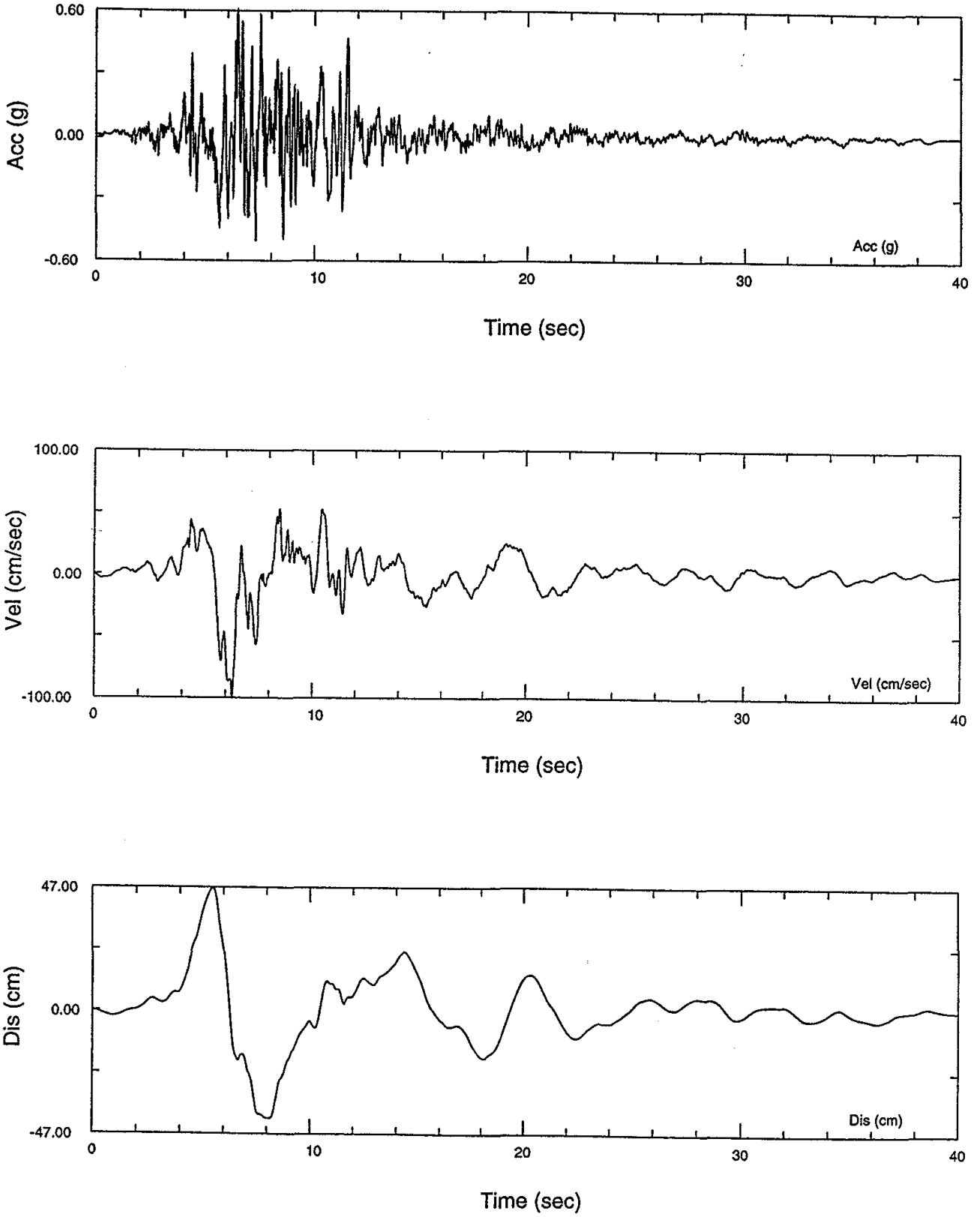

Figure E49Set6 Initial Fault Parallel Time History.

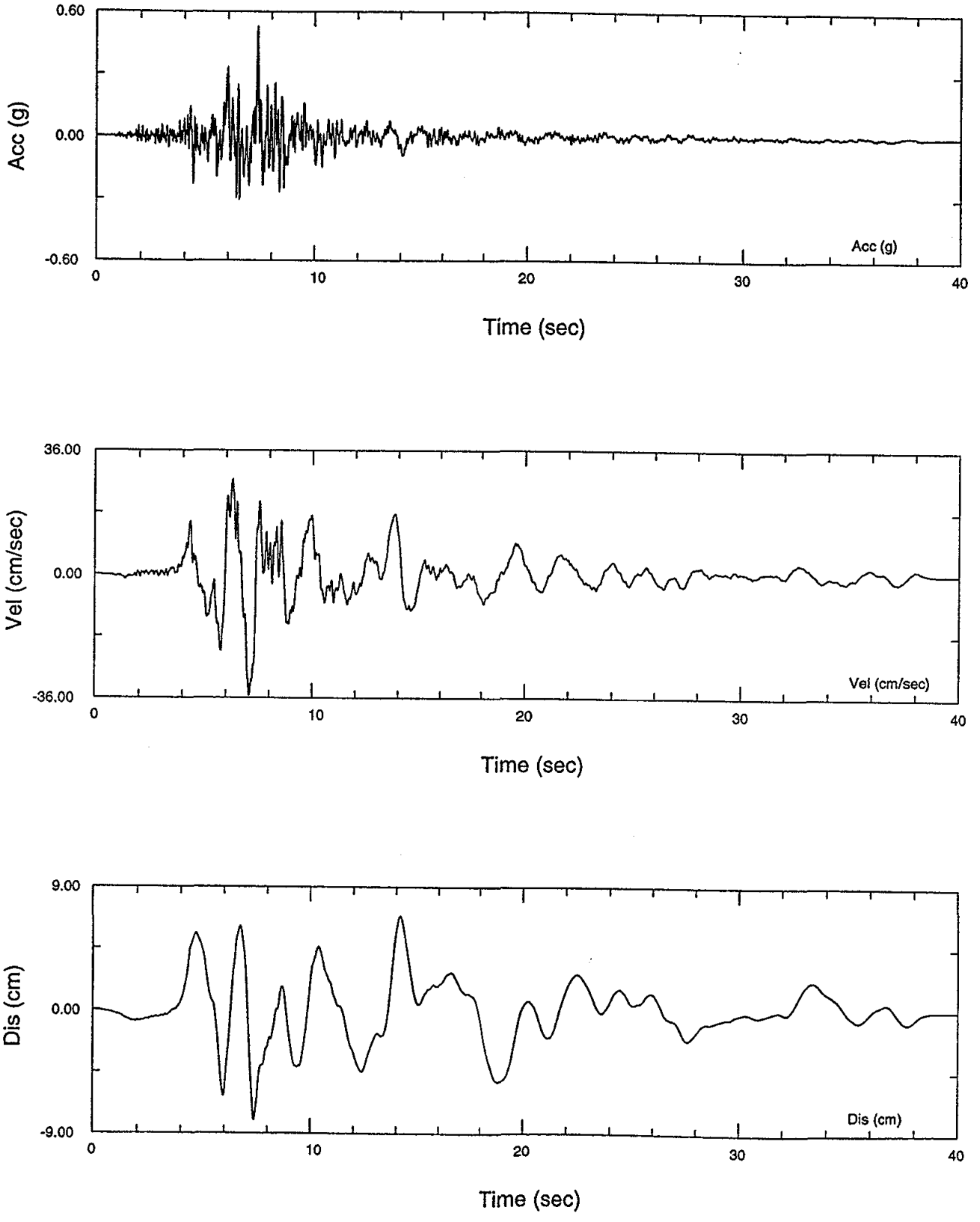

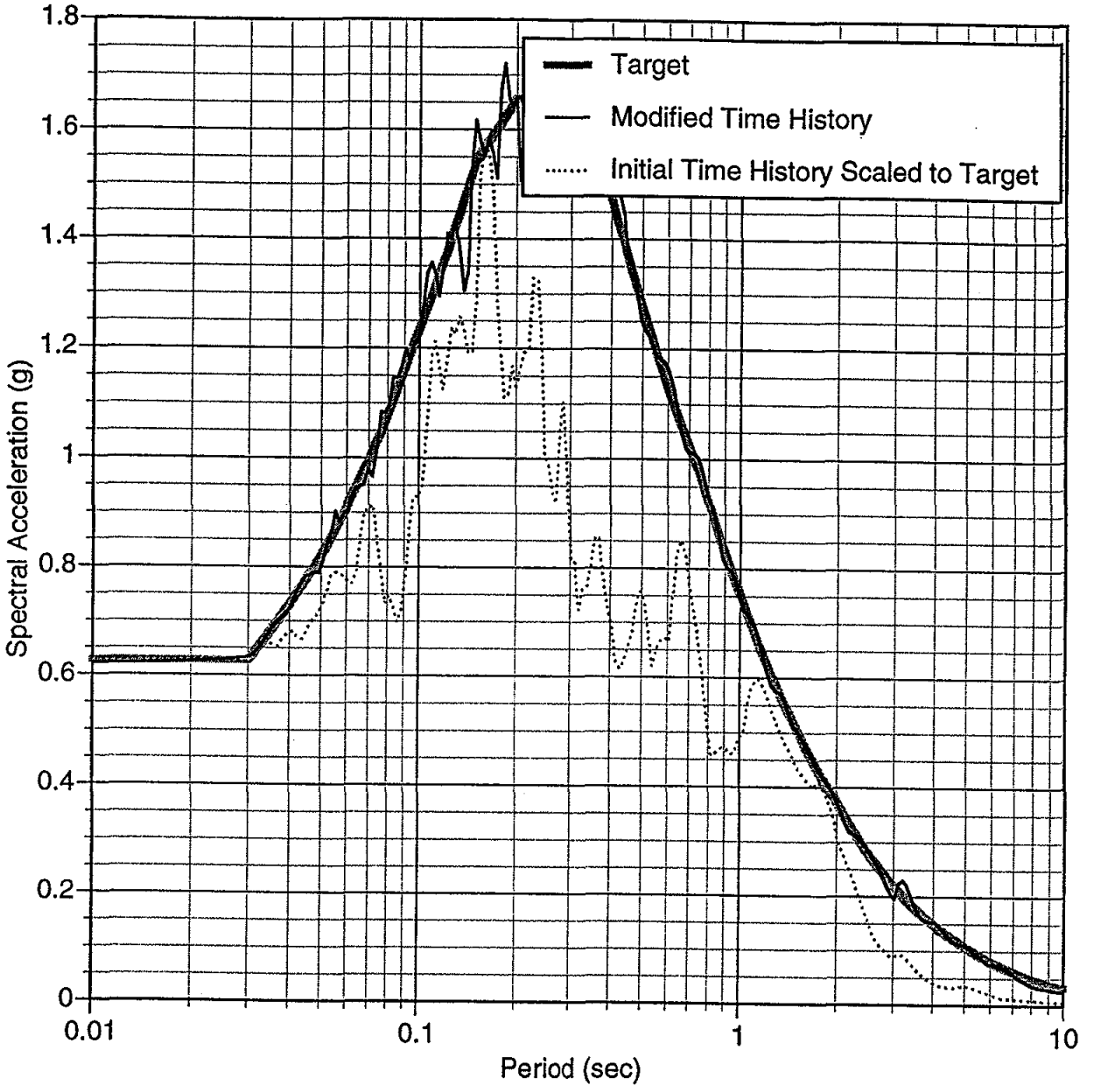

Figure E50Set6 5% damped response spectra for the modified Fault Parallel component and initial time history scaled to the target PGA.

...3:Data1:East_BBridge_RefMotions:Report_Figures:Set6:Set6_rsp.dg

Figure E51 Set6 Spectrum Compatible Fault Parallel Reference Time History.

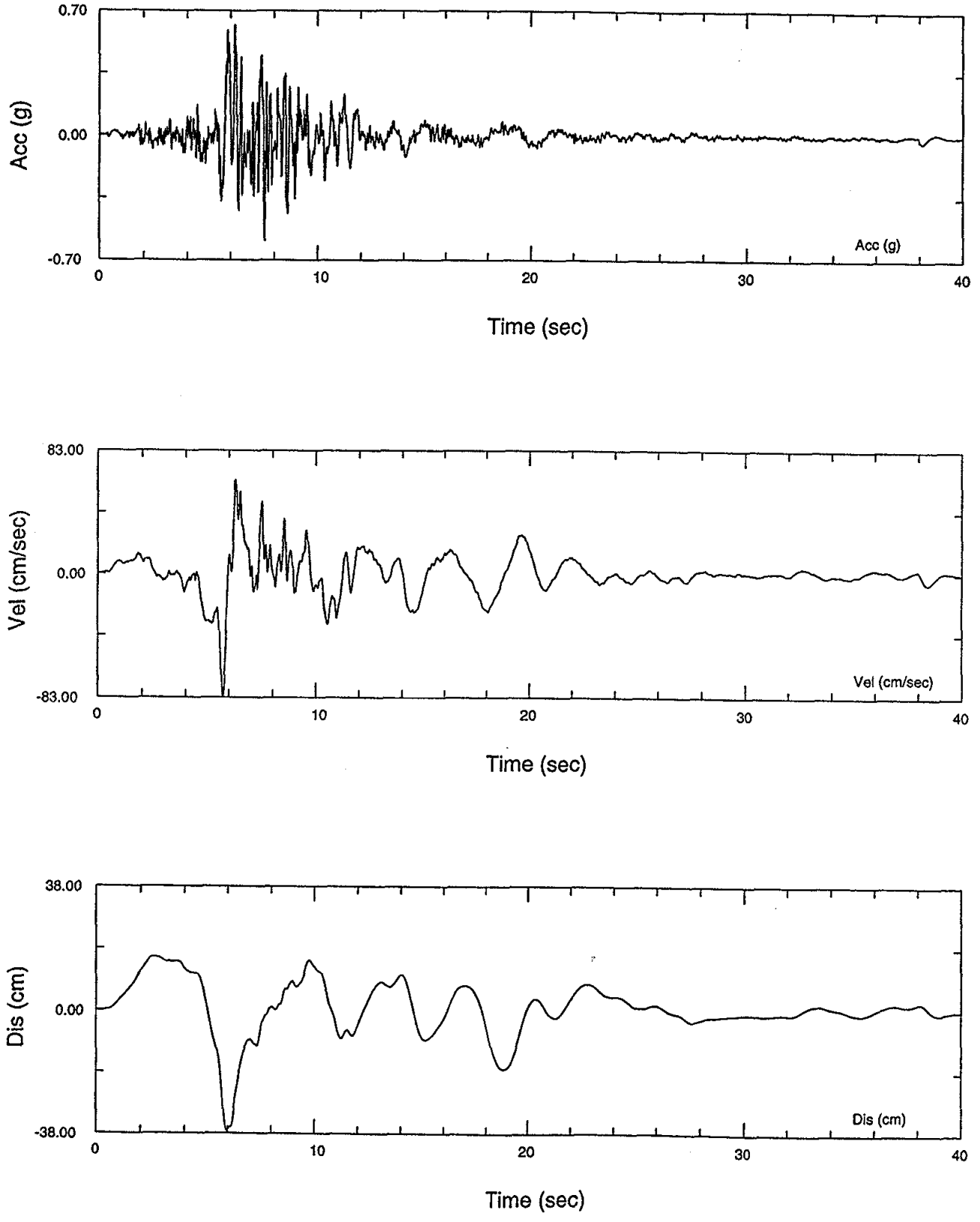

Figure E52 Set6 Initial Vertical Time History.

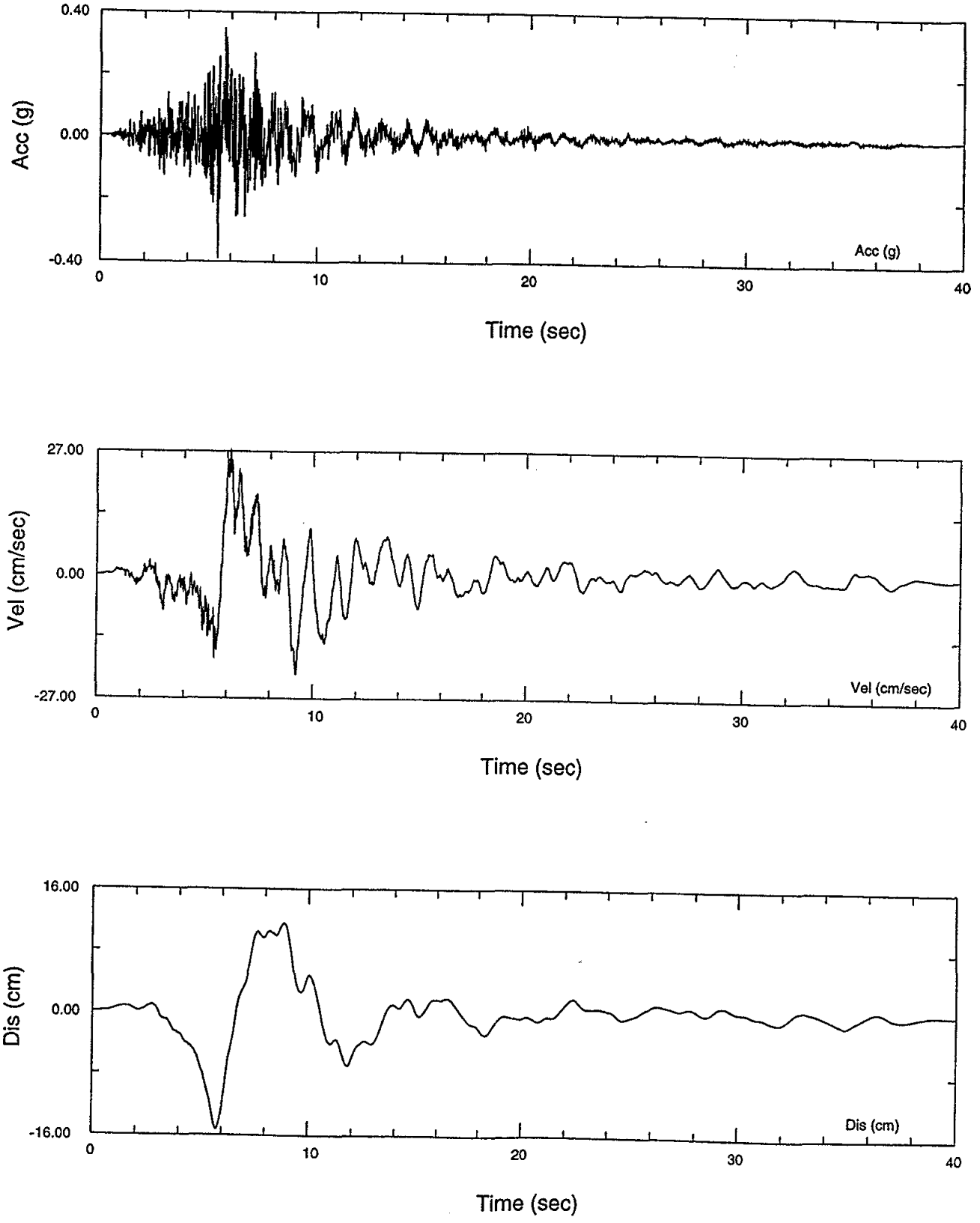

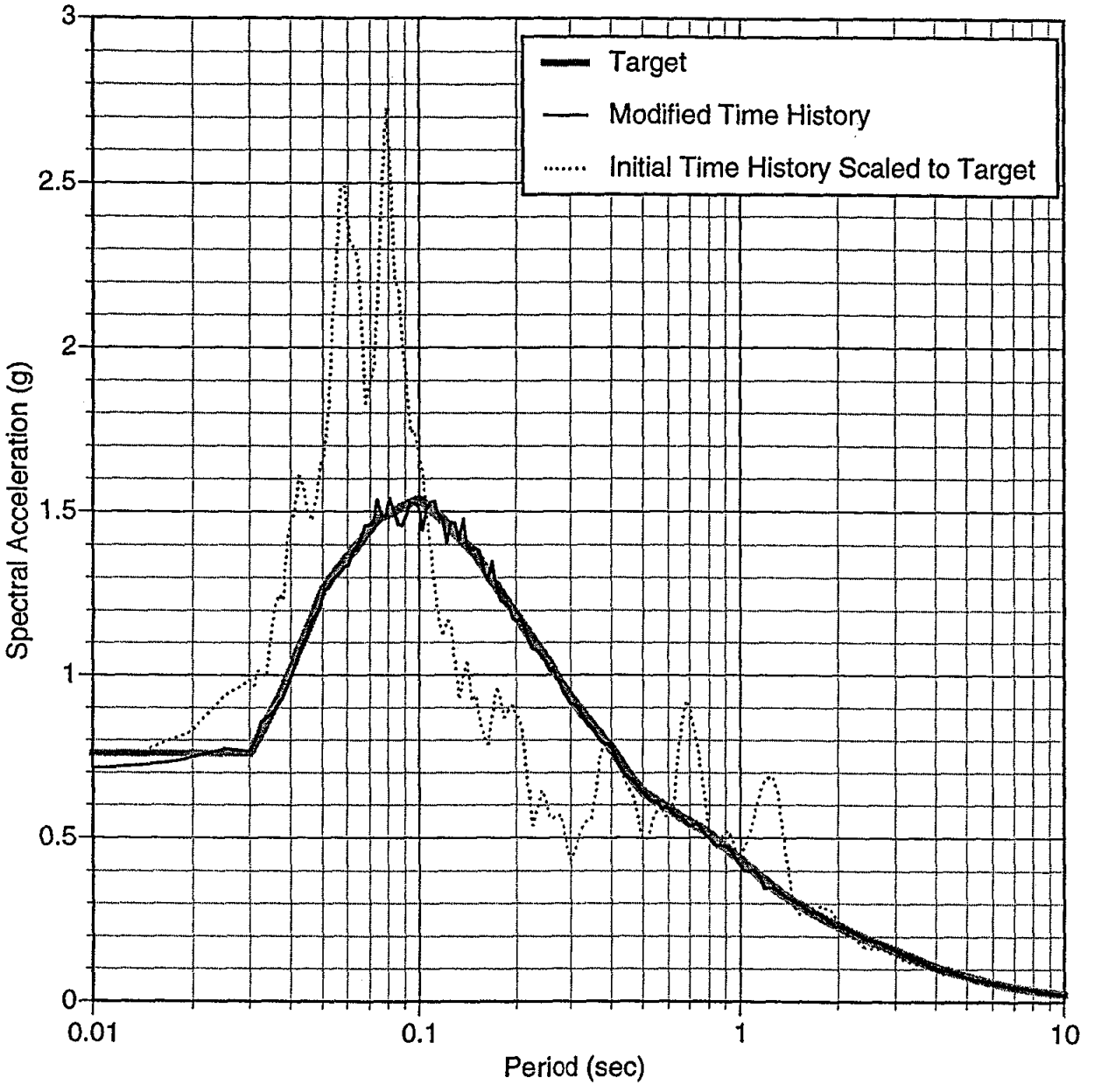

Figure E53Set6 5% damped response spectra for the modified Vertical component and initial time history scaled to the target PGA.

J3:Data1:East_BBridge_RefMotions:Report_Figures:Set6:Set6_rsp.dg

Figure E54. Set6 Spectrum Compatible Vertical Reference Time History.

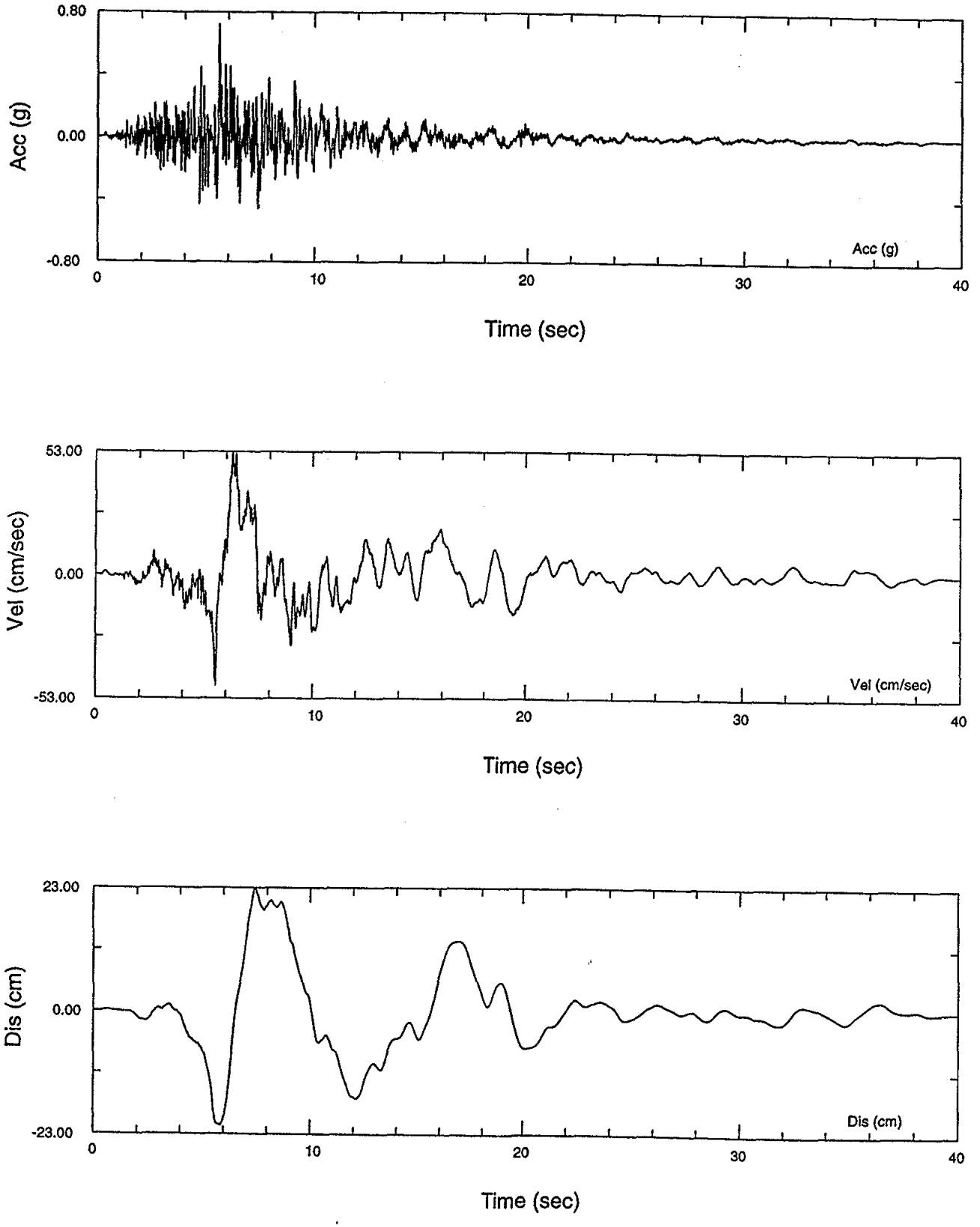

APPENDIX F
EMPIRICAL PLANE-WAVE COHERENCY MODELS FOR HORIZONTAL AND VERTICAL COMPONENTS

Appendix F

Spatial Coherency Functions

Introduction

Scattering and complex wave propagation can lead to significant variations in the ground motion along the length of large structures even if the site conditions are similar (e.g. rock). This variability typically includes variability in both the Fourier phases the Fourier amplitudes; however, since each ground motion is modified to be spectrum compatible, the variation in the Fourier amplitude is not considered. The variation in the Fourier phase affects the shape of the time history. This variation can be described by the spatial coherency which is a statistical model of the ground motion variability.

Coherency

The coherency of ground motion is parameterized by a coherency function. The coherency is a complex number given by

$$\gamma_{ij}(\omega) = \frac{S_{ij}(\omega)}{S_{ii}(\omega)S_{jj}(\omega)}$$

where

$$S_{ij}(\omega) = \sum_{m=-M}^{M} a_m u_i(\omega_m)\bar{u}_j(\omega_m),$$

The absolute value of the complex coherency is called the "lagged coherency" because it is equivalent to lining up (lagging) the ground motion at the two locations so that the wave passage effect is removed.

$$|\gamma_{ij}(\omega)| = \left| \frac{S_{ij}(\omega)}{S_{ii}(\omega)S_{jj}(\omega)} \right|$$

The lagged coherency does not restrict the alignment of the ground motions to be consistent from frequency to frequency; that is the apparent wave speeds can be different at each frequency. At high frequencies, the wave speed implied by the complex coherency becomes more random. However, in the application of the wave passage (see section 4), a constant wave speed is used for all frequencies. To be consistent with this application, the coherency function needs to correspond to the coherency that would be computed by aligning the ground motion to a single wave speed. This coherency is called the "plane-wave coherency".

$$|\gamma_{pw}(\omega,\xi,\xi_r)| = |\gamma(\omega,\xi)|\, h(\omega,\xi_r)$$

where

$$\frac{\mathrm{Re}\,\gamma_{jk}(\omega,\xi_r)}{|\gamma_{jk}(\omega,\xi)|} = h(\omega,\xi_r)\cos(2\pi f\xi_r s)$$

Coherency Model

Array data from the dense arrays listed in Tables F-1 were used to develop the spatial coherency model. A previous evaluation (Abrahamson, 1992) has shown that the coherency is does not depend strongly on earthquake

magnitude, distance, or site condition. Therefore, all of the array data was used to develop a single generic coherency model that is applicable to the Bay Bridge site. A summary of the data set from each array is given in Table F-2.

The empirical modeling is developed using $\tanh^{-1}$ of coherency during the curve fitting. The final model is presented in terms of the linear coherency for ease of application. This final model is listed in Table F-3 and is plotted in Figures F-1 and F-2.

References

Abrahamson, N. A. (1992). Generation of spatially incoherent strong motion time histories, Proc. Tenth World Conf. Earth. Engin., Madrid, Spain, 845-850.

TABLE F-1

Dense Array Characteristics

Array	Location	Site Class	Surface Stations	Spacing (m) Min	Max
EPRI LSST	Taiwan	Soil	15	3	85
EPRI Parkfield	CA	Rock	13	10	191
Chiba	Japan	Soil	15	5	319
USGS Parkfield	CA	Rock	14	25	952
Imperial Valley Diff	CA	Soil	5	18	213
Hollister Diff	CA	Soil	4	61	256
Stanford (temp)	CA	Soil	4	32	185
Coalinga (temp)	CA	Rock	7	48	313
UCSC ZIYA (temp)	CA	Rock	6	25	300
Pinyon Flat (temp)	CA	Rock	58	7	340
SMART 1	Taiwan	Soil	39	100	4000
SMART 2	Taiwan	Rock	8*	200	750*

TABLE F-2

Dense Array Data Sets

Array	No.of Eqk Analyzed	Mag Min	Mag Max	Dist (km) Min	Dist (km) Max	Max GM
EPRI LSST	15	3.0	7.8	5	113	0.26g
EPRI Parkfield	12	3.0	3.9	13	15	0.04g
Chiba	19	4.8	6.7	61	105	0.41g
USGS Parkfield	9	2.2	3.5	18	45	0.04g
Imperial Valley Diff	2	5.1	6.5			0.89g
Hollister Diff	1	5.3		17		0.20g
Stanford (temp)	4		<4	40		0.007g
Coalinga (temp)	1	5.2		12		0.21g
UCSC ZIYA (temp)	3	2.3	3.0	9	19	
Pinyon Flat (temp)	6	2.0	3.6	14	39	
SMART 1	20	4.0	7.8	5	80	0.33g
SMART 2	2	4.0	5.5	15	60	0.06g

Table F-3. Empirical Functions for Plane-Wave Coherency

$$\gamma_{pw}(f,\xi) = \left[1 + \left(\frac{f}{a_1 f_c(\xi)}\right)^{n_1}\right]^{-1/2} \left[1 + \left(\frac{f}{a_2 f_c(\xi)}\right)^{n_2(\xi)}\right]^{-1/2}$$

where

Coeff	Horizontal	Vertical
a1	1.647	3.15
a2	1.01	1.0
n1	7.02	4.95
n2(ξ)	5.1 - 0.51 ln(ξ+10)	1.685

where f is frequency in Hz and ξ is the separation distance in m.

For the horizontal component:

$$f_c(\xi) = -\left[1.886 - 2.2209 \ln\left(\frac{4000}{\xi} + 1.5\right)\right]$$

For the vertical component:

$$f_c(\xi) = \exp\left(2.43 - 0.025 \ln(\xi+1) - 0.048 \left[\ln(\xi+1)\right]^2\right)$$

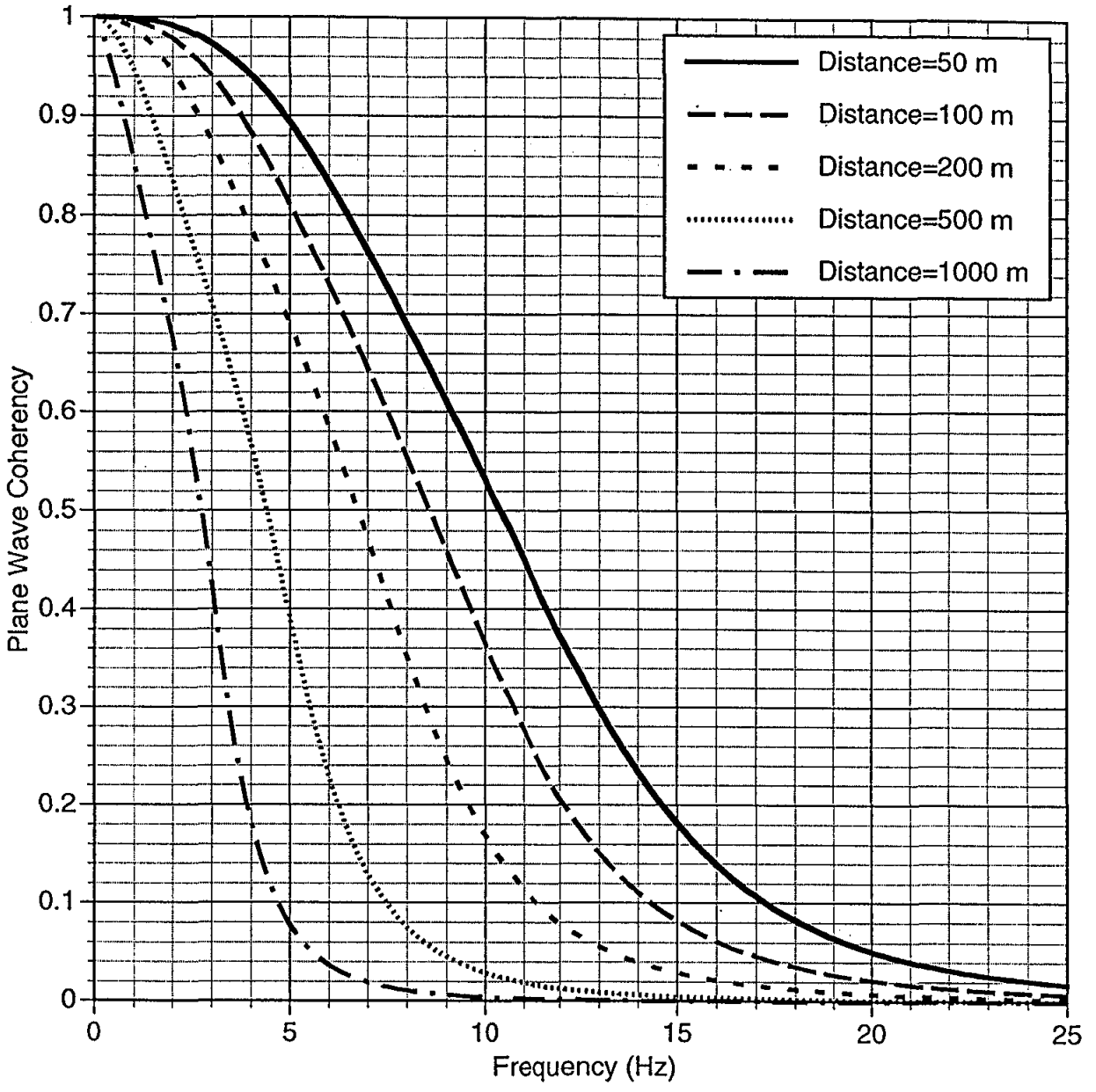

Figure 3-14a. Plane wave coherency model for the horizontal component.

FIG F-1

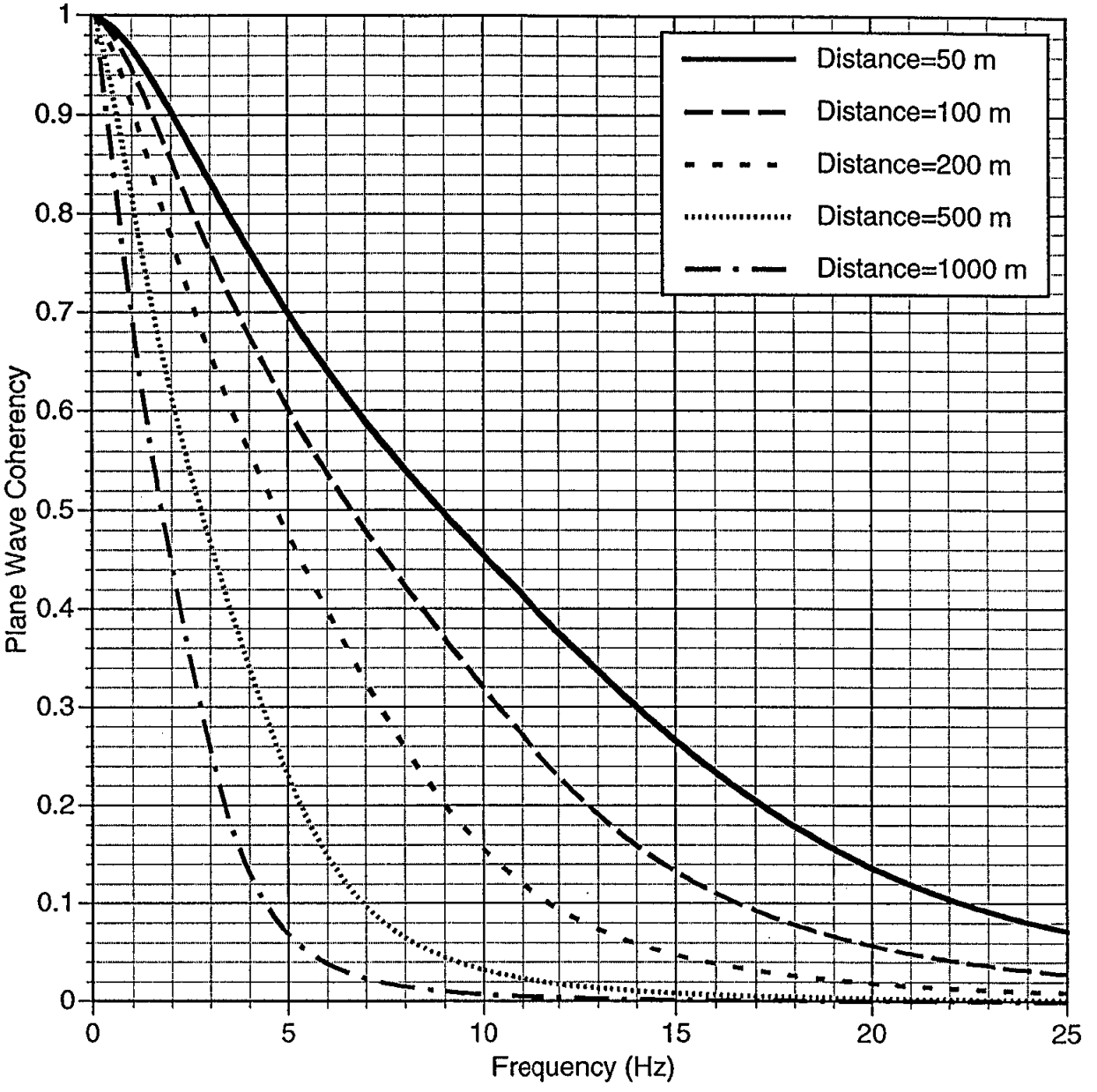

Figure 3-14b. Plane wave coherency model for the vertical component.

APPENDIX G
GUIDELINES FOR GENERATION OF RESPONSE-SPECTRUM COMPATIBLE ROCK MOTION TIME HISTORIES FOR APPLICATION TO CALTRANS TOLL BRIDGE SEISMIC RETROFIT PROJECT

GUIDELINES FOR GENERATION OF RESPONSE-SPECTRUM-COMPATIBLE ROCK MOTION TIME HISTORIES FOR APPLICATION TO CALTRANS TOLL BRIDGE SEISMIC RETROFIT PROJECTS

by

The Caltrans Seismic Advisory Board
Ad Hoc Committee on Soil-Foundation-Structure Interaction

August 9, 1996

INTRODUCTION

Currently one three-component set of synthetic rock motion time histories has been generated for each of the seven state-owned toll bridges (five in Northern California and two in Southern California) for use in the seismic retrofit program. These time histories have been adjusted to make them compatible with the corresponding horizontal and vertical site-specific "target" response spectra developed for a selected "reference" pier location at each bridge site. Because extensive inelastic nonlinear behavior can be expected in each retrofitted bridge during a future Safety Evaluation Earthquake (SEE), the Caltrans Seismic Advisory Board (SAB) and the toll bridge Peer Review Panel (PRP) have recommended that two additional three-component sets of response-spectrum-compatible rock motion time histories be generated for each reference location and that corresponding response-spectrum-compatible and coherency-compatible sets be generated for other pier locations for use in further validating seismic bridge performances. Seismic performance evaluations using these additional sets of input motions are considered necessary due to the high sensitivity of history-dependent inelastic response to variations in the input motions from one set to another, even when they are all fully compatible with the same specified target response spectra. Such evaluations for different sets of inputs will result in increased confidence in the final retrofit measures of each bridge, including the installation of energy-dissipation devices and/or seismic isolation bearings.

To provide a consistent and unified approach for all toll bridge seismic retrofit projects and to serve as a guide for Caltrans and its designated design contractors in developing phase-

independent sets of time histories for each bridge, it is recommended that the guidelines presented herein be followed. It should be noted that they are limited to the generation of rock outcrop motions which are required to be compatible with the prescribed site-specific target response spectra for the selected reference locations. They do not cover the generation of response-spectrum-and-coherency-compatible multiple-support rock-motion time histories. This procedure is covered in various ground-motion reports submitted to Caltrans on toll-bridge projects (Geomatrix, 1993a). Also, these guidelines do not cover site-response analyses which will be covered in a separate document.

OVERVIEW OF RESPONSE-SPECTRUM-COMPATIBLE TIME-HISTORY DEVELOPMENT PROCEDURES

Given prescribed target acceleration response spectra (ARS) and a set of associated controlling earthquake and ground motion parameter values (details of which will be described later), the methods currently used in developing ground motion time histories compatible with prescribed target ARS may be classified as follows:

Method 1 - Response-Spectrum Compatibility Time-History Adjustment Method. (Gasparini and Vanmarcke, 1976; Silva and Lee, 1987; Lilhanand and Tseng, 1988; Bolt 1994). This method as generally practiced starts by selecting a suitable 3-component set of initial or "starting" accelerograms and proceeds to adjust each of them iteratively, using either a time-domain (Lilhanand and Tseng 1988; Abrahamson 1992) or a frequency-domain (Gasparini and Vanmarcke 1976; Silva and Lee 1987; Bolt and Gregor, 1993) procedure, to achieve compatibility with a specified target ARS and other associated parameter values. The time-domain adjustment procedure usually produces only small local adjustments to the selected starting time histories, thereby producing response-spectrum-compatible time histories closely resembling the initial motions. Thus, the general "phasing" of the seismic waves in the starting time history is largely maintained while achieving close compatibility with the target ARS, but results in minor changes in the phase relationships. The frequency domain procedure commonly used retains the phase relationships of an initial motion, but does not always provide as close a fit to the target spectrum as does the time domain procedure. Also, the motion

produced by the frequency domain procedure shows greater visual differences from the initial motion.

Method 2 - Source-to-Site Numerical Model Time-History Simulation Method (Boore and Akinson 1987; Sommerville and Helmberger 1990, Papageorgiou and Aki 1983; Silva and Lee 1987; Bolt 1987). This method generally starts by constructing a numerical model to represent the controlling-earthquake source and source-to-site transmission and scattering functions and then accelerograms are synthesized for the site using numerical simulations based on various plausible fault-rupture scenarios. Each individual accelerogram produced by this simulation procedure generally does not produce a time history having its ARS and other characteristics closely matching those specified. Even when applying certain constraints on the modelling parameters of this method, which are consistent with those represented by the target spectra, a large number of simulations are usually required to achieve reasonable consistency with the target values on an ensemble average basis. This method, however, can produce a time history having a desired characteristic such as having a large velocity pulse, or "fling", as expected for a near source site. Therefore, this method can be used to generate suitable starting motions for use in Method 1. Because of the large number of time-history simulations required in order to achieve a "stable" average ARS for the ensemble, this method is generally not practical for developing multiple set of time histories for direct engineering applications; rather it is generally used for developing a set of time histories to be used directly, or to supplement a set of actual recorded accelerograms, in developing site-specific target response spectra and associated ground motion parameter values. This method is useful for assessing various earthquake scenarios and for examining the effects of various seismologic parameters on the resulting ground motions.

Method 3 - Multiple Actual Recorded Time-History Scaling Method (NRC Standard Review Plan 1989; UBC, 1994). This method starts by selecting multiple 3-component sets (generally $\geq$ 7) of actual recorded accelerograms which are subsequently scaled in such a way that the average of their response spectral ordinates over the specified frequency (or period) range of interest matches the target ARS. Experience in applying

this method shows that its success depends very much on the selection of time histories. Because of the lack of suitable recorded time histories, individual accelerograms often have to be scaled up or down by large multiplication factors (sometimes as large as 2.5), thus raising questions about the appropriateness of such scaling. Experience also indicates that unless a large ensemble of time histories (typically > 20) is selected, it is generally difficult to achieve matching of the target ARS over the entire spectral frequency (or period) range of interest.

Method 4 - Connecting Accelerogram Segments Method (Seed and Idriss 1969). This method produces a synthetic time history by connecting together segments of a number of actual recorded accelerograms in such a way that the ARS of the resulting time history fits reasonably well the target ARS. This method generally requires producing a number of synthetic time histories to achieve acceptable matching of the target spectrum over the entire frequency (or period) range of interest.

For the current toll bridge seismic retrofit projects, Method 1 has been used in generating the first set of rock motion time histories for each controlling seismic event of each bridge. Among the four methods described above, it is the consensus of the Ad Hoc Committee that, until more rigorous comparative studies of all current methods are completed, Method 1 is most suitable and practical for the toll bridge seismic retrofit applications and that, in the interest of maintaining consistency, this method should be used for generating the three sets of rock motion time histories representing the SEE event applicable to each toll bridge project.

TARGET RESPONSE SPECTRA AND ASSOCIATED GROUND MOTION PARAMETERS

For generating sets of time histories, the existing target acceleration response spectra developed for rock-outcrop motions at a selected reference location representing the controlling SEE event for each toll bridge project should continue to be used. For the Northern California toll bridges (San Francisco-Oakland Bay Bridge, Richmond-San Rafael Bridge, San Mateo-Hayward Bridge, Benicia-Martinez Bridge, and Carquinez Bridge), the target ARS are those developed by Geomatrix Consultants, Inc. (Geomatrix, 1993b) in collaboration with International Civil

Engineering Consultants, Inc. For the Southern California toll bridges (Vincent Thomas Bridge and Coronado Bridge), the target ARS are those developed by CWPGeosciences, Inc. (CWPGeosciences, 1994). The target response spectra for each controlling seismic event should be supplemented by a set of ground motion parameters representing relevant target controlling seismic events, which should include (1) magnitude and source-to-site distance (closest distance from the site to the controlling fault plane), (2) peak ground (rock-outcrop) acceleration (PGA), peak ground velocity (PGV), and peak ground displacement (PGD), and (3) duration of strong shaking defined to be the time duration between 5 to 95% of cumulative energy measured by $\int a^2(t)dt$; where $a(t)$ is the acceleration time history. For any site having the controlling source-to-site distance less than about 10 km, the requirement of a fling in the ground motions should also be specified. Example values of these target ground motion parameters for the Richmond-San Rafael Bridge are shown in Tables 1 and 2.

The target ARS and associated controlling earthquake and ground-motion parameters form the basic requirements for generating response-spectrum-compatible time histories using Method 1.

SELECTION OF STARTING TIME HISTORIES OF MOTION

Since the Method 1 recommended for generating response-spectrum-compatible time histories produces only local disturbances to the starting time histories selected for modification, especially when using the time-domain adjustment procedure, the phasing (seismic wave sequence or pattern) characteristics of the starting motions are largely maintained. Thus, it is important to select the starting time histories carefully. For generating the additional sets of spectrum-compatible reference rock-motion time histories for the toll bridge projects, the starting time histories should be selected using the following guidelines:

(1) Each set of starting accelerograms for a given toll bridge should preferably be selected from sets of recorded accelerograms for different past seismic events with similar fault mechanism and it should possess a significantly different ground motion pattern from other selected sets.

(2) Each past seismic event selected should have a magnitude, where possible, within ± 0.5 of the target controlling earthquake magnitude; and, the closest distance from the site of the recorded motions to the earthquake source should generally be within 10 km of the target source-to-site distance.

(3) The selected recorded accelerograms should have their PGA, PGV, and PGD values and their strong shaking durations within the ranges (-25% and +50%) of the corresponding target guideline values.

(4) These selected accelerograms should be free-field surface recordings on a rock, rock-like, or stiff soil site; no recordings on a soft soil site should be used.

(5) For a close-in controlling seismic event, i.e. within about 10 km of the site, the selected accelerograms should contain a large velocity pulse or "fling". When such recordings are not available, Method 2 can be used to generate a starting set of time histories having a fling or recorded motions can be modified to include a large directional velocity pulse.

A sample data base of available free-field strong motion recordings on rock, rock-like, and stiff soil sites for past earthquakes having magnitudes ≥ 6.5 and source-to-site distances ≤ 30 km, from which a set of starting time histories may be selected, is shown in Appendix A compiled by Abrahamson. A discussion of the appropriate ground motion selection process is given by Bolt and Gregor (1993) as they applied it to the seismic condition of the East Crossing of the San Francisco-Oakland Bay Bridge.

GUIDELINES FOR GENERATION OF RESPONSE-SPECTRUM-COMPATIBLE TIME HISTORIES

Having selected a three-component set of recorded time histories representing the starting motion, the horizontal components should be transformed into principal components and their corresponding principal directions should be evaluated using the procedures shown in Appendix B by Penzien. These principal components should then be made response-spectrum compatible

using the previously described Method 1 following the standard time-domain adjustment procedure (Kaul, 1978; Lilhanand and Tseng, 1988; Abrahamson, 1992) or the standard frequency-domain adjustment procedure (Hao, Oliviera, and Penzien, 1989; Silva and Lee, 1987; Bolt and Gregor, 1993). Using the latter procedure, only the Fourier amplitude spectrum, not the phase spectrum, is adjusted. Generation of the response-spectrum-compatible time histories should conform to the following guidelines:

(1) For each principal component of motion, response-spectrum matching should be carried out for at least 75 spectral frequencies (or periods) over the range 0.1 to at least 20 cps which corresponds to the period range 10.0 to at least 0.05 seconds. A recommended standard set of spectrum-matching frequencies and corresponding periods is given in Table 3.

(2) After each response-spectrum-compatible acceleration time history is generated, its acceleration response spectral values should be computed for the minimum number (75) of specified spectrum-matching frequencies (or periods) and these values should be compared with the corresponding target response spectral values to determine levels of spectrum compatibility. Then additional response spectral values should be generated for comparison with the corresponding target spectral values for an additional minimum set of 75 spectral frequencies (or periods) chosen approximately midway between each pair of consecutive spectral-matching frequencies (or periods) plus the frequency of 40 cps (period of 0.025 second). A recommended set of such additional spectral frequencies (and corresponding periods) for back checking response-spectrum compatibility of a generated time history is given in Table 4.

(3) Each generated response-spectrum-compatible acceleration time history should have its response spectral values matching the corresponding target spectral values at the specified set of spectrum-matching frequencies to within -5% to +10% of the target values.

(4) The peak values of each generated acceleration time history and its integrated velocity and displacement time histories should fall within their target ranges of values mentioned previously. Likewise, its 5-95% strong-motion duration should fall within its target range.

(5) Each generated acceleration time history should be checked for a broad distribution of motion contents with frequency (or period) by examining its response spectral values for a low and a high damping ratio such as 2 and 10%.

(6) For any response-spectrum-compatible motion generated from a starting acceleration time history containing a fling, the corresponding velocity and displacement time histories should be checked against the velocity and displacement time histories of the starting motion to make sure that the time-history modification process did not substantially alter the characteristics and amplitude of the fling.

(7) For each generated three-component set of response-spectrum-compatible time histories, the cross-correlation coefficient of each pair of acceleration, velocity, or displacement time histories should be computed and checked to ensure that it has a relatively low value, say ≤ 0.1 for the acceleration time histories, ≤ 0.2 for the integrated velocity time histories, and ≤ 0.3 for the integrated displacement time histories.

(8) The generated response-spectrum-compatible time histories should be digitized at time intervals not greater than 0.01 second.

(9) The integrated velocity and displacement time histories of each generated response-spectrum-compatible acceleration time history should be checked to ensure that they do not have numerically-generated baseline drifts. Such baseline drifts should be corrected using an appropriate procedure, e.g. by introducing an acceleration impulse (Lilhanand and Tseng 1988), by high-pass filtering, or by

the classical baseline correction scheme (Brady 1966). After each baseline correction, the resulting baseline-corrected acceleration time history should be checked again for response-spectrum compatibility. Further iterations may be required to achieve simultaneously no baseline drifts and satisfactory response-spectrum compatibility.

The additional sets of three-component response-spectrum-compatible time histories generated for a single reference point following the above guidelines will show different visual characteristics.

UTILIZATION OF GENERATED RESPONSE-SPECTRUM-COMPATIBLE TIME HISTORIES

The target acceleration response spectra are in general identical for the two horizontal principal components of motion; however, a distinct target spectrum is specified for the vertical component. In such cases, a generated three-component (two horizontal and one vertical) set of response-spectrum-compatible time histories can be oriented horizontally along any two orthogonal coordinate axes in the horizontal plane considered suitable for structural analysis applications. However, for the toll bridge projects which have controlling seismic events with close-in seismic sources, the two horizontal target response spectra representing motions along a specified set of orthogonal axes are somewhat different, especially in the low frequency (long period) range; thus, the response-spectrum-compatible time histories must have the same definitive orientation. In this case, the generated three-component set of response-spectrum-compatible time histories should be used in conjunction with their defined orientation. The application of this three-component set of motions in a different coordinate orientation requires transforming these motions to the new coordinate system. It should be noted that such a transformation of the components will generally result in time histories which are not fully compatible with the original target response spectra. Thus, if response-spectrum compatibility is desired in a specific coordinate orientation (such as fault normal and fault parallel), target response spectra in the specific orientation should be generated first and then a three-component set of fully response-spectrum-compatible time histories can be generated for this specific coordinate system.

For application to the toll bridge seismic retrofit projects, each 3-component set of response-spectrum-compatible time histories generated for each selected reference location representing the controlling SEE event of each bridge should be used to generate the corresponding sets of multiple-support response-spectrum-and-coherency-compatible rock-outcrop motion time histories applicable to each pier of the bridge using an appropriate procedure (Hao, Oliviera, and Penzien, 1989; Abrahamson, 1992a; Tseng, Lilhanand, and Yang, 1993). These rock-outcrop time histories generated should then be used in appropriate site response analyses to develop the corresponding free-field site soil response motions required for conducting the soil-foundation-structure interaction analyses for each pier.

CONCLUDING STATEMENT

The guidelines recommended herein are based on data and knowledge presently available and on experience gained to date (August 1996). As changes take place in the future through research and development, they should be reviewed and modified as deemed appropriate.

ACKNOWLEDGEMENT

In response to a joint recommendation by the Caltrans toll bridge Peer Review Panel and the Seismic Advisory Board that two additional sets of input motions be used in validating the retrofit measures of each toll bridge, the Board's Ad Hoc Committee on Soil-Foundation-Structure Interaction was requested by Caltrans on April 16, 1996 to develop, on a high-priority basis, guidelines for the generation applicable to the toll bridge seismic retrofit projects. In response, the Committee prepared the guidelines presented herein.

Membership on the Committee consists of Abbas Abghari, Engineering Service Center, Caltrans, John F. Hall, California Institute of Technology, I. M. Idriss, University of California, Davis, Ignatius P. Lam, Earth Mechanics, Inc., Brian H. Maroney, Engineering Service Center, Caltrans, Joseph P. Nicoletti, URS Consultants, Frieder Seible, University of California, San Diego, Wen S. Tseng, International Civil Engineering Consultants, Inc., and Joseph Penzien, International Civil Engineering Consultants, Inc. who served as Chairman of the Committee.

For this particular task, Norman A. Abrahamson, Engineering Seismology Consultant, met with the committee and made valuable contributions. Bruce A. Bolt, member of the Seismic Advisory Board, reviewed this document and made valuable suggestions.

REFERENCES

Abrahamson, N.A. (1992), "Non-Stationary Spectral Matching," Presented at 87th Annual Meeting of Seismological Society of America, also Seismological Research Letter, Vol. 63, No. 1.

Abrahamson, N.A. (1992a), "Generation of Spatially Incoherent Strong Motion Time Histories," Proceedings of the Tenth World Conference on Earthquake Engineering, Madrid, Spain, July 19-24, pp. 845-850.

Bolt, B.A. (Editor) (1987), "Seismic Strong Motion Synthetics," New York Academic Press, pp. i-328.

Bolt, B.A. and Gregor, N.J. (1993), "Synthesized Strong Ground Motions for the Seismic Condition Assessment of the Eastern Portion of the San Francisco Bay Bridge," UCB/EERC-93/12 Report, pp. 1-217.

Bolt, B.A. (1994), "The State of the Art in Synthesis of Strong Ground Motion for Earthquake Engineering," Proceedings of the Tenth World Conference on Earthquake Engineering, July, 1992, Madrid, pp. 6487-6492.

Boore D. and Akinson, G. (1987), "Stochastic Prediction of Ground Motion and Spectral Response Parameters at Hard-Rock Sites in Eastern North America," Bulletin of the Seismological Society of America, Vol. 77, pp. 440-467.

Brady, A.G. (1966), "Studies of Responses to Earthquake Ground Motion," Earthquake Engineering Research Laboratory, California Institute of Technology, Pasadena, California.

Gasparini, D. and Vanmarcke, E.H. (1976), "SIMQKE: A Program for Artificial Motion Generation, Department of Civil Engineering, Massachusetts Institute of Technology.

Hao, H., Oliviera, C.S., and Penzien, J. (1989), "Multiple-Station Ground Motion Processing and Simulation based on SMART-1 Array Data," Nuclear Engineering and Design, Vol. 111, No. 6, pp. 2229-2244.

Kaul, M.K. (1978), "Spectrum-Consistent Time-History Generation," Journal of American Society of Civil Engineers, Vol. 104, No. 3M4, pp. 781-788.

Lilhanand, K. and Tseng, W. S. (1988), "Development and Application of Realistic Earthquake Time Histories Compatible with Multiple-Damping Design Spectra," Proceedings of the 9th Work Conference of Earthquake Engineering, Tokyo-Kyoto, Japan, August 2-9.

Nuclear Regulatory Commission (1989), "Standard Review Plan," Section 3.7.1, Revision 2, August.

Papageorgiou, A.S. and Aki, K. (1983), "A Specific Barrier Model to the Quantitative Description of Inhomogeneous Faulting and the Prediction of Strong Motion," Bulletin of the Seismological Society of America, Vol. 73, pp. 693-722 and 953-978.

Silva, W.J. and Lee, K. (1987), "WES RASCAL Code for Synthesizing Earthquake Ground Motions," State-of-the-Art for Assessing Earthquake Hazards in the United States, Report 24, U.S. Army Engineers Waterway Experimental Station, Miscellaneous Paper 5-73-1.

Sommerville, P.G. and Helmberger, D.V. (1990), "Modelling Earthquake Ground Motion at Close Distances," EPRI/Stanford/USGS Workshop on Modeling Earthquake Ground Motion at Close Distances, August 32

Tseng, W. S., Lilhanand, K., and Yang, M. S. (1993), "Generation of Multiple-Station Response-Spectrum-and-Coherency-Compatible Earthquake Ground Motions for Engineering

Applications," Proceedings of the Twelfth International Conference on Structural Mechanics in Reactor Technology, Paper No. K01/3, Stuttgart, Germany, August 15-20.

TABLE 1

RICHMOND-SAN RAFAEL BRIDGE

CONTROLLING MAXIMUM CREDIBLE EARTHQUAKE PARAMETERS

Controlling Earthquake Source	Maximum Credible Earthquake Magnitude (M_w)	Closest Distance to Selected Reference Location (Km)	
		West End of Bridge	East End of Bridge
San Andreas	8	16½	21
Hayward	7¼	11½	7

Source: "Seismic Ground Motion Study for Richmond-San Rafael Bridge," prepared by Geomatrix Consultants, Inc. in Cooperation with International Civil Engineering Consultants, Inc. for Caltrans, Division of Structures, under State Contract No. 59N772, June 1993.

TABLE 2

RICHMOND-SAN RAFAEL BRIDGE

GUIDELINE VALUES FOR SELECTED GROUND MOTION PARAMETERS

Controlling Earthquake Source	Ground Motion Component	Peak Ground Acceleration (PGA) (g)	Peak Ground Velocity (PGV) (cm/sec)	Peak Ground Displacement (PGD) (cm)	Duration of Strong Shaking* (sec)
San Andreas	Longitudinal	0.55	65-79	37-45	42
	Transverse	0.55	65-79	37-45	42
	Vertical	0.48	45-59	35-39	42
Hayward	Longitudinal	0.70	68-84	30-36	20
	Transverse	0.70	68-84	30-36	20
	Vertical	0.66	39-55	22-28	20

Source: "Seismic Ground Motion Study for Richmond-San Rafael Bridge," prepared by Geomatrix Consultants, Inc. in Cooperation with International Civil Engineering Consultants, Inc. for Caltrans, Division of Structures, under State Contract No. 59N772, June 1993.

*Note: "Duration of strong shaking" is defined as the time duration between 5 to 95% of cumulative energy measured by $\int a^2(t)dt$, where $a(t)$ is acceleration time history.

TABLE 3

MINIMUM SET OF 75 SPECTRAL-MATCHING FREQUENCIES AND PERIODS

Frequency (cps)	Period (sec)	Frequency (cps)	Period (sec)	Frequency (cps)	Period (sec)
0.1	10.0	1.8	0.56	5.75	0.174
0.111	9.0	1.9	0.53	6.0	0.167
0.125	8.0	2.0	0.50	6.25	0.16
0.143	7.0	2.1	0.48	6.5	0.154
0.167	6.0	2.2	0.46	6.75	0.148
0.2	5.0	2.3	0.44	7.0	0.143
0.222	4.5	2.4	0.42	7.33	0.136
0.25	4.0	2.5	0.40	7.67	0.130
0.286	3.5	2.6	0.385	8.0	0.125
0.333	3.0	2.7	0.37	8.5	0.117
0.385	2.6	2.8	0.355	9.0	0.111
0.435	2.3	2.9	0.34	9.5	0.105
0.5	2.0	3.0	0.33	10.0	0.1
0.555	1.8	3.2	0.31	11.0	0.091
0.625	1.6	3.4	0.29	12.0	0.083
0.714	1.4	3.6	0.28	13.0	0.077
0.833	1.2	3.8	0.265	14.0	0.073
1.0	1.0	4.0	0.25	16.0	0.063
1.1	0.91	4.2	0.24	18.0	0.055
1.2	0.83	4.4	0.23	20.0	0.05
1.3	0.77	4.6	0.22	22.0	0.045
1.4	0.70	4.8	0.21	25.0	0.04
1.5	0.67	5.0	0.20	28.0	0.036
1.6	0.63	5.25	0.19	31.0	0.033
1.7	0.60	5.5	0.18	34.0	0.030

TABLE 4

MINIMUM SET OF 75 ADDITIONAL SPECTRAL FREQUENCIES AND PERIODS TO BE USED FOR BACK-CHECKING RESPONSE-SPECTRUM COMPATIBILITY

Frequency (cps)	Period (sec)	Frequency (cps)	Period (sec)	Frequency (cps)	Period (sec)
0.105	9.5	1.85	0.54	6.1	0.164
0.118	8.5	1.95	0.51	6.35	0.157
0.133	7.5	2.05	0.49	6.65	0.15
0.154	6.5	2.15	0.465	6.85	0.146
0.182	5.5	2.25	0.44	7.15	0.14
0.211	4.75	2.35	0.425	7.5	0.133
0.235	4.25	2.45	0.41	7.85	0.127
0.267	3.75	2.55	0.39	8.25	0.121
0.308	3.25	2.65	0.38	8.75	0.114
0.357	2.8	2.75	0.364	9.25	0.108
0.4	2.5	2.85	0.35	9.75	0.103
0.46	2.2	2.95	0.34	10.5	0.095
0.53	1.9	3.1	0.32	11.5	0.087
0.59	1.7	3.3	0.30	12.5	0.080
0.67	1.5	3.5	0.285	13.5	0.075
0.77	1.3	3.7	0.27	14.5	0.070
0.91	1.1	3.9	0.256	15.0	0.067
1.05	0.95	4.1	0.244	17.0	0.059
1.15	0.89	4.3	0.233	19.0	0.053
1.25	0.8	4.5	0.222	21.0	0.048
1.35	0.74	4.7	0.213	23.5	0.043
1.45	0.69	4.9	0.204	26.5	0.038
1.55	0.65	5.4	0.185	29.5	0.034
1.65	0.61	5.65	0.177	32.0	0.031
1.75	0.57	5.85	0.171	36.0	0.028

APPENDIX A

STRONG MOTION RECORDINGS FOR EVENTS WITH M ≥ 6.5 AND DIST < 30 KM

Compiled by
N. A. Abrahamson

Yr	Event	Station Designation	Mag	Mech	Dist (km)	Site*	Ave H 5-75% Dur (sec)	Ave H 5-95% Dur (sec)	Ave H PGA (g)	Ave H PGV (cm/s)	Ave H PGD (cm)
1940	Imperial Valley	El Centro	6.9	SS	8.3	2	14.09	24.03	0.259	30.00	17.85
1971	San Fernando	Castatic	6.6	RV	24.9	1	6.59	14.94	0.295	20.10	3.28
1971	San Fernando	Fairmont Dam	6.6	RV	29.1	0	2.91	12.56	0.088	5.53	0.89
1971	San Fernando	Hollywood Storage Lot	6.6	RV	21.2	2	4.97	10.84	0.191	16.78	8.80
1971	San Fernando	Lake Hughes #1	6.6	RV	25.8	2	5.84	15.61	0.126	15.56	2.36
1971	San Fernando	Lake Hughes #4	6.6	RV	24.2	0	3.86	12.80	0.171	6.86	1.30
1971	San Fernando	Lake Hughes #9	6.6	RV	23.5	0	2.85	10.61	0.145	4.19	1.20
1971	San Fernando	Lake Hughes #12	6.6	RV	20.3	1	2.64	11.31	0.322	14.69	2.21
1971	San Fernando	Pacoima Dam	6.6	RV	2.8	1	5.64	7.15	1.193	78.16	20.41
1971	San Fernando	Palmdale FS	6.6	RV	25.4	2	9.29	17.38	0.135	9.98	2.21
1971	San Fernando	Old Seismo Lab	6.6	RV	19.1	0	4.53	9.02	0.134	7.60	1.43
1971	San Fernando	Santa Anita	6.6	RV	27.0	0	5.83	11.16	0.179	5.35	2.58
1971	San Fernando	Santa Felita Dam	6.6	RV	27.5	0	6.22	19.89	0.150	7.82	4.93
1976	Gazli	Gazli	6.8	RV	3.0	0	4.94	6.63	0.661	68.43	24.49
1978	Tabas	Dayhook	7.4	RV	17.0	0	6.83	12.33	0.365	23.36	10.48
1978	Tabas	Tabas	7.4	RV	3.0	2	7.91	16.31	0.844	108.96	59.09
1979	Imperial Vly	Aeropuetro	6.5	SS	8.5	2	5.16	7.04	0.292	32.65	6.20
1979	Imperial Vly	Agarias	6.5	SS	12.9	2	6.66	12.90	0.286	38.85	10.83
1979	Imperial Vly	Bonds Corner	6.5	SS	2.5	2	5.37	9.71	0.675	45.55	15.81
1979	Imperial Vly	Brawley	6.5	SS	8.5	2	4.04	14.46	0.188	37.37	17.38
1979	Imperial Vly	Calexico	6.5	SS	10.6	2	6.49	12.81	0.236	18.42	9.11
1979	Imperial Vly	Calipatria FS	6.5	SS	23.8	2	11.72	24.20	0.100	14.31	8.24
1979	Imperial Vly	Cerro Prieto	6.5	SS	26.5	0	18.09	32.97	0.163	14.69	5.81
1979	Imperial Vly	Chihuahua	6.5	SS	28.7	2	12.75	21.05	0.262	27.38	10.82
1979	Imperial Vly	Cucapah	6.5	SS	23.6	2	6.78	15.03	0.140	3.10	1.37
1979	Imperial Vly	El Centro CC	6.5	SS	7.6	2	4.20	11.78	0.224	50.79	25.08
1979	Imperial Vly	Meloland	6.5	SS	0.5	2	2.22	7.49	0.305	80.55	28.45
1979	Imperial Vly	El Centro #1	6.5	SS	15.5	2	6.27	17.28	0.136	13.08	8.33
1979	Imperial Vly	El Centro #2	6.5	SS	10.4	2	4.06	8.92	0.315	31.50	14.34
1979	Imperial Vly	El Centro #3	6.5	SS	9.3	2	4.73	13.01	0.242	43.21	21.00
1979	Imperial Vly	El Centro #4	6.5	SS	4.2	2	3.06	8.48	0.418	53.52	34.55
1979	Imperial Vly	El Centro #5	6.5	SS	1.0	2	3.60	8.83	0.444	65.15	47.20
1979	Imperial Vly	El Centro #6	6.5	SS	1.0	2	4.67	9.97	0.424	84.42	42.71
1979	Imperial Vly	El Centro #7	6.5	SS	0.6	2	2.06	5.81	0.396	72.13	33.23
1979	Imperial Vly	El Centro #8	6.5	SS	3.8	2	2.93	6.30	0.523	51.63	33.92
1979	Imperial Vly	El Centro #10	6.5	SS	8.6	2	4.74	12.39	0.196	44.13	24.55

Yr	Event	Station Designation	Mag	Mech	Dist (km)	Site*	Ave H 5-75% Dur (sec)	Ave H 5-95% Dur (sec)	Ave H PGA (g)	Ave H PGV (cm/s)	Ave H PGD (cm)
1979	Imperial Vly	El Centro #11	6.5	SS	12.6	2	4.56	8.31	0.372	38.11	17.34
1979	Imperial Vly	El Centro #12	6.5	SS	18.2	2	9.64	19.26	0.129	19.59	11.67
1979	Imperial Vly	El Centro #13	6.5	SS	21.9	2	8.34	21.27	0.128	13.82	6.54
1979	Imperial Vly	EC Diff Array	6.5	SS	5.3	2	3.36	6.77	0.411	53.90	25.36
1979	Imperial Vly	Holtville PO	6.5	SS	7.5	2	4.72	12.46	0.236	49.30	31.75
1979	Imperial Vly	Parachute Test Site	6.5	SS	14.2	2	6.49	17.41	0.150	16.93	11.08
1979	Imperial Vly	SAHOP	6.5	SS	11.1	2	5.53	8.72	0.381	24.61	3.91
1979	Imperial Vly	Superstition mtn	6.5	SS	26.0	0	4.28	9.14	0.146	6.76	2.48
1979	Imperial Vly	Westmorland	6.5	SS	15.1	2	13.32	24.93	0.090	21.55	12.88
1985	Nahanni	Site 1	6.8	RV/OBL	6.0	0	7.10	7.99	1.035	46.05	11.87
1985	Nahanni	Site 2	6.8	RV/OBL	8.0	0	4.80	9.61	0.397	31.14	7.05
1985	Nahanni	Site 3	6.8	RV/OBL	16.0	0	7.01	11.28	0.143	4.49	1.82
1987	Superstition Hills B	El centro CC	6.7	SS	13.9	2	7.30	17.55	0.304	43.56	18.80
1987	Superstition Hills B	Westmorland FS	6.7	SS	13.3	2	10.88	18.21	0.191	26.99	16.24
1987	Superstition Hills B	Wildlife	6.7	SS	24.4	2	16.47	31.35	0.194	32.12	20.44
1988	Spitak	Gukasian	6.8	RV/OBL	30.0	0	5.35	9.11	0.187	20.78	6.49
1989	Loma Prieta	Agnew	6.9	RV/OBL	28.2	2	8.00	19.92	0.165	21.39	11.10
1989	Loma Prieta	Anderson Dam DS	6.9	RV/OBL	21.4	0	5.18	10.68	0.242	19.33	7.21
1989	Loma Prieta	Branteforte	6.9	RV/OBL	10.3	0	6.27	9.40	0.476	47.83	6.38
1989	Loma Prieta	Capitola	6.9	RV/OBL	14.5	2	5.65	12.54	0.484	32.70	7.08
1989	Loma Prieta	Corralitos	6.9	RV/OBL	5.1	2	4.00	7.38	0.555	49.95	11.12
1989	Loma Prieta	Coyote Lake Dam	6.9	RV/OBL	22.3	2	4.76	12.37	0.169	17.14	8.98
1989	Loma Prieta	Gilroy - Gal Col	6.9	RV/OBL	11.6	1	1.46	4.91	0.341	25.25	5.40
1989	Loma Prieta	Gilroy Historic Bldg	6.9	RV/OBL	12.7	2	3.70	10.92	0.262	31.75	6.37
1989	Loma Prieta	Gilroy #1	6.9	RV/OBL	11.2	0	1.72	5.11	0.441	32.73	7.16
1989	Loma Prieta	Gilroy #2	6.9	RV/OBL	12.7	2	2.34	10.25	0.344	35.87	9.29
1989	Loma Prieta	Gilroy #3	6.9	RV/OBL	14.4	2	2.40	8.87	0.451	39.95	12.57
1989	Loma Prieta	Gilroy #4	6.9	RV/OBL	16.1	2	4.56	14.31	0.297	38.35	8.45
1989	Loma Prieta	Gilroy #6	6.9	RV/OBL	19.9	0	4.50	12.77	0.146	13.48	4.24
1989	Loma Prieta	Gilroy #7	6.9	RV/OBL	24.2	1	4.09	10.27	0.270	16.50	2.87
1989	Loma Prieta	Hollister City Hall	6.9	RV/OBL	28.2	2	5.56	15.51	0.230	41.62	21.57
1989	Loma Prieta	Hollister Diff Array	6.9	RV/OBL	25.8	2	3.76	12.81	0.274	39.53	15.53
1989	Loma Prieta	Hollister South & Pine	6.9	RV/OBL	28.8	2	7.16	22.57	0.256	42.61	23.43
1989	Loma Prieta	LGPC	6.9	RV/OBL	6.1	0	5.49	9.00	0.584	69.53	21.76
1989	Loma Prieta	Saratoga, Aloha Ave	6.9	RV/OBL	13.0	2	3.97	8.83	0.407	41.89	21.12
1989	Loma Prieta	Saratoga W Vly Col	6.9	RV/OBL	13.7	2	4.13	10.90	0.291	51.06	26.68
1989	Loma Prieta	Sunnyvale - Colten Ave	6.9	RV/OBL	28.8	2	9.78	23.23	0.208	36.64	17.97
1989	Loma Prieta	UCSC	6.9	RV/OBL	18.1	0	5.52	8.78	0.350	11.66	2.55
1989	Loma Prieta	UCSC Lick Obs	6.9	RV/OBL	17.9	1	6.08	9.58	0.422	18.14	4.38
1989	Loma Prieta	WAHO	6.9	RV/OBL	16.9	2	7.11	10.74	0.486	32.15	4.74
1992	Cape Menocino	Cape Mendocino	7.1	RV	8.5	0	2.69	7.98	1.247	73.15	22.54
1992	Cape Menocino	Fortuna	7.1	RV	23.6	2	9.95	18.44	0.115	25.51	18.78
1992	Cape Menocino	Petrolia	7.1	RV	9.5	2	4.61	16.91	0.625	65.89	25.35
1992	Cape Menocino	Rio Dell	7.1	RV	18.5	2	3.09	13.11	0.460	42.99	20.25
1992	Landers	Coolwater	7.3	SS	21.2	2	38.91	74.65	0.344	32.91	13.75
1992	Landers	Desert Hot Springs	7.3	SS	23.2	2	21.75	31.89	0.162	20.55	10.38
1992	Landers	Joshua Tree	7.3	SS	11.6	2	21.32	26.65	0.279	34.47	11.94

Yr	Event	Station Designation	Mag	Mech	Dist (km)	Site*	Ave H 5-75% Dur (sec)	Ave H 5-95% Dur (sec)	Ave H PGA (g)	Ave H PGV (cm/s)	Ave H PGD (cm)
1992	Landers	Lucerne	7.3	SS	1.1	0	8.31	13.50	0.771	44.57	27.37
1992	Landers	Yermo	7.3	SS	24.9	2	8.99	18.24	0.193	39.11	32.89
1994	Northridge	Arleta	6.7	RV	9.2	2	6.02	13.23	0.326	30.69	12.72
1994	Northridge	Canoga Park	6.7	RV	15.5	2	6.35	12.77	0.401	45.74	10.95
1994	Northridge	Castaic	6.7	RV	22.6	1	5.31	8.81	0.540	52.15	3.19
1994	Northridge	Jensen Filter Plant	6.7	RV	6.2	2	3.59	9.18	0.501	102.69	32.15
1994	Northridge	Century City North	6.7	RV	25.7	2	7.13	13.42	0.238	23.06	6.17
1994	Northridge	Hollywood Storage	6.7	RV	25.5	2	6.11	11.34	0.300	20.15	4.87
1994	Northridge	Lake Hughes #9	6.7	RV	26.8	0	4.31	8.60	0.189	9.21	3.55
1994	Northridge	Lake Hughes #12	6.7	RV	22.8	2	5.14	9.76	0.212	11.85	5.38
1994	Northridge	Moorpark FS	6.7	RV	28.0	2	7.54	15.18	0.237	20.45	4.51
1994	Northridge	Newhall FS	6.7	RV	7.1	2	2.83	5.71	0.586	85.67	25.86
1994	Northridge	Saticoy, USC 003	6.7	RV	12.8	2	6.11	13.57	0.406	42.77	11.92
1994	Northridge	Pacoima Dam DS	6.7	RV	8.0	1	1.31	4.22	0.424	37.78	4.93
1994	Northridge	Kagel Canyon	6.7	RV	8.2	1	5.67	9.97	0.361	40.21	8.85
1994	Northridge	Rinaldi Rec Sta	6.7	RV	7.1	2	3.69	7.45	0.629	110.11	23.85
1994	Northridge	Santa Monica CH	6.7	RV	27.6	2	5.80	9.75	0.572	32.35	10.39
1994	Northridge	Santa Susana	6.7	RV	19.3	2	3.95	7.67	0.284	19.55	5.53
1994	Northridge	Sepvuleda VA	6.7	RV	8.9	2	4.40	8.02	0.841	80.60	16.71
1994	Northridge	Stone Canyon	6.7	RV	22.2	0	5.11	7.89	0.313	32.62	3.80
1994	Northridge	Roscoe, USC 006	6.7	RV	10.7	2	5.90	14.67	0.343	29.83	7.85
1994	Northridge	Sylmar Conv Sta	6.7	RV	6.2	2	4.44	11.28	0.741	109.86	50.13
1994	Northridge	Sylmar Conv Sta East	6.7	RV	6.1	2	3.62	7.21	0.639	93.62	31.33
1994	Northridge	Sylmar Olive View	6.7	RV	6.4	2	2.56	6.07	0.714	100.67	22.90
1994	Northridge	Tarzana	6.7	RV	17.5	1	6.82	11.60	1.327	93.73	32.68
1994	Northridge	Topanga FS	6.7	RV	23.4	2	5.12	9.08	0.311	15.07	1.96
1994	Northridge	Vasquez Rocks	6.7	RV	24.2	0	4.14	7.80	0.145	14.39	2.90

Site classification: 0 = rock, 1 = shallow soil, 2 = deep soil

APPENDIX B

TRANSFORMATION OF GROUND MOTION

by

Joseph Penzien

INTRODUCTION

The transformation of three-dimensional ground motion into components along an orthogonal set of principal axes, which have maximum, minimum, and intermediate values of variance and zero values of covariance, has been treated in the literature (Penzien and Watabe, 1974; Penzien and Watabe, 1975). For this report, only the basic relations used in transforming two dimensional ground motion into principal components will be presented; and, the influence of such transformation on response spectral values of the resulting principal components of motion will be discussed.

BASIC RELATIONS

Consider two components of horizontal ground motion $a_x(t)$ and $a_y(t)$ along orthogonal axes x and y, respectively. This motion can be transformed into components along a new set of orthogonal axes x' and y' located in the rotated position shown below. Knowing the time histories of motion $a_x(t)$ and $a_y(t)$, the components of motion along the x' and y' axes can be evaluated using the relations

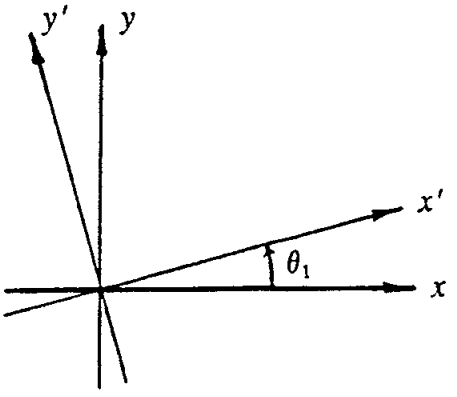

$$a_{x'}(t) = a_x(t) \cos\theta + a_y(t) \sin\theta$$

$$a_{y'}(t) = -a_x(t) \sin\theta + a_y(t) \cos\theta \qquad \text{(B-1)}$$

Variances of the components of motion $a_x(t)$ and $a_y(t)$ and the corresponding covariance are defined as

$$\sigma_x^2 \equiv \frac{1}{t_d}\int_0^{t_d}\left[a_x(t) - \overline{a_x(t)}\right]^2 dt$$

$$\sigma_y^2 \equiv \frac{1}{t_d}\int_0^{t_d}\left[a_y(t) - \overline{a_y(t)}\right]^2 dt \qquad \text{(B-2)}$$

$$\mu_{xy} = \frac{1}{t_d}\int_0^{t_d}\left[a_x(t) - \overline{a_x(t)}\right]\left[a_y(t) - \overline{a_y(t)}\right] dt$$

where the bars above quantities $a_x(t)$ and $a_y(t)$ indicate average (or mean) values over duration t_d. When both average values equal zero, the corresponding variances represent mean-square intensities of the components of motion. Substituting x' and y' for x and y, respectively, in Eqs. (2), yield the corresponding relations defining the variances and covariance of components $a_{x'}(t)$ and $a_{y'}(t)$.

It can be shown that the variance of the component of motion along the x' axis is given by

$$\sigma_{x'}^2 = \left(\frac{\sigma_x^2 + \sigma_y^2}{2}\right) + \left(\frac{\sigma_x^2 - \sigma_y^2}{2}\right)\cos 2\theta + \mu_{xy} \sin 2\theta \qquad \text{(B-3)}$$

and that its maximum (major principal) value is given when $\theta = \theta_1$ where

$$\tan 2\theta_1 = \frac{2\mu_{xy}}{(\sigma_x^2 - \sigma_y^2)} \qquad \text{(B-4)}$$

Further, it can be shown that the covariance of the components of motion along the x' and y' axes is given by

$$\mu_{x'y'} = -\left(\frac{\sigma_x^2 - \sigma_y^2}{2}\right) \sin 2\theta + \mu_{xy} \cos 2\theta \qquad \text{(B-5)}$$

and that, when θ_1 as expressed by Eq. (B-4) is substituted into this relation, the covariance of the components along the major principal axis at $\theta = \theta_1$ and the minor principal axis at $\theta = \theta_1 + 90°$ equals zero.

One should note that the above transformation of variances and covariance of two-dimensional ground motion is identical to the transformation of the two normal stresses and the shear stress associated with a set of orthogonal axes x and y in defining a two-dimensional state of stress; thus, the same Mohr's circle used in transforming components of two-dimensional stress can be used in transforming the variances and covariance of any two orthogonal components of two-dimensional ground motion. In this latter case, the Mohr's circle is constructed as shown below.

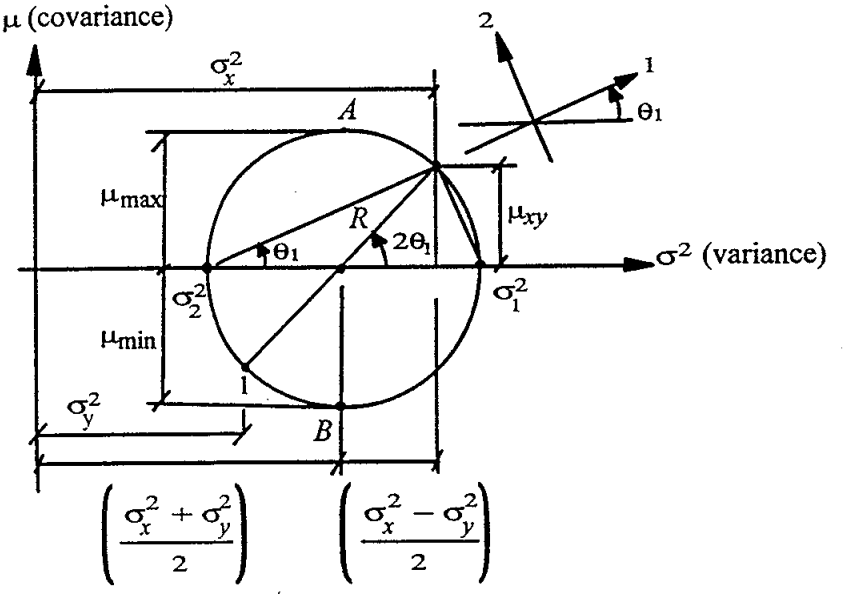

First, the center of the circle is located on the variance axis at $(\sigma_x^2 + \sigma_y^2)/2$; then, a point on the circle is located at coordinates σ_x^2 and μ_{xy}. Completing the circle of radius

$$R = \left[\left(\frac{\sigma_x^2 - \sigma_y^2}{2}\right)^2 + \mu_{xy}^2\right]^{1/2} \qquad \text{(B-6)}$$

the major and minor variances (σ_1^2 and σ_2^2) for components of motion along principal axes 1 and 2, respectively, are given by the abscissa values at the two points on the circle where it crosses the variance axis, namely the values

$$\sigma_{1,2}^2 = \left(\frac{\sigma_x^2 + \sigma_y^2}{2}\right) \pm \left[\left(\frac{\sigma_x^2 - \sigma_y^2}{2}\right)^2 + \mu_{xy}^2\right]^{1/2} \tag{B-7}$$

The covariances (ordinates) associated with these two points both equal zero indicating that (1) the covariance μ_{12} of the principal components of motion along axes 1 and 2 equals zero, and (2) the covariance of components of motion along axes in the negative 1 and 2 directions (i.e. the $\theta = \theta_1 + 180°$ and $\theta = \theta_1 + 270°$ directions) also equals zero.

Using Eq. (B-5), one can show that the values of θ which give maximum and minimum values of covariance $\mu_{x'y'}$ are $\theta_1+45°$ and $\theta_1+135°$ and that the corresponding values of $\mu_{x'y'}$ are given by

$$\mu_{\substack{\max \\ \min}} = \pm\left[\left(\frac{\sigma_x^2 - \sigma_y^2}{2}\right)^2 + \mu_{xy}^2\right]^{1/2} \tag{B-8}$$

which correspond to Pts. A and B on Mohr's circle as shown above. The variances of the components of motion along these axes, which produce maximum and minimum values of covariance, are both equal to $(\sigma_x^2 + \sigma_y^2/2)$.

INFLUENCE OF TRANSFORMATION ON RESPONSE SPECTRAL VALUES

Transforming the components of horizontal ground motion for use as inputs to a structure has great significance from a seismic performance point of view. To illustrate, consider the simple single-lumped-mass oscillator shown here which is assumed to experience identical response in the x′ direction when subjected to a single component of input in that same direction, regardless of the angle θ, i.e. the system responds in an uncoupled manner to any two orthogonal components of input motion, namely $a_x(t)$ and $a_y(t)$ or $a_{x'}(t)$ and $a_{y'}(t)$, acting simultaneously. The maximum absolute values of the

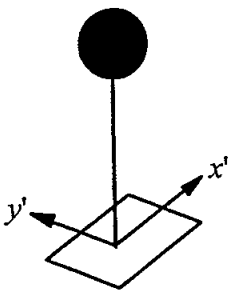

system's uncoupled responses in these directions are given by the corresponding response spectral values of the inputs. These spectral values for components of motion in the x, y, x', and y' directions will be designated herein as $S_x(T,\xi)$, $S_y(T,\xi)$, $S_{x'}(T,\xi)$, and $S_{y'}(T,\xi)$, respectively. Plots of these spectral values as functions of oscillator period T for discrete values of damping ξ yield the corresponding sets of response spectra. For the above uncoupled simple system, each response spectral value produced by a single component of input will be nearly proportional to the standard deviation (square root of the variance) of that input motion; thus, the following relations will be satisfied approximately:

$$S_1(T,\xi)/S_x(T,\xi) \doteq \sigma_1/\sigma_x$$

$$S_2(T,\xi)/S_y(T,\xi) \doteq \sigma_2/\sigma_y \qquad \text{(B-9)}$$

in which the subscripts indicate directions of input and corresponding directions of oscillator response.

Let us define two dimensionless ratios as follows:

$$\alpha_{xy} \equiv \sigma_y/\sigma_x \qquad 0 \leq \sigma_{xy} \leq 1$$

$$\rho_{xy} \equiv \mu_{xy}/\sigma_y\sigma_x \qquad -1 \leq \rho_{xy} \leq 1 \qquad \text{(B-10)}$$

It is assumed here that the variance on component $a_x(t)$, σ_x^2, is always greater than the variance on component $a_y(t)$, σ_y^2, i.e. motion $a_x(t)$ is always stronger than motion $a_y(t)$ in which case the ratio α_{xy} must fall in the range zero to one as indicated above. The ratio ρ_{xy} as defined above is referred to as the cross-correlation coefficient of motions $a_x(t)$ and $a_y(t)$. In accordance with this definition, it must always be in the range -1 to +1 as indicated. Making use of Eqs. (B-7), (B-9), and (B-10), one can obtain

$$\left(\frac{S_1(T,\xi)}{S_x(T,\xi)}\right) \doteq \left(\frac{\sigma_1}{\sigma_x}\right) = \left\{\left(\frac{1+\alpha_{xy}^2}{2}\right) + \left[\left(\frac{1-\alpha_{xy}^2}{2}\right)^2 + (\rho_{xy}\alpha_{xy})^2\right]^{1/2}\right\}^{1/2}$$

(B-11)

$$\left(\frac{S_2(T,\xi)}{S_y(T,\xi)}\right) \doteq \left(\frac{\sigma_2}{\sigma_y}\right) = \left\{\left(\frac{1+\alpha_{xy}^2}{2\alpha_{xy}^2}\right) - \left[\left(\frac{1-\alpha_{xy}^2}{2\alpha_{xy}^2}\right)^2 + \left(\frac{\rho_{xy}}{\alpha_{xy}}\right)^2\right]^{1/2}\right\}^{1/2}$$

Equations (B-11) are plotted in Fig. B-1 as functions of ρ_{xy} over the range $0 \leq \rho_{xy} \leq 0.2$ for discrete values of α_{xy} equal to 1.0, 0.9, 0.8, 0.7, and 0.0. Since these functions are symmetric about $\rho_{xy} = 0$, the abscissa scale in this figure can also represent negative values of ρ_{xy}. If all of the functions plotted were extended to $\rho_{xy} = \pm 1$, the ordinates at those limiting values of ρ_{xy} would be equal to $(1 + \alpha_{xy}^2)^2$ for the upper functions representing $S_1(T,\xi)/S_x(T,\xi)$ and would be to zero for the lower functions representing $S_2(T,\xi)/S_y(T,\xi)$. Note that when the cross-correlation coefficient of components $a_x(t)$ and $a_y(t)$ is controlled to values in the range -0.10 to +0.10, the response spectrum ratios will remain in the range -0.95 to +1.05, even for the largest value of α_{xy}. Normally such control would be considered adequate for engineering purposes.

Using Eqs. (B-10), Eq. (B-4) can be expressed in the form

$$\tan 2\theta_1 = \frac{2\rho_{xy}\alpha_{xy}}{(1-\alpha_{xy}^2)} \qquad \text{(B-12)}$$

Angle θ_1 is plotted in Fig. B-2 as a function of ρ_{xy} over the range $0 \leq \rho_{xy} \leq +0.2$ for discrete values of α_{xy}. All functions represented are antisymmetric about $\rho_{xy} = 0$; thus, plots for negative values of ρ_{xy} are not shown. The values of θ_1 for $\rho_{xy} \pm 1$ can be obtained using the relation $\tan\theta_1 = \pm\alpha_{xy}$. Should ρ_{xy} be controlled to values in the range -0.10 to +0.10, as mentioned

above, the corresponding values of θ_1 may cover a wide range, depending upon the value of α_{xy}. For $\alpha_{xy}=+1$, this range is from -45° to +45°; however, for decreasing values of α_{xy}, this range narrows rapidly.

CONCLUDING STATEMENT

In assessing the severity of two-dimensional seismic ground motion on the performance of a structural system, it is not sufficient to simply characterize each of its two orthogonal components independently of each other, unless they are the actual principal components of motion having zero cross-correlation. Any significant cross-correlation of the selected components should be taken into consideration appropriately. Consistent with this position, it is strongly recommended that when using two recorded (or generated) components as the starting seismic motion they should first be transformed into principal components of motion which act in the corresponding principal directions. These principal components may then be made response-spectrum-compatible with specified design spectra.

REFERENCES

Penzien, J. and Watabe, M. (1974), "Simulation of 3-Dimensional Earthquake Ground Motions," Bulletin of the International Institute of Seismology and Earthquake Engineering, Vol. (1974), pp. 103-115.

Penzien, J. and Watabe, M. (1975), "Characteristics of Three-Dimensional Earthquake Ground Motions," Earthquake Engineering and Structural Dynamics, Vol. 3, pp. 365-373, 1975.

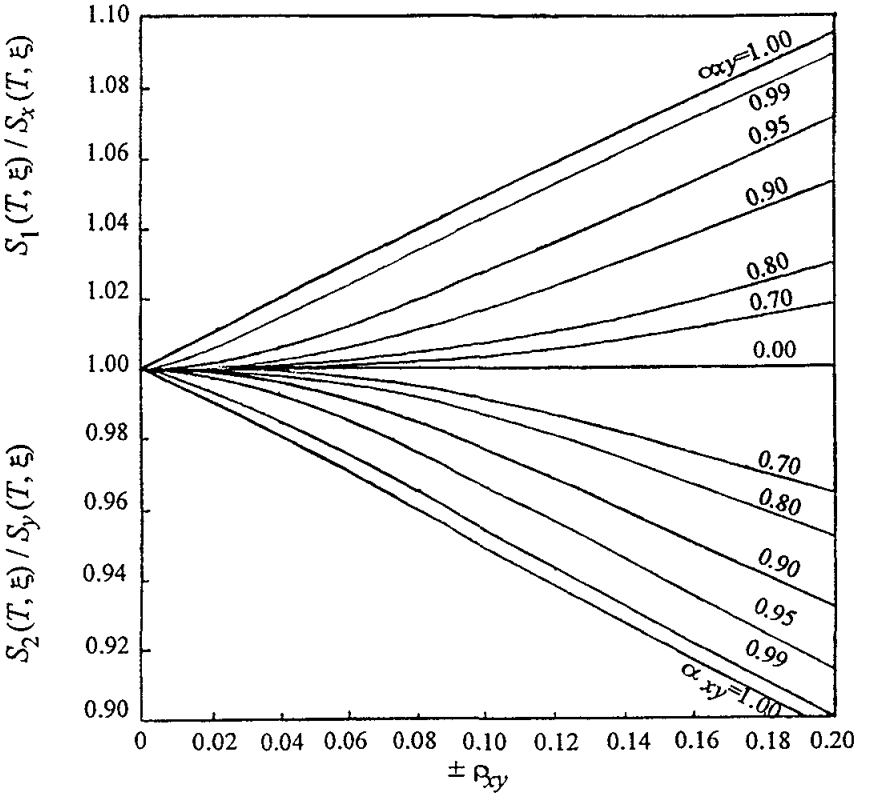

Fig. B-1 Response spectrum ratio vs. cross-correlation coefficient of $a_x(t)$ and $a_y(t)$ for discrete values of α_{xy}.

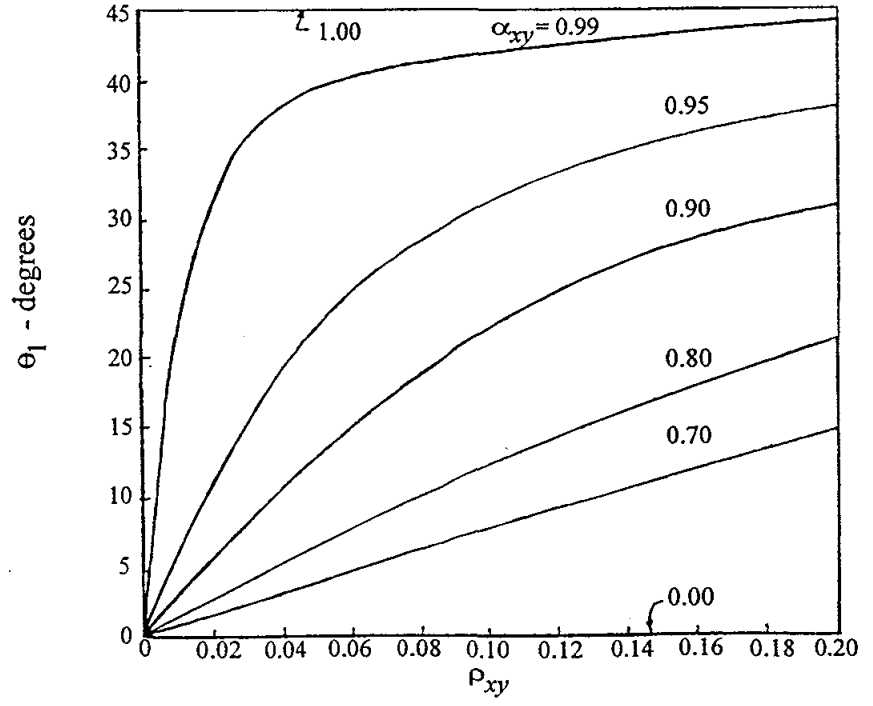

Fig. B-2 Angle θ_1 to the major principal axis vs. cross-correlation coefficient of $a_x(t)$ and $a_y(t)$ for discrete values of α_{xy}.